UNIVERSITY OF STRATHCLYDE

Investigation and Validation of Vibratory Methods for Stress Relieving and Weld Conditioning

This thesis is presented for the Degree of

Doctor of Philosophy

February 1999

ASM Younus Munsi

Department of Mechanical Engineering,
University of Strathclyde, Glasgow, UK

To my mother and father,

My wife Anju and

My beloved daughter Lisa.

and also

To my brothers and sisters

ACKNOWLEDGEMENTS

I am particularly grateful to my supervisors, Dr. Alex J. Waddell and Dr. Colin A. Walker who throughout the work, have given me invaluable guidance, inspiration, challenge and well-founded criticism. I would like to extend my gratitude to Professor Thomas G. F. Gray, Professor Alan Hendry, Dr. Andrew J. McLaren, Mr. Donald A. Forbes, and to the many other academic staff for their help and co-operation in this work.

I would like to thank Mr. Chris Cameron, Mr. Alex Cairney, Mr. John Low, Mr. Ronny McKenzie, Mr. Ted Silvers, Mr. Jack Sivewright, Mr. Andrew Crockett, Mr. John C. Barnes and other laboratory assistants for their help in preparing necessary jigs and fixtures and also their help in using laboratory equipment. I would also like to thank Mr. James Kelly for his help and co-operation in the metallurgical investigations.

None of this work described within could have been carried out without the financial support given to me by the University of Strathclyde and ORS Award Scheme as tuition fees and scholarship. I would like to special thank to my supervisors Dr. Alex J. Waddell and Dr. Colin A. Walker, and Head of Mechanical Engineering Dept. Professor Thomas G. F. Gray and Administrative Officer Miss. Janet Harbidge for their support of this matter. I would also like to thank to EPSRC for its support for different equipment especially for the X-ray diffractometer.

Above all, it is to my wife Anju, that I must express sincere appreciation for boundless patience, understanding, encouragement, and help throughout the work; also to my beloved daughter Lisa whose dad was always busy and did not spend enough time with her.

ABSTRACT

Manufacturing processes inevitably induce a state of residual stress into materials and products. These residual stresses pose a large potential problem, in terms of dimensional stability and reduced fatigue life. Ideally, residual stresses should be reducible to low levels. There are three methods in general usage for the relaxation of these stresses, - Annealing, Shakedown and Vibratory Stress Relief (VSR). A previous study had suggested that vibration during and/or after welding may usefully modify residual stresses due to welding. This has been termed *Vibratory Weld Conditioning* (VWC). A comparative study of the methods is presented in section 1.4.

The use of VSR, though widespread, has been adopted on a case-by-case basis, due to the lack of understanding of the processes at work. The purpose of this work was to investigate and validate the VSR/VWC method as a proposed alternative to the processes mentioned above. In order to do this a series of tests were devised in which the specimens were welded as a mechanism of stress induction. The residual stresses were measured before and after welding and vibration by means of a scanning X-ray diffractometer.

In Chapter 1, the study of Residual Stress (source, formation etc), Welding Metallurgy and a comparison of VSR/VWC with other treatment methods are presented. In Chapter 2, a detailed review of literature is presented, where the accessible literature on VSR/VWC to date are included. In Chapter 3, the theoretical background of Modal Analysis, the Measurement of Dynamic Induced Stress and Measurement of Residual Stresses is discussed. In Chapter 4, the FE analysis of different structures is presented. In the FE analysis, different properties of the structures were determined using the FE model to aid the VSR/VWC study.

The experimental investigations are presented in Chapter 5, which is divided into the following parts: Modal Analysis (experimental), Calibration of the X-ray measurements, VSR/VWC treatments, Cryogenic treatment, Fatigue Test and Metallurgical Investigation of VSR/VWC treated specimens. At the outset of the experimental work, the calibration of the X-ray diffractometer was carried out. After calibration of the X-ray and the X-ray Elastic Constant the error band of the diffractometer was significantly reduced. The practical modal analysis of the "8" frame was carried out to determine the modal characteristics of the frame to aid the VSR investigation of the frame.

The VSR/VWC treatments are divided into **"during welding"** and **"post weld"** treatments and are presented in 10 different experiments. First, the "during welding" treatments were carried out. Investigation was started with application of tensile and compressive static stress to the specimens during welding and cooling. It was observed that the tensile induced stress decreased, and compressive induced stress increased the residual stresses. Rigid body motion (RBM) vibration showed no effect on the residual stresses. The cantilever beam test of the flexural vibration test showed some important characteristics, where the longitudinal residual stresses were found to decrease with application of small-induced stress. An increase in applied stress or time of vibration did not cause any more reduction. The transverse residual stresses increased with application of small-induced stresses. With increase in the applied stress the residual stresses decreased. High frequency vibration in both RBM and flexural vibration was found to be ineffective in reducing the residual stresses. The flexural vibration of the Four-Roller Supported beam showed a very confusing result, where no particular trend of the residual stresses was found. The combined mode of vibration (longitudinal and flexural) treatment showed no effect on residual stresses.

The "post weld" treatment of the specimens showed a significant reduction in the residual stresses, where the reduction in the residual stresses were found to be a function of applied stress, while the vibration time effect was found to be negligible. A complex shape of reduction in the residual stresses were found along the width of the specimens, which made it impossible to develop any plastic flow model for the reduction in the residual stresses. Torsional test revealed a very important property of the residual stresses, where the residual stresses were found to decrease by a significant amount with application of very small induced stress. High induced stress only redistributed the residual stresses.

Cryogenic treatment caused no reduction in the residual stresses. Contrarily the same specimen showed a significant reduction after VSR treatment. The fatigue test showed an increased fatigue life of the VSR treated specimens, while the thermally treated specimens showed a decreased fatigue life. The vibrated specimens showed highly oriented ferrite crystals in directions with Miller [111] to the stress axis. The hardness of the VSR treated specimens was found to increase significantly in comparison to the unvibrated specimens.

Table of Contents

Index Notation

ω	Frequency
t	Time
ω_n	Natural frequency
k	Spring stiffness
m	Mass of the system
f	Applied force
ζ	Damping ratio
c	Damping coefficient
h	Structural damping factor
η	Structural damping loss factor
x	Displacement
$\dot{x}$	Velocity
$\ddot{x}$	Acceleration
λ	Wave length
θ	Angle
ψ	Angle
σ	Stress and /or free energy change per unit area
δ	Dilatational component of shape deformation
τ	Shear stress
s	Shear component of the shape deformation
α	Thermal expansion coefficient and/or ferrite
α_1	Parabolic rate constant
M_s	Martensite start temperature
M_f	Martensite finish tempetature
N	Number of cycles
A	Strain energy factor and/or Ampere (current unit)
γ	Surface energy and /or Austenite phase
μ	Non zero mean of applied stress
ΔG	Molar free energy
T	Temperature

ν	Poisons ratio
E	Modulus of Elasticity
R	Resistance
V	Voltage
ε	Strain
G_f	Gauge factor
λ	Wave length of X-ray
d	Spacing of the reflecting planes of atoms
$\mu\varepsilon$	Microstrain
M	Moment
I	Moment of inertia
K_c	Corrected elastic constant
AC	Alternating current
DC	Direct current
MPa	Mega Pascal
GPa	Giga Pascal
RMS	Root Mean Square
Sp	Specimen
HAZ	Heat Affected Zone
FRF	Frequency response function

Chapter 1

Introduction

Introduction

1.1 General Introduction

There is an increasing interest in the dynamic behaviour of structures based on the fact that the mechanical properties, especially the residual stress, can be changed during the application of controlled vibration. Residual stress is a major problem in the production and construction industries, since it reduces component fatigue life. If the residual stress is not relieved or redistributed in a suitable manner, i.e. the component is not conditioned before starting its life, it is certain that the fatigue life of the component would be decreased significantly, or would distort to some degree.

It is generally accepted that fatigue strength is significantly increased by a compressive residual stress and lowered by a tensile residual stress. The residual stress state influences the propagation of micro and macro cracks which presents considerable problems during the service life of a component. The combination of tensile residual stress with service loading effectively raises the mean stress level. The total state of stress (including residual stresses) directly affects the rate of crack propagation. Extension tests have demonstrated that fracture conditions can be related to the total state of stress in a structure including the full effects of stress concentrations and residual stresses. Compressive residual stresses on either side of the heat affected zone in welded components can become problematic in thin steel structures due to the risk of buckling.

Distortion is the most apparent result of thermal stress induced by the welding process. Primary distortion is the result of the initial welding process which tends to misalign the welded components. Secondary distortion is the result of additional warpage when welds are machined so as to unbalance the stress equilibrium. Heat affected zone (HAZ) hydrogen cracking in welds is the most common form of fabrication cracking. These cracks generally initiate at the stress concentration point which is formed at the weld toe or root and propagates in the heat affected zone material.

As a preliminary to the main study, the origins of residual stress and the fundamentals of welding metallurgy were studied and a brief discussion of them will be presented

here. Methods of relieving residual stress in metals include (i) thermal treatment and (ii) mechanical treatment. Thermal treatment of residual stress can be further divided into the following: (a) annealing, (b) cryogenic treatment, (c) parallel heat source welding. Mechanical treatment can be further divided into: (a) plastic deformation stress relief, and (b) vibratory stress relief (VSR) and/or vibratory weld conditioning (VWC). All of these treatment methods will be briefly discussed in this chapter.

In this study several types of specimens were used for different studies. First of all, a rectangular "8" frame specimen measuring 400 mm × 200 mm was chosen as a simple structure for modal analysis and preliminary VSR investigation. In this connection a brief theoretical study of Modal Analysis was carried out, the result of which is presented in section 3.1. The dynamic properties of the specimens were investigated where a detailed modal analysis was carried out and some important modal and dynamic characteristics were determined and is presented in section 5.8. The "8" frame was prepared from a solid plate, although there were very little residual stresses present in the structure, and no residual stress was applied externally, i.e. the frames were treated as homogeneous materials. The VSR treatment of "8" frame was stopped as it was decided to reduce the number of variables in the working structure and it was decided to keep the specimens as simple as possible.

A cantilever beam and a dynamic four point bending beam of cross-section 76.2-mm × 6.35-mm were chosen for different treatment methods. Some specimens were treated by applying static stress. These specimens were pre-stressed by bending with either tensile or compressive stress in order to investigate the effect of applied static pre-stress on welding residual stress. For the VSR and VWC treatment, a lower frequency (25 Hz) was selected to induce a higher dynamic stress because it was thought that relaxation of residual stress occurs in VSR treatment due to applied stress. In addition, some specimens were VSR treated using high mechanical frequencies to investigate their effect on welding residual stress. In the treatment process two approaches were used; during welding treatment and post weld treatment.

In the during-welding treatments, two different modes of vibration were used; rigid body motion vibration and flexural motion vibration. In the rigid body motion

vibration the specimens were clamped rigidly to the vibration table and vibration was applied while the specimens were being welded (virtually no flexural motion occurred). In the flexural motion vibration, three different kinds of set-up were used. In the first kind, one end of the specimen was clamped to a rigid frame and vibratory forcing was applied to the other end by an electromagnetic shaker. In the second kind, four-point roller supports were used to vibrate the structures, where two pieces of flat bars were joined together using a single pass weld. Vibration was applied to the specimens while the specimens were being welded. In that set-up two sets of rollers were used to apply vibration to the specimens and the other two kept the specimens in position. In both of the set-ups above, pure flexural vibrations were applied to the specimens. In the third kind of set-up, two pieces of flat bars were welded together in a single pass weld as in the previous set-up. In this set-up both ends of the specimens were clamped to a rigid frame, vibration was applied to the specimens using two connecting rods from the vibrator. A combined mode of vibration (longitudinal and flexural) was applied to the specimens.

In the post-weld treatment the specimens were treated after cooling down to room temperature, where two types of vibration were used; flexural vibration and torsional vibration. The flexural vibration set-up was similar to the flexural (during welding) vibration set-up (first kind). Cylindrical shafts of different dimensions (presented in Section 5.2.3) were processed where torsional stresses were applied to the shafts to investigate the effect of pure shear stress to the residual stresses. In the torsion test, one end of the shaft was clamped to a rigid frame and torsional forcing was applied to the other end.

A cryogenic treatment was carried out using some flat bar specimens, where the specimens were submerged into liquid Nitrogen to observe the effect of cryogenic temperature on the residual stresses. A fatigue test of as-welded, thermally treated and vibratory treated specimens was carried out for comparison of the fatigue life of differently treated specimens. A metallurgical investigation of the vibrated and unvibrated specimens was carried out, where the crystal structures and the hardness of the vibrated and unvibrated specimens was studied. All the results of the experiments mentioned above are presented in Chapter 5, where the investigation is subdivided into

fourteen different experimental sections. At the start of each experimental section, the '*abstract*' of the experiment is presented, where a brief procedure and findings are included to provide an overview of the experiment.

In the different experiments the set-up was changed/modified according to the objective and requirement of the experiment. Prior to the onset of the experimental work the variables such as displacement, applied stress etc. were calibrated. The details of the calibration processes are presented in the relevant experiments. Finite Element (FE) analyses of the specimens was also carried out in order to determine the values of the applied static/dynamic stresses and to determine the modal characteristics which are presented in Chapter 4.

The residual stresses of the specimens were measured using an X-ray diffractometer. In this connection, different residual stress measurement methods were briefly studied, and are discussed in Chapter 3.

1.2 Residual Stress

Residual stress is a severe problem in the production/construction industries. It arises in the production processes of the components and may cause premature failure. In every step of production some residual stress is induced within the specimens/product. If materials are externally loaded, the real stress state would be the summation of the external and residual stresses.

Compressive residual stress is usually beneficial, since it will cause a mean stress displacement in the direction of compressive stresses - thereby inhibiting crack propagation. On the other hand, a tensile residual stress will cause a shift of the mean stress towards tension, hence helping to promote the possibility of crack propagation and likely fracture.

1.2.1 Definition

Residual stress is the self-equilibrating stress which exists in materials under uniform temperature conditions, without any external traction. This stress would always be produced if regions of a material are inhomogeneously elastically or plastically

deformed in such a permanent manner that strain incompatibility occurs. Of course these deformations occur due to internal or external loading. This loading might arise either from thermal processes of diffusion or as a result of phase transformations in such a way that internal stress fields are set up. In fulfillment of the conditions of equilibrium, volumetric and shape change takes place. Such conditions of residual stress may be caused by shrinkage processes and damage may arise through the formation of cracks and fractures, the positive and negative effects on the properties of strength of components, the reduced resistance to stress corrosion and corrosion fatigue and finally on the wear behaviour of mating components.

1.2.2 Classification of Residual Stress

Several categories of residual stress may be distinguished according to the characteristic dimension of the regions upon which they act.

Residual Stress of First Kind

In the first kind, or type-I, the magnitude and direction of the internal stresses are nearly homogeneous or vary slowly over a macroscopic region (several millimetres to a large area) of the body and are equilibrated within the whole body (Figure 1.1). Macro residual stress and applied stress add algebraically at least up to the elastic limit and thus are important in determining load-carrying capabilities. This stress may develop from mechanical processes such as surface working, forming, assembly, thermal processes such as welding or casting and oxidation or corrosion.

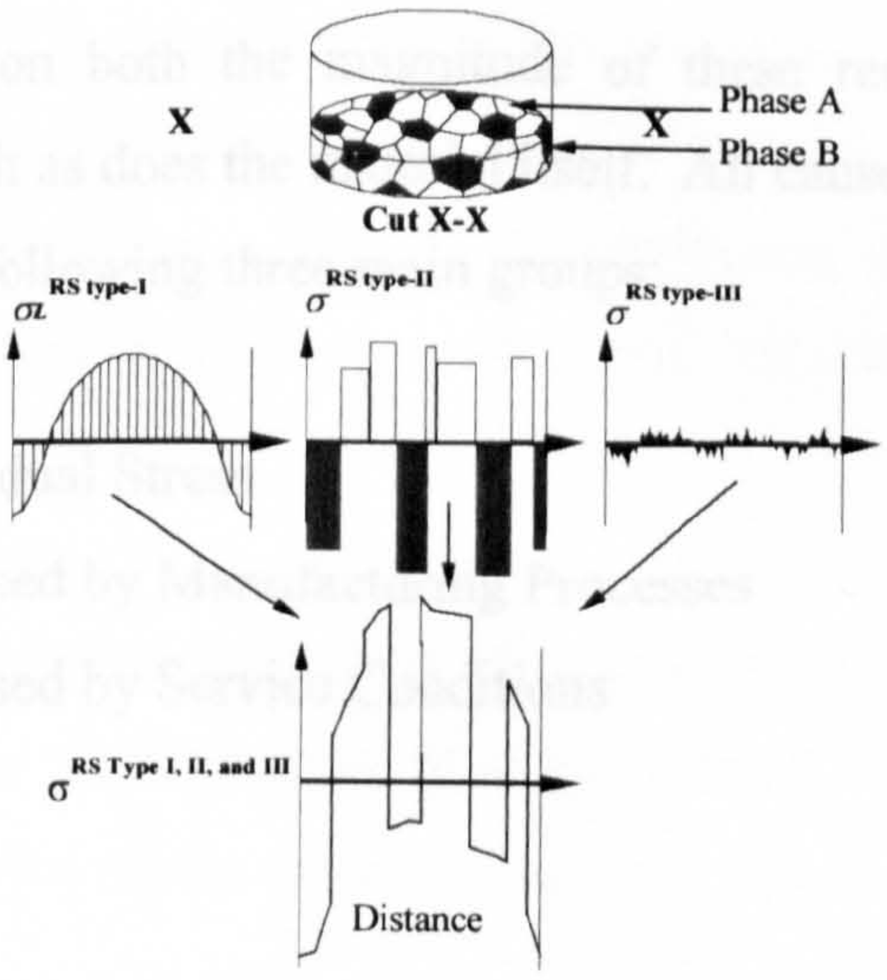

Figure 1.1 – Residual stresses in a multi-phase system

Residual Stress of Second Kind

In the second kind, or type-II, the residual stresses are nearly homogeneous in a sub-volume (say one grain or part of a grain) of the body and are equilibrated across a sufficient number of grains (Figure 1.1). Discontinuities in the grain boundaries may arise from mismatching lattice parameter; the scale of such stresses is similar to that of the granular microstructure. Crystal lattice dislocations, interstices, substitutional elements and similar imperfections cause these types of stresses. Micro stresses are mainly caused by the phase transformation of metals during cooling or due to aging of metastable phases.

Residual Stress of Third Kind

In the third kind, or Type-III, the residual stresses are inhomogeneous across a submicroscopic range (over dimensions of 1-1000 $\mathring{A}$, areas) of a material, say several atomic distances within a grain, and are equilibrated across small parts of a grain (Figure 1.1). This stress arises from varying stress fields of individual dislocation pile-ups, kink boundaries and other microstructural phenomena of a discontinuous nature.

1.2.3 Formation of Residual Stress

In structural metals, residual stresses are commonly associated with inhomogeneous plastic deformation; whether due to large temperature gradients, volume change due to phase transformations, or from metal flow. The specific process causing these effects has a large influence on both the magnitude of these residual stresses and their distributions in the depth as does the material itself. All causes of residual stresses can be classified under the following three main groups:

1. Material Based Residual Stress
2. Residual Stress Caused by Manufacturing Processes
3. Residual Stress Caused by Service Conditions

1.2.3.1 Material Based Residual Stress

Residual stress may be created if there are two or more phases present in a material, i.e. due to multi-phase systems, non-metallic inclusions, lattice defects etc.

Stress due to Multi-Phase Systems

In a multi-phase system two or more phases form from their highly heated parent metal (which in steel is an austenitic state) when it passes through the transformation temperature. To be specific, steel can be considered, because it is the most widely used metal in civilisation. In steels, austenite transforms into its preceding phases, these transformations can be classified into two broad categories according to the mechanism of transformation; these are reconstructive transformation and displacive transformation. Reconstructive transformation occurs with the uncoordinated diffusion of all the atoms, including iron. They need not be accompanied by a change in chemical composition, but it is worth emphasizing that reconstructive transformation cannot be sustained without the diffusion of all the atoms. In the displacive transformation the pattern of atomic arrangement is altered by deformation. There is no diffusion of iron or substitutional solutes during displacive transformations in iron alloys. Both kinds of transformations lead to change in shape. In the displacive transformations the shape change is in general described as an *invariant-plane strain* (IPS) with a large shear component. Such a deformation leaves the plane of contact between the parent and product phases undistorted and unrotated. This plane is called the *habit plane*. The strain energy associated with a constrained invariant-plane strain (IPS) is minimised when the product phase has a thin-plate shape. This is why Widmanstätten ferrite, bainite, acicular ferrite and martensite in steels grow in the form of plates. Detailed descriptions of the above aspects are presented in Bhadeshia [15]. These phases will be discussed in the welding metallurgy section.

Phase transformation is the main reason of formation of micro residual stress in metals. The reasons for the formation of residual stress at a microstructural level during phase transformation are described below.

1. If there is a large difference in the thermal expansion coefficients of different phases (martensite, bainite, ferrite and cementite), then there will be a large micro residual stress in the metal. When steel cools down from its austenitic state, it forms bainite, martensite, ferrite and cementite etc. depending on the cooling condition and presence of alloying elements. Some austenite does not transform to its preceding phases mainly due to lack of driving force or other kinetic restrictions such as heterogeneous nucleation. It therefore remains as residual or retained austenite. If the austenite to ferrite transformation begins at 720 ^{0}C, then, due to cooling to ambient temperature (20 ^{0}C), there will be a large elastic or plastic strain in the metal which would cause the residual stress. The final stress level would depend on the difference between the transformation temperature and the ambient temperature. If the difference between the two temperatures is small there would be lower stress, or if the difference is big there would a higher stress.

2. The austenite to ferrite transformation is accompanied by an atomic volume change of approximately 1%, which can lead to the generation of residual stress. Details of this phenomenon are discussed in Honeycombe [65].

3. The packing density of atoms in the space lattice of austenite and ferrite is different. The calculation of packing density shows that when austenite transforms to ferrite it expands its volume by 8.86%. This phenomenon is applicable to all product phases of austenite except martensite, because this transformations is displacive, i.e. diffusionless, and there is no volume change.

4. Evidence has been found that the volume changes due to transformation from austenite to other phases are not uniformly reflected in linear change in all dimensions. It was observed by Bhadeshia [15] that the thickness of a flat disc specimen actually decreased as the volume increased, i.e. the strain due to transformation is not isotropic. This phenomenon happens if the material is crystallographically textured, or transformations occur under the influence of stress which induces some non uniformity of strain, hence residual stress forms in the metal.

A phase change in a stress free material is usually triggered if the metal passes through a transformation temperature. Alternatively, the application of a stress in the isothermal condition can trigger a transformation in circumstances where it would not otherwise occur.

The permanent strain caused by any transformation is called *transformation plasticity*. A paper by Bhadeshia [15], which included transformation plasticity in the solution of engineering problems, has focused on the role of the volume changes due to transformation (originally *Greenwood & Johnson* carried out this work). For a longitudinal stress σ the longitudinal plastic strain would be

$$\varepsilon = \frac{5}{6}\frac{\Delta V}{V}\frac{\sigma}{\sigma_Y} \qquad 1.1$$

where: σ_Y is the yield stress of the weaker phase and $\Delta V/V$ is the transformation volume strain. Clearly, it is the volume strain which is assumed to enable a transformation to interact with an externally applied or internally generated stress. This is a reasonable approach when considering reconstructive transformations. If the metal specimen subjected to phase transformation transforms completely to its preceding phases then there will be a small residual stress. The value of the residual stress would increase with an increase in the amount of retained austenite and again the value should be very small or negligible in a completely austenitic metal piece. This explains why there must be a certain proportion of retained austenite which causes a maximum value of residual stress.

Work has been carried out by Bhadeshia [15] at the University of Cambridge where a polycrystalline sample was stressed at a temperature above its normal martensite start temperature M_S. The amount of martensite obtained was seen to vary directly with the magnitude of the applied stress. The stress manifests itself as a mechanical driving force whose contribution assists the chemical driving force, which on its own is inadequate to trigger transformation. Also, it was found that most of the crystal plates tended to grow on those planes which were close to the plane of maximum shear stress (45^0 to the applied tensile stress).

For reconstructive transformations, it is only the hydrostatic component of stress that can interact with the shape change (which is due only to a density change). The response to an arbitrary stress cannot therefore be as large as that for displacive transformation in steels. In that case the shear component of the IPS is relatively large and so is the corresponding mechanical driving force component.

The total driving force can be partitioned into 'mechanical driving force' and 'chemical driving force'. This is based on the reasoning that the movement of a glissile interface is a combined deformation and transformation process. The work done by external stress may be added to the chemical free energy change in order to obtain the net free energy difference. The mechanical driving force is assumed to be given as the work done (ΔG_{mech}) by the external stress in producing the macroscopic shape deformation:

$$\Delta G_{mech} = \sigma_N \delta + \tau s \qquad 1.2$$

Where σ_N is the normal stress on the habit plane and τ is the component of the shear stress on the habit plane which is parallel to the direction along which the shear displacements of the shape deformation occur. The strains δ and s are the dilatational and shear component of the shape deformation. There is a limitation of mechanical driving force because the magnitude of stress that can be applied is limited by the yield stress of austenite, which is much lower at higher temperature. So, it is not possible to apply a large mechanical driving force to combine with the chemical driving force for transformation.

Non-metallic Inclusions and Lattice Defects

Non metallic inclusions and lattice defects are another cause of residual stress. These defects and inclusions cause the third kind of residual stress i.e. stress which is in only few atomic distances. The mechanism of induction of this residual stress can be explained as if there is a dislocation or a small inclusion particle in the metal of which the diameter is not equal in diameter to the Fe atom. Thus the surrounding atoms cannot keep the standard distances between them and an atomic force is applied due to the imbalance of surface energy of the atoms. This results in an induced residual stress.

1.2.3.2 Residual Stress Caused by Manufacturing Processes

The manufacturing process is an important cause of residual stresses. There are different manufacturing systems such as Casting, Forming, Machining, Heat Treating, Joining (Welding, Brazing, Soldering), Coating etc. all of which are liable to cause residual stresses. These processes will be briefly discussed.

Casting

In metal casting, the residual stress forms due to non-uniform cooling i.e. thermal gradient in the metal. In casting, the mould exterior solidifies and progressively becomes capable to carry load due to rapid cooling but the interior remains liquid. The interior cools and contracts, but the solid exterior does not allow the metal to flow and fill up the gap until the stress approaches its yield point - hence residual stresses form. Finally, the outer skin is left in a state of compressive residual stress which is balanced by the tensile stress in the core.

Forming

Forming causes residual stress of the first kind i.e. macro residual stress. In forming, in-homogeneous and anisotropic plastic deformation occurs, which causes residual stress. The magnitude and distribution of the formed residual stress is dependent on the actual conditions of deformation and metal flow during forming.

Machining

The combined rapid heating and surface deformation of machining processes produce surface residual stresses. The final distribution of residual stresses being strongly dependent on the exact details of the machining operation, cutting speed, lubrication, type and sharpness of the cutting tool etc. A high value of residual stress forms during rough machining but it reduces significantly during careful low feed machining. This phenomenon is very clear in grinding where the formation of residual stress can be reduced almost to zero.

Shot Peening and Rolling

During shot peening and rolling, surface layers are extended, and due to the resistance of the interior to this extension, the surface is put into compression. This process is

therefore particularly useful in reducing crack propagation because the surface compressive stress shifts the average stress towards compression hence reducing the possibility of crack initiation and propagation.

Welding

To understand residual stresses due to welding, the process and its metallurgical aspects should be understood. A brief discussion of welding metallurgy will follow. There are a number of reasons why residual stresses are generated in welds. The main reasons are: phase transformation, microstructural problems/defects and thermal expansion/contraction. The final residual stress is the summation of all stresses which are formed for different reasons (Figure 1.1). Steel welding is always a multi-phase system, so the discussion in Section 1.2.3.1 would be valid for considering residual stress in welds. At the macro structural level, thermal contraction and hindered expansion generates residual stress due to a very steep temperature profile.

In welding, an intense moving point heat source generates a high temperature gradient. In the fusion zone, the molten metal solidifies at around 1200 ^{0}C and shrinks with decreasing temperature, but the shrinkage is hindered by the surrounding solid metal. In both the transverse and longitudinal directions (to the weld) the shrinkage compensation is controlled by the boundary conditions, which also control the heat flow and temperature gradient.

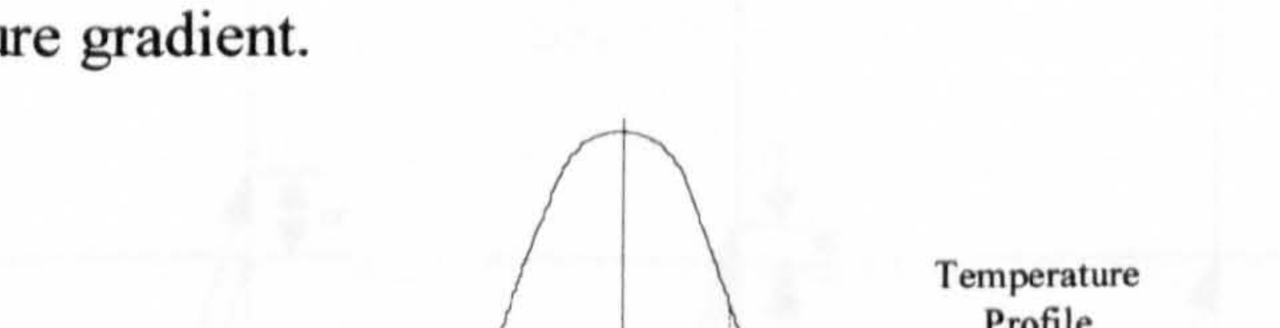

Figure 1.2 – Schematic temperature distribution in the fusion and weld HAZ

Schematic Diagram of Thermal Stress Induction

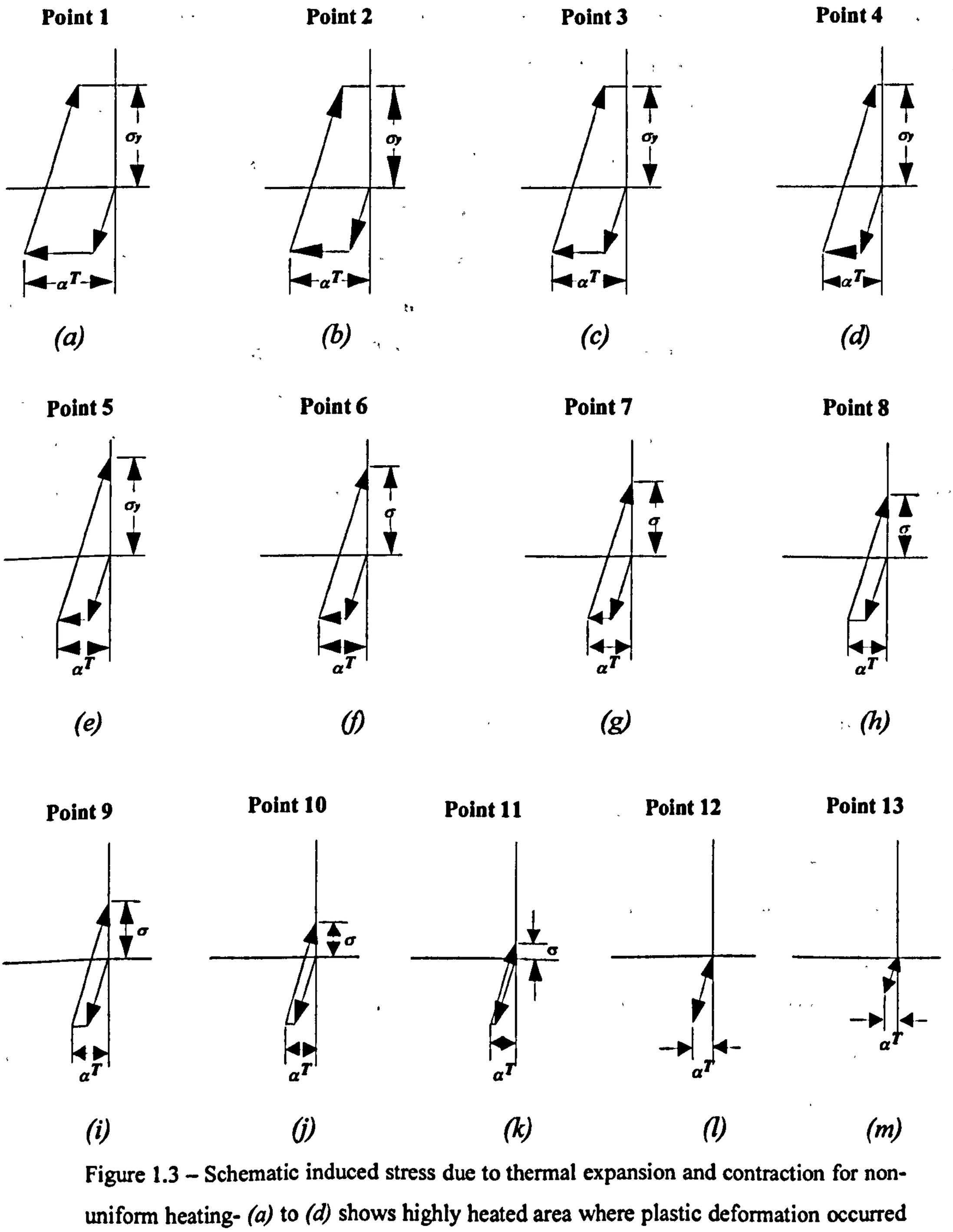

Figure 1.3 – Schematic induced stress due to thermal expansion and contraction for non-uniform heating- *(a)* to *(d)* shows highly heated area where plastic deformation occurred in the HAZ in both halves of the thermal cycle and the residual stress is equal to the yield point of the material. *(e)* to *(k)* shows medium heated area where plastic deformation occurred in the first half of the thermal cycle, and the residual stress is equal or less than the yield point. *(l)* and *(m)* shows the low heated area where plastic deformation did not occur, thus no residual stress is formed.

The major residual stress in the heat affected zone comes from hindered thermal expansion. Due to intense localized heating, the heat affected zone tries to expand, but its expansion is constrained by the surrounding cooler solid metal and plastic deformation occurs at a lower stress. At elevated temperatures, the yield stress is smaller than that which exists at normal room temperatures. When the metal cools, it shrinks, but the metal is completely solid and progressively becomes capable of carrying higher loads as its temperature decreases. So, it cannot flow to fill the gap due to contraction until it reaches its yield stress. A temperature distribution in the fusion and heat affected zone and its effect on the HAZ, 'the stress history' schematically shown in Figure 1.2 and 1.3 explains the reason for residual stress in the heat affected zone. The stress induction history in all 13 points (Figure 1.3) is illustrated by schematic stress-strain diagrams, where the vertical axis shows the formed stresses due to heating and cooling and the horizontal line shows strain/deformation due to the thermal stress. In the schematic diagrams of the highly heated zones it is shown that due to localized heating the heated metal expands but the expansion is constrained by the surrounding cold metal which causes deformation due to compressive stress. On cooling, the deformed metal shrinks but is again constrained by the surrounding cold metal so it cannot fill the gap created by the shrinkage. Hence residual stress forms. If the formed stress reaches the yield point then another plastic deformation occurs and the residual stress becomes very close to the yield stress of the metal. If it does not reach the yield point, then the formed residual stress depends on the deformation of the first half of the thermal cycle and is usually equal or less than the yield stress of the metal. In the very low heated zone, plastic deformation does not occur since the formed stress does not reach the yield point, hence residual stress does not form. A detail study of this phenomenon is presented by Gray [60]. In this model the material property is assumed as elastic then perfectly plastic.

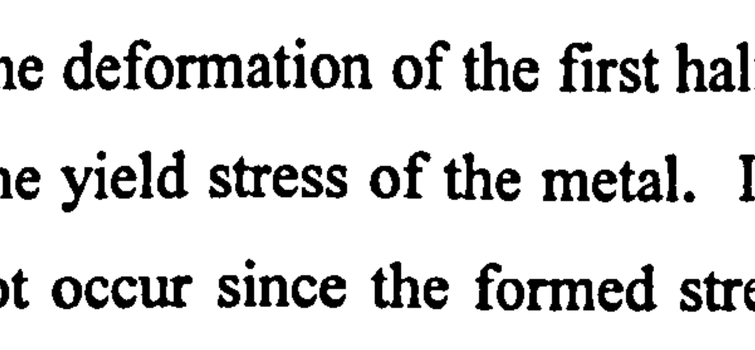

Figure 1.4 - Stress profile due to thermal expansion for non-uniform heating

The expected stress distribution in the HAZ along a line transverse to the weld is given below. This stress profile should be valid for both longitudinal and transverse directional stresses.

Generally, a large stress is induced in the longitudinal direction due to shrinkage of the weld. Due to equilibrium of formed stresses, the large stresses in the longitudinal direction change the transverse stresses to zero or compressive stresses a little distance away from the weld toe. A typical longitudinal and transverse welding residual stress plot is shown in Figure 1.5 below.

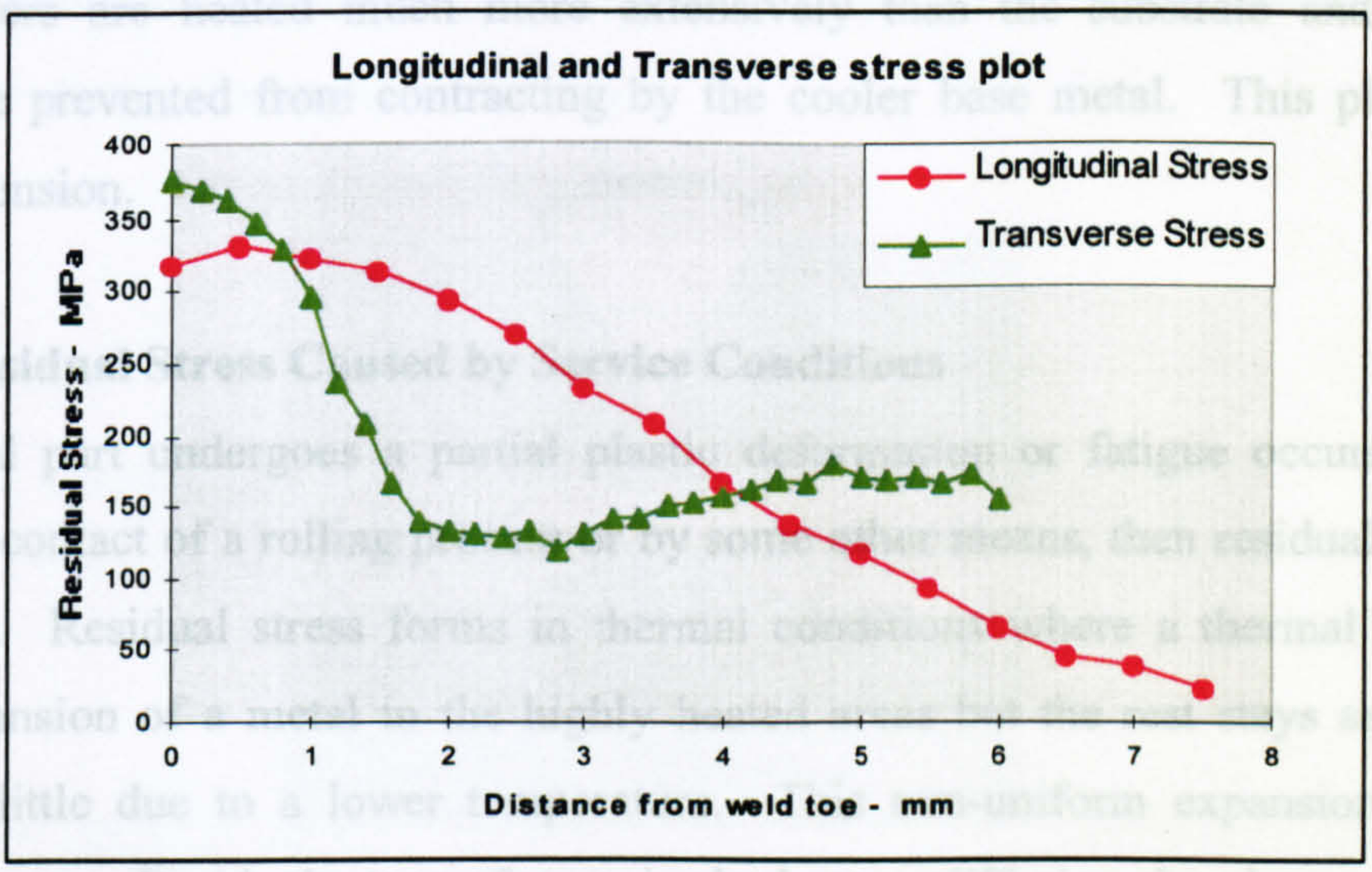

Figure 1.5 - Typical welding residual stress distribution

Heat Treatment

During heating and cooling, stresses may arise due to differences in the rate of temperature change between the surface and internal volume or from differences in the coefficient of expansion of the different phases present. The local yield strength may be exceeded at some temperature and result in non-uniform plastic flow. Large stresses may also occur.

In materials that undergo phase changes, even more complex stress states may develop. For example in hardenable steels, martensite may form first at the surface (on cooling), causing plastic extension at the centre. When this phase subsequently forms in the centre of the piece, the surface is put in tension.

Surface Coating

Protective surface layers for various environments can be produced for example by electro-plating, spraying, flame deposition and explosive cladding. Electro-plating often seems to produce residual tensile stresses which are sensitive to small layer thickness and are a function of the additive concentrations in the plating solution.

Stress patterns are found in other methods of depositing protective coatings such as flame deposition. Deposition of the powdered nickel or copper oxides is brought about by the detonation of a gaseous mixture over a base of nickel or titanium. The surface layers are heated much more extensively than the substrate and, during coating, are prevented from contracting by the cooler base metal. This places the surface in tension.

1.2.3.3 Residual Stress Caused by Service Conditions

If the metal part undergoes a partial plastic deformation or fatigue occurs due to continuous contact of a rolling process or by some other means, then residual stresses are formed. Residual stress forms in thermal conditions where a thermal gradient causes expansion of a metal in the highly heated areas but the rest stays as it is or expands a little due to a lower temperature. This non-uniform expansion creates residual stress. Residual stress forms in hydrogen diffusion in electrochemical corrosion.

1.3 Welding Metallurgy

A basic knowledge of welding metallurgy is essential for any investigator who wishes to investigate the effect of vibration treatment on welded joints. In this chapter a concise discussion of the welding metallurgy of mild steel is followed by a reasonably detailed discussion of phase transformations during weld cooling, because the residual stress forms during cooling while a diversity of phase transformation occurs; to understand residual stress, the phase transformations of welding should be understood. In welding, residual stress is very much dependent on the actual situations that occur during and after welding.

There are different types of welding, of which fusion welding is of the greatest importance in the fabrication of engineering structures. There are different ways that fusion welding may be carried out, but in all of these processes the principle is always the same, melting a small portion of both metal pieces to be joined and adding some molten metal into the weld pool (Figure 1.6). When the molten metal solidifies it welds the components together. The metallurgy of welding can be classified in two major regional categories which are designated as the Fusion Zone and the Heat Affected Zone (HAZ). The fusion zone represents the deposited and molten parent metal, its solidification, microstructure, properties etc. The Heat Affected Zone (HAZ) represents the parent metal which is not melted but affected by heat which causes many chemical and physical changes.

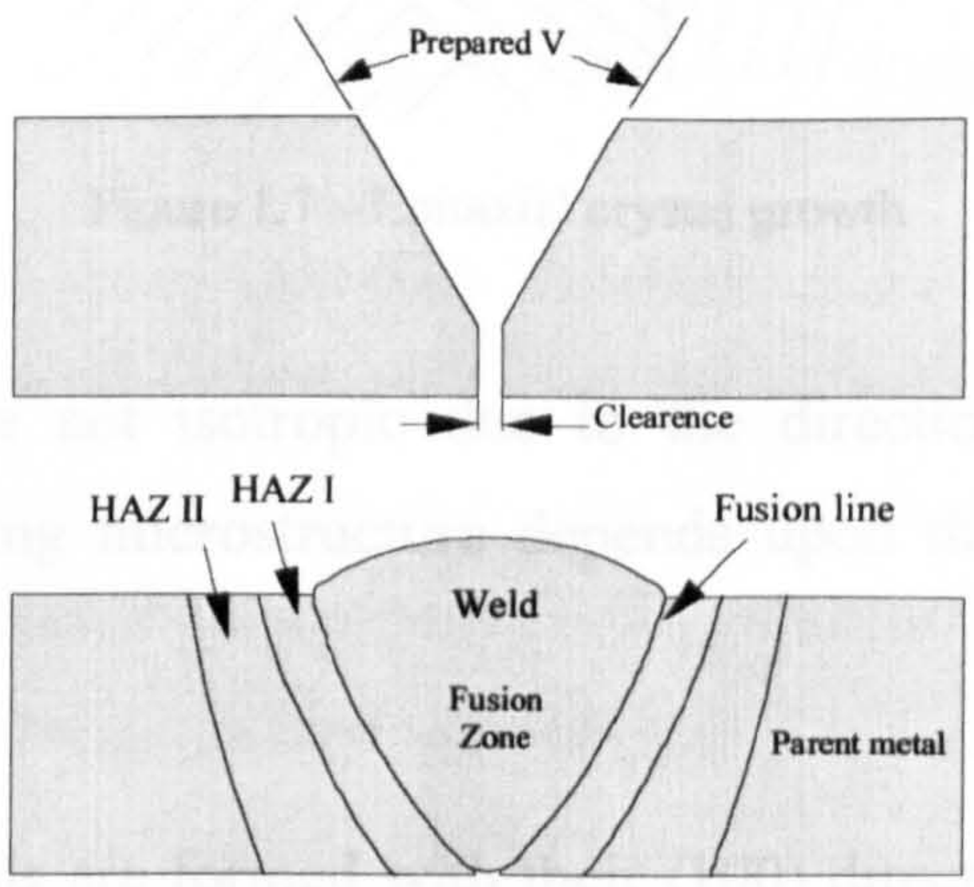

Figure 1.6 – Different zones in welding

1.3.1 The Fusion Zone

Iron is in the delta ferrite phase (BCC structure) just after solidification, when it cools further, delta ferrite transforms to austenite (FCC structure). It reverts back to ferrite again (alpha ferrite) when it cools further. A phase transformation diagram is presented in Figure 1.17. The microstructure and properties of the solidified phases depends on the alloying elements and cooling conditions etc. Mild Steel contains very small amounts of carbon, manganese, vanadium, etc, so its properties may be considered as being similar to pure iron.

The weld deposit begins to solidify with the epitaxial growth of columnar delta ferrite grains from the hot grain structure of the parent plate at the fusion surface. Epitaxial solidification is a heterogeneous process in which a solid embryo of the weld metal

forms at the molten-back surface of the base metal. The shape of the embryo depends on the various surface energies of the system, γ_{ML} (the base metal-liquid surface energy), γ_{SL} (the solidified weld metal-liquid surface energy) and γ_{SM} (the surface energy between the solid weld metal and the base metal). Assuming γ_{SL} is isotropic, it can be shown that, for a given volume of the embryo, the interfacial energy of the whole system can be minimised if the embryo has the shape of a spherical cap.

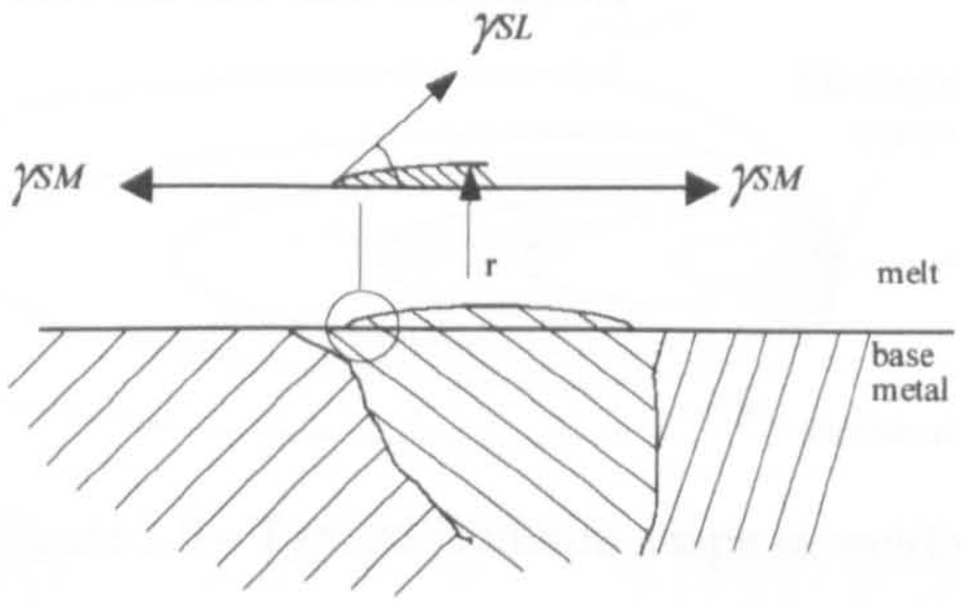

Figure 1.7 – Epitaxial crystal growth

The formed crystals are not isotropic due to the direction of flow of heat. The orientation of the welding microstructure depends upon the isotherms of the weld pool.

It is observed that crystals are formed with their ⟨100⟩ directions perpendicular to the isotherms i.e. parallel to the direction of the heat flow.

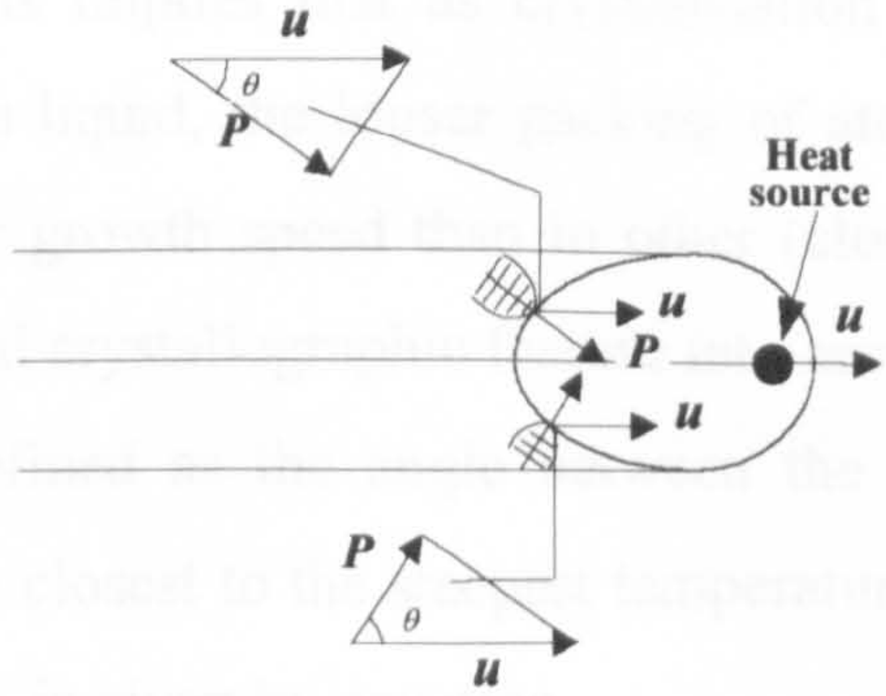

Figure 1.8 - The relationship between crystal growth and welding speed

If the velocity of welding is u and speed of solidification P then the relation of these two will be,

$$P = u\cos\theta \qquad 1.3$$

Given a constant velocity of welding u, the solidification speed varies with the angle θ on the liquidus isotherms of the weld. This explains that the solidification is a maximum on the line of weld centre ($\theta = 0^0$) and a minimum on the isotherm perpendicular to the weld line ($\theta = 90^0$). In continuous welding the shape of the weld pool and the isotherms depend upon the materials conductivity, heat input, welding speed and of course the specimen geometry, which is discussed in detail in Gray [60]. A typical set of weld isotherms are shown below

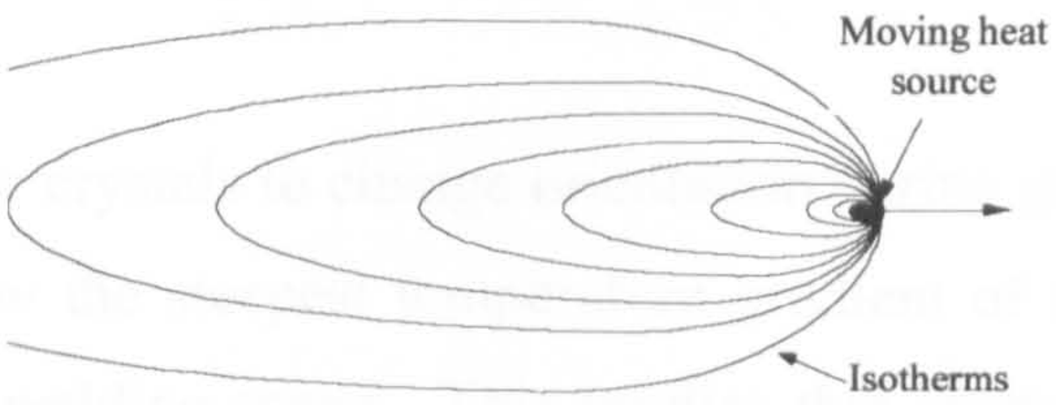

Figure 1.9 - Typical isotherm shape in welding

The isotherms of the weld pool vary with the speed of welding, which characterizes many properties of the welding. If the speed of the welding is too high the isotherms of the welding reach a critical shape such that the growing crystals have to make sudden changes in direction at the weld centre line in order to maintain the continuity of the weld. Abrupt change in the growth direction can be detrimental to the toughness of the weld due to increased risk of segregation at the weld centre line. The preferential growth in the ⟨100⟩ direction is thought to be because this direction is the least closed packed. This implies that as crystallisation occurs from the random atomic arrangement in the liquid, the looser packing of atoms in the ⟨100⟩ direction effectively allows a faster growth speed than in other (closed packed) directions. In order to take this additional crystallographic feature into account, equation (1.3) has to be modified. If θ^d is defined as the angle between the appropriate ⟨100⟩ growth direction and the direction closest to the steepest temperature gradient, then the actual crystal growth velocity, P', is given by equation

$$P' = P\cos\theta^d \qquad 1.4$$

Hence, the fastest growth speeds occur when the ⟨100⟩ direction coincides with the steepest temperature gradient, i.e. when $\theta^d = 0$.

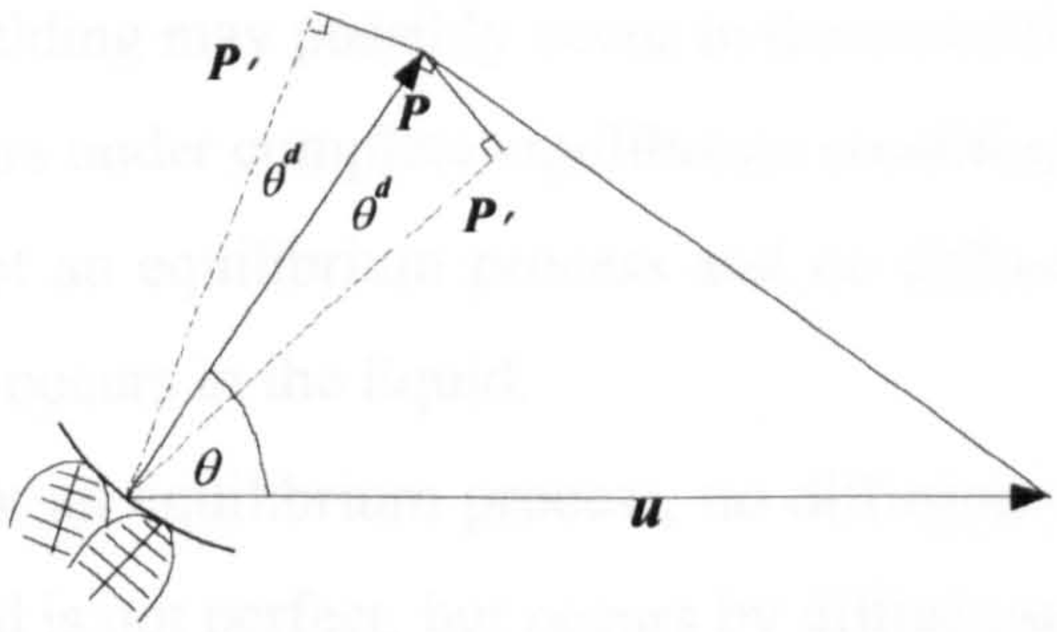

Figure 1.10 - Relationship between crystal growth normal to the maximum temperature gradient (P), and along the approximate ⟨100⟩ direction.

It is often necessary for crystals to change orientation during growth in order that they may continue to follow the steepest temperature gradient of the weld pool, and this occurs irrespective of welding speed. This implies that crystals growing in a certain ⟨100⟩ direction are unable to maintain this direction, because as the heat source is moving away, the direction of the steepest temperature gradient is effectively changing. From equation 1.4, as θ^d approaches θ, so that $P' \rightarrow 0$ i.e. the growth cannot continue when the angle θ^d becomes as large as θ. In order to maintain growth continuity, the solidifying crystals have to change orientation and this requires them to re-nucleate another more appropriate ⟨100⟩ direction. The mechanism is not properly understood, although it seems likely that re-nucleation at an atomic level on the surface of the existing crystals can occur without difficulty.

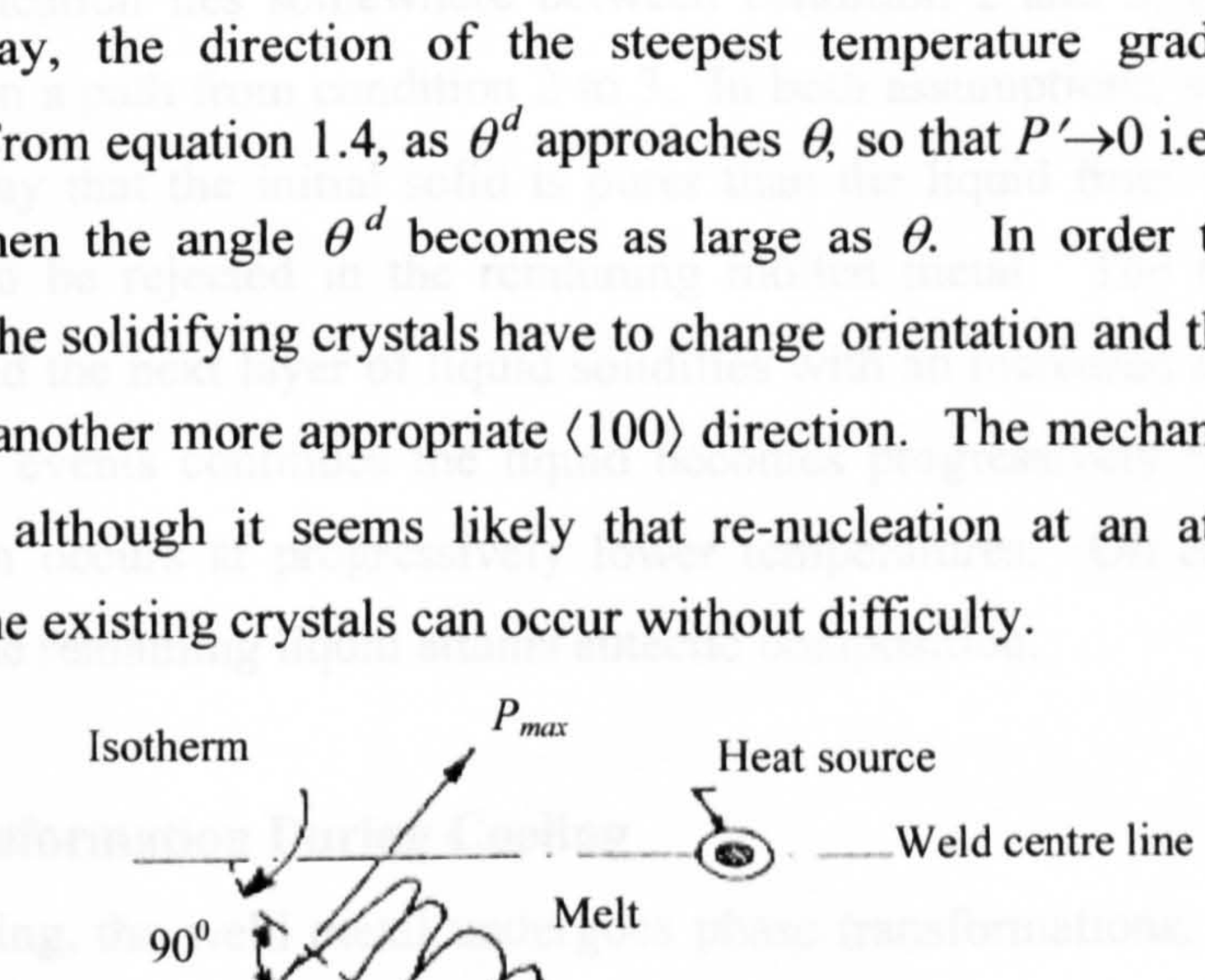

Figure 1.11 - Crystal growth occurs along ⟨100⟩ directions that correspond most closely to the steepest temperature gradient of the weld pool. After Easterling [43].

Solidification during welding may possibly occur in three conditions,

1. Solidification occurs under complete equilibrium conditions.
2. Solidification is not an equilibrium process and no diffusion occurs in the solid, but perfect mixing occurs in the liquid.
3. Solidification is not an equilibrium process, no diffusion occurs in the solid, and mixing in the liquid is not perfect, but occurs by diffusional processes only.

The rapid rates of cooling of fusion welds imply that weld solidification cannot occur under equilibrium conditions, so condition 1 may be ruled out. In the initial stages of solidification, good mixing of the liquid seems likely due to the turbulence of the melt, but when the heat source moves away and solidification goes to completion, it seems likely that the mixing occurs by diffusion. On this basis it may be conjectured that weld solidification lies somewhere between condition 2 and 3, or more accurately, progresses on a path from condition 2 to 3. In both assumptions, solidification occurs in such a way that the initial solid is purer than the liquid from which it forms, i.e. solute has to be rejected in the remaining molten metal. The temperature further decreases and the next layer of liquid solidifies with an increased solute level. As the sequence of events continues the liquid becomes progressively richer in solute and solidification occurs at progressively lower temperatures. On completion it might occur that the remaining liquid attains eutectic composition.

Phase Transformation During Cooling

During cooling, the weld metal undergoes phase transformations. The rapid cooling rates of the weld metal determines the transformation and its products, which usually does not occur under equilibrium conditions. In fact, there is a need for a certain degree of free energy for nucleation and transformation. The energy required comes from the surface and strain energy. The Figure 1.12 shows the molar energy balance of the transforming weld.

$$\Delta G \geq -\Delta G_V + \Delta G_S + \Delta G_E - \Delta G_D \qquad 1.5$$

Where ΔG molar free energy,

ΔG_V is the chemical free energy of the nucleus and is negative because it assists transformation.

ΔG_S refers to the increase in surface energy between γ and α phases,

ΔG_E is the increase in strain energy due to lattice dilatation.

ΔG_D implies that the transformation is heterogeneous and refers to the energy donated to nucleation by an existing heterogeneity in the high temperature phase. ΔG_D can thus refer, for example, to a grain boundary.

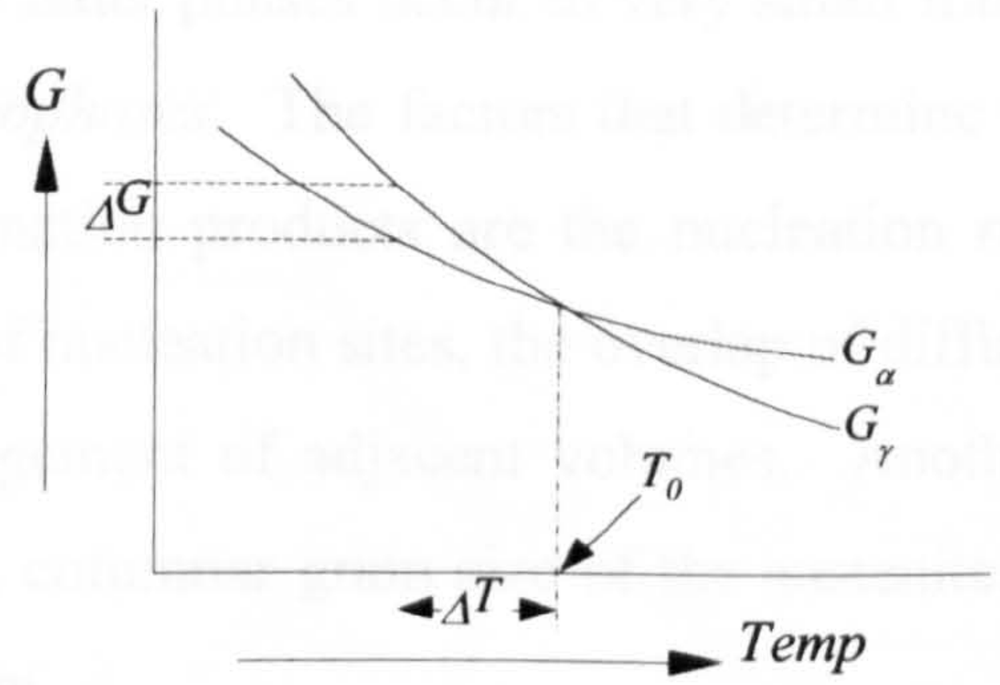

Figure 1.12 - The molar free energies of the two solid phases γ and α

T_0 in the figure above refers to the temperature at which the free energy of γ and α phases are equal. The equation 1.5 and the Figure 1.12 imply that for transformation, some degree of under cooling is necessary to make ΔG positive. From the free energy consideration the most potent nucleation sites in decreasing order are:

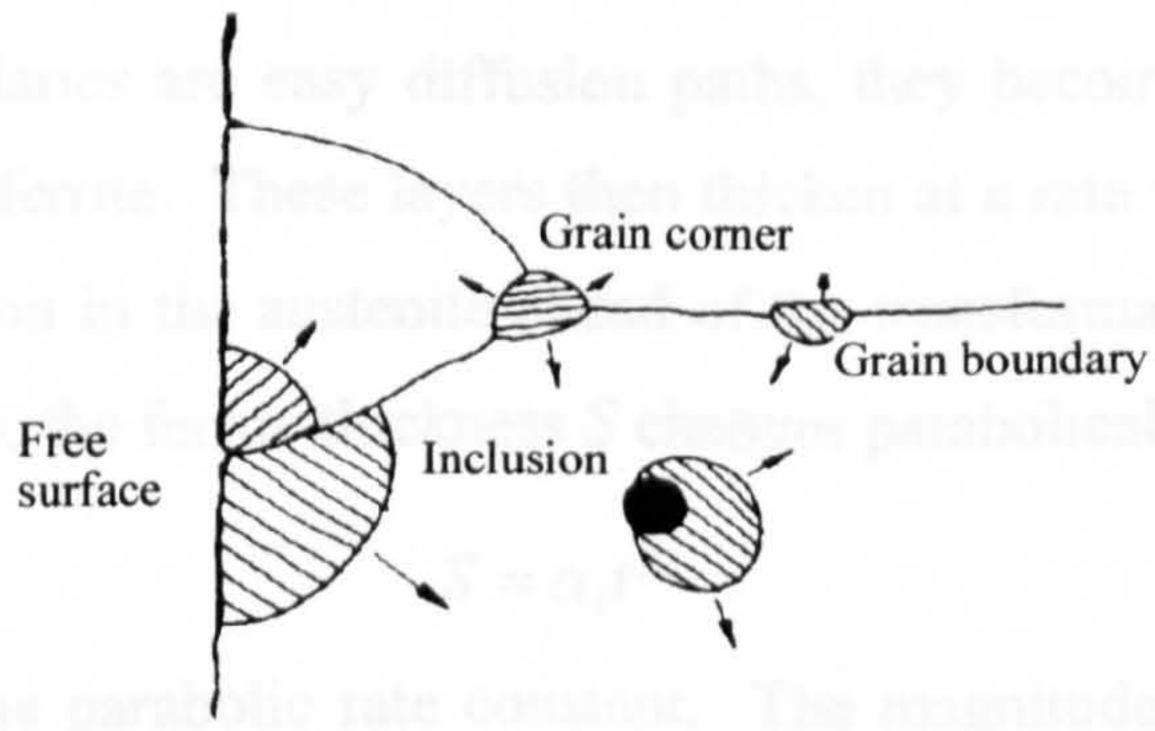

Figure 1.13 - The most potent sites of nucleation. After Easterling [43].

1. Free surfaces
2. Grain corners
3. Grain boundaries
4. Inclusions
5. Dislocations, including stacking faults.
6. Vacancy clusters.

In practice, the relative amount of transformation as a whole is also a function of the total number of sites available. The microstructure obtained as the weld cools from the liquid phase to ambient temperature is called the as-deposited or primary microstructure. Its major components include allotriomorphic ferrite, widmanstätten ferrite, and acicular ferrite. There may also be some martensite, retained austenite or degenerate pearlite. The latter phases occur in very small fractions, and are known by the collective term *microphases*. The factors that determine the final volume fraction of the various transformation products are the nucleation rate, the growth rate, the density and dispersion of nucleation sites, the overlap of diffusion fields from adjacent products and the impingement of adjacent volumes. Another important variable in weld metal is the initial columnar grain size of the austenite, from which the various eutectoidal products form.

Bainite, consisting of sheaves of parallel platelets, is not generally found in well-designed welding alloys. A phase transformation diagram in presented in Figure 1.17.

Allotriomorphic ferrite (α) is the first phase to form on cooling the austenite grains below the Ae_3 temperature. It nucleates at the columnar austenite grain boundaries. Because these boundaries are easy diffusion paths, they become decorated with thin continuous layers of ferrite. These layers then thicken at a rate which is controlled by the diffusion of carbon in the austenite ahead of the transformation interface. Under isothermal conditions, the ferrite thickness S changes parabolically with time t:

$$S = \alpha_1 t^{1/2} \qquad 1.6$$

where α_1 is called the parabolic rate constant. The magnitude of the parabolic rate constant depends on the equilibrium compositions of the austenite and ferrite and on the diffusivity of carbon in austenite. Alloying elements such as manganese, which stabilise austenite, are associated with a smaller value of α_1. In welding, transformations are not isothermal, but nevertheless, because nucleation is not rate limiting, the fraction of allotriomorphic ferrite obtained correlates directly with the parabolic rate constant. The thickness of the ferrite varies with the square root of time, meaning that the rate of growth decreases as the ferrite layer gets thicker. This is because the distance over which carbon has to diffuse increases with time. The

growth rate for a given alloy goes through a maximum as a function of temperature, because the driving force for transformation increases with undercooling whereas the diffusivity decreases. Consequently, as the weld cools to temperatures less than 600^0C, the diffusional growth of ferrite slows down so much that the layer of allotriomorphic ferrite reaches a limiting thickness.

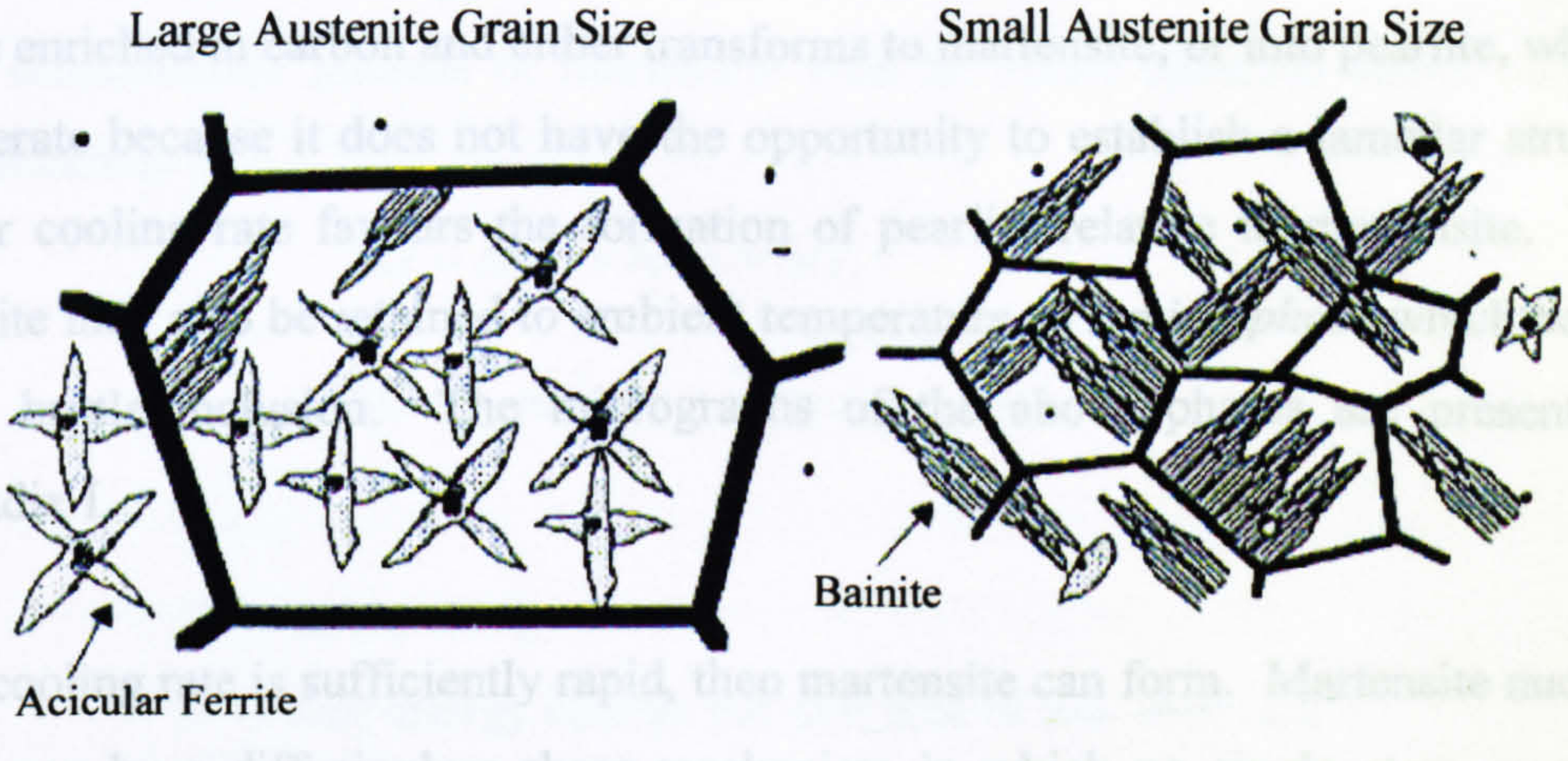

Figure 1.14 - Schematic illustration of the effect of prior-austenite grain size on the formation of acicular ferrite. After Easterling [43].

Widmanstätten ferrite formation does not involve the diffusion of substitutional solutes, and therefore its growth is not sluggish at low temperatures. The remaining ferrite therefore begins to transform to Widmanstätten ferrite. Although substitutional solutes and iron atoms do not diffuse during the growth of Widmanstätten ferrite, carbon does partition during transformation. Because of its plate shape, much of the carbon can be accommodated at the sides of the growing plate, so that the plate tip always encounters fresh austenite. This is unlike the case for allotriomorphic ferrite, where the partitioned carbon builds up ahead of the interface and progressively slows down the rate of growth. Widmanstätten ferrite plates therefore lengthen at a constant rate. The growth rates are found to be so large for typical weld compositions, that the formation of Widmanstätten ferrite is usually completed within a fraction of a second. Widmanstätten ferrite that forms in weld deposits correlates badly with the plate lengthening rate. This is because there is an interference between the plates of Widmanstätten ferrite that grow from the austenite grain boundaries, and *acicular ferrite* plates which nucleate at non-metallic particles dispersed throughout the weld. The formation of Widmanstätten ferrite and *acicular ferrite* is therefore competitive.

Anything that increases the number density of inclusion nucleation sites, relative to austenite grain nucleation sites, favours the formation of acicular ferrite at the expense of Widmanstätten ferrite. Hence, the refinement of austenite grain size, or a reduction in the oxide content of the weld below a limiting value, both lead to a decrease in the acicular ferrite content. By the time the weld deposit cools to about 500 ^{0}C, most of the austenite has been consumed. The small quantity of remaining austenite (about 5%) is enriched in carbon and either transforms to martensite, or into pearlite, which is degenerate because it does not have the opportunity to establish a lamellar structure. Slower cooling rate favours the formation of pearlite relative to martensite. Some austenite may also be retained to ambient temperature as a *microphase* which behaves like a brittle inclusion. The micrographs of the above phases are presented in Appendix I.

If the cooling rate is sufficiently rapid, then martensite can form. Martensite nucleates and grows by a diffusionless shear mechanism in which no single atom moves by more than one lattice spacing.

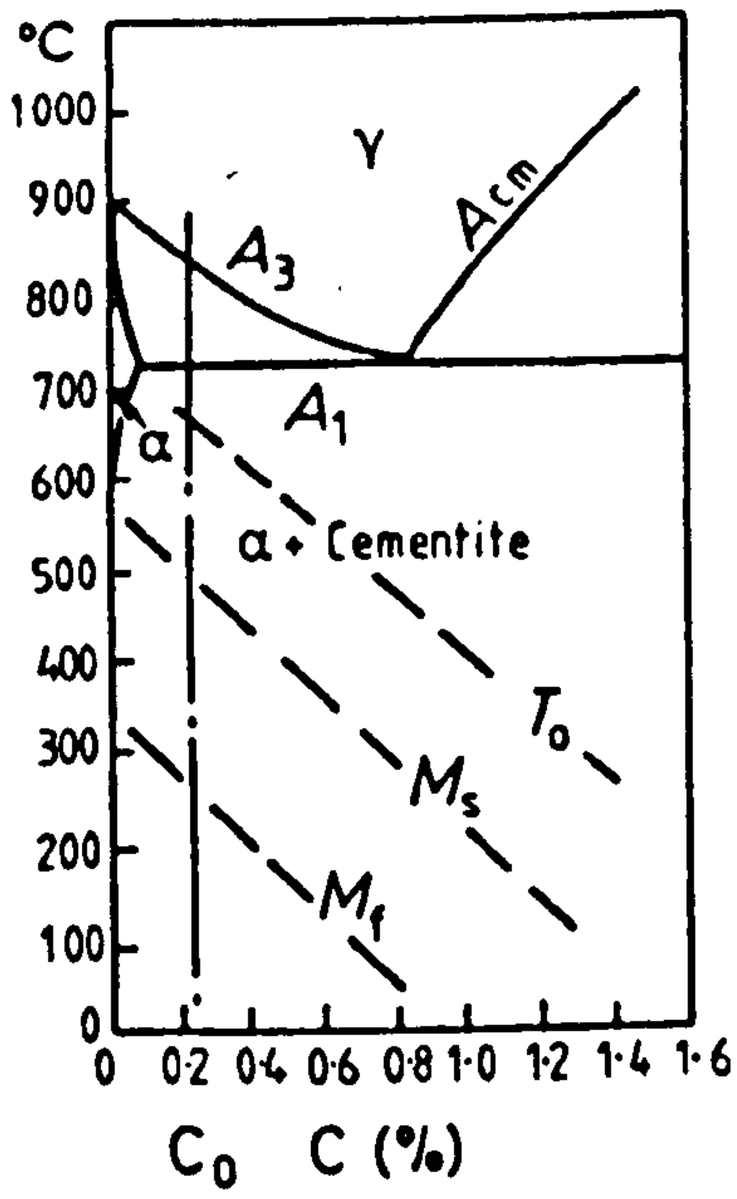

Figure 1.15 - The M_s and M_f temperature in steel as a function of carbon content. After Easterling [43].

Therefore, the martensite has the same composition as the parent austenite. The overall free energy change, ΔG, when nucleation takes place, is a result of three components:

- The change in chemical free energy, ΔG_V
- The strain energy ΔG_E
- The interfacial energy between matrix and martensite. ΔG_s

For a semicoherent nucleus of martensite with an oblate spheroid shape, radius a, semi-thickness c:

$$\Delta G = \Delta G_V + \Delta G_E + \Delta G_S \qquad 1.7$$

$$\Delta G = \frac{4}{3}\pi a^2 c\Delta g + \frac{4}{3}\pi a c^2 A + 2\pi a^2 \sigma \qquad 1.8$$

where

A = strain energy factor

σ = free energy change per unit area of γ/α' interface

Δg = chemical free energy change per unit volume. ($\Delta g = g^{\alpha'} - g^{\gamma}$)

The critical nucleus size is determined by a^* and c^*, at which the free energy change is ΔG^*, which defines a saddle on the free energy- c-a-curve, thus

$$c^* = -2\sigma / \Delta g \qquad 1.9$$

$$a^* = 4A\sigma / \Delta g^2 \qquad 1.10$$

and

$$\Delta G^* = 32\pi A^2 \sigma^3 / 3(\Delta g)^4 \qquad 1.11$$

In the transformation energy equation, the elastic strain energy ΔG_E is much larger than the surface energy ΔG_S, since σ is small. This means 'surfaces' such as grain boundaries or inclusions are not particularly good nucleation sites for martensite. Instead martensite prefers to nucleate at dislocations, or group of dislocations, within the grain where it can utilize the strain energy of the dislocation as an aid to nucleation. The potency of the dislocation as a nucleation site depends on the size of its contribution to strain. It is found that an increase in the dislocation density only slightly increases the number of martensite nucleation sites at the martensite start (M_S) temperature; the M_S is raised slightly. Martensite transformation is not a thermally activated process and it can occur very rapidly, reaching speed of *ca.* 1000 ms^{-1}. The

mode of growth is not properly understood except that to achieve the lattice structure of body centred tetragonal (BCT) iron, both a homogeneous shear and an inhomogeneous shear in the form of slip or twining is needed. The mode of inhomogeneous shear adopted depends on the transformation temperature and carbon content. For carbon contents up to *ca.* 0.4 wt % the dominant mode is by slip and the growth morphology is then *lath*, i.e. elongated thin plates, which is usually observed in steel weld metals, grows in packets on $\{111\}_\gamma$ *habit planes*, with a *Kurdjumov-Sachs* orientation relationship, i.e.:

$$\{1\ 1\ 1\}_\gamma \ //\ \{0\ 1\ 1\}_{\alpha'} \quad \{1\ 1\ 1\}_\gamma \text{ habit plane}$$

$$\langle 1\ 0\ \bar{1}\rangle_\gamma \ //\ \langle\ \bar{1}\ 1\ \bar{1}\rangle_{\alpha'} \quad (\alpha' = \text{martensite})$$

Lath martensite has a very high dislocation density, partly as a result of inhomogeneous shear, but also because of the large plastic strain. The high hardness of the lath martensite is mainly due to this high dislocation density, but there is also some contribution to hardening by the carbon in solution.

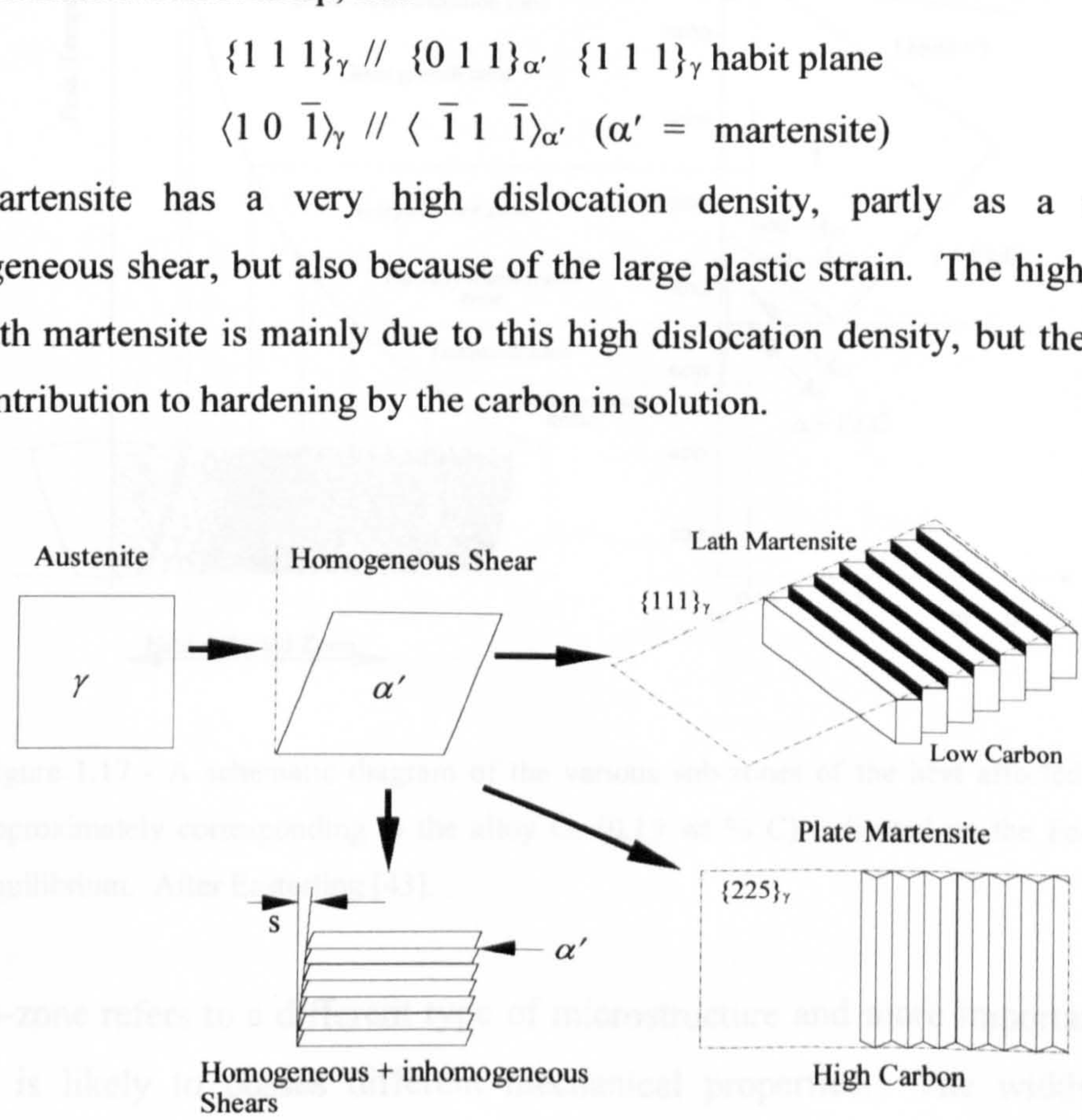

Figure 1.16 - Morphologies of martensite. The habit plane of martensite in steel depends on the carbon content. After Easterling [43].

1.3.2 The Heat Affected Zone

The heat affected zone can be divided into a number of sub-zones (depending on the material being welded). For the case of steel, the different zones are shown in the figure below.

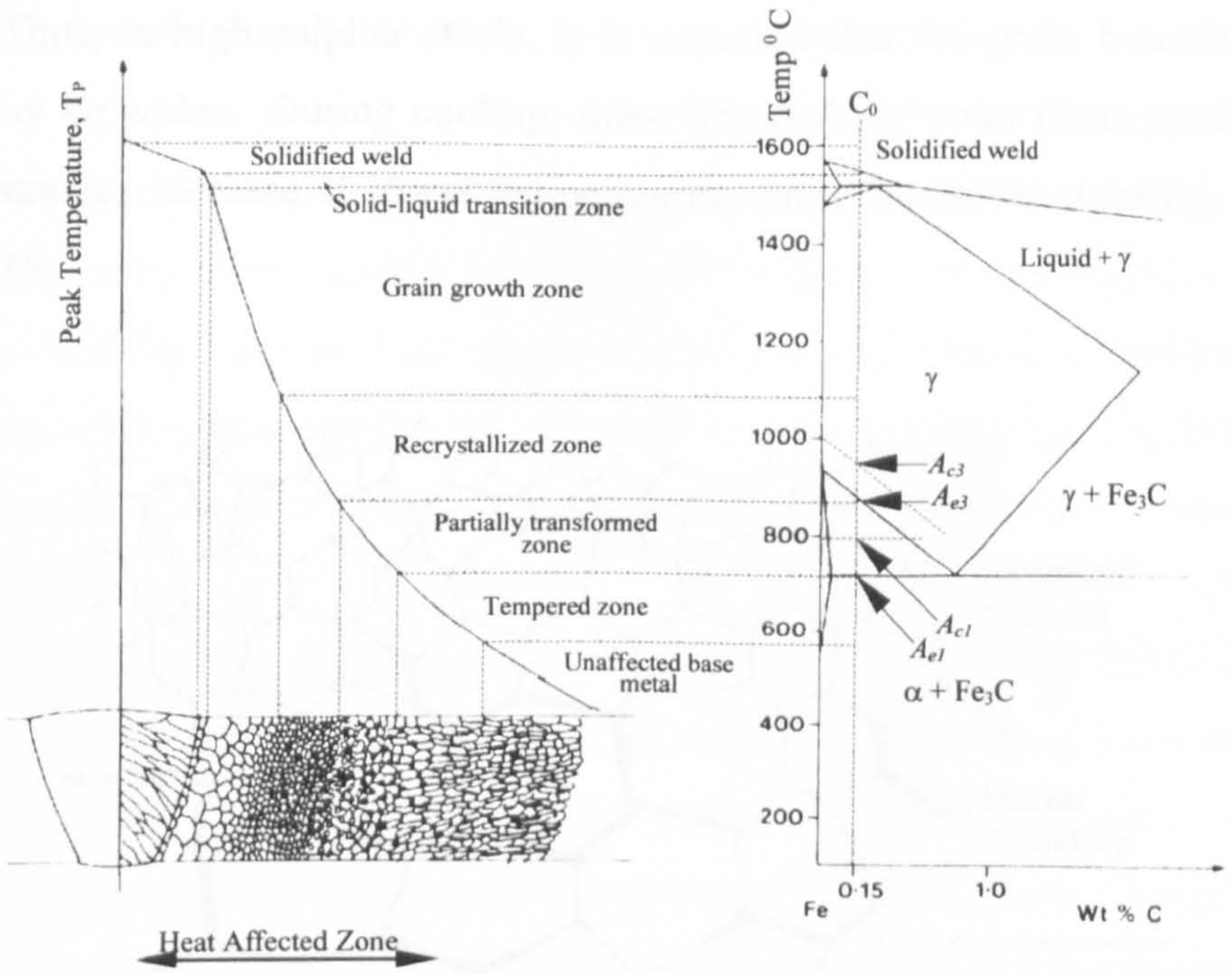

Figure 1.17 - A schematic diagram of the various sub-zones of the heat affected zone approximately corresponding to the alloy C_0 (0.15 wt % C) indicated on the Fe-Fe_3C equilibrium. After Easterling [43].

Each sub-zone refers to a different type of microstructure and more importantly each structure is likely to posses different mechanical properties. The widths of the different zones can be determined by the thermal cycles. Before discussing different zones and their properties the history of the parent metals should be discussed in order to obtain a reasonable understanding of the reaction in the base metal due to the thermal cycle. The severity of effect of the heating and cooling cycle on the base metal depends on the distance from the fusion boundary. The cooling rate of the metal depends on the boundary conditions, and the cooling time can be stated as $\Delta t_{8\text{-}5}$ (800-500 ^{0}C) because for many weldable steels in this temperature range austenite decomposes to its succeeding phases.

Reaction at the Fusion Line

In the fusion line (Figure 1.6) the base metal transforms to δ-ferrite and liquid in the grain boundaries. Because of the lower solubility of C and Mn in ferrite these elements tend to segregate to the melted grain boundaries and in some cases, they may produce compounds, e.g. (MnFe)S, which lower the melting point of the boundary region. Thus, in high sulphur steels, it is expected that the grain boundary melted region may be wider. During cooling, these low melting point films persist, and as residual stresses increase at lower temperatures, cause *liquation cracking*, shown in Figure 1.18.

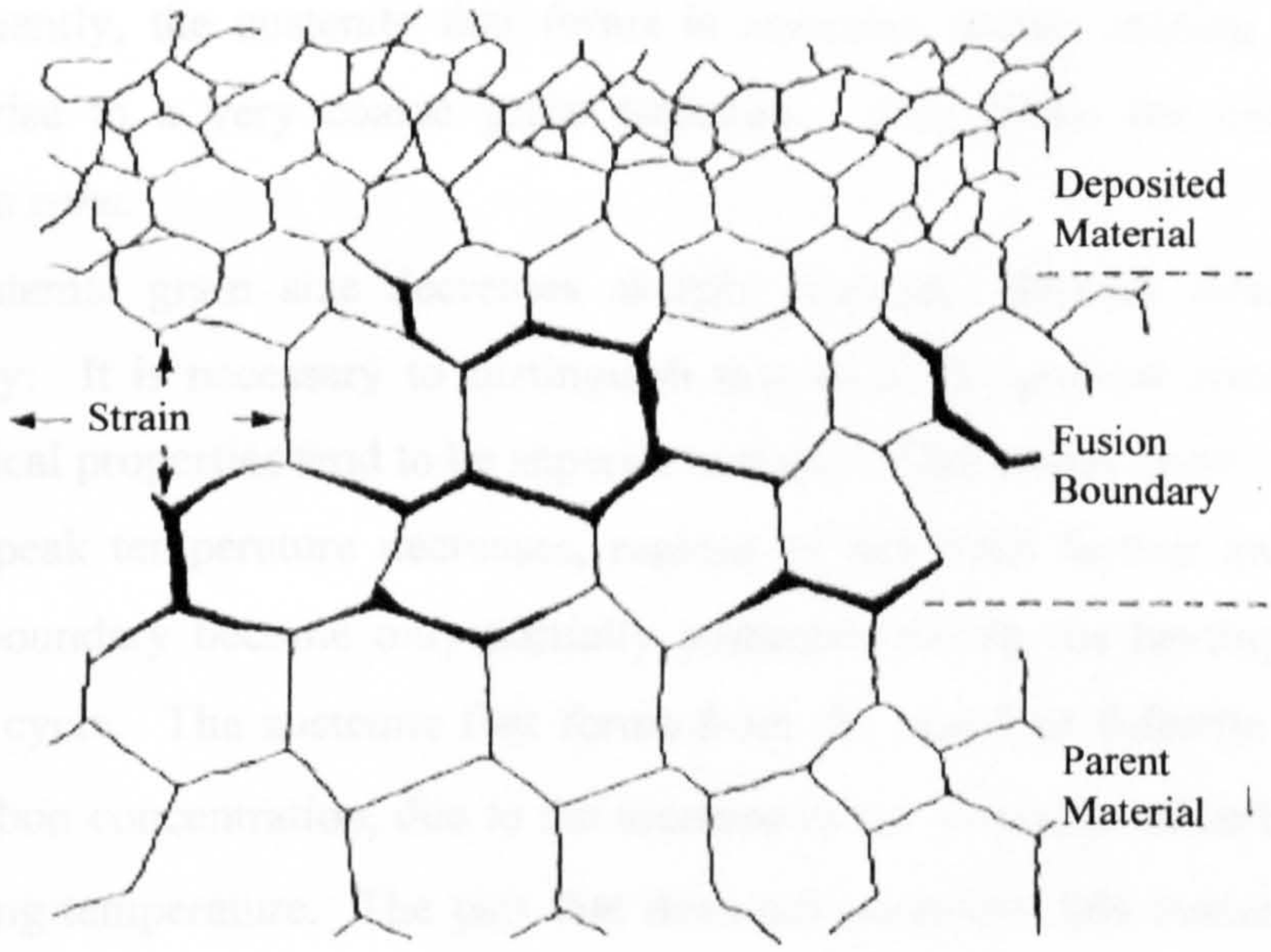

Figure 1.18 - Schematic illustration of liquation cracking at the fusion line. After Easterling [43].

On transforming back to austenite during the cooling cycle, the high degree of segregation at the boundaries increases boundary drag and thus reduces grain growth. It also effectively modifies the composition of austenite, and this, together with the effect of smaller grain size, affects the austenite transformation products, compared with the larger austenite grains away from the fusion line, by transforming at higher temperatures. This accounts for a more equiaxed ferritic structure at the fusion line.

Microstructural Zones

There is a well-defined gradient of microstructure in the heat affected zone, as a function of the distance from the fusion boundary.

1. Those regions immediately adjacent to the fusion boundary are heated to very high temperature and hence transform completely to austenite. During continuous heating, austenite begins to form at a temperature $Ac_1 \approx 800^0$C, and the samples become fully austenitic at $Ac_3 \approx 950^0$C (Figure 1.17). These temperatures are different from the corresponding equilibrium temperatures Ae_1 and Ae_3 because they increase with the heating rate. The peak temperatures in the HAZ close to the fusion boundary are well in excess of the Ac_3 temperature of weldable steels. Consequently, the austenite that forms is annealed during heating beyond Ac_3, giving rise to a very coarse grain structure. This forms the *coarse grained austenite zone.*
2. The austenite grain size decreases sharply with the distance from the fusion boundary. It is necessary to distinguish this as a fine-grained zone because its mechanical properties tend to be superior to those of the coarse zone.
3. As the peak temperature decreases, regions of the HAZ further away from the fusion boundary become only partially austenitic during the heating part of the thermal cycle. The austenite that forms from the liquid or δ-ferrite has a rather high carbon concentration, due to the increase in the solubility of carbon in γ with decreasing temperature. The part that does not transform into austenite becomes tempered.
4. When the peak temperature becomes less than the Ac_1 temperature, the only effect of the heat input is to temper the microstructure, the extent of tempering decreases with distance from the fusion boundary.

The individual microstructures are illustrated in Figure 1.19, and discussed in detail in the section below.

Grain Growth Zone

The transformation rate of austenite to its succeeding phases depends upon the supercooling below the equilibrium temperature, alloying elements, and inclusions.

Since the peak temperature in this zone is much higher than Ac_3, the austenite grains coarsen rapidly as they approaches a temperature a range 1200–1500 ^{0}C. In steels which are microalloyed, it may be necessary for the grain boundary pinning particles (e.g. niobium carbonitrides) to dissolve before substantial grain coarsening occurs. In any case, once the coarsening begins, it proceeds very rapidly because the effect of temperature increases exponentially during heating.

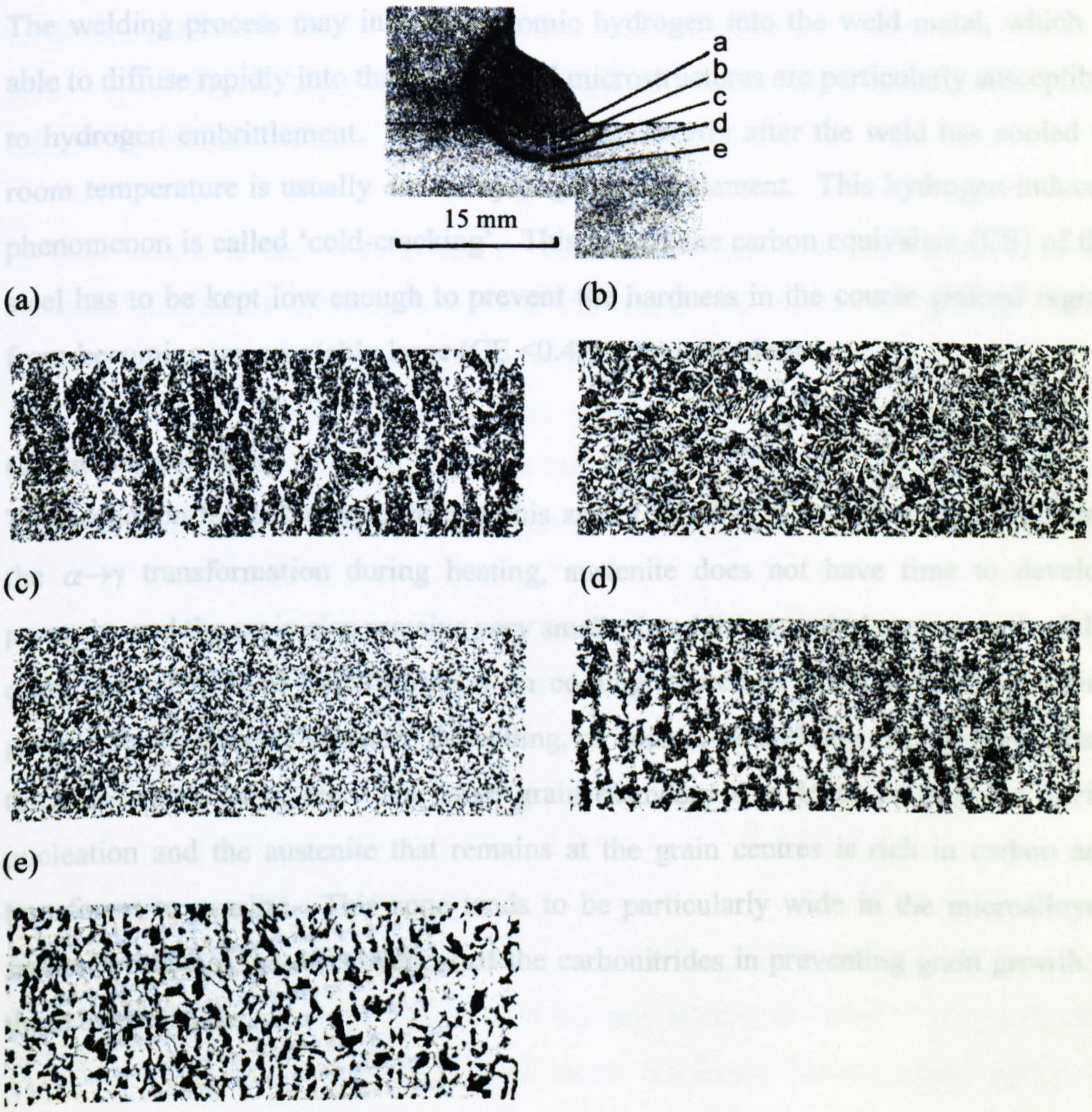

Figure 1.19 - A series of optical micrograph showing various zones in the HAZ of a MMA-welded normalised pearlitic steel (a) fusion zone (b) grain growth zone (c) grain refined zone (d) partially transformed zone and zone of spherodized carbides (e) unchanged base metal. After Easterling [43].

The importance of the coarse grained austenite is in the mechanical properties which develop as the austenite transforms during the cooling part of the thermal cycle. The coarse grain structure leads to an increase in hardenability, because it becomes easier to avoid intermediate transformation products, so that untempered martensite or other hard phases can form during cooling.

The welding process may introduce atomic hydrogen into the weld metal, which is able to diffuse rapidly into the HAZ. Hard microstructures are particularly susceptible to hydrogen embrittlement. Fracture occurring shortly after the weld has cooled to room temperature is usually due to hydrogen embrittlement. This hydrogen-induced phenomenon is called 'cold-cracking'. This is why the carbon equivalent (CE) of the steel has to be kept low enough to prevent the hardness in the course grained region from becoming unacceptably large (CE <0.4% recommended).

Grain Refined Zone

The reduction in peak temperature in this zone (*ca.* 1100 ^{0}C) implies that, following the $\alpha \rightarrow \gamma$ transformation during heating, austenite does not have time to develop properly, and the grain size remains very small. In addition, carbides may not be fully dissolved. The $\gamma \rightarrow \alpha$ transformation on cooling, therefore, tends to produce a fine grained ferrite-pearlite structure depending, of course, on welding energy-input, plate thickness (boundary), etc. The large grain boundary area tends to promote ferrite nucleation and the austenite that remains at the grain centres is rich in carbon and transforms to pearlite. This zone tends to be particularly wide in the microalloyed steels, because of the effectiveness of the carbonitrides in preventing grain growth at these temperatures.

Partially Transformed and Spheroidized Zone

In the temperature range 750-900 ^{0}C, the pearlite in the base metal quickly austenitizes because of its lower $\alpha \rightarrow \gamma$ transformation temperature, the austenite being enriched in C and Mn. This is because the solubility of C and Mn in austenite, which is in equilibrium with ferrite, increases as the temperature decreases. For this reason, the $\gamma \rightarrow \alpha$ transformation on cooling can yield a wide range of possible structure,

depending on cooling rate, $\Delta t_{8\text{-}5}$, e.g. pearlite, upper bainite, autotempered martensite or high carbon (twinned) martensite.

The spheroidized carbide zone corresponds approximately to the temperature range 700-750 ^{0}C. There is relatively little $\alpha \rightarrow \gamma$ transformation during the rapid heating cycle, so that the most notable changes concern degradation of the lamellar pearlite to spheroidal particles of Fe_3C. The agglomeration of spheroidized cementite particles at grain boundaries and triple junction, emphasises the role of grain boundaries as high diffusivity channels for carbon at these low temperatures.

In both zones, if the cooling rate is sufficiently high, then the carbon-enriched austenite transforms partially into hard martensite, the remaining austenite being retained to ambient temperature. These minute regions of hard martensite are known as 'local brittle zones'. They are located in much softer surroundings consisting of tempered ferrite. Consequently they do not cause a general reduction of toughness, but lead to an increase in the scatter associated with toughness tests.

When the cooling rate in this region is not high enough to induce martensite transformation, the carbon-enriched austenite can decompose into a mixture of coarse cementite and ferrite. The cementite particles again constitute local brittle zones and increase the variability in mechanical properties.

Zone of 'Unchanged' Base Metal

The unchanged zone concerns temperatures in the range up to ca. 650 ^{0}C, in which changes in morphology of constituents do not appear to occur. However, the combined effect of heating and residual stress can cause *dynamic strain ageing* to occur. This phenomenon is associated with moving dislocations sweeping up interstitial impurities such as C and N. On cooling, the solute enriched dislocations are strongly locked in position, thus embrittling the structure. The problem can be intensified by additional welding runs, as in multi-run welds, or during reheat annealing.

1.4 Residual Stress Relief

Residual stress relief can be achieved by removing the causes of residual stress, which include phase transformation, reducing dislocation density or local plastic flow. There are mainly two methods used to relieve residual stress, namely Thermal Stress Relief and Mechanical Stress Relief.

Thermal Stress Relief

There are two different types of thermal stress relieving treatments, they are (1) Annealing – to relieve micro and macro residual stresses, (2) Cryogenic treatment – to relieve micro residual stresses.

Annealing

Traditionally, the solution to the residual stress problems outlined in the general introduction has been to apply a thermal annealing process. At elevated temperatures, the hardness of the material is reduced so that it cannot support internal stresses of significant magnitude. In addition, creep processes are greatly accelerated at high temperature, allowing viscous flow to occur over a short time scale (hours rather than weeks). Upon quasi-static cooling, (to avoid steep thermal gradients) the material exists in a state of low residual stress. Although this procedure has become a de facto standard, and is considered mandatory in many safety-critical applications, thermal annealing suffers from limitations to its applicability; it is also expensive, lacks convenience, and may generate a variety of undesirable side effects.

The modification of material properties to meet exacting standards can impose severe constraints upon subsequent thermal treatments. The use of stress relief annealing in such cases may be restricted if not entirely precluded. Temperatures, dwell times, heating and cooling rates must all remain within limits imposed by the requirements for ultimate material properties, effectively curtailing the achievement of successful stress relief in many cases. This limitation is accentuated by the lack of quantitative data concerning the effect of elevated temperature upon the hardness (yield point) of many materials: as a result, the optimum parameters for effective and efficient thermal stress relief may be ill defined.

It should also be noted that stress relief temperatures cannot be allowed to exceed the crystalline phase transformation point of the material in question, since in this case volume changes associated with lattice re-organisation may cause massive localised straining - even during quasi-static cooling. All too often the effect of such rapid straining is to reintroduce residual stresses comparable with those present before the treatment.

The cost of thermal annealing in terms of energy, equipment and time is non-negligible (5-8% of final cost is typical). Effective stress relief requires the use of slow heating and cooling cycles, in conjunction with an extended period during which components must be maintained at a constant high temperature. Larger structures, in particular, require longer "soak" times and lower heating/cooling rates to ensure minimal internal temperature gradients throughout the process. This necessarily involves a large expenditure of energy, much of which escapes through furnace walls and is wasted.

Capital costs of furnace equipment suitable for components of large dimensions is also high, whilst the use of outside contractors for the operation incurs additional costs of transportation and may create delays in the production process. In large scale manufacturing operations the maximum output rate from a given plant may exceed the capacity of thermal annealing facilities. This results in a production bottleneck and the expense involved in installing suitable additional furnace equipment may well preclude the possibility of a cost-effective solution to this problem.

Stress relief annealing, by its very nature, involves dramatic softening of the affected material. During the process it is common for large deformations of treated structures to occur. Atmospheric control in large industrial furnaces is not routine, with the result that annealing often causes heavy oxidation of the treated material. Grain growth and related metallurgical changes occur rapidly during treatment, and may cause severe degradation of the mechanical properties of the material. Processes must be undertaken after stress relief to rectify the foregoing defects; such measures must be taken into account as an integral part of the design process. The availability of a

stress relief method free from side effects would therefore promote more efficient design and manufacturing processes.

Cryogenic Treatment

Some tool producers use cryogenic treatment to increase tools fatigue life. In this method metals are treated (quenched) in liquid nitrogen before putting them to service. The possible reason of increase in fatigue life would be transformation of all retained austenite to martensite or other phases which reduces micro residual stresses (residual stress type-II) by cooling the metal to cryogenic temperature. Frey [52] claimed that cryogenic treatment of Drills and powder metal parts improved fatigue life to 1.5 to 2 times. For small parts or components this process can be used to reduce micro residual stresses, but for large parts this process is not possible to use. Also type-I and type-III residual stresses cannot be relieved by this method. This is also an expensive method of treatment for larger components.

Mechanical Treatment

There are two types of mechanical treatments, they are (1) shake down, and (2) vibratory stress relief (VSR).

Shakedown

In this process the component is stressed over its yield point, preferably mid way between the yield point and ultimate strength, then the load is released. As a result, a partial local plastic deformation occurs in the component especially in the tensile residual stressed zone, which relieves residual stress. The problems with this method are (a) it needs a system for load application, (2) it is not easy to apply stresses on specimens of complex geometry. Due to the above factors, its application is limited to a very few products like pressure vessels, where the vessel is pressurised above its working pressure and the pressure is then released to reduce the residual stresses.

Vibratory Stress Relief

Vibratory stress relief (VSR) is a generic term applied to certain mechanical treatments intended to reduce the problems associated with residual stress. Cyclic loading is applied to the residual stress affected component, inducing periodic straining. It has been the contention of commercial practitioners of VSR for many years that this process would bring great benefits over other methods of stress relief. The accessible literature on VSR associated with cyclic loading has been reviewed, and is discussed in the next chapter.

In cases where untreated components are subject to spontaneous dimensional changes over time, VSR treatments have been reported to increase stability. No single factor can be presented as the cause for this effect, and in the absence of detailed investigation various authors have postulated work hardening, stress relief, lattice slip or accelerated "shakedown" as primary mechanisms.

VSR operators often claim improved tolerances i.e. less distortion in parts vibrated before finish machining. The reduced distortion of the material upon release from machining restraints must depend upon the lowering of surface residual stresses in treated components. Increased hardness, often cited as a probable cause, is not a relevant factor, since strains occurring upon removal of residually stressed material are generally elastic in nature.

The ultimate claim of researchers is that stress relief occurs in treated material. In a number of articles, a variety of direct and indirect evidence is presented to support this postulate. The majority of cases are indicative of localised effects, restricted to regions of high initial stress and large dynamic strain amplitudes. Few instances of widespread stress reduction have been reliably documented.

In industrial scale processes, the source of applied loading is most commonly an electric motor with unbalanced eccentric masses mounted on the rotating shaft. Electronic speed controllers control the motors. The nature of the force generated by this system is determined by the geometry of the eccentric masses and the motor mounting. The magnitude of the generated force is proportional to the square of the

treatment frequency, which is difficult to control independently. High strain amplitudes within the treating material may be achieved by matching the motor speed to a natural frequency of the system. Vibration in several resonant modes allows different patterns of dynamic strain to be excited, ensuring better overall coverage of the subject than may be achieved by means of a single treatment.

The potential advantages of VSR over thermal annealing and its effectiveness needs to be proven. Equipment and energy costs are likely to be negligible in comparison with industrial scale furnaces. VSR equipment is generally much more portable than furnaces, allowing structures to be treated in situ and thus avoiding transportation costs. The time required is generally much shorter than for thermal treatment: VSR processes typically require between a few seconds and 1 hour, as compared with up to 24 hours for annealing. Side effects associated with thermal stress relief such as distortion and reduction of mechanical properties are largely avoided in the VSR process. Although a certain degree of distortion may occur during vibration, this is relatively small compared with the massive warping which often accompanies annealing.

It is believed that no overall phase transformations in metallurgical structure are initiated by cyclic loading (although this needs to be investigated in detail). Thermal treatments may unacceptably alter the mechanical properties of the metal whereas the VSR process improves them. Designers of heat-treated alloy components must make compromises between the degradation in strength, toughness and hardness during annealing, and the problems associated with residual stresses in subsequent service. In certain duplex stainless steels the degree of thermal stress relief is limited.

The major problem associated with mechanical conditioning is the possibility of fatigue damage to the material. This is clearly a significant factor for consideration, in selection of an appropriate treatment method particularly in safety-critical applications. Until the mechanisms involved in VSR are properly understood, fatigue predictions will remain uncertain. Reduced residual stresses may in some measure counteract the adverse effects of cyclic loading, so that the overall effect of treatment might be beneficial in some cases.

Over the past three decades, the use of VSR has become widespread throughout industry world wide, despite a lack of reliable data necessary for scientific understanding of the phenomena involved. The results of laboratory scale investigations to date are inconclusive: although VSR has been shown to accomplish stress reductions in some circumstances, its applicability to certain classes of material remains doubtful. Heavily cold worked metals and quenched alloys in particular have been reported to be largely unresponsive to cyclic loading.

Several classes of model have been proposed in reports of previous research. A simplistic theory in which bulk plastic flow occurs in response to the superposition of residual and applied stresses is cited in many references (discussed in Chapter 2), where it is referred to as a standard model. Other authors ascribe stress relief to phase transformation from retained austenite to martensite or other phases. Some of the authors write VSR as 'an alternative mechanism', although details of the proposed theories are absent, the rather vague term 'dislocation effects' is commonly used, with little or no further explanation. Another prevalent proposal is "cyclic hardening softening"; once again, no details are forthcoming, and no clear indication is made of the role played by these effects in the VSR process. A detailed discussion of the situation currently occupied by VSR research will be presented in chapter two.

1.5 Objectives of This Study

There is a degree of controversy between researchers about the effectiveness of vibratory methods of stress relieving. The cause of that controversy can be explained as most of the researchers did not have a full understanding of the stress states of their structures, because of the complexity of stress measurement methods. Presently available experimental data does not provide conclusive evidence in support of a specific theory of VSR. Little attention has been paid to the effects of vibration upon the microstructure and mechanical properties of the treated material. Consequently, VSR is widely perceived as somewhat of a "black art" rather than as a well-defined engineering process. In order to negate this situation it is necessary to place its fundamental mechanism upon a firm scientific basis. Additionally, it should be noted that the vibratory response of real commercial structures and components is

considerably more complex than that of simple test specimens. Successful application to real-life situations must therefore rely upon detailed analysis of the compliance of each part and upon careful engineering of the vibratory response of the entire system.

With the development of modern X-ray technique, the stress measurement method has been improved significantly, which provided scope to observe the change in residual stress in detail in the experimental specimens due to vibratory treatment. The current investigation is aimed at providing a satisfactory rational explanation for VSR, based upon the observed changes in material properties and residual stress state due to cyclic loading. Experimental techniques used to investigate the effects of vibration include the use of an X-ray diffractometer to measure residual stress before and after treatment in order to observe the effect. Prior to the onset of this experimental work, the residual stress was calibrated using a standard method, where the Effective Elastic Constant of the material was calibrated to obtain the confidence of the stress measurements. Although the error band specified by the manufacturer of the X-ray diffractometer was ±20.67 MPa, it was reduced to almost ±10 MPa by the calibration method which is discussed in Section 5.1.

In this study, welding residual stress was chosen as the prime aspect of investigation, because the fabrication industries all over the world use welding and face residual stress problems. VSR or VWC methods can be applied to the structure in situ to relieve the residual stress. If the effectiveness of VSR or VWC is proven then they will be the most useful alternative to the other methods of stress relieving.

Acknowledgement

The author of this thesis acknowledges that the Metallurgy section of this thesis is mainly taken from four different sources; they are Bhadeshia [15], Gray [60], Easterling [43], and Honeycombe [65].

Chapter 2

Literature Review

Literature Review

2.1 Introduction

Vibratory stress relief is not a new concept: an extensive body of literature, dating from 1943 (McGoldrick and Saunders [94]), is devoted to the subject. Published works include several review articles, which present critical evaluations of various studies by other authors. The most comprehensive of these to date is that of Dawson [39], which is an exhaustive chronological survey of research publications concerning VSR before 1975. A brief summary of the methodology, results and conclusions of each author is supplemented, where appropriate, by discussion of possible sources of error or confusion. In many cases Dawson was able to explain negative results as the consequence of defects in the experimental procedures adopted by the authors of the reports.

In order to present a more structured overview of the literature, it is divided according to the materials or method of materials processing. In this chapter, a brief summary of the relevant aspects of previous research within each class will be presented. This will be arranged according to the date of publication and features common to all or most of the works belonging to each category will form the basis for tentative hypotheses and conclusions. Although in many cases the published results appear negative, this does not necessarily indicate fundamental ineffectiveness of the VSR process: careful consideration of the materials and techniques adopted by the researchers often provides some indication of methodological difficulties.

A sizeable quantity of the literature on VSR has been excluded from this review (although it is listed in the *References*) because of the nature of the publications. Those publications were mainly from the manufacturers of VSR equipment, where, in the absence of any reasonable data, success was claimed and the methodology of VSR was supplied.

2.2 Classification of Investigation

This investigation is categorised according to the materials used, process of loading or type of previous treatments, i.e. the methods used for induction of residual stress. Such methods include casting, welding, heat treatment and plastic deformation; elastic stresses due to the influence of separate members in complex structures may also be classified as residual stress. Various research groups have been involved in efforts to investigate the effects of cyclic loading upon the properties of materials in each of these groups. A brief summary of the findings published by each group will be presented in the treatment of this category. Subsequent sections represent the same research classified according to different criteria, and therefore only features common to all or most publications will be highlighted.

2.2.1 Cast Materials

It is inherent in the nature of products cast from molten metal that, upon cooling, residual stresses develop. Material close to the surface cools and hardens faster than the core metal, which is forced to yield due to thermal contraction of the surface layer. Subsequently, the core material cools and contracts further, until finally the outer skin is left in a state of compressive residual stress, balanced by tensile stress in the core. Several research groups have utilised this natural aspect of castings in their investigations of VSR.

The earliest available publication reporting the practical application of vibratory treatment on stressed material was that of McGoldrick and Saunders [94] in 1943. Since circumstances did not permit quantitative observations of residual stress or distortion of cast components, this article cannot be considered as evidence for or against the effectiveness of VSR. Instead the authors concentrated upon developing resonant/subresonant techniques for the application of controlled high amplitude loading, accepting that stress relief due to plasticity would occur most effectively under such conditions.

McGoldrick and **Saunders** [94]: This work was carried out at the David W. Taylor Model Basin, USA in 1938 and 1939, published in 1943. Iron castings were subjected to vibration in order to relieve residual stress and provide dimensional stability. The castings were rough machined, vibrated, annealed then again vibrated. The specimens were vibrated in different ways. (1) Suspended clear of the floor and struck with a maul, sledge or ram. (2) Rolled along the shop floor by parbuckling, i.e. by winding a rope around them and then pulling on the rope. (3) Carried around in a springless wagon over rough pavements or roads. (4) Lifted a short distance off their support and dropped, repeating this operation a number of times. The annealing was carried out in a furnace at 538 to 565 ^{0}C and maintained that temperature for 6 hours, then was allowed to cool down at a rate of 11.5 ^{0}C per hour. The dimensions of these treated castings were checked at intervals for more than a year, and they did not show any measurable dimensional change.

Bühler and **Pfalzgraf,** [25]: Publications by Bühler and Pfalzgraf in the early 1960's included reports of their experience in applying VSR techniques to cast iron test pieces. Complex castings exhibiting stresses of approximately 100 MPa were subjected to cyclic stresses of ±40 MPa where no significant change in residual stresses was observed as a result of this treatment. Additional tests performed using cast tension rings (residual stress around 11 MPa, cyclic stress ±40 MPa) yielded similar results. It should be noted here that the cyclic loading methods used were non-resonant, resulting in cyclic stress amplitudes lower than those attainable using resonant techniques. In the second set of tests, the combination of low residual stress levels with intermediate amplitude loading was unremarkable due to its lack of effect.

The measurement of the residual stresses was carried out using two processes. One of them was measuring the length of the experimenting bar before and after treatment. The other was using the strain gauge to monitor changes due to treatment.

Campbell, [28]: This is a detailed publication about the effect of vibration on solidification of metals from Cosworth Research and Development Ltd, Worchester and was published in 1981. In this work, castings of different metals were vibrated

during the solidification process, and the properties of the cast materials investigated. It is reported that due to vibration, the inclusions in the cast iron are reduced. Carbide precipitation has been observed to decorate slip planes in austenitic steel containing 0.5C-1.8Mn-5Cr. Grain refinement occurred in steel due to vibration. The precise mechanisms of that fragmentation as was described may be that of root bending and subsequent recrystallization to form a high angle boundary across the root with consequent penetration by the liquid due to the favourable energy driving force. Ductile shearing is not likely since the available force is too low. The remelting of the roots (as a direct consequence of vibration) seems unlikely since, among other reasons, the energy requirements are high for this to happen. For grain refinement the described frequency range was below 100-200 Hz and was concluded that there was no special advantage in the choice of ultrasonic frequencies.

The reason that grain refinement was not mentioned in the publication as that is possibly due to the fact that an applied stress was present. At higher frequencies the amplitude of vibration was low and so was the magnitude of the applied dynamic stresses - thus the effect of vibration was not observed. Contrarily at lower frequencies the amplitudes of vibration/applied stress to the experimenting specimen was high which refined the grains.

Due to vibration the metal became more chemically uniform on a microscopic scale. Improved structural homogeneity combined with improved chemical uniformity was reported to yield uniformity of properties over substantial volumes of the cast material. Improved uniformity of mechanical properties was found in several bronzes; improved uniformity of hardness was found in cast iron. Also, improved ductility was found in a magnesium alloy in the cast condition and after rolling to sheet. Reduced anisotropy of ductility was observed in the rolled steel.

Significant increases in mechanical properties of most alloys were reported. Typical improvements were shown as (i) yield strength 10 to 30% (ii) ultimate tensile strength 20-40% (iii) elongation 20-40%. The increase in the yield strength was explained as a

combined effect of better alloying distribution on a microscale and finer grain size. Measurement of residual stress was not carried out.

Balasingh et. al. [10]: This work was carried out at the Indian Institute of Science in 1983. A self-created standard specimen geometry was adopted for use in this research, exhibiting residual stresses due to differential cooling and mould restraint, where the specimen was kept lightweight and simple in design. The quality of the castings was controlled by maintaining the same conditions of the moulds (mould hardness, dryness etc). Also, the pouring temperature of the metal was controlled to obtain the same level of residual stress. Grey cast iron having a carbon equivalent (CE = %C + 1/3%Si + 1/3%P) values in the range 3-4 % were used, with two separate silicon-based inoculants. Residual stresses were measured by strain gauge sectioning and X-ray diffraction techniques. A combination of diffraction measurements with sectioning techniques resulted in good agreement between the two methods. Dynamic strain amplitudes during treatment were measured using resistance strain gauges.

Castings were clamped on a vibration table in various different orientations until a satisfactory method was found which could introduce high dynamic strain amplitudes. Non-resonant or forced vibration was applied at various amplitudes for periods of up to 6 hours. One end of the casting was clamped to the vibrator table and loads were fixed on the other end. By changing the load on the end the applied dynamic stress was varied.

At the resonant vibration of castings, fatigue failure occurred after 25 minutes. Residual stress reduction was found to occur within the first 5 minutes of treatment with only marginal changes being observed before 2 minutes. Consequently, the standard treatment duration was chosen to be 10 minutes. The authors studied the effect of varying the chemical composition of the cast material. It was found that up to 33.5 % reduction in residual stress (8.57 $kg/mm^2 \rightarrow 5.69\ kg/mm^2$) could be achieved in certain materials. The stress levels tended towards a constant value which was independent of the material's carbon equivalent (CE) value. The relative stress reduction in the samples varied according to the initial residual stress levels. Initial

stresses, and hence stress relief, fell with increasing carbon content for irons inoculated with similar substances. In one case, uninoculated (plain carbon) material of low carbon content (CE=3.2) failed to respond well to vibration. Although no specific interpretation of this observation was offered, it was clear that materials of different internal composition exhibited distinctive characteristics in their response to the mechanical stress relief processes.

It was reported by this research group that vibration caused slight increases in hardness. The author also stated that no deterioration in fatigue life occurred, although no evidence was presented in support of this claim. The significance of the observation that stress relief is only slight within the first 2 minutes of vibration cannot be over emphasised. Clearly, the model of plastic flow in response to combined dynamic and residual stress predicts rapid stress relief within the first few cycles of loading at high amplitude. Balasingh's observation displayed contrary behaviour to this postulate because he found residual stress reduction within the first 5 minutes of treatment, with only marginal changes before 2 minutes - therefore providing clear contradictory evidence against this postulate.

Nakagiri, et. al. [99]: This work was carried out in Japan in 1984, on FC25 pearlitic cast iron (3.58% C, 2.1% Si, 0.4% Mn, 0.21% S) rectangular specimens measuring $300 \times 40 \times 6$ mm. The mechanical properties of the metal were reported as: $E = 110$ GPa, $\sigma_U = 385$ MPa, $\sigma_{0.2} = 340$ MPa, and $\sigma_{0.02} = 170$ MPa. The residual stress was measured using an X-ray diffractometer. Using a large electromagnetic shaker, the specimens were vibrated in a flexural vibration mode at a resonant frequency of 153 Hz. It was reported that when the sum of the vibratory stress and the residual stress was more than 0.02% offset stress of the material, residual stress was found to be relieved. This certainly explained the plastic deformation of the stressed area of the metal due to the combination of the applied and residual stresses, i.e. describing the plastic flow model. In another observation vibratory treated specimens were exposed in the open air for a month for natural ageing, no increase or decrease of residual stresses was recorded. This review is based on the abstract – not from the complete paper because this paper is in Japanese.

Maekawa, et. al. [90]: This work was carried out in Japan in 1986, where the behaviour of the surface residual stress relief and lattice defect density were studied with the application of mechanical vibration. The material used was FC25 cast iron (3.45% C, 1.87% Si, 0.4% Mn, 0.166% P, 0.146% S) and the specimen was a rectangular bar of dimensions 300 × 40× 6 mm. The mechanical properties of the metal was reported as E=160 GPa, σ_U = 380 MPa, $\sigma_{0.2}$ = 340 MPa, and $\sigma_{0.025}$ = 170 MPa. An X-ray diffractometer was used to measure the residual stress. Similar to Nakagiri [99] the authors reported that when the sum of the applied stress and the residual stress was more than 0.025%-offset stress of the specimen, residual stress and lattice defect density were relieved simultaneously. When the summation was less than 0.025% offset stress then the residual stress and lattice defect density did not change. The authors of this article also explained VSR with a plastic flow model. This review is based on the abstract – not from the complete paper because this paper is in Japanese.

Ananthagopal et. al. [3]: This study was undertaken to establish if VSR could replace thermal stress relieving for components in M/s Larsen & Toubro Ltd, Bangalore, India in 1986. A commercially available "Formula 62" stress reliever was used to relieve the residual stress of the iron castings. Formula 62 uses a 0–100 Hz exciter, which was capable to pick the resonant/subresonant frequency automatically. A strip chart recorder was used to record the component response during vibration. The specimens were vibrated for 15 minutes at their resonant/sub-resonant frequencies. The components were machined and the dimensions were monitored over a two-month period. Some components were thermally stress relieved. The authors concluded that VSR was highly cost effective as compared to thermal stress relieving. The applied stress to the components or the relieved stresses were not reported.

Zhang et. al. [145]: Work was carried out in 1989 at the Shenyang Foundry, China. Iron castings were subjected to vibratory treatment in order to relieve residual stress. Subresonant (on the lower flank) frequency of vibration was used to excite the specimen to maximise the energy input into the casting. As a result of the treatment,

the residual stress values were found to be more uniform, i.e. the peak stresses were reduced and the stress distribution became more uniform. This review also based on the abstract of the literature. The details of this paper were not accessible because the article is in Chinese.

2.2.2 Summary

Although several research groups have investigated the use of VSR techniques in relation to cast materials, only a few of these have presented quantitative data concerning its effects. Of these, Balasingh [10], Nakagiri [98], Maekawa [90] report significant changes as a result of vibration. Research performed by Bühler and Pfalzgraf [25] is more important, though it reported a negative result. Similar experiments conducted by Balasingh also produced no observable change in residual stress. An increase in the applied dynamic stress amplitude using resonant vibration resulted in a reduction in the residual stress. The work of Balasingh appears to have been carefully controlled and well monitored. Two contradictory opinions were found from different researchers about the frequency of vibration. Balasingh used resonance frequency and found significant stress reduction. On the other hand Zhang [145] used subresonant frequency and again found significant reduction in residual stress. At the resonance frequency the amplitude is high but the absorption of vibration energy by the specimen is very low, so if energy absorption was the cause of stress reduction then Balashing would not see any change in residual stress. This suggests that the frequency of vibration is not very important for VSR.

Although the publications reviewed in this section provide ample evidence of the potential of the VSR process, in no case was there any investigation into the fundamental mechanisms underlying this phenomenon. In any attempt to provide a coherent theory, attention must be paid to the observation of Balasingh [10] that certain types of material shows less response in reduction of residual stress in VSR treatment than others. Comparison between the responsiveness of different metals may provide some insight into the nature of stress relief processes.

Works carried out in Japan by Maekawa [90] and Nakagiri [98] are very similar, in both cases VSR was reported as the effect of plastic flow of metal under the effect of total stress (residual stress + applied stress). It was shown that if the total stress is more than 0.025%-offset stress then VSR works, otherwise the treatment has no effect. Although there is controversy about this model, it is the most widely accepted concept of stress relieving in VSR treatment. Campbell [28] vibrated castings of different metal during solidification and found a large improvement of mechanical properties and refinement of microstructure.

Work carried out by Ananthagopal [3] claimed a big success in dimension control, where VSR was concluded to be more effective than thermal treatment. Since there is no direct measurement of residual stress, this result cannot be taken as full evidence. Zhang [145] used subresonant vibration frequency to maximise energy input to the specimens, and the results exhibited an increase in the uniform residual stress after treatment.

2.2.3 Welded Structures

Residual stresses are inevitably created during the manufacture of welded fabrications, in a manner analogous to that involved in castings. Intense localised heating forms the essence of all welding operations, resulting in high stress levels in the weld metal and the immediate surrounding material upon cooling. The magnitude of such stresses often approaches the yield strength of the material used. In general, the weld metal itself is left in a state of residual tension, balanced by compressive stresses in the parent material. Welding stresses may be localised within the heat affected zone (HAZ) of the material, or may extend their influence throughout the entire welded structure -depending upon the geometry of the specimen.

McGoldrick and Saunders [94]: This work was carried out at the Taylor Model Basin, USA and was published in 1943. Large fabricated carriage frames could not be annealed in a furnace due to their size and were subjected to vibration in order to relieve residual strain, i.e., to stabilise the frame dimensionally. Vibration was applied

to the specimens using two parallel shaft out-of-balance motors - geared together to run in opposite directions at the same speed. The vibrator generated 440 lbs. driving force in a speed range of from 250 to 3000 rpm. The test specimens were supported near the ends on two knife-edges made from structural angles which in turn were bolted down to a special vibration-testing foundation anchored to bed rock. The applied stresses were measured using Tuckerman optical strain gauges and SR-4 Metalectric strain gauges. The vibrational frequency was chosen slightly below the natural frequency of the test specimen. The dynamic stress applied to the specimen was ±15000 lbf/in^2 (103 MPa) at a frequency of 14 Hz. The specimens were treated in this condition for 8 hours.

Another attempt at VSR treatment of a huge frame (about 68 ft long 56 ft wide and 9 ft high) was undertaken by the Taylor Model Basin. Before any vibration was carried out on the frame, deflection measurements were taken with all the construction supports in place under the whole frame. The same frame was then supported under the driving wheel and steady wheel locations only, where the reactions would come in service. Deflection of the centre was measured followed by calibration using dead weights. The vibrator was mounted at the centre of the frame and the natural frequency of the system was found to be 10 Hz. At this frequency the vibratory amplitude (at the centre of the frame) was found to be 0.05 inch pk/pk. The frame was vibrated for 15 hours at 10 Hz.

In both cases the reduction of residual stress was not measured - due to the unavailability of a non-destructive testing method. Only the dimensional stability of the frames was measured. It was considered that if the part or structure showed no large distortion due to a vibratory treatment process then the structure would not distort or change in dimension in actual subsequent operation. It was found that due to the vibratory treatment, no large distortion of the structures occurred. In most of the batches there was not any control specimen left for comparison with vibrated specimens. It is unfortunate that the earliest available publication on VSR shows incomplete results and thus the comments are inconclusive, though the authors concluded that "the result is negative, but the feeling of safety is positive".

Bühler and **Pfalzgraf** [23]: This work was carried out in the early 60's. In addition to their investigations using iron castings, Bühler and Pfalzgraf also conducted a series of experiments on welded specimens. Their specimens consisted of simple rectangular bars, 540-mm long 40-mm wide and 20-mm thick with a weld seam placed along the long narrow face in order to introduce localised residual stress. The vibratory equipment consisted of an eccentric mass type motor which was used in two different arrangements - allowing both longitudinal (compression-tension) and transverse (longitudinal bending) modes to be excited. Due to the high stiffness of the specimens in the longitudinal mode, resonant conditions could not be attained using their equipment, with the result that relatively low dynamic stress amplitudes were used in this mode (≤ 10 MPa).

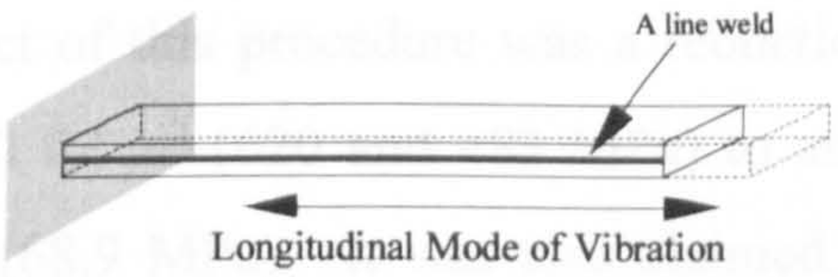

Figure 2.1 – Longitudinal mode of vibration of the discussed structure.

In the flexural mode of vibration, cyclic stress levels varied linearly across the length and depth of the specimen - reaching maximum amplitude at the surface. Cyclic stress amplitudes excited using this arrangement was unreported, except in one case where the dynamic stress imposed upon the specimen was found to be ±120 MPa.

Residual stresses within the welded specimens were measured by a strain gauge sectioning method. It was found that slightly mismatched tensile stresses of 175 MPa and 110 MPa on upper and lower faces were balanced by a compressive core stress of 150 MPa (the reported yield strength of the material was ≥250 MPa). No change in these values was effected by the longitudinal vibration treatment. Bending mode vibration was similarly ineffective, except in one case where it was found that the use of the highest available dynamic stress amplitude was capable of causing a 20% reduction in residual stress value throughout the specimen cross-section. No reference was made to the frequency or duration of vibratory treatment employed in this study.

The possibility that negative results were due to insufficient dynamic stress or numbers of cycles cannot be eliminated, but neither can it be confirmed on the basis of the published report. The observation of some stress relief in one case is encouraging, but clearly not conclusive proof of the success of the process.

Houck, [67]: This work was carried out in the Ohio State University, Columbus, Ohio, USA in 1966. A single example of the application of resonant vibration to a welded structure was presented by this literature. Residual stresses were measured by X-ray diffraction methods before and after treatment of a complex workpiece - using commercially available VSR equipment. The duration of the treatment was 25 minutes; no details of the response amplitude or the frequency of the applied load were supplied. The effect of this procedure was a reduction of anisotropic residual stresses 90000 and 70000 lbf/in^2 (620 and 482 MPa) to an isotropic distribution of magnitude 10000 lbf/in^2 (68.9 MPa). It was also claimed that the distortion of the structure was greatly reduced as a result of the treatment, although no evidence in support of this assertion was presented.

Wozney and **Crawmer** [139]: This work was carried out in the General Electric Co., Schenectady, USA in 1968, where the research was directed in two fronts: investigation of the mechanism of VSR, and its application to large scale welded fabrications. In the work using welded material, flat plates of mild steel (ASTM A7) were thermally stress relieved for two hours at 648 ^{0}C before being welded at either end into a large rigid frame. This procedure resulted in uniform long range tensile residual stress throughout the body of the plate, supported by concomitant compressive stress in the frame. Specimen dimensions were 900-mm in length 250-mm in wide and 6-mm thick; welds ran on the 6 mm × 250 mm faces. The direction of the measured residual stress was parallel to the 900 mm edges: its magnitude before vibration was 140 MPa, determined from the change in strain occurring in the plate upon completion of the welding process. The 0.02% yield stress of the material was determined to be 275 MPa.

Vibratory treatment applied to these structures involved the use of an eccentric mass type electric motor. This was clamped to the centre of the test plate in such a manner as to promote longitudinal bending vibration. Loading was applied for 5 minutes at each of two resonant frequencies: one of these corresponded to a purely flexural mode of vibration, while the second incorporated an additional degree of torsional motion. Peak stress amplitudes in the bending mode were ±90 MPa. In the hybrid mode, higher strain values at one edge of the plate resulted in gauge failure: it was estimated, based upon the relative deflections of the two edges, that a maximum stress amplitude of 200 MPa had been achieved. Control specimens were also investigated, one undergoing thermal stress relief for 1 hour at 621 ^{0}C whilst no treatment was applied to another. Residual stress after treatment was measured by observing the change in strain due to cutting the plate from its frame.

No observable reduction in residual stress occurred as a result of the vibratory treatment, in contrast with almost 100% relief in the thermally treated plate. On the basis of the estimated vibration amplitude and the known yield strength of the material, the authors declared that plastic yielding must have occurred in the outer layers of the plate. The core material was of sufficient cross-section to support the increased load with negligible change to the overall strain. Thus, the degree of spring-back occurring upon sectioning was largely unaffected. This argument depends upon uncertain assumptions concerning dynamic stress amplitudes and the material cyclic yield strength, either of which may be in error. Cyclic hardening characteristics of the test material were cited as a possible factor affecting the degree of stress relief. It was concluded that stress reduction should not be expected to occur uniformly throughout vibrated structures, and that the possibility of fatigue damage during treatment cannot be neglected.

Rich [114]: This work was carried out in Vibratronics Division of Lodding Engineering Corp., Auborn, Massachusetts, USA in 1969. This work involved the vibration of two different steels, a plain carbon steel (AISI 1020) and AISI 304 stainless steel. Long plate specimens of each material (1900-mm in length 100-mm in wide and 25-mm thick) had residual stresses induced by placing two parallel weld

beads along the length of one of the 1900-mm × 100-mm plate surfaces. Each was then treated by one of three methods, one being vibrated using commercial VSR equipment, another subjected to thermal stress relief, whilst the third was retained as a control sample. For thermal stress relief, the AISI 1020 steel specimens were heated to 626 ^{0}C for an hour then furnace cooled, and the AISI 304 stainless steel specimens were heated to 482 ^{0}C for 2 hours then furnace cooled. Residual stresses within each specimen were measured by the strain gauge sectioning technique.

Mechanical treatment applied to each material involved resonant vibration at ±72 MPa for 10 minutes - this amplitude falling comfortably below the long term fatigue stress of each material. In the case of plain carbon steel, welding stresses of 200 MPa were reduced to 38 MPa by vibration as compared to 40 MPa as a result of thermal treatment. Even more impressive results were obtained using the stainless material: 133 MPa fell to 11 MPa after vibration, 19 MPa being the level remaining following annealing.

Although the available information lacks details concerning the frequency of treatment, and therefore the number of applied load cycles, these results are nevertheless outstanding. The measurement procedure for residual stresses was found to be reproducible, yielding results in good agreement with the residual stress calculated from the observed curvature change occurring upon welding. Despite the fact that only one sample of each material was treated by vibration, the potential of mechanical stress relief was clearly demonstrated by this research. Of paramount importance is the observation that these results were achieved without exceeding the fatigue limits of the materials in question, so that the risk of damage occurring during treatment may be considered to be negligible.

Cheever & Rowlands [30]: This experimental work was carried out in Battelle-Columbus Laboratories in 1977. Two different types of welded specimens were subjected to vibration. One was a rolled and welded ring, the other a T-section. The rolled and welded rings (Figure 2.2) were fabricated by rolling sheets of furnace flattened 1020 steel to join opposite edges.

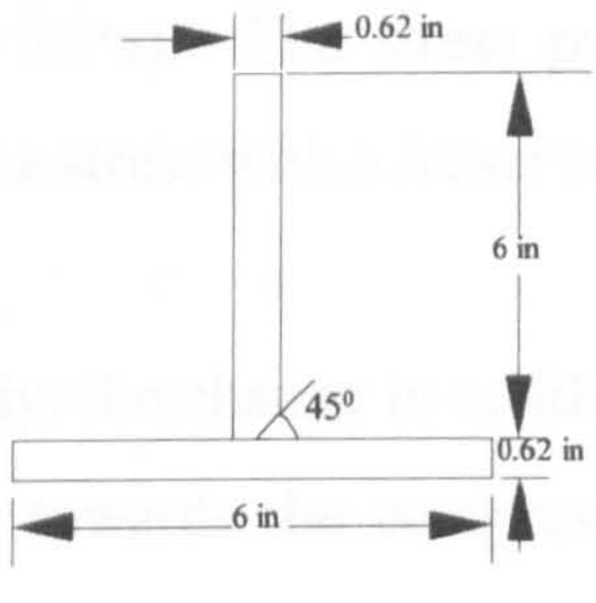

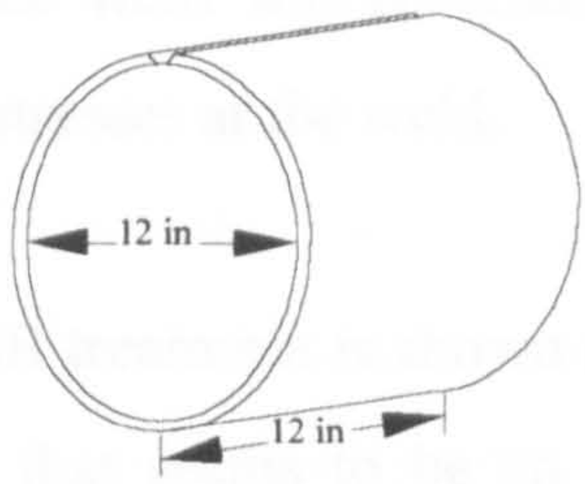

Figure 2.2 – The 'T' section and circular welding ring.

The edges were bevelled, then Gas Metal Arc welded in two passes. Three specimens were welded at the seam while they were being vibrated, the amplitude of vibration was 1 mm (pk/pk) at 56.7 Hz. The other three specimens were welded without any vibration. The roundness of the specimens was checked and it was found that the vibrated rings were more round than the unvibrated rings. However, further studies with a second set of rings using the same processing sequence gave contradictory results.

Welded T-sections (12 of them) were made from hot rolled steel plate (AISI 1020). Each specimen was welded at the T-junction while it was vibrated at a frequency of 71.7 Hz with 1-mm amplitude (pk/pk). Vibration started before welding and continued for 20 minutes after the first pass. It was reported that the unvibrated specimens distorted more after machining. In both kinds of specimens the applied stress or mode of vibration was not mentioned.

Botros [19]: This work was carried out in the N. C. Agricultural and Technical State University, USA in 1980. In this study the specimens were prepared from structural hot rolled A36 bars. The width of the bars were 4, 6 & 8 inch and the thicknesses were ¼ and ½ inch. The residual stresses of the bar were measured where very small amounts of residual stresses were found. Square boxes 3 ft × 3 ft were formed by welding. Vibration was applied to the specimens using an electro-magnetic shaker with a frequency range 5 to 3000 Hz. Vibration frequencies were chosen between 50 to 80 Hz. The residual stress distribution before vibratory treatment was measured using strain gauges. The reported stress level on the weld was shown as 30,000 lbf/in^2 (206 MPa), which was dropped rapidly due to VSR treatment to – 3,000/5,000 lbf/in^2

(20.6/34.4 MPa). The stress pattern away from the weld was reversed with high compressive stress with a lesser to a degree than the stresses at the weld.

In this study, the change in residual stress due to VSR treatment is shown only in one direction - towards the compressive stresses - and that seems to be an incomplete picture.

Shankar, Wood and **Khan** [118]: This work was carried out in the University of Portland, Oregon, USA in 1980. During the course of his research, Shankar worked on residual stress relief of simple butt welds. Three specimens were formed by welding together six plates of annealed mild steel (ASTM A36) in pairs - forming plates 900-mm in length 400-mm in wide and 13-mm thick. All specimens were prepared identically: annealing was performed at 852 ^{0}C for 1 hour; welding was performed in two passes, with the plates remaining firmly clamped during cooling to minimise distortion. Stress measurements were made using a strain gauge sectioning method, supplemented by tests using X-ray diffractometry to ensure that the sectioning process yielded accurate values of residual stress.

Vibration was applied by clamping the test pieces to a shaker table driven by an eccentric-mass direct current motor. Both resonant and sub-resonant vibratory treatment was applied to the test specimens, although no indication was made in the article of the stress amplitudes induced during these processes, or of the number of applied cycles. As a result of resonant vibration, the peak residual stress level was found to be reduced from 295 MPa to 255 MPa, a change of 13%: the yield strength of the material in the welded condition was approximately 300 MPa. Sub-resonant treatment was found to cause a smaller reduction. Numerical values of residual stress measurement were not published: the data presented here were taken from a graphical representation. Although the authors' extrapolation of this graph to the weld centre indicates a larger stress reduction as a result of vibration, this inference does not rest upon solid experimental evidence. It was nevertheless concluded that residual stress levels close to the yield strength of welded material may be reduced by the application of cyclic loading - even without achieving resonant vibratory conditions.

Gifford [55]: This work was carried out in Auckland Industrial Development Division, New Zealand in 1983. In this investigation T-butt welded specimens was studied by Gifford using a variety of techniques. The expected resonant behaviour of specimens having the chosen geometry was modelled using finite element methods: the results of this analysis were then compared with natural frequencies found by Fourier transformation of experimental impulse response data. This stage was followed by excitation of several resonant modes of vibration using commercial eccentric mass motors. The maximum stress amplitude achieved using this method was ±21 MPa - well below the material's known yield strength of 305 MPa. Although there was a considerable degree of scatter in the residual stress values (measured by a hole drilling method), no systematic variation was detected as a result of vibration.

It was concluded by the author that the chosen measurement points were perhaps not sufficiently close to the weld region, with the possible result that stress re-distribution occurring at points removed from the measurement sites may have failed to influence the observed residual stress. Furthermore, it is a known feature of the hole drilling stress measurement technique that stresses in excess of one third of the material yield strength will not be reliably measured, due to plastic distortion of the material under the stress concentrating influence of the hole. Steep stress gradients also contribute to scatter in the values yielded by this method. Failure to observe a clear trend in measured residual stress may therefore be attributed to the chosen measurement process. Clearly, though the low amplitude of applied dynamic stresses is a prime additional factor contributing to the lack of positive results.

Larsson & Tronsker [82]: Experiments carried out by "VERITEC - Marine Technology Consultant" in 1984, included two types of specimens: namely Window and Cruciform. The specimens were vibrated using a commercially available VSR vibrator. The specimens were vibrated during welding at their resonant frequency. Vibration started at the start of welding and continued for 5 minutes after completion. The electrodes used were baked in a desiccator to control hydrogen content.

Window test specimens (two) were preheated to 85 ^{0}C then cooled to 75 ^{0}C prior to the weld being started. The temperature was measured using a Cromel-Alumel thermocouple and strain due to welding was measured using a temperature compensated strain gauge – located 67-mm from the weld centre. In this test the frequency of vibration was between 42-83 Hz.

For the Cruciform test specimen the steel plate was NVE 36 quality. No preheating was carried out on these specimens. The frequency of vibration was between 76-81 Hz.

Five sections were taken from each completed weldment for microstructural examination. The sections were polished, etched and measured in an optical metallurgical microscope. Hardness tests were also carried out on the sections. No significant effect of vibration was observed on the weld geometry and hardness of the weld. The residual stress was found to have dropped by 8% due to VSR treatment.

Ankirskii, [4]: The effect of vibration and heat treatment on the properties of 20K (Russian expression – not known to the writer of this thesis) sheet steel (GOST5520-69) was studied in the *All-union Scientific Research and Design Technological Institute of Chemical Engineering, Penza* in 1985. The sheets used were 40 mm thick. These were welded manually using UONI-13/45A electrodes. One end of the welded panel was fixed with the column raised on a base plate and a vibrator was fixed to the other end. Vibration treatment was carried out at resonant frequencies between 24 to 32 Hz. The time of vibration was 20 to 25 minutes and the applied stresses to the specimens were 200-400 MPa. A diagram of the set-up was not supplied. The reference specimens were heat-treated (tempered) at 625±10 ^{0}C, held at that temperature for 2 hours and then cooled in air. Crystal structure, hardness, impact toughness and fatigue life was investigated. Tempering resulted in the usual changes: reduced yield stress and hardness, along with increased impact toughness. Vibratory treatment resulted in an increase in strength and a reduction in ductility. The result of the fatigue test indicated that the fatigue life was decreased in both cases (tempered and vibrated) compared with the unwelded parent metal but the vibratory treated

specimens showed higher fatigue life than tempered specimens. No initiative was taken to measure the residual stress.

This work illustrates a salient point in favour of VSR treatment in that VSR can relieve residual stress from the most vulnerable or suspected areas of the specimen without harming other necessary properties of the specimen that is needed for its service life. On the other hand, tempering or annealing relieves residual stress at the expense of some essential mechanical properties of the specimen.

Ernst, et. al. [47]: Experiments were carried out in 1986 to observe the vibration effect on solidifying weld metal. To study this, welds were made in four alloys - with and without the application of mechanical vibration. The alloys studied were Type AISI 304L austenitic stainless steel with a ferrite number 0, Type 304L with a ferrite number of 5, 2219 aluminium-copper alloy and cupro-nickel. Mechanical vibration was introduced using a rotating eccentric load. The vibration was induced in the base plate by clamping it to a table on which the frequency generator was connected. For each base plate, the frequency was adjusted until a resonant peak was found. Welds were then produced using a semi-automatic Gas Tungsten Arc Welding process. The welds were sectioned and mounted transversely - top side up. For the cupro-nickel specimens it was observed that vibrations yielded a refined microstructure and showed many changes in growth directions. The cupro-nickel specimens were vibrated at 100% of the "resonant peak" and showed a grain size refinement similar to the welds made at 40% but to a lesser extent. The details of the vibration methods were not delivered. For the stainless steels and aluminium-copper alloys no change in the solidification structure was observed after the application of vibration.

The mechanism of grain refinement was described as follows. In order for structural refinement to occur, two factors must be present. The first is the ability for a dendrite tip to break off and float into the melt, thus acting as a site for heterogeneous nucleation. The second factor is the survival of the newly formed solid in the melt. For a dendrite to break off, long fragile dendrites are necessary. Once fragmented,

remelting of the solid cannot occur as it floats into the melt if new growth is to occur. New growth can occur if the solid is in a region of constitutionally undercooled liquid.

Jesenský, [68]: This work was carried out in The Welding Researchers Institute, Bratislava, CSSR in 1983, where vibration was applied to reduce residual stress of welded structures. A box section measuring 200 mm high by 170 mm wide was prepared using 15 mm thick plates by welding a top and bottom flange to the vertical plates. Manual arc welding was used to prepare the box. The overall length of the beam was 1.5 m. The material of the beam was Fe 510 B /CSN 41 1523.1/ steel, and the electrode was according to CSN standard (E 52.33 coated). The vibration was applied to the specimens using a mechanical eccentric vibrator with frequency range of 1 to 200 Hz. One beam was kept as a control specimen (as welded) and the other one was vibrated in its first four resonant frequencies (highest resonant frequency - 120 Hz). The surface residual stresses were measured by the tensometric method which consists of cutting prisms 20 mm × 20 mm in size along the beam circumference. An HBM strain gauge (type 1.5/120 LY 11) was cemented onto the material surface in the shape of a rosette of 0^0 and 90^0. The reduction in residual stresses was shown to be very significant. The two peaks of residual stresses 430 MPa and 375 MPa were shown as being reduced to 260 MPa and 220 MPa respectively.

Though great success was claimed, some questions arise from this work: the modes of vibration were not reported and the types and value of applied stresses were not supplied. Only two specimens were prepared, one specimen was treated and then compared with the untreated one.

A fatigue test was also carried out, where two batches of welded joints were tested. The test result of the unvibrated specimens were compared with the vibratory treated specimens. The test result showed that the fatigue life of the vibratory stress relieved specimens was not less than the unvibrated specimens.

Klotzbücher and **Kraft** [78]: This work was carried out by Klotzbücher and Kraft in Nuremberg, Germany in 1987 where two separate types of welded structure were

involved with this research. Their first approach was an attempt to relieve the overall long range residual stress within steel rings (ST 52-3N) - closed elastically and welded along the closure seam. Specimens were divided into three groups, each to be treated differently: control specimens were left unprocessed, while one group were subjected to vibration using a shaker table. Another specimen was thermally stress relieved for 2 hours at 602 ^{0}C. After treatment, each specimen was machined in a predetermined manner: the deviation from true circularity after machining was taken as a measure of dimensional stability. Rings were subsequently slit along the weld seam and the degree of spring-back measured: this was taken as a measure of long range (type I) residual stress. No direct measurement of the residual stresses was carried out. The duration of vibration or amplitude of applied dynamic stress was not mentioned in their report.

Although no change in residual stress levels could be determined in specimens subjected to cyclic loading, those which underwent the thermal process were almost completely free from spring-back. In addition, it was observed that the roundness of the vibrated rings was similar to that of the control group, whereas thermal stress relief caused significant improvement in this respect.

Following their unsuccessful tests on welded rings, the authors shifted their attention to welded T-joints - fabricated from the same material. These specimens were also vibrated at resonance while clamped on the shaker table; in this case the amplitude of applied cyclic stress (±17 MPa) was recorded. Comparisons were made with control groups consisting of untreated and thermally annealed materials. The only observation made on these test pieces was the degree of deviation from flatness of the material after one surface was milled. As each group consisted of only two specimens, it is necessary to discount the significance of the author's observation that vibration slightly reduced the distortion which occurred upon machining (0.65 mm and 0.40 mm on the vibrated specimens against 0.60 mm and 0.80 on the control group specimens). The effect of thermal annealing was much more dramatic (0.05 mm to 0.10 mm).

Observations of motor input currents during the vibration of test specimens were also recorded. The authors noted substantial reductions throughout the course of each treatment with no corresponding decrease occurring during vibration of the annealed material. It was speculated that this effect was indicative of reduction in the internal friction of the treated material. This interpretation cannot be reconciled without a proper understanding of the phenomenon of resonance and the current versus load characteristics of electric motors.

Ohol et. al. [102]: The application of VSR processes to larger structures was attempted by Ohol [102] in 1988, using structural steel (IS:2062-69). The yield strength of the material was 235 MPa. A massive gear box bed plate assembly was fabricated by welding together steel plates. Residual stress levels in one region were determined by a blind hole drilling technique. The principal stresses were found as 88.5 MPa and 41.7 MPa. Vibration was applied using commercially available eccentric mass a.c. motors, and was carried out at four distinct resonant frequencies for 30 seconds each. Dynamic strain amplitudes were measured using resistance strain gauges. The authors recorded reductions in residual stress between 30% and 55%. Principal stresses reduced to 63.2 MPa and 18.2 MPa.

Following the treatment of the bedplate, the authors applied their equipment to a large austenitic stainless steel bowl assembly - strengthened by welded mild steel support members. In this case no measurements of residual stress or dynamic stress amplitudes were made, nor was there any indication of the material yield strength. The criterion for success of the treatment was the dimensional tolerance achieved in the structure after finish machining. It was stated that satisfactory results were achieved, but it should be noted that no control experiment was performed. The role of vibration in maintaining tolerance remains unclear in this case.

Bouhelier et. al. [20]: This work was carried out by Bouhelier's group in France in 1988, where a series of tests were performed upon large welded parts – gear box casings fabricated from E-26-4 grade steel. Only two test specimens were used: one was subjected to vibration using eccentric mass motors, the other thermally stress

relieved at 602 ^{0}C for one hour as a control specimen. Residual stress levels within treated weldments were measured using X-ray diffraction techniques. Although several different resonant frequencies were used, it was found that the lowest of these corresponded to simple rigid body motion of the workpiece, resulting in very low induced stress amplitudes (≤1.5 MPa). Despite this observation, it was stated that application of this process for 15 minutes was capable of effecting significant reduction in residual stress levels within the component. Peak tensile stresses were reduced from 100 MPa to 60 MPa, although no change in compressive stress was noted. No additional change was recorded after further resonant vibration at stress amplitudes up to 200 times those used in this first process. Thermally annealed material exhibited significantly greater stress reductions, and the maximum residual stress after thermal treatment was found to be 30 MPa. Further measurements were made to determine whether distortion during vibration could be used as an indicator of the effectiveness of the process. No changes in specimen geometry were detected after cyclic loading.

Similar tests were performed upon a smaller welded component manufactured from E-24 grade steel, with comparable results. Variable reductions (up to 40%) of tensile residual stress were detected after vibration: the original values were ~100 MPa. As before, no changes in compressive residual stress levels were noted. In this case no indication of the applied cyclic load amplitude was given, nor were any results presented concerning the thermal treatment of the control specimen.

Consideration of the results presented by these authors raises various questions concerning their experimental techniques. Since only one specimen of each type was used, the statistical significance of data thus obtained is minimal. No indication of the expected scatter in experimental values was made available.

The authors observed a significant reduction in residual stress by application of a very small dynamic stress. The observation of stress reduction as a result of extremely low amplitude vibration would suggest that the plastic flow model of residual stress reduction is not valid in certain types of residual stresses and their reductions.

Finally, it is not possible for a reduction in tensile residual stress to occur with no accompanying change in compressive stress. Failure to observe such changes were explained by the authors as the result of the localised nature of their stress measurement process.

Polnov, et. al. [108]: This work was carried out by All-Union Scientific-Research Institute of Fittings Technology, former USSR in 1992. Vibratory treatment was carried out on 250 mm length, 110 mm wide and 5 mm thick rectangular plates of low-carbon steel. Torsional variable stress was applied to the specimens for this treatment. The frequency of vibration was 48 Hz and the vibratory shear stress was ±90 MPa. The residual stresses in the transverse cross section of the plate were measured by the magnetoelastic method. The decrease in residual stress in the plate in relation to the time of vibration treatment was found to be non-linear and the main portion of the decrease in stresses was in the first minute of the treatment. Subsequently, the residual stresses were stabilised and did not reduce further. The details of their experiments were not delivered. Also, the stress levels before and after the treatment were not mentioned.

Tewary & Shanker, [126]: This work was carried out in the Banaras Hindu University, India in 1993. In this work the change in mechanical properties of welded joints due to vibration were investigated. Mild steel plates of 8 mm thick were machined to a size of 25 cm × 25 cm on a milling machine. Two plates were positioned and clamped on the vibrator table, then welded under stationary and dynamic conditions using the frequency and amplitude range of 0 – 400 Hz and 0 – 40 μm respectively. The type of vibration was reported as 'longitudinal' but the mode of vibration was not mentioned. However the set-up of their experiment indicates that it was rigid body mode vibration. Tensile and hardness tests of the specimens were carried out where it was observed that the yield strength, ultimate strength and hardness increased significantly due to the treatment. The increase in the mechanical properties was observed in the frequency range of 80–400 Hz and amplitude range of 5–30 μm. Microstructural examination of the specimens was also carried out where it was found that the grain size was refined and the material became more uniform in the

vibratory treated specimens. It was concluded that the improvement of mechanical properties was due to the uniformity and refinement of the microstructure.

Fenghua & Dexin [49]: This work was carried out in Dalian University of Technology, China in 1994. A mild steel pipe was welded in a T junction format and the residual stress at five points on the joint was measured using the hole drilling method. To reduce the scatter of the data the measurements and application of the treatment was carried out by same person using the same instruments. Three groups of specimens were prepared. The first group without any treatment, the second group was treated with vibration and the third group was treated with artificial ageing. Due to the vibratory treatment the peak residual stress was reduced from 203 MPa to 80 MPa and the average stress reduction was shown as from 91.7 MPa to 49 MPa. The residual stress distribution was reported to become more uniform after the treatment. A fatigue test of the specimens was carried out where it was found that the fatigue life of the vibratory treated specimens was increased. Details of the vibratory treatment were not given.

Aoki & Nishimura, [7]: This work was carried out in Japan in 1995. In this experiment, mild steel bar 100 mm by 6 mm cross-section and 280 mm length was used. Two bars were welded while they were vibrated. The outer ends of the two specimens were rigidly fixed and the inner ends were connected to a small shaker. Small amplitude (0.09 mm to 0.669 mm) longitudinal flexural vibration was applied to the specimens while they were being welded. Two different frequencies (60 Hz and 100 Hz) were chosen to treat the specimens. The natural frequency of the specimens was 60 Hz. The duration of vibration was not reported. The residual stress was measured using a parallel beam X-ray diffractometer with a scintillation counter. For the two different frequencies the reported reduction in residual stresses on the weld are shown below.

Table 2.1 – Reduction in residual stresses on the weld due to VSR treatment

Frequency 60 Hz			Frequency 100 Hz	
Vibration amplitude	Residual stress		Vibration amplitude	Residual Stress
No vibration	290		No vibration	290
0.09	175		0.062	230
0.375	170		0.129	160
0.669	110		0.184	270

The residual stress on the weld was found to have decreased significantly. On the weld toe, the stress was found to have decreased, but to a lesser degree. A small distance away from the weld toe the stresses were found to have increased, which was certainly redistribution of residual stresses. Residual stresses were found to have decreased as the amplitude of vibration increased, but when the amplitude of vibration was large the reduction effect was small, which is shown in Table 2.1. An elasto-plastic model was also created to show the plastic deformation during vibratory treatment. In that model the stress-strain characteristic of the metal was assumed to be elastic up to the yield point, then completely plastic. The reduction in the residual stresses was explained as being due to plastic deformation of the stressed area.

Sonsino, et. al. [123]: This work was carried out in Germany in 1996 where experiments were carried out using two different types of specimens: T-joints and egg-box type cruciform joints. The details of the specimens are shown in Figure 2.3.

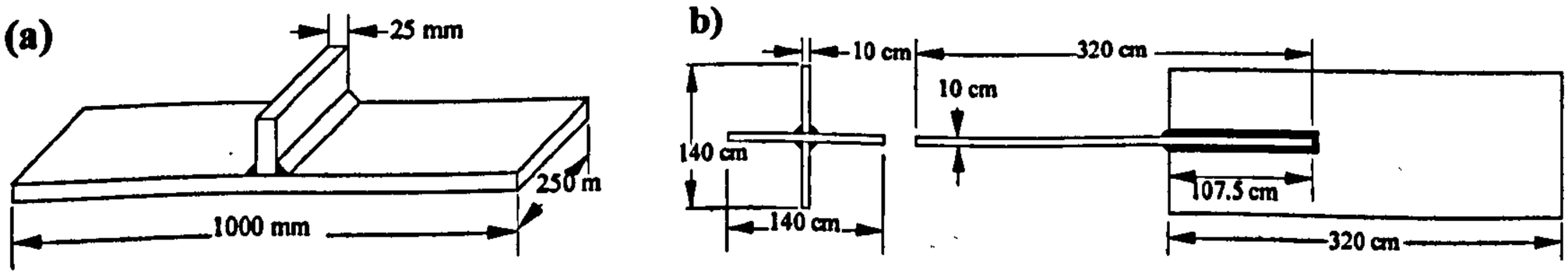

Figure 2.3 – T-joint and egg box type welded joints.

Three different types of steels were chosen for this investigation. The yield strengths of the three steels were 380 MPa, 774 MPa and 777 MPa. High yield strength materials were chosen to exhibit a high tensile residual stress after welding. The frequency of vibration of the specimens was chosen as 100 Hz. The time of vibrations was 10 to 15 minutes and 10 to 25 minutes. The mode of vibration or applied stresses to the specimens was not delivered. The reduction in residual stresses in the vibratory

treated specimens was found to be small in comparison with the thermally treated specimens.

A fatigue test was also carried out using both kinds of specimens. The authors found that the fatigue life was higher in the thermally treated specimens. The authors concluded with the statement:- 'VSR cannot act as a substitute for thermal treatment'.

The author's comment about VSR may be valid for the materials that they have used in their treatment, but their comment about the fatigue life seems contradictory to the works of most researchers, which casts a strong doubt over their experimental methods.

2.2.4 Summary

Published research into the effect of cyclic loading on welded material and structures has been directed exclusively at steel specimens, particularly ferritic plain carbon steels. Going through the findings of different experimenters the reader must have mixed feelings, because of the controversy between different experimenters, about the effectiveness of VSR. The majority of investigations have yielded positive findings, reporting the reduction of residual stress levels or improved dimensional stability as a result of vibratory treatment. Some of them found an increase in residual stress or no change due to the treatment. Because of the complexity of the stress measurement methods, most of the previous researchers took a limited number of point measurements which always gave a partial picture of the residual stress distribution. So the change due to the treatment was not seen as a complete picture. The residual stress is highly self-equilibrating, which can be increased in some areas due to a reduction in others. In some areas the stress may not change without a radical redistribution. This explains why there is so much disagreement between the researchers about the subject. The findings and comments from different experimenters depended on the position of the point that they measured. Nobody measured/scanned the changes in residual stresses in the whole stress field or in the whole specimen to obtain a full picture.

Programmes which contradict these findings may be divided into two classes: those in which the stress amplitude of the applied vibration was very low and those in which the applied stress amplitude was not adequately documented.

Bühlar and Pfalzgraf [23] reported negative results; the most probable explanation for this result was the magnitude of the applied stress and/or number of cycle was not sufficient enough to relieve residual stress. Houck [67] and Botros [19] claimed a large success in reducing residual stress from a high tensile value to an isotropic distribution of negative stress, which seems a partial result. Wozney and Crawmer [139] reported no change in residual stress as a result of vibratory treatment. They concluded that stress reduction should not be expected to occur uniformly throughout the structure, and that the possibility of fatigue damage during treatment cannot be neglected. Though there was a lack of information concerning the frequency of treatment, Rich [114] claimed a large success in reducing the residual stress from 200 MPa to 38 MPa. Cheever and Rowlands [30] vibrated their specimens while they were being welded and found a confusing result. In the first batch they found that the distortion was decreased due to the vibratory treatment but in the second batch they found the reverse. Shanker [118] used resonant and subresonant vibratory treatment, where subresonant treatment showed a smaller reduction in residual stress than the resonant treatment. Shanker's findings are contradictory to the comment of Claxton [32-37] who explains VSR as an energy concept, at sub-resonance frequency higher energy is absorbed by the structure hence stress reduces. Gifford [55] applied a small dynamic stress (±21 MPa) to his specimens and found no reduction in residual stress. Jesenský [68] claimed a large success in reducing the residual stress but the mode of vibration and/or applied stress was not reported, which made his findings confusing.

Klotzbücher and Kraft [78] found some indication of dimensional stability and concluded that VSR cannot be considered as an alternative to thermal stress relieving in cases where the aim is to effectively reduce distortion during machining. Ohol [102] found a reduction in residual stress between 30% to 55%. Bouhelier [20] claimed to achieve significant stress reduction by applying extremely low amplitude vibration. Fenghua & Dexin [49] found a significant reduction in residual stress due

to vibratory treatment, whereas artificial ageing showed a lower reduction than the VSR treatment. Aoki & Nishimura [7] vibrated their specimen during welding using low amplitude and found a significant reduction in the residual stress. Sonsino [123] found a very small or negligible reduction in residual stress and commented that VSR could not replace heat-treatment. Tewary & Shanker [126] and Ernst [47] vibrated their specimens during welding and found improved mechanical and microstructural properties of the vibrated samples. Ankirskii [4] treated his specimens after welding and found an improvement in the mechanical properties of the specimens.

The remainder of the published research on the subject supports the contention that cyclic loading of welded specimens at sufficiently high amplitudes is capable of reducing the peak levels of residual stress within the material. Maximum effectiveness is achieved by resonant vibration of material which exhibits initial stresses comparable with its yield strength. In common with research based upon cast specimens, no attempt was made by any of the authors to form a theory explaining the fundamental nature of the VSR process.

2.2.5 Plastic Deformation Stresses

Residual stresses may be induced into ductile materials by non-uniform plastic deformation. Neighbouring regions, which exhibit different strain responses during this process, may be left in a state of incompatibility with one another. This mismatch must be accommodated by residual elastic strain, supported by an accompanying residual stress field. Documented investigations of VSR methods include several studies of the effect upon such material of various cyclic loading processes.

Moore [97]: This work was carried out in the University of Illinois, USA in 1944. The material chosen by Moore for his study on the effect of fatigue cycling upon metals was shot peened structural steel. Specimens took the form of tapered cantilever beams, so shaped to ensure uniform applied surface stresses during resonant loading. It was not possible to measure the residual stress due to unavailability of a proper measurement method. Residual stress was calculated from curvature change occurring

upon splitting the shot peened strips where they were free to bend. Some stress relief was achieved as a result of cycling loading, the degree of reduction being dependent upon the amplitude and duration of the loading regime. In an extreme case, one load cycle of magnitude sufficient to cause 0.2% permanent surface strain was observed to effect approximately 76% reduction in residual stress.

Further investigation involving different material (carburised and quenched steel) indicated that such effects were not repeatable. It was thought that this was due to the brittle nature of the material, and the conclusion was drawn that stress relief was dependent upon a degree of plastic deformation occurring during loading.

Fuchs and **Mattson** [53]: This work was carried out in the General Motors Corporation, USA in 1946 where shot peened material was adopted for investigation. In this case, however, additional residual stress was induced by plastic twisting of long steel bar specimens. The reason for applying two separate stress induction processes was not made clear. In contrast with the earlier work by Moore, the authors observed no changes in residual stress levels as a result of cyclic torsional loading. This discrepancy may be resolved by observing that, in the latter work, imposed cyclic stresses acted in one sense only, and were not reversed. The direction of fatigue loading was the same as that applied during stress induction: the effect of such treatment would be expected to be minimal. Applied loads sufficient to cause permanent distortion of the test pieces would tend to contribute towards the previously induced stress pattern, rather than to cause its reduction. The residual stresses were calculated by measuring the distortion of the specimens after removing some layers off by machining.

Pattinson and **Dugdale** [105]: This work was carried out at the University of Sheffield, UK in 1962. Residual stresses are known to have a detrimental effect upon fatigue life, although this phenomenon is less pronounced in ductile materials. The authors postulated that this might be due to the rapid fading of residual stresses during cyclic loading, reducing the time during which additional damage occurs. In order to investigate this claim, specimens of two materials 0.17% carbon steel and aluminium

alloy L65 (4.5% copper) were plastically straightened to induce residual stress. These were then cycled using bending fatigue testing equipment at a variety of amplitudes below their (reduced) fatigue limits. Residual stress levels in the treated and untreated specimens were determined by a strain gauged sectioning method.

For the steel test pieces, the plastic bending was found to induce surface residual stress of 98.9 MPa. Compared with a yield strength of 233.5 MPa this was found to have only a marginal influence upon the fatigue limit of the material, reducing this quantity from 230 MPa to 204 MPa. Imposed dynamic stresses as low as ±61 MPa were found to be capable of reducing residual stress levels by as much as 15% after 10^7 cycles. Higher amplitudes caused correspondingly greater changes: up to 35% reduction after 10^7 cycles at ±200 MPa. Stress relief was found to vary linearly with the logarithm of the number of applied cycles, up to and including the upper limit of 10^4 cycles.

In the case of the aluminium alloy, the effect of cyclic loading was significantly more complex than in the steel specimens. Although the residual stress, at 116 MPa, was much lower in comparison with the 0.1 proof stress (482 MPa), the endurance limit at 10^7 cycles was more strongly affected by plastic bending (207 MPa → 150 MPa). For loading regimes involving less than 10^7 cycles, applied loads as high as ±125 MPa had no discernible effect upon internal stress. Beyond this point, relatively rapid decreases began to occur: over 10^8 cycles, cyclic stresses of ±40 MPa caused almost 20% reduction; loading to ±125 MPa increased this figure to 75%. Within this region, stress reduction varied linearly with the logarithm of the number of applied cycles, continuing regularly up to the limit of the applied treatments.

The authors concluded, as a result of their work, that significant reductions in residual stress were attainable by means of cyclic loading below the fatigue limits of the materials concerned. They attributed the disparity between the effects of residual stress upon fatigue life in steel and aluminium alloy to differences in the vibratory stress reduction behaviour of the two materials. It was noted that, in the case of the alloy specimens, testing to determine the effect of cyclic loading upon material properties ought to be continued for at least 10^8 cycles.

Wozney and **Crawmer** [139]: This work was carried out in the General Electric Co., Schenectady, USA in 1968 where two different types of specimens were processed. Their results concerning large scale welded fabrications were discussed earlier (section 2.2.3): they also performed tests upon much smaller specimens, loaded using fatigue testing equipment. In common with many researchers before them, the authors chose shot peening as their method for introducing residual stress into a small scale test piece (a thin Almen strip, 76 mm × 19 mm × 1.3 mm). This strip was fabricated from a steel (SAE 1070) of exceptionally high strength (σ_U = 1600 MPa, σ_p = 1250 MPa, hardness = 48.5 RC): compressive surface residual stress levels due to the shoot peening were correspondingly high, at -350 MPa. Following stress induction, the specimen was subjected to cyclic bending in a standard fatigue testing machine at various amplitudes and durations, the surface residual stress being determined after each treatment stage by X-ray diffractometry.

No discernible effect of loading at ±240 MPa for 27000 cycles could be determined. Increasing the applied stress amplitude to ±480 MPa for a further 27000 cycles resulted in a decrease in the magnitude of surface residual stress to -282 MPa or a reduction of 68 MPa from the original condition. This treatment was followed by 100 cycles at ±585 MPa, stimulating an additional 27 MPa reduction in residual stress. Increasing the number of applied cycles to 27,000 at this amplitude provoked still more stress relief, resulting in a final surface residual stress of -234 MPa or a reduction of 21 MPa.

The authors noted that the sum of the applied and residual stresses in the material did not exceed the previously determined value of its yield stress: they attempted to reconcile this observation with the fact of residual stress reduction by postulating cyclic softening of the material. Using the recorded values of applied stress amplitudes and the residual stresses before and after each treatment, they derived several points upon the cyclic strain-strain curve of the material. Comparison of these data with the results of previous research into the cyclic behaviour of a similar steel (SAE 1045) resulted in reasonably good correlation being established. The conclusion was drawn that VSR effects could be adequately explained by and predicted from the

cyclic elastic/plastic properties of the subject material. The dependence of stress relief upon treatment duration was attributed to the fact that full softening was not achieved and that stable hysteresis was not established immediately upon commencement of cyclic loading. It was noted that fatigue damage must be considered likely as a result of prolonged vibration at the amplitudes used in the course of this research.

Dawson [39, 40, 41]: The research undertaken by Dawson in the course of his doctoral degree at the University of Liverpool in 1975, involved consideration of the effect of cyclic loading upon three separate materials. Each was subjected to a similar method of residual stress induction, namely strain-controlled plastic bending to near collapse. Specimens in the form of long square bars 450 mm × 13 mm × 13 mm were vibrated in resonant cantilever modes using an electromagnetic shaker. The three materials chosen were cold drawn bright mild steel (σ_Y = 400 MPa), hot rolled mild steel (σ_Y = 280 MPa) and aluminium alloy BS1474:HE30TF (σ_Y = 200 MPa). Surface residual stress levels immediately following plastic bending were measured by strain gauge sectioning techniques, and were found to be 250 MPa, 100 MPa and 100 MPa respectively. Theoretical calculations based upon the assumption of perfect elastic/plastic behaviour predicted that the surface residual stress should be exactly half of the material yield strength, in broad general agreement with these observations.

Dawson found that, by application of sufficiently high dynamic strain amplitudes, surface residual stresses in these materials could be reduced essentially to zero. No dependence upon the frequency of applied vibration was observed within the range 30-90 Hz. In the case of each material a minimum strain amplitude was determined below which no changes in residual stress occurred as a result of loading: these lower limits represent applied stress amplitudes somewhat less than half of the quoted yield strengths of the materials involved. Application of higher amplitude cyclic loading produced ultimate residual stress levels, which were found to decrease linearly with applied strain amplitude. It is significant, however, that the sum of applied dynamic strain and ultimate surface residual stress is not a constant value, but rather increases with the degree of stress reduction achieved. This observation may indicate the

occurrence of work hardening during the VSR process. All three test materials exhibited this characteristic behaviour, regardless of their cyclic hardening/softening properties.

Careful observation of material behaviour during the first few cycles of vibration was achieved by simulating the process using fatigue testing machinery. It was found that cycling about a fixed position resulted in stress changes, which stabilised very quickly, whereas unconstrained cycling allowed redistribution of residual stress to continue during many load cycles. Although the majority of the residual stress relief occurred during the first 10 cycles of vibration, significant changes were observed throughout the process: the upper limit used in the course of this research was 10^4 cycles. Estimates made concerning the effect upon the fatigue life of vibratory treatment sufficient to effect complete surface stress relief suggested that approximately 25% reduction in this quantity might be expected, although no experimental data were presented in support of this assertion.

The programme of research accomplished by this author was both rigorous and comprehensive in achieving its objectives: it was conclusively demonstrated that residual stress relief could be accomplished by cyclic loading. Observation of continuing reduction for many cycles constitutes evidence that a simple overload mechanism is insufficient to explain the phenomenon in its entirety, as does the fact that the sum of applied stress and final residual stress is dependent upon the degree of stress reduction achieved. (The latter quantity may perhaps tend towards a constant value as the number of cycles is increased beyond Dawson's self-imposed limit of 10^4 cycles.) Although a lower limit of applied stress amplitude was noted below which stress reduction was found not to occur, this value may well arise from nothing more significant than the chosen method of stress induction. Since the plastic bending method is incapable of causing surface residual stress levels greater than half of the material yield strength, stress reduction might be expected to depend upon exceeding a threshold amplitude: the use of higher initial residual stresses might eliminate this requirement.

Taggert, et. al [124]: This work was carried out at the University of Washington, USA 1982, where copper single crystals were studied to observe their response in VSR treatment. Residual stress was induced to the crystals by uniform bending of the crystal along its [111] tensile axis. The specimens were vibrated as cantilevers so that the effect of various stress ranges on a fixed value of residual stress could be assessed. Sinusoidal excitation near a resonance frequency was used in the test. Copper crystals were chosen to make sure that the specimen was free from stresses other than due to dislocation. The quantitative indication of the internal stress existing close to the surface was inferred by comparing the change in hardness from the initial stress free condition. The author commented that VSR can be obtained in controlled conditions.

Kuo and **Cohen** [79]: This work was carried out in Northwestern University, Evanston, USA in 1983. In this work where research was under taken into the effects of fatigue cycling upon both annealed and cold worked low carbon steel AISI 1008 was directed mainly at elucidating changes in microstructural properties by means of X-ray diffractometry. Specimens were of standard fatigue testing geometry, the test section of interest being 62 mm × 6.35 mm × 5.08 mm. Two sets of samples were prepared, one annealed for 1 hour in argon gas at 920 ^{0}C and air cooled, the other having been cold rolled to 50% reduction in thickness in 0.5% increments. All specimens were subjected to mechanical and electropolishing processes in order to prepare their surfaces for X-ray diffraction.

The authors commented that the effect of cyclic loading, until failure occurred, appeared to be to introduce compressive residual stress throughout the thickness of these specimens. This is clearly an incomplete picture of the true state of affairs, since it is impossible for compressive residual stresses to exist without corresponding tensile stresses, required to maintain equilibrium. In view of this observation, residual stress profiles presented for cold worked material must be regarded with some doubt. Nevertheless, the authors observed some small degree of residual stress reduction in cold worked material during both low - and high-cycle fatigue loading of their material. In addition, the internal dislocation density was found to fall slightly during the process.

It is important that proper care is taken in assessing these results; the issue raised earlier concerning residual stress measurement accuracy weakens the evidence presented in this article. Nevertheless, it may be concluded on the basis of this report that significant changes in both the residual stress and microstructure may be initiated by cyclic loading of low carbon steel.

Nakagiri, et. al. [98]: This study was carried out at Kansai University, Osaka, Japan in 1994. In this study Copper and Brass 150 mm × 40 mm × 3 mm specimens were tested, whose elastic limit was considered to be approximately equal to the 0.025 % offset stress (yield stress). The authors mentioned that to improve the accuracy of X-ray diffraction analysis the specimens were annealed in a vacuum for 1 hour then shot-peened to induce residual stress. The detail of this phenomenon is not delivered. The X-ray measurement area was electropolished then the specimens were vibrated. The authors concluded that if the sum of the residual stress and vibrational stress exceeds 0.025 %-offset stress, the excessive part of the residual stress is relieved. Otherwise, no relief of the residual stress can be expected. It was also concluded that for lower applied stresses (1/4 to 1/10 times than elastic limit), the residual stress does not change but dimensional stability occurs.

Eigenmann, et al. [44]: This work was carried out at the Universität Karlsruhe (TH), F. R. G. in 1994. Residual stress relaxation by cyclic deformation of 42CrMo steel was investigated. The samples with a diameter of 5 mm were oil quenched and tempered for two hours at 620 ^{0}C. Compressive surface residual stresses were introduced by shot peening. The samples were subjected to cyclic tensile-compressive loading with triangular load-time functions having a frequency of 5 Hz. Servo-hydraulic testing machines were used to create stress amplitudes σ_a = 400, 500, 600, and 700 MPa. The surface residual stresses in the axial direction were measured by X-ray diffraction after unloading the sample from compressive half cycles. In all cases, most significant reductions of compressive surface macro residual stresses were observed after the first loading cycle. The reason for that reduction was explained as quasi-static plastic deformation. Since the sum of compressive surface residual stresses and loading stresses exceeds the yield strength of the shot peened surface layer

during the compressive half cycle. In this case, the resistance against residual stress relaxation during the first cycle is given by

$$R_{e,surface} \leq \sigma_a + \left|\sigma^{RS}{}_{surface}\right|$$

The further reduction of the residual stress was reported to be proportional to the log *N*, residual stress changes being pronounced with increasing stress σ_a. The reason for the cyclic residual stress relaxation in the case of shot peened materials states are micro plastic cyclic deformations which occurs if

$$R^{cyc}{}_{e,surface} \leq \sigma_a + \left|\sigma^{RS}{}_{surface}\right|.$$

Which is valid with $R^{cyc}{}_{e,surface}$ the materials resistance against micro plastic cyclic deformation in the surface layers. The plastic deformation causing cyclic residual stress relaxation can be looked upon in an integral way as cyclic creep of the material. It can be described by the logarithmic creep law

$$\sigma^{RS}{}_{surface} = A - B\log N$$

where constants A and B can be determined for each stress amplitude from experimental data. In case of σ_a = 400 MPa, after first cycle no further residual stress relaxation is observed with increasing number of cycles *N*. Obviously this stress amplitude is smaller than the materials resistance against cyclic residual stress relaxation $R^{cyc}{}_{surface}$ at the surface. For stress amplitudes σ_a = 600, and 700 MPa, the macro residual stress appears to relax faster in the final stage of the lifetime of the sample just before failure. The reason is cyclic work softening which is accompanied by relaxation of micro residual stresses, represented by the half width value of [211] diffraction profiles. It is shown from the experimental data that with exception of cyclic softening, the micro residual stress remain almost constant during the lifetime of the samples.

Fenghua & Dexin [49]: This work was carried out in Dalian University of Technology, China in 1994. C90 steel oil tubes of specifications 34CrMo4 and 28CrMoTi were used in this investigation. The residual stress was measured using the hole drilling method. To reduce the scatter of the data the measurements and application of treatments were carried out by the same person and the same

instruments. Residual stress was introduced by cold plastic deformation. The first group of specimens were treated with vibration and the second group with artificial ageing. As a result of the vibratory treatment the maximum residual stress was found to have reduced from 346.6 MPa to 155 MPa, a reduction of 55%, and the average stress was reduced from 160 MPa to 60 MPa, a reduction of 60%. On the other hand the artificial ageing showed a reduction from 160 MPa to 99.5 MPa, a reduction of 38.5%. A fatigue test of the specimens was carried out where it was shown that the fatigue life of the vibratory treated specimens was increased. The details of the treatment were not provided.

Walker, et. al. [133]: This work was carried out at the University of Strathclyde in 1995, where the effect of vibration on rectangular mild steel bars (BS970:EN3b) was studied. Residual stress was introduced to the specimen by cold rolling, where they were deformed plastically to obtain a high level of residual stress. VSR treatment was carried out using an electromagnetic shaker, which was controlled by a resonance-seeking phase-locked loop controller. This maintained resonance frequency during vibration and gave an accurate measurement of resonance frequencies (~100 ± 0.001 Hz). A sectioning technique was used to measure the residual stress. The changes in mechanical properties (elastic modulus and internal friction) were monitored by the use of the electronic instrumentation in the vibration controller. A detailed analysis of X-ray diffraction was carried out to obtain the necessary information concerning the internal microstructure and dislocation density within the materials before and after treatment. It was demonstrated that 40 % of peak residual stress was reduced by resonant cyclic loading of cold rolled mild steel. With some evidence the authors concluded that dislocation motion is one of the mechanism of residual stress relieving on a microscopic scale.

Lutes & Sarkani, [89]: This work was carried out at George Washington University, USA in 1996. In this study welded T-joint specimens of 406 mm in length were investigated for fatigue life. Low frequency cyclic load was applied to the specimens. The shape and size of each specimen is shown in Figure 2.4 below.

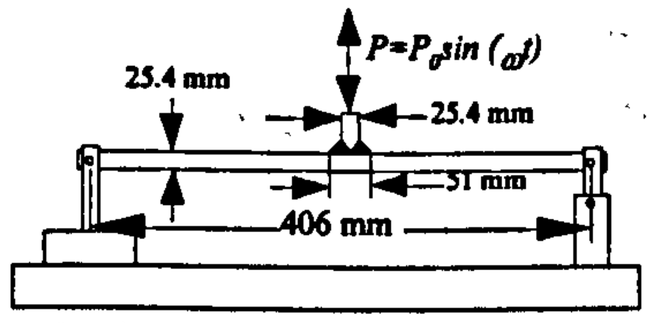

Figure 2.4 – Specimen for fatigue testing

A residual stress model of the specimens was delivered

$$\sigma_{mean} = \sigma_{yield} - \sigma_{\max} + \mu \text{ ; for } \sigma_{max} - \mu < \sigma_{yield}$$

$$\sigma_{mean} = 0 \text{ ; for } \sigma_{max} - \mu > \sigma_{yield}$$

Where σ_{max} = the largest tensile nominal stress applied prior to the current cycle, and μ = Non zero mean of applied cyclic stress.

Two groups of specimens were processed in two different situations. The first group was pre-cycled with high amplitude stress (σ_y) and then the fatigue life of the specimens was tested. For the second group, the specimens were left as welded then the fatigue life was tested. In the fatigue test three different applied stresses were used ($0.4\sigma_y$, $0.8\sigma_y$, and σ_y). Linear regression of log (N) on $\left({}^{S_{eff}}/_{S_{yield}}\right)$ for the result of 16 tests of pre-cycled specimens gave $N = 270000\left({}^{S_{eff}}/_{S_{yield}}\right)^{-4.039}$. Similar constant amplitude test for the as welded specimens gave $N = 166000\left({}^{S_{eff}}/_{S_{yield}}\right)^{-3.300}$. For applied stress $S = \sigma_y$ fatigue life appeared to be the same in both cases but for lower applied stresses was larger in the pre-cycled specimens. The measurement of residual stress was not carried out.

2.2.6 Summary.

Moore [97] found a 76% reduction of residual stress in a specimen, but found that result is non repeatable to other specimens. Fuchs & Mattson [53] did not find any stress reduction using cyclic torsional loading. Its possible cause might be the amount of applied stress was not sufficient to change the value of stress or they were not

measured properly. The work of Pattinson and Dugdale [105] indicates that the phenomenon of VSR may not be attributed to simple plastic flow in accordance with the superposition principle, but rather involves a continuing process. Their work also reveals that low carbon steels are not the only suitable candidates for such treatment, as does that of Dawson [39]. Dawson used cold rolled, hot rolled steel and aluminium and found stress reduction in first 10 cycles with a relatively high applied stress, which indicates superposition of stress caused stress relaxation. Wozney and Crawmer [139] have shown that some degree of residual stress relief may be accomplished even in extremely hard materials. Although not indicative of dramatic changes, the report of Kuo and Cohen [79] claimed that due to fatigue loading, compressive stress was introduced all over the specimens. They also revealed interesting effects upon the internal microstructure of cold worked steel as a result of fatigue loading. Taggert [124] used single copper crystal to obtain only residual stresses due to dislocations, and claimed that VSR can be obtained in a controlled condition. Nakagiri [98] used copper and brass and concluded that when total stress exceeds 0.025% offset stress, stress relaxation occurs. Eigenmann [44] found that stress relieves if the applied stress exceeds a threshold value, and he explained VSR by a superposition of stress theory. Fenghua & Dexin [49] found a stress reduction of 55% for VSR treatment. Walker [133] used a cold rolled mild steel and claimed a 40% reduction of residual stress. Lutes & Sarkani [89] carried out a fatigue test of two types; vibratory treated and non treated specimens, and found that the fatigue life of vibratory treated specimens are much higher than non-treated specimens.

Consensus between the majority of research groups investigating these materials is indicated: it may be concluded that properly controlled VSR treatment of cold worked metal is effective in reducing residual stress.

2.2.7 Heat treated materials

Heat treatment of metals is often implemented in order to improve certain material properties. In many cases this objective is achieved by means of rapid cooling from a high temperature, leaving the material in a meta-stable configuration. It is inherent in

the nature of such processes that uniform cooling rates throughout the body of the metal cannot be maintained, and so residual stresses are created during the treatment. Stresses induced in this manner are essentially similar to those formed during casting or welding, although the properties of the supporting material may be significantly altered by the applied heat treatment.

Bühler and **Pfalzgraf** [25]: Research by Bühler and Pfalzgraf in the early 60's in Germany was directed mainly at the investigation of VSR in cast and welded structures, but included brief reports of work carried out using quenched bars of various cross sections. A combination of static and dynamic axial loading (34 MPa± 3 MPa) had no discernible effect upon residual stress, as determined by strain monitored sectioning techniques, even after 5×10^6 cycles: this absence of change was attributed to the low amplitude of the dynamic loading component. Increasing this factor to ± 23 MPa by means of resonant bending methods caused specimens to suffer fatigue failure after 2.5×10^4 cycles, but had no beneficial effect upon residual stress levels within the material. Finally, the authors introduced a stress concentrating notch into their specimens, increasing the maximum dynamic stress to ±30 MPa: application of 2.5×10^4 cycles resulted in cracking and failure. At this point the compressive surface residual stress had been reduced by 50% from its original level of -160 MPa.

It should be noted that the initial residual stress levels in the material under investigation were not high in comparison with the expected yield strength of a quenched steel: the same is also true of the dynamic loading stresses. In addition to this factor, it might be expected that the brittle nature of the chosen material would engender fatigue failure well before the occurrence of significant stress relief during cyclic loading. Consequently, the author's failure to effect changes in the residual stress pattern except by cycling to destruction is unsurprising. Their conclusion was that significant stress reduction was achieved only at amplitudes in excess of the material's fatigue limit: it was supposed that stress reduction was dependent upon the dynamic stress amplitude, the number of applied cycles, and the magnitude of static stress loading imposed upon the specimen during treatment.

The number of tests performed using quenched material was rather low: this lack of comprehensive data renders the author's conclusions less authoritative than might otherwise have been the case. Despite these reservations, however, this work demonstrates quite conclusively that stress relief may be achieved in quenched materials by the application of appropriate cyclic loading treatments.

Larsson and **Spiegelberg** [81]: This work was carried out in the Swedish Institute for Metal Research, Sweden in 1973. Residual stresses were introduced into cylindrical rods of 0.4% carbon steel by induction hardening, and partially relieved by tempering for 1 hour at 455 K. The authors used a notched specimen geometry, which allowed controlled high amplitude loading to be applied using bending fatigue equipment. Measurement of the residual stress achieved by this method performed by X-ray diffractometry, with a quoted uncertainty of ±50 MPa.

Initial stress levels were extremely high, in accordance with the carbon content of the chosen steel, reaching peak values in the region of -1500 MPa at a depth of 0.5 mm below the specimen surface. Two different loading treatments were applied to the material, each for various numbers of cycles. It was found that fatigue loading at ±1400 MPa was capable of reducing surface residual stresses by almost 75% after 10^4 cycles: correspondingly smaller reductions were achieved by loading at ±1000 MPa. A considerable degree of scatter was present in the data, but the general trend remained clear: stress reduction continued at a decreasing rate throughout the fatigue process, being approximately proportional to the logarithm of the number of applied cycles.

Stress relief was attributed by the authors to a general yield mechanism, although no information was presented concerning the yield strength or proportional limit of the chosen material. Their observation of continued change throughout the duration of the process must cast doubt upon any postulate involving simple plastic flow behaviour, although gradual softening of the material during cycling may be supposed to be responsible for this phenomenon. Several anomalous observations were reported: the authors attempted to explain these as the result of premature cracking

during the fatigue process, resulting in lower effective applied dynamic stresses. The implications of this theory are rather important, since it is precisely those materials, which are most vulnerable to cracking under load which have the greatest need for stress relief treatments. If proven to be correct, this conjecture may well preclude the use of VSR in the treatment of hardened high carbon steels.

2.2.8 Summary.

All of the authors contributing to the literature survey relating to the VSR treatment of thermally-induced residual stress have concluded that some improvement is possible. Of the two available publications, the least encouraging is that of Bühler and Pfalzgraf [25], in which it was stated that significant fatigue damage must occur as a necessary consequence of any effective stress reduction process. The work of Larsson and Spiegelberg [81] cannot be taken as evidence in contradiction with this view, although no estimate of the effective fatigue limit of their material was made. It appears, therefore, that simple cyclic loading of this class of material is a proven technique for residual stress reduction, but that the possibility of fatigue damage should not be neglected in assessing the possible benefits of the process.

2.2.9 Externally Imposed Stress

Although true residual stress arises internally within the affected material, it is possible to simulate such stresses by the imposition of external loading. In such cases, the internal stress pattern is due to forces imposed by external members upon the stressed component. Provided that the external loading system is rigid in comparison with the stressed part, the behaviour of the stressed material closely models a situation in which true residual stresses are present. Research concerning the response of such systems to cyclic loading has been reported by two authors.

Volkov & Orzhekauskas, [131]: This work was carried out in 1988, to investigate the effect of vibration treatment on titanium structures (VT6). The residual stress was measured using X-ray diffraction methods. Special samples of constant and variable cross sections were prepared from the alloy to apply a constant tensile/compressive stress over the specimens upper and lower surfaces. The frequency of vibration was

not mentioned. The applied vibratory stress to the specimen was 60% of the material yield stress, which caused an average 40% reduction in residual stress. However, for the specimens with high levels of initial stresses the effect of stress relief reached 60-70%. It was also reported that most of the stress was relieved during the first 1000 – 2000 cycles.

Vlasenko & Senyukov [130]: This work was carried out at the Academy of Science of the Uhrainian SSR, Kiev in 1990. Experiments were carried out on chromium-nickel steel cylindrical specimens with a diameter of 6 mm and a working portion length of 50 mm. For the purpose of the elimination of residual stresses, which might occur on the surface of specimens during their preparation, they were held for 30 days before finish machining. The surface of the working portion of the specimen was finish-machined with a depth of cut of ~0.1 mm and then polished with emery paper. The mechanical properties of the material were determined by tensile tests. The properties at the room temperature were σ_u = 1002 MPa, σ_p = 590 MPa, and $\sigma_{0.2}$ = 682 MPa and at 300 ^{0} C the properties were σ_u = 875 MPa, σ_p = 650 MPa, and $\sigma_{0.2}$ = 705 MPa. The specimens were axially stressed with a static load (close to the yield stress) to imitate the residual stress, then a vibratory axial stress was applied. A multifactorial experiment was designed to obtain a mathematical model reflecting the contribution of each of the factors. In the described experiment the factors were the amplitude of the cyclic load, the frequency, the maximum cyclic stress and the temperature. Considering the experimental results it was reported that the frequency had no effect on stress relief. The temperature had a significant influence on the reduction of stress due to thermally activated dislocation motion but had practically no influence on the accumulated deformation. And it was also concluded that in the static or dynamic condition each type of loading was capable of reducing the same amount of residual stress, so one another could replace them.

2.2.10 Summary

Although only two publications are available concerning the use of VSR to reduce elastically imposed stresses, it is nonetheless clear that some degree of improvement in

the material is possible. Volkov & Orzhekauskas [131] used a titanium structure in the VSR treatment and found 60-70% residual stress relief. Vlasenko & Senyukov [130] used chromium-nickel cylindrical steel, and used axial vibration. The conclusion of their work was that either static or dynamic loading both was capable of reducing the same amount of residual stress.

2.3 Conclusion

One factor which emerges predominantly from the preceding discussion is the tendency of VSR treatment to be effective only at high dynamic stress amplitudes. This trend is most pronounced in the case of hard materials (heat-treated and cast metals), but is nevertheless apparent even in the case of welded structures - fabricated from ductile mild steel.

The application of resonant vibration to cast materials is likely to induce cracking after a relatively low number of cycles if the amplitude of vibration is high: to avoid fatigue failure the applied stress must be kept lower than the fatigue limit. Similarly, materials hardened by heat treatment exhibit a tendency towards cracking during cyclic loading at amplitudes sufficient to induce stress reduction. In common with cast metals subjected to purely internal residual stress, these components proved susceptible to cracking during treatment. Results obtained from cast iron specimen were not very encouraging: two Japanese publications claimed success using a very high applied stress, which might be damaging to the structure considering crack formation and propagation. The documented benefit from most of the researchers was that the process improved stability during subsequent service. This was attributed to accelerated (strain) ageing of components, that were significantly distorted during the course of the treatment. The work of Balasingh indicates that the response of cast material to the VSR process depends strongly upon its chemical composition, although the nature of this relationship was not investigated.

The majority of work conducted using vibration to reduce residual stress was on welded joints. Most of the investigations using welded joints have yielded positive findings and have reported on the reduction of residual stress levels or improved dimensional stability as a result of vibratory treatment. Some of them found an increase in residual stress or no change due to the treatment. The cause of these findings is discussed in section (2.2.4). In addition to stress reduction, improved mechanical properties of the weld was found due to the application of vibration during welding.

Those reports concerning the application of cyclic loading to plastically deformed materials contain some of the most detailed information yet available. Despite statements by commercial VSR operators that plastically deformed materials are less susceptible to the process than those exhibiting heat induced residual stress, every scientific research effort has achieved positive results. A common observation is that stress relief depends critically upon achieving sufficiently high cyclic strain amplitudes during treatment, and that changes continue to occur throughout many cycles. Bouhelier found a significant reduction of residual stress by applying very little dynamic stress. The latter two factors strongly suggest that VSR should not be modelled as simply a process of plastic flow in response to superimposed dynamic and residual stresses.

Chapter 3

Techniques Used in This Work

Techniques Used in This Work

To carry out this study, three principal techniques were used. These were:

1. Modal Analysis
2. Dynamic Stress Measurement - using strain gauging
3. Residual Stress Measurement - using X-ray diffraction

3.1 Modal Analysis

Modal Analysis is a structural study of vibration which verifies the theoretical models and predictions. It is a test where the structure or component is vibrated with a known excitation - often out of its normal service environment. It is generally made under closely controlled conditions which yields more accurate and detailed information. This type of test, including both data acquisition and its subsequent analysis, is called Modal Analysis.

The name Modal Analysis is relatively new but the principals of modal testing were laid down many years ago. These have evolved through various phases with descriptions such as *'Resonance Testing'* and *'Mechanical Impedance Methods'* being used to describe the general area of activity. At its primitive stage it was very time consuming so it was not so interesting in practical application. There was a rapid advancement in measurement and analysis technique in the 1960's which paved the way for more precise measurements and thus more powerful applications. However, by 1970 there has been major advances in transducers, electronics and digital analysers and the current techniques of Modal Analysis were established.

Modal Analysis can be divided into theoretical and experimental analysis. In the theoretical analysis the mass, damping and stiffness of the structure are known whereas the natural frequencies, the mode shapes and finally frequency response function are unknown parameters. In the experimental Modal Analysis a mathematical model is sought which describes how the test structure is vibrating. The

parameters of interest are natural frequencies, together with the mass, damping, stiffness and mode shapes associated with each mode of vibration.

In Modal Analysis, experiments are carried out on the test structure by vibrating it with a known excitation to measure its response. The response should be measured at enough points on the structure to ensure that all modes will display their resonant characteristics in the response curve of at least one of the points. The response i.e. displacements, velocity and/or acceleration is measured at the same time - at several points of the structure. From the data generated one can easily calculate the frequency response function (FRF), which is a plot of the response as a function of the frequency. A typical FRF plot is shown below (inertance vs. frequency).

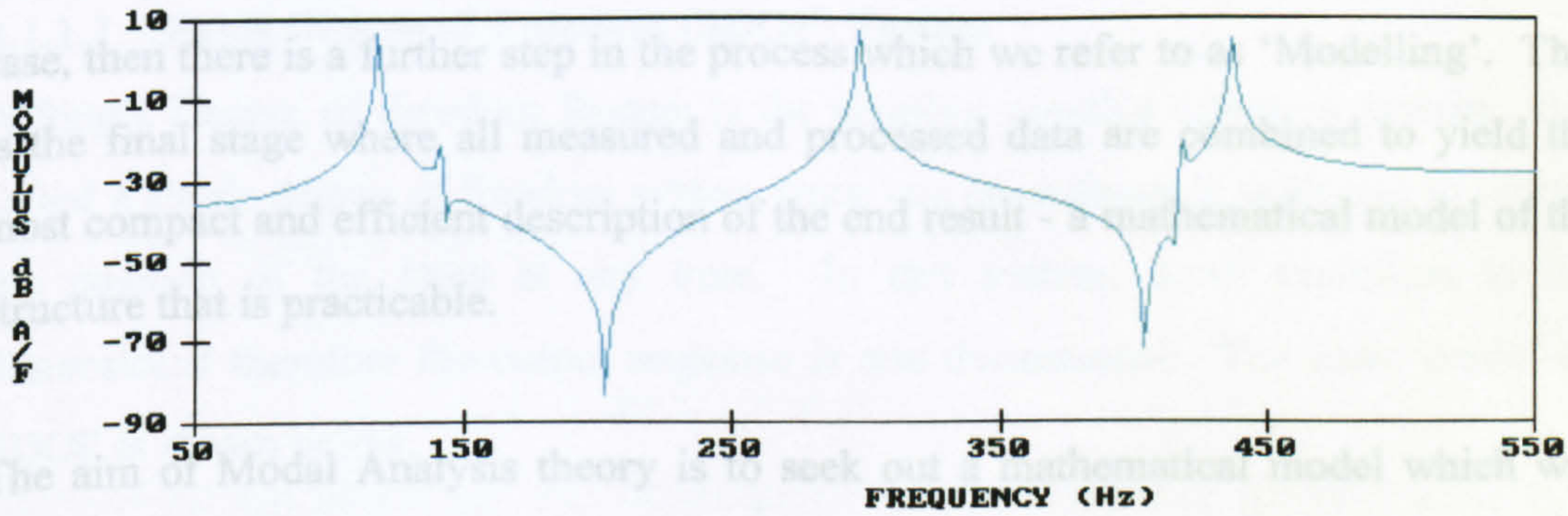

Figure 3.1 - A typical FRF plot

The frequency response function may be defined as the Fourier transform of output divided by the Fourier transform of input (force). So,

$$\frac{X(\omega)}{f(\omega)} = \text{Receptance}$$

$$\frac{\dot{X}(\omega)}{f(\omega)} = \text{Mobility}$$

$$\frac{\ddot{X}(\omega)}{f(\omega)} = \text{Inertance}$$

Where $X(\omega)$ = Fourier transform of displacement

$\dot{X}(\omega)$ = Fourier transform of velocity

$\ddot{X}(\omega)$ = Fourier transform of acceleration

$f(\omega)$ = Fourier transform of force input

In the analysis stage, the measured data (invariably, frequency response function or mobilities) are subjected to a range of curve fitting procedures in an attempt to find the mathematical model which provides the closest description of the actually observed behaviour. There are many approaches or algorithms for this phase and, as is usually the case, no single one is ideal for all problems. Thus, an appreciation of the alternatives is a necessary requirement for the experimenter wishing to make optimum use of his time and resources.

Generally, an analysis is conducted on each measured curve individually. If this is the case, then there is a further step in the process which we refer to as 'Modelling'. This is the final stage where all measured and processed data are combined to yield the most compact and efficient description of the end result - a mathematical model of the structure that is practicable.

The aim of Modal Analysis theory is to seek out a mathematical model which will explain the closest description of the observed behaviour allowing the modal parameters (natural frequency, damping factor and modal vector) to be calculated more accurately than directly from the transfer function. A practical Modal Analysis is presented in Section 5.8.

In the theoretical analysis there needs to be three phases. In the first phase a knowledge is required of the structures physical characteristics usually in terms of mass, stiffness and damping properties and this is referred to as the *SPATIAL MODEL*. The second phase leads to a description of the structure as a set of vibration modes: the *MODAL MODEL*. This model is defined as a set of natural frequencies with corresponding vibration mode shapes and modal damping factors. The third phase is generally that in which we have the greatest interest, namely the analysis of exactly how the structure will vibrate under given excitation condition - especially the

amplitudes. Clearly this will depend not only upon the structures inherent properties but also on the nature and magnitude of the imposed excitation, hence there will be innumerable solutions. However, it is convenient to present an analysis of the structure response to a 'standard' excitation and to describe this as the *RESPONSE MODEL.*

This analysis will focus on these three stages and types of model – *SPATIAL, MODAL* and *RESPONSE* - and it is essential to understand fully their interdependence as it upon this characteristic that the principles of modal testing are founded.

3.1.1 Dynamic Theory

3.1.1.1 Single Degree of Freedom (SDOF) System

A Single Degree of Freedom System is the simplest possible vibratory system. It is called a single degree of freedom system since one co-ordinate is sufficient to specify the position of the mass at any time. In this system, input excitation is one dimensional therefore the output response is one dimensional. The basic model for SDOF is shown below.

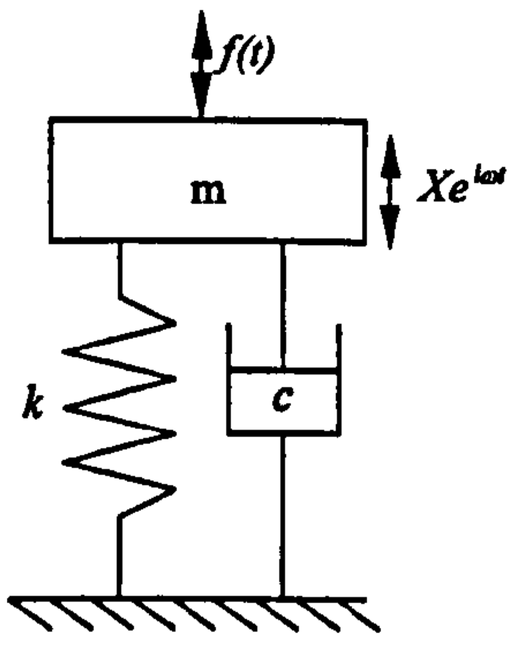

Figure 3.2 - Model - a single degree of freedom system.

Where *f(t)* and *x(t)* are general time varying force and displacement response quantities. For the SDOF system a free vibration analysis yields its natural frequency and damping factor while a particular type of forced response analysis, assuming a harmonic excitation, leads to the definition of the frequency response function - such as mobility - the ratio of velocity response to force input.

$$x_p(t) = \frac{f}{\left[\left(k - m\omega^2\right)^2 + \left(c\omega\right)^2\right]^{\frac{1}{2}}} e^{i(\omega t - \varphi)} \qquad 3.5$$

3.1.1.1.2 Hysteretic (Structural) Damping (SDOF)

A large variety of materials, when subjected to cyclic stress exhibit a stress/strain relationship which is characterised by a hysteresis loop.

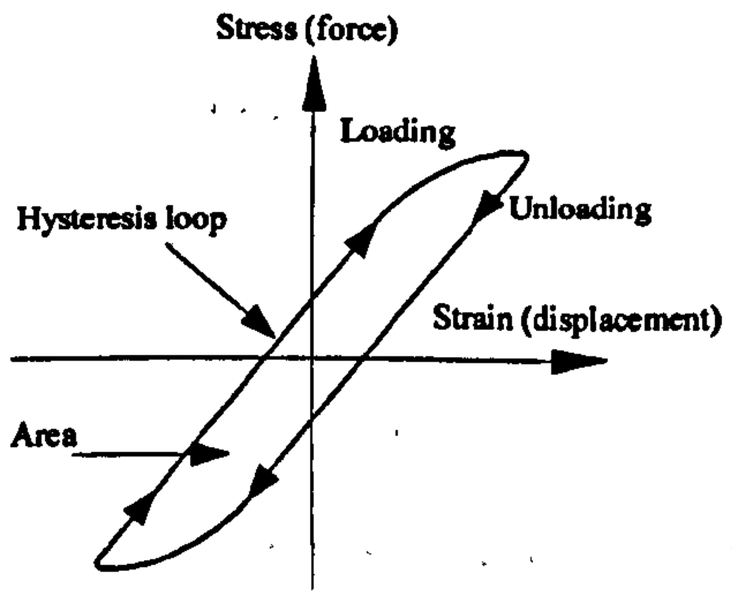

Figure 3.4 - Hysteresis loop for elastic materials

The energy dissipated per cycle due to internal friction in the materials is proportional to the area within the hysteresis loop. It has been found that the internal friction is independent of the rate of strain (i.e. independent of frequency) and over a significant frequency range is proportional to the displacement. Thus the damping force is proportional to the elastic force but, since energy is dissipated, it must be in phase with the velocity. Thus for simple harmonic motion the damping force is given by

$$hk\frac{\dot{x}}{\omega} = ihkx$$

where h is called the structural damping factor.

Then the equation of motion becomes

$$m\ddot{x} + hk\frac{\dot{x}}{\omega} + kx = fe^{i\omega t}$$

or $$m\ddot{x} + ihkx + kx = fe^{i\omega t}$$

or $$-m\omega^2 e^{i\omega t}X + ihkXe^{i\omega t} + kXe^{i\omega t} = fe^{i\omega t}$$

or $$Xk\left\{-\frac{m}{k}\omega^2 + 1 + i\frac{h}{k}\right\} = f$$

$$\text{or} \qquad \frac{X}{f} = \frac{1}{k\left\{1 - \frac{\omega^2}{\omega_n{}^2} + i\eta\right\}} \qquad 3.6$$

where η is the structural damping loss factor.

and the phase angle $\varphi = \tan^{-1}\left[\frac{\eta}{\left(1-\omega^2/\omega_n{}^2\right)}\right]$

1. The amplitude ratio $\frac{Xk}{f}$ attains its maximum value of $\frac{f}{k\eta}$ at the resonance frequency ($\omega = \omega_n$) in the case of hysteresis damping, which occurs at a frequency below the resonance ($\omega < \omega_n$) in the case of viscous damping.

2. The phase angle φ has a value of $\tan^{-1}\eta$ at $\omega = 0$ in the case of hysteresis damping, while it has a value of zero at $\omega = 0$ in the case of viscous damping. This indicates that the response can never be in phase with the forcing function in the case of hysteresis damping.

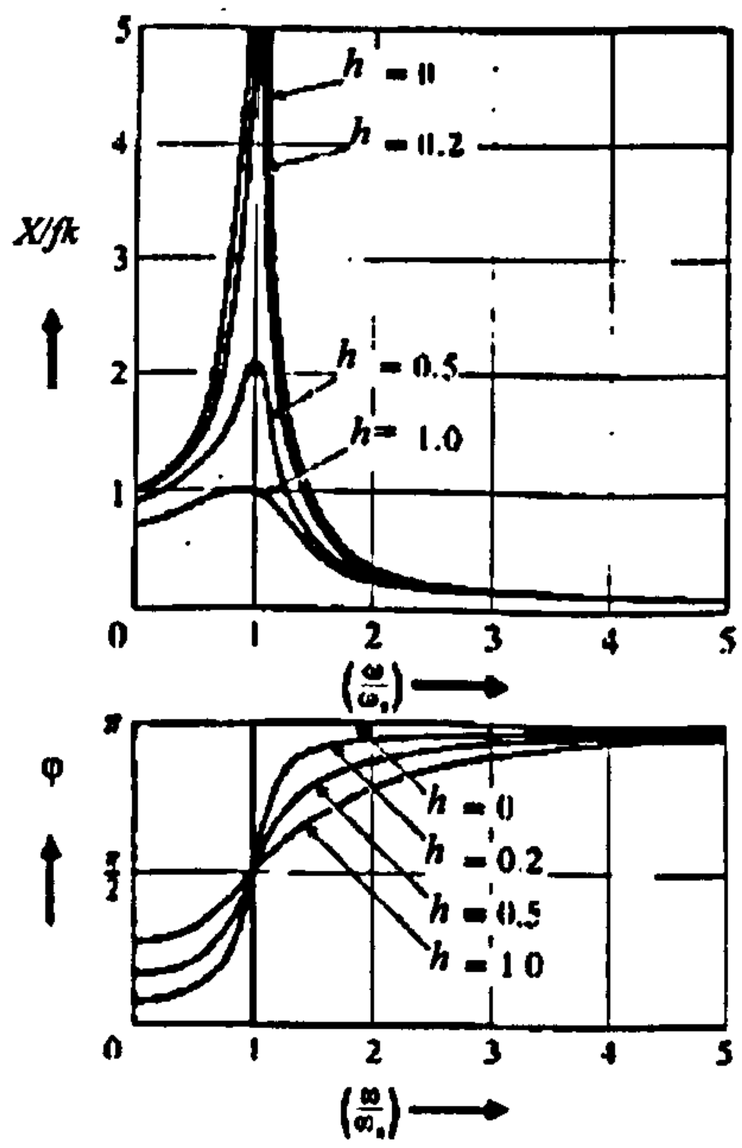

Figure 3.5 - Comparison of different values of structural damping factor *h*.

3.1.1.1.3 Frequency Response Function of SDOF

The receptance frequency response function (FRF) $\alpha(\omega)$ is the ratio between a harmonic displacement response, and the harmonic force. From Equation (3.3), the FRF can be found.

$$\alpha(\omega) = \frac{X}{f} = \frac{1}{\left(k - m\omega^2\right) + ic\omega} \qquad 3.7$$

Which is now complex, containing magnitude and phase information.

$$\text{or} \qquad \alpha(\omega) = \frac{1}{m\left\{\left(\frac{k}{m} - \omega^2\right) + i\frac{c\omega}{m}\right\}}$$

where $\omega_n^2 = \frac{k}{m}$

The damping part $\frac{c\omega}{m}$ may be written in different ways depending on the type of damping.

The mobility frequency response function can be represented as the ratio of velocity, $\dot{x}(t)$ and the input force, i.e.

$$\text{Mobility} = \frac{\dot{x}(t)}{f}$$

Similarly the inertance can be defined as the ratio of acceleration frequency response function and harmonic force, i.e.

$$\text{Inertance} = \frac{\ddot{x}(t)}{f}$$

For a single degree of freedom, the frequency response function (FRF) is plotted on a x-y graph, as FRF vs. Frequency. A typical FRF plot is shown below.

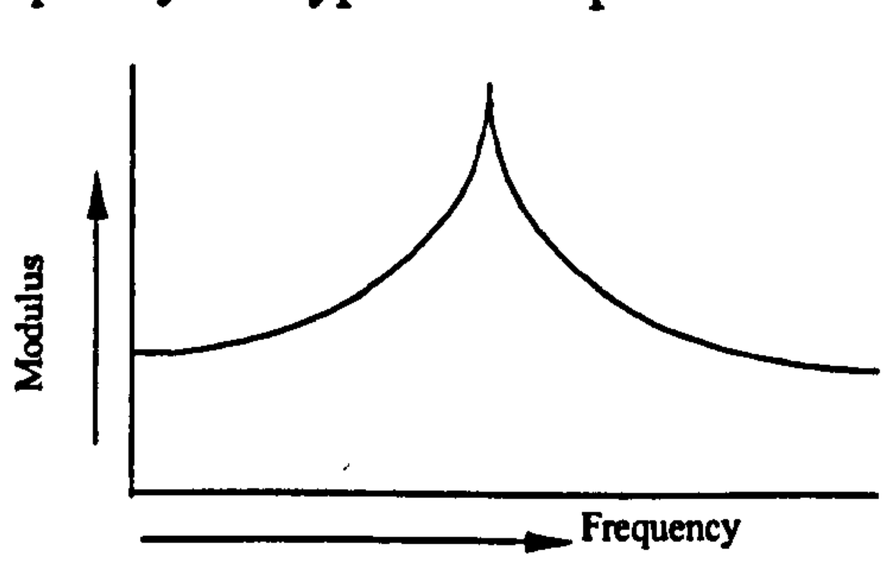

Figure 3.6 - A typical plot of FRF

The effect of damping on the FRF curve is very important. For light damping (typically less than 1%) the mobility FRF plots exhibit a degree of symmetry about a vertical line passing through the resonance frequency. The amplitude of the resonance frequency varies with damping i.e. if the damping is high, the resonance amplitude is low and if damping is low, the resonance amplitude is high.

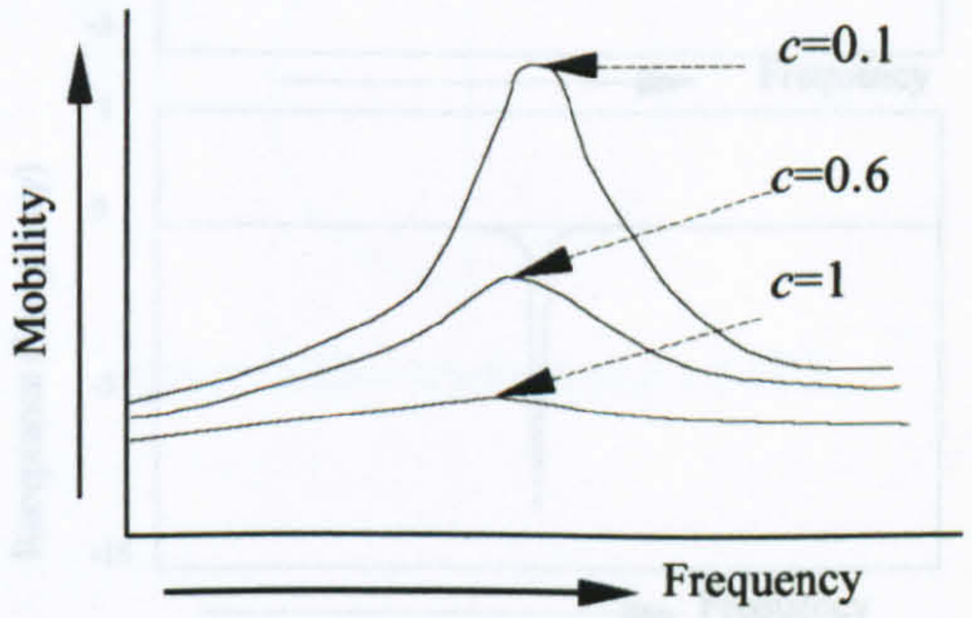

Figure 3.7 - Effect of damping on FRF curve

Since almost all the frequency response functions are complex quantities, they cannot be fully displayed on a standard x-y graph. So, there are some options used in practice.

(I) Modulus of FRF vs. Frequency and Phase vs. Frequency.

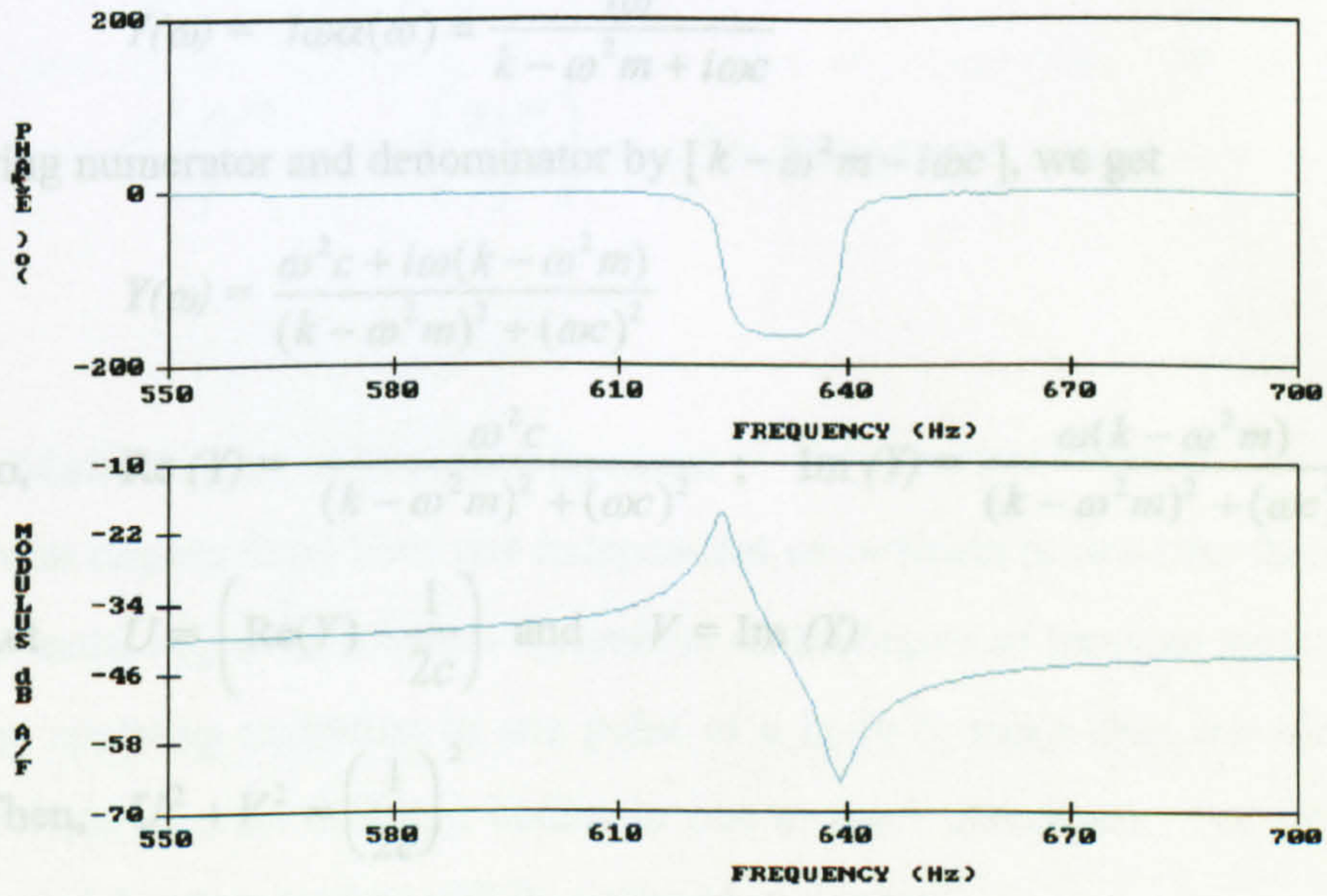

Figure 3.8 - A typical plot of modulus vs. frequency and Phase vs. Frequency

(ii) Real part vs. Frequency

Imaginary part vs. Frequency.

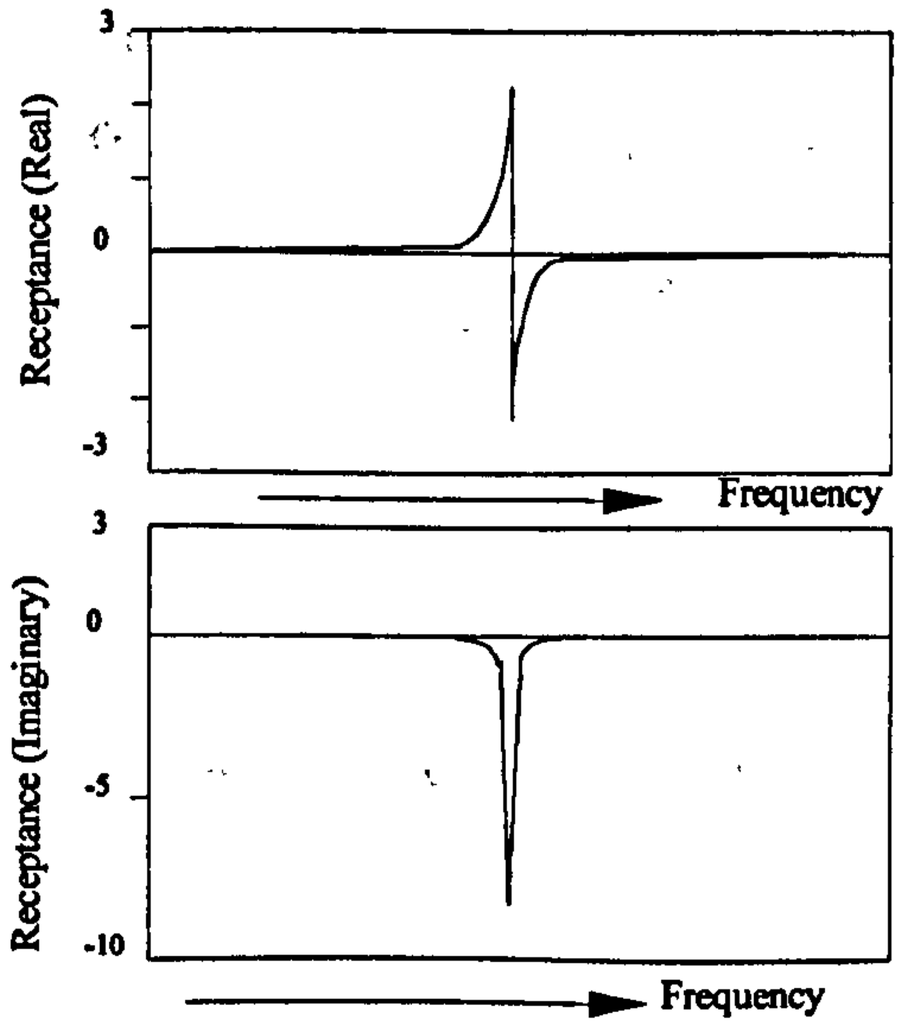

Figure 3.9 - A typical plot of Real part vs. frequency and Imaginary part vs. frequency

(iii) Real part vs. Imaginary parts (Nyquist plot)

A Nyquist plot is given below.

Nyquist Plot

Multiplying Equation (3.7) by $i\omega$, we get

$$Y(\omega) = i\omega\alpha(\omega) = \frac{i\omega}{k - \omega^2 m + i\omega c}$$

Multiplying numerator and denominator by $[k - \omega^2 m - i\omega c]$, we get

$$Y(\omega) = \frac{\omega^2 c + i\omega(k - \omega^2 m)}{(k - \omega^2 m)^2 + (\omega c)^2}$$

so, $\text{Re}\,(Y) = \dfrac{\omega^2 c}{(k - \omega^2 m)^2 + (\omega c)^2}$; $\text{Im}\,(Y) = \dfrac{\omega(k - \omega^2 m)}{(k - \omega^2 m)^2 + (\omega c)^2}$

Let $U = \left(\text{Re}(Y) - \dfrac{1}{2c}\right)$ and $V = \text{Im}\,(Y)$

Then, $U^2 + V^2 = \left(\dfrac{1}{2c}\right)^2$

A plot of *Re (Y(ω))* vs. *Im (Y(ω))* for $\omega = 0$ to ∞ will trace out a circle of radius $1/2c$ and with its centre at ($Re = 1/2c$, $Im = 0$), which is called Nyquist plot. In the Nyquist plot, one portion of information (frequency) is missing, which must be added by identifying the values of frequency corresponding to particular points on the curve.

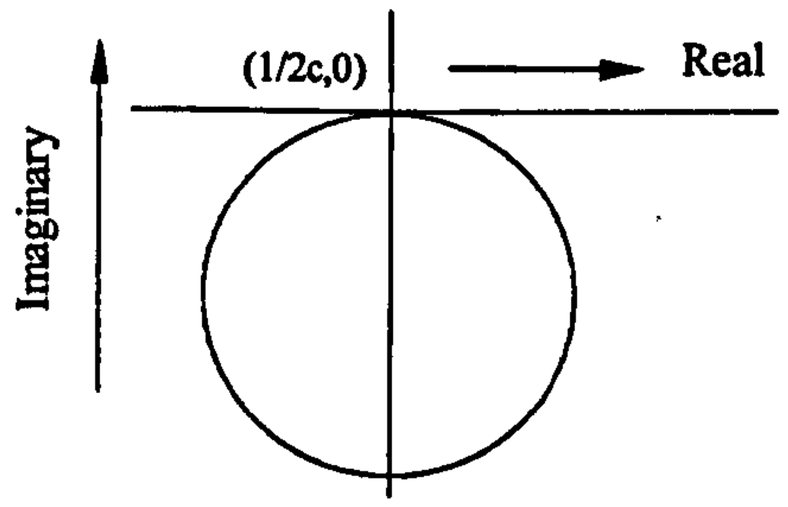

Figure 3.10 - Nyquist plot of FRF

3.1.1.1.4 Relation Between Receptance, Mobility and Inertance

If we consider a sinusoidal vibration (i.e. $x(t) = Xe^{i\omega t}$), it is possible to convert the FRF between receptance, mobility and inertance.

Displacement = $Xe^{i\omega t}$

Velocity = $i\omega Xe^{i\omega t}$

Acceleration = $i^2\omega^2 Xe^{i\omega t} = -\omega^2 Xe^{i\omega t}$

$$\text{Mobility} = \frac{i\omega Xe^{\omega t}}{f} = i\omega\left(\frac{Xe^{i\omega t}}{f}\right) = i\omega \times \text{Receptance.} \qquad 3.8$$

$$\text{Inertance} = -\frac{\omega^2 Xe^{i\omega t}}{f} = -\omega^2\left(\frac{Xe^{i\omega t}}{f}\right) = -\omega^2 \times \text{Receptance.} \qquad 3.9$$

3.1.1.2. Multi-Degree of Freedom Systems

Systems that require more than one independent co-ordinate to describe their motions are called multi-degree of freedom system. A multi-degree of freedom system may be created by applying excitation in one point of a body in more than one direction or applying excitations on different bodies in one or more directions. For simplicity a two degree of freedom system will be analysed in this text.

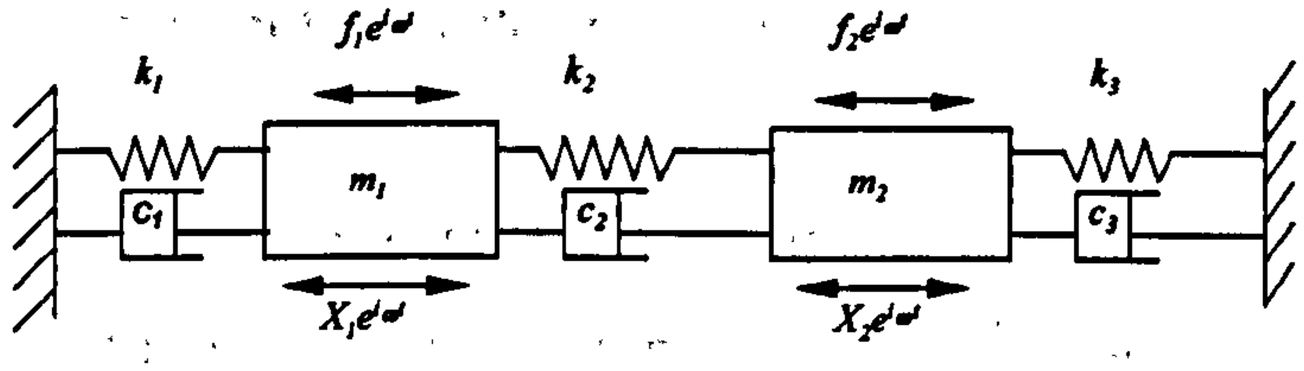

Figure 3.11 - Multi-degree of freedom system

The equation of motion of the two-degree of freedom system with damping and excitation is given below

$$\begin{bmatrix} m_1 & 0 \\ 0 & m_2 \end{bmatrix}\begin{Bmatrix} \ddot{x}_1 \\ \ddot{x}_2 \end{Bmatrix} + \begin{bmatrix} c_1+c_2 & -c_2 \\ -c_2 & c_2+c_3 \end{bmatrix}\begin{Bmatrix} \dot{x}_1 \\ \dot{x}_2 \end{Bmatrix} + \begin{bmatrix} k_1+k_2 & -k_2 \\ -k_2 & k_2+k_3 \end{bmatrix}\begin{Bmatrix} x_1 \\ x_2 \end{Bmatrix} = \begin{bmatrix} f_1 \\ f_2 \end{bmatrix} e^{i\omega t} \qquad 3.10$$

In short form they can be written as

$$[m]\{\ddot{x}\} + [c]\{\dot{x}\} + [k]\{x\} = [f]e^{i\omega t} \qquad 3.11$$

The main obstacle in solving these equations is the coupling between equations, but the coupling depends on the choice of co-ordinates. If the system of equations could be uncoupled, so that diagonal mass, stiffness matrices are obtained then each equation would be similar to that of single degree of freedom system, and could be solved independent of each other. In Modal Analysis the system response is derived by transforming the equations of motion into an independent set of equations. Choosing transformation matrix $[\varphi]$, the x co-ordinates are transformed to η by the equation

$$\{x\} = [\varphi]\{\eta\} \qquad 3.12$$

where the columns of matrix $[\varphi]$ are the mode shapes. Substituting this equation in Equation (3.11), we obtain

$$[m][\varphi]\{\ddot{\eta}\} + [c][\varphi]\{\dot{\eta}\} + [k][\varphi]\{\eta\} = \{f\}e^{i\omega t}$$

Pre-multiplying the above equation by the transpose of the modal matrix, i.e. $[\varphi]^T$, we obtain

$$[\varphi]^T[m][\varphi]\{\ddot{\eta}\} + [\varphi]^T[c][\varphi]\{\dot{\eta}\} + [\varphi]^T[k][\varphi]\{\eta\} = [\varphi]^T\{f\}e^{i\omega t} \qquad 3.13$$

Two assumptions are taken for granted before attempting solution of these equations. Firstly the type of damping is viscous, and secondly the distribution of damping is proportional. By proportional damping it is implied that the damping matrix [*c*] is proportional to the stiffness matrix or the mass matrix - or to some linear combination of these two matrices. Mathematically it means that

$$\text{either} \qquad [c] = \alpha[m]$$

$$\text{or} \qquad [c] = \beta[k]$$

$$\text{or} \qquad [c] = \alpha[m] + \beta[k] \qquad 3.14$$

Where α and β are constants.

Considering Equation (3.14) i.e.

$$[c] = \alpha[m] + \beta[k]$$

$$\text{so,} \qquad [\varphi]^T[c][\varphi] = [\varphi]^T\alpha[m][\varphi] + [\varphi]^T\beta[k][\varphi]$$

$$[\varphi]^T[c][\varphi] = \alpha[M] + \beta[K]$$

$$\text{i.e.} \qquad [C] = \alpha[M] + \beta[K] \qquad 3.15$$

where $[M]$, $[C]$ and $[K]$ are diagonal matrices.

So, from Equations (3.13) and (3.15), we obtain

$$[M]\{\ddot{\eta}\} + [C]\{\dot{\eta}\} + [K]\{\eta\} = [\varphi]^T\{f\}e^{i\omega t}$$

The above equation represents an uncoupled set of equations for damped forced single degree of freedom. The i^{th} equation is

$$M_i\ddot{\eta} + C_i\dot{\eta} + K_i\eta = [\varphi_i]f_ie^{i\omega t} = f_ie^{i\omega t} \qquad 3.16$$

which represents the equation of motion of a system shown in Figure 3.12 below.

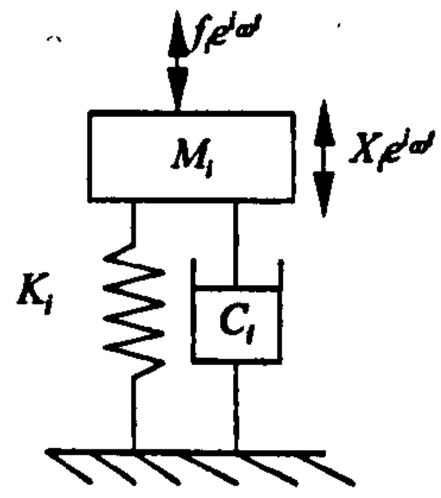

Figure 3.12 - Multi-degree of freedom system equivalent to SDOF system.

3.1.1.2.1 Hysteretic (Structural) Damping (MDOF)

The damping force is proportional to the elastic force and is in phase with the velocity. For simple harmonic motion (SHM) the damping force is given by $hk\frac{\dot{x}}{\omega}$. Thus for the multi degree of freedom, the equation of motion is given by

$$[m][\ddot{x}] + ih[k]\{\dot{x}\} + [k]\{x\} = \{f\}e^{i\omega t}$$

Changing to principal co-ordinates we obtain

$$[M]\{\ddot{\eta}\} + ih[K]\{\dot{\eta}\} + [K]\{\eta\} = [\varphi_i]\{f\}e^{i\omega t}$$

Thus the equations above are uncoupled in that they are very similar to the single degree of freedom system of equations, hence each equation can be solved independently. In general form the equation can be written as

$$M_i\ddot{\eta}_i + ihK_i\dot{\eta}_i + K_i\eta_i = f_i e^{i\omega t} \qquad 3.17$$

The solution of this equation is similar to the solutions of single degree of freedom systems.

3.1.1.2.2 Multi-Degree of Freedom FRF

In multi-degree of freedom systems the FRF curve is obtained from the summation of all the individual curves. The exact shape of the curve is not quite so easy to deduce, because some sections of the curve are actually positive in sign and some are negative. But there is no indication of this on the logarithmic plot which only shows the modulus. There is a fundamental rule which has great value: if two consecutive modes have the same sign for the modal constants, then there will be an anti-resonance at some frequency between the natural frequencies of those two modes. If

they have the opposite signs, there will not be anti-resonance but just minimum amplitude.

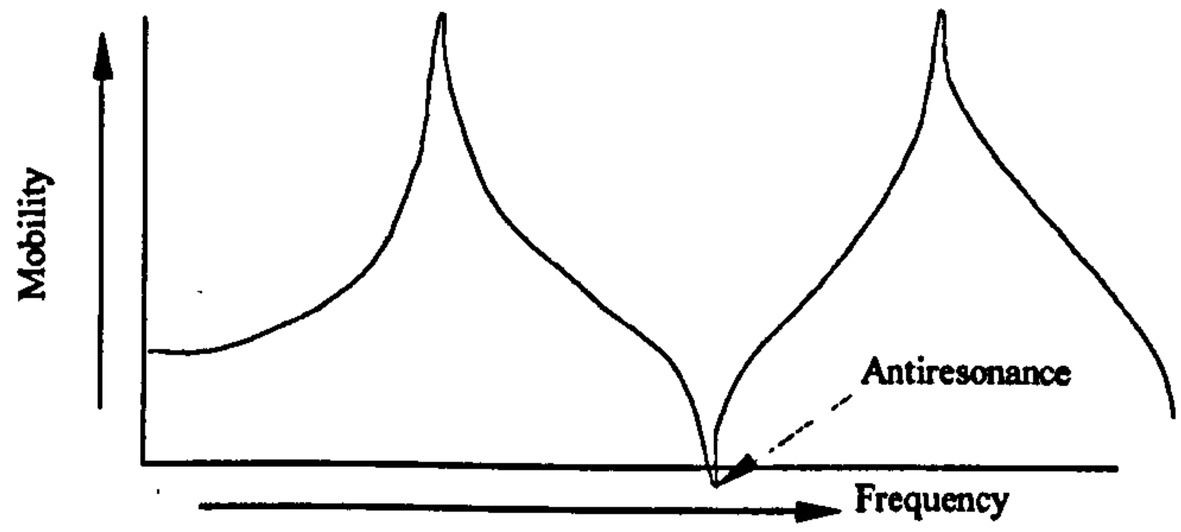

Figure 3.13 - Antiresonance created by same sign of FRF

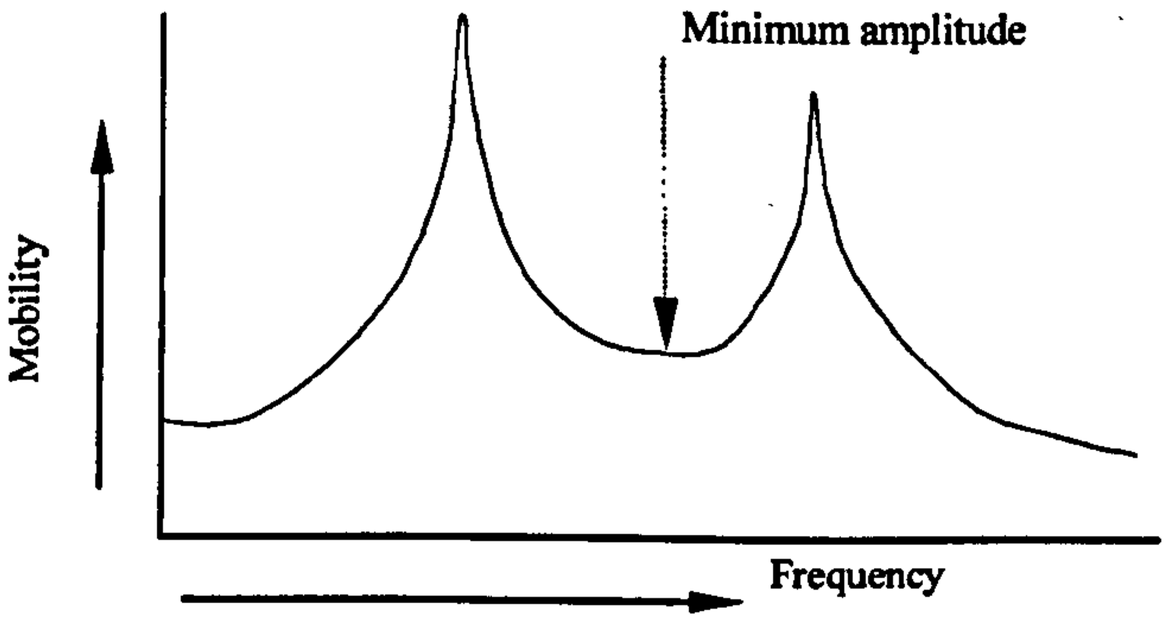

Figure 3.14 - Minimum value of amplitude created by opposite sign of FRF

In a similar way to the Undamped Multi-Degree of Freedom system, the FRF curve can be obtained. Due to damping, the resonance and anti-resonance region will be blunted, and the phase angle (not shown) will change from 0 or 180 to elsewhere depending on the degree of damping.

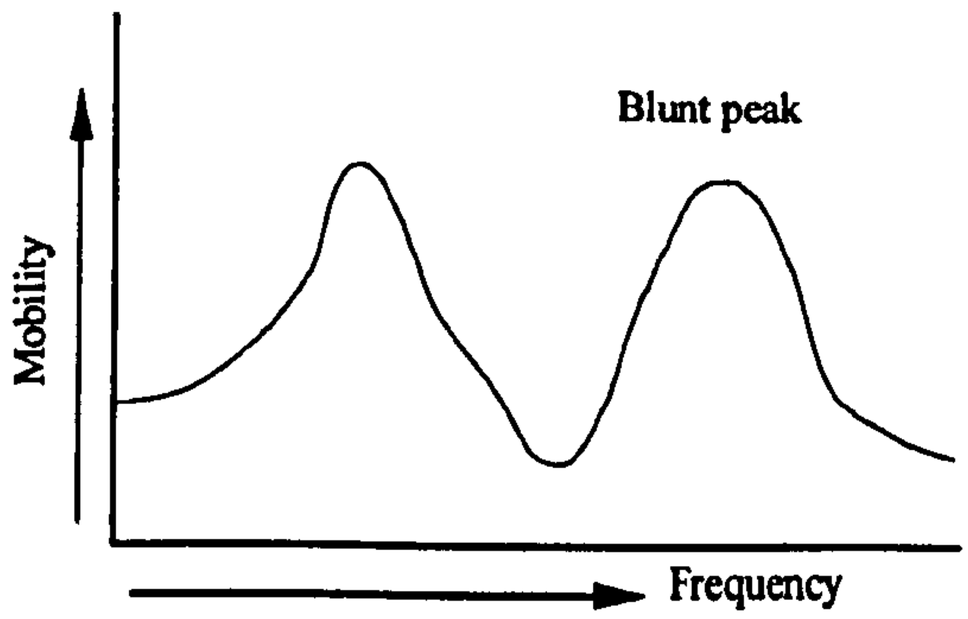

Figure 3.15 - FRF of damped MDOF system.

In similar way to the SDOF system a Nyquist plot can be plotted for both types of MDOF systems, in both cases exact circles can be formed.

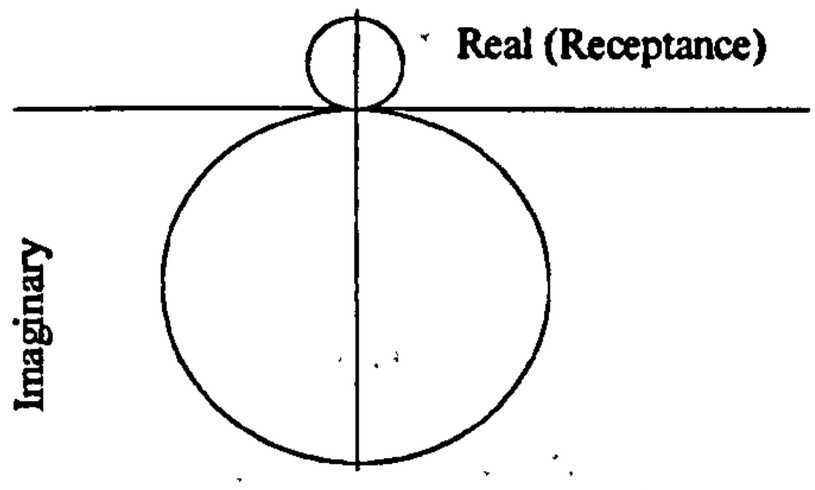

Figure 3.16 - Nyquist plot of MDOF system.

3.1.2 Measurement Method

The measurement methods for Modal Analysis are divided and developed to make direct measurements of the various mobility properties of the structure. For the structure one directional excitation was used. Essentially, there are a number of aspects of measures and measurement processes, which demand particular attention in order to ensure the acquisition of the high quality data, which are required for the next stage - data analysis.

1 Supporting the structure
2 Selecting force input point
3 Selecting force input clamp
4 Selecting proper size of accelerometer
5 Excitation method
6 Conditioning amplifier
7 Analyser
8 Controlling software

3.1.2.1 Supporting The Structure

For a free-free vibration, the structure should be supported by low stiffness springs, which needs some special arrangements for holding and fixing the structure against the springs. A very simplified form of supporting the structure is by using some highly flexible thin elastic bands or ropes instead of springs. If the supporting elastics are highly flexible, and easily extended then the positions of the supports become independent of natural frequency and mode shapes. If elastic ropes are used which are relatively thick then the FRF curves become damped and this will affect the natural

frequency. The detailed analysis of supporting points is shown in Section 5.8.3.1 and 5.8.3.4.

3.1.2.2 Selecting The Force Input Point

To obtain the correct mode shapes, the force input point is very important. This aspect depends on the size and shape of the structure. It has been found that positioning the force input point on or near the maximum deflection point gives better mode shapes. The force input point on a stationary point does not give any reasonable mode shapes. The detailed analysis is shown in Section 5.8.3.6.

3.1.2.3 Selecting Force Input Clamp

Usually the accelerometers are positioned on the measurement points of the structure. The accelerometer positions do not affect natural frequencies if the force input clamp is properly tightened against the structure. But it is very difficult because over tightened clamps make the structure rigid which affects the natural frequencies and mode shapes. In the same way under-tightened clamps cause different natural frequencies of the structure and the force input point/clamp. A detailed study of accelerometer position is shown in Section 5.8.3.2.

3.1.2.4 Selecting Accelerometer Size

The selection of the size of the accelerometer is very important in determining the exact natural frequency of the structure, because the accelerometer increases the mass of the structure and hence decreases the natural frequency. A detailed study of the effect of accelerometer size is shown in Section 5.8.3.5. The weight of the accelerometer should be less than 1-2 percent of the experimenting structure for accurate measurement. The accelerometer sensitivity is also very important in the selection process, high sensitivity accelerometer should be selected in all cases. The sensitivities vary from 1 to 10000 pC/g. Larger accelerometers give higher sensitivity and at the same time they increase the total mass of the structure, hence natural frequency. There should be a compromise between these two factors.

3.1.2.5 Excitation Method

A source is needed to vibrate the structure. Various types of vibrators are available of which there are three in use: mechanical (out-of balance rotating mass), electromagnetic (moving coil in magnetic field), and electrohydraulic. Each has its advantages and disadvantages. The mechanical exciter is capable of generating a prescribed force at a variable frequency although there is relatively little flexibility or control in its use. The magnitude of the force is restricted by the out-of–balance and is only variable by making adjustments to this quantity – not something which can be done while the vibration is continuing. Also this type of exciter is relatively ineffective in low frequencies. In the electromagnetic shaker the supplied input signal is converted to an alternating magnetic field and drives the vibrator. In this case, the frequency and amplitude of excitation are controlled independently of each other. The electrohydraulic exciter generates a much higher force and is able to apply a simultaneous static load as well as a dynamic vibratory load.

3.1.2.6 Conditioning Amplifier

The choice of amplifier depends heavily on the type of accelerometer/transducer used. In all cases, its role is to straighten the small signals generated by the acclerometers/transducers so that they can be fed to the analyser for measurement.

3.1.2.7 Analyser

Each mobility measurement system incorporates an analyser in order to measure the specific parameters of interest – force, response levels. In principle, each analyser is a form of voltmeter although the signals processing required to extract the necessary information concerning magnitude and phase of each parameter leads to a very complex and sophisticated device. Different measurement systems employ different types of analysers. The choice will depend again on the type of excitation which has been used: sinusoidal, random, transient and/or periodic. The data are supplied to the analyser in analogue form. But with a digital instrument the first stage of the signal processing is analogue to digital (A to D) conversion so that the quantities to be processed are then in the form of a string of discrete values, as opposed to a

continuous function. The subsequent processing stages are then performed digitally using a computer or other means.

3.1.2.8 Controlling Software

To communicate with the analyser and vibrator amplifier a computer is used, which is controlled by software. The computer controls the vibration (frequency, amplitude etc.) and receives the digital signal from the analyser as raw data. The obtained data is then processed to obtain a mathematical model of the vibration response. In this investigation the software package ICATS was used as a controlling tool (a specialised software package developed by Imperial College, London). The software has some problem in its practical use but it is very helpful and very useful in determining the modal properties of the structure.

3.1.3 Summary of Signal Analysis

In the analysis of the FRF raw data, a mathematical model is sought out, which explains the FRF characteristics. A major part of this analysis consists of curve-fitting a theoretical expression for an individual FRF to the actual measured data. There are three methods to fit the curves, they are

1. The circle fit
2. The line fit
3. The IDENT fit

3.1.3.1 The Circle Fit

The Nyquest plot in Section 3.1.1.1.3 showed a circle fit of a single degree of freedom system which can be generalised for a multi-degree of freedom system. In this case the interactions between each other (two or more modes) is to be taken into account. Indeed, when two modes are close, the circle corresponding to the first one will not be totally drawn, but 'interrupted' by the plot of the second circle for the following mode. The details of this method are available in Kennedy and Pancu [75a]. Given a set of data, ICATS plots a circle passing by the highest number of measurement points.

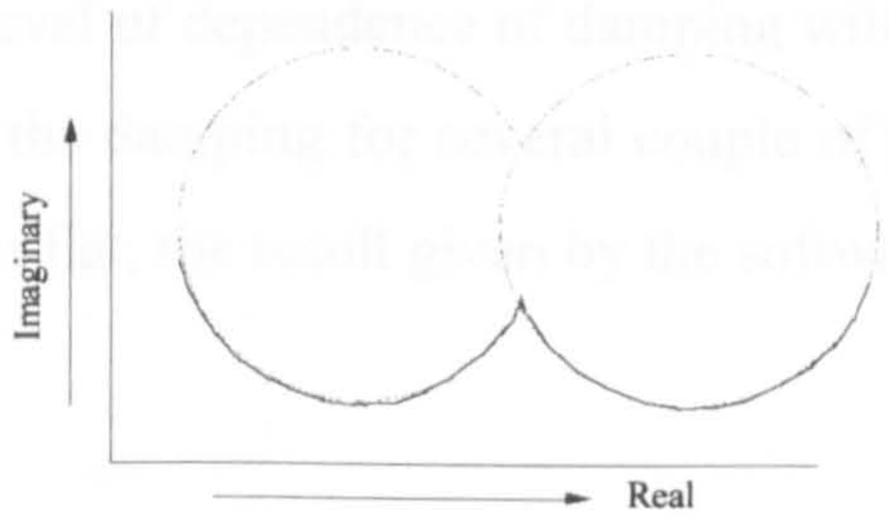

Figure 3.17 - Influence of one mode over another mode

If a lot of points do not lie well on a circle, or if there is too big gap between two points, the analysis has to be refined by adding more points around the resonance.

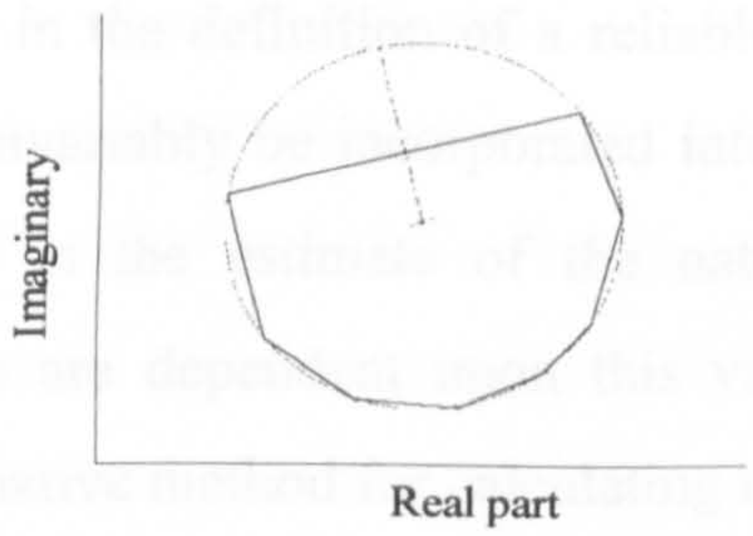

Figure 3.18 - Example of a bad circle fit having gap between two points

To evaluate the natural frequency, ICATS uses the highest arc length found between two points. Indeed when the natural frequency is reached, the changes in response are very quick with respect to the frequency, and the closer the natural frequency, the quicker is the change. For this reason, the natural frequency can only be between the two points defining the longest arc. The results given in this way are very reliable.

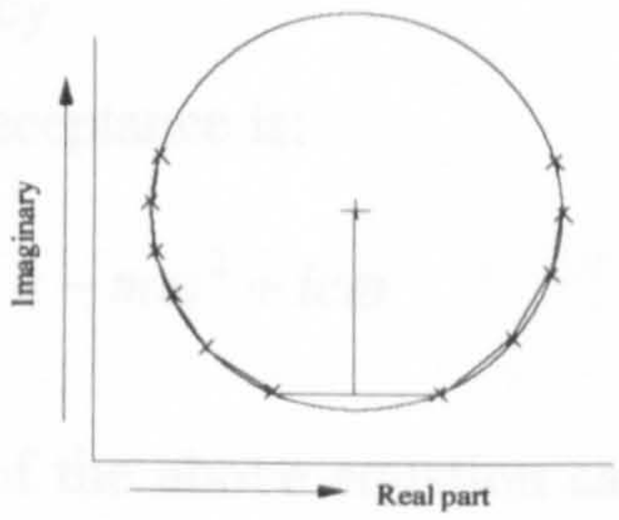

Figure 3.19 - Location of resonance on the longest arc

This method gives also an evaluation of the damping, using two points around the resonance frequency. Normally the result should be independent of the points taken. If it is not, a further analysis has to be done.

In order to evaluate the level of dependence of damping with respect to the two points, a plot gives the value of the damping for several couple of points before and after the resonance. If the graph is flat, the result given by the software is reliable.

3.1.3.2 The Line Fit

In the circle fit, the calculation of the natural frequency from the maximum sweep rate of the locus can also be complicated by the presence of scatter in the experimental data points. Typical experimental data can produce a plot in which a number of maxima are present. The extraction of a reliable value for the natural frequency can pose significant difficulties in the definition of a reliable algorithm. Some form of extrapolation process will invariably be incorporated into such algorithm which will inevitably introduce errors in the estimate of the natural frequency. Since the remaining modal properties are dependent upon this value any errors will have a cumulative effect. An alternative method for calculating the modal properties is based upon the use of dynamic stiffness data (1/receptance). Details of this method are described in Dobson [42a]. Considering a single degree of freedom system, with a damping noted c, the receptance can be written as

$$\alpha(\omega) = \frac{1}{k - m\omega^2 + ic\omega} \qquad 3.21$$

where $k =$ stiffness

$m =$ mass

$\omega =$ frequency

From this, the inverse of the receptance is:

$$\frac{1}{\alpha(\omega)} = k - m\omega^2 + ic\omega \qquad 3.22$$

The real and imaginary part of the above equation can be plotted against ω^2 over a range of frequency, where the real component curves will intersect at a point equivalent to the natural frequency and the imaginary component curves will be parallel lines. Details of the method is provided in Dobson [42a]

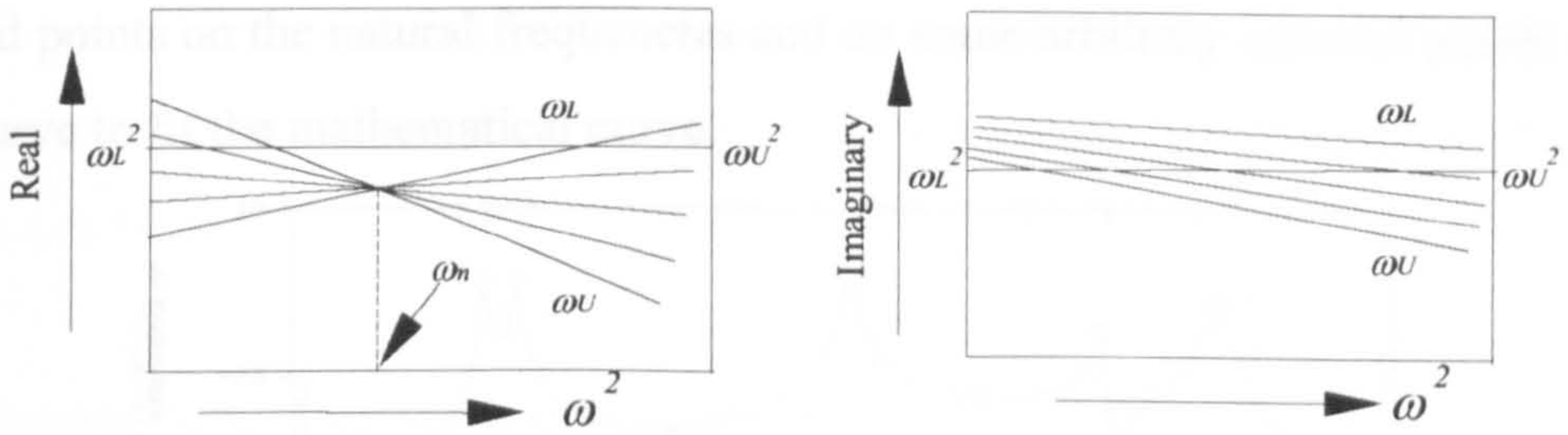

Figure 3.20 - Lines obtained from theoretical plots of the real and imaginary part of the inverse of the receptance

3.1.3.3 The IDENT Method

This method is appropriate for very lightly damped structures. In this method a mathematical model is created which is very similar to the measured FRF plot. When several modes with modal constants of differing magnitude are combined, the resultant mobility plot will be some way similar to Figure 3.21, which illustrates a 7-mode system. The identification calculation requires the knowledge of seven natural frequencies from ω_1 to ω_7 and the frequency response data at 7+1 response frequencies. The selection of the response frequencies is quite arbitrary, usually the points are chosen at the level of the antiresonance and far away from the resonance in order to have a better fit of the curves. A sample of the selected points is shown in Figure 3.21. The software makes the curve pass through the locations of presumed resonances and selected points. The final aspect of the regenerated curve has to be superimposed on the experimental FRF within a close tolerance which is directly related to the error in measurement of inertance or mobility. Details of this method is provided in Ewins [48a].

In the majority practical cases, vibration data are acquired by measurement over a limited frequency range on structures which, being continuous, have a great many degrees of freedom and a corresponding number of modes. Thus it is generally impossible to carry out a complete modal analysis which encompasses all the modes, and in general case an *N*-mode representation has to approximate to a greater-than-*N* set of data. These errors can be reduced by increasing N, i.e. the curve should be fitted in a wide range of frequency to minimise error. Figure 3.21 below shows the

selected points on the natural frequencies and on some arbitrary selected points on the FRF curve to fit the mathematical curve.

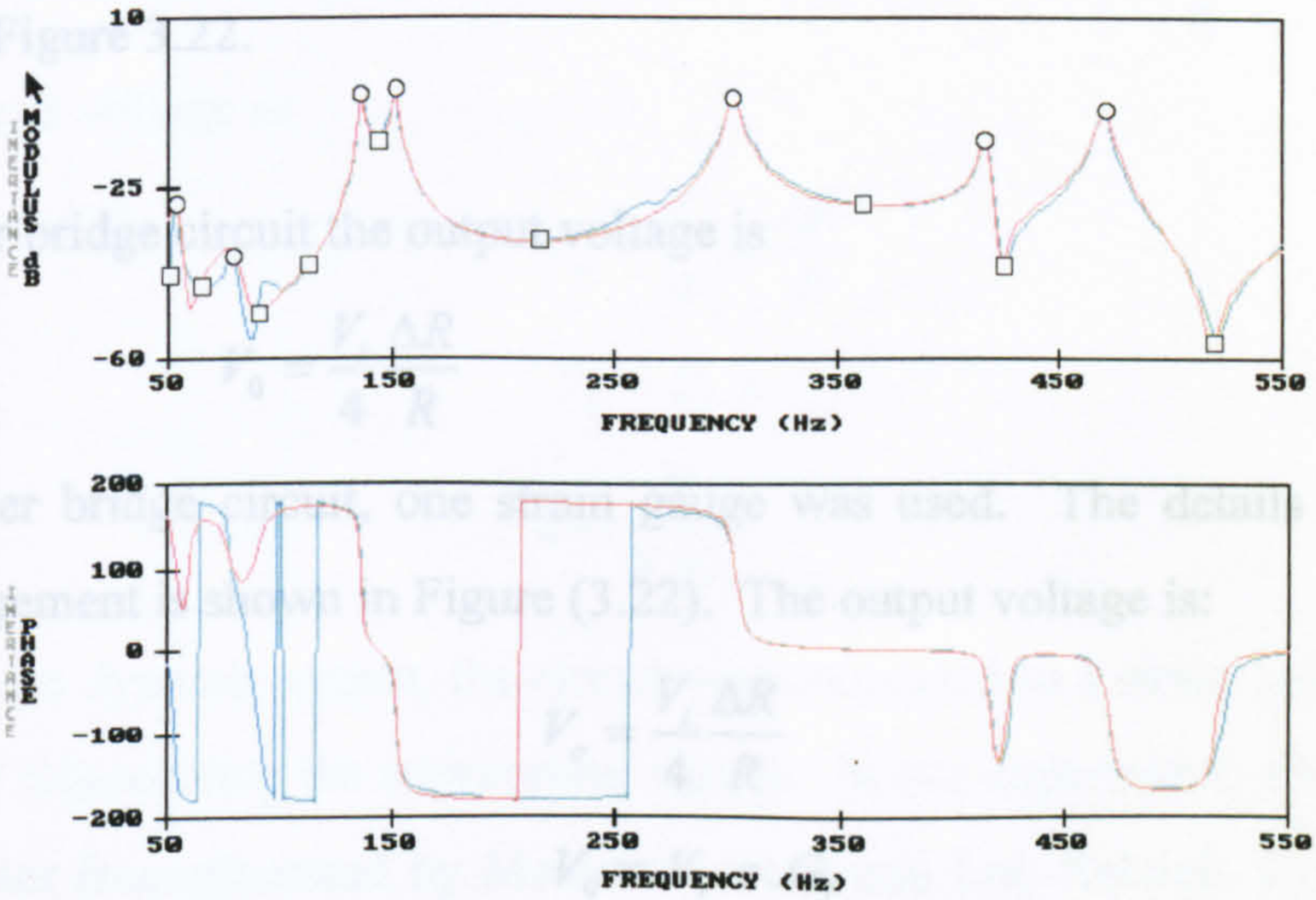

Figure 3.21 - Example of an IDENT fit of FRF curve

The data extractable from the new curve are the damping ratio, the natural frequencies and the mode shapes. The validity of the results obtained is very dependent on the measurement intervals used during the experimental work.

3.2 Measurement of Dynamic Stress

In vibratory stress relief a dynamic stress is applied to the experimenting structure to relieve/level the residual stress. The dynamically induced stress generated in the structure is a function of the vibratory amplitude, frequency, resonance, anti-resonance, mode of vibration, etc. Strain gauges were used in order to determine the level of induced dynamic stress. In this investigation, quarter and full bridge circuits were used to measure static and dynamic induced stresses.

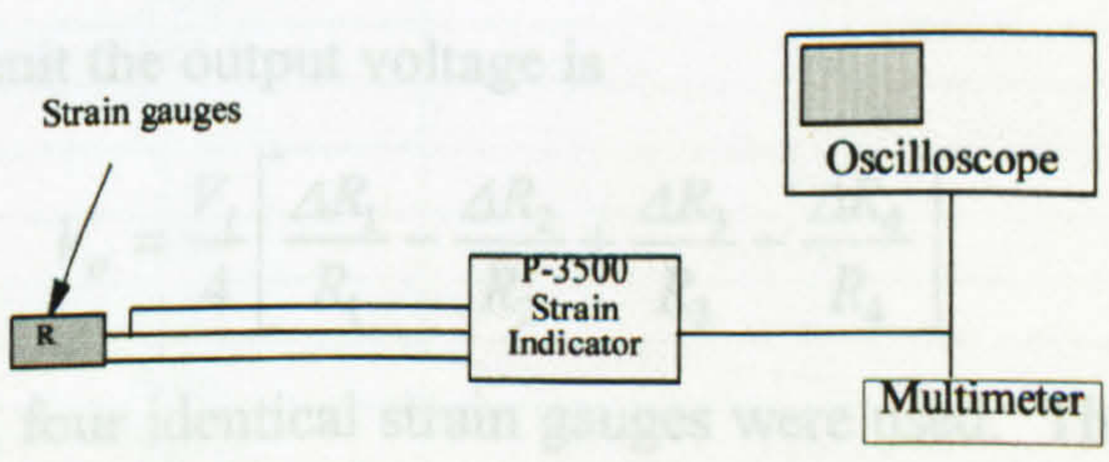

Figure 3.22 - Set-up for measuring dynamically induced stress - quarter bridge

Full bridge circuitry was used where the strain output was low, to minimise relative error. A quarter bridge circuit was used in all other cases. The quarter bridge circuit is shown in Figure 3.22.

For a quarter bridge circuit the output voltage is

$$V_0 = \frac{V_i}{4}\frac{\Delta R}{R} \qquad 3.23$$

In the quarter bridge circuit, one strain gauge was used. The details of the strain gauge arrangement is shown in Figure (3.22). The output voltage is:

$$V_o = \frac{V_i}{4}\frac{\Delta R}{R}$$

$$V_0 = V_i \,.\, \varepsilon \,.\, G_f$$

$$\text{i.e.} \qquad \varepsilon = \frac{V_o}{V_i . G_f} \qquad 3.24$$

where V_i Input Voltage

V_o Output Voltage

G_f Gauge Factor

ε Strain

For the full bridge the circuit is shown below

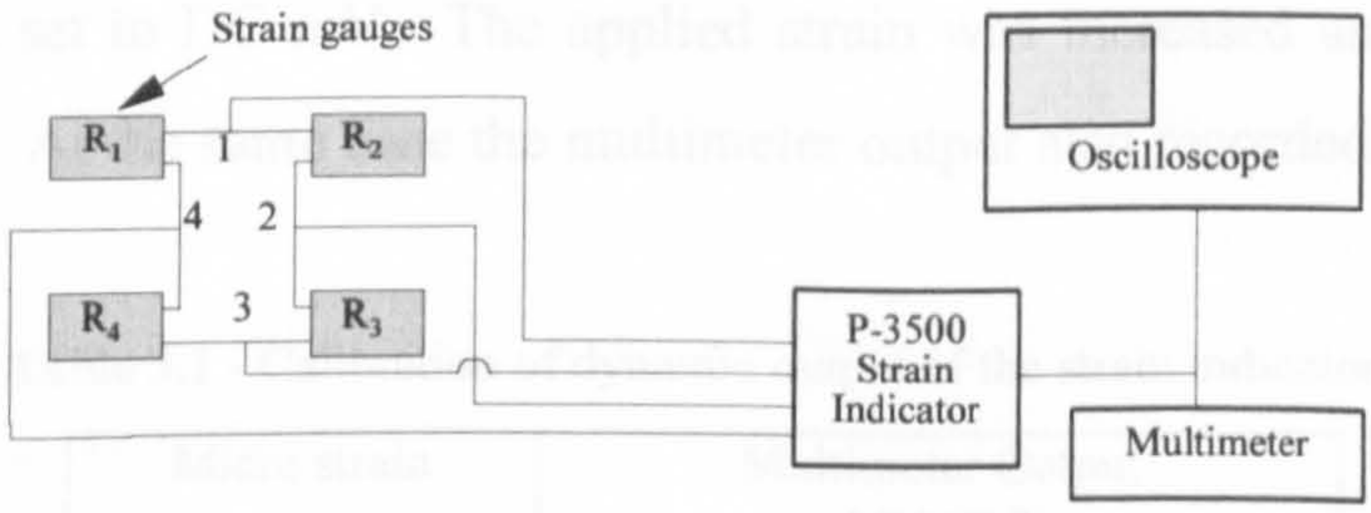

Figure 3.23 - Set-up for measuring dynamically induced stress - full bridge

For a full bridge circuit the output voltage is

$$V_o = \frac{V_i}{4}\left[\frac{\Delta R_1}{R_1} - \frac{\Delta R_2}{R_2} + \frac{\Delta R_3}{R_3} - \frac{\Delta R_4}{R_4}\right] \qquad 3.25$$

In the bridge circuit, four identical strain gauges were used. They were positioned on the structure such that their respective signals were not cancelled out - i.e. diagonally positioned strain gauges were positioned on the same side of the structure (R_1 and R_3

on one side and R_2 and R_4 on the other side). The detail of the strain gauge arrangement is shown in Figure 3.23). So, all the components of $\frac{\Delta R}{R}$ were added and gave the output voltage as

$$V_o = \frac{V_i}{4}.4.\frac{\Delta R}{R}$$

$$V_0 = V_i.\varepsilon.G_f$$

i.e. $$\varepsilon = \frac{V_o}{V_i.G_f} \qquad 3.26$$

To measure the dynamic output, the circuit was connected to a strain indicator, which is capable of regenerating the appropriate signals. In this experiment, a P-3500 digital strain indicator (manufactured by Measurement Group Ltd, Raleigh, North Carolina, USA) was used. That was able to measure dynamic strain up to the frequency of 4 kHz. The output of the strain indicator was AC/DC signals, which needed to be connected to a suitable output device to read the signals. In this experiment, a Multimeter was used as the display instrument. A Proto four point bending rig with quarter bridge circuit specimen was used to calibrate the strain indicator output. The specimen was mounted and positioned on the four point bend. The quarter bridge (on the specimen) and the multimeter were connected to the strain indicator, and the multimeter was set to DC mV. The applied strain was increased and read from the strain indicator. At the same time the multimeter output also recorded.

Table 3.1 - Calibration of dynamic output of the strain indicator

Micro strain	Multimeter Output MV (DC)
0	0.35
44.5	15.42
78.5	27.05
112.5	38.85
204.5	70.48
248	85.4
291	100.12
353	121.6
426.5	146.7
463.5	159.38

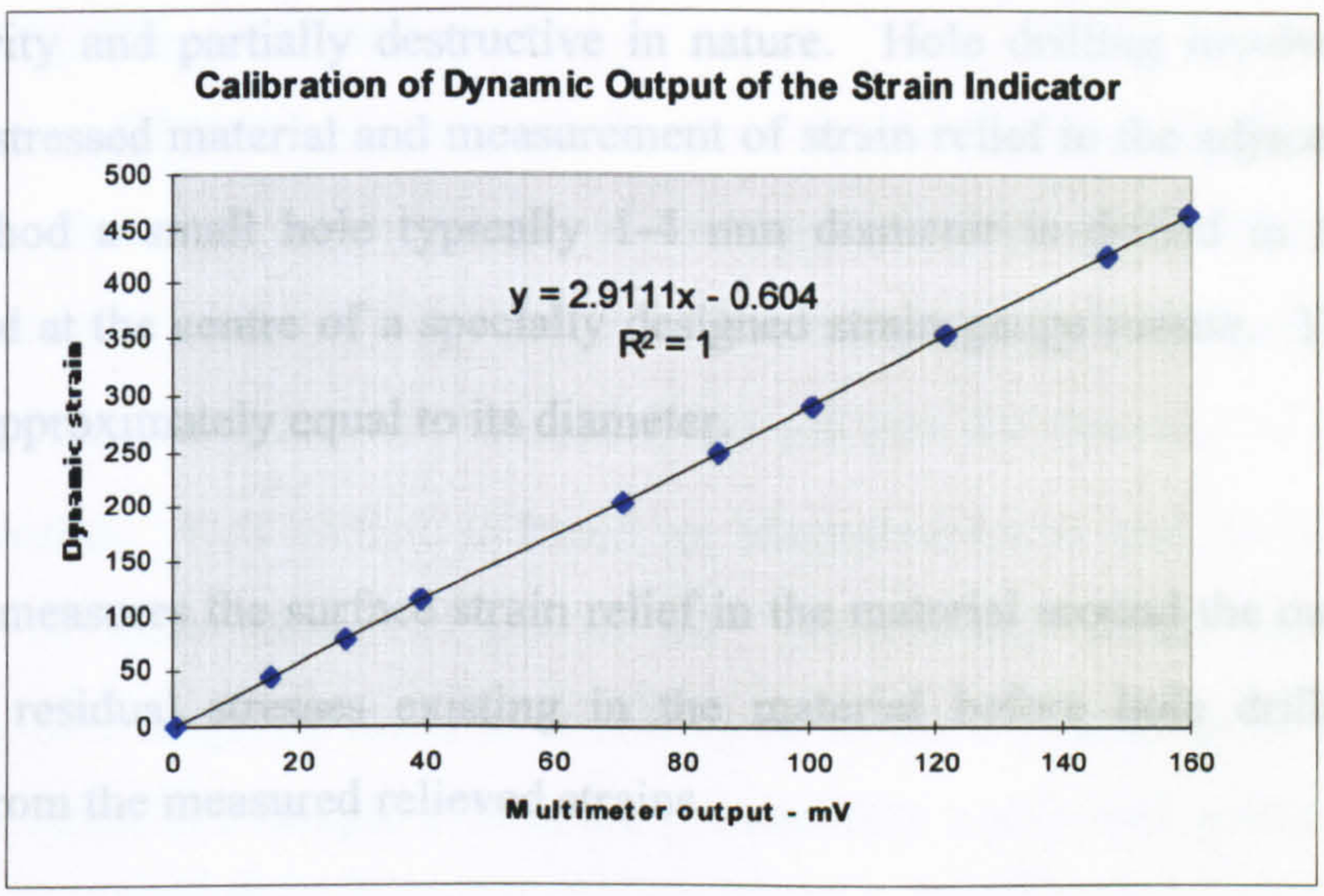

Figure 3.24 - Calibration of P-3500 strain indicator – dynamic strain v multimeter output

From the graph, the calibration factor, 1 mV = 2.9111 micro strain. The values of the multimeter output and the strain, are both DC, so this conversion factor does not need any more conversion. But measuring the dynamic strain/stress using a multimeter (which shows RMS value) will need another conversion. The peak value of the signal is obtained by multiplying RMS value by the factor 1.4144.

3.3 Residual Stress Measurement

Various methods of measuring the residual stress distributions are currently used in industry. The following techniques have been examined to determine the suitability of each for the purposes of validation of the VSR process.

1. Dissection Method (Hole Drilling)
2. Ultrasonic
3. Magnetic Methods (Barkhausen Noise Analysis and Sigmatron CP2000)
4. Diffraction Methods (Neutron & X-ray)

3.3.1 Hole Drilling Method

The hole drilling method is a widely used technique for measuring residual stress. Simplicity, reliability in practice and limited damage to the specimen are among the reasons for the popularity of this method. On the other hand its disadvantages are,

low sensitivity and partially destructive in nature. Hole drilling involves localised removal of stressed material and measurement of strain relief in the adjacent material. In this method a small hole typically 1-4 mm diameter is drilled in the residual stressed field at the centre of a specially designed strain gauge rosette. The depth of the hole is approximately equal to its diameter.

The rosette measures the surface strain relief in the material around the outside of the hole. The residual stresses existing in the material before hole drilling can be calculated from the measured relieved strains.

Holographic hole drilling is another technique which involves using an optical interference fringe pattern to determine the residual stresses. In this method, a small hole is drilled into the part containing residual stress, and the displacement caused by localised stress relief is (noted) registered using holographic interferometry. The resulting fringe pattern is analysed to calculate the residual stress, using a simple 'fringe counting' method. Taper hole drilling improves the strain sensitivity and stress calculation accuracy without exceeding the limit for the hole size at the surface of the specimen. In this method a truncated cone shape hole is drilled instead of a conventional cylindrical hole.

3.3.2 Barkhausen Noise Analysis

Barkhausen noise is discontinuous changes in the magnetisation of ferromagnetic material under an applied alternating magnetising field. The intensity of Barkhausen 'jumps' is known to be dependent on elastic stress whether it is residual or applied. When a magnetic field or mechanical stress is applied to a ferromagnetic material, changes take place in its domain structure by abrupt movements of domain walls or rotation of domain magnetisation vectors. These changes in turn produce changes in the overall sample magnetisation, as well as in sample dimension. Barkhausen noise is sensitive to grain size, dislocations, precipitates, texture and hardness that can give spurious result for anisotropic/inhomogeneous material. This method is still in development.

3.3.3 The Sigmatron CP2000

The Sigmatron CP2000 is designed for use in the measurement of stress in ferromagnetic materials where changes in the magnetic properties of the material act as a stress sensitive sensor. The output from this technique gives the magnitude of the differential of the two principal stresses (σ_1-σ_2) and also the direction of the principal stresses σ_1 and σ_2. This method is based on Magnetostriction and the Villari Effect where both of these cause changes in the permeability of the material. The permeability of a magnetic material is analogous to the conductivity in an electrical circuit. The stress in a sample affects the permeability and in turn produces changes in the magnetic properties.

3.3.4 Ultrasonic Methods

In this method the velocity of propagation of ultrasound in a solid medium is influenced by the state of strain in the medium. The main advantage of this method is it can obtain information about stresses in the interior of the material. And the main drawback is susceptibility to competing source of velocity shift. Again, practical applications are still being developed.

3.3.5 Neutron Diffraction

In this method, the interatomic spacing of a selected crystal reflection is used as a strain gauge and stresses are determined using appropriate elastic stress/strain relations. The main advantages of this method are that it is non-destructive, can measure stresses throughout the thickness of the specimen, can measure stresses in different phases of a structure and can provide information regarding macrostress and microstress. And the main drawbacks are due to the complexity of the machine, it must be highly automated, hence become extremely expensive. Other drawbacks are it takes long measurement time (2 hours for a point measurement), the error band is relatively high (±30 MPa), limited to some material.

3.3.6 X-ray Diffraction Method (XRD)

It is widely recognised that X-ray diffraction (XRD) is the only truly non-destructive method presently available that can be reliably applied to the measurement of residual stress. This method can measure stress within 0.0006 inch (0.016 mm) of the surface of most metals, due to rather soft (less than 10 Kev) X-radiation.

3.3.6.1 Principle of X-Ray Diffraction Measurement

When a monochromatic X-ray beam irradiates a solid material, it is scattered by the atoms composing the material. For a perfect crystalline material, atoms are packed regularly into a three-dimensional periodic lattice. XRD techniques exploit the fact that when a metal is under stress, applied or residual, the resultant elastic strain cause the atomic planes in the metallic crystal structure to change their interplaner spacing. From the measurement of this interplaner distance the total stress on the metal (residual and applied) can be calculated. When a polycrystalline metal is placed under stress, the resultant elastic strains are manifest in the crystal lattice of the individual crystallites. In other words, the stress applied externally or residual in the material, when below its yield strength, is taken up by interatomic strain. X-ray diffraction techniques are capable of actually measuring the interatomic spacing, which is indicative of the macro elastic strain experienced by the specimen. Stress values are obtained from these elastic strains in the crystals by knowing the elastic constants of the material and assuming that stress is proportional to strain.

Bragg Equation

The most important parameters involved in the mechanics of X-ray diffraction are described by the Bragg relation.

$$n\lambda = 2d\sin\theta \qquad 3.27$$

where $n = 1$ for stress work

λ = wave length of the X-ray

d = Spacing of the reflecting planes of atoms

θ = Bragg angle

This relation is illustrated in Figure 3.25 below

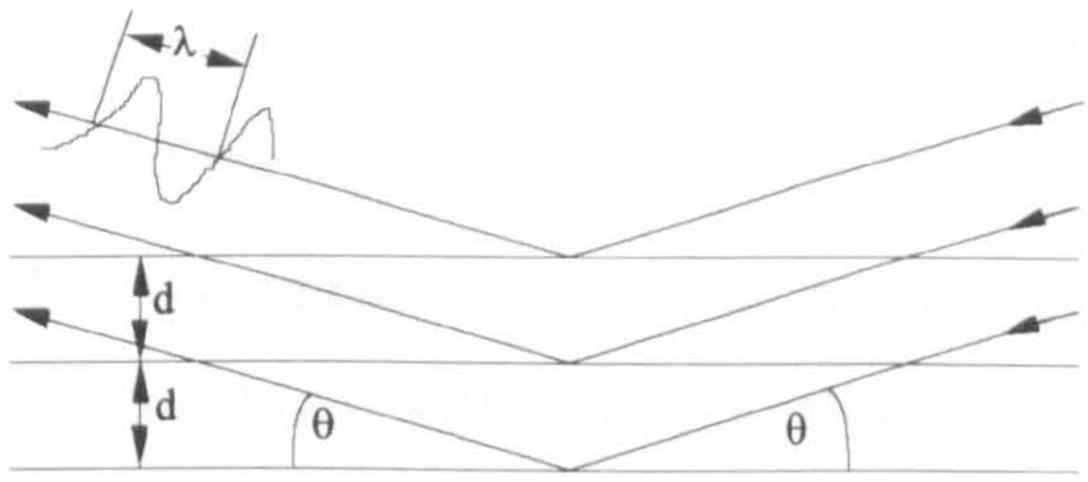

Figure 3.25 - Bragg relation

In X-ray stress analysis, λ is a known constant and 2θ is measured. In a powder, or fine grained metal, where particles show no preferred orientation, an X-ray beam only a few square millimeters in cross section is diffracted as a cone of many individual X-ray beams. Figure 3.26 shows the X-ray diffracted cone.

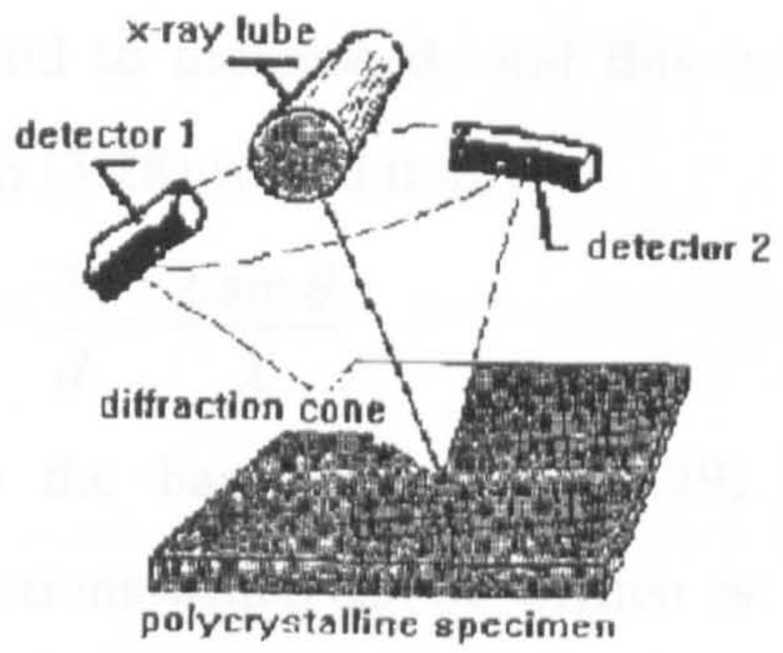

Figure 3.26 - Diffraction cone

This cone is composed of many individual beams, each about the size of the grains in the specimen; however they are so numerous that they overlap and form a continuous cone, except when the grain size is too large. The cones semi-apex angle ($180 - 2\theta$) is not infinitely sharp, in that a plane perpendicular to the cones axis would show that the diffracted X-ray intensity is distributed over a few tenths to several degrees of 2θ. Therefore the angular distribution of the diffracted beam intensity must be ascertained as a function of 2θ. In other words, the diffracted X-ray intensity must be measured at several angular positions, or a continuum of positions, in order to determine the mean diffraction angle 2θ.

This measurement is conventionally collected by two methods. One exposes photographic film to X-radiation. The other uses an electronic X-ray detector which is moved through a segment of the cone as to produce an intensity versus θ reading (in practice 2θ is used). The instrument incorporating this moving detector is called an X-ray Diffractometer. The Proto XRD stress analyser uses a position sensitive scintillation detector (PSSD) which does not require the motion of 2θ vs. intensity measurement. The PSSD is capable of performing multi-channel measurements simultaneously and quickly.

The effect that elastic strain, caused by applied or residual stress, has on these diffracted X-rays is to change the theta value (Bragg angle).

An applied stress would tend to increase d, and this in turn would decrease θ as rewriting the Bragg Equation (3.28) would imply.

$$\frac{1}{d} = \frac{2.\sin\theta}{\lambda} \qquad 3.28$$

This concept will lead to the basic Equation (3.29) relating X-ray diffraction principals to stress-strain relations which can be written as:

$$\varepsilon_{\phi\psi} = \left(\frac{1+\nu}{E}\right)\sigma_{\phi}\sin^2\psi - \frac{\nu}{E}(\sigma_1+\sigma_2) \qquad 3.29$$

where:

$E/(1+\nu)$ = the elastic constant

σ_{ϕ} = $\sigma_1 \cos^2\phi + \sigma_2 \sin^2\phi$ = stress in the plane of the surface of the specimen at an angle of ϕ with a principal stress direction in the specimen surface.

ψ = angle between the surface normal and the normal to the plane of the specimen and the direction of stress measurement in the plane.

$\varepsilon_{\phi\psi}$ = strain in the direction defined by the angles

$\sigma_1+\sigma_2$ = principal stresses in the surface plane of the specimen

ν = Poisson's ratio

θ = angle between a reference direction in the surface plane of the specimen and the direction of stress measurement in the same plane.

The symbols in Equations 3.28 and 3.29 are explained in Figure 3.27.

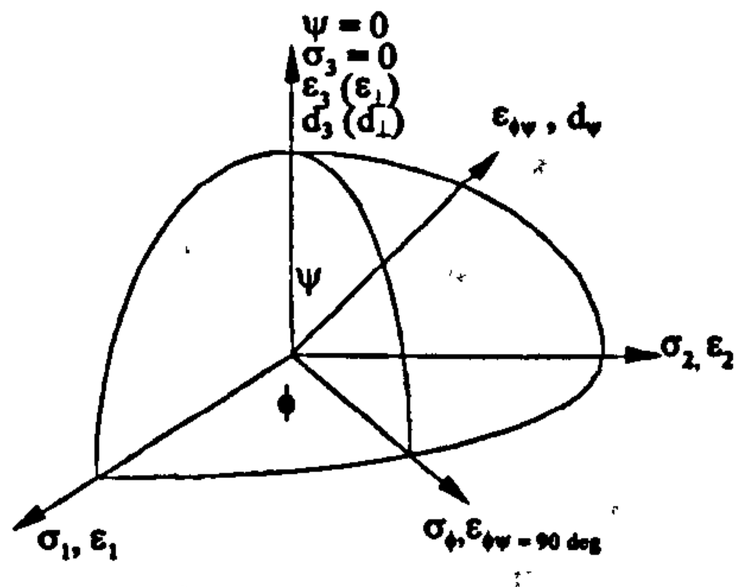

Figure 3.27 - Ellipsoid of Stress and Strain.

Equation 3.29 may be written as:

$$\sigma_\phi = \frac{(d_\psi - d_\perp)E}{d_\perp.(1+\nu)\sin^2\psi} \qquad 3.30$$

Where:

d_ψ = interatomic planar spacing for crystal planes in which the normal is defined by the angle ψ.

$d_\perp$ = interplanar atomic spacing for crystal planes parallel to the specimen surface

Now since the difference between d_ψ and $d_\perp$ is small, then from Bragg's relation

$$\frac{\delta d}{d} = -\cot\frac{\delta 2\theta}{2} \qquad 3.31$$

and Equation (3.30) may be written in terms of θ as

$$\sigma_\phi = (2\theta_\perp - 2\theta_\psi)\frac{\cot\theta}{2}\left(\frac{E}{1+\nu}\right)\frac{1}{\sin^2\psi}\left(\frac{\pi}{180}\right) \qquad 3.32$$

where $2\theta_\perp$ = Bragg angle of the $d_\perp$ planes expressed in degrees

$2\theta_\psi$ = Bragg angle of the d_ψ planes expressed in degrees

It should be noted that for a residual stress measurement the diffracting angle, θ, of interatomic planes of at least two different ψ angles with respect to the surface normal must be measured. These planes are crystallographically equivalent (same Miller indices) and in the unstressed state of the metal would have the same interatomic (d) spacing.

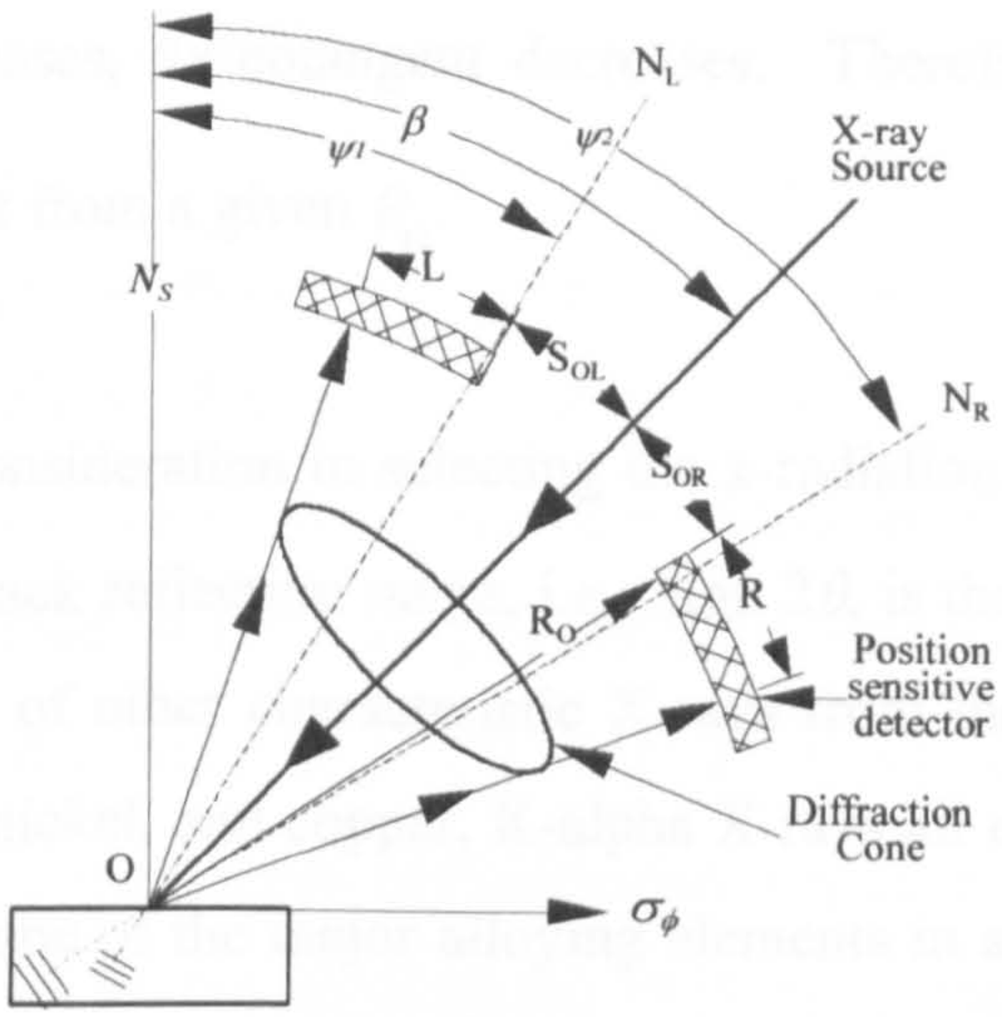

Figure 3.28 - One angle arrangement in Single Exposure Technique.

In Figure 3.28 N_S is the specimen surface normal; β is the angle subtended by the incident beam. N_L and N_R are the normals to the diffracting planes; ψ_1 and ψ_2 the angles between N_S and N_L and N_R, respectively. R_o is the focusing circle; O is the point of incidence of the X-ray beam. L and R are the measured parameters representing the distance from the confident mark of known distance from the incident beam position. S_{OL} and S_{OR} are the distances from the incident X-ray beam to the aforementioned marks.

However, in a stressed material two or more orientations of diffracting planes are selected, so that they are at different angles to the surface and therefore their normals are at some angles ψ to the surface normal. Depending upon the angle of these planes to the surface direction, their interplaner atomic spacing is increased or decreased by varying amounts.

3.3.6.2 Selection of X-Radiation

It should be noted that in any XRD stress measurement technique, X-ray peaks in the far back-reflection range, i.e., peaks with 2θ angles near 180^o, are much preferred because they show the greatest X-ray peak 2θ shift with a given amount of applied or residual stress. The advantage of a large 2θ is illustrated in Equation (3.31) where it is

noted that as θ_1 increases, its cotangent decreases. Therefore, a larger difference $(2\theta_1\text{-}2\theta_\psi)$ would result from a given θ_o.

The other important consideration in selecting the x-radiation is providing an intense X-ray peak in the far back reflection range, i.e., high 2θ, is that the radiation does not cause the fluorescence of other characteristic X-rays from the stress specimen. For example, iron, cobalt, nickel, and copper, K-alpha X-rays all exhibit the disadvantage of fluorescing at least one of the major alloying elements in austenitic stainless steel. Thus they produce high background radiation which degrades the diffracted X-ray peak clarity. For that reason it is important to use different x-radiation for different materials.

A chromium target tube was used to provide the characteristic x-radiation source for the PROTO XRD stress analyzer in this investigation. The characteristic x-radiation from the chromium tube does not fluoresce the major alloying elements in steel, stainless steel, or aluminium, and it provides two useful x-radiations. Chromium K-beta diffracts from a 2θ of approximately 147^o from austenitic stainless steel. Chromium K-alpha reflects from a 2θ of about 156^o for ferritic steels, martensitic steels, and aluminium alloys and can analyse plane (211) if wavelength $\lambda = 2.2911$Å is used. These high 2θ angles allow for a compact stress head design - an important advantage in the Proto XRD system. They can be operated in confined spaces, even within 4-inch diameter pipes.

3.3.6.3 Stress Measurement Techniques

There are three basic techniques for measuring stresses based on the X-ray diffraction method. These are the double exposure or two angle technique (DET); the single exposure or one angle technique (SET); and the $\sin^2\psi$ or multi angle technique. The angle of exposure which is referred to is that between the incident X-ray beam and the specimen surface normal, i.e., beta (β) in Figure 3.28.

Single Exposure Technique (SET)

As stated earlier in order to measure residual stress, the diffracting angle (θ) from the same type of crystallographic plane, (i.e., same Miller indices), at two different angles with respect to the surface need to be measured (see Figure 3.28). This can be accomplished using a single incident X-ray beam angle because, as shown in Figure 3.26, X-rays are diffracted from a fine-grained polycrystalline surface as a cone of beams. By measuring the Bragg angle (θ) on two opposite sides of the cone, stress can be measured using a single beta (β) angle (see Figure 3.28). Note that the two positions of measurement on the approximate circle produced by the intersection of the cone of X-rays and a plane normal to the incident beam, are the closest and farthest away (i.e., opposite sides of the circumference) from the specimen surface normal, respectively. Actually, when β is not equal to zero, the plane-cone intersection forms a circle only when the metal is unstressed; for a stressed metal the circle is deformed into a skewed ellipse. As described in the previous paragraph, a single incident angle (β) can be used to provide readings at two ψ angles using the equation:

$$\sigma = \left(\frac{E}{1+\nu}\right)\frac{\cdot(R+S_{OR})-(L+S_{0L})}{\cdot 4\cdot R_0\cdot\sin^2\theta_0\cdot\sin 2\beta} \qquad 3.33$$

Where: E = Young's modulus

ν = Poisson's ration and the other parameters are defined in Figure 3.28.

Double Exposure Technique (DET)

The Double Exposure Technique (DET) measures the interplanar spacing (d) of planes at two different angular positions (ψ_1 and ψ_2) with the specimen surface. One set of planes are those which are parallel to the surface, and thus the ψ angle is zero, i.e., $\psi_1 = 0$. The second set of planes are those that make a reasonably steep angle with the surface, e.g., $\psi_2 = 45^o$ or 60^o. These angles are often chosen because their sin values are 0.05 and 0.75. This simplifies the calculation using Equation 3.32.

The DET has been applied to film, camera and laboratory diffractometer stress measurement. However, significant errors can be introduced when the stress measuring head is moved from one (ψ) angle to another on any instrument except a diffractometer, where the specimen to detector distance is rigidly maintained at a constant R_o (Figure 3.28). Even with this error potential, the DET is used because most conventional instrumentation, including most other stress measurement devices, is incapable of measuring two angles simultaneously.

The major parametric difference between the single and double exposure techniques is that one ψ angle, ψ_L in Figure 3.28, is usually equal to zero degrees for the double exposure technique. The PROTO stress analyser is conventionally used to apply the single exposure technique.

Multiple Exposure Technique (MET)

This method is also called sine square ψ technique. In a stressed, untextured metal the interplanar atomic spacing (d) of crystallographic equivalent planes (i.e., identical Miller indices, hkl) will vary consistently with their ψ angle. Furthermore, a plot of this (d) spacing versus $\sin^2\psi$ will produce a straight line (Figure 3.29). In order to calculate the residual stress from such a plot, the data must be plotted as d_ψ vs. $\sin^2\psi$ and the slope of the best fitted straight line should be calculated.

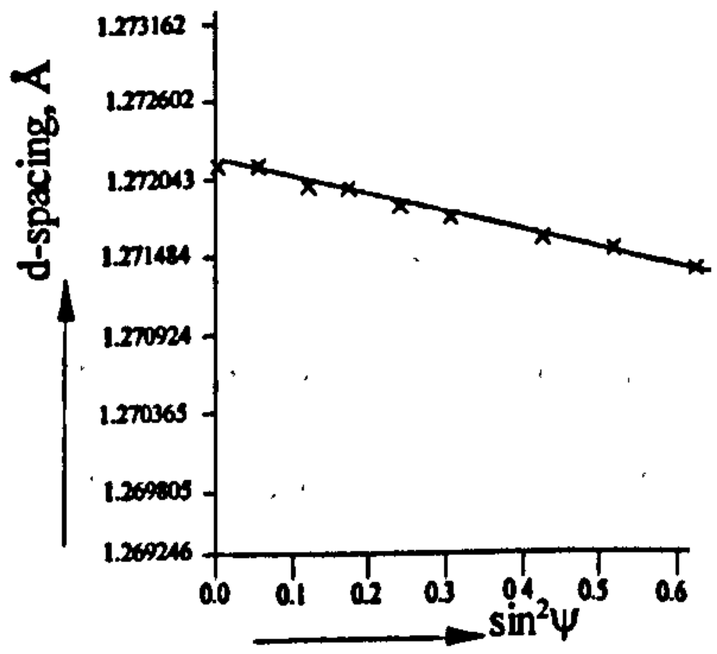

Figure 3.29 - d spacing versus $\sin^2\psi$

Equation 3.30 can be rewritten as

$$d_\psi = \frac{1+\nu}{E} d_\perp \sigma_\phi \sin^2\psi - d_\perp \qquad 3.34$$

Differentiating Equation 3.34 with respect to $\sin^2\psi$ would give the slope (m) of the plot.

$$\frac{d(d_\psi)}{d(\sin^2\psi)} = \frac{1+\nu}{E} d_\perp \sigma_\phi = m \qquad 3.35$$

Thus the residual stress

$$\sigma_\phi = \frac{mE}{(1+\nu)d_\perp} \qquad 3.36$$

3.3.6.4 Application Considerations

There are a number of considerations that affect the nature and viability of XRD stress measurements. This section discusses those limitations and possible data collection enhancements.

Specimen Condition

There are a number of error sources and problems that are produced by the condition of the specimen.

Surface Condition

Any XRD stress measurement technique measures only surface stresses. The maximum depth of penetration of the chromium K-alpha (Kα) or K-beta (Kβ) X-ray beam into a steel, aluminium, or stainless steel surface is about 0.0006 inches (.016 mm). This means that processes such as grinding or polishing which disturb; (i.e., cold work), the surface, affect the measured stress. These processes give rise to their own particular stress field to depths of several thousandths of an inch (0.001 inches = 0.0254 mm) into the surface. Polymer coatings, heavy grease or paint as well as thick corrosion layers can also affect the reliability of the XRD stress measurement.

Care must be exercised in removing any of these coatings since the cleaning processes may cause cold working of the surface. Electro-polishing is the recommended method of removal of work hardened metal or any corrosion product before XRD stress measurement.

Microstructure

The idea of measurement of residual stress using X-ray is based upon the assumption that the material is polycrystalline, homogeneous, macroscopically isotropic and the grain size is small. In practice these assumptions are not always valid as grain size, multiphase material, anisotropy crystallographic texture often cause problems. To overcome these problems additional measures should be taken. A brief overview of the difficulties is presented here.

Grain Size

Grain size can broaden the X-ray peak, i.e., produce a wider peak, if it is of the order of a few tenths of a micrometer or less. However, such small grain sizes are seldom encountered which can cause error in the measurement. Too large a grain size is more often the problem. If the grains are too large, there are insufficient amounts of grains in the area of the specimen which is irradiated by the X-ray beam to provide a continuous cone of X-rays. Grain sizes much larger than about 80 microns, approximately ASTM 4-5, will certainly cause problems in stress measurement with any stress analyser. Also, on ferritic and martensitic steels, the effective grain size of the ferrite and martensite are likely to be much smaller than the austenitic grain size usually reported in the certifications or specifications.

The most straightforward method of detecting a large grain problem with the stress analyser is to determine if movements of R_o about 0.020 inches (0.5 mm) significantly change the value or the shape or intensity of either peak. The (R-L) peak change (Figure 3.28) should not exceed 0.8 pixels, and the relative intensity ratio of the two peaks, after background subtraction, should not change more than five percent. XRD peaks from large grains are characteristically very intense and sharp. However, no peak at all may be evident in extreme cases. The effect of large grain size might be observed by taking stress measurements on cast or forged steels and aluminium or extruded aluminium.

Multiphase Material

When a measurement is made on a multiphase material, usually only one phase is analysed. The measured strain is therefore the elastic strain of this particular phase, coming partly from the macroscopic stress and partly from the stresses of other phases on the analysed one. The stress determined by the $\sin^2\psi$ technique is not the macroscopic strain but the average stress of the analysed phase. Moreover, if, in addition, the mechanical and thermal loadings on the sample are strongly anisotropic, plastic anisotropy problems will also arise. In other respects, an experimental problem can be a superposition of the peaks of several phases.

Plastic Anisotropy Problem

The plastic deformation of polycrystalline materials originates in gliding or twining within the grains. These processes are highly anisotropic at a microscopic scale and lead to strain incompatibilities which are accommodated by local strains. The average over the whole material of these elastic strains is equal to zero but, in a similar way as the diffracting volume retains some of the elastic anisotropy of the crystallites, it retains part of these elastic strains coming from deformation incompatibilities. In a great majority of cases it is negligible, but for highly textured material with strong plastic deformation it is not.

Cold Working

Cold working causes increased disorder in the crystalline structure as this introduces dislocations and microstrains. This is manifested in the X-ray diffraction peak by broadening, and in extreme cases can cause the peak to be distributed over such a large two-theta (2θ) range, that it is indistinguishable from the background. Fortunately, this extreme is seldom encountered in stress measurement of engineering components. With a surface that has been highly cold worked before welding, the X-ray peaks are often less broad near the weld fusion line. This is due to the annealing effect that the heat of welding has on metal immediately adjacent to the weld.

Texture

Preferred orientation, or texture, may be caused in metals by plastic work, heat treating, plating or casting. It is an alignment of the tiny crystalline grains along preferred directions. Anomalous results may appear when XRD stress measurements are attempted on a metal with preferred orientation (texture). The presence of texture may be detected by plotting the stress data as θ versus $\sin^2\psi$.

Stress Constant

The bulk values of E and ν may be found in any one of a number of handbooks. However, as noted in SAE it is generally recognised by XRD stress users that application of these bulk values for stress calculation can cause substantial error.

The X-ray elastic constant can be derived experimentally by applying known loads and measuring the stress using XRD. An experimental curve can be plotted and the X-ray elastic constant can be determined from the slope. In this study the Effective Elastic Constant was determined for the material used in this investigation to minimise the error in measurements, which is discussed in Section 5.1.

Chapter 4

Finite Element Analysis

Finite Element Analysis

Finite Element (FE) Analysis was carried out to determine structural, thermal, modal and dynamic properties of different structures. FE was done on different occasions for different specimens. Whenever any geometry of the test specimen was changed, FE modeling was carried out in order to understand the characteristics of the structures. The derived data was used in the different experiments. The objective of each FE model is provided in the detailed description of the models.

Weld FE modeling was initiated, but was given up half way through the analysis because of time limitation. The thermal part of the analysis was converging well but the structural part did not converge due to the non-linear properties of steel at higher temperature. Also, designing the moving heat source made the model very lengthy and was taking a long time to solve. Modal and Harmonic Analysis of the different structures are given below.

4.1 Cantilever Beam

For the Cantilever beam, a Modal and Harmonic analysis were carried out to determine modal properties, i.e. mode shapes natural frequencies etc. The Cantilever Beam model is shown in Figure 4.1. For the cantilever beam a modal analysis was carried out to determine the natural frequencies of the experimenting structure. The most important aim for the cantilever beam analysis was a determination of the applied dynamic stresses due to application of simple flexural vibration to the specimens. In the harmonic analysis a detailed study of the weld toe and the side opposite the weld was carried out because these two areas were investigated in the Experiments VIII and XIII.

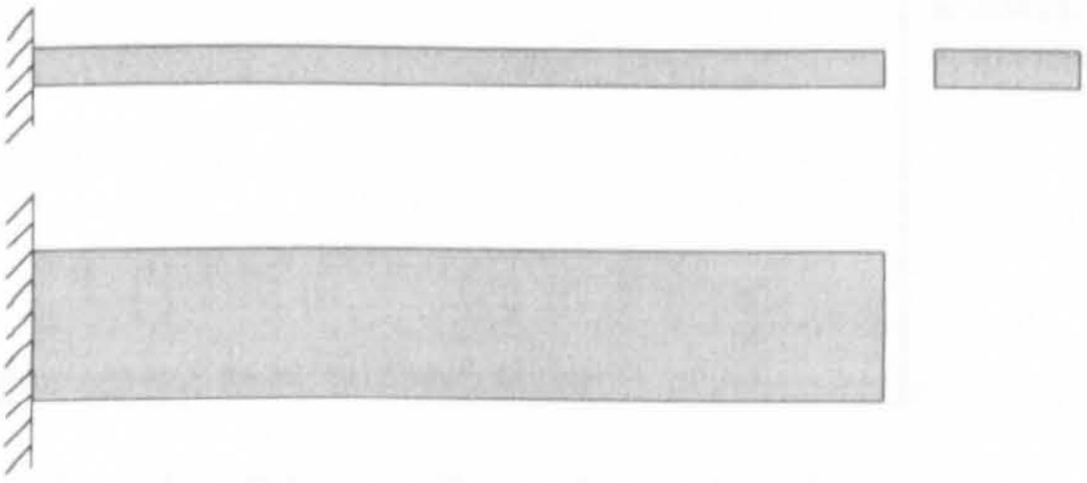

Figure 4.1 - Cantilever FE model

4.1.1 Modal Analysis

Modal analysis of the cantilever beam showed the following characteristic of the model. The mode shapes and the natural frequencies of the first five modes:

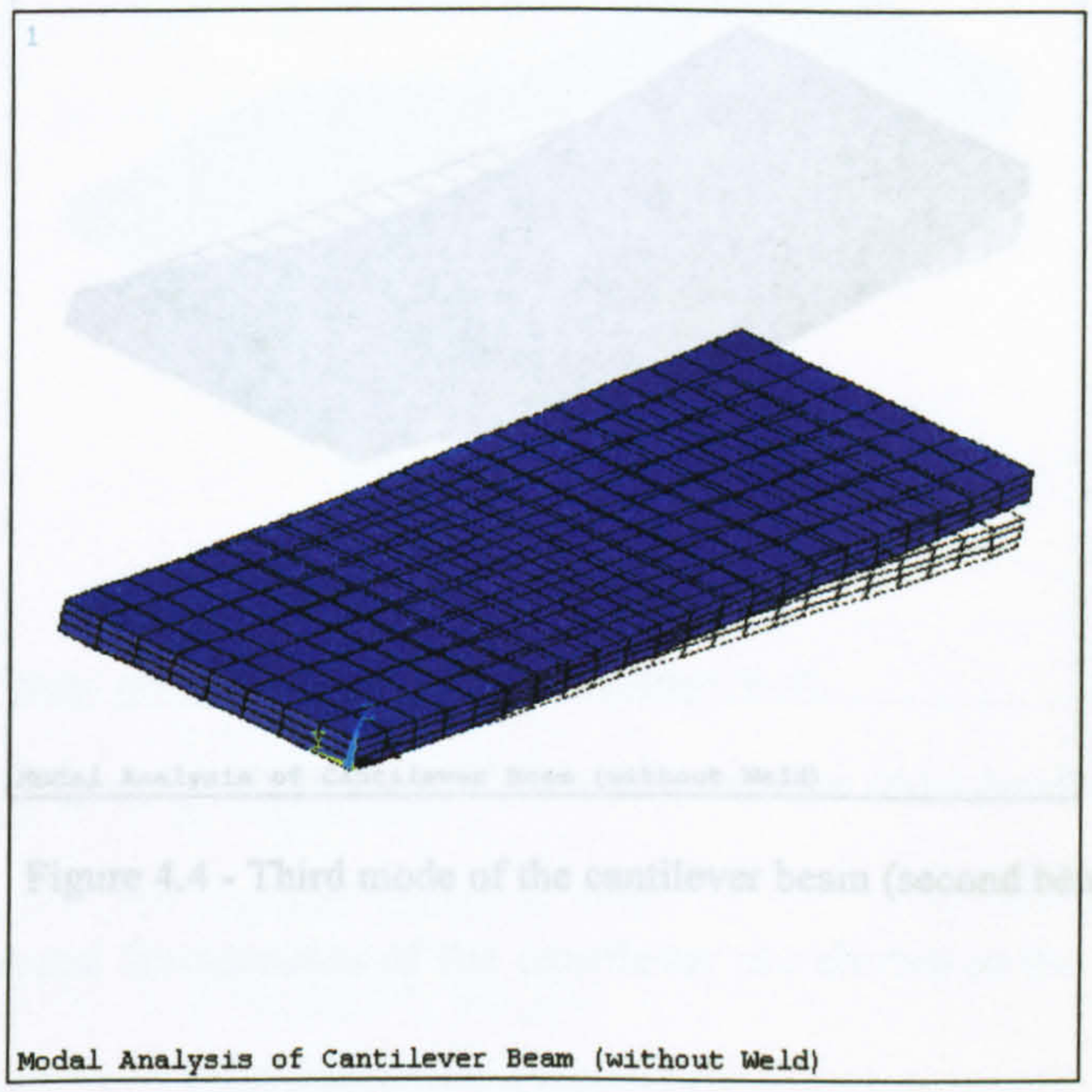

Figure 4.2 - First mode of the cantilever beam (bending)

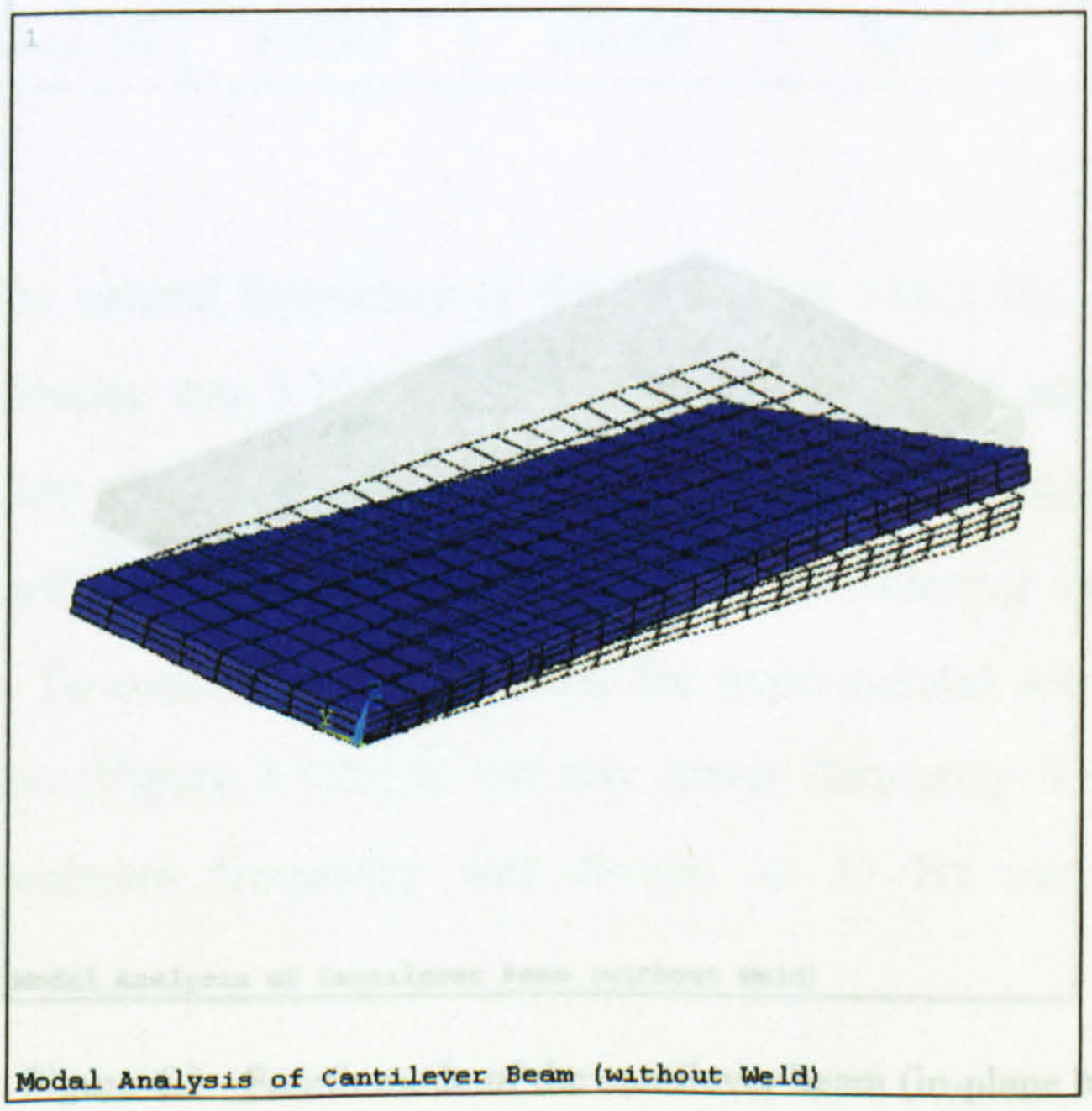

Figure 4.3 - Second mode of the cantilever beam (torsional)

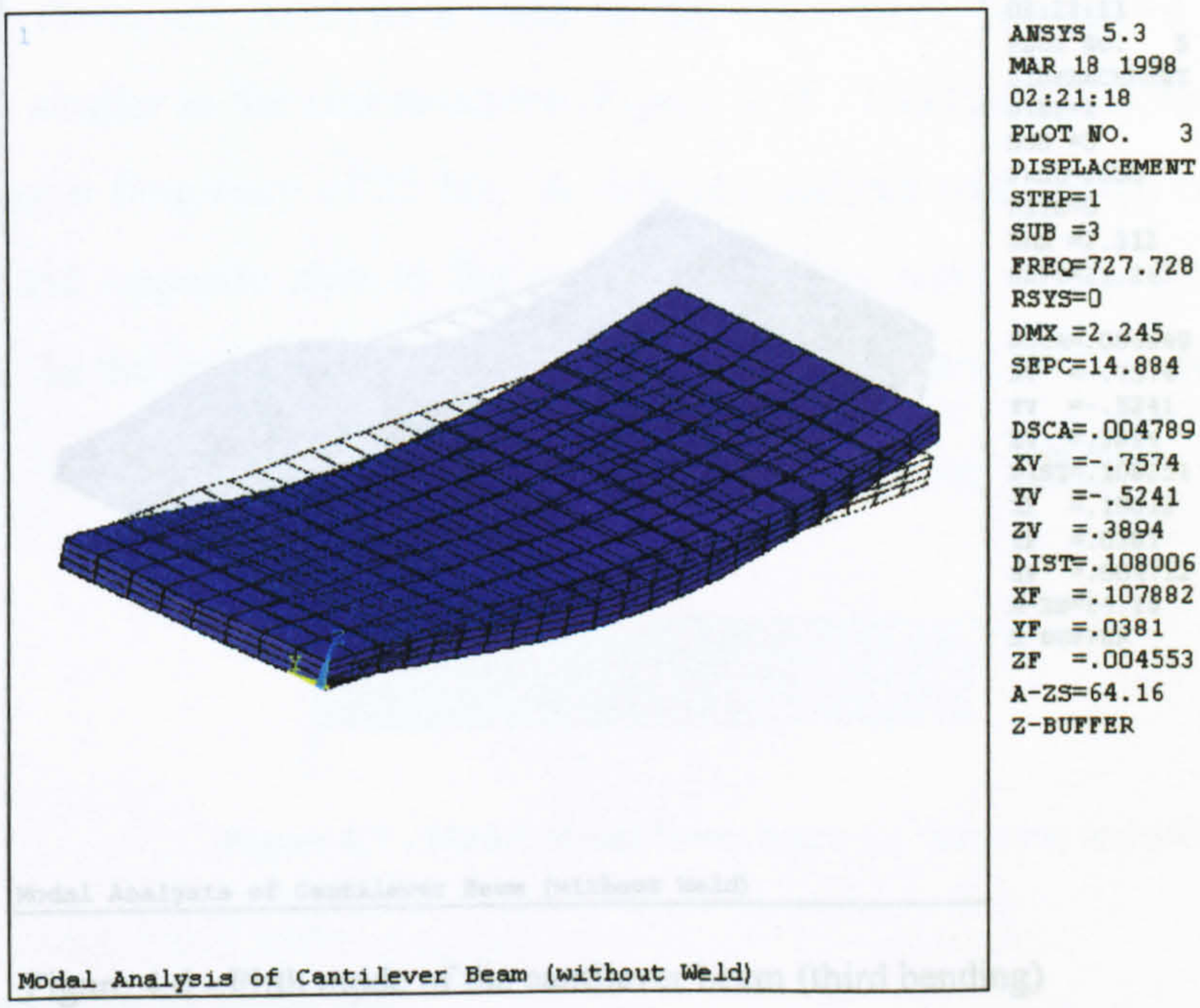

Figure 4.4 - Third mode of the cantilever beam (second bending)

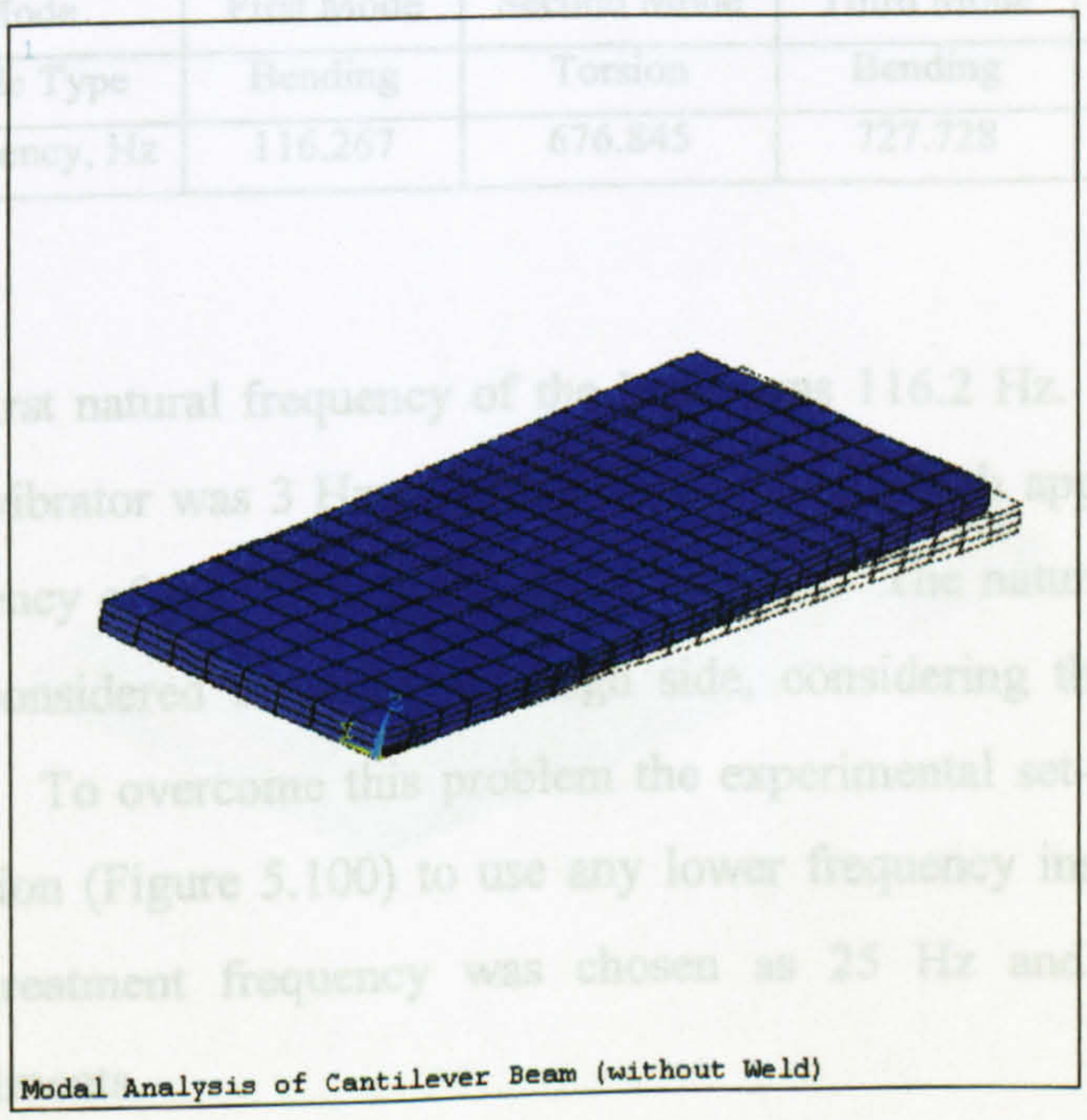

Figure 4.5 - Fourth mode of the cantilever beam (in-plane bending)

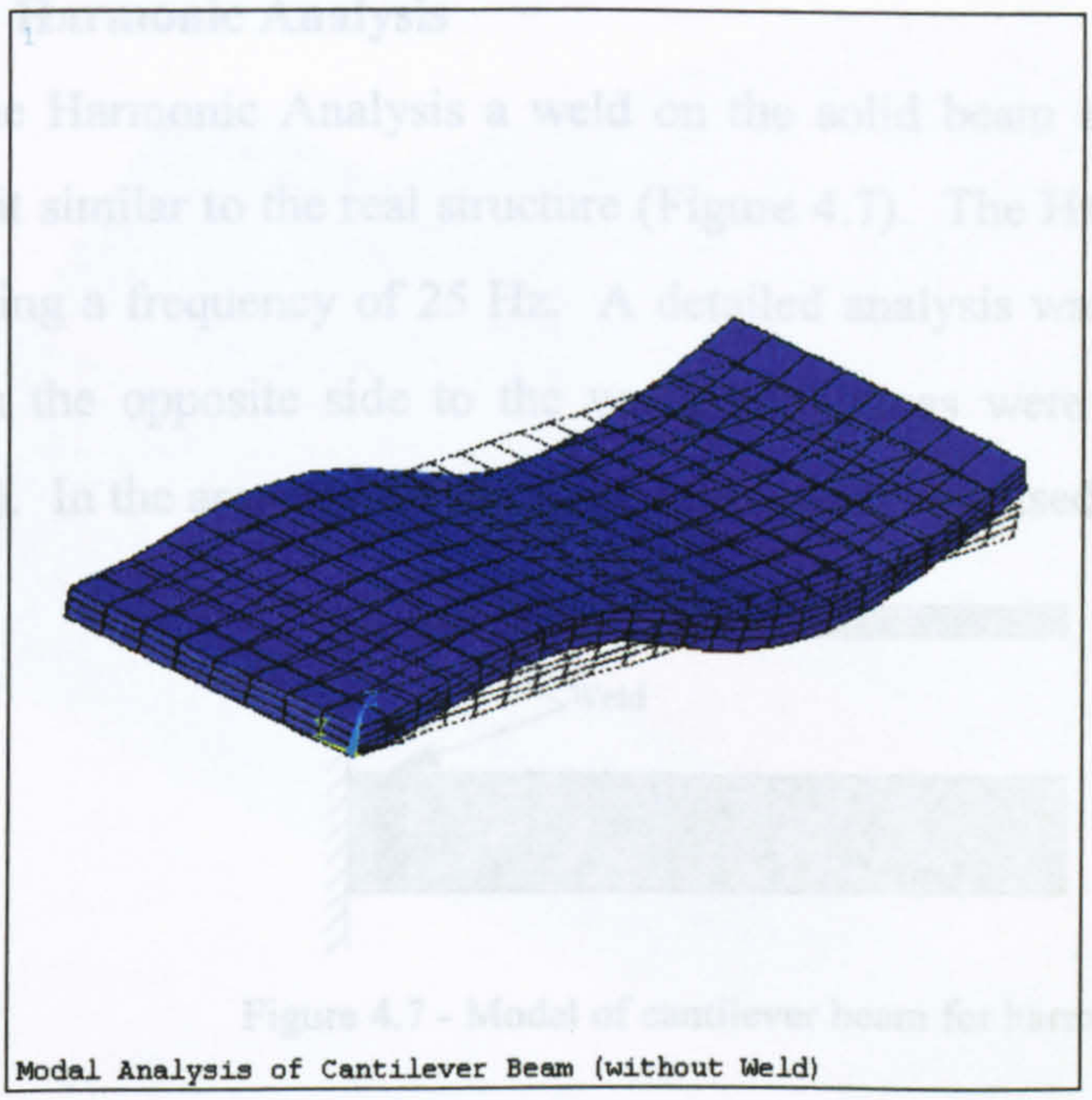

Figure 4.6 - Fifth mode of the cantilever beam (third bending)

The natural frequencies of the cantilever are shown in the table below.

Table 4.1 - Modes and frequency of vibration of the cantilever beam

Mode	First Mode	Second Mode	Third Mode	Fourth Mode	Fifth Mode
Mode Type	Bending	Torsion	Bending	In-plane	Torsion
Frequency, Hz	116.267	676.845	727.728	1266	2050

The first natural frequency of the beam was 116.2 Hz. The frequency range of the used vibrator was 3 Hz to 3 kHz. To induce a high applied vibratory stress a lower frequency of the vibrator should be selected. The natural frequency of the structure was considered to be on the high side, considering the required applied dynamic stress. To overcome this problem the experimental set-up was adapted for a forced vibration (Figure 5.100) to use any lower frequency instead of a natural frequency. The treatment frequency was chosen as 25 Hz and was used in most of the experiments.

4.1.2 Harmonic Analysis

For the Harmonic Analysis a weld on the solid beam was added in the analysis to make it similar to the real structure (Figure 4.7). The Harmonic Analysis was carried out using a frequency of 25 Hz. A detailed analysis was carried out in the weld toe and in the opposite side to the weld, both areas were in the Heat Affected Zone (HAZ). In the area around the weld a fine mesh was used in the model.

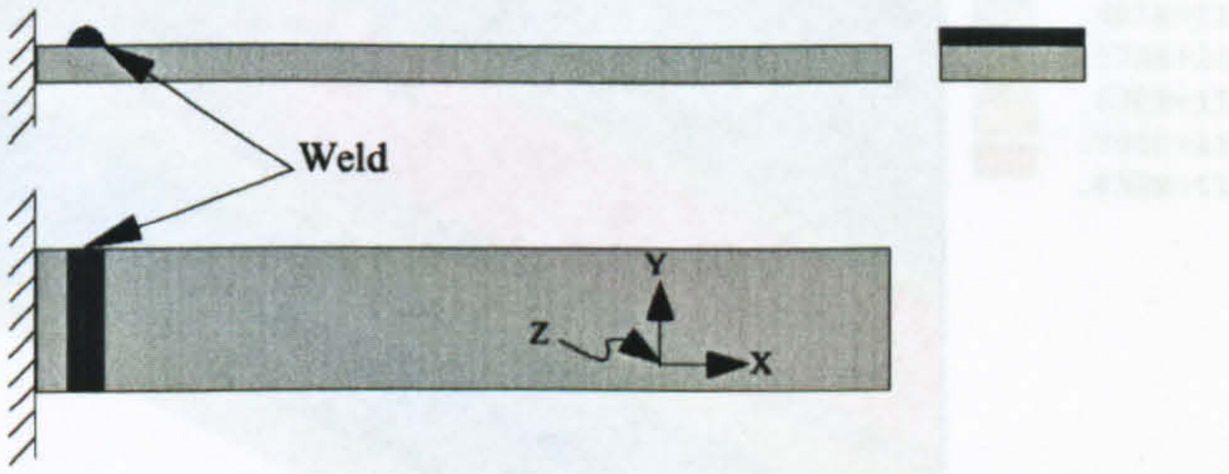

Figure 4.7 - Model of cantilever beam for harmonic analysis

Investigation of Weld toe

The equivalent applied dynamic stress to the specimen are shown in the two Figures 4.8 and 4.9 below where the mid width in the HAZ shows the maximum applied stresses. This analysis was carried out to co-relate with the analysis in Experiment VIII.

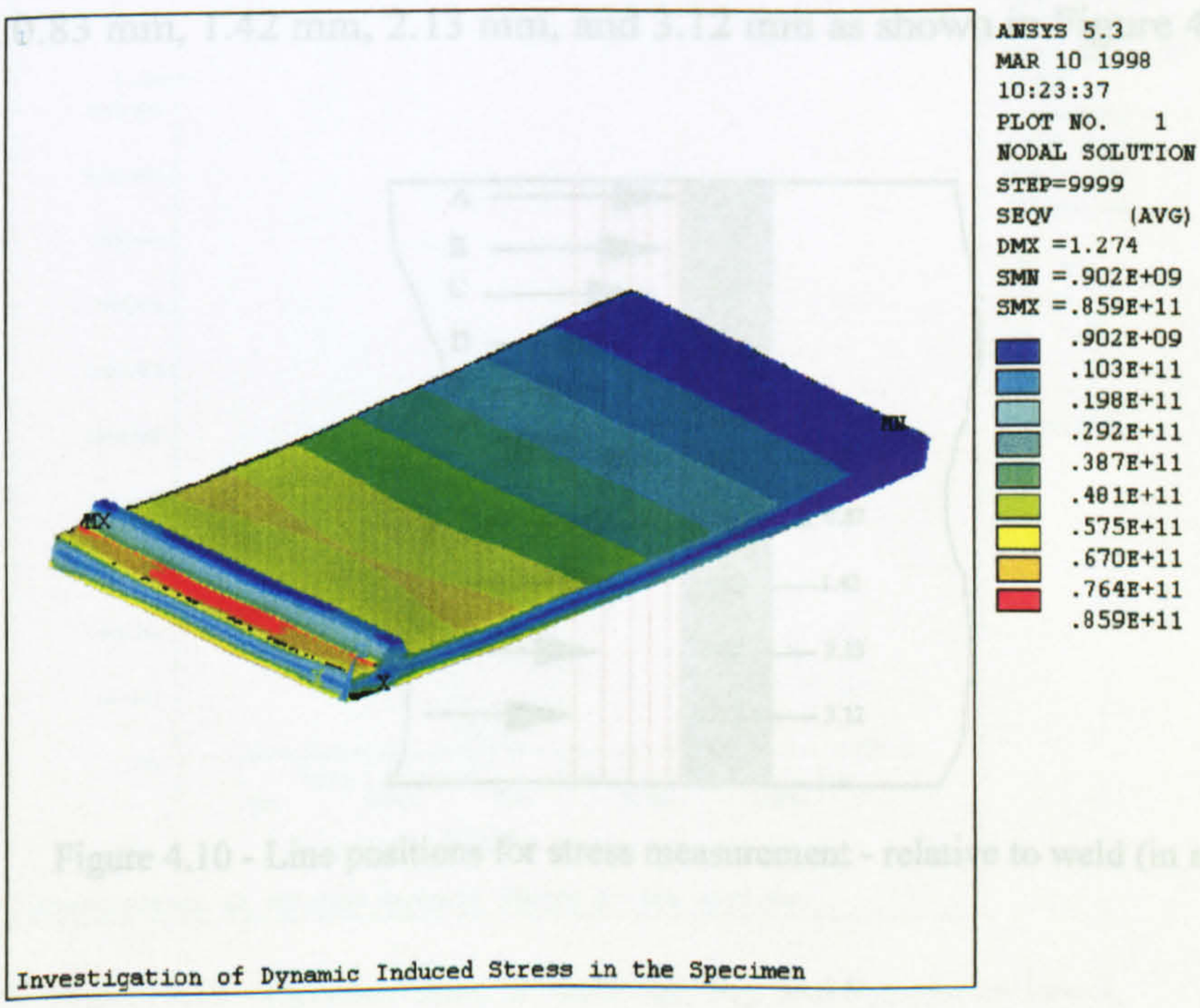

Figure 4.8 - Equivalent stress plot of cantilever beam

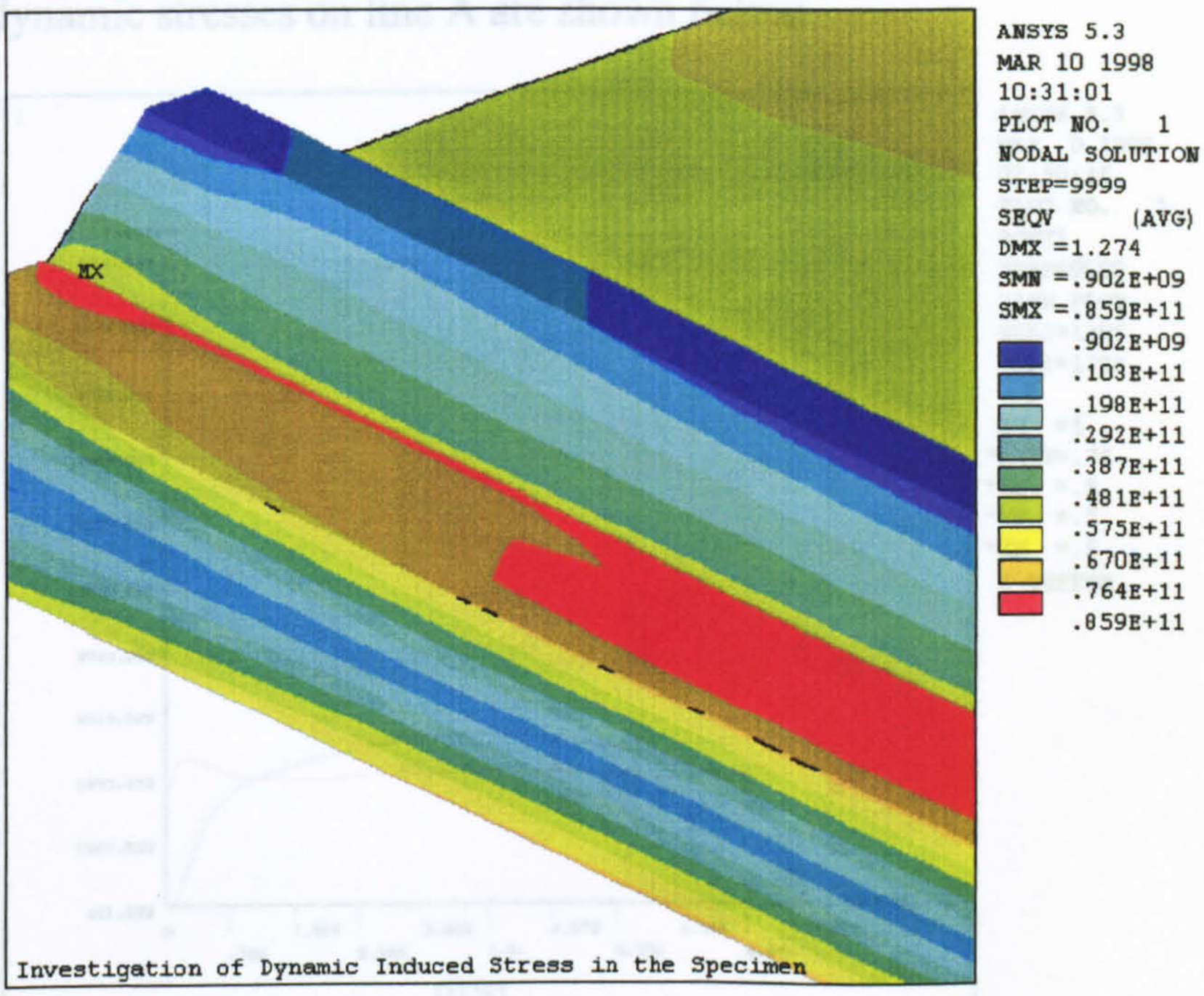

Figure 4.9 - Equivalent stress plot of cantilever beam (zoomed half of the plate width)

To analyse the applied dynamic stresses, strains, etc. in the HAZ (where X-ray measurements were carried out to investigate VSR effects), six lines were selected (line A, B, C, D, E and F). The distances of the lines from the weld toe were 0.37 mm, 0.83 mm, 1.42 mm, 2.13 mm, and 3.12 mm as shown in Figure 4.10 below.

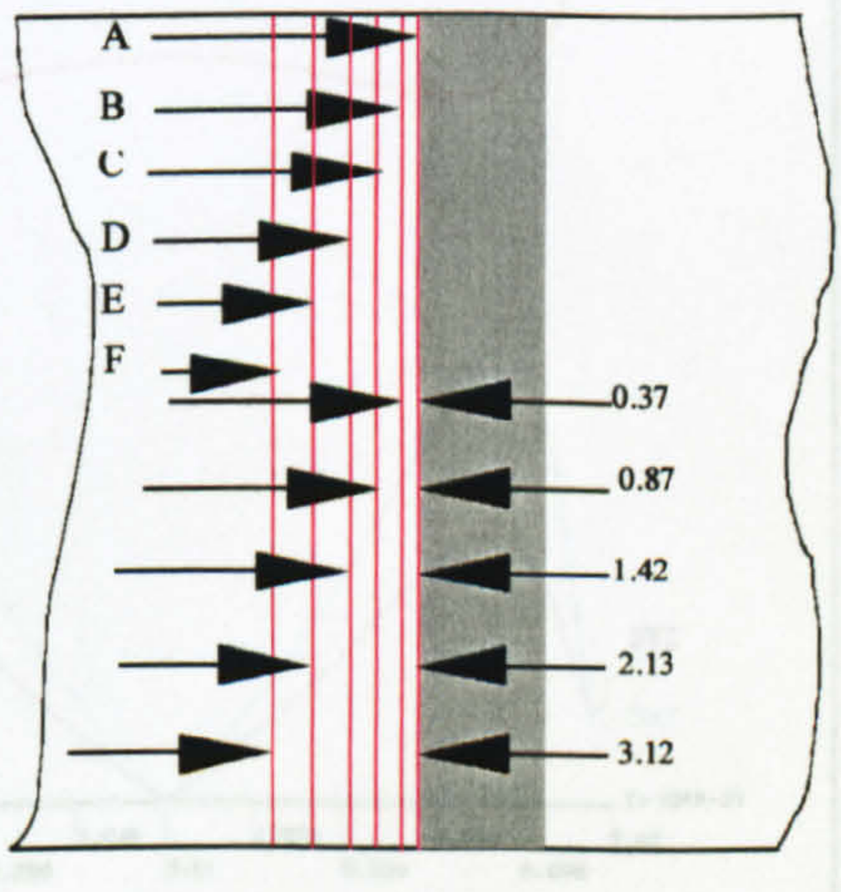

Figure 4.10 - Line positions for stress measurement - relative to weld (in mm)

The dynamic stresses on line A are shown below

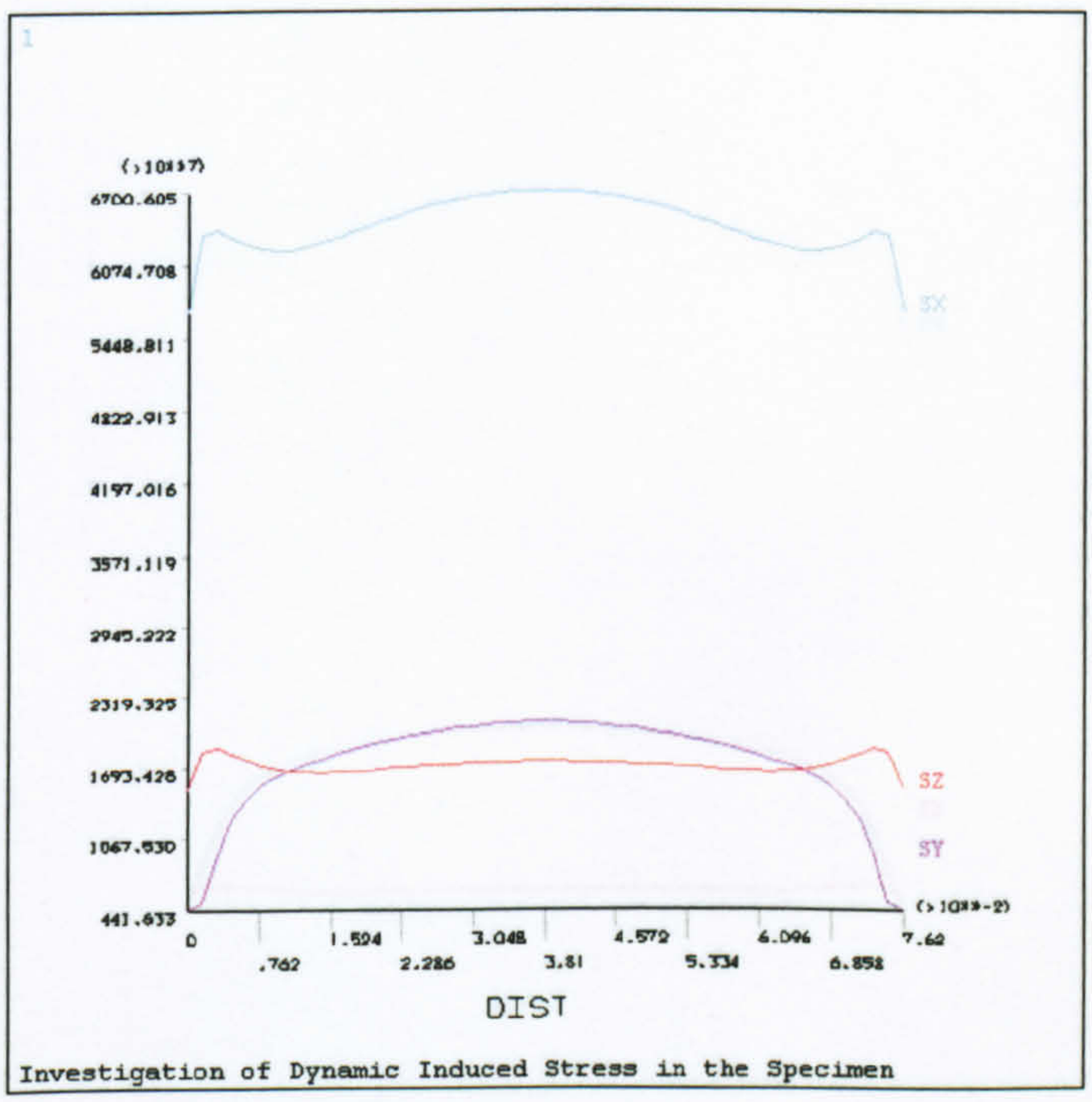

Figure 4.11 - Dynamic stresses S_X, S_Y, and S_Z plot on line A

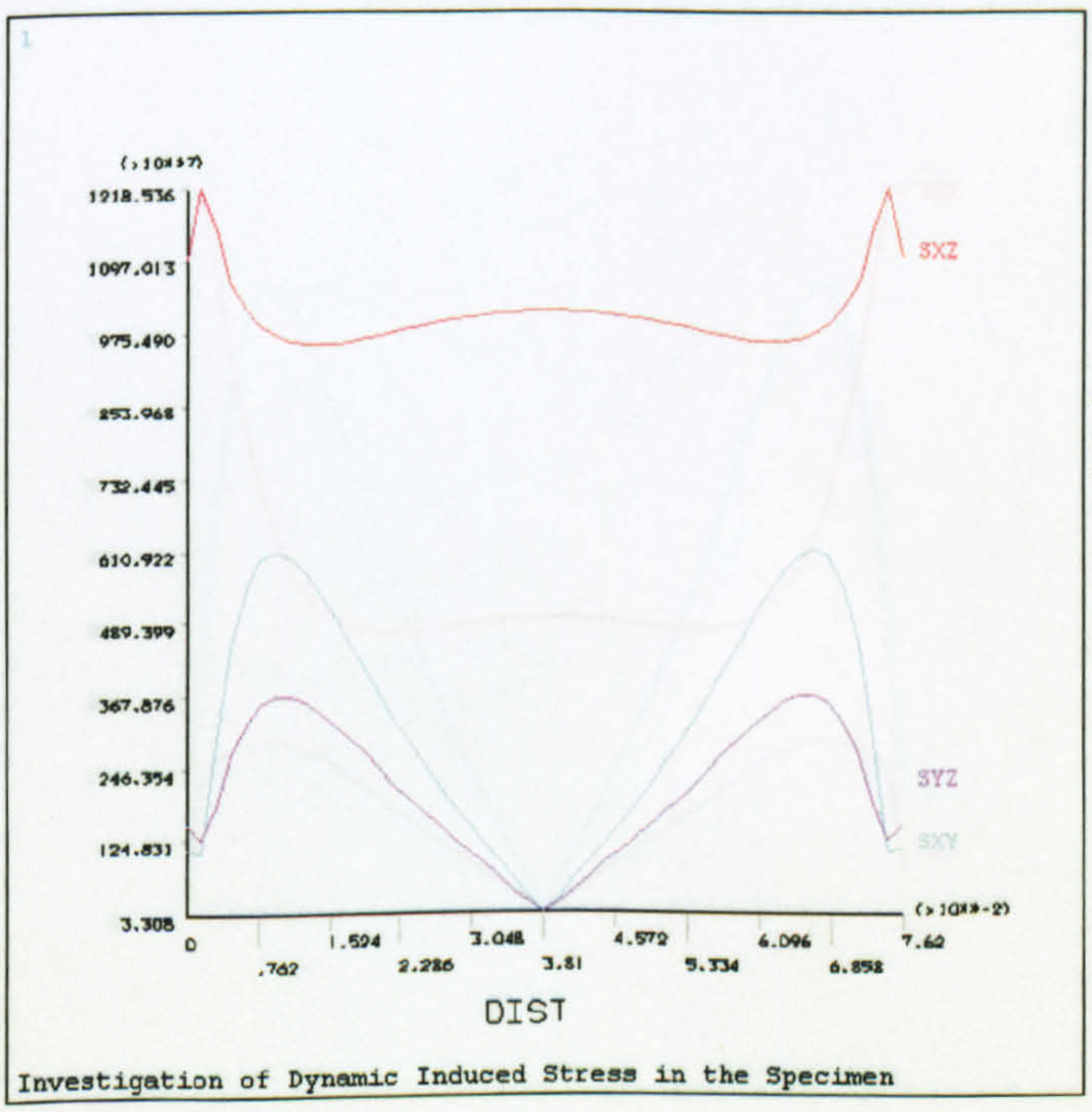

Figure 4.12 - Dynamic shear stresses S_{XY}, S_{YZ}, and S_{ZX} plot on line A

The dynamic stresses for line B are shown below

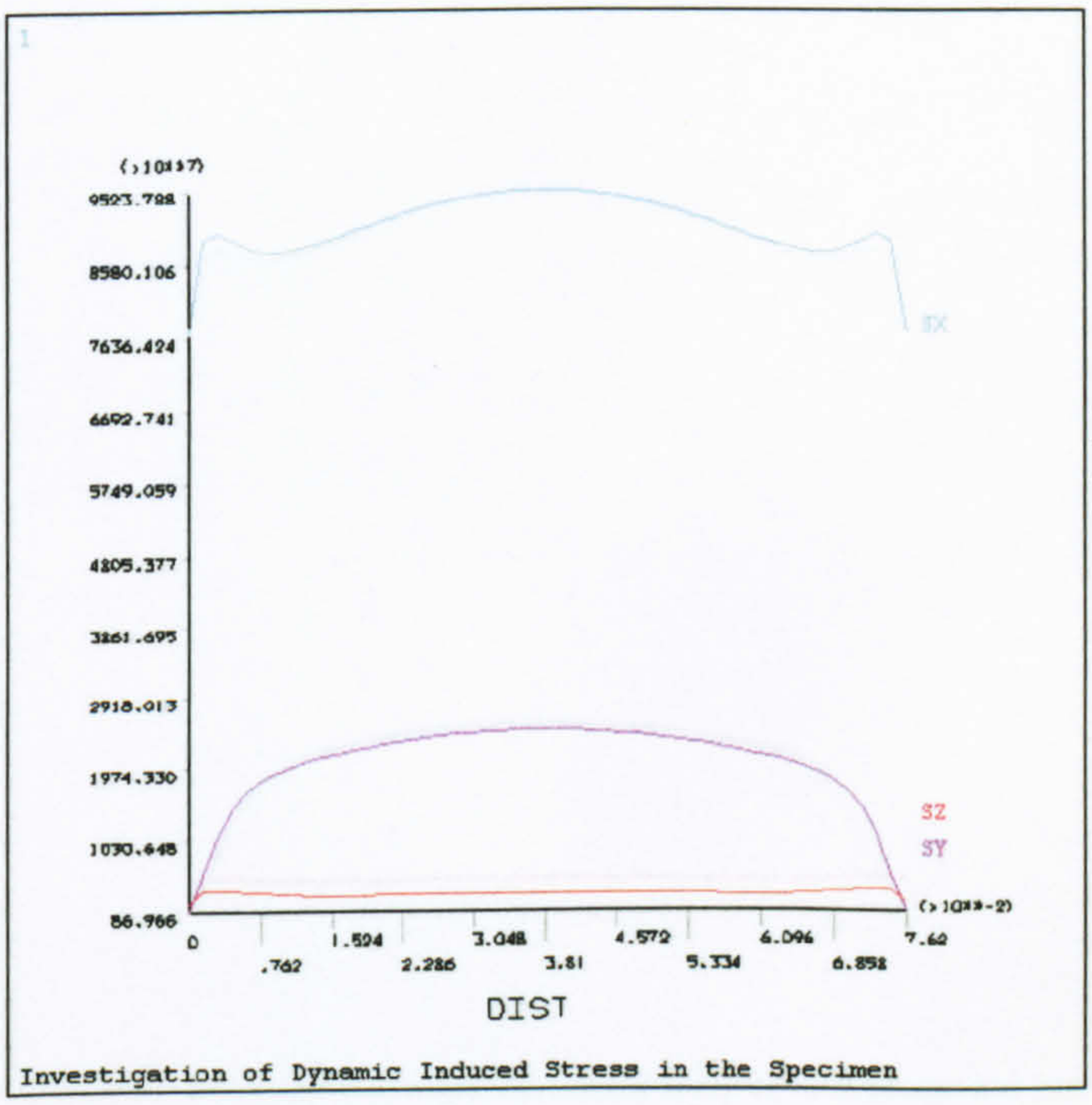

Figure 4.13 - Dynamic stresses S_X, S_Y, and S_Z plot on line B

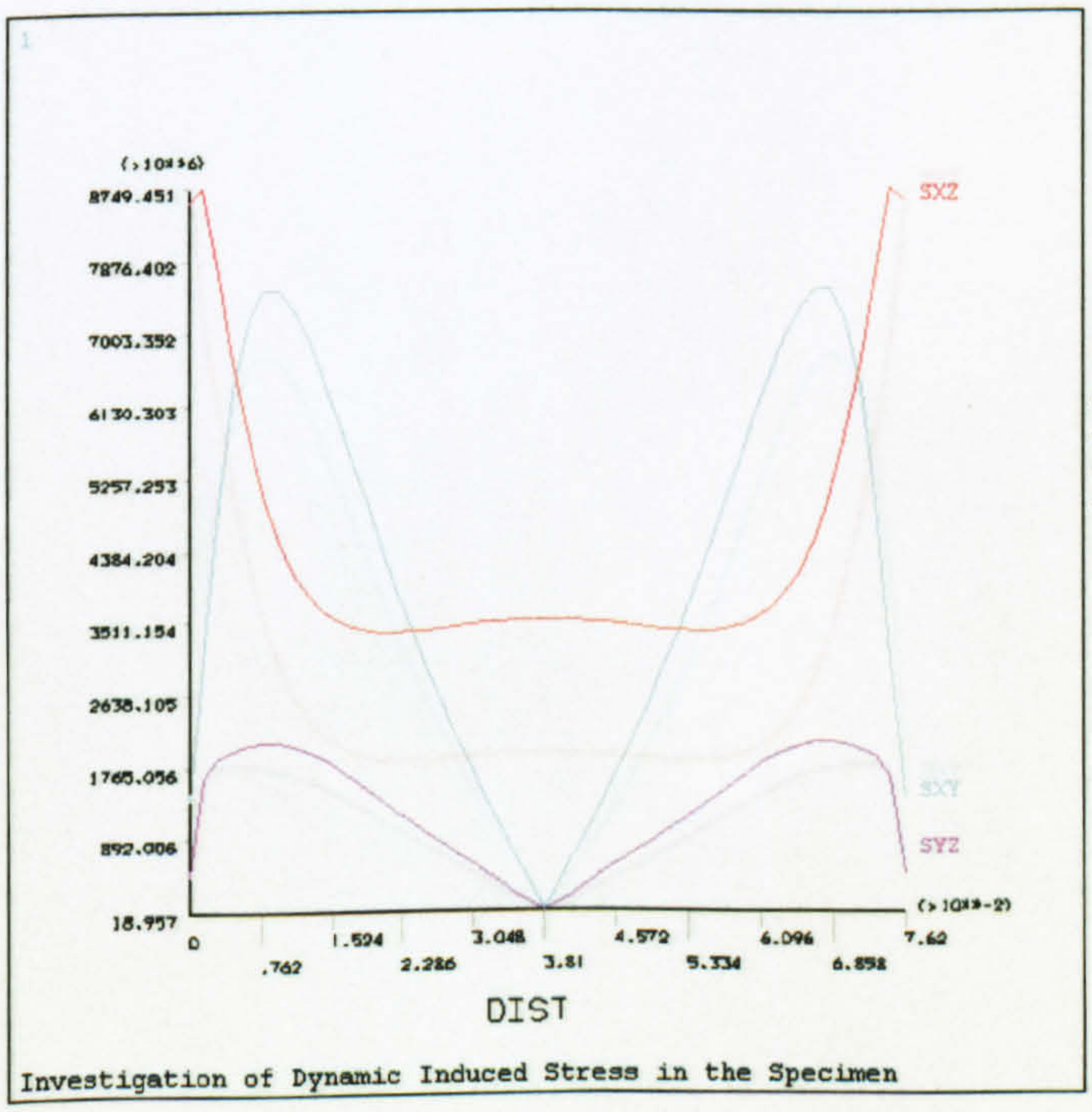

Figure 4.14 - Dynamic shear stresses S_{XY}, S_{YZ}, and S_{ZX} plot on line B

The dynamic stresses for line C are shown below

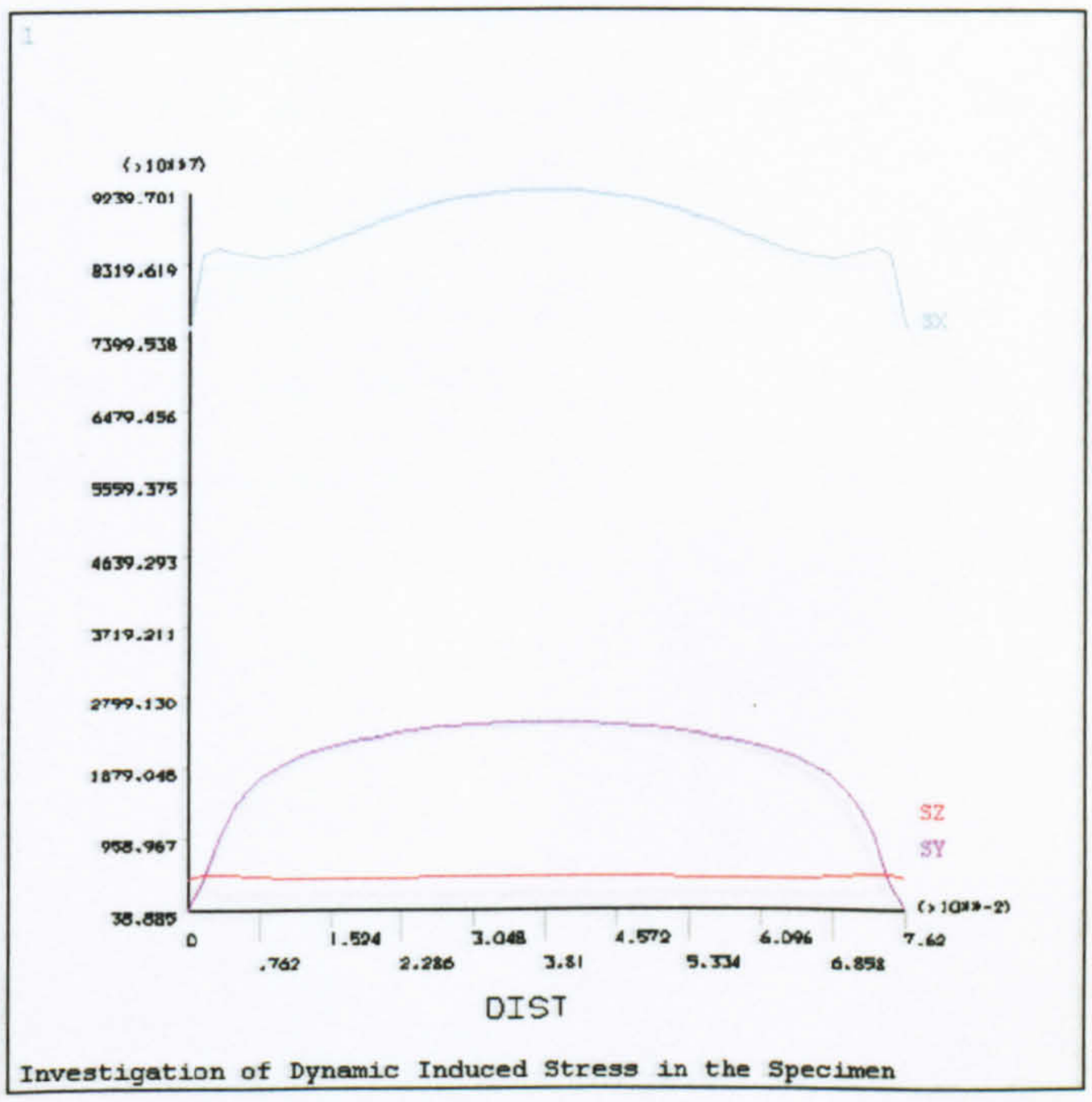

Figure 4.15 - Dynamic stresses S_X, S_Y, and S_Z plot on line C

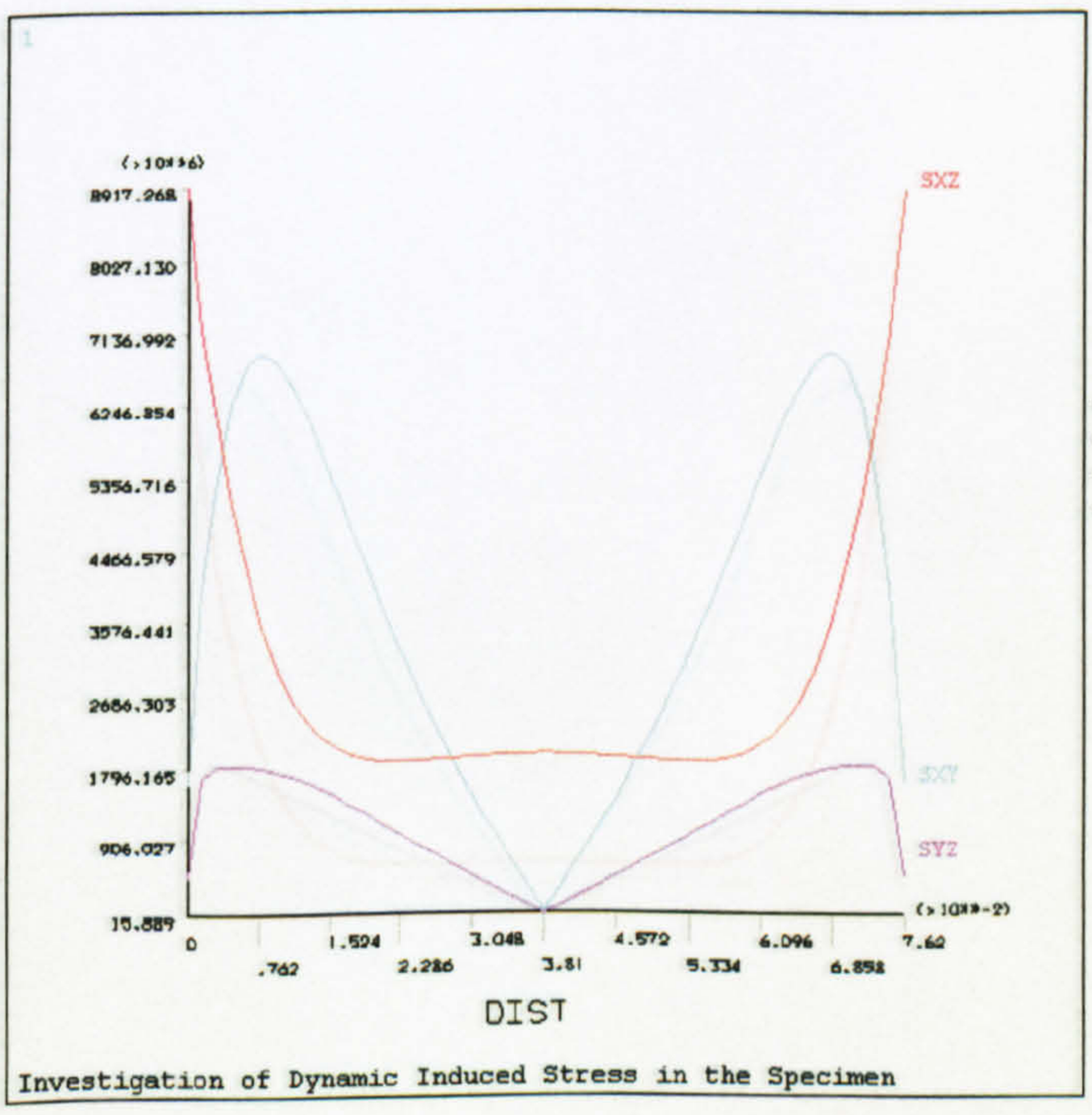

Figure 4.16 - Dynamic shear stresses S_{XY}, S_{YZ}, and S_{ZX} plot of line C

The dynamic stresses for line D are shown below

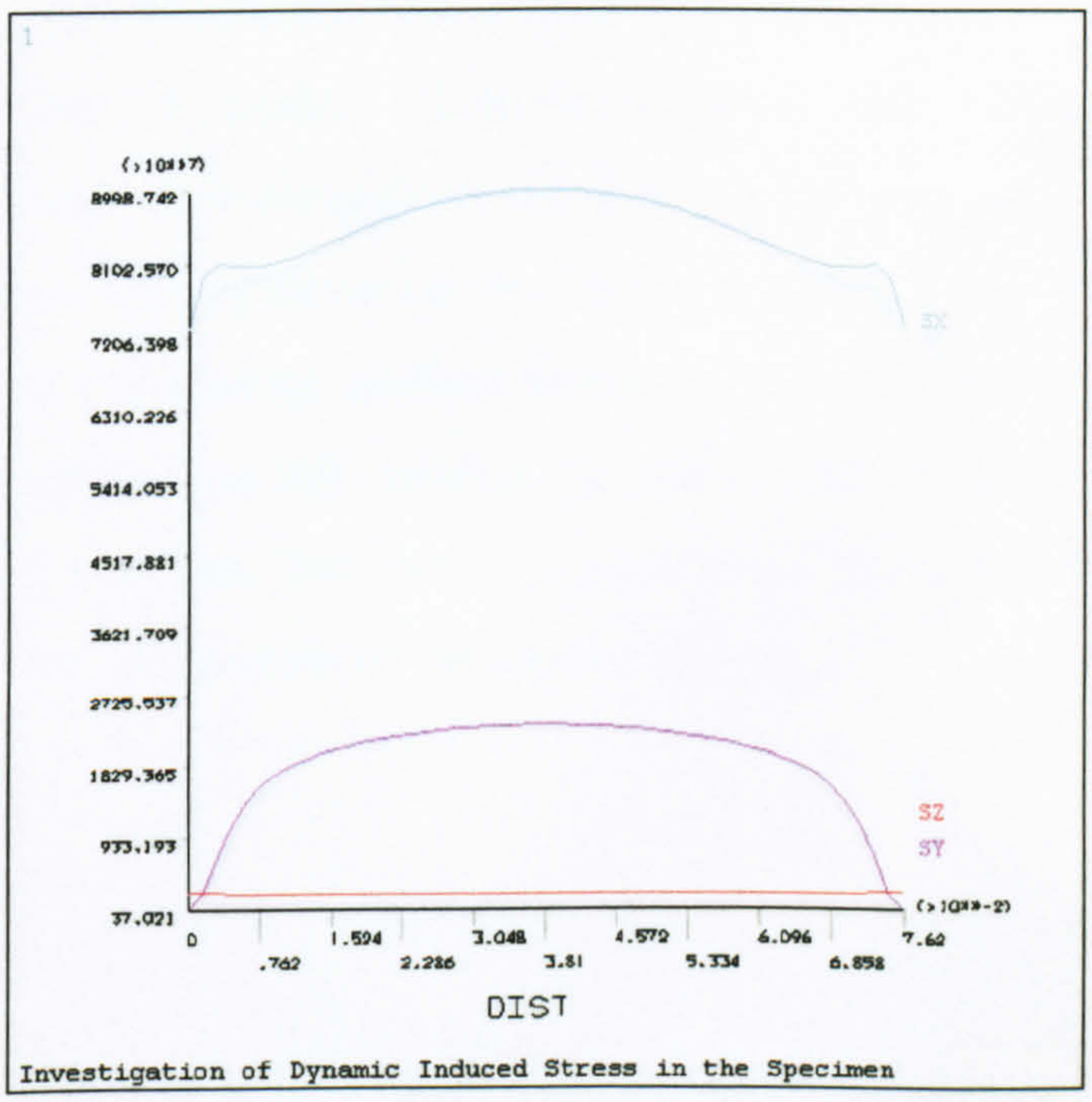

Figure 4.17 - Direct stress plot on line D

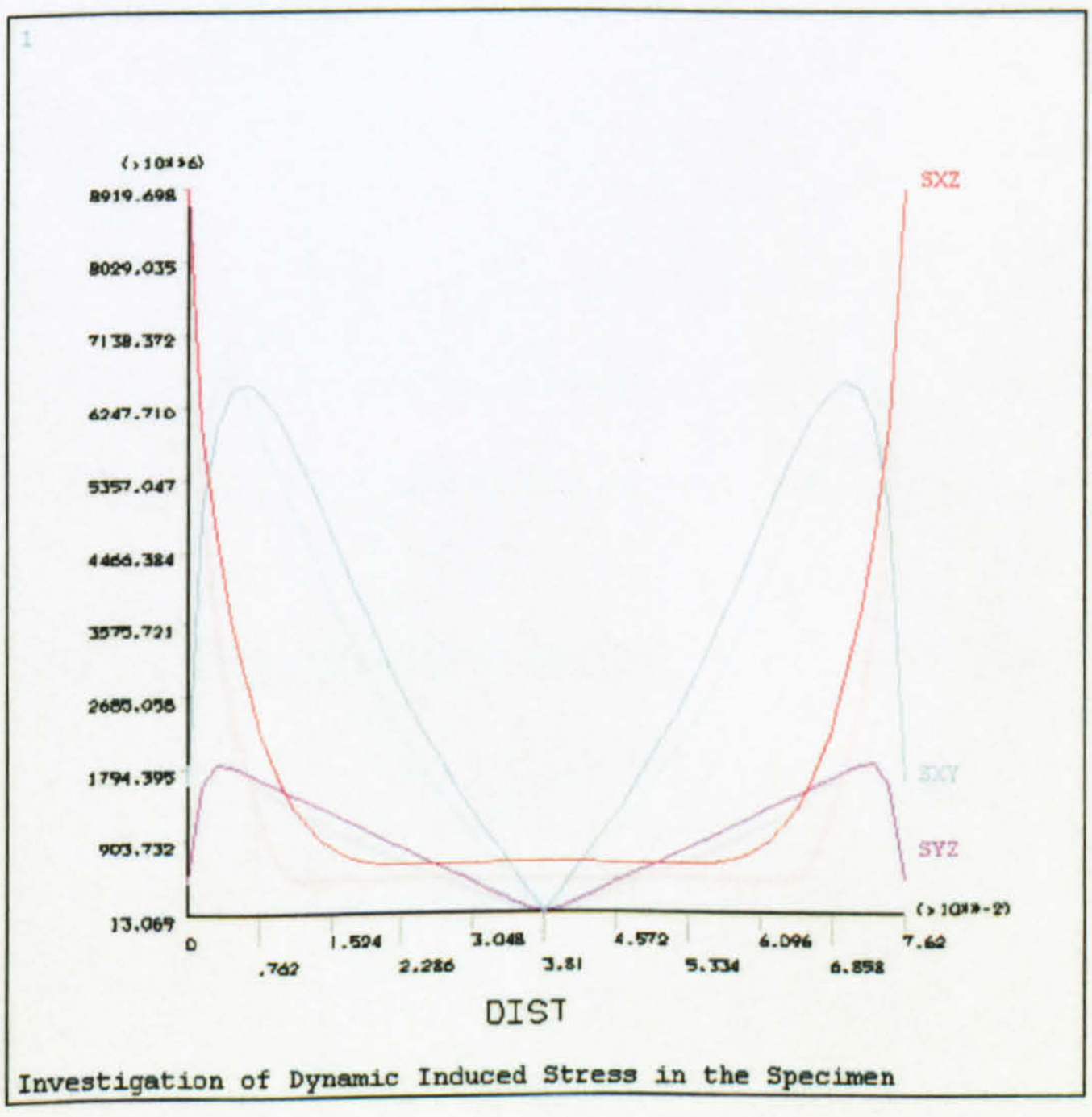

Figure 4.18 - Applied shear stresses on line D

The dynamic stresses for line E are shown below

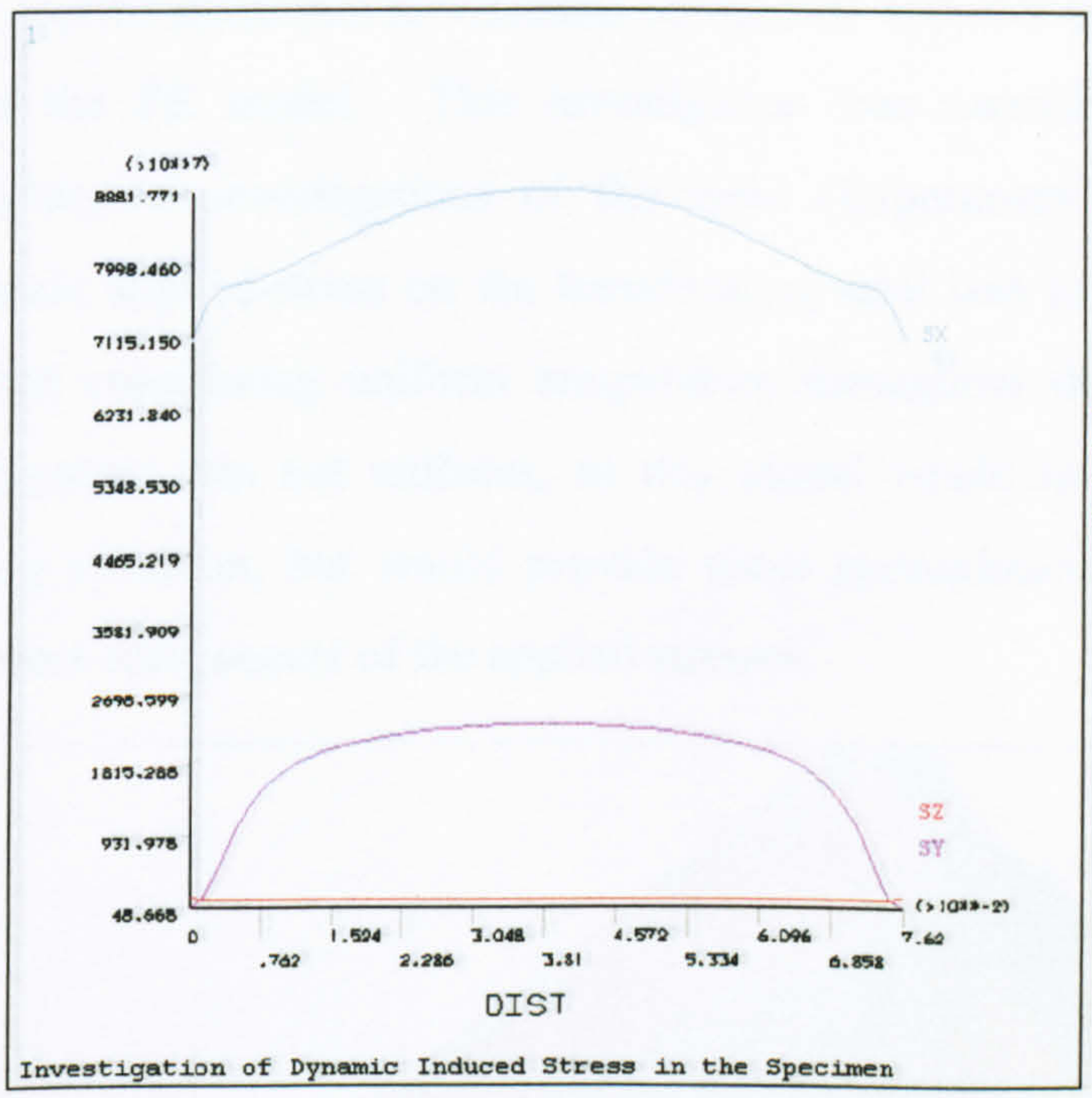

Figure 4.19 - Applied direct stresses on line E

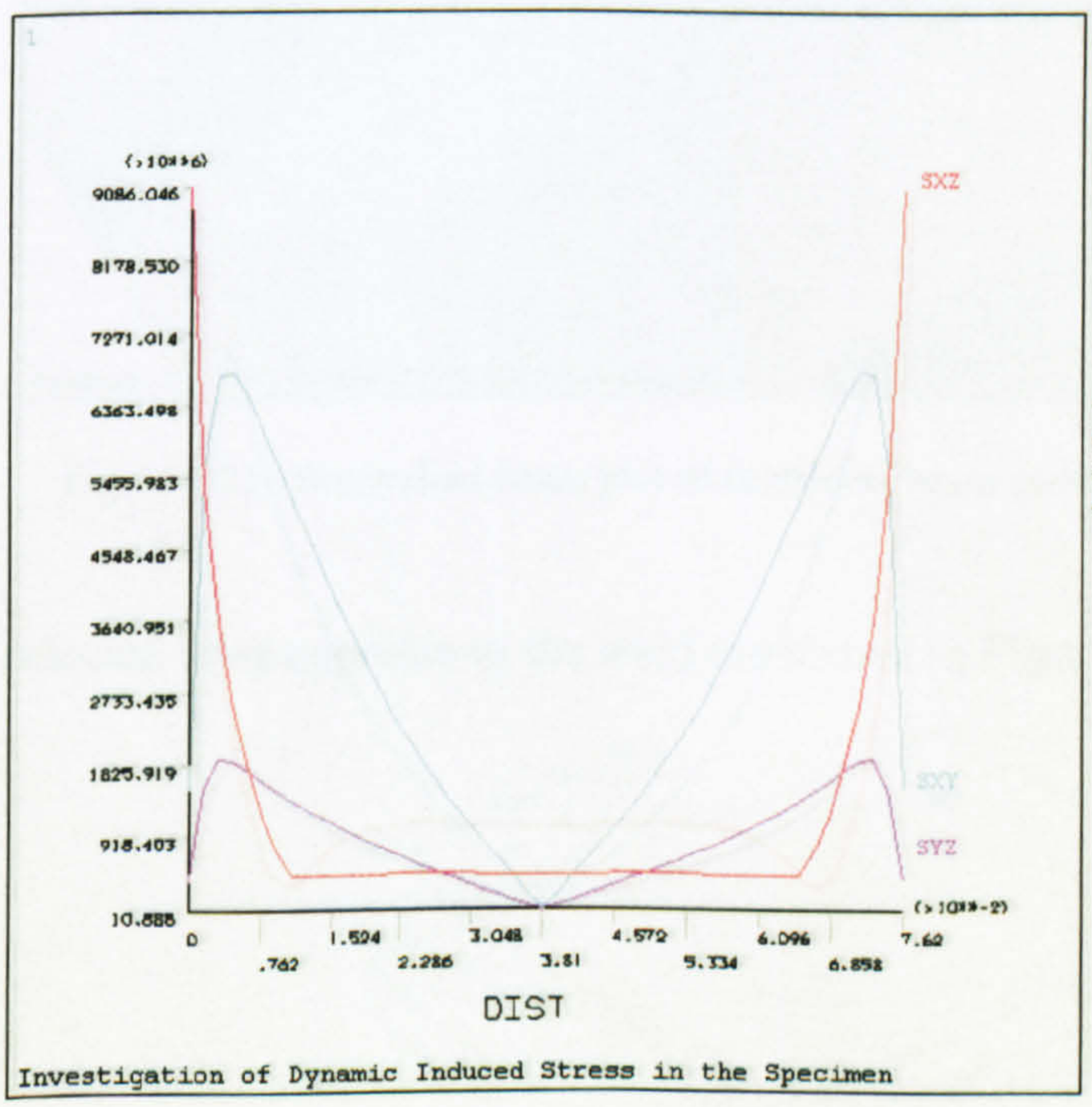

Figure 4.20 - Applied shear stresses on line E

The dynamic stresses for line F are shown below

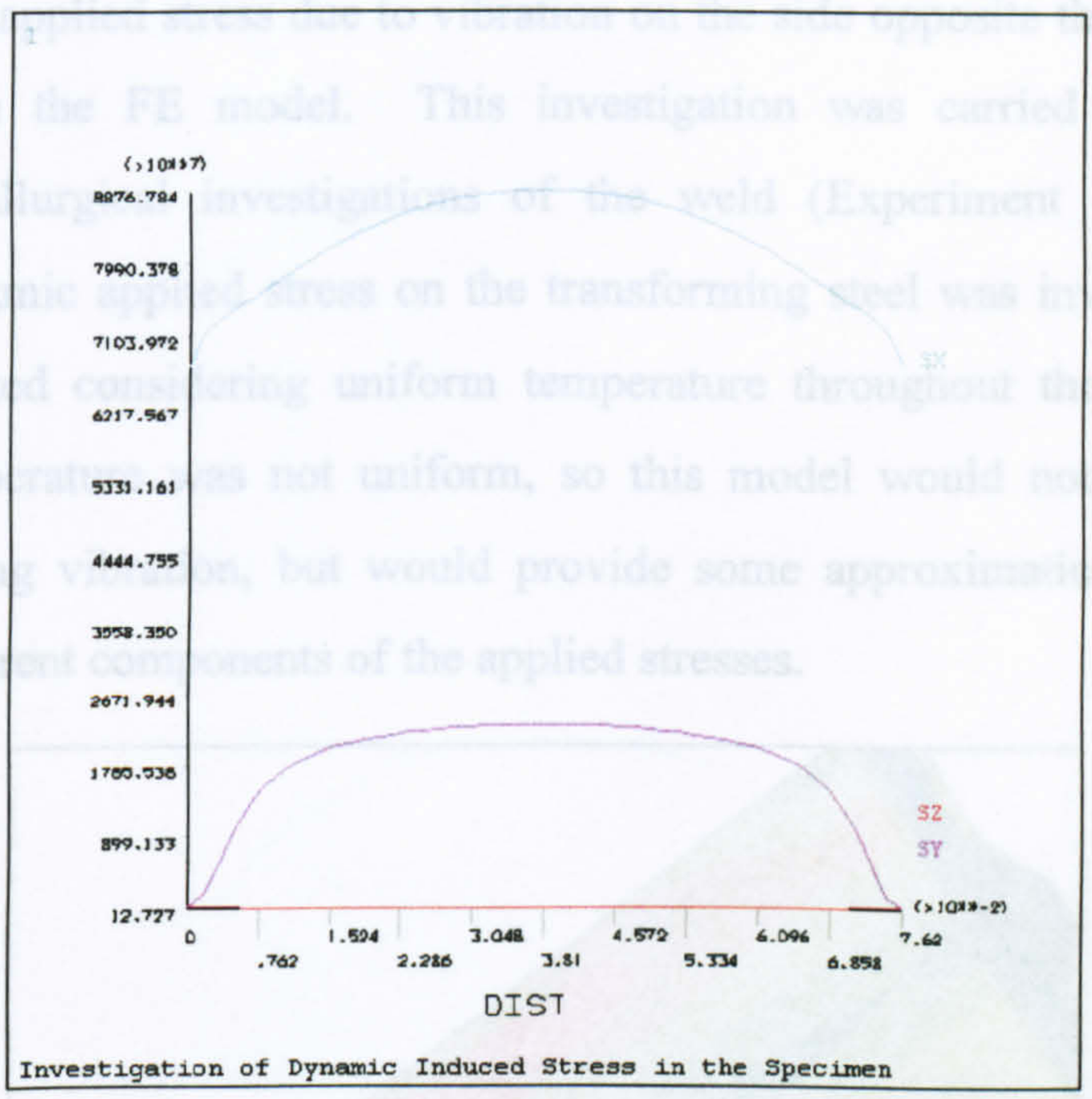

Figure 4.21 - Applied direct stresses on line F

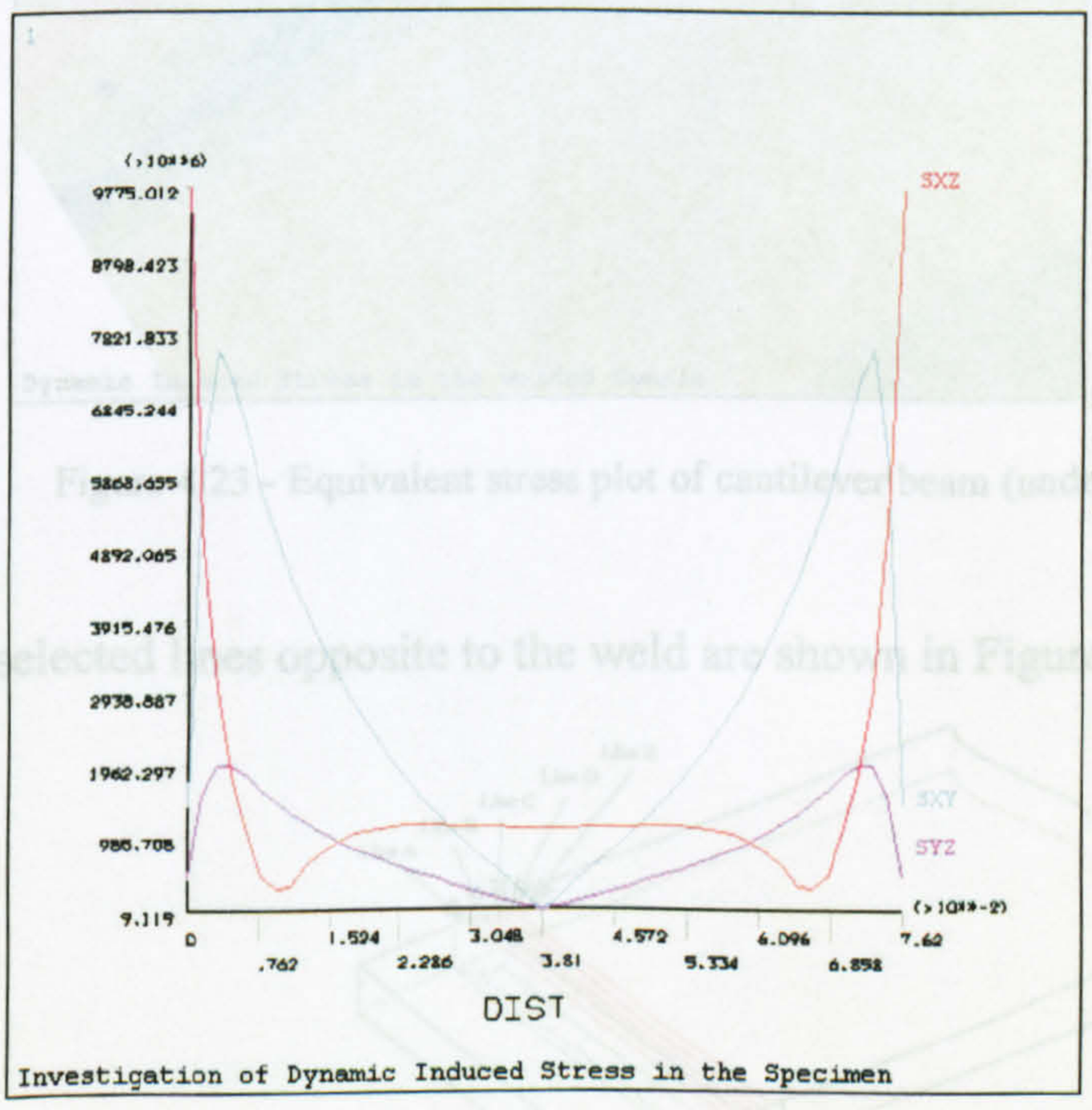

Figure 4.22 - Applied shear stresses of line F

Investigation of the Side Opposite the Weld

The applied stress due to vibration on the side opposite the weld was also determined from the FE model. This investigation was carried out to co-relate with the metallurgical investigations of the weld (Experiment XIII) where the effect of dynamic applied stress on the transforming steel was investigated. This model was created considering uniform temperature throughout the specimen. In reality the temperature was not uniform, so this model would not provide the exact stresses during vibration, but would provide some approximation about the distribution of different components of the applied stresses.

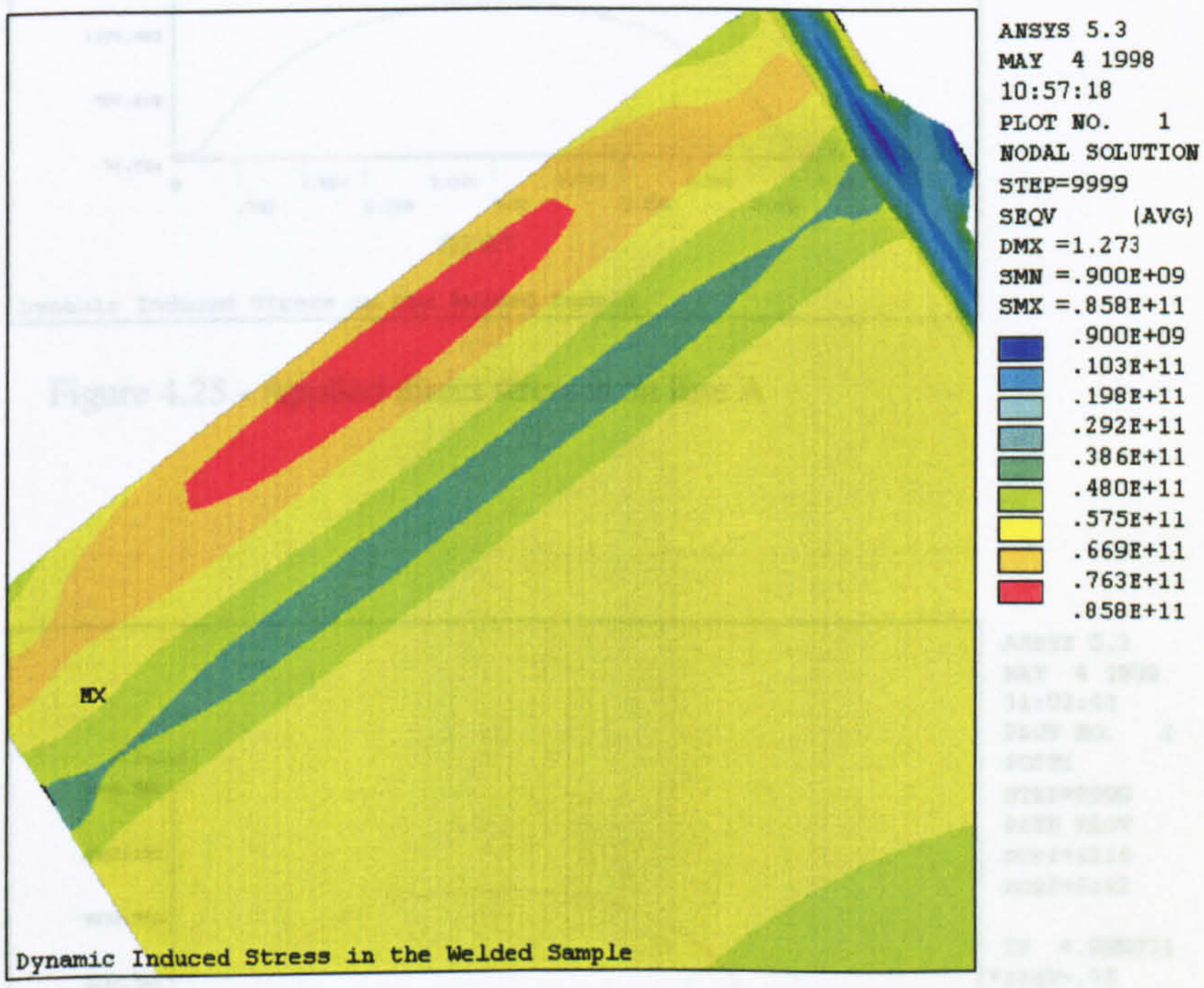

Figure 4.23 - Equivalent stress plot of cantilever beam (underside of weld bead)

The selected lines opposite to the weld are shown in Figure 4.24 below.

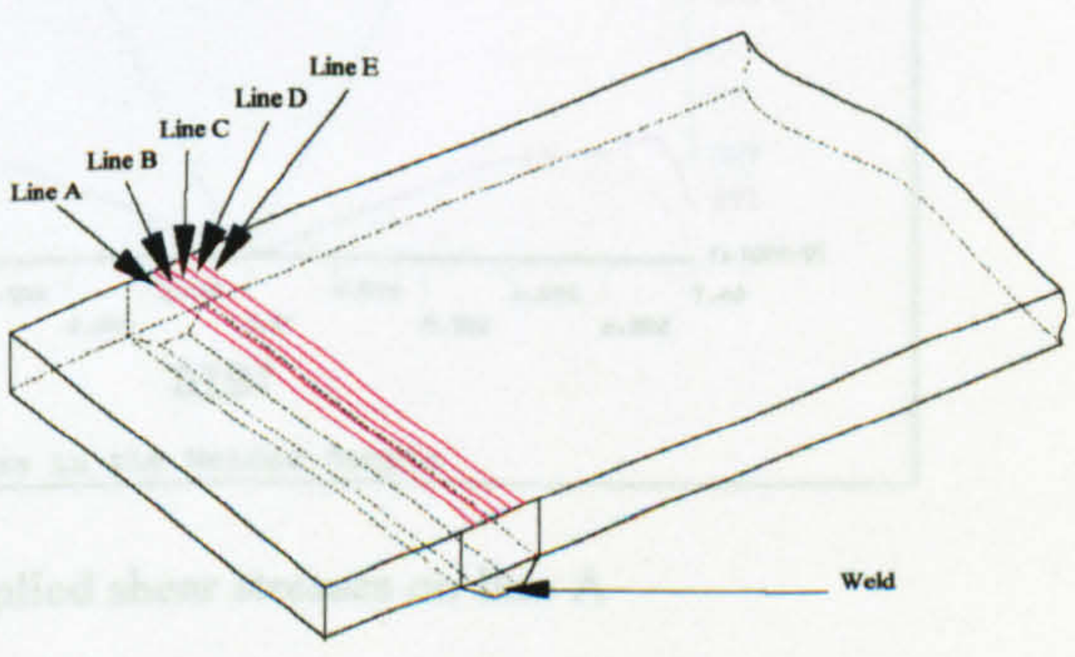

Figure 4.24 - Position of investigated lines in the heat affected parent metal.

Applied dynamic stresses on line A

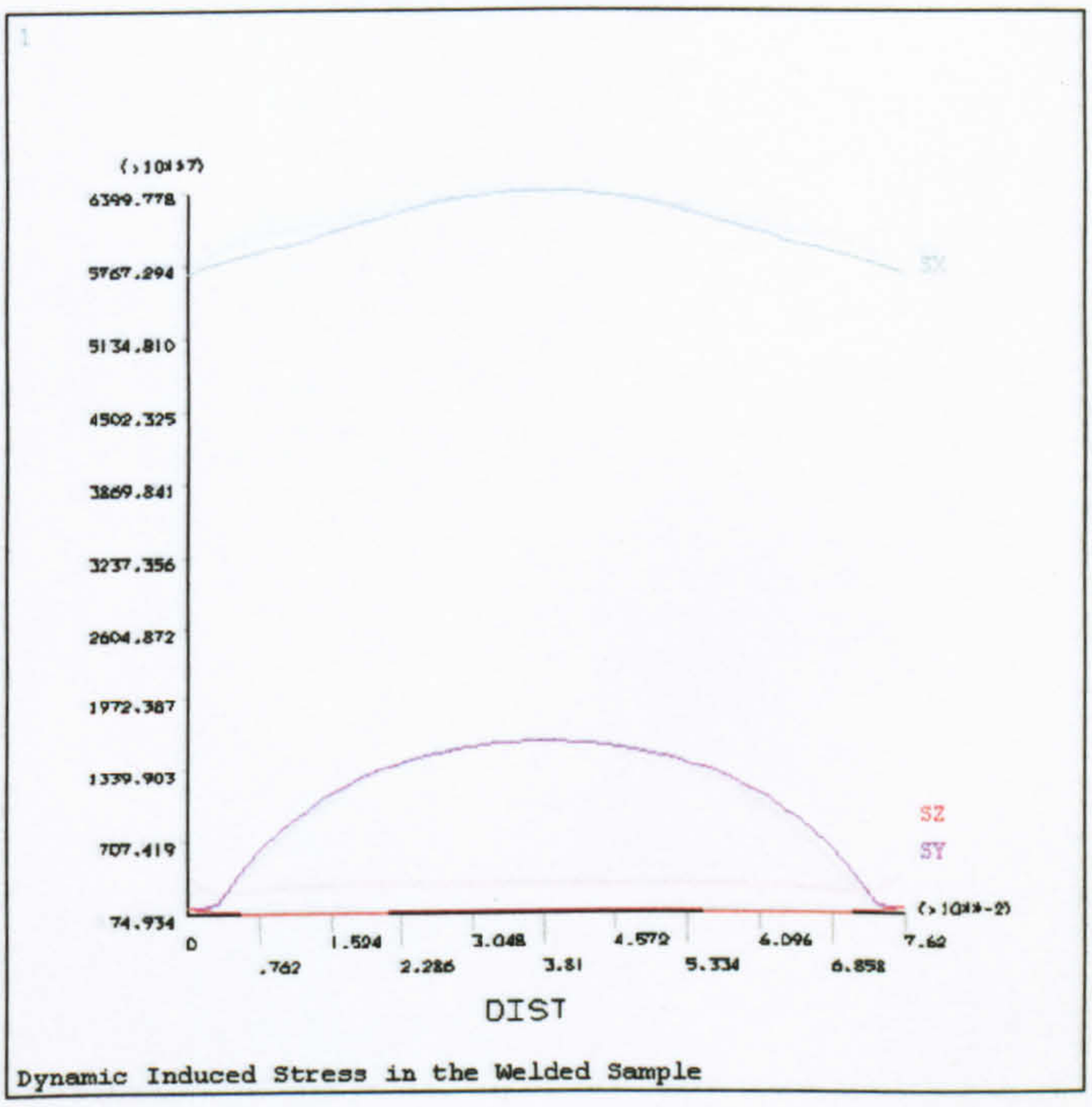

Figure 4.25 - Applied direct stresses on line A

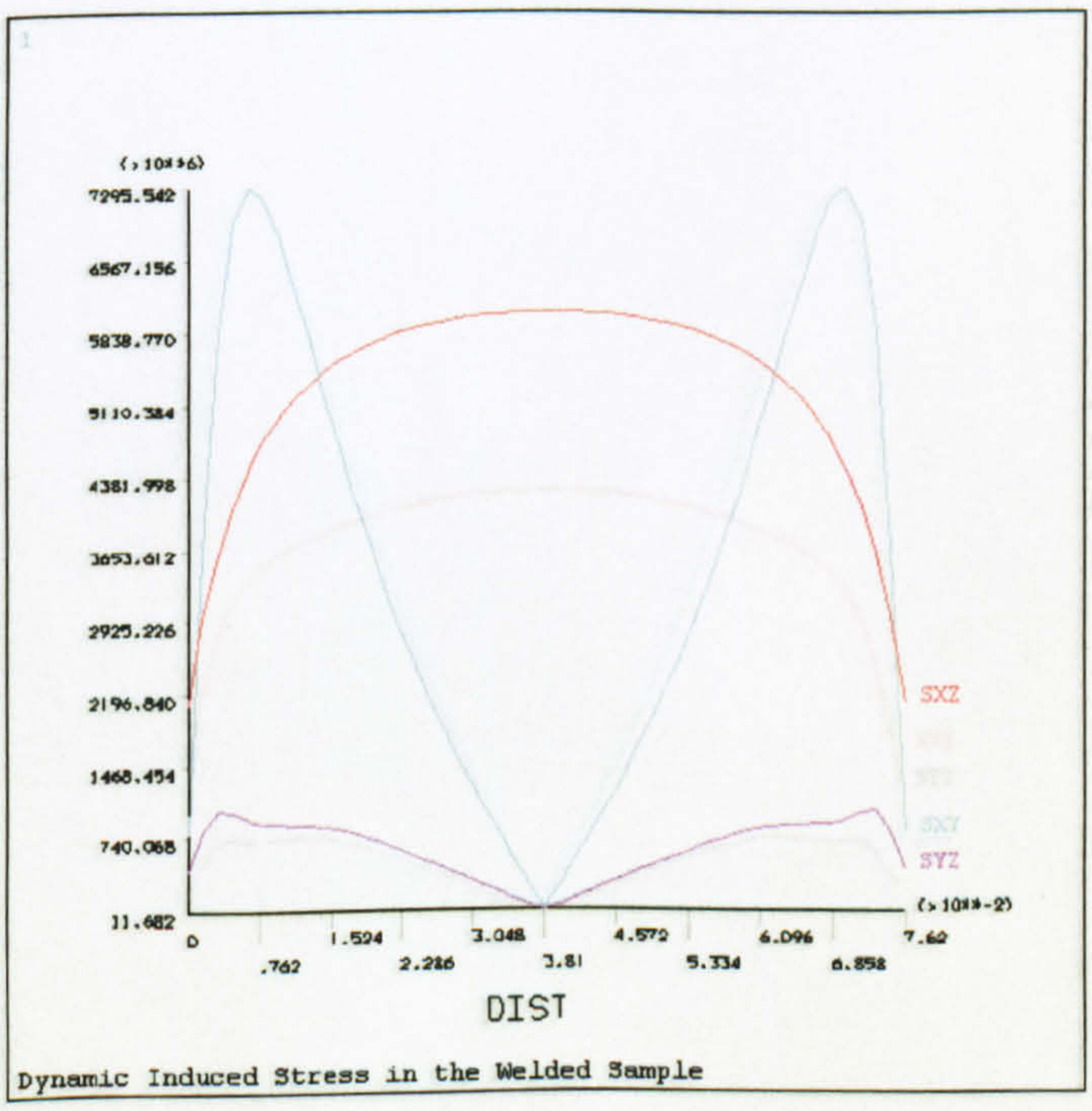

Figure 4.26 - Applied shear stresses on line A

Applied dynamic stresses on line B

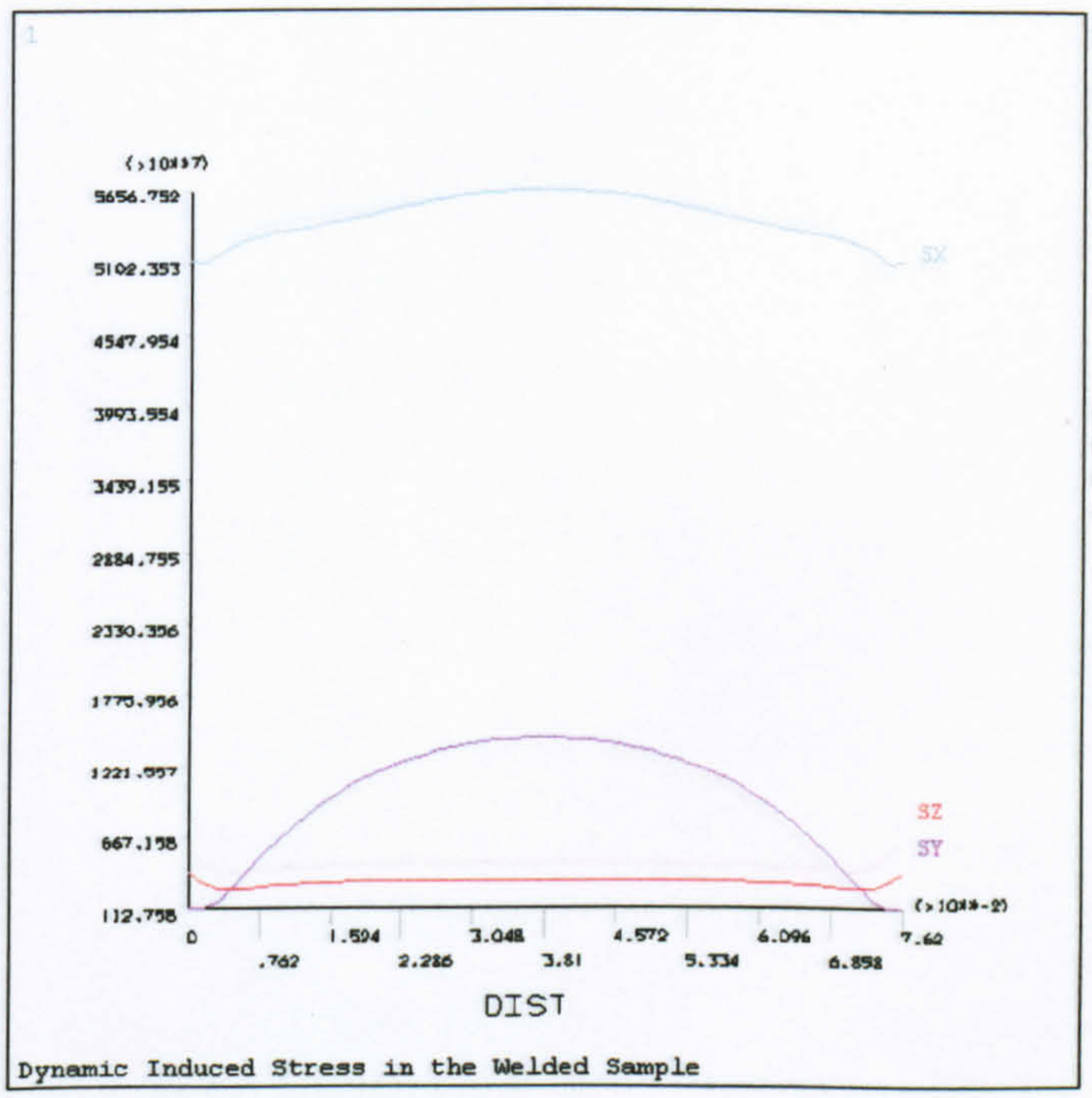

Figure 4.27 - Applied direct stresses on line B

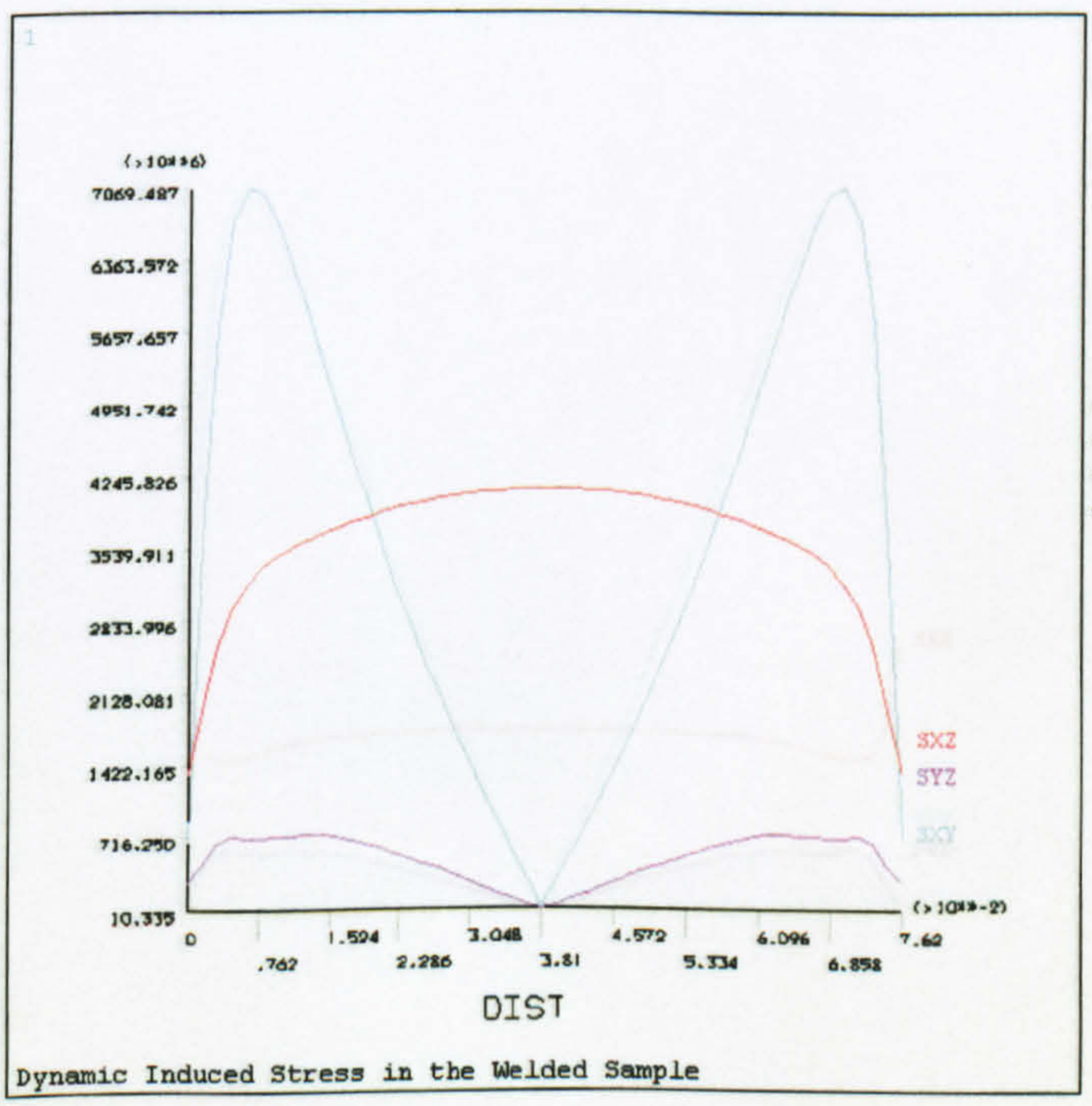

Figure 4.28 - Applied shear stresses on line B

Applied dynamic stresses on line C

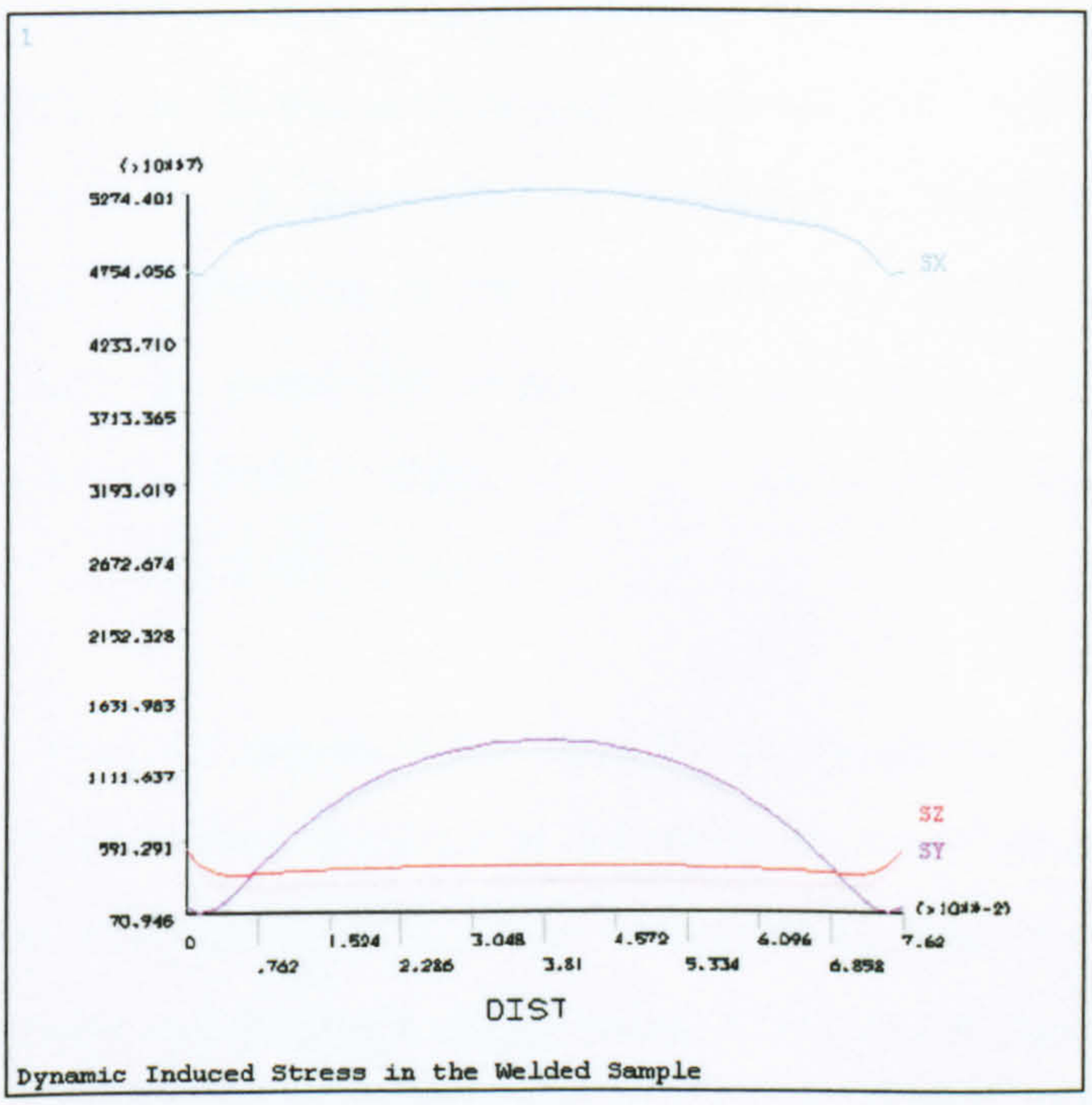

Figure 4.29 - Applied direct stresses on line C

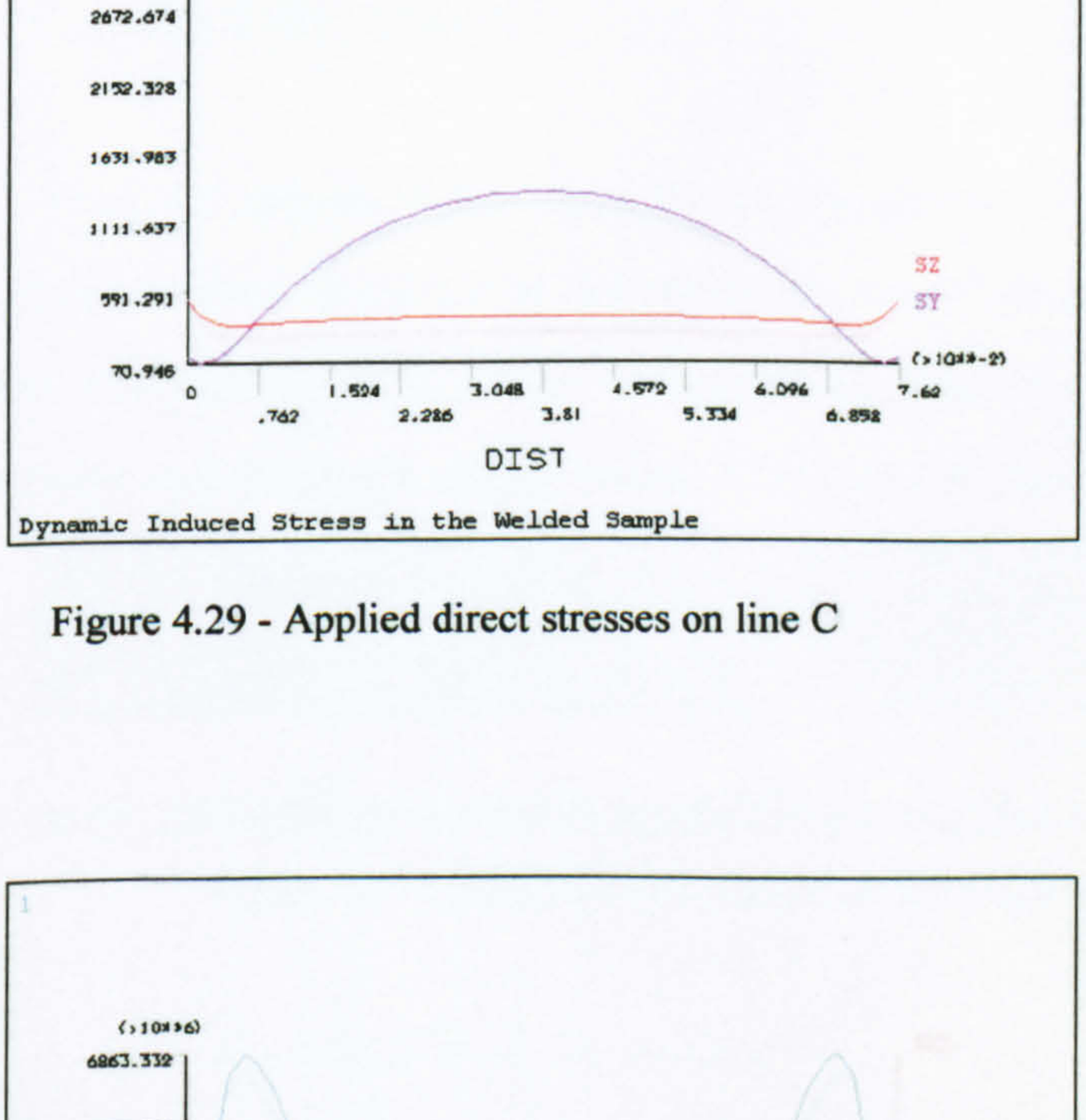

Figure 4.30 - Applied shear stresses on line C

Applied dynamic stresses of line D

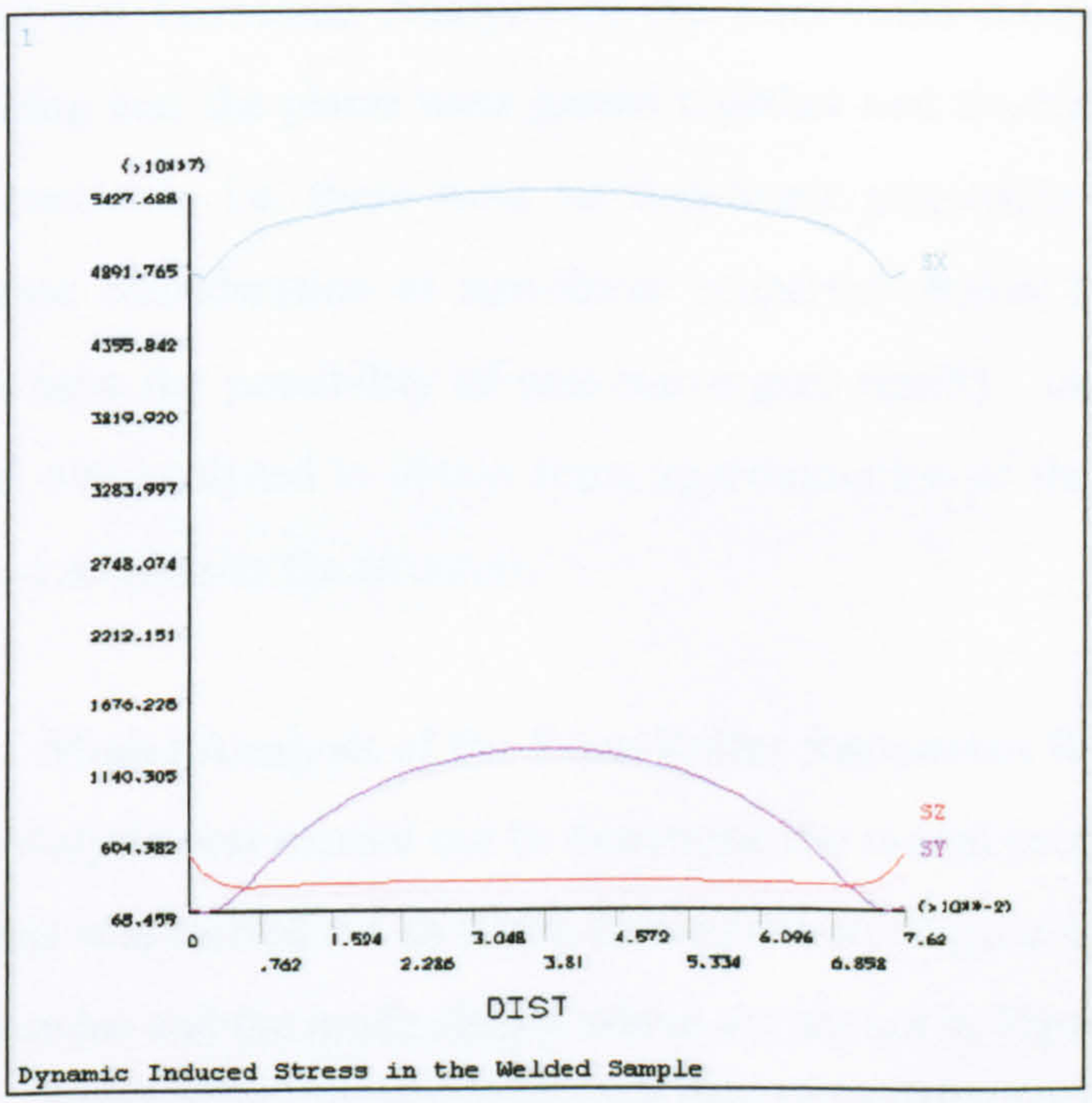

Figure 4.31 - Applied direct stresses on line D

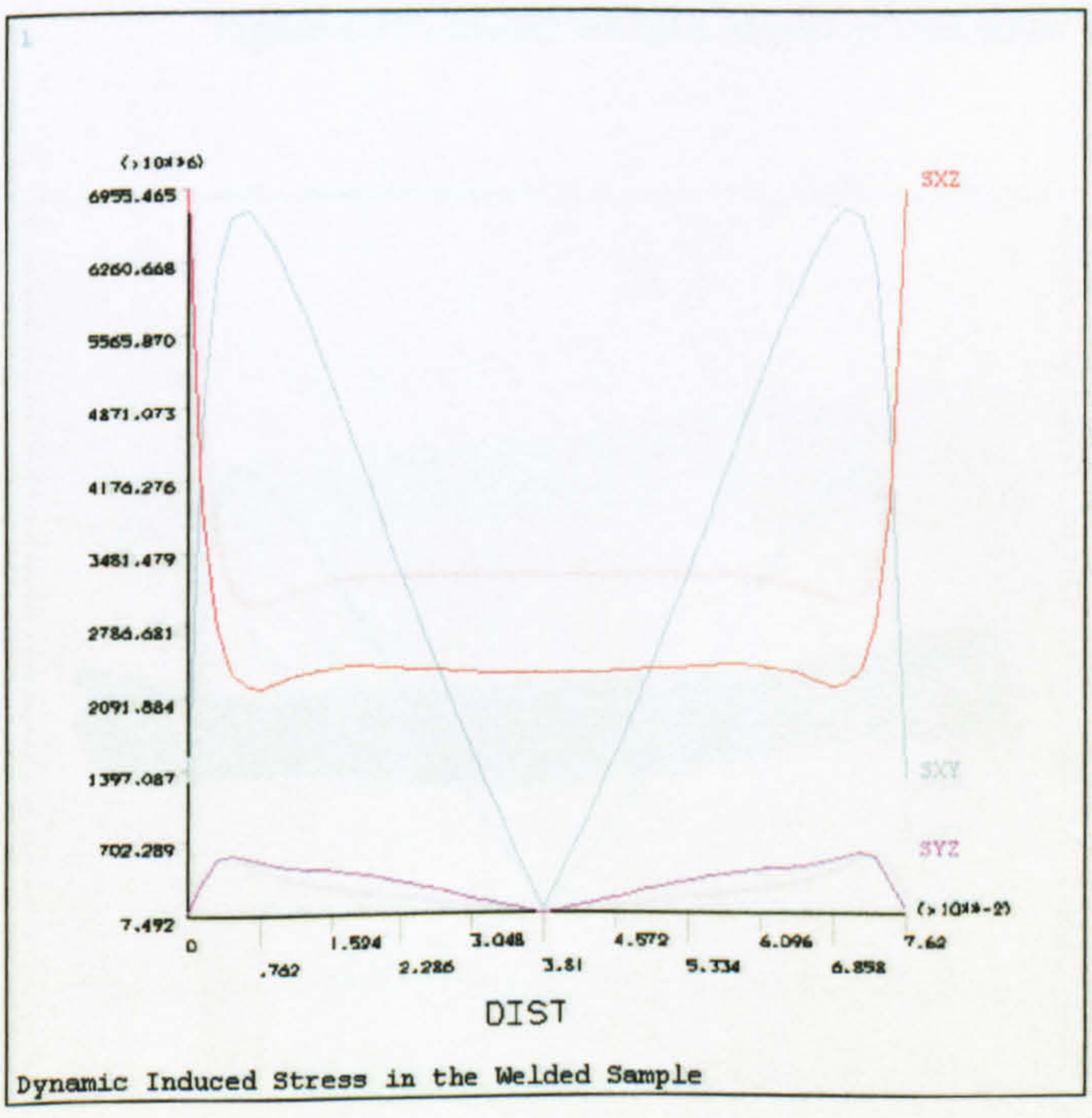

Figure 4.32 - Applied shear stresses on line D

Applied dynamic stresses on line E

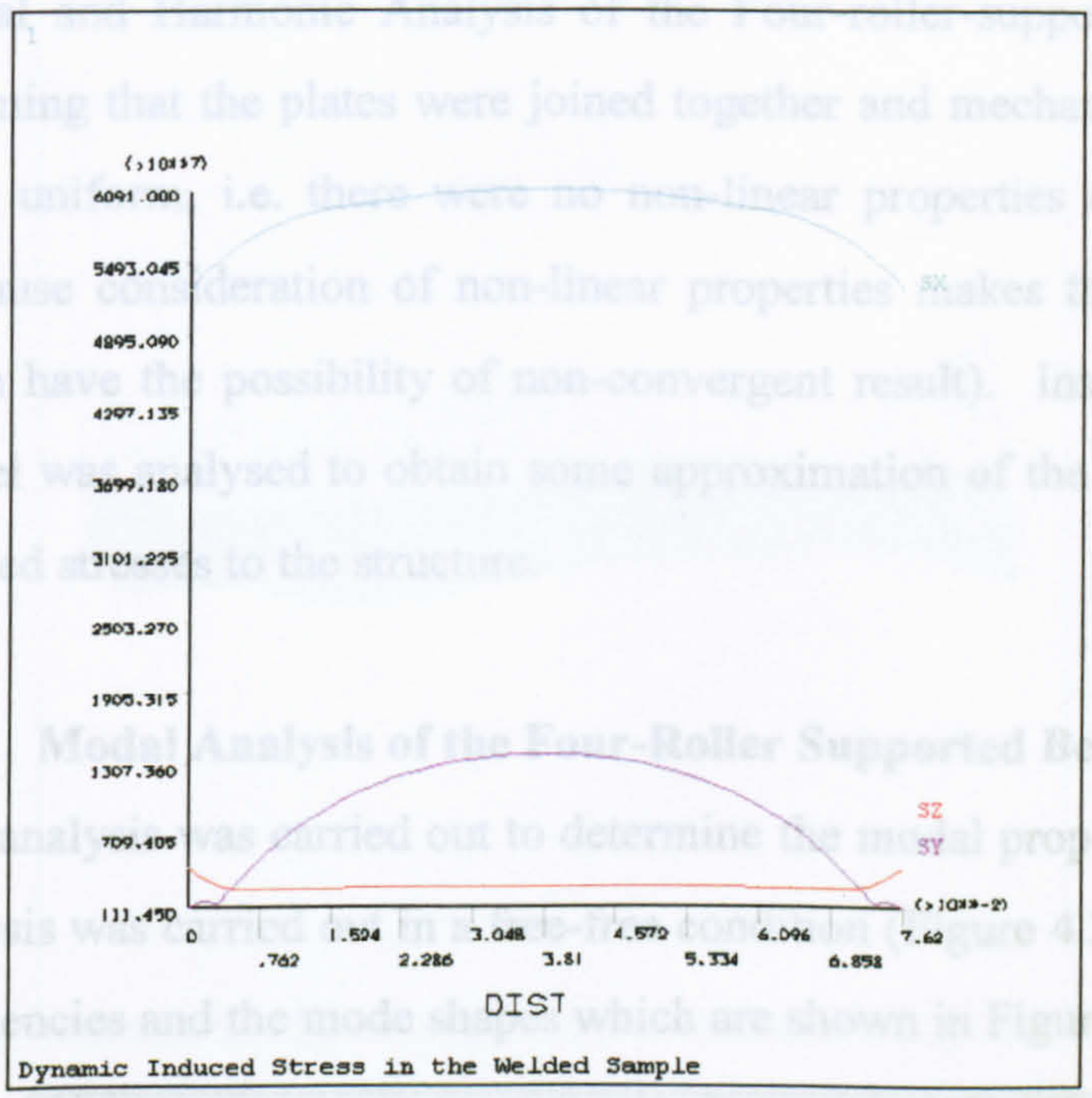

Figure 4.33 - Applied direct stresses on line E

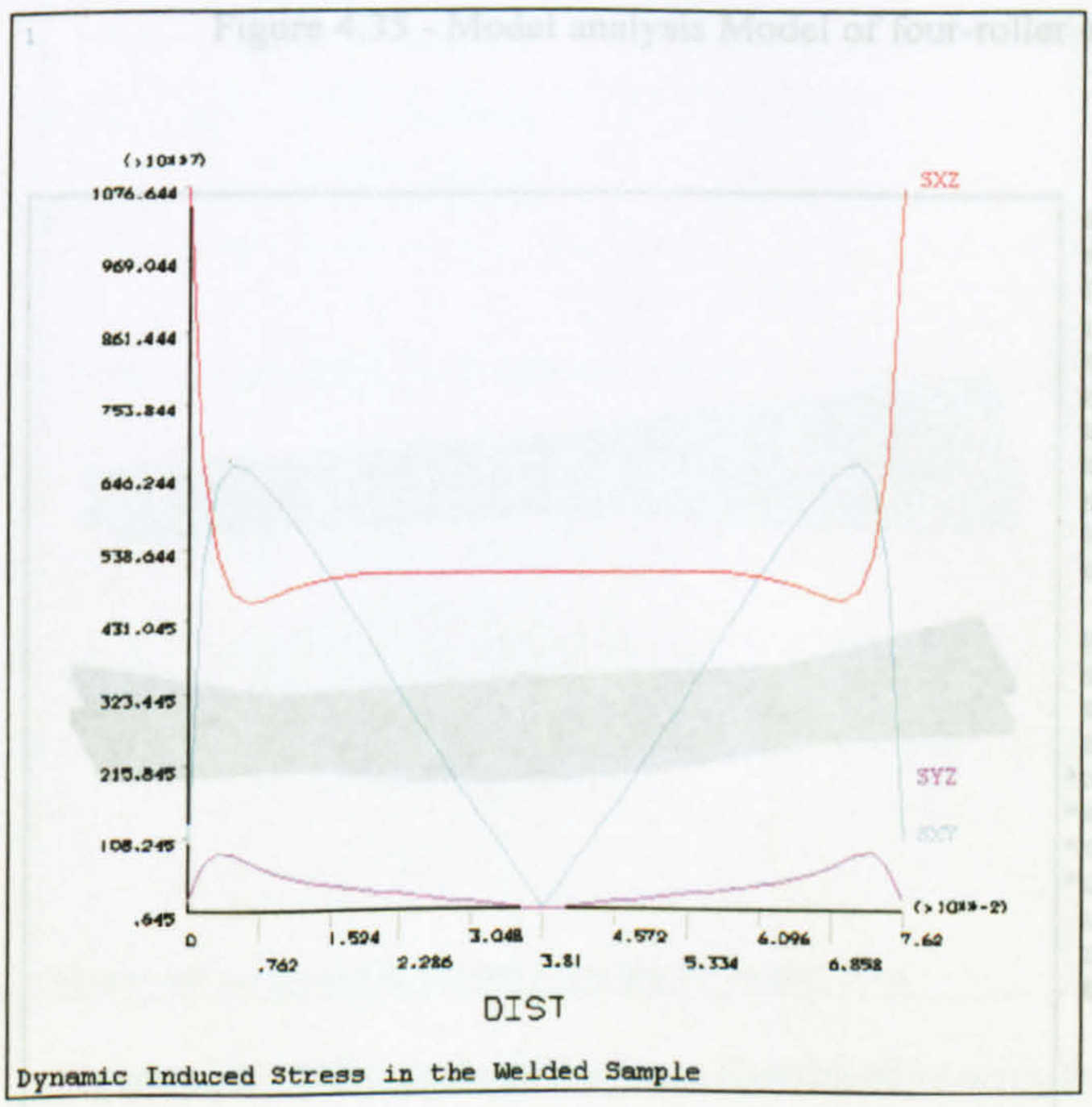

Figure 4.34 - Applied shear stresses on line E

4.2 Four roller Supported Beam

Modal and Harmonic Analysis of the Four-roller-supported beam was carried out assuming that the plates were joined together and mechanical properties of the beam were uniform, i.e. there were no non-linear properties due to higher temperatures (because consideration of non-linear properties makes the model highly complex - again have the possibility of non-convergent result). Instead a uniform-temperature model was analysed to obtain some approximation of the natural frequencies and the applied stresses to the structure.

4.2.1 Modal Analysis of the Four-Roller Supported Beam

This analysis was carried out to determine the modal properties of the structure. This analysis was carried out in a free-free condition (Figure 4.35) to determine the natural frequencies and the mode shapes which are shown in Figures 4.36 to 4.39.

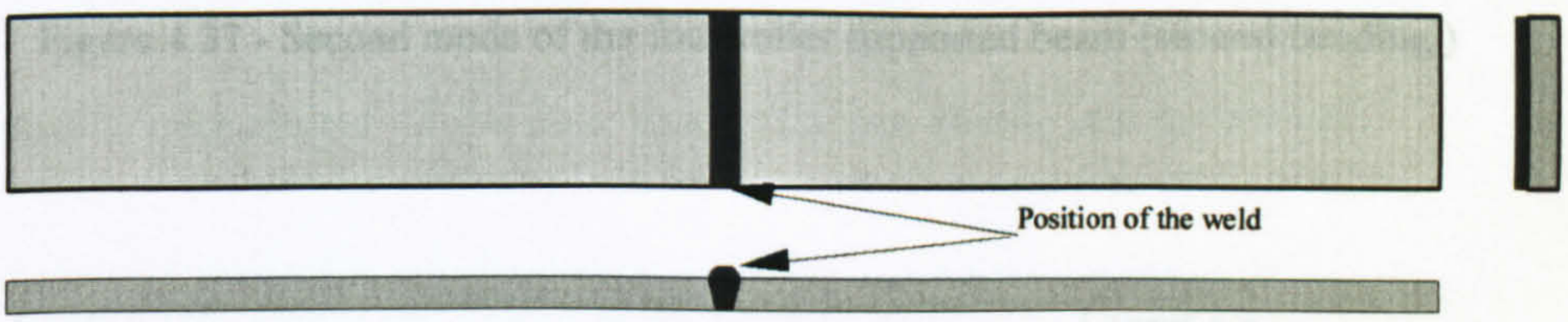

Figure 4.35 - Modal analysis Model of four-roller supported beam

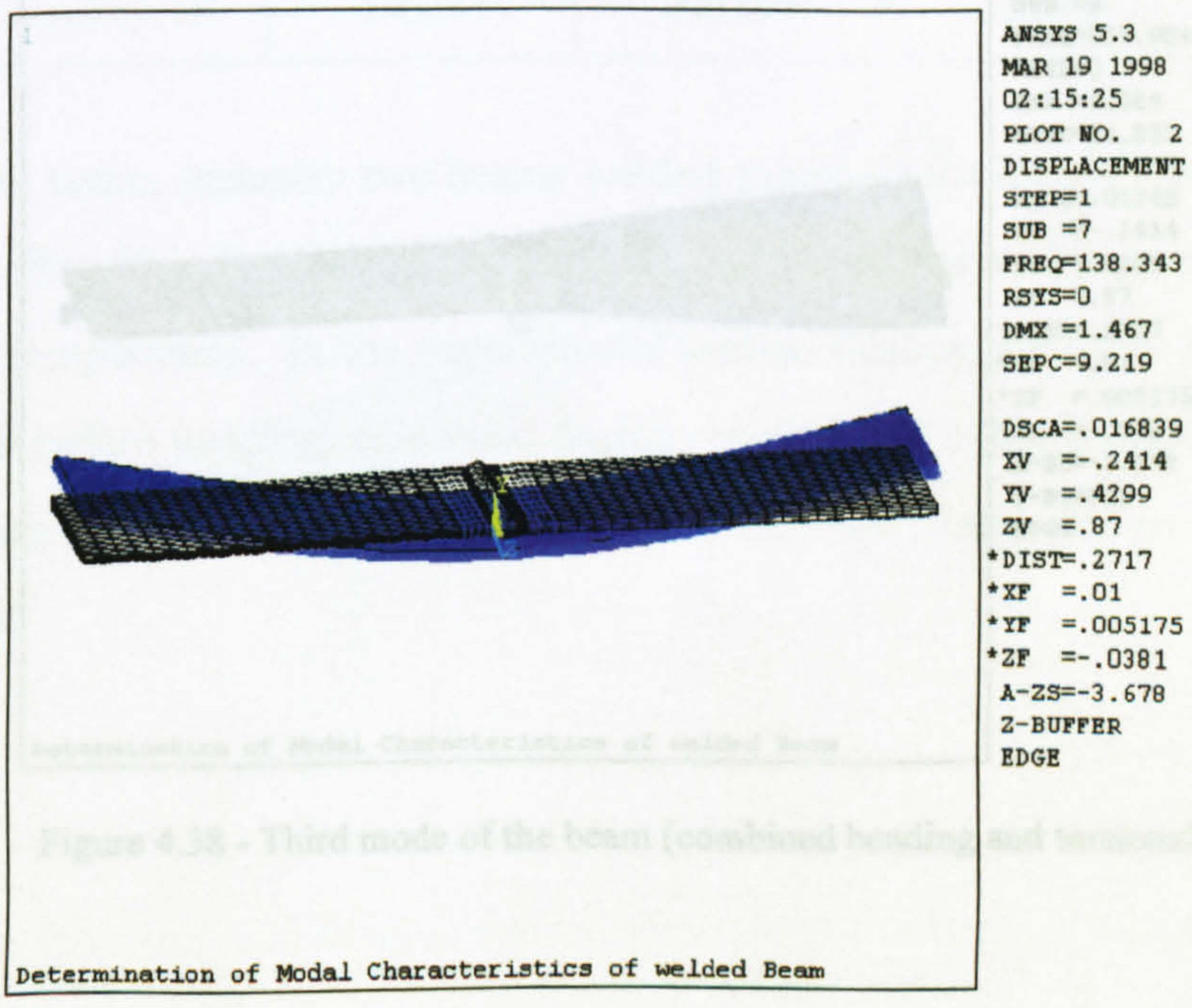

Figure 4.36 - First mode of four-roller supported beam (bending)

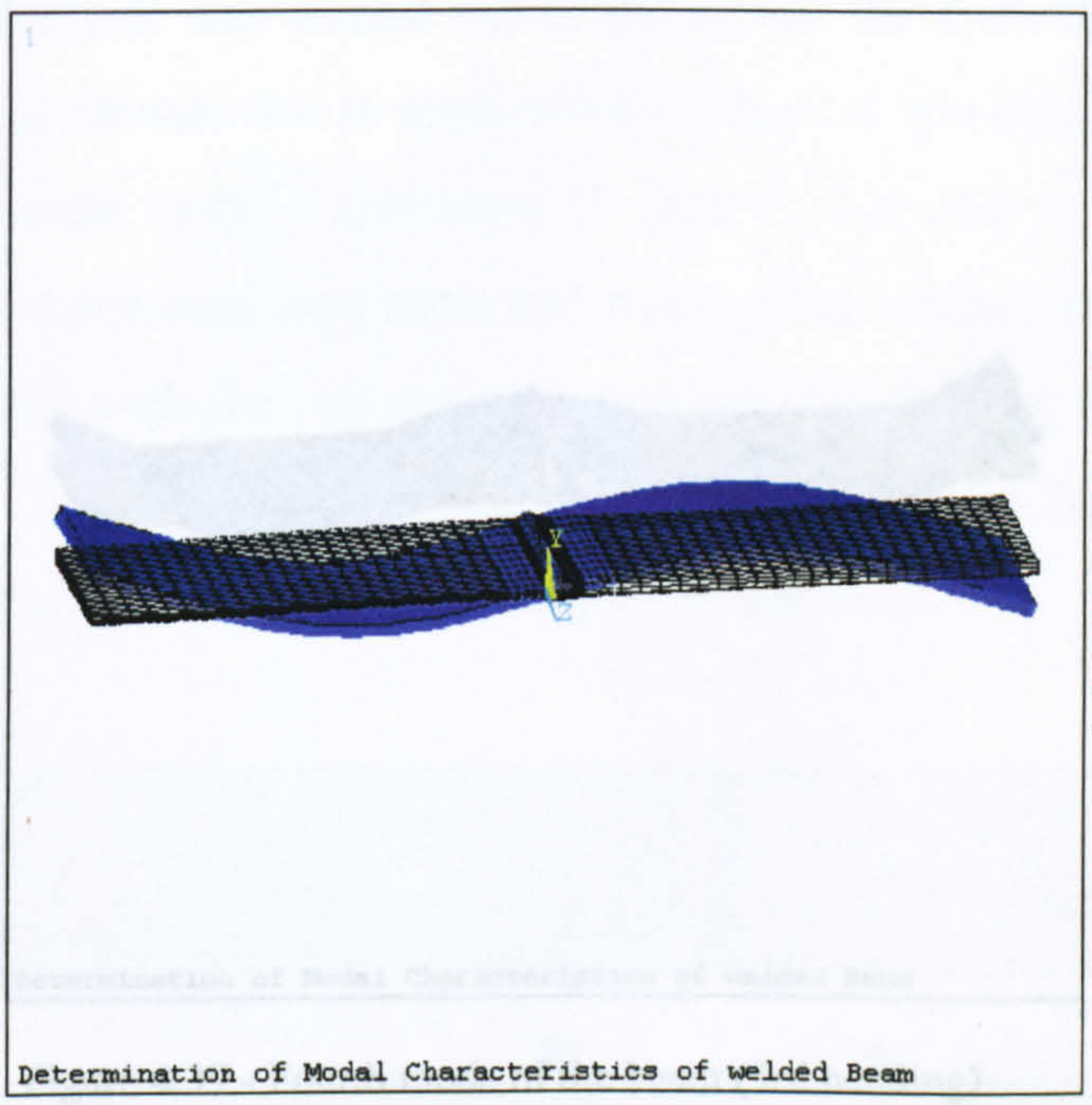

Figure 4.37 - Second mode of the four-roller supported beam (second bending)

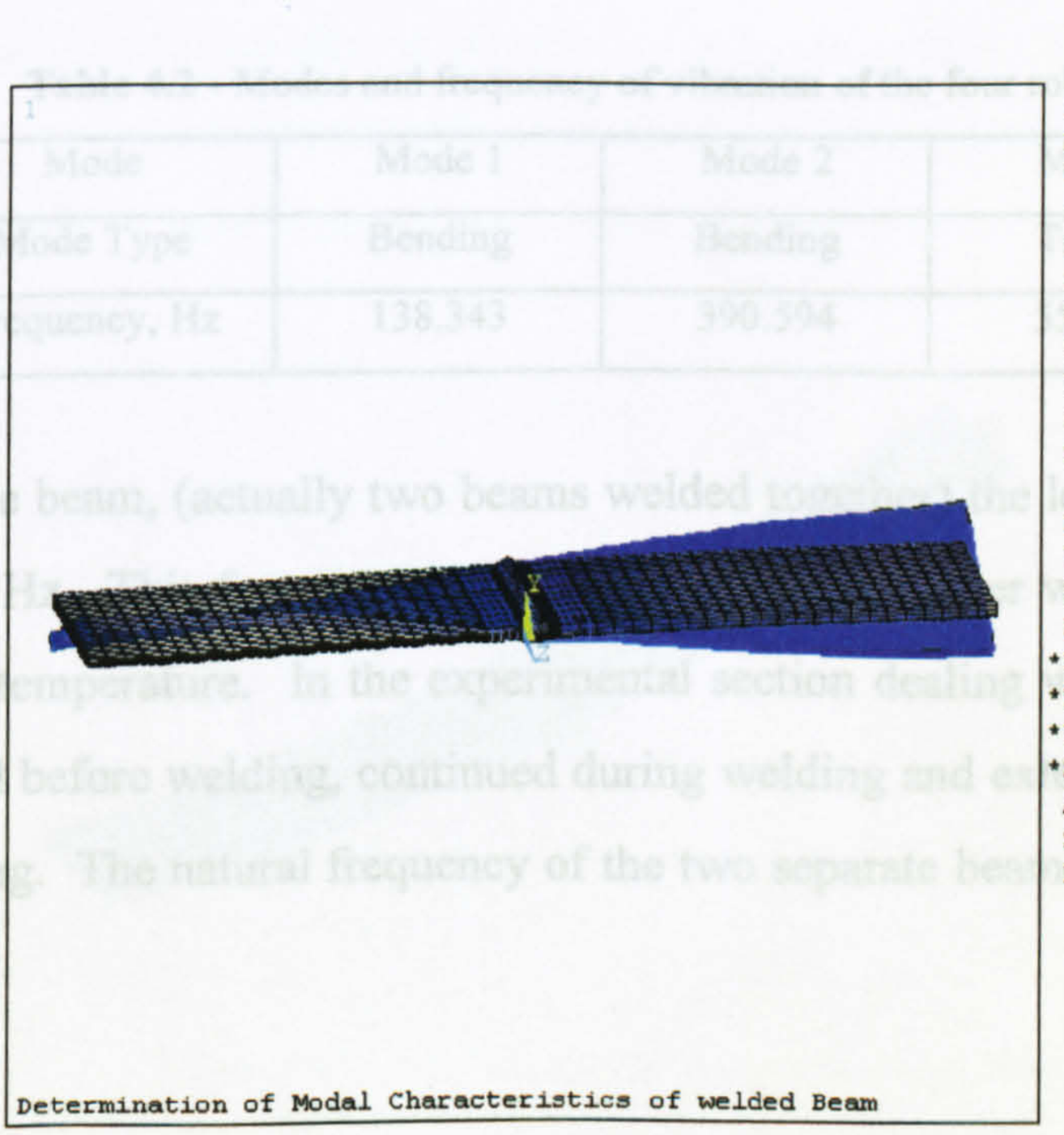

Figure 4.38 - Third mode of the beam (combined bending and torsional)

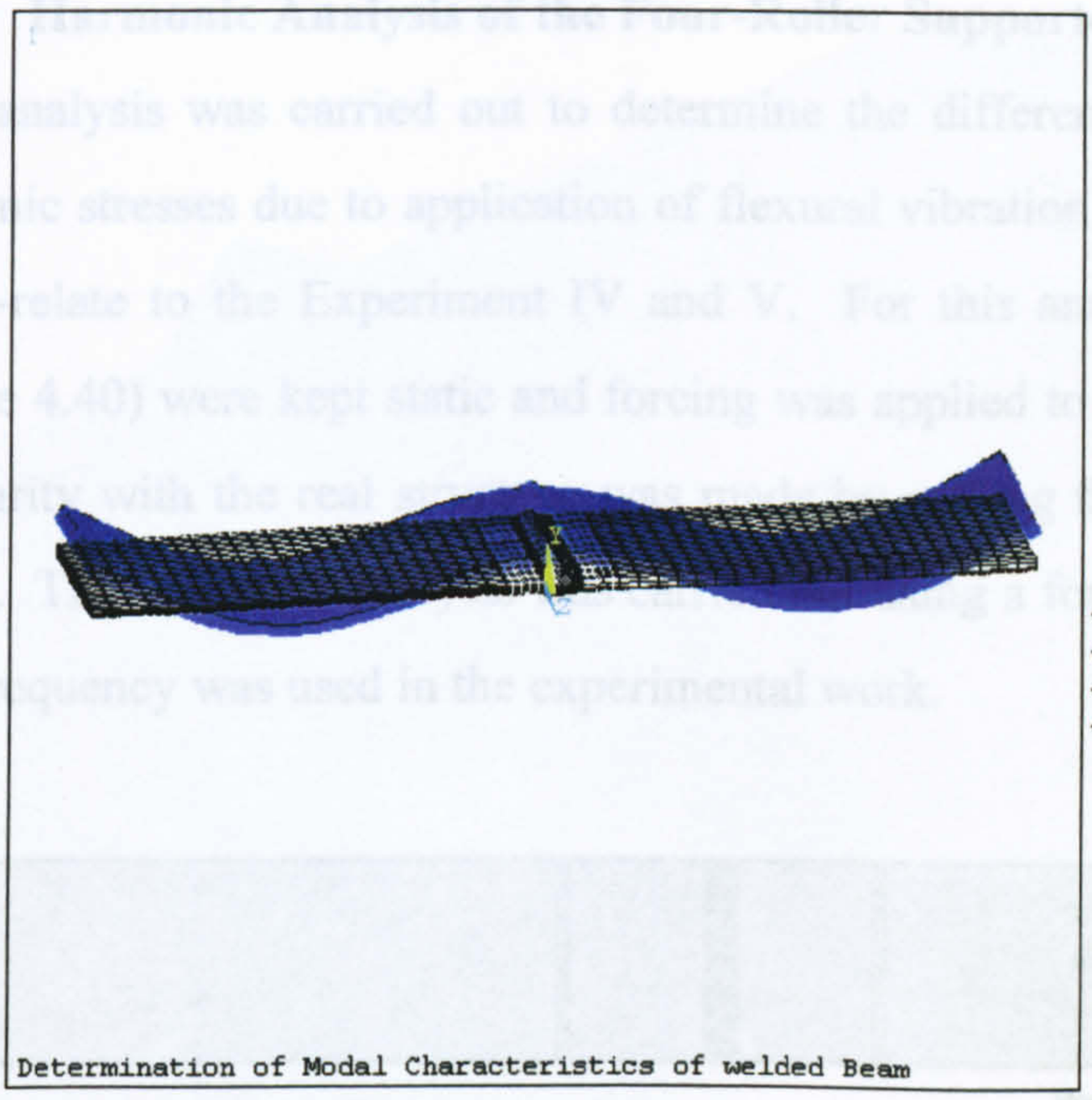

Figure 4.39 - Fourth mode of the beam (3rd bending)

The natural frequencies of the four modes shown above are as follows.

Table 4.2 - Modes and frequency of vibration of the four roller supported beam

Mode	Mode 1	Mode 2	Mode 3	Mode 4
Mode Type	Bending	Bending	Torsion	Bending
Frequency, Hz	138.343	390.594	554.984	771.614

For the beam, (actually two beams welded together) the lowest natural frequency was 138.3 Hz. This frequency was valid for the beam after welding and cooling down to room temperature. In the experimental section dealing with this specimen, vibration started before welding, continued during welding and extended for 2 - 4 minutes after welding. The natural frequency of the two separate beams (before welding) was even higher.

4.2.2 Harmonic Analysis of the Four-Roller Supported Beam

This analysis was carried out to determine the different components of the applied dynamic stresses due to application of flexural vibration to the specimens, which was to co-relate to the Experiment IV and V. For this analysis, the middle rollers (of Figure 4.40) were kept static and forcing was applied to the end rollers. Geometrical similarity with the real structure was made by putting the weld at mid length of the beam. The harmonic analysis was carried out using a forcing frequency of 25 Hz and this frequency was used in the experimental work.

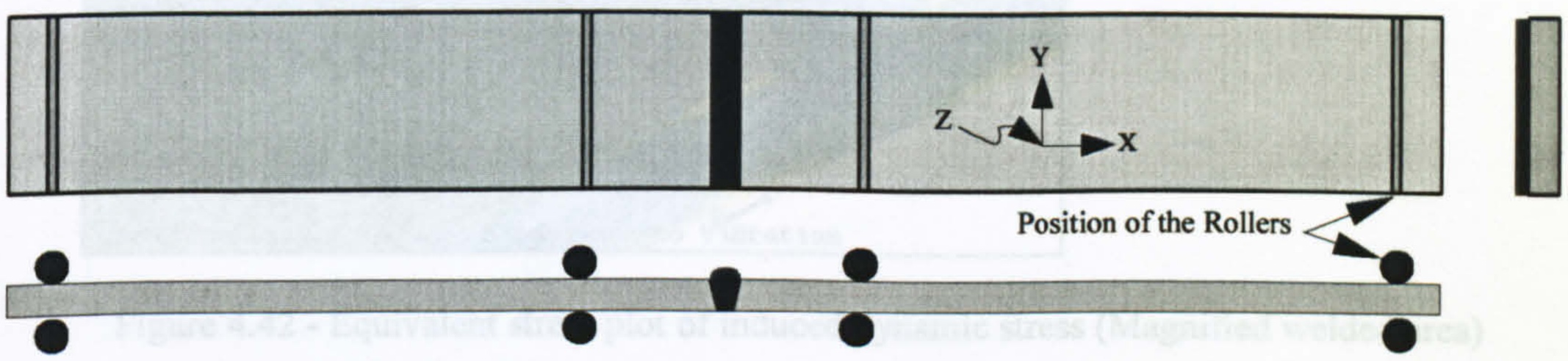

Figure 4.40 – Boundary conditions of the four-roller supported beam (harmonic analysis)

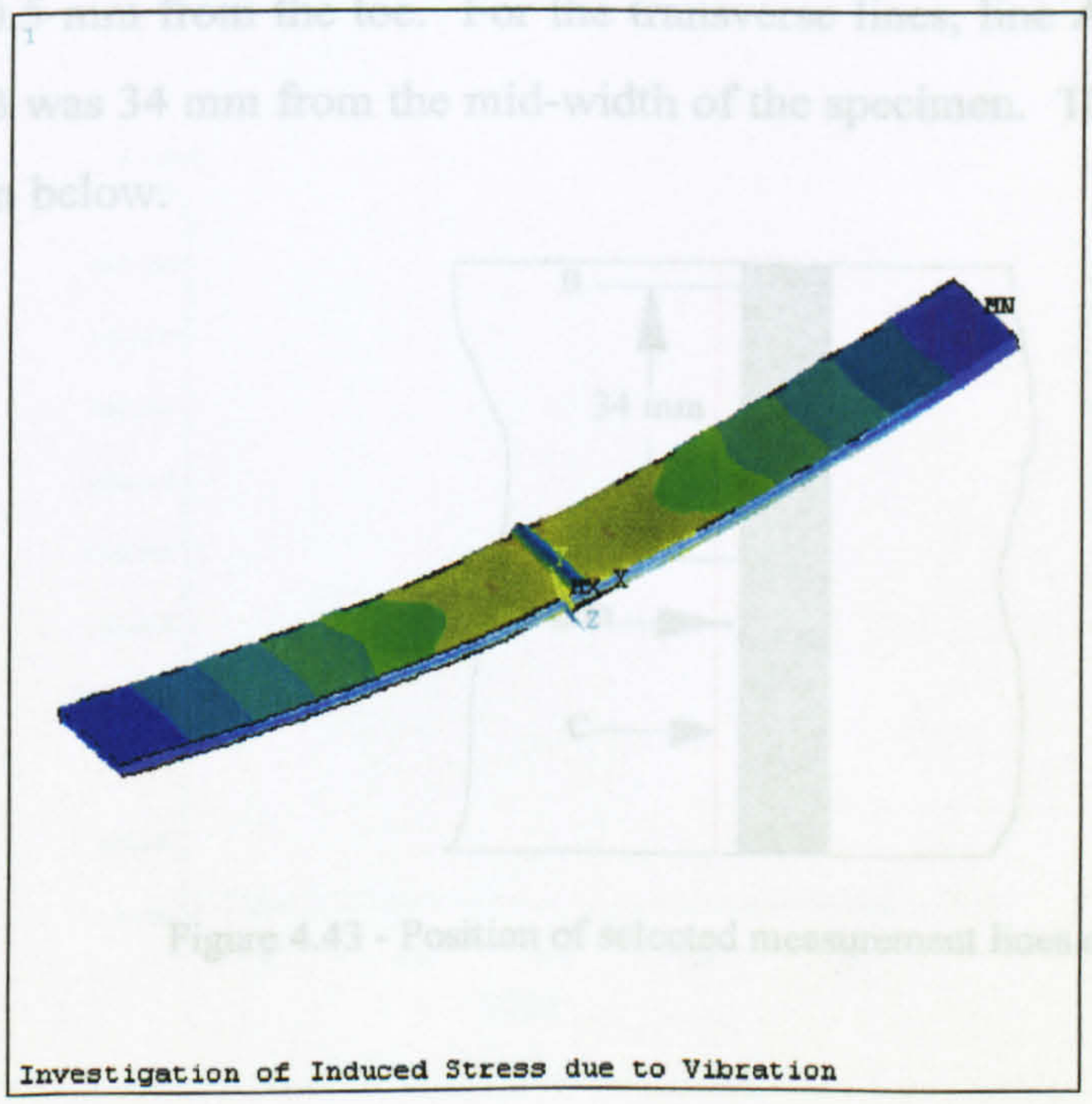

Figure 4.41 - Equivalent stress plot of applied dynamic stress in the beam

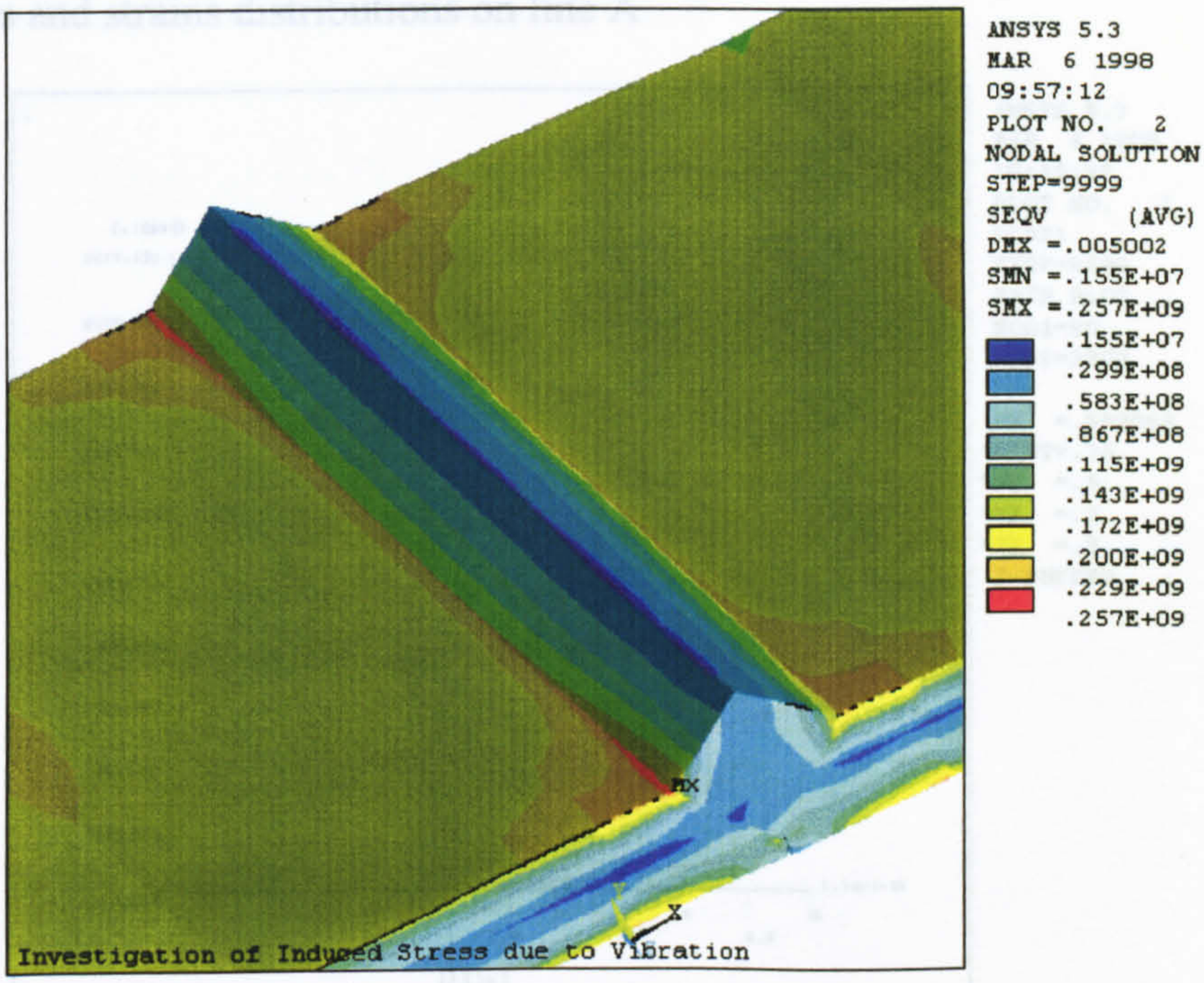

Figure 4.42 - Equivalent stress plot of induced dynamic stress (Magnified welded area)

To analyse the applied dynamic stress a total of three lines were selected (two transverse lines and one longitudinal line to the weld). The longitudinal line (line C) was 0.5 mm from the toe. For the transverse lines, line A was at the mid-width and line B was 34 mm from the mid-width of the specimen. The positions of the lines are shown below.

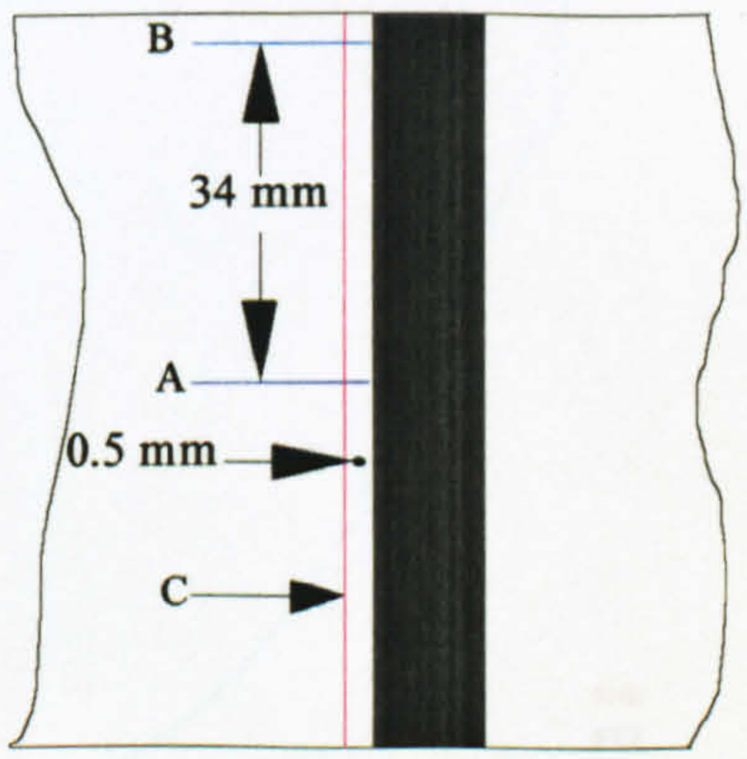

Figure 4.43 - Position of selected measurement lines on the specimen

Stress and strains distributions on line A

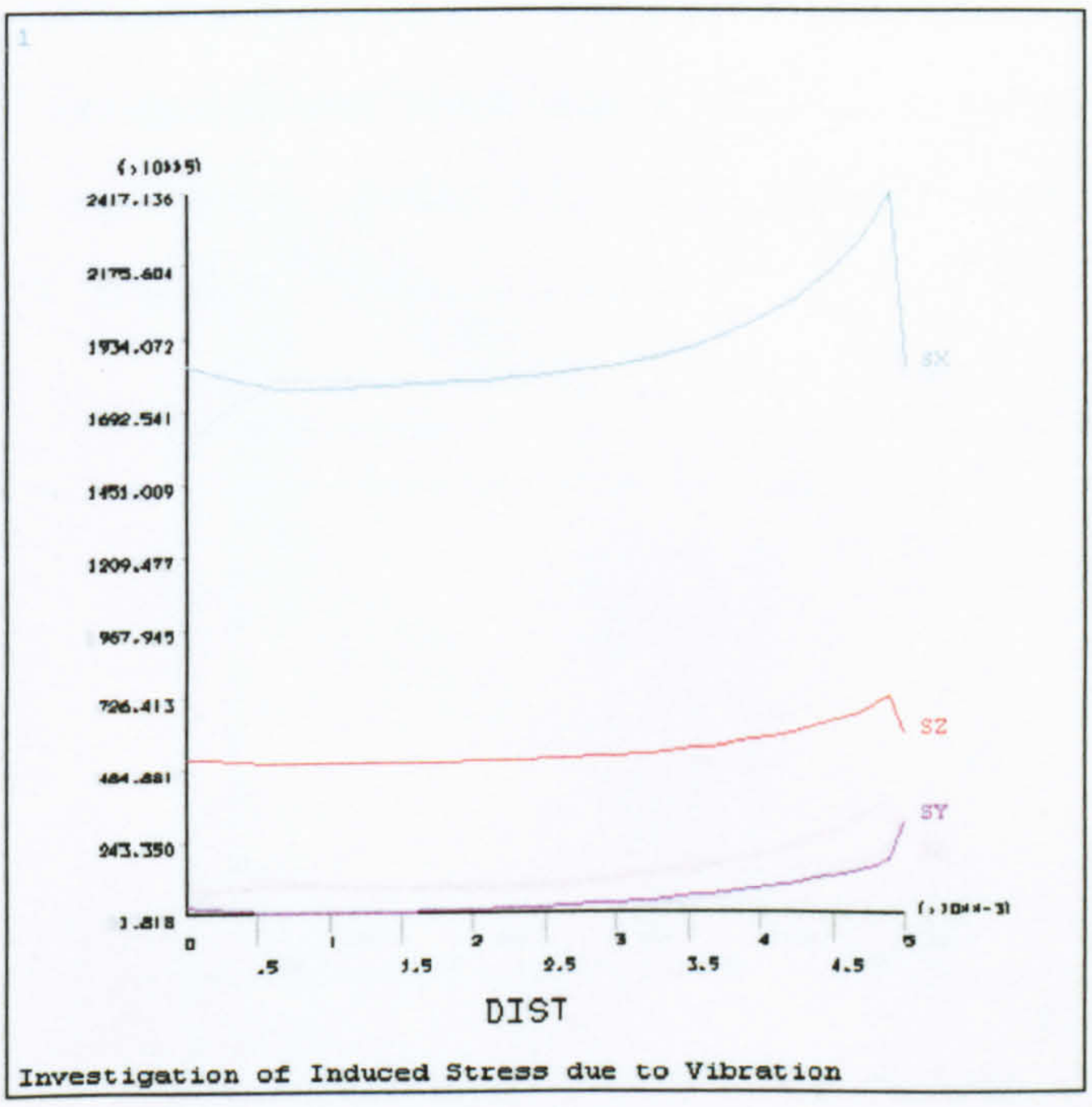

Figure 4.44 - Direct applied stresses on line A

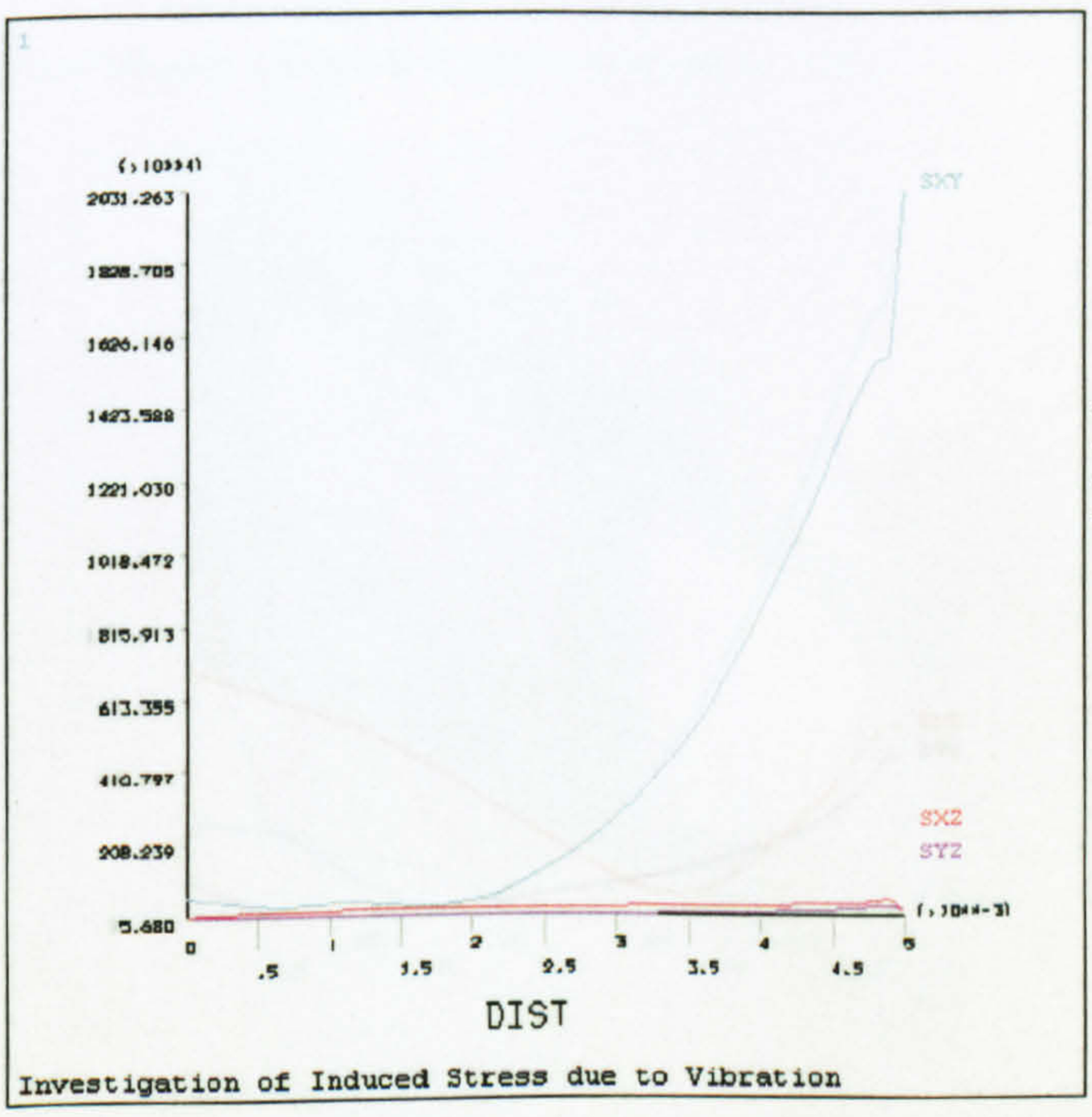

Figure 4.45 - Applied shear stresses on line A

Dynamic applied stress and strains on line B

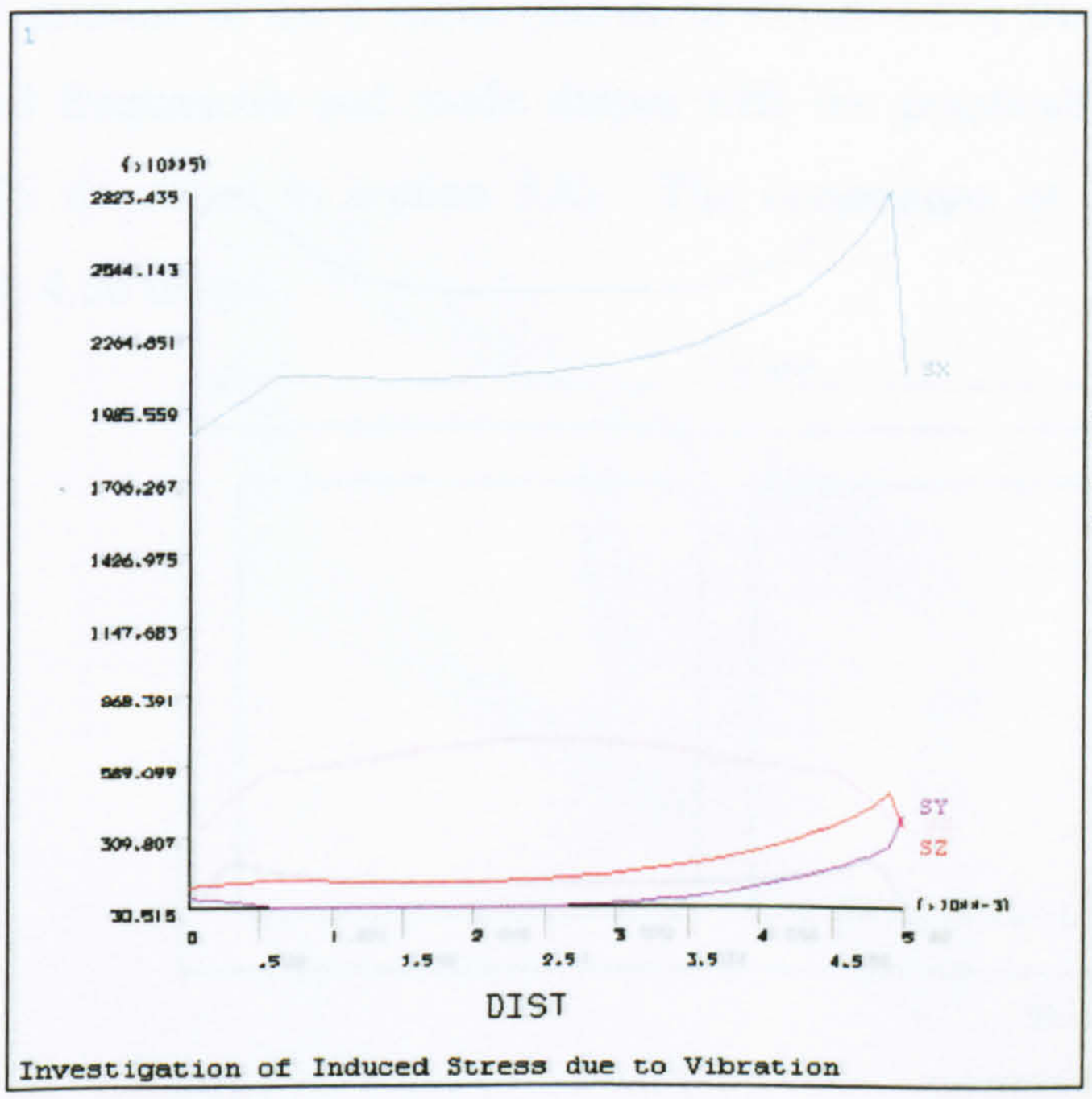

Figure 4.46 - Direct applied stress on line B

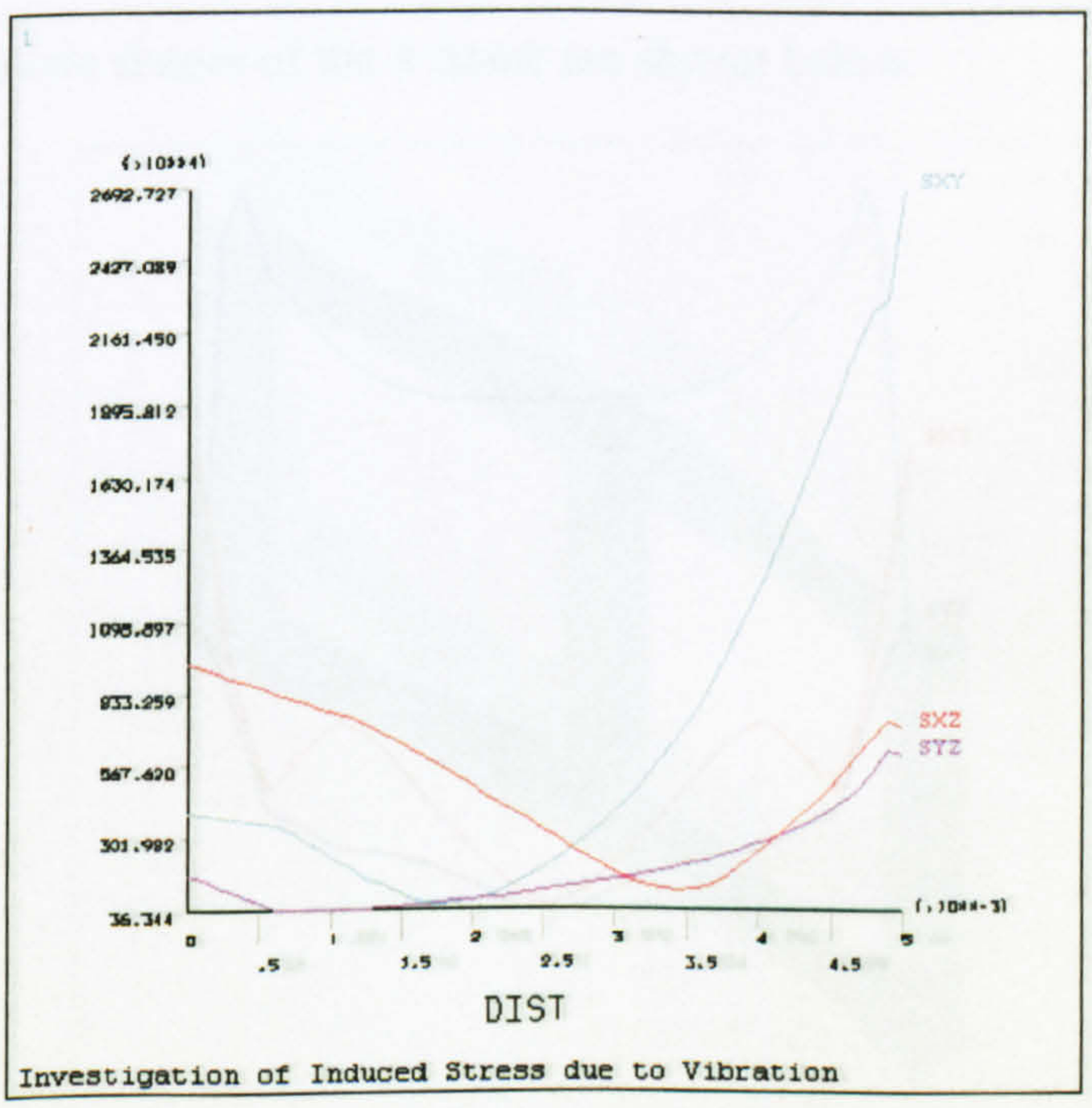

Figure 4.47 - Applied shear stresses of line B

Applied stresses and strains of line C

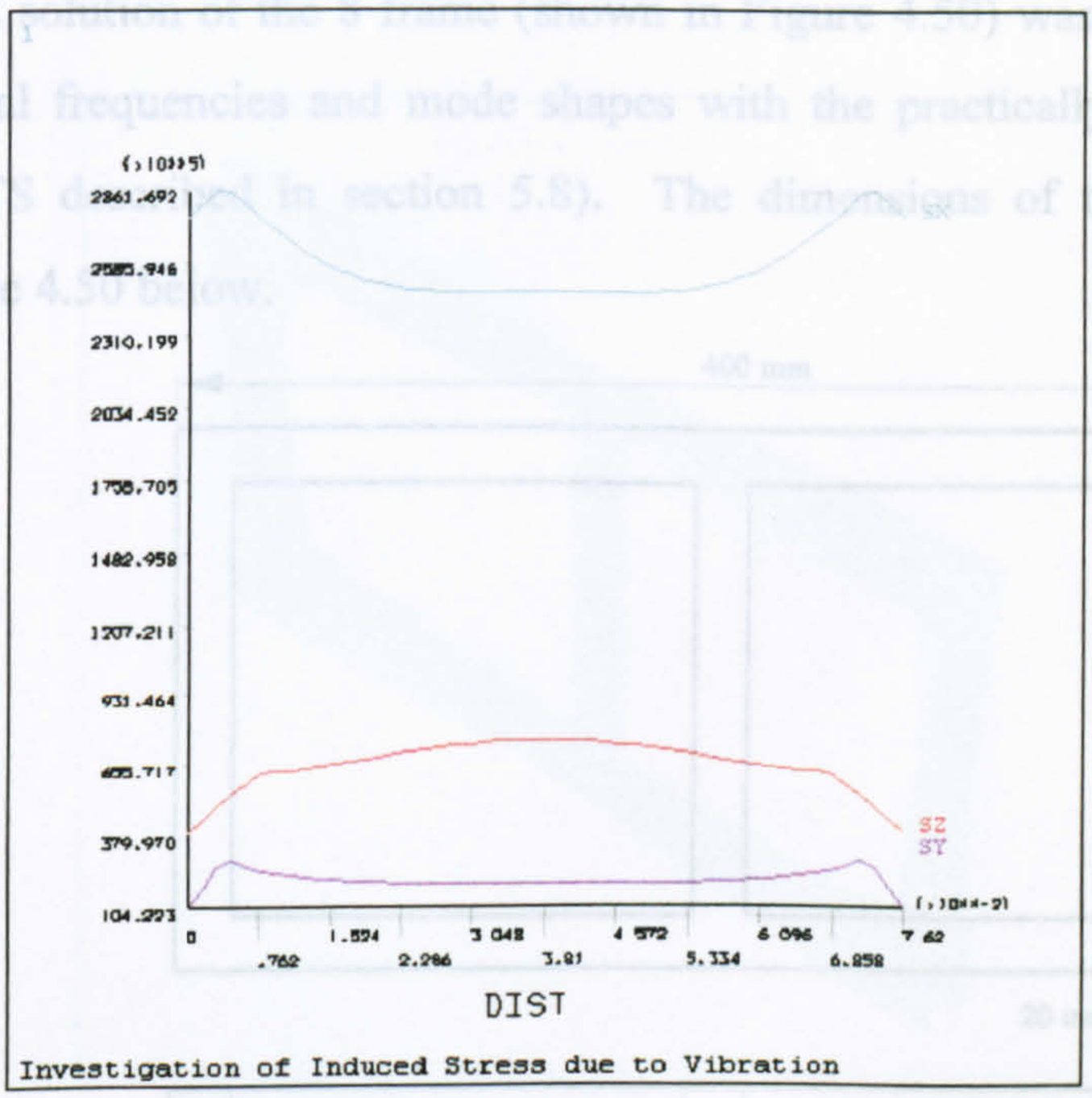

Figure 4.48 - Direct applied stresses on line C

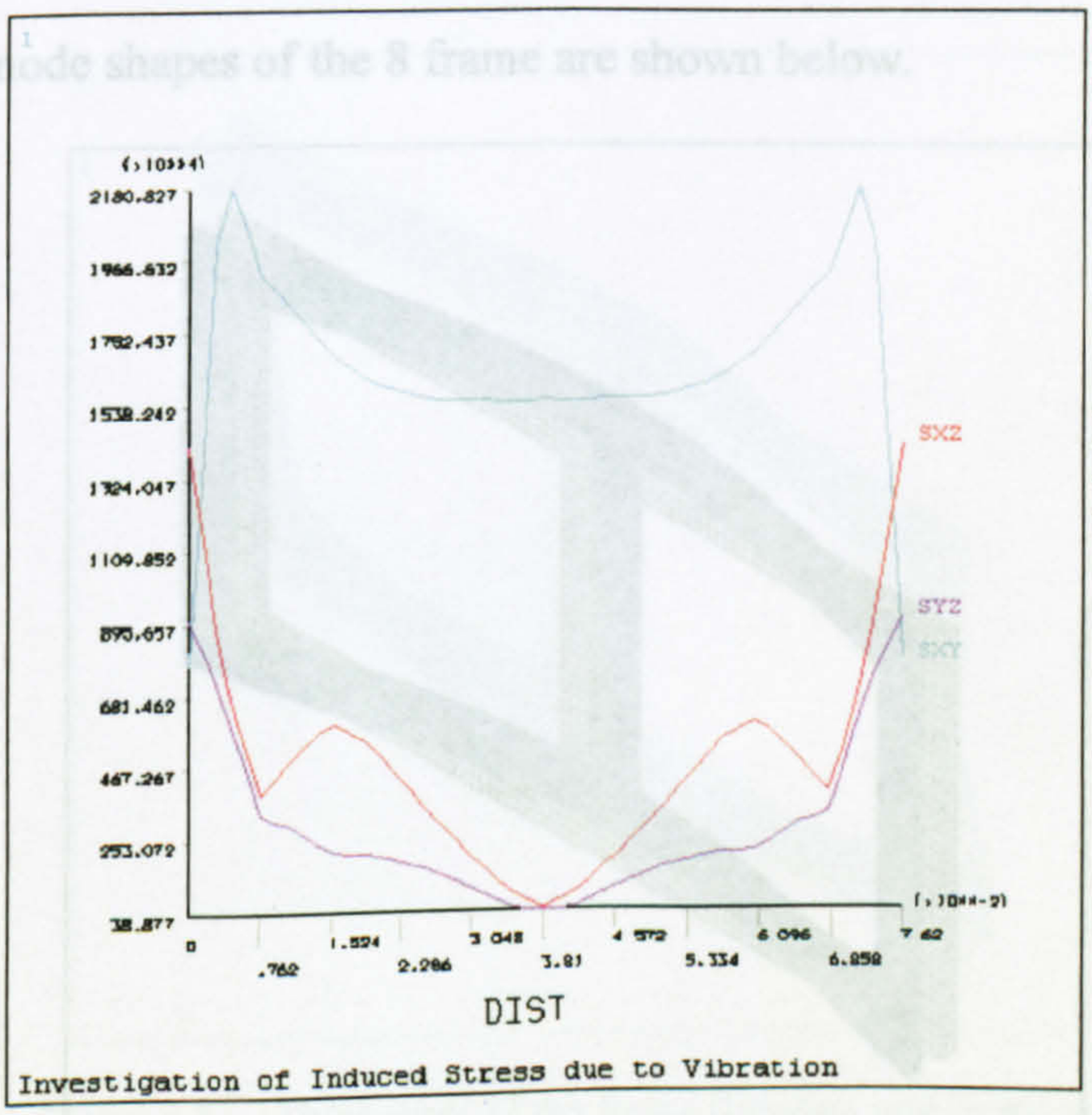

Figure 4.49 - Applied shear stresses on line C

4.3 8 Frame

A FE solution of the 8 frame (shown in Figure 4.50) was carried out to compare the natural frequencies and mode shapes with the practically determined values (using ICATS described in section 5.8). The dimensions of the model are described in Figure 4.50 below.

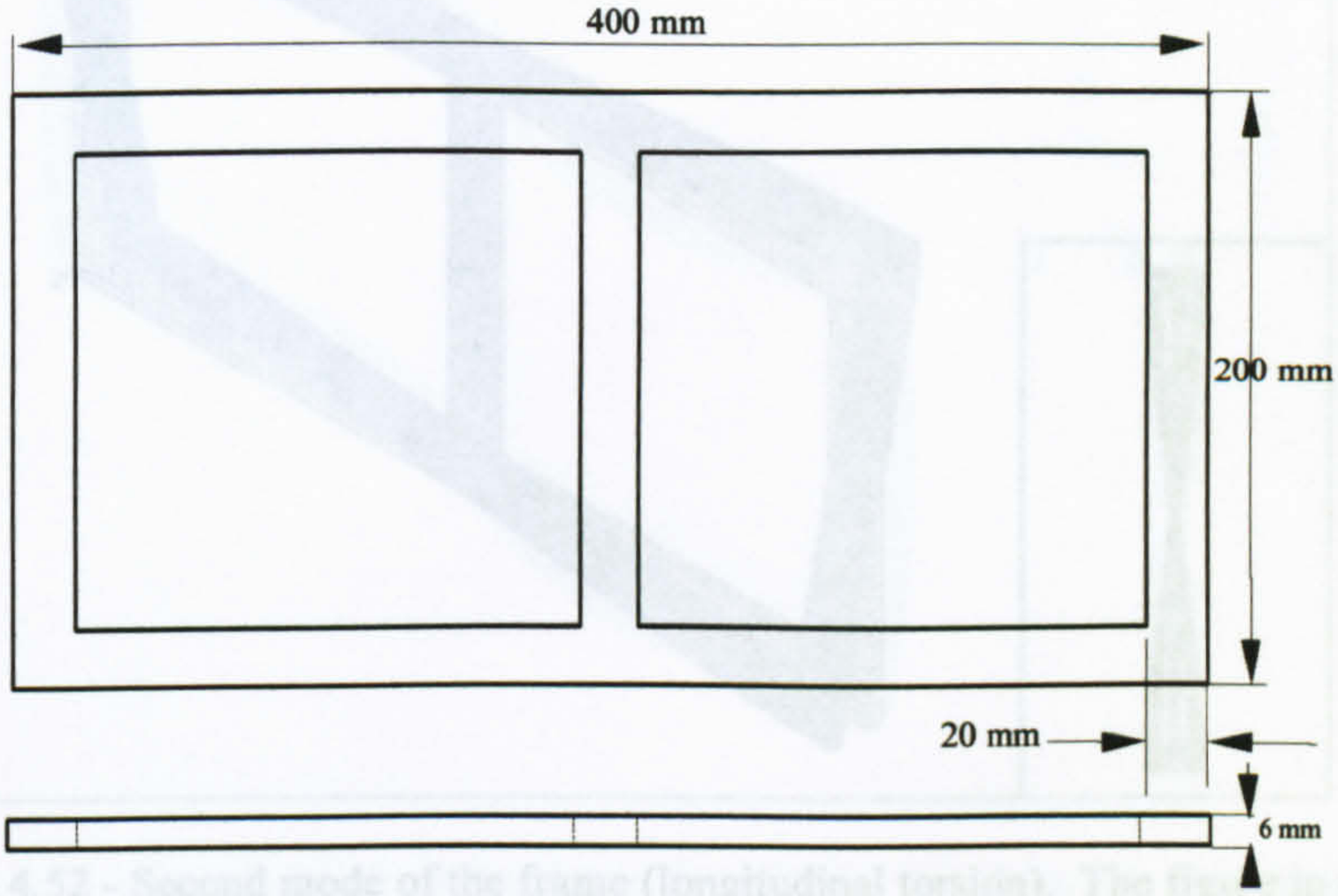

Figure 4.50 – Dimensions of the experimenting "8" frame

The mode shapes of the 8 frame are shown below.

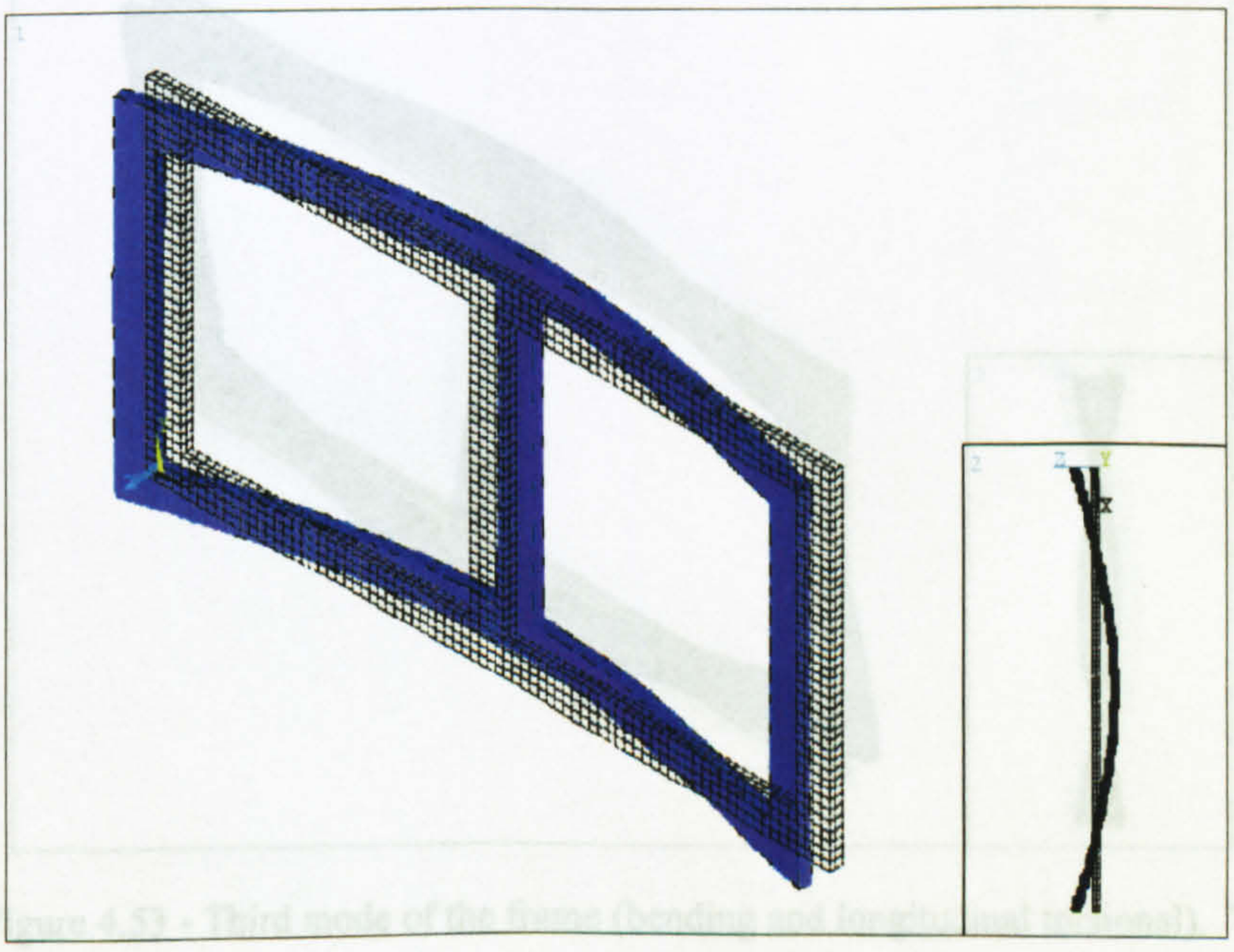

Figure 4.51 - First mode of the frame (transverse bending). The figure in the inset is viewed from the top.

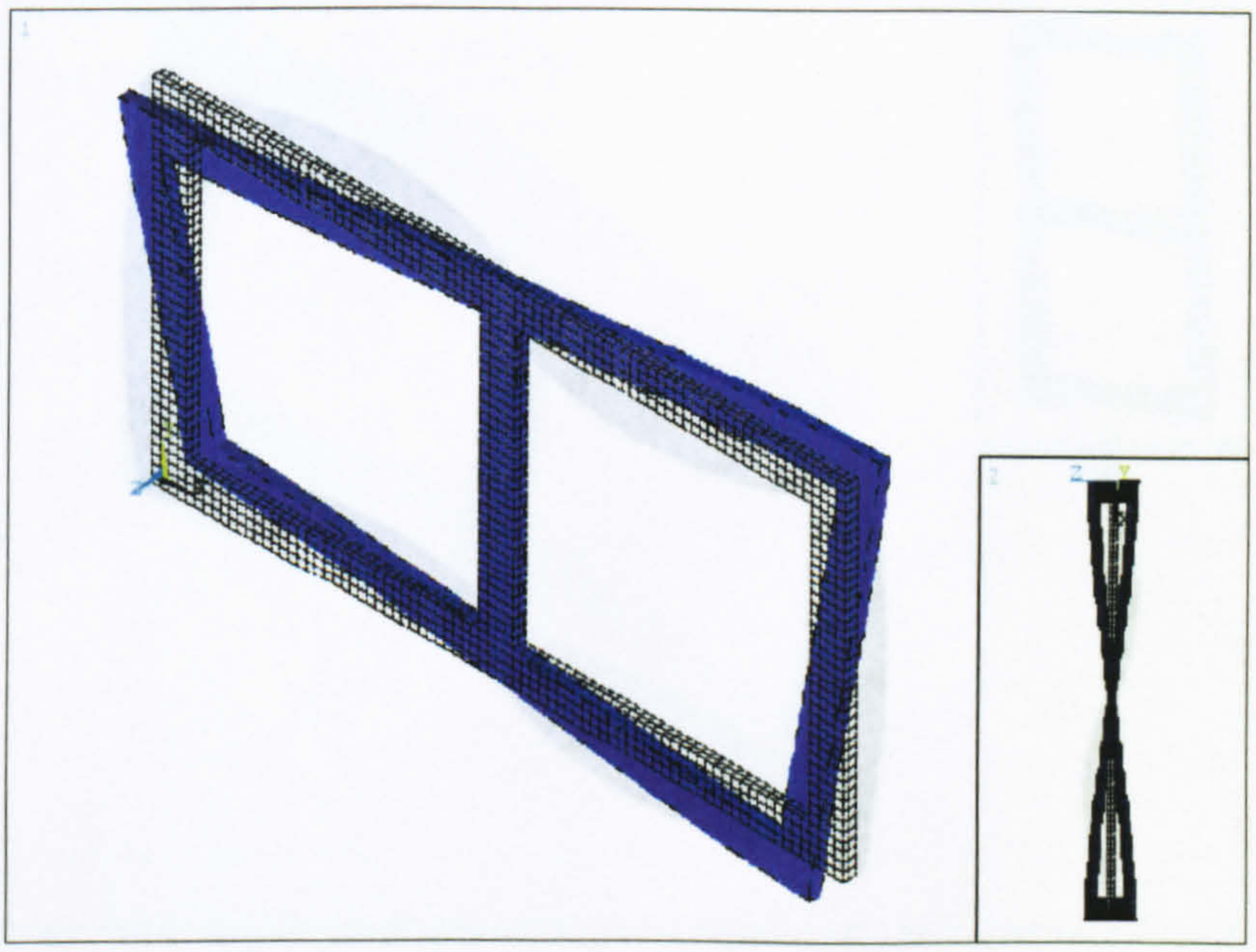

Figure 4.52 - Second mode of the frame (longitudinal torsion). The figure in the inset is viewed from right side.

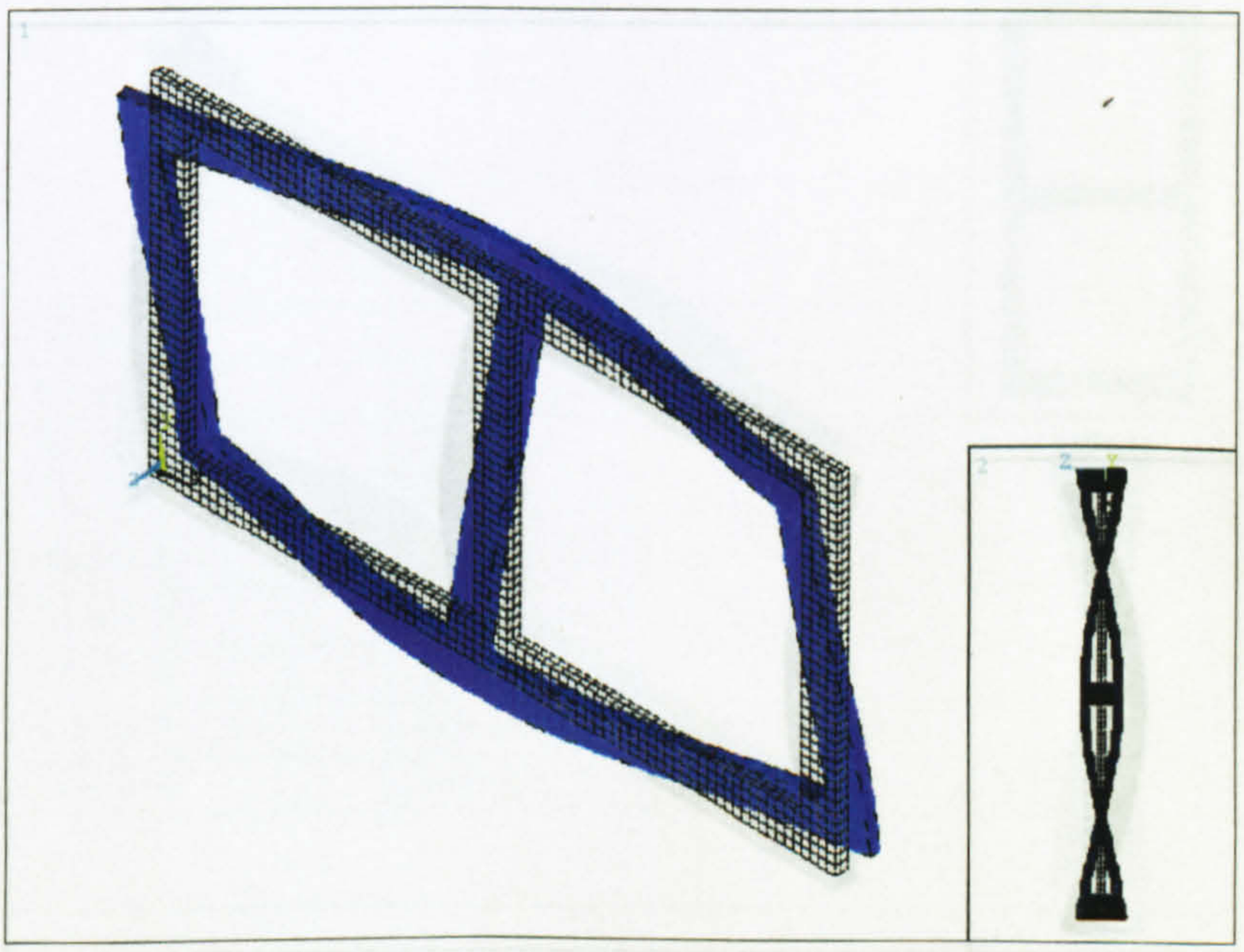

Figure 4.53 - Third mode of the frame (bending and longitudinal torsional). The figure in the inset is viewed from the top.

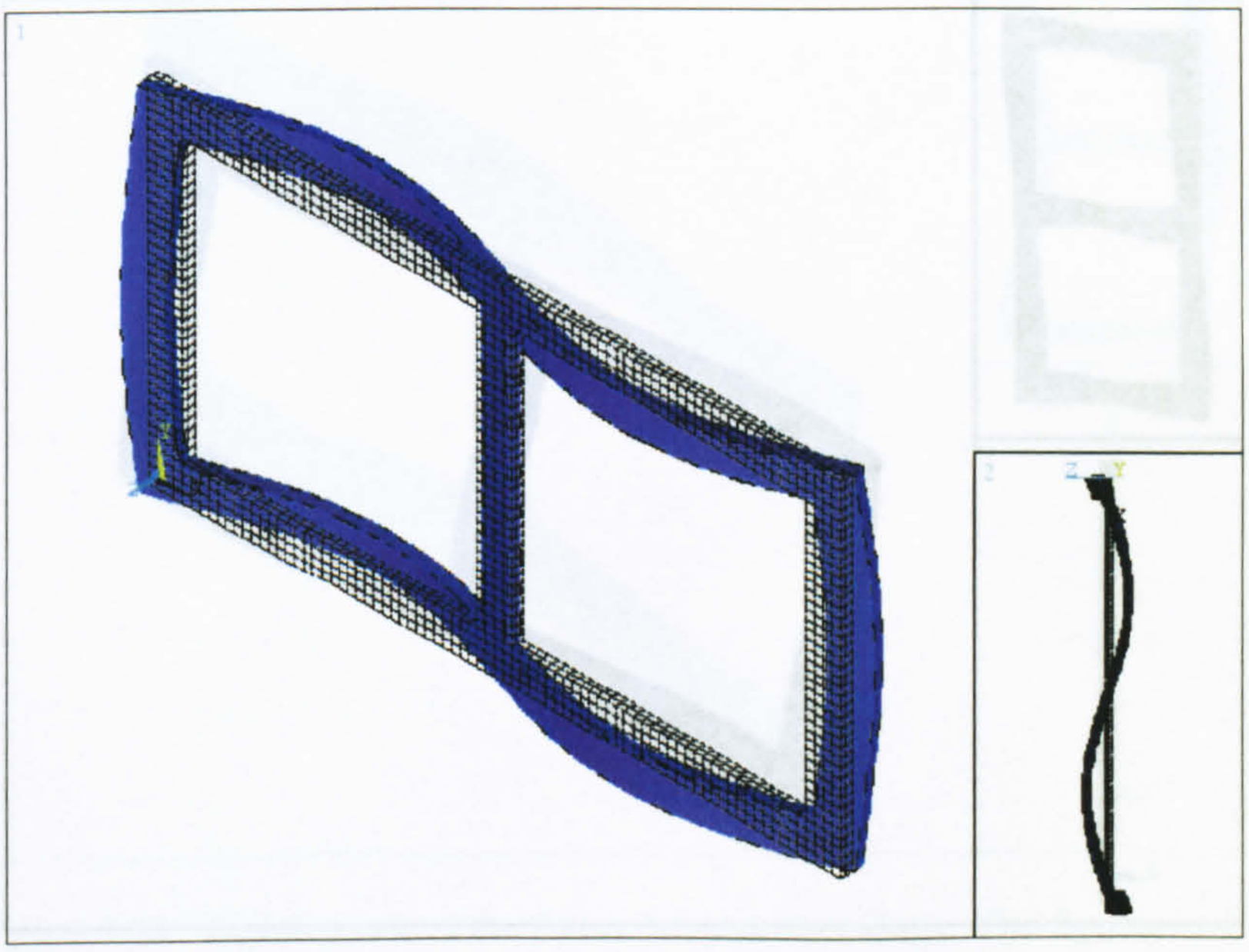

Figure 4.54 - Fourth mode of the frame (bending). The figure in the inset is viewed from the top.

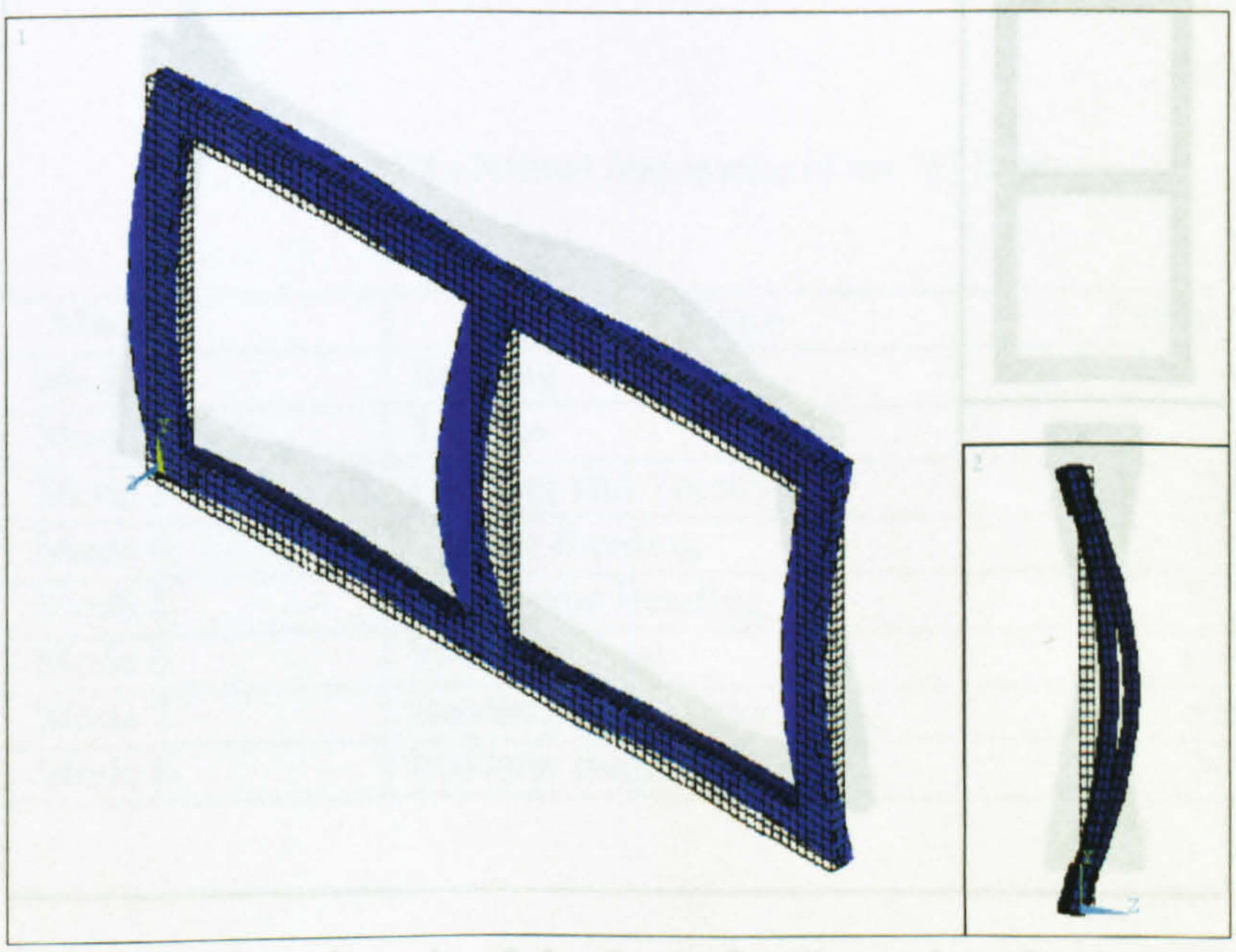

Figure 4.55 - Fifth mode of the frame (longitudinal bending). The figure in the inset is viewed from the side.

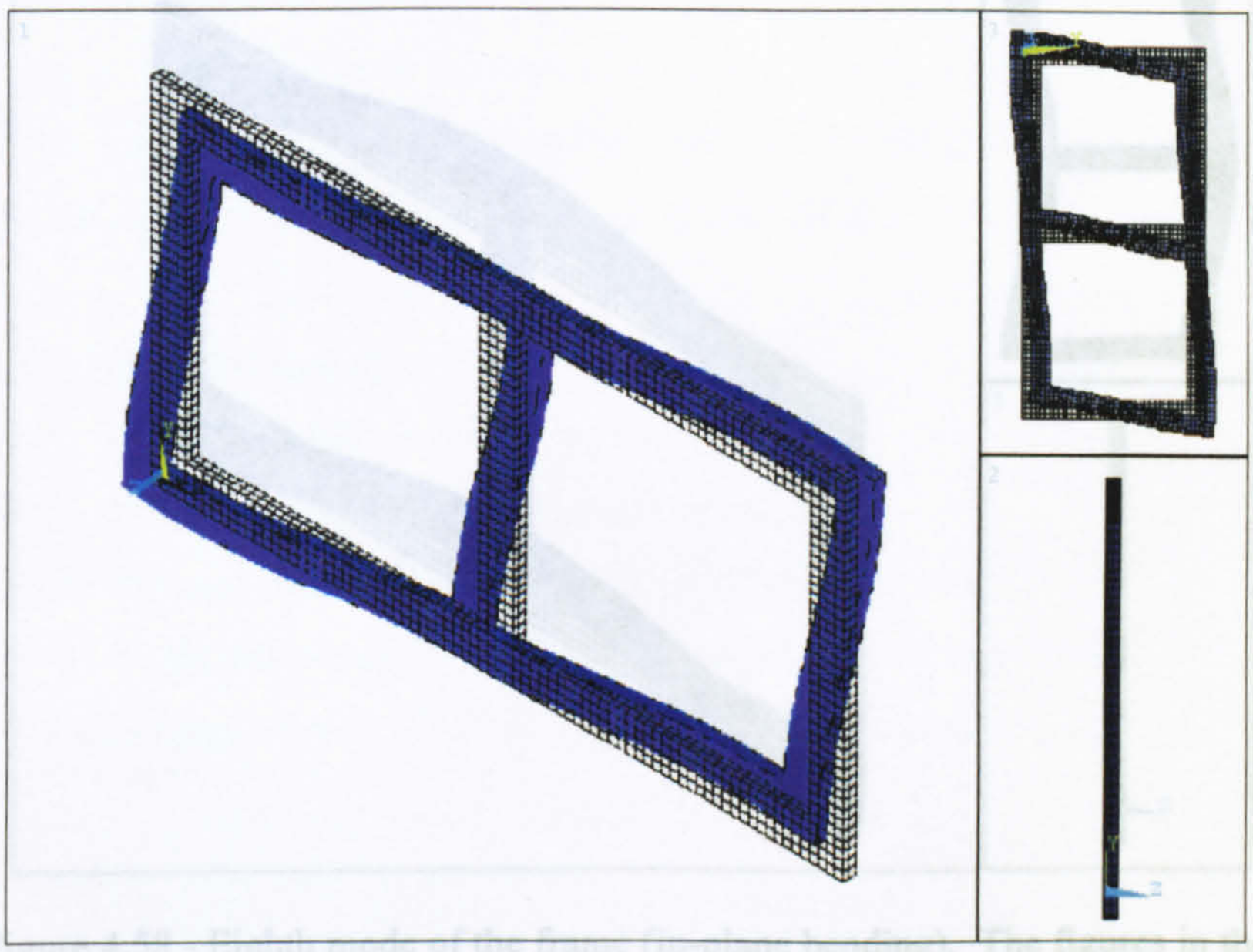

Figure 4.56 - Sixth mode of the frame (in-plane - shear mode). The figures in the two insets - the top is viewed from the front and bottom is from the top

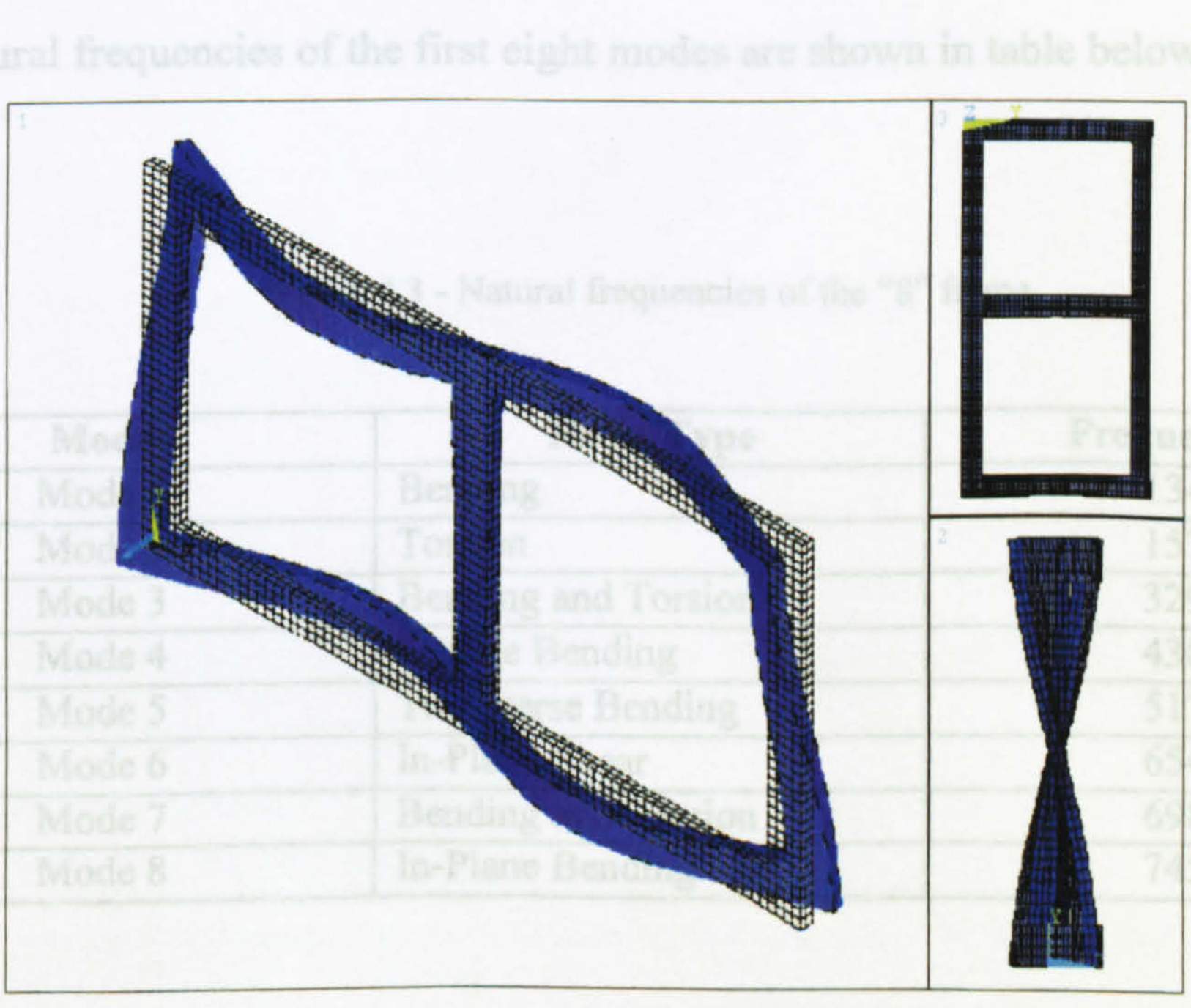

Figure 4.57 - Seventh mode of the frame (bending and torsional combined). The figures in the two insets – the top is viewed from the front and the bottom is viewed from right side

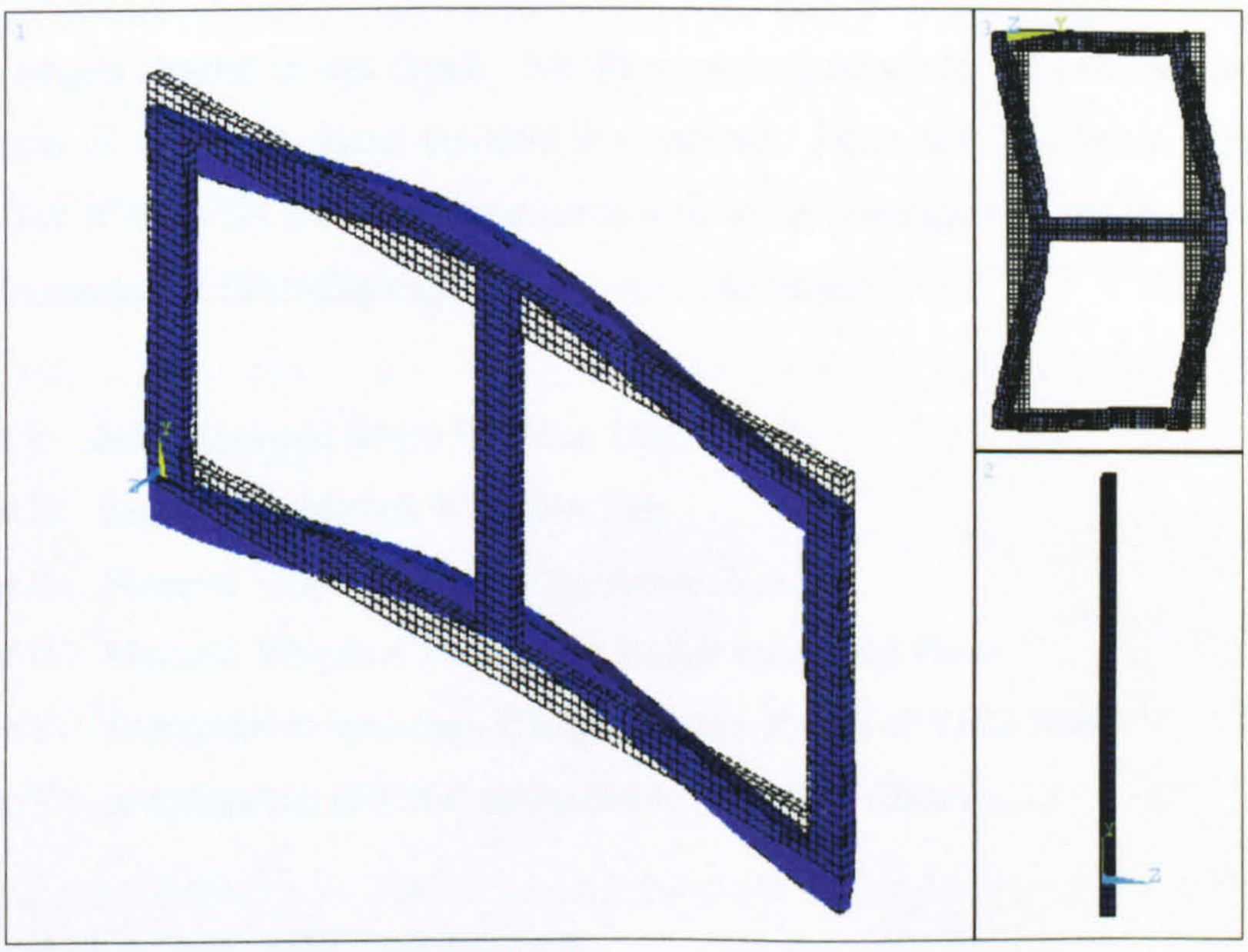

Figure 4.58 - Eighth mode of the frame (in-plane bending). The figures in the two insets - the top is viewed from the front and the bottom is viewed from the side

The natural frequencies of the first eight modes are shown in table below.

Table 4.3 - Natural frequencies of the "8" frame

Mode	Mode Type	Frequency, Hz
Mode 1	Bending	134.42
Mode 2	Torsion	157.08
Mode 3	Bending and Torsion	329.03
Mode 4	Double Bending	438.94
Mode 5	Transverse Bending	517.23
Mode 6	In-Plane Shear	654.69
Mode 7	Bending and Torsion	698.04
Mode 8	In-Plane Bending	745.77

Chapter 5

Experimental Programmes

Overview of Chapter 5

This is the largest chapter in this thesis. All the experimental works are included here. First of all, the calibration of the X-ray elastic constant is presented. Next, the description of the specimens is included. The VWC/VSR and other treatments and some investigations are presented. In **"during welding"** treatment the following experiments were carried out.

Experiment I: Static Induced Stress Welding Test

Experiment II: Rigid Body Motion Vibration Test

Experiment III: Flexural Vibration Test – Cantilever Beam

Experiment IV: Flexural Vibration Test – Four Roller Supported Beam

Experiment V: Treatment of Specimen Using a Certain Range of Yield Stress

Experiment VI: Investigation of VWC in Combined Mode of Vibration

The experiments in **"post weld"** treatment are

Experiment VII: VSR Treatment of As-welded Specimens (Batch Treatment)

Experiment VIII: VSR Treatment of As-welded Specimens

Experiment IX: Investigation of Residual Stress Characteristics During Fatigue Failure.

Experiment X: Investigation of Torsional Stress Effect on Residual Stress and VSR.

The **"other"** experiments are

Experiment XI: Cryogenic Treatment Test

Experiment XII: Fatigue Test

Experiment XIII: Metallurgical Investigation of Vibratory Treated Specimens

Experiment XIV: Modal Analysis

The residual stress measurements were carried out using an X-ray diffractometer. The manufacturer specified the error band of the diffractometer in general as ±21 MPa. After calibration of the machine and the Material Elastic Constant the error band for this method was less than ±10 MPa. In the experiments where the specimens were processed in batches, though the same mild steel was used in the experiments there remains a possibility of different material properties in different specimens. Considering this fact, the error band may be therefore taken as ±21 MPa overall. In the experiments where the residual stresses of the same specimen was measured before and after treatment, the material properties were the same, so the error band may be taken as ±10 MPa. The error bands are introduced in some selected plots for easy observation.

5.1 Calibration of X-ray Elastic Constant

Calibration of the X-ray measurements is important in order to obtain the exact value of residual stress measured - otherwise the measured value cannot be assured as an absolute residual stress. In this calibration process there are two steps involved. The steps are, (1) Calibration of the X-ray diffractometer and (2) Calibration of X-ray elastic constant. In step 1, the X-ray diffractometer is calibrated using very fine Fe powder. In this calibration the X-ray source hits the Fe powder from five different perpendicular distances and the two detectors pick the angular 2θ positions of the diffracted rays. The diffracted angles are then plotted against the distance of the X-ray source. From that plot, the position of the diffracted angle for zero stress is calculated. The process of the calibration is very straightforward, and, with the Proto system, the user friendly software guides the user through a proper calibration routine. There is an option of calibration check, which ensures the correctness of the calibration.

In step 2, the calibration of X-ray elastic constant is carried out. This calibration is very important because when a measurement is made on a multiphase material, usually only one phase is analysed. The measured strain is therefore the elastic strain of this particular phase, coming partly from the macroscopic stress and partly from the stresses of the other phases on the analysed one. Since the modulus of elasticity of the particular phase is different from the bulk modulus of elasticity of the material, thus the calculated stress is obviously different from the absolute residual stress present in the material. To determine the absolute value of the residual stress, the effective elastic constant for stress analysis should be determined.

In this calibration, the specimen was stressed (applying a bending load) in several steps. In every step of bending, the total stress (residual + applied) of the specimen was measured using the X-ray diffractometer and at the same time increase in bending stress was measured with the installed strain gauge (Figure 5.4). With the combination of Mechanical Modulus of Elasticity, Poisson's ratio and the ratio of the X-ray measured stress and strain gauge measured stress, the Effective Elastic Constant was calculated. The details of this calibration are discussed in this section.

5.1.1 Modification of Four-point Bend to Determine the X-ray Elastic Constant

To calculate the X-ray Elastic Constant, using a four-point bending jig, a known force has to be applied to the specimen. The applied load and the strain gauge on the specimen would give the measured Mechanical Modulus of Elasticity, which would be used in the X-ray diffractometer stress computation process.

In the four-point bending jig, purchased with the X-ray Diffractometer, as normal, no facility was provided for determining the applied force. It was however felt necessary to determine the magnitude of this force and an experimental programme was undertaken to do so. Four strain gauges were installed on the four-point bend and it was then calibrated using a Zwick testing machine and a P-3500 digital strain indicator. For the installation of the strain gauges on the four-point bend jig, a full bridge circuit was chosen to obtain a maximum output. Four strain gauges were installed on the four corners of the four-point bend jig (diagonally two gauges were on the top surface and the other two were on the bottom surface) to compensate for the change in strain readings for a small movement of the specimen.

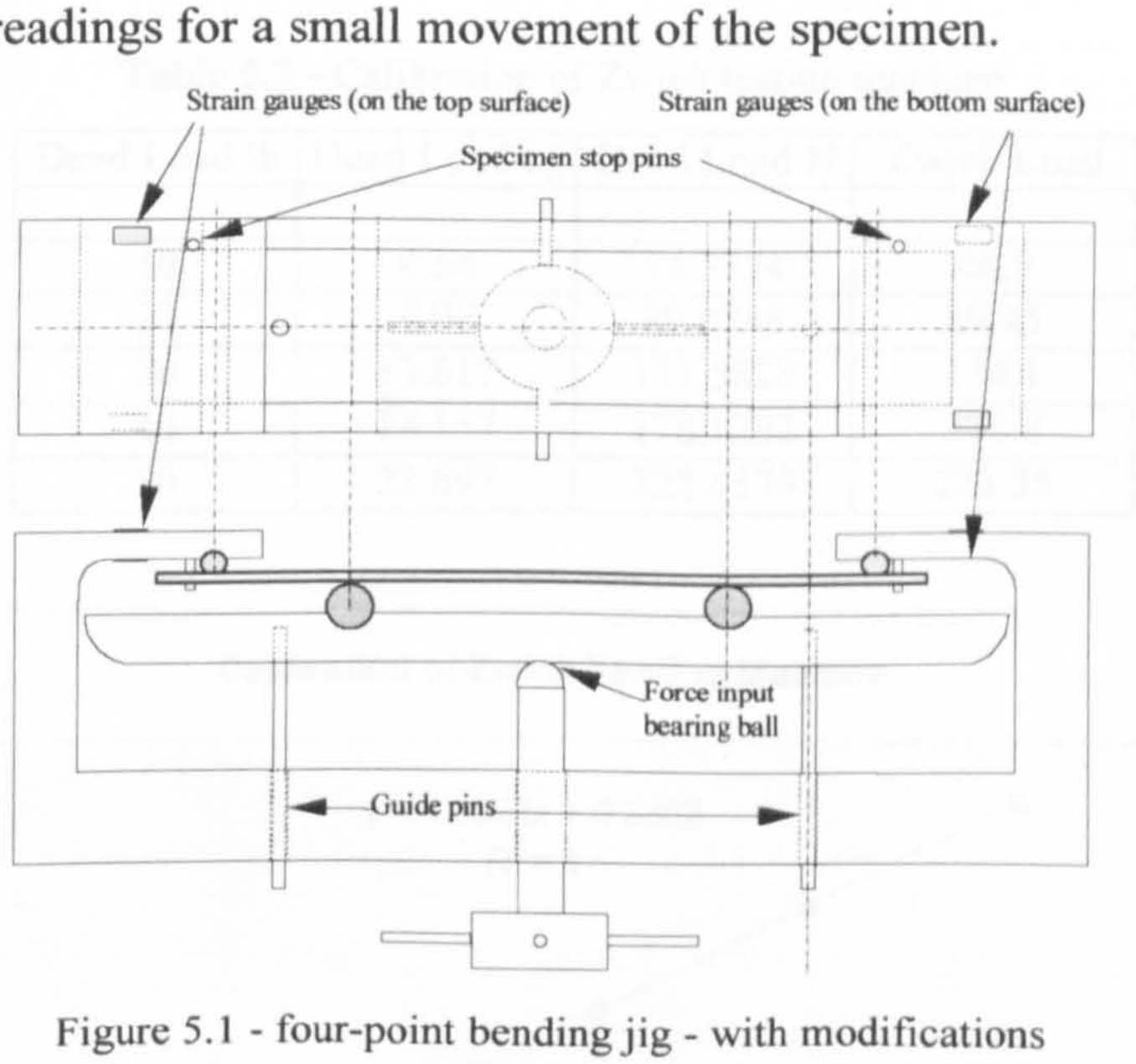

Figure 5.1 - four-point bending jig - with modifications

The guide pins of the four-point bend jig were replaced by another set of precise sliding fit pins which gave almost zero movement other than the force axis of the lower force input rollers. Two specimen stop pins were installed on the jig to avoid specimen movement, which gave a more consistent response from the strain gauges.

The force-input point was changed to a bearing ball to obtain the exact point of force input in every loading of the jig. The changes are described in Figure 5.1.

A calibration of the Zwick Testing Machine was carried out using calibrated dead loads (Table 5.1). In the calibration of the testing machine the calibrated dead loads were applied on the testing machine head and the corresponding readings from the load cell were recorded and are shown in Table 5.2. The readings were then plotted as Zwick load against applied load where a very good linearity was found which provided confidence in the calibration process.

Table 5.1 - Verification of dead weights with a calibrated scale

No. of Load	Load	Verified load
	lb	kg
0	10	4.54
3	10	4.54
12	10	4.537
25	10	4.54
34	10	4.54

Table 5.2 - Calibration of Zwick testing machine

Dead Load lb	Dead Load kg	Dead Load N	Zwick Load
10	4.54	44.5374	44.9
20	9.08	89.0748	89.45
30	13.617	133.5828	134.1
40	18.157	178.1202	178.8
50	22.697	222.6576	223.35

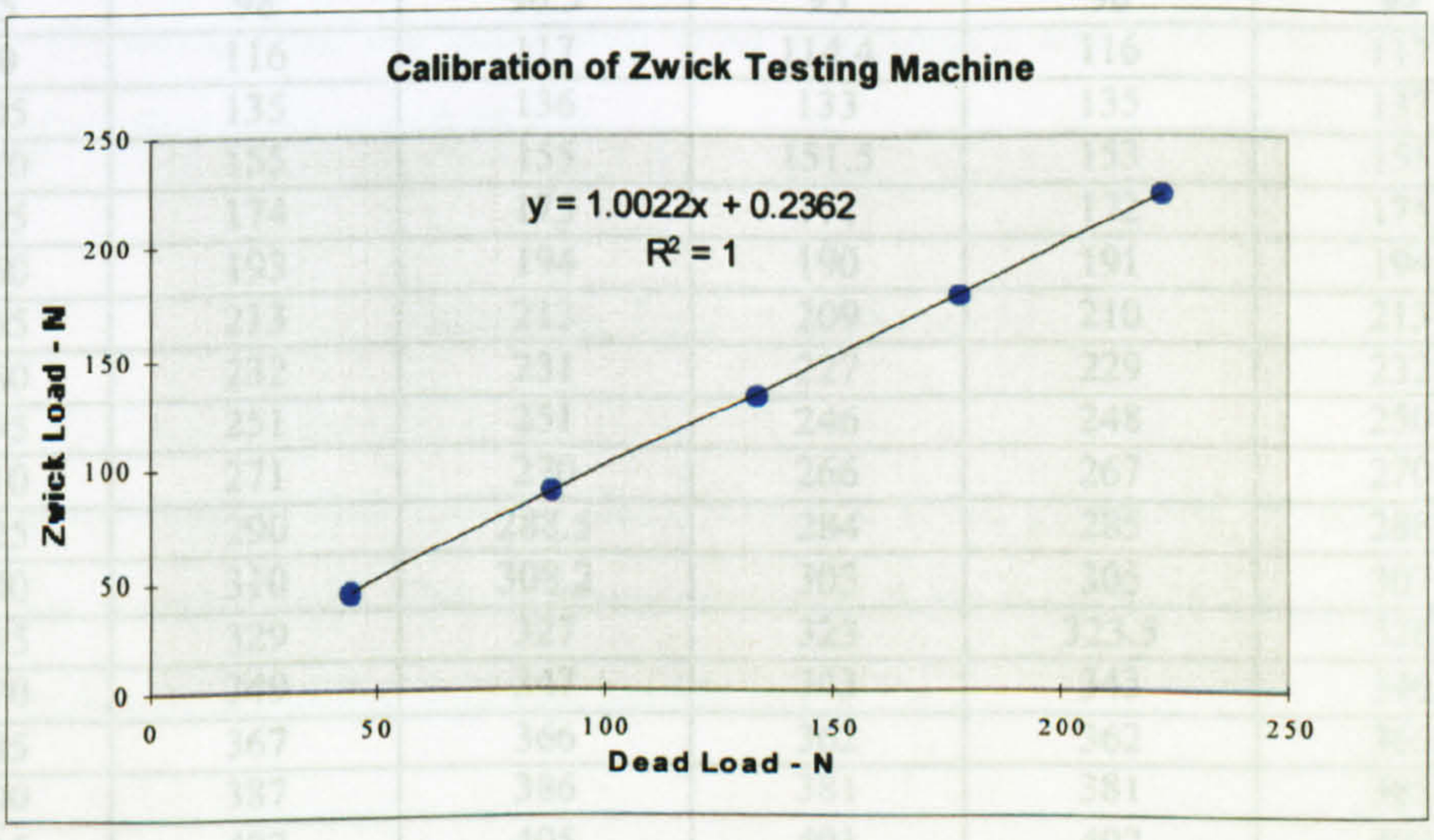

Figure 5.2 - Calibration of Zwick testing machine

The slope of the straight line was 1.0022 (Figure 5.2) which means that the ratio between the Zwick load and the applied load was 1.0022, i.e. only 0.22 % error in applied load was found which was negligible.

5.1.2 Calibration of Four-point Bending Jig Force Input

The four-point bend jig was calibrated to determine the relationship between the input force and its strain response from the full bridge - fitted to the jig. The Zwick testing machine was used as a force-input device and a P-3500 digital strain indicator (manufactured by Measurement Group Ltd, Raleigh, North Carolina, USA) was used to measure the strain bridge response. The steel specimen was 81 mm length, 19.05 mm wide and 1.59 mm thick. This width and thickness of the specimen was chosen to fit them into the four point bend and to position them on the four point bend such that symmetry is maintained on both sides of the four point bend. The maximum possible thickness of the specimen to be inserted into the four point bend was 1.8 mm and the allowable width of the specimen was 19.05±0.05 inch according to the design of the four point bend.

Table 5.3 - Five sets of data of strain response for same load steps

Force N	Micro Strain	Micro Strain	Micro Strain	Micro Strain	Micro Strain
	Set-1	Set-2	Set-3	Set-4	Set-5
15	19	18	18	19	18
30	39	38	37.5	38.5	38
45	58	58	57.5	58	58
60	77.5	78	77	77	77
75	98	96.5	95	96	97
90	116	117	114.4	116	117
105	135	136	133	135	137
120	155	155	151.5	153	155
135	174	175	171	172	175
150	193	194	190	191	194
165	213	213	209	210	213
180	232	231	227	229	232
195	251	251	246	248	250
210	271	270	266	267	270
225	290	288.5	284	285	288
240	310	308.2	303	305	307
255	329	327	323	323.5	326
270	349	347	343	343	346
285	367	366	362	362	365
300	387	386	381	381	385
315	407	405	401	402	404
330	426	424	420	421	424

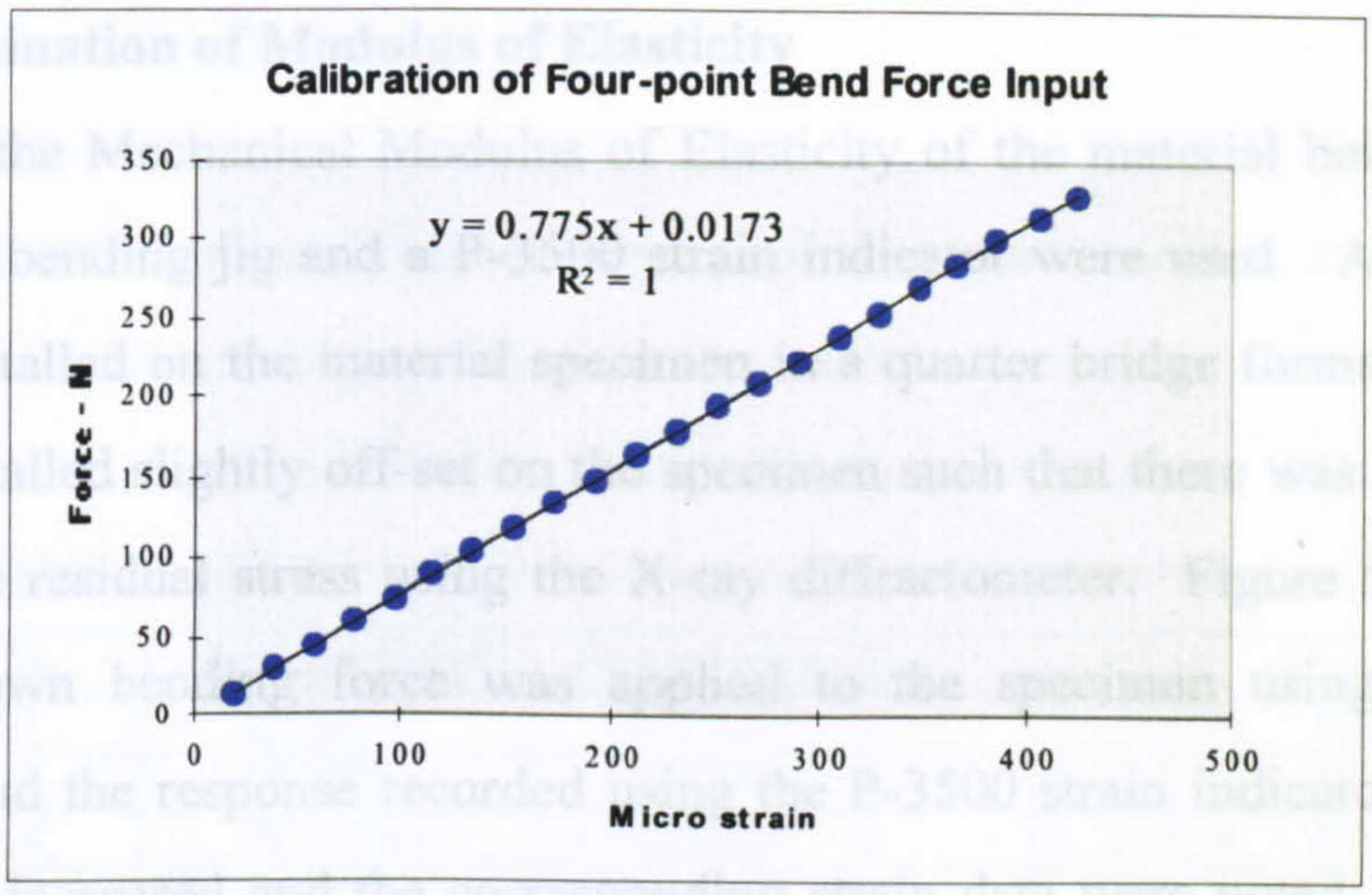

Figure 5.3 - Typical calibration of four-point bend force Input (set-1)

The input force was applied to the specimen using the Zwick testing machine and corresponding strain readings were taken from the strain indicator. The force to the specimen was gradually increased and corresponding strain readings were recorded. Five sets of data were taken (load in N and strain gauge reading in $\mu\varepsilon$) for the load steps shown in Table 5.3. The data were then plotted as load against strain and are shown in Figure 5.3.

The plots of all five sets of data (only one plot is shown here) shown in Table 5.3 above illustrated a good linearity and provided confidence in all these measurements. The slope of any plot could be considered as the calibration constant. To minimise the error in calibration, the average of all five constants were accepted as the calibration constant. By doing this, the maximum error anticipated was 0.867 %. The average gradient of all five plots was 0.78178.

$$\text{Therefore, } 1\ \mu\varepsilon = 0.78178 \text{ N.}$$

The above calibration was used to determine the force generated by the four-point bending jig thumbscrew. This information was further utilised in calculating the Modulus of Elasticity of the material loaded in the jig.

5.1.3 Determination of Modulus of Elasticity

To determine the Mechanical Modulus of Elasticity of the material being measured, the four-point bending jig and a P-3500 strain indicator were used. A strain gauge bridge was installed on the material specimen in a quarter bridge format. The strain gauge was installed slightly off-set on the specimen such that there was enough space to measure the residual stress using the X-ray diffractometer. Figure 5.4 shows the set-up. A known bending force was applied to the specimen using the integral thumbscrew and the response recorded using the P-3500 strain indicator. The force was gradually increased and the corresponding strain data were noted. Two sets of data were taken from two specimens; both specimens were prepared from the same steel bar; one of them was spot electropolished for the X-ray diffractometer measurement and other was simply emery finished. Using the applied force information obtained from the strain indicator readings, the induced bending stresses were calculated as follows.

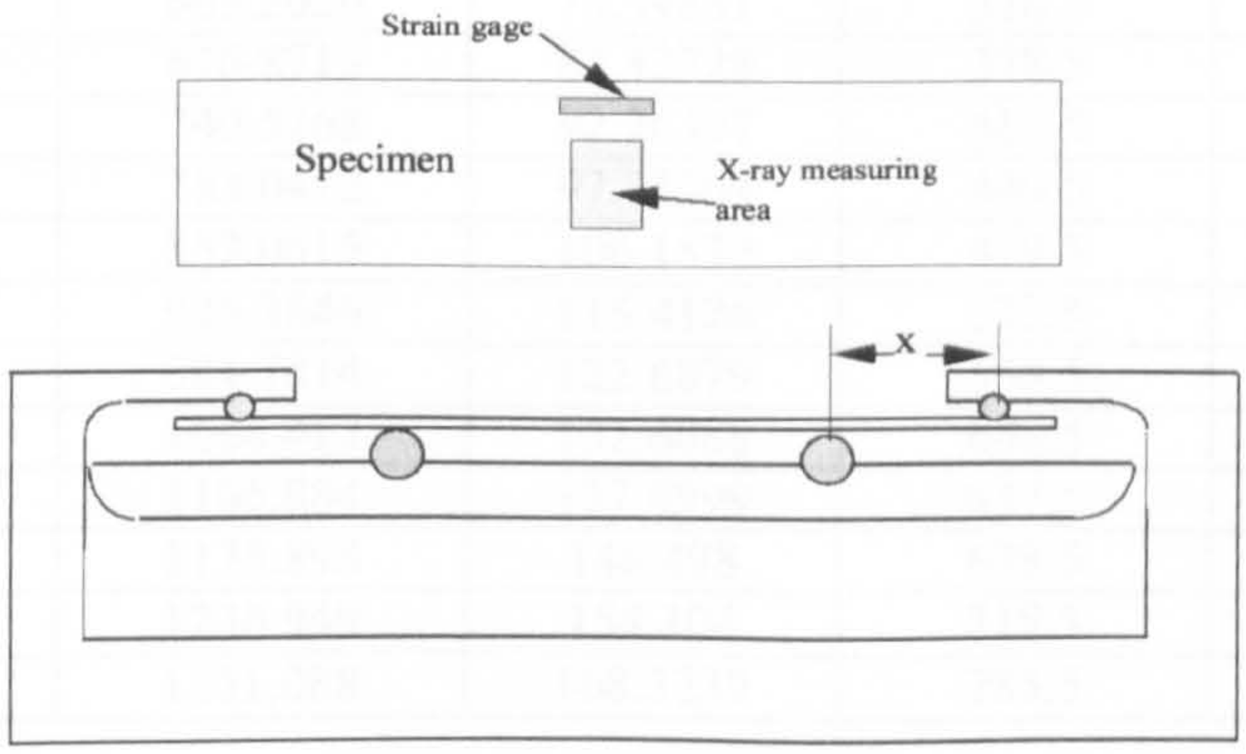

Figure 5.4 - four-point bending and strain gauge position on specimen

The induced stress on the specimen due to bending load was

$$\sigma = \frac{My}{I}$$

Where σ - Induced stress due to bending load

M - Moment applied to the specimen = (F × x)/2

y - Distance of the top-most fibre from the neutral axis of the specimen.

I - Moment of Inertia = $(bh^3)/12$

F - Applied load

x - Distance between two rollers = 13.5813 mm

b - width of the specimen = 19.05 mm

h - thickness of the specimen = 1.57 mm

All the parameters mentioned above were measured and the stress and strain values calculated. Table 5.4 and Figure 5.5 show the results.

Table 5.4 - Stress - Strain table of specimen - 1 (Electropolished

Force, N	Moment, Nmm	Stress, MPa	$\mu\varepsilon$	ε
4.29979	29.19837	3.637648	12	0.000012
9.38136	63.70553	7.936685	28	0.000028
16.41738	111.4847	13.8892	55	0.000055
24.23518	164.5726	20.5031	86	0.000086
28.92586	196.4254	24.47145	104	0.000104
35.57099	241.5501	30.09327	129.5	0.00013
40.65256	276.0573	34.3923	148.5	0.000149
46.9068	318.5277	39.68343	174	0.000174
54.7246	371.6156	46.29733	202.5	0.000203
62.15151	422.0492	52.58054	231.5	0.000232
66.84219	453.9019	56.54888	251.5	0.000252
73.87821	501.6811	62.5014	278.5	0.000279
80.91423	549.4602	68.45391	305	0.000305
89.12292	605.2026	75.39851	336.5	0.000337
99.67695	676.8713	84.32728	378.5	0.000379
109.0583	740.5768	92.26397	413.5	0.000414
115.3126	783.0472	97.55509	440.5	0.000441
125.4757	852.0615	106.1532	479.5	0.00048
136.4206	926.3846	115.4126	523.5	0.000524
145.0202	984.7814	122.6879	558.5	0.000559
156.7469	1064.413	132.6088	608.5	0.000609
163.0011	1106.884	137.8999	637.5	0.000638
173.1643	1175.898	146.498	678.5	0.000679
182.1547	1236.949	154.104	718.5	0.000719
198.963	1351.088	168.3239	785.5	0.000786

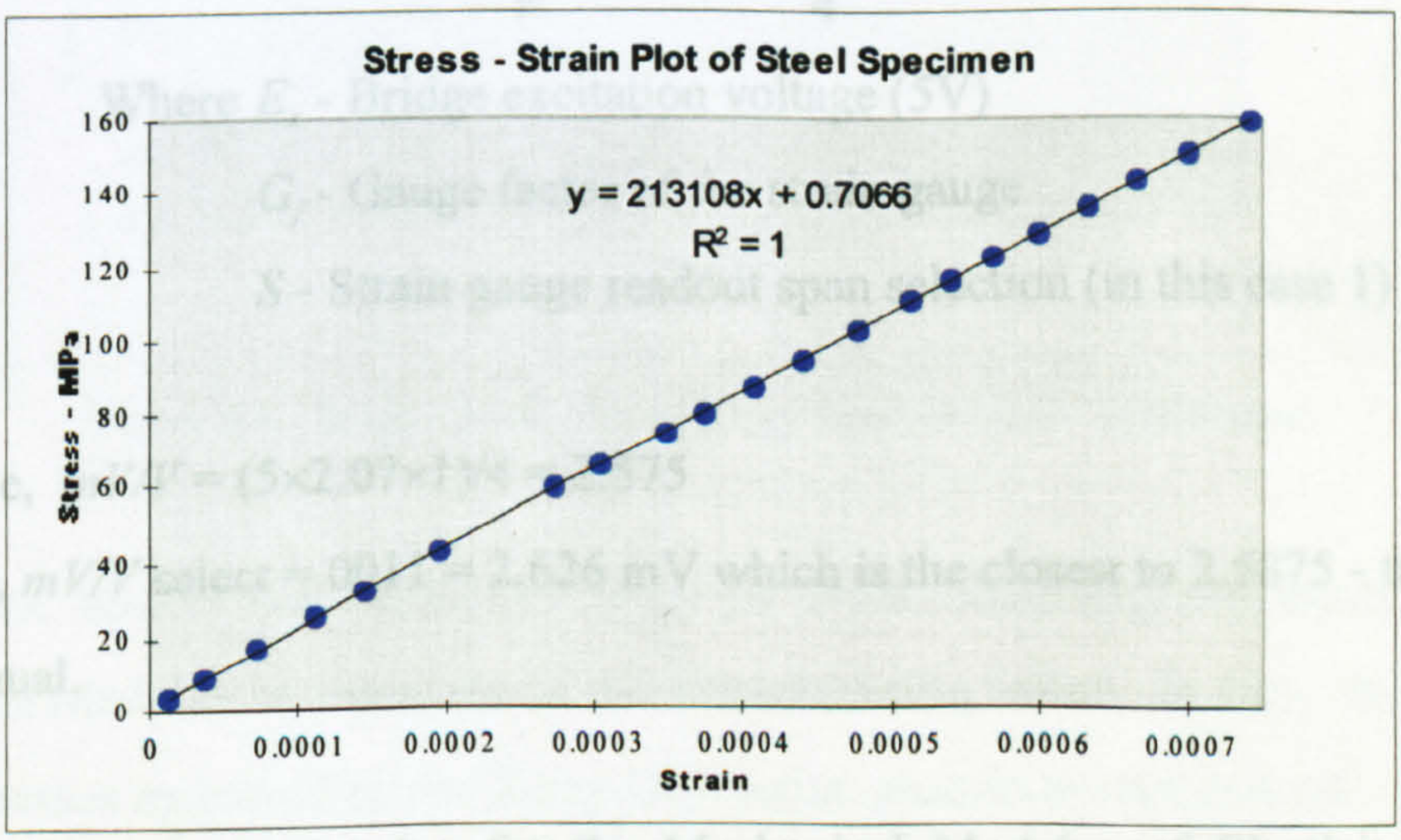

Figure 5.5 - Stress - Strain plot of specimen - 1 (Electropolished)

The Mechanical Modulus of Elasticity of the specimen is the slope of the stress-strain plot. The Mechanical Modulus of Elasticity of the electro-polished specimen was calculated as 213108 MPa. In the emery finished specimen the value was found as 213095 MPa (the table and the plot of the emery finished specimen are not shown here). The Modulus of Elasticity was taken as the average value of the two values found in two specimens.

The value of Mechanical Modulus of Elasticity can therefore be taken as 213.1 GPa for the specimen.

5.1.4 Determination of X-ray Elastic Constant

To calibrate the X-ray elastic constant, the four-point bending jig was suitably positioned on the goniometer table of the X-ray diffractometer. The specimen was placed on the four-point bending jig. The strain bridge indicating the applied force to the specimen was connected to the P-3500 strain indicator and strain gauge bridge on the specimen was connected to the Proto strain indicator.

Calibration of strain gauge bridge attached to the specimen was carried out using the equation:

$$\frac{mV}{V} = \frac{E_x G_f S}{4}$$

Where E_x - Bridge excitation voltage (5V)

G_f - Gauge factor of the strain gauge

S - Strain gauge readout span selection (in this case 1)

In this case, $mV/V = (5 \times 2.07 \times 1)/4 = 2.575$

Therefore, mV/V select = 0011 = 2.626 mV which is the closest to 2.5875 - taken from Proto manual.

The previously obtained value for the Mechanical Modulus of Elasticity (213100 MPa) was entered in the material chart part of the XRDWIN program. The bending

stress was applied to the specimens using the force input screw of the four point bend (Figure 5.1). Before taking any measurement a little stress was induced in the specimen as an initial stress to get linearity in the measured stresses. Using the X-ray diffractometer the stress in the specimen was measured and same time a strain value from the Proto strain indicator was recorded. The bending stress to the specimen was applied in several steps which were below the yield strength of the material. More bending stress to the specimen was applied and the residual stress (using the X-ray diffractometer) and strain increment (from Proto strain indicator) were measured. This process was continued for several steps to obtain a reasonable set of data. The applied stresses to the specimens were kept below the yield strength of the specimen.

The value of the assumed X-ray Elastic Constant (E/(1+ν) = 213100/1.29) and the Mechanical Modulus of Elasticity value 213100 MPa were inserted into the material property chart of the Proto strain program and a stress - strain graph was plotted. The stress - strain plot is shown below.

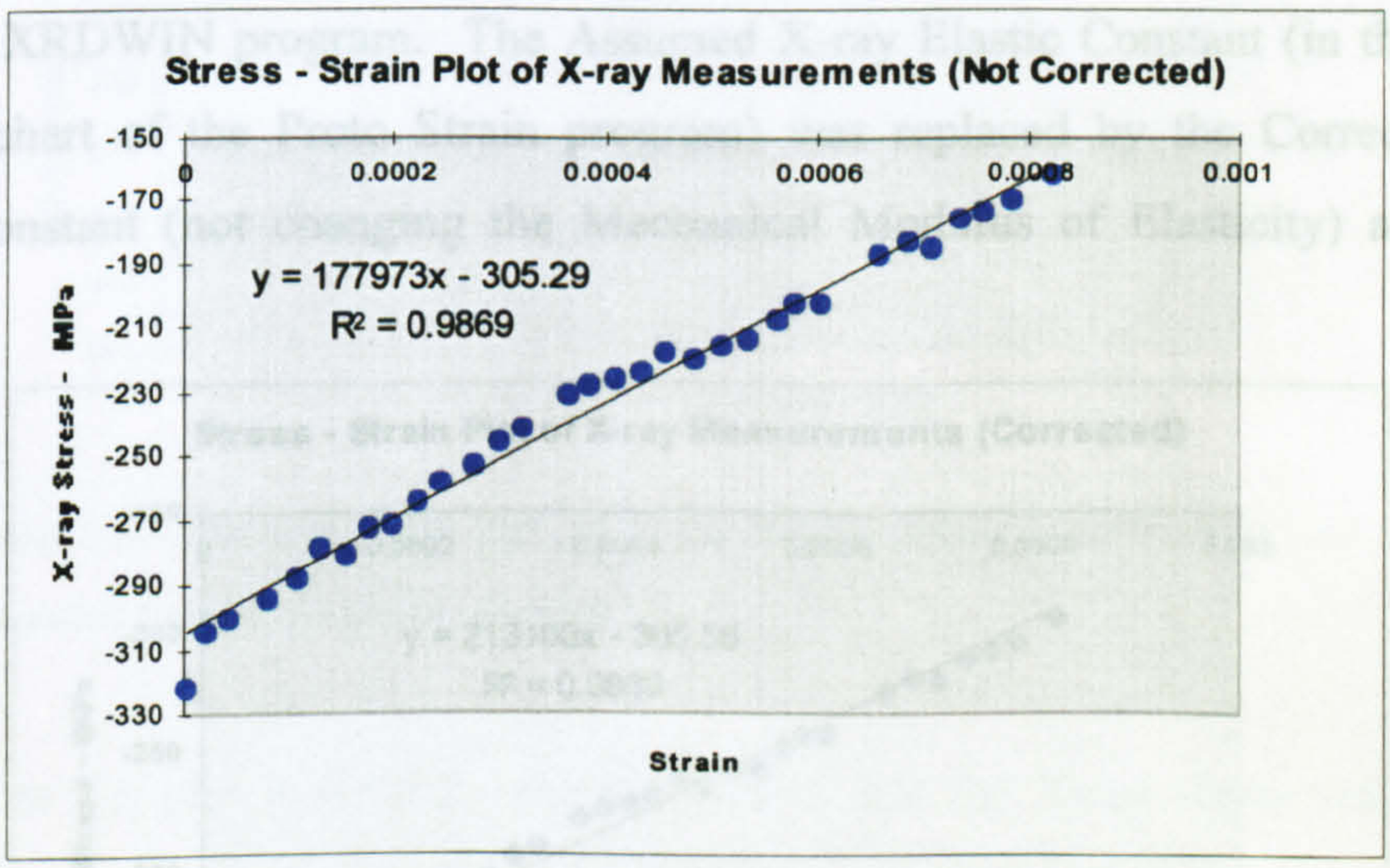

Figure 5.6 - Stress - strain plot of X-ray measurements - uncorrected

In the plot above, the calculated slope is lower than the previously obtained Mechanical Modulus of Elasticity of the material being tested. In turn, this indicates that the stresses measured by the X-ray Diffraction process are not correct.

The plot of the XRDWIN software programme provided two important pieces of data, in determining the actual residual stresses obtained using the X-ray Diffractometer.

They were

Slope = 177973.268 MPa.

Corrected X-ray Elastic Constant = 197798.484 MPa.

To obtain the corrected stress values, the K_c value of the X-ray and the effective Young's Modulus were calculated

K_c = (Corrected X-ray Elastic Constant)/(Assumed X-ray Elastic Constant)

K_c = 197798.484/165193.7984 = 1.197372

E_{eff} = 213100 × 1.197372 MPa = 36961.98 ksi

Young's Modulus in the Material property chart of the XRDWIN program was then replaced by the new value of E_{eff} (as shown above) and stresses were calculated again using the XRDWIN program. The Assumed X-ray Elastic Constant (in the material property chart of the Proto Strain program) was replaced by the Corrected X-ray Elastic Constant (not changing the Mechanical Modulus of Elasticity) and plotted again.

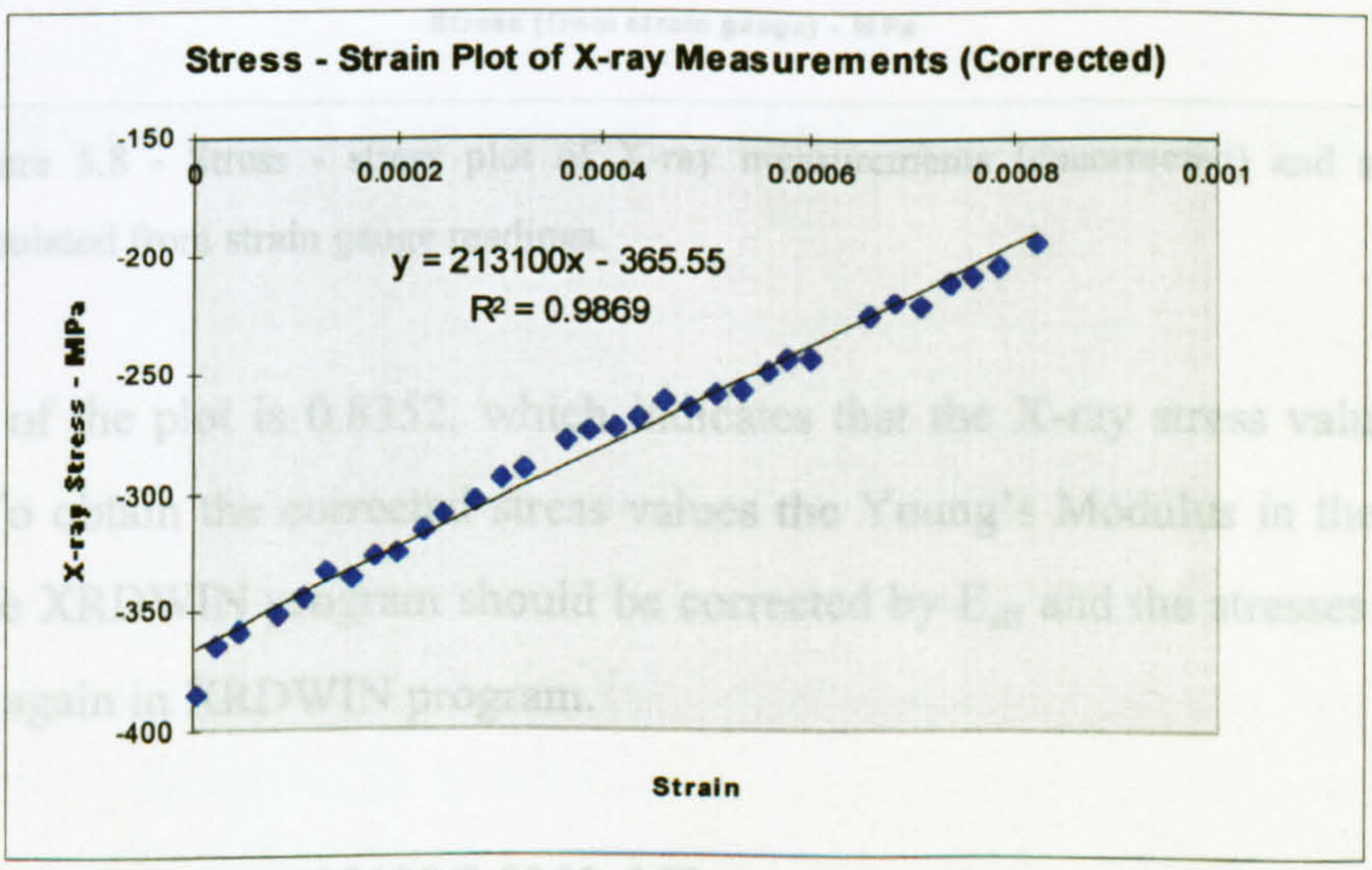

Figure 5.7 - Stress - strain plot of X-ray measurements – corrected

The plot above is showing its slope as 213100 MPa, which is the same as the value of the Mechanical Modulus of Elasticity, and the K_c value in the second plot is 1, which indicates that the measured stress values are correct.

5.1.5 Alternative Method of Calibration

The measured X-ray stress can be plotted against stress (calculated from strain gauge readings, $\sigma = E \times \varepsilon$), in which the slope would determine the status of the X-ray measured stresses. If the X-ray measured stresses are correct then the slope of the plot should be 1. In this test the X-ray measured stress against stress from the strain gauge was plotted.

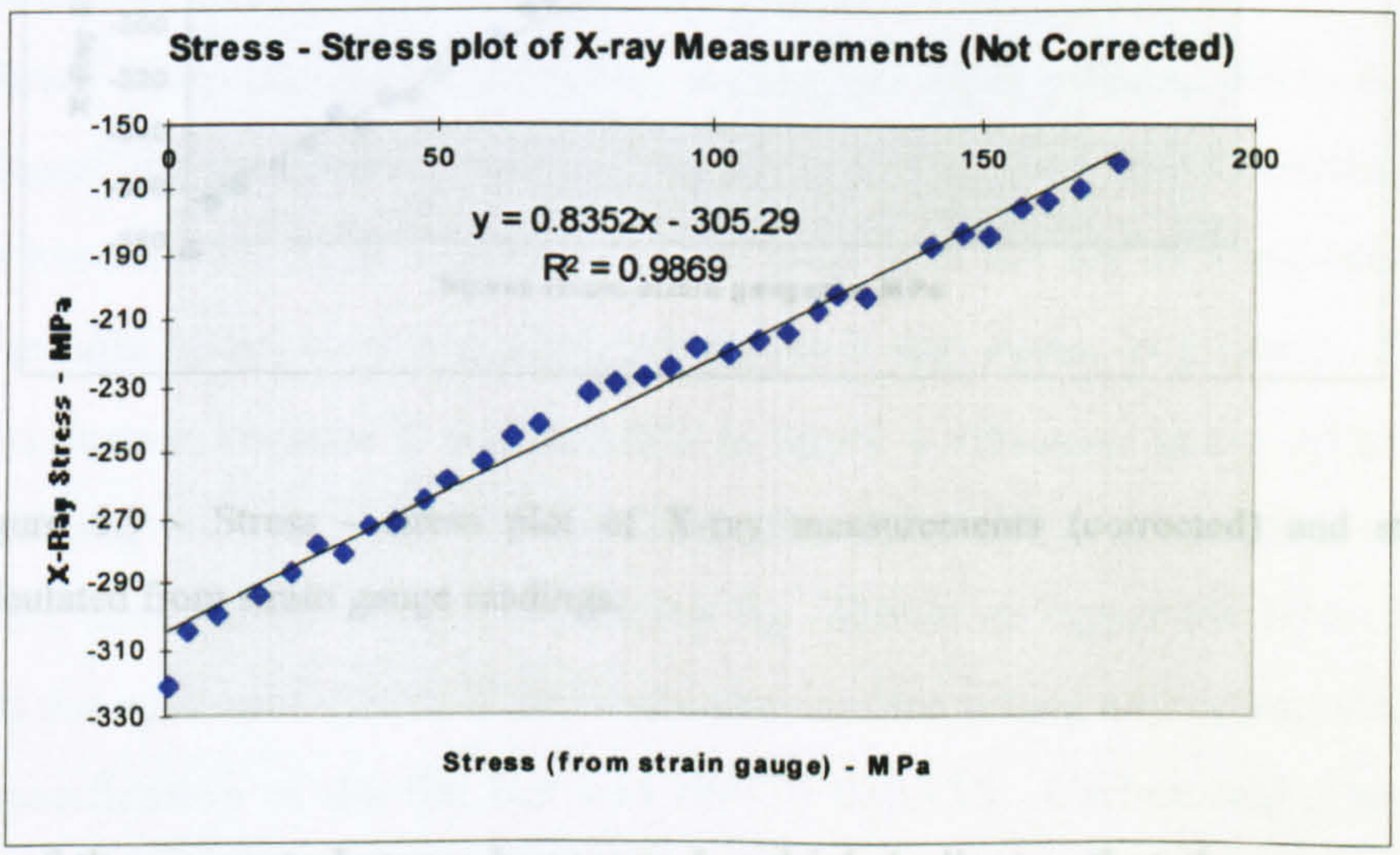

Figure 5.8 - Stress - stress plot of X-ray measurements (uncorrected) and stresses calculated from strain gauge readings.

The slope of the plot is 0.8352, which indicates that the X-ray stress values are not correct. To obtain the corrected stress values the Young's Modulus in the materials chart of the XRDWIN program should be corrected by E_{eff} and the stresses should be calculated again in XRDWIN program.

$$E_{eff} = 213100/0.8352 \text{ MPa}$$
$$= 213100 \times 0.144858029/0.8352 \text{ ksi}$$
$$= 36960.3 \text{ ksi}$$

and $E_{eff}/(1+\nu)$ $= 213100/(1.29 \times 0.8352)$ MPa.

$= 197789.51$ MPa.

The corrected X-ray stress values are again plotted as X-ray stress against stress (from the strain gauge), which are given below

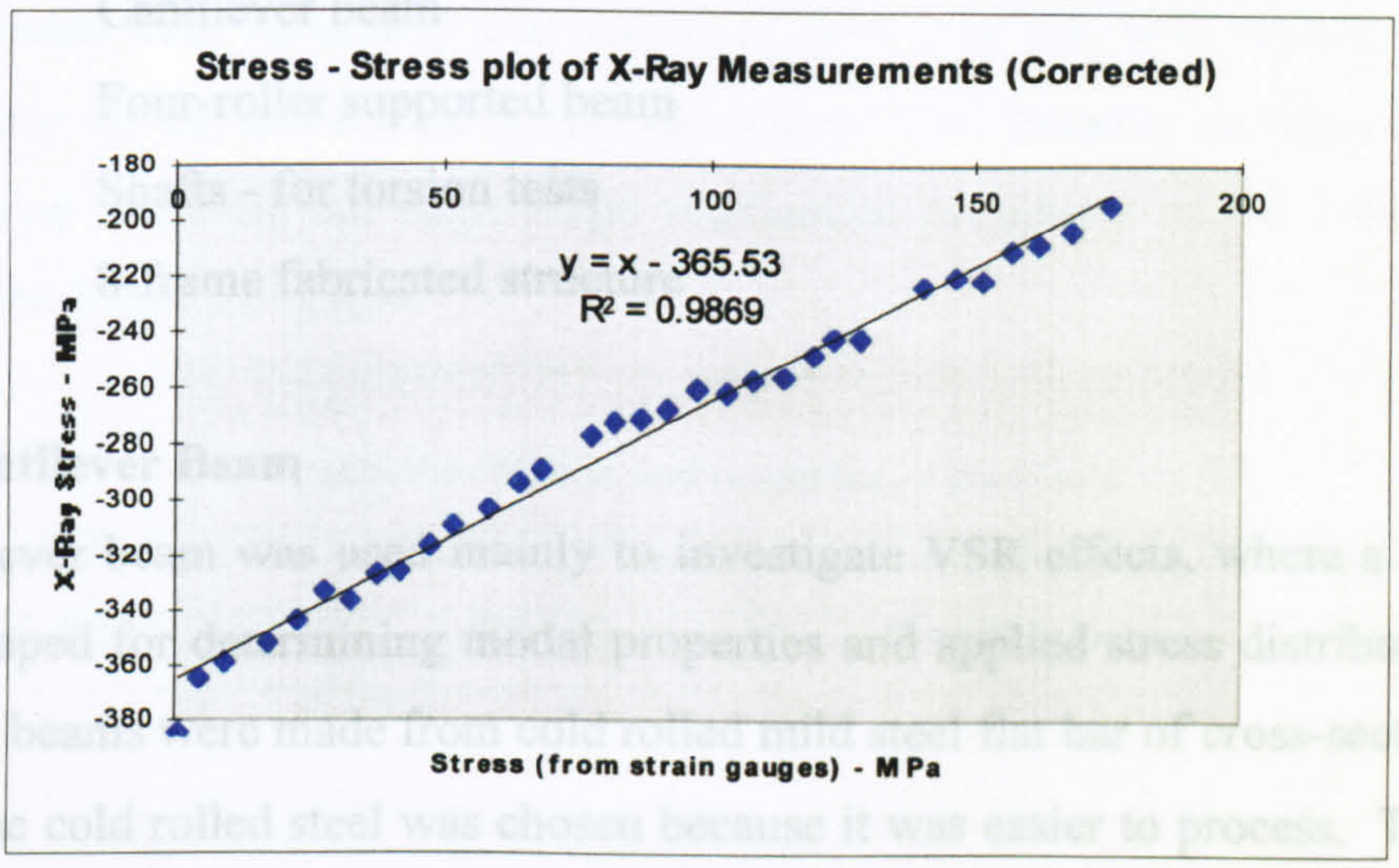

Figure 5.9 - Stress - stress plot of X-ray measurements (corrected) and stresses calculated from strain gauge readings.

The slope of the corrected stress becomes 1, which indicates that the stress values are correct.

5.2 Test Specimen Specification - Dimensions, Chemical and Mechanical Properties)

Due to the restricted space in the X-ray cabinet, fairly small specimens had to be used. It was also decided to use simple specimens and locate them kinematically - within the cabinet. These factors would decrease the variability of the test results and allow them to be processed more efficiently. In this study mainly four different types of specimens were used:

1. Cantilever beam
2. Four-roller supported beam
3. Shafts - for torsion tests
4. 8-frame fabricated structure

5.2.1 Cantilever Beam

The cantilever beam was used mainly to investigate VSR effects, where a FE model was developed for determining modal properties and applied stress distribution. The Cantilever beams were made from cold rolled mild steel flat bar of cross-section 1/4 in $\times$ 3 in. The cold rolled steel was chosen because it was easier to process. This cross-section was chosen because it was suitable to apply a vibratory stress up to 380 MPa with the existing vibrator and was easy to handle. Also due to its width it was easy to locate on the goniometer using the locating jig (shown in Appendix II) and to check the level of the specimen (using a dial indicator) before taking any measurements. The material specification of the flat bar was BS970 080A15. Carbon and other alloying elements are shown in the Table (5.5) below.

Table 5.5 - Alloying elements of the cantilever beam specimen

% C	% Si	% Mn	% P	% S
0.18	0.23	0.88	0.013	0.011

Total length of the specimen was 290 mm which included clamping length and free length for vibration. It was decided to put a single pass bead weld line near the clamp (Figure 5.10) of the specimen to induce some residual stress. The free length of the specimen was chosen considering the requirement of the applied stress and the capacity of the vibrator. The designed specimen is shown in Figure 5.10 below.

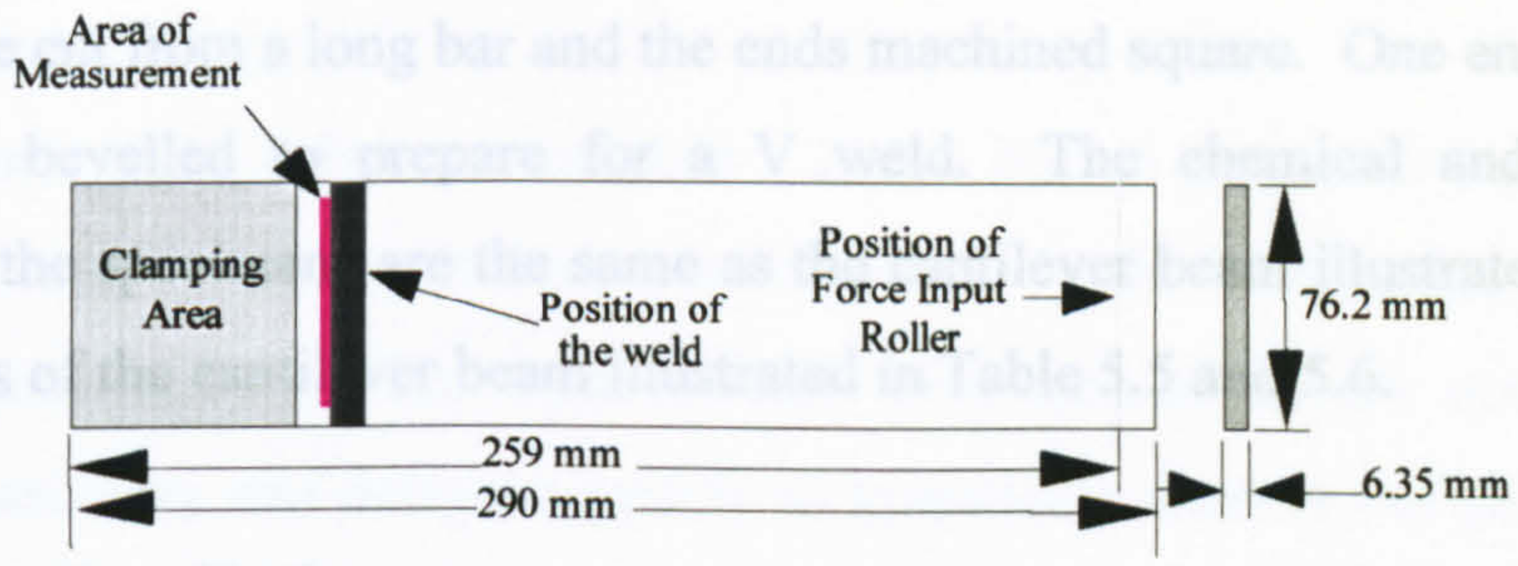

Figure 5.10 - Cantilever beam specimen.

The specimens were accurately cut from a 12 foot long bar, with special care being taken to keep the cut end square in both directions - thus ensuring an equal distance of the weld line from the cut edge. The mechanical properties of the specimens are shown in the Table 5.6 below.

Table 5.6 - Mechanical properties of used steel

Ultimate tensile strength, R_m	Yield point, $R_{P(0.2\%)}$	Modulus of Elasticity, E	Poisson's ratio, ν
611 MPa	607 MPa	210609 MPa	0.265

5.2.2 Four-Roller Supported Beam

The same cross section and material choice was used for the four-roller supported specimen. The material specification and alloying elements were the same as the cantilever beam specimens (section 5.2.1). One complete specimen comprised of two identical pieces of bar, joined by MIG welding. The specimen dimensions are given below.

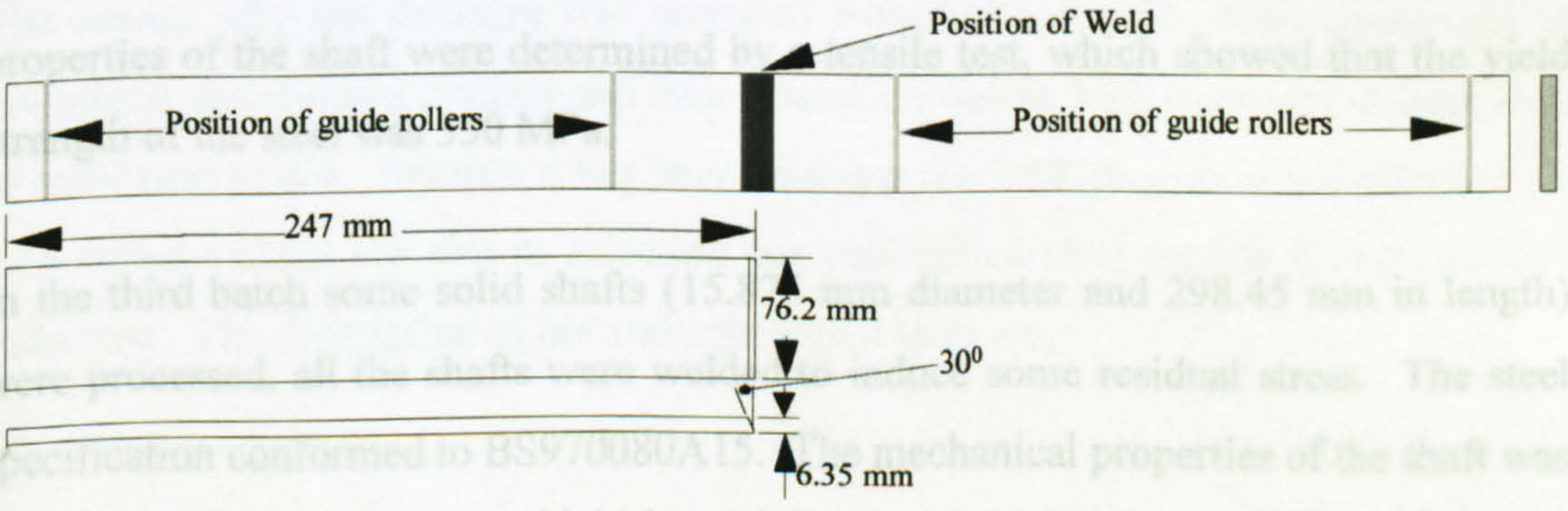

Figure 5.11 - Four-roller supported beam specimen

The bars were cut from a long bar and the ends machined square. One end of each bar was suitably bevelled to prepare for a V weld. The chemical and mechanical properties of the specimens are the same as the cantilever beam illustrated in same as the specimens of the cantilever beam illustrated in Table 5.5 and 5.6.

5.2.3 Torsion Test Shaft

For torsional test, hollow and solid, both kinds of shafts were used. Considering the requirement of the applied stress to the specimen for VSR treatment, the experimental set-ups along with the dimensions of shafts were modified. First of all some hollow shafts (25.4 mm OD and 22 mm ID and 430 mm in length - mild steel oddments properties not known) were used for treatment. Some of them were welded to induce residual stress, others were treated without any welding, i.e. treated as a homogeneous material. There was not enough length left after preparing the specimens for VSR treatment to carry out a tensile test to obtain the yield stress, so a hardness test was carried out. The Rockwell hardness was found to be B-56. From that hardness value, the ultimate tensile strength was assumed to be 370 MPa (from the Materials Handbook). There is no particular relationship between the yield stress and ultimate strength of any material. Which means that the yield strength cannot be determined directly. To obtain an approximate yield stress, 70 - 75% of the ultimate strength can be considered which is a reasonable approach. In that case the yield strength would be 277 MPa.

In the second batch hollow steel shafts having the dimensions 21.3 mm OD, 13.9 mm ID and 430 mm in length were treated - some of them welded before vibratory treatment. The steel specification of the shafts conformed to BS1387. The mechanical properties of the shaft were determined by a tensile test, which showed that the yield strength of the steel was 350 MPa.

In the third batch some solid shafts (15.875 mm diameter and 298.45 mm in length) were processed, all the shafts were welded to induce some residual stress. The steel specification conformed to BS970080A15. The mechanical properties of the shaft was determined by a tensile test, which showed that the Yield Strength was 401 MPa.

5.2.4 8-Frame

The dimensions of the 8-Frame were 400 × 200 × 20 × 6 mm and it was decided to prepare the frame by cutting it from a solid plate. In this connection hot and cold rolled solid plates (200 × 6 mm cross section) were used as the raw material for this frame. The structure was designed mainly to investigate some out of plane modes of vibration. A previous finite element parametric study was carried out to aid selection of the cross-section.

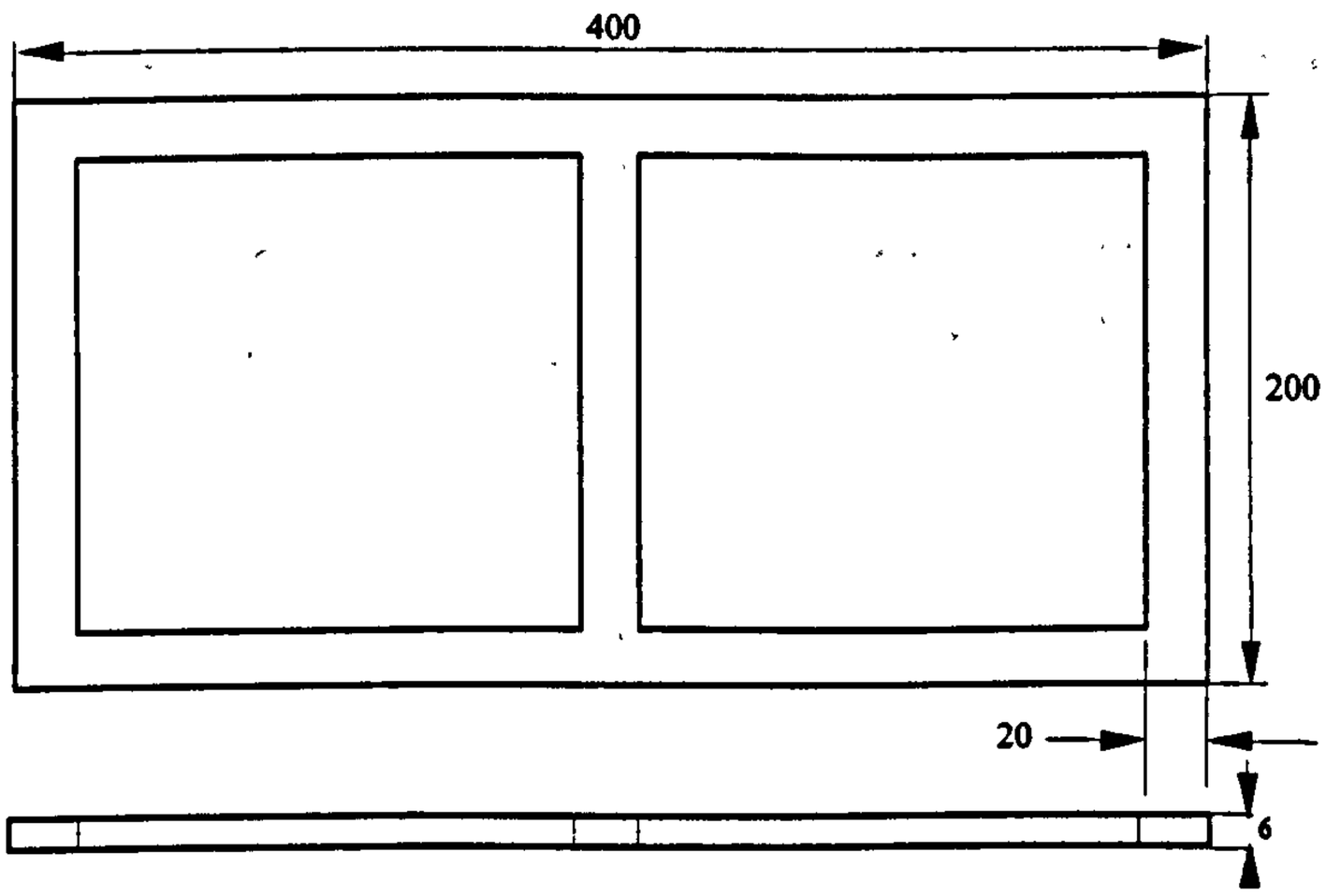

Figure 5.12 - 8-Frame specimen

To prepare the frame the rectangular sections were cut by drilling 1.5 mm diameter holes at each corner and therafter a band saw was used to cut the straight parts. The inside edges were finish machined by a milling cutter. The outside edges were also cut by band saw and finished by a milling cutter.

The reason why the structure was prepared from hot and cold rolled plates was to investigate the residual stresses and their relaxation due to VSR treatment in both kind of solid steel plates. Because it has been said that the VSR process is not effective on cold rolled metals, the aim in selecting the cold rolled steel was to investigate this statement. The description of hot and cold rolled steel are;

Cold rolled steel BS 970 080A15 (Cross section 8 in × 0.25 in)

Table : 5.7 - Chemical properties of cold rolled steel

C % (m/m)	Si % (m/m)	Mn % (m/m)	P % (m/m)	S % (m/m)
0.16	0.14	0.81	0.013	0.008

Density (measured) 7.714×10^3 kg/m^3

The mechanical properties are not specified for 080A15 (in BS970).

To obtain the mechanical properties, the hardness of the material was tested. The tested hardness number was recorded as HRB 84 to 86. The equivalent ultimate tensile stress was noted as 562 MPa. The yield stress of the material can be taken as 71 % of the ultimate stress - giving a yield stress = 399 N/mm^2

Hot rolled Steel BS 4360 43A (cross section 200 × 6 mm)

Table 5.8 - Chemical properties of the hot rolled steel

C % (m/m)	Mn % (m/m)	S % (m/m)	P % (m/m)	Si % (m/m)
0.0900	0.5800	0.0360	0.0450	0.1800

Table 5.9 - Mechanical properties of the hot rolled steel

Ultimate tensile strength, R_m, MPa	Yield stress, R_e, MPa	Elongation, A_{min}, %
465	345	29.6

5.3

"During Welding" Treatment

5.3.1 Experiment I: Static Induced Stress Welding Test

Abstract

In this experiment some bar specimens were welded while they were in a pre-stressed condition with either tensile or compressive stresses to investigate their effect. The peak longitudinal residual stresses were found to decrease and transverse residual stresses were found to increase with the application of tensile static stresses. Residual stresses away from the weld toe were also decreased with the application of tensile stresses. Compressive applied static stresses caused general increase in residual stresses all along the measurement line. Thus, the effect of compressive induced stresses was found to be adverse to the reduction in the residual stresses.

5.3.1.1 Introduction

This experiment was designed to investigate the effect of pre-stress on residual stresses formed in a welded structure. Some researchers have shown that the presence of stress during cooling and phase transformation can change the appearance of the transformation products. It was shown that austenite can be retained in steel due to insufficient transformation energy, which can cause additional residual stress in metal. The presence of stresses during transformation can cause a well organised crystal structure of the metal. Applied stress does not always work in favour of transformation - sometimes it works against it. Details of this phenomenon are described in Bhadeshia [15].

For VWC, this study is important because the welding transformation is always stress influenced. During cooling, the weld and surrounding HAZ experience either tensile or compressive stress that modify the transformation products and possibly cause some change in the residual stress state.

5.3.1.2 Experimental Procedure

In this experiment, static stresses were applied to the specimens prior to the weld, in order to observe its effect on residual stresses. It was decided to use a bead weld on flat mild steel bar (76.2 mm × 6.35 mm) to investigate the residual stress in the HAZ.

A small line (3 to 5 mm length) at the mid-width of the specimen started from the weld toe was selected for observation. The mid-width was chosen to minimise boundary effects.

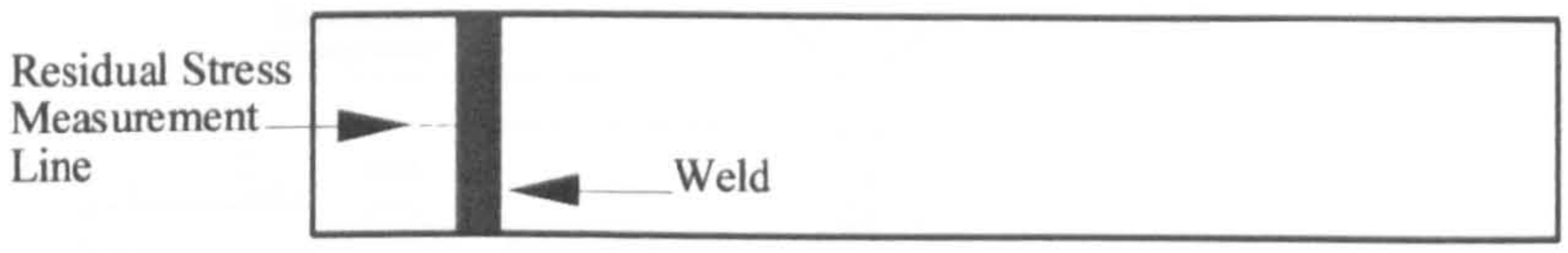

Figure 5.13 - Position of the stress measurement line

In this experiment, two batches of specimens were processed. In the first batch, different levels of tensile stresses were induced on the top surface of the specimens where the bead welding was carried out (shown in Figure 5.14) and the induced stress effect to the welding residual stress was investigated. The details of the experimental set-up are shown in Figure 5.14. To induce static tensile stress on the top surface, the specimens were clamped as a cantilever beam and a static bending load was applied on the top surface of the far end of the specimens. Details of the loading conditions are shown in the experimental result (Section 5.3.1.4) batch 1. The static applied stresses to the specimens were determined by measuring the deflection at a certain point on the specimens. The deflection was then calibrated for applied stresses which are shown in Section 5.3.1.3.

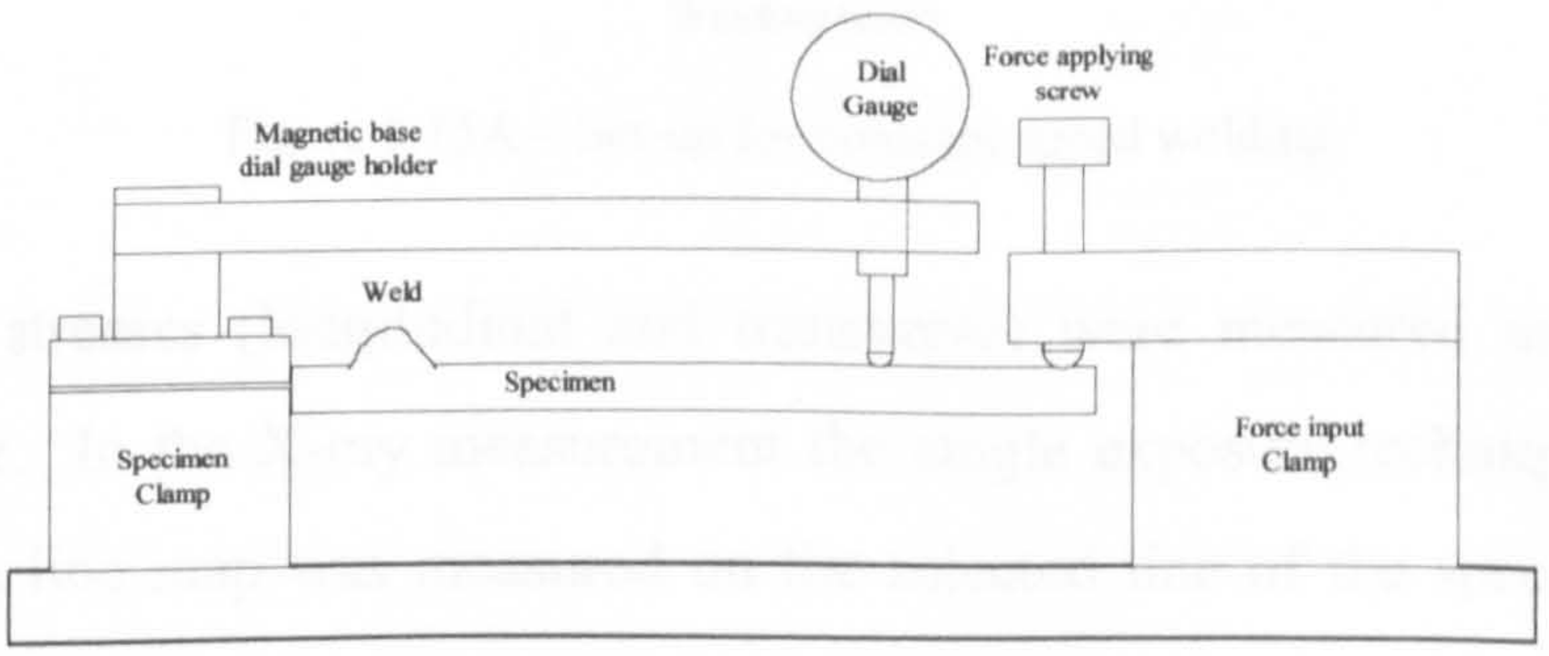

Figure 5.14 - Applied stress set-up - static tensile at weld - top surface

In the second batch, different levels of tensile and compressive stresses were induced on the top surface of the specimens and their effect on the welding residual stresses investigated. To induce compressive static stress on the top surface, the specimens were clamped and the static loads were applied at the bottom of the far end of the

specimens (Figure 5.15). The details of the loading conditions are shown in the experimental results (Section 5.3.1.4) batch 2.

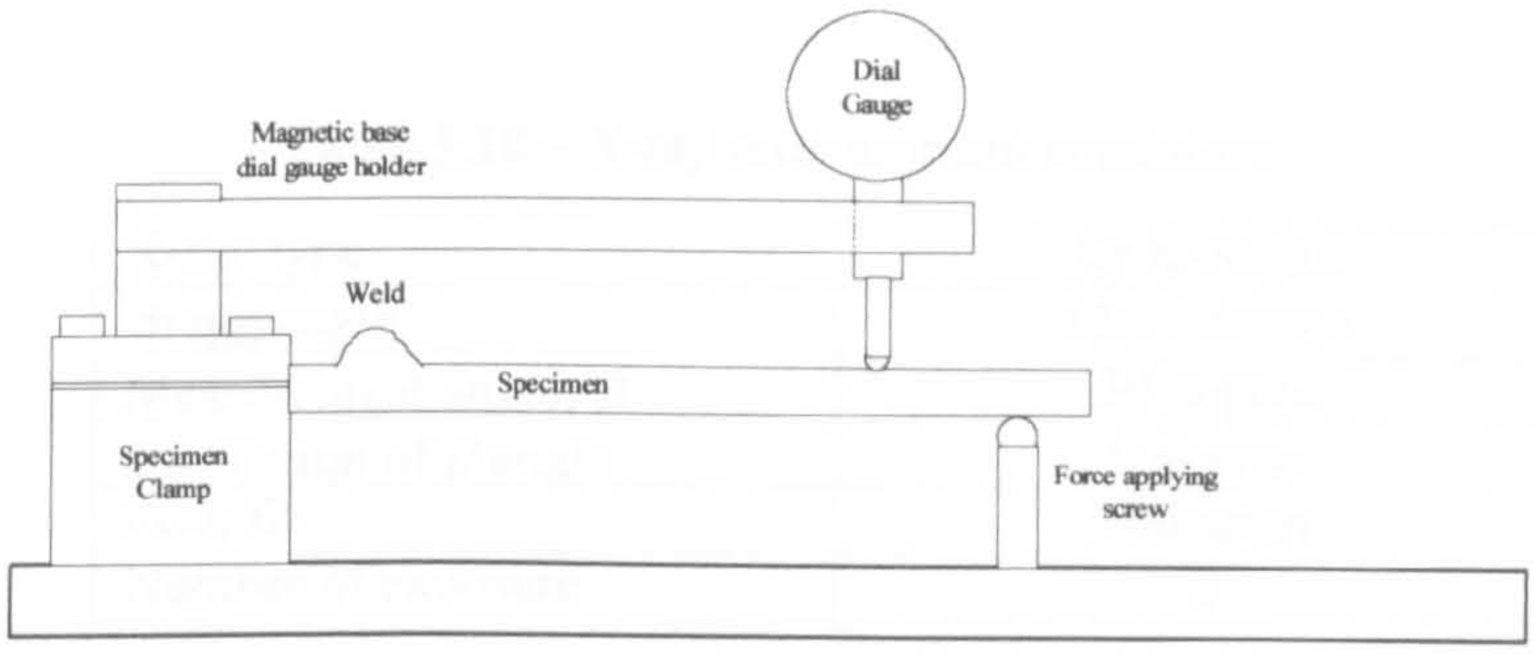

Figure 5.15 - Applied stress set-up - static compressive at weld - top surface

The welding speed was controlled by a torch holder which was connected to a stepper motor. An external resistance-controlled speed controller controlled the speed of the stepper motor. The set-up for controlling the welding speed is shown in Figure 5.15A.

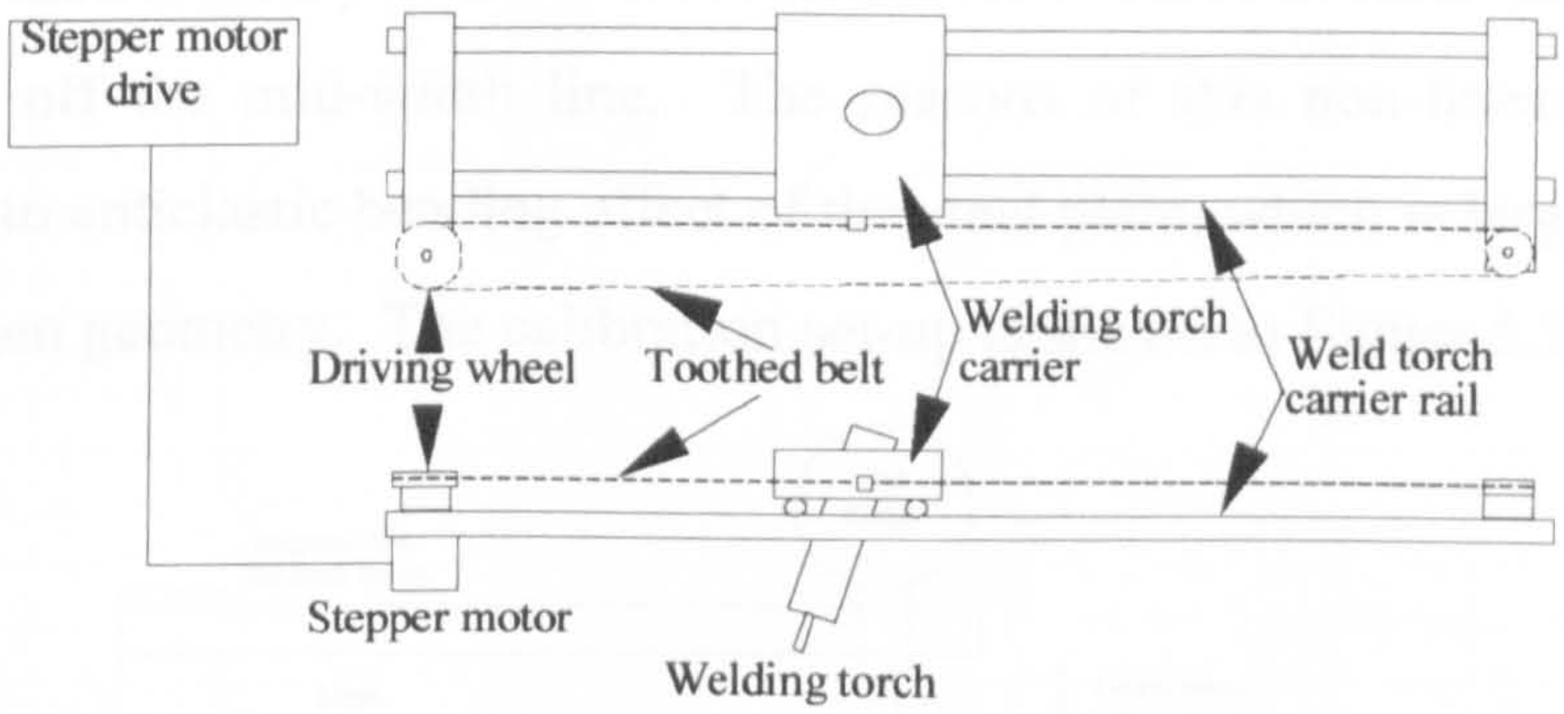

Figure 5.15A – Set-up for constant speed welding

The residual stresses (longitudinal and transverse) were measured using an X-ray diffractometer. In the X-ray measurement the single exposure technique (SET) was used, where a line map was measured on the selected line of the specimens (Figure 5.13). The measurements were carried out using a fixed position X-ray head where the goniometer table moved to locate the measurement point under the head. The movement of the goniometer under the X-ray head was controlled by a computer. The specimens were located on the goniometer table using a positioning jig, where six points were used to locate the specimens in the exact position every time. After positioning the specimens on the jig they were clamped using a clamping screw, which prevented from any movement of the specimens relative to the goniometer

table/clamping jigs. The measurement jig is shown in Appendix II. The conditions of the X-ray measurements are shown in the table below.

Table 5.10 – X-ray measurement conditions

X-ray type	Cr K-Alpha
Bragg angle	156.1 degree
Measurement angle, β	30 degree
Oscillation of β angle	0 degree
Peak fit	Gaussian
Number of exposure	2

5.3.1.3 Calibration of Induced Stresses

The induced stress due to bending the specimen was calibrated using a strain gauge positioned at the mid-width line of the specimen. The mid-width line was selected because some non-linearity of the induced stress was observed when the strain gauge was installed off the mid-width line. The reasons of this non-linearity was most probably due to anticlastic bending effect of the steel plate, which is largely dependent on the specimen geometry. The calibration set-up is shown in Figure 5.16.

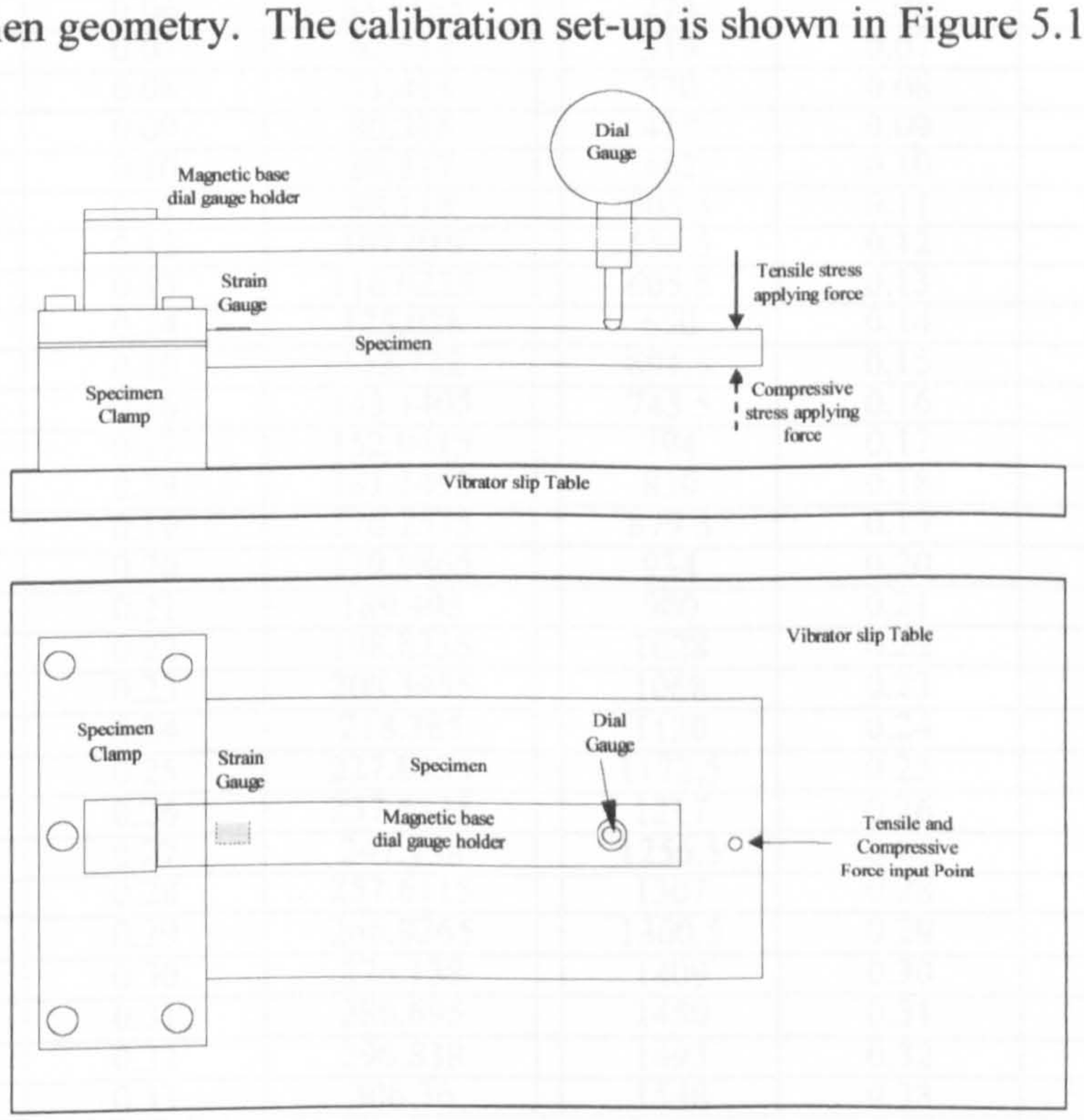

Figure 5.16 - Calibration set-up for pre-induced tensile and compressive stress

By installing the strain gauge at the mid-width, the average stress was found. The bending force (tensile and compressive) was applied to the specimen by a screw (Figure 5.16). The deflection of the specimen was measured using a precision dial gauge (1 div = 0.0001 inch) and at the same time, the strain was measured using a P-3500 digital strain indicator (manufactured by Measurement Group, Raleigh, North Carolina, USA). The deflection was gradually increased and the corresponding deflection and strain readings were recorded. The deflection of the specimen was plotted against the applied stress in order to obtain the calibration constant. The calibration table and plots are shown below.

Table 5.11 - Calibration Table - tensile and compressive applied stress

Tensile Stress			Compressive Stress		
Mic Strain	Deflection	Stress	Mic Strain	Deflection	Stress
	inch	MPa		inch	MPa
0	0	0	0	0	0
48	0.01	9.936	46	0.01	9.522
90	0.02	18.63	90.5	0.02	18.7335
132	0.03	27.324	136	0.03	28.152
175	0.04	36.225	182.5	0.04	37.7775
217	0.05	44.919	229.5	0.05	47.5065
259.5	0.06	53.7165	274	0.06	56.718
302	0.07	62.514	319	0.07	66.033
345	0.08	71.415	370	0.08	76.59
388	0.09	80.316	417	0.09	86.319
431	0.10	89.217	462	0.10	95.634
474	0.11	98.118	505.5	0.11	104.638
517	0.12	107.019	556.5	0.12	115.195
560.5	0.13	116.0235	605.5	0.13	125.338
604	0.14	125.028	650	0.14	134.55
646	0.15	133.722	691.5	0.15	143.140
691.5	0.16	143.1405	745.5	0.16	154.318
734.5	0.17	152.0415	794	0.17	164.358
778.5	0.18	161.1495	839	0.18	173.673
822.5	0.19	170.2575	879.5	0.19	182.056
869.5	0.20	179.9865	934	0.20	193.338
915	0.21	189.405	980	0.21	202.86
960.5	0.22	198.8235	1028	0.22	212.796
1006.5	0.23	208.3455	1068	0.23	221.076
1055	0.24	218.385	1120	0.24	231.84
1100.5	0.25	227.8035	1172.5	0.25	242.707
1147.5	0.26	237.5325	1217	0.26	251.919
1194	0.27	247.158	1256.5	0.27	260.095
1244.5	0.28	257.6115	1307	0.28	270.549
1289.5	0.29	266.9265	1360.5	0.29	281.623
1334	0.30	276.138	1409	0.30	291.663
1385	0.31	286.695	1450	0.31	300.15
1434	0.32	296.838	1493	0.32	309.051
1480	0.33	306.36	1548	0.33	320.436

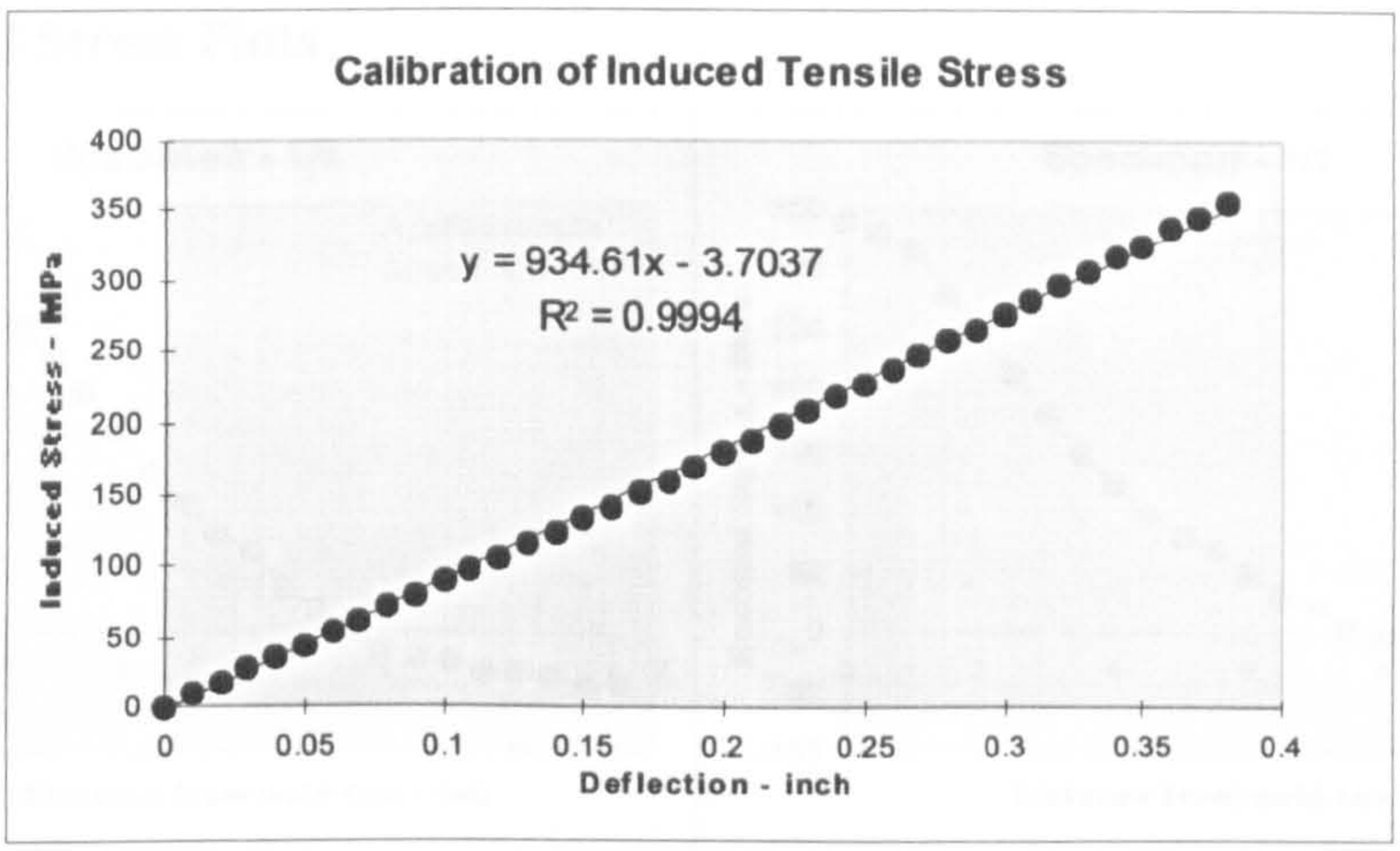

Figure 5.17 - Calibration plot of tensile applied stress

Calibration constant : 1 inch deflection = 934.61 MPa induced Stress

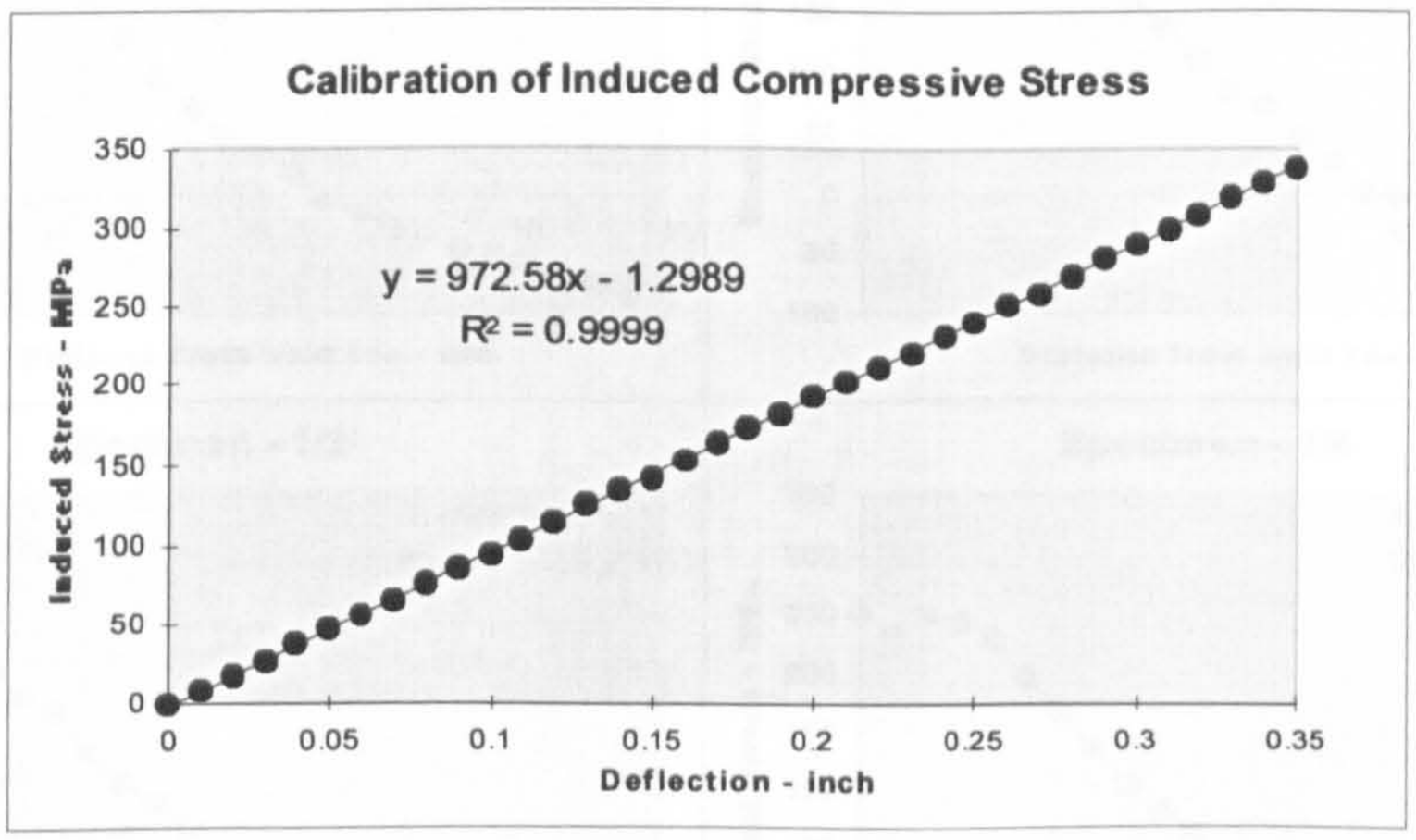

Figure 5.18 - Calibration plot of compressive applied stress

Calibration constant : 1 inch deflection = 972.58 MPa induced Stress

5.3.1.4 Experimental Results

Batch 1

In this batch, a total of 8 specimens were processed, where different levels of tensile bending stress were applied to the top surface of the specimens. In the pre-stressed condition a single pass bead weld on the top surface of the specimen was carried out and the pre-stress was maintained until the specimens cooled down to room temperature. The measured longitudinal and transverse residual stresses and also the summary plot are shown below. A description of the summary plot is provided in the discussion of results section of this batch.

Longitudinal Stress Plots

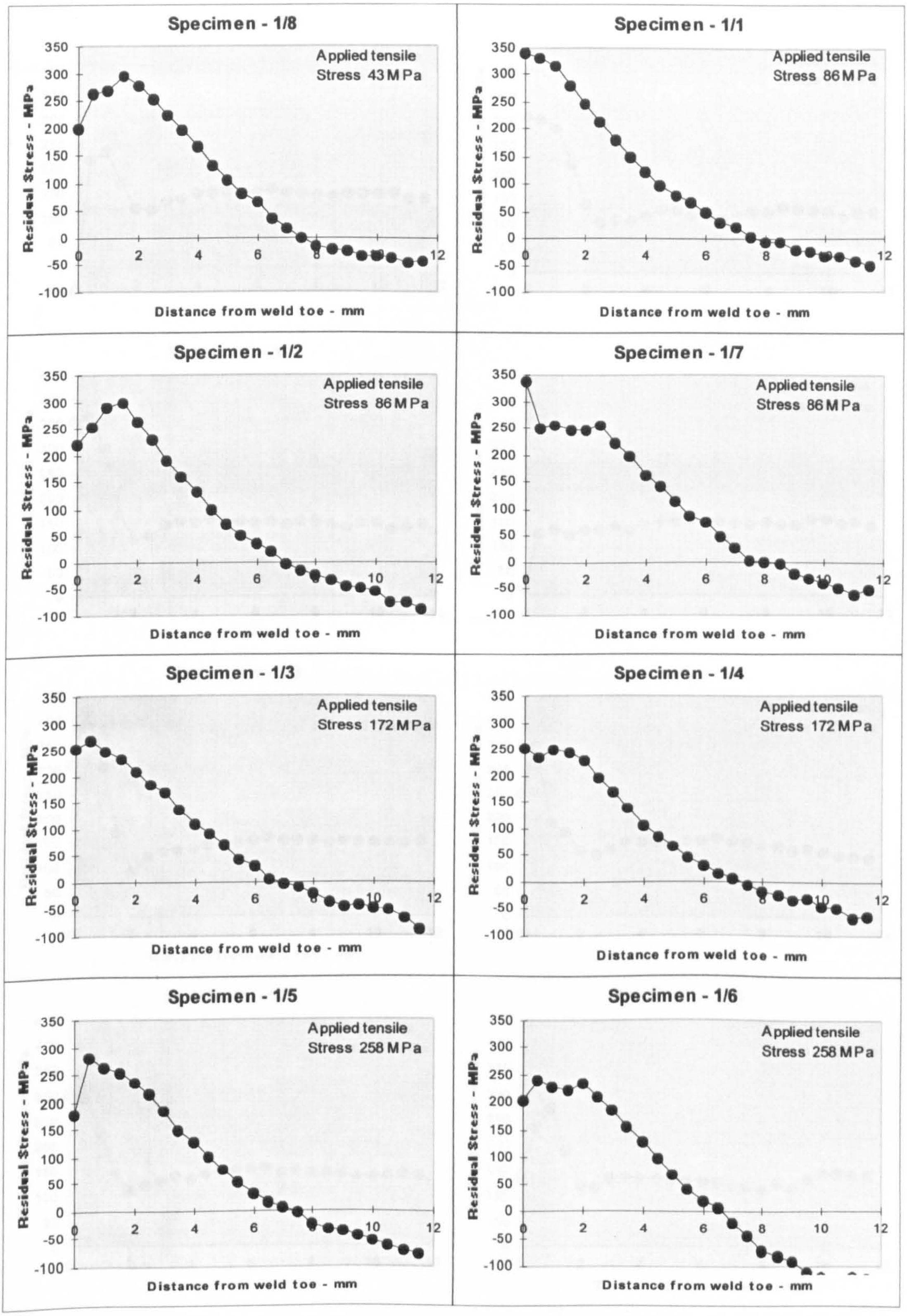

Figures 5.19 to 5.26 - Longitudinal stress plots - specimens 1/1 to 1/8

Transverse Stress Plots

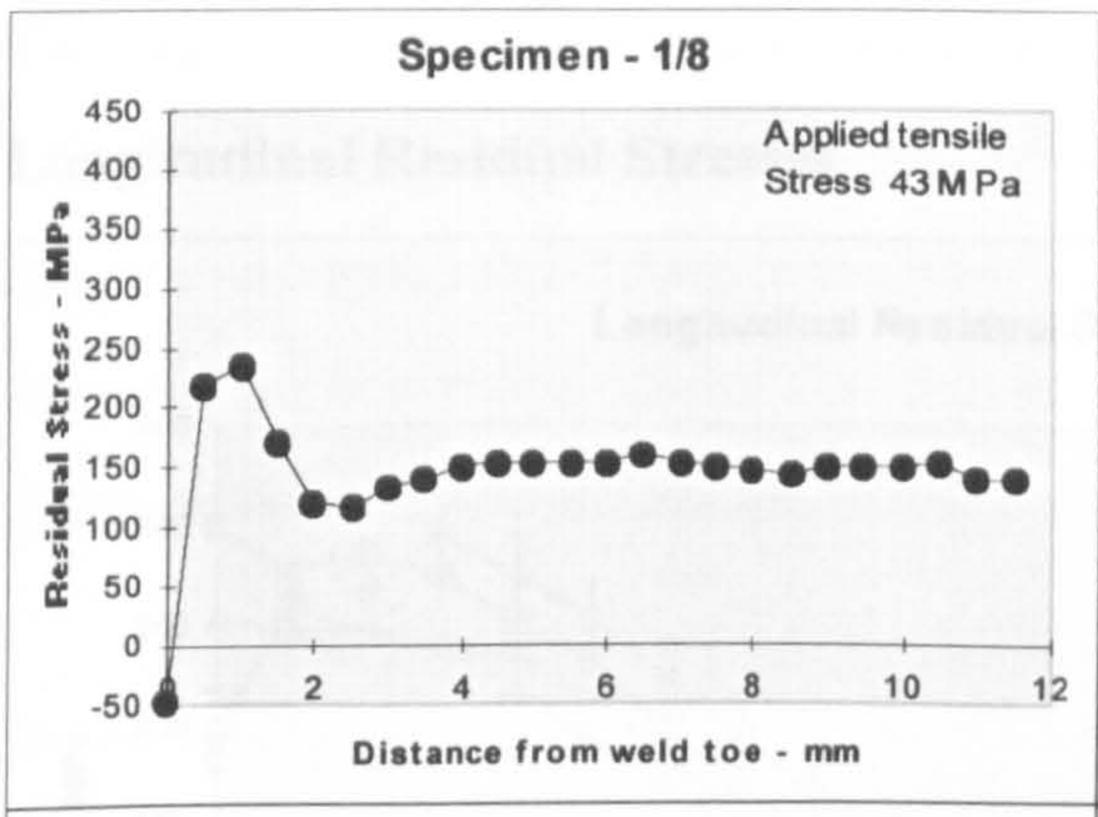

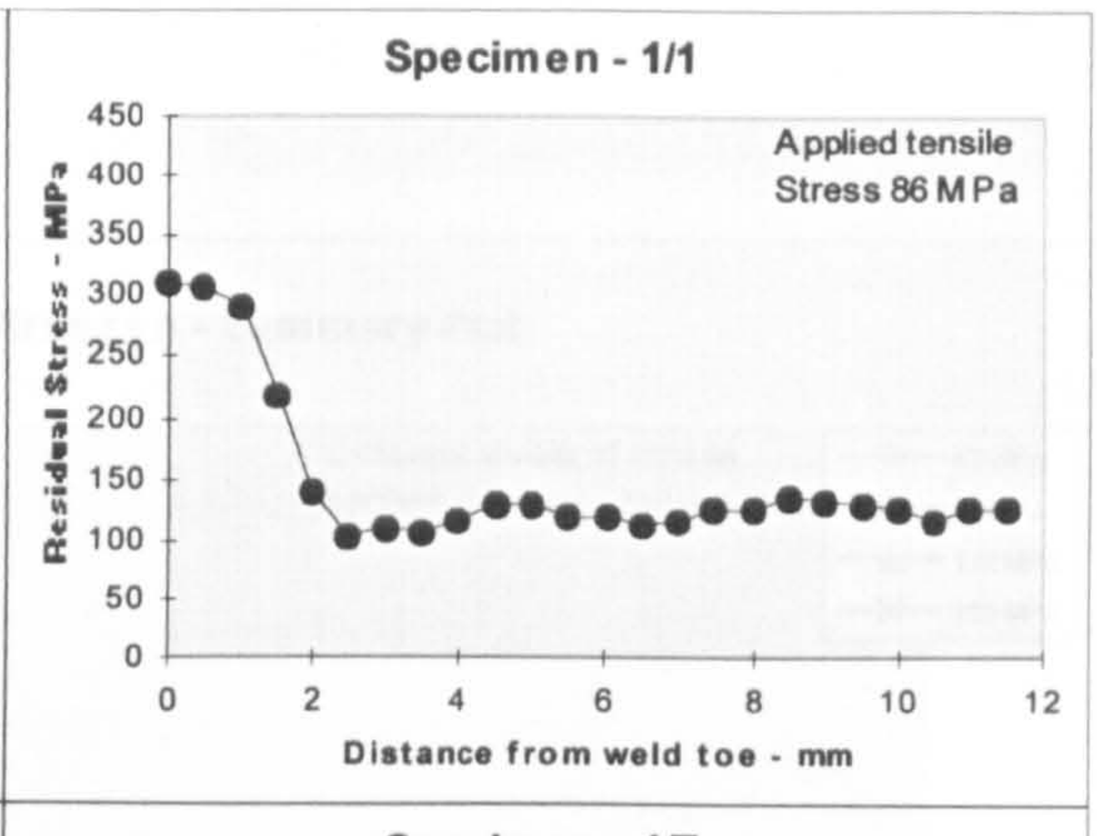

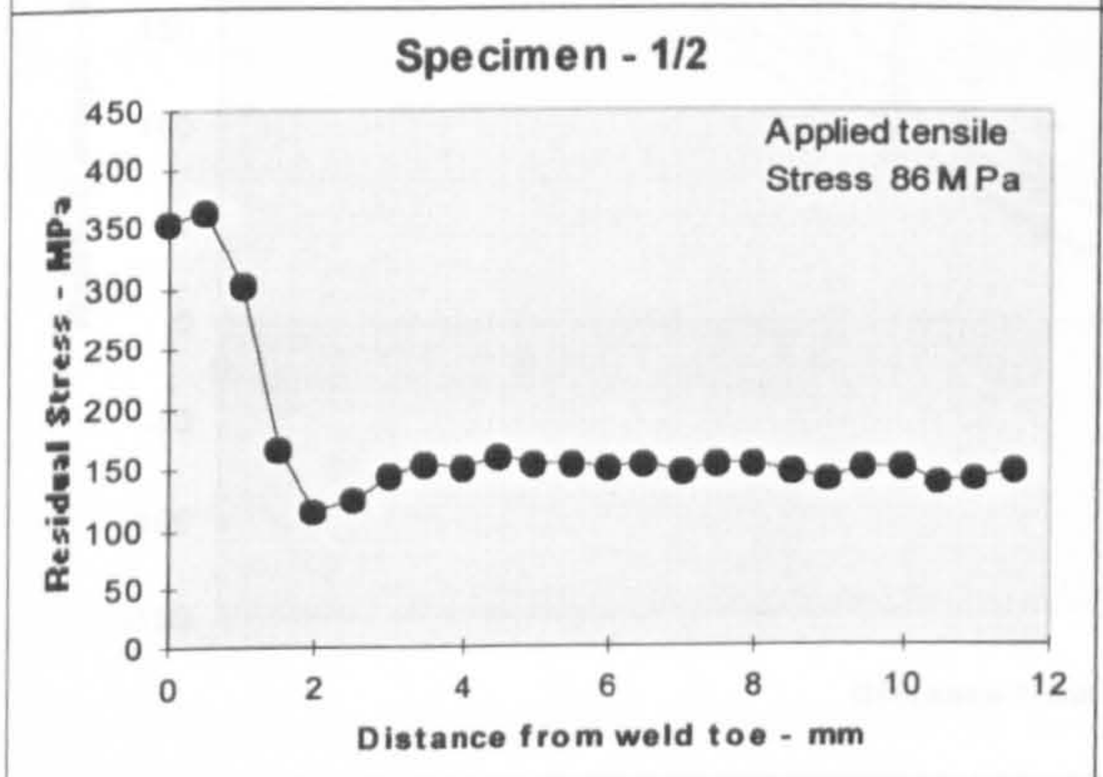

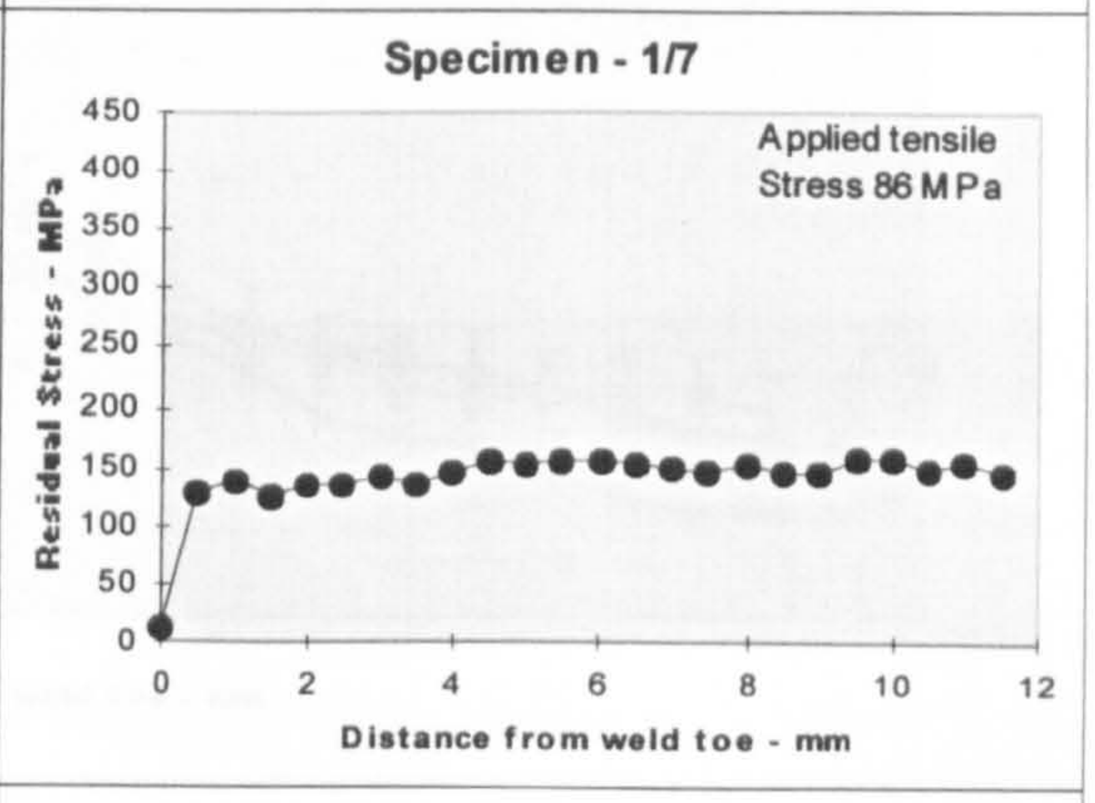

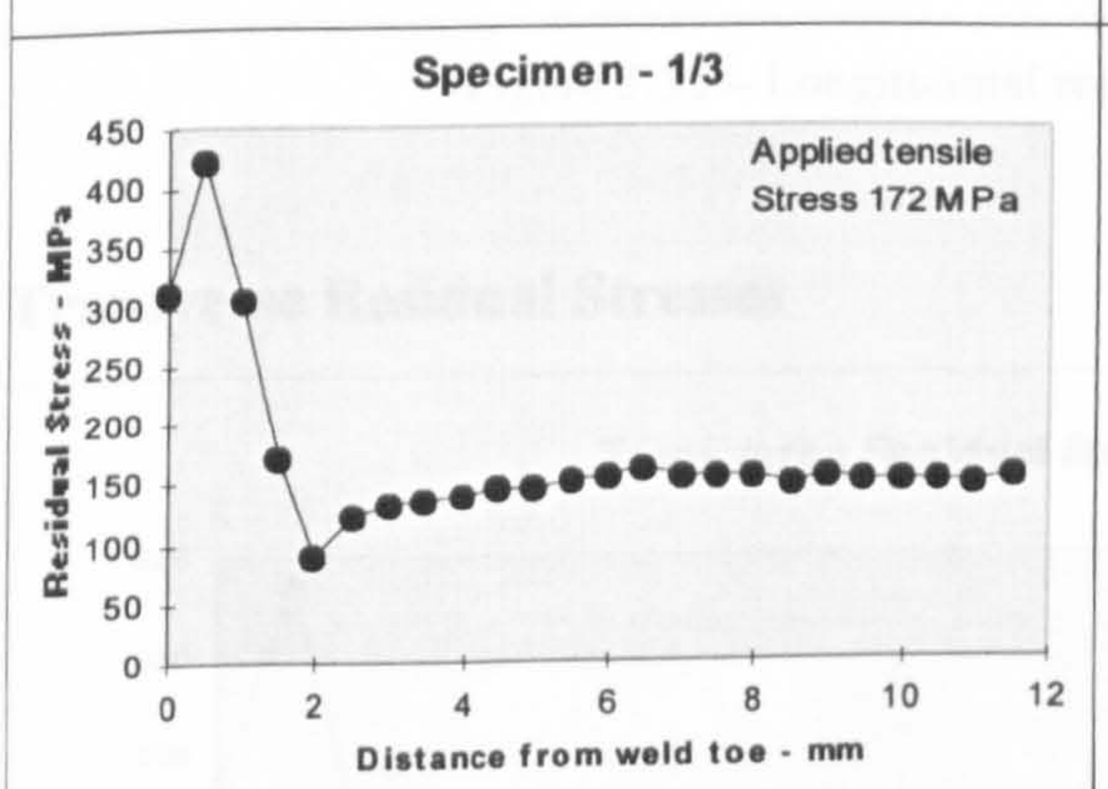

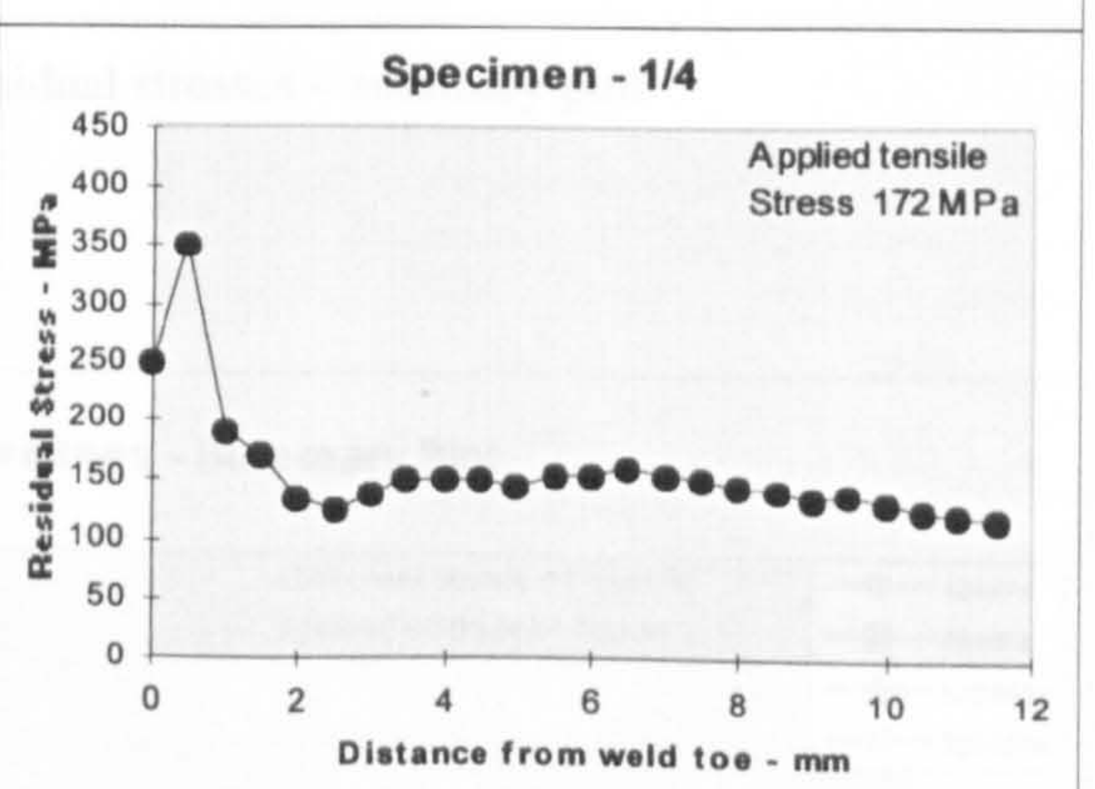

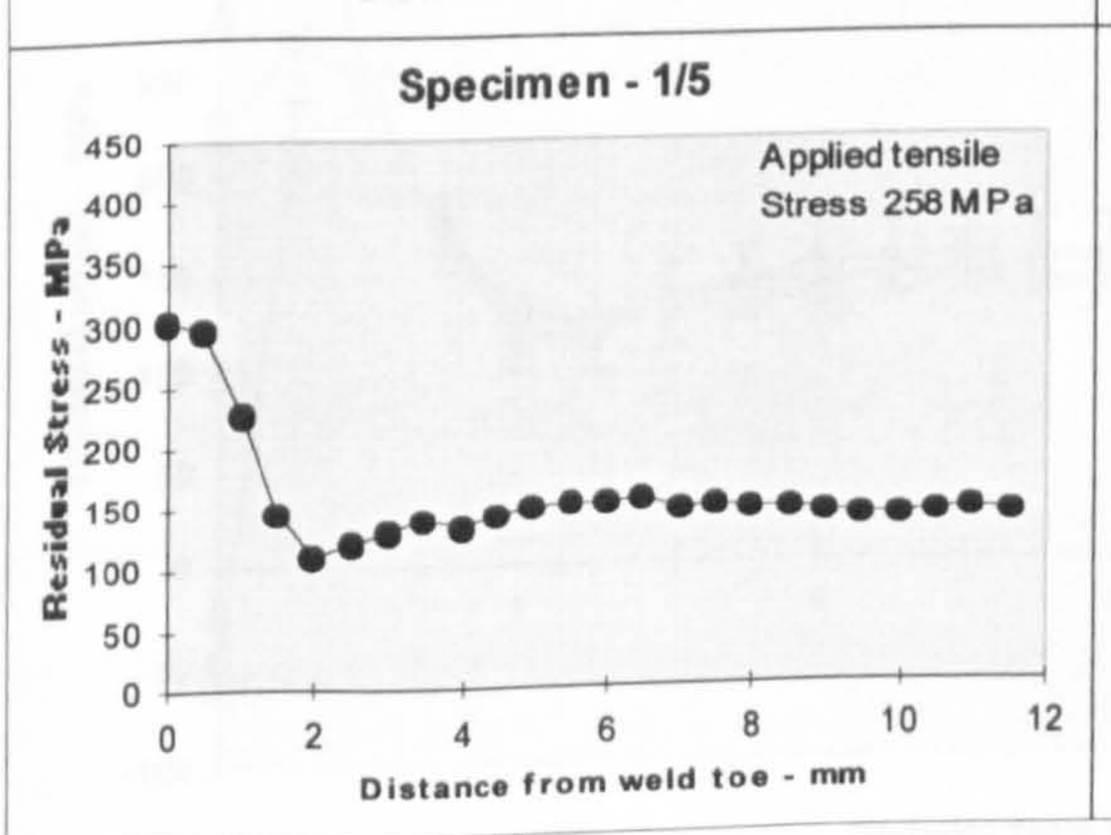

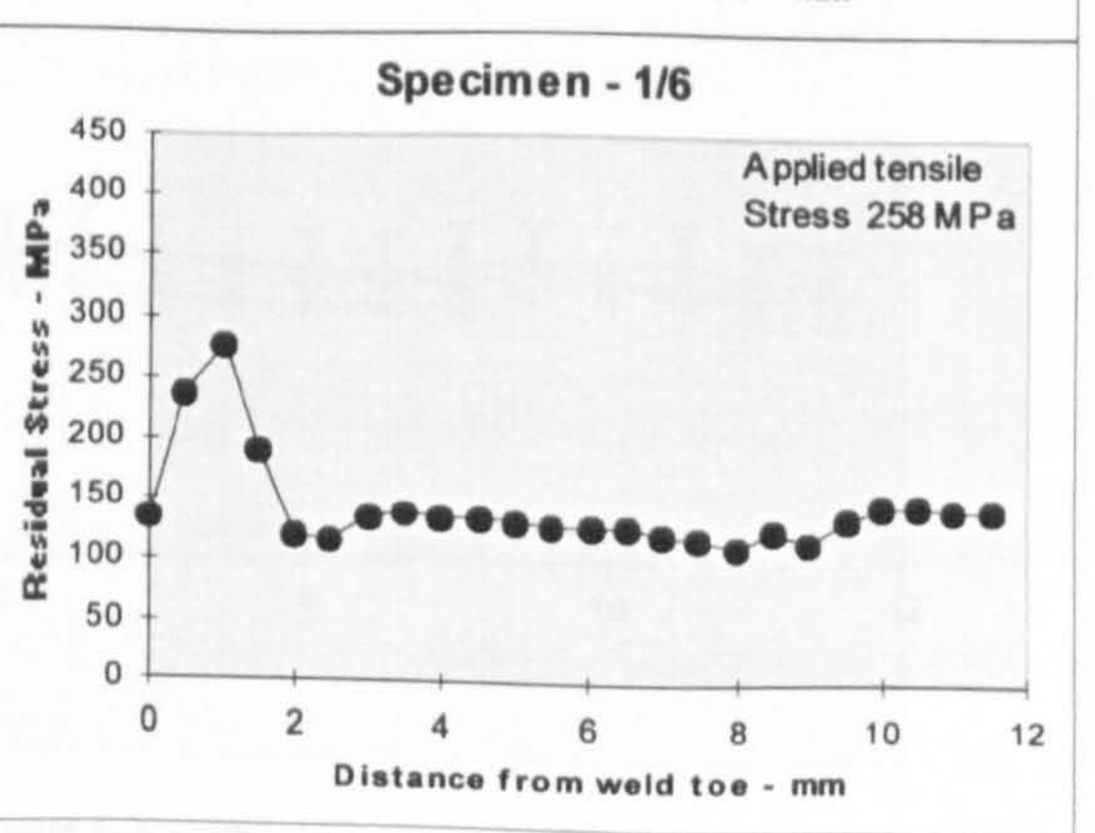

Figures 5.27 to 5.34 - Transverse stress plots - specimens 1/1 to 1/8

Summary Plots

Longitudinal Residual Stresses

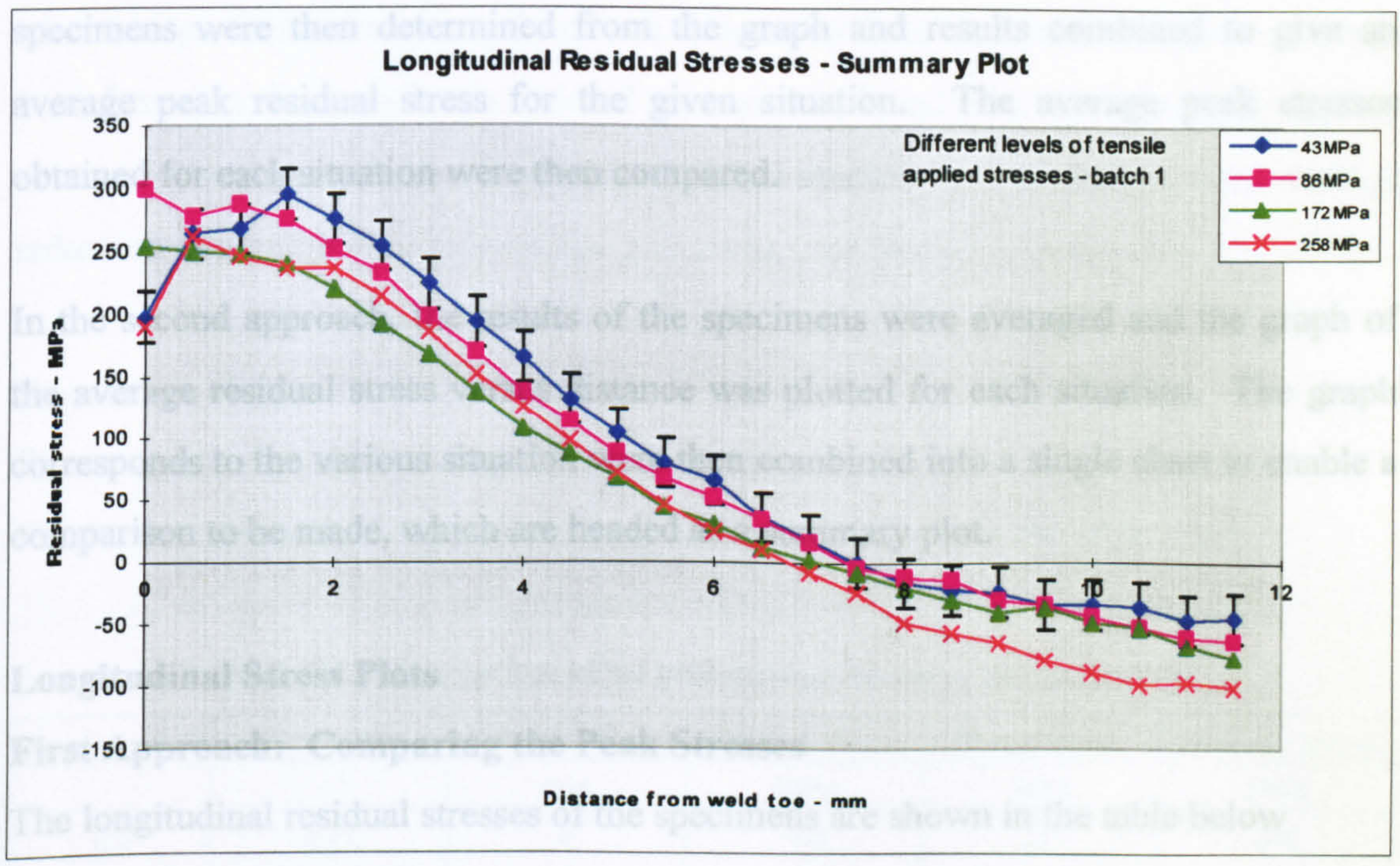

Figure 5.35 – Longitudinal residual stresses – summary plot

Transverse Residual Stresses

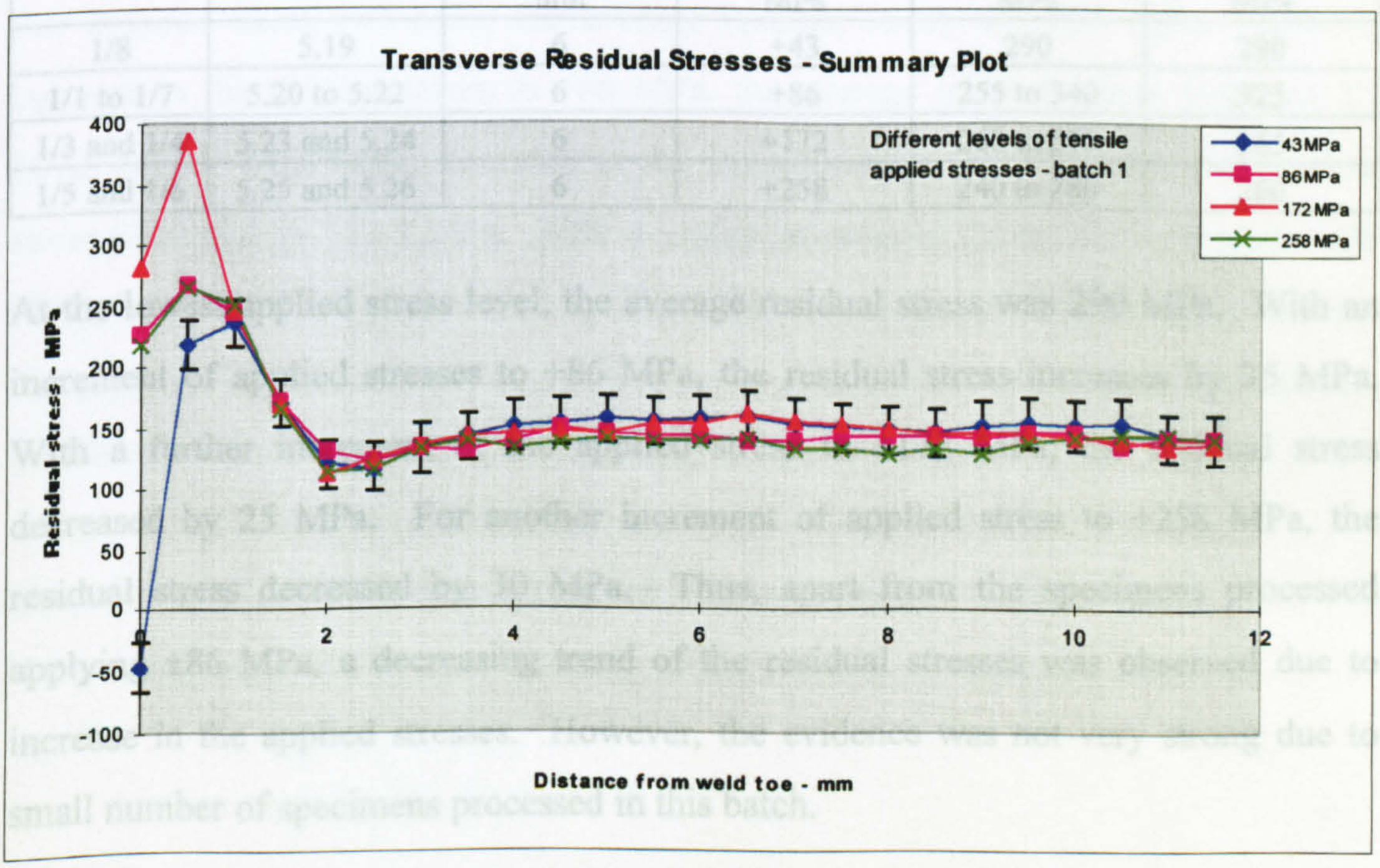

Figure 5.36 – Transverse residual stresses – summary plot

Discussion of Result - Batch 1

Two approaches were used in the analysis of the results. In the first approach, a separate graph was plotted for each specimen. The peak residual stress for each specimens were then determined from the graph and results combined to give an average peak residual stress for the given situation. The average peak stresses obtained for each situation were then compared.

In the second approach, the results of the specimens were averaged and the graph of the average residual stress versus distance was plotted for each situation. The graph corresponds to the various situation were then combined into a single chart to enable a comparison to be made, which are headed as a summary plot.

Longitudinal Stress Plots

First Approach: Comparing the Peak Stresses

The longitudinal residual stresses of the specimens are shown in the table below

Table 5.12 – Comparison of the peak residual stresses – longitudinal stress

Specimen No.	Figure No.	Stressed Time.	Applied Stress	Stress Range	Average Stress
		min	MPa	MPa	MPa
1/8	5.19	6	+43	290	290
1/1 to 1/7	5.20 to 5.22	6	+86	255 to 340	325
1/3 and 1/4	5.23 and 5.24	6	+172	260 to 270	265
1/5 and 1/6	5.25 and 5.26	6	+258	240 to 280	260

At the lowest applied stress level, the average residual stress was 290 MPa. With an increment of applied stresses to +86 MPa, the residual stress increases by 35 MPa. With a further increment of the applied stress to +172 MPa, the residual stress decreased by 25 MPa. For another increment of applied stress to +258 MPa, the residual stress decreased by 30 MPa. Thus, apart from the specimens processed applying ±86 MPa, a decreasing trend of the residual stresses was observed due to increase in the applied stresses. However, the evidence was not very strong due to small number of specimens processed in this batch.

Second Approach: Analysing the Summary Plot

In the summary plot (Figure 5.35), the residual stresses near the weld toe (distance range 0-1 mm) increased and decreased with increase in the applied static stresses, where no particular trend was found. A little away from the weld toe (distance range 1-11.5 mm), a decrease in the residual stresses was found with increase in the applied stresses. The maximum decrease in the residual stresses was ~60 MPa and the average reduction was ~45 MPa.

Transverse Stress Plots

First Approach: Comparing the Peak Stresses

The transverse residual stresses of the specimens are shown in the table below

Table 5.13 – Comparison of the peak residual stresses – transverse stress

Specimen No.	Figure No.	Stressed Time.	Applied Stress	Stress Range	Average Stress
		min	MPa	MPa	MPa
1/8	5.27	6	+43	235	235
1/1 to 1/7	5.28 to 5.30	6	+86	315 to 370	342.5
1/3 and 1/4	5.31 and 5.32	6	+172	350 to 425	387.5
1/5 and 1/6	5.33 and 5.34	6	+258	275 to 300	287.5

For induced stress +43 MPa, the average residual stress was 235 MPa. With an increase in the induced stress to +86 MPa, the average residual stress increased by 107.5 MPa. With further increase in the induced stress to +172 MPa, the residual stress increased by 152.5 MPa. With a further increase in the induced stress to +258 MPa, the residual stress increased by 52.5 MPa. Specimen 1/7 (Figure 5.30), showed the peak to be missing which possibly as a result of some other effects or the measurement points were not precise enough to pick up the sharp peak.

Thus, from this batch the transverse peak residual stresses were found to increase with increase in the applied stresses.

Second Approach: Analysing the Summary Plot

The transverse residual stresses near the weld toe (distance range 0-1 mm) were found to increase with increase in the applied static stresses (Figure 5.36). The specimens subjected to induced stress of ±43 MPa showed the lowest residual stresses. With increase in the induced stress to ±86 MPa, ±172 MPa, and ±258 MPa, the residual stresses near the weld toe (distance range 0-1 mm) significantly increased. Away from the weld toe (distance range 1-3 mm), no change in residual stresses was observed. Further away from the weld toe (distance range 3-11.5 mm), the residual stresses decreased, but the decrease in this case was smaller than that of the longitudinal stresses.

Thus, in both longitudinal and transverse residual stress plots, a very similar trend of change in residual stresses were observed. In this batch the resolution of the measurement points was not sufficient to pick the actual stress profile near the weld toe. This caused a confused pattern of change in residual stresses near the weld toe. To resolve this confusion, batch 2 were processed applying both tensile and compressive stresses, which are shown below.

Batch 2

In this batch, 14 specimens were processed at different levels of tensile and compressive static stress - applied to the line of measurement specified. The specimens were pre-stressed prior to welding and maintained in this condition until being allowed to cool down to room temperature. The applied stress levels were 258 MPa, 172 MPa, 86 MPa, 0 MPa, -86 MPa, -172 MPa, and -258 MPa. The plots which follow, show the results of the longitudinal and transverse residual stresses measured along a central longitudinal line - as illustrated in Figure 5.13 - from the toe of the weld.

Longitudinal Stress Plots

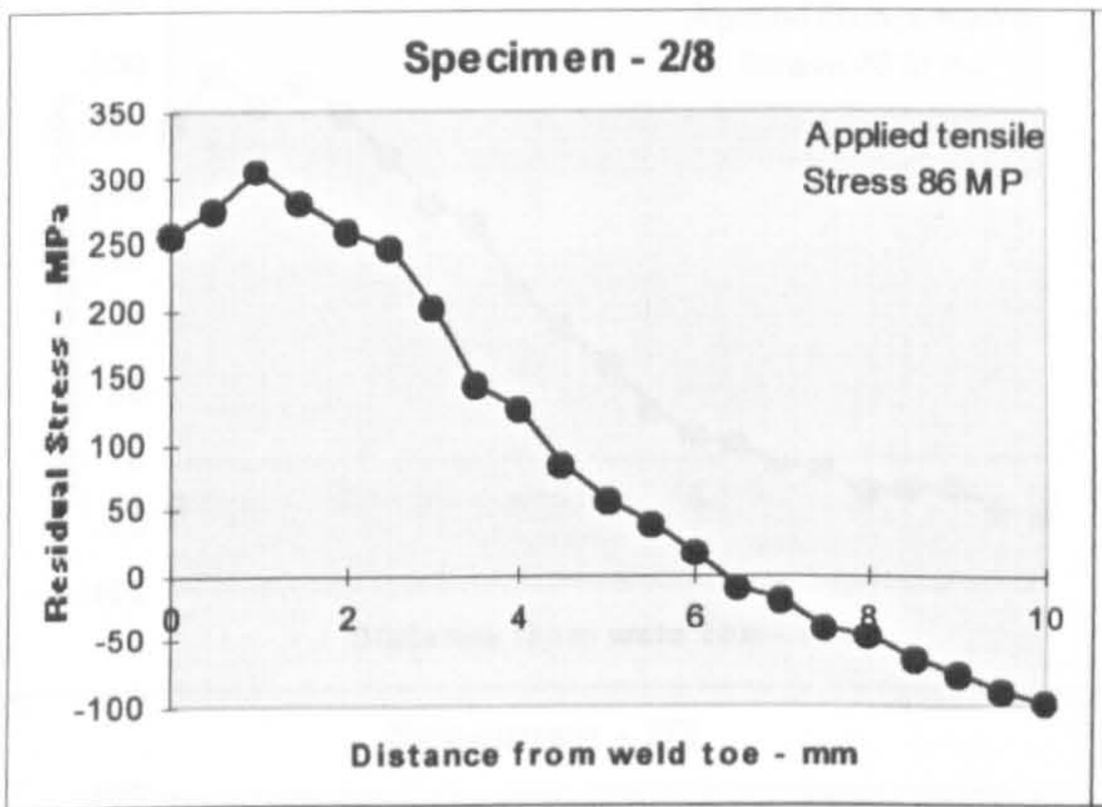

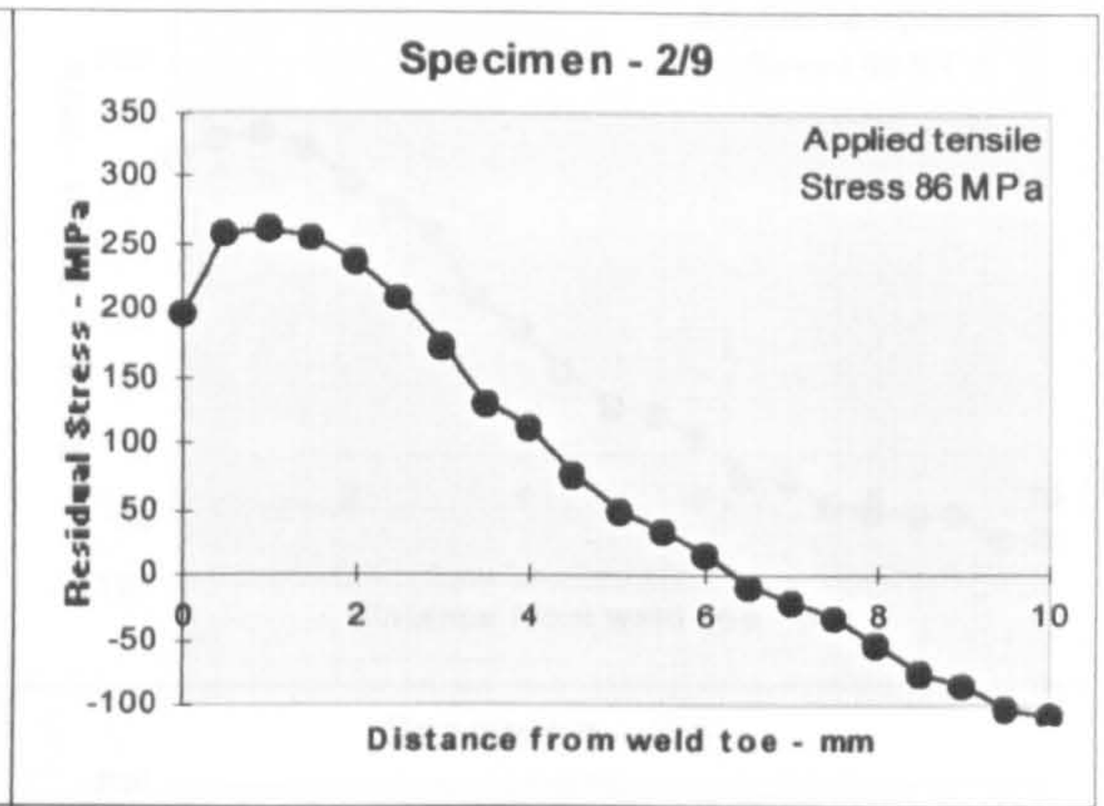

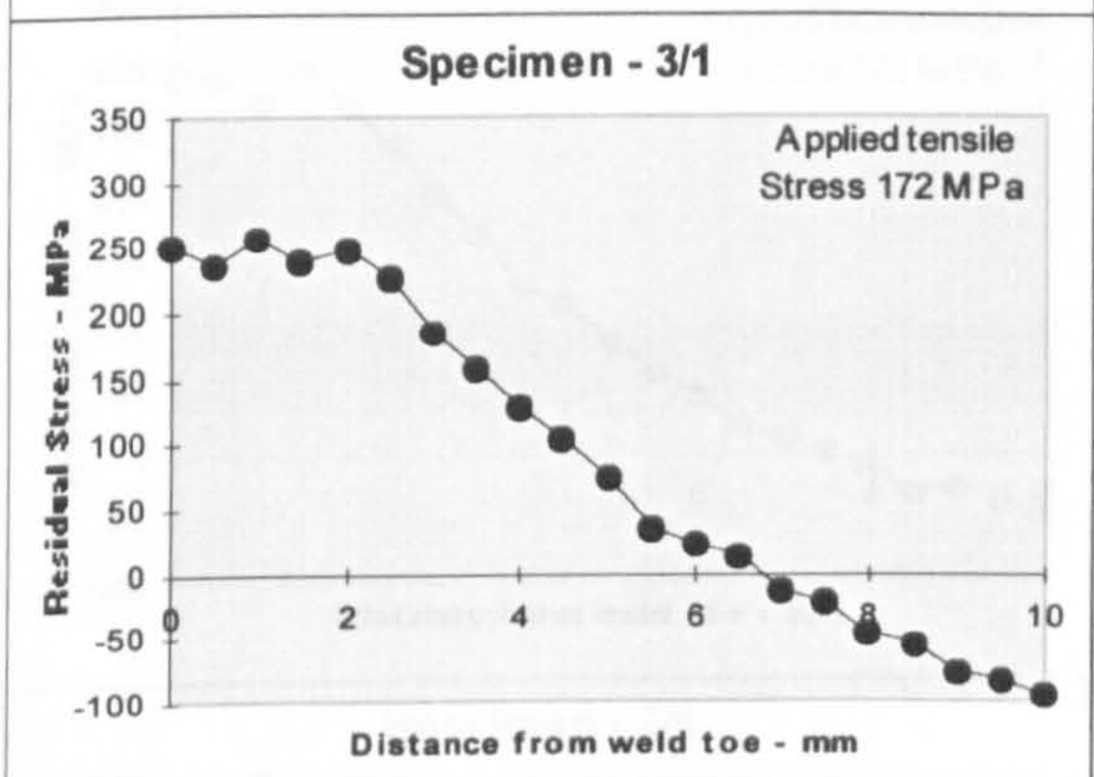

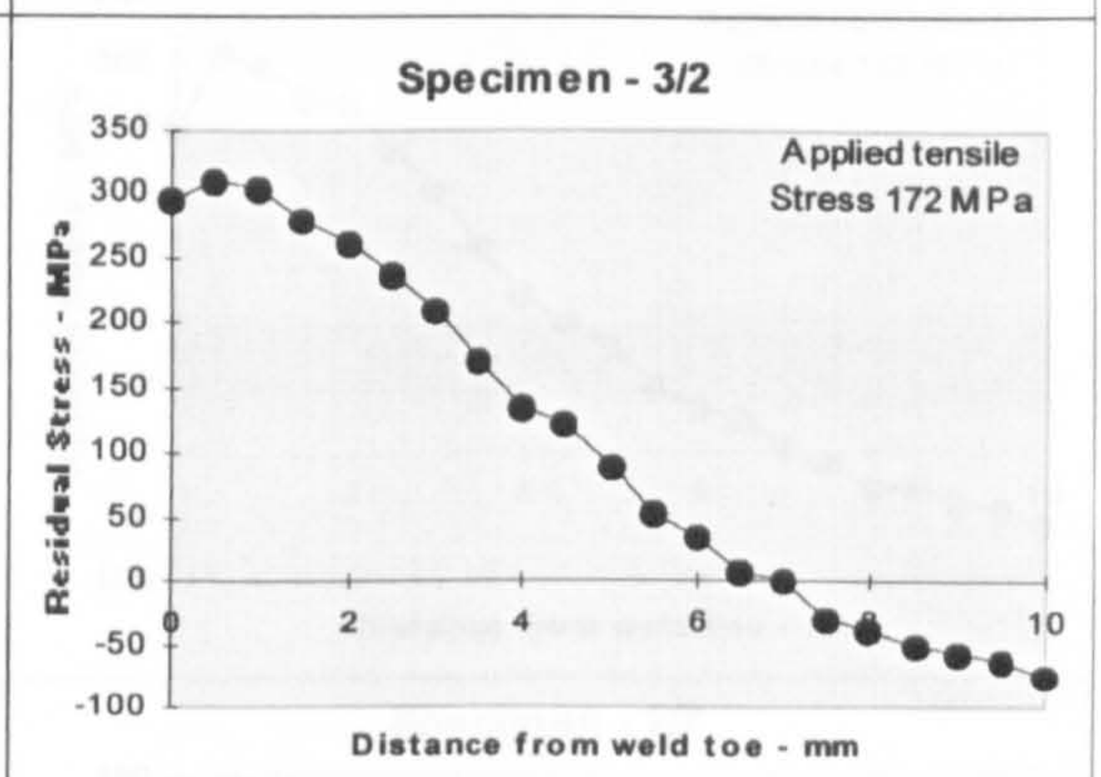

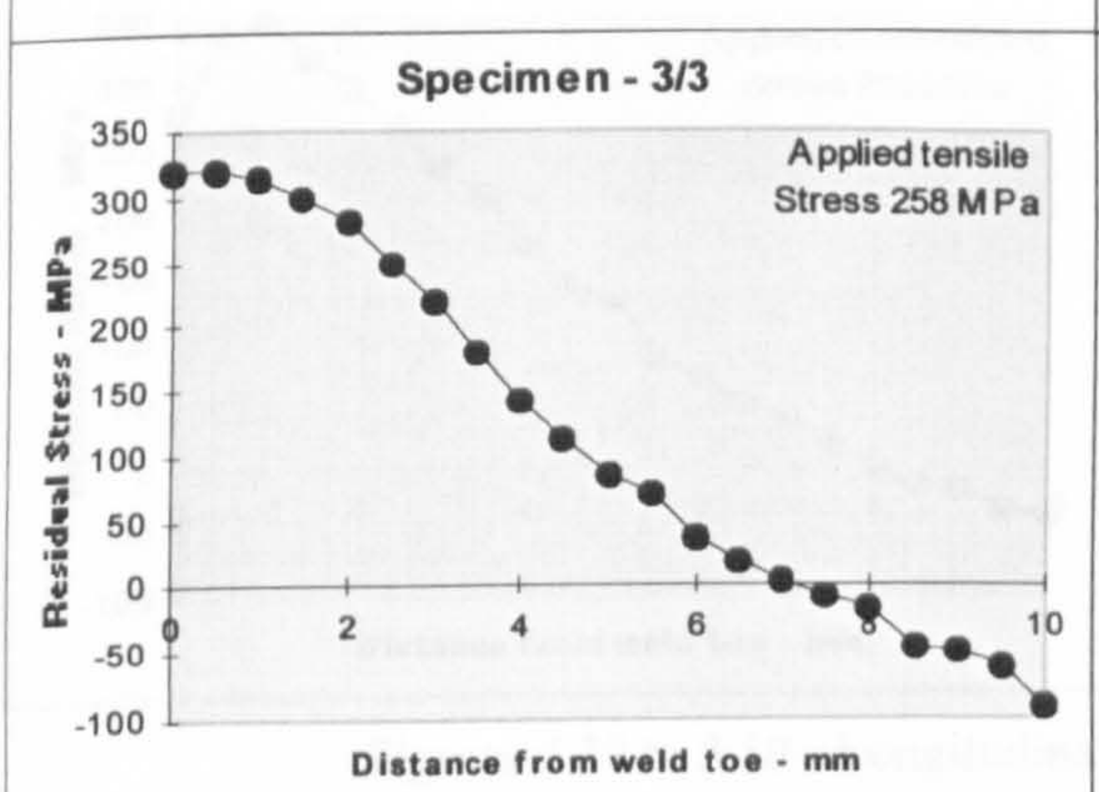

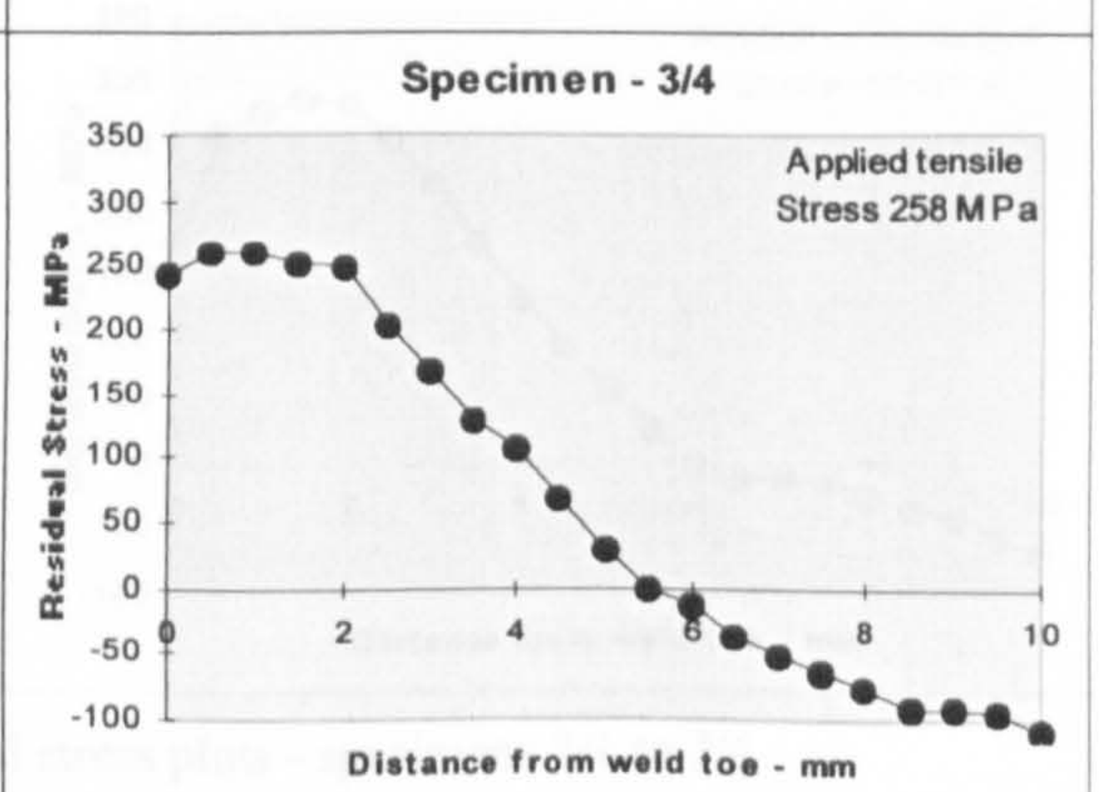

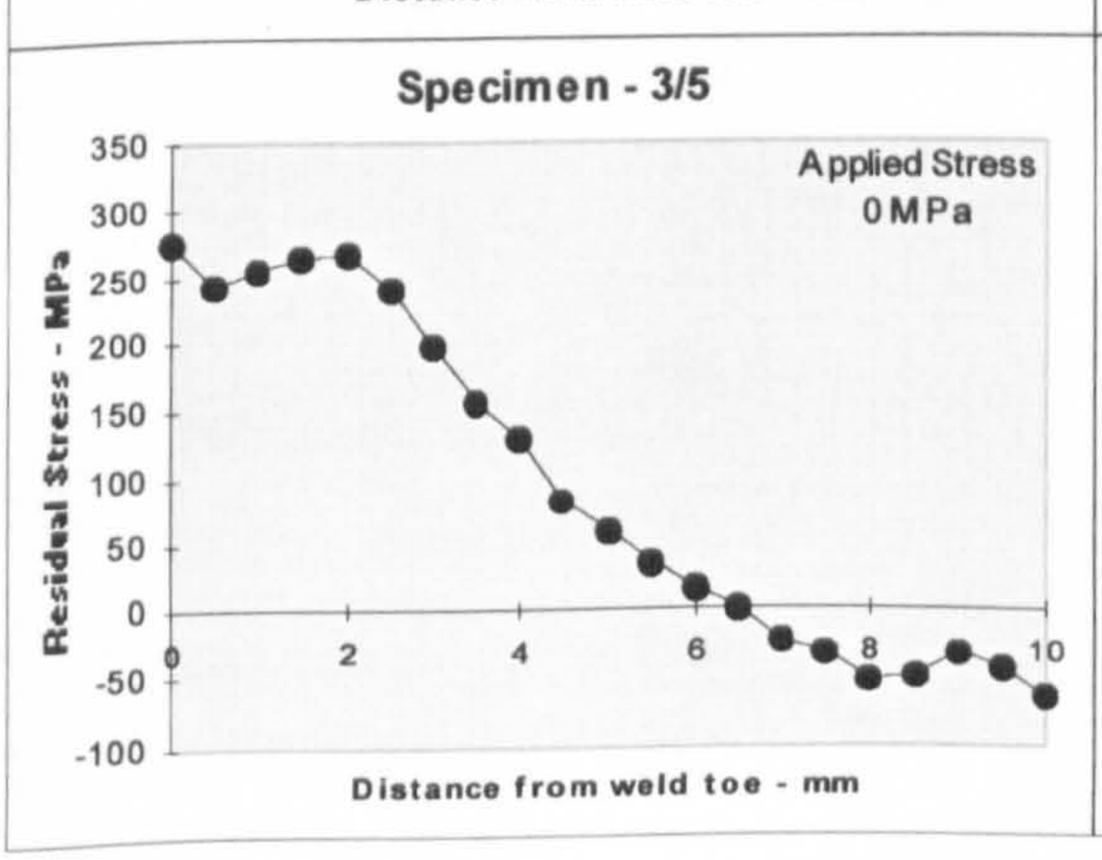

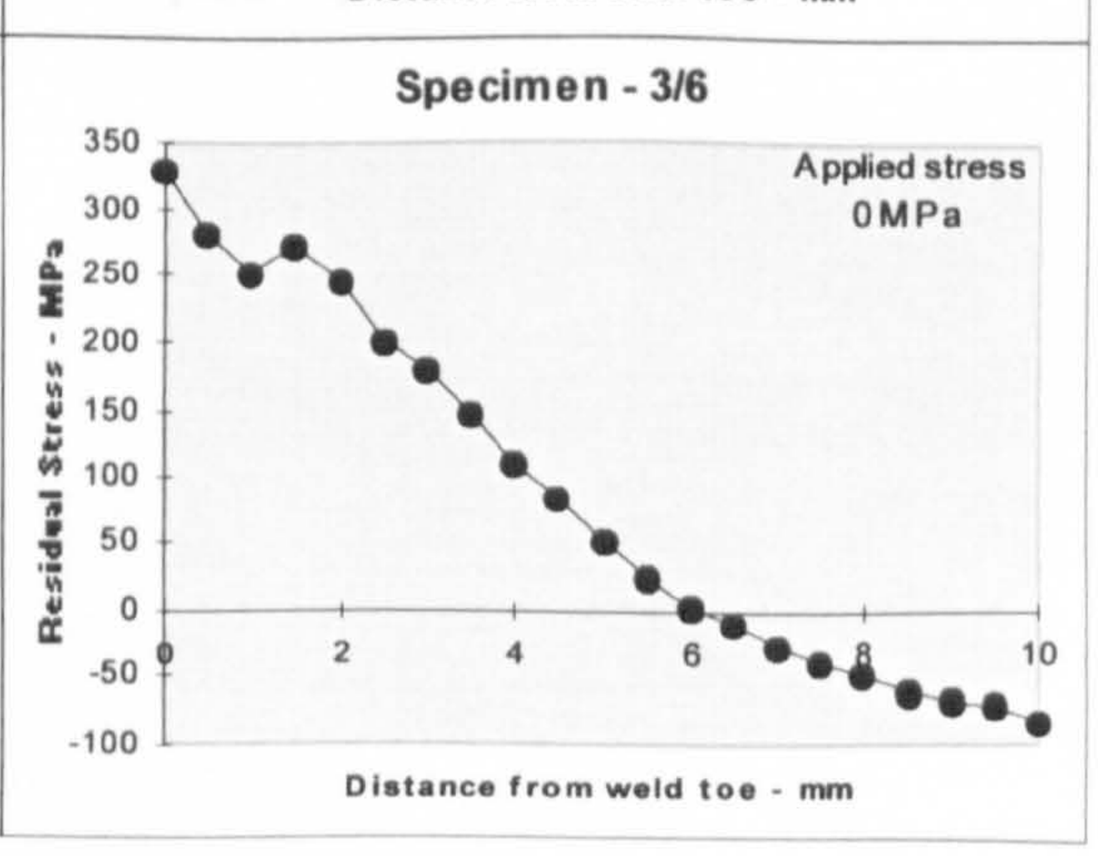

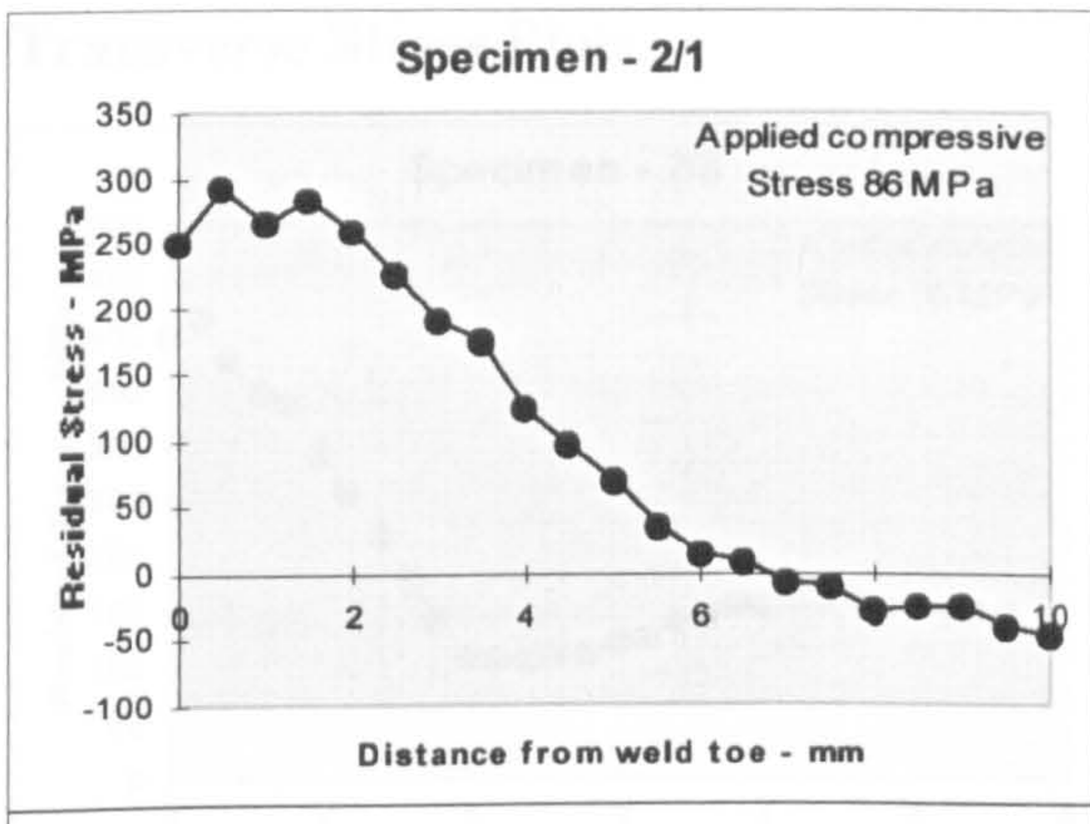

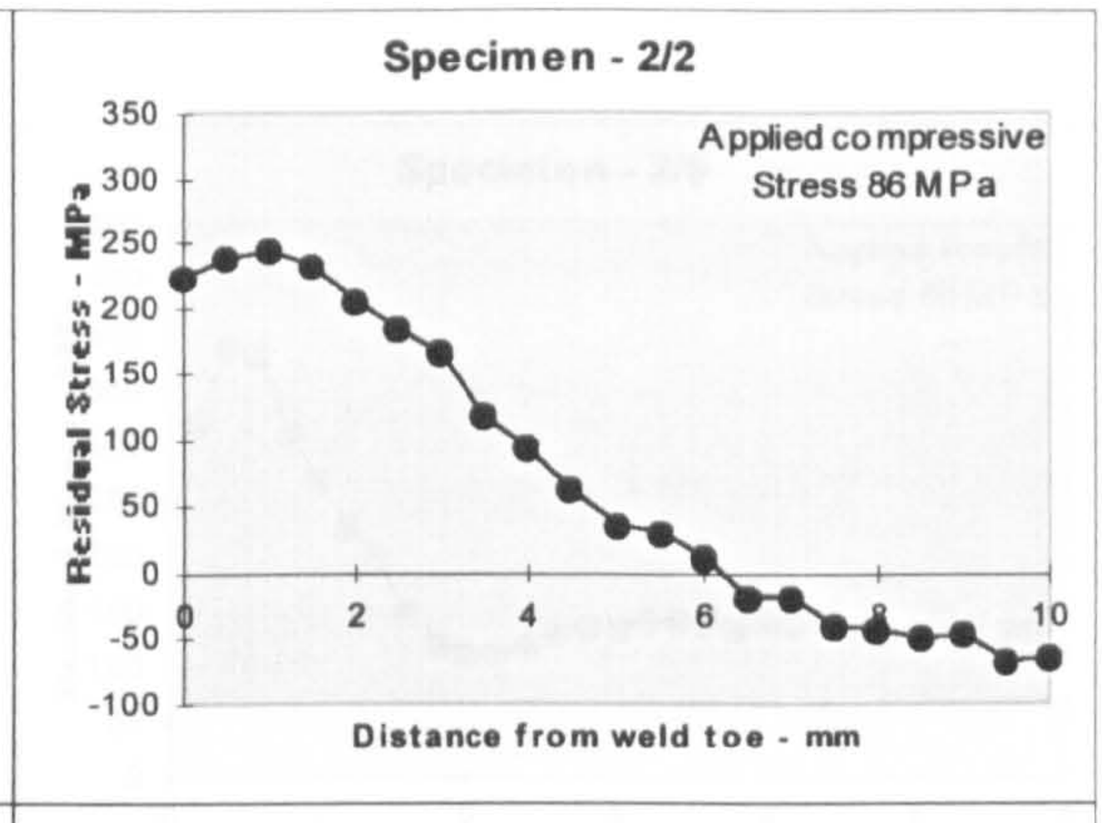

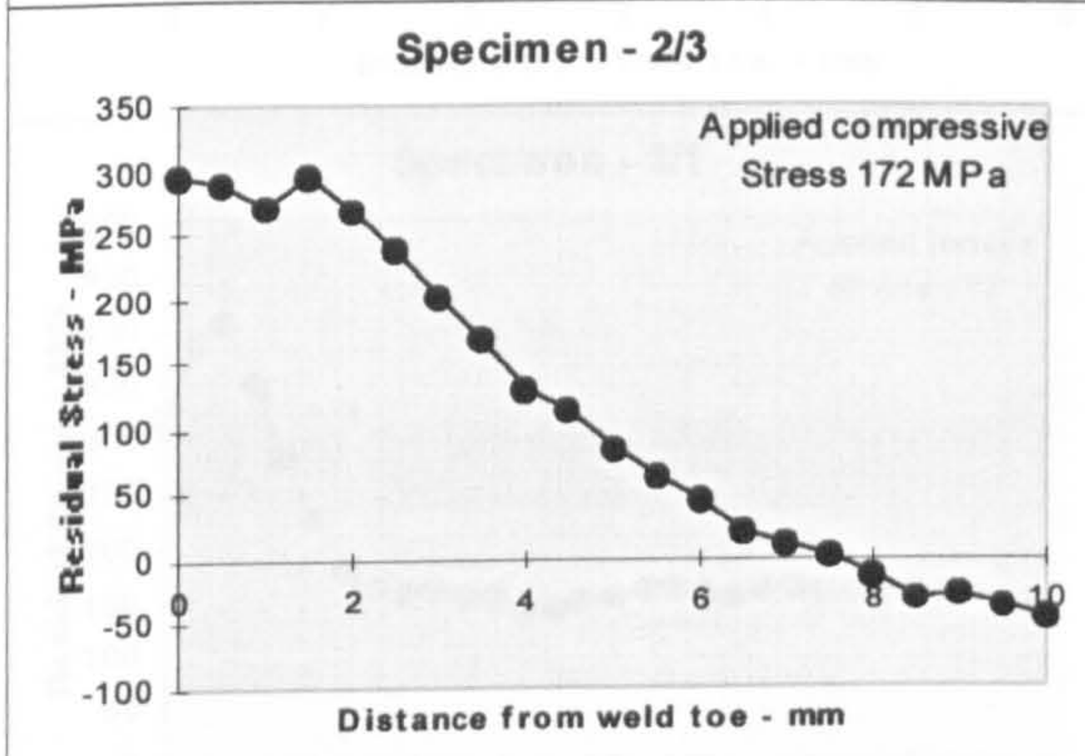

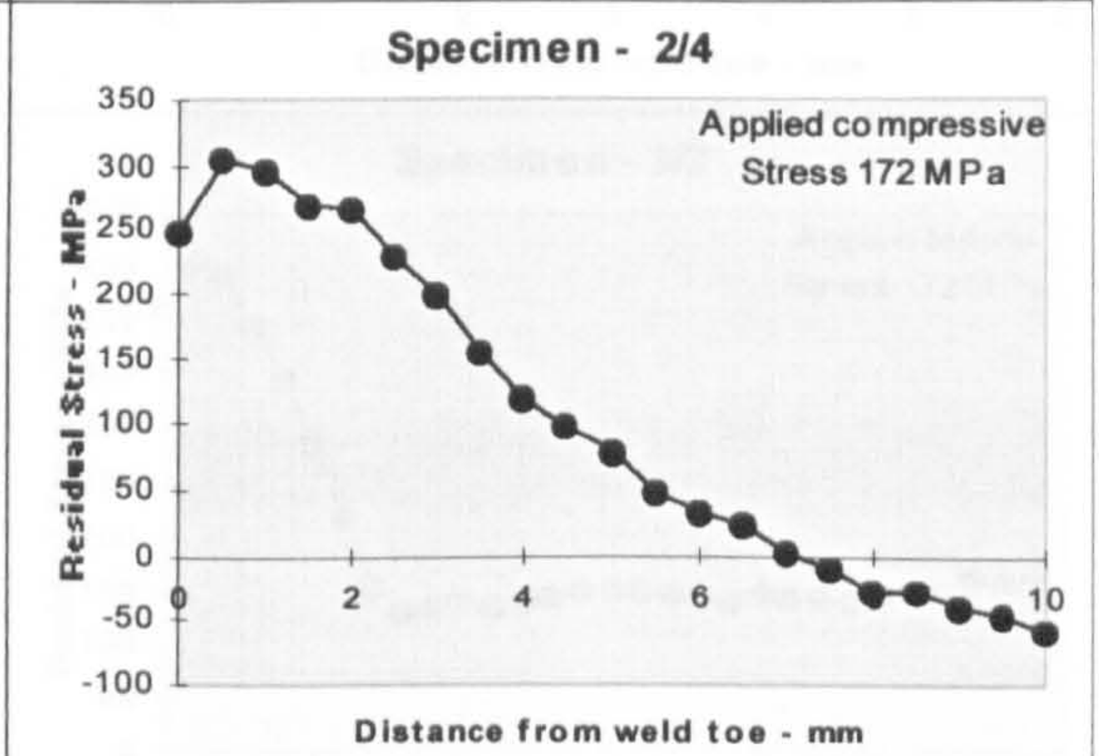

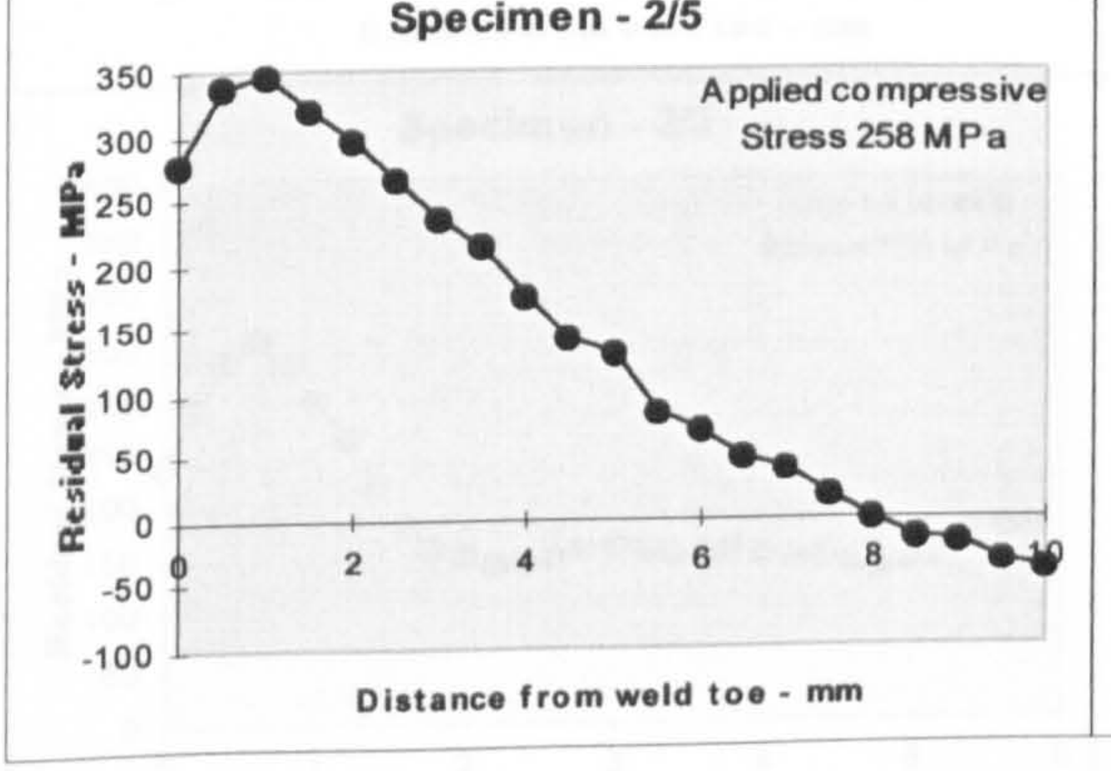

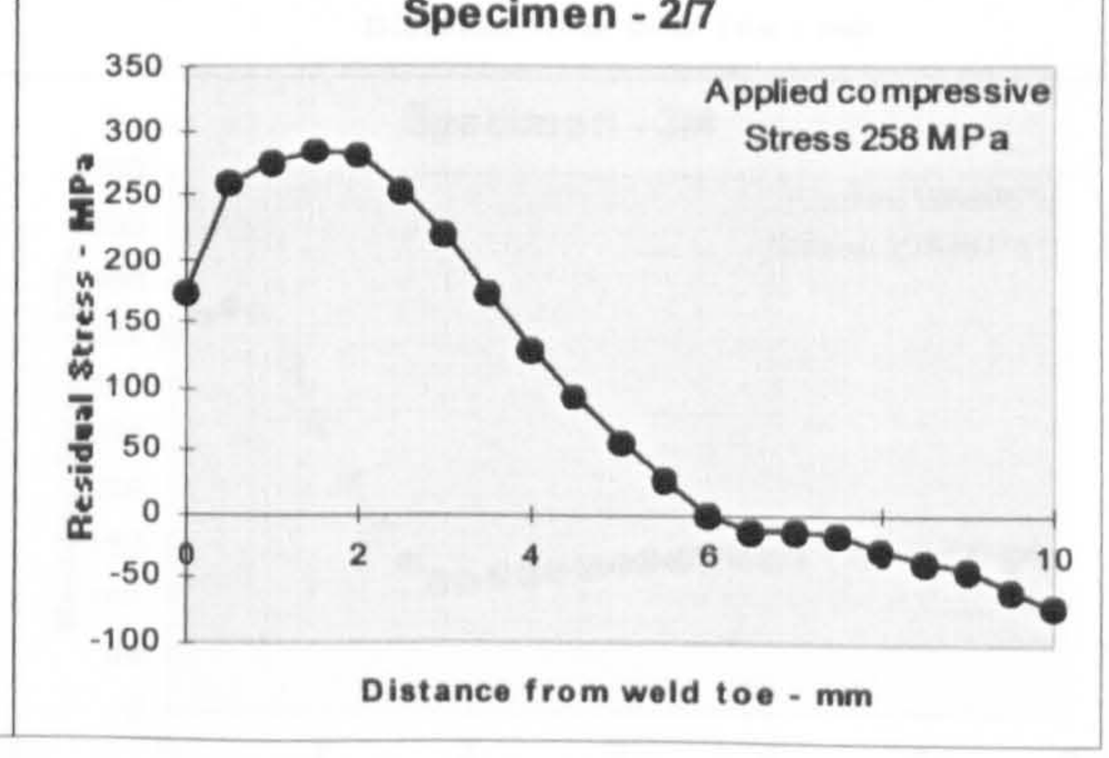

Figures 5.37 to 5.50 - Longitudinal stress plots - specimens 2/1 to 3/6

Transverse Stress Plots

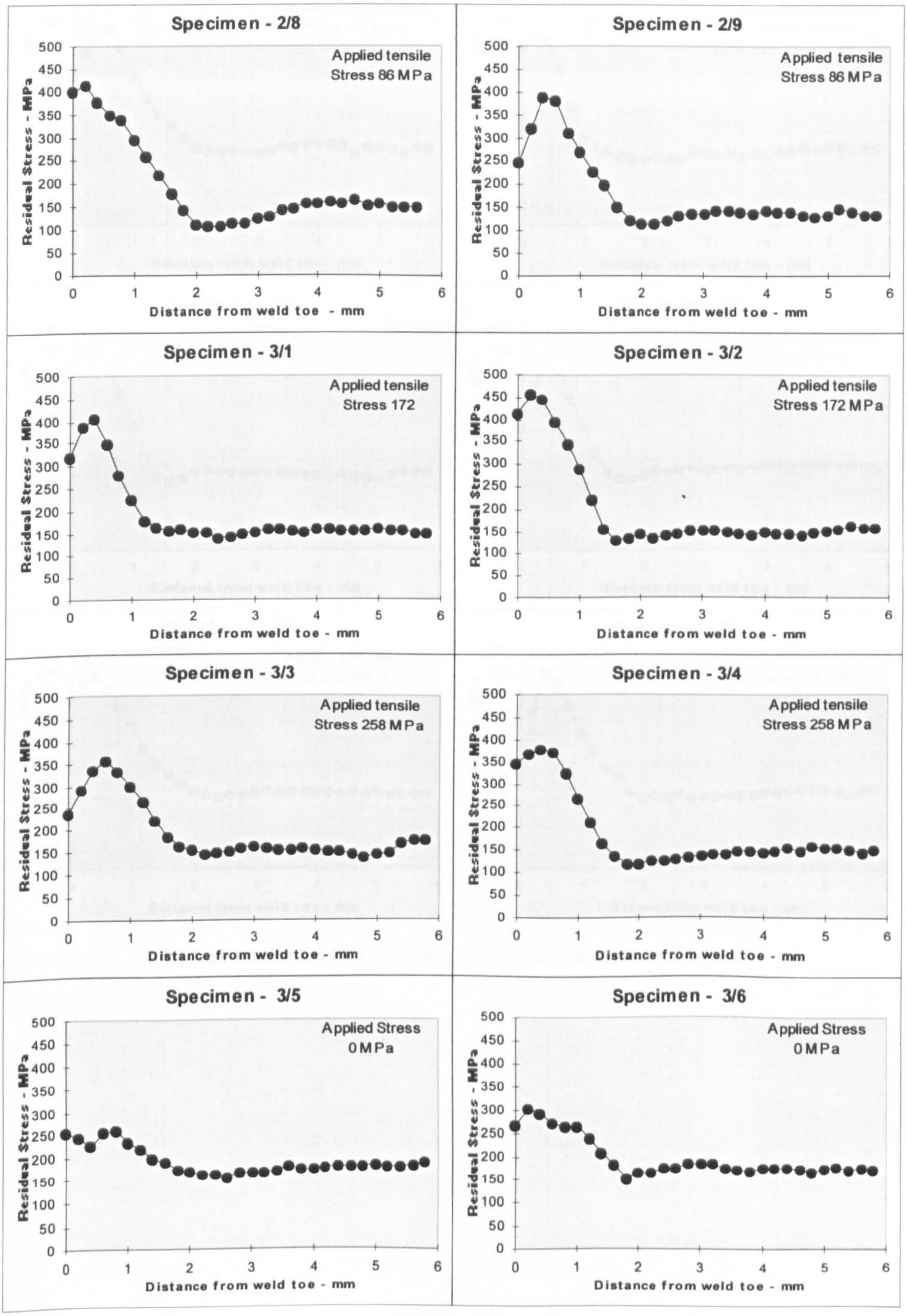

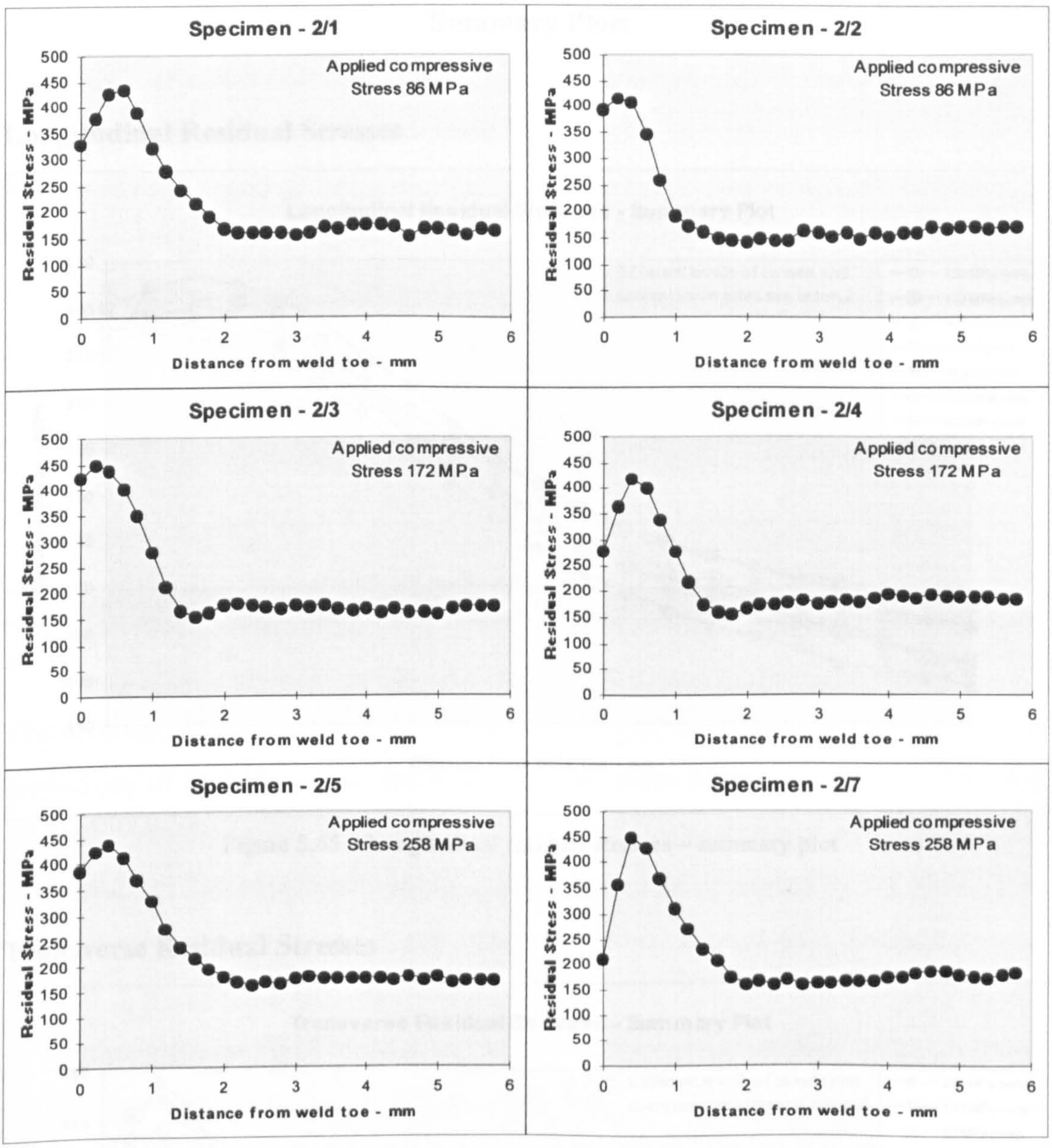

Figures 5.51 to 5.64 - Transverse stress plots - specimens 2/1 to 3/6

Summary Plots

Longitudinal Residual Stresses

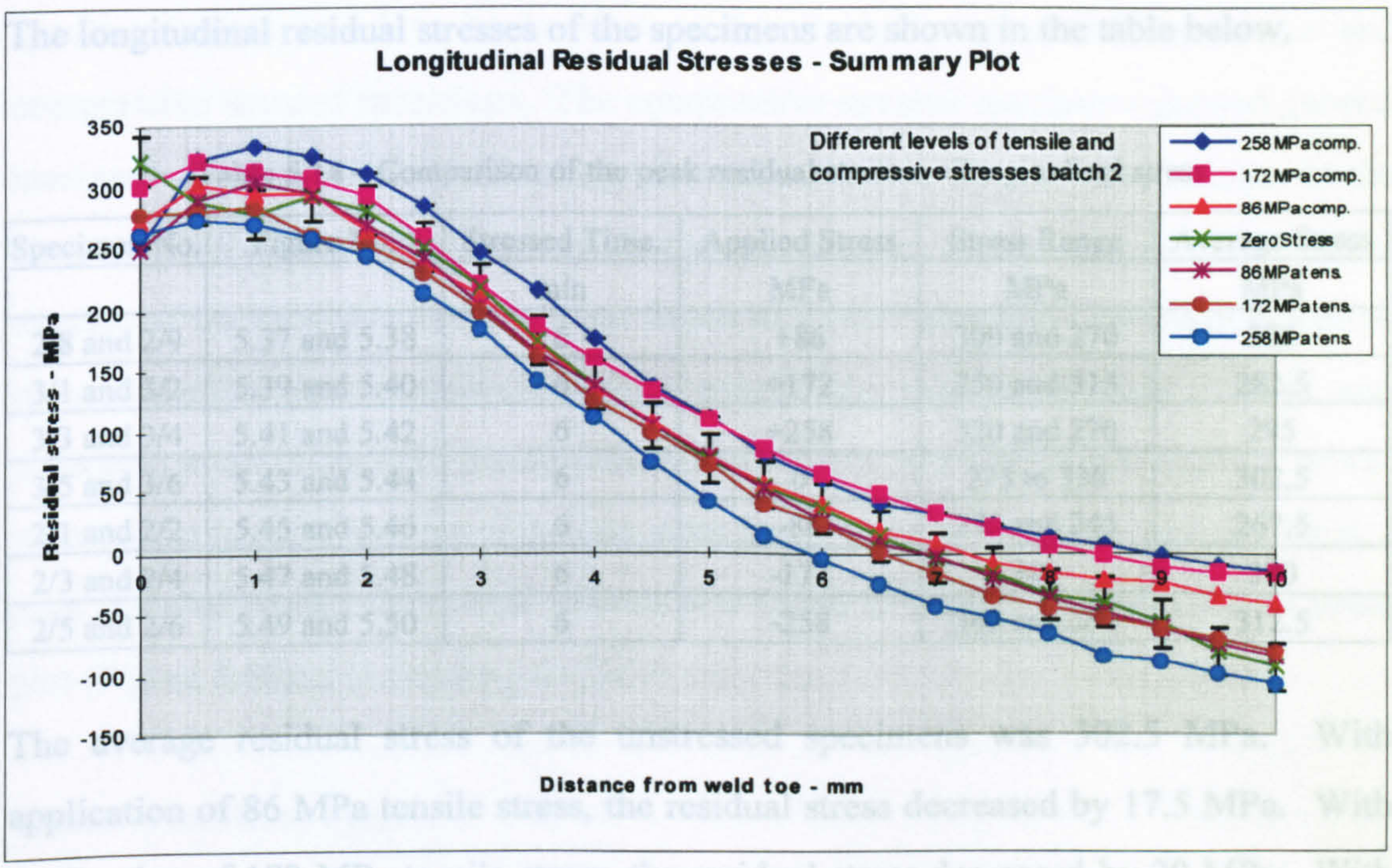

Figure 5.65 – Longitudinal residual stresses – summary plot

Transverse Residual Stresses

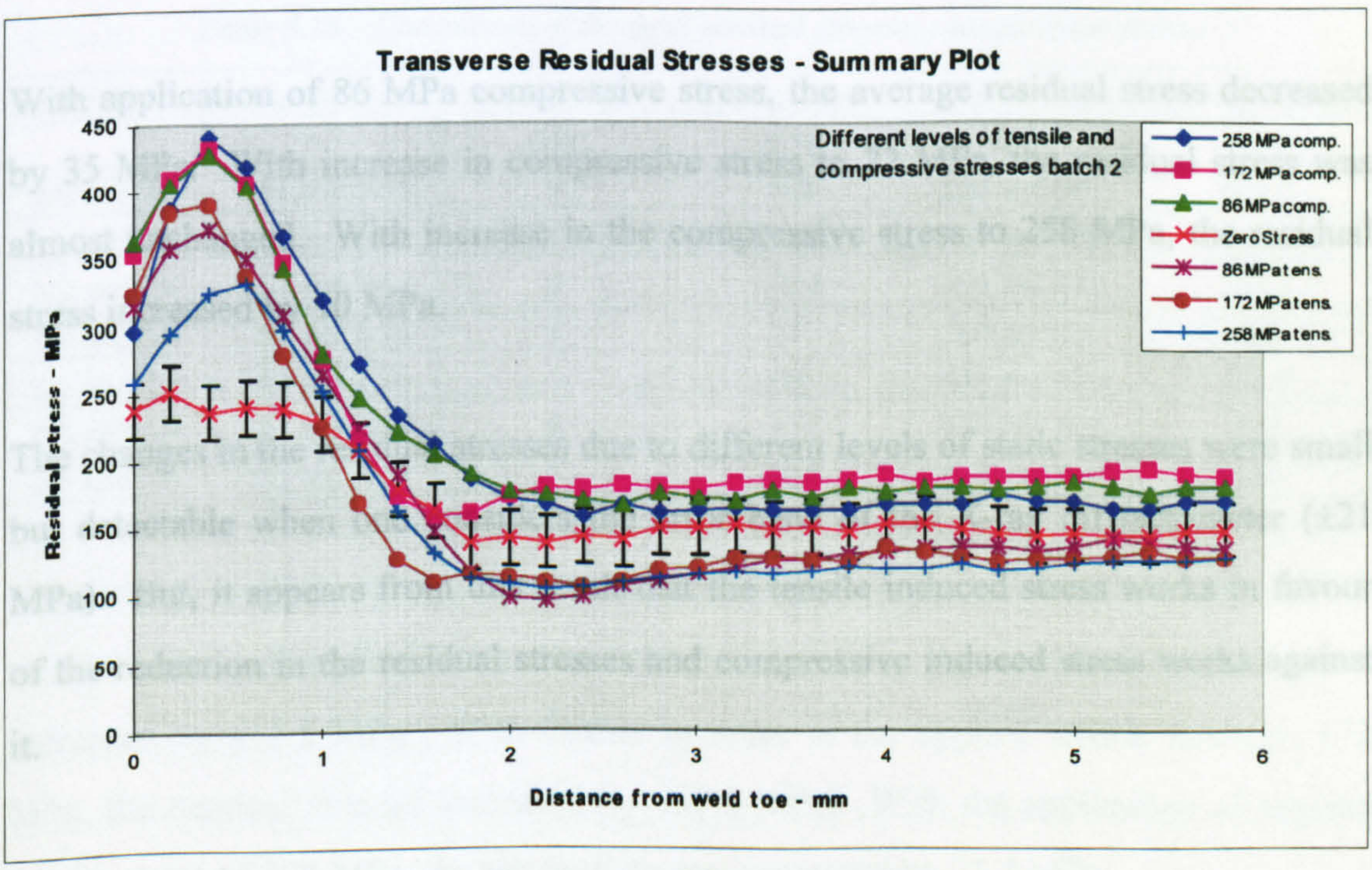

Figure 5.66 – Transverse residual stresses – summary plot

Discussion of Result - Batch 2

Longitudinal Stress Plots

First Approach: Comparing the Peak Stresses

The longitudinal residual stresses of the specimens are shown in the table below.

Table 5.14 – Comparison of the peak residual stresses – longitudinal stress

Specimen No.	Figure No.	Stressed Time.	Applied Stress	Stress Range	Average Stress
		min	MPa	MPa	MPa
2/8 and 2/9	5.37 and 5.38	6	+86	300 and 270	285
3/1 and 3/2	5.39 and 5.40	6	+172	250 and 315	282.5
3/3 and 3/4	5.41 and 5.42	6	+258	320 and 270	295
3/5 and 3/6	5.43 and 5.44	6	0	275 to 330	302.5
2/1 and 2/2	5.45 and 5.46	6	-86	290 and 245	267.5
2/3 and 2/4	5.47 and 5.48	6	-172	300	300
2/5 and 2/6	5.49 and 5.50	6	-258	345 and 280	312.5

The average residual stress of the unstressed specimens was 302.5 MPa. With application of 86 MPa tensile stress, the residual stress decreased by 17.5 MPa. With application of 172 MPa tensile stress, the residual stress decreased by 20 MPa. With application of 258 MPa tensile stress, the residual stress decreased by 7.5 MPa. Thus, in all tensile stressed specimens, reductions in residual stresses were observed.

With application of 86 MPa compressive stress, the average residual stress decreased by 35 MPa. With increase in compressive stress to 72 MPa, the residual stress was almost unchanged. With increase in the compressive stress to 258 MPa, the residual stress increased by 10 MPa.

The changes in the residual stresses due to different levels of static stresses were small but detectable when one considers the error band of the X-ray diffractometer (±21 MPa). But, it appears from this result that the tensile induced stress works in favour of the reduction in the residual stresses and compressive induced stress works against it.

Second Approach: Analysing the Summary Plot

A general trend of residual stresses all over the measurement line was observed in the longitudinal residual stress plot (Figure 5.65). The residual stresses of the unstressed specimens were found to be in-between the residual stresses of the tensile and compressive stressed specimens. The compressive stressed specimens showed general increased residual stresses all along the measurement line in comparison to the unstressed specimens. With increase in the compressive applied stresses, the residual stresses of the measurement line were found to further increase. The tensile applied stresses showed the opposite, where a general decrease in residual stresses was observed on all along the measurement line. With increase in the applied tensile stresses, the residual stresses of the line were found to have further decreased. Thus, a clear trend of change in residual stresses was found in the longitudinal residual stress plot (Figure 5.65).

Transverse Stress Plots

First Approach: Comparing the Peak Stresses

The transverse residual stresses of the specimens are shown in the table below.

Table 5.15 – Comparison of the peak residual stresses – longitudinal stress

Specimen No.	Figure No.	Stressed Time.	Applied Stress	Stress Range	Average Stress
		min	MPa	MPa	MPa
2/8 and 2/9	5.51 and 5.52	6	+86	420 and 385	402.5
3/1 and 3/2	5.53 and 5.54	6	+172	405 and 470	437.5
3/3 and 3/4	5.55 and 5.56	6	+258	350 and 375	365.5
3/5 and 3/6	5.57 and 5.58	6	0	265 to 315	290
2/1 and 2/2	5.59 and 5.60	6	-86	438 and 425	431.5
2/3 and 2/4	5.61 and 5.62	6	-172	450 and 420	435
2/5 and 2/6	5.63 and 5.64	6	-258	438 and 450	444

The average residual stress of the unstressed/control specimens was 290 MPa. With an increment of applied stresses to 86 MPa tensile, the average residual stress increased by 112.5 MPa. With further increase in the applied tensile stress to 172 MPa, the residual stresses increased by 137.5 MPa. With the application of applied tensile stress of 258 MPa, the residual stresses increased by 75.5 MPa.

The specimens subjected to compressive applied stresses showed higher residual stresses than the unstressed specimens. The effect of the different magnitude of compressive applied stresses was found to be very small - the residual stresses of all compressive applied stress plots showed very similar stress values (average 431.5 MPa, 435 MPa, and 444 MPa). Although the differences between the average residual stresses were small, there was a clear trend of increase in the residual stresses due to increases in the compressive applied stresses.

Thus, the transverse residual stresses were found to increase with application of both tensile and compressive stresses, but the rate of increment was higher for the compressive applied stresses.

Second Approach: Analysing the Summary Plot

The transverse residual stresses of the summary plot in Figure 5.66 showed a different picture from the longitudinal residual stresses of plot in Figure 5.65. The transverse residual stresses on and near the weld toe (distance range 0-1 mm) were found to increase with application of both tensile and compressive stresses. The residual stresses of the unstressed specimens were lower than that of the residual stresses of the stressed specimens in the mentioned range. With application of stresses (both tensile and compressive) the residual stresses increased but the degree of increment in the tensile stressed specimens was lower than that of the increment in the compressive stressed specimens. Away from the weld toe the residual stresses were found to decrease with application of tensile stresses. With increase in the tensile stresses the residual stresses were found to further decrease. The compressive stressed specimens showed an increase in the residual stresses. Further increase in the applied stress showed a further increase in the residual stresses. Thus, a clear pattern of change in the residual stresses was found from the result of this batch.

5.3.1.5 Summary of Results

In both types of analysis, the longitudinal residual stresses in the first batch was found to decrease with increase in the applied stress. The transverse stresses showed the

reverse, where the residual stresses increased with the induced stresses. Away from the weld toe, the longitudinal and transverse residual stresses were found to decrease with increase in the applied tensile stress.

In batch 2, the longitudinal residual stresses decreased with application of tensile stresses. The compressive induced stresses showed the opposite – the residual stresses were found to increase with application of compressive stresses. Away from the weld toe, the residual stresses decreased with the application of tensile stresses and increased with the application of compressive stresses.

Away from the weld toe, the increase or decrease in the residual stresses in this experiment seemed relatively small, but above the error band of the X-ray diffractometer. In all four summary plots, a similar trend of the residual stresses were observed, where the tensile applied stresses caused decrease in the residual stresses and compressive applied stress caused the opposite.

The yield stress of the as-rolled flat bar was 611 MPa. At higher temperature, the yield stress of the specimen was much lower than 611 MPa. Also, it was non-linear over the wide range of temperature change during cooling. A tensile test at 700 ^{0}C showed that the yield stress of the steel was ~70 MPa, so that there was every likelihood that yielding would take place during the weld – cooling process.

5.3.2 Experiment II: Rigid Body Motion Vibration Test

Abstract

In this experiment the effect of rigid body motion vibration on welding residual stresses was investigated. The specimens were welded while they were being vibrated in a rigid body motion mode. The specimens were vibrated using two different frequencies (50 Hz and 500 Hz). In the low frequency (50 Hz) vibration, the residual stresses were found to be very confusing where no particular trend was observed. In the high frequency (HF) vibration, very small reductions in the residual stresses were observed in the longitudinal stresses and in the transverse direction, no reduction was found.

5.3.2.1 Introduction

Essentially, three forms of vibratory motion have been investigated relating to VSR and VWC, these being Rigid Body Motion (RBM), Flexural Motion and Torsional Motion. This part of the study relates to the RBM investigation. Tewary & Shanker [126] noticed that the properties of the material improves by the use of RBM vibration during welding. Even though the mechanism whereby this improvement occurs is not at all clear or obvious. In this experiment, the changes in residual stresses were investigated after the application of different levels of RBM vibration. Essentially, this part of the study involves the specimen being vibrated under conditions of RBM - during and after the welding process.

5.3.2.2 Experimental Procedure

In this experiment, the specimens were subjected to vibration at the start of welding process and continued for three and half minutes. In this investigation the optimum welding parameters (voltage, current, speed and time) were established initially and thereafter kept constant. A single pass bead weld on the specimen was performed. The frequency and amplitude of vibration were varied to investigate their effect on residual stresses. Details of the vibratory conditions are provided in the residual stress plots (in the experimental results, Section 5.3.2.4). The experimental set-up for this investigation is shown in Figure 5.67. The amplitude of vibration was measured using an accelerometer, which is shown in Figure 5.67.

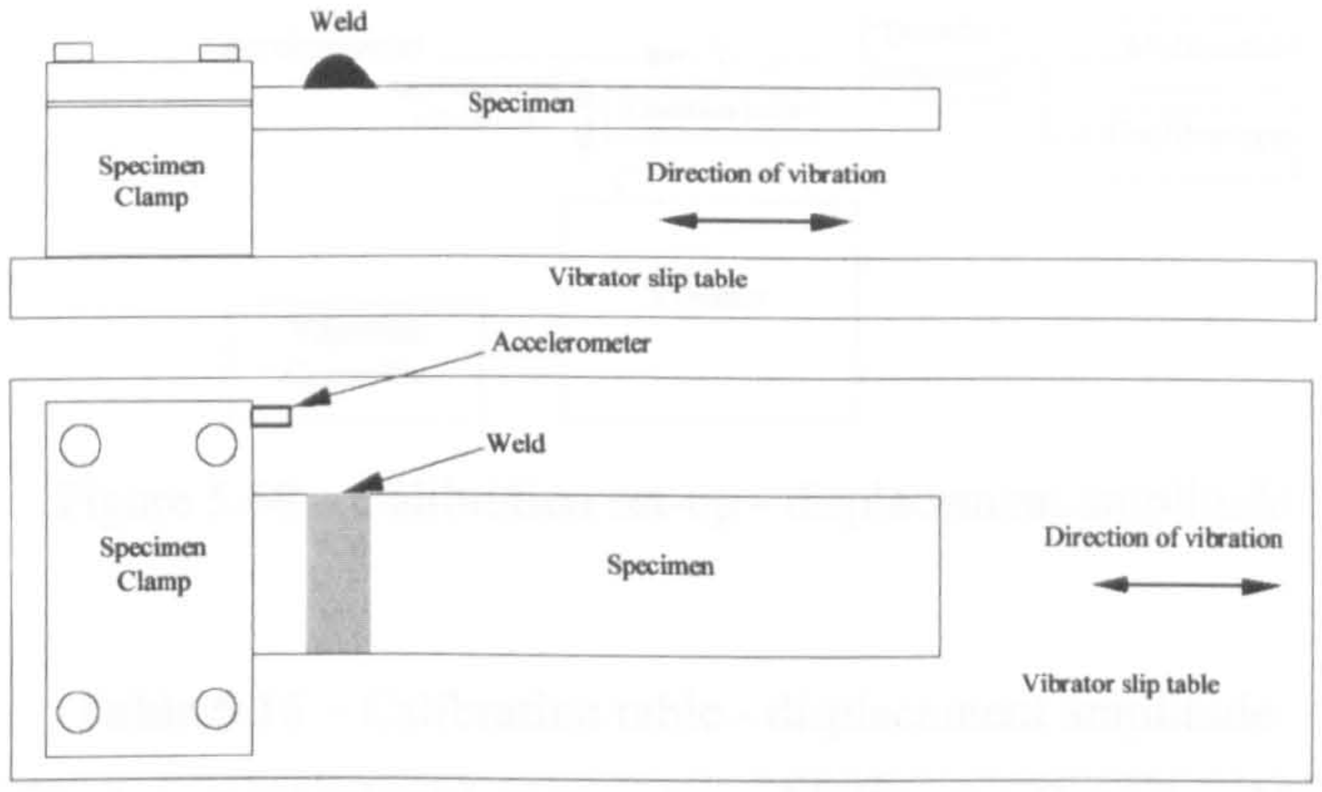

Figure 5.67 - Experimental set-up for rigid body motion - during welding

The welding speed was controlled by the stepper motor drive controller (Figure 5.15A). When the specimens cooled down to room temperature, the residual stresses on the selected line (Figure 5.13) were measured using the X-ray diffractometer. Similar to the previous experiment the single exposure technique (SET) was used to measure the residual stresses in the stress mapping technique. The X-ray measurement jig is shown in Appendix II. The X-ray measurement conditions were similar to that of Table 5.10.

5.3.2.3 Displacement Calibration

Calibration of the displacement amplitude of vibration was carried out to determine the exact amplitude of vibration. This involved a calibrated vibrator, an accelerometer, a double integrator, a multimeter and an oscilloscope. The accelerometer was attached to the vibratory table and was connected to a double integrator. The calibration set-up is shown in Figure 5.68. The output of the double integrator was connected to a multimeter set read the RMS value of the displacement and also to an oscilloscope to monitor the output of the multimeter. The signal input to the vibrator was connected to the second channel of the oscilloscope for observation. The RMS value of the displacement was read from the multimeter which was then converted to a peak/peak value. The applied displacement of the vibration table was recorded from the vibration controller. The displacement was gradually increased and the corresponding displacement and multimeter output was recorded. The output of the multimeter was then plotted against the displacement. The calibration plot is shown in Figure 5.69.

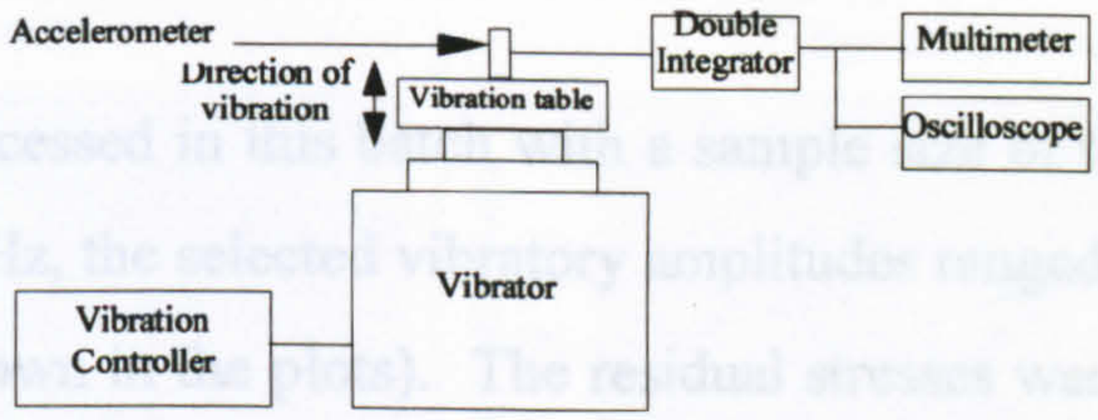

Figure 5.68 – Calibration set-up - displacement amplitude

Table 5.16 – Calibration table - displacement amplitude

Displacement (pk/pk), mm	Multimeter Output, mV
0.25	70.4
0.35	99.35
0.4	112.5
0.5	141.1
0.6	170
0.7	201.5
0.8	232.7
0.9	266.1
1	296.3
1.1	327
1.2	355.5
1.3	382.1
1.4	417
1.5	446.5

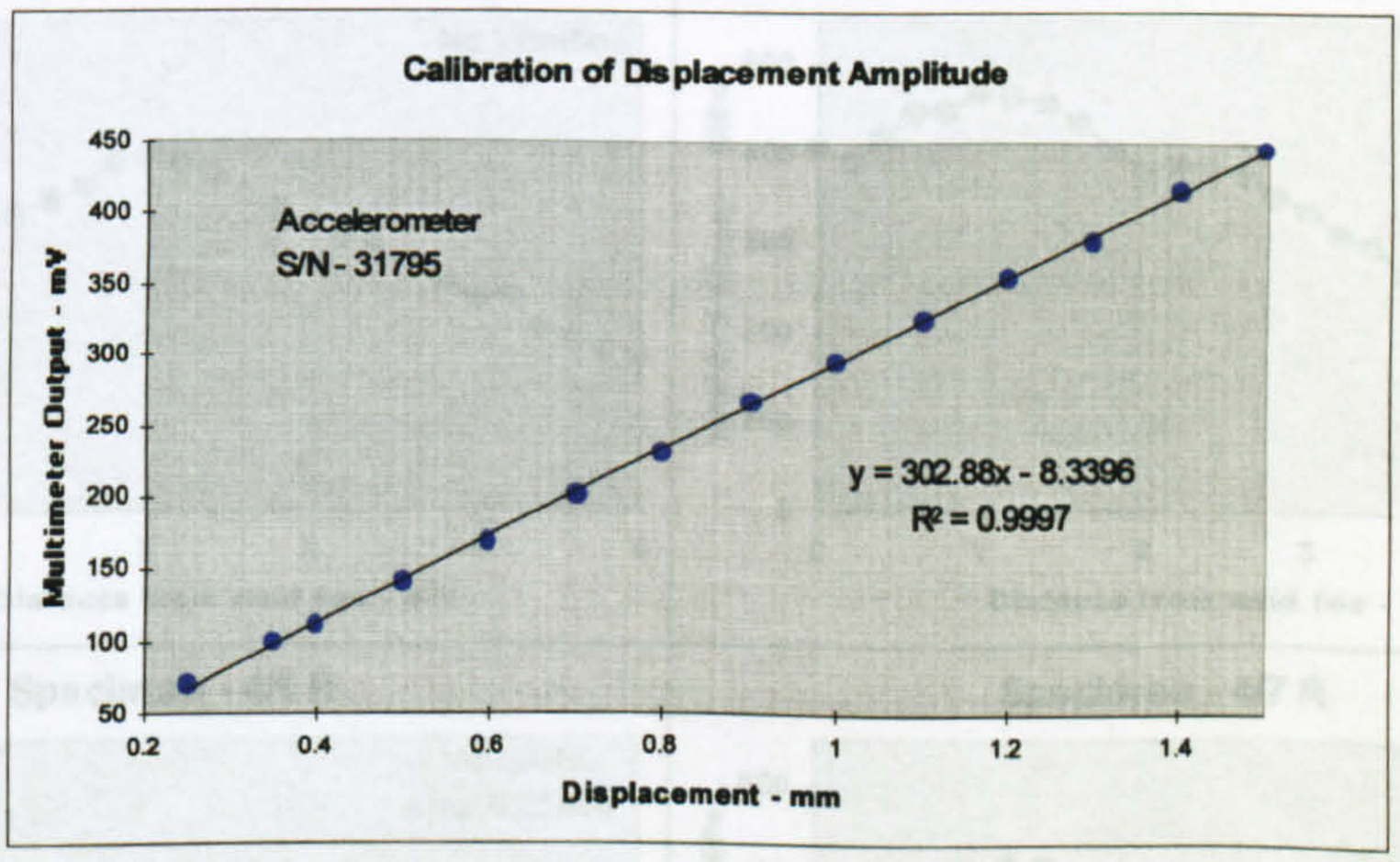

Figure 5.69 – Calibration plot – displacement amplitude

The calibration constant was calculated as 302 mV output (RMS) = 1 mm (pk/pk)

5.3.2.4 Experimental Results

In this experiment, four batches of specimens were processed. In the first three batches, the same experimental procedure was used. The results of all three batches were very similar with no particular trend of change in residual stresses being observed. The results are shown below for batch 3 only. In batch 4 the high frequency effect was investigated and the results are shown below.

Batch 3

Nine specimens were processed in this batch with a sample size of three. Keeping the frequency constant at 50 Hz, the selected vibratory amplitudes ranged from 0 to 0.5 mm (pk/pk) in three steps (shown in the plots). The residual stresses were measured on the selected line shown in Figure 5.13. The results from this batch are shown below.

Longitudinal Stress Plots

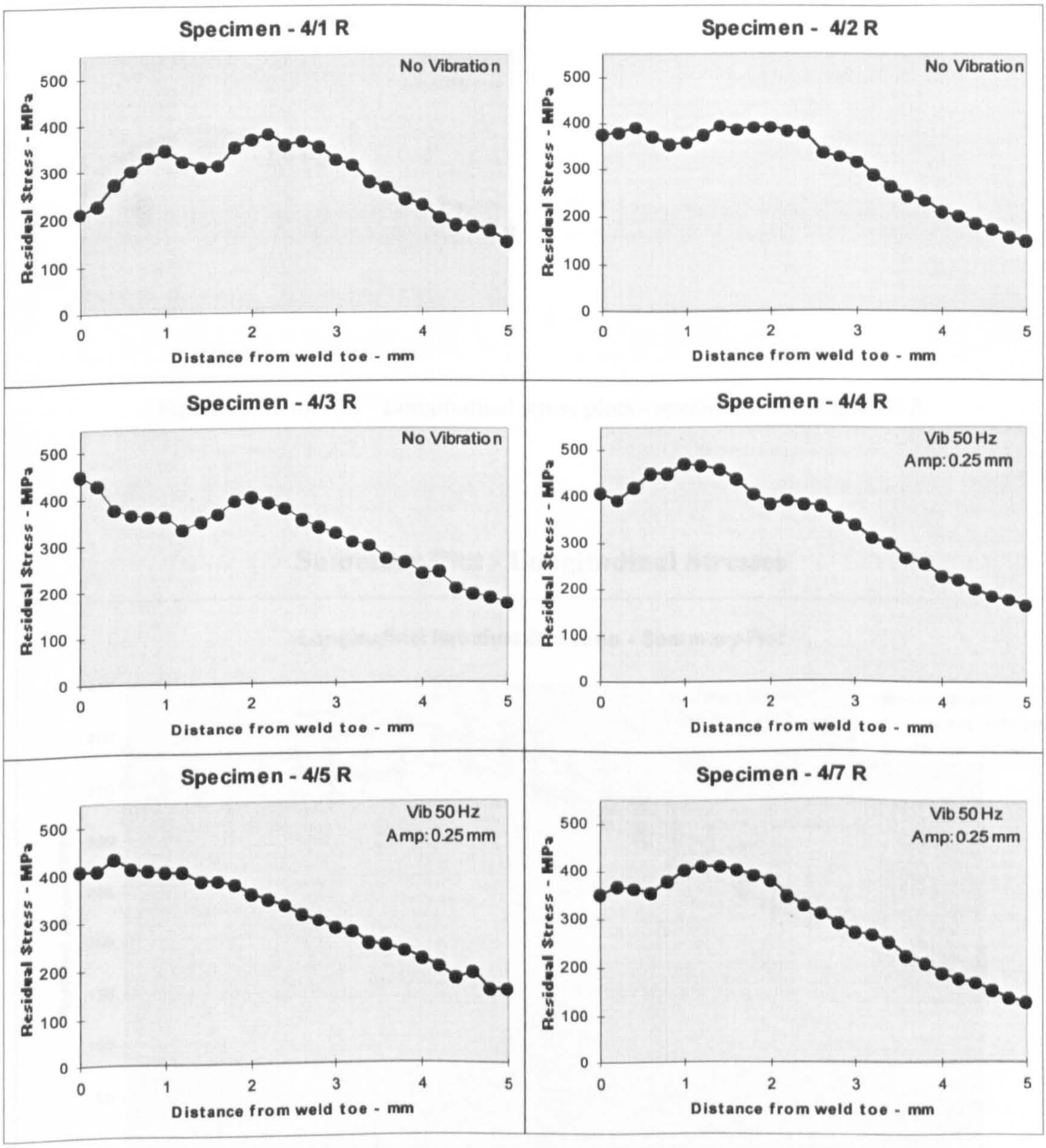

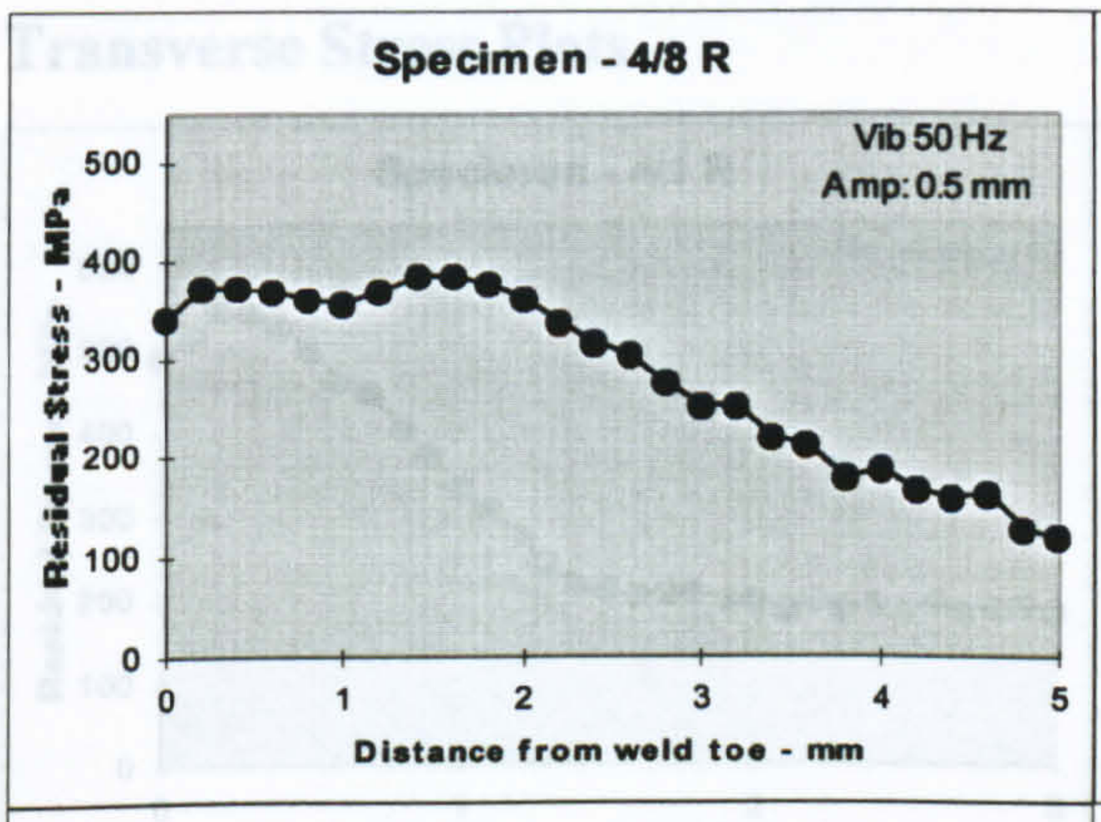

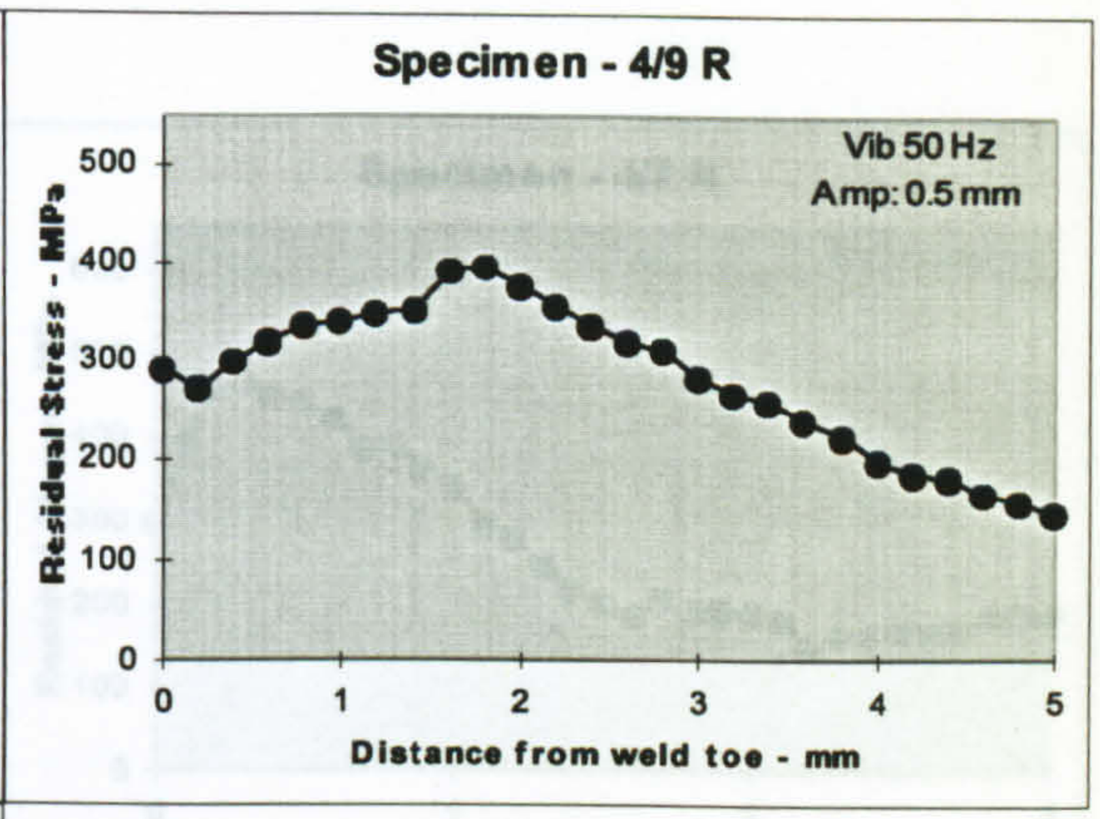

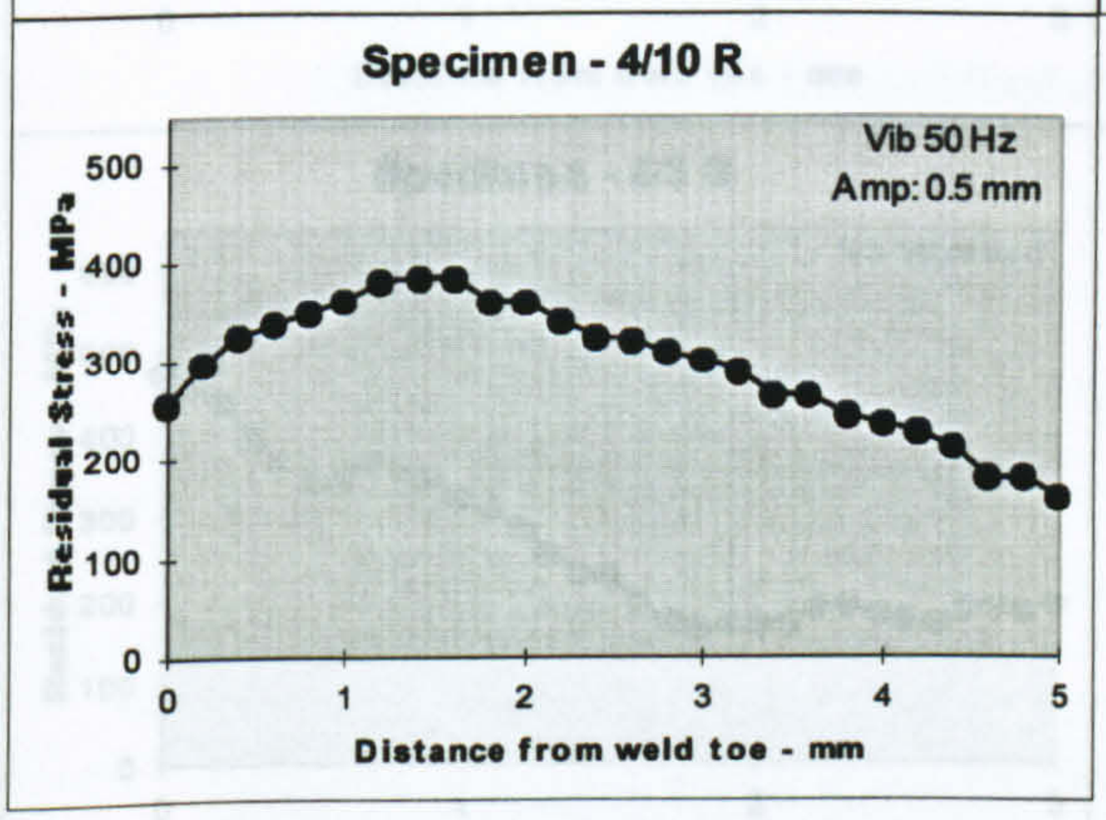

Figures 5.70 to 5.78 - Longitudinal stress plots - specimens 4/1 R to 4/10 R

Summary Plot - Longitudinal Stresses

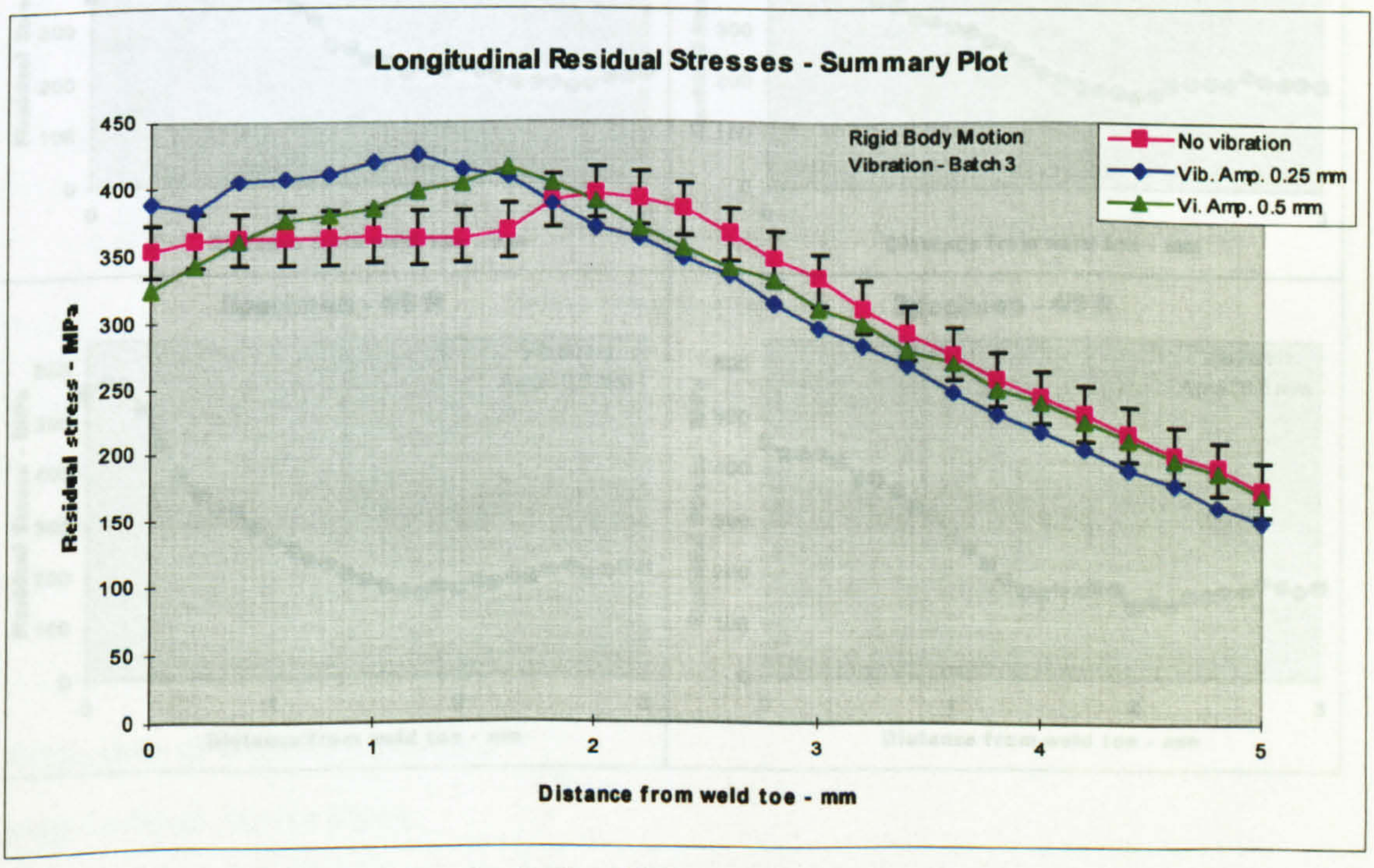

Figure 5.79 – Longitudinal residual stresses of batch 3 – summary plot

Transverse Stress Plots

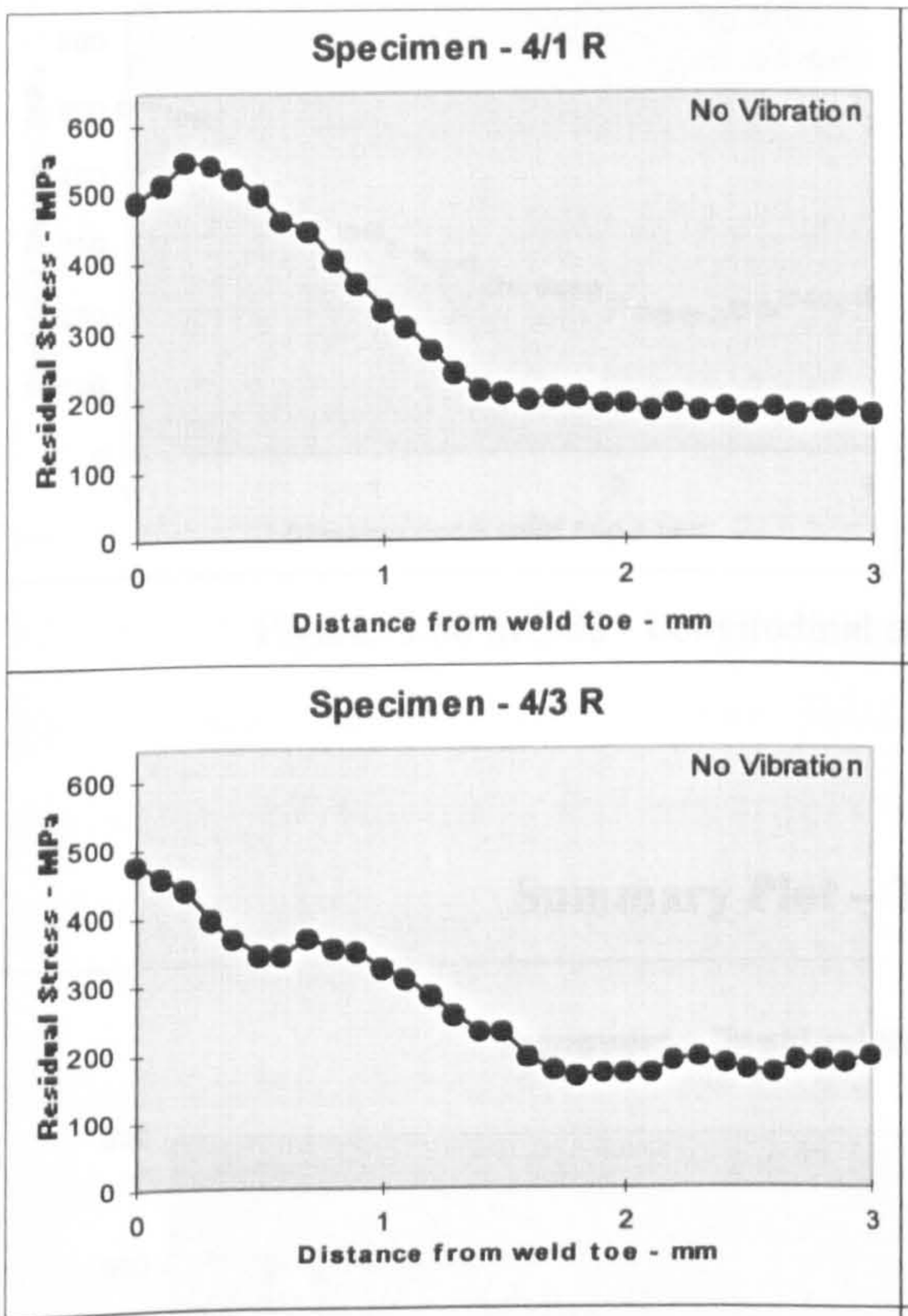

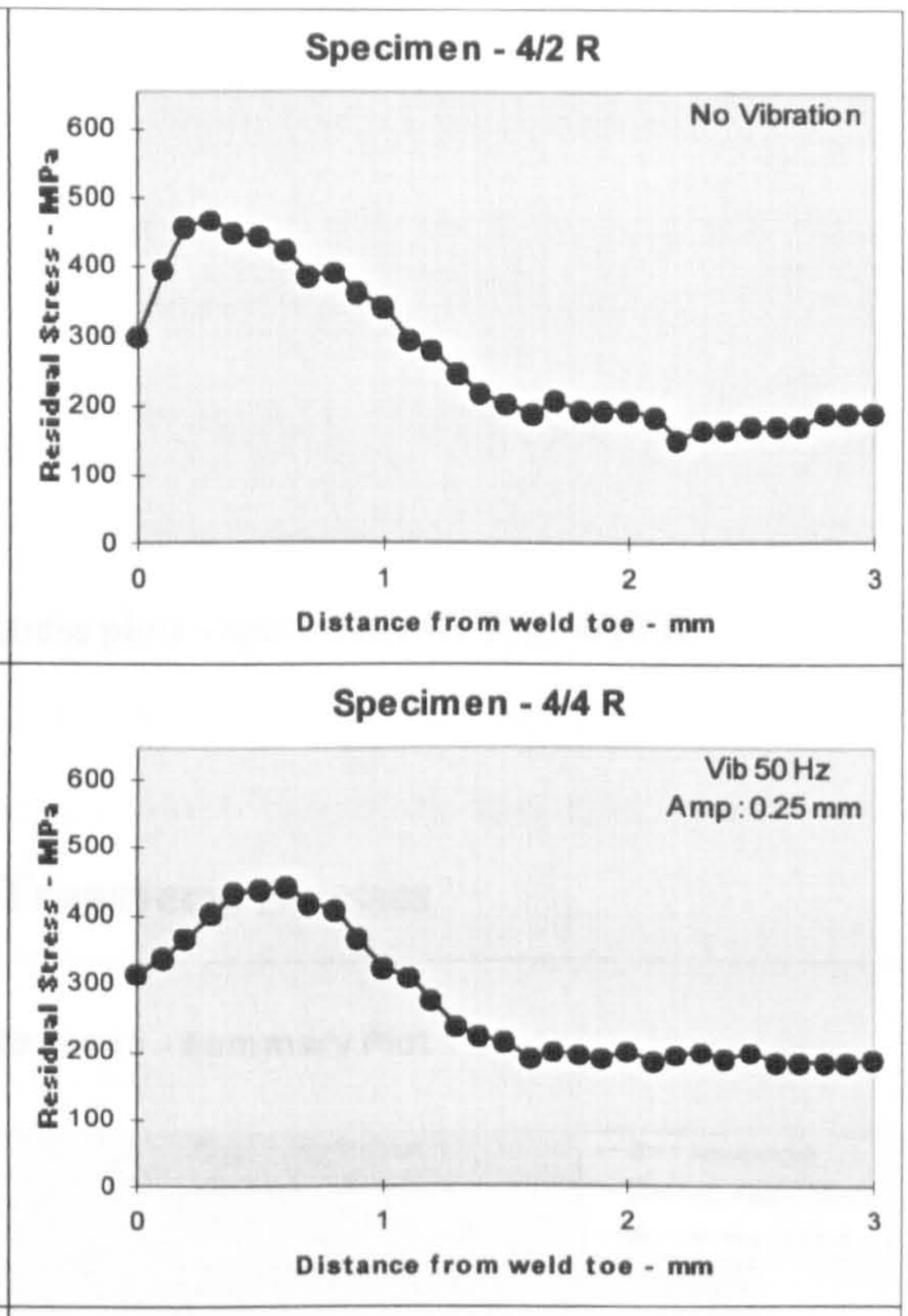

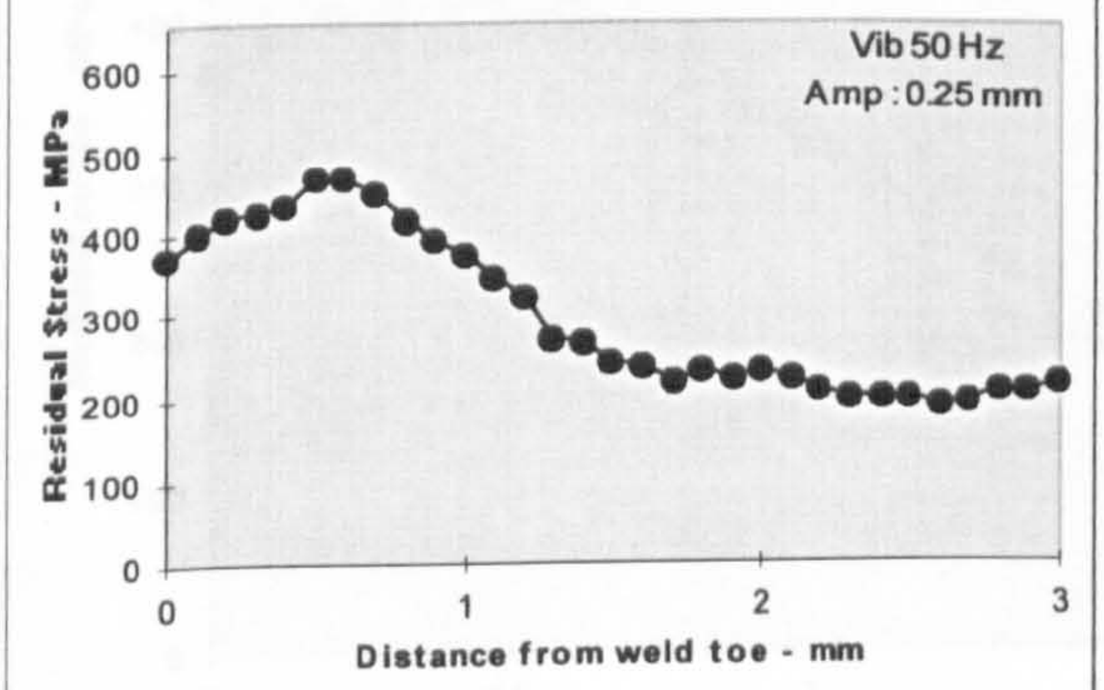

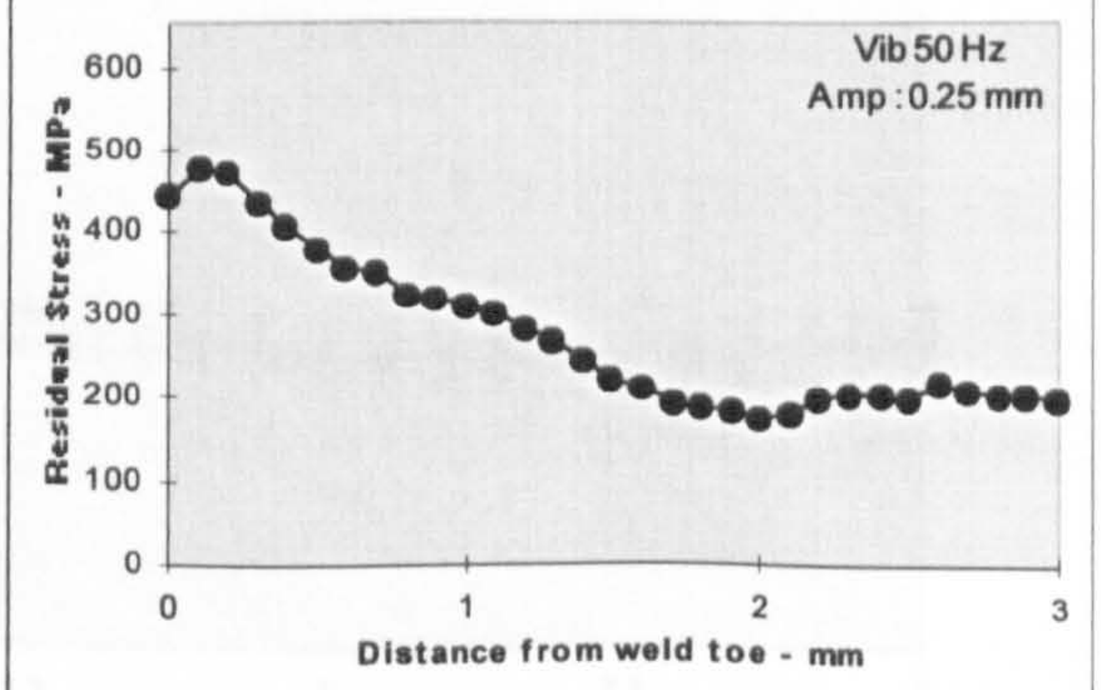

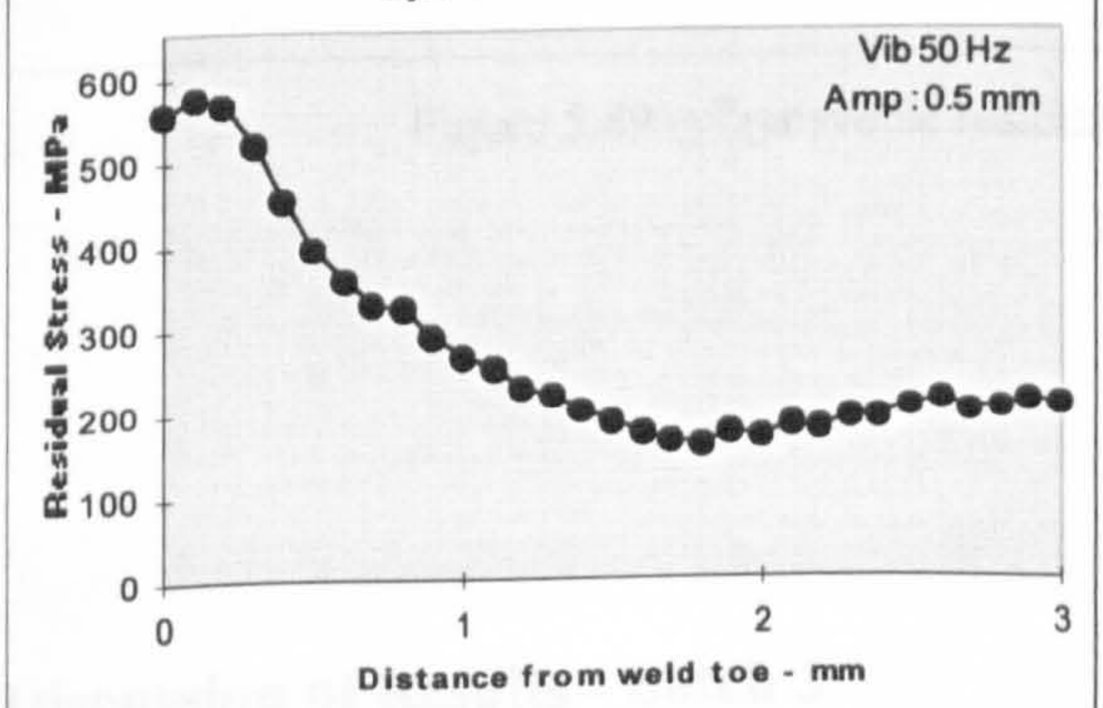

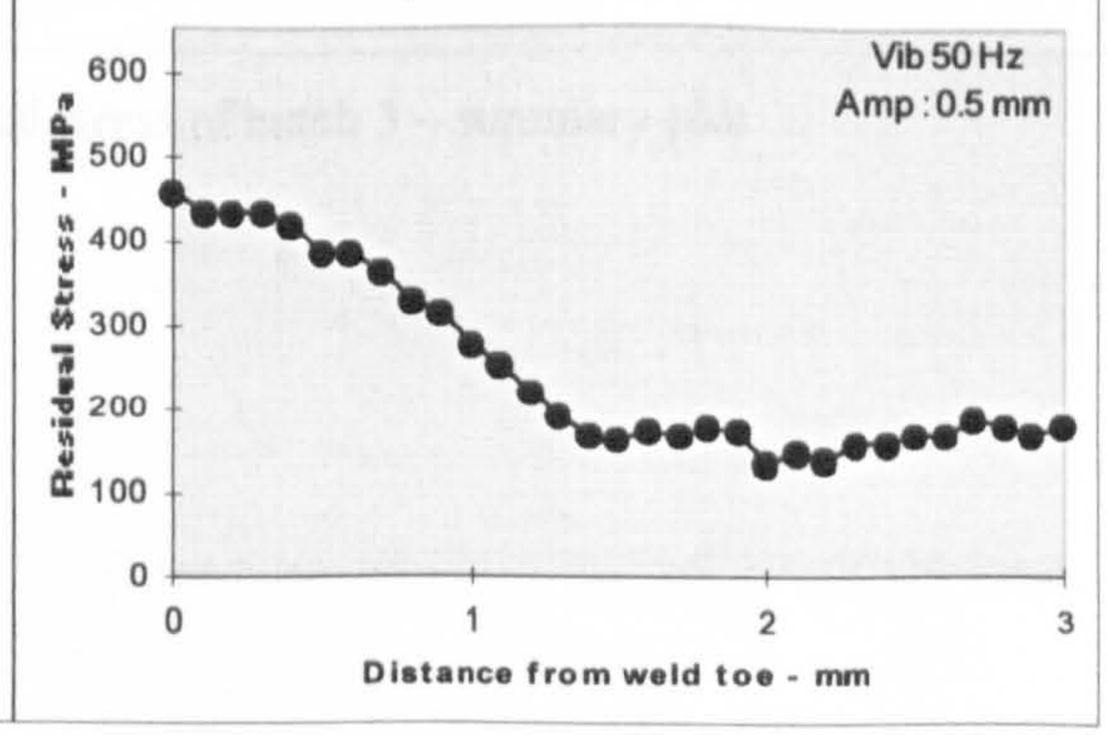

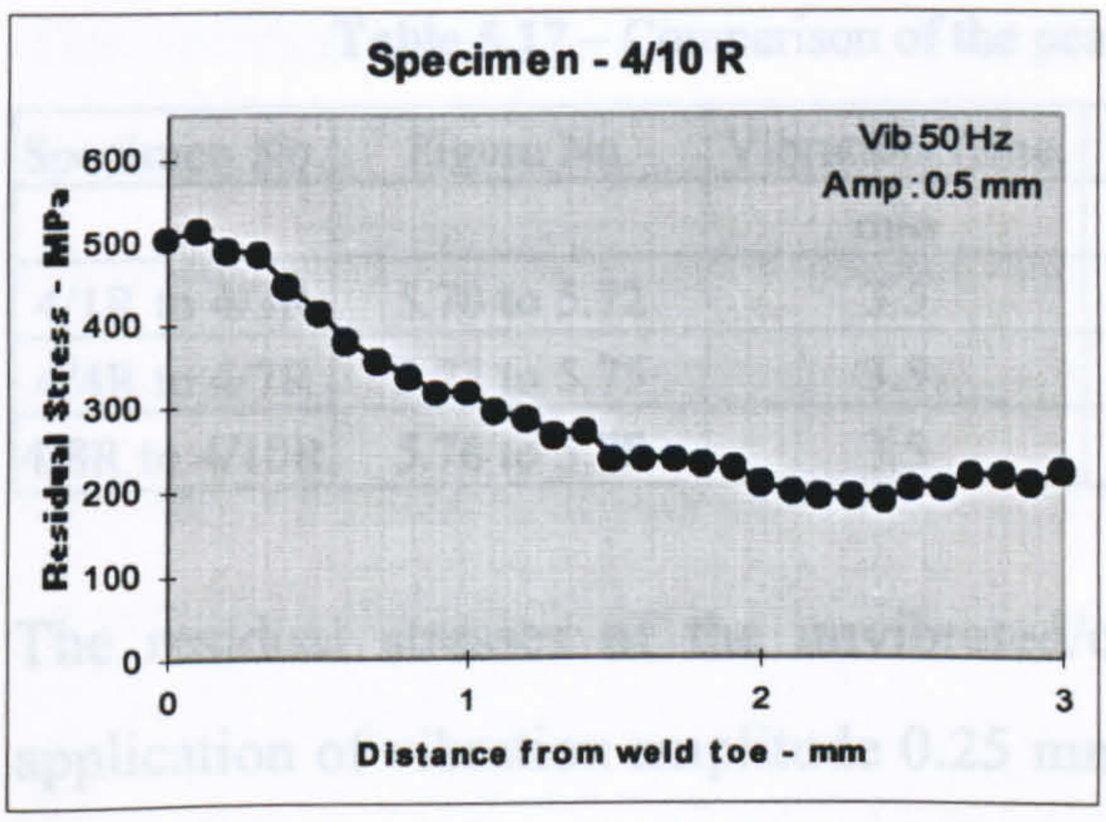

Figures 5.80 to 5.88 - Longitudinal stress plots - specimens 4/1 R to 4/10 R

Summary Plot – Transverse Stresses

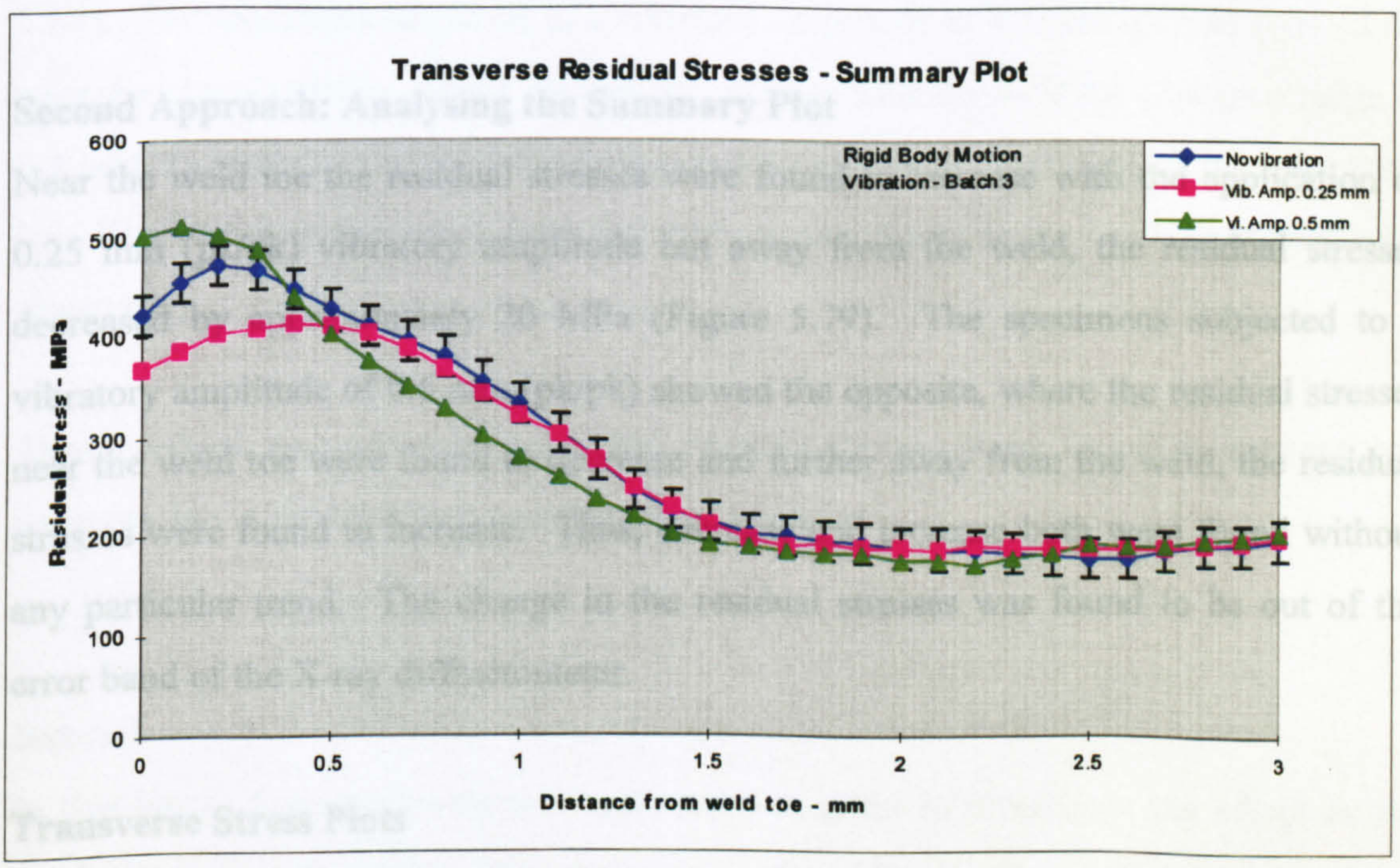

Figure 5.89 – Transverse residual stress of batch 3 – summary plot

Discussion of Results - Batch 3

Longitudinal Stress Plots

First Approach: Comparing the Peak Stresses

The longitudinal residual stresses of the specimens are shown in the table below

Table 5.17 – Comparison of the peak residual stresses – longitudinal stress

Specimen No.	Figure No.	Vibration Time.	Vibration Amp.	Stress Range	Average Stress
		min	mm (pk/pk)	MPa	MPa
4/1R to 4/3R	5.70 to 5.72	3.5	0	370 to 450	406.6
4/4R to 4/7R	5.73 to 5.75	3.5	0.25	400 to 460	428.33
4/8R to 4/10R	5.76 to 5.78	3.5	0.5	380 to 390	385

The residual stresses of the unvibrated/control specimens were 406.6 MPa. With application of vibration amplitude 0.25 mm (pk/pk), the residual stresses were found to increase by 22 MPa. With further increase in the vibration amplitude to 0.5 mm (pk/pk), the residual stresses were found to decrease by 21 MPa. Thus, due to application of vibration, the residual stresses were found to increase and decrease without any particular trend.

Second Approach: Analysing the Summary Plot

Near the weld toe the residual stresses were found to increase with the application of 0.25 mm (pk/pk) vibratory amplitude but away from the weld, the residual stresses decreased by approximately 20 MPa (Figure 5.79). The specimens subjected to a vibratory amplitude of 0.5 mm (pk/pk) showed the opposite, where the residual stresses near the weld toe were found to decrease and further away from the weld, the residual stresses were found to increase. Thus, decrease and increase both were found without any particular trend. The change in the residual stresses was found to be out of the error band of the X-ray diffractometer.

Transverse Stress Plots

First Approach: Comparing the Peak Stresses

The transverse residual stresses of the specimens are shown in the table below

Table 5.18 – Comparison of the peak residual stresses – longitudinal stress

Specimen No.	Figure No.	Vibration Time.	Vibration Amp.	Stress Range	Average Stress
		min	mm (pk/pk)	MPa	MPa
4/1R to 4/3R	5.80 to 5.82	3.5	0	460 to 550	496.6
4/4R to 4/7R	5.83 to 5.85	3.5	0.25	440 to 475	461.6
4/8R to 4/10R	5.86 to 5.88	3.5	0.5	455 to 575	513

The residual stresses of the unvibrated/control specimens were 496.6 MPa. With application of vibration amplitude 0.25 mm (pk/pk), the residual stresses were found to decrease by 30 MPa. With further increase in the vibration amplitude to 0.5 mm (pk/pk), the residual stresses were found to increase by ~17 MPa. Thus, the residual stresses were found to increase and decrease due to application of different amplitudes of vibration, where no particular trend was present.

Second Approach: Analysing the Summary Plot

The residual stresses on and near the weld toe (distance range 0-0.6 mm) of the specimens vibrated at 0.25 mm (pk/pk) decreased by ~60 MPa, but a little away from the weld toe, the residual stresses were very similar to the unvibrated specimens (Figure 5.89). The specimens subjected to a vibratory amplitude of 0.5 mm (pk/pk) showed the opposite characteristics, where the residual stresses near the weld toe (distance range 0-0.4 mm) increased. The residual stresses in the distance range of 0.5-1.5 mm decreased by ~40 MPa but further away from the weld toe no changes in the residual stresses were observed.

Thus, without any particular trend the residual stresses were found to increase and decrease due to increase in the amplitude of vibration.

Batch 4

In this batch, four specimens were processed in order to investigate the effect on the residual stress of the higher frequencies - namely ~500 Hz. Due to the high frequency of vibration the amplitude was reasonably small. This was due to a large mass (slip table, clamping jigs and specimens) connected to the vibrator and the limited power of the system. Four specimens were vibrated at a frequency of ~500 Hz, with vibratory amplitude being set at 0.08 mm, 0.06 mm, 0.045 mm, and 0.045. The longitudinal and transverse residual stress plots and the summary plots are shown below.

Longitudinal Stress Plots

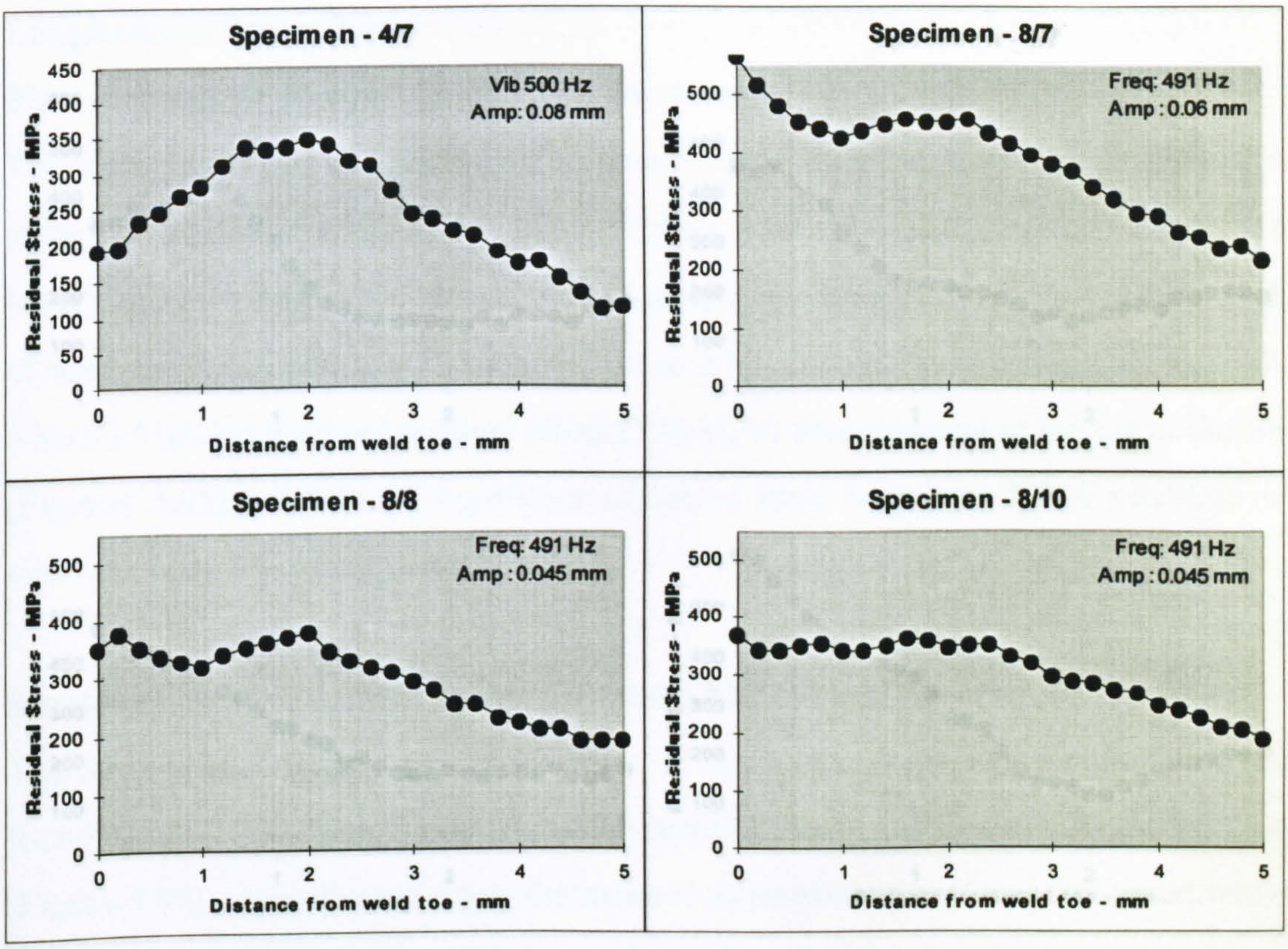

Figures 5.90 to 5.93 - Longitudinal stress plots - specimens 4/7, 8/7, 8/8 and 8/10.

Summary Plot

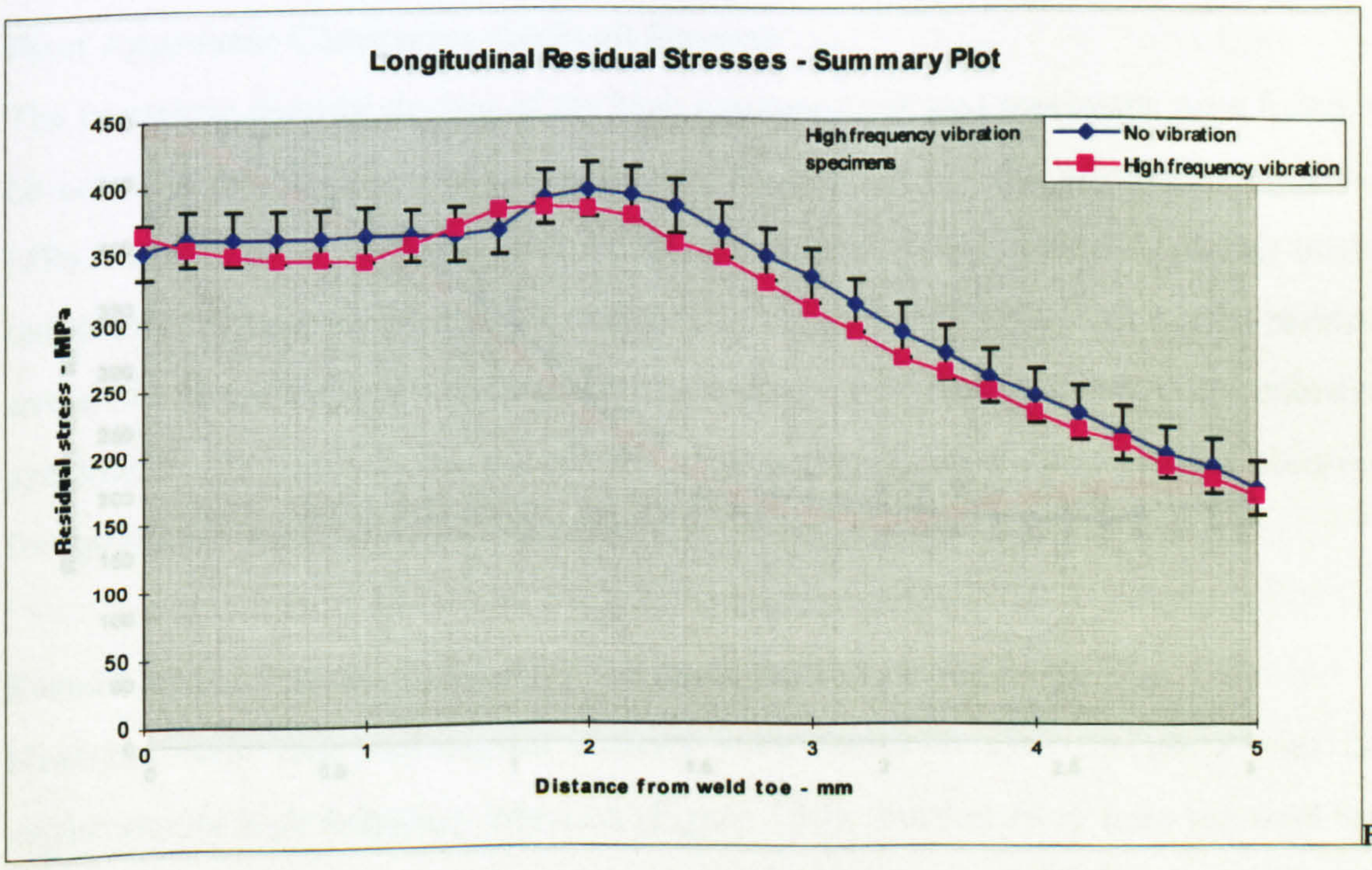

Figure 5.94 – Longitudinal residual stresses - high frequency vibrated specimens.

Transverse Stress Plots

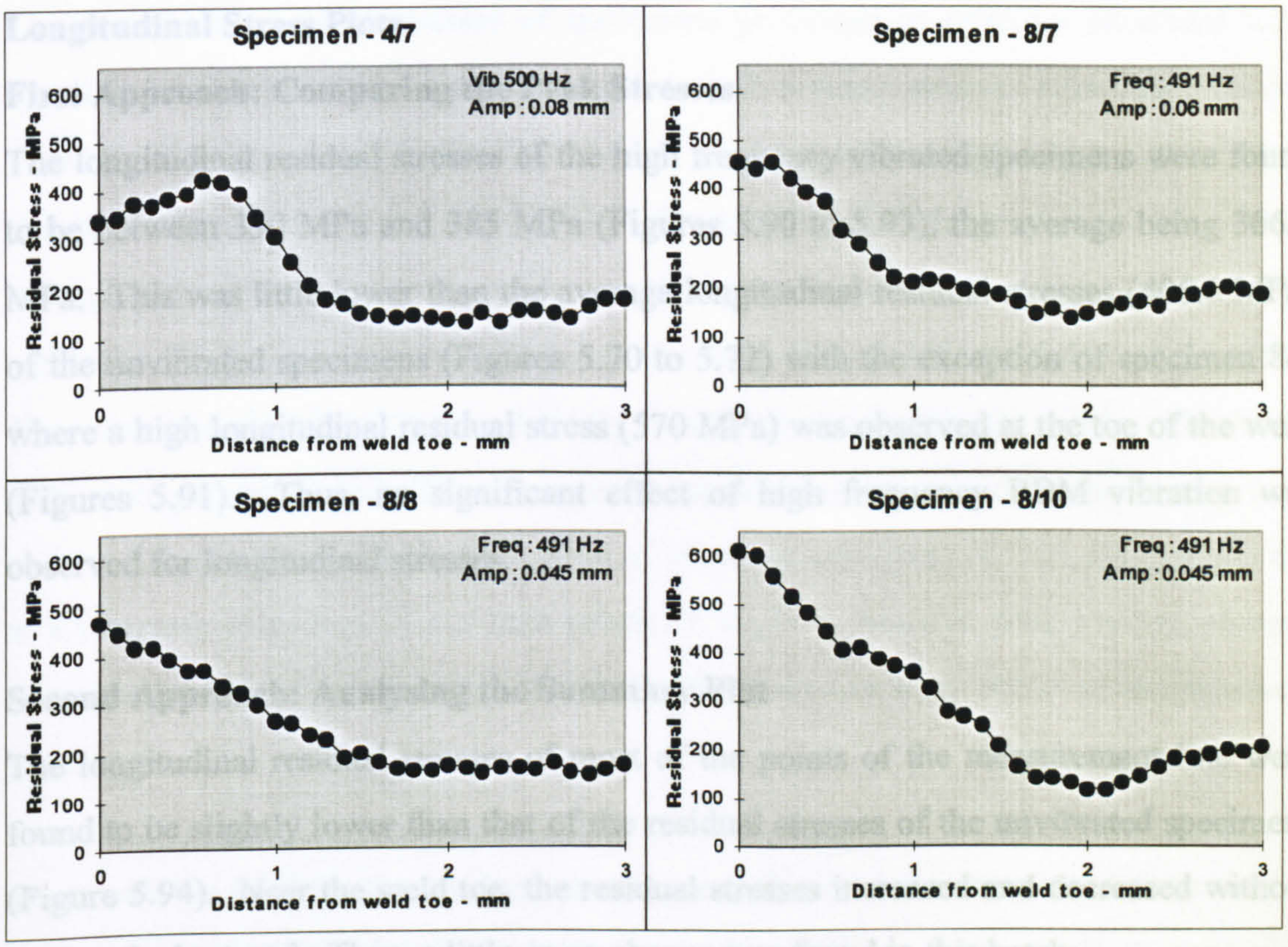

Figures 5.95 to 5.98 - Transverse stress plots – specimens 4/7, 8/7, 8/8 and 8/10.

Summary Plot

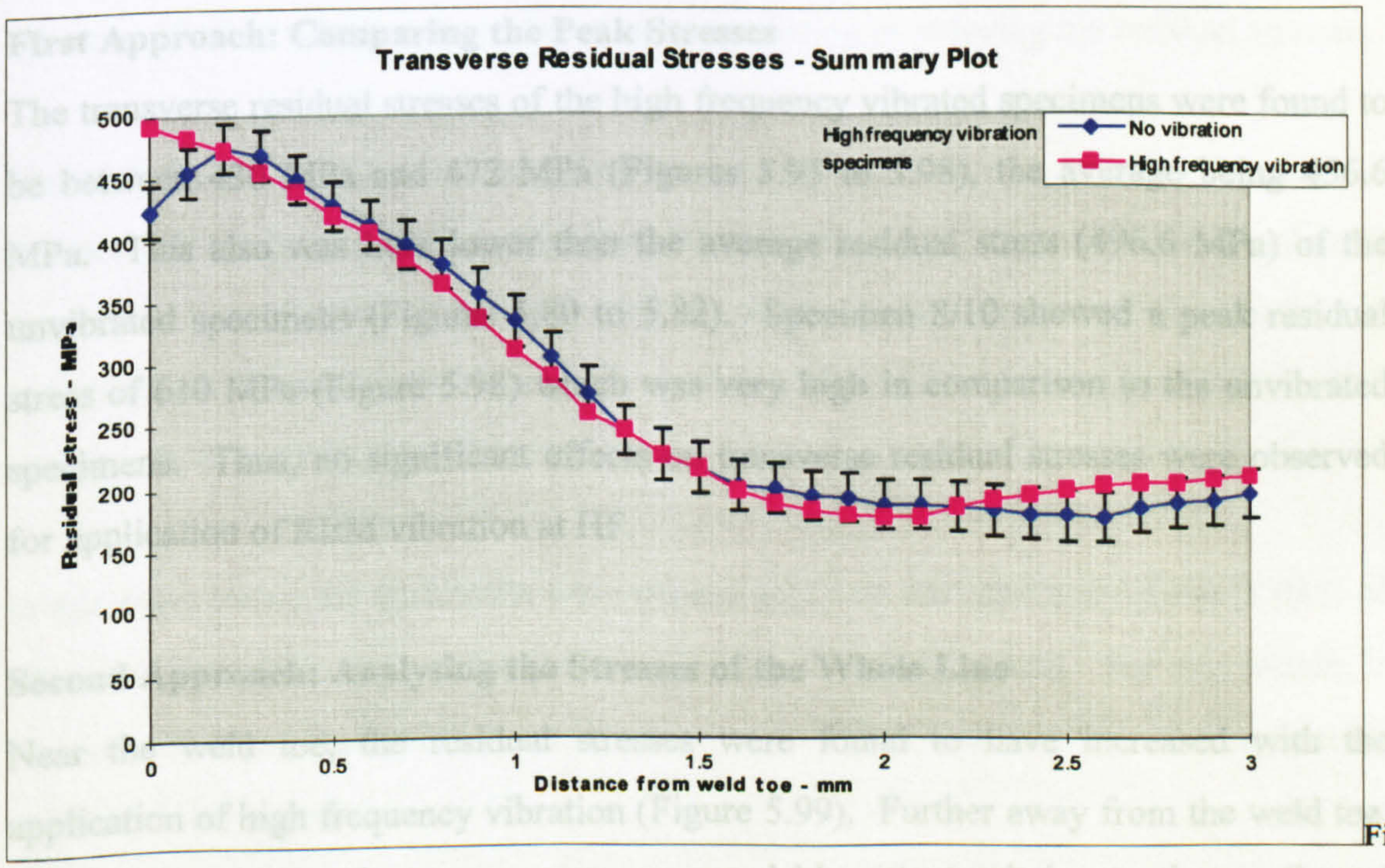

Figure 5.99 – Transverse residual stresses - high frequency vibrated specimens.

Discussion of Results - Batch 4

Longitudinal Stress Plots

First Approach: Comparing the Peak Stresses

The longitudinal residual stresses of the high frequency vibrated specimens were found to be between 350 MPa and 385 MPa (Figures 5.90 to 5.93), the average being 366.6 MPa. This was little lower than the average longitudinal residual stresses (406.6 MPa) of the unvibrated specimens (Figures 5.70 to 5.72) with the exception of specimen 8/7 where a high longitudinal residual stress (570 MPa) was observed at the toe of the weld (Figures 5.91). Thus, no significant effect of high frequency RBM vibration was observed for longitudinal stresses.

Second Approach: Analysing the Summary Plot

The longitudinal residual stresses of most of the points of the measurement line were found to be slightly lower than that of the residual stresses of the unvibrated specimens (Figure 5.94). Near the weld toe, the residual stresses increased and decreased without any particular trend. Thus, a little or no change was found in this batch.

Transverse Stress Plots

First Approach: Comparing the Peak Stresses

The transverse residual stresses of the high frequency vibrated specimens were found to be between 430 MPa and 472 MPa (Figures 5.95 to 5.98), the average being 456.6 MPa. This also was little lower than the average residual stress (496.6 MPa) of the unvibrated specimens (Figures 5.80 to 5.82). Specimen 8/10 showed a peak residual stress of 610 MPa (Figure 5.98) which was very high in comparison to the unvibrated specimens. Thus, no significant effects on transverse residual stresses were observed for application of RBM vibration at HF.

Second Approach: Analysing the Stresses of the Whole Line

Near the weld toe, the residual stresses were found to have increased with the application of high frequency vibration (Figure 5.99). Further away from the weld toe, the stresses did not decrease to any commendable extent relative to the unvibrated specimens.

5.3.2.5 Summary of Results

The changes in residual stresses of specimens processed in different situations were found to be contradictory. No particular trends in residual stresses were observed due to the application of RBM vibration. In the third batch the longitudinal peak residual stresses decreased due to 0.5 mm (pk/pk) vibration, but at a vibratory amplitude of 0.25 mm (pk/pk); an increase in the average residual stresses were observed. Away from the weld, the residual stresses were found to decrease in both HF and LF configurations. The decrease however was relatively small and considered within the X-ray diffractometer error band. The transverse peak residual stresses of the third batch were observed to decrease with an application of vibration amplitude of 0.25 mm (pk/pk) but at a vibratory amplitude of 0.5 mm (pk/pk) a slight increase in peak residual stresses was found. Away from the weld toe, the residual stresses were observed to decrease a little.

Thus, near the weld toe the residual stresses were observed to increase and decrease due to the application of vibration. Away from the weld toe, very small or negligible reductions were found relative to the error band of the X-ray diffractometer (±21 MPa) in both the transverse and longitudinal stresses. So, the effects of the rigid body motion vibration (RBM) vibration were found to be confusing in reducing the residual stresses.

The high frequency vibration was also found to be ineffective in reducing the residual stresses. The longitudinal residual stresses of the high frequency RBM vibrated specimens were found to be very similar to the peak stresses of the unvibrated specimens. There was however a slight trend towards reduction in longitudinal residual stresses. In the transverse residual stresses no reduction in the stresses were found.

In this experiment, the specimens were treated applying the rigid body mode (RBM) of vibration, thus there were not any induced stress in the specimens. For this reason, it was expected that the residual stress reduction would not occur. The obtained result confirmed the expectation.

5.3.3 Experiment III: Flexural Vibration Test – Cantilever Beam

Abstract

In this experiment flexurally induced stresses were generated by vibration – during the welding period. The experiment was carried out in three phases: (1) investigation of the level of applied stress, (2) investigation of the time of vibration and (3) investigation of the high frequency (HF) flexural vibration effect.

The longitudinal residual stresses were found to decrease with application of small induced stresses. The increase in the time of vibration showed no effect on residual stresses.

The transverse residual stresses were found to increase with the application of small-induced stresses and were found to further increase with increase in the applied stresses. Beyond a certain level of applied stress, a decrease in the residual stresses was observed.

The longitudinal residual stresses were found to decrease in the specimens subjected to 2 minutes of vibration. The transverse residual stresses were found to increase with increase in the time of vibration when the induced stress was small and found to decrease when the induced stress was large.

In the high frequency (HF) vibration, the longitudinal residual stresses showed no reduction whereas the transverse residual stresses showed a slight increase due to vibration.

5.3.3.1 Introduction

The effect of Rigid Body Motion vibration was investigated in the previous experiment where no particular trend of residual stresses were observed due to vibration. In this experiment the effect of flexural vibration was investigated. This investigation is very important because flexural vibration can induce dynamic stresses and may result in reduction in the residual stresses. Also, flexural vibration can induce a pre-selected stress in the specimens at pre-selected locations. Most researchers in VSR recommended flexural vibration to relieve residual stresses. From the work carried out in the early 60's by Bühler and Pfalzgraf [22, 24, and 25] to the most recent work by Sonsino et. al. [123], most of the publications related to VSR/VWC used flexural vibration to relieve the residual stresses. In this experiment the time and

amplitude of vibration both were varied to observe its effect. Initiation was taken to observe the effect of flexural high frequency vibration on the residual stress.

5.3.3.2 Experimental Procedure

In this experiment the specimens were subjected to vibration during welding at a non-resonant frequency of 25 Hz (the natural frequency of the specimens was *ca.* 115 Hz). This frequency was selected to aid the displacement amplitude of vibration of the system. It was not possible to obtain high vibratory amplitude using the natural frequency of the specimens. The experimental set-up is shown in Figure 5.100.

In this set-up, one end of the specimen was inserted into the vibrating clamp where it was clamped by two rollers. The rollers were loaded by compression springs which were tightened with screws. The springs were used to capacitate the translational and rotational movement of the specimens during vibration. The other end of the specimen was rigidly clamped to a fixed frame. The roller clamp was connected to the vibrator with a 1 inch diameter steel rod which was guided with a brass bush. The specimens were welded while being vibrated at pre-selected conditions – the details of which are described in the experimental results section. A single pass bead weld was performed on the specimens. The stepper-motor-driven weld-torch carrier (Figure 5.15A) controlled the welding speed. The welding speed was kept constant for all the specimens.

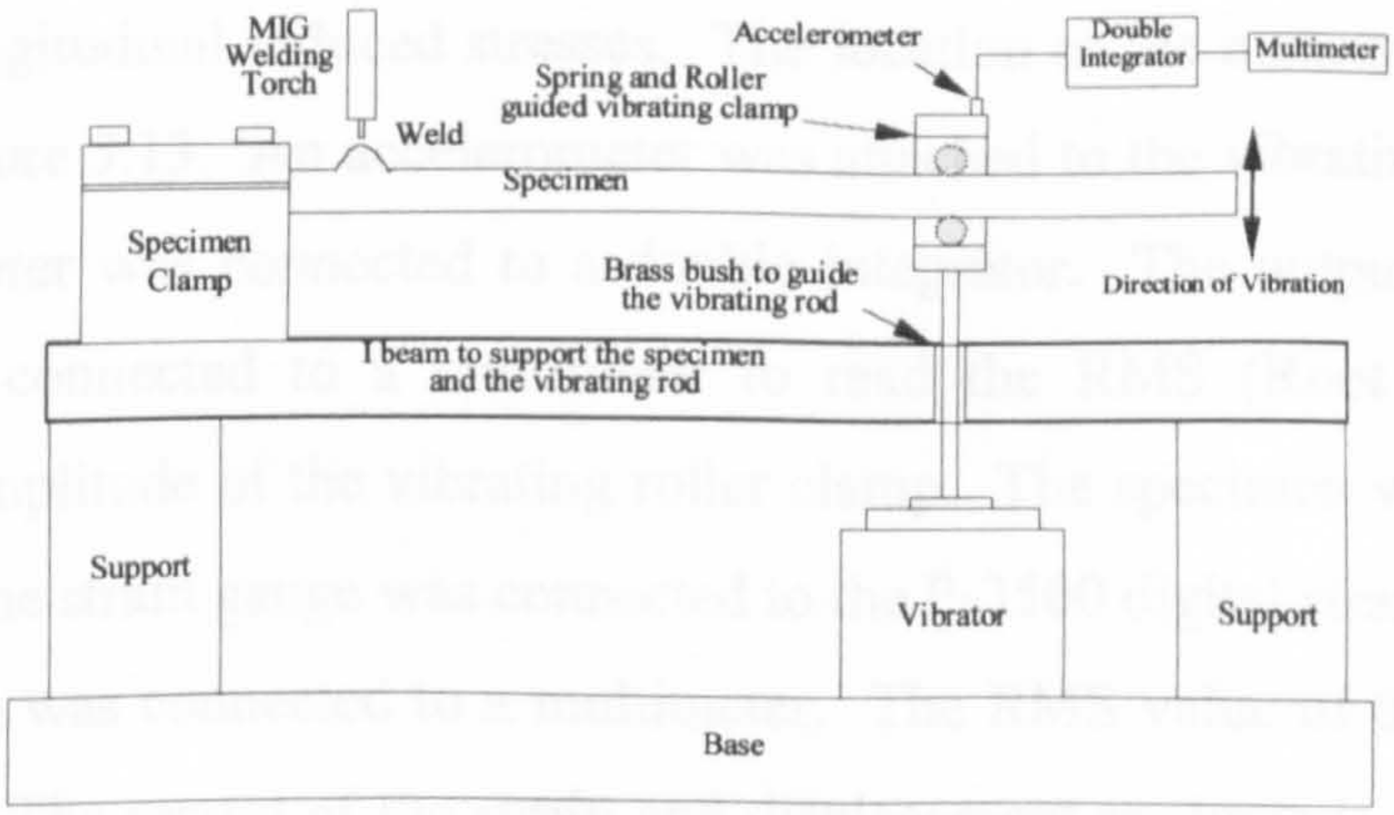

Figure 5.100 - Experimental set-up - flexural vibration treatment of cantilever beam

When the specimens cooled down to room temperature, the longitudinal and transverse directional residual stresses were measured on the selected line shown in

Figure 5.13 using the X-ray diffractometer. The conditions of X-ray measurement are shown in Table 5.10. A line map was measured on the selected line using the single exposure technique (SET). The residual stress levels for the specimens are shown in Section 5.3.3.4. The X-ray measurement jig was also the same as in previous experiments and is shown in Appendix II.

5.3.3.3 Induced Stress Calibration

The dynamically induced stress was calibrated using a P-3500 digital strain indicator, an accelerometer, a double integrator and a multimeter. The calibration set-up is shown in Figure 5.101.

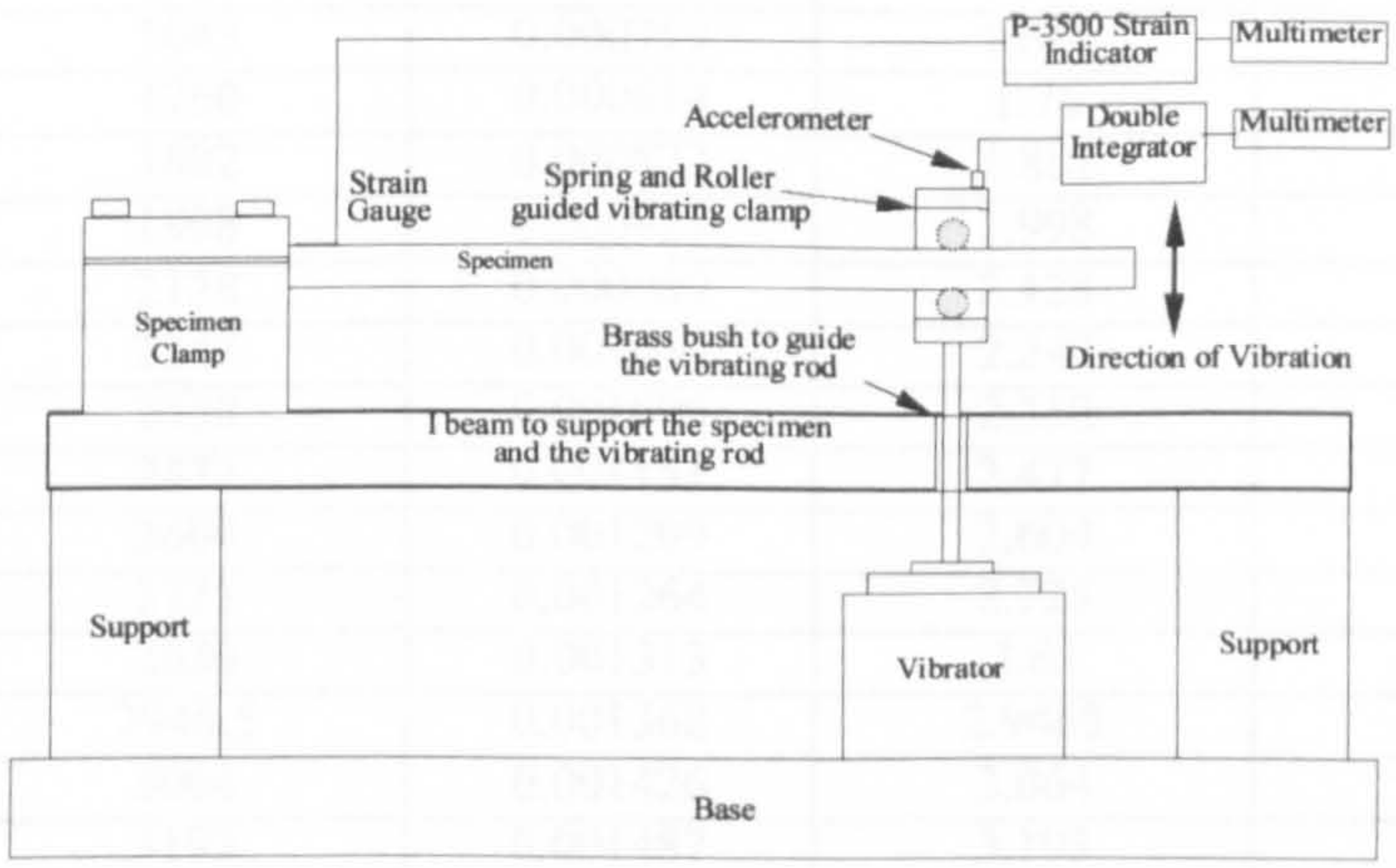

Figure 5.101 - Calibration set-up - applied stress to the specimens

A strain gauge was fixed on the X-ray measurement targeted area of the specimen to measure the longitudinal induced stresses. The location of the measurement area/line is shown in Figure 5.13. An accelerometer was attached to the vibrating roller clamp. The accelerometer was connected to a double integrator. The output of the double integrator was connected to a multimeter to read the RMS (Root Mean Square) displacement amplitude of the vibrating roller clamp. The specimen was mounted on the set-up and the strain gauge was connected to the P-3500 digital strain indicator, the output of which was connected to a multimeter. The RMS value of the strain output was measured. The record of the strain and displacement readings is shown in Table 5.19. The data were plotted as stress against displacement to obtain the calibration constant of the applied stresses in terms of displacements.

Table 5.19 - Calibration table - applied dynamic stress, accelerometer S/N : 31795

Micro Strain	Displacement	Strain	Displacement	Induced Stress
V	V (RMS)		mV	MPa
16.7	104.8	5.11E-05	0.1048	10.76493
38.15	240.9	0.000117	0.2409	24.59174
58.2	369	0.000178	0.369	37.5161
78	513.5	0.000239	0.5135	50.27931
96	630.5	0.000294	0.6305	61.88223
115	762	0.000352	0.762	74.12975
133.5	879.5	0.000409	0.8795	86.05497
152	1008	0.000465	1.008	97.98019
166	1100	0.000508	1.1	107.0047
188	1245.5	0.000575	1.2455	121.186
211	1396	0.000646	1.396	136.012
229	1519	0.000701	1.519	147.6149
248	1643	0.000759	1.643	159.8624
266	1760	0.000814	1.76	171.4653
285	1882	0.000872	1.882	183.7129
303	1998	0.000927	1.998	195.3158
323	2128	0.000989	2.128	208.2079
341	2247	0.001044	2.247	219.8108
358	2358	0.001096	2.358	230.7691
376	2477	0.001151	2.477	242.3721
395	2604	0.001209	2.604	254.6196
413	2725	0.001264	2.725	266.2225
429	2830	0.001313	2.83	276.5362
447	2946.5	0.001368	2.9465	288.1391
466	3064	0.001426	3.064	300.3866
486	3193	0.001487	3.193	313.2788
502.5	3297	0.001538	3.297	323.9148

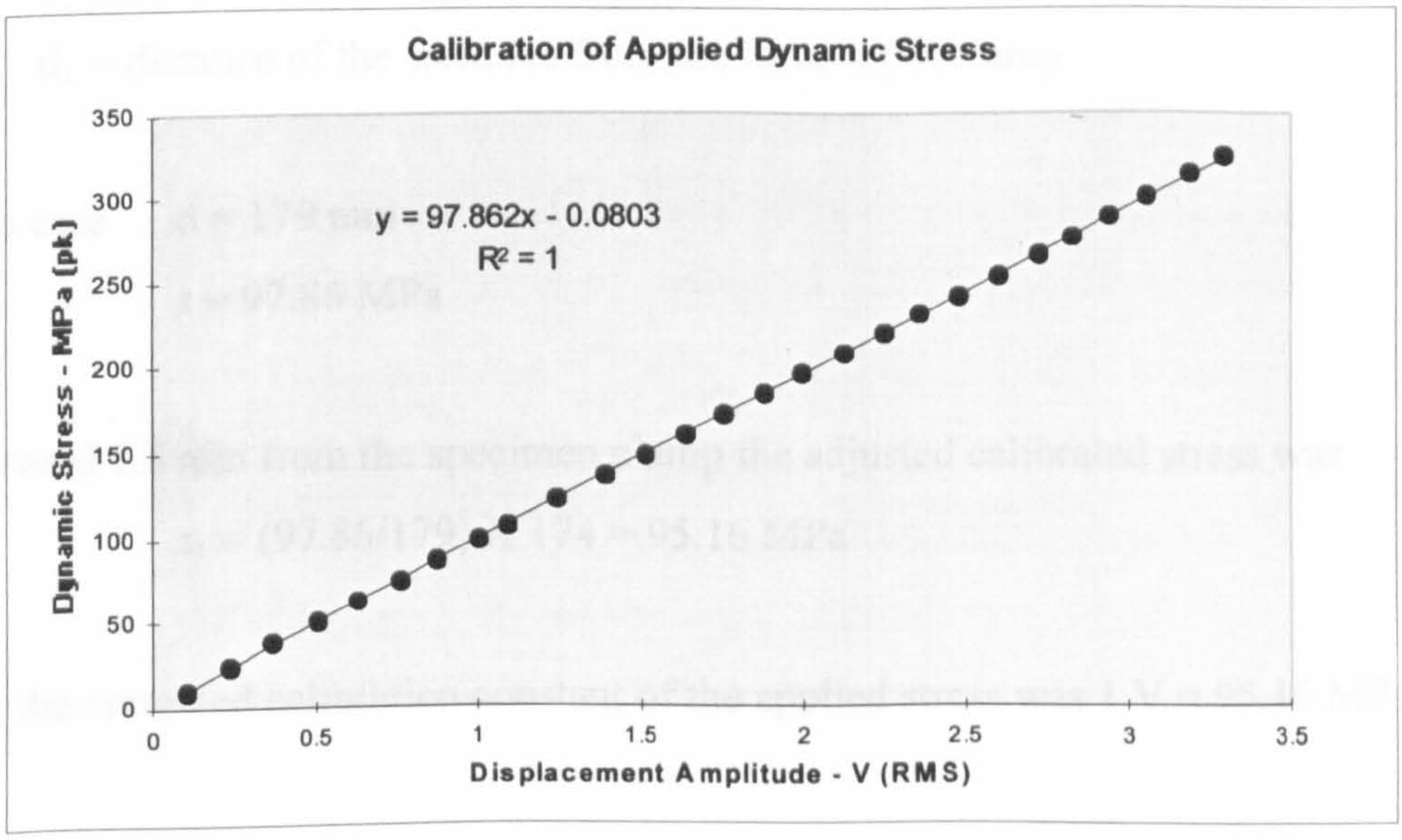

Figure 5.102 - Calibration plot - applied dynamic stress

Calibration Constant, 1 V (RMS) = 97.862 MPa

The dynamic stress due to vibration was not constant along the specimen length and the weld line tended to move in the transverse direction from specimen to specimen - due to the displacement of the welding torch. This movement could not be avoided because (a) it was necessary to clean the welding torch or change the torch tip due to wear and (b) any attempt to clean the torch or change the tip caused movement of the torch position. Because of this movement of the weld line, the calibration constant was adjusted by measuring the distance of the weld toe from the clamp.

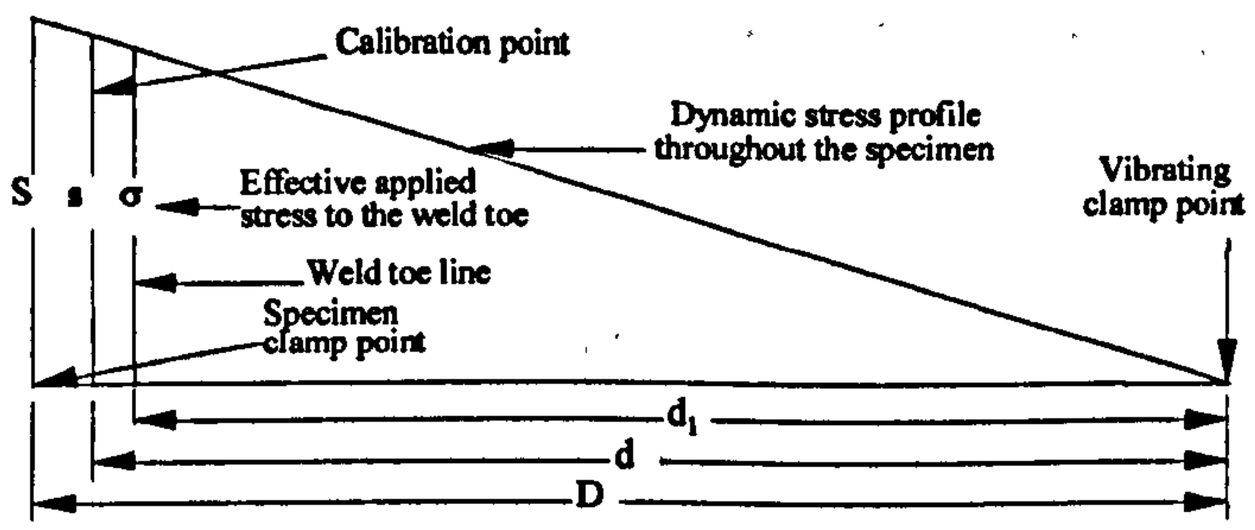

Figure 5.103 - Correction of calibration constant for the weld toe

The bending stress on the weld toe σ was calculated by the equation.

$$\sigma = \frac{s}{d} \times d_1$$

where s = calibrated stress from the strain gauge

d = distance of strain gauge from the force input clamp

d_1 = distance of the weld toe from the force input clamp

In this case d = 179 mm

s = 97.86 MPa

For a weld 7.5 mm from the specimen clamp the adjusted calibrated stress was

$s_1 = (97.86/179)\ X\ 174 = 95.16$ MPa

Thus, the corrected calibration constant of the applied stress was 1 V = 95.16 MPa.

5.3.3.4 Experimental Results

In this experiment, five batches of specimens were processed where the frequency and amplitude were varied independently. In the first batch a relatively large number of specimens (28 specimens) were processed where the frequency and time of vibration were kept constant and the amplitude of vibration was varied. In the second, third and fourth batches the time of vibration was increased, applying different levels of applied stresses. The details of the treatment conditions are shown in the relevant batches. In the fifth batch, high frequency (HF) vibration was applied to the specimens to observe its effect. The residual stresses were measured on the selected line shown in Figure 5.13.

Batch 1: Change in Applied Stress Amplitude

In total, 28 specimens were processed; grouping four in a sample, seven situations were created. The first sample was welded without any vibration, i.e. the control sample. The other six samples were vibrated while they were being welded. The dynamic applied stresses to the samples due to the vibration were ±48 MPa, ±96 MPa, ±144 MPa, ±192 MPa, ±240 MPa, and ±288 MPa. The longitudinal and transverse residual stresses were measured.

Longitudinal Stress Plots

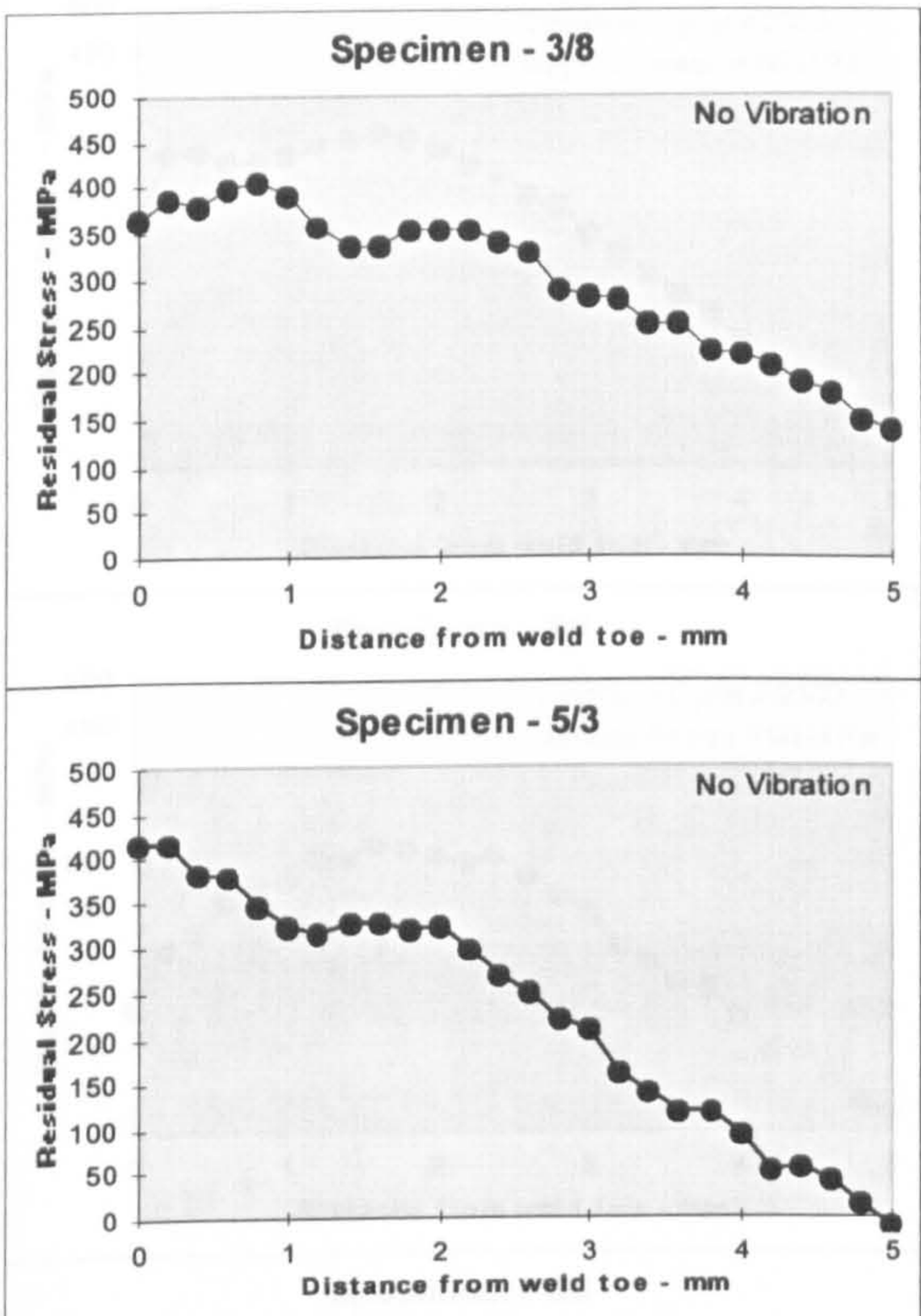

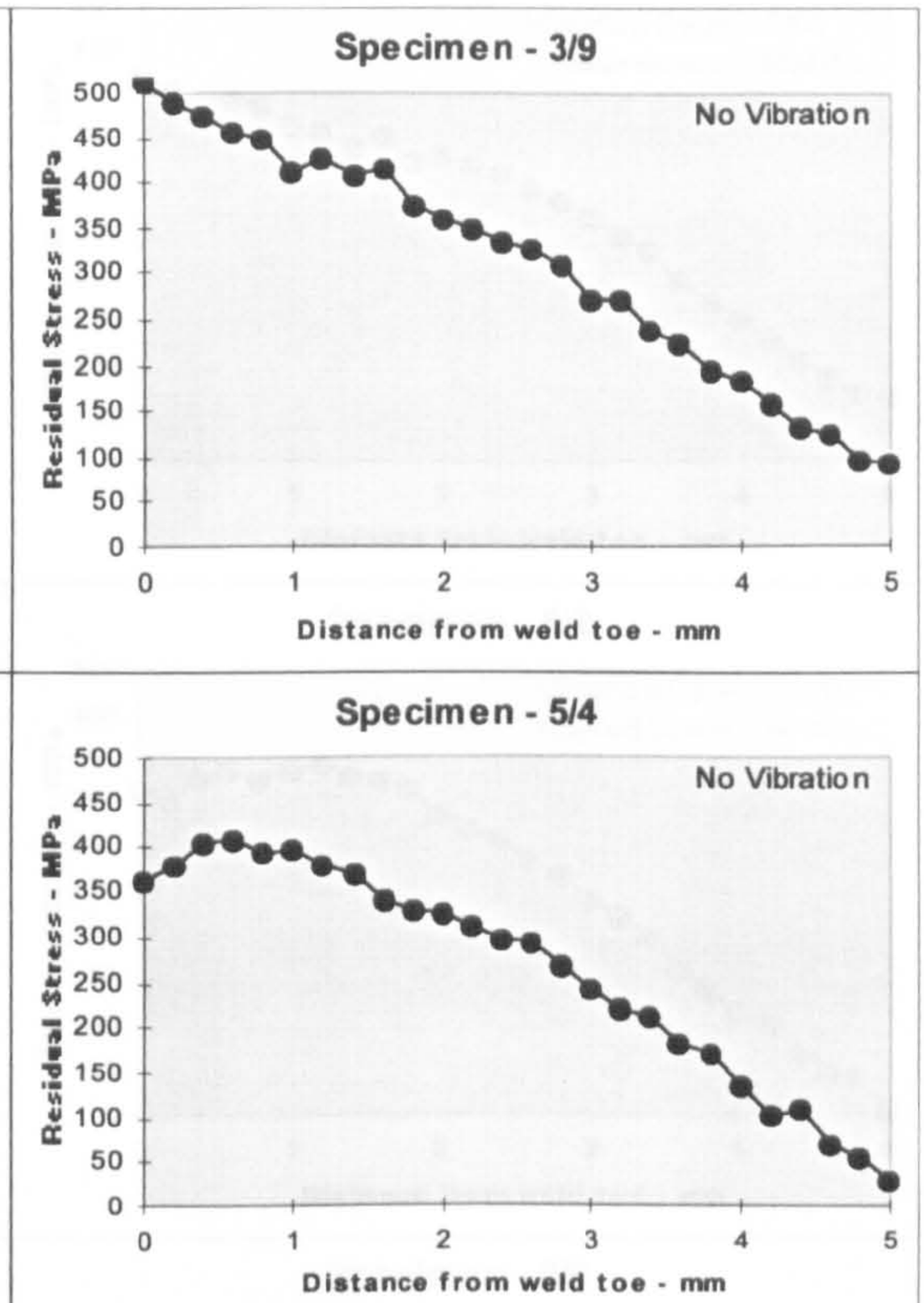

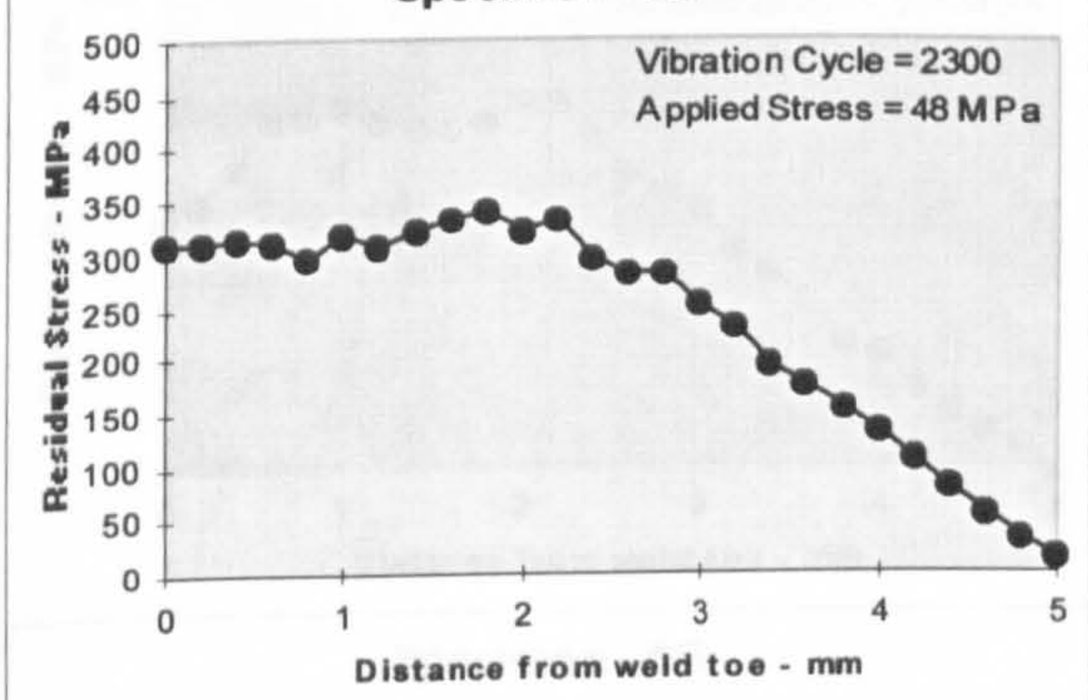

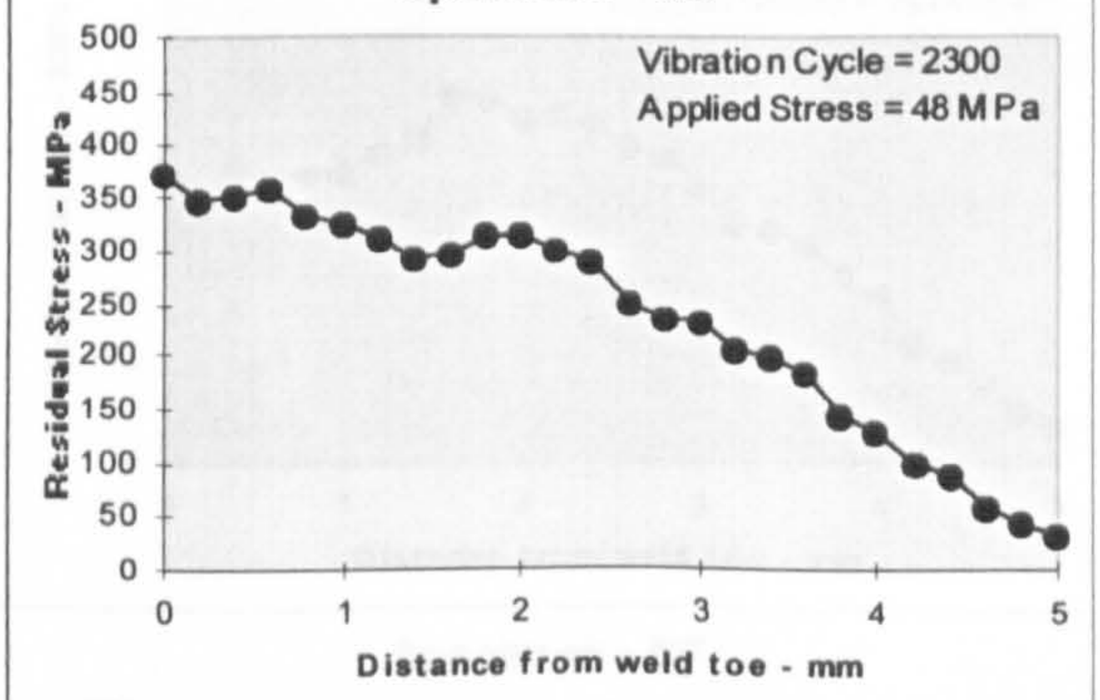

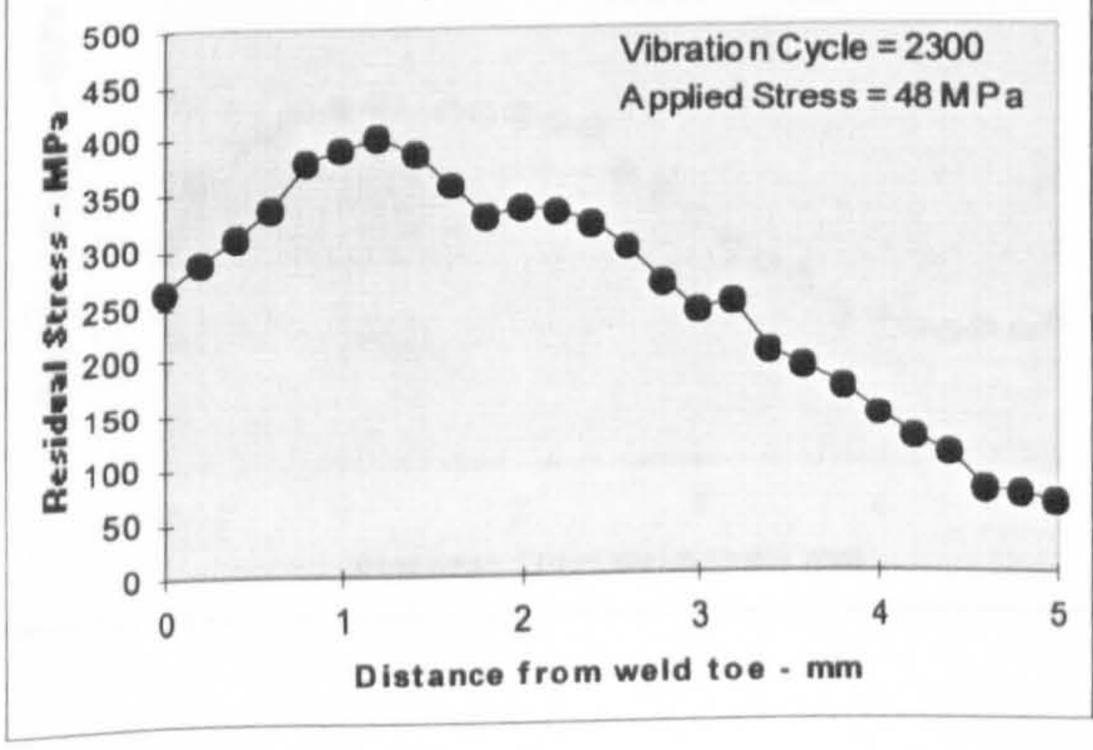

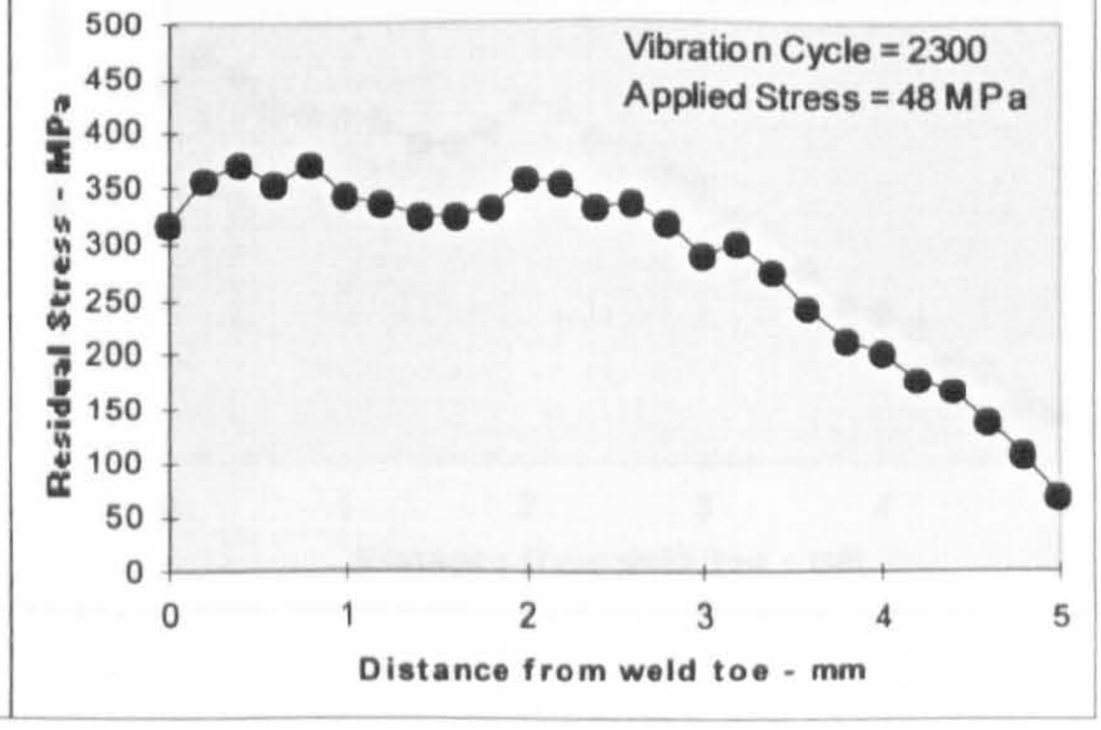

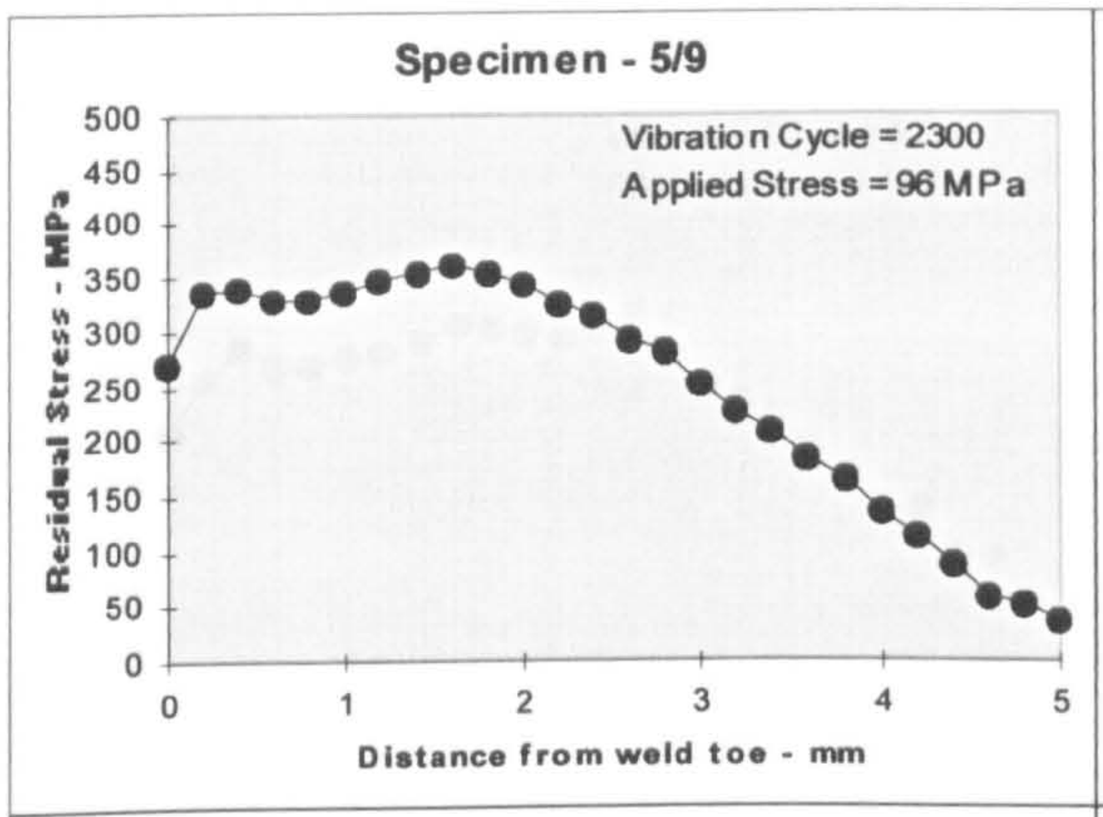
Specimen - 5/9
Vibration Cycle = 2300
Applied Stress = 96 MPa
Residual Stress - MPa
Distance from weld toe - mm

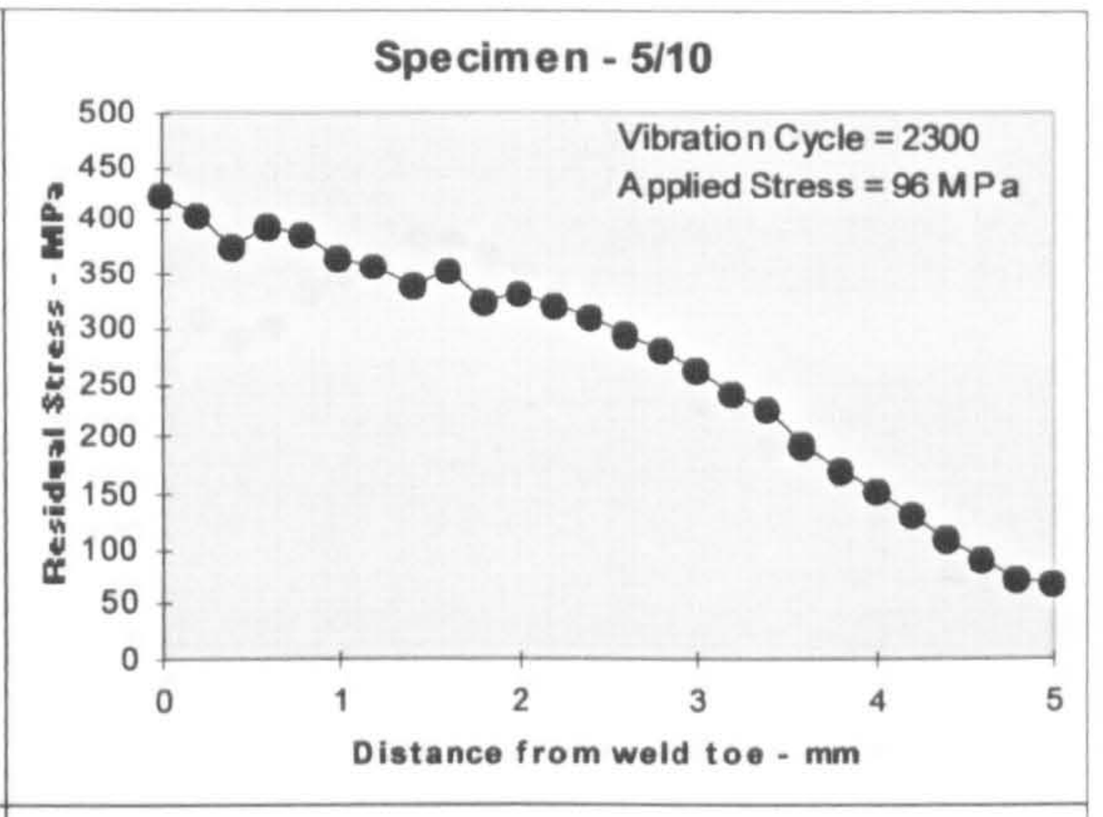
Specimen - 5/10
Vibration Cycle = 2300
Applied Stress = 96 MPa
Residual Stress - MPa
Distance from weld toe - mm

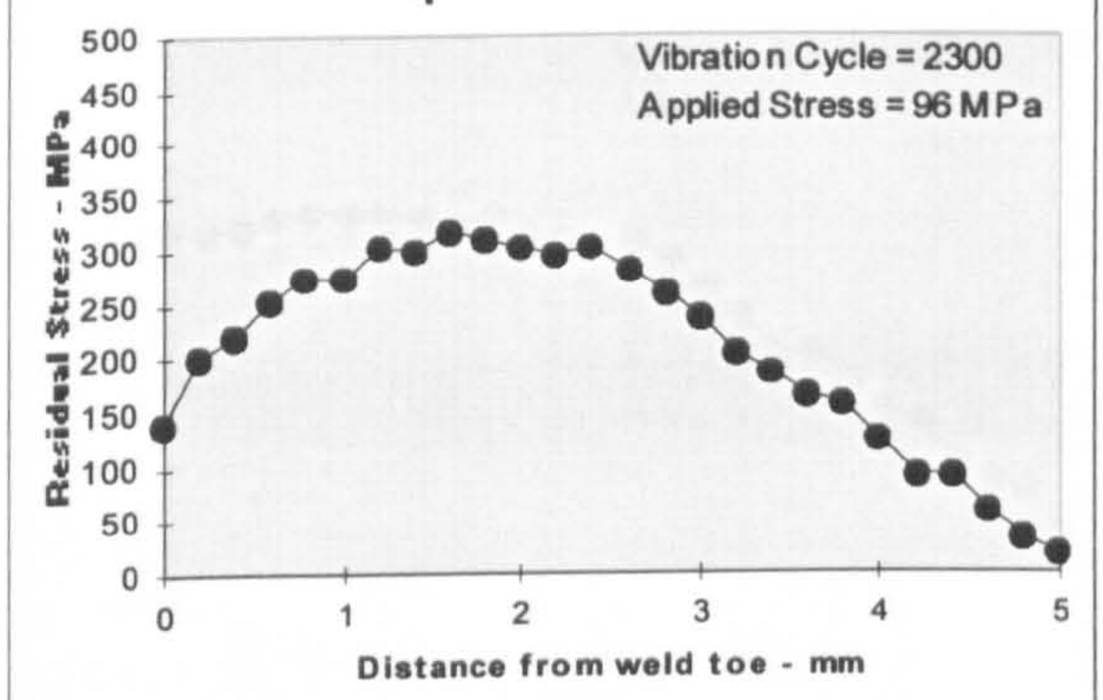
Specimen - 6/1
Vibration Cycle = 2300
Applied Stress = 96 MPa
Residual Stress - MPa
Distance from weld toe - mm

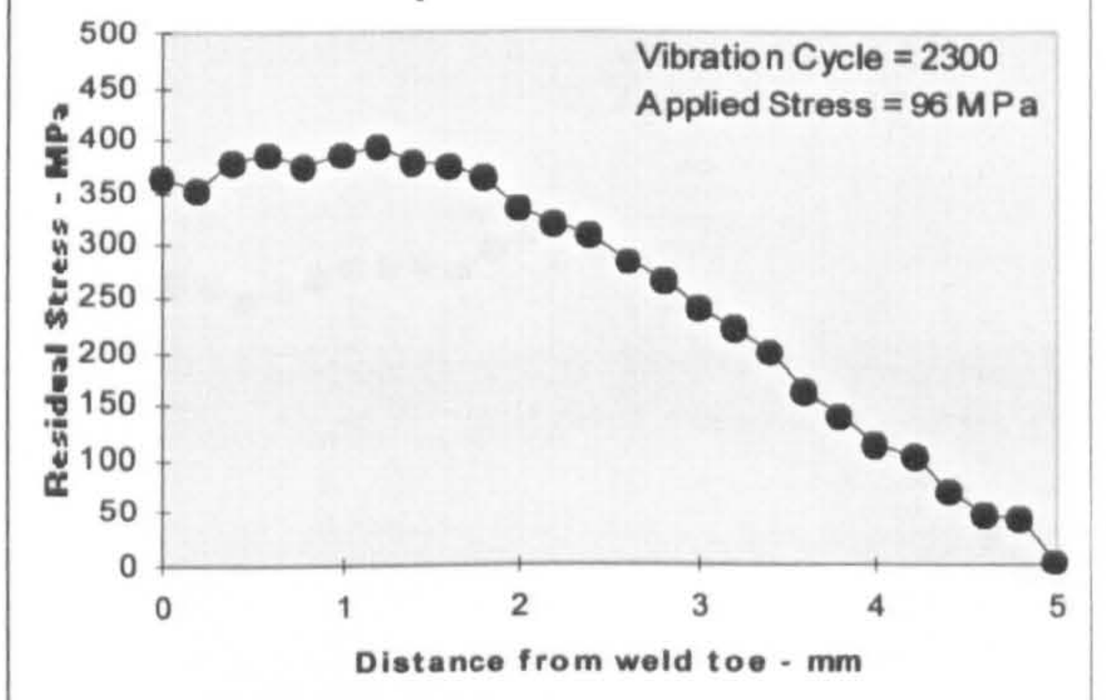
Specimen - 6/2
Vibration Cycle = 2300
Applied Stress = 96 MPa
Residual Stress - MPa
Distance from weld toe - mm

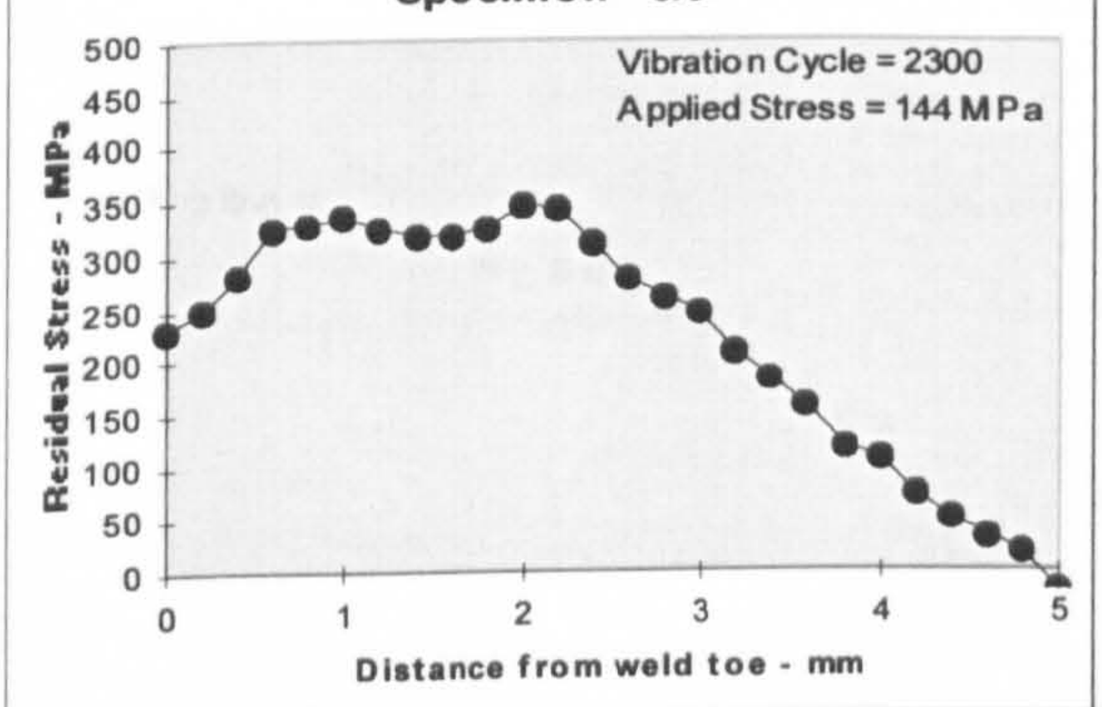
Specimen - 6/3
Vibration Cycle = 2300
Applied Stress = 144 MPa
Residual Stress - MPa
Distance from weld toe - mm

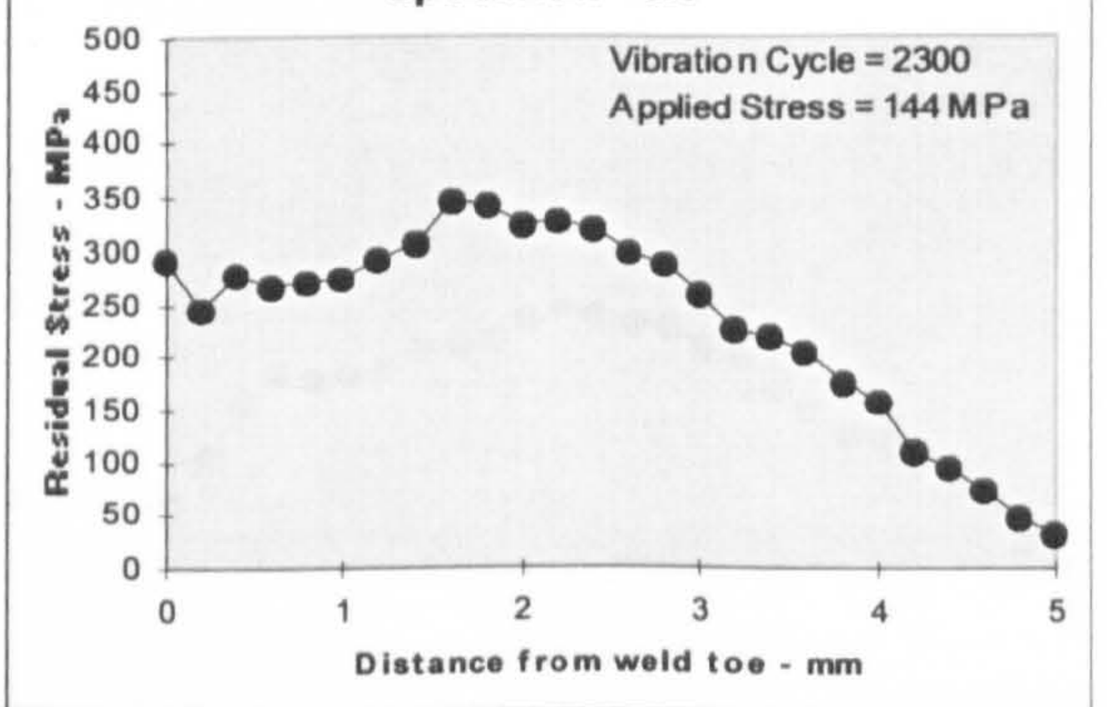
Specimen - 6/5
Vibration Cycle = 2300
Applied Stress = 144 MPa
Residual Stress - MPa
Distance from weld toe - mm

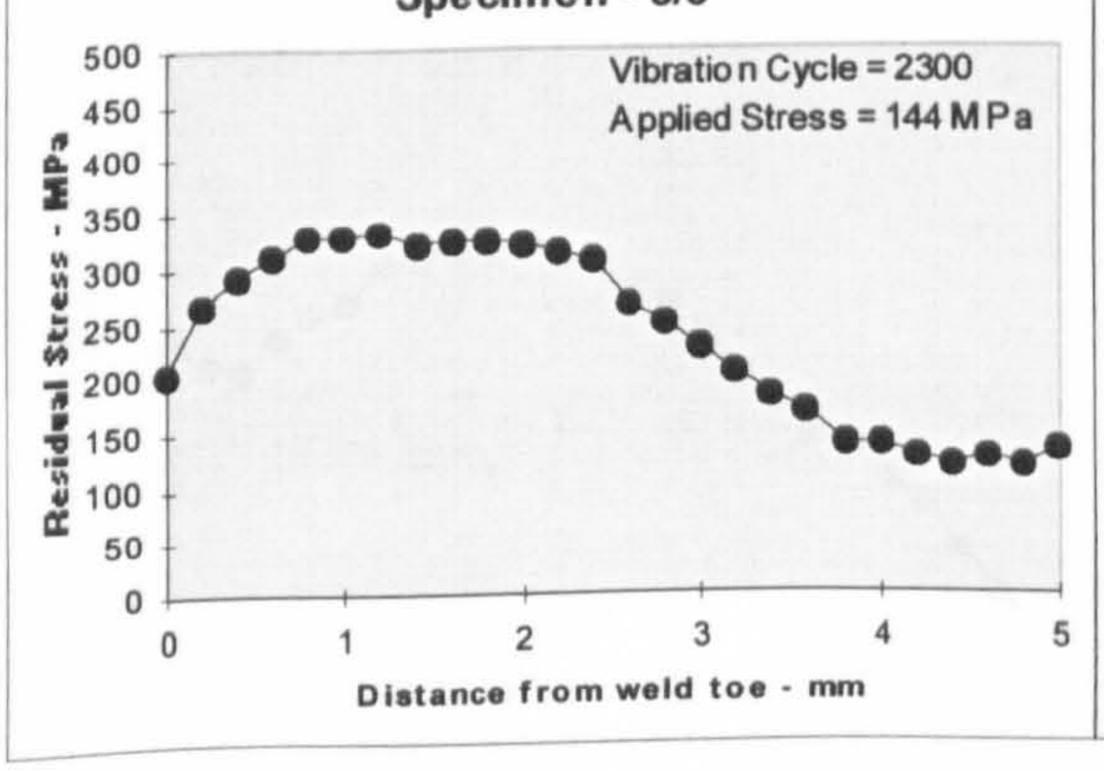
Specimen - 6/6
Vibration Cycle = 2300
Applied Stress = 144 MPa
Residual Stress - MPa
Distance from weld toe - mm

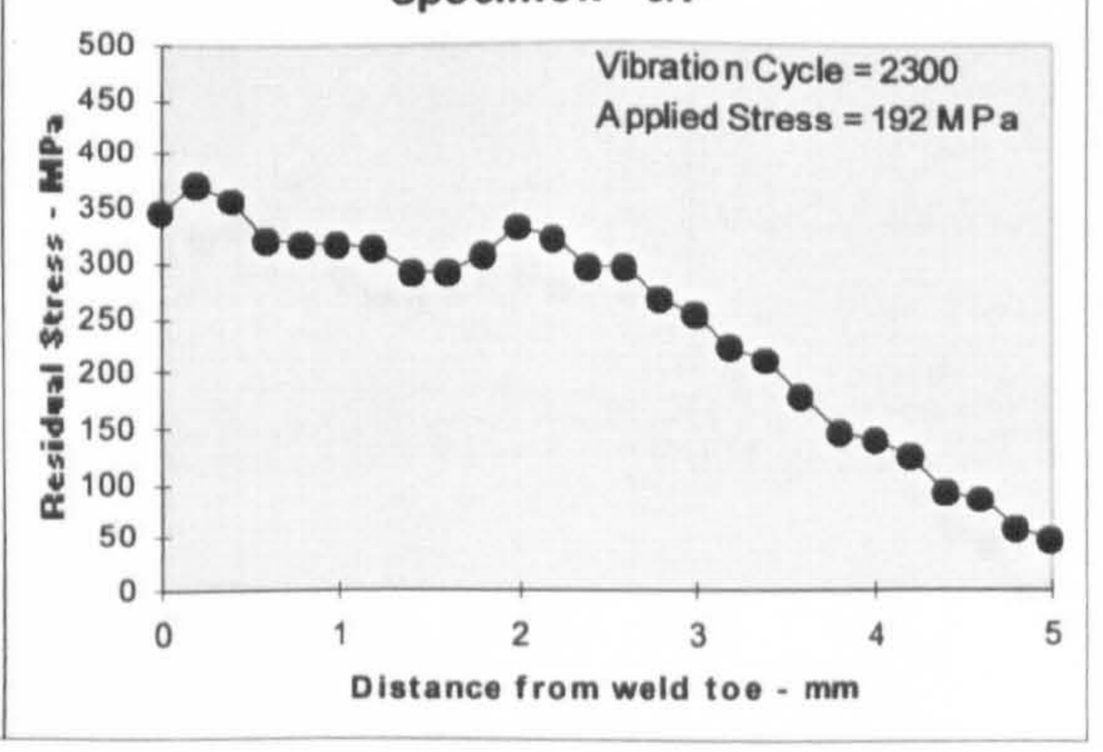
Specimen - 6/7
Vibration Cycle = 2300
Applied Stress = 192 MPa
Residual Stress - MPa
Distance from weld toe - mm

Specimen - 6/8
Vibration Cycle = 2300
Applied Stress = 192 MPa
Residual Stress - MPa
Distance from weld toe - mm
Specimen - 6/9
Vibration Cycle = 2300
Applied Stress = 192 MPa
Residual Stress - MPa
Distance from weld toe - mm
Specimen - 7/1
Vibration Cycle = 2300
Applied Stress = 192 MPa
Residual Stress - MPa
Distance from weld toe - mm
Specimen - 7/2
Vibration Cycle = 2300
Applied Stress = 240 MPa
Residual Stress - MPa
Distance from weld toe - mm
Specimen - 7/3
Vibration Cycle = 2300
Applied Stress = 240 MPa
Residual Stress - MPa
Distance from weld toe - mm
Specimen - 7/4
Vibration Cycle = 2300
Applied Stress = 240 MPa
Residual Stress - MPa
Distance from weld toe - mm
Specimen - 7/5
Vibration Cycle = 2300
Applied Stress = 240 MPa
Residual Stress - MPa
Distance from weld toe - mm
Specimen - 7/6
Vibration Cycle = 2300
Applied Stress = 288 MPa
Residual Stress - MPa
Distance from weld toe - mm

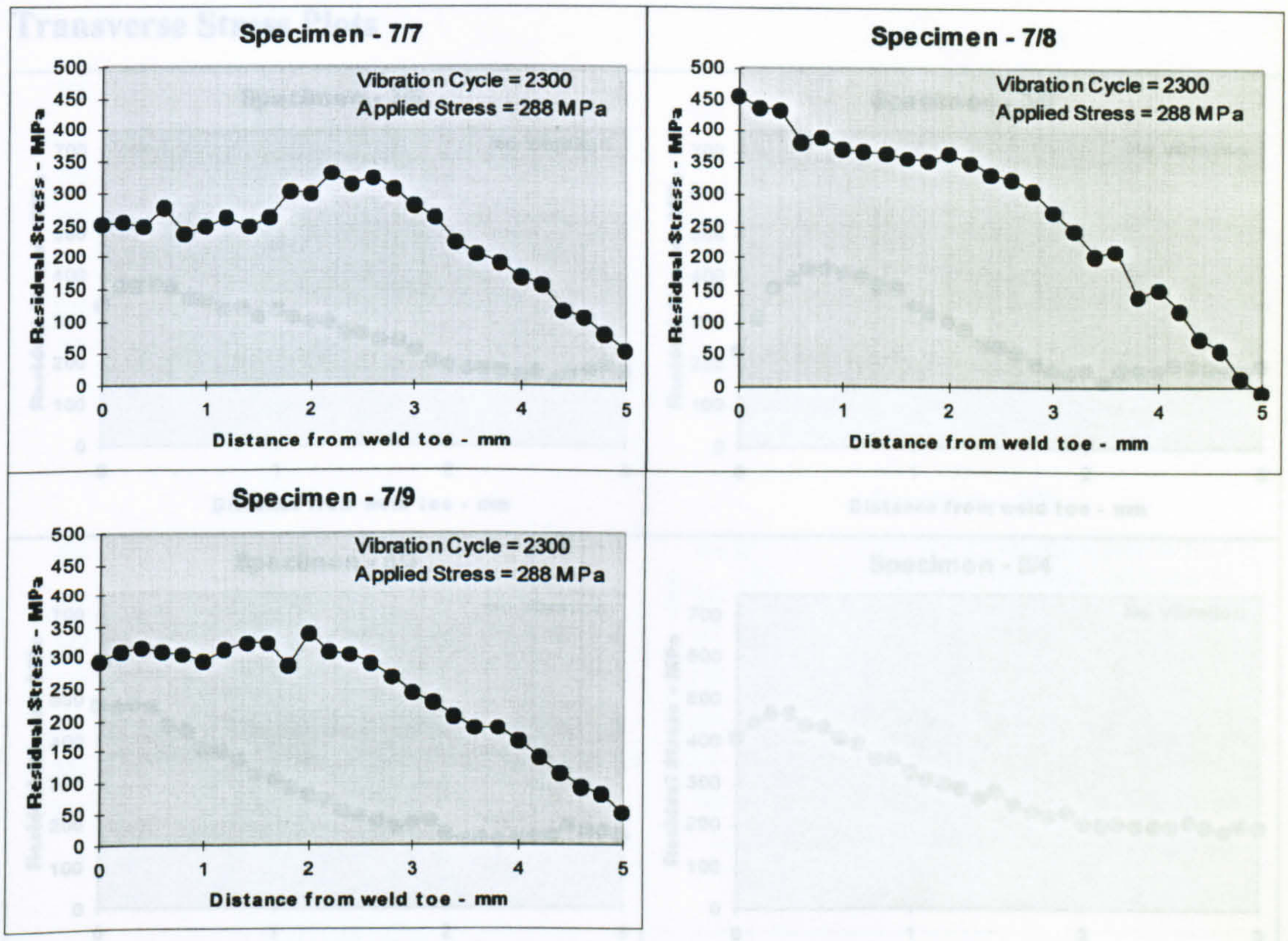

Figures 5.104 to 5.130 - Longitudinal stress plots - specimens 3/8 to 7/9

Summary Plot

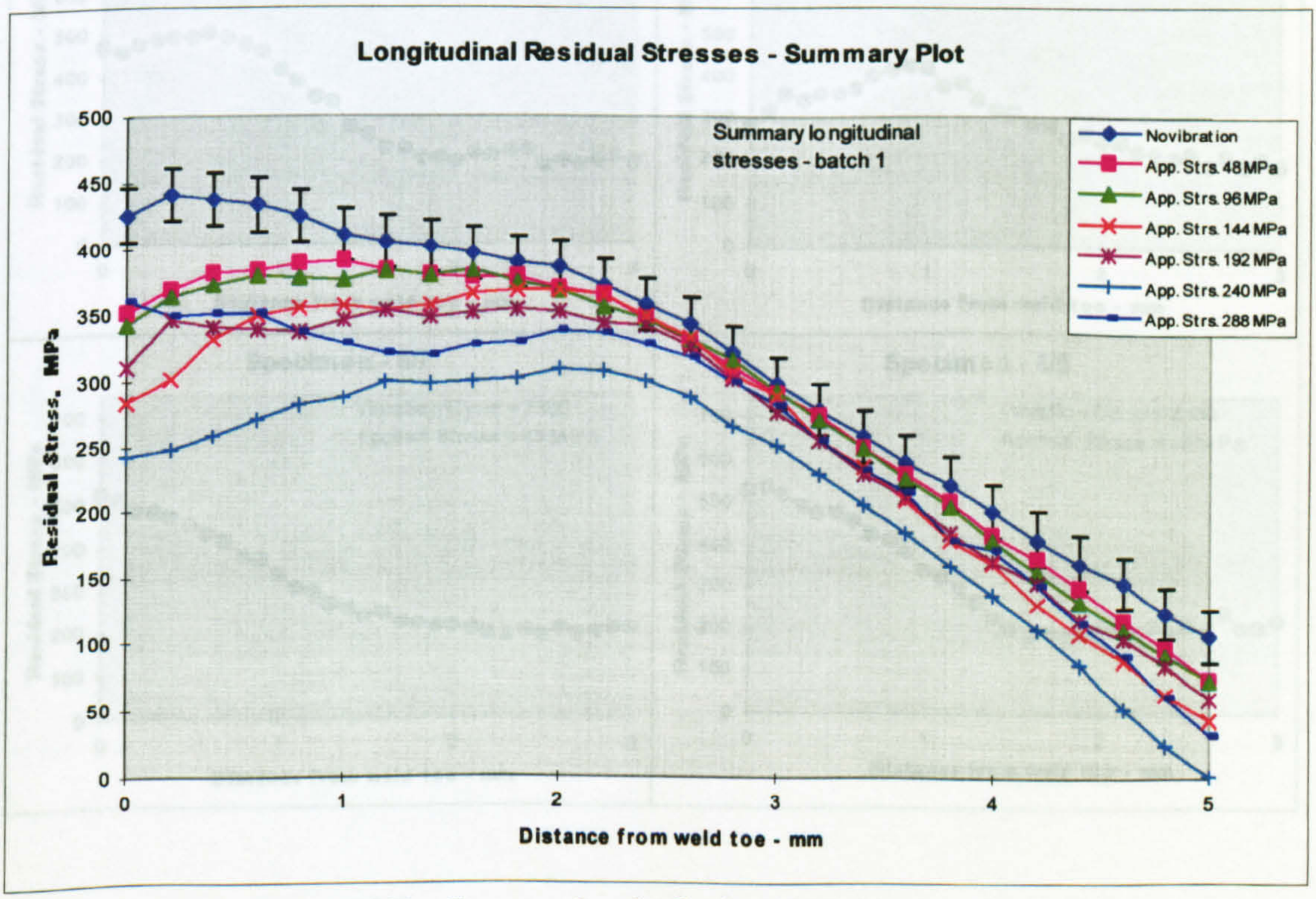

Figure 5.131 – Summary longitudinal residual stresses – batch 1

Transverse Stress Plots

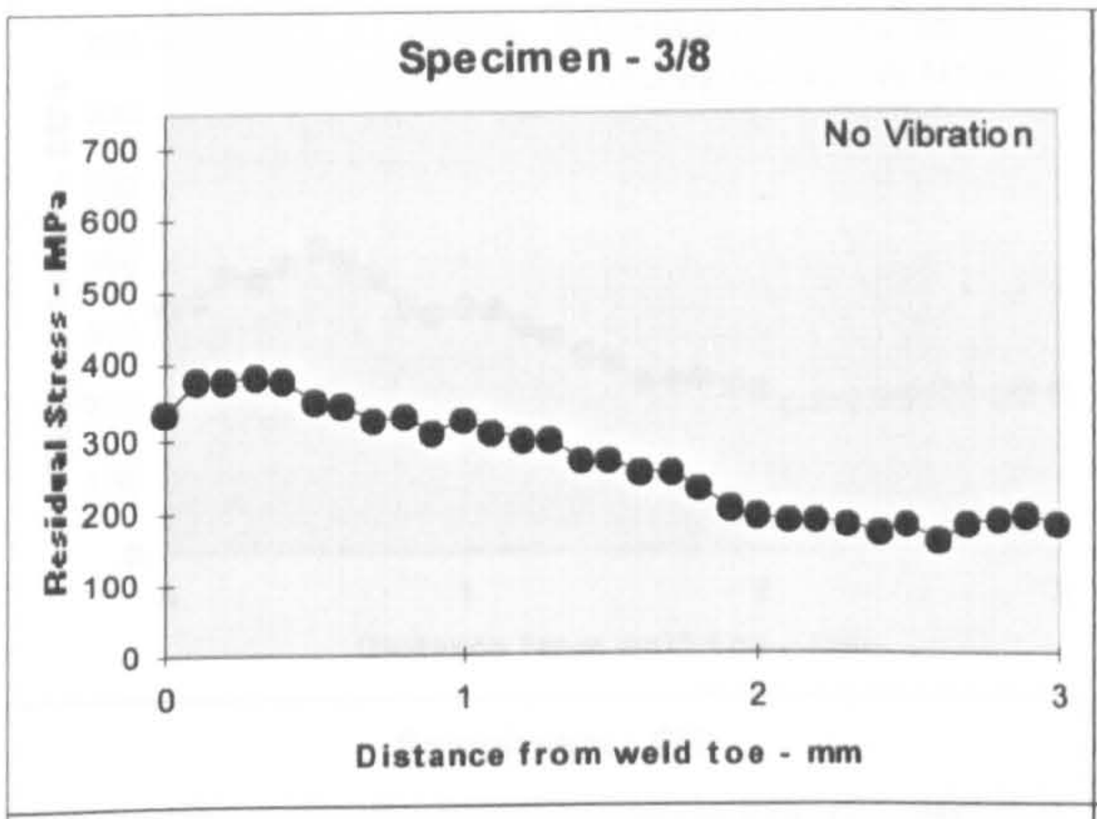

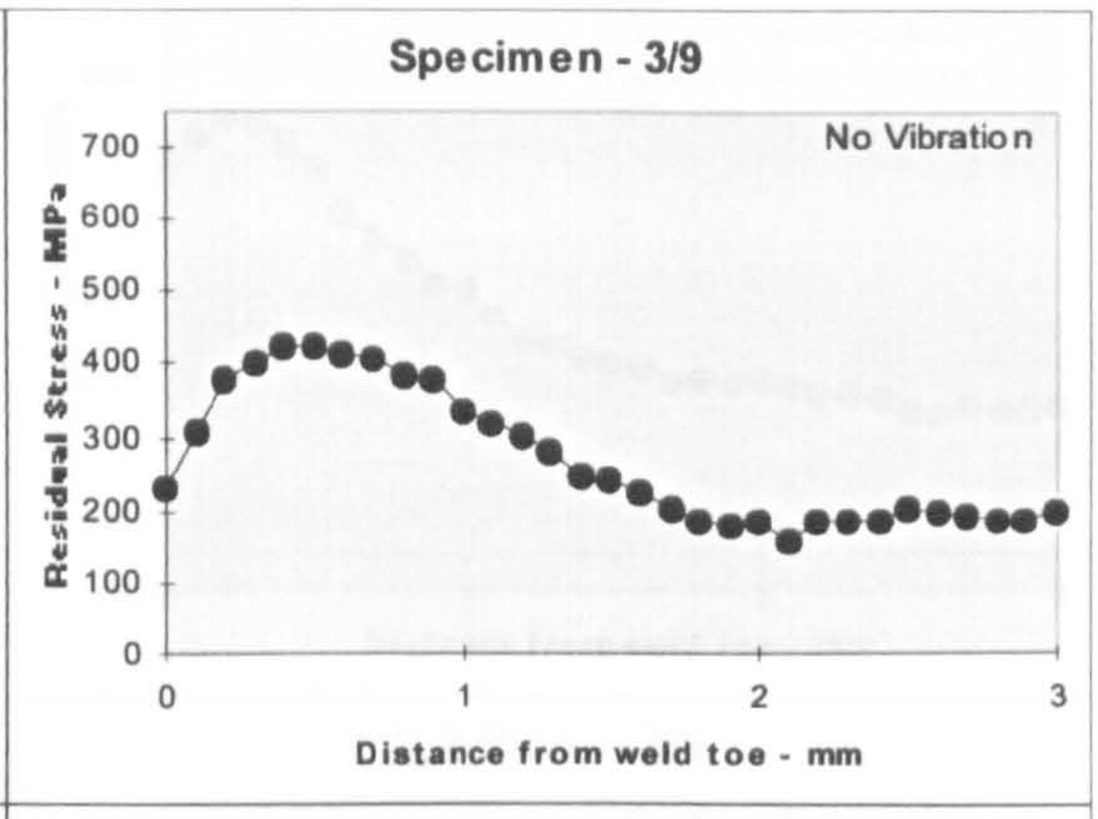

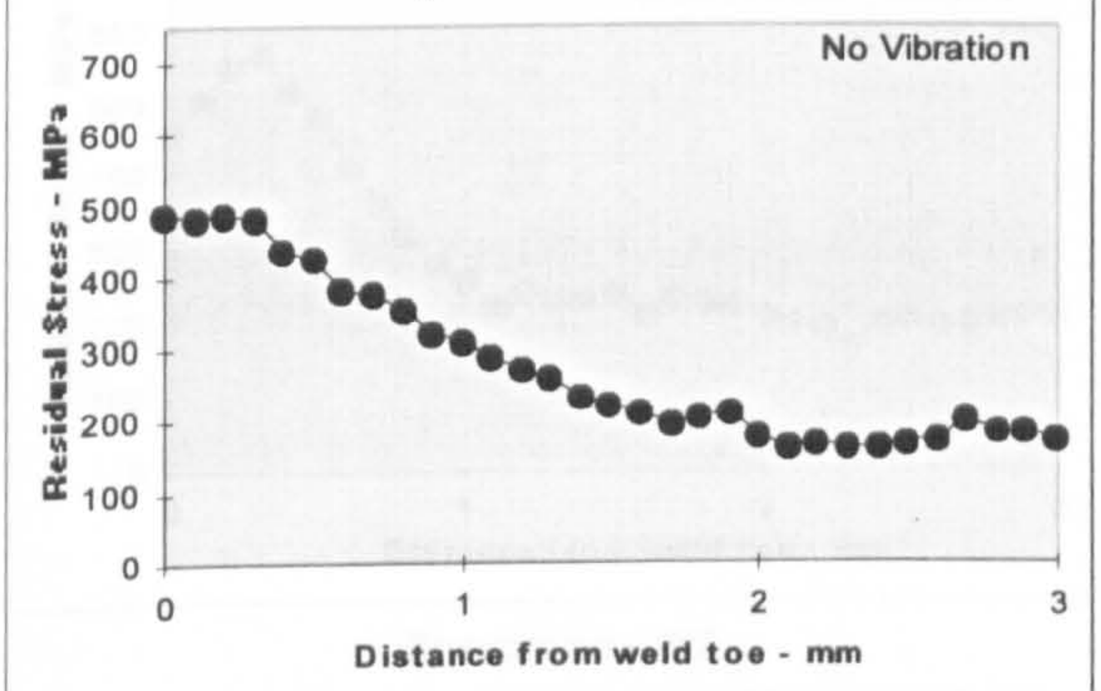

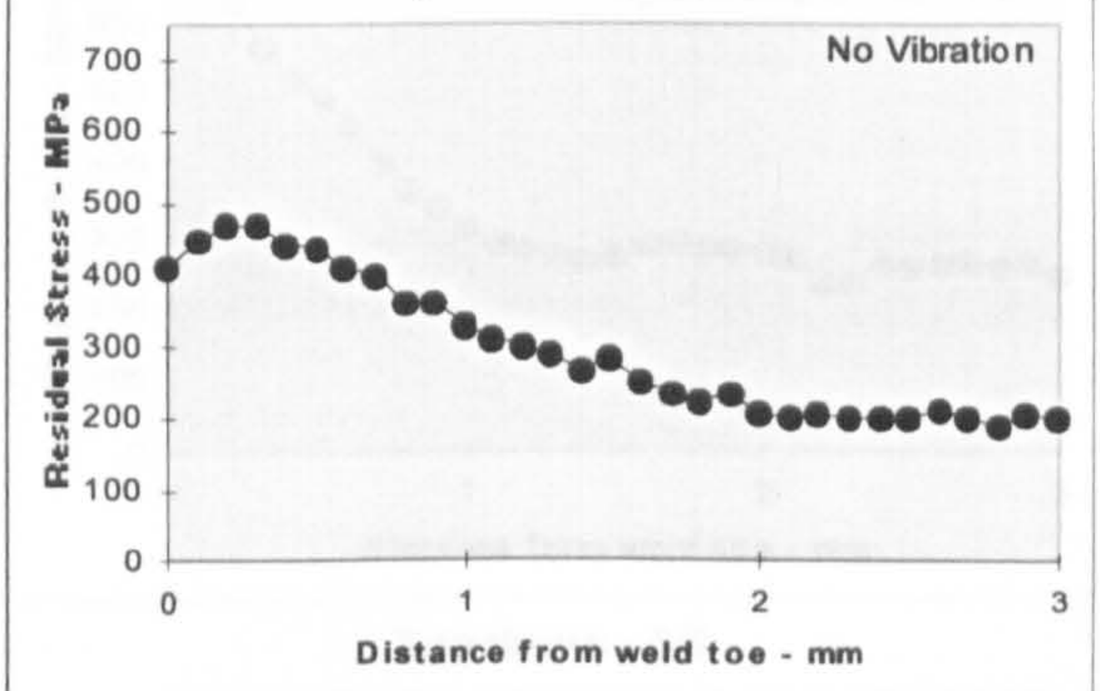

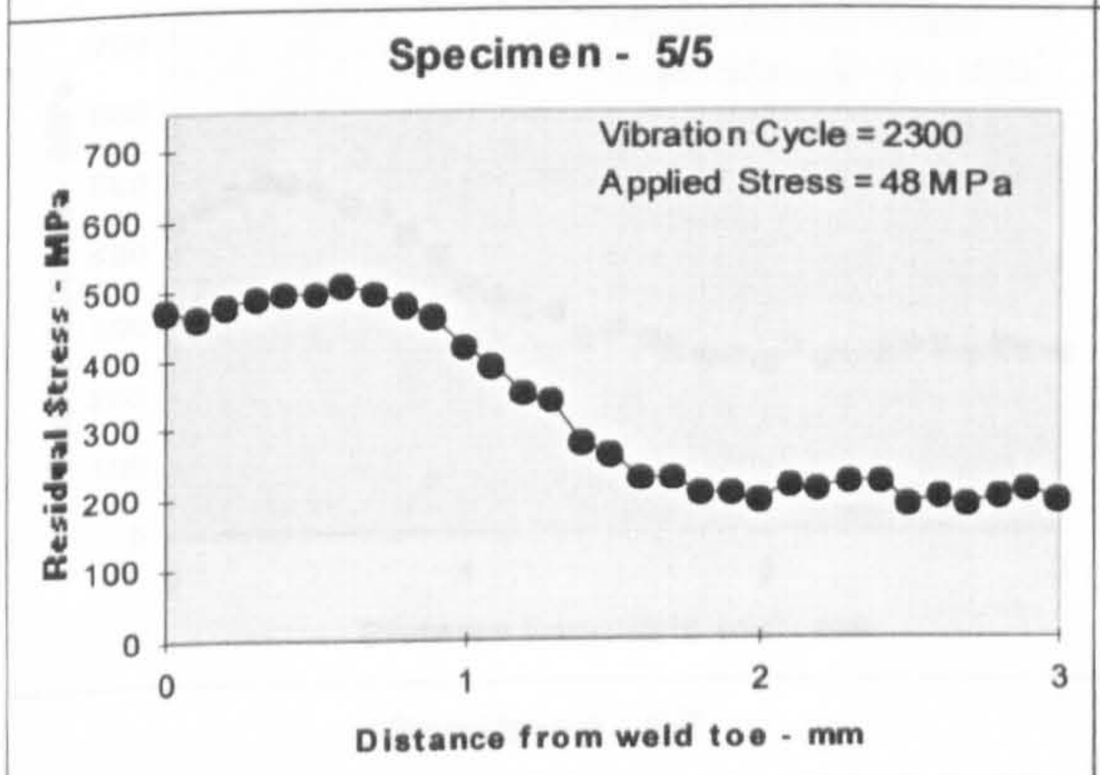

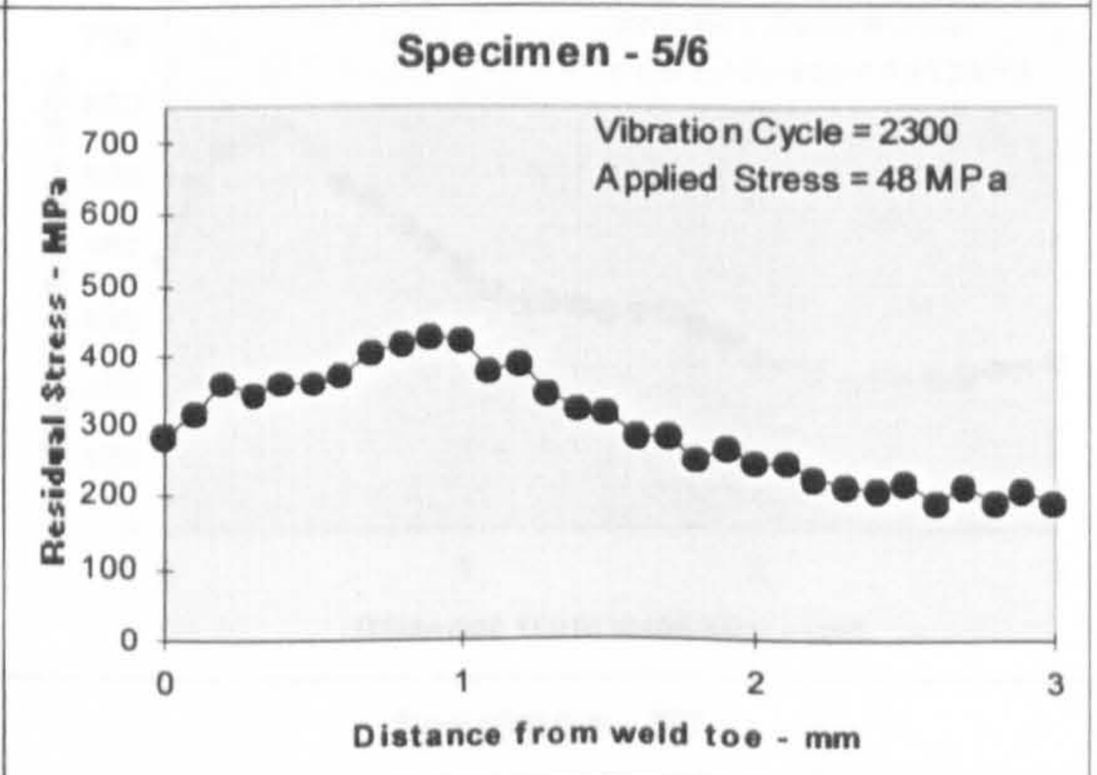

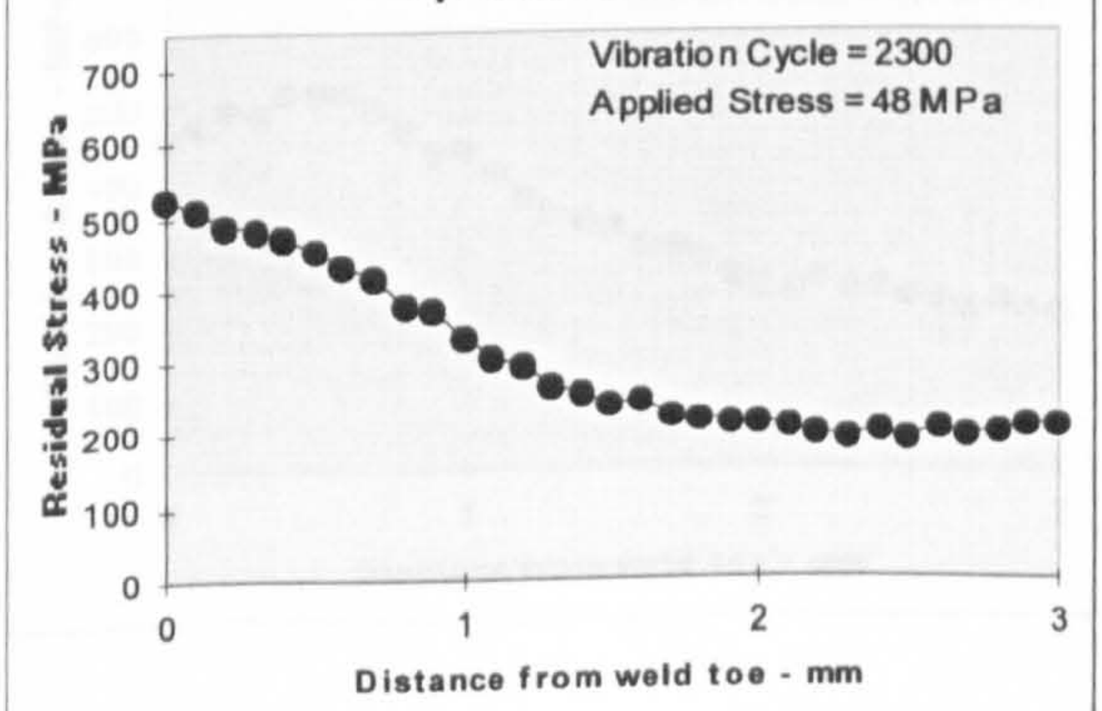

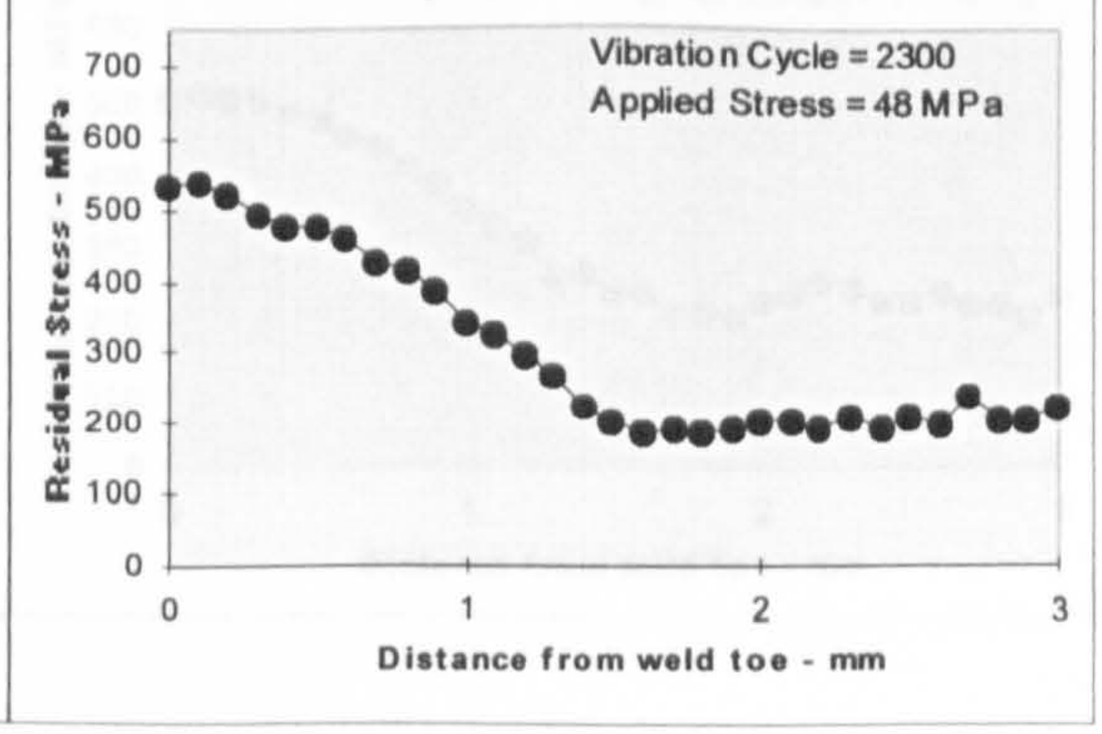

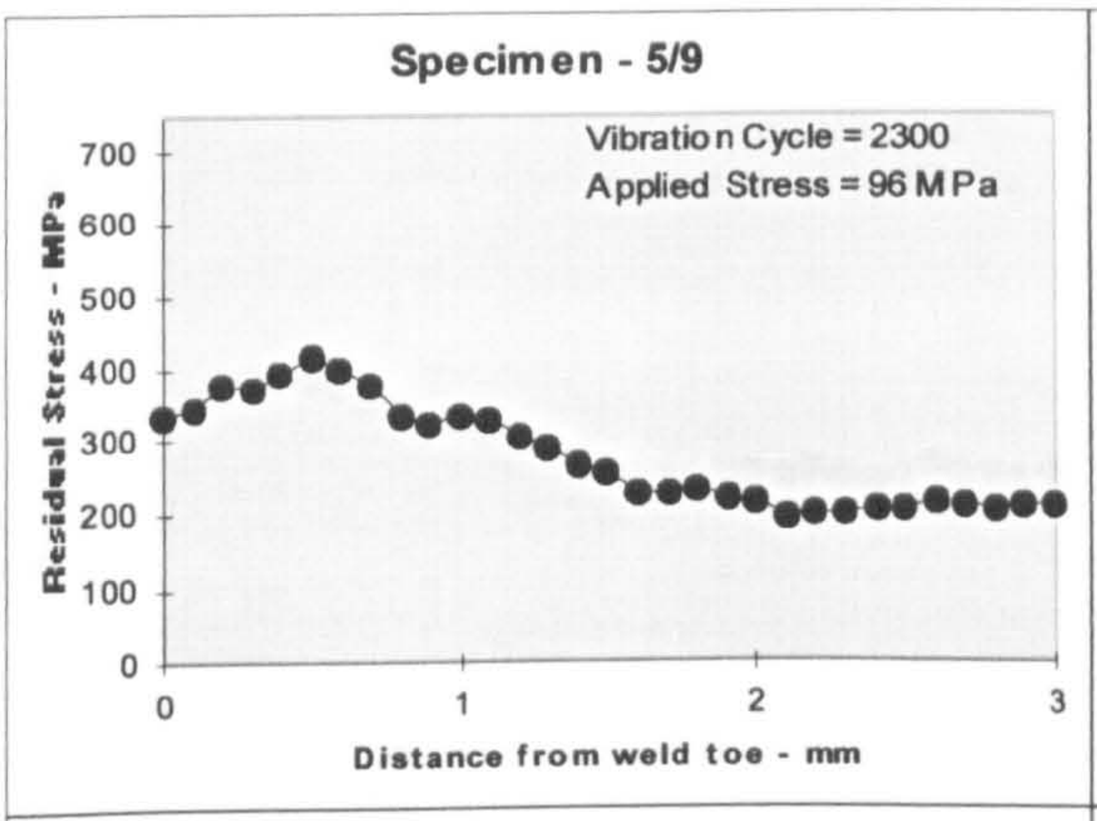
Specimen - 5/9
Vibration Cycle = 2300
Applied Stress = 96 MPa
Residual Stress - MPa
Distance from weld toe - mm

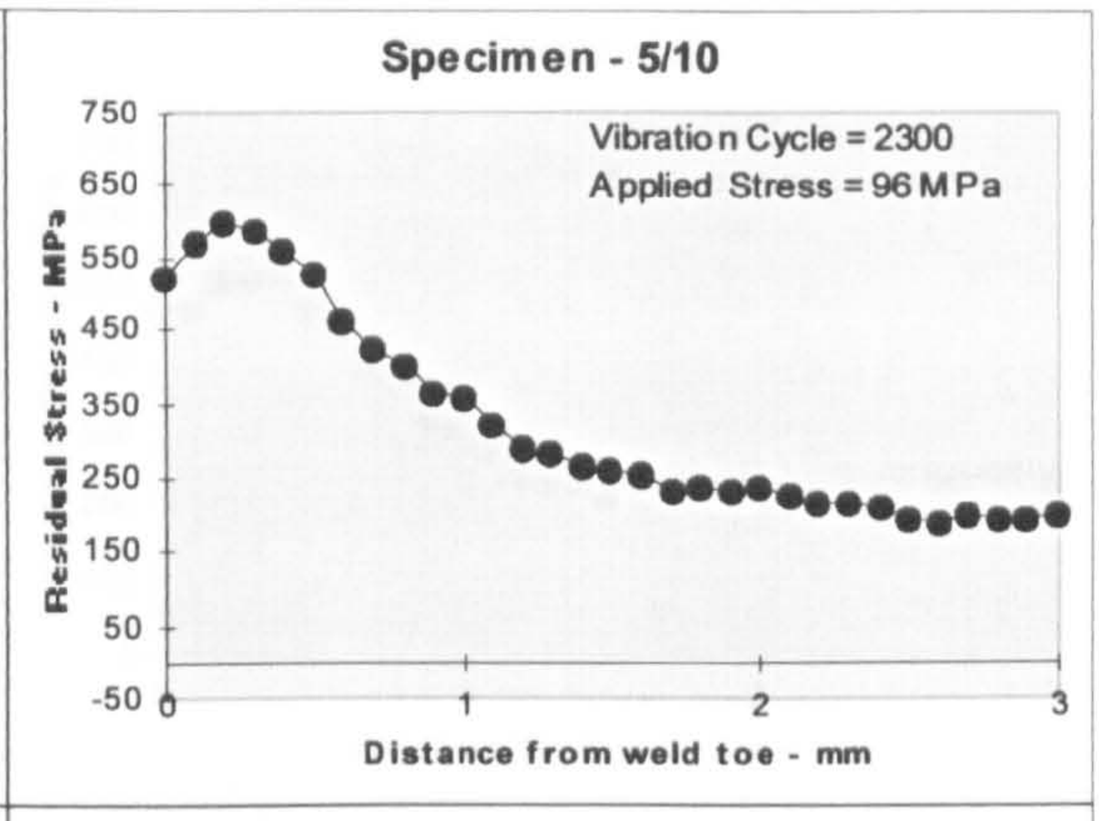
Specimen - 5/10
Vibration Cycle = 2300
Applied Stress = 96 MPa
Residual Stress - MPa
Distance from weld toe - mm

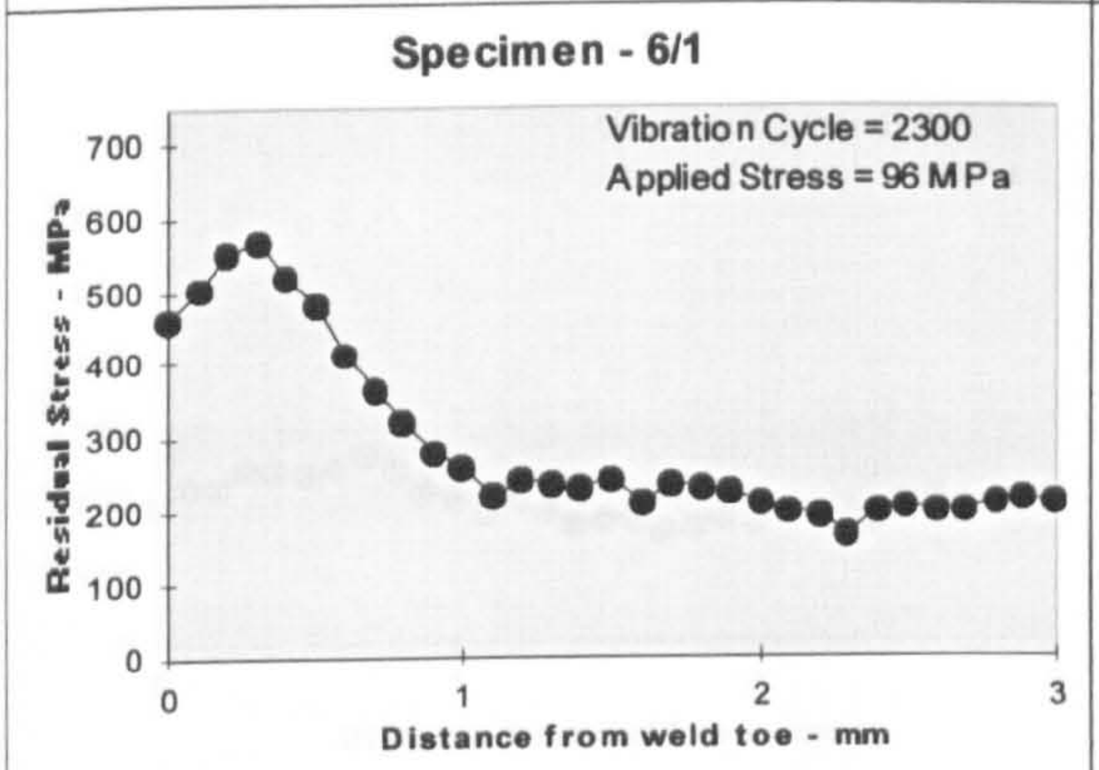
Specimen - 6/1
Vibration Cycle = 2300
Applied Stress = 96 MPa
Residual Stress - MPa
Distance from weld toe - mm

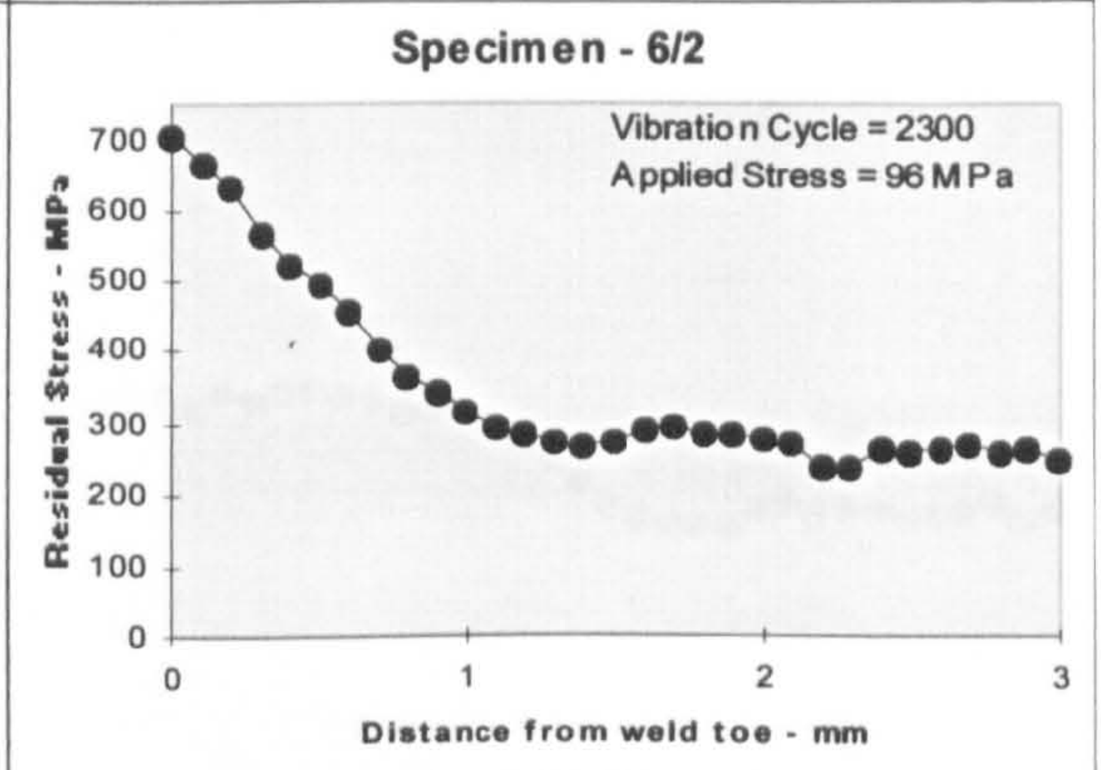
Specimen - 6/2
Vibration Cycle = 2300
Applied Stress = 96 MPa
Residual Stress - MPa
Distance from weld toe - mm

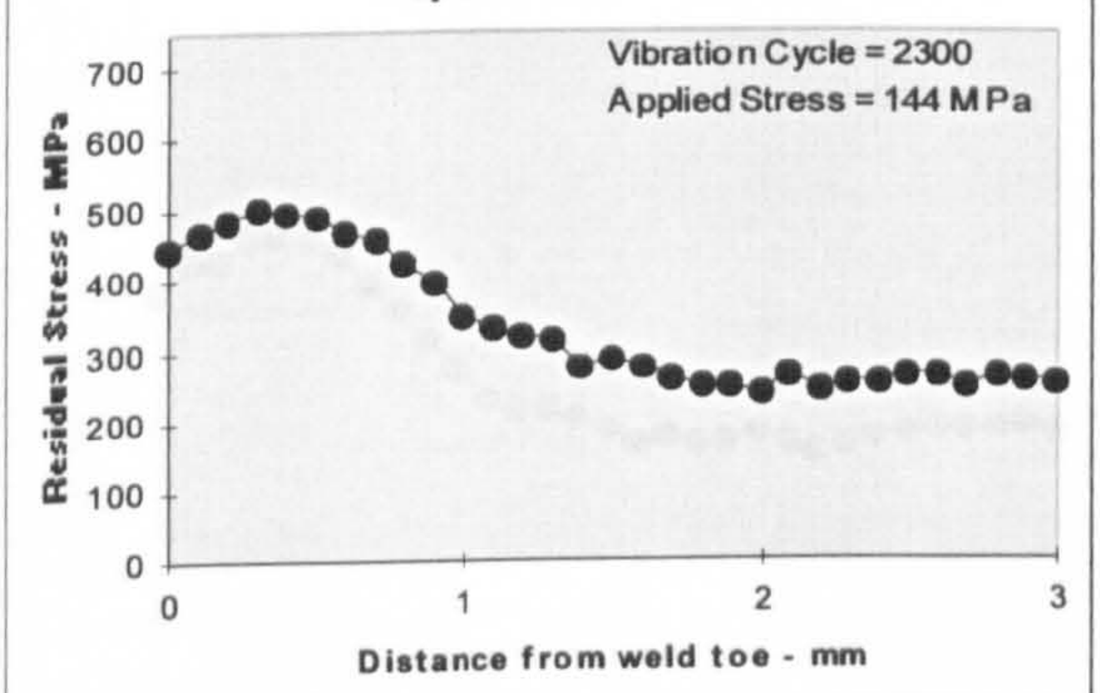
Specimen - 6/3
Vibration Cycle = 2300
Applied Stress = 144 MPa
Residual Stress - MPa
Distance from weld toe - mm

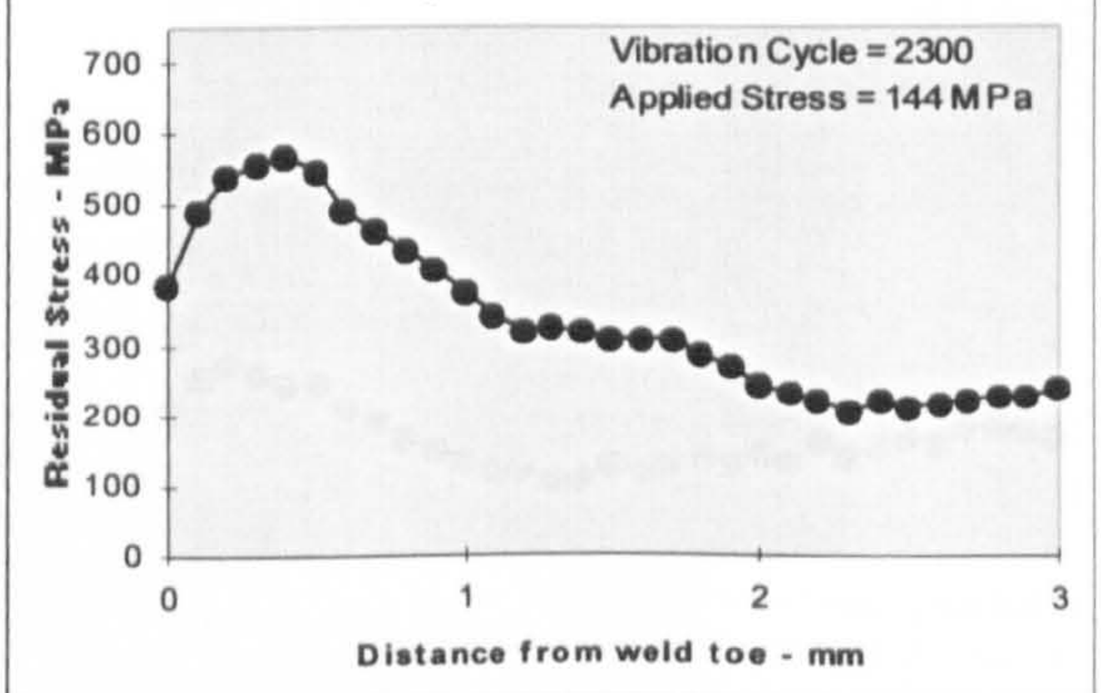
Specimen - 6/5
Vibration Cycle = 2300
Applied Stress = 144 MPa
Residual Stress - MPa
Distance from weld toe - mm

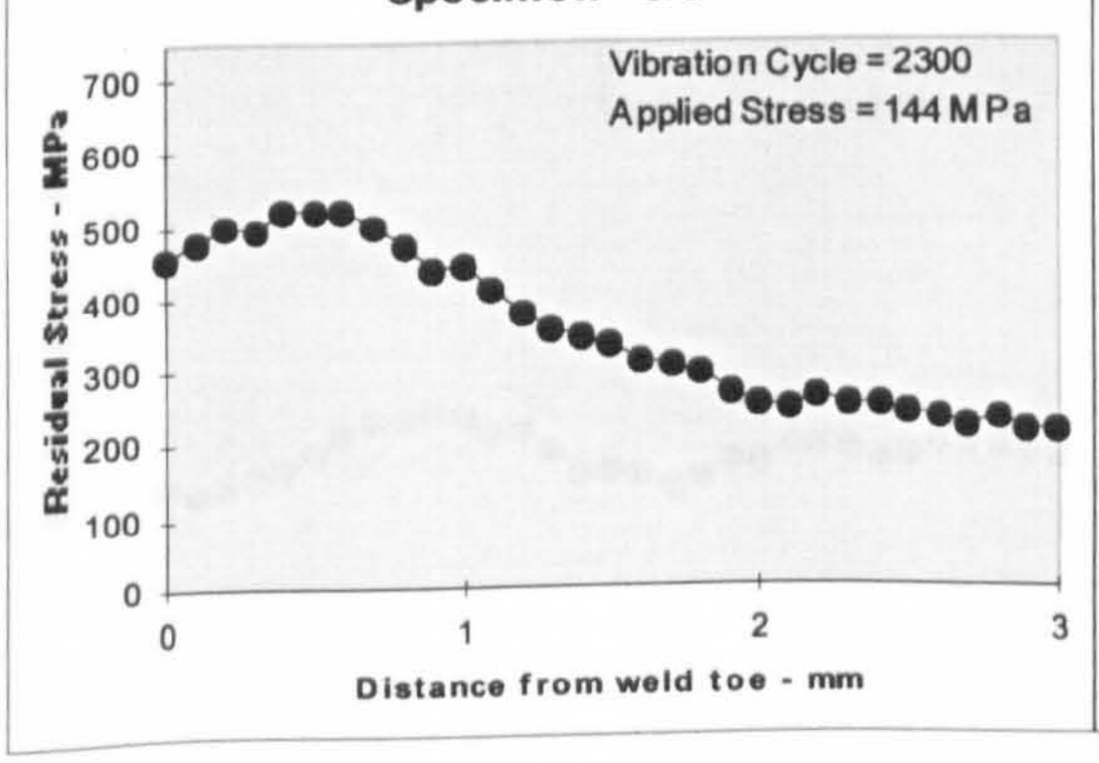
Specimen - 6/6
Vibration Cycle = 2300
Applied Stress = 144 MPa
Residual Stress - MPa
Distance from weld toe - mm

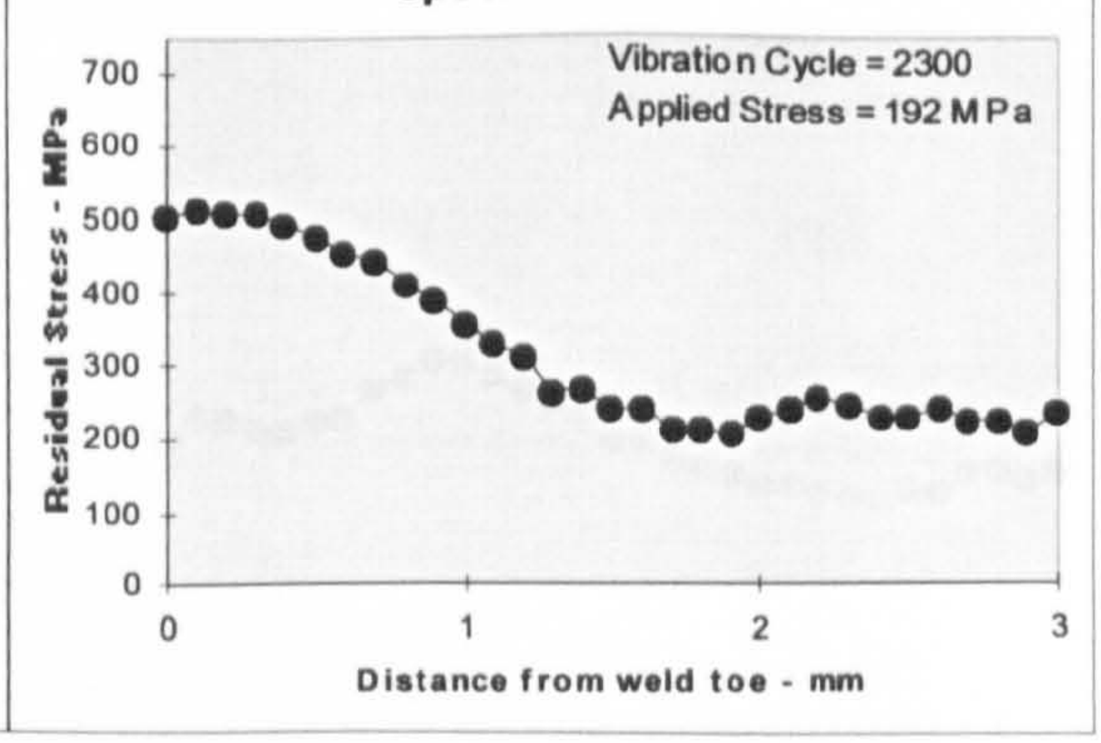
Specimen - 6/7
Vibration Cycle = 2300
Applied Stress = 192 MPa
Residual Stress - MPa
Distance from weld toe - mm

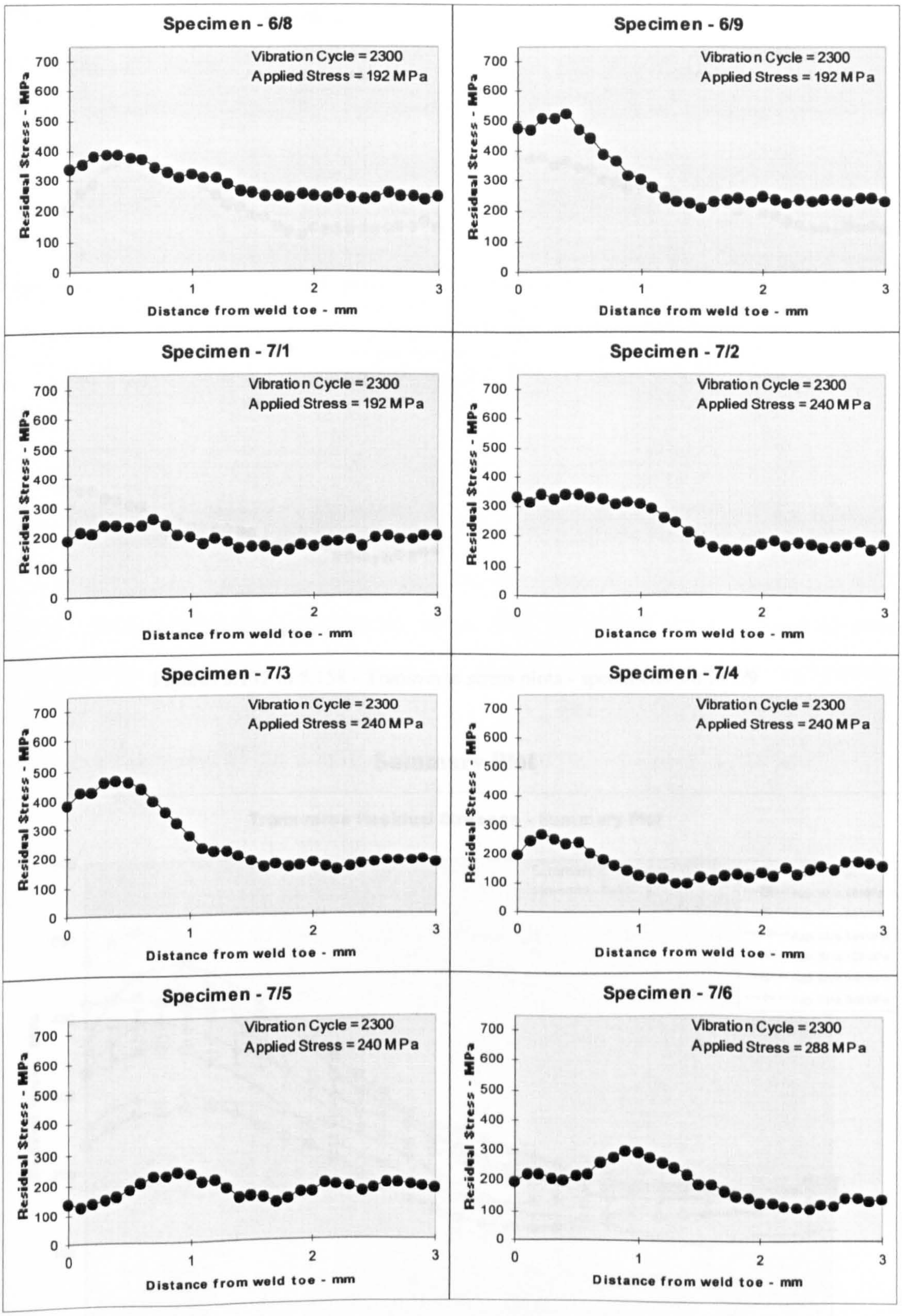
Specimen - 6/8
Vibration Cycle = 2300
Applied Stress = 192 MPa
Residual Stress - MPa
Distance from weld toe - mm
Specimen - 6/9
Vibration Cycle = 2300
Applied Stress = 192 MPa
Residual Stress - MPa
Distance from weld toe - mm
Specimen - 7/1
Vibration Cycle = 2300
Applied Stress = 192 MPa
Residual Stress - MPa
Distance from weld toe - mm
Specimen - 7/2
Vibration Cycle = 2300
Applied Stress = 240 MPa
Residual Stress - MPa
Distance from weld toe - mm
Specimen - 7/3
Vibration Cycle = 2300
Applied Stress = 240 MPa
Residual Stress - MPa
Distance from weld toe - mm
Specimen - 7/4
Vibration Cycle = 2300
Applied Stress = 240 MPa
Residual Stress - MPa
Distance from weld toe - mm
Specimen - 7/5
Vibration Cycle = 2300
Applied Stress = 240 MPa
Residual Stress - MPa
Distance from weld toe - mm
Specimen - 7/6
Vibration Cycle = 2300
Applied Stress = 288 MPa
Residual Stress - MPa
Distance from weld toe - mm

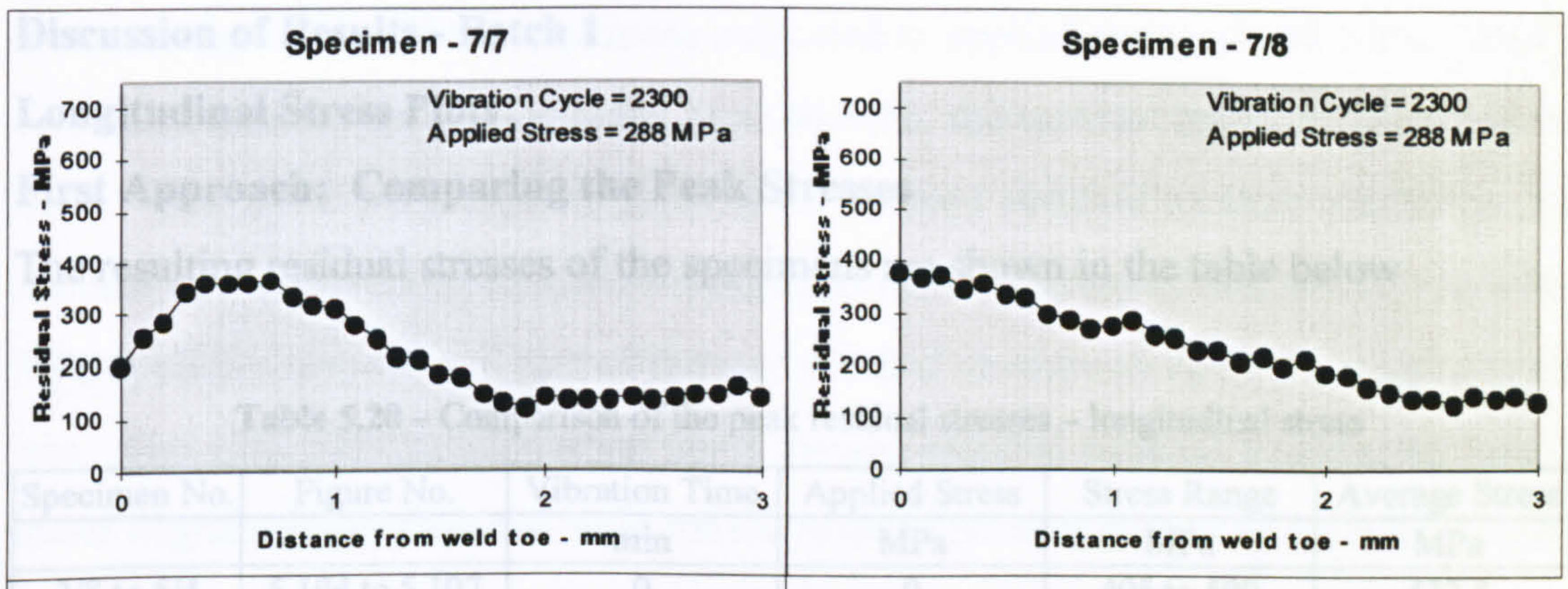

Figures 5.132 to 5.158 - Transverse stress plots - specimens 3/8 to 7/9

Summary Plot

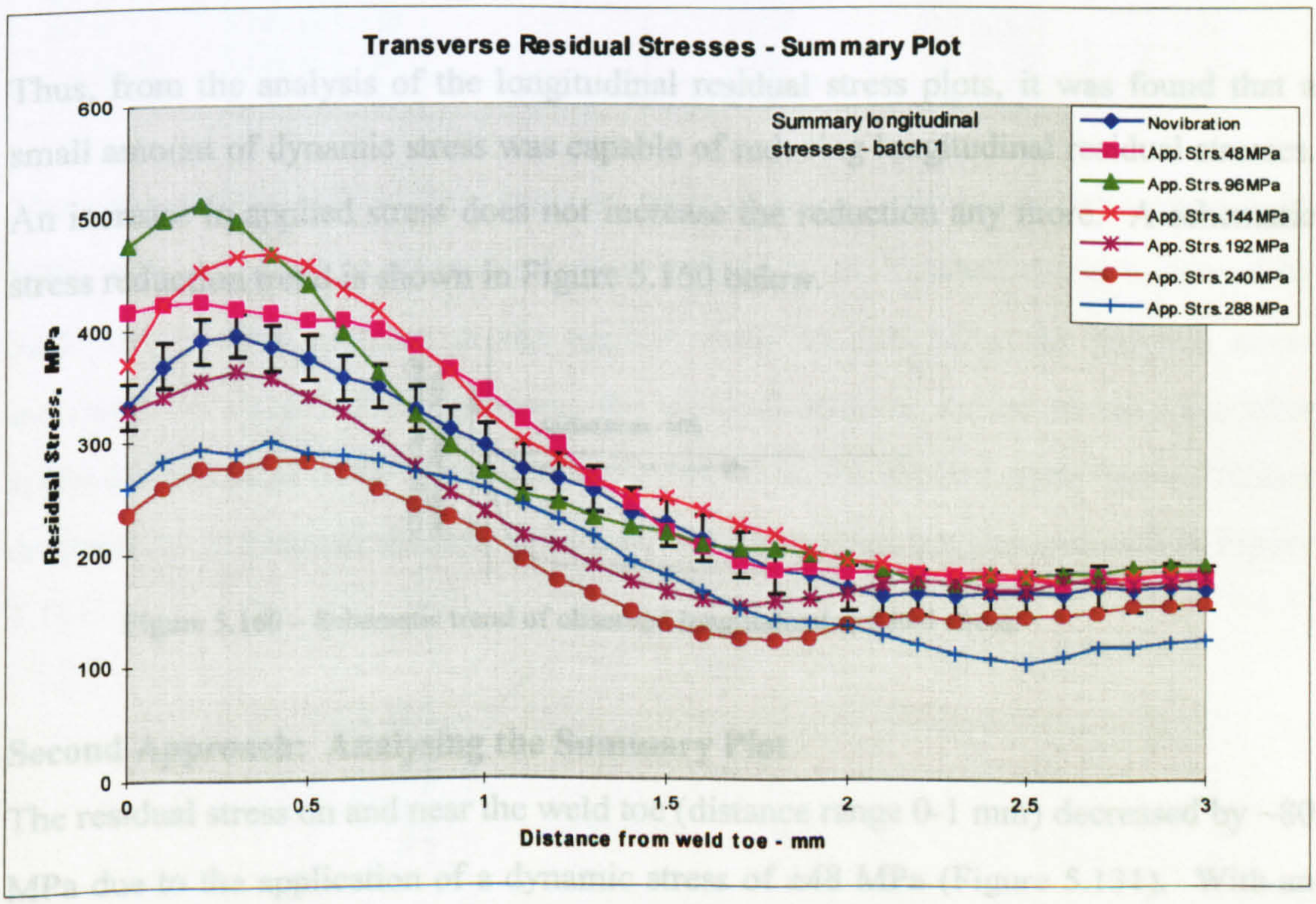

Figure 5.159 – Summary transverse residual stresses – batch 1

Discussion of Results - Batch 1

Longitudinal Stress Plots

First Approach: Comparing the Peak Stresses

The resulting residual stresses of the specimens are shown in the table below

Table 5.20 – Comparison of the peak residual stresses – longitudinal stress

Specimen No.	Figure No.	Vibration Time	Applied Stress	Stress Range	Average Stress
		min	MPa	MPa	MPa
3/8 to 5/4	5.104 to 5.107	0	0	405 to 500	432.5
5/5 to 5/8	5.108 to 5.111	1.5	±48	335 to 400	368
5/9 to 6/2	5.112 to 5.115	1.5	±96	320 to 425	376.25
6/3 to 6/6	5.116 to 5.118	1.5	±144	330 to 350	343.3
6/7 to 7/1	5.119 to 5.122	1.5	±192	320 to 375	351.25
7/2 to 7/5	5.123 to 5.126	1.5	±240	248 to 365	314.5
7/6 to 7/9	5.127 to 5.130	1.5	±288	330 to 440	367.5

The average longitudinal residual stress of the unvibrated/control specimens was 432.5 MPa. With application of induced stress ±48 MPa, the average residual stress decreased by ~64.5 MPa. In the next five applied stress levels the average residual stresses were 376.25 MPa, 343.3 MPa, 351.25 MPa, 314.25 MPa and 367.5 MPa, they were lower than that of the average residual stress of the unvibrated specimens.

Thus, from the analysis of the longitudinal residual stress plots, it was found that a small amount of dynamic stress was capable of reducing longitudinal residual stresses. An increase in applied stress does not increase the reduction any more. A schematic stress reduction trend is shown in Figure 5.160 below.

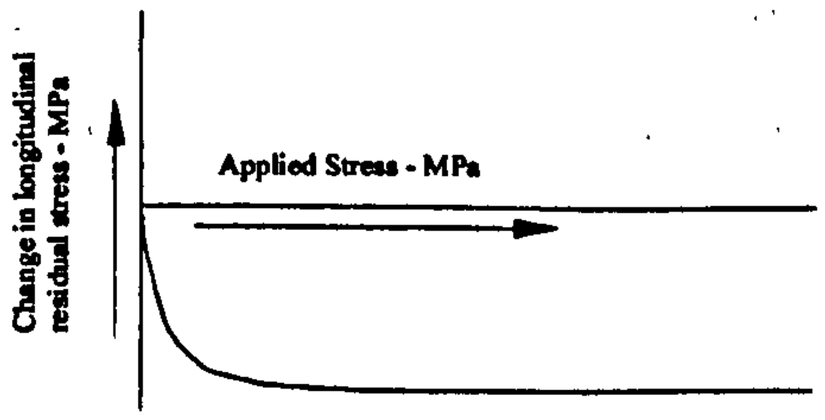

Figure 5.160 – Schematic trend of observed longitudinal residual stress.

Second Approach: Analysing the Summary Plot

The residual stress on and near the weld toe (distance range 0-1 mm) decreased by ~80 MPa due to the application of a dynamic stress of ±48 MPa (Figure 5.131). With an increase in the dynamic stress to ±96 MPa, the residual stress was found to be similar

to the residual stress of the specimens subjected to applied stress of ±48 MPa. With a further increase in the applied stress to ±144 MPa, the residual stress decreased by 56 MPa. The ±192 MPa applied stress level showed residual stresses similar to the residual stresses of the specimens subjected to induced stress of ±96 MPa. The ±240 MPa applied stress showed further reduced residual stresses all along the measurement line. The ±288 MPa applied stress level showed reduced residual stresses, but with a lesser degree. Away from the weld toe the residual stresses decreased but with a lesser degree.

Transverse Stress Plots

First Approach: Comparing the Peak Stresses

The resulting residual stresses of the specimens are shown in the table below

Table 5.21 – Comparison of the peak residual stresses – longitudinal stress

Specimen No.	Figure No.	Vibration Time	Applied Stress	Stress Range	Average Stress
		min	MPa	MPa	MPa
3/8 to 5/4	5.132 to 5.135	0	0	380 to 480	439.25
5/5 to 5/8	5.136 to 5.139	1.5	±48	420 to 530	493.75
5/9 to 6/2	5.140 to 5.143	1.5	±96	415 to 705	570
6/3 to 6/6	5.144 to 5.146	1.5	±144	505 to 570	525
6/7 to 7/1	5.147 to 5.150	1.5	±192	260 to 520	420
7/2 to 7/5	5.151 to 5.154	1.5	±240	220 to 480	330
7/6 to 7/9	5.155 to 5.158	1.5	±288	300 to 380	347.5

The average transverse residual stress of the unvibrated/control specimens was 439.25 MPa. With application of induced stress ±48 MPa, the residual stress increased by 54.5 MPa. With increase in the applied stress to ±96 MPa, the residual stress increased by ~130 MPa. However, the residual stresses started to decrease after applied stress level ±144 MPa. Further increases in the applied stress caused further decrease in the residual stresses. The trend of the residual stresses is shown in Figure 5.161.

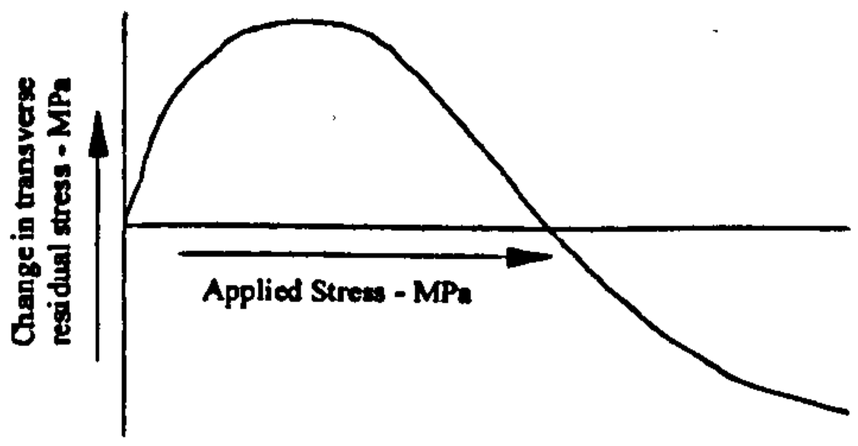

Figure 5.161 – Schematic trend of observed transverse residual stresses.

Second Approach: Analysing Summary Plot

The transverse residual stresses on and near the weld toe (distance range 0-1 mm) increased with application of a dynamic stress of ±48 MPa (Figure 5.159). An increase in the applied stress to ±96 MPa caused a further increase in the residual stresses. The ±144 MPa applied stress level caused an increase in the residual stresses but with a lesser degree. The applied stress level ±192 MPa and above showed further decreased residual stresses. Away from the weld toe (distance range 2-3 mm), no reductions in residual stresses were observed until applied stress level ±144 MPa. The ±240 MPa applied stress level showed a decrease of residual stress of 25 MPa and the applied stress ±288 MPa showed a decrease of ~50 MPa.

Thus, the trend of residual stresses on and near the weld toe (distance range 0-1 mm) was found to be similar to the trend found in the peak stress analysis. Away from the weld toe (distance range 2-3 mm), the residual stresses decreased in high applied stresses.

Batch 2: Constant Induced Amplitude – 80 MPa

In this batch, nine specimens were processed. The frequency of vibration was maintained at 25 Hz and the applied induced stress set at 80 MPa. The time of vibration was varied from 0 to 8 minutes. One specimen was welded without any vibration. The remaining eight specimens were vibratory treated during/after welding. The treatment times for the eight specimens ranged from 2 minutes to 8 minutes in 2 minute increments.

The longitudinal and transverse residual stresses of the samples on the selected line were measured. In this batch the longitudinal measurement line was moved a little towards the weld. The measurement line was similar to the measurement line in Figure 5.13 but it was moved a little (0.3~0.4 mm) towards the weld, which made the longitudinal residual stress peaks slightly different from residual stress peaks of other batches. The residual stress plots are shown below.

Longitudinal Stress Plots

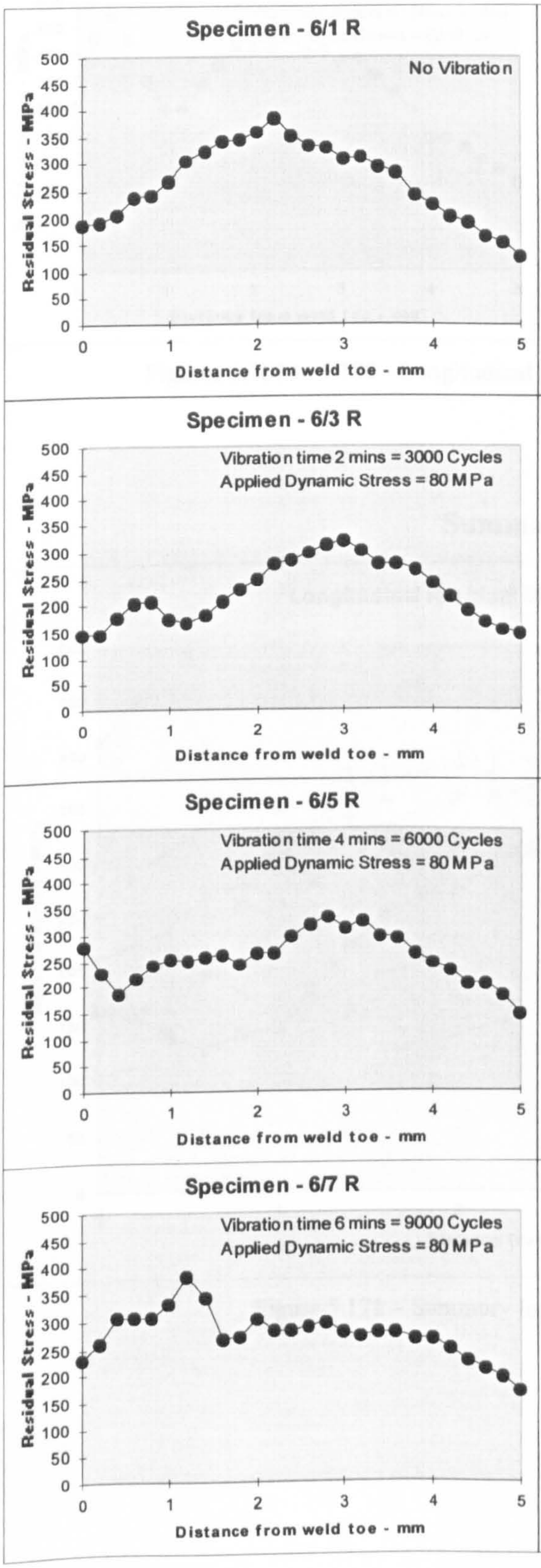

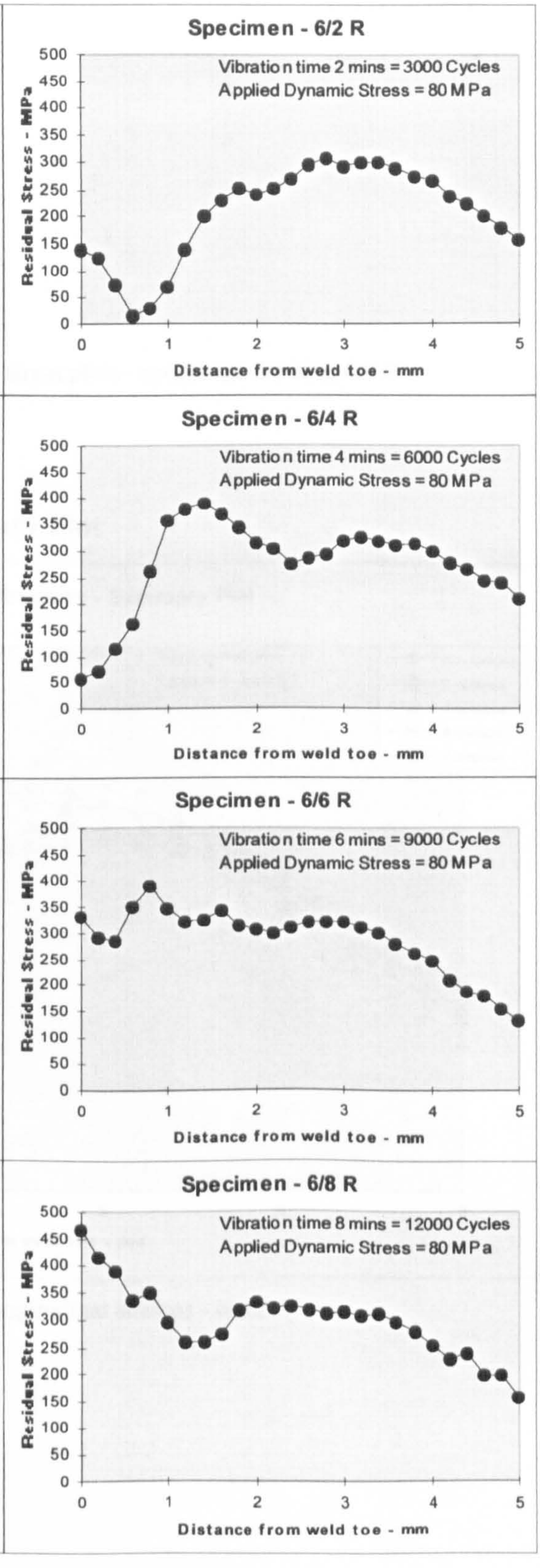

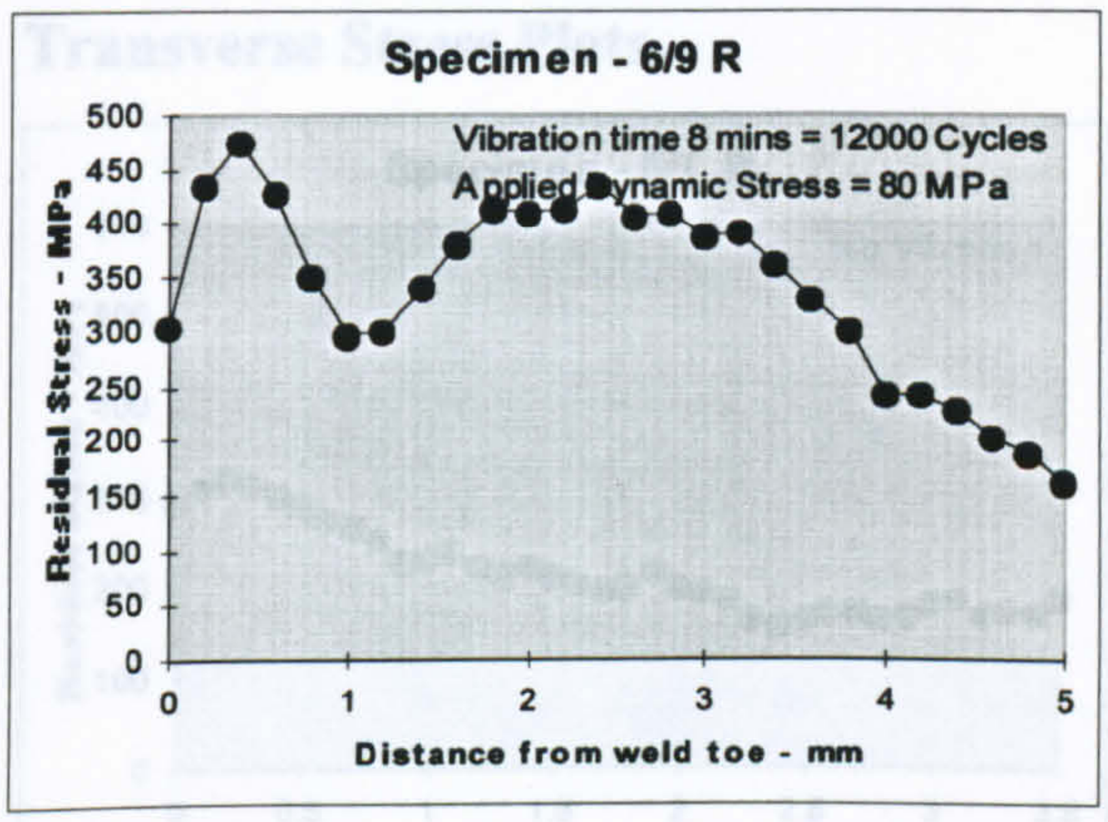

Figures 5.162 to 5.170 - Longitudinal stress plots - specimens 6/1 R to 6/9 R

Summary Plot

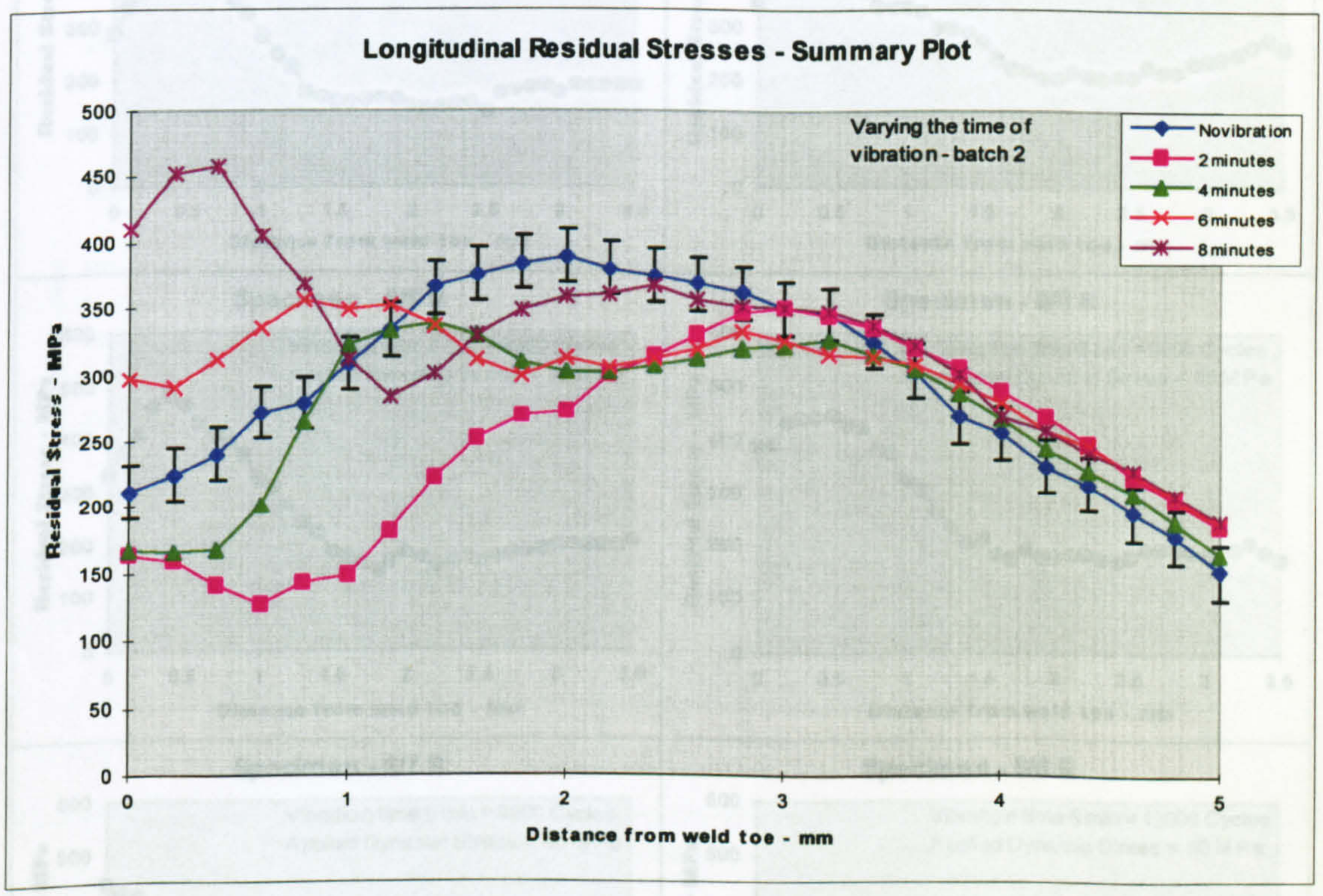

Figure 5.171 – Summary longitudinal stresses - batch 2

Transverse Stress Plots

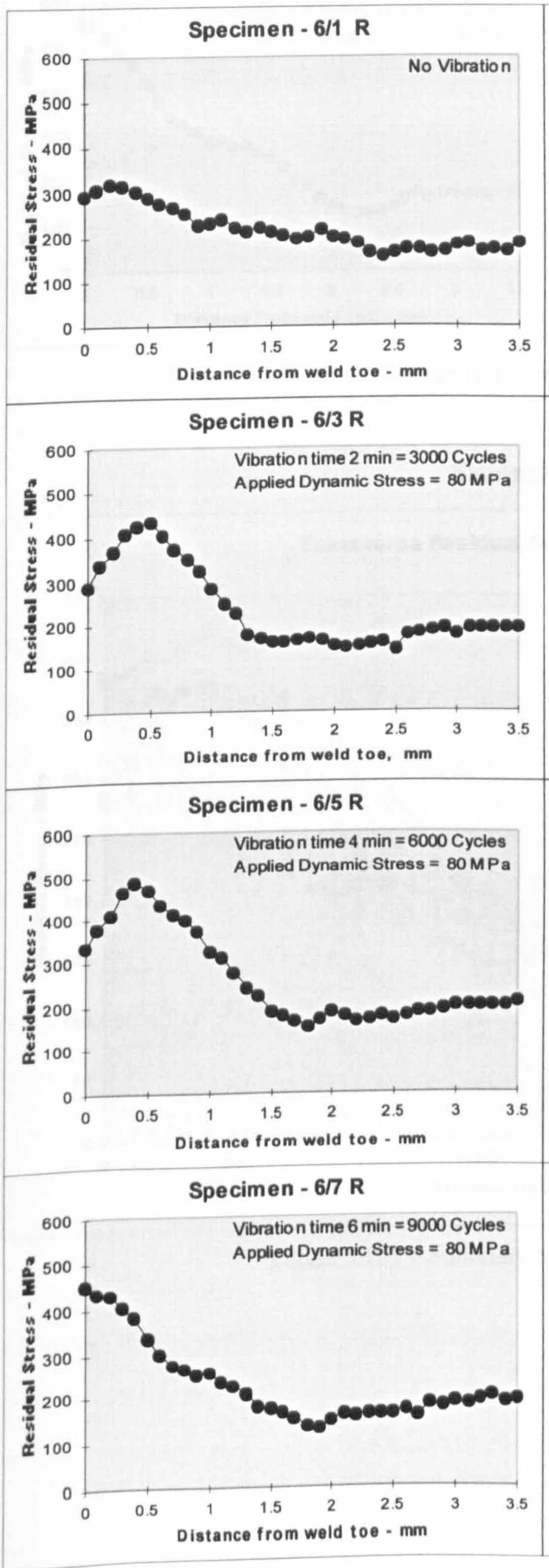

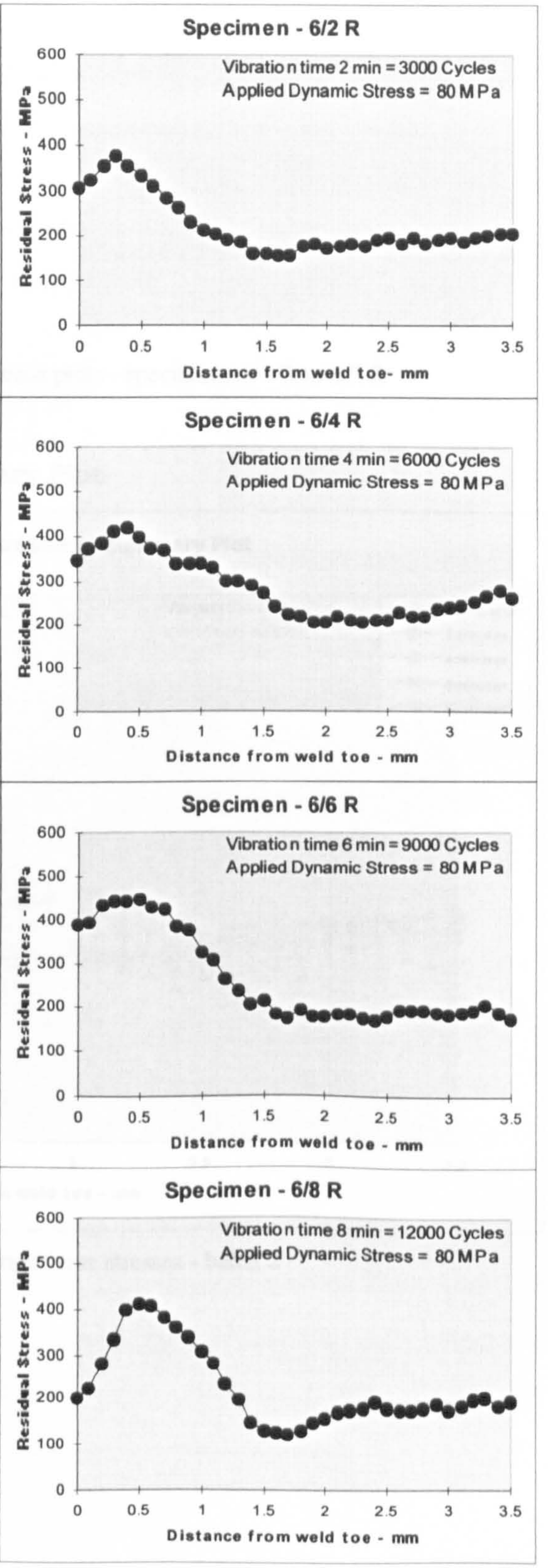

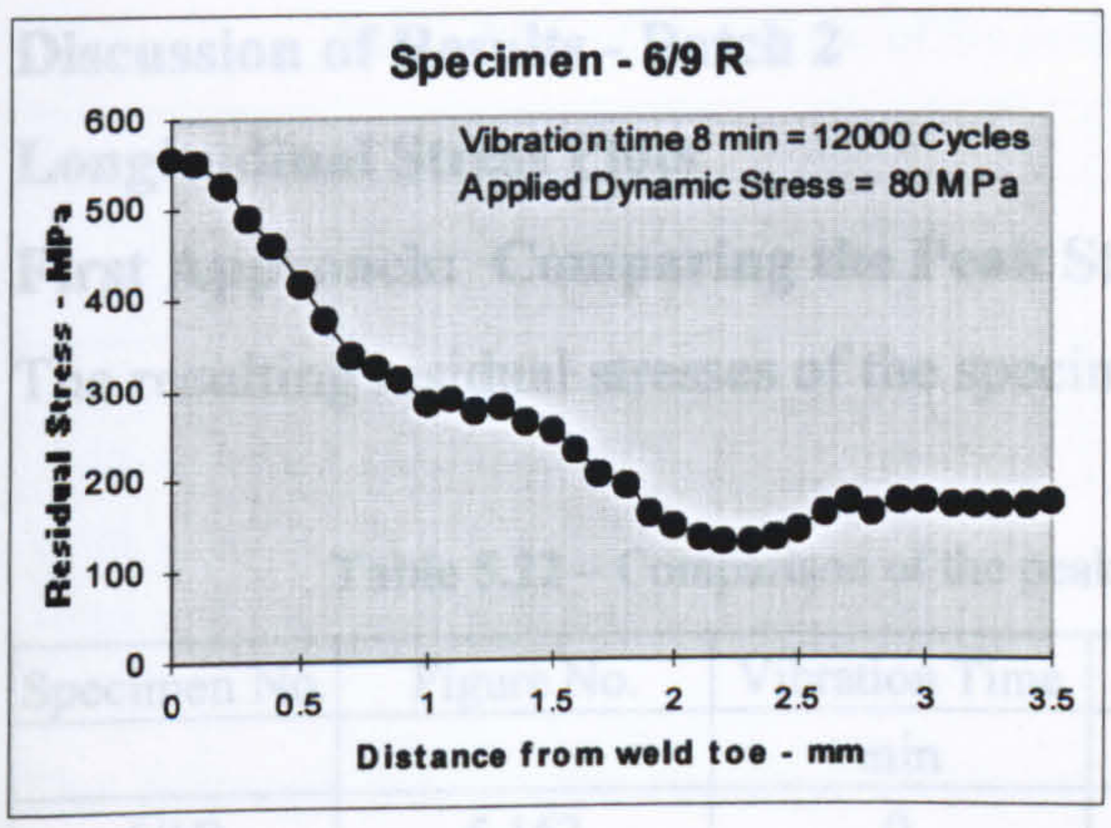

Figure 5.172 to 5.180 - Transverse stress plots - specimens 6/1 R to 6/9 R

Summary Plot

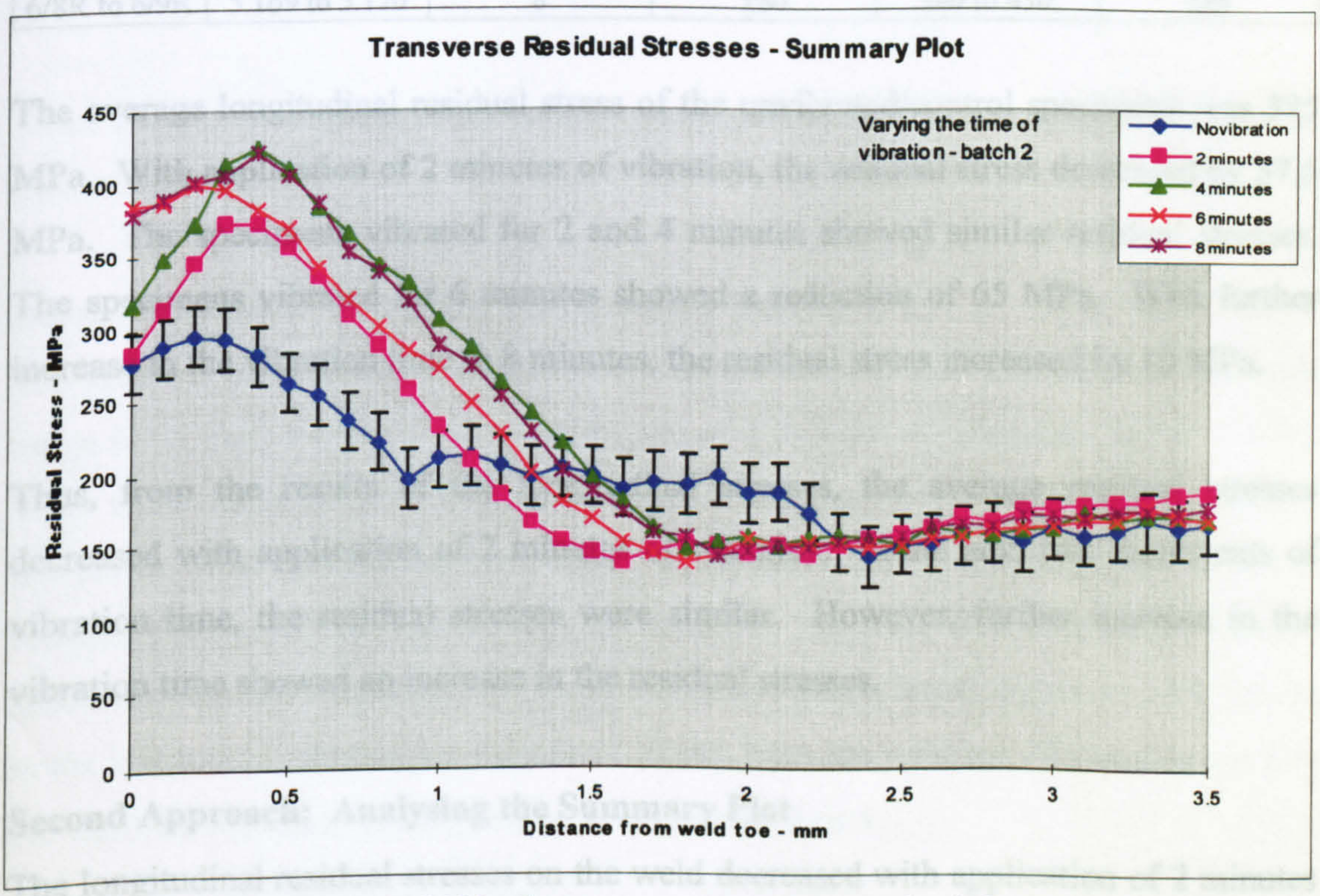

Figure 5.181 – Summary transverse stresses - batch 2

Discussion of Results - Batch 2

Longitudinal Stress Plots

First Approach: Comparing the Peak Stresses

The resulting residual stresses of the specimens are shown in the table below

Table 5.22 – Comparison of the peak residual stresses – longitudinal stress

Specimen No.	Figure No.	Vibration Time	Applied Stress	Stress Range	Average Stress
		min	MPa	MPa	MPa
6/1R	5.162	0	0	375	375
6/2R to 6/3R	5.163 to 5.164	2	±80	310 to 325	317.5
6/4R to 6/5R	5.165 to 5.166	4	±80	325 to 330	327.5
6/6R to 6/7R	5.167 to 5.168	6	±80	300 to 320	310
6/8R to 6/9R	5.169 to 5.170	8	±80	340 to 430	385

The average longitudinal residual stress of the unvibrated/control specimens was 375 MPa. With application of 2 minutes of vibration, the residual stress decreased by 57.5 MPa. The specimens vibrated for 2 and 4 minutes showed similar residual stresses. The specimens vibrated for 6 minutes showed a reduction of 65 MPa. With further increase in the vibration time to 8 minutes, the residual stress increased by 10 MPa.

Thus, from the results of the longitudinal stresses, the average residual stresses decreased with application of 2 minutes of vibration. In the next two increments of vibration time, the residual stresses were similar. However, further increase in the vibration time showed an increase in the residual stresses.

Second Approach: Analysing the Summary Plot

The longitudinal residual stresses on the weld decreased with application of 2 minutes of vibration (Figure 5.171). With an increase in the vibration time to 4 minutes, the residual stresses decreased but with a lesser degree. Further increase in the vibration time showed increased residual stresses. Away from the weld toe (distance range 3-5 mm), the residual stresses were found to increase with a smaller degree.

Transverse Stress Plots

First Approach: Comparing the Peak Stresses

The resulting residual stresses of the specimens are shown in the table below

Table 5.23 – Comparison of the peak residual stresses – longitudinal stress

Specimen No.	Figure No.	Vibration Time	Applied Stress	Stress Range	Average Stress
		min	MPa	MPa	MPa
6/1R	5.171	0	0	330	330
6/2R to 6/3R	5.172 to 5.173	2	±80	375 to 427	401
6/4R to 6/5R	5.174 to 5.175	4	±80	422 to 488	455
6/6R to 6/7R	5.176 to 5.177	6	±80	~450	~450
6/8R to 6/9R	5.178 to 5.179	8	±80	412 to 560	486

The average transverse residual stress of the unvibrated/control specimens was 330 MPa. With application of 2 minutes of vibration, the peak residual stress increased by 71 MPa. Next increments in the time of vibration showed the increase in the average residual stresses by 125 MPa, 120 MPa and 156 MPa.

Thus, a trend of increase in the residual stresses was observed due to increase in the time of vibration.

Second Approach: Analysing the Summary Plot

The residual stresses of the measurement points on and near the weld toe (distance range 0-1.2 mm) increased with application of 2 minutes of vibration (Figure 5.181). With an increase in the vibration time to 4 minutes, the residual stresses further increased. The specimens vibrated for 8 minutes showed a similar stress to the residual stresses of the specimens vibrated for 4 minutes. The 6 minutes vibrated specimens showed increased residual stresses, but with a lesser degree in comparison to the specimens vibrated for 4 minutes. Away from the weld toe (distance range 2.4-3.5 mm), no reduction in the residual stresses were found.

Batch 3: Constant Induced Vibratory Stress – 160 MPa

In this batch, ten specimens (two in a sample) were welded during vibration. Keeping the vibration frequency to 25 Hz and induced stress to 160 MPa, the time of vibration was varied from 0 to 8 minutes in increments of 2 minutes. The results of these tests are shown below.

Longitudinal Stress Plots

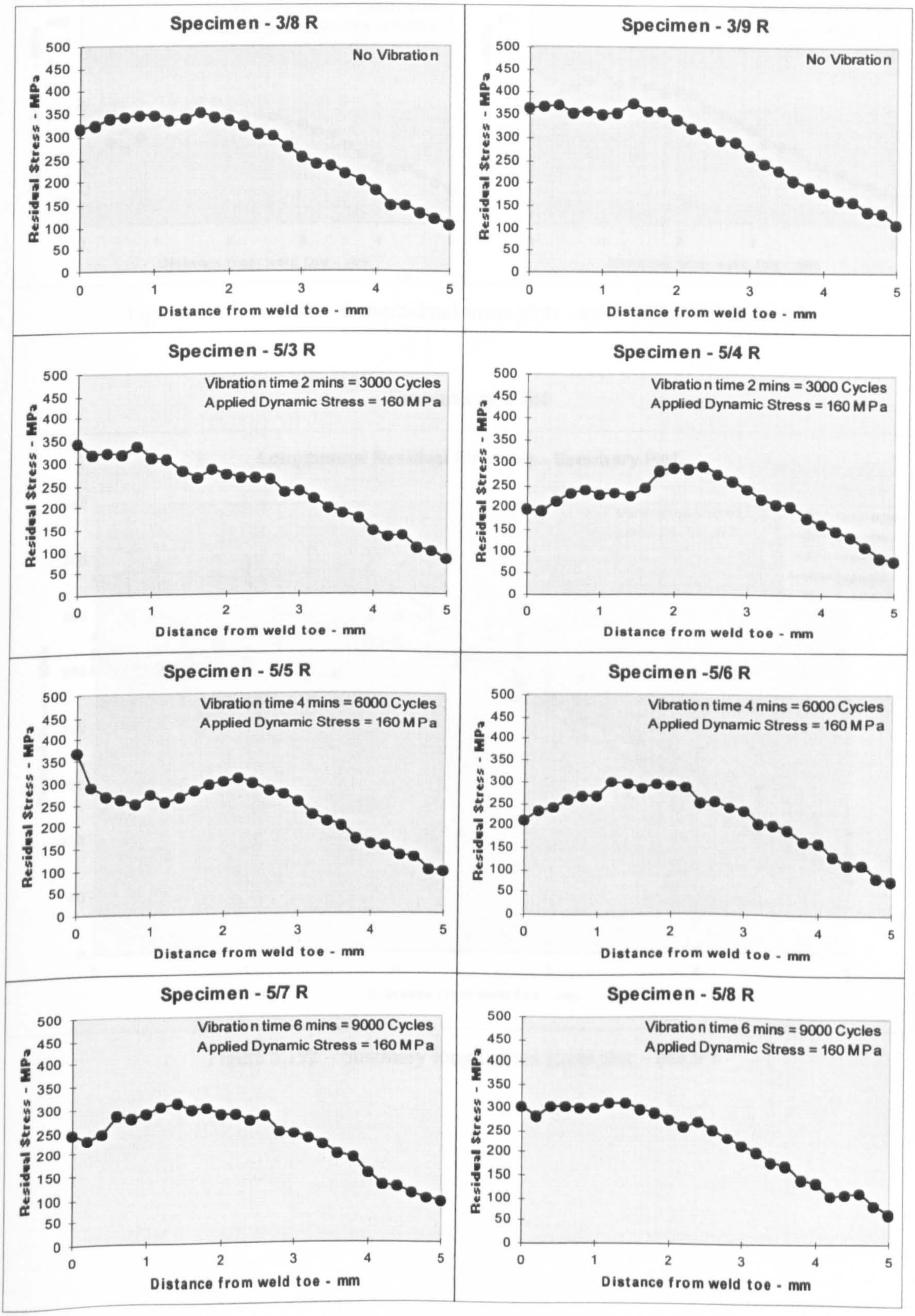

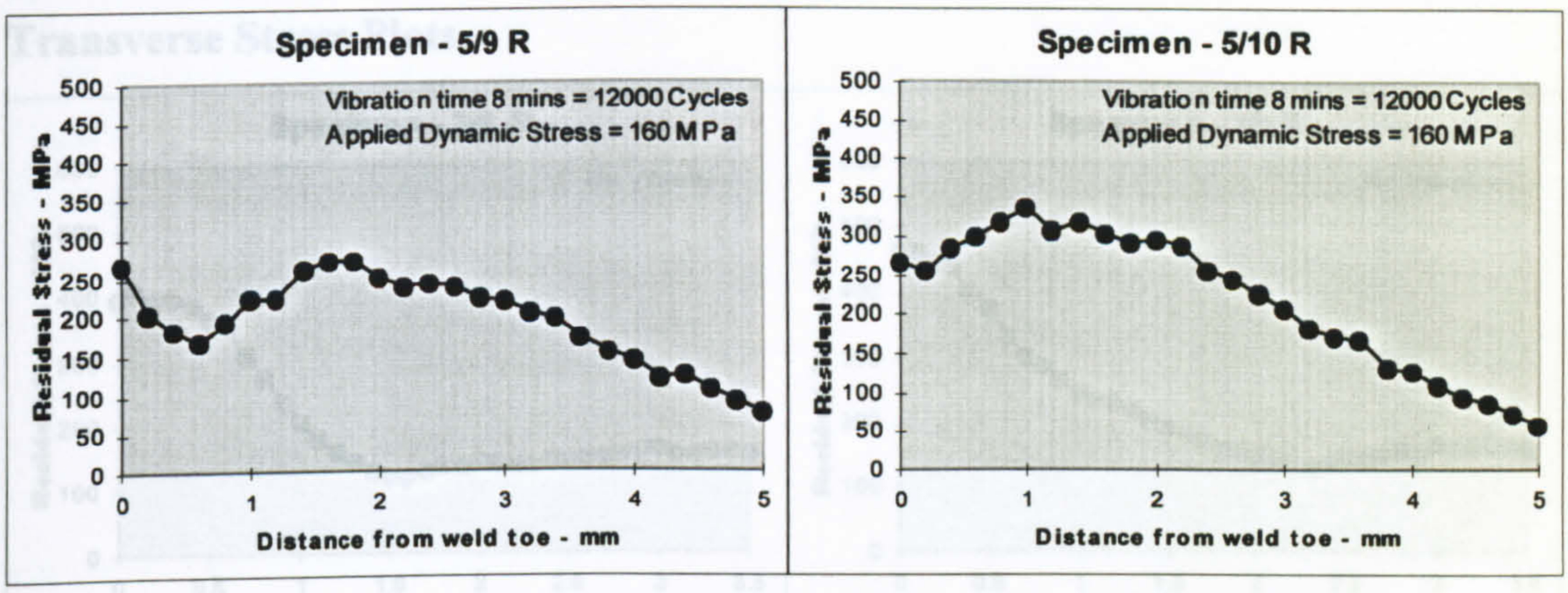

Figures 5.182 to 5.191 - Longitudinal stress plots - specimens 3/8 R to 5/10 R

Summary Plot

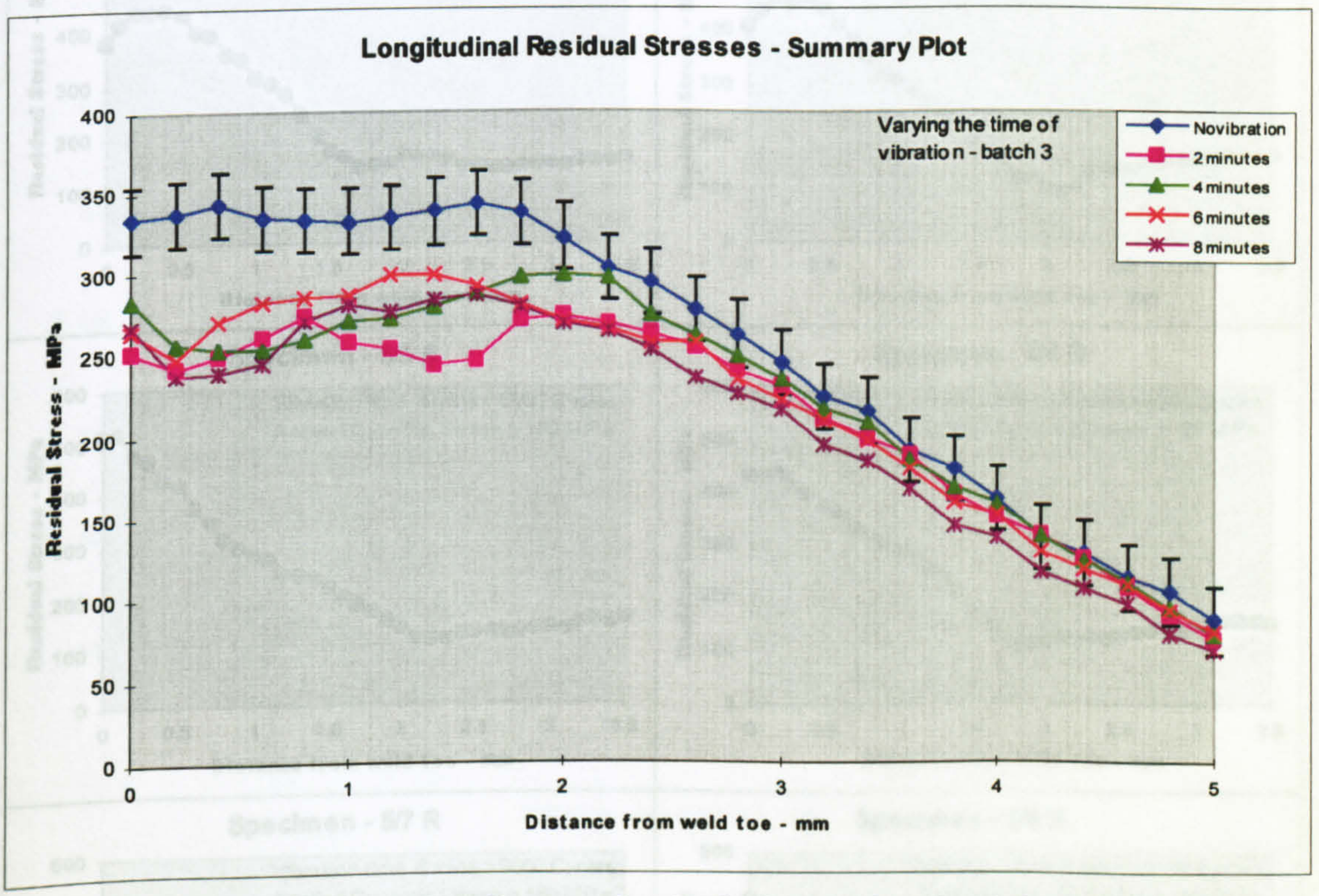

Figure 5.192 – Summary longitudinal stress plot – batch 3

Transverse Stress Plots

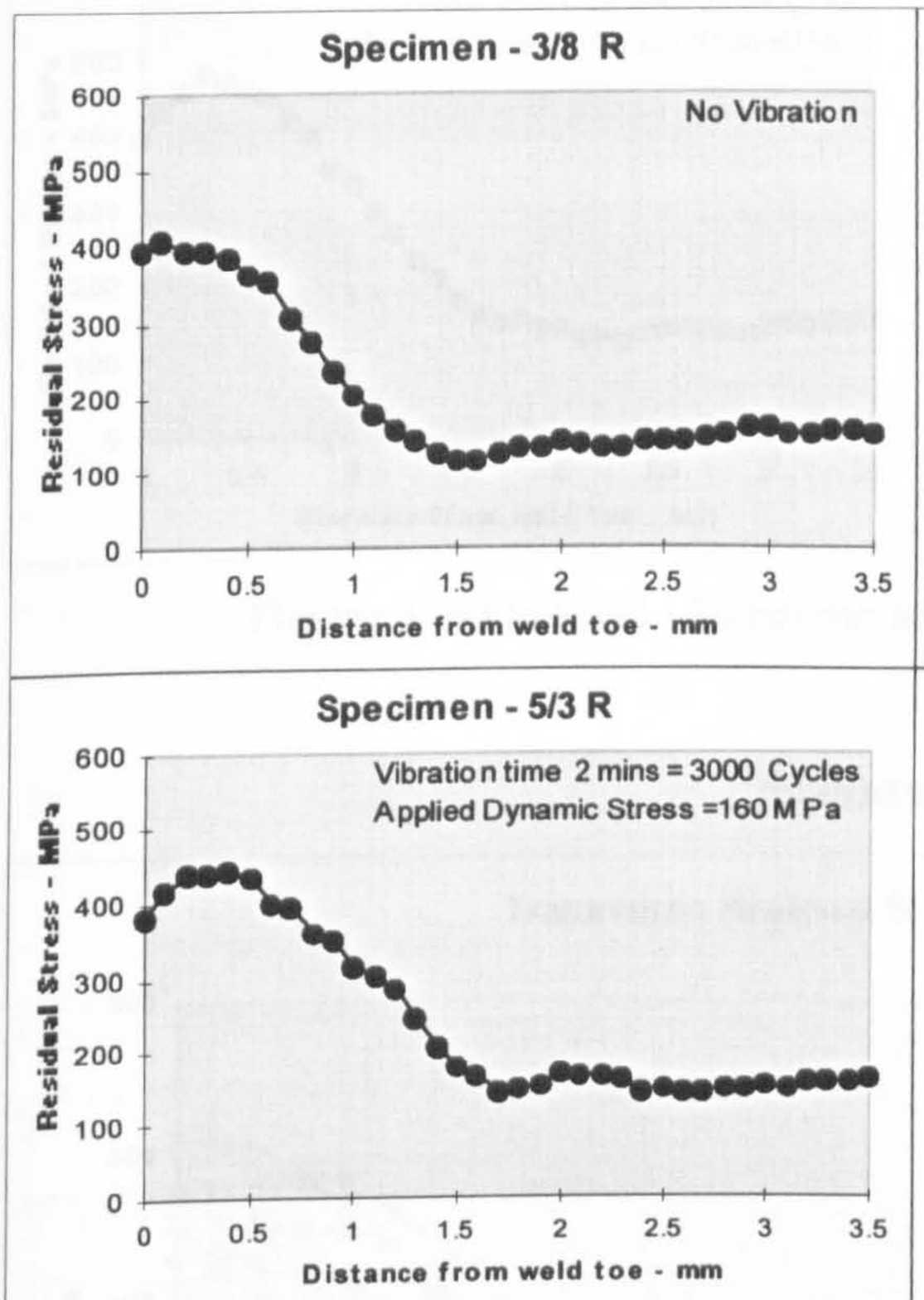

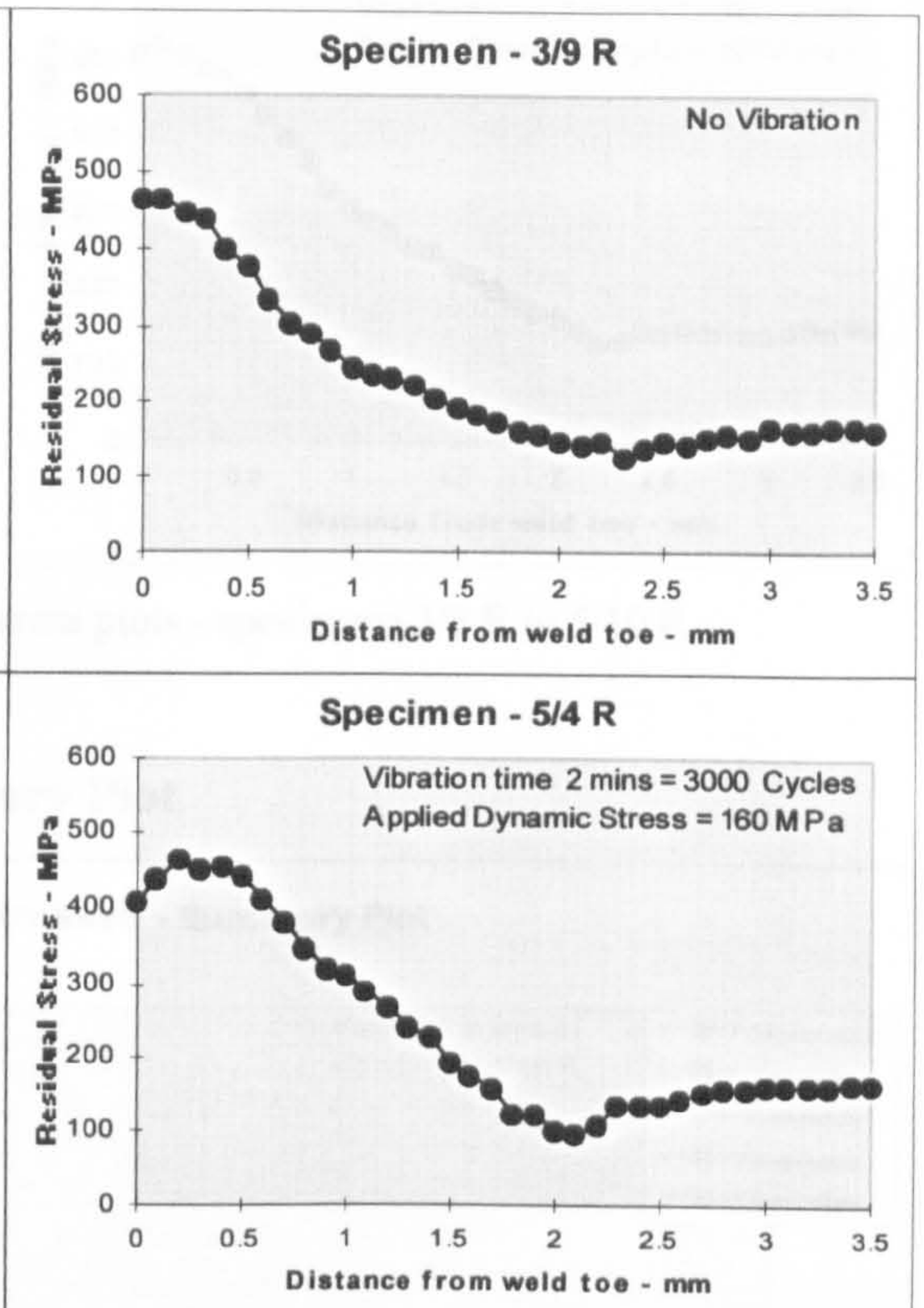

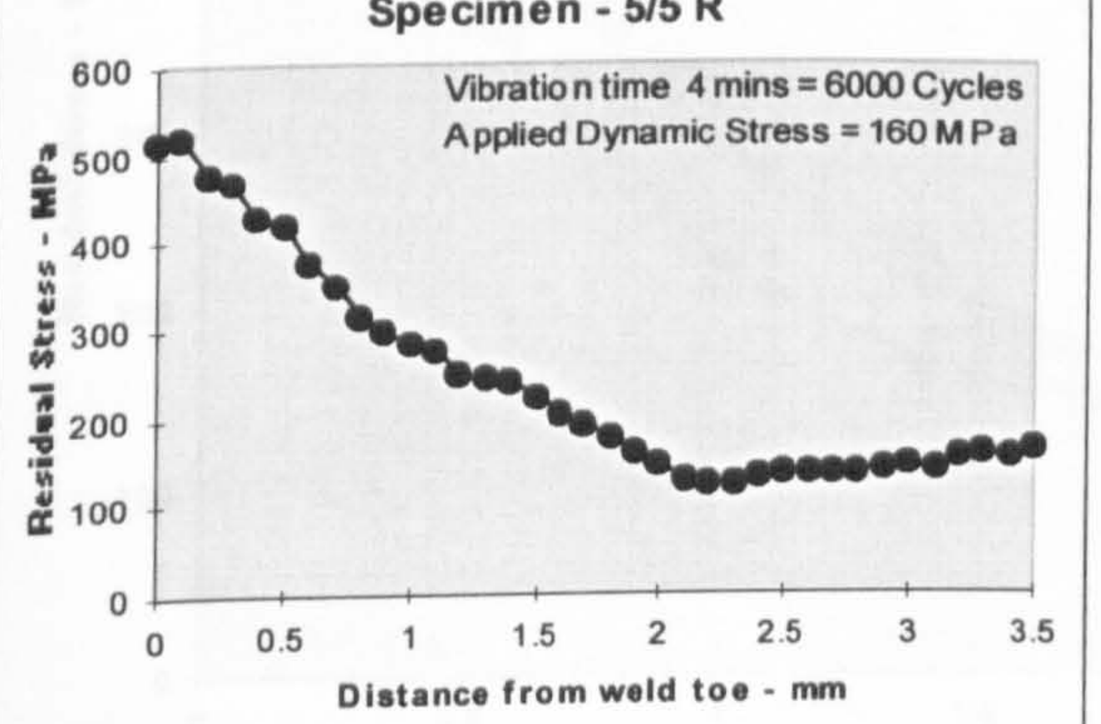

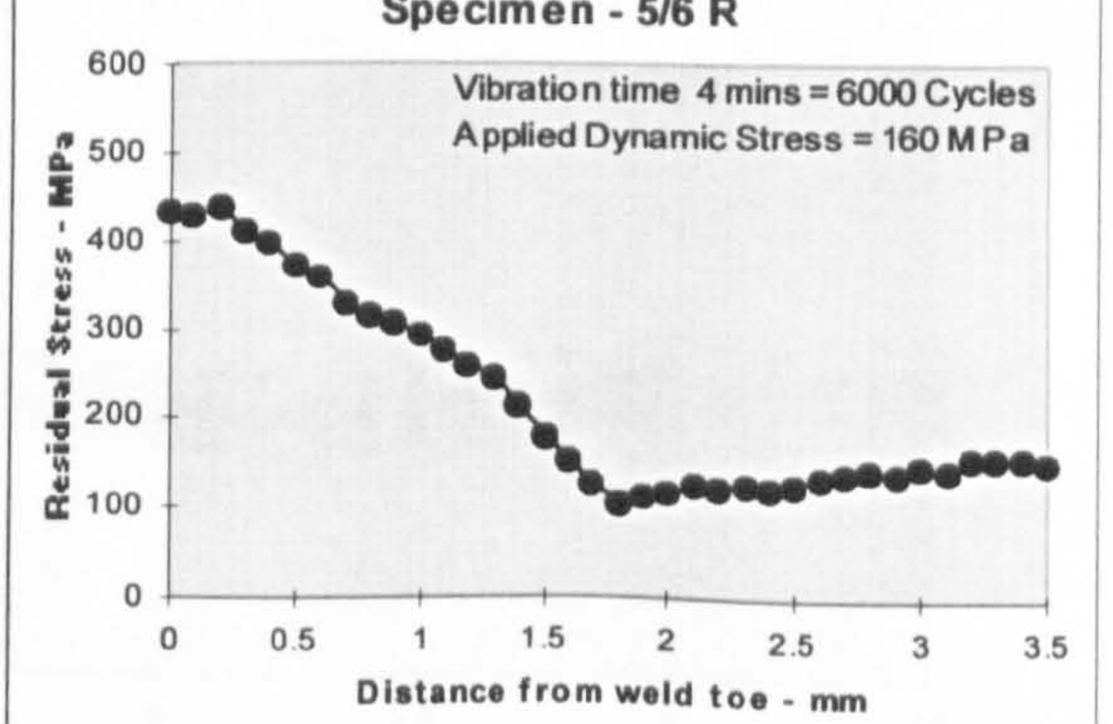

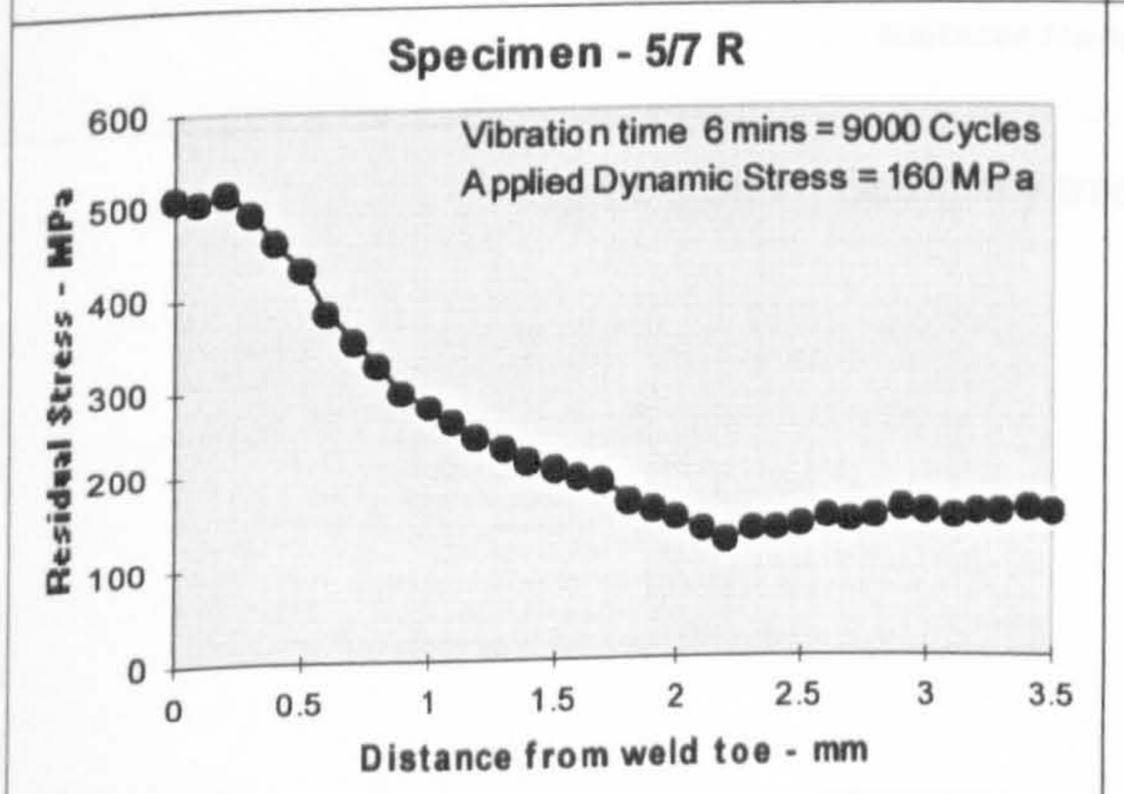

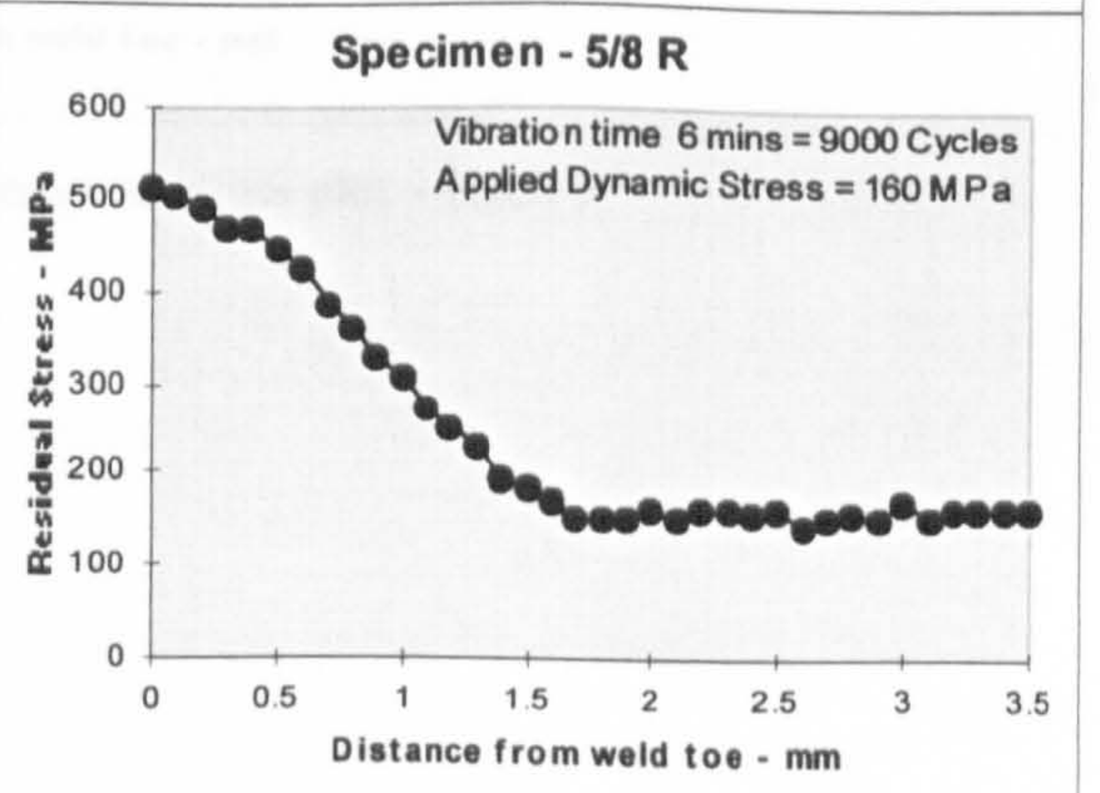

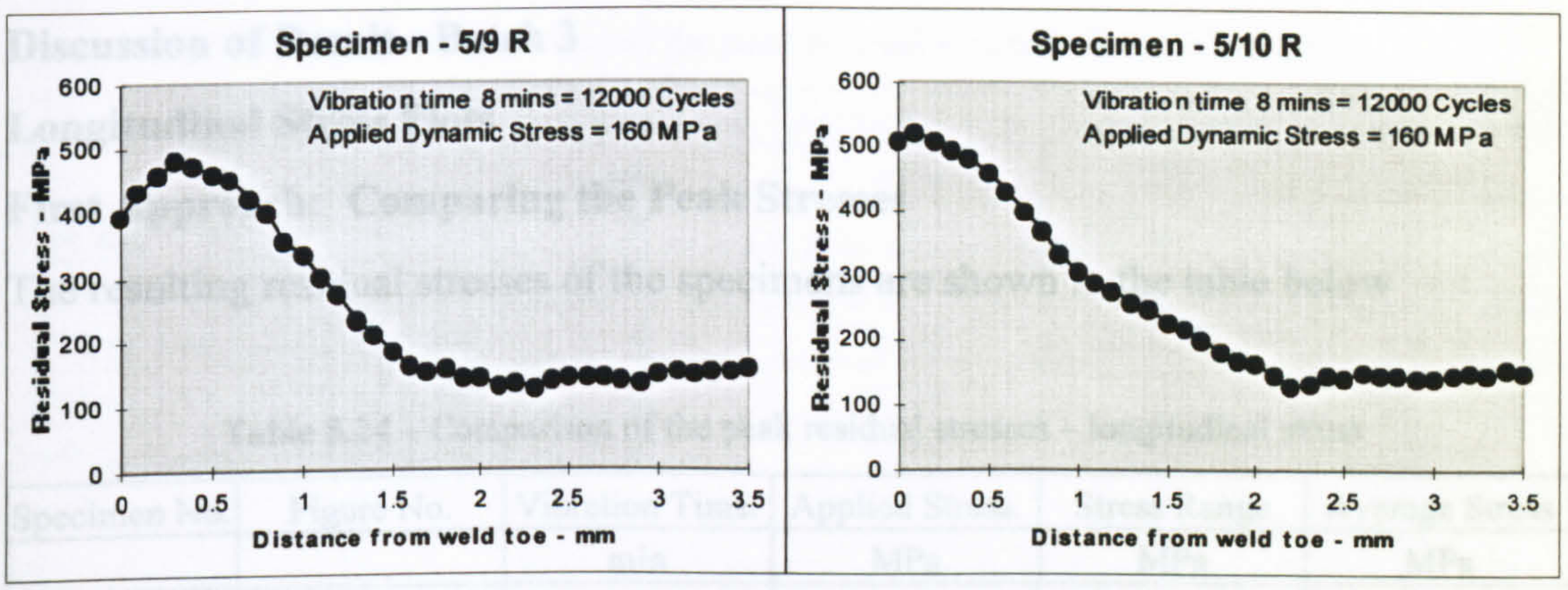

Figures 5.193 to 5.202 - Transverse stress plots - specimens 3/8 R to 5/10 R

Summary Plot

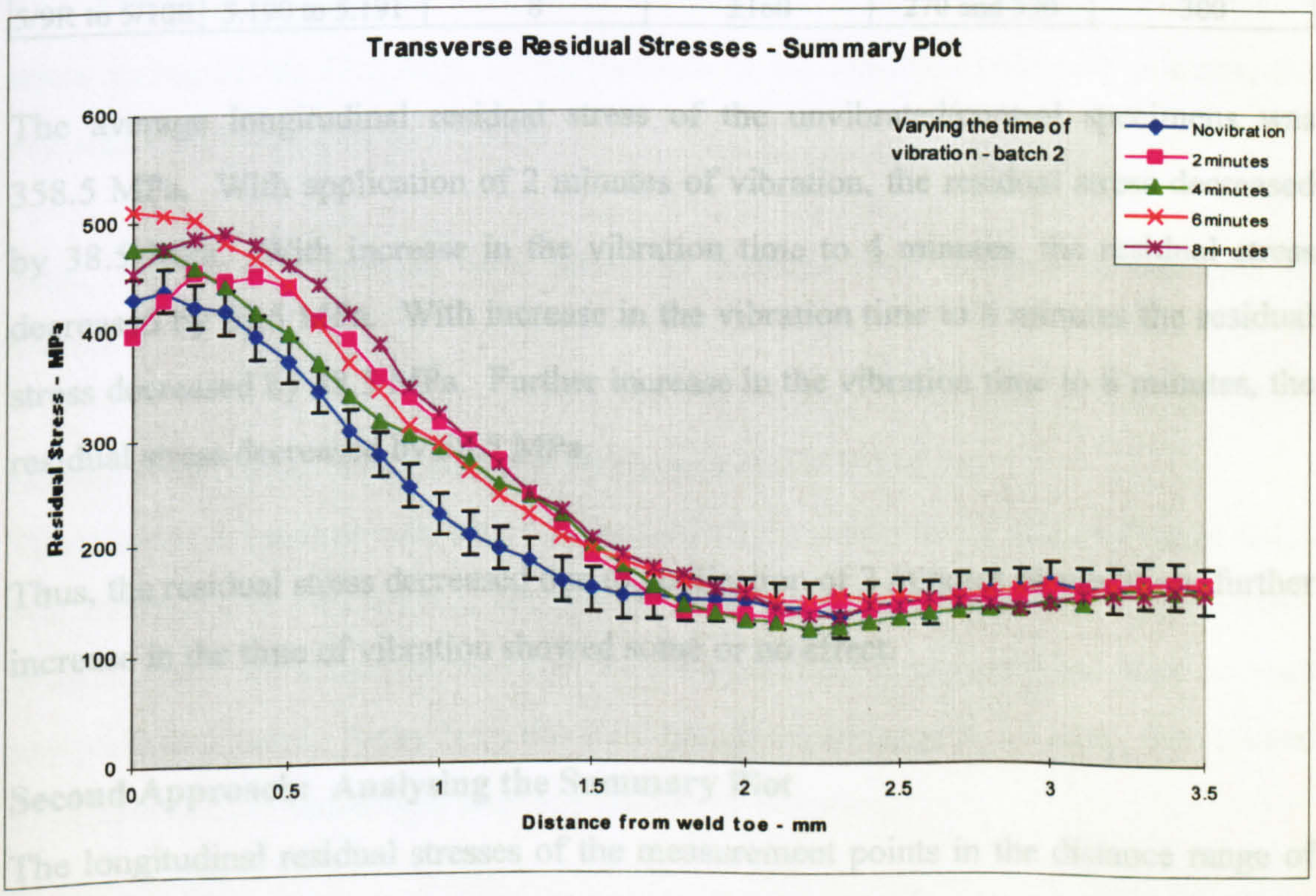

Figure 5.203 – Summary transverse stress plot – batch 3

Discussion of Result - Batch 3

Longitudinal Stress Plots

First Approach: Comparing the Peak Stresses

The resulting residual stresses of the specimens are shown in the table below

Table 5.24 – Comparison of the peak residual stresses – longitudinal stress

Specimen No.	Figure No.	Vibration Time.	Applied Stress.	Stress Range	Average Stress
		min	MPa	MPa	MPa
3/8R and 3/9R	5.182 and 5.183	0	0	345 and 372	358.5
5/3R to 5/4R	5.184 to 5.185	2	±160	350 and 290	320
5/5R to 5/6R	5.186 to 5.187	4	±160	310 and 300	305
5/7R to 5/8R	5.188 to 5.189	6	±160	~310	~310
5/9R to 5/10R	5.190 to 5.191	8	±160	270 and 330	300

The average longitudinal residual stress of the unvibrated/control specimens was 358.5 MPa. With application of 2 minutes of vibration, the residual stress decreased by 38.5 MPa. With increase in the vibration time to 4 minutes, the residual stress decreased by 53.5 MPa. With increase in the vibration time to 6 minutes the residual stress decreased by 48.5 MPa. Further increase in the vibration time to 8 minutes, the residual stress decreased by 58.5 MPa.

Thus, the residual stress decreased due to application of 2 minutes of vibration, further increase in the time of vibration showed some or no effect.

Second Approach: Analysing the Summary Plot

The longitudinal residual stresses of the measurement points in the distance range of 0-2 mm decreased by ~80 MPa in application of 2 minutes of vibration (Figure 5.192). Further increases in the vibration time showed no effect. Away from the weld toe (distance range 2.5-5 mm), a little or no reduction in residual stresses were found.

Transverse Stress Plots

First Approach: Comparing the Peak Stresses

The resulting residual stresses of the specimens are shown in the table below

Table 5.25 – Comparison of the peak residual stresses – longitudinal stress

Specimen No.	Figure No.	Vibration Time.	Applied Stress.	Stress Range	Average Stress
		min	MPa	MPa	MPa
3/8R and 3/9R	5.193 and 5.194	0	0	420 and 465	442.5
5/3R to 5/4R	5.195 to 5.196	2	±160	450 and 460	455
5/5R to 5/6R	5.197 to 5.198	4	±160	430 and 520	475
5/7R to 5/8R	5.199 to 5.200	6	±160	~520	~520
5/9R to 5/10R	5.201 to 5.202	8	±160	485 and 520	502.5

The average transverse residual stress of the unvibrated/control specimens was 442.5 MPa. With application of 2 minutes of vibration, the residual stress increased by 12.5 MPa. With increase in the vibration time to 4 minutes, the residual stress increased by 32.5 MPa. With a further increase in the vibration time to 6 minutes, the residual stress increased by 77.5 MPa. With increase in the vibration time to 8 minutes, the residual stress increased by 60 MPa.

Thus, the residual stresses were found to increase with increase in the time of vibration.

Second Approach: Analysing the Stresses of the Whole Line

The transverse residual stresses of the measurement points in the distance range 0-1.5 mm increased by ~65 MPa in application of 2 minutes of vibration (Figure 5.203). With increase in the time of vibration the residual stresses increased but there was not any particular trend. Away from the weld toe (distance range 2-3.5 mm), the residual stresses remained unchanged after application of vibration.

Batch 4: Constant Induced Vibratory Stress – 240 MPa

In this batch fifteen specimens (three in a sample) were welded during vibration. In all these specimens induced stress was 240 MPa and frequency of vibration was 25 Hz. Similar to previous two batches, the vibration time was varied from 0 to 8 minutes in 2 minutes increment. The details of the vibration time are shown in the residual stress plots. The longitudinal and transverse residual stresses of the selected line (Figure 5.13) were measured and plotted, which are shown below.

Longitudinal Stress Plots

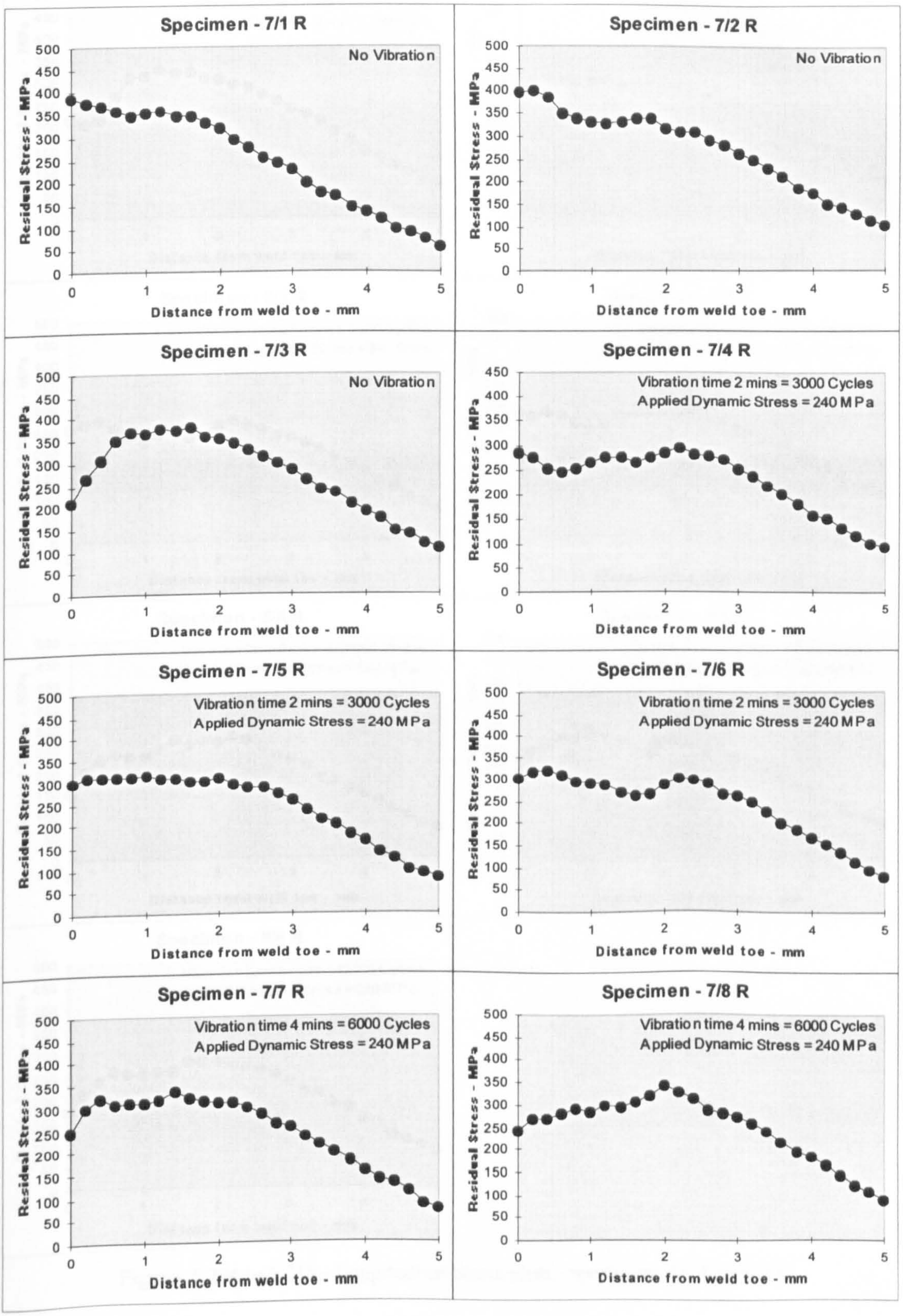

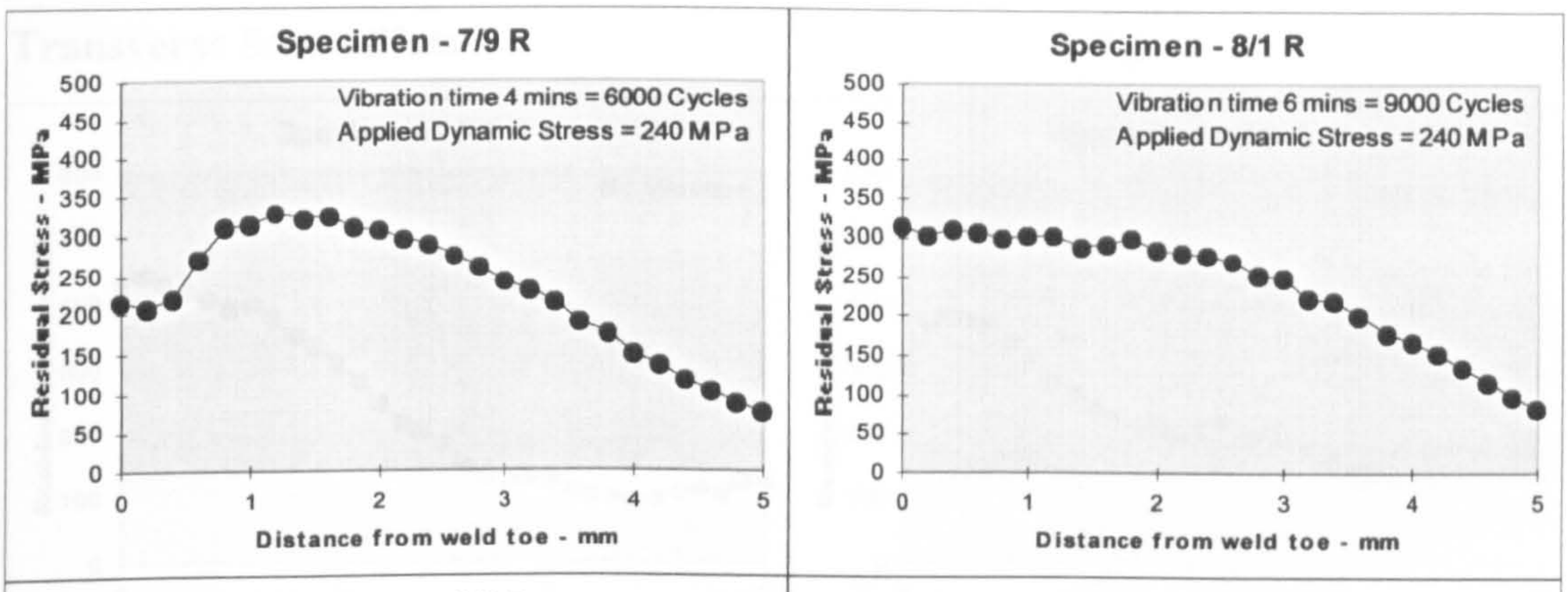

Figures 5.204 to 5.218 - Longitudinal stress plots - specimens 7/1 R to 8/8 R

Transverse Stress Plots

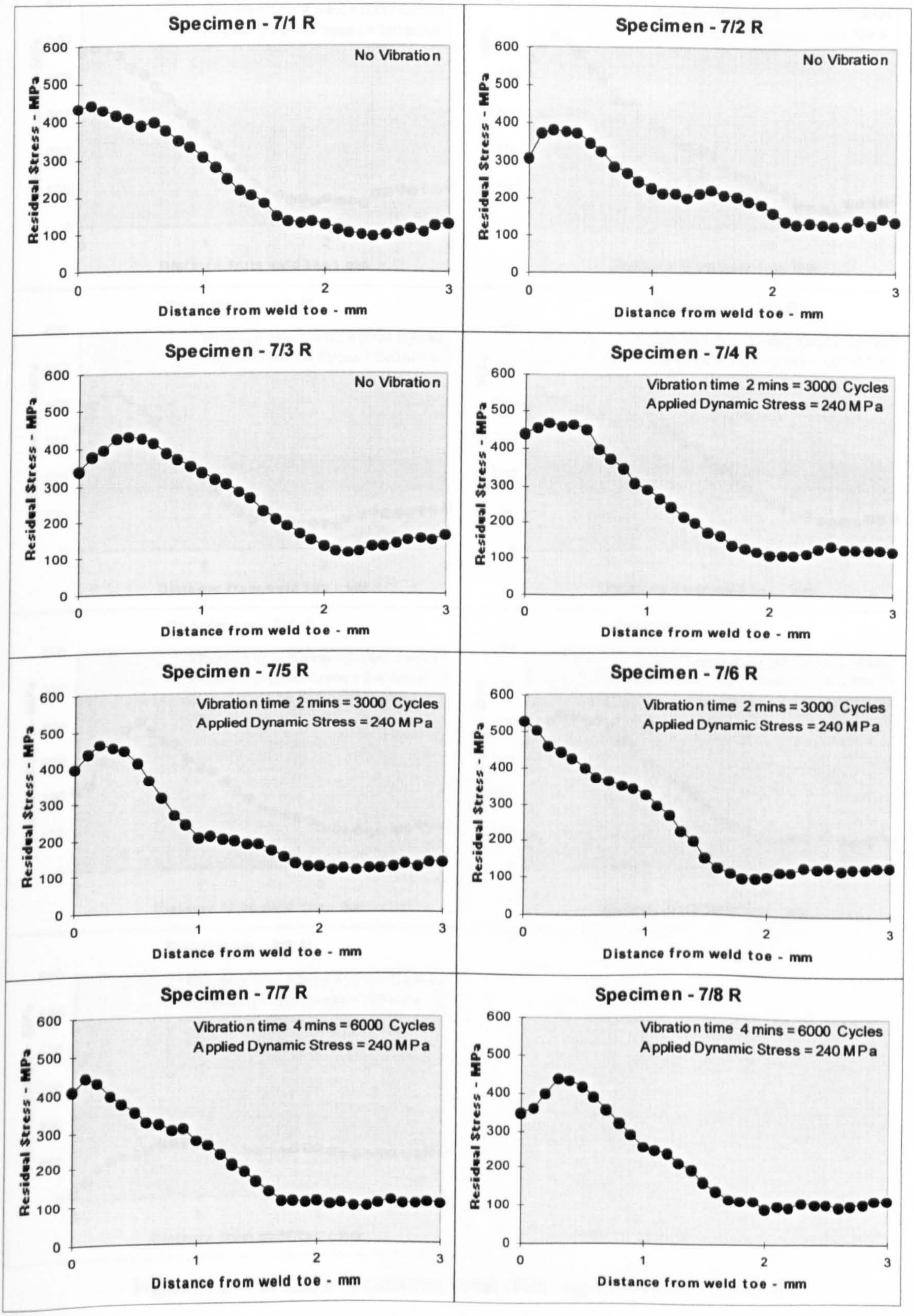

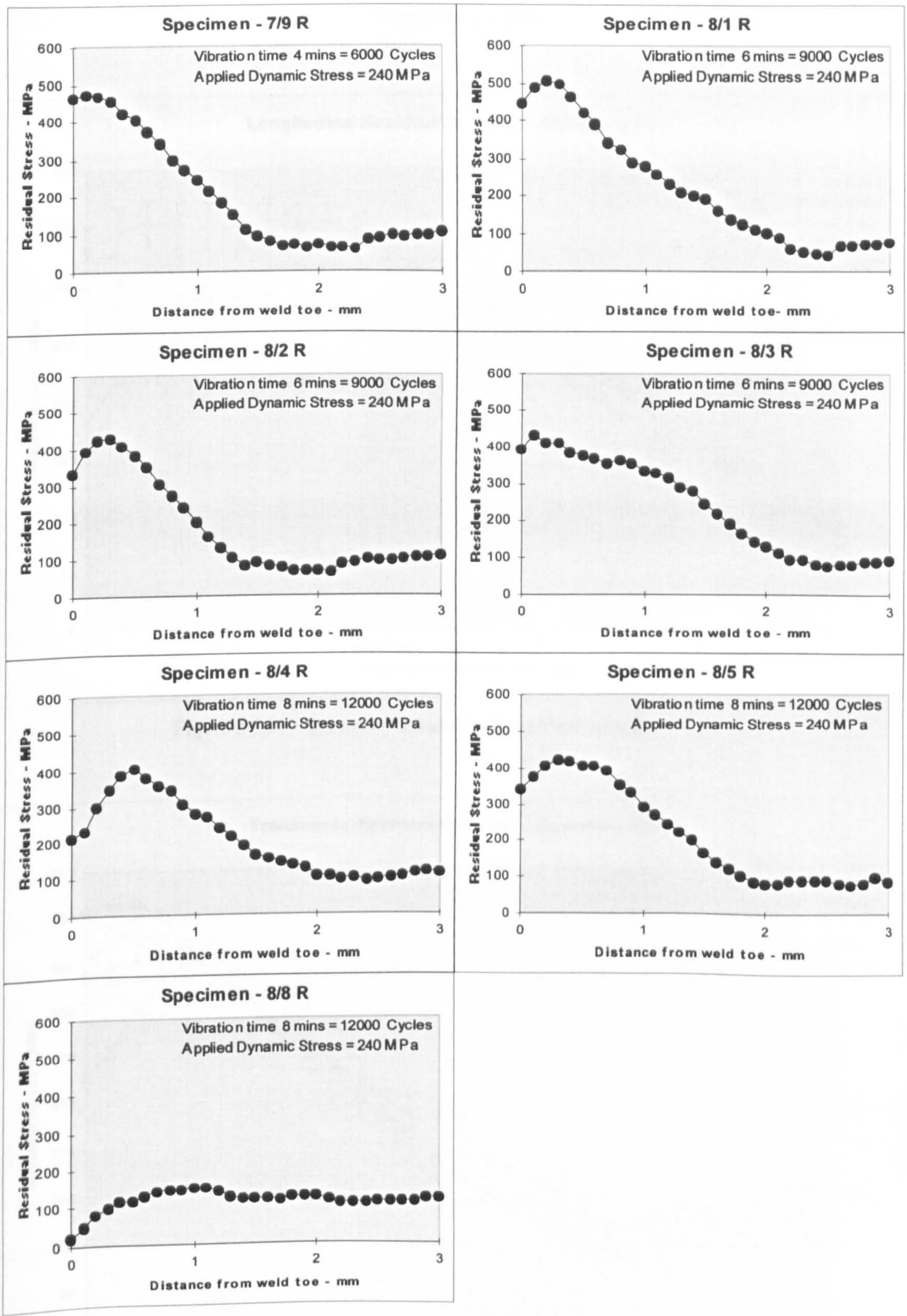

Figures 5.219 to 5.233 - Transverse stress plots - specimens 7/1 R to 8/8 R

Summary Plots

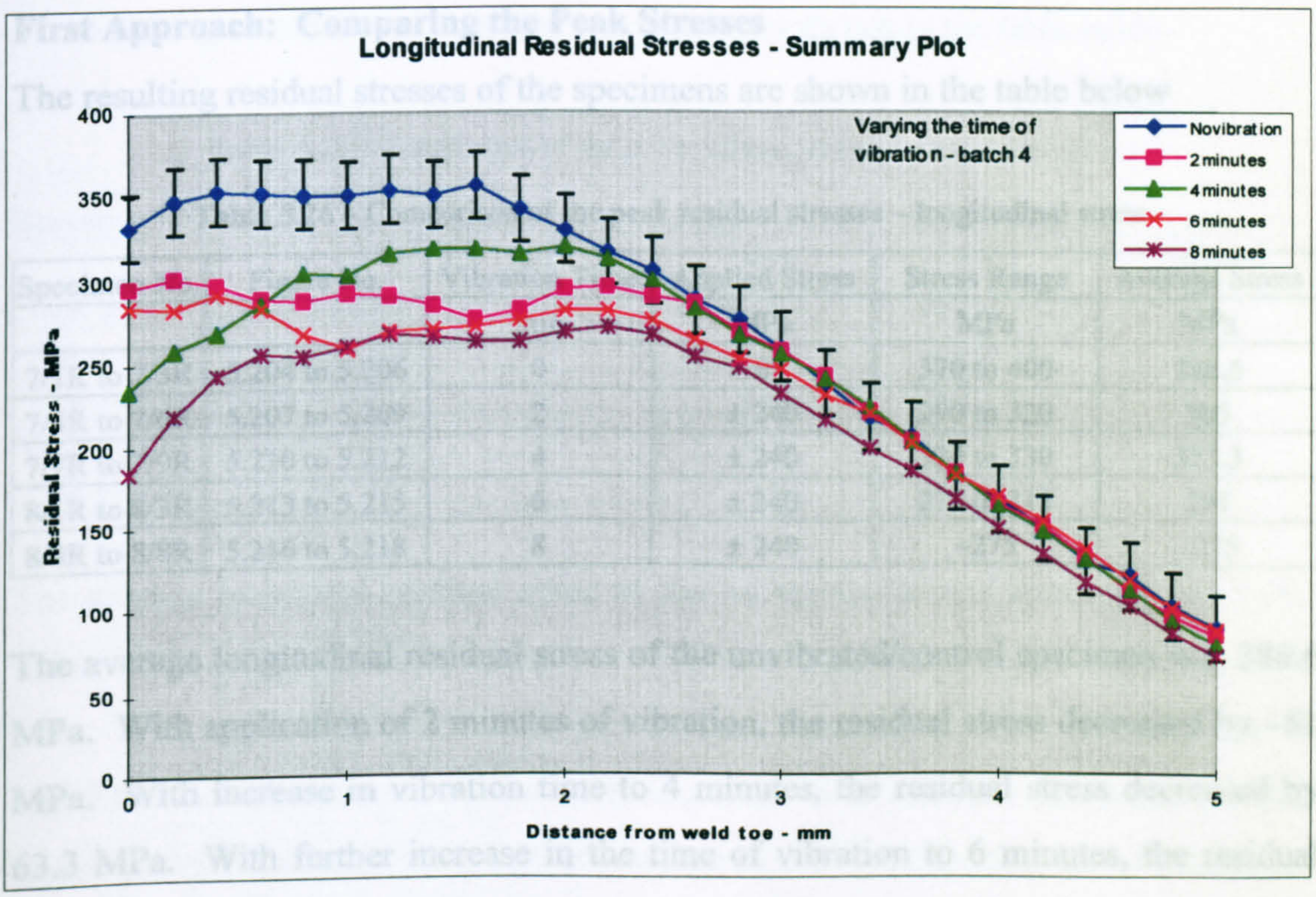

Figure 5.234 – Summary longitudinal residual stresses – batch 4

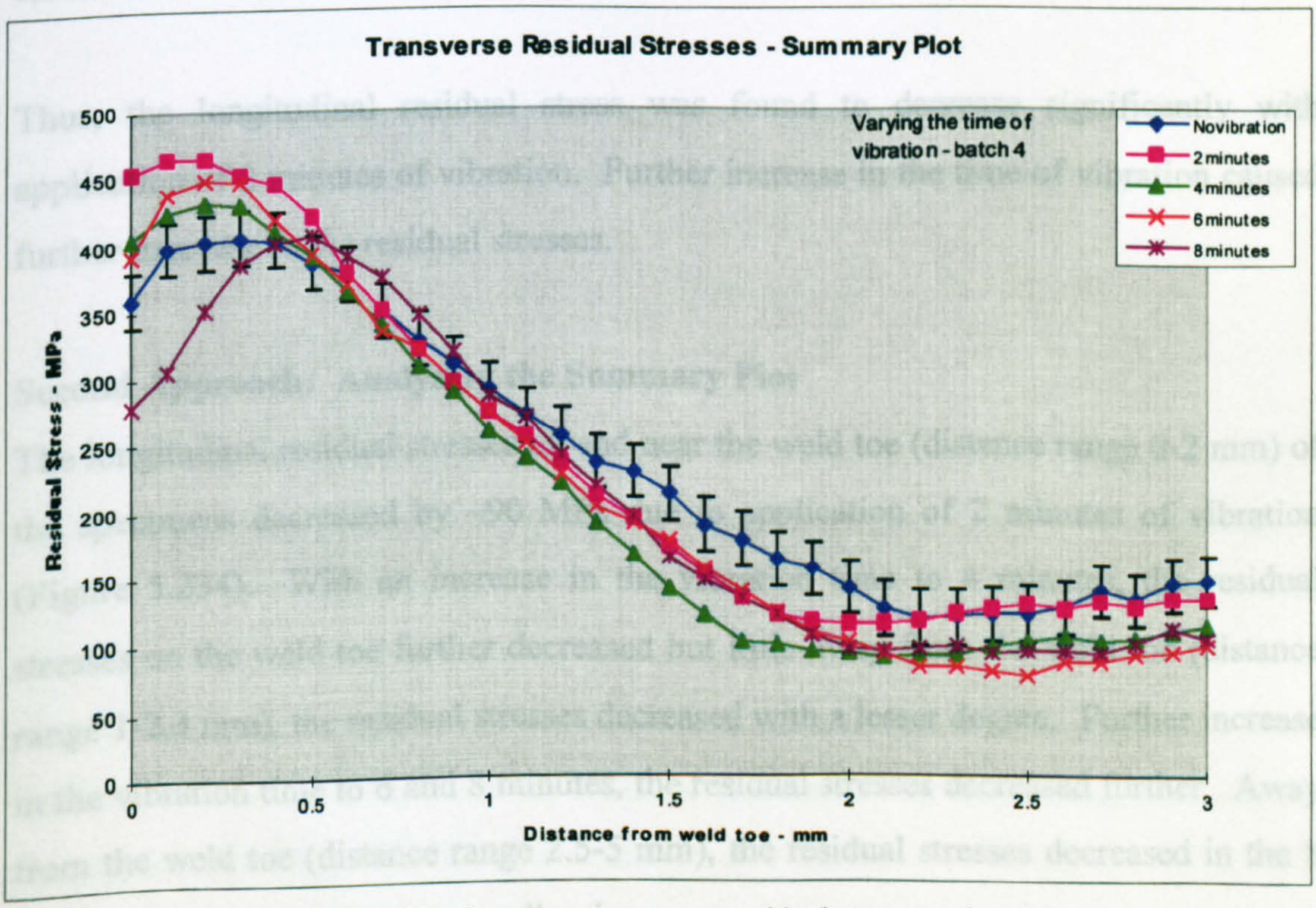

Figure 5.235 – Summary transverse residual stresses – batch 4

Discussion of Result - Batch 4

Longitudinal Stress Plots

First Approach: Comparing the Peak Stresses

The resulting residual stresses of the specimens are shown in the table below

Table 5.26 – Comparison of the peak residual stresses – longitudinal stress

Specimen No.	Figure No.	Vibration Time	Applied Stress	Stress Range	Average Stress
		min	MPa	MPa	MPa
7/1R to 7/3R	5.204 to 5.206	0	0	370 to 400	386.6
7/4R to 7/6R	5.207 to 5.209	2	± 240	290 to 320	305
7/7R to 7/9R	5.210 to 5.212	4	± 240	320 to 330	323.3
8/1R to 8/3R	5.213 to 5.215	6	± 240	275 to 315	291
8/4R to 8/8R	5.216 to 5.218	8	± 240	~275	~275

The average longitudinal residual stress of the unvibrated/control specimen was 386.6 MPa. With application of 2 minutes of vibration, the residual stress decreased by ~81 MPa. With increase in vibration time to 4 minutes, the residual stress decreased by 63.3 MPa. With further increase in the time of vibration to 6 minutes, the residual stress decreased by ~95 MPa. With increase in the vibration time to 8 minutes, the residual stress decreased by ~111.6 MPa.

Thus, the longitudinal residual stress was found to decrease significantly with application of 2 minutes of vibration. Further increase in the time of vibration caused further decrease in the residual stresses.

Second Approach: Analysing the Summary Plot

The longitudinal residual stresses on and near the weld toe (distance range 0-2 mm) of the specimens decreased by ~90 MPa due to application of 2 minutes of vibration (Figure 5.234). With an increase in the vibration time to 4 minutes, the residual stresses on the weld toe further decreased but little away from the weld toe (distance range 1-2.3 mm), the residual stresses decreased with a lesser degree. Further increase in the vibration time to 6 and 8 minutes, the residual stresses decreased further. Away from the weld toe (distance range 2.5-5 mm), the residual stresses decreased in the 8 minutes of vibration, but to a smaller degree.

Transverse Stress Plots

First Approach: Comparing the Peak Stresses

The resulting residual stresses of the specimens are shown in the table below

Table 5.27 – Comparison of the peak residual stresses – transverse stress

Specimen No.	Figure No.	Vibration Time	Applied Stress	Stress Range	Average Stress
		min	MPa	MPa	MPa
7/1R to 7/3R	5.219 to 5.221	0	0	380 to 445	418.3
7/4R to 7/6R	5.222 to 5.224	2	±240	460 to 535	488.3
7/7R to 7/9R	5.225 to 5.227	4	±240	440 to 470	450
8/1R to 8/3R	5.228 to 5.230	6	±240	430 to 500	453.3
8/4R to 8/8R	5.231 to 5.233	8	±240	140 to 430	415

The average transverse residual stress of the unvibrated/control specimen was 418.3 MPa. With application of 2 minutes of vibration, the residual stress increased by 70 MPa. With increase in the vibration time to 4 minutes, the residual stress increased by ~32 MPa. With increase in the vibration time to 6 minutes, the residual stress increased by 35 MPa. With a further increase in the vibration time to 8 minutes, the residual stress was found to be similar to the residual stresses of the unvibrated specimens.

Thus, the transverse residual stresses increased significantly with a smaller time of vibration. Increase in the time of vibration showed increase in the residual stresses but with a lesser degree.

Second Approach: Analysing the Summary Plot

The transverse residual stresses on and near the weld toe (distance range 0-0.5 mm) increased with application of 2 minutes of vibration (Figure 5.235). The specimens vibrated for 4 and 6 minutes showed an increase but with a lesser degree. The specimens vibrated for 8 minutes showed a decrease in residual stresses by ~75 MPa. Little away from the weld toe (distance range 0.5-1.3 mm), the residual stresses were unchanged. Further away from the weld toe (distance range 1.3-3 mm), the residual stresses decreased by ~35 MPa after 4 minutes of vibration.

Thus, on and near the weld toe, the residual stresses increased with small induced stresses and decreased with in high applied stresses. Away from the weld toe the residual stresses decreased with increase in the time of vibration.

Batch 5: Investigation of High Frequency Vibration Effect

In this experiment two specimens were processed in order to investigate the effect of high frequency flexural mechanical vibration on welding residual stress. The specimens were vibrated at a frequency of 341.5 Hz and the applied stress was ~2 MPa. The vibration was started before welding and was continued for 5 minutes from the welding start time. The resulting residual stresses are shown below.

Longitudinal Stress Plots

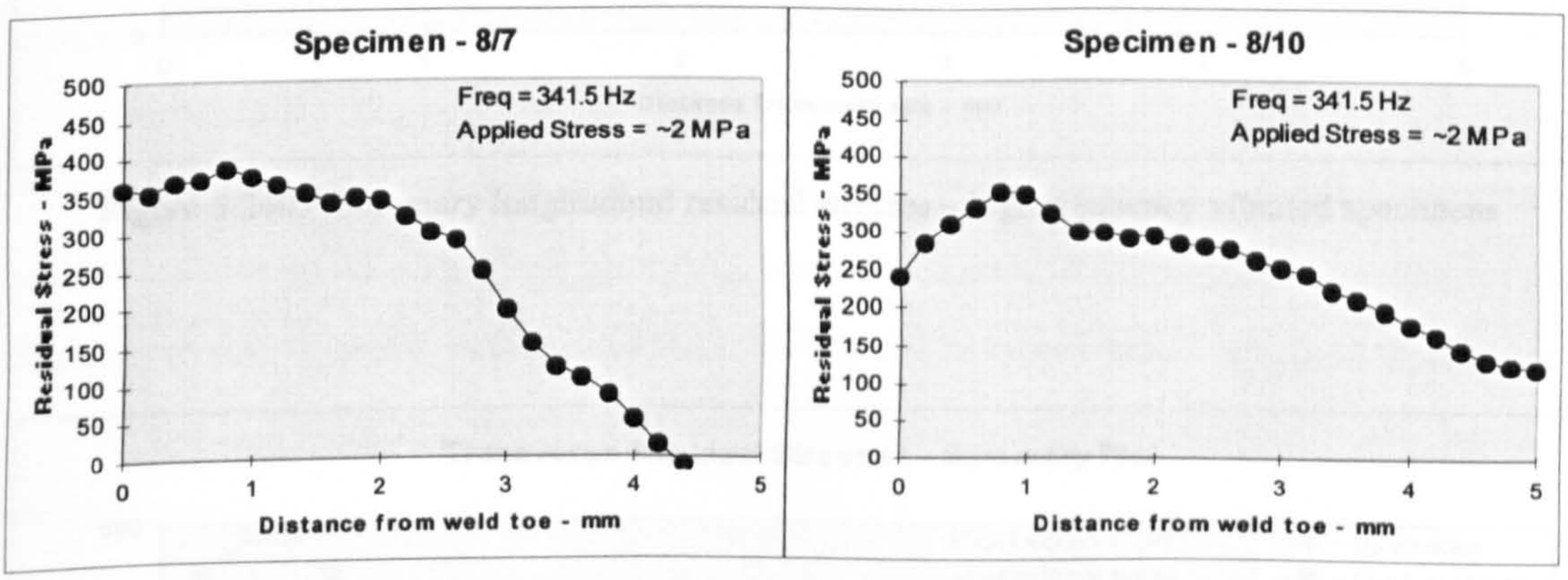

Figure 5.236 and 5.237 - Longitudinal stress plot - specimens 8/7 & 8/10

Transverse Stress Plots

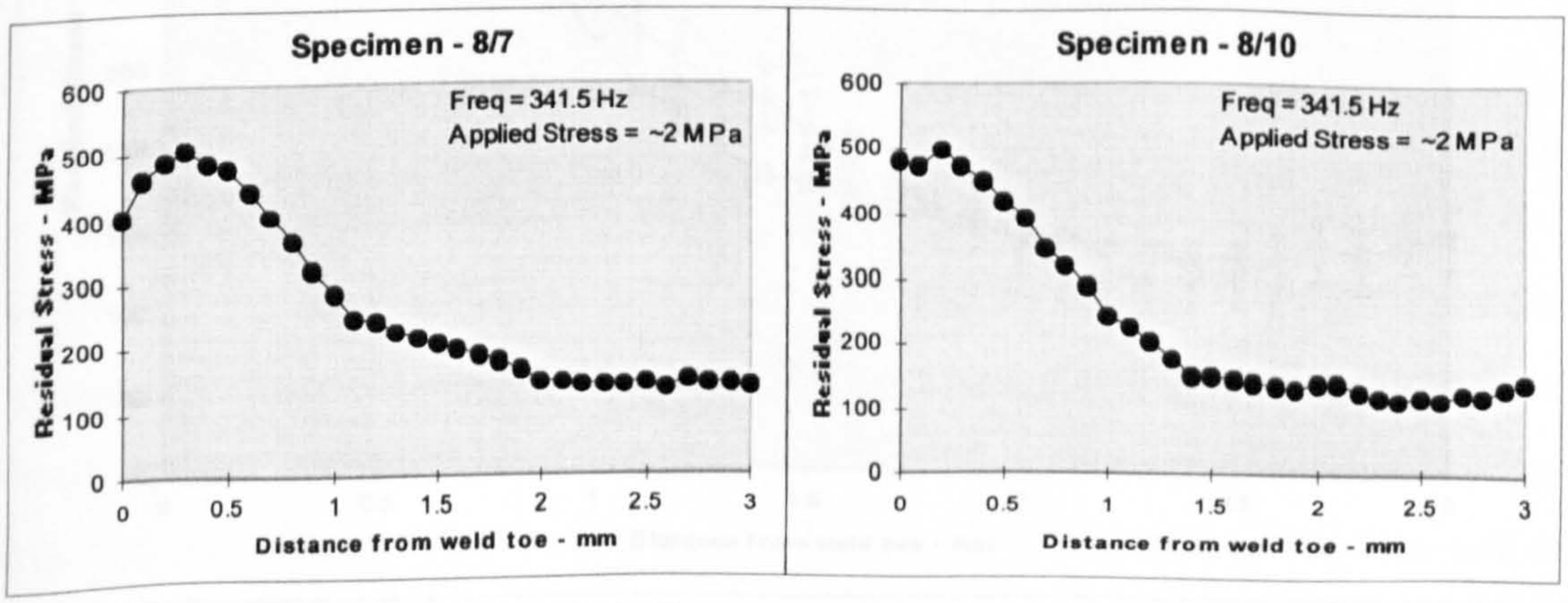

Figure 5.238 and 5.239 - Transverse stress plot - samples 8/7 & 8/10

Summary Plot

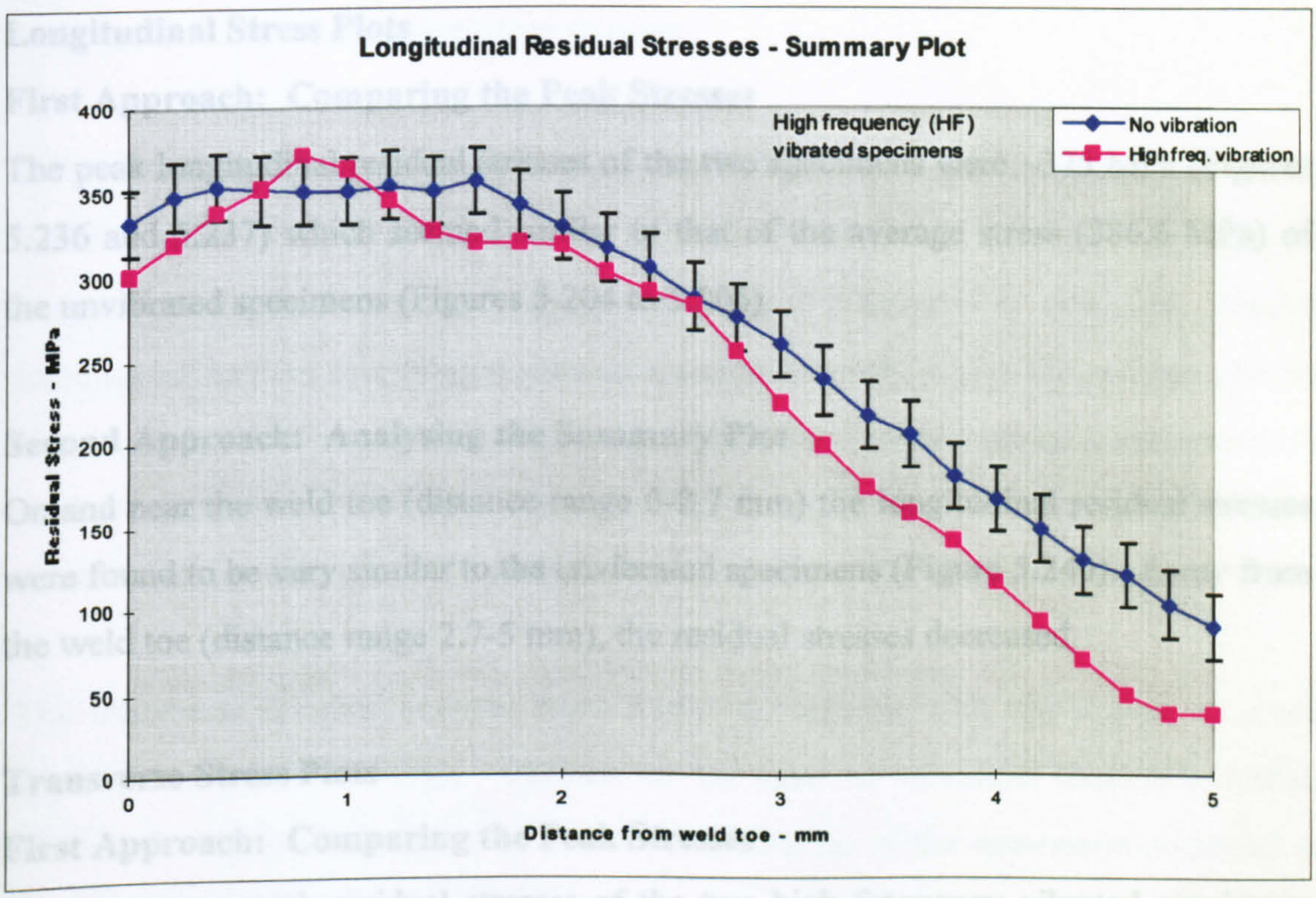

Figure 5.240 – Summary longitudinal residual stresses – high frequency vibrated specimens

Figure 5.241 – Summary transverse residual stresses – high frequency vibrated specimens

Discussion of Results - Batch 5

Longitudinal Stress Plots

First Approach: Comparing the Peak Stresses

The peak longitudinal residual stresses of the two specimens were ~375 MPa (Figures 5.236 and 5.237) which seemed similar to that of the average stress (386.6 MPa) of the unvibrated specimens (Figures 5.204 to 5.206).

Second Approach: Analysing the Summary Plot

On and near the weld toe (distance range 0-2.7 mm) the longitudinal residual stresses were found to be very similar to the unvibrated specimens (Figure 5.240). Away from the weld toe (distance range 2.7-5 mm), the residual stresses decreased.

Transverse Stress Plots

First Approach: Comparing the Peak Stresses

The transverse peak residual stresses of the two high frequency vibrated specimens were found to be ~510 MPa (Figure 5.238 to 5.239), which was higher than that of the average peak residual stresses (418.3 MPa) of the unvibrated specimens (Figures 5.219 to 5.221). It seems that the HF vibration caused an increase in the residual stresses.

Second Approach: Analysing the Summary Plot

The residual stresses on and near the weld toe (distance range 0-0.5 mm) increased by ~85 MPa with application of high frequency (HF) vibration (Figure 5.241). Away from the weld toe no change in the residual stresses were found.

5.3.3.5 Summary of Results

In batch 1, the applied stress to the specimens was varied. The longitudinal residual stresses of the specimens were found to decrease with small applied stresses. With increase in the applied stresses, the residual stresses did not decrease any more. Thus, the small-applied stresses were found to be effective in reducing the longitudinal residual stresses. The transverse residual stresses were found to increase with

application of small stresses, however, the residual stresses were found to decrease with application of higher vibratory stresses.

In batch 2, 3 and 4 the time of vibration was varied. The applied stresses to the three batches were ±80 MPa, ±160 MPa and ±240 MPa. In all three batches the longitudinal residual stresses decreased in the first 2 minutes of vibration. Further increase in the time of vibration showed a confused result, where the residual stresses were found to increase and also decrease. The three different stress levels showed a similar reduction in the residual stresses. This concludes that the longitudinal residual stress decreases with small vibratory induced stresses applied for a short time.

The transverse residual stresses were found to increase with application of small applied stresses (±80 MPa). Increase in the time of vibration showed a further increase in the residual stresses. The residual stresses of the specimens subjected to ±160 MPa applied stresses showed an increase in the residual stresses but with a lesser degree in comparison to the specimens subjected to applied stress ±80 MPa. With increase in the time of vibration caused a further increase in the residual stresses. The specimens subjected to applied stresses of ±240 MPa also showed an increase in the residual stresses on and near the weld toe. With increase in the time of vibration, the residual stresses decreased. Away from the weld toe the residual stresses decreased with increase in time of vibration. Thus, the transverse residual stresses were found to increase with increase in the time of vibration when the induced stress was small and found to decrease when the induced stress was large.

In application of high frequency vibration, the longitudinal and transverse both residual stresses were found to increase. The reason of this increment is unknown.

Similar to experiment I and II, the yield stress of the as rolled bar was 611 MPa. Due to welding the yield stress was decreased to ~0 MPa at ~1300 ^{0}C. The yield stress was increased in a non-linear pattern from ~0 MPa to 350 MPa over the wide range of the temperature decrease from 1300 ^{0}C to 20 ^{0}C (Figure 5.334).

5.3.4 Experiment IV: Flexural Vibration Test – Four Roller Supported Beam

Abstract

In this experiment, two identical metal bars were welded together using a single pass weld while they were being vibrated. Both time and amplitude of vibration were varied to observe their effect. Two groups of specimens were processed. In the first group, the time of vibration was varied, the residual stress was found to increase and decrease with increase in the time of vibration, where no particular trend was present. In the second group, the amplitude of vibration was varied, and similar to the previous, the results showed no particular trend. In both groups, away from the weld toe, the residual stress was found to decrease due to the treatment.

5.3.4.1 Introduction

This experiment was designed to observe the effect of flexural motion vibration during welding. In the previous experiments a bead weld was carried out on a 76.2 mm by 6.35 mm cross-section steel plate during vibration. In this experiment, two pieces of metal were joined together with a single pass weld thus simulating a real weld. The vibration was applied to the specimens while they were being welded. The cross section of the material used was kept the same as the previous experiments. Aoki & Nishimura [7], Maekawa [90] and Nakagiri [99] used a combined mode (longitudinal and flexural) of vibration in their study and found significant reduction in the residual stresses. In this study it was decided to apply pure flexural vibration to the specimens to observe its effect. In order to flexurallly vibrate these specimens a new experimental set-up was prepared. The details of the set-up are provided in the next section.

5.3.4.2 Experimental Procedure

In this experimental set-up, four sets of rollers were used - two used to vibrate the specimens and the other two hold the specimen in position. The rollers were fitted to vibrating/holding jigs and were guided by a set of compression springs. The specimens were inserted into the jigs and the compression springs tightened them using screws. The springs were compressed almost fully in order to hold the specimens tightly. The used springs tightened the specimens but it did not make them so rigid that it prevents the rotational movement of the specimens caused by the flexural vibration.

While carrying out this experiment, it was found that this set-up was not capable of applying high dynamic stress to the specimen during welding, because at high amplitudes of vibration, the molten metal solidified in a distorted shape. Thus, the set-up had to be modified to overcome the problem. To obtain the optimum condition, the set-up was changed twice and these changes are discussed later. In the first set-up, the end rollers were fixed to the frame and the middle rollers were vibrated. During welding, the specimens were vibrated in different situations to observe its effects on the welding residual stresses. The first experimental set-up is shown in Figure 5.242 below.

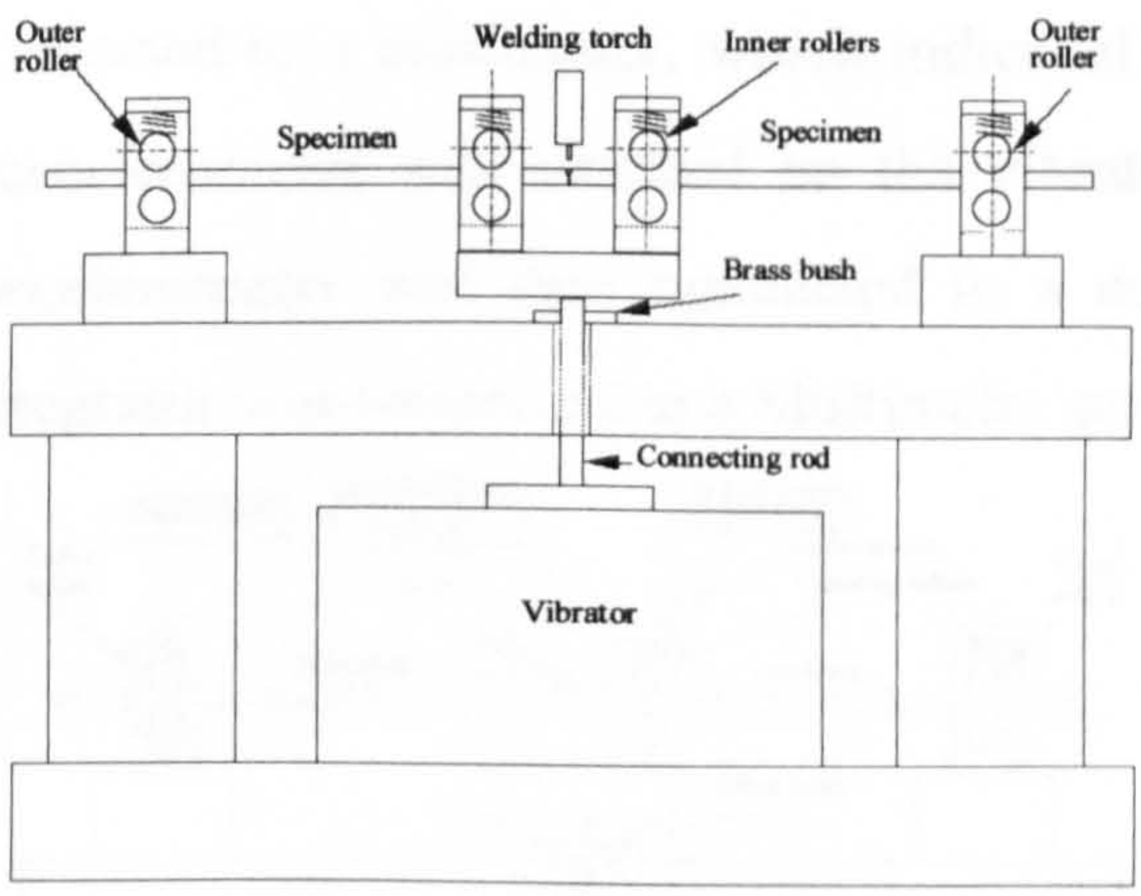

Figure 5.242 - Experimental set-up #1 - flexural vibration test

The welding torch was supported and controlled in the same manner as that described in previous experiment. The specimens cooled down to room temperature and the residual stresses were measured using the X-ray diffractometer. The X-ray measurement conditions were similar to that shown in Table 5.10. A single exposure technique (SET) was used, where a line map was measured on the selected line shown in Figure 5.243. In the residual stress measurement, a specially prepared jig was used to locate the specimen on the goniometer table where a six-point locator was used. A screw clamp was used to secure the specimen to the jig. The measurement jig for these specimens is shown in Appendix II.

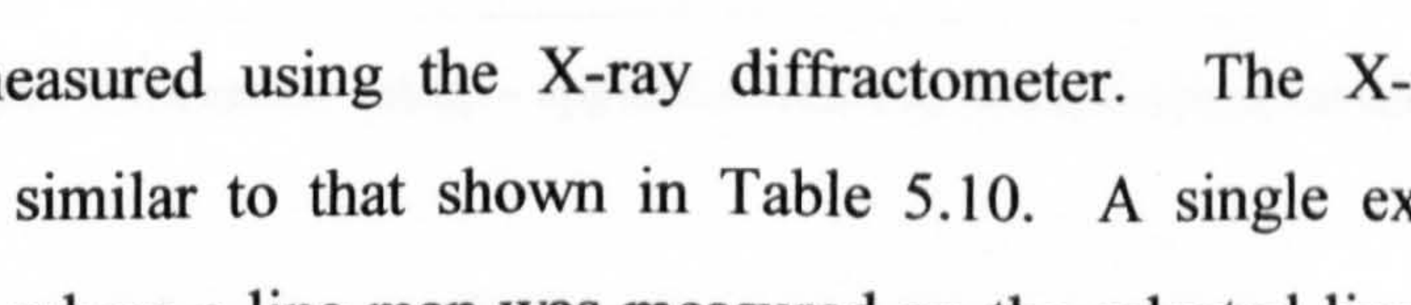

Figure 5.243 - Residual stress measurement lines on the specimens

5.3.4.3 Calibration of Induced Stresses

The calibration of induced stress was carried out on the same set-up. A strain gauge was attached at the mid-width and near the weld (on line A in Figure 5.243) of the steel plate such that the bending stress in the longitudinal direction was measured. The specimen was then inserted and tightened on the set-up shown in Figure 5.244. It was necessary to set the strain gauge between the two inner rollers, not necessarily at the mid-length between the rollers, because the set-up was designed to produce a constant bending moment throughout the length between the two inner rollers. The strain gauge was connected to a calibrated P-3500 digital strain indicator. The output of the P-3500 strain indicator was connected to a multimeter, which indicated the RMS value of the dynamic strain. An accelerometer was attached on the vibrating head as shown in Figure 5.244. The accelerometer was then connected to a double integrator. The output of the double integrator was connected to a Multimeter set to the RMS output.

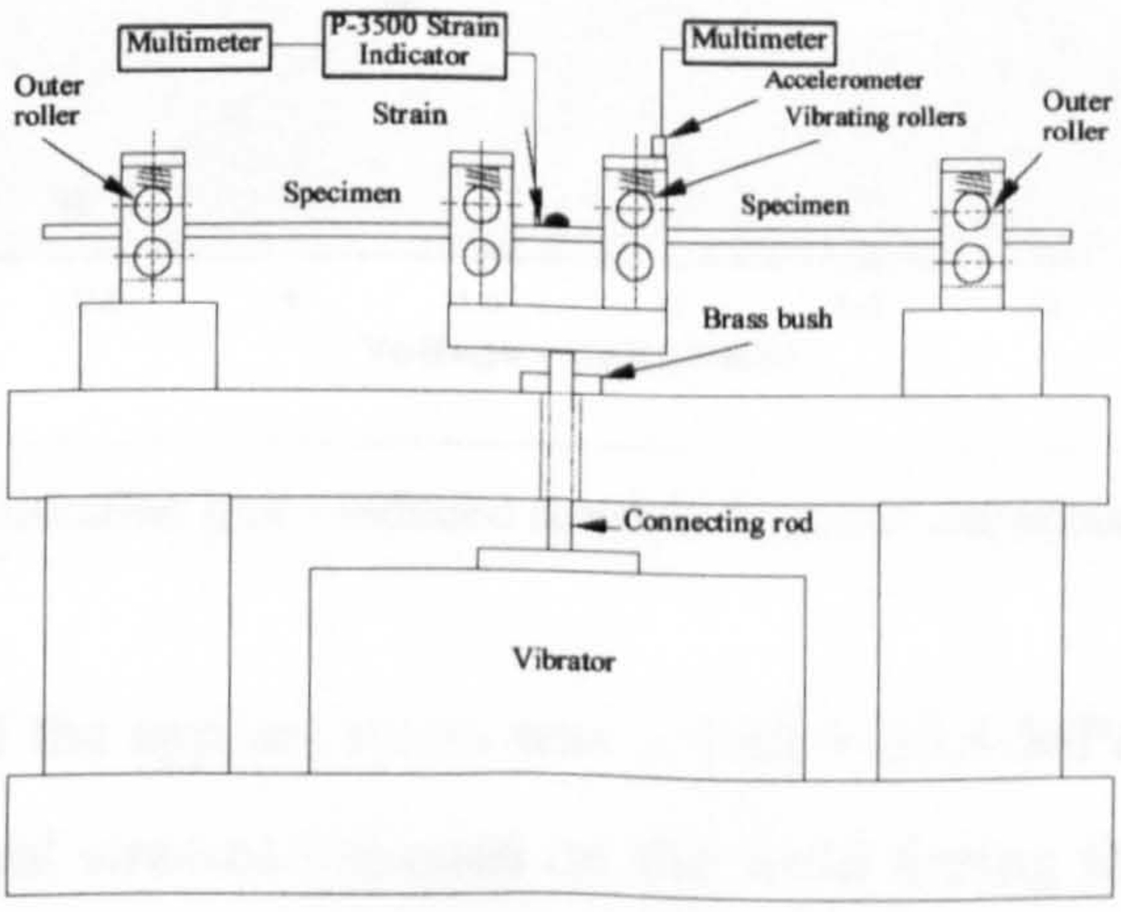

Figure 5.244 - Calibration set-up - applied stresses in flexural vibration during welding

In the calibration the frequency of vibration was kept constant and the amplitude was increased in several steps and the corresponding values of strains and displacements (on the jig) were recorded from the multimeter. The RMS strain was converted to peak stress using the pre-determined Modulus of Elasticity. Then the peak stresses were plotted against the deflection amplitudes (in RMS) which gave the calibrated induced stress values in terms of deflection. The data of the calibration and the calibration plot are shown in Table 5.28 and Figure 5.245.

Table 5.28 - Calibration table - induced dynamic stress for true flexural vibration. Double Integrator, S/N - 786. Accelerometer - 31795

Micro Strain	Strain	Stress	Displacement	Applied Stress
MV (RMS)		MPa (pk)	mV (RMS)	MPa
9	6.18E-05	13.02118	0.419	13.02118
27	0.000185	39.06353	0.861	39.06353
46	0.000316	66.55268	1.288	66.55268
69	0.000474	99.82902	1.742	99.82902
86	0.000591	124.4246	2.191	124.4246
105	0.000721	151.9137	2.616	151.9137
122	0.000838	176.5093	3.018	176.5093

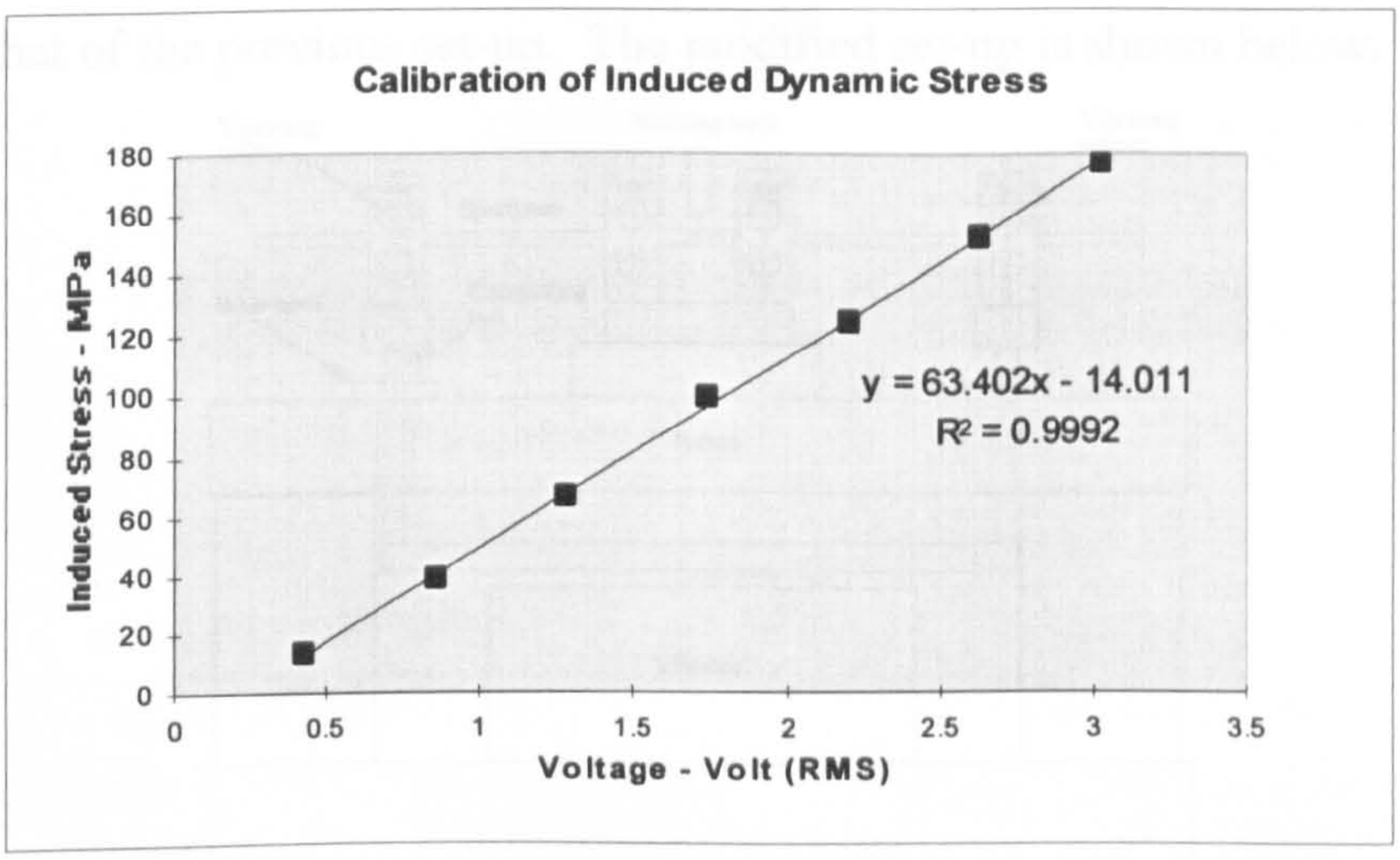

Figure 5.245 - Calibration plot - induced stress in terms of deflection of the specimen

The calibrated value of the applied stress was 1 Volt = 63.4 MPa. It should be bear in mind here that the actual stresses imposed on the weld during the cooling process will be quite different from this calibrated value. Nevertheless, to enable similar amounts of vibration to be given to the different welds, the approach is acceptable.

5.3.4.4 Experimental Results

In this experiment, three different set-ups were used. In set-up #1, two batches of specimens (batch 1 and 2) were processed. In set-up #2, batch 3 was processed. In batch 1, 2 and 3, the time of vibration was varied and in all three batches, a similar result was found. Thus, instead of all three batches, batch 3 is shown here. In batch 4, the set-up was again modified (set-up #3) where the amplitude of vibration was varied and is also shown here.

Set-up #2

In the previous set-up it was not possible to induce higher dynamic stress to the specimens because at the higher amplitudes the weld was deforming. After observing this it was decided to modify the set-up to induce higher stress in the weld region - without higher amplitude of weld pool vibration. It was decided to apply vibration at the two end rollers instead of the two inner rollers. The inner rollers were fixed to the frame. The calibration of applied stress relating to this set-up was carried out in a fashion to that of the previous set-up. The modified set-up is shown below.

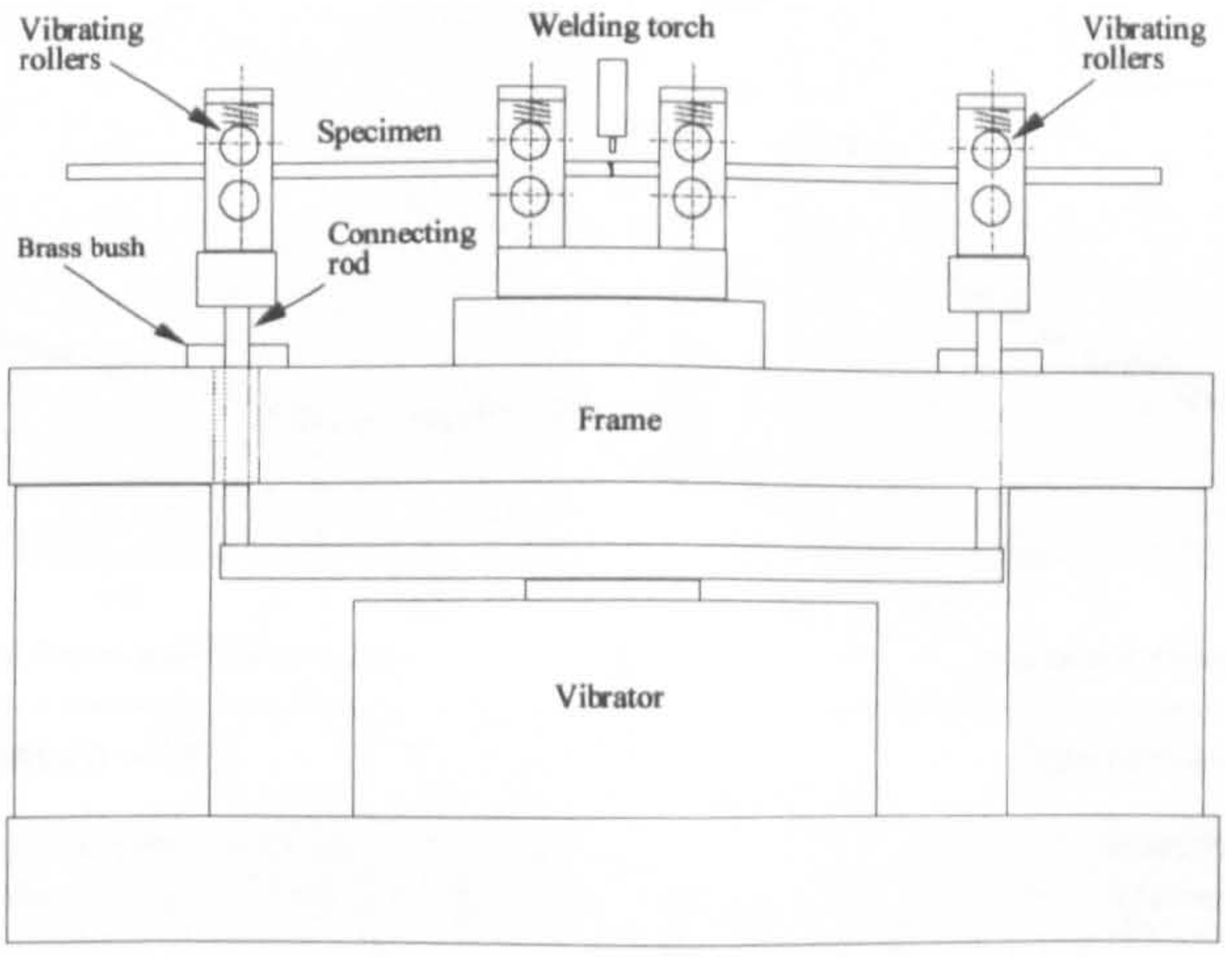

Figure 5.246 – Flexural vibration treatment of flat bar – set-up #2

Batch 3

In this batch fifteen specimens were processed (three in a sample). Keeping the applied stress and frequency at 61.08 MPa and 25 Hz respectively the time of vibration was varied. The first sample was welded without vibration. The next sample was vibrated during welding only. In the next three samples, the time of vibration was increased from 30 seconds to 1.5 minutes as shown in the plots. As shown in Figure (5.243), two lines were selected to measure the residual stresses and the results are shown below.

Transverse Residual Stresses of line A

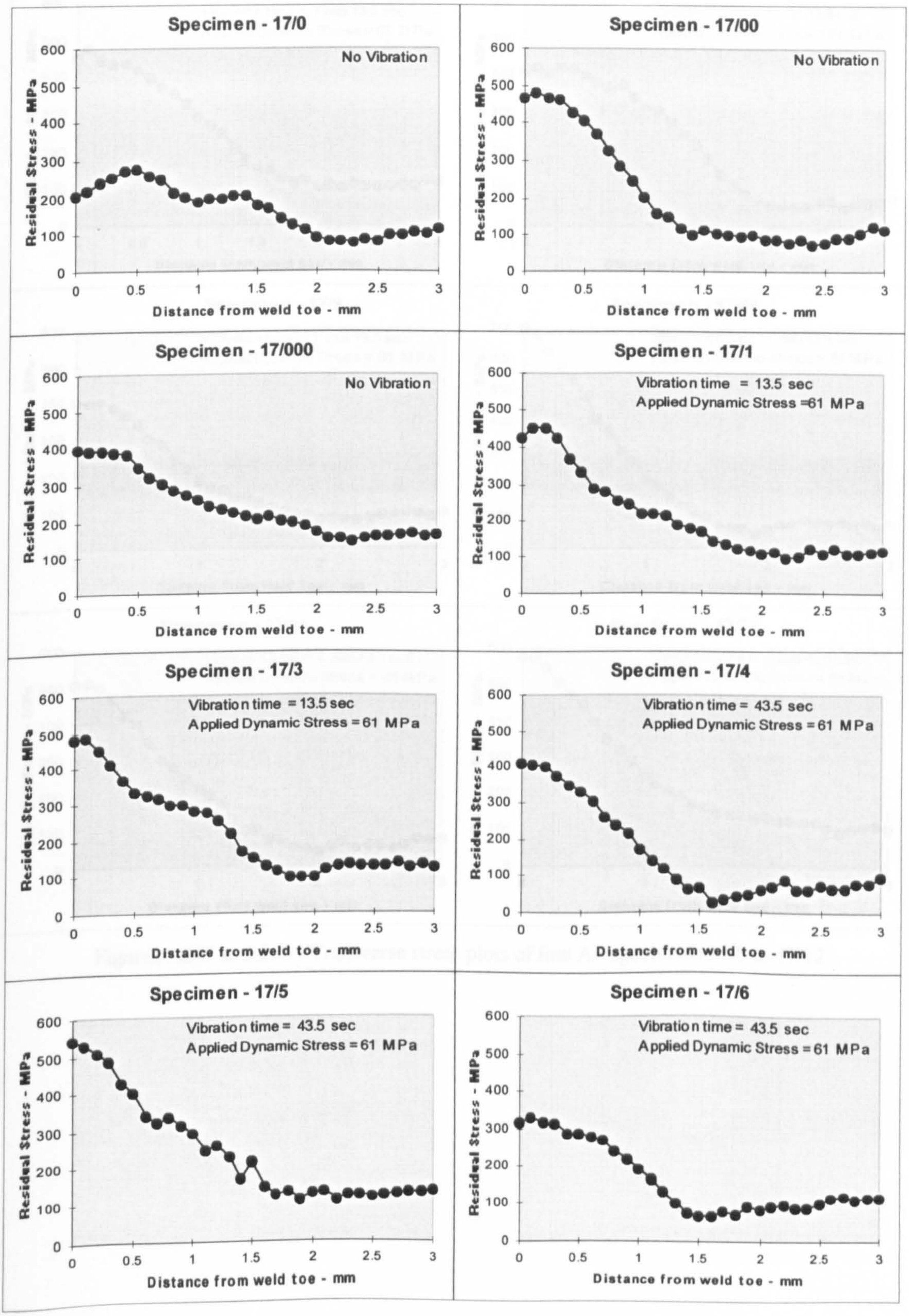

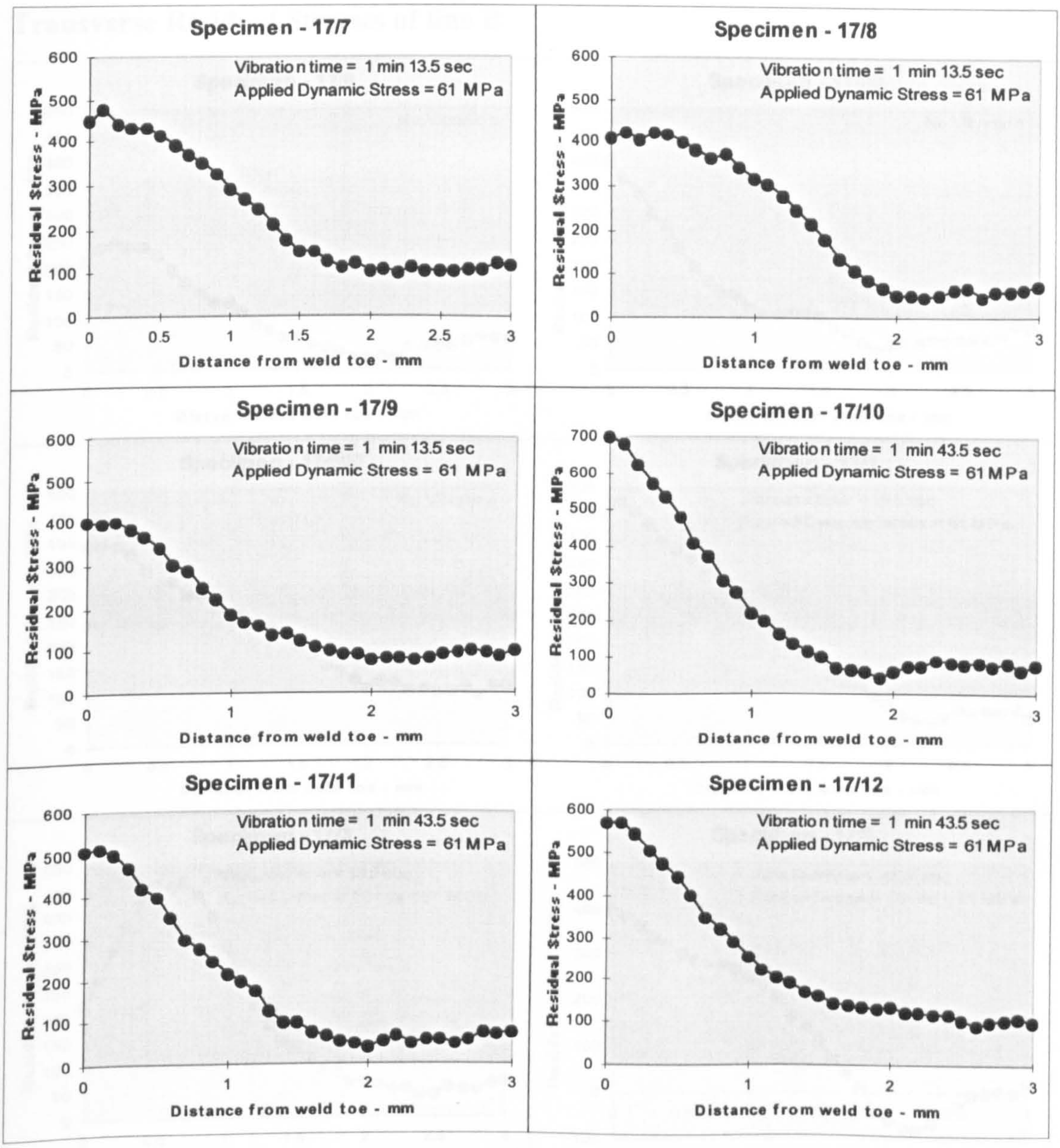

Figures 5.247 to 5.260 - Transverse stress plots of line A - specimens 17/0 to 17/12

Transverse Residual Stresses of line B

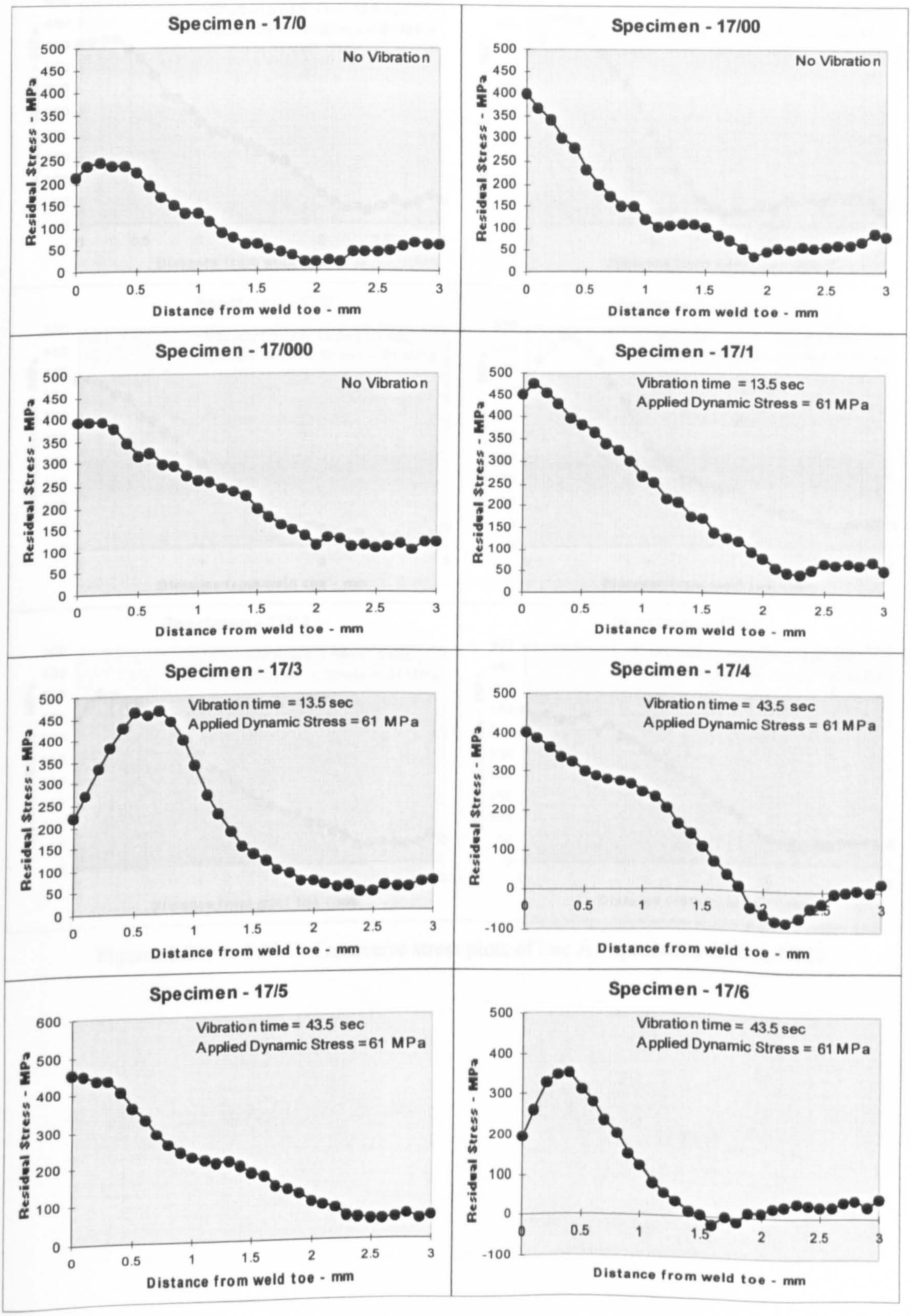

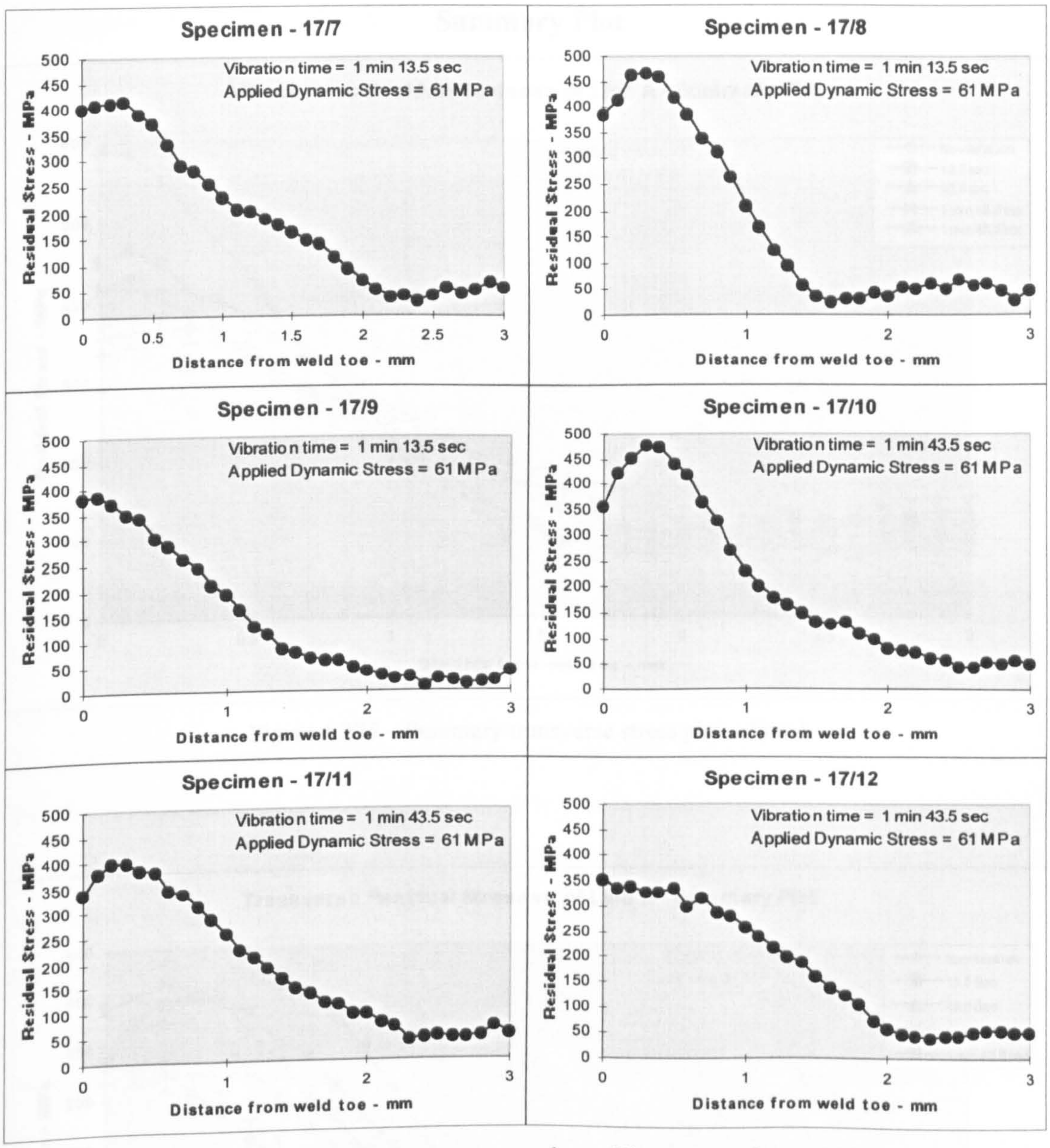

Figures 5.261 to 5.274 - Transverse stress plots of line A - specimens 17/0 to 17/12

Summary Plot

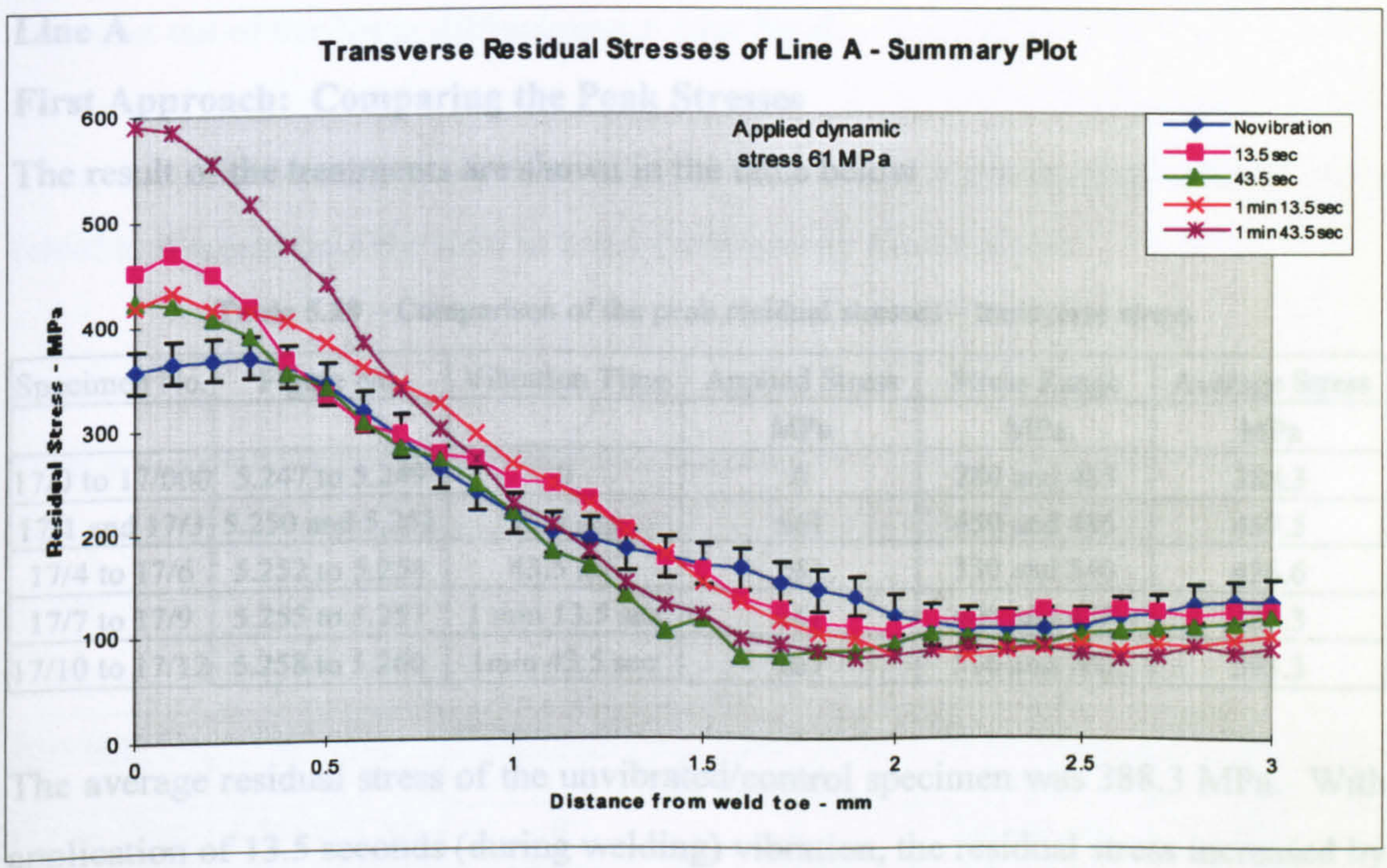

Figure 5.275 – Summary transverse stress plot – line A

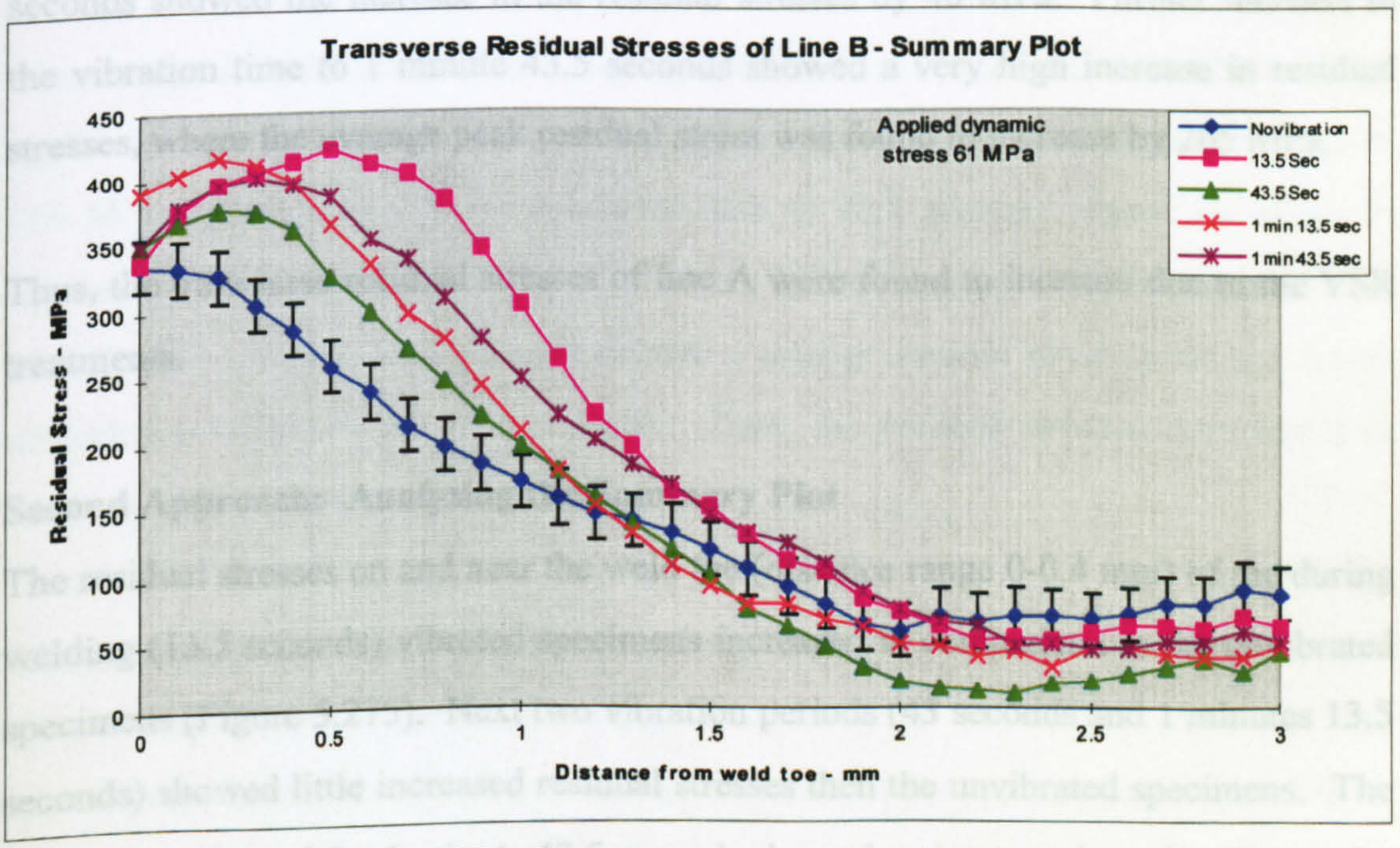

Figure 5.276 – Summary transverse stress plot – line B

Discussion of Results - Batch 3

Line A

First Approach: Comparing the Peak Stresses

The result of the treatments are shown in the table below

Table 5.29 – Comparison of the peak residual stresses – transverse stress

Specimen No.	Figure No.	Vibration Time	Applied Stress	Stress Range	Average Stress
			MPa	MPa	MPa
17/0 to 17/000	5.247 to 5.249	0	0	280 and 485	388.3
17/1 and 17/3	5.250 and 5.251	13.5 sec	±61	450 and 485	467.5
17/4 to 17/6	5.252 to 5.254	43.5 sec	±61	330 and 540	426.6
17/7 to 17/9	5.255 to 5.257	1 min 13.5 sec	±61	400 and 475	428.3
17/10 to 17/12	5.258 to 5.260	1min 43.5 sec	±61	510 and 700	593.3

The average residual stress of the unvibrated/control specimen was 388.3 MPa. With application of 13.5 seconds (during welding) vibration, the residual stress increased by 79.2 MPa. The increase in the vibration time to 43.5 seconds showed an increase in the residual stresses by 38.3 MPa. Further increase in vibration time to 1 minute 13.5 seconds showed the increase in the residual stresses by 40 MPa. Further increase in the vibration time to 1 minute 43.5 seconds showed a very high increase in residual stresses, where the average peak residual stress was found to increase by 205 MPa.

Thus, the transverse residual stresses of line A were found to increase due to the VSR treatments.

Second Approach: Analysing the Summary Plot

The residual stresses on and near the weld toe (distance range 0-0.4 mm) of the during welding (13.5 seconds) vibrated specimens increased in comparison to the unvibrated specimens (Figure 5.275). Next two vibration periods (43 seconds and 1 minutes 13.5 seconds) showed little increased residual stresses then the unvibrated specimens. The specimens vibrated for 1 minute 43.5 seconds showed an increase in residual stress by ~220 MPa in comparison to the unvibrated specimens. In the distance range 0.4–1.3 mm a very confusing stresses were found, where no particular trend was present. Away from the weld toe (distance range 1.3-3 mm), the residual stresses decreased

with application of vibration but with a lesser degree – the change in residual stresses were just out of the X-ray diffractometer error band.

Thus, a mixed result was observed in this batch, where the residual stresses were found to increase near the weld to and decrease away from the toe.

Line B

First Approach: Comparing the Peak Stresses

The result of the residual stresses are shown in the table below

Table 5.30 – Comparison of the peak residual stresses – transverse stress

Specimen No.	Figure No.	Vibration Time	Applied Stress	Stress Range	Average Stress
			MPa	MPa	MPa
17/0 to 17/000	5.261 to 5.263	0	0	245 and 410	351.5
17/1 and 17/3	5.264 and 5.265	13.5 sec	±61	460 and 475	467.5
17/4 to 17/6	5.266 to 5.268	43.5 sec	±61	345 and 460	401.6
17/7 to 17/9	5.269 to 5.271	1 min 13.5 sec	±61	385 and 470	425
17/10 to 17/12	5.272 to 5.274	1min 43.5 sec	±61	350 and 475	406.6

The average residual stress of the unvibrated/control specimens was 351.5 MPa. With application of 13.5 seconds (during welding) vibration, the residual stress increased by 116 MPa. An increase in the vibration time to 43.5 seconds caused the stress to increase by 50 MPa. Further two increments in the vibration time to 1 minute 13.5 seconds and 1 minute 43.5 seconds showed a similar residual stress to the specimens subjected to vibration for 43.5 seconds. Thus, the residual stresses were found to increase with application of vibration.

Second Approach: Analysing the Summary Plot

The residual stresses of the distance range 0-1.4 mm from the weld toe increased with application of 13.5 sec (during welding) vibration, where a maximum increase of ~185 MPa was found (Figure 5.276). Further increase in vibration time to 43.5 sec, 1 min 13.5 sec and 1 min 43.5 sec showed increase in the residual stresses but with a lesser degree. In the distance range of 1.4-1.9 mm the residual stresses increased and decreased with application of vibration, where no particular trend was observed. In

the distance range 1.9-3 mm the residual stresses decreased with application of vibration, where the maximum decrease of ~60 MPa was observed and that occurred the in vibration time of 43.5 seconds. Thus, similar to line A the residual stresses were found to increase on and near the weld toe and away from the weld toe the residual stresses were found to decrease.

Set-up #3

Changing the set-up by end vibration in set-up #2, the applied stress situation was improved but still the same problem remained in increasing the applied stresses, it was not possible to increase the applied stress above ~60 MPa. To improve this situation another trial was given, this time the distance between the two inner roller sets were decreased from 9 cm to 6 cm, to decrease the weld pool vibration amplitude. The modified set-up is shown in Figure 5.277. The calibration of the new set-up was carried out, where the calibrated value was 1 Volt = 62.76 MPa.

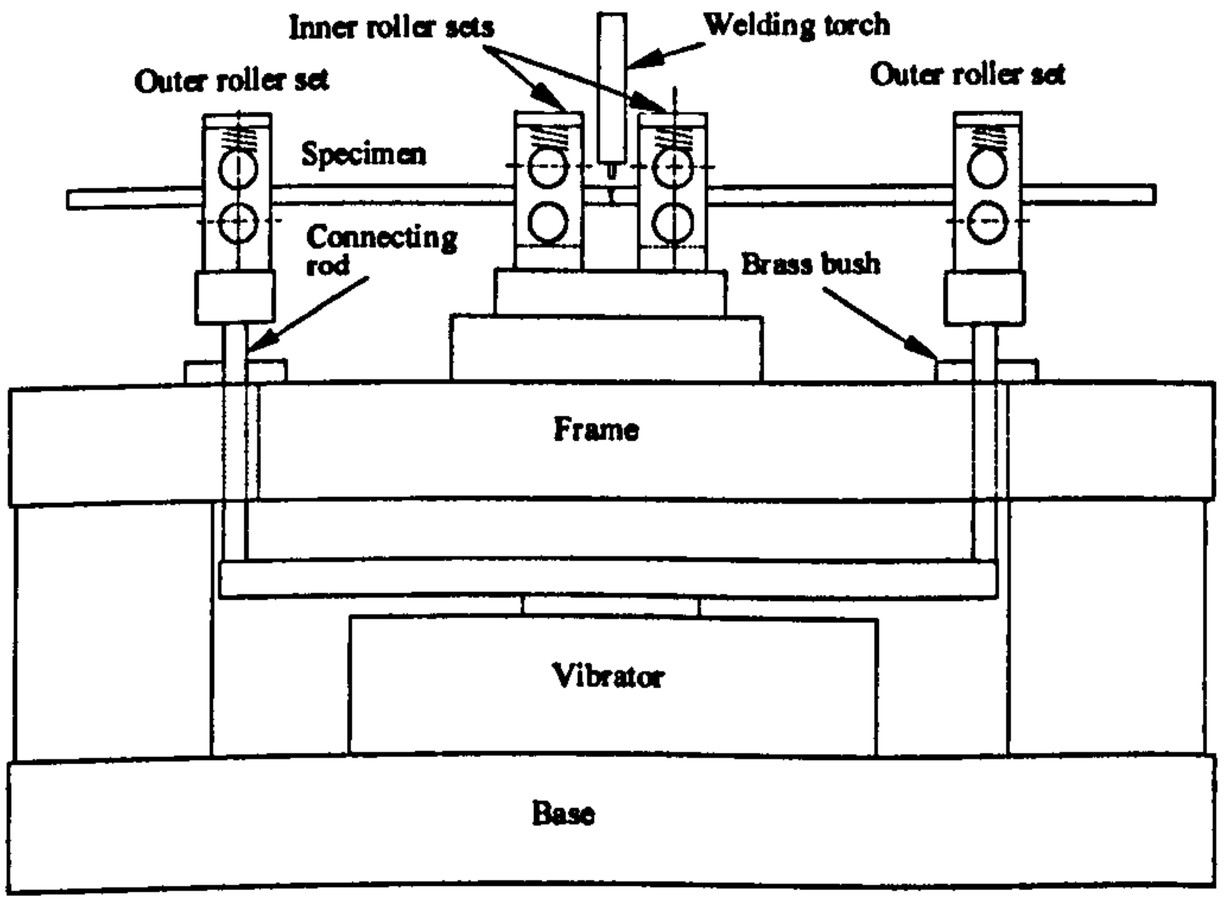

Figure 5.277 - Modified set-up for flexural motion vibration test – set-up #3

Batch 4

In this batch, twenty-eight specimens were processed. Keeping the frequency constant to 25 Hz, the amplitude of vibration was varied. The vibration time was kept constant to 3 minutes 13.5 seconds. Three specimens were welded without any vibration. Others were vibrated in different intervals and are shown in the plots. During vibration in stress level 64.76 MPa the specimens broke. The transverse residual stresses of line A and line B (Figure 5.243) were measured.

Residual Stresses of line A

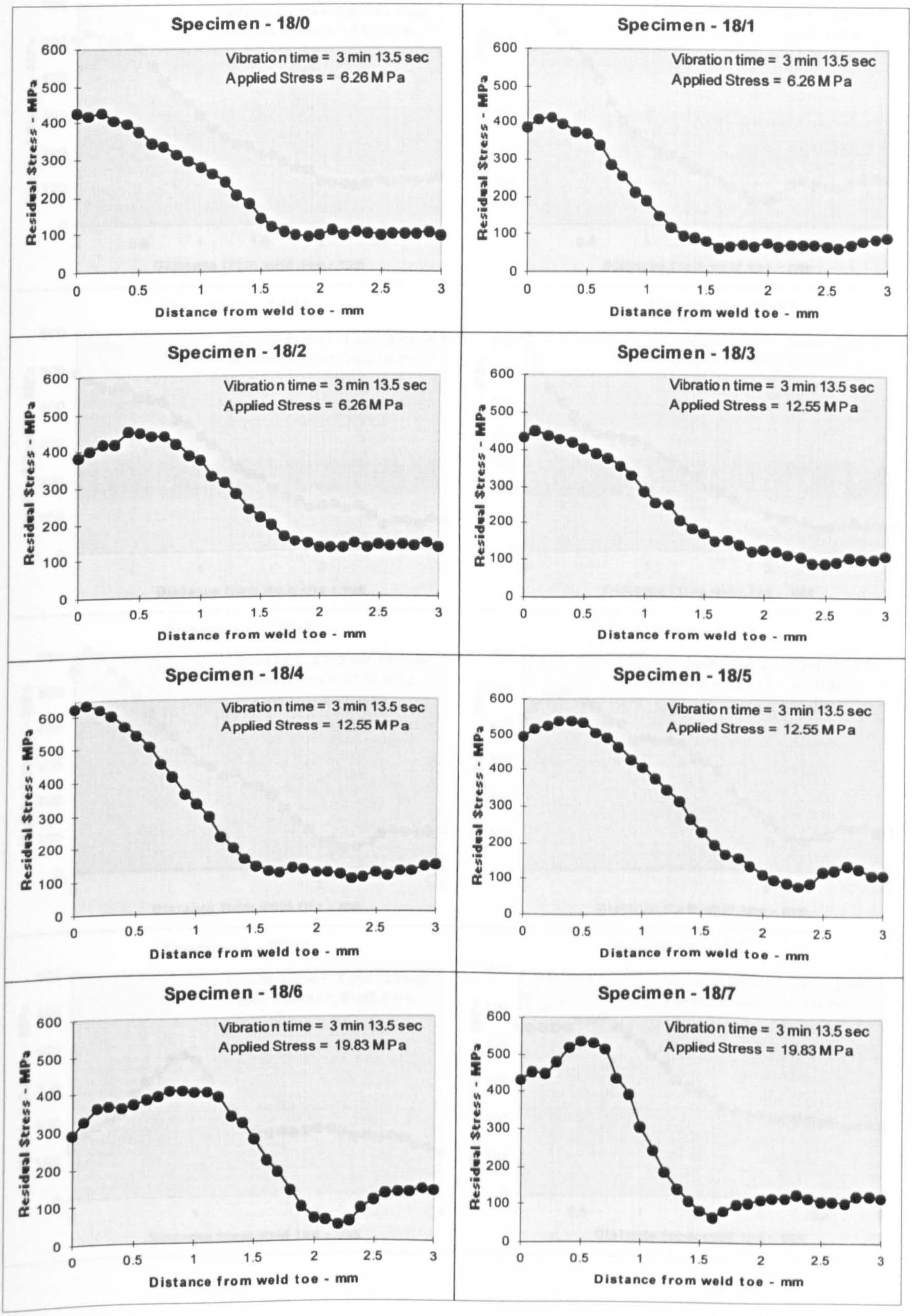

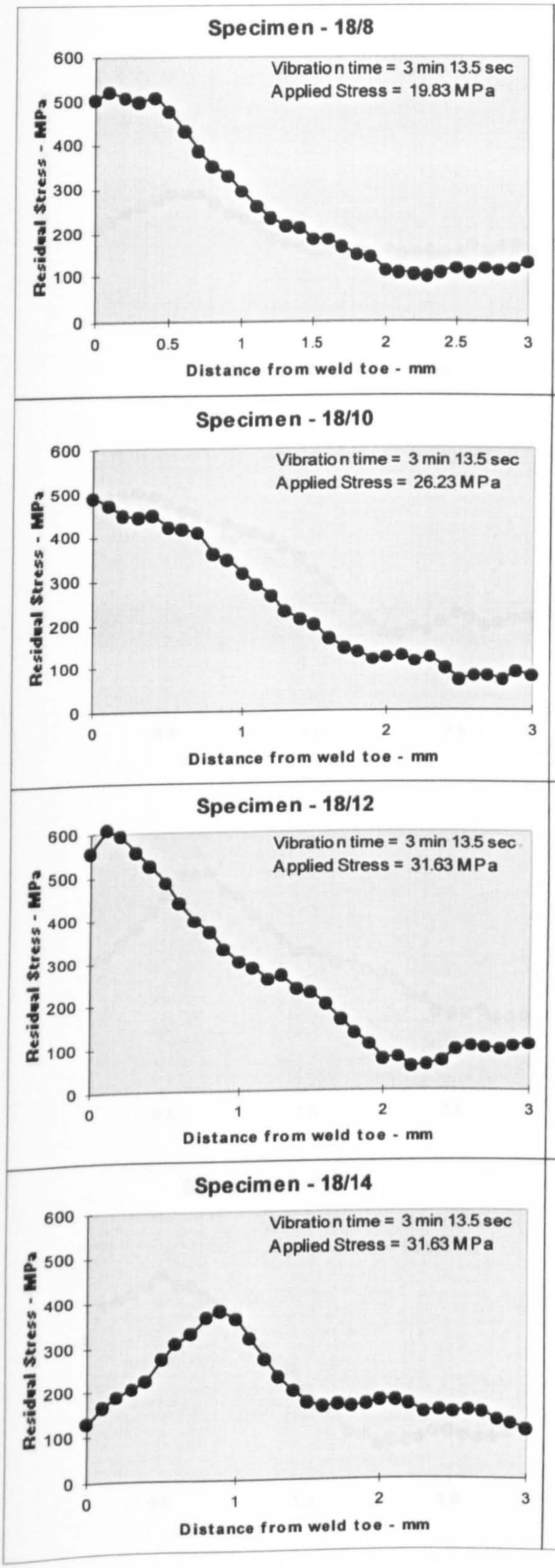
Specimen - 18/8
Vibration time = 3 min 13.5 sec
Applied Stress = 19.83 MPa
Residual Stress - MPa
Distance from weld toe - mm

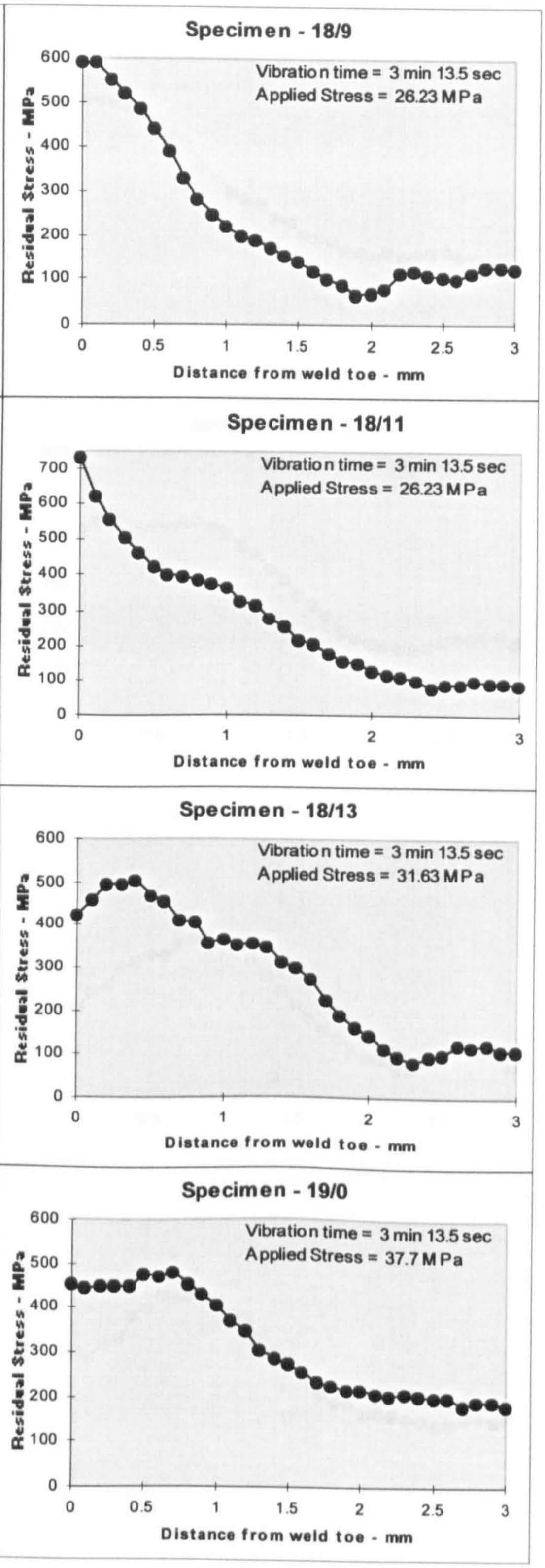
Specimen - 18/9
Vibration time = 3 min 13.5 sec
Applied Stress = 26.23 MPa
Residual Stress - MPa
Distance from weld toe - mm

Specimen - 18/10
Vibration time = 3 min 13.5 sec
Applied Stress = 26.23 MPa
Residual Stress - MPa
Distance from weld toe - mm

Specimen - 18/11
Vibration time = 3 min 13.5 sec
Applied Stress = 26.23 MPa
Residual Stress - MPa
Distance from weld toe - mm

Specimen - 18/12
Vibration time = 3 min 13.5 sec
Applied Stress = 31.63 MPa
Residual Stress - MPa
Distance from weld toe - mm

Specimen - 18/13
Vibration time = 3 min 13.5 sec
Applied Stress = 31.63 MPa
Residual Stress - MPa
Distance from weld toe - mm

Specimen - 18/14
Vibration time = 3 min 13.5 sec
Applied Stress = 31.63 MPa
Residual Stress - MPa
Distance from weld toe - mm

Specimen - 19/0
Vibration time = 3 min 13.5 sec
Applied Stress = 37.7 MPa
Residual Stress - MPa
Distance from weld toe - mm

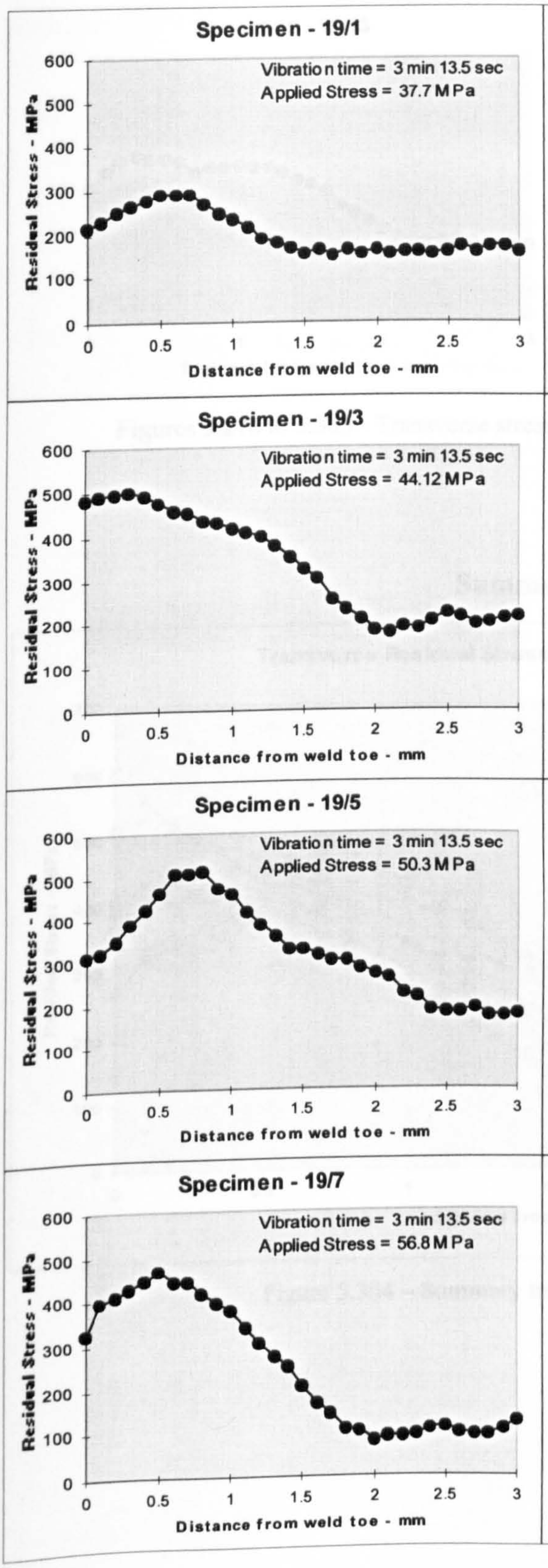
Specimen - 19/1
Vibration time = 3 min 13.5 sec
Applied Stress = 37.7 MPa
Residual Stress - MPa
Distance from weld toe - mm

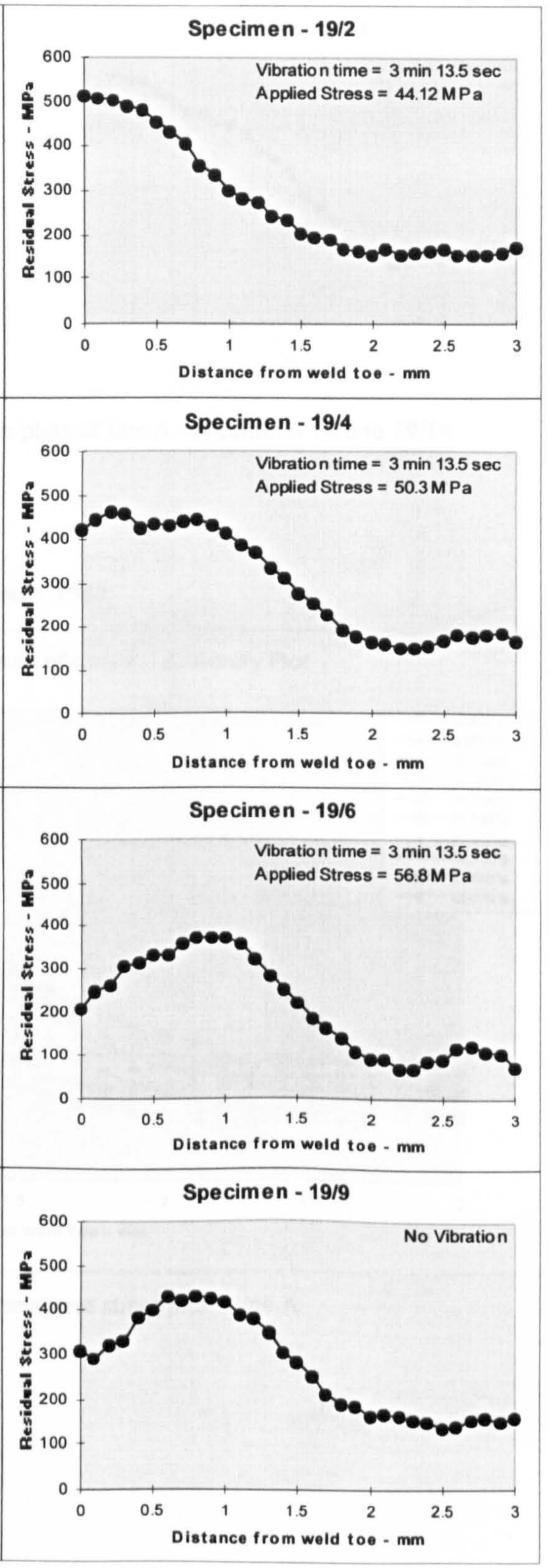
Specimen - 19/2
Vibration time = 3 min 13.5 sec
Applied Stress = 44.12 MPa
Residual Stress - MPa
Distance from weld toe - mm

Specimen - 19/3
Vibration time = 3 min 13.5 sec
Applied Stress = 44.12 MPa
Residual Stress - MPa
Distance from weld toe - mm

Specimen - 19/4
Vibration time = 3 min 13.5 sec
Applied Stress = 50.3 MPa
Residual Stress - MPa
Distance from weld toe - mm

Specimen - 19/5
Vibration time = 3 min 13.5 sec
Applied Stress = 50.3 MPa
Residual Stress - MPa
Distance from weld toe - mm

Specimen - 19/6
Vibration time = 3 min 13.5 sec
Applied Stress = 56.8 MPa
Residual Stress - MPa
Distance from weld toe - mm

Specimen - 19/7
Vibration time = 3 min 13.5 sec
Applied Stress = 56.8 MPa
Residual Stress - MPa
Distance from weld toe - mm

Specimen - 19/9
No Vibration
Residual Stress - MPa
Distance from weld toe - mm

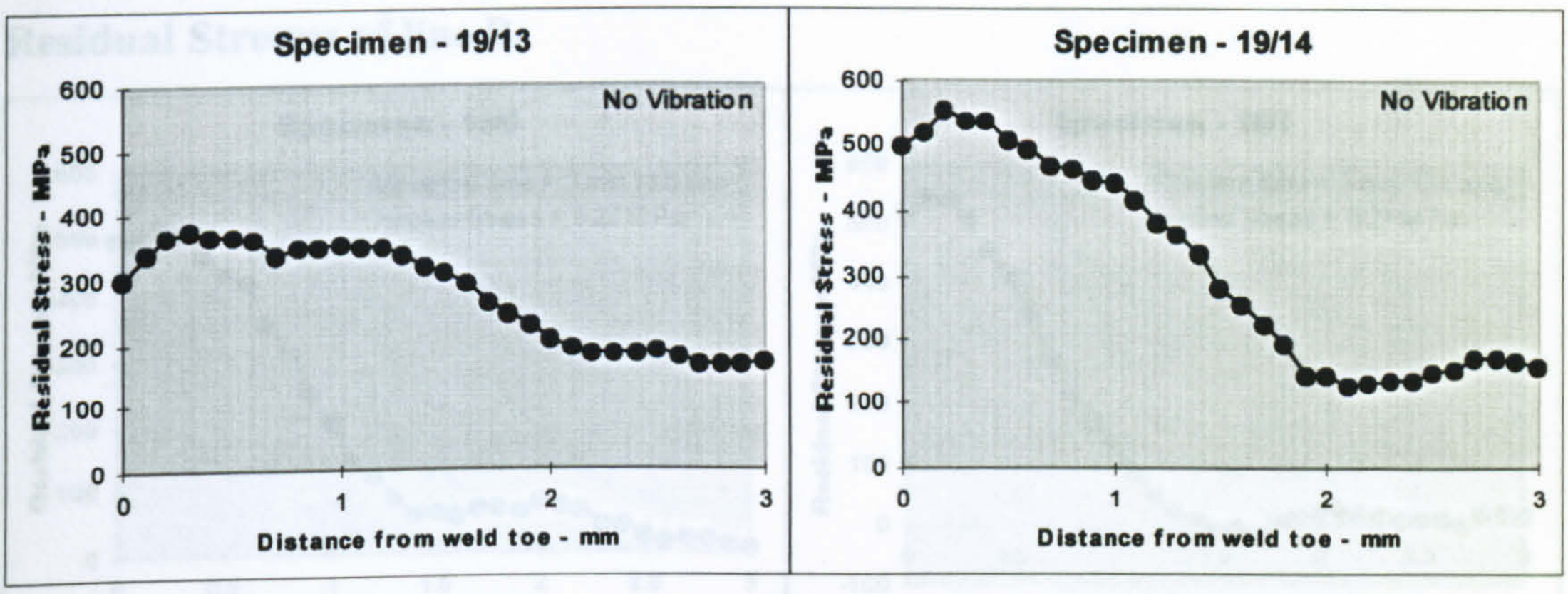

Figures 5.278 to 5.303 - Transverse stress plots of line A - specimens 18/0 to 19/14

Summary Plot

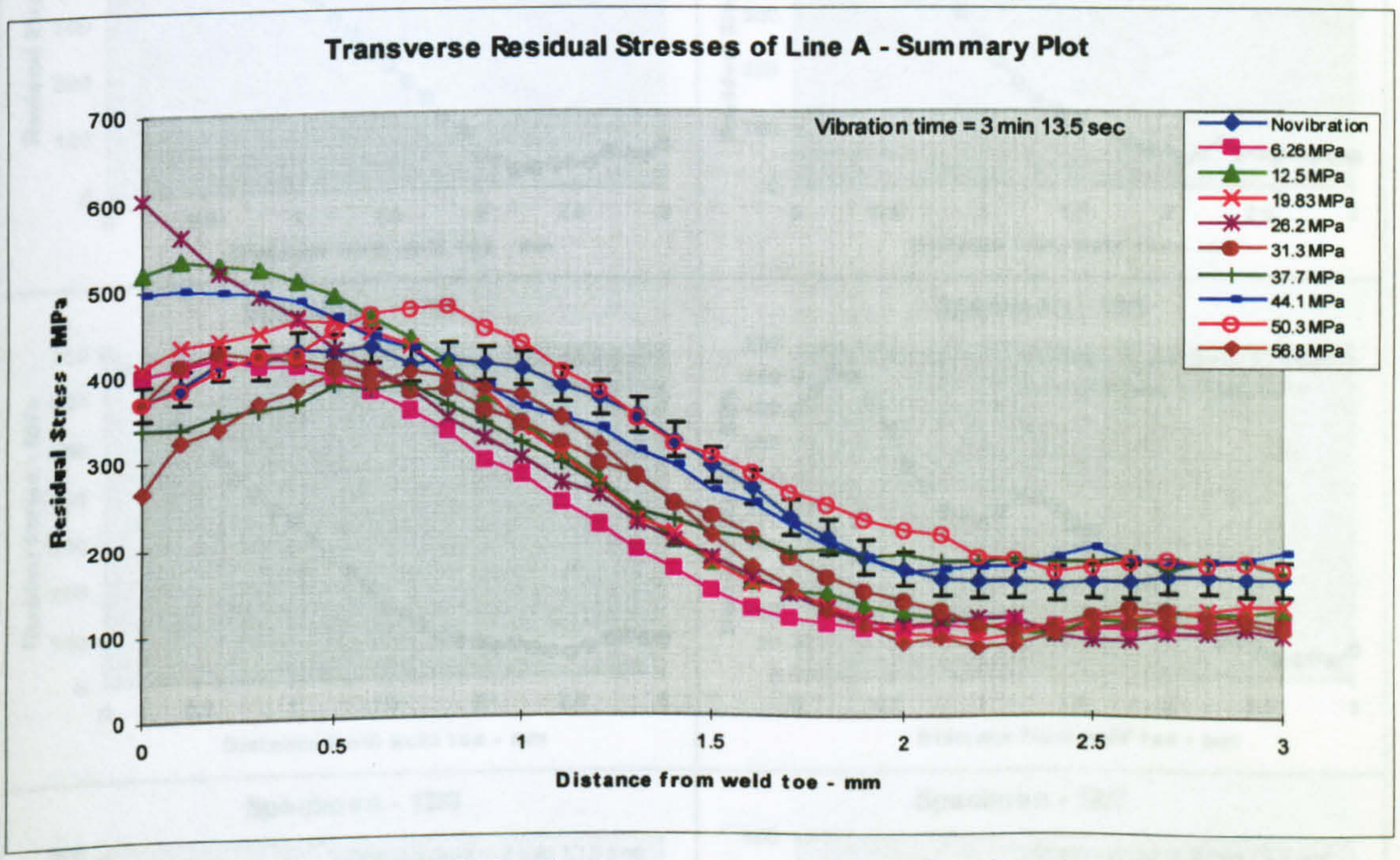

Figure 5.304 – Summary transverse stress plot – line A

Residual Stresses of line B

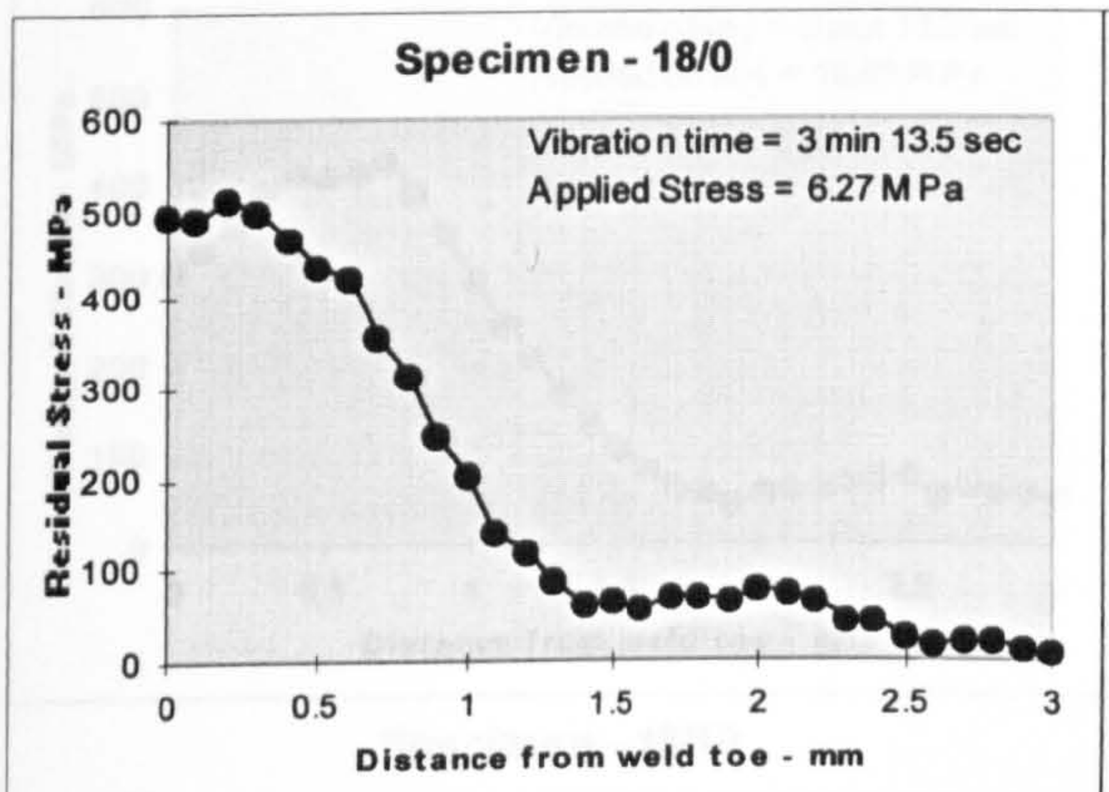

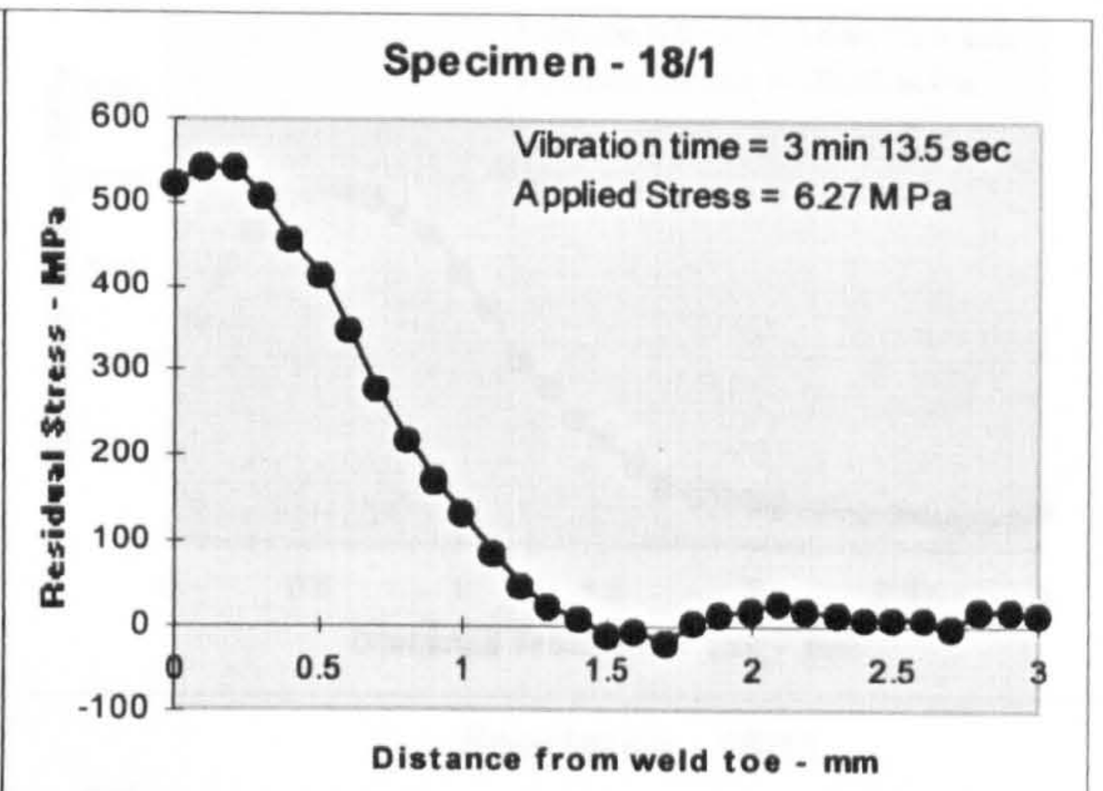

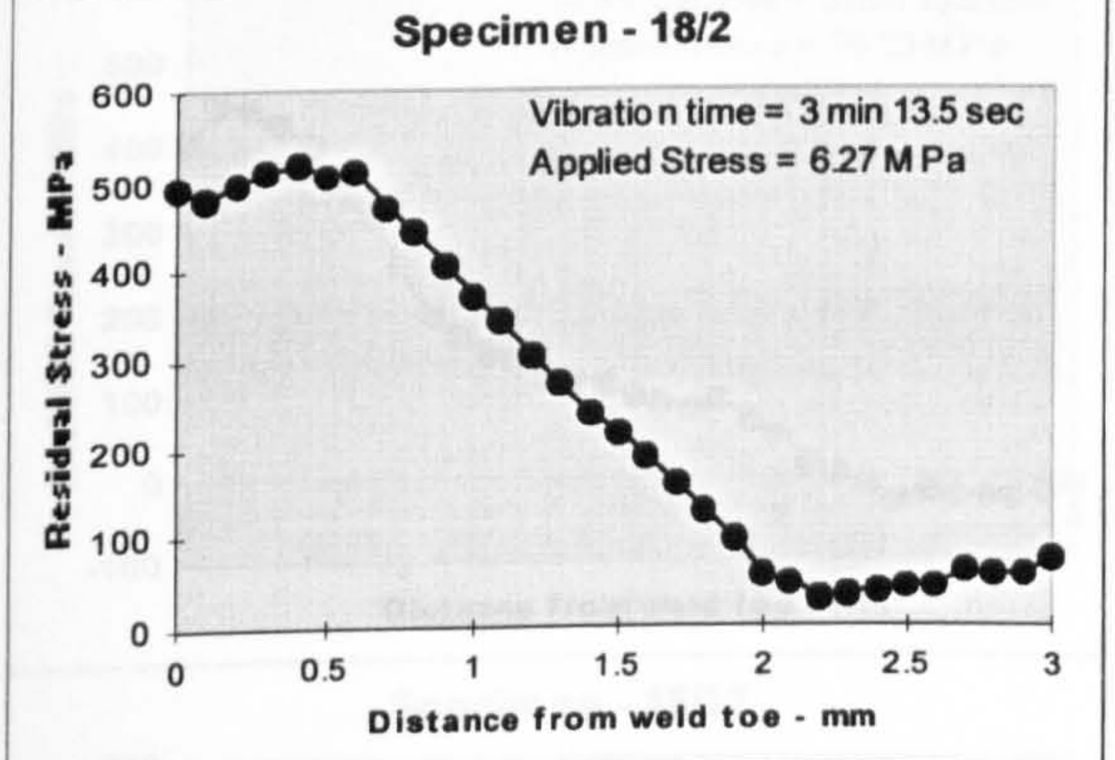

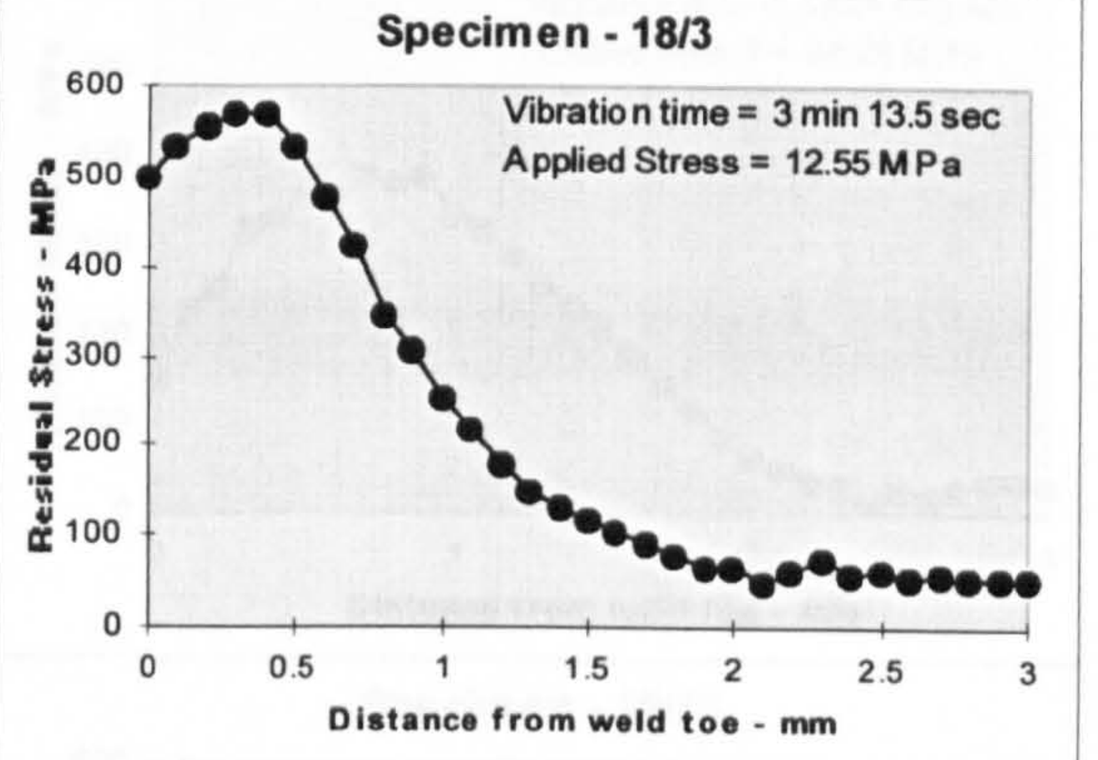

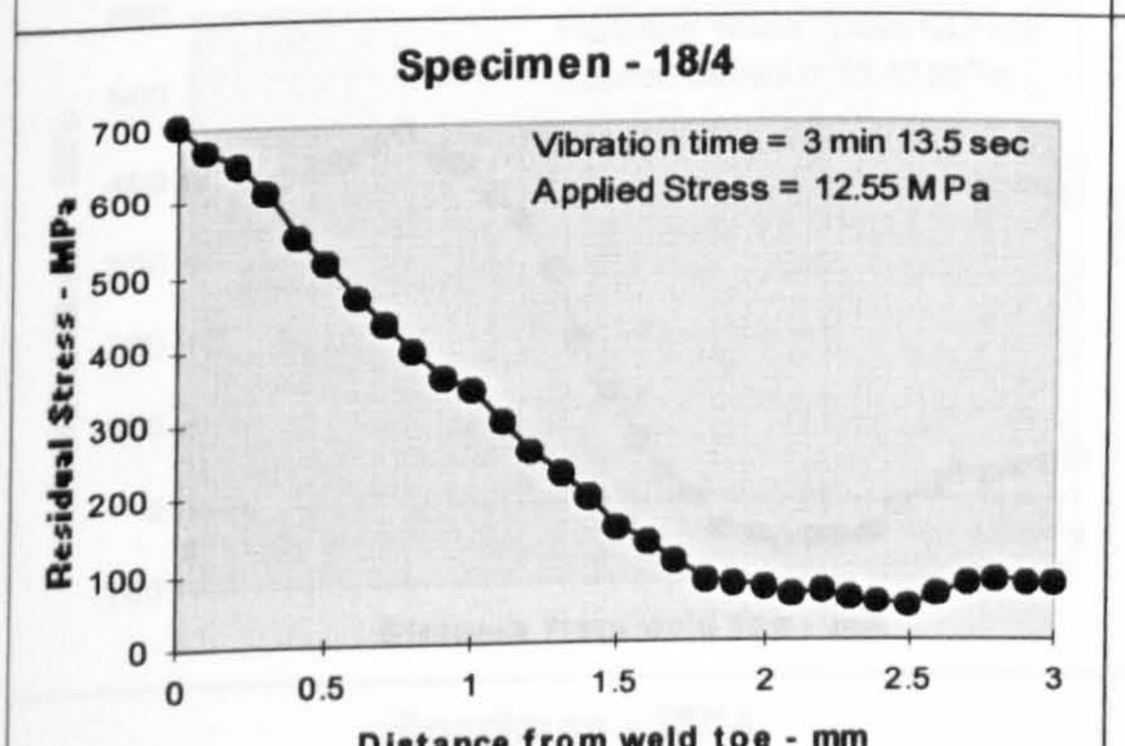

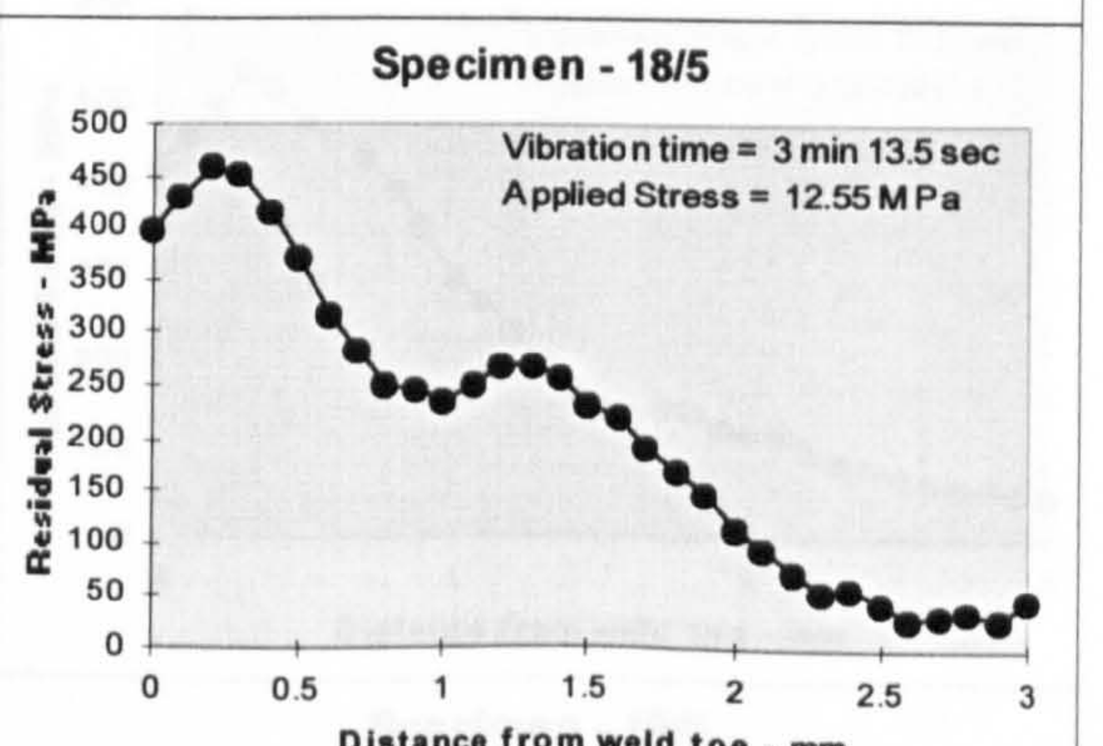

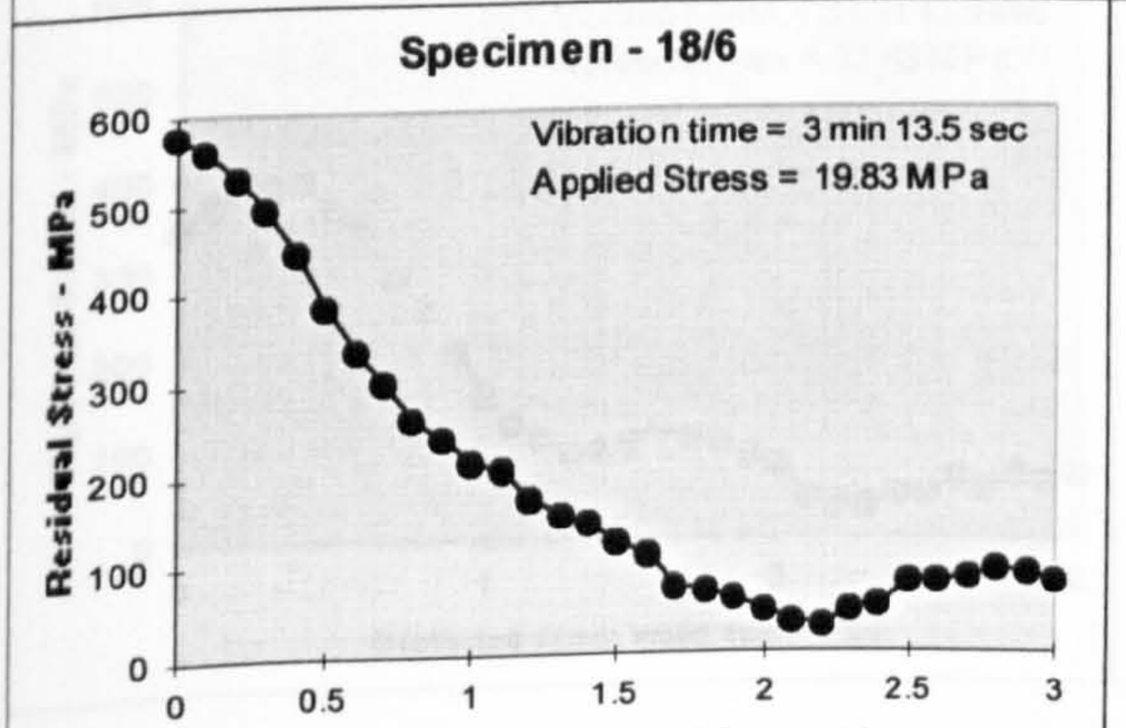

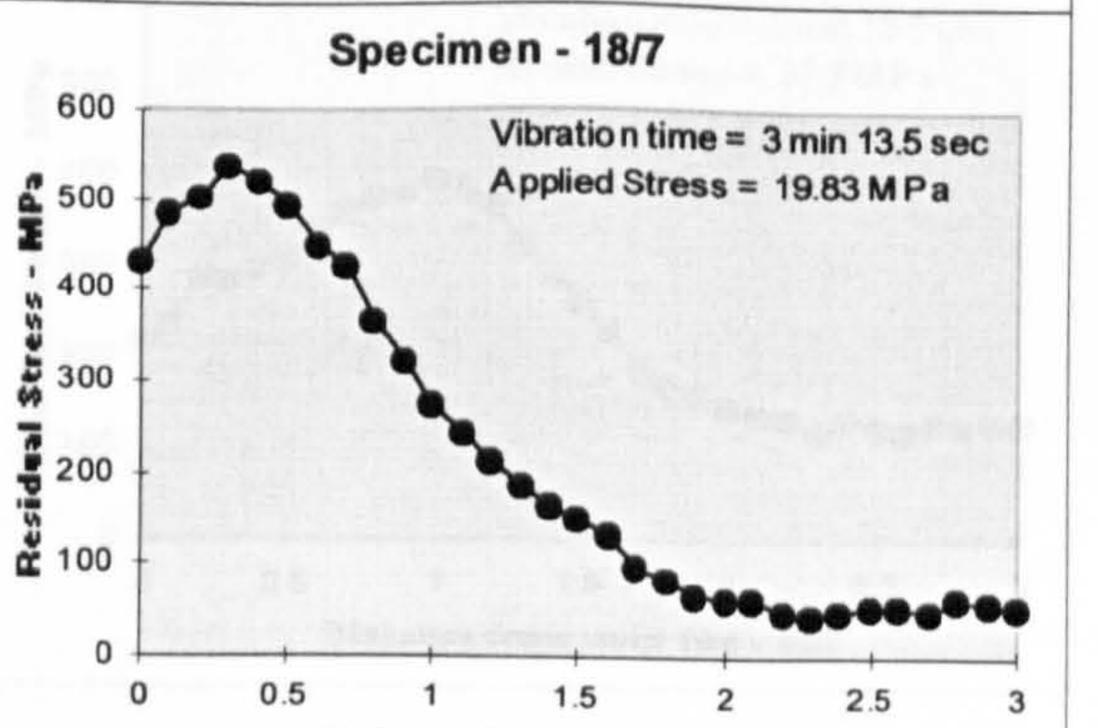

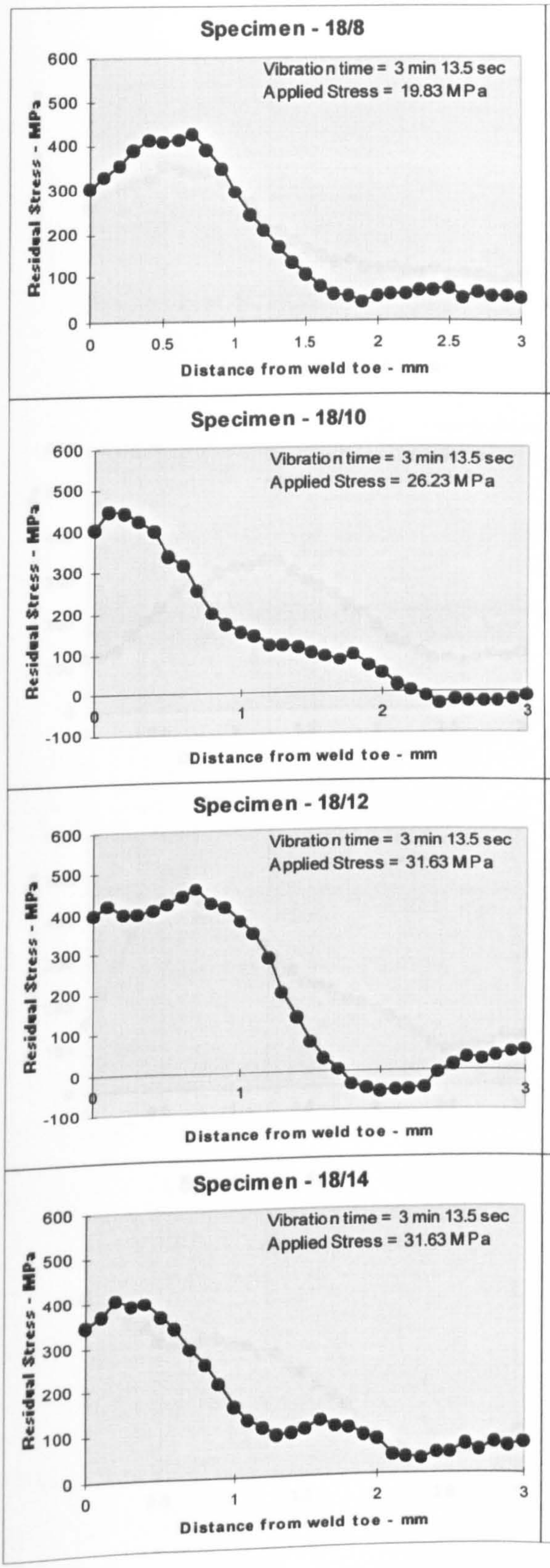
Specimen - 18/8
Vibration time = 3 min 13.5 sec
Applied Stress = 19.83 MPa
Residual Stress - MPa
Distance from weld toe - mm

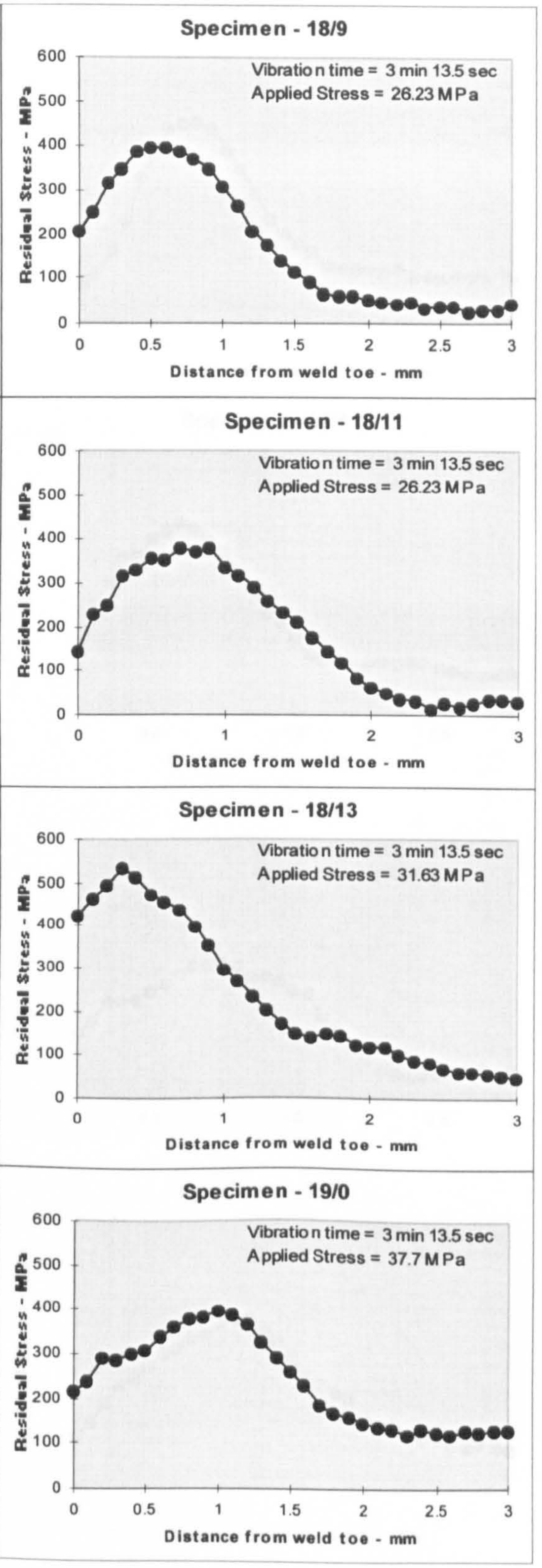
Specimen - 18/9
Vibration time = 3 min 13.5 sec
Applied Stress = 26.23 MPa
Residual Stress - MPa
Distance from weld toe - mm

Specimen - 18/10
Vibration time = 3 min 13.5 sec
Applied Stress = 26.23 MPa
Residual Stress - MPa
Distance from weld toe - mm

Specimen - 18/11
Vibration time = 3 min 13.5 sec
Applied Stress = 26.23 MPa
Residual Stress - MPa
Distance from weld toe - mm

Specimen - 18/12
Vibration time = 3 min 13.5 sec
Applied Stress = 31.63 MPa
Residual Stress - MPa
Distance from weld toe - mm

Specimen - 18/13
Vibration time = 3 min 13.5 sec
Applied Stress = 31.63 MPa
Residual Stress - MPa
Distance from weld toe - mm

Specimen - 18/14
Vibration time = 3 min 13.5 sec
Applied Stress = 31.63 MPa
Residual Stress - MPa
Distance from weld toe - mm

Specimen - 19/0
Vibration time = 3 min 13.5 sec
Applied Stress = 37.7 MPa
Residual Stress - MPa
Distance from weld toe - mm

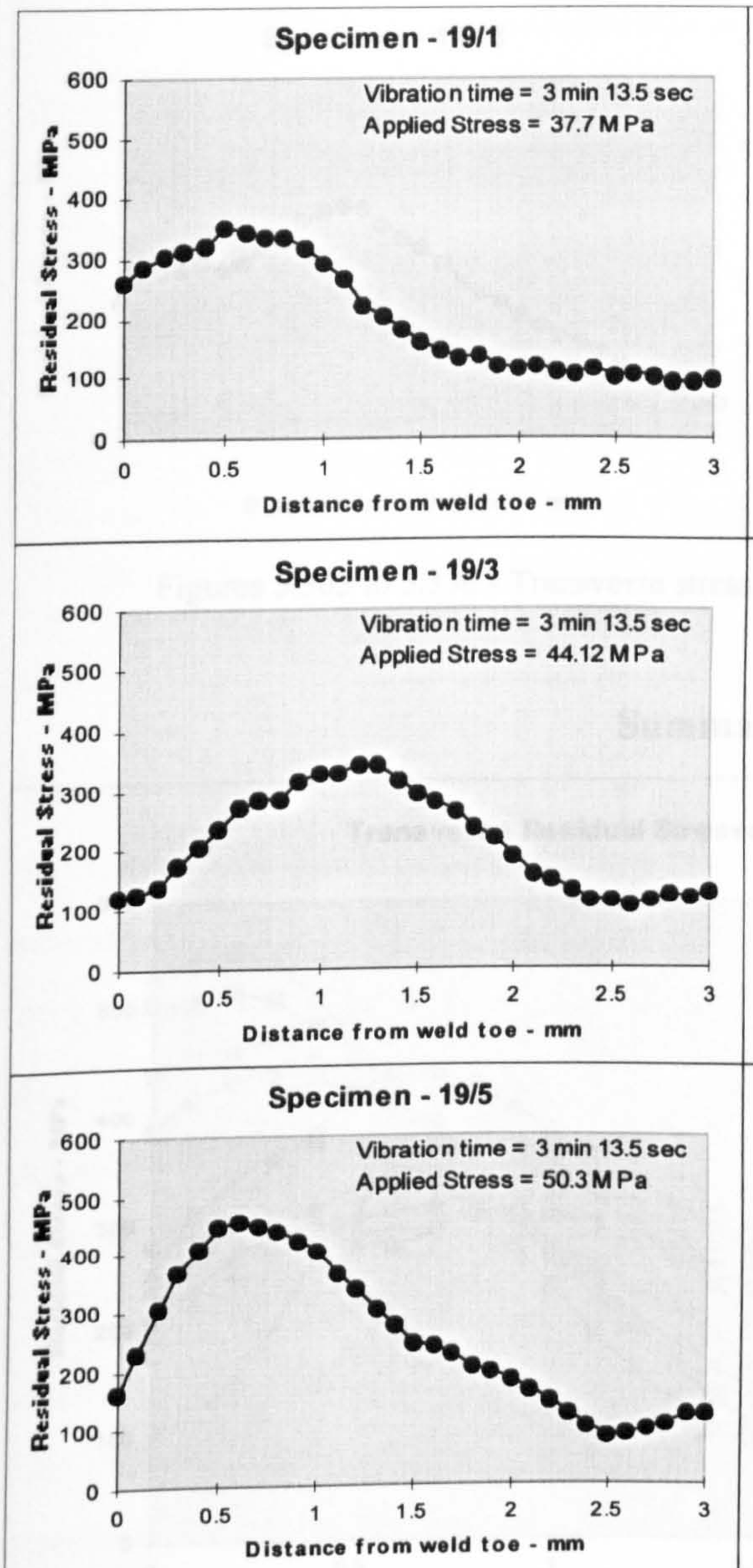
Specimen - 19/1
Vibration time = 3 min 13.5 sec
Applied Stress = 37.7 MPa
Residual Stress - MPa
Distance from weld toe - mm

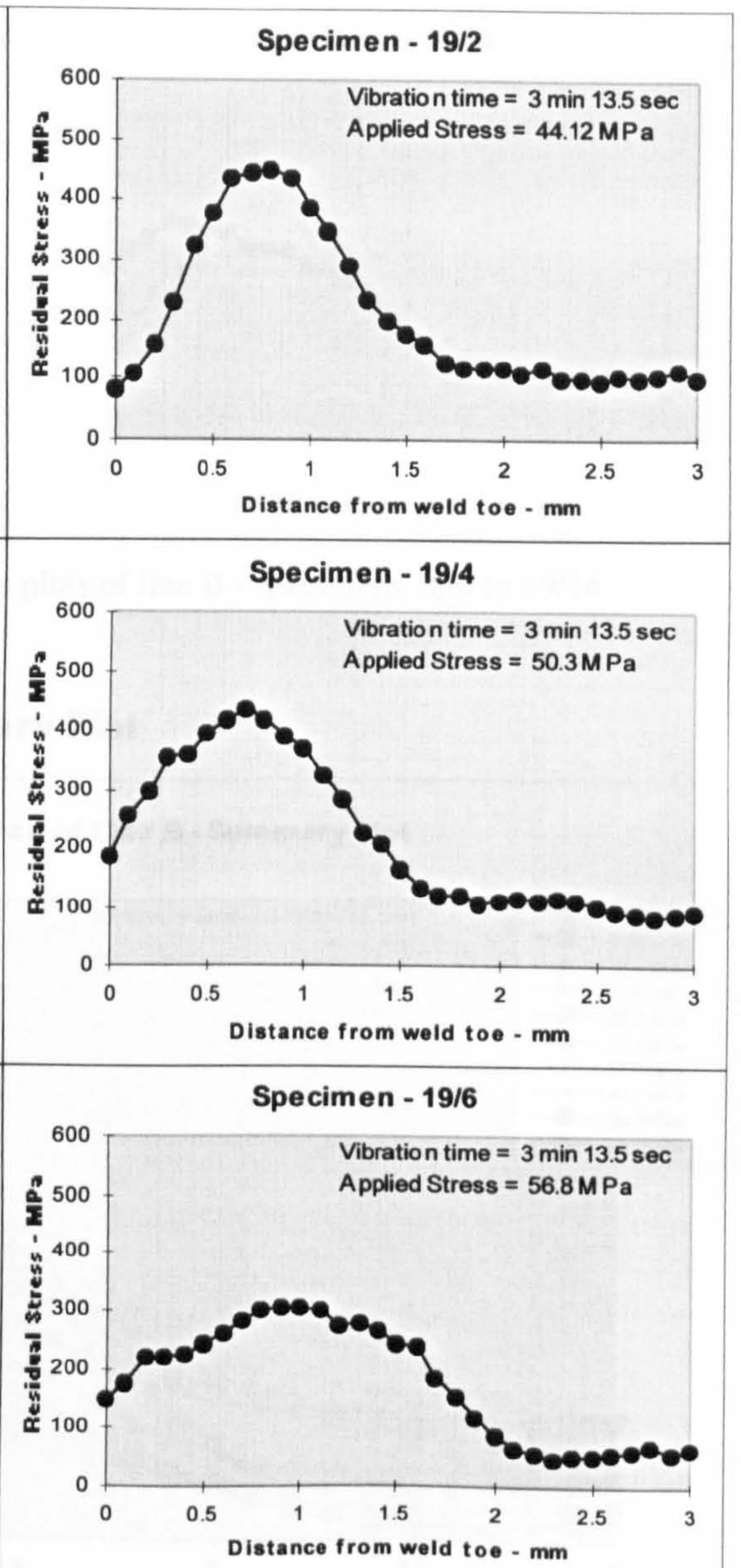
Specimen - 19/2
Vibration time = 3 min 13.5 sec
Applied Stress = 44.12 MPa
Residual Stress - MPa
Distance from weld toe - mm

Specimen - 19/3
Vibration time = 3 min 13.5 sec
Applied Stress = 44.12 MPa
Residual Stress - MPa
Distance from weld toe - mm

Specimen - 19/4
Vibration time = 3 min 13.5 sec
Applied Stress = 50.3 MPa
Residual Stress - MPa
Distance from weld toe - mm

Specimen - 19/5
Vibration time = 3 min 13.5 sec
Applied Stress = 50.3 MPa
Residual Stress - MPa
Distance from weld toe - mm

Specimen - 19/6
Vibration time = 3 min 13.5 sec
Applied Stress = 56.8 MPa
Residual Stress - MPa
Distance from weld toe - mm

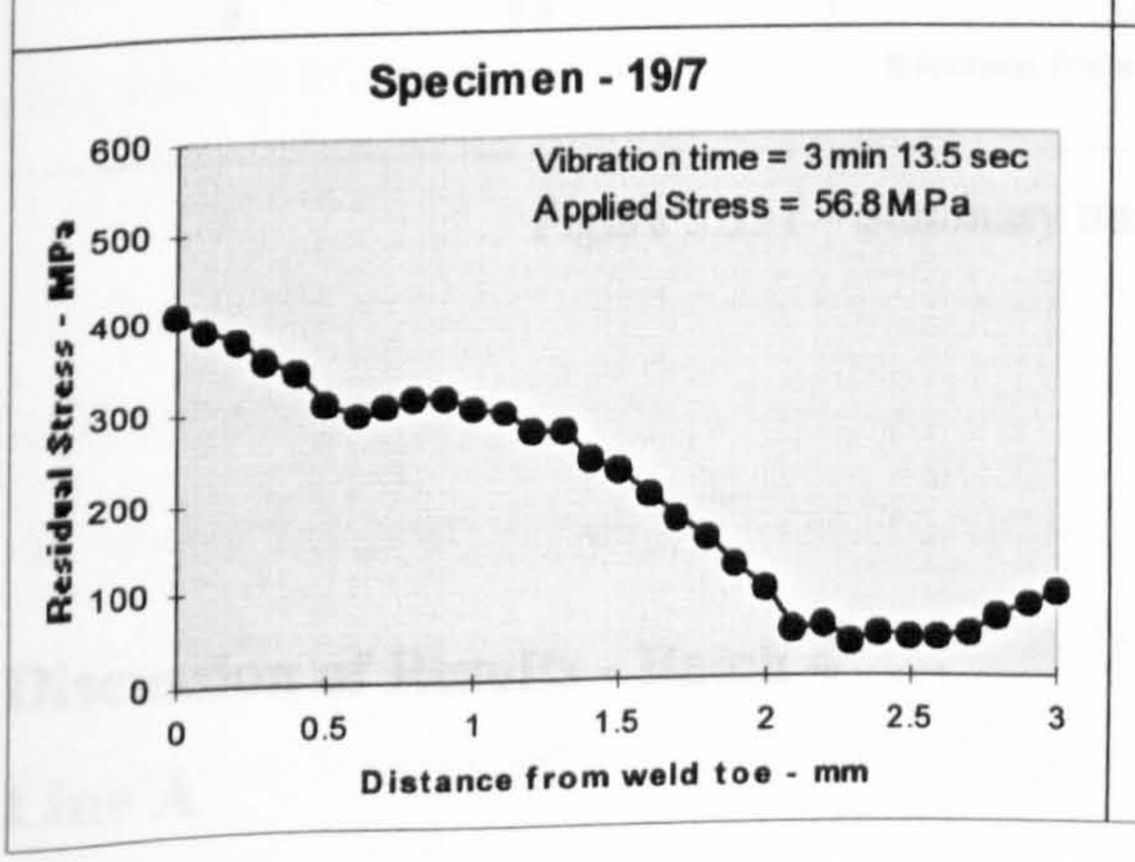
Specimen - 19/7
Vibration time = 3 min 13.5 sec
Applied Stress = 56.8 MPa
Residual Stress - MPa
Distance from weld toe - mm

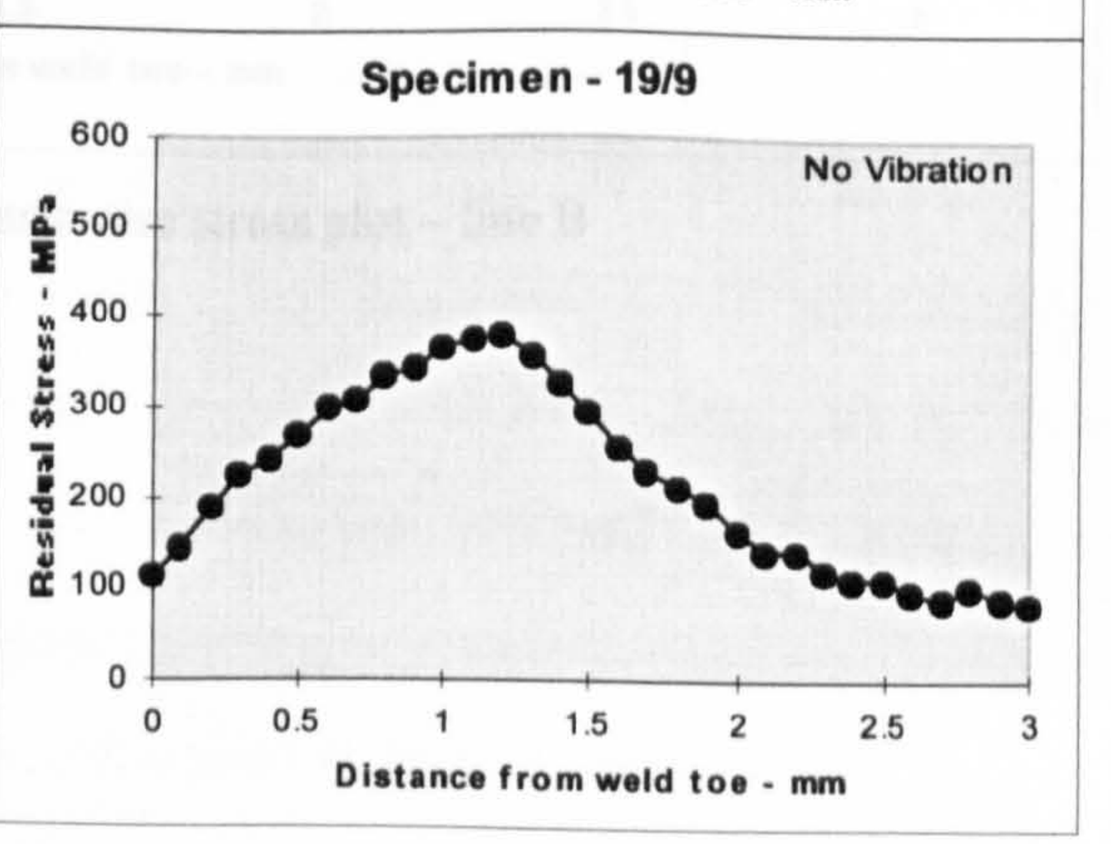
Specimen - 19/9
No Vibration
Residual Stress - MPa
Distance from weld toe - mm

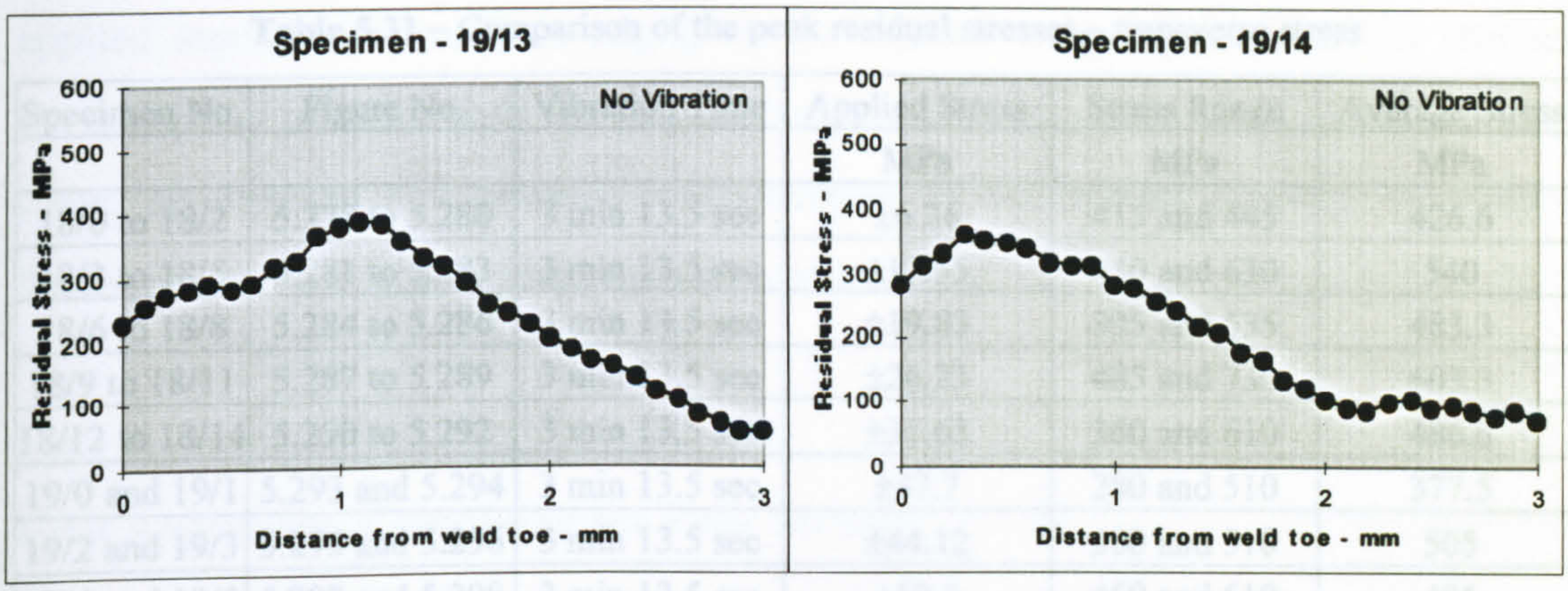

Figures 5.305 to 5.330 - Transverse stress plots of line B - specimens 18/0 to 19/14

Summary Plot

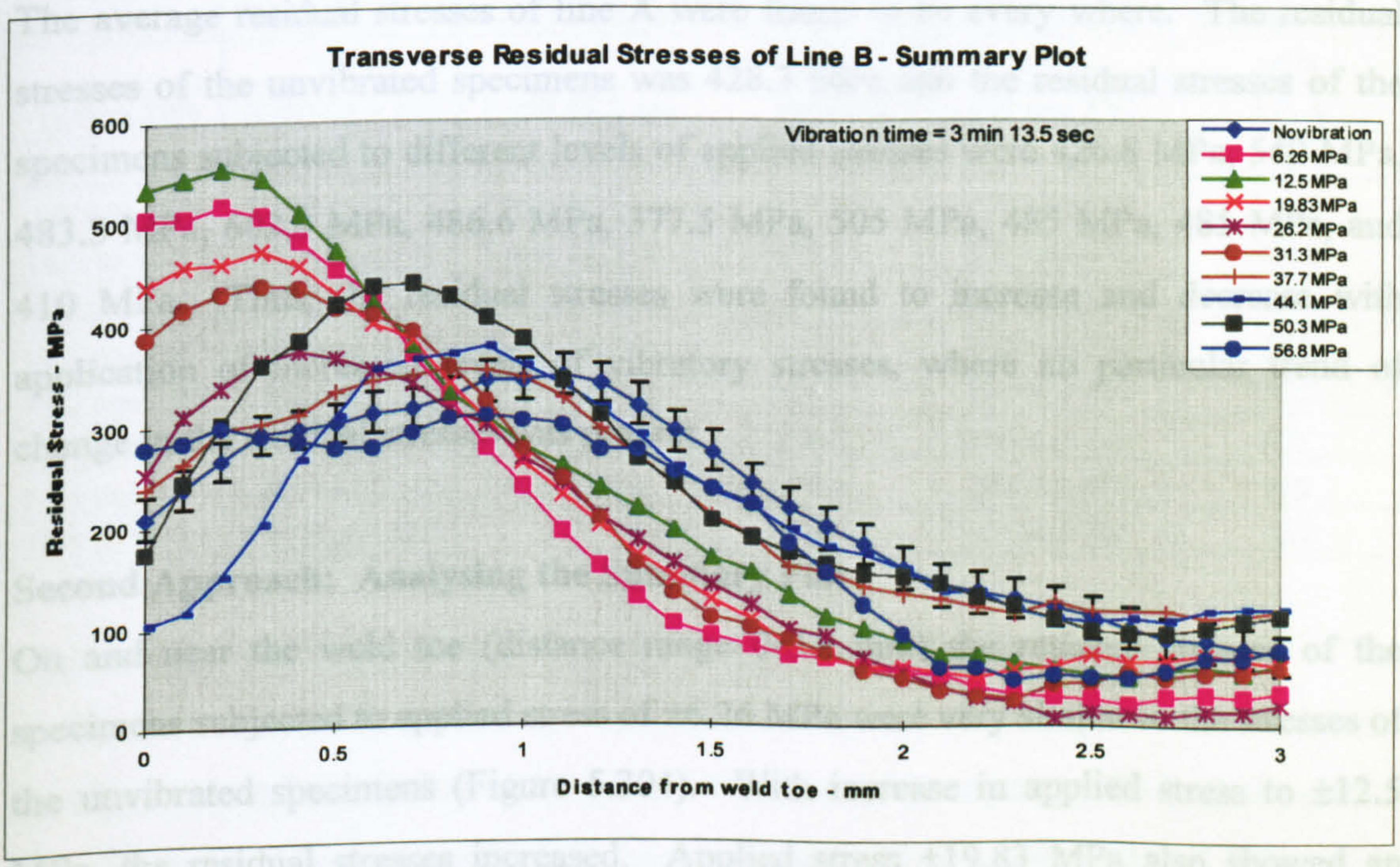

Figure 5.331 – Summary transverse stress plot – line B

Discussion of Results - Batch 4

Line A

First Approach: Comparing the Peak Stresses

The residual stresses of the specimens are shown in the table below.

Table 5.31 – Comparison of the peak residual stresses – transverse stress

Specimen No.	Figure No.	Vibration Time	Applied Stress	Stress Range	Average Stress
			MPa	MPa	MPa
18/0 to 18/2	5.278 to 5.280	3 min 13.5 sec	±6.26	415 and 445	426.6
18/3 to 18/5	5.281 to 5.283	3 min 13.5 sec	±12.55	450 and 630	540
18/6 to 18/8	5.284 to 5.286	3 min 13.5 sec	±19.83	395 and 535	483.3
18/9 to 18/11	5.287 to 5.289	3 min 13.5 sec	±26.23	485 and 730	603.3
18/12 to 18/14	5.290 to 5.292	3 min 13.5 sec	±31.63	360 and 610	486.6
19/0 and 19/1	5.293 and 5.294	3 min 13.5 sec	±37.7	280 and 510	377.5
19/2 and 19/3	5.295 and 5.296	3 min 13.5 sec	±44.12	500 and 510	505
19/4 and 19/5	5.297 and 5.298	3 min 13.5 sec	±50.3	460 and 510	485
19/6 and 19/7	5.299 and 5.300	3 min 13.5 sec	±56.8	360 and 460	410
19/9 to 19/14	5.301 to 5.303	0	0	365 and 560	428.4

The average residual stresses of line A were found to be every where. The residual stresses of the unvibrated specimens was 428.3 MPa and the residual stresses of the specimens subjected to different levels of applied stresses were 426.8 MPa, 540 MPa, 483.3 MPa, 603.3 MPa, 486.6 MPa, 377.5 MPa, 505 MPa, 485 MPa, 485 MPa, and 410 MPa. Thus, the residual stresses were found to increase and decrease with application of increased levels of vibratory stresses, where no particular trend of change in the residual stresses was present.

Second Approach: Analysing the Summary Plot

On and near the weld toe (distance range 0-0.8 mm) the residual stresses of the specimens subjected to applied stress of ±6.26 MPa were very similar to the stresses of the unvibrated specimens (Figure 5.304). With increase in applied stress to ±12.5 MPa, the residual stresses increased. Applied stress ±19.83 MPa also showed an increase but with a lesser degree. Applied stress ±31.3 MPa and ±37.7 MPa showed decreased residual stresses, but applied stress ±44.1 MPa showed increased residual stresses. Applied stress ±50.3 MPa showed similar residual stresses to the unvibrated specimens but applied stress ±56.8 MPa showed decreased residual stresses. Thus, on and near the weld toe no consistent trend in residual stresses was observed.

Away from the weld toe (distance range 0.5-1.5 mm) the residual stresses decreased with application of small applied stresses (±6.26 MPa). The effects of increased

applied stress were small or negligible for further reducing the residual stresses. Further away from the weld toe (distance range 1.5-3 mm), the residual stresses were found to increase and decrease with increase in the applied stresses, however a decreasing trend of the residual stresses was observed.

Line B

First Approach: Comparing the Peak Stresses

The residual stresses of the specimens were

Table 5.32 – Comparison of the peak residual stresses – transverse stress

Specimen No.	Figure No.	Vibration Time	Applied Stress	Stress Range	Average Stress
			MPa	MPa	MPa
18/0 to 18/2	5.305 to 5.307	3 min 13.5 sec	±6.26	520 and 550	533.3
18/3 to 18/5	5.308 to 5.310	3 min 13.5 sec	±12.55	460 and 700	578.3
18/6 to 18/8	5.311 to 5.313	3 min 13.5 sec	±19.83	420 and 580	513.3
18/9 to 18/11	5.314 to 5.316	3 min 13.5 sec	±26.23	375 and 450	403.3
18/12 to 18/14	5.317 to 5.319	3 min 13.5 sec	±31.63	400 and 530	460
19/0 and 19/1	5.320 and 5.321	3 min 13.5 sec	±37.7	340 and 390	365
19/2 and 19/3	5.322 and 5.323	3 min 13.5 sec	±44.12	430 and 440	435
19/4 and 19/5	5.324 and 5.325	3 min 13.5 sec	±50.3	430 and 440	435
19/6 and 19/7	5.326 and 5.327	3 min 13.5 sec	±56.8	290 and 410	350
19/9 to 19/14	5.328 to 5.330	0	0	355 and 365	360

The average residual stresses of the unvibrated/control specimens were 360 MPa. The residual stresses of the specimens subjected to different levels of applied stress showed mostly increased residual stresses. The difference in the average residual stresses of the vibrated and control/unvibrated specimens were +173.3 MPa, +218.3 MPa, +153 MPa, +43 MPa, +100 MPa, +5 MPa, +75 MPa, +75 MPa, and –10 MPa. In applied stress ±56.8 MPa, the residual stresses were found to decrease by –10 MPa. The above data indicate that the residual stresses increased significantly with application of smaller applied stresses. With increased applied stresses the residual stresses also increased but with a lesser degree.

Second Approach: Analysing the Summary Plot

On and near the weld toe (distance range 0-0.8 mm), the residual stresses of the specimens subjected to applied stress of ±6.26 MPa increased in comparison to the stresses of the unvibrated specimens (Figure 5.331). The applied stresses ±12.5 MPa, ±19.83 MPa and ±31.3 MPa showed a significant increase in the residual stresses. With increase in the applied stresses to ±37.7 MPa, the residual stresses increased but with a lesser degree. With applied stress ±44.1 MPa the residual stresses decreased. With further increase in the applied stresses, the residual stresses increased.

Away from the weld toe (distance range 0.8-2 mm), the residual stresses decreased with application of small stresses. With increase in the applied stresses the residual stresses decreased but with a lesser degree. Further away from the weld toe (distance range 2-3 mm), the residual stresses decreased but with a lesser degree.

Thus, the residual stresses on and near the weld toe increased and also decreased with application of different levels of applied stresses. And away from the weld toe a small reduction in the residual stresses was observed.

5.3.4.5 Summary of Results

In batch 3, time of vibration was varied. The average peak residual stresses of the selected lines (line A and B) were found to increase with application of small induced stresses, with increase in the applied stresses the residual stresses were increased but with a lesser degree. A similar result was found in the summary plot analysis. The residual stresses on and near the weld toe was found to increase with application vibration. Away from the weld toe the residual stresses were found to decrease. Further away from the weld toe the residual stresses were found to decrease but with a lesser degree.

The residual stresses of this batch was found to increase with application of vibration but the increase in the time of vibration seems did not have any effect.

In batch 4, the applied stresses to the specimens were varied. The peak residual stresses of line A were found to be confused, where no particular trend was present. In line B, the residual stresses were found to increase significantly with application of small stresses. With increase in the applied stresses the residual stresses were found to increase but with a lesser degree. In higher applied stresses (±56.8 MPa), the residual stresses were found to decrease.

In the summary plot a similar result was found. Due to increase in the applied stresses the average residual stresses of line A (on and near the weld toe) were found to increase and decrease without any particular trend. Away from the weld toe the residual stresses were found to decrease. Further away from the weld toe the residual stresses decreased but with a lesser degree.

Thus, the peak residual stresses of both batches were found to be very similar – the residual stresses were increased with increase in the applied stresses. Due to further increase in the applied stress the residual stresses increased but with a lesser degree. The trend of the peak residual stress of line B indicates that the residual stresses would decrease with further increase in the applied stresses. In the summary plot of both batches, the residual stresses on and near the weld toe were found to decrease and also increase without any particular trend. Away from the weld toe the residual stresses of the specimens were found to decrease with application of vibration. A further detailed investigation is necessary for this experiment.

5.3.5 Experiment V:

Treatment of Specimens Using a Certain Range of Yield Stress.

Abstract

The specimens in this experiment were welded without any vibration. While the specimens were cooling down, vibration was applied to them for a certain period selecting the range of yield stress of the metal. Three batches of specimens were processed using different range of yield stresses. The residual stresses were found to be very confusing, where both increase and decrease in the residual stresses were found due to the treatments.

5.3.5.1 Introduction

This experiment was designed considering the fact that the property of mild steel at elevated temperature is different from its normal temperature properties. After welding the yield strength of the weld and surrounding metal decreases to very lower values and increases with decrease in temperature. This is illustrated in Figure 5.334. A tensile test of the experimenting steel showed that the yield strength at 700 ^{0}C was ~70 MPa.

Eigenmann [44], Fenghua [49], Nakagiri [98] and many others explained stress relief in VSR treatment as a result of plastic deformation. At room temperature the yield stress is high, thus requires higher induced stress for plastic deformation. On the other hand at higher temperature a lower induced stress is capable to cause plastic deformation. In this experiment vibration was applied to the specimens in three different temperature ranges to observe their effect. The experimental set-up for this experiment was same as Experiment IV (Figure 5.277).

5.3.5.2 Experimental Procedure

In this experiment the specimens were mounted on the set-up (Figure 5.277), a single pass bead weld was carried out without any vibration or induced stress. In the

welding process, the stepper motor driven welding carrier maintained constant speed of the welding torch. The vibratory treatment was applied to the specimens using a pre-selected temperature range, i.e. using a pre-selected range of yield stress. In the treatment process, the applied stress to the selected line (line A in Figure 5.243) was varied.

To carry out this experiment, the temperature profile of the specimen during cooling was determined. To measure the temperature, a calibrated thermocouple was used. The calibration of the thermocouple was carried out using melting ice and boiling water.

The thermocouple was inserted into a blind hole where it was tightened using a metal plug. This was done to obtain maximum conduction between the specimen and the thermocouple and thus minimise the error. Three specimens were welded to measure the temperature. In all three specimens, a 1 mm diameter hole was drilled near the prepared V of the specimens. The hole was located at the mid-width of the specimens (Figure 5.332). In the first specimen the hole was drilled 3 mm from the edge. In the second specimen the hole was drilled 5 mm from the edge and in the third specimen the hole was 7 mm from the edge.

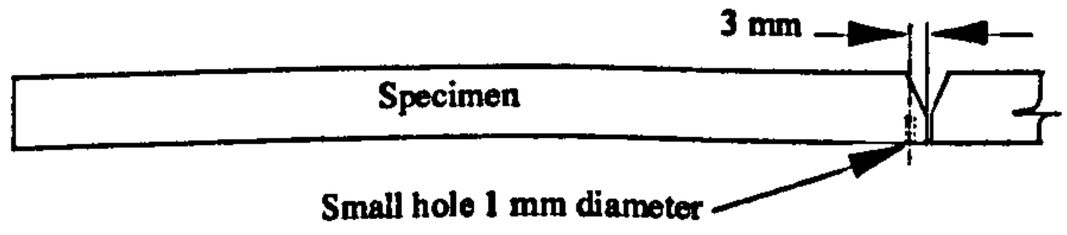

Figure 5.332 - Dimension of the specimen to obtain the cooling curve

The specimens were located on the welding rig and the thermocouple connected to a Protek 506 Multimeter. The multimeter output was connected to the computer. Using the software of the multimeter (Protek 506) the temperature variation of the specimen was plotted against time. The specimens were welded and the temperature profile of the three distances were recorded and printed. All three plots were then reproduced using *Microsoft Excel*. The data and the plot are shown in Table 5.33 and Figure 5.333.

Table 5.33 - Study of temperature history in HAZ of weld joints. Multimeter Protek-506, Thermocouple: local prepared

Sp- 20/0 3 mm		Sp- 19/11 5 mm		Sp- 19/12 7 mm	
Time, S	Temperature ^{0}C	Time, S	Temperature	Time, S	Temperature ^{0}C
0	49	0	28.62	0	51.85
0.62	87.5	6.18	660	1.03	145.18
2.47	350	7.71	671.7	1.9	338.3
4.14	561	9.27	660	3.71	525
5.27	650	12.36	602.2	4.02	553.5
6.3	665.5	19.44	525	4.87	608
7.14	667	27.78	437.5	5.98	626
8.24	653	33.96	386	6.91	623.5
9.24	647.8	40.11	350	8.87	605
11.74	612.5	48.84	306.25	16.67	525
18.64	525	63.06	262.5	24.63	448.5
25.64	437.5	72.36	241.9	28.87	412.2
30.14	395	81.36	225.1	35.67	365.5
37.02	350	102.36	199.4	38.87	346
41.14	324.6	148.08	156.98	48.87	304.6
49.04	293.38	162.36	149.26	58.87	268.3
54.14	275.3	192.36	131	68.87	245
64.14	252	222.36	119.5	78.87	226.8
74.14	233	252.36	104.2	88.87	210
84.14	218	282.36	100		

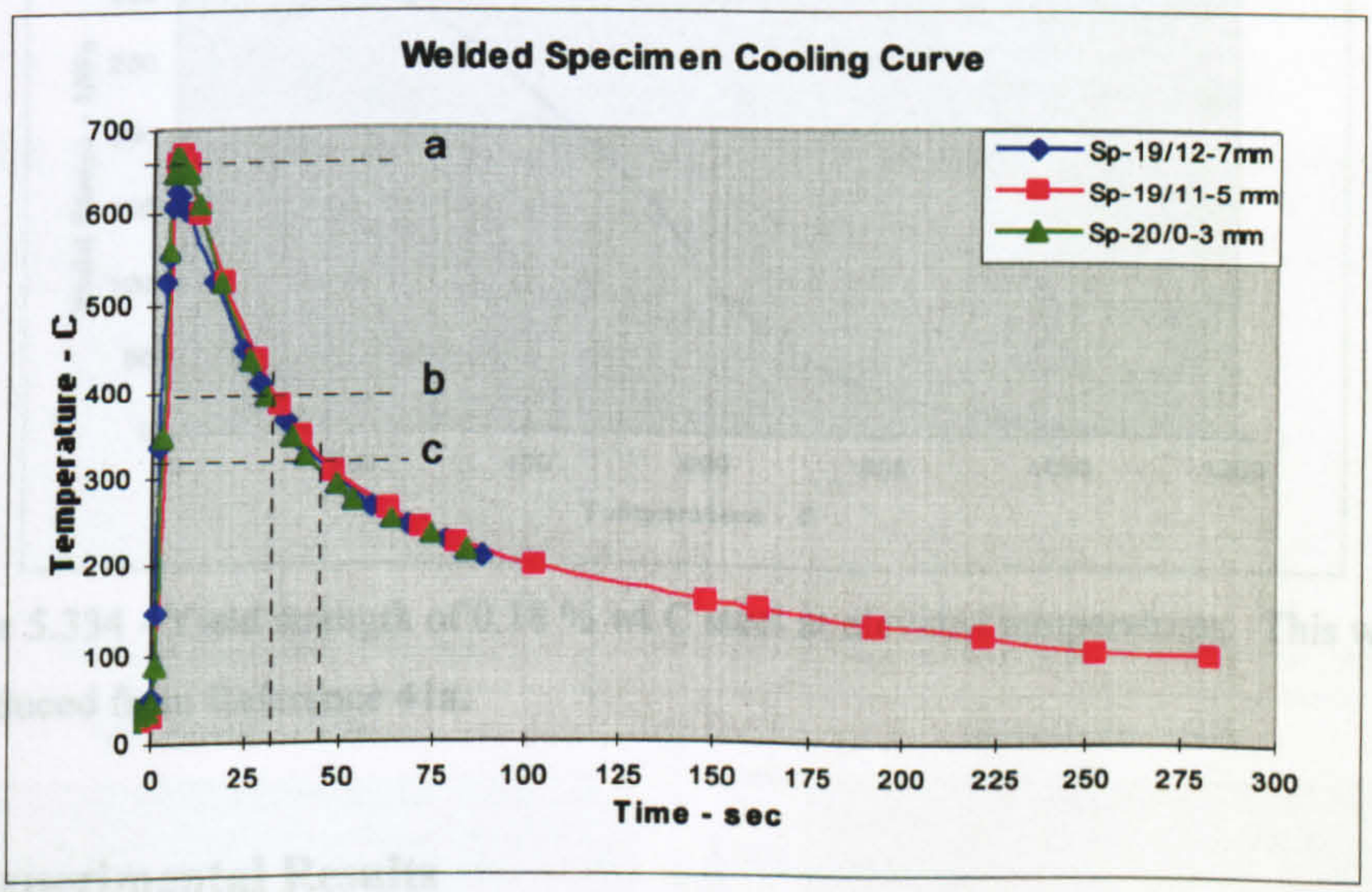

Figure 5.333 - Welded specimen cooling curve

In this experiment three batches of specimens were processed. In the first batch, vibration started just after finishing of the welding. The temperature of the specimens just after weld finishing was 660 ^{0}C or above. In the second batch, vibration started after 31 seconds of the weld finishing, in this waiting time the temperature reduced to 395 ^{0}C. In the third batch vibration started after 45 seconds of the weld finishing.

The waiting time reduced the temperature to 320 ^{0}C. This three vibration times were chosen to find appropriate timing of VSR treatment in relation to the yield strength of the cooling mild steel welds. The yield stress of the metal at different temperatures was determined from the temperature-yield stress relationship in Figure 5.334, which was re-produced from Reference 41a.

After vibratory treatment of the specimens, the transverse residual stresses on the two lines (Figure 5.243) were measured. The residual stresses were measured using an X-ray diffractometer where a line map was measured using the single exposure technique (SET). The X-ray measurement conditions were similar to that described in Table 5.10. The X-ray measurement jig was similar to the previous experiment (shown in Appendix II).

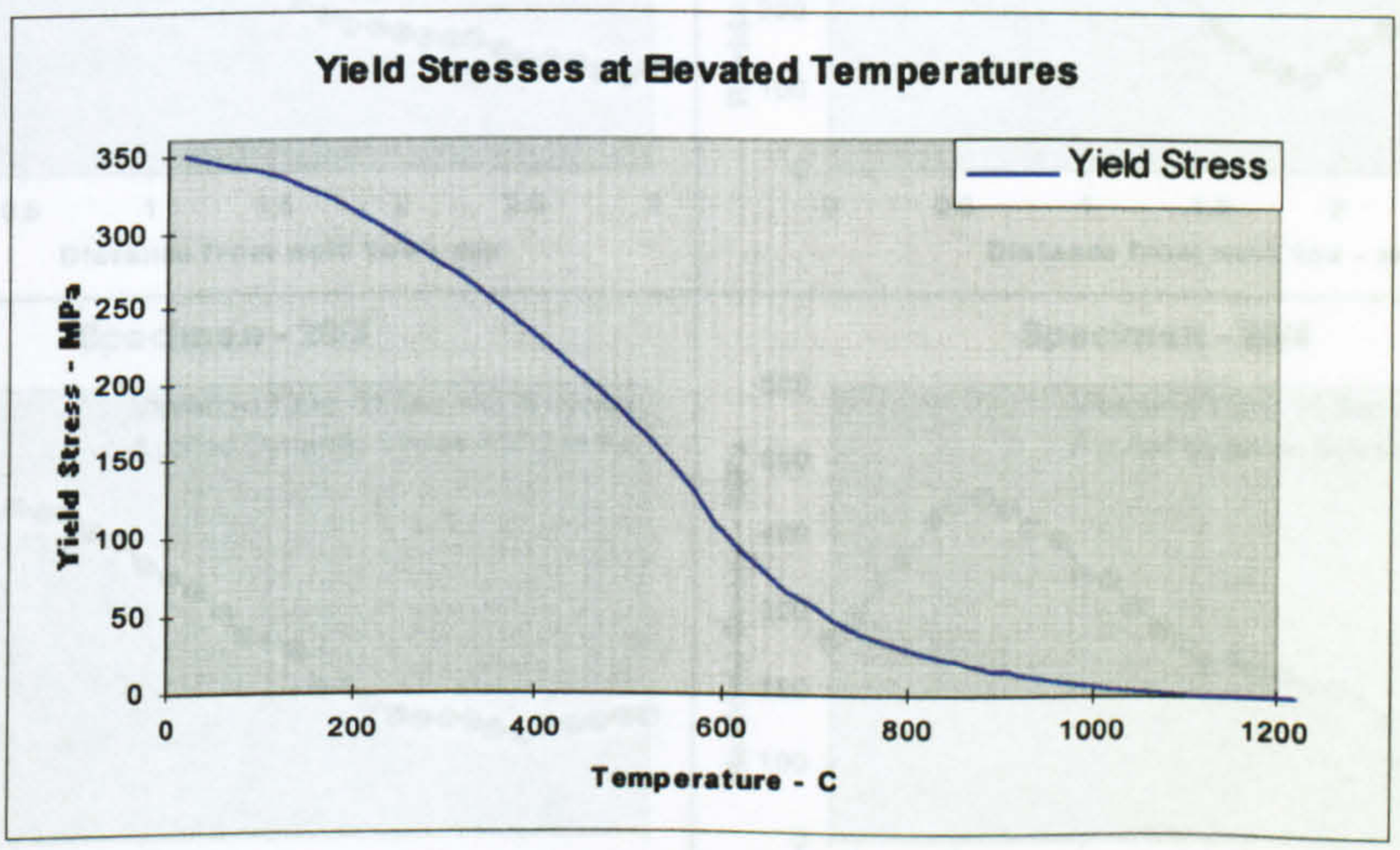

Figure 5.334 - Yield strength of 0.18 % wt C steel at elevated temperatures. This was reproduced from Reference 41a.

5.3.5.3 Experimental Results

Batch 1

In this batch, eleven specimens were processed, in which vibration started just after completion of welding and continued for 51 seconds. In this time the temperature decreased from 660~700 ^{0}C ("a" in Figure 5.333) to 295~305 ^{0}C and the corresponding yield stress increased from ~72 MPa to ~278 MPa as shown in Figure 5.334. Keeping the time of vibration and frequency (25 Hz) constant the amplitude of vibration was varied. The applied stresses to the specimens are shown in the plots.

Residual Stress Plots of Line A

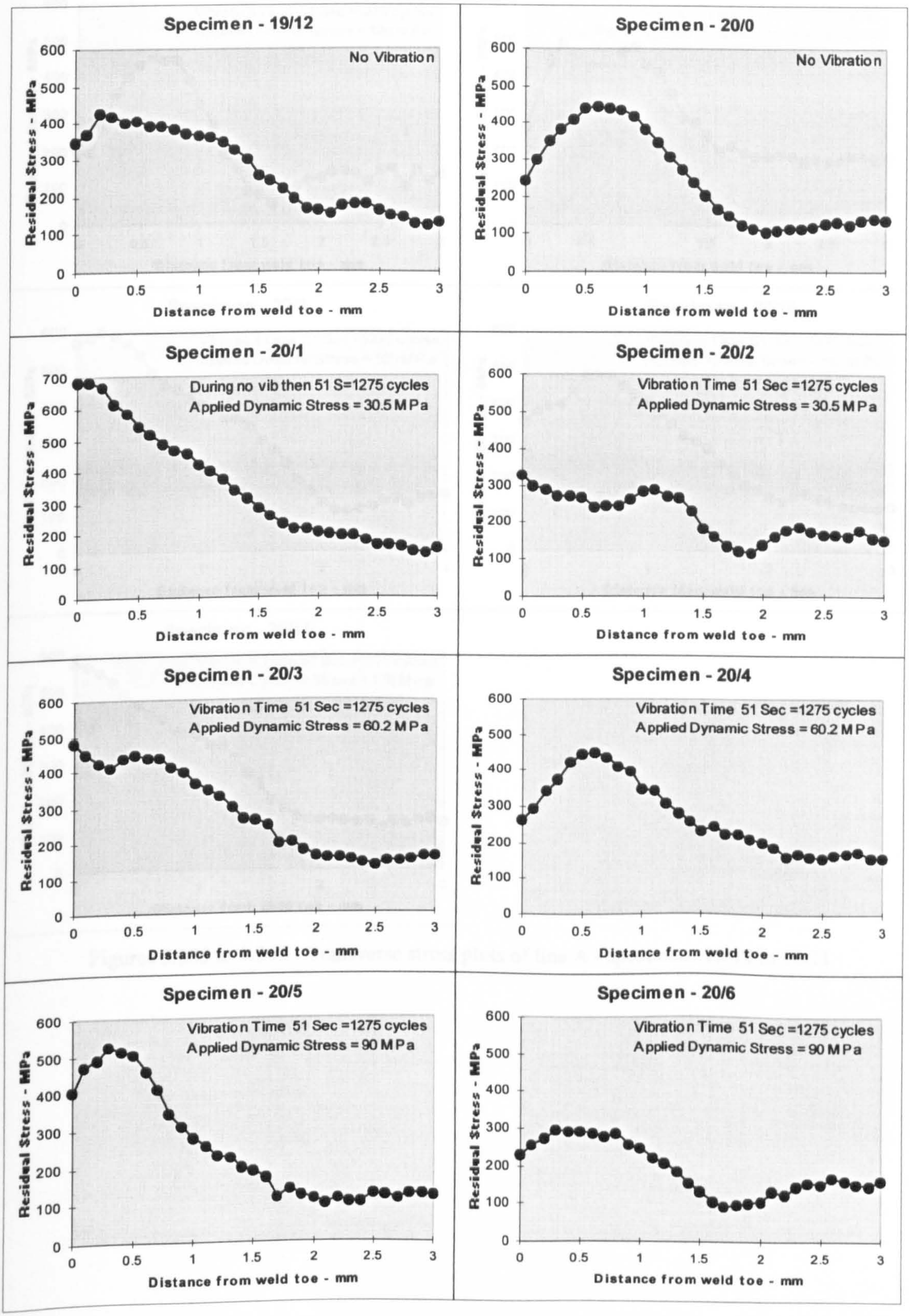

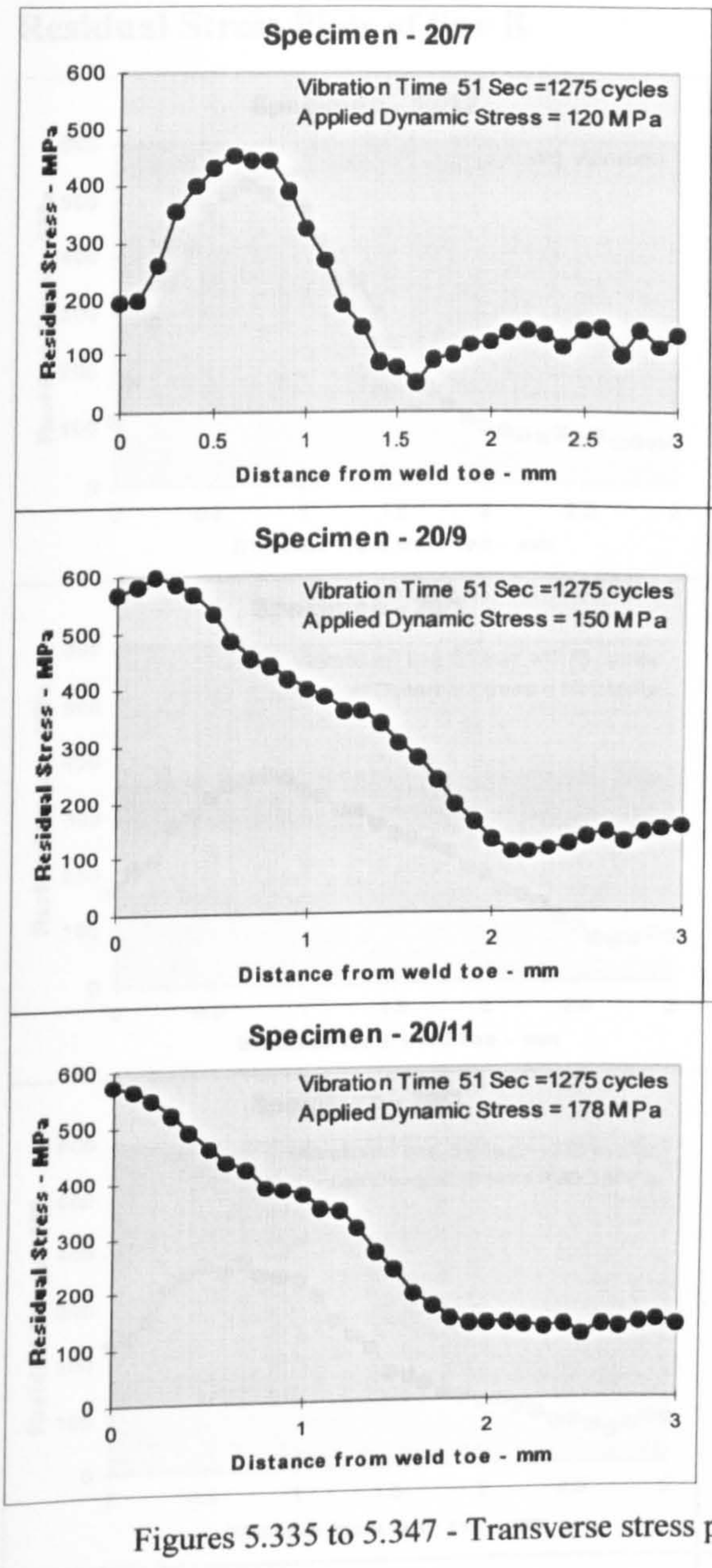

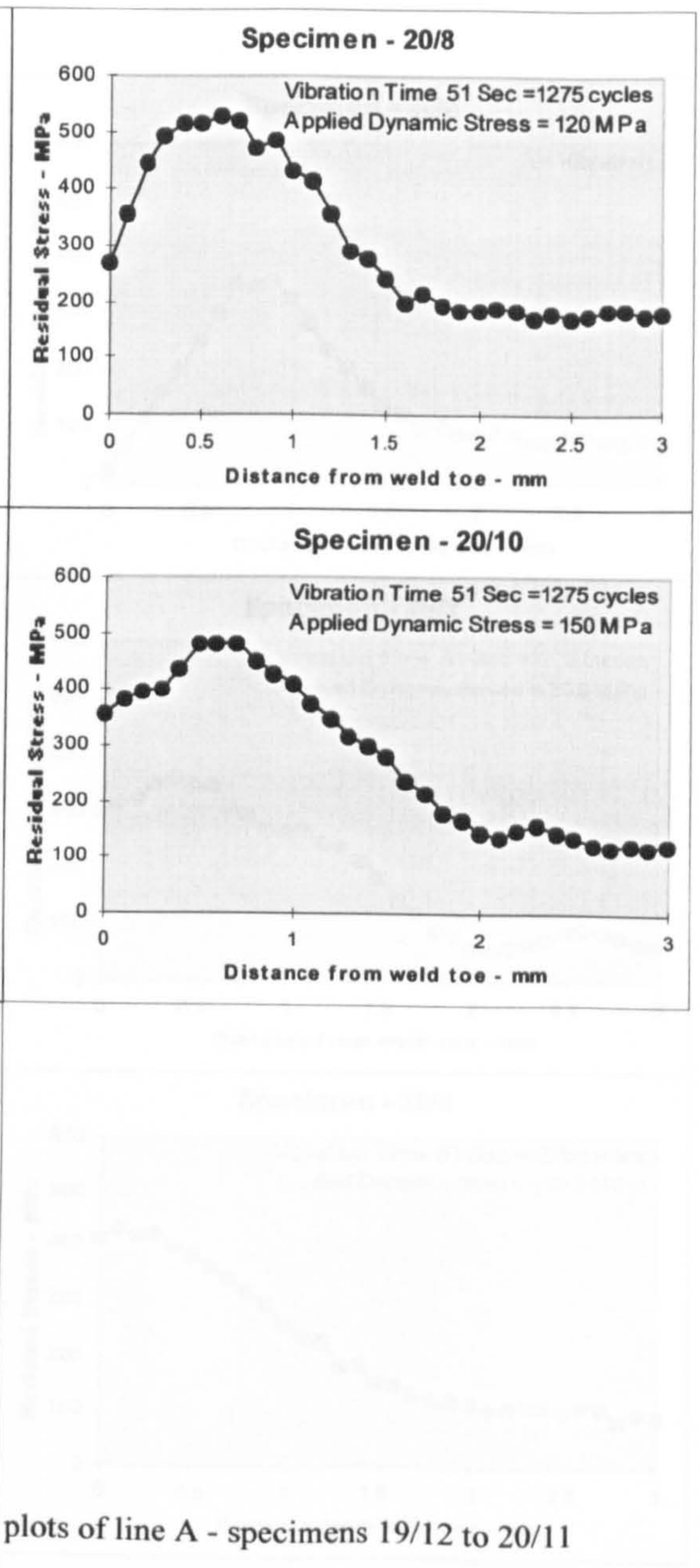

Figures 5.335 to 5.347 - Transverse stress plots of line A - specimens 19/12 to 20/11

Residual Stress Plots of line B

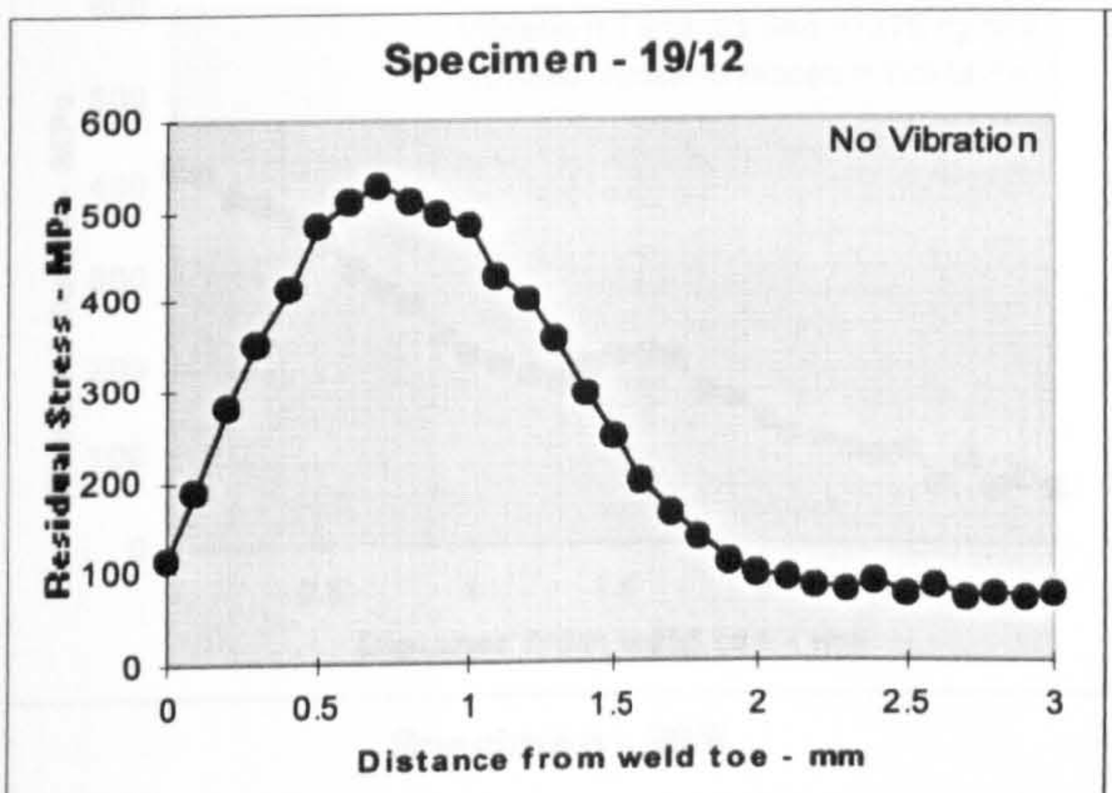

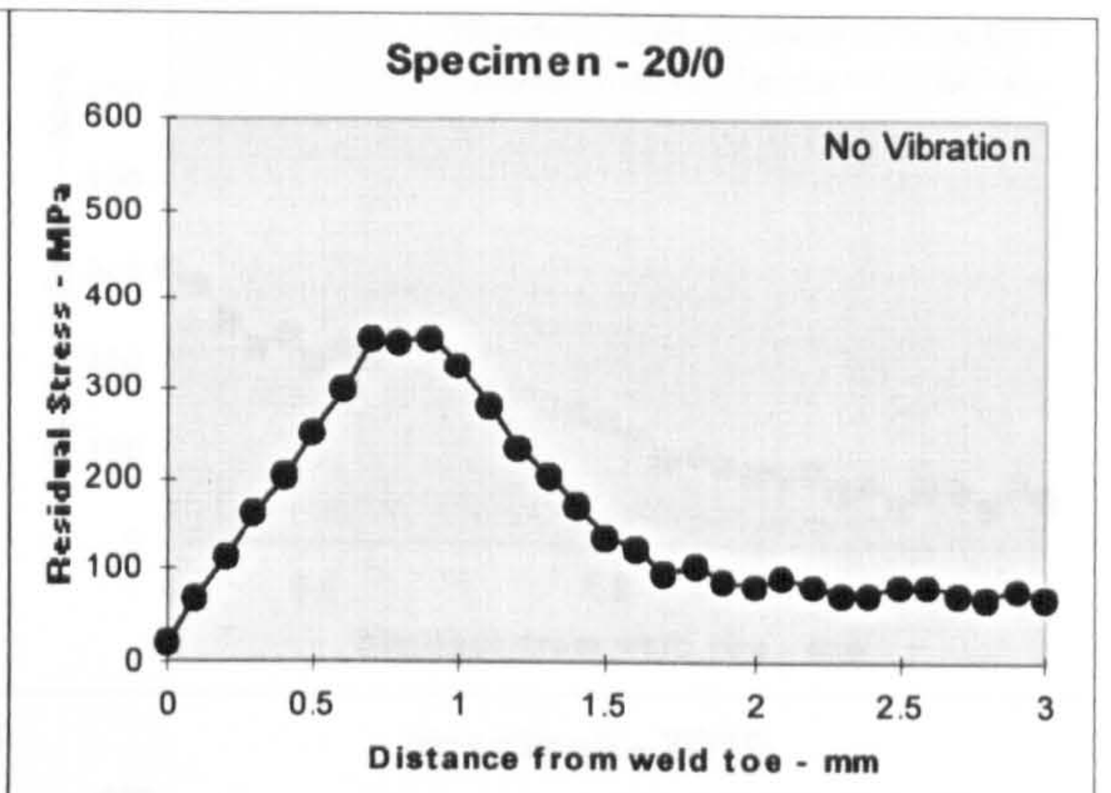

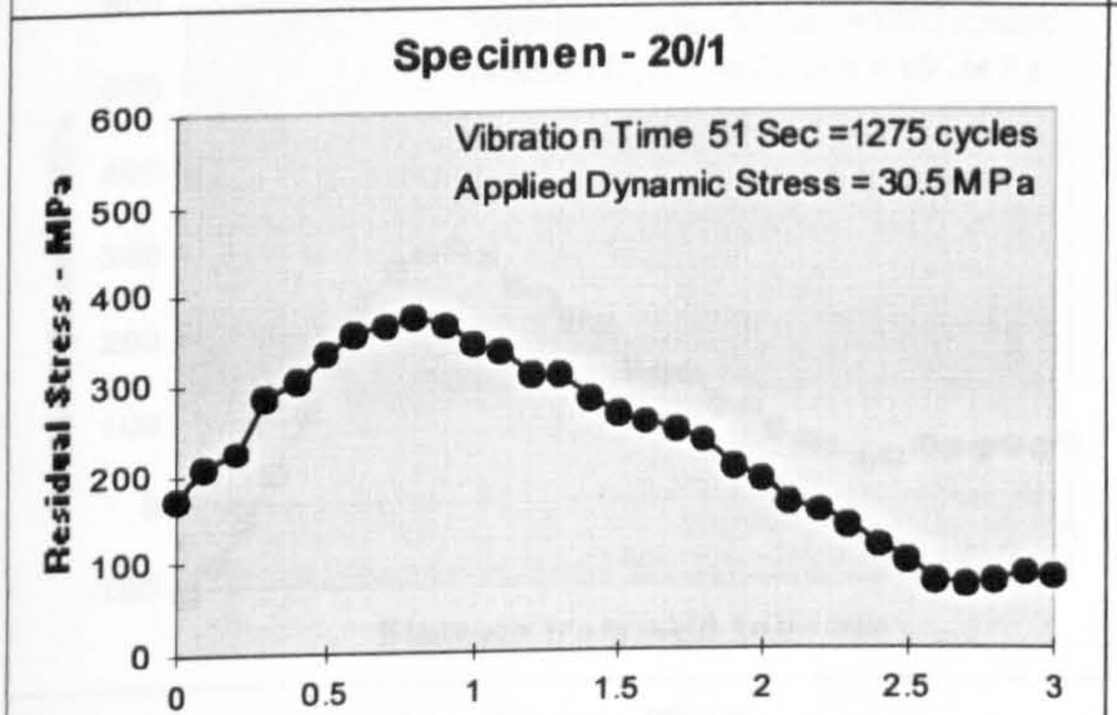

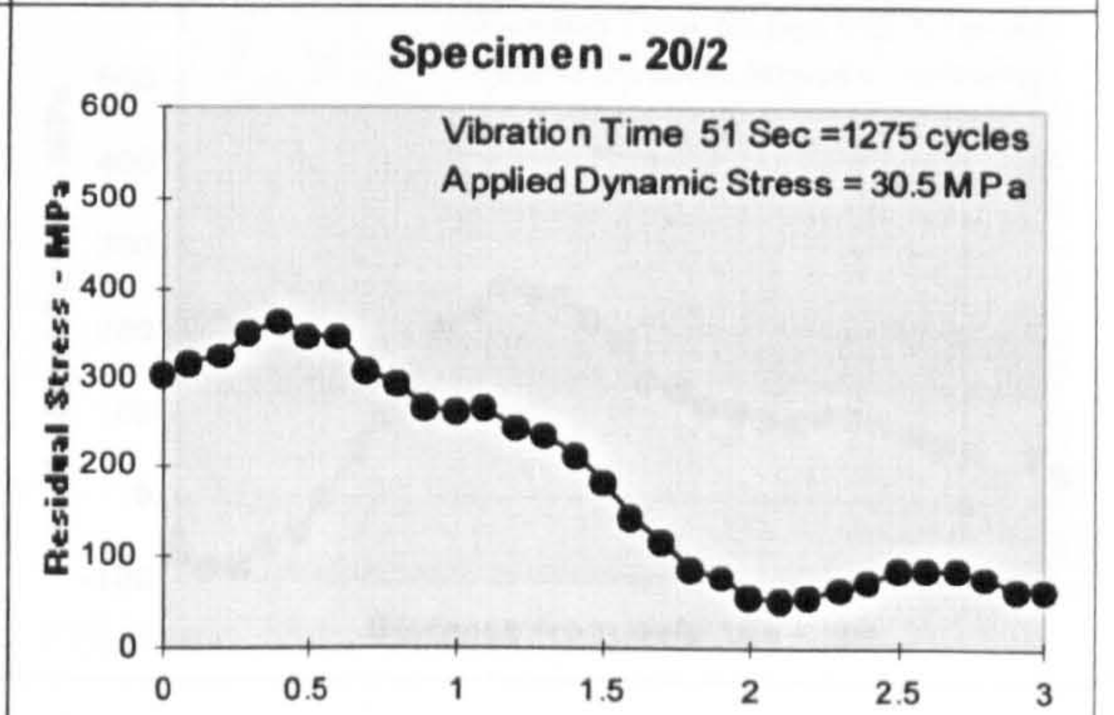

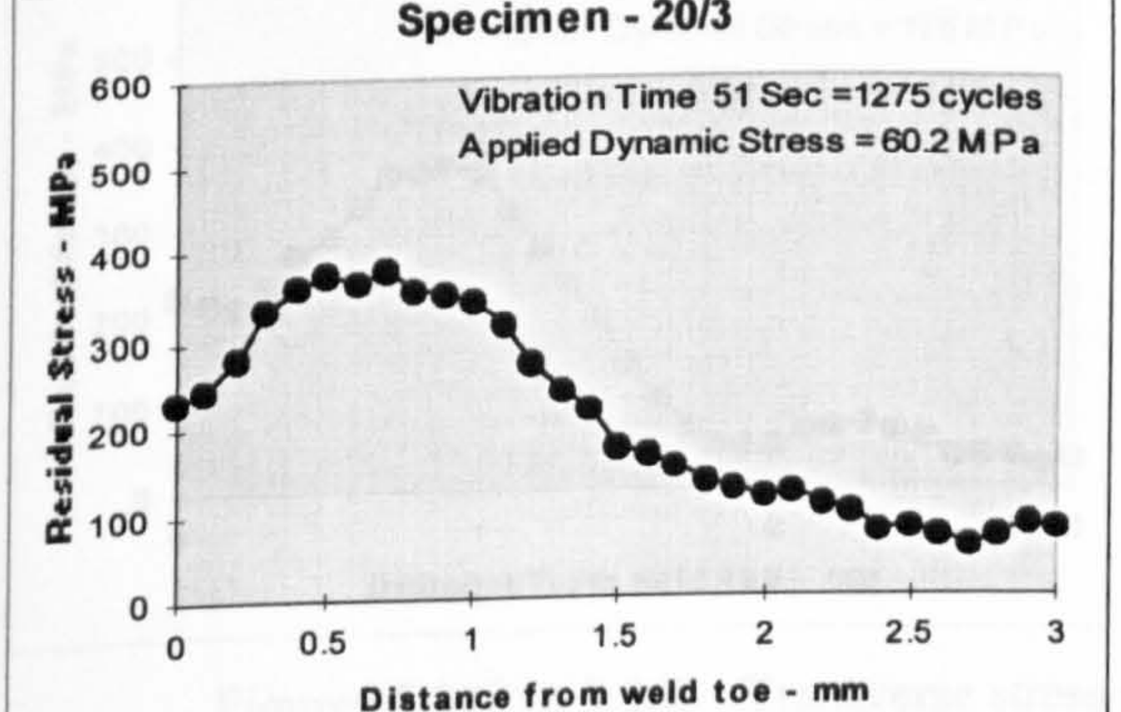

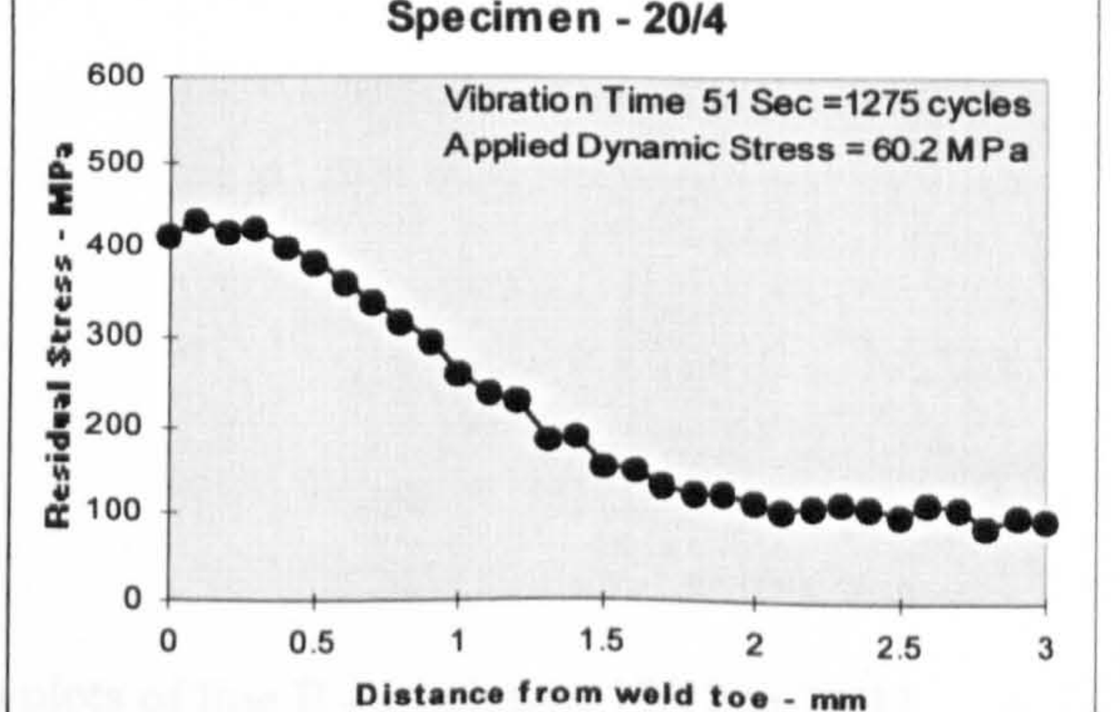

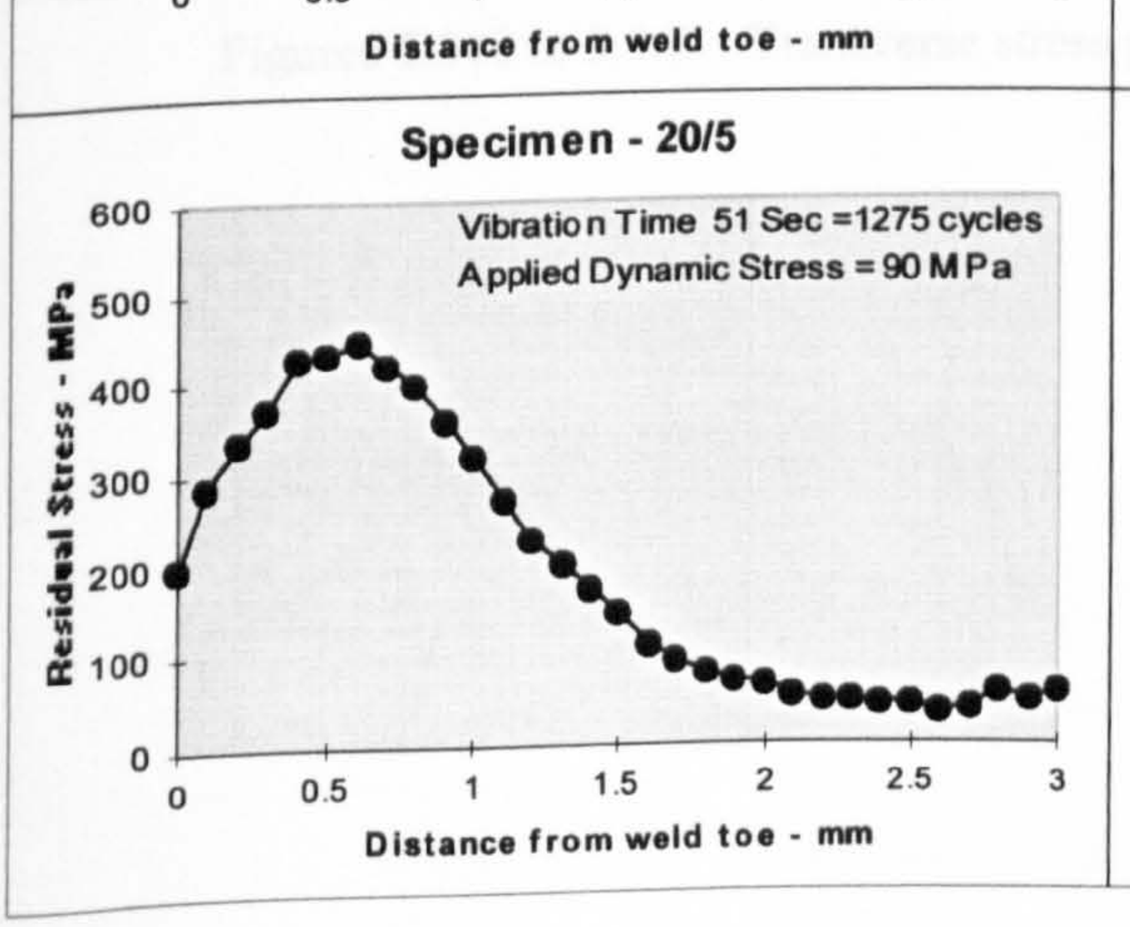

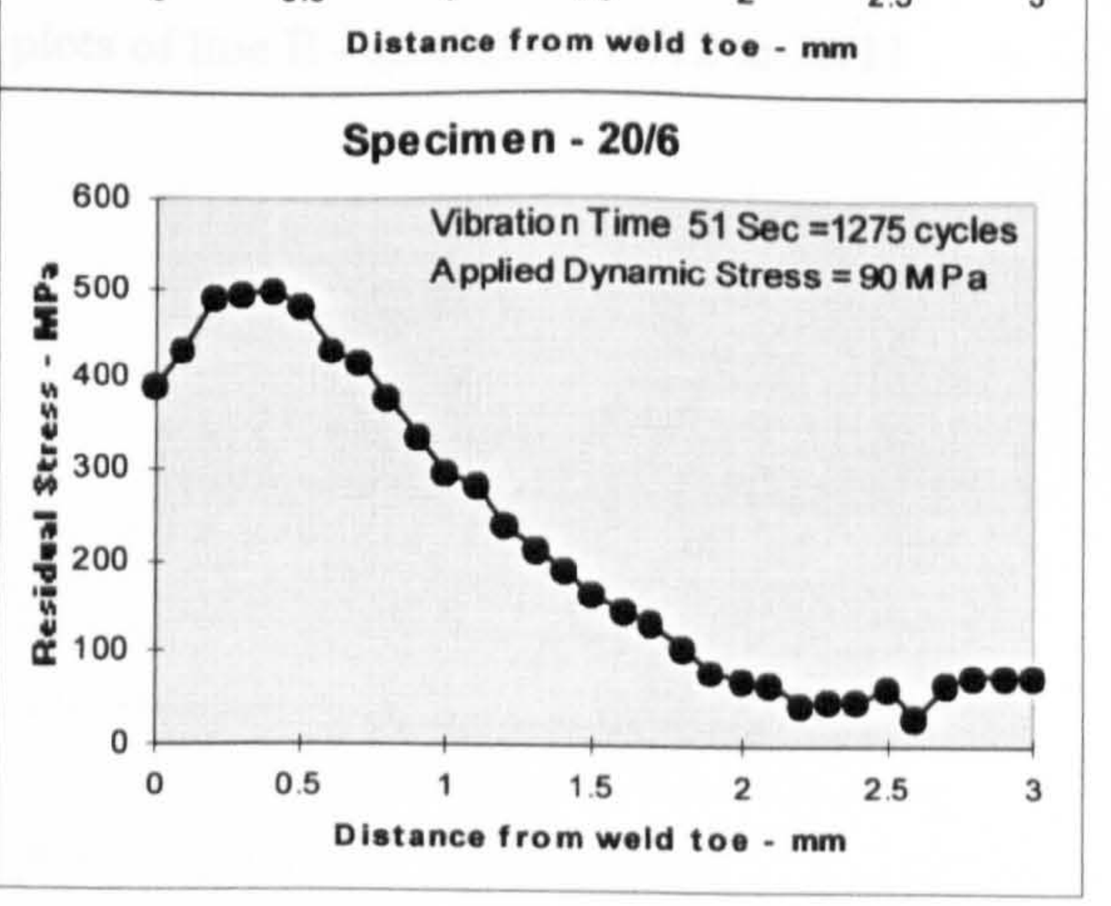

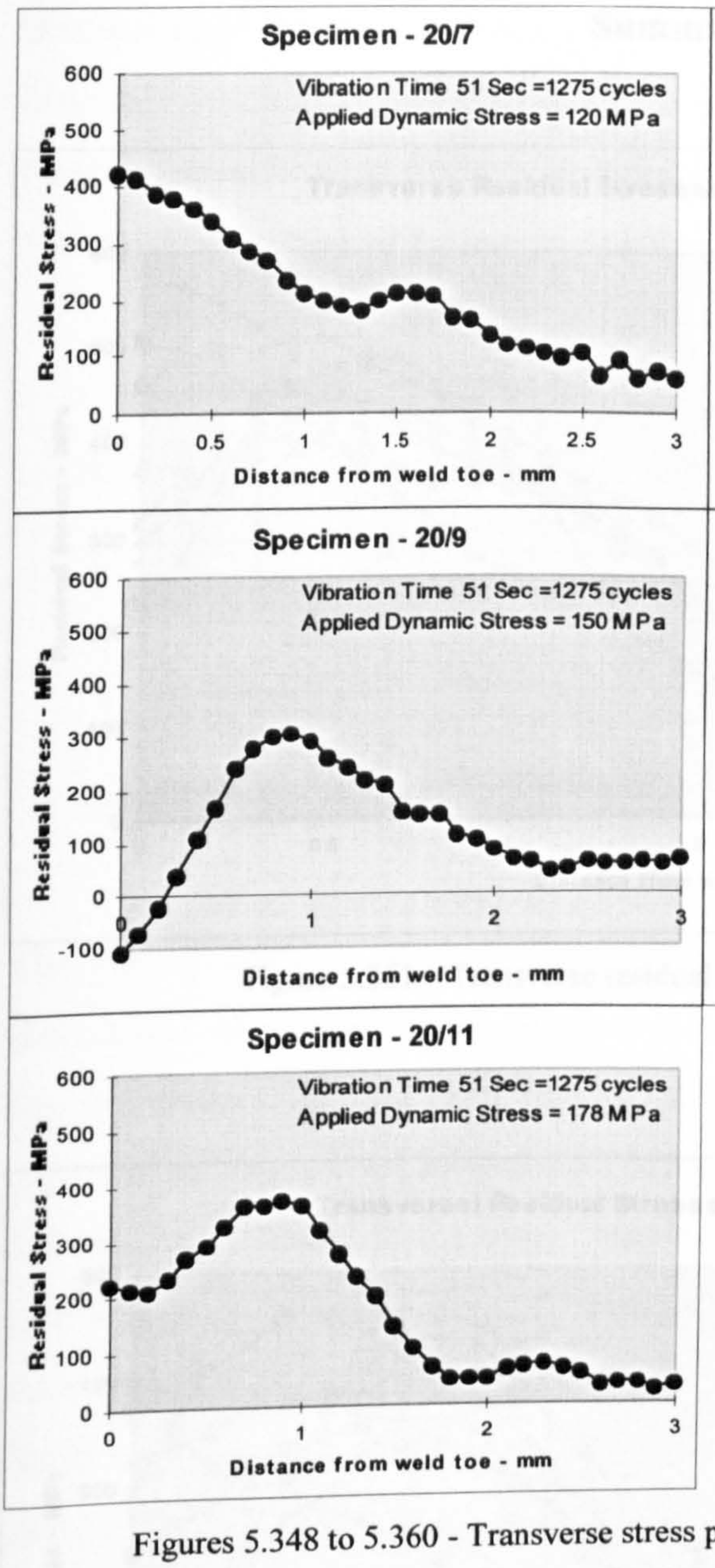

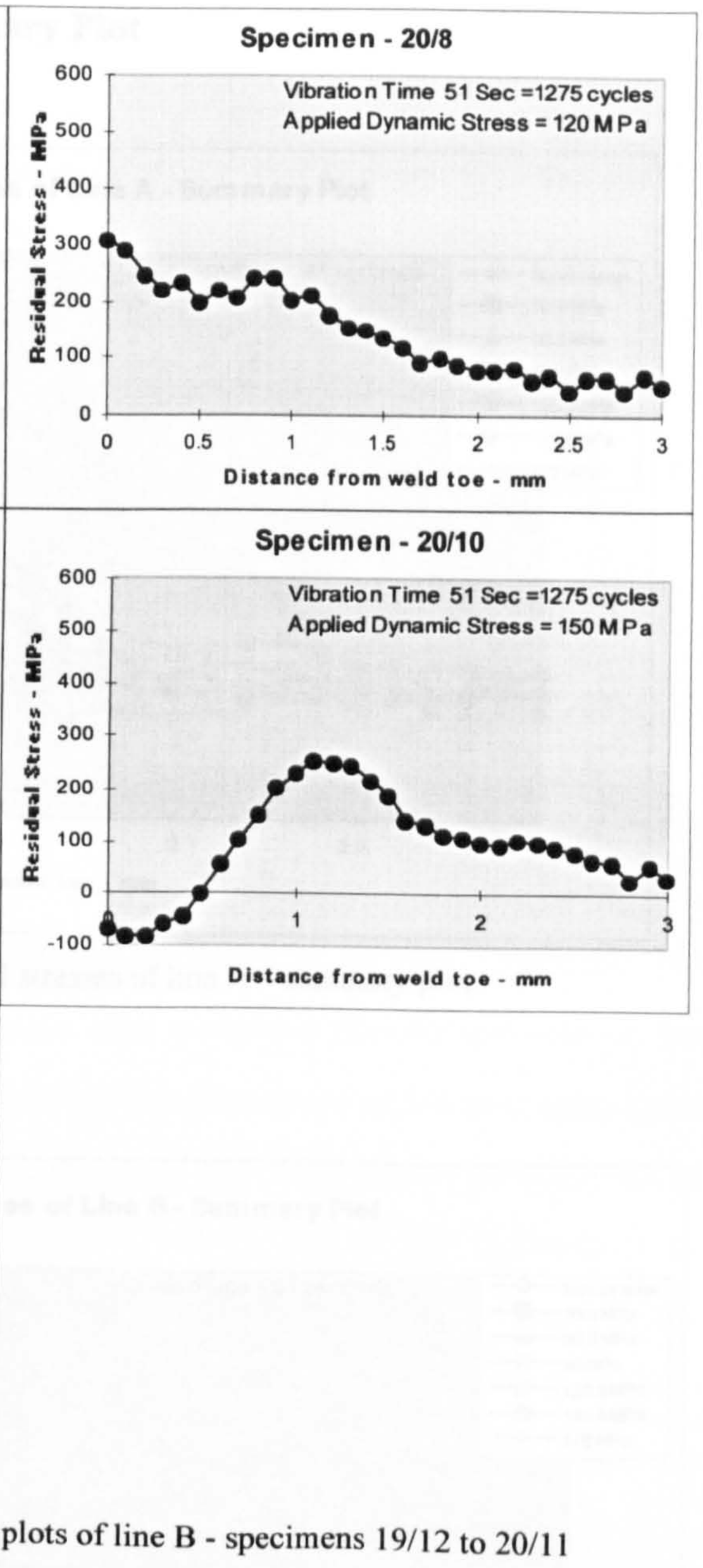

Figures 5.348 to 5.360 - Transverse stress plots of line B - specimens 19/12 to 20/11

Summary Plot

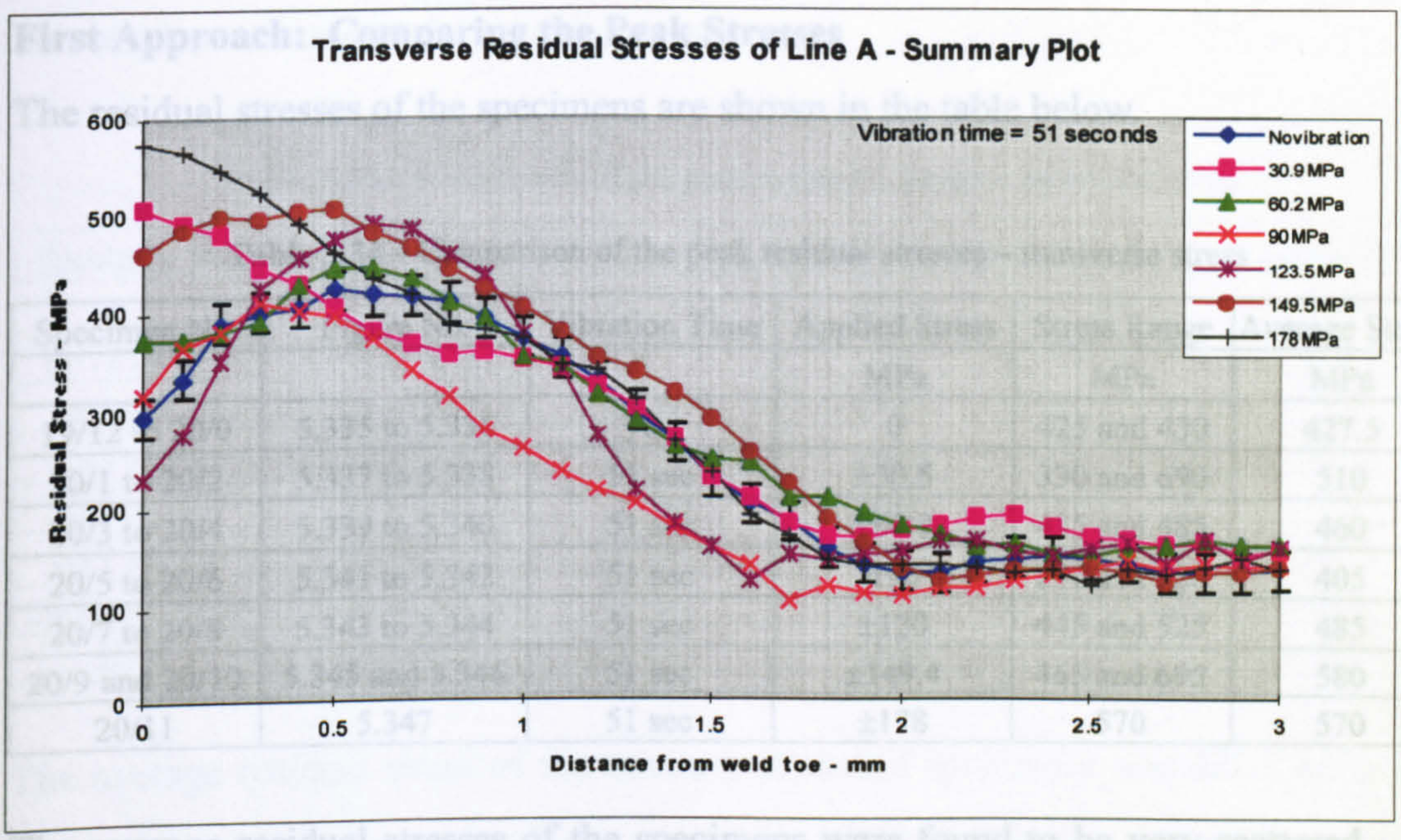

Figure 5.361 – Transverse residual stresses of line A – summary plot

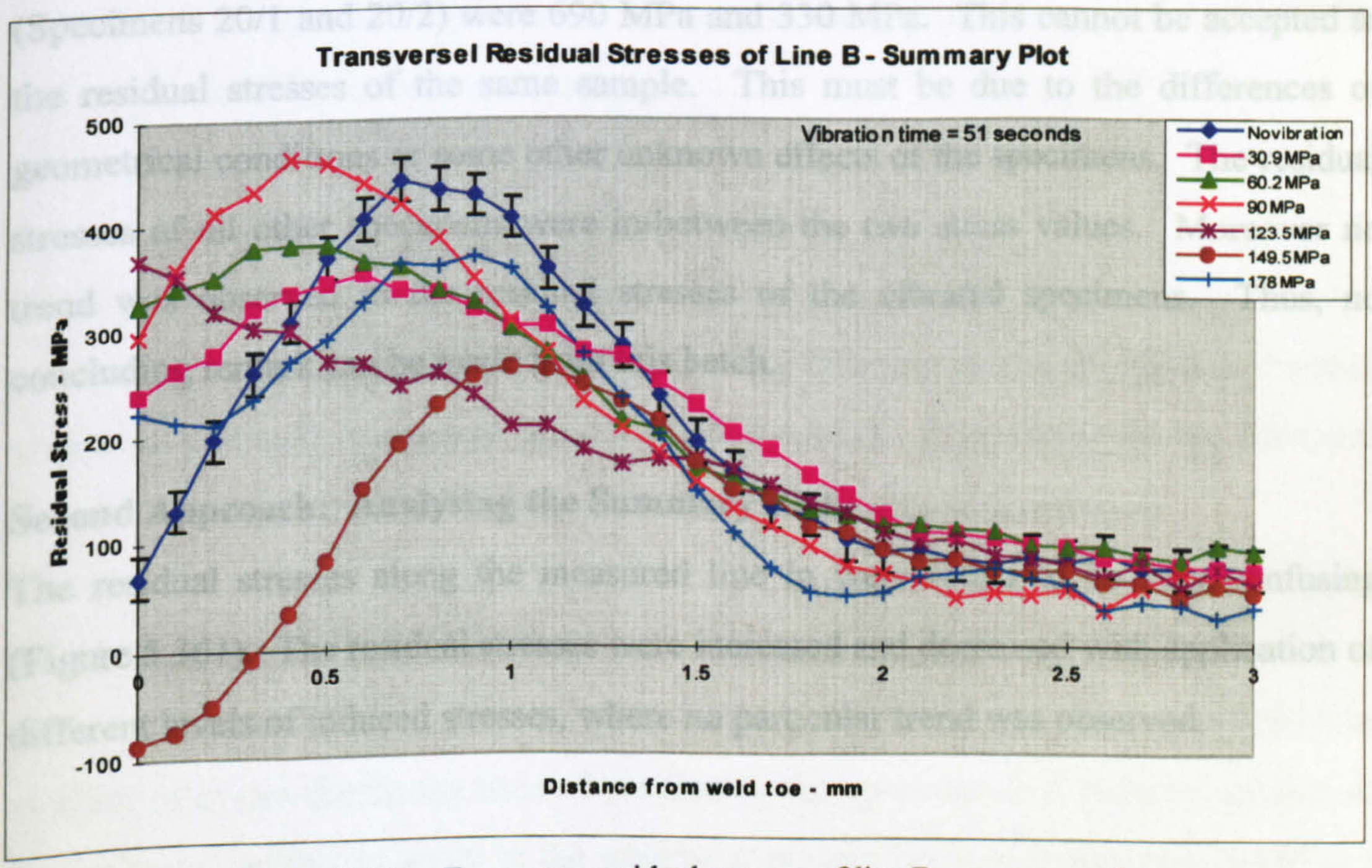

Figure 5.362 – Transverse residual stresses of line B – summary plot

Discussion of Results - Batch 1

Line A

First Approach: Comparing the Peak Stresses

The residual stresses of the specimens are shown in the table below.

Table 5.34 – Comparison of the peak residual stresses – transverse stress

Specimen No.	Figure No.	Vibration Time	Applied Stress	Stress Range	Average Stress
			MPa	MPa	MPa
19/12 to 20/0	5.335 to 5.336	0	0	425 and 430	427.5
20/1 to 20/2	5.337 to 5.338	51 sec	±30.5	330 and 690	510
20/3 to 20/4	5.339 to 5.340	51 sec	±60.2	435 and 485	460
20/5 to 20/6	5.341 to 5.342	51 sec	±90	290 and 520	405
20/7 to 20/8	5.343 to 5.344	51 sec	±120	445 and 525	485
20/9 and 20/10	5.345 and 5.346	51 sec	±149.4	465 and 695	580
20/11	5.347	51 sec	±178	570	570

The average residual stresses of the specimens were found to be very scattered. No clear trend of change in the residual stresses was observed due to increase in the applied stresses. In the same situation the peak residual stresses of the two specimens (Specimens 20/1 and 20/2) were 690 MPa and 330 MPa. This cannot be accepted as the residual stresses of the same sample. This must be due to the differences of geometrical conditions or some other unknown effects of the specimens. The residual stresses of all other specimens were in-between the two stress values. Moreover no trend was observed in the residual stresses of the vibrated specimens. Thus, no concluding remark can be made from this batch.

Second Approach: Analysing the Summary Plot

The residual stresses along the measured line in were found to be very confusing (Figure 5.361). The residual stresses were increased and decreased with application of different levels of induced stresses, where no particular trend was observed.

Line B

First Approach: Comparing the Peak Stresses

The residual stresses of the specimens were

Table 5.35 – Comparison of the peak residual stresses – transverse stress

Specimen No.	Figure No.	Vibration Time.	Applied Stress	Stress Range	Average Stress
			MPa	MPa	MPa
19/12 to 20/0	5.348 to 5.349	0	0	345 and 520	432.5
20/1 to 20/2	5.350 to 5.351	51 sec	±30.5	350 and 360	355
20/3 to 20/4	5.352 to 5.353	51 sec	±60.2	375 and 420	397.5
20/5 to 20/6	5.354 to 5.355	51 sec	±90	440 and 500	470
20/7 to 20/8	5.356 to 5.357	51 sec	±~120	310 and 425	367.5
20/9 and 20/10	5.358 and 5.359	51 sec	±149.4	240 and 300	270
20/11	5.360	51 sec	±178	370	370

The average residual stress of the unvibrated/control specimens was 432.5 MPa and the average residual stresses of the specimens vibrated inducing different amplitude stresses were 355 MPa, 397.5 MPa, 470 MPa, 367.5 MPa, 270 MPa and 370 MPa. Thus, apart from the specimens processed applying ±90 MPa, the residual stresses were found to decrease, however the increase in the applied stress above ±30.5 MPa did not increase the reduction any more.

Second Approach: Analysing the Summary Plot

On and near the weld toe (distance range 0-1 mm), the residual stresses were found to increase and also decrease with application of different levels of applied stresses, where no particular trend was present (Figure 5.362). Away from the toe (distance range 1-3 mm), the residual stresses were found to be almost unchanged.

Batch 2

In this batch the vibration frequency was reduced to 7 Hz in order to apply a reduced number of cycles during the time of processing the specimens. A reduced number of cycles were decided to apply to the treatment process because it was considered that there might be a strain hardening during treatment which re-increased residual stress after dropping in the first few cycles of treatment.

In this batch six specimens were processed without any treatment. After 31 seconds of the weld finishing, vibration started and continued for 5 seconds, i.e. 35 cycles of vibration. In this waiting time (31 seconds) the HAZ temperature decreased to ~395 ^{0}C ("b" in Figure 5.333), the yield stress at that temperature was ~235 MPa (shown in Figure 5.334). The applied stresses to the specimens are shown in the plots. The transverse residual stresses on the two lines (line A and line B as in Figure 5.243) were measured.

Residual Stress of Line A

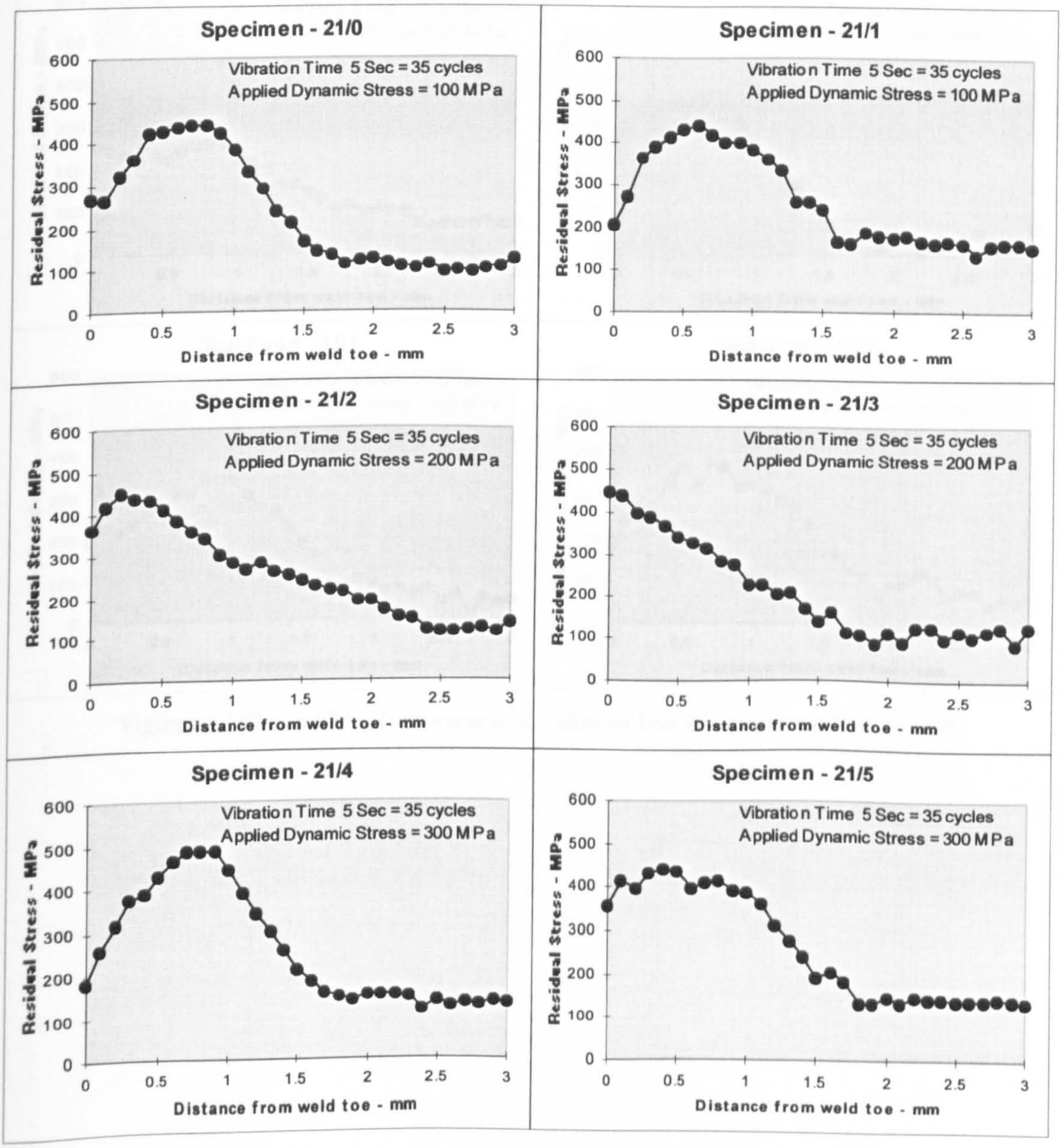

Figure 5.363 to 5.368 - Transverse stress plots of line A - specimens 21/0 to 21/5

Residual Stress of Line B

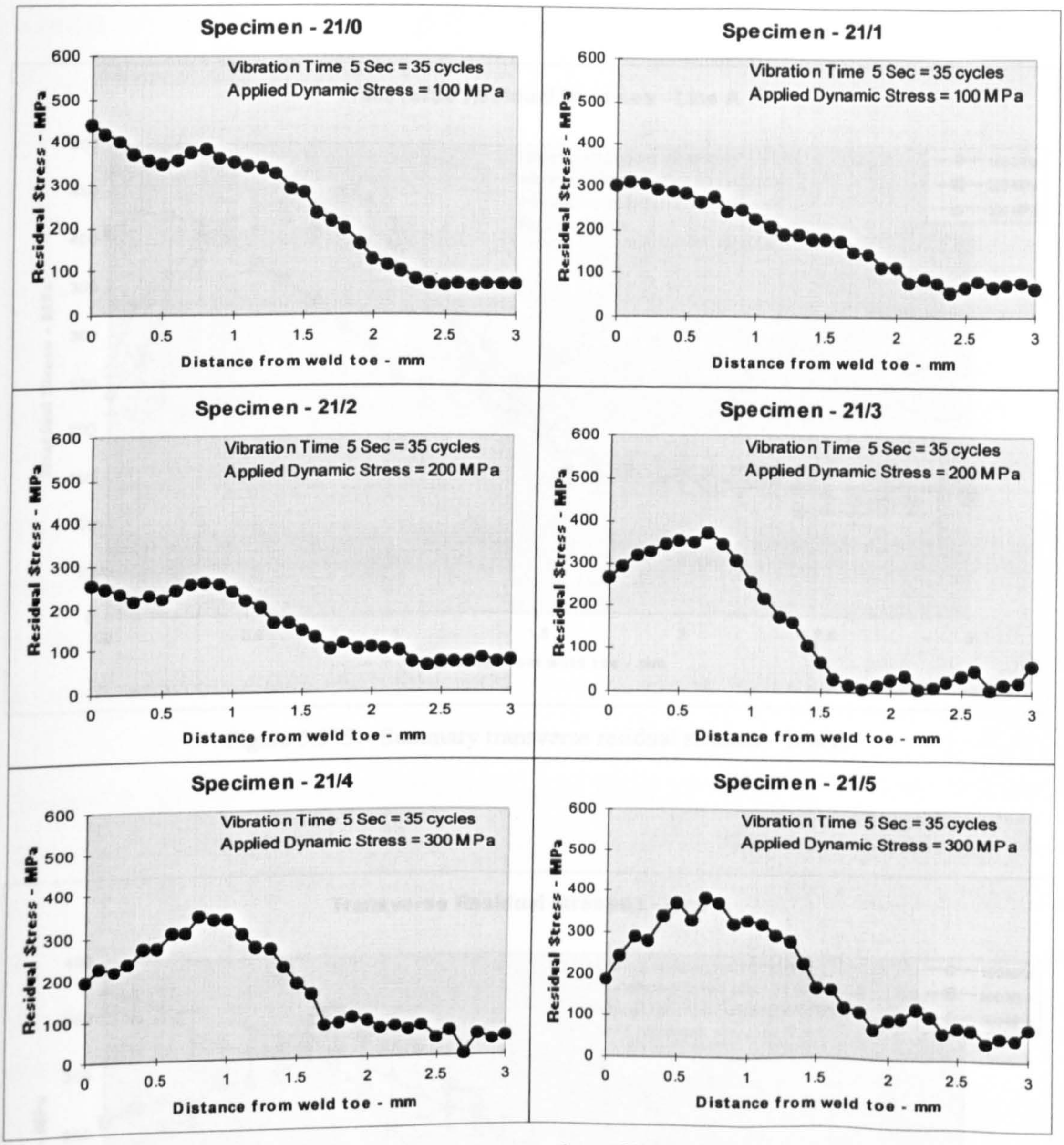

Figures 5.369 to 5.374 - Transverse stress plots of line B - specimens 21/0 to 21/5

Summary Plots

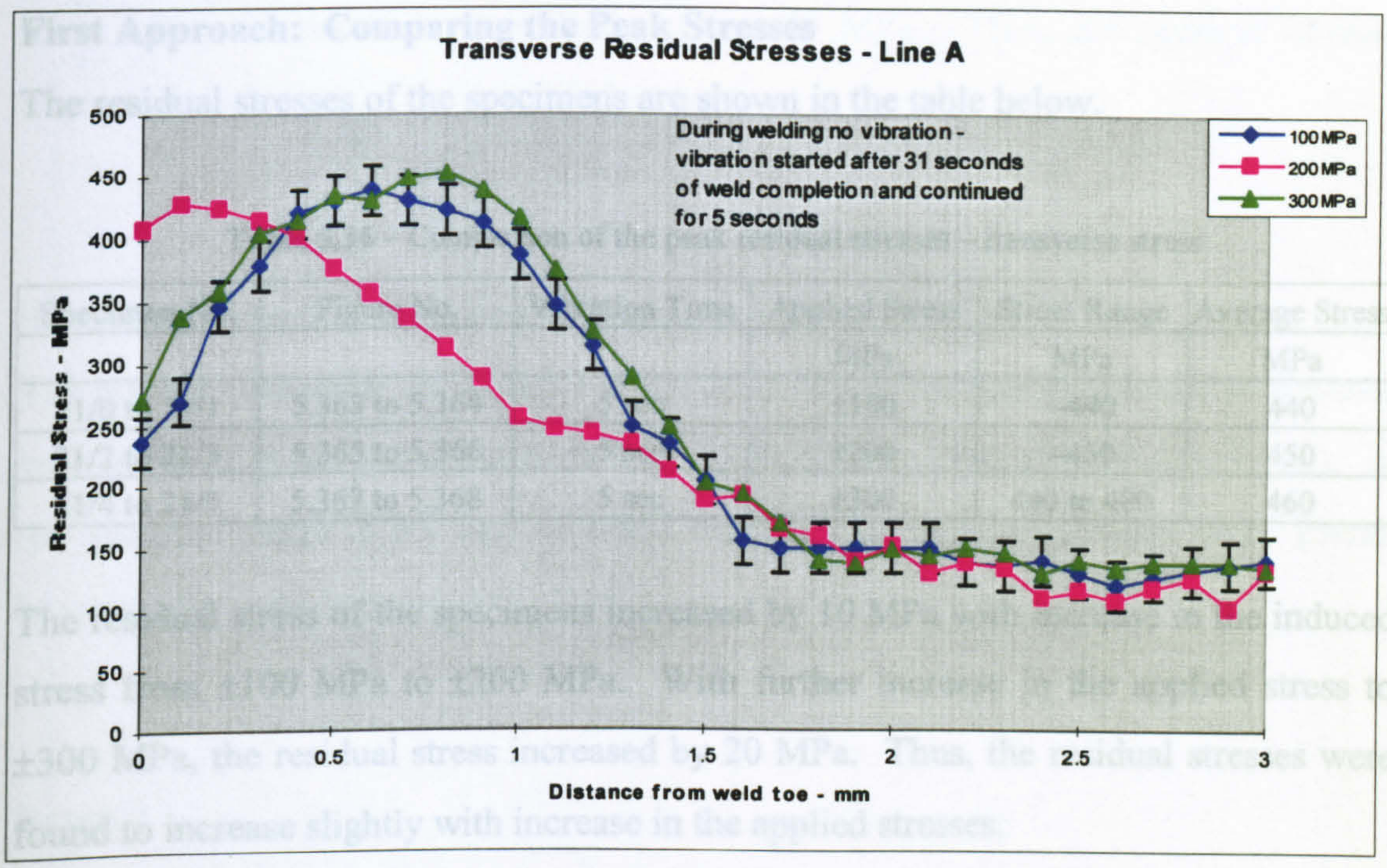

Figure 5.375 – Summary transverse residual stresses – line A

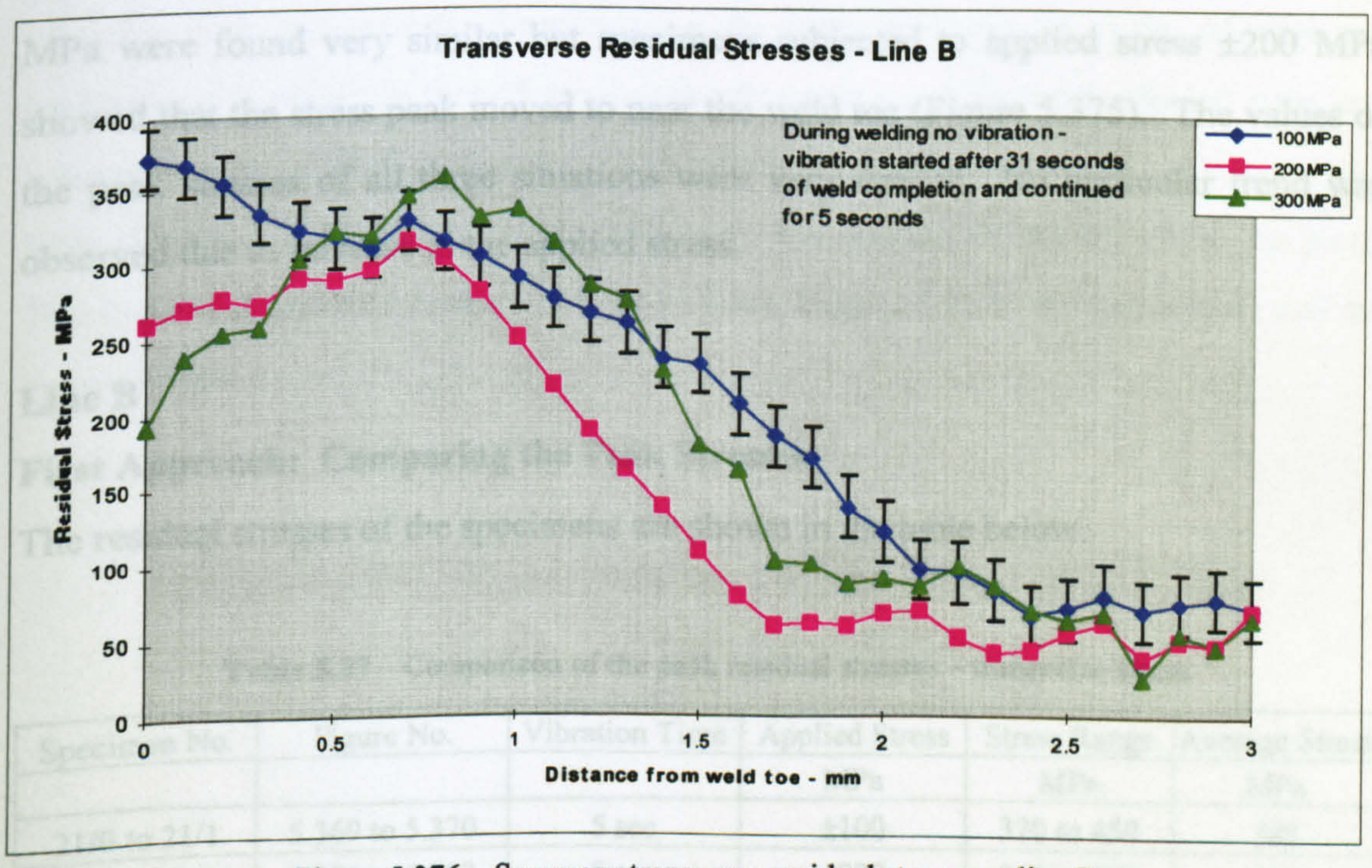

Figure 5.376 – Summary transverse residual stresses – line B

Discussion of Results - Batch 2

Line A

First Approach: Comparing the Peak Stresses

The residual stresses of the specimens are shown in the table below.

Table 5.36 – Comparison of the peak residual stresses – transverse stress

Specimen No.	Figure No.	Vibration Time	Applied Stress	Stress Range	Average Stress
			MPa	MPa	MPa
21/0 to 21/1	5.363 to 5.364	5 sec	±100	~440	440
21/2 to 21/3	5.365 to 5.366	5 sec	±200	~450	450
21/4 to 21/5	5.367 to 5.368	5 sec	±300	440 to 480	460

The residual stress of the specimens increased by 10 MPa with increase in the induced stress from ±100 MPa to ±200 MPa. With further increase in the applied stress to ±300 MPa, the residual stress increased by 20 MPa. Thus, the residual stresses were found to increase slightly with increase in the applied stresses.

Second Approach: Analysing the Summary Plot

The residual stresses of the specimens subjected to applied stress ±100 MPa and ±300 MPa were found very similar but specimens subjected to applied stress ±200 MPa showed that the stress peak moved to near the weld toe (Figure 5.375). The values of the peak stresses of all three situations were very similar. No particular trend was observed due to increase in the applied stress.

Line B

First Approach: Comparing the Peak Stresses

The residual stresses of the specimens are shown in the table below.

Table 5.37 – Comparison of the peak residual stresses – transverse stress

Specimen No.	Figure No.	Vibration Time	Applied Stress	Stress Range	Average Stress
			MPa	MPa	MPa
21/0 to 21/1	5.369 to 5.370	5 sec	±100	320 to 450	385
21/2 to 21/3	5.371 to 5.372	5 sec	±200	260 to 370	315
21/4 to 21/5	5.373 to 5.374	5 sec	±300	340 to 378	359

The residual stress of the specimens decreased by 70 MPa with increase in the induced stress from ±100 MPa to ±200 MPa. With further increase in the applied stress to ±300 MPa, the residual stress decreased by 26 MPa. Thus, the residual stresses decreased with application in applied stresses.

Second Approach: Analysing the Summary Plot

The residual stresses in the distance range 0-2.2 mm of the line were found to decrease with increase in the applied stresses from ±100 MPa to ±300 MPa (Figure 5.376). In the distance range 2.2-3 mm, a small decreases in residual stresses were found, however the trend was not very clear.

Batch 3

Similar to batch 2, the frequency of vibration of this batch was 7 Hz. In this batch six specimens were processed. The specimens were welded without any treatment. Vibratory treatment was started after 45 seconds of finishing of the welding. The vibration was continued for 5 seconds, i.e. on every specimen 35 cycles of vibratory loading was applied. In that 45 seconds the temperature of the heat affected zone was reduced to 320 ^{0}C ("c" in Figure 5.333), which corresponds to a yield stress of ~267 MPa (Figure 5.334). The applied stresses to the specimens are shown in the plots. The transverse residual stresses of the two lines (Figure 5.243) were measured and are shown below.

Residual Stress of Line A

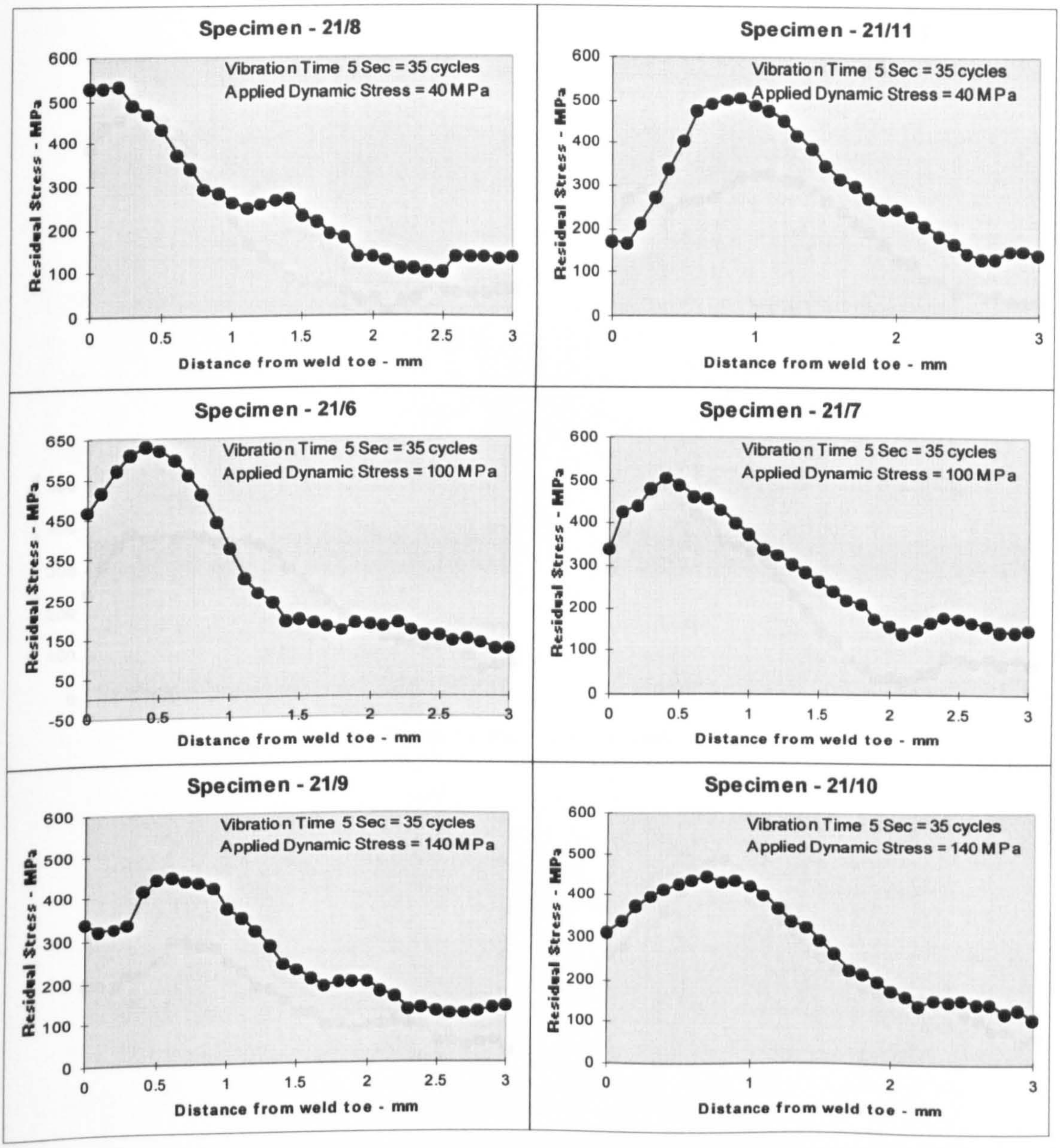

Figures 5.377 to 5.382 - Transverse stress plots of line A - specimens 21/6 to 21/11

The Residual Stress of Line B

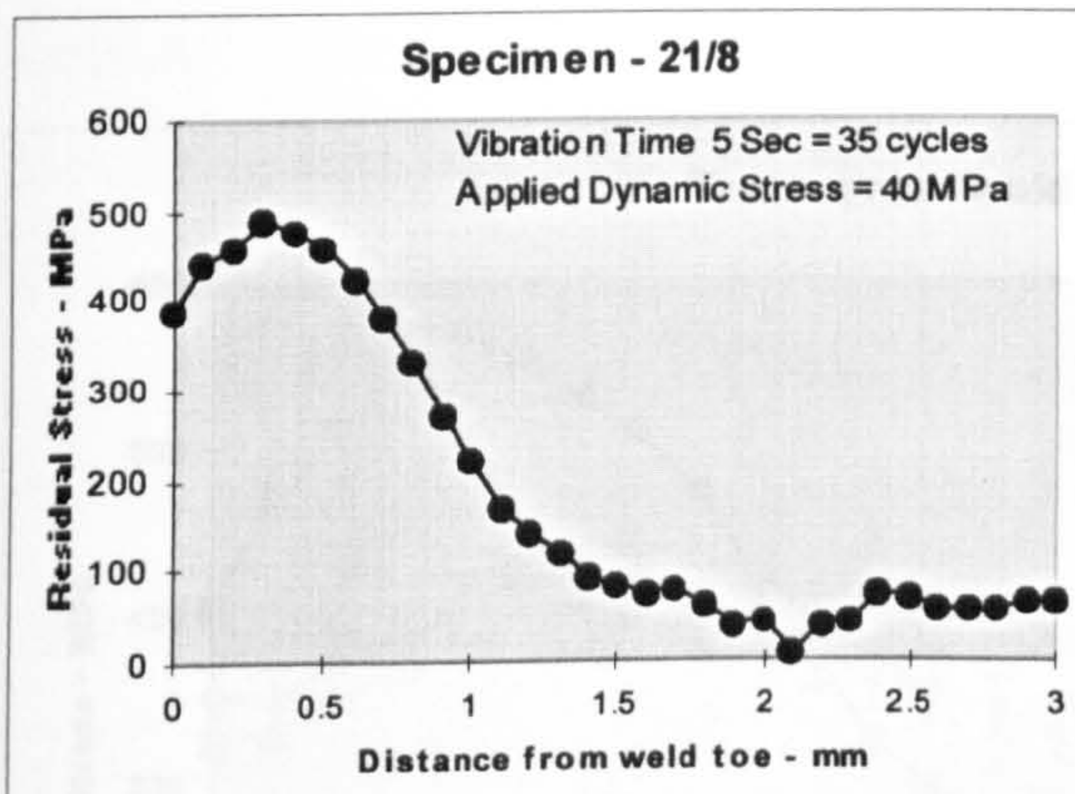

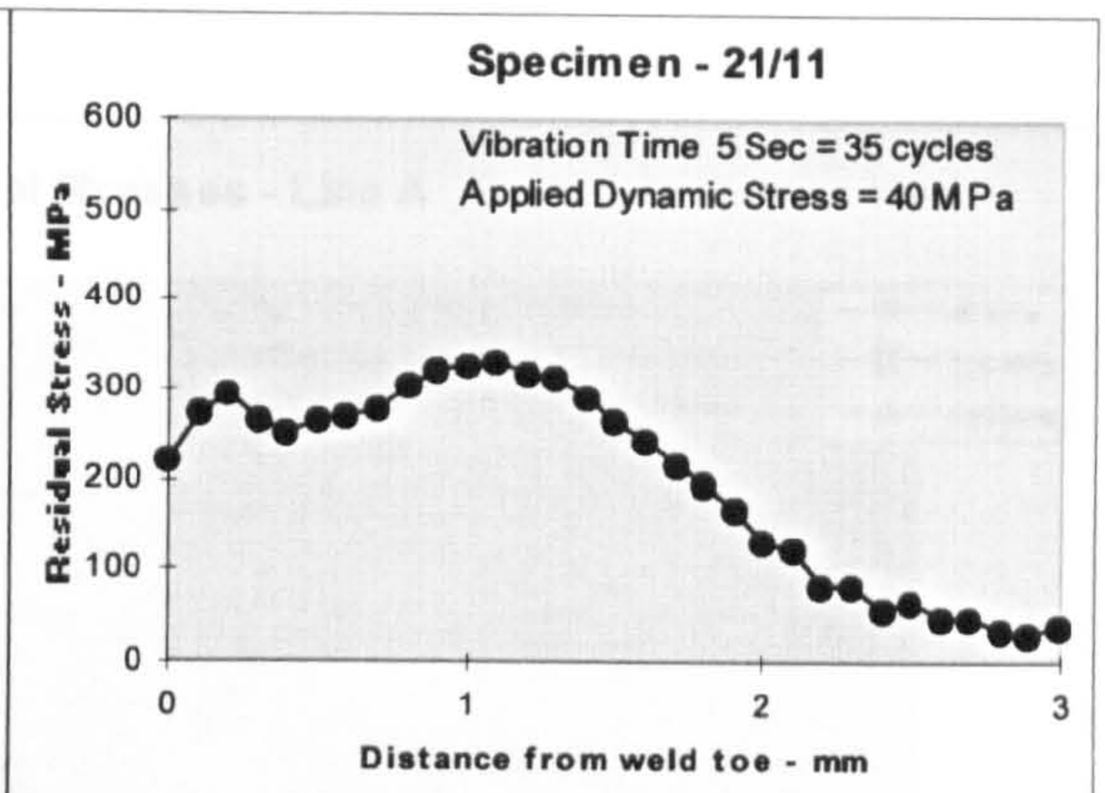

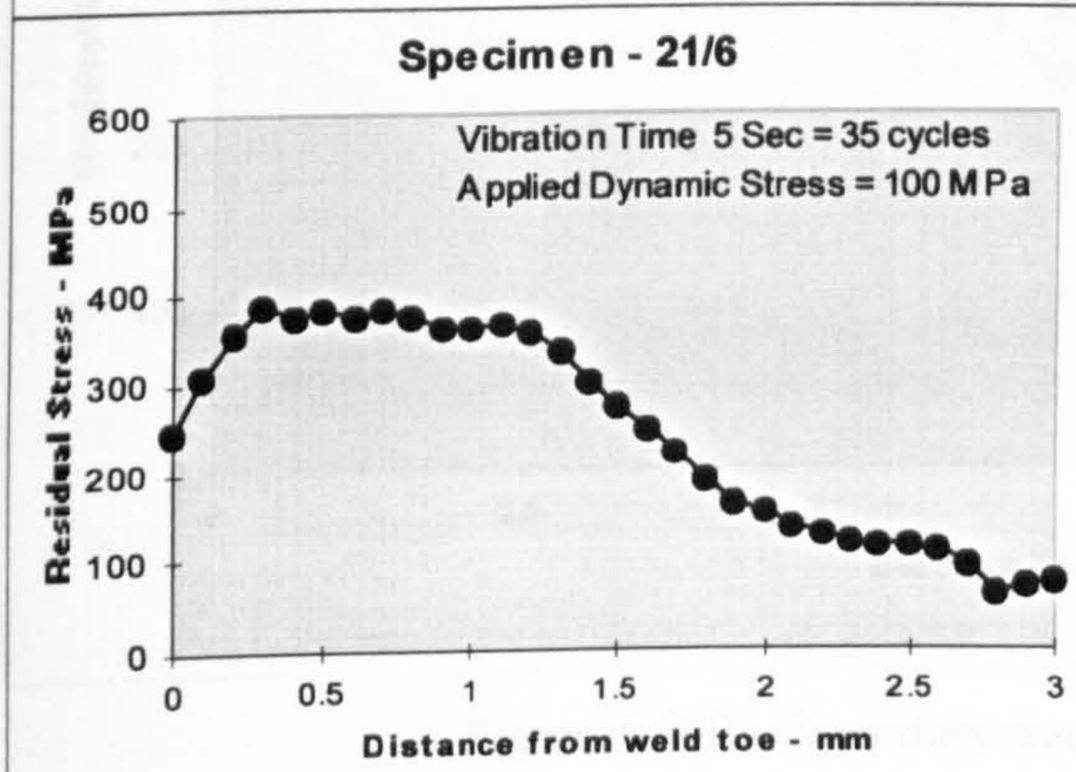

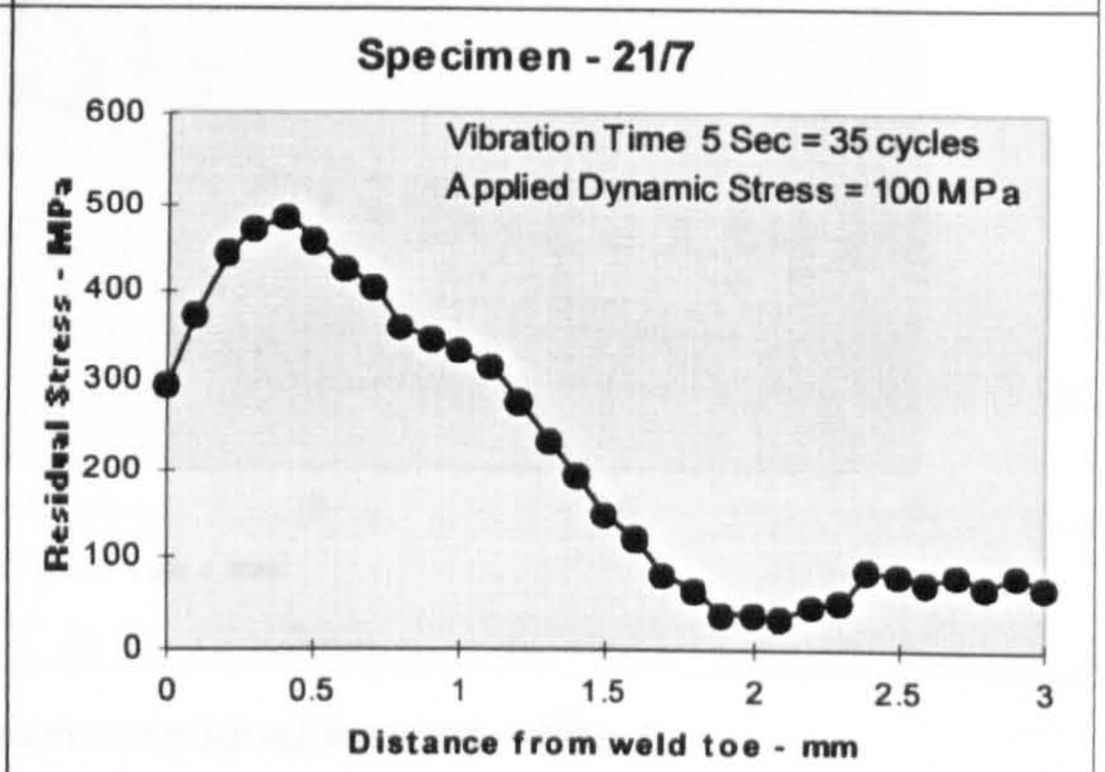

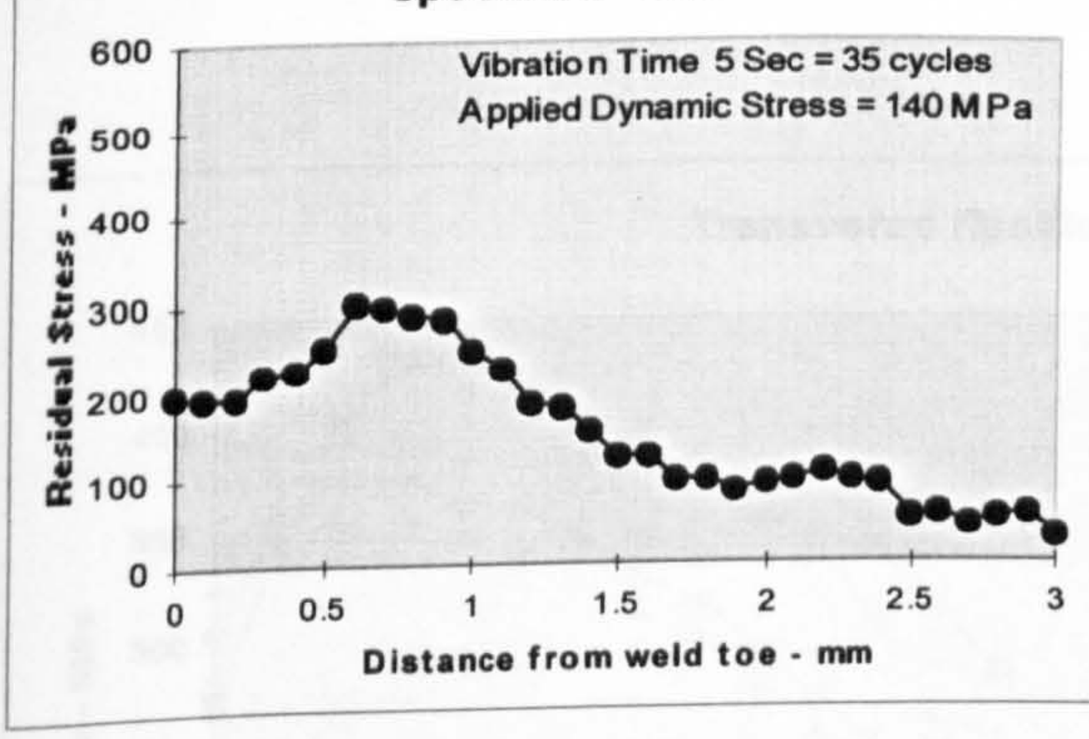

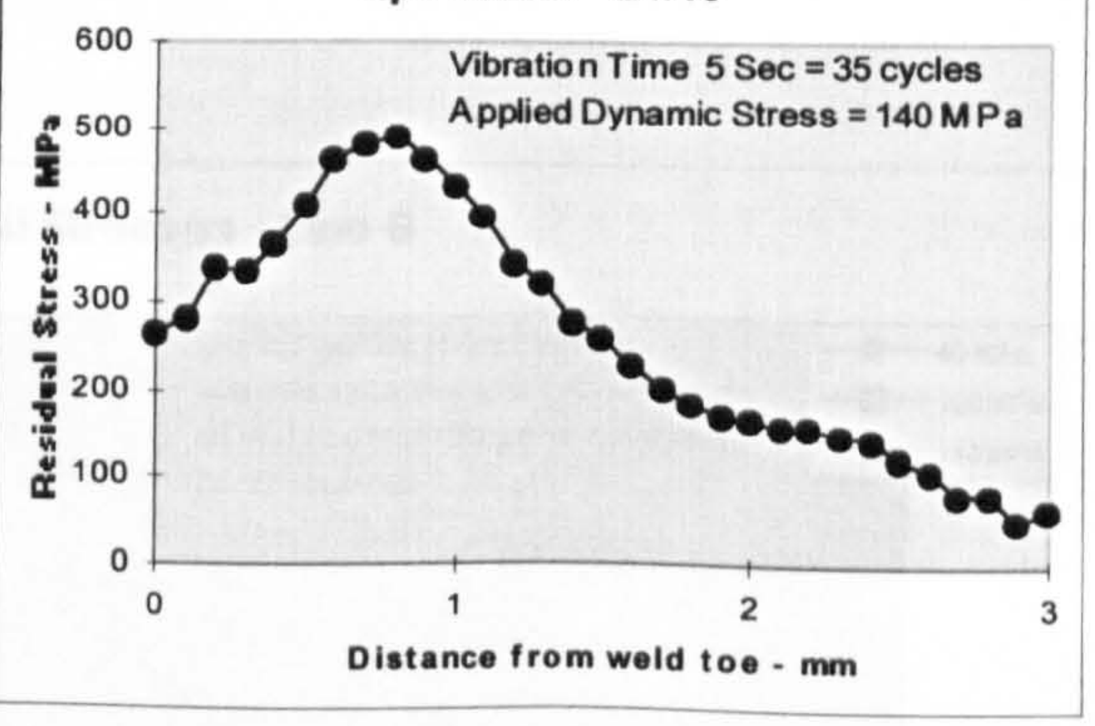

Figures 5.383 to 5.388 - Transverse stress plots of line B - specimens 21/6 to 21/11

Summary Plots

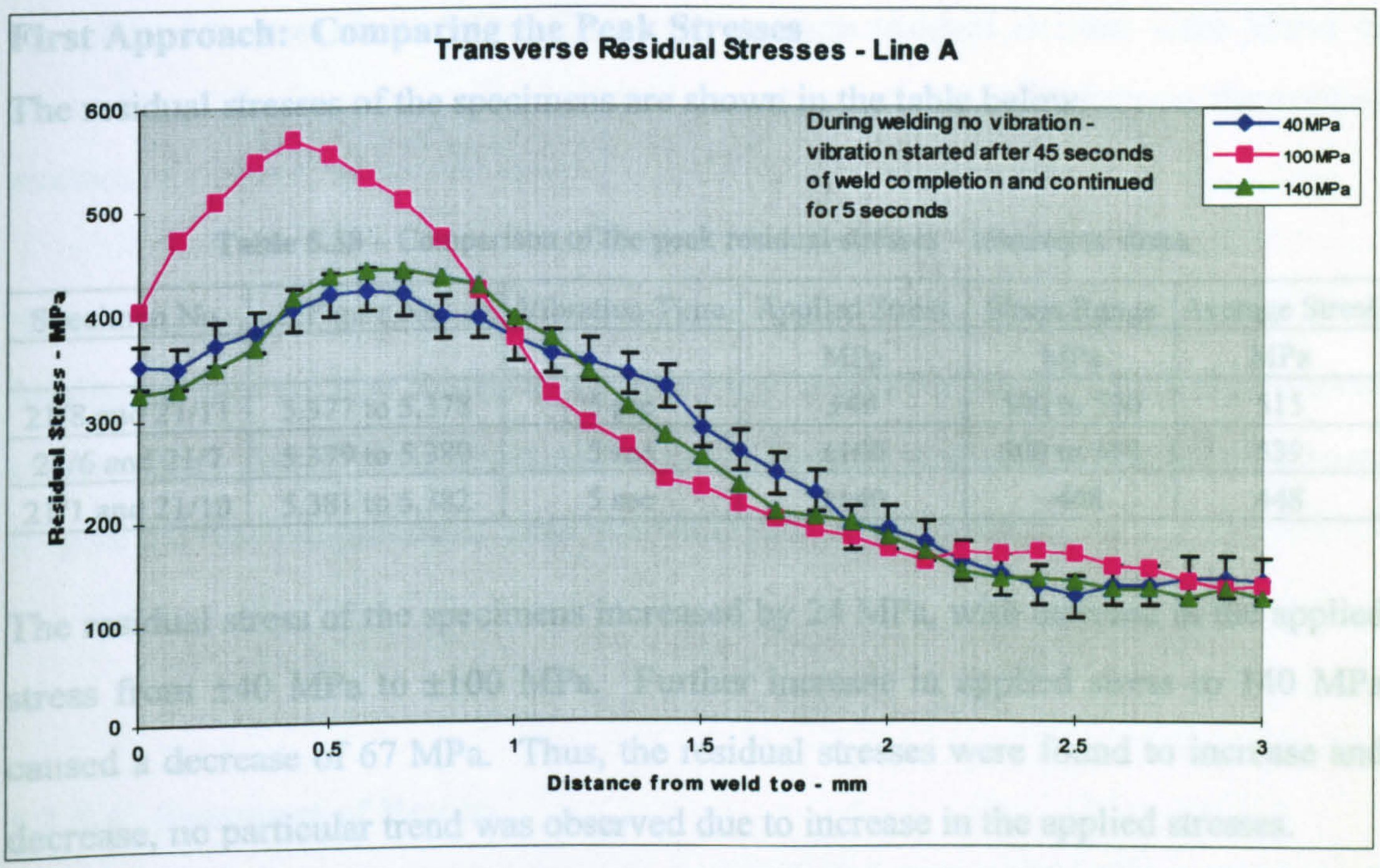

Figure 5.389 – Summary transverse residual stresses – line A

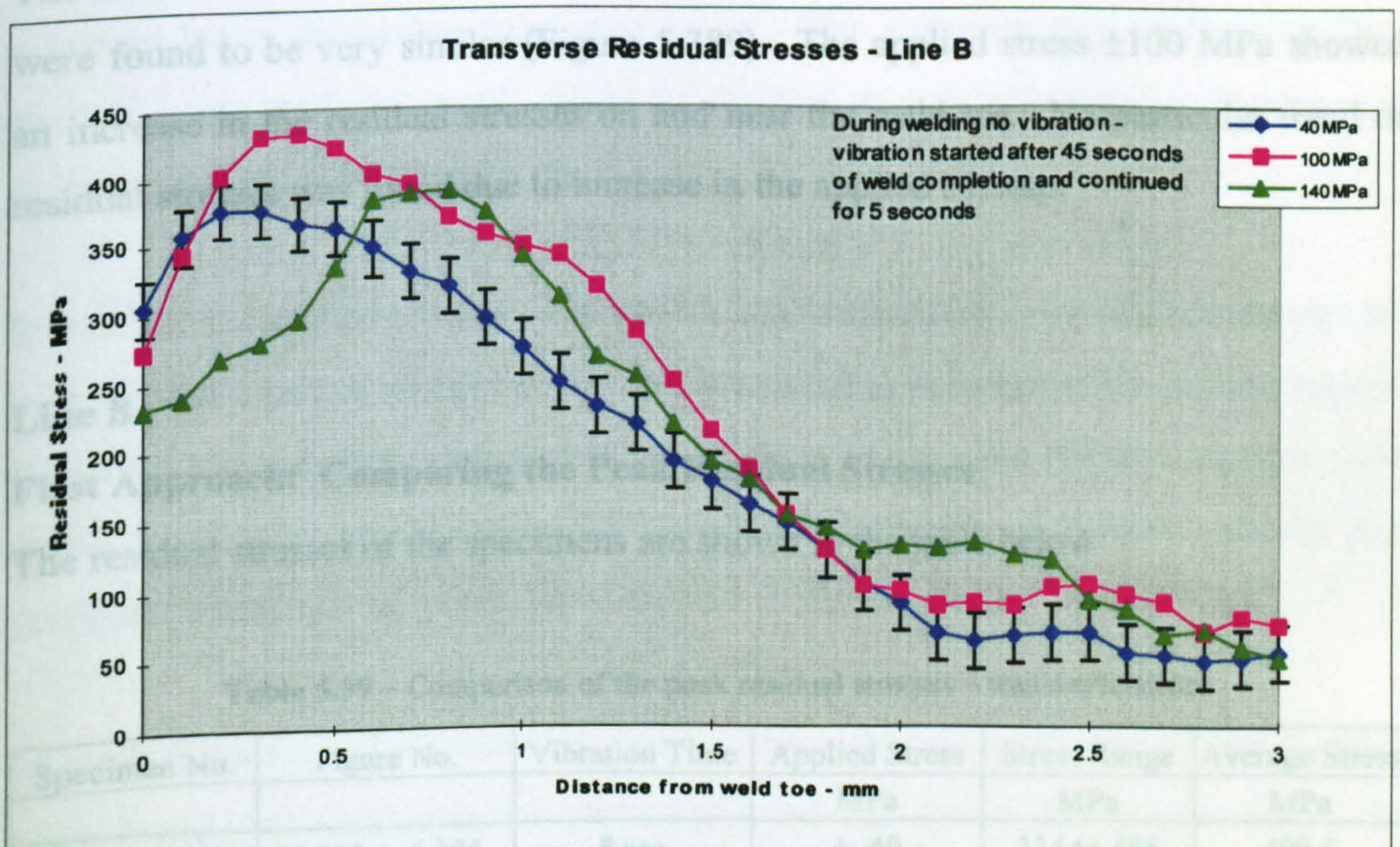

Figure 5.390 – Summary transverse residual stresses – line A

Discussion of Results - Batch 3

Line A

First Approach: Comparing the Peak Stresses

The residual stresses of the specimens are shown in the table below.

Table 5.38 – Comparison of the peak residual stresses – transverse stress

Specimen No.	Figure No.	Vibration Time	Applied Stress	Stress Range	Average Stress
			MPa	MPa	MPa
21/8 and 21/11	5.377 to 5.378	5 sec	±40	500 to 530	515
21/6 and 21/7	5.379 to 5.380	5 sec	±100	500 to 578	539
21/1 and 21/10	5.381 to 5.382	5 sec	±140	~448	448

The residual stress of the specimens increased by 24 MPa, with increase in the applied stress from ±40 MPa to ±100 MPa. Further increase in applied stress to 140 MPa caused a decrease of 67 MPa. Thus, the residual stresses were found to increase and decrease, no particular trend was observed due to increase in the applied stresses.

Second Approach: Analysing the Summary Plot

The residual stresses of the specimens with applied stresses ±40 MPa and ±140 MPa were found to be very similar (Figure 5.389). The applied stress ±100 MPa showed an increase in the residual stresses on and near the weld toe. No particular trend of residual stresses was found due to increase in the applied stresses.

Line B

First Approach: Comparing the Peak Residual Stresses

The residual stresses of the specimens are shown in the table below

Table 5.39 – Comparison of the peak residual stresses – transverse stress

Specimen No.	Figure No.	Vibration Time	Applied Stress	Stress Range	Average Stress
			MPa	MPa	MPa
21/8 and 21/11	5.383 to 5.384	5 sec	±~40	334 to 485	409.5
21/6 and 21/7	5.385 to 5.386	5 sec	±100	380 to 480	430
21/1 and 21/10	5.387 to 5.388	5 sec	±140	293 to 490	391.5

The residual stress of the specimens increased by 20 MPa, with increase in the applied stress from ±40 MPa to ±100 MPa. Further increase in applied stress to 140 MPa caused a decrease of 18 MPa. Thus, the average residual stresses were found to increase and decrease, no particular trend was observed due to increase in the applied stresses.

Second Approach: Analysing the Summary Plot

Similar to line A, line B also showed a very confusing result, where the residual stresses were found to decrease and increase due to increase in the applied stresses (Figure 5.390). No particular trend was observed from this batch.

5.3.5.4 Summary of Results

In batch 1, the dynamic applied stress to the specimens were varied. The average peak residual stresses of line A were found to be very scattered. The scatter was so high that any comparison was impossible. In line B, the residual stresses were also scattered but a decreasing trend was found. The summary plot of the two lines showed a very confusing result, where the residual stresses were found to increase and decrease without any particular trend.

In batch 2, the applied stresses were varied. Due to increase in the applied stresses the average peak residual stresses of line A were found to increase with a smaller degree. However, the summary plot showed a different result - the residual stresses were found to increase and decrease with application of induced stresses without any particular trend.

In batch 3, the applied stresses were varied. The peak residual stresses of line A and B were found very confusing, no particular trend was found due to increase in the applied stresses. A similar result was found in the summary plot of the two lines.

The results of this experiment showed a high scatter, which must be the effect of some unknown factors, might be due to different geometrical condition or different metallurgical properties. In all three batches, no particular trend of residual stresses were observed. Thus, no global conclusion may be drawn these results.

The importance of this experiment demanded an extensive study, which was not done due to the time limitation of this experimenter. In this experiment only three batches of specimens were processed also the number of specimens in the batches were not so large. This experiment was just a start of investigation of the effect of dynamic induced stresses on the changing yield stresses of the metal. A further detailed investigation is necessary by following the yield stresses of the cooling material/steel.

5.3.6 Experiment VI:

Investigation of VWC in Combined Vibration Mode (Flexural and Longitudinal)

Abstract

In this experiment the findings of a Japanese paper was investigated. Two batches of specimens were processed where the vibratory amplitude was varied. The resulting longitudinal residual stresses of both batches were found to be very confusing where the stresses were found to increase and decrease with application of vibration - no particular trend of change in residual stresses were observed. The transverse residual stresses were found to increase on and near the weld toe, but away from the weld, no particular trend of change in the residual stresses was observed.

5.3.6.1 Introduction

This experiment was designed to investigate the findings in a Japanese paper produced by Shigeru Aoki and Tadashi Nishimura [7], "Analytical Model for Improvement of Residual Stress of Welding Joint using Vibration". In this paper it is claimed that vibration during welding reduces residual stress significantly on the weld and part of the heat affected zone. In their experiment two identical flat bar specimens were welded together where the far ends of the specimens were fixed and the other two ends were welded (Figure 5.391). During welding, the specimens were vibrated with a small shaker. The longitudinal residual stress was shown to be significantly down on the welds and some part of the heat affected zone. Residual stress on the parent metal some distance away from the weld was shown to be increased. The time of vibration or number of cycles applied was not mentioned in that paper. The transverse residual stress was not measured or was not presented in that paper. It was decided to investigate/repeat that work because the flexural vibration treatment in Experiment IV and V (little different from their set-up) did not show any significant change in the residual stresses.

5.3.6.2 Experimental Procedure

In this experiment, the experimental procedures described in the Japanese paper were copied. The set-up shown in their paper was amended a little to adapt with the existing X-ray diffractometer and the vibrator. The set-up is shown in Figure 5.391.

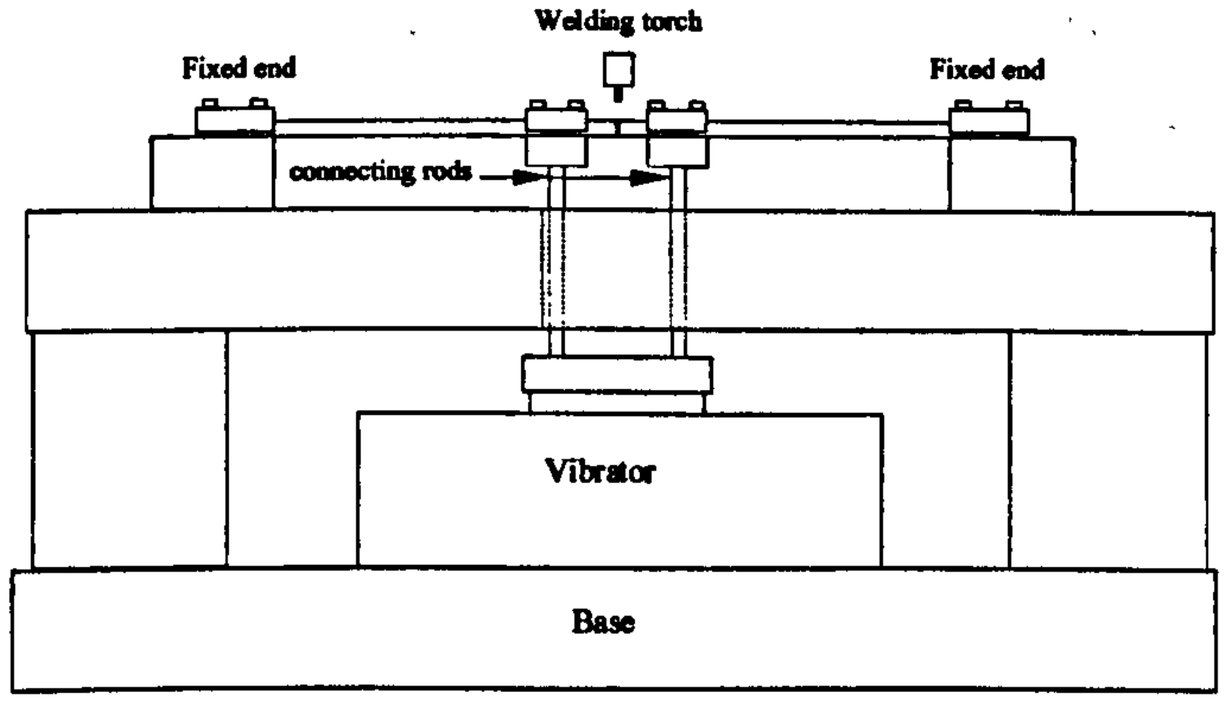

Figure 5.391 – Amended experimental set-up - investigation of a Japanese work

In this experiment, two batches of specimens were processed. In the first batch, longitudinal and transverse residual stresses were measured to obtain the full picture of the residual stresses changes due to the treatment. In the second batch, only longitudinal residual stresses were measured.

Similar to the previous experiments, two pieces of metal bar were welded together to make a weld joint. One end of the of metal pieces were bevelled 30^0 to prepare V for welding. The specimens were mounted on the set-up and different levels of vibration were applied to the specimens. While the specimens were vibrating, a single pass weld was carried out. After welding, two bars of metals were joined together and the mode of vibration was changed from flexural mode to combined longitudinal and flexural mode. The stepper motor driven welding torch carrier maintained a constant speed weld. The time of vibration was kept constant and the amplitude varied. The residual stresses were measured on the mid-width line (line A in Figure 5.243) using the X-ray diffractometer utilising the single exposure technique (SET). The measurement conditions were similar to the conditions described in Table 5.10. The specimens were positioned on the goniometer table using the same jig as used in experiment IV and V is described in Appendix II.

5.3.6.3 Calibration of Displacement Amplitudes

The calibration of displacement amplitude was carried out using a very crude method, in which an accelerometer was attached on the vibration clamp (Figure5.392) and connected to a double integrator. The output of the double integrator (displacement

amplitude) was connected to a multimeter to obtain the displacement in mV (RMS). The displacement (pk/pk) of the vibratory clamp was measured using a steel rule. Sufficient light and other arrangements were made to minimise error in measurement.

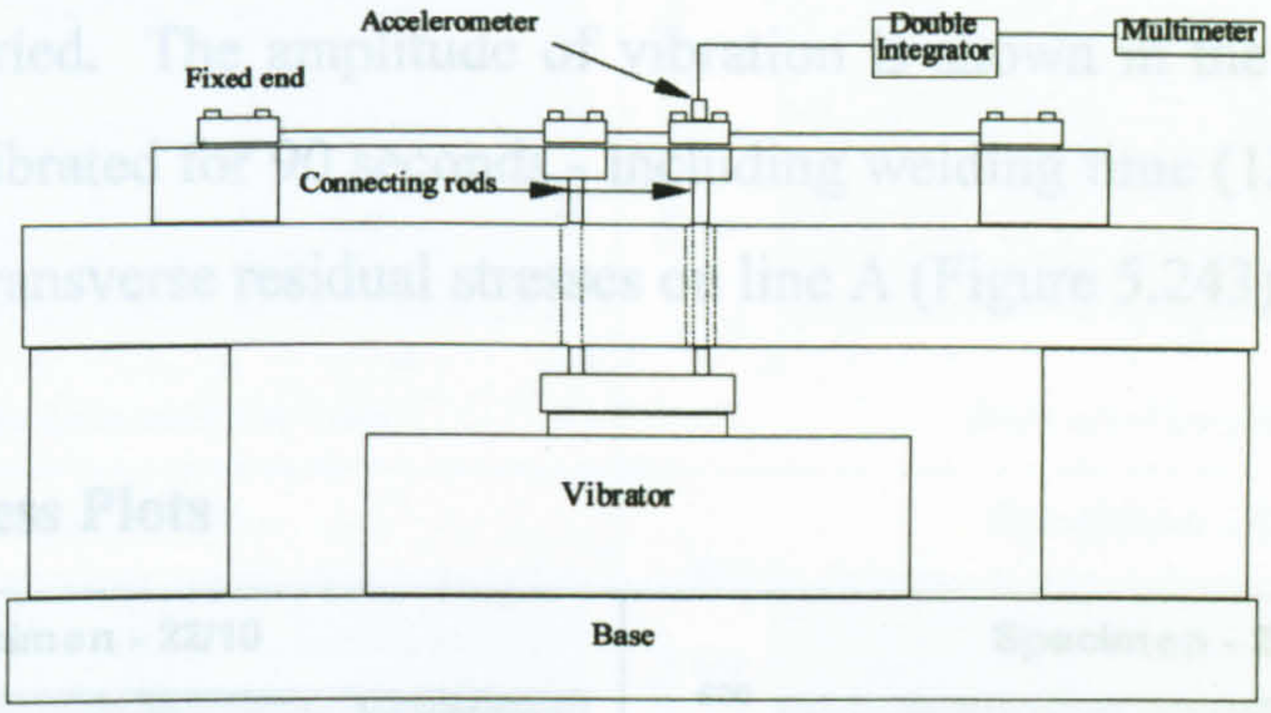

Figure 5.392 – Calibration set-up - displacement amplitude

Table 5.40 - Calibration of displacement amplitude

Multimeter Output - mv (rms)	Disp. Amp. - mm (pk/pk)
594	3.4
995	5.5
1485	8
1912	10
2775	14.5
3177	16.7

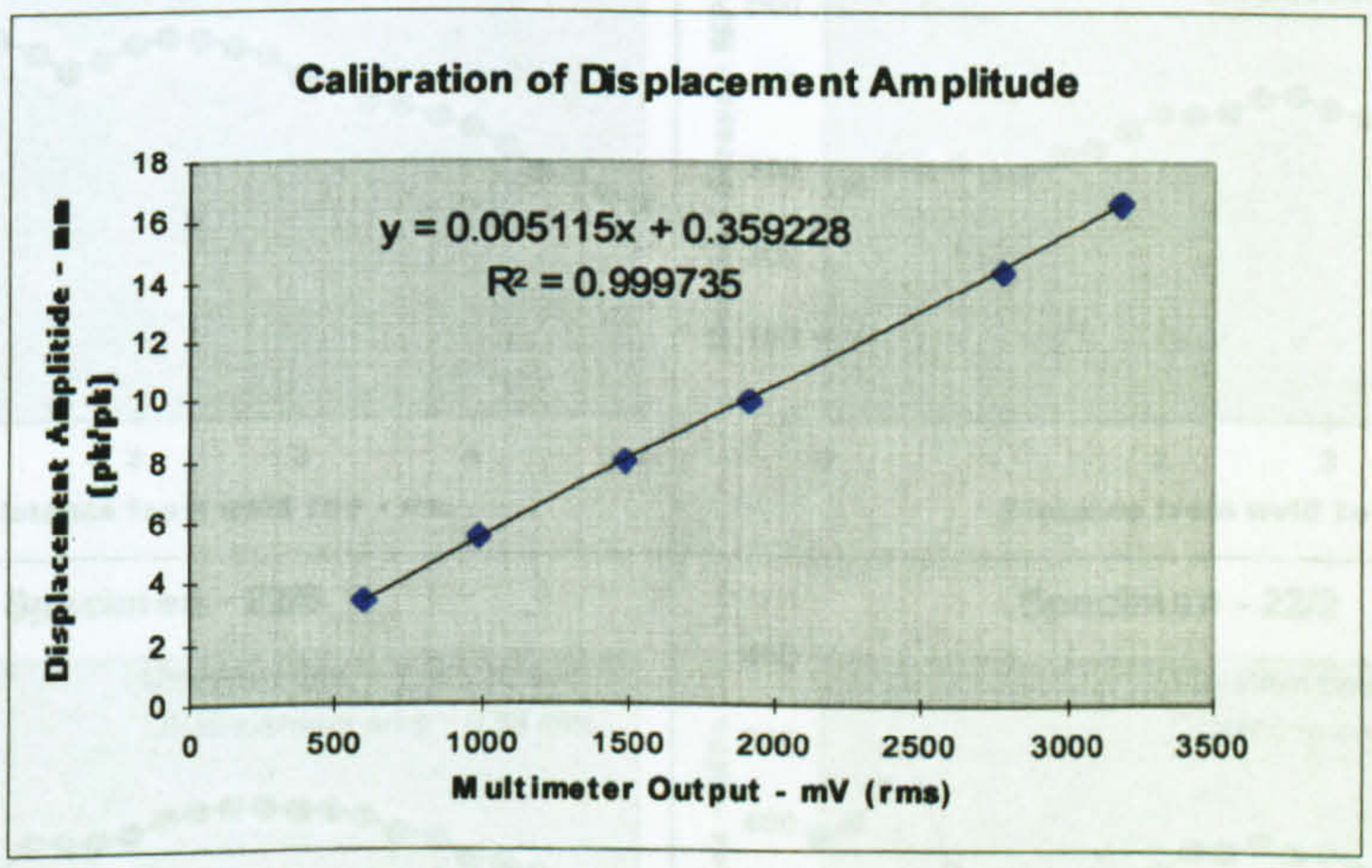

Figure 5.393 - Calibration of displacement amplitude

The vibration amplitude was gradually increased and the corresponding multimeter output and the displacement were recorded and are shown in Table 5.40. The measured displacement was then plotted against the multimeter output to obtain the calibration constant. The good linearity of the data and increased confidence in the calibration processes (Figure 5.393).

5.3.6.4 Experimental Results

Batch 1

In this batch 10 specimens processed. Keeping the frequency of vibration constant the amplitude was varied. The amplitude of vibration is shown in the stress plots. The specimens were vibrated for 90 seconds - including welding time (13.5 seconds). The longitudinal and transverse residual stresses on line A (Figure 5.243) were measured.

Longitudinal Stress Plots

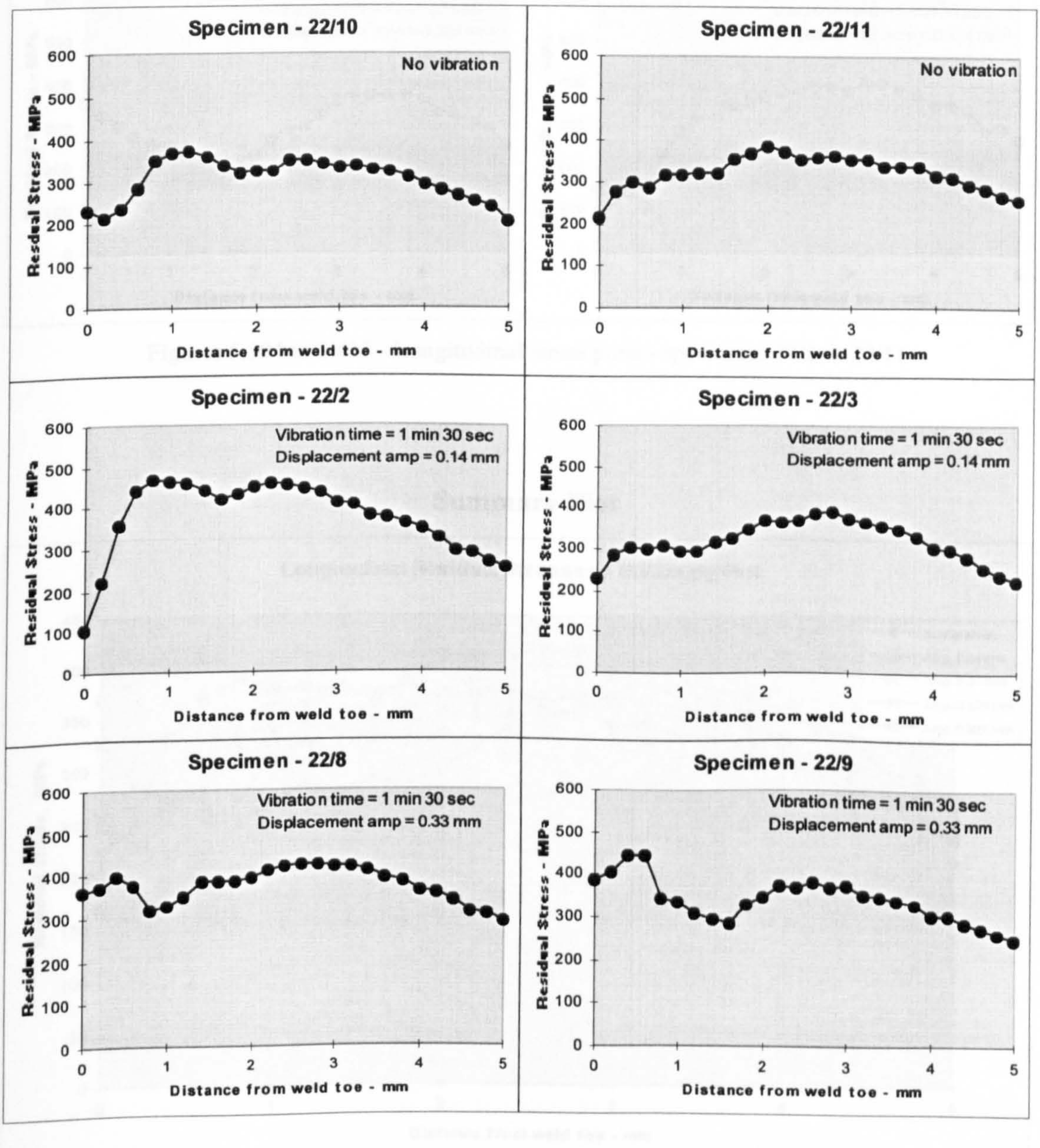

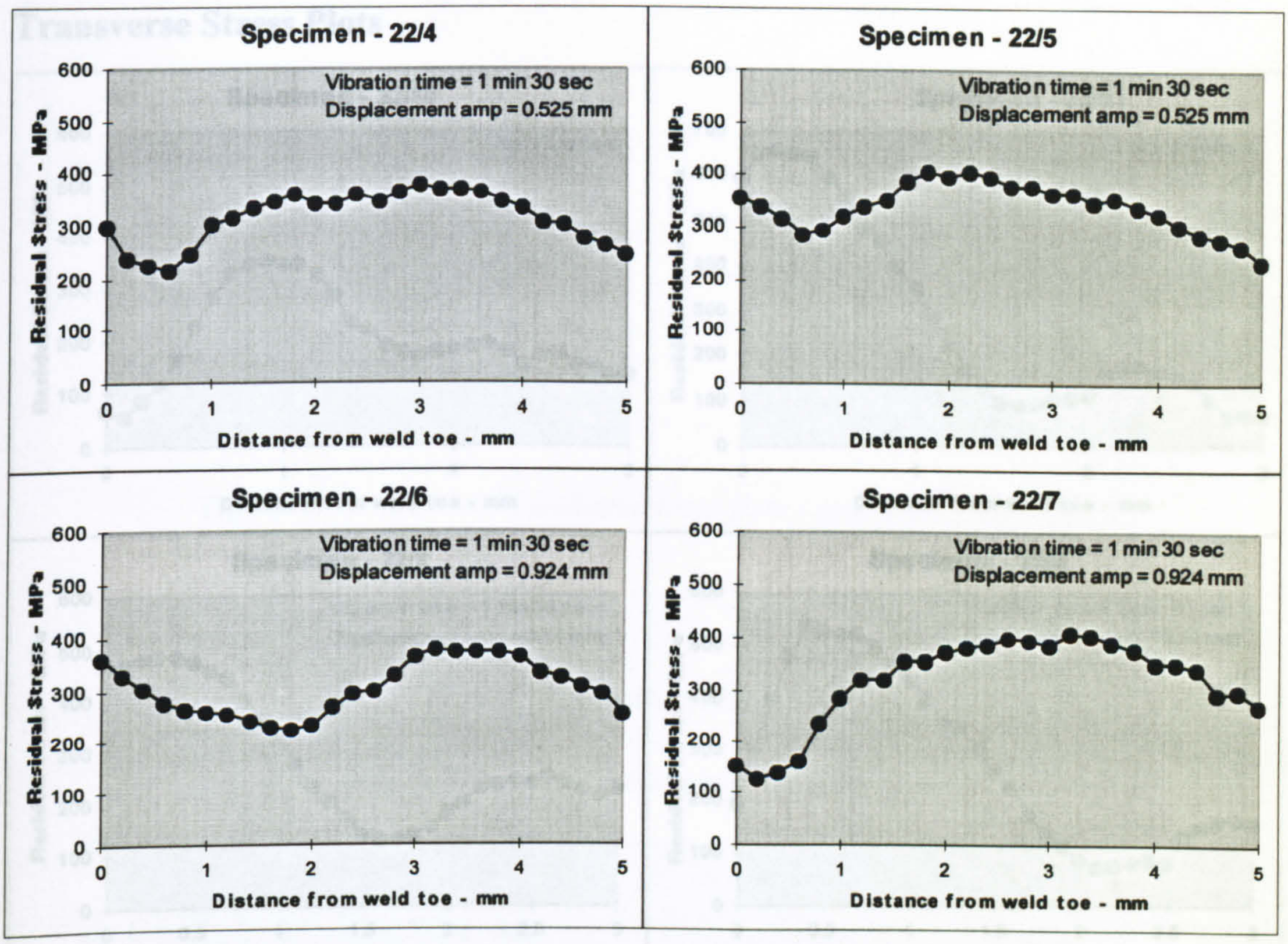

Figures 5.394 to 5.403 - Longitudinal stress plots - specimens 22/2 to 22/11

Summary Plot

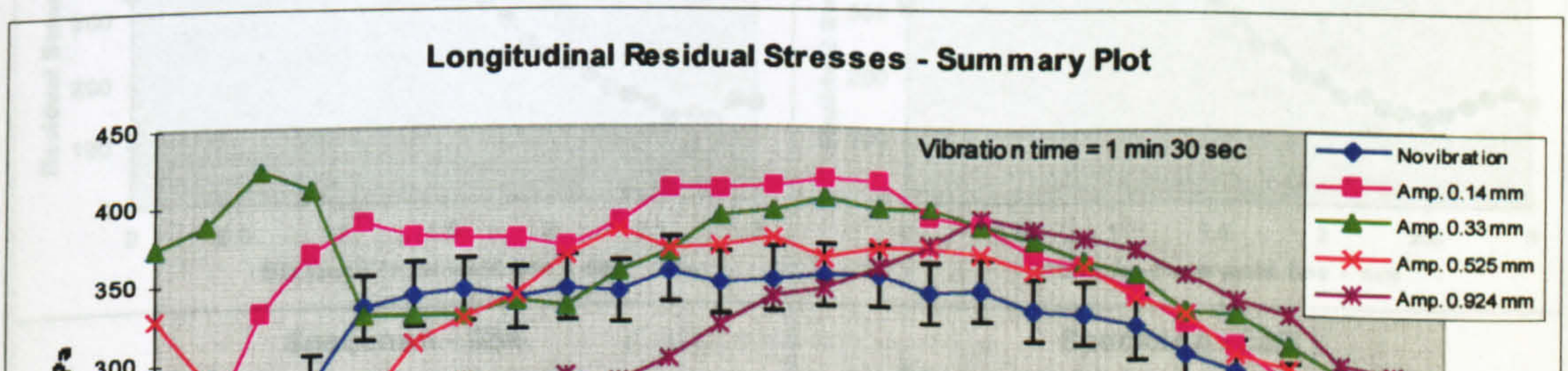

Figures 5.404 – Summary longitudinal residual stresses – specimens 22/2 to 22/11

Transverse Stress Plots

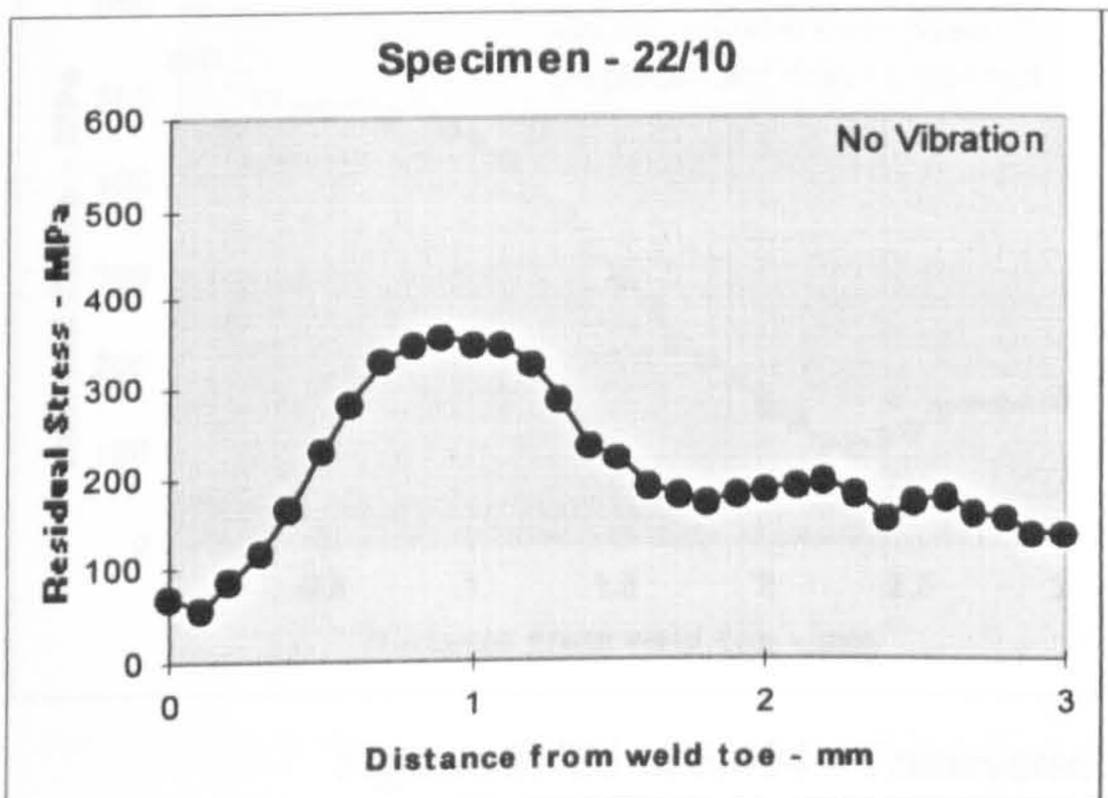

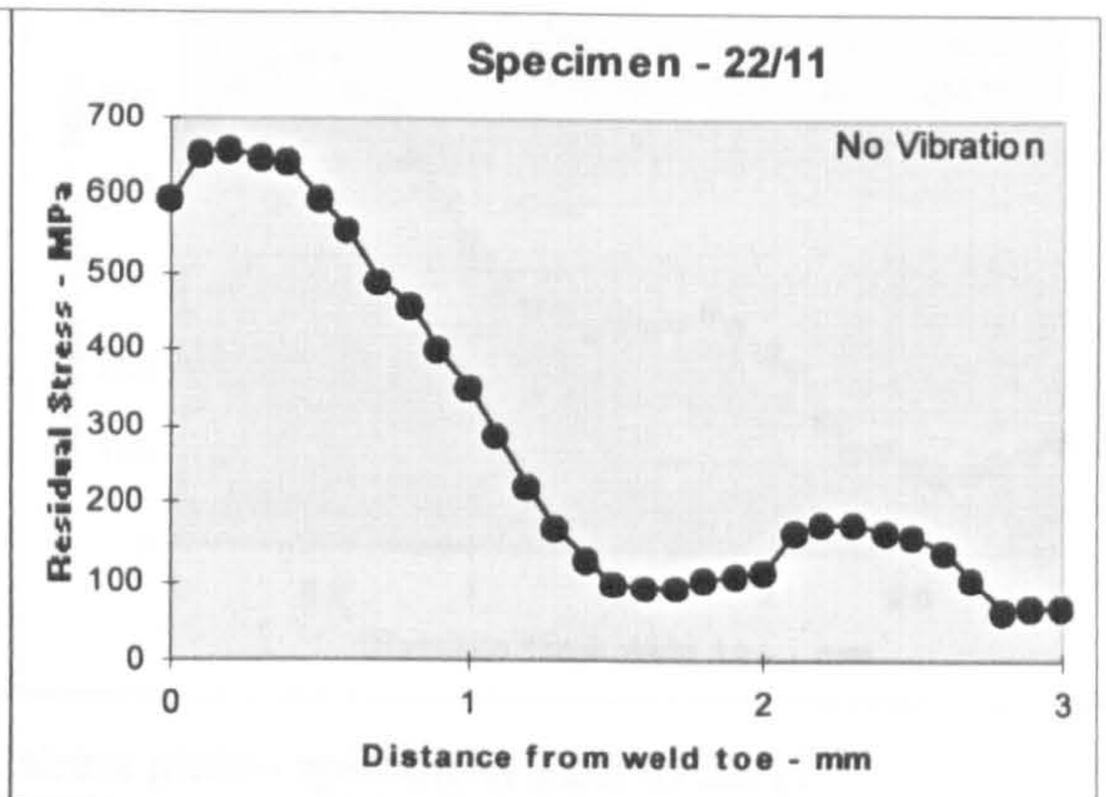

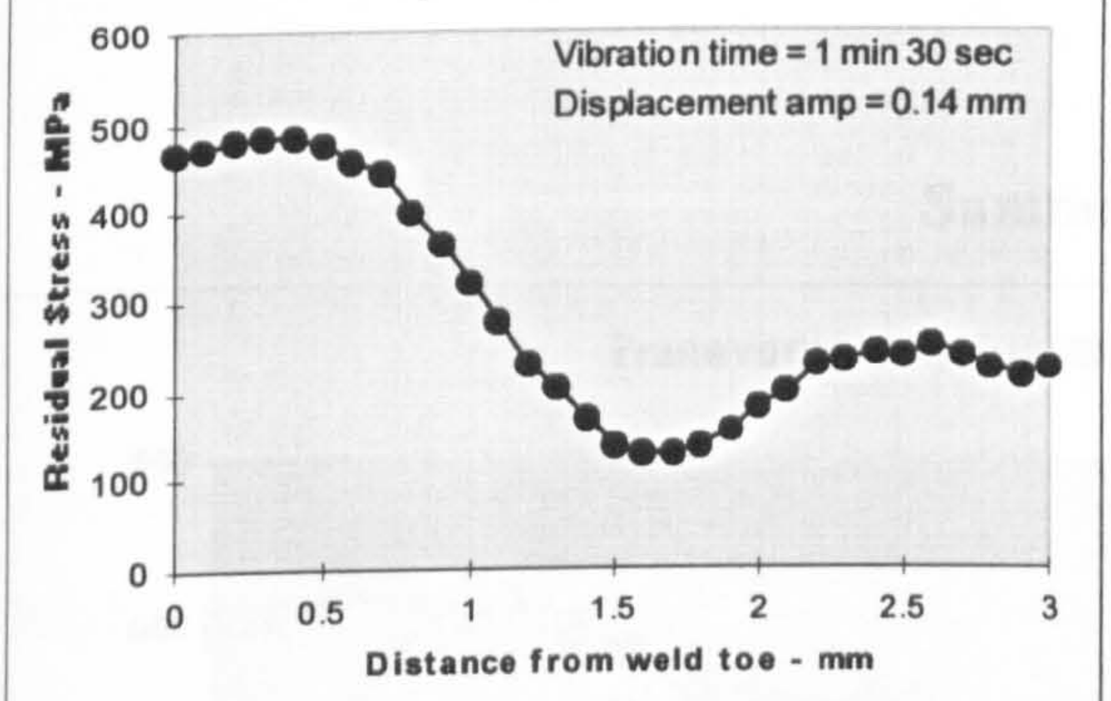

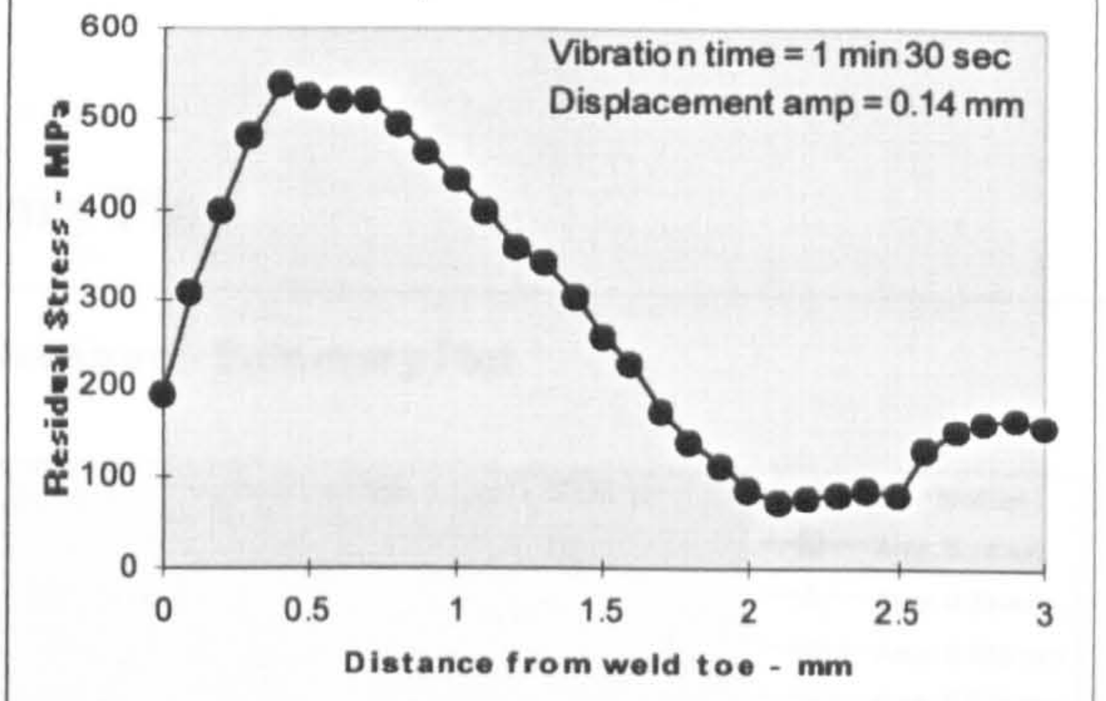

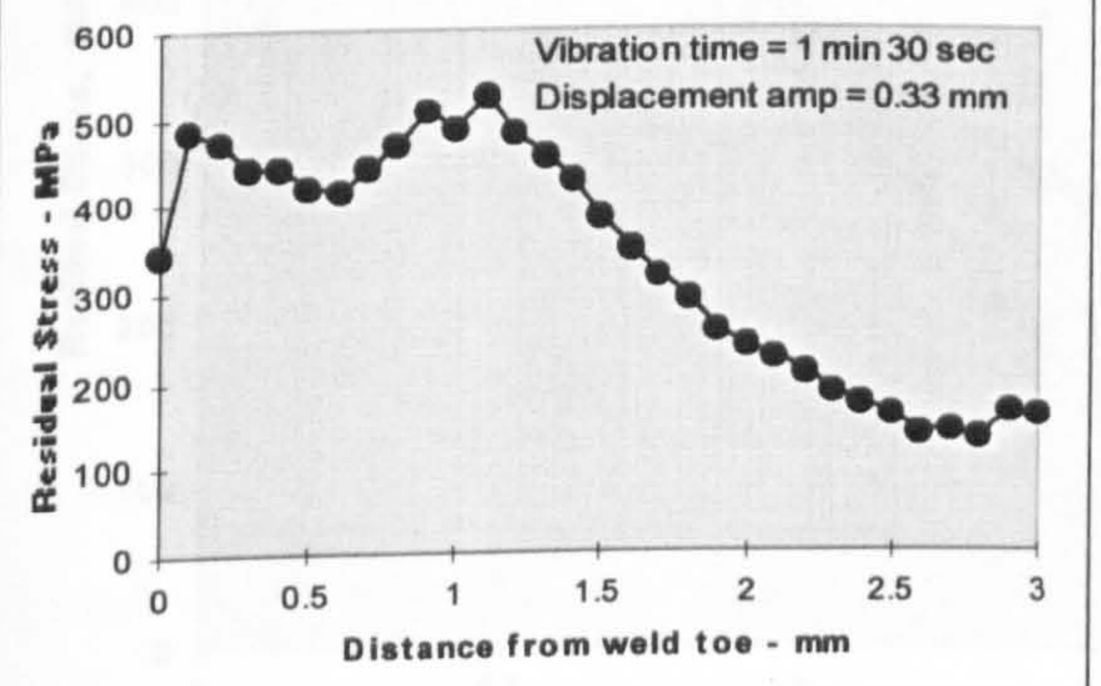

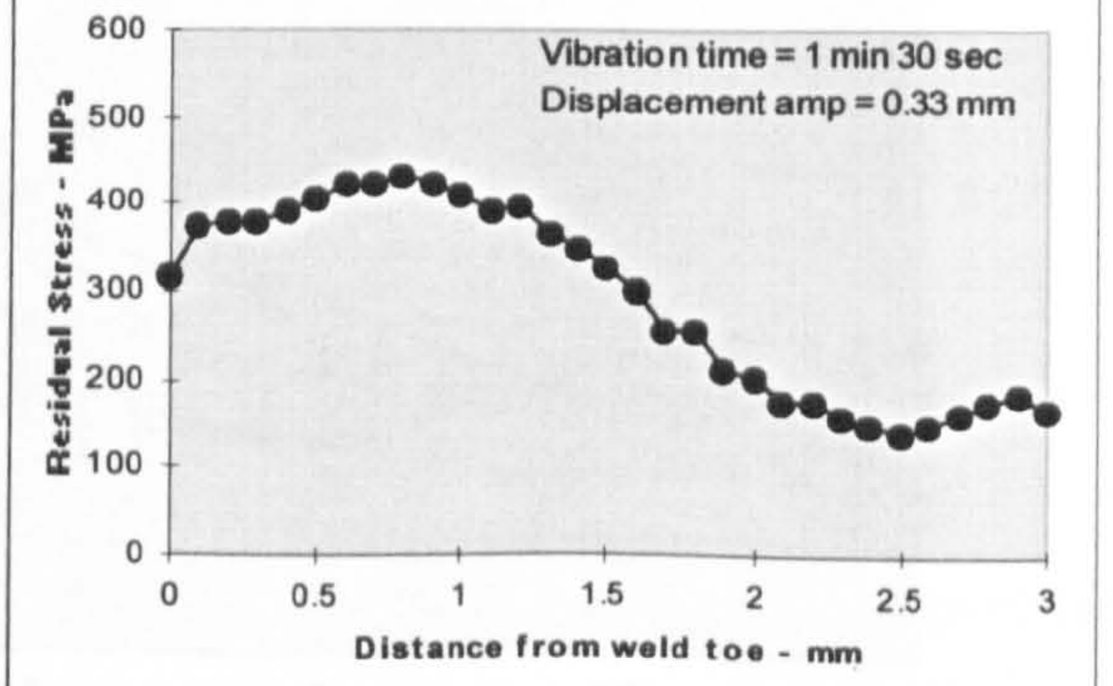

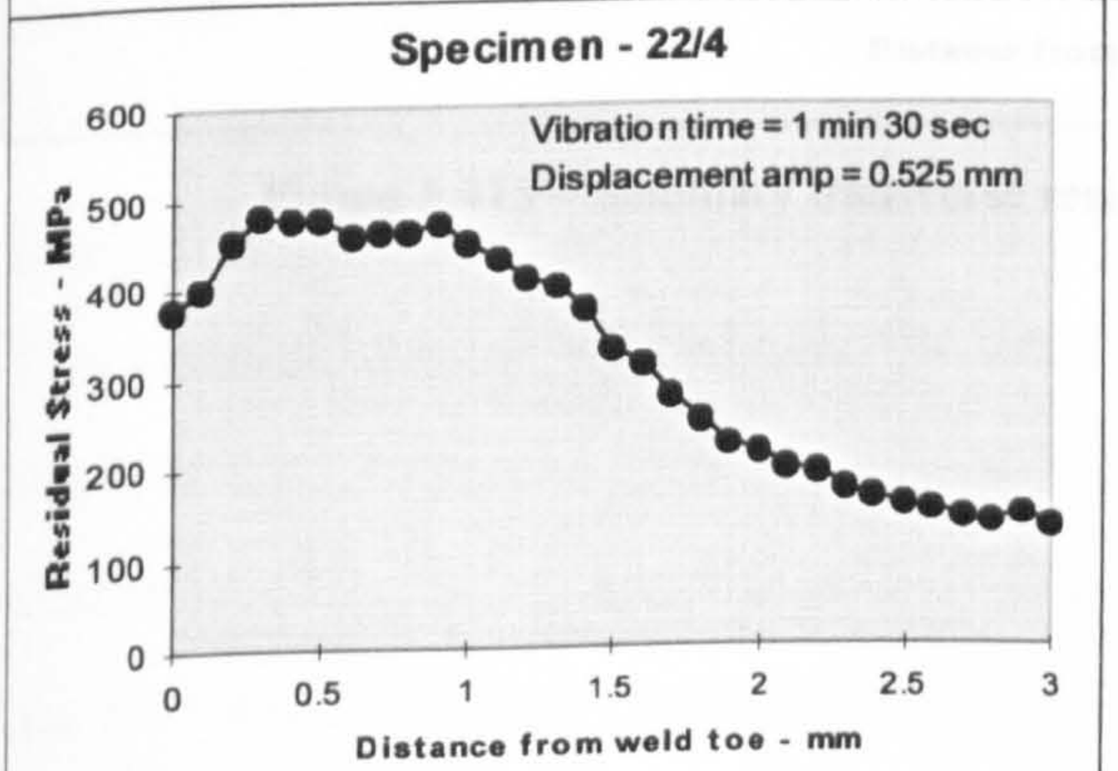

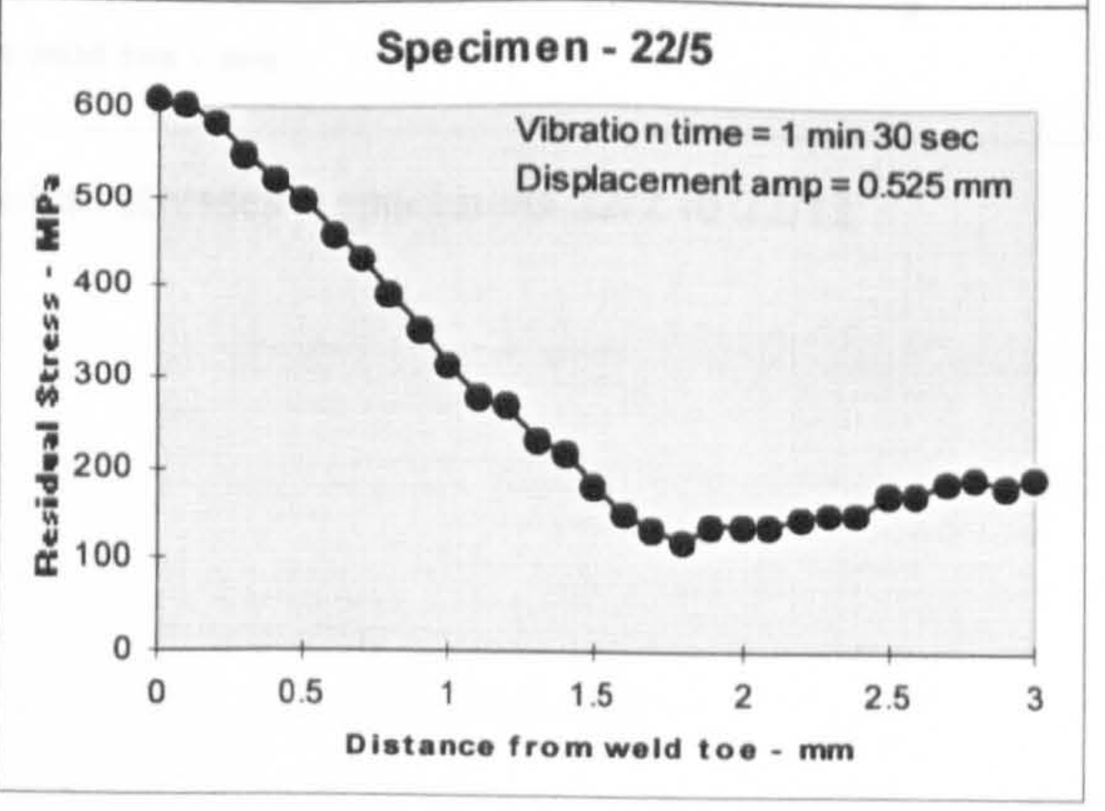

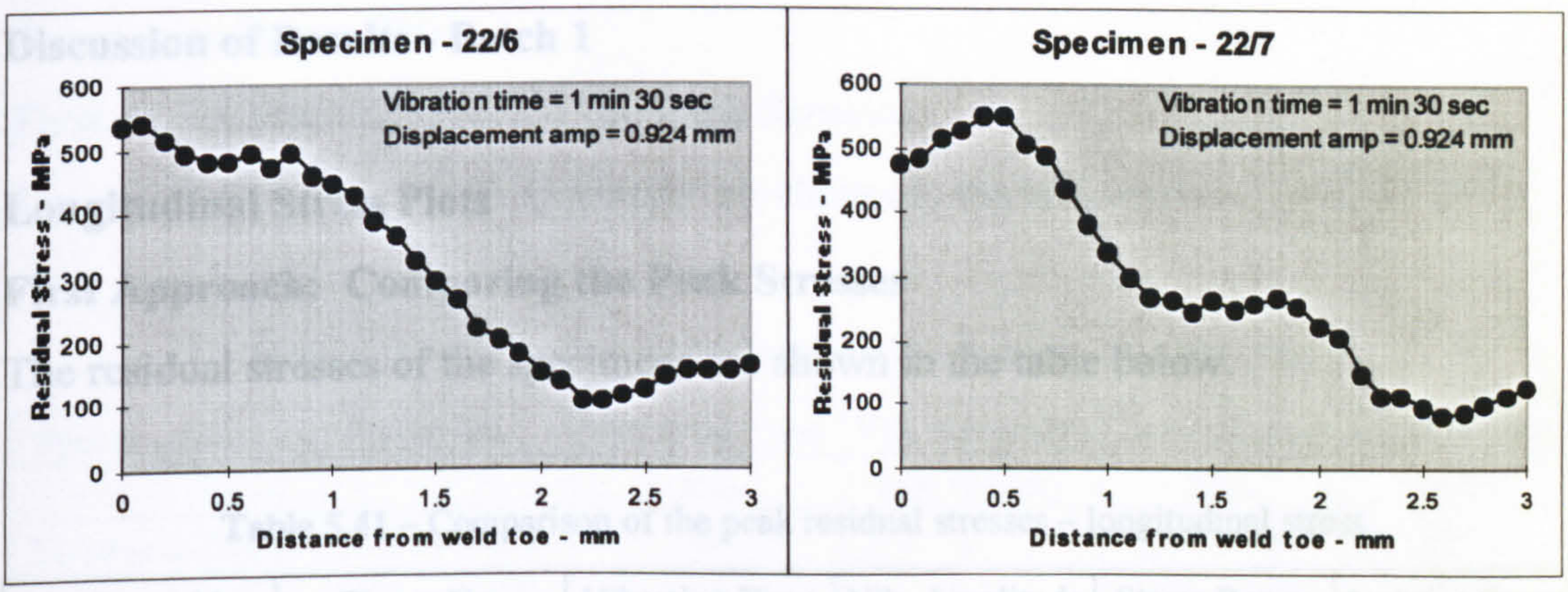

Figures 5.405 to 5.414 - Transverse stress plots - specimens 22/2 to 22/11

Summary Plot

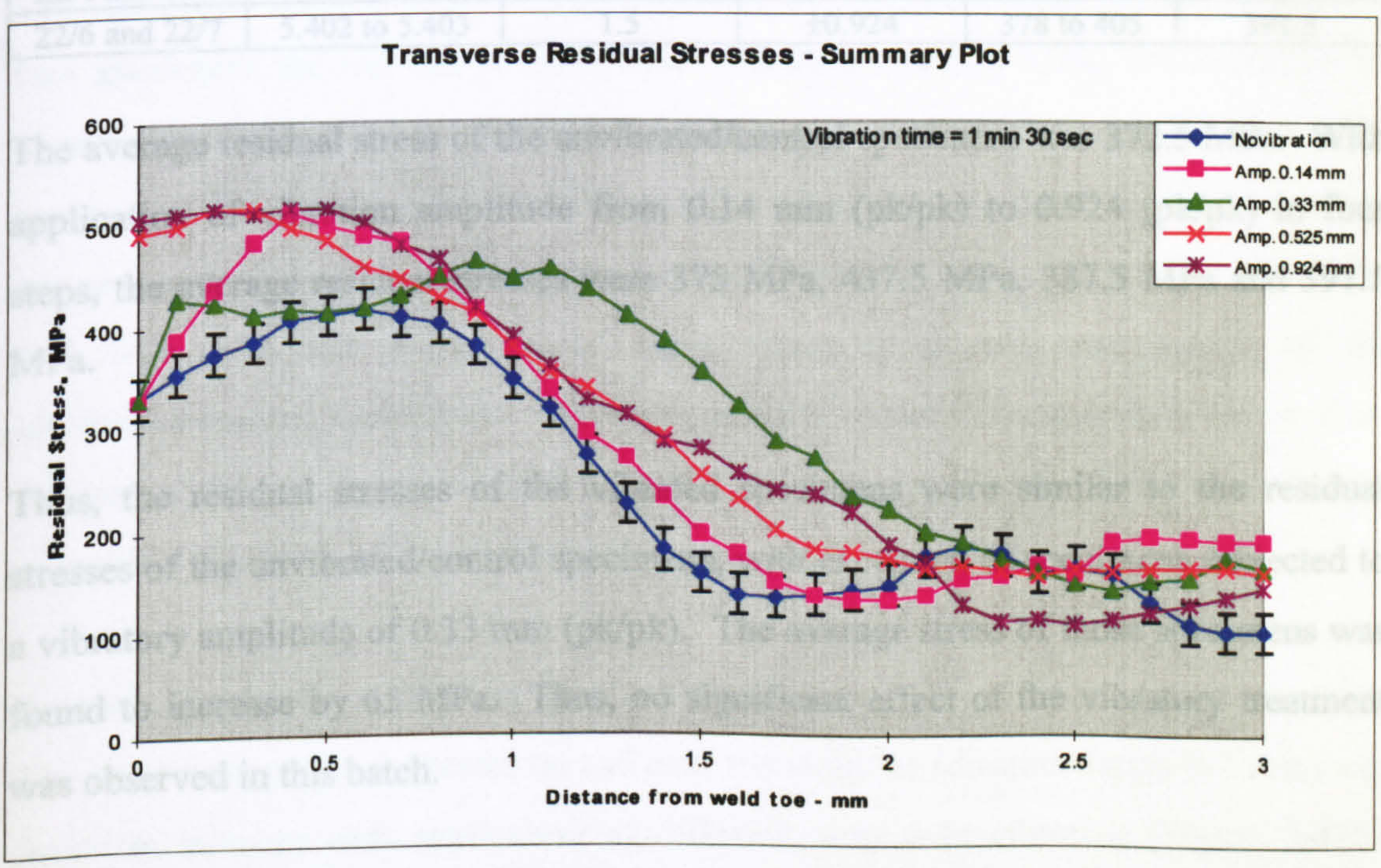

Figure 5.415 – Summary transverse residual stresses – specimens 22/2 to 22/11

Discussion of Results - Batch 1

Longitudinal Stress Plots

First Approach: Comparing the Peak Stresses

The residual stresses of the specimens are shown in the table below.

Table 5.41 – Comparison of the peak residual stresses – longitudinal stress

Specimen No.	Figure No.	Vibration Time	Vib. Amplitude	Stress Range	Average Stress
		min	mm (pk/pk)	MPa	MPa
22/10 and 22/8	5.394 to 5.395	0	0	365 to 380	372.5
22/2 and 22/3	5.396 to 5.397	1.5	±0.14	370 to 380	375
22/8 and 22/9	5.398 to 5.399	1.5	±0.33	420 to 455	437.5
22/4 and 22/5	5.400 to 5.401	1.5	±0.525	375 t0 400	387.5
22/6 and 22/7	5.402 to 5.403	1.5	±0.924	378 to 405	391.5

The average residual stress of the unvibrated/control specimens was 372.5 MPa. With application of vibration amplitude from 0.14 mm (pk/pk) to 0.924 (pk/pk) in four steps, the average residual stresses were 375 MPa, 437.5 MPa, 387.5 MPa and 391.5 MPa.

Thus, the residual stresses of the vibrated specimens were similar to the residual stresses of the unvibrated/control specimens, with exception of specimens subjected to a vibratory amplitude of 0.33 mm (pk/pk). The average stress of those specimens was found to increase by 65 MPa. Thus, no significant effect of the vibratory treatment was observed in this batch.

Second Approach: Analysing the Summary Plot

The residual stresses on and near the weld toe was found to be very confusing, where the stresses increased and decreased with application of different amplitude of vibration (Figure 5.404). No particular pattern was observed. Away from the weld toe the residual stresses were found to increase with smaller degrees.

Transverse Stress Plots

First Approach: Comparing the Peak Stresses

The residual stresses of the specimens are shown in the table below

Table 5.42 – Comparison of the peak residual stresses – transverse stress

Specimen No.	Figure No.	Vibration Time	Vib. Amplitude	Stress Range	Average Stress
		min	mm (pk/pk)	MPa	MPa
22/10 and 22/8	5.405 to 5.406	0	0	355 to 660	507.5
22/2 and 22/3	5.407 to 5.408	1.5	±0.14	485 to 540	512.5
22/8 and 22/9	5.409 to 5.410	1.5	±0.33	425 to 525	475
22/4 and 22/5	5.411 to 5.412	1.5	±0.525	480 t0 600	540
22/6 and 22/7	5.413 to 5.414	1.5	±0.924	550 to 555	552.5

The transverse residual stresses were found to be very confusing. In the unvibrated two specimens the residual stresses were 355 MPa and 660 MPa, which cannot be expected as the residual stresses of the specimens processed in the same situation. The average of the two stresses was 507.5 MPa. The average residual stresses of the specimens subjected to different amplitude of vibration were 512.5 MPa, 475 MPa, 540 MPa and 552 MPa, all of them were within the two values of the unvibrated/control specimens. Also, no particular trend was present in the residual stresses of the specimens vibrated applying different amplitudes. Thus, no reduction in residual stresses was found from this batch.

Second Approach: Analysing the Peak Stresses

The transverse residual stresses on and near the weld toe (distance range 0-2 mm) was found to increase with application of different amplitude vibration (Figure 5.415). Away from the weld toe the residual stresses increased but with a lesser degree.

Batch 2

In this batch, nine specimens were processed. Keeping the frequency of vibration constant the amplitude was varied. The amplitude of vibration is shown in the stress plots. The specimens were vibrated for 120 seconds including welding time (13.5 seconds). The longitudinal residual stresses of the selected line (line A of Figure 5.243) were measured. The plotted results are shown below.

Longitudinal Stress Plots

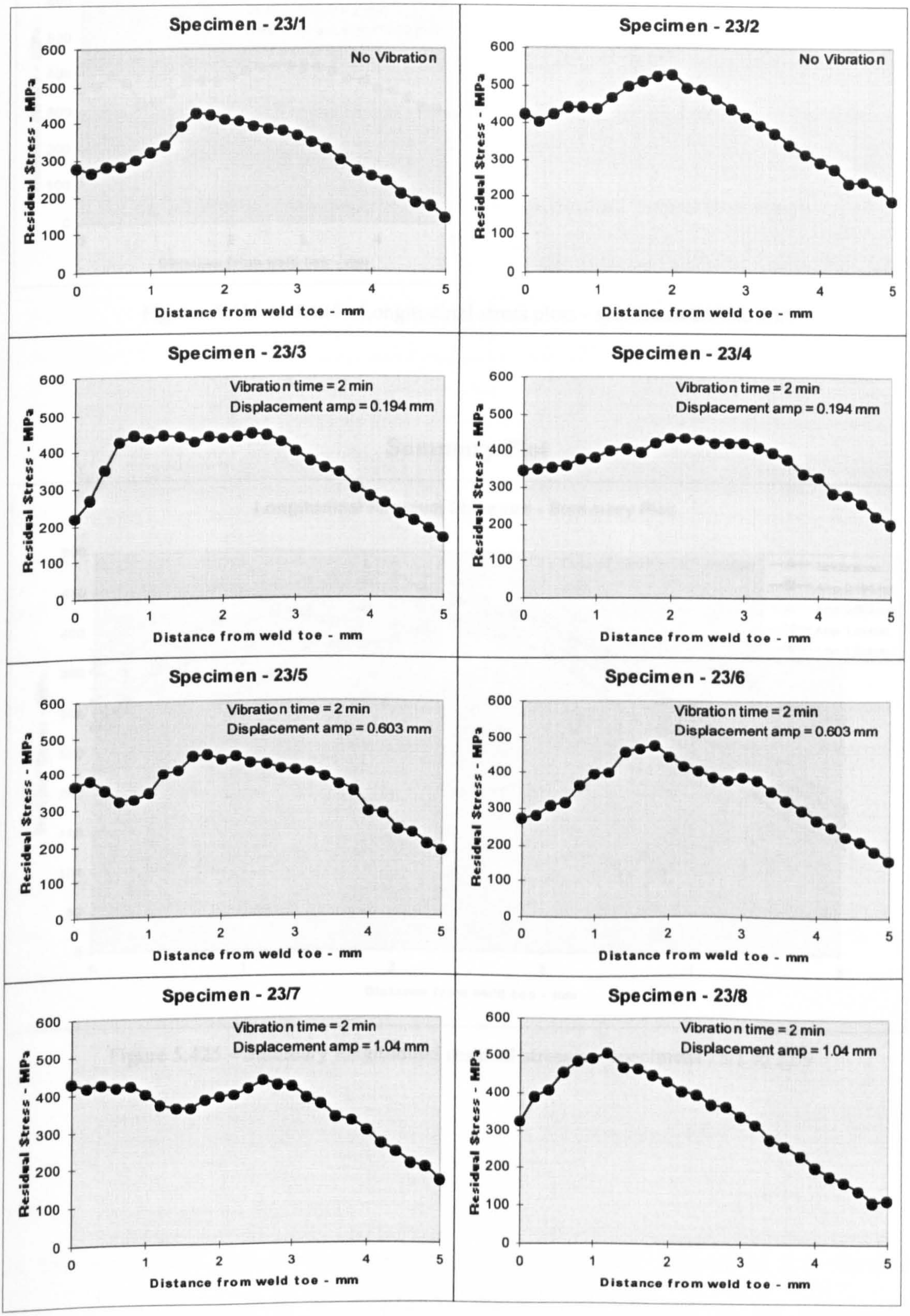

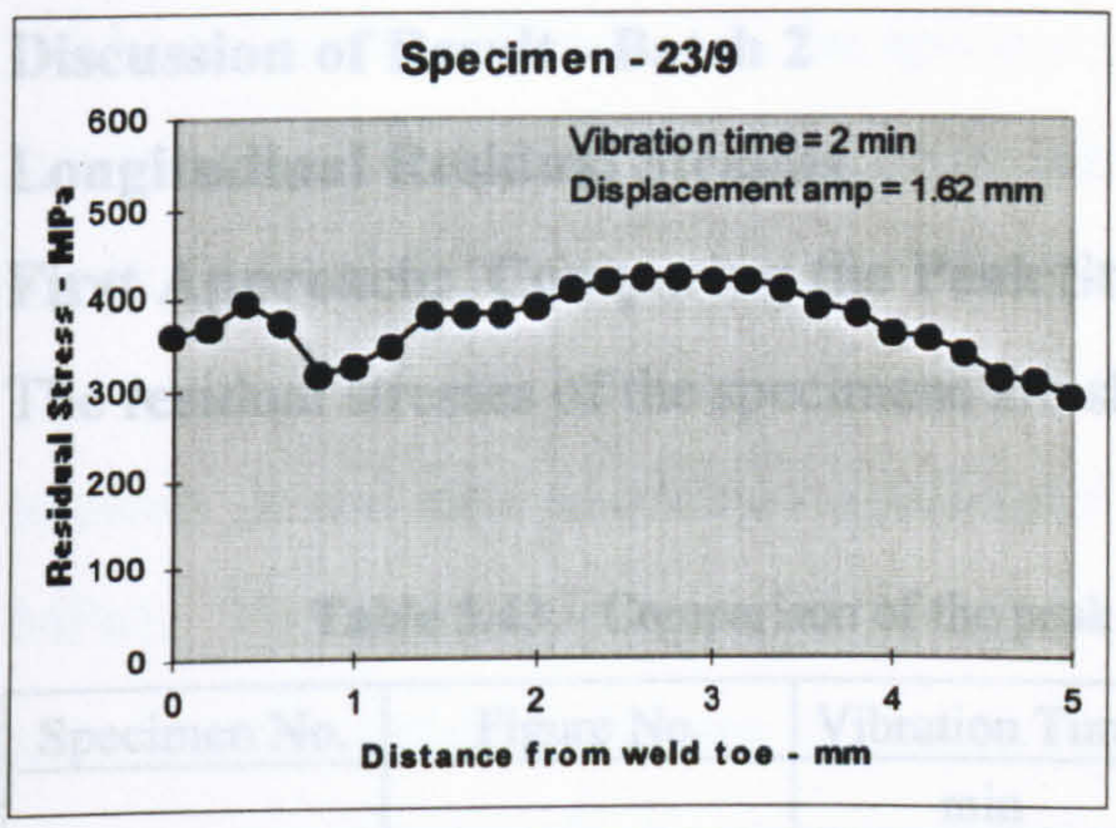

Figures 5.416-to 5.424 - Longitudinal stress plots - specimens 23/1 to 23/9

Summary Plot

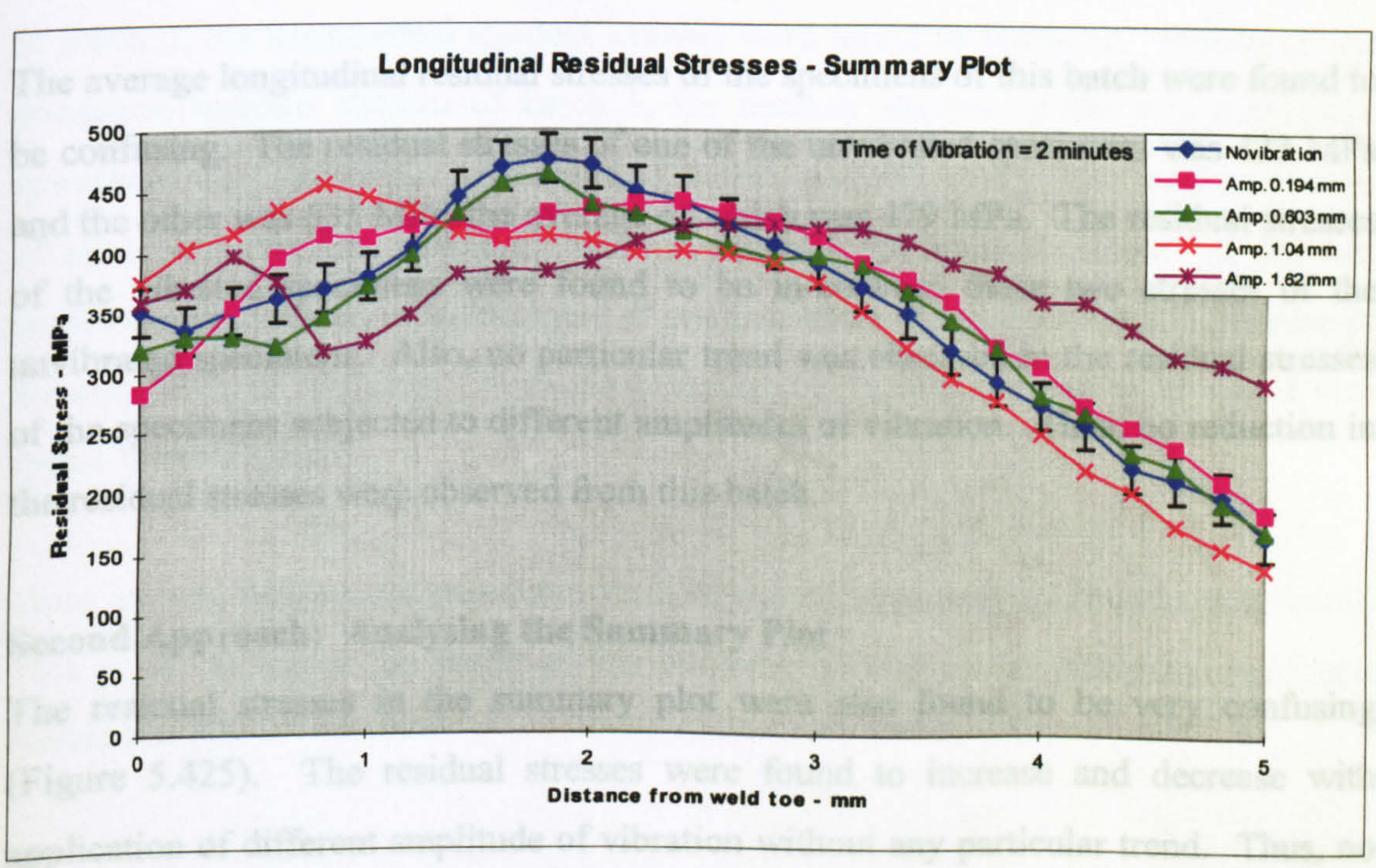

Figure 5.425 – Summary longitudinal residual stresses – specimens 23/1 to 22/9

Discussion of Result - Batch 2

Longitudinal Residual Stresses

First Approach: Comparing the Peak Stresses

The residual stresses of the specimens are shown in the table below

Table 5.43 – Comparison of the peak residual stresses – longitudinal stress

Specimen No.	Figure No.	Vibration Time	Vib. Amplitude	Stress Range	Average Stress
		min	mm (pk/pk)	MPa	MPa
23/1 and 23/2	5.416 to 5.417	0	0	423 to 535	479
23/3 and 23/4	5.418 to 5.419	2	±0.194	430 to 460	445
23/5 and 23/6	5.420 to 5.421	2	±0.603	450 to 478	464
23/7 and 23/8	5.422 to 5.423	2	±1.04	430 t0 515	472.5
23/9	5.424	2	±1.62	425	425

The average longitudinal residual stresses of the specimens of this batch were found to be confusing. The residual stresses of one of the unvibrated specimens was 423 MPa and the other was 535 MPa, the average of which was 479 MPa. The residual stresses of the vibrated specimens were found to be in-between those two stresses of the unvibrated specimens. Also, no particular trend was observed in the residual stresses of the specimens subjected to different amplitudes of vibration. Thus, no reduction in the residual stresses were observed from this batch.

Second Approach: Analysing the Summary Plot

The residual stresses in the summary plot were also found to be very confusing (Figure 5.425). The residual stresses were found to increase and decrease with application of different amplitude of vibration without any particular trend. Thus, no reduction in the residual stresses was observed from this limited investigation.

5.3.6.5 Summary of Results

In the first batch, the average peak longitudinal residual stresses of the vibrated specimens were found to be similar to the residual stresses of the unvibrated specimens. The two specimens subjected to a vibration amplitude of 0.33 mm (pk/pk) showed a higher peak residual stress. The reason of this increase is unknown. This

might be due to difference in the specimen geometry or the material property. In the summary plot, the residual stresses were found to increase and decrease with application of different amplitude vibration, where no particular trend was observed. The pattern of the transverse residual stresses were more confusing, the residual stresses of the two unvibrated specimens were in a wide range (355 MPa and 660 MPa). The residual stresses of all of the vibrated specimens were found to be in-between the residual stresses of the two unvibrated specimens. Also, no trend was present in the residual stresses of the specimens vibrated applying different displacement amplitudes. In the summary plot the scatter is clear, where no trend was found.

In batch 2, the longitudinal residual stresses were found so scattered. Similar to the transverse residual stresses of batch 1, the residual stresses of the two unvibrated specimens were found in a wide range (423 MPa and 535 MPa). The residual stresses of all of the vibrated specimens were in-between the residual stresses of the two unvibrated specimens. Also, no trend of residual stresses was found due to increase in the amplitude of vibration. Thus, no reduction in residual stresses or any trend was found from this batch.

Thus, in both batches, no particular trend of reduction in residual stresses was found. This result increases the doubt of the success claimed in the paper by Aoki and Nishimura [7].

5.4

"Post-weld" Treatment

5.4.1 Experiment VII:

VSR Treatment of As-welded Specimens (Batch Treatment)

Abstract

In this experiment the welded specimens were processed as a post weld treatment. The specimens were vibrated varying both amplitude and time of vibration. Four batches of specimens were processed. In all four batches substantial reduction in the residual stresses were found. The residual stresses were found to decrease with increase in the amplitude of vibration, i.e. applied stresses. The effect of increase in the time of vibration was found to be negligible.

5.4.1.1 Introduction

In the previous experiments the vibratory treatment was carried out while the specimens were being welded. In those experiments the effect of rigid body motion (RBM) vibration and flexural vibrations were investigated. The results of those experiments were mixed, where decrease as well as increase in the residual stresses was found due to the treatments. The rigid body motion treatment did not show any significant change in residual stresses due to the treatments. On the other hand the flexural vibration showed some reduction in the residual stresses but the reductions were not so significant. The reason why during welding treatment was less effective in reducing the residual stresses has not yet been established. After those welding treatments it was decided to carry out experiment on welded specimens after cooling down to room temperature, i.e. post-weld treatment. Processing the specimens at room temperature reduced some variables (mainly non-linear mechanical properties caused by changing temperature). In the post weld treatment it was easy to apply a higher level of dynamic stress to the specimens due to the fact that the yield stress of the specimens at room temperature was much higher than the yield stresses of the solidifying metal after welding.

5.4.1.2 Experimental Procedure

In these experiments generally, specimens were welded without any treatment. The welding was carried out on the specimens using the same setting as in experiment III. The specimen geometry was similar to Figure 5.13. A single pass weld was performed on the specimen using a MIG welding torch. A constant speed of the welding torch

carrier was maintained by a stepper motor drive (Figure 5.15A). When the specimens cooled down to room temperature the residual stresses of the selected line (Figure 5.13) was measured using the X-ray diffractometer. The conditions of the X-ray measurements were similar to as described in Table 5.10. The residual stresses were measured using the single exposure technique (SET) as a line map on the selected line.

After measuring the residual stresses the specimens were vibrated as a post weld treatment. The specimens were vibrated varying the applied dynamic stress and number of cycles. In this experiment the frequency of vibration was kept constant at 25 Hz. The experimental set-ups and induced stress calibration were the same as described in experiment III. The X-ray measurement jig was also similar to the jig used in experiment I, II and III (shown in Appendix II).

5.4.1.3 Experimental Results

Batch 1

Six specimens were processed in this batch, where during welding treated specimens were reprocessed as a preliminary test of post weld treatment. The specimens with higher level of residual stresses were selected for the preliminary investigation. In order to put the results of the current batch into perspective, a brief summary of the of the during-welding treatment follows.

Sp-5/3: This specimen was welded without any treatment.

Sp-5/5: This specimen was vibratory treated for 1.5 minutes at a frequency of 25 Hz. The applied stress to the specimen was ±48 MPa.

Sp-5/10: This specimen was treated in exactly the same way as specimen 5/5 with the exception of the induced stress - this was increased to 96 MPa.

Sp-6/1: The during-weld treatment of this specimen is same as specimen 5/10.

Sp-6/2: The during-weld treatment of this specimen is same as specimen 5/10.

Sp-6/5: This specimen was treated in exactly the same way as specimen 6/2 with the exception of the induced stress - this was increased to 144 MPa.

In this batch, the dynamically induced stress was kept constant and the time of vibration was varied. The details of the vibratory conditions are shown in the plots. The residual stresses of the specimens were again measured after the post-weld treatment. The measured stresses are shown below. The blue line represents the residual stresses before vibratory treatment and the pink represents after treatment.

Longitudinal Stress Plots

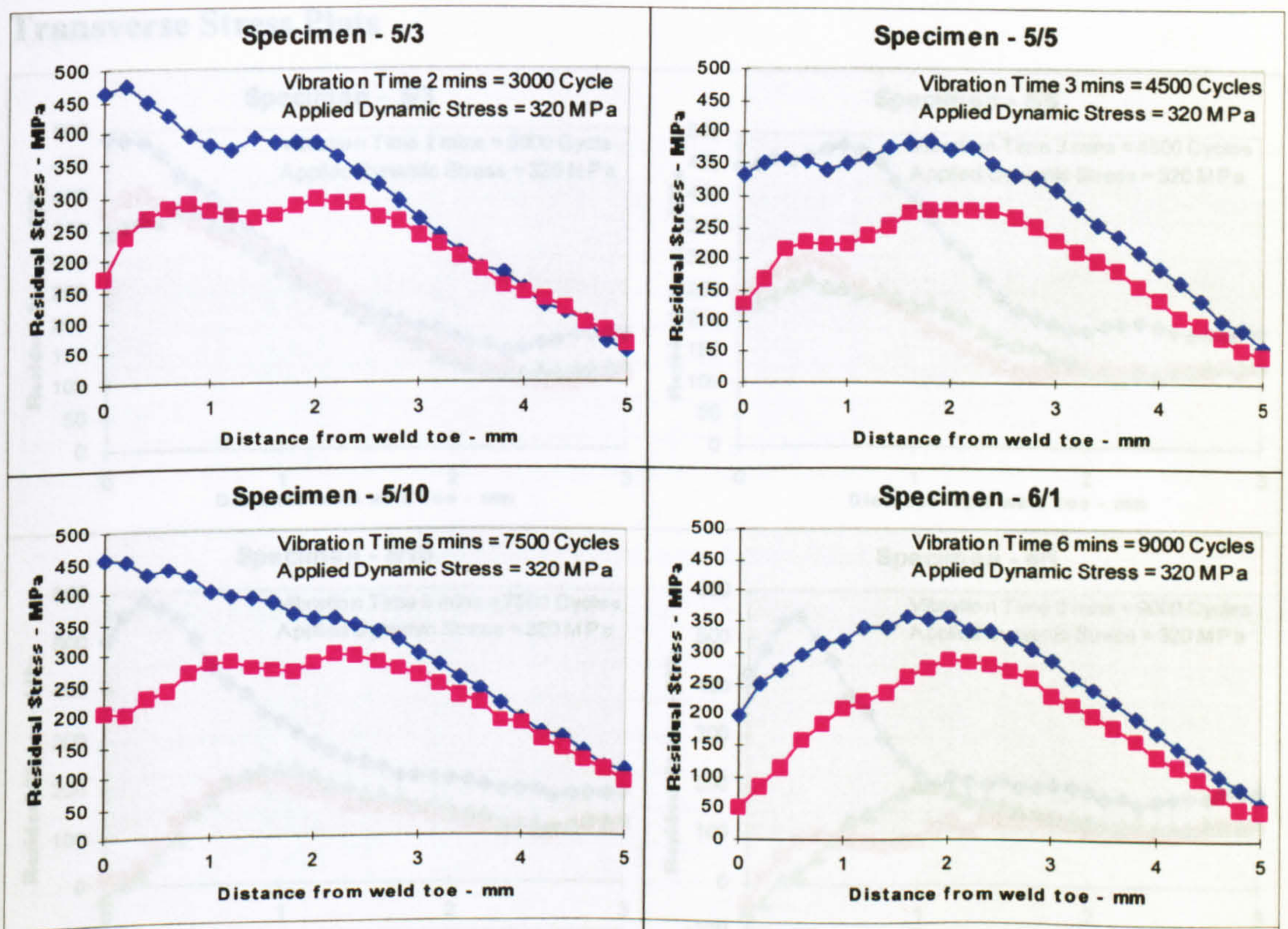

Figures 5.426 to 5.431 - Longitudinal stress plots - specimens 5/3 to 6/5

The transverse residual stress in all of the specimens was measured before the post-weld treatment and again re-measured after 21 days in order to see if the residual stress tends to return to its original state. The blue line is the residual stress profile before the post-weld treatment. The pink line is the residual stress measured just after treatment and the green line is the stress plot after 21 days. The stress plots are shown below.

Transverse Stress Plots

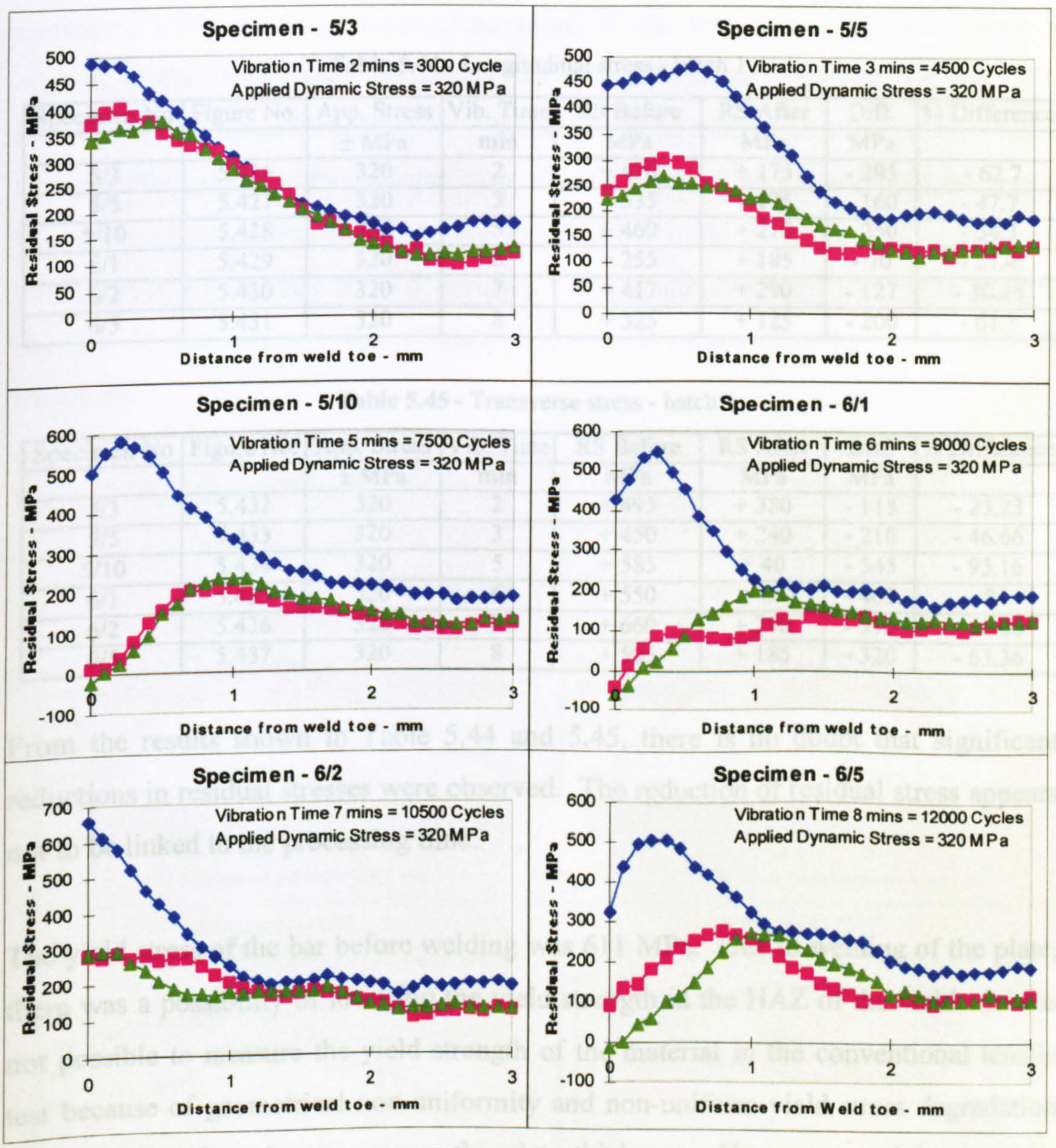

Figures 5.432 to 5.437 - Transverse stress plots - specimens 5/3 to 6/5

Discussion of Results - Batch 1

Table 5.44 and 5.45 shows the longitudinal and transverse stress results of maintaining a constant induced stress of ±320 MPa and varying the processing time. In the tables the maximum reduction in residual stresses of the plots are included for comparison. For the residual stresses (RS) in the tables below the (+ve) and (-ve) signs indicate tensile and compressive stresses respectively. In the difference column in the tables, the (-ve) and (+ve) signs indicate a decrease and an increase in the residual stresses respectively.

Table 5.44 - Longitudinal stress - batch 1

Specimen No	Figure No.	App. Stress	Vib. Time	RS Before	RS After	Diff.	% Difference
		± MPa	min	MPa	MPa	MPa	
5/3	5.426	320	2	+ 470	+ 175	- 295	- 62.7
5/5	5.427	320	3	+ 335	+ 175	- 160	- 47.7
5/10	5.428	320	5	+ 460	+ 210	- 250	- 54.3
6/1	5.429	320	6	+ 255	+ 185	- 70	- 27.4
6/2	5.430	320	7	+ 417	+ 290	- 127	- 30.45
6/5	5.431	320	8	+ 325	+ 125	- 200	- 61.5

Table 5.45 - Transverse stress - batch 1

Specimen No	Figure No.	App. Stress	Vib. Time	RS Before	RS After	Diff.	% Difference
		± MPa	min	MPa	MPa	MPa	
5/3	5.432	320	2	+ 495	+ 380	- 115	- 23.23
5/5	5.433	320	3	+ 450	+ 240	- 210	- 46.66
5/10	5.434	320	5	+ 585	+ 40	- 545	- 93.16
6/1	5.435	320	6	+ 550	+ 88	- 462	- 84
6/2	5.436	320	7	+ 660	+ 290	- 370	- 56.06
6/5	5.437	320	8	+ 505	+ 185	- 320	- 63.36

From the results shown in Table 5.44 and 5.45, there is no doubt that significant reductions in residual stresses were observed. The reduction of residual stress appears not to be linked to the processing time.

The yield stress of the bar before welding was 611 MPa. Due to welding of the plate, there was a possibility of lowering the yield strength in the HAZ of the weld. It was not possible to measure the yield strength of the material in the conventional tensile test because of geometrical non-uniformity and non-uniform yield stress degradation due to non-uniform heating across the plate thickness. However, no initiation was taken to measure the yield strength of the metal. If the yield strength of 611 MPa is considered then there was a possibility of local yielding in most of the specimens. In

that re-measurement of the residual stresses after 21 days, a little difference between the two plotted lines were observed in (Figure 5.432 to 5.437) which might be due to the movement of the measurement lines in either ways. The differences were negligible in comparison to the error band (±10 MPa) of the X-ray diffractometer.

Batch 2

In the last batch the applied stress was maintained at 320 MPa, and it was found that 5-6 minutes of vibration reduced the stress significantly. Claxton [32 to 37], Habel [62] explained VSR as energy input phenomena, if this was right then lower level of applied stress would take bit longer time to relieve the residual stresses. To investigate this, some specimens were processed using smaller induced stresses where the specimens vibrated for a longer time. In this batch 11 specimens were processed. The induced stress was kept constant to ±300 MPa and the time of vibration was varied from 1.5 minutes to 13.5 minutes. The longitudinal and transverse residual stresses of the selected line (Figure 5.13) were measured before and after the treatment.

Longitudinal Stress Plots

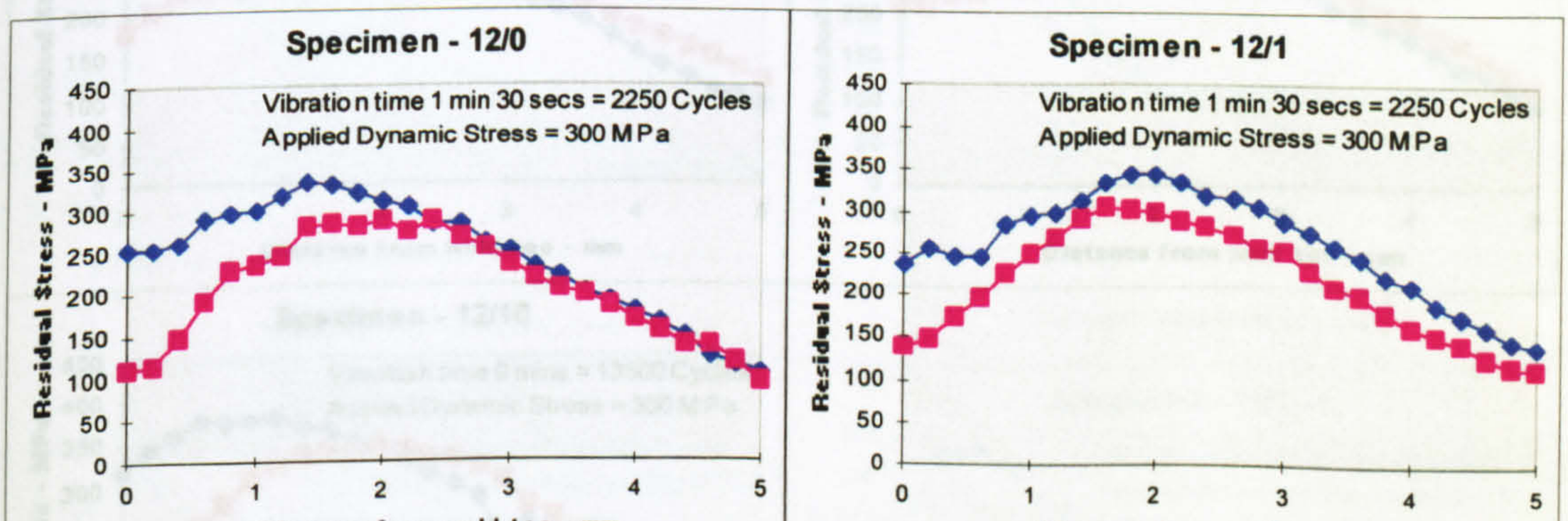

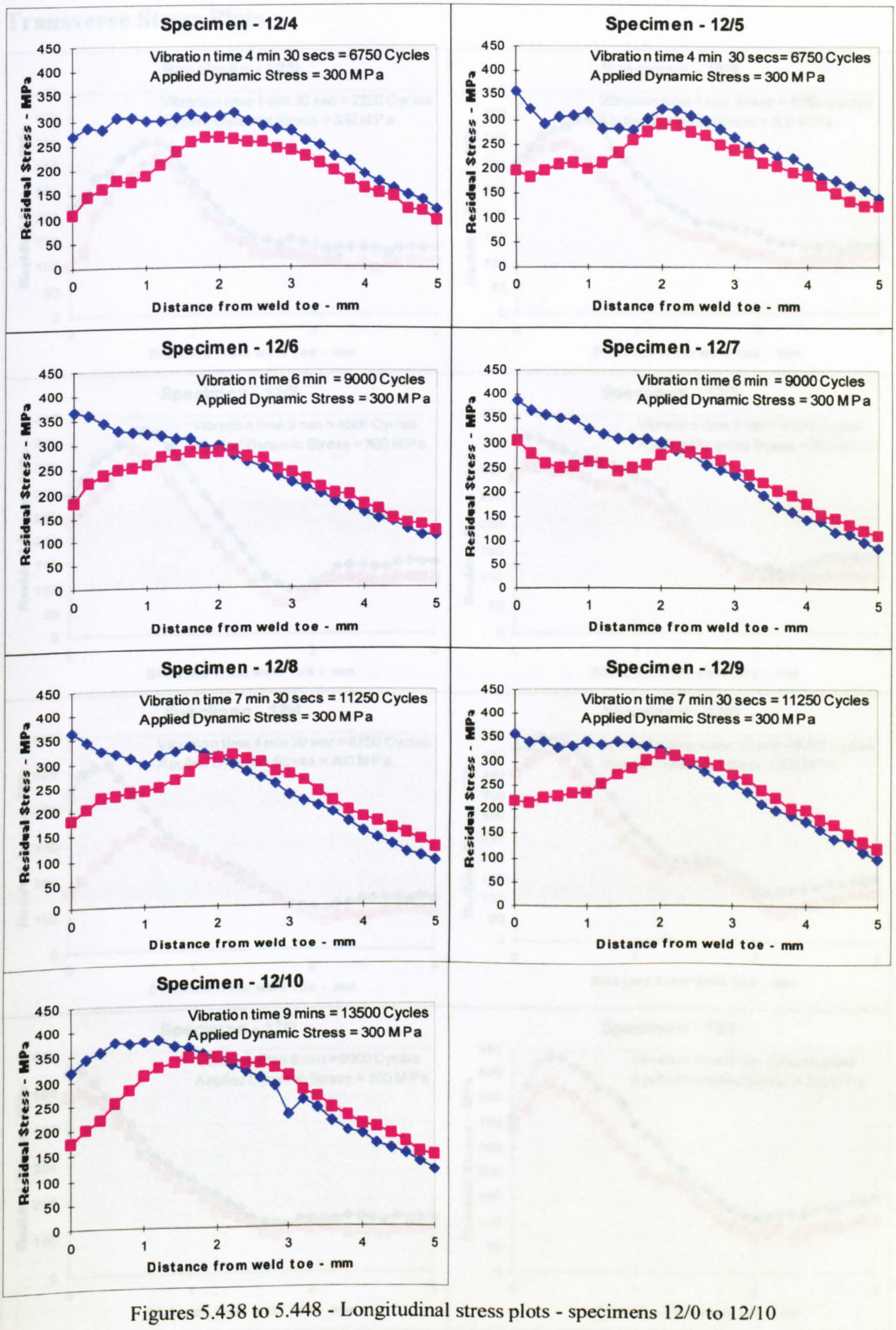

Figures 5.438 to 5.448 - Longitudinal stress plots - specimens 12/0 to 12/10

Transverse Stress Plots

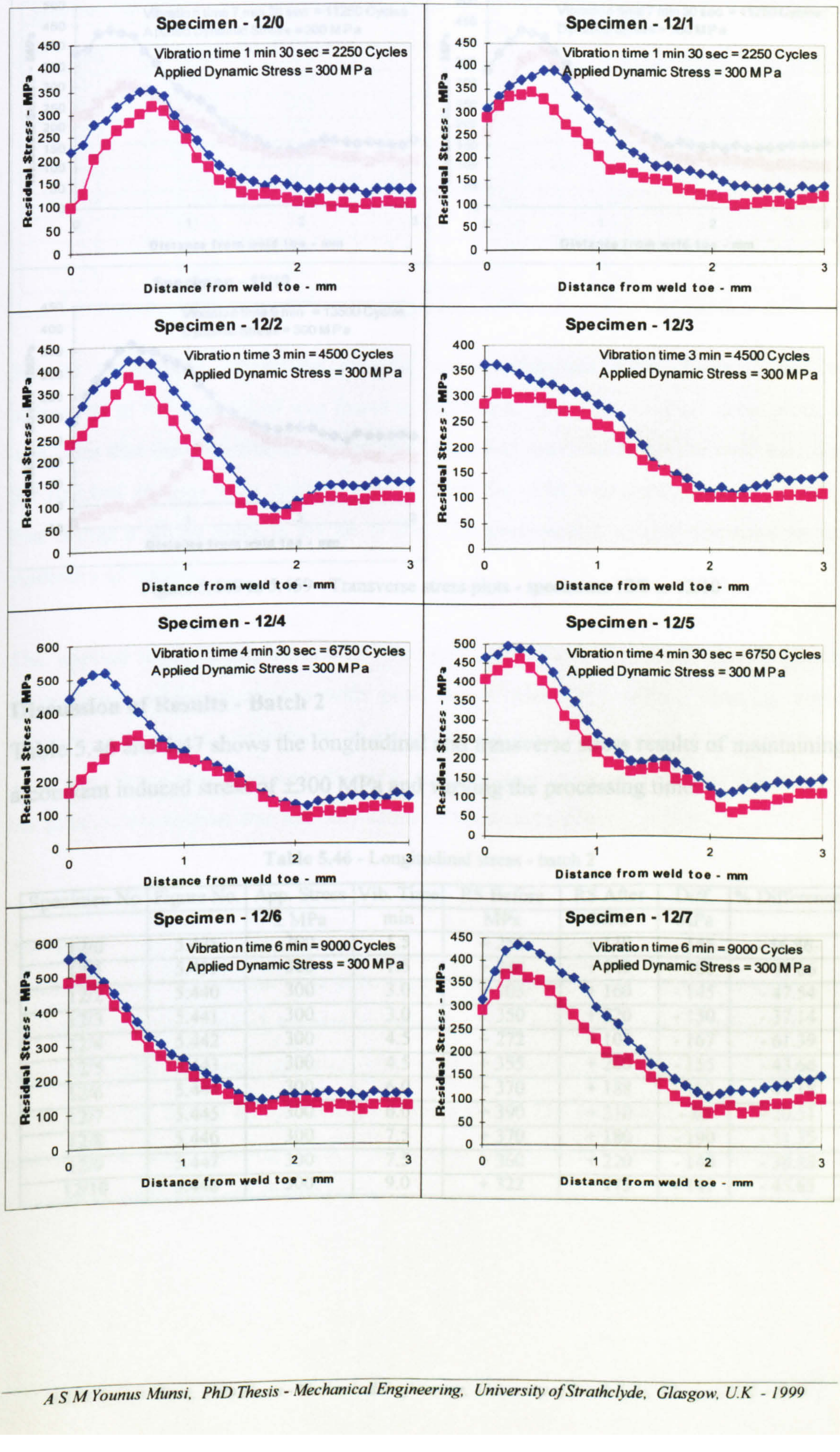

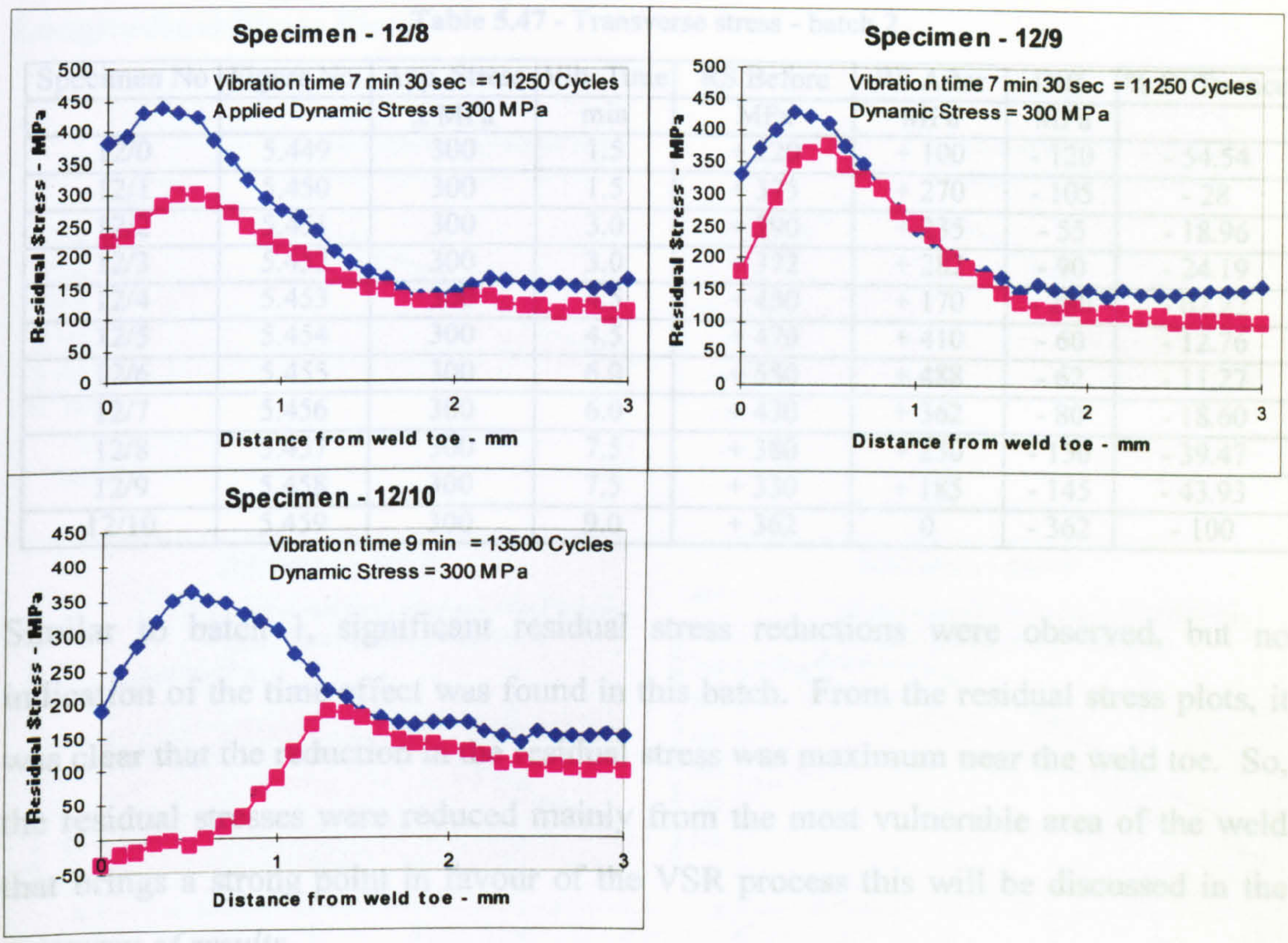

Figure 5.449 to 5.459 - Transverse stress plots - specimens 12/0 to 12/10

Discussion of Results - Batch 2

Table 5.46 and 5.47 shows the longitudinal and transverse stress results of maintaining a constant induced stress of ±300 MPa and varying the processing time.

Table 5.46 - Longitudinal stress - batch 2

Specimen No	Figure No.	App. Stress	Vib. Time	RS Before	RS After	Diff.	% Difference
		± MPa	min	MPa	MPa	MPa	
12/0	5.438	300	1.5	+ 255	+ 110	- 145	- 56.86-
12/1	5.439	300	1.5	+ 240	+ 140	- 100	- 41.66
12/2	5.440	300	3.0	+ 305	+ 160	- 145	- 47.54
12/3	5.441	300	3.0	+ 350	+ 220	- 130	- 37.14
12/4	5.442	300	4.5	+ 272	+ 105	- 167	- 61.39
12/5	5.443	300	4.5	+ 355	+ 200	- 155	- 43.66
12/6	5.444	300	6.0	+ 370	+ 188	- 182	- 49.18
12/7	5.445	300	6.0	+ 390	+ 310	- 80	- 20.51
12/8	5.446	300	7.5	+ 370	+ 180	- 190	- 51.35
12/9	5.447	300	7.5	+ 360	+ 220	- 140	- 38.88
12/10	5.448	300	9.0	+ 322	+ 175	- 147	- 45.65

Table 5.47 - Transverse stress - batch 2

Specimen No	Figure No.	App. Stress	Vib. Time	RS Before	RS After	Diff.	% Difference
		± MPa	min	MPa	MPa	MPa	
12/0	5.449	300	1.5	+ 220	+ 100	- 120	- 54.54
12/1	5.450	300	1.5	+ 375	+ 270	- 105	- 28
12/2	5.451	300	3.0	+ 290	+ 235	- 55	- 18.96
12/3	5.452	300	3.0	+ 372	+ 282	- 90	- 24.19
12/4	5.453	300	4.5	+ 450	+ 170	- 280	- 62.22
12/5	5.454	300	4.5	+ 470	+ 410	- 60	- 12.76
12/6	5.455	300	6.0	+ 550	+ 488	- 62	- 11.27
12/7	5.456	300	6.0	+ 430	+ 362	- 80	- 18.60
12/8	5.457	300	7.5	+ 380	+ 230	- 150	- 39.47
12/9	5.458	300	7.5	+ 330	+ 185	- 145	- 43.93
12/10	5.459	300	9.0	+ 362	0	- 362	- 100

Similar to batch 1, significant residual stress reductions were observed, but no indication of the time effect was found in this batch. From the residual stress plots, it was clear that the reduction in the residual stress was maximum near the weld toe. So, the residual stresses were reduced mainly from the most vulnerable area of the weld that brings a strong point in favour of the VSR process this will be discussed in the *summary of results*.

The applied stress of this batch was ±300 MPa, thus there should not be any plastic deformation in the specimens with peak stress below 311 MPa. Thus, in some specimens there was a possibility of plastic deformation and in other specimens there were not. Stress reduction was observed in all the specimens, it concludes that may be the plastic deformation was not only cause of stress reduction.

Batch 3

In this batch, 11 specimens were processed. The specimens were welded without any treatment and the residual stresses measured. Then specimens were vibrated with a constant applied dynamic stress of ±300 MPa and the number of cycles of vibration varied in order to find an optimum processing time. The specimens were vibrated as indicated in the following plots - with two per sample. The longitudinal and transverse stress plots are shown below.

Longitudinal Stress Plots

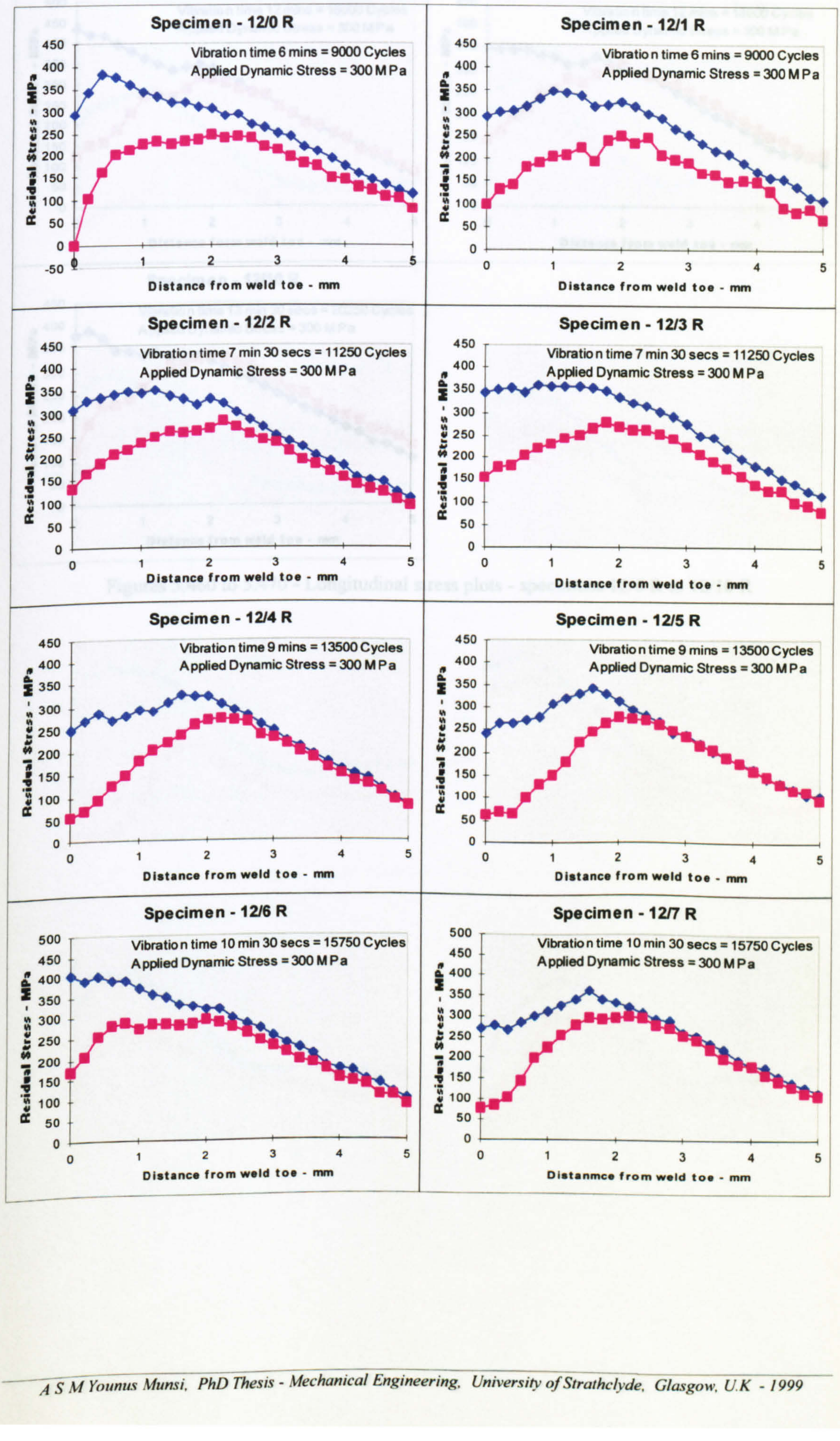

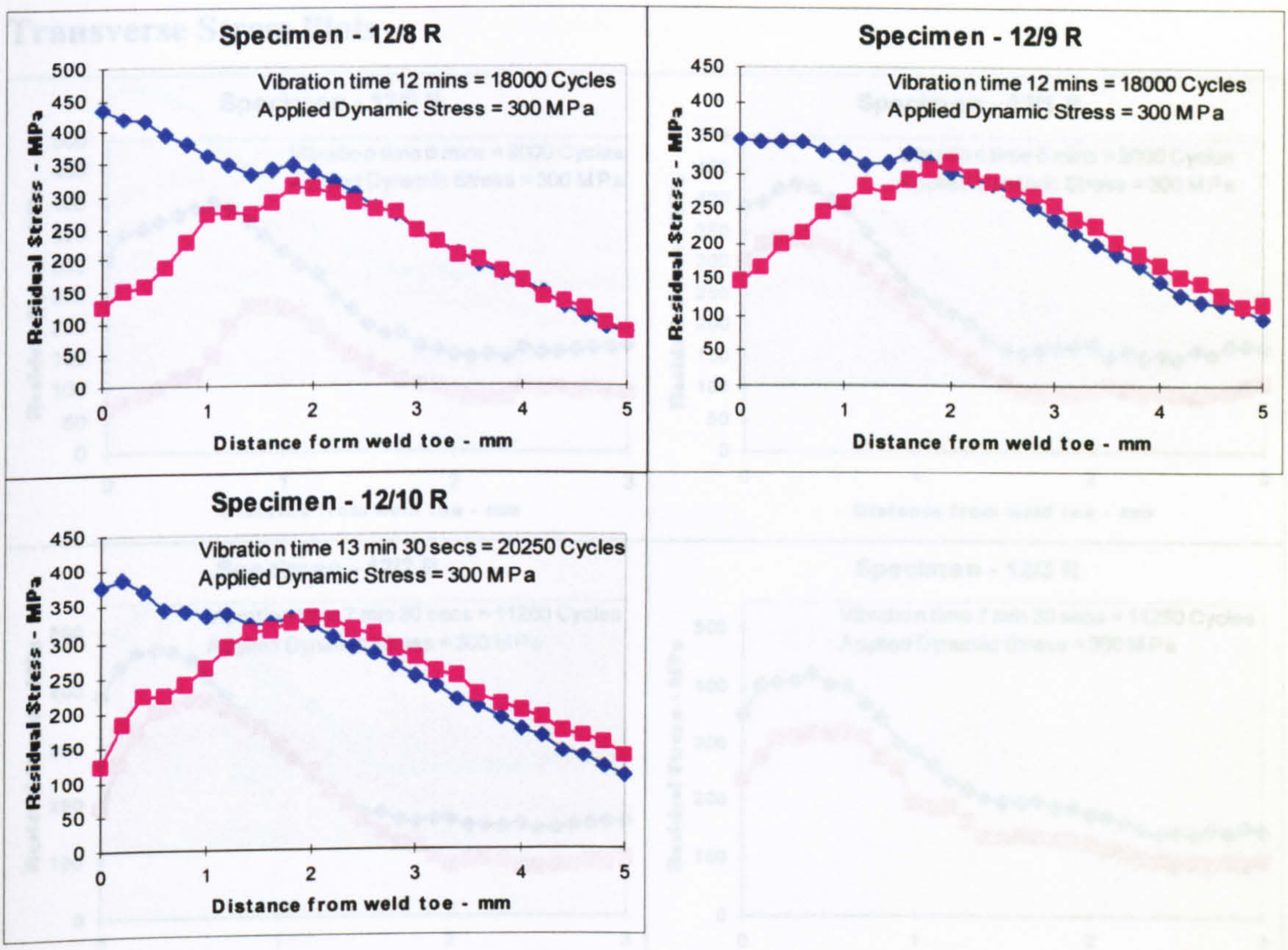

Figures 5.460 to 5.470 - Longitudinal stress plots - specimens 12/0 R to 12/10 R

Transverse Stress Plots

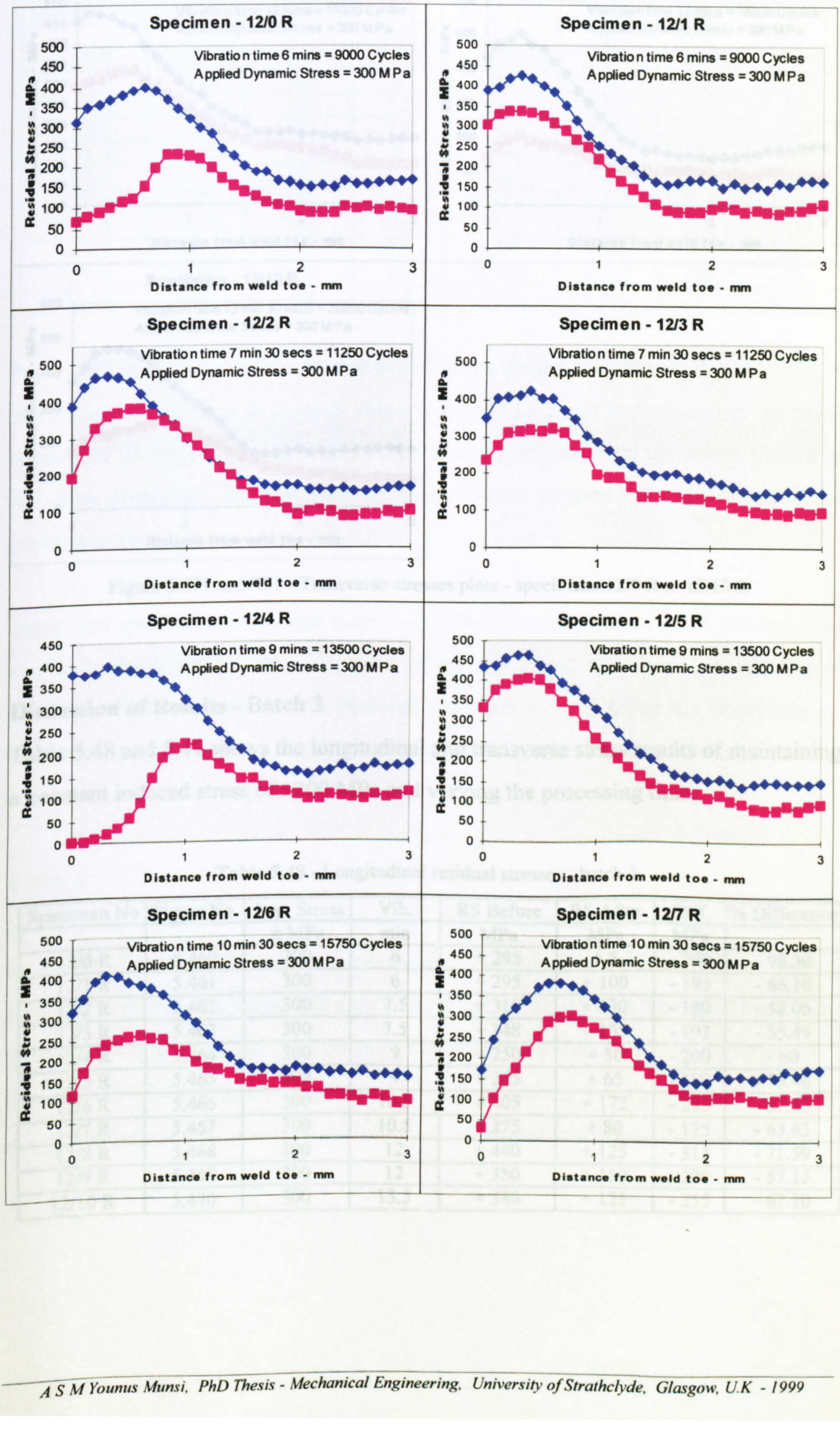

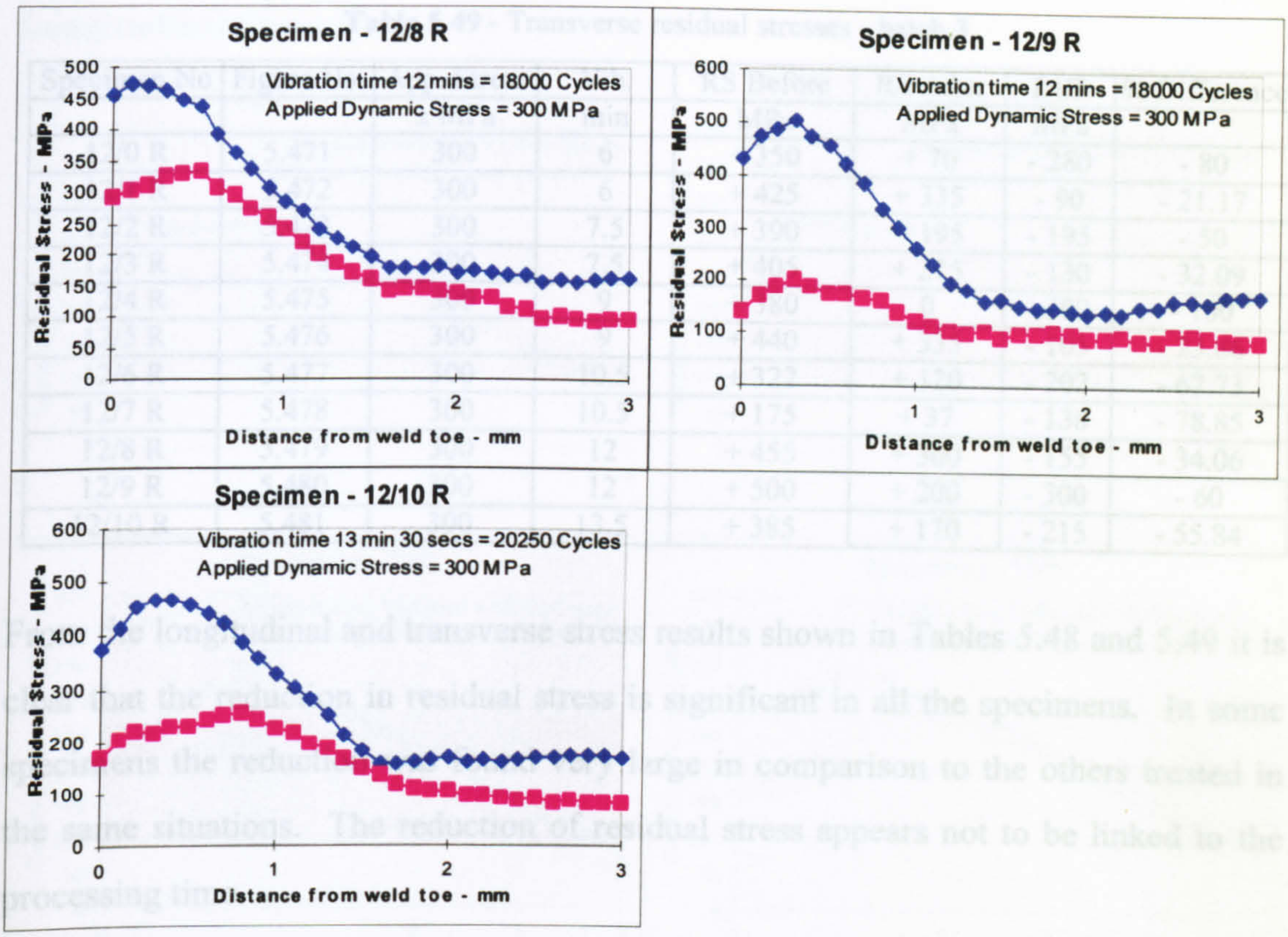

Figure 5.471 to 5.481 - Transverse stresses plots - specimens 12/0 R to 12/10 R

Discussion of Results - Batch 3

Table 5.48 and 5.49 shows the longitudinal and transverse stress results of maintaining a constant induced stress of ±300 MPa and varying the processing time.

Table 5.48 - Longitudinal residual stresses - batch 3

Specimen No	Figure No.	App. Stress	Vib.	RS Before	RS After	Diff.	% Difference
		± MPa	min	MPa	MPa	MPa	
12/0 R	5.460	300	6	+ 295	+ 5	- 290	- 98.30
12/1 R	5.461	300	6	+ 295	+ 100	- 195	- 66.10
12/2 R	5.462	300	7.5	+ 310	+ 130	- 180	- 58.06
12/3 R	5.463	300	7.5	+ 348	+ 155	- 193	- 55.49
12/4 R	5.464	300	9	+ 250	+ 50	- 200	- 80
12/5 R	5.465	300	9	+ 245	+ 65	- 180	- 73.46
12/6 R	5.466	300	10.5	+ 405	+ 172	- 233	- 57.53
12/7 R	5.467	300	10.5	+ 275	+ 80	- 175	- 63.63
12/8 R	5.468	300	12	+ 440	+ 125	- 315	- 71.59
12/9 R	5.469	300	12	+ 350	+ 150	- 200	- 57.15
12/10 R	5.470	300	13.5	+ 380	+ 125	- 255	- 67.10

Table 5.49 - Transverse residual stresses - batch 3

Specimen No	Figure No.	App. Stress ± MPa	Vib. min	RS Before MPa	RS After MPa	Diff. MPa	% Difference
12/0 R	5.471	300	6	+ 350	+ 70	- 280	- 80
12/1 R	5.472	300	6	+ 425	+ 335	- 90	- 21.17
12/2 R	5.473	300	7.5	+ 390	+ 195	- 195	- 50
12/3 R	5.474	300	7.5	+ 405	+ 275	- 130	- 32.09
12/4 R	5.475	300	9	+ 380	0	- 380	- 100
12/5 R	5.476	300	9	+ 440	+ 335	- 105	- 23.86
12/6 R	5.477	300	10.5	+ 322	+ 120	- 202	- 62.73
12/7 R	5.478	300	10.5	+ 175	+ 37	- 138	- 78.85
12/8 R	5.479	300	12	+ 455	+ 300	- 155	- 34.06
12/9 R	5.480	300	12	+ 500	+ 200	- 300	- 60
12/10 R	5.481	300	13.5	+ 385	+ 170	- 215	- 55.84

From the longitudinal and transverse stress results shown in Tables 5.48 and 5.49 it is clear that the reduction in residual stress is significant in all the specimens. In some specimens the reduction was found very large in comparison to the others treated in the same situations. The reduction of residual stress appears not to be linked to the processing time.

Since, the applied stress to this batch was 300 MPa, the condition of yielding was similar to the batch 2. Thus, for most of the specimens, there was a possibility of yielding. In specimens 12/7 R (residual peak stress +175 MPa) the possibility of yielding appears to be very small, but a significant stress reduction was found.

Batch 4

In this batch 11 specimens were processed. The specimens were welded without any treatment and the residual stress measured. The specimens were vibrated with a constant amplitude that generated a dynamic stress of ±250 MPa. The specimens were vibrated - two in a sample. The times of vibration were 9 minutes, 10.5 minutes, 13.5 minutes, 15 minutes, and 16.5 minutes. The longitudinal and transverse stress plots are shown below.

Longitudinal Stress Plots

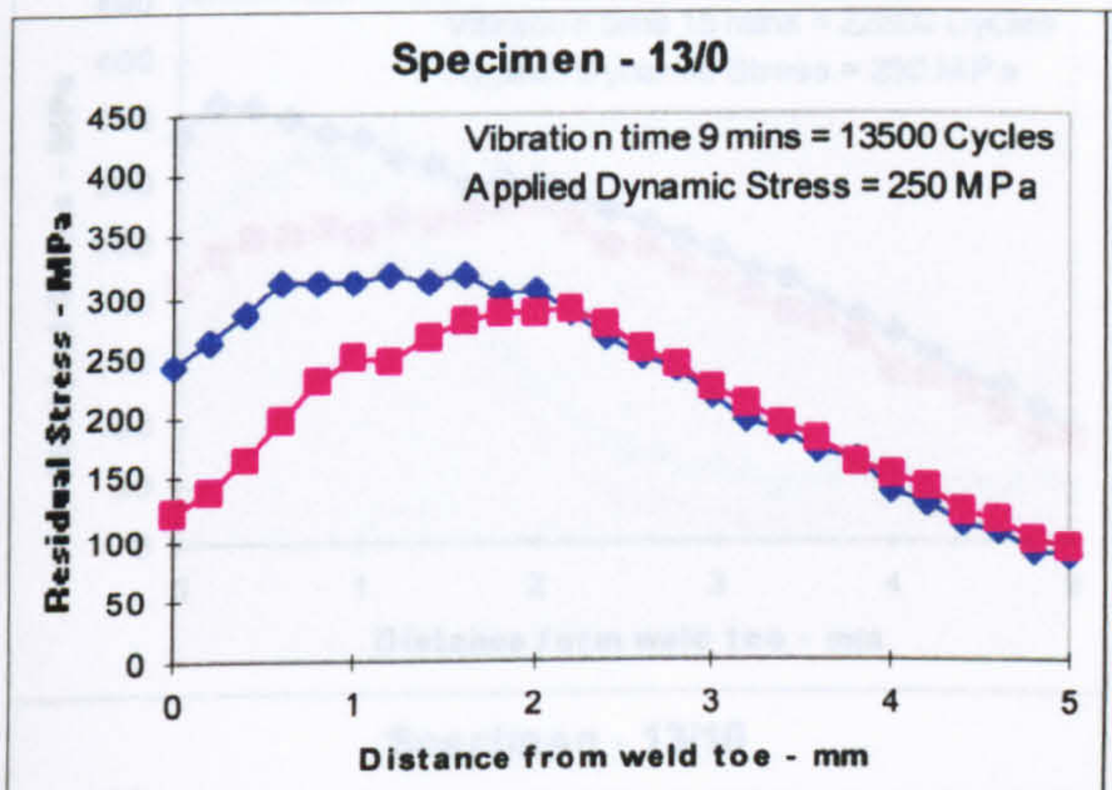

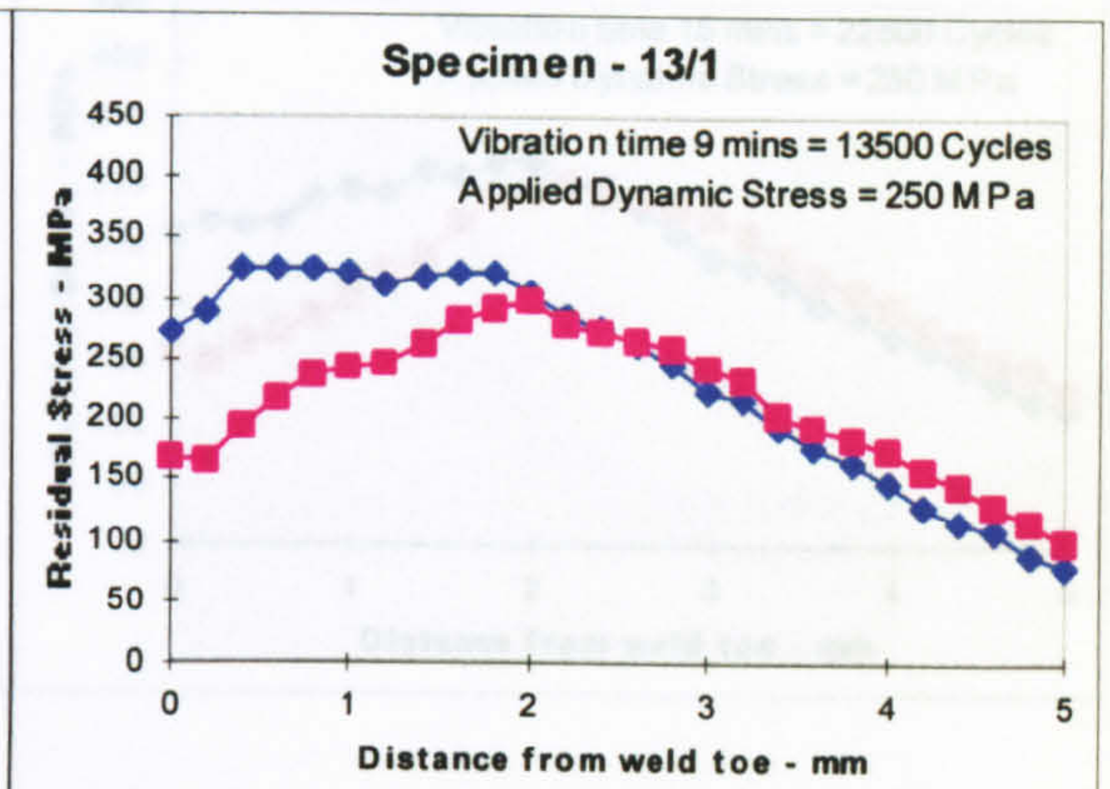

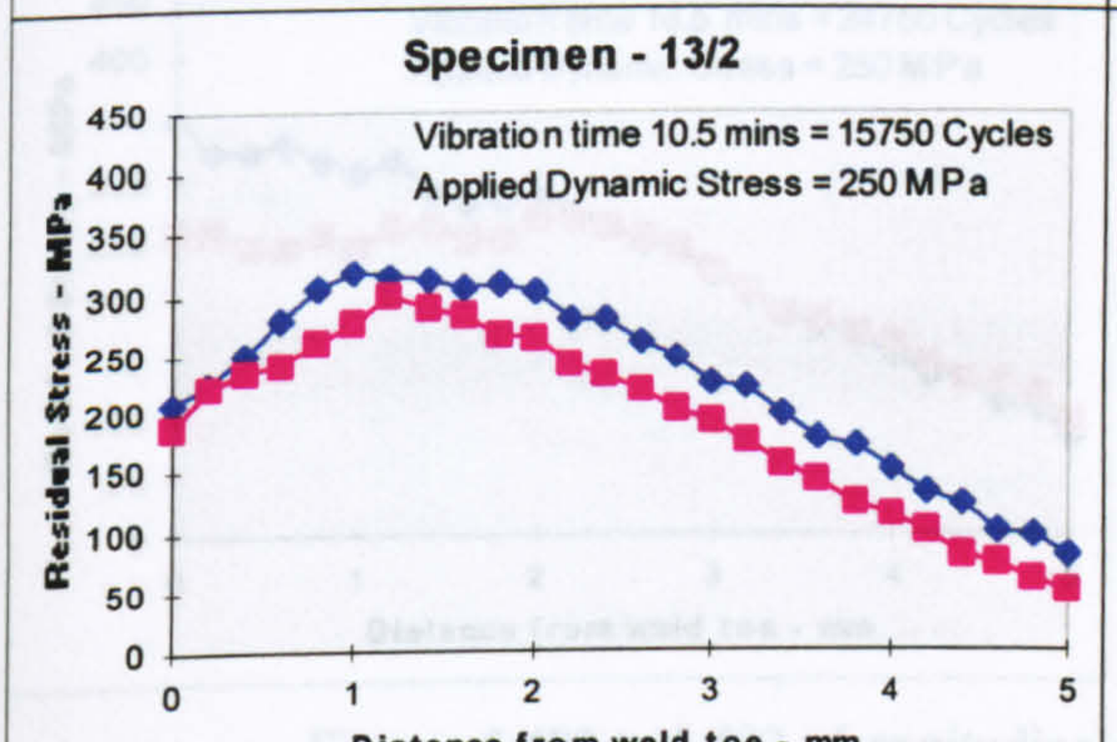

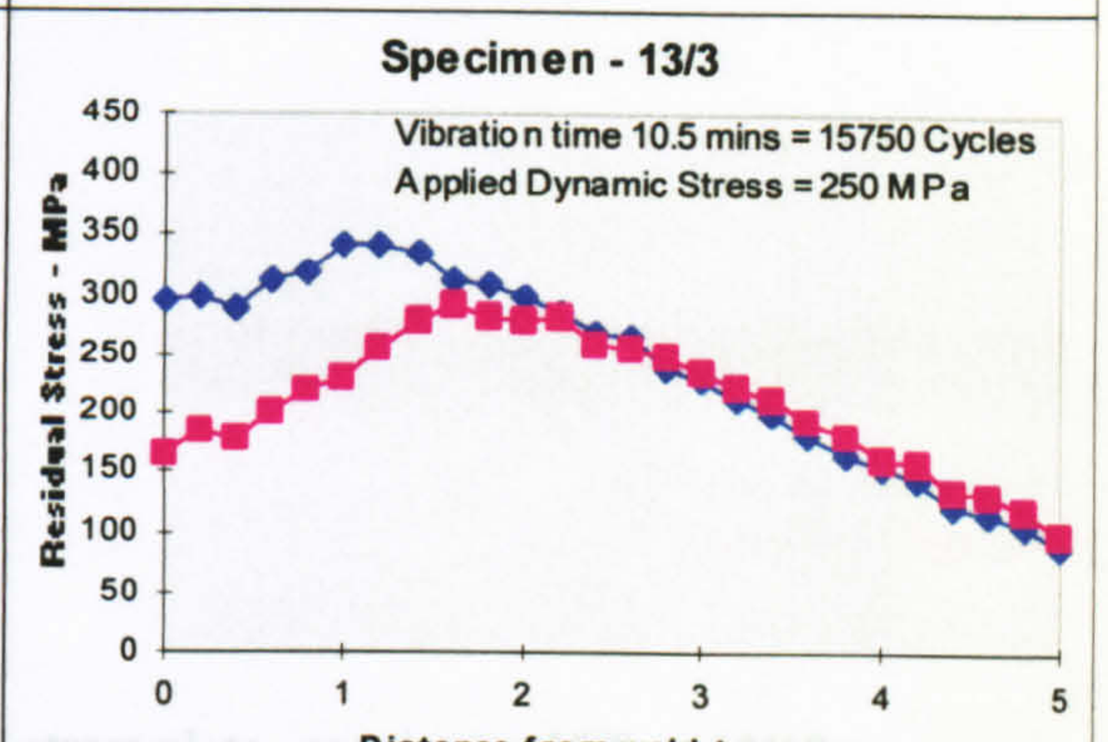

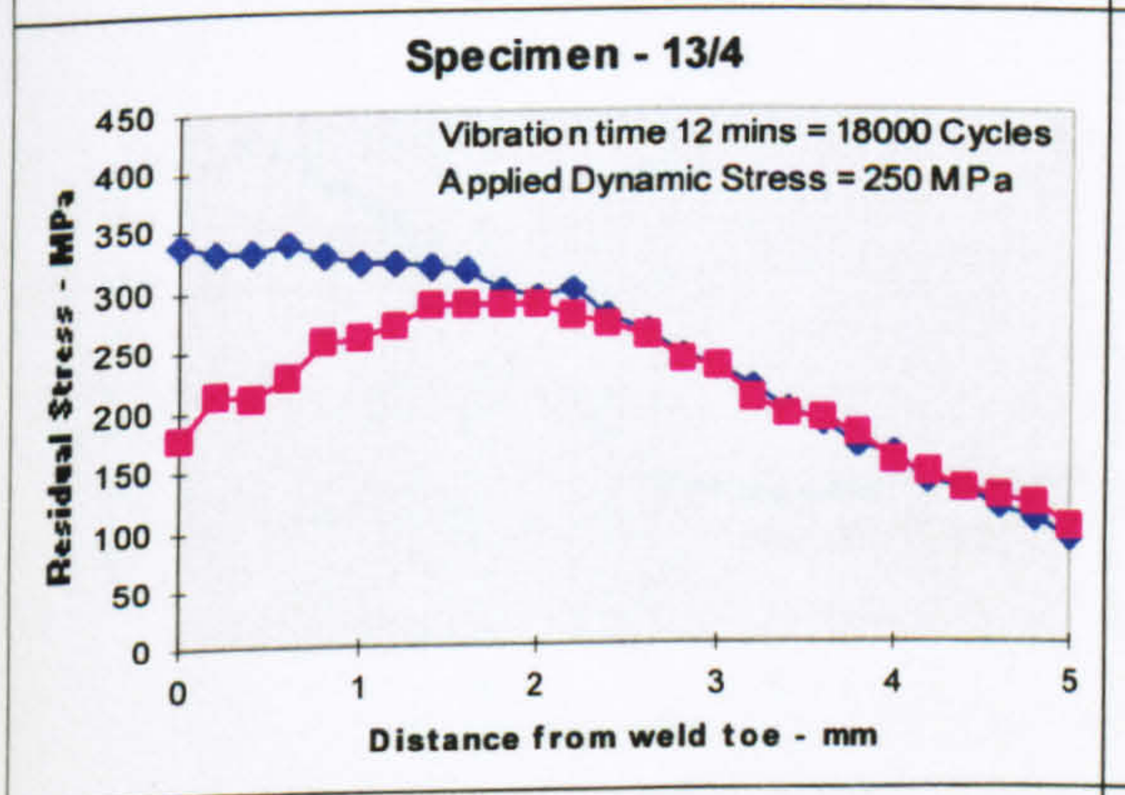

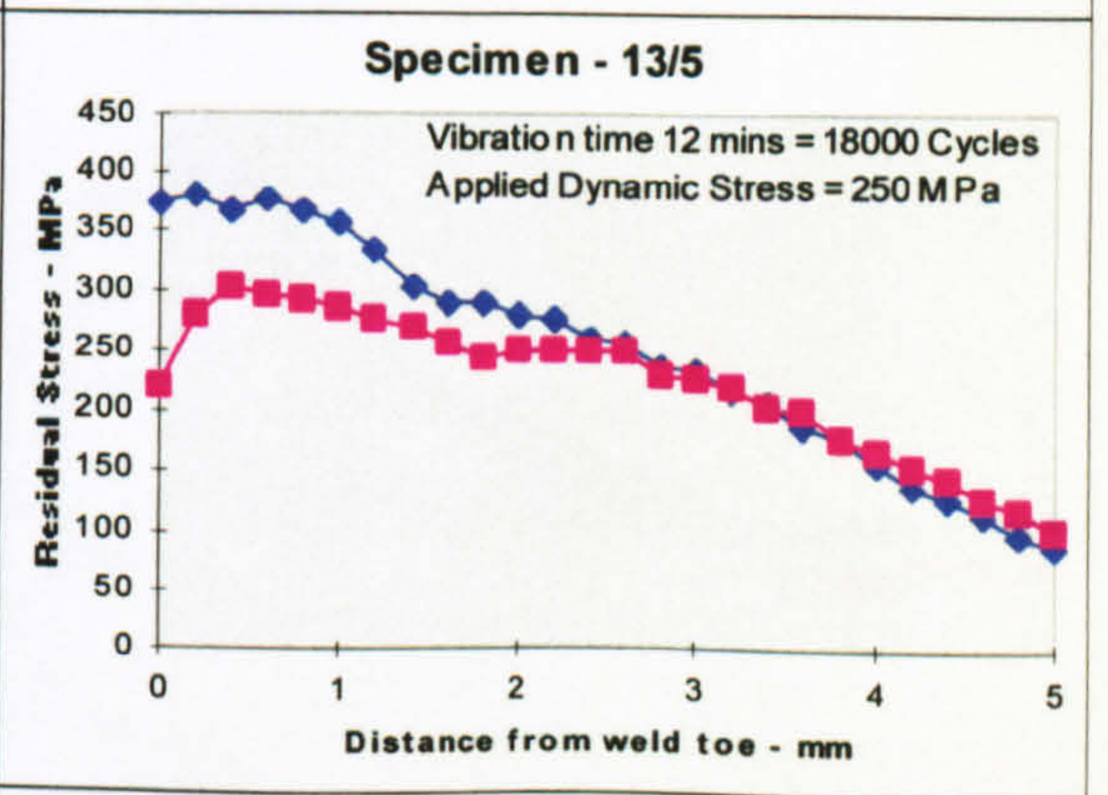

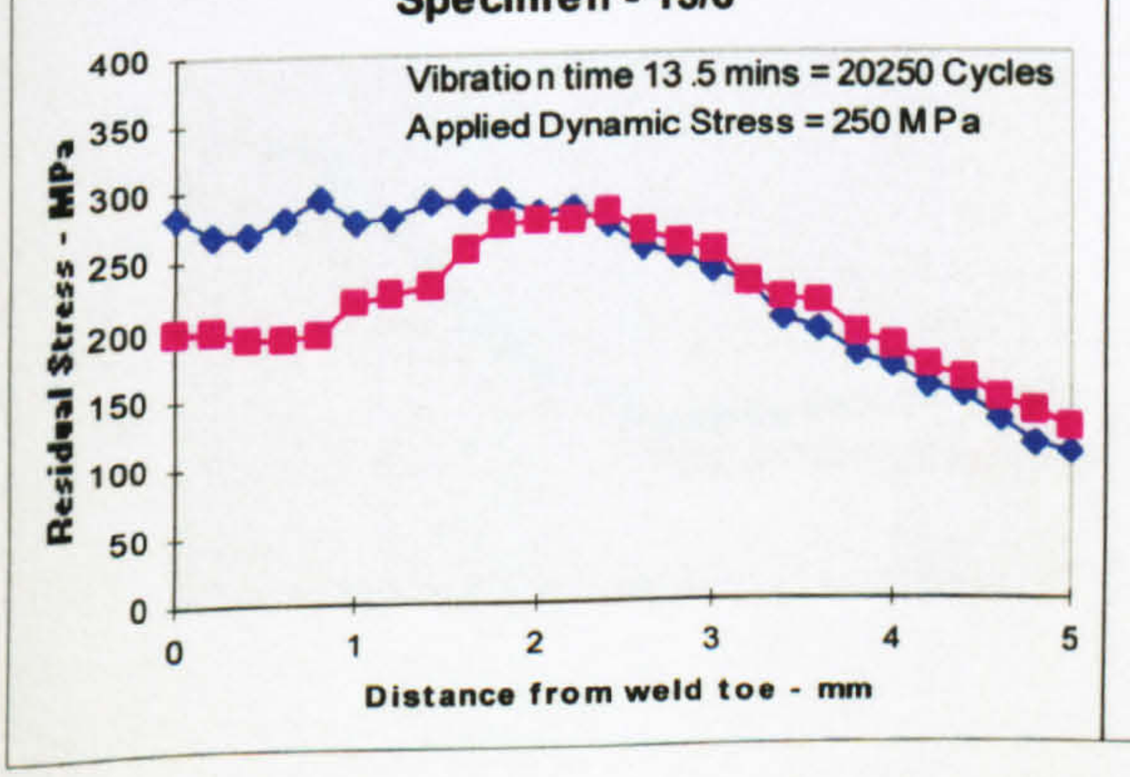

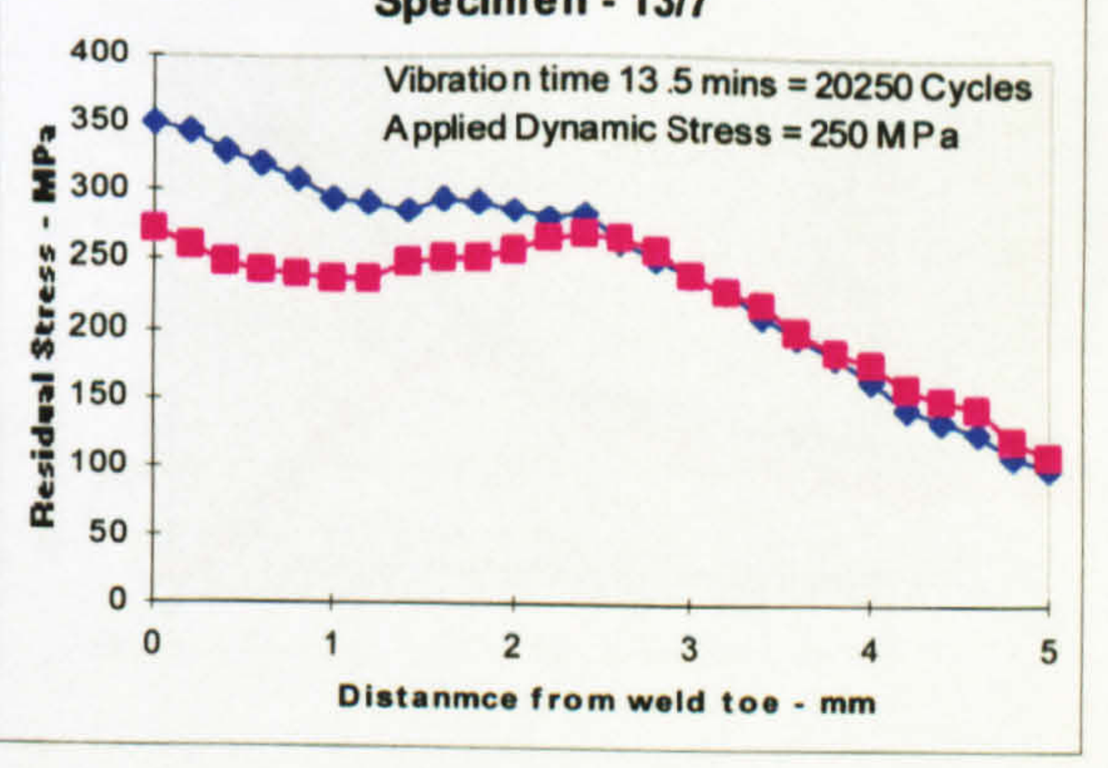

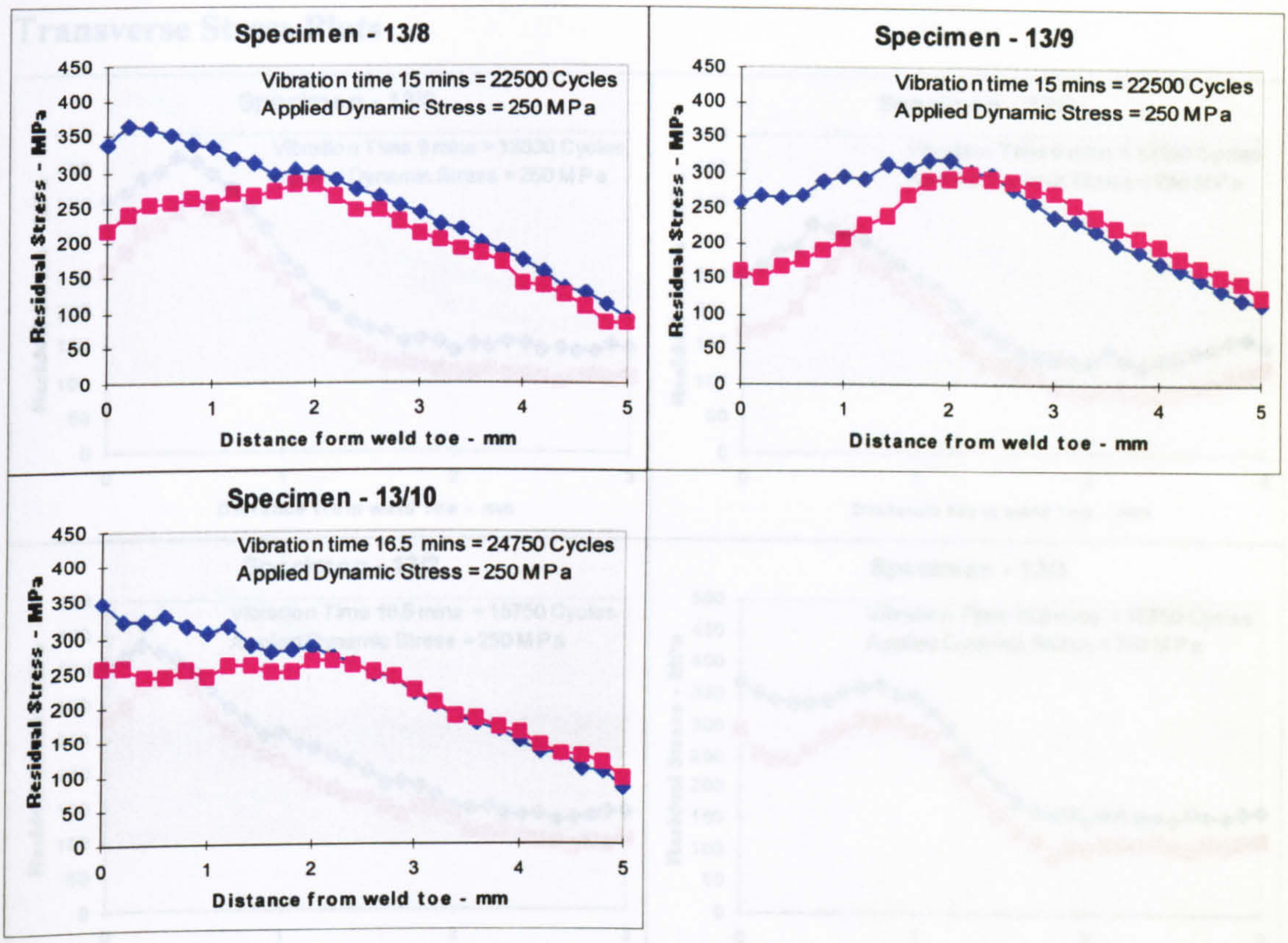

Figures 5.482 to 5.492 - Longitudinal stress plots - specimens 13/0 to 13/10

Transverse Stress Plots

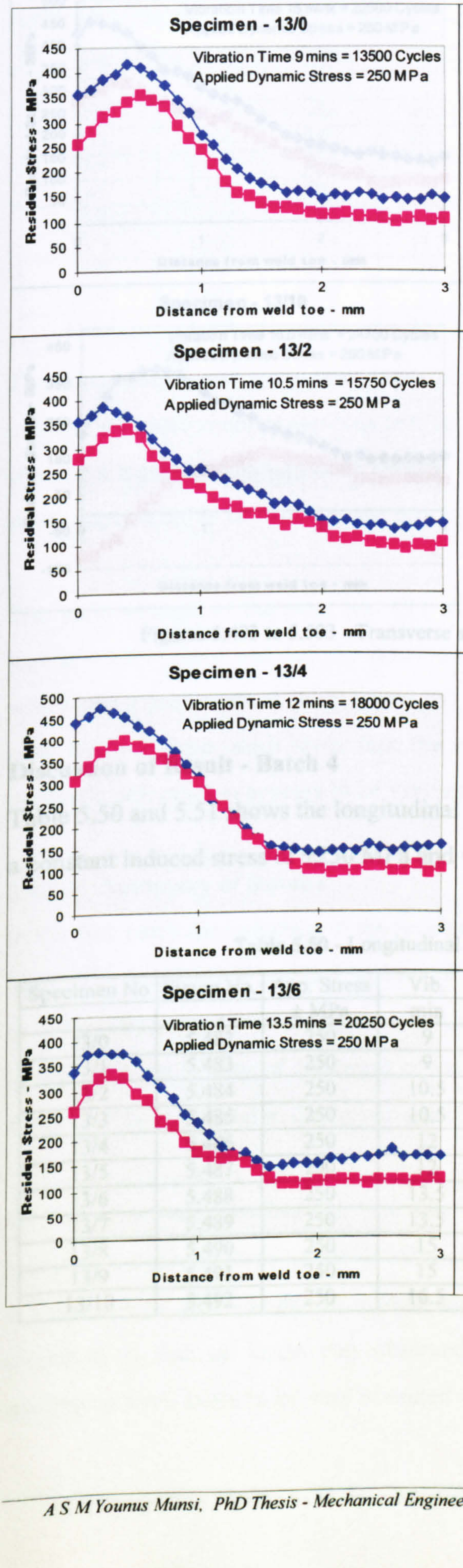

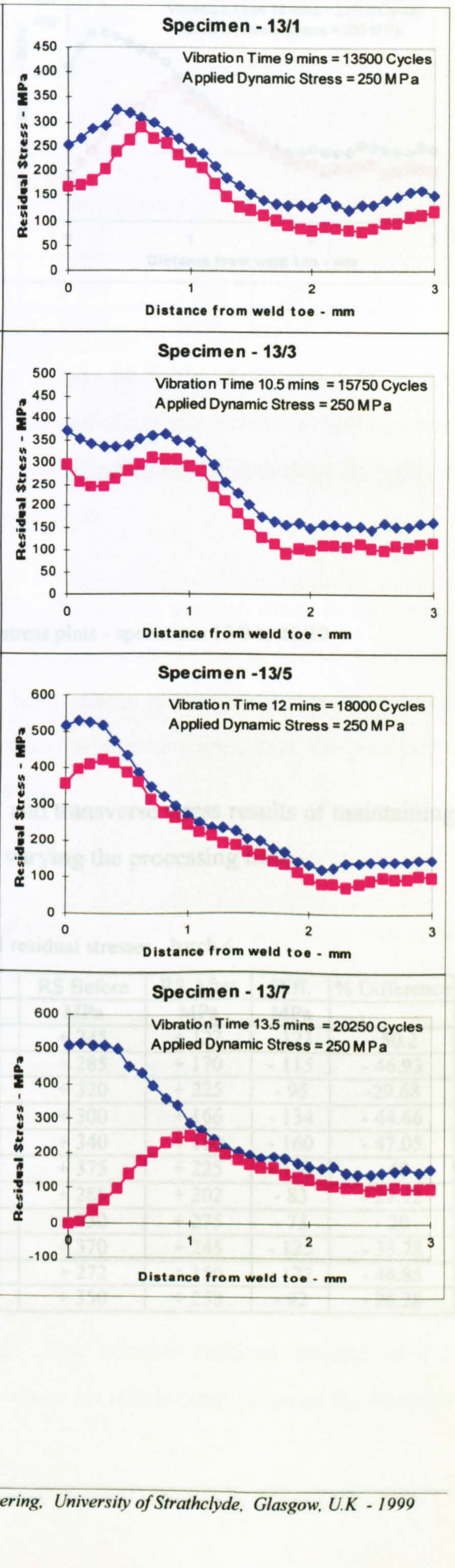

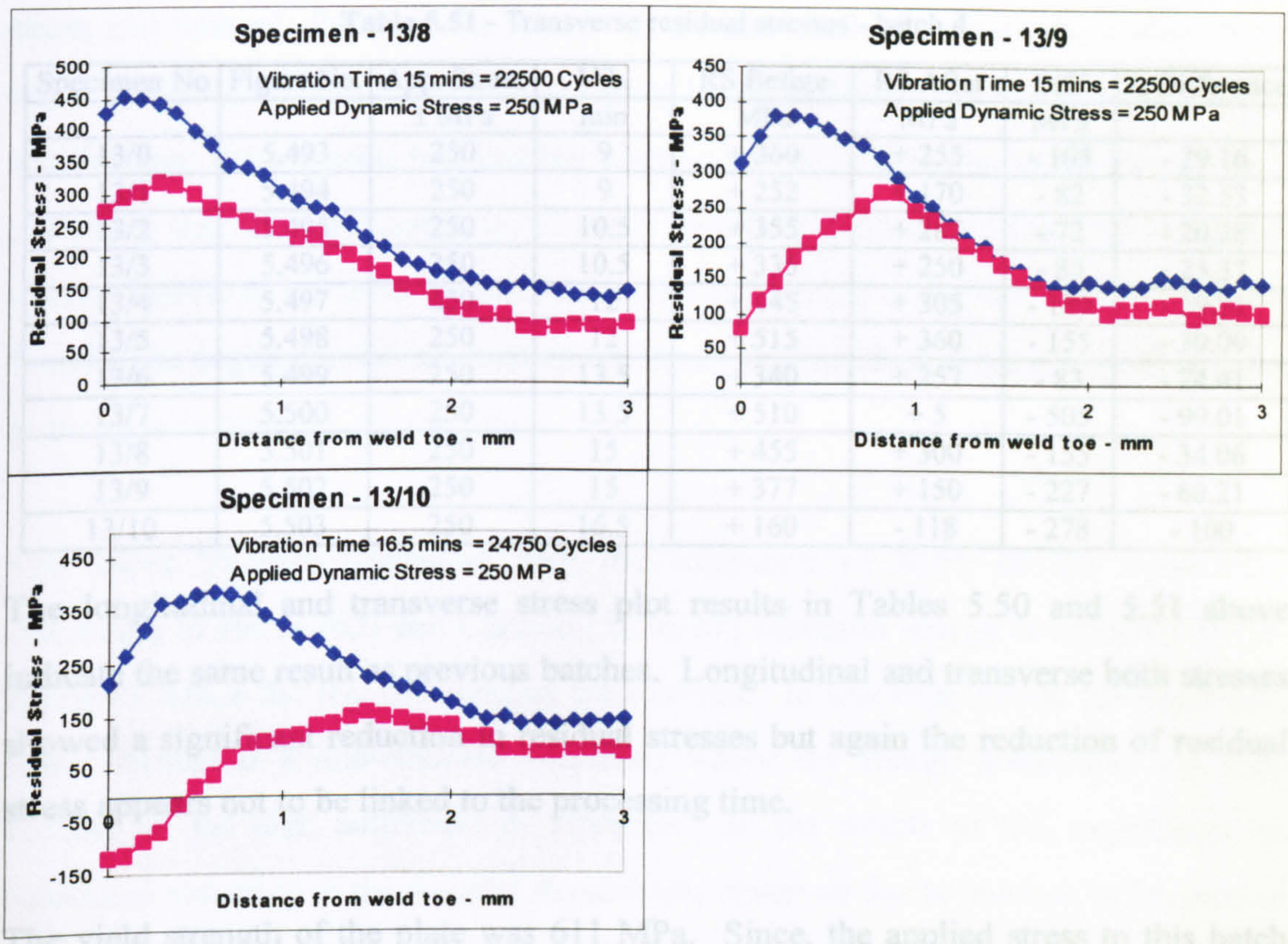

Figures 5.493 to 5.503 - Transverse stress plots - specimens 13/0 to 13/10

Discussion of Result - Batch 4

Table 5.50 and 5.51 shows the longitudinal and transverse stress results of maintaining a constant induced stress of ±250 MPa and varying the processing time.

Table 5.50 - Longitudinal residual stresses - batch 4

Specimen No	Figure No.	App. Stress	Vib.	RS Before	RS After	Diff.	% Difference
		± MPa	min	MPa	MPa	MPa	
13/0	5.482	250	9	+ 245	+ 122	- 123	- 50.2
13/1	5.483	250	9	+ 285	+ 170	- 115	- 46.93
13/2	5.484	250	10.5	+ 320	+ 225	- 95	-29.68
13/3	5.485	250	10.5	+ 300	+ 166	- 134	- 44.66
13/4	5.486	250	12	+ 340	+ 180	- 160	- 47.05
13/5	5.487	250	12	+ 375	+ 225	- 150	- 40
13/6	5.488	250	13.5	+ 285	+ 202	- 83	- 29.12
13/7	5.489	250	13.5	+ 350	+ 275	- 75	- 20
13/8	5.490	250	15	+ 370	+ 245	- 125	- 33.78
13/9	5.491	250	15	+ 272	+ 150	- 122	- 44.85
13/10	5.492	250	16.5	+ 350	+ 258	- 92	- 26.28

Table 5.51 - Transverse residual stresses - batch 4

Specimen No	Figure No.	App. Stress	Vib.	RS Before	RS After	Diff.	% Difference
		± MPa	min	MPa	MPa	MPa	
13/0	5.493	250	9	+ 360	+ 255	- 105	- 29.16
13/1	5.494	250	9	+ 252	+ 170	- 82	- 32.53
13/2	5.495	250	10.5	+ 355	+ 283	- 72	- 20.28
13/3	5.496	250	10.5	+ 335	+ 250	- 85	- 25.37
13/4	5.497	250	12	+ 445	+ 305	- 130	- 29.21
13/5	5.498	250	12	+ 515	+ 360	- 155	- 30.09
13/6	5.499	250	13.5	+ 340	+ 257	- 83	- 24.41
13/7	5.500	250	13.5	+ 510	+ 5	- 505	- 99.01
13/8	5.501	250	15	+ 455	+ 300	- 155	- 34.06
13/9	5.502	250	15	+ 377	+ 150	- 227	- 60.21
13/10	5.503	250	16.5	+ 160	- 118	- 278	- 100

The longitudinal and transverse stress plot results in Tables 5.50 and 5.51 above indicate the same result as previous batches. Longitudinal and transverse both stresses showed a significant reduction in residual stresses but again the reduction of residual stress appears not to be linked to the processing time.

The yield strength of the plate was 611 MPa. Since, the applied stress to this batch was 250 MPa, there was not any possibility of plastic deformation in the specimens which had a peak residual stress below 361 MPa. Some specimens in this batch had a peak residual stress much lower than the value mentioned above, thus the possibility of plastic deformation appears to be very small.

5.4.1.4 Summary of Results

In the first batch the reduction in the residual stress of most of the specimens was very high. The longitudinal residual stresses of this batch were found to decrease by 27% to 63%. The transverse residual stresses were found to decrease by 23% to 93%. Due to the different history of treatment of this batch, the stress reduction of this batch should not be compared to the reductions of the other batches.

Of the other three batches the first two batches (batch 2 and 3) were processed applying a dynamic stress of ±300 MPa where the vibration times were varied from 1.5 minutes to 16.5 minutes in several steps. In all of the specimens a significant reduction in residual stress was observed. The reduced residual stresses of the specimens were found to be very scattered where no relationship between the residual

stress and time of vibration was found. In the last batch, (batch 4) the applied stress was ±250 MPa. In this batch, the reduction in the residual stresses were found to be smaller than the previous two batches where ±300 MPa dynamic stress was applied, indicating that stress reduction in vibratory treatment method is a function of applied stress. Similar to the other batches, the effect of increase in the time of vibration was found to be negligible, i.e. no decrease or increase of residual stresses were found due to increase in the time of vibration.

The above findings contradict with the comments of some of the researchers. According to Habel [62] and Claxton [32 to 37] vibration energy is absorbed by the specimen hence the residual stresses are relieved. In this experiment, the specimens were vibrated at a non-resonant frequency where the energy absorption was high because of the high amplitude of vibration. In the results of this experiment no additional reduction in the residual stresses was observed due to increase in the time of vibration. The energy input to the specimens was increased by increasing the time of vibration but the reduction in the residual stresses were not achieved. Thus, this result concludes that the energy concept of VSR may not be true.

Contrarily the residual stresses were found to decrease more in the specimens subjected to higher dynamic stress which indicates that most possibly plastic flow occurred in the stressed area of the specimens hence the residual stresses were relieved.

The yield strength of the plate was 611 MPa. Due to welding, there was a possibility of lowering the yield strength. The applied stresses to the specimen were varied from ±250 MPa to ±320 MPa. It appears form the peak residual stresses and the applied stresses that there was a possibility of local yielding in some specimens and in other specimens there were not, but stress reduction was observed in all the specimens. This concludes two possible situations.

1. Although the peak residual stresses appear to be small in the measured data where the possibility of yielding seemed very small, the residual stresses in some other areas were high where plastic deformation might have occurred, hence residual stresses were relieved.
2. Except yielding there was any other reason of reduction in the residual stresses, which is not known.

5.4.2 Experiment VIII:

VSR Treatment of As-Welded Specimens

Abstract

In this experiment the welded specimens were processed after cooling down to room temperature. The specimens were processed varying the amplitude/applied stress and time of vibration. An increase in the applied stresses lead to a significant decrease in the residual stresses. The time of vibration effect was found to be a very small effect for the lower applied stresses - an increase in the time of vibration found no effect on residual stresses. At the higher applied stresses the residual stresses were found to increase due to increase in the time of vibration.

An another important characteristic was observed from the result of this experiment. The reduction in the residual stresses was found to be maximised in two points equidistant from the mid-width of the specimen. This might be due to the equilibrium characteristics of the residual stresses or the shear component of the applied stresses caused that reduction.

5.4.2.1 Introduction

In all of the foregoing experiments, specimens were processed in batches where some specimens were vibratory treated and some were kept as control specimens. The residual stresses of the treated specimens were compared with the unvibrated specimens. Unfortunately, there are some problems associated with multiple specimen experiments and these are:

1. It was impossible to keep the weld line in the same position for all of the specimens within the group. Measuring the residual stress using an X-ray diffractometer needs a fairly plane surface. If the measurement area is rough or inclined then there is a possibility of substantial error in the X-ray measurements. The acceptable distance of the X-ray measurement point from the X-ray head is 40±0.1 mm. If the distance were different from the mentioned value then there would be a substantial error in the measurements. So, if a line measurement was carried out from weld to the HAZ then it would result in different distances of the measurement points from the accepted value (40±0.1 mm) and without doubt cause an error. Thus, any

movement of the weld line would cause an error in the X-ray measurements if the measurement start point (weld toe) was not relocated by moving the specimen.

2. The residual stress on a welded specimen is a function of specimen geometry. If the weld line moves or if there is a little difference of weld geometry between the specimens (due to starting and finishing of the weld), certainly there would be difference in residual stresses from specimen to specimen.
3. The formation of residual stresses in a welded specimen is a function of temperature gradient in the welded area during cooling. If the weld line moves then the boundary condition changes and so changes the thermal gradient which caused different level of residual stresses. So, it is extremely difficult to compare two or more specimens which have apparently been treated in the same way.

The aforementioned problems can be overcome by processing the same specimen in a number of steps - varying different parameters and measuring the residual stress before and after each step of treatment. By this method, it is possible to measure the residual stress on the same points before and after treatment, so the question of different material property would be neglected because it would compare the treatment effect with the same specimen.

5.4.2.2 Experimental Procedure

In this experiment the specimens were welded without any treatment and the residual stresses were measured. The welding speed was controlled with the stepper motor controlled welding torch carrier (Figure 5.15A). A single pass weld was carried out on the specimen as shown in Figure 5.13. In the X-ray measurement the single exposure technique (SET) was used. The measurement conditions were similar to that described in Table 5.10. A line map was measured on the selected line (Figure 5.13). The X-ray measurement jig was the same as the jig used in Experiment-I, II and III (shown in Appendix II). The experimental set-up and calibration constant was similar to the set-up and calibration constant of Experiment-III.

In some specimens, the measurement surface was prepared by electropolishing. The descriptions of the electropolishing processes are provided in the description of the respective specimens.

In this experiment the specimens were processed - varying different parameters, i.e. time of vibration, applied dynamic stress etc. The residual stresses on the selected line were measured before and after every step of the treatment. The residual stresses were plotted in two forms - namely line and point stress plots.

In the line stress plot, the residual stresses of every measurement point on the line was plotted as stress against distance. This plot was showing the change in the residual stresses of the whole line due to the treatment.

In the point stress plots, every single point on the measurement line was focused. In the point stress plots, the change in residual stress of each point due to the treatment was shown by plotting residual stress against time of vibration or residual stress against the applied dynamic stresses. This plot was showing a clear picture of change in residual stresses of every single point due to different treatment.

5.4.2.3 Experimental Results

Specimen 13/1 and 13/2

These two specimens were welded without any treatment. As a post-weld treatment, the specimens were vibrated for different time intervals. The vibration intervals are shown in the plots.

In both specimens, the applied stress was ±300 MPa. The frequency of vibration was 25 Hz, and the specimens were vibrated until they fractured and broke. The transverse residual stress was measured on the selected line (Figure 5.13) before and after every step of the treatment. The line and point stresses of the two specimens are shown in Figure 5.504 to 5.507.

Residual Stress Plots of Specimen 13/1

Line Stress Plot

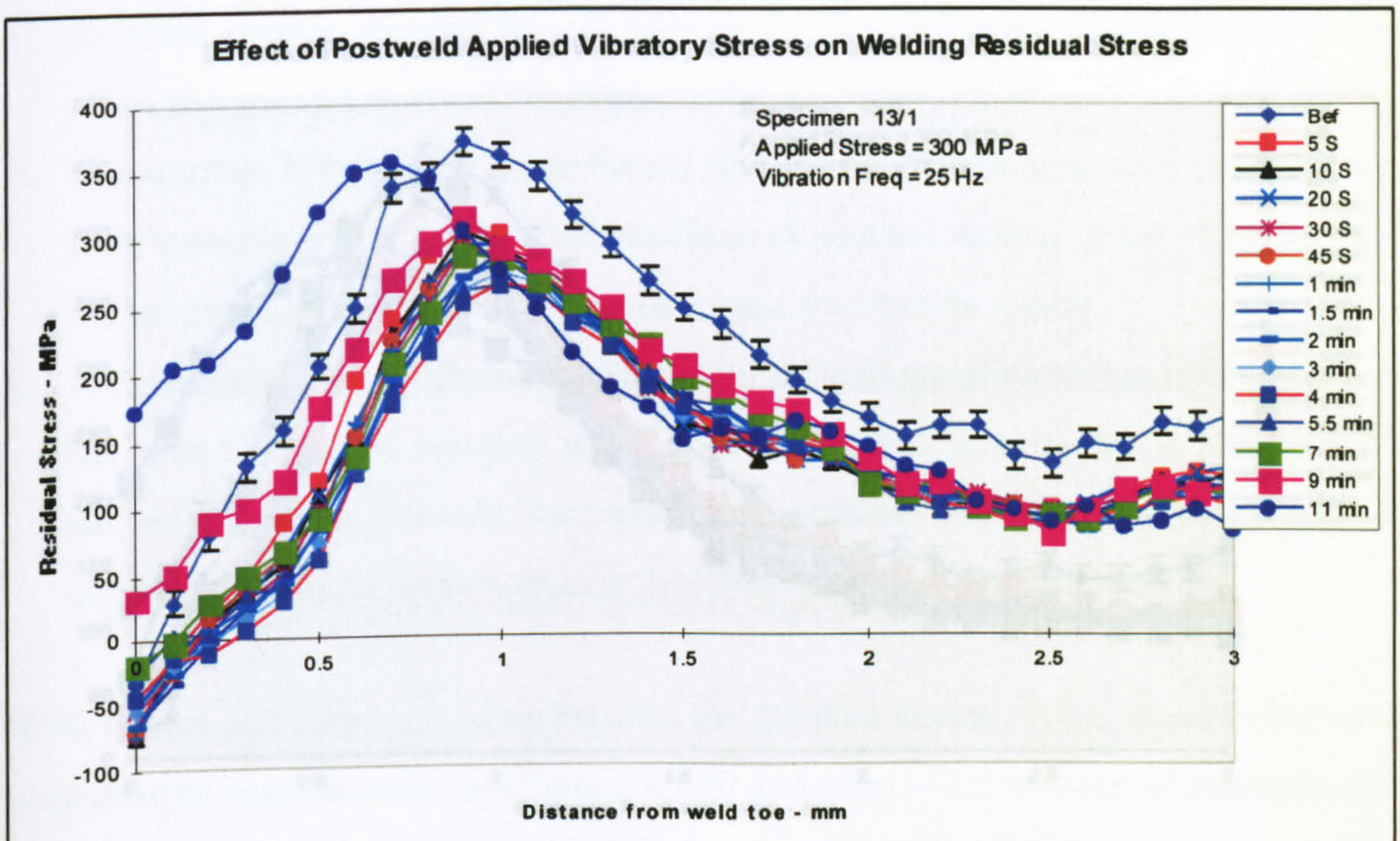

Figure 5.504 – Transverse line stress plot - specimen 13/1

Point Stress Plot

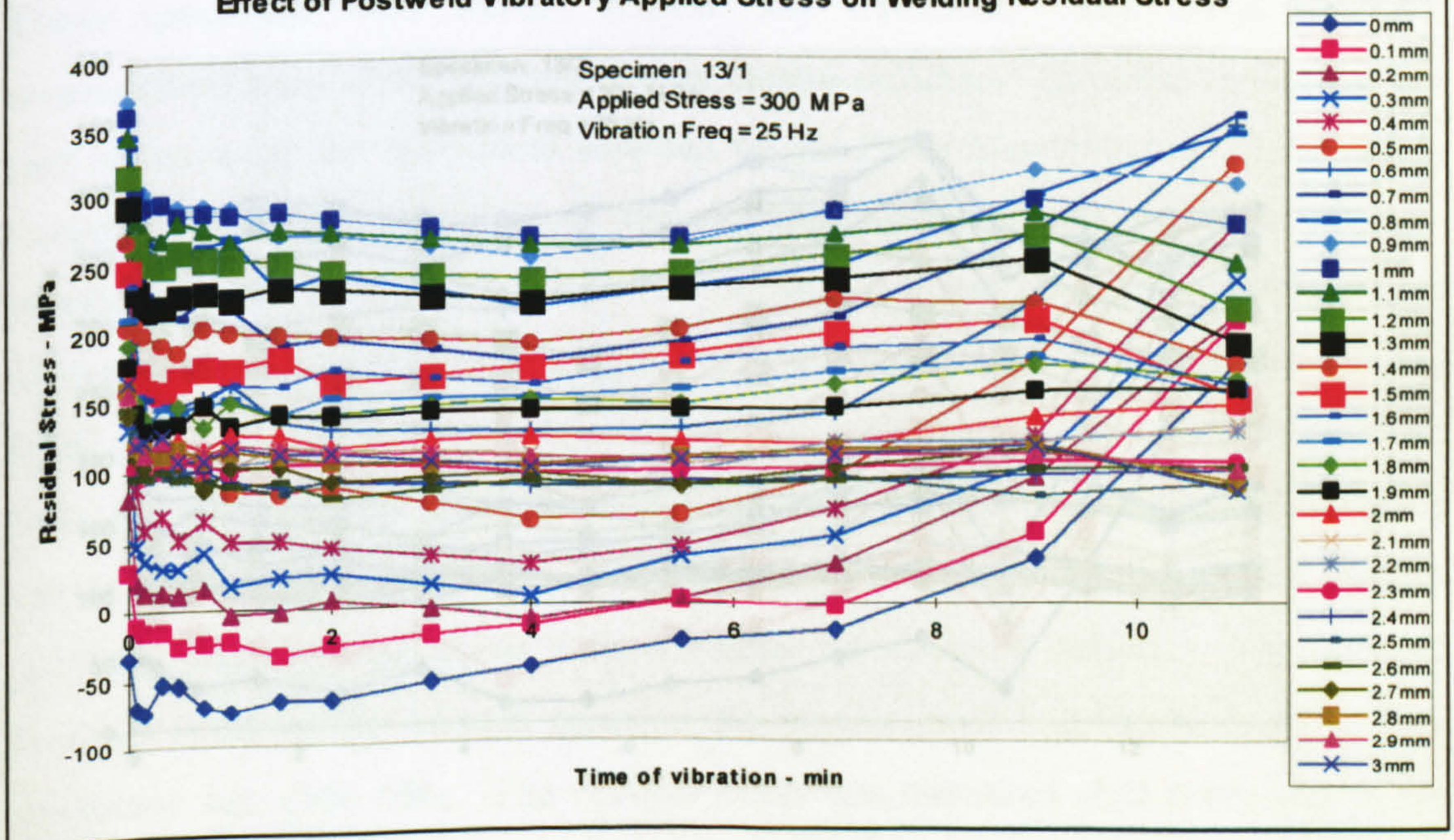

Figure 5.505 – Transverse point stress plot - specimen 13/1

Residual Stress Plots of Specimen 13/2

Line Stress Plot

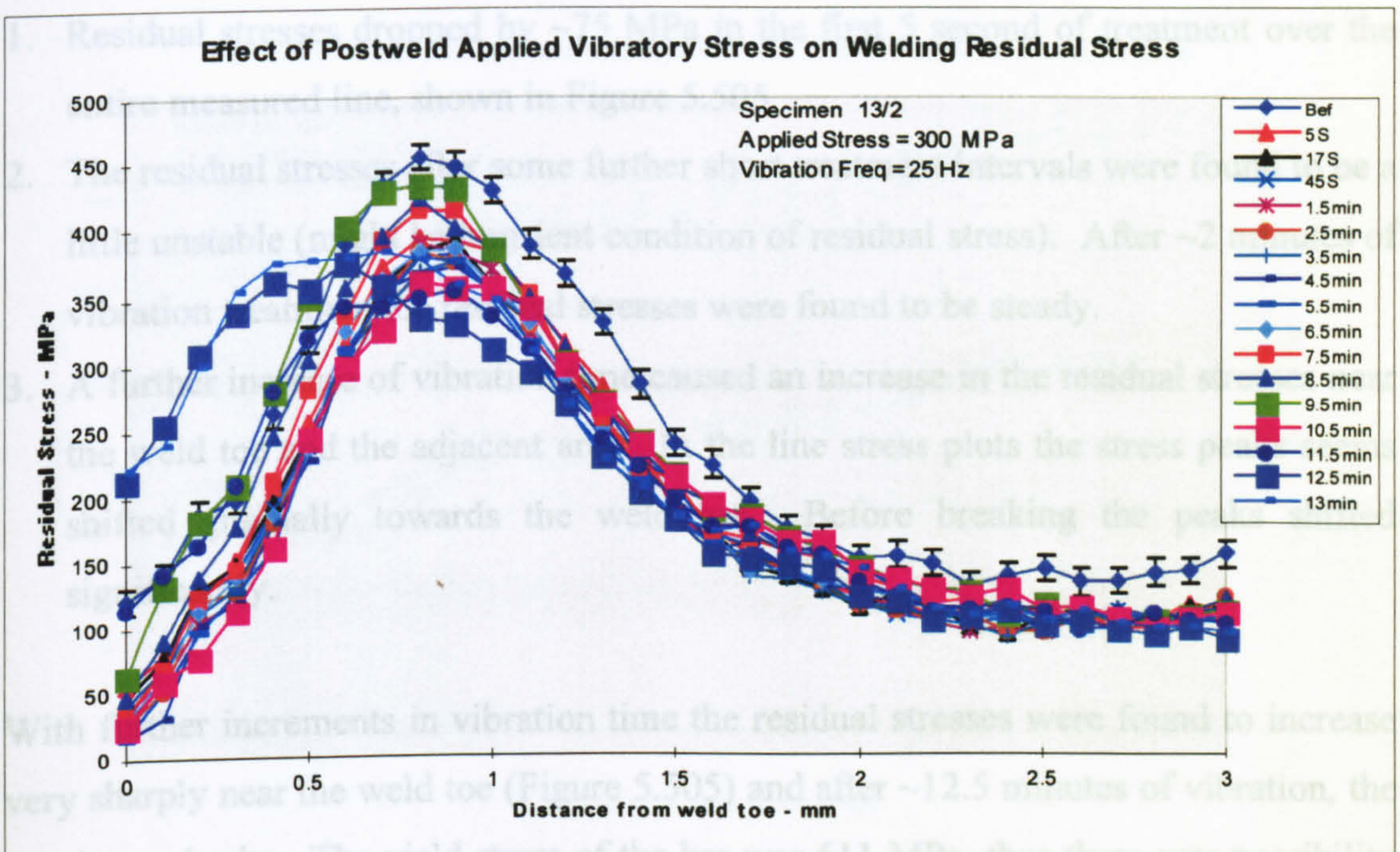

Figure 5.506 – Transverse line stress plot - specimen 13/2

Point Stress Plot

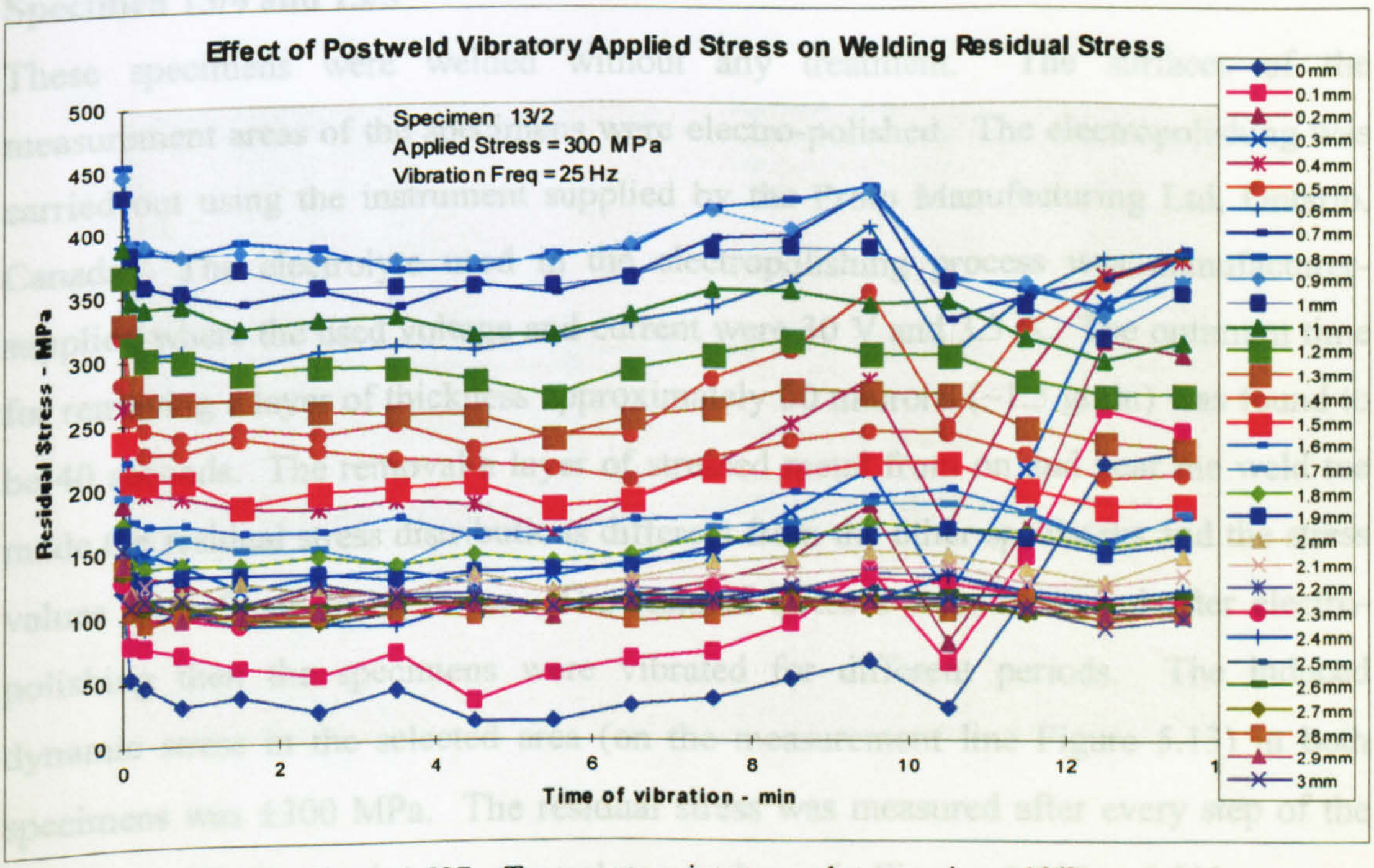

Figure 5.507 – Transverse point stress plot - specimen 13/2

Discussion of Result - Specimen 13/1 and 13/2

From the plots of the two specimens the following observations were made

1. Residual stresses dropped by ~75 MPa in the first 5 second of treatment over the entire measured line, shown in Figure 5.505.
2. The residual stresses after some further short treatment intervals were found to be a little unstable (might be transient condition of residual stress). After ~2 minutes of vibration treatment the residual stresses were found to be steady.
3. A further increase of vibration time caused an increase in the residual stresses near the weld toe and the adjacent area. In the line stress plots the stress peaks seems shifted gradually towards the weld toe. Before breaking the peaks shifted significantly.

With further increments in vibration time the residual stresses were found to increase very sharply near the weld toe (Figure 5.505) and after ~12.5 minutes of vibration, the specimens broke. The yield stress of the bar was 611 MPa, thus there was possibility of local yielding in both of the specimens.

Specimen 13/4 and 13/5

These specimens were welded without any treatment. The surfaces of the measurement areas of the specimens were electro-polished. The electropolishing was carried out using the instrument supplied by the Proto Manufacturing Ltd, Ontario, Canada. The electrolyte used in the electropolishing process was manufacturer-supplied where the used voltage and current were 30 V and 3.3 A. The optimum time for removing a layer of thickness approximately 50 microns (~1.5 grain) was found to be 40 seconds. The removal a layer of stressed metal from on and near the weld toe made the residual stress distributions different from the other specimens and the stress values were found to be lower. The residual stresses were measured after electro-polishing then the specimens were vibrated for different periods. The induced dynamic stress in the selected area (on the measurement line Figure 5.13) in both specimens was ±300 MPa. The residual stress was measured after every step of the treatment. The line and point stress plots are shown in Figures 5.508 to 5.511.

Residual Stress Plots of Specimen 13/4

Line Stress Plot

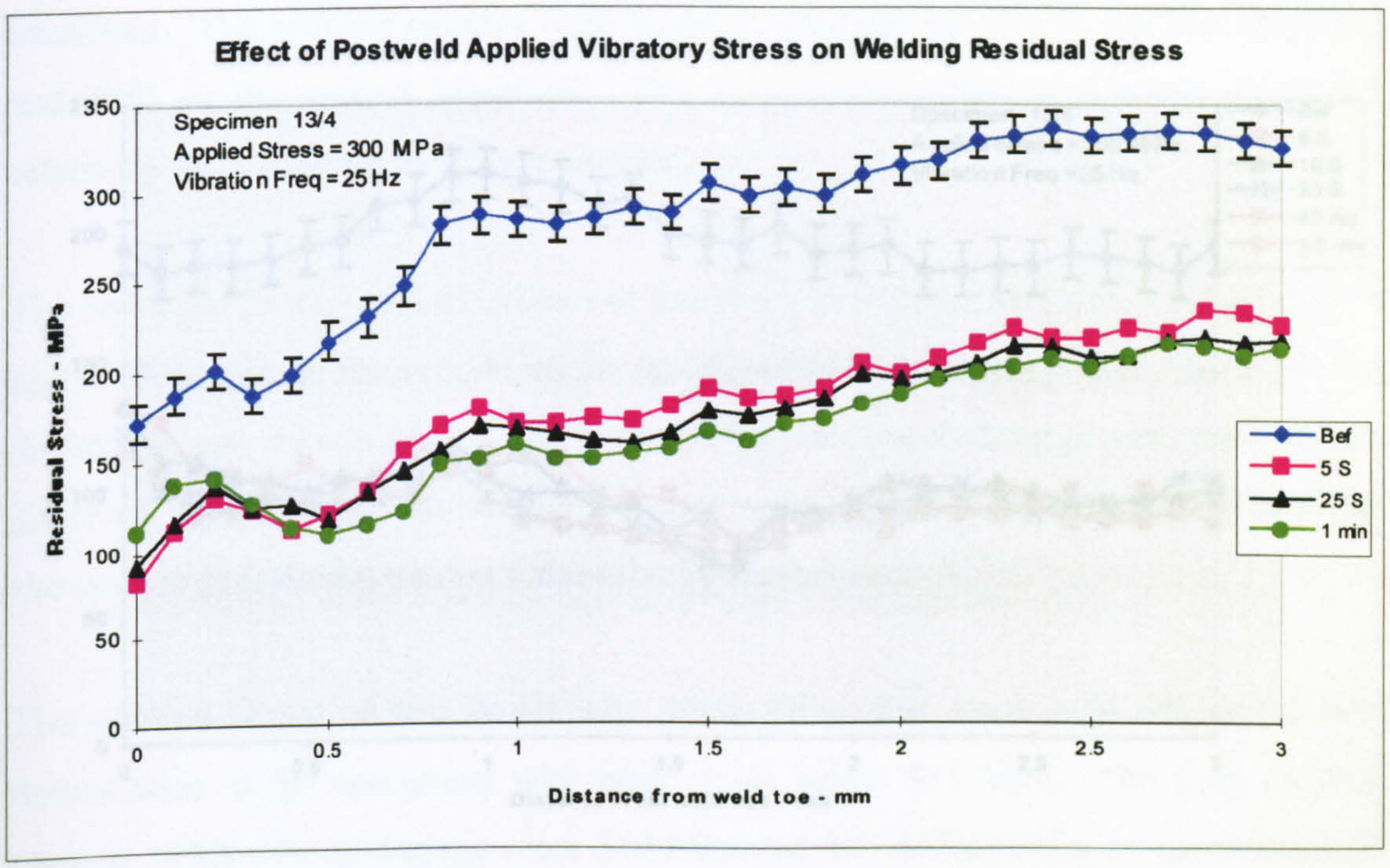

Figure 5.508 – Transverse line stress plot - specimen 13/4

Point Stress Plot

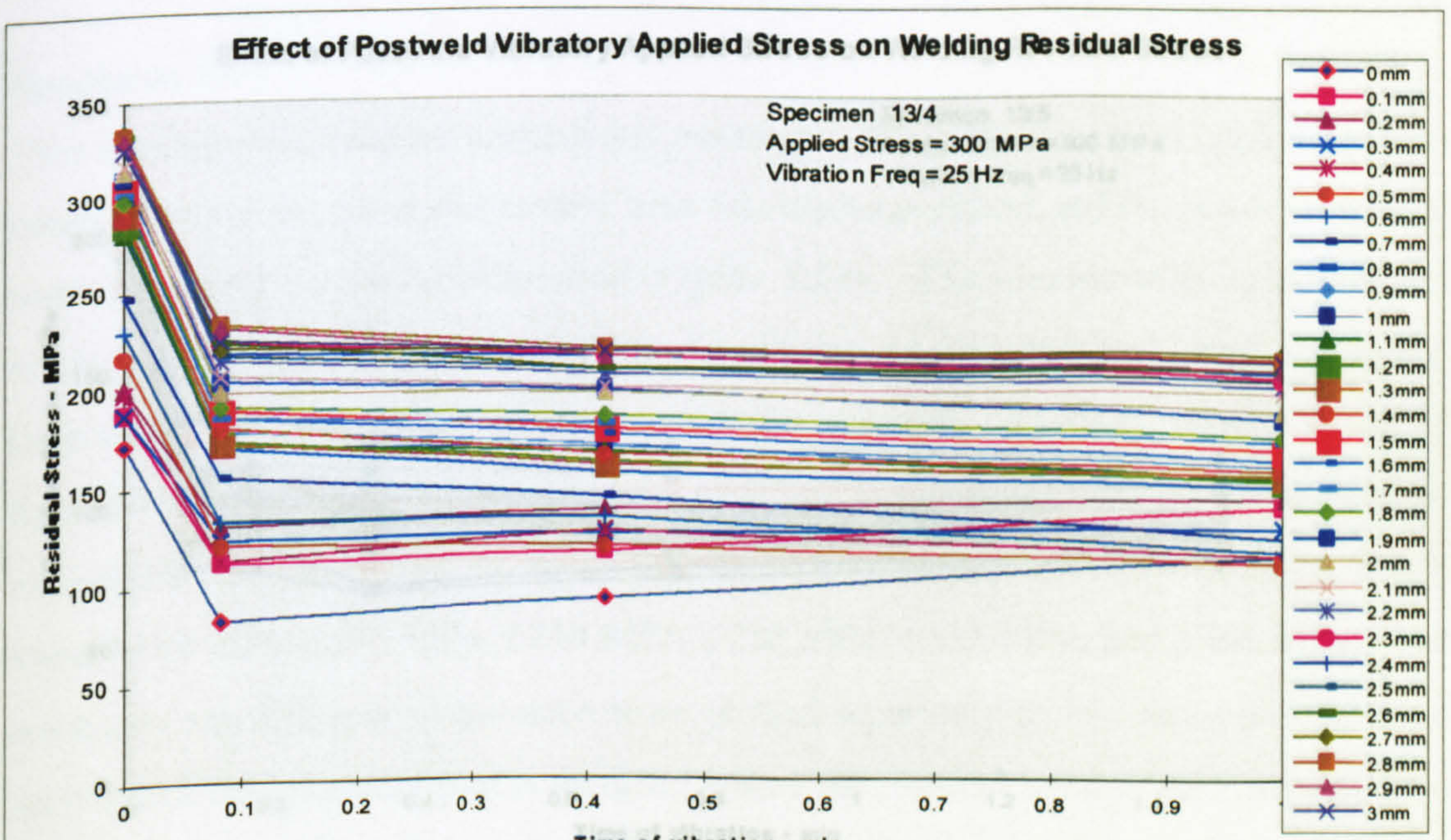

Figure 5.509 – Transverse point stress plot - specimen 13/4

Residual Stress Plots of Specimen 13/5

Line Stress Plot

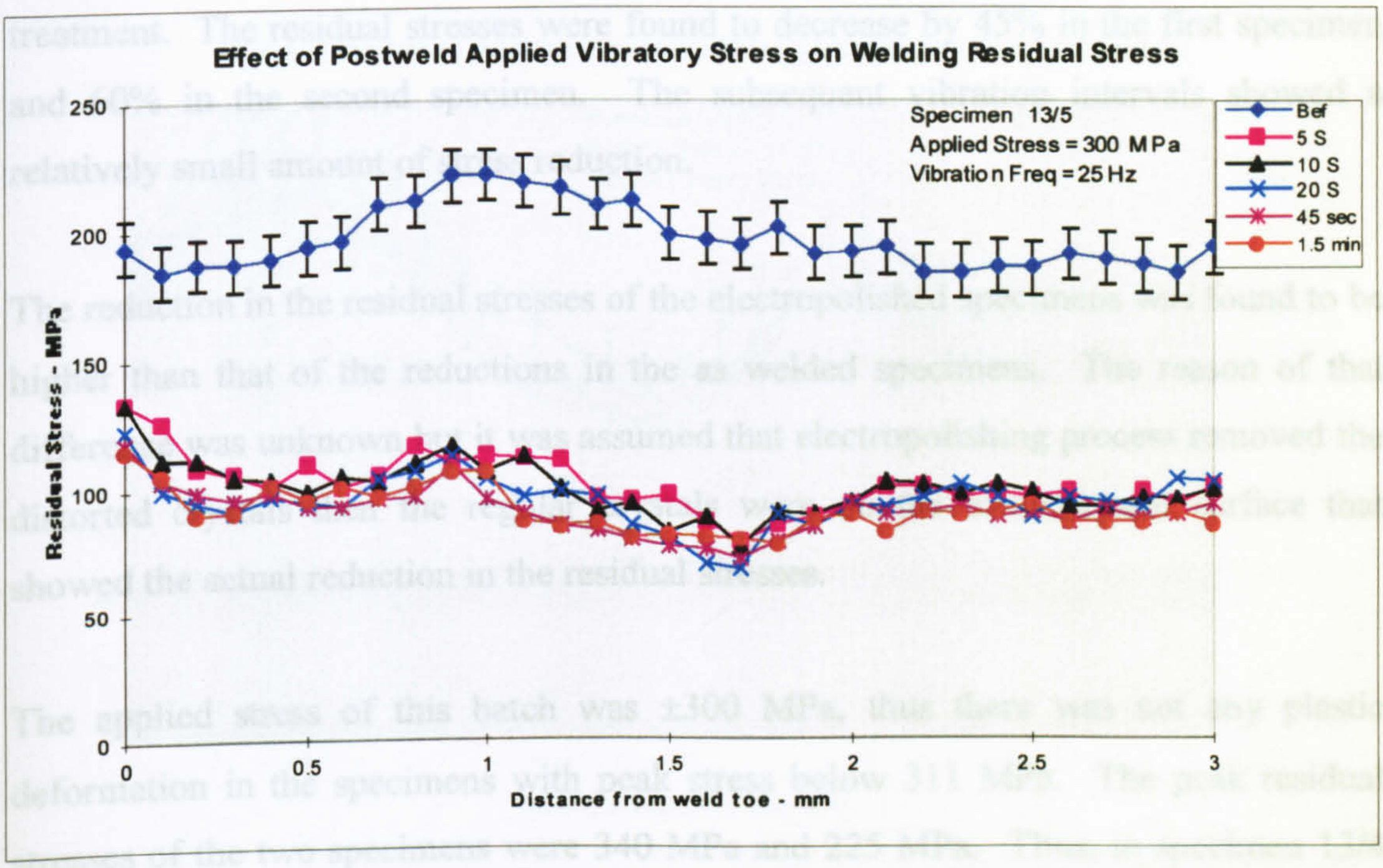

Figure 5.510 – Transverse line stress plot - specimen 13/5

Point Stress Plot

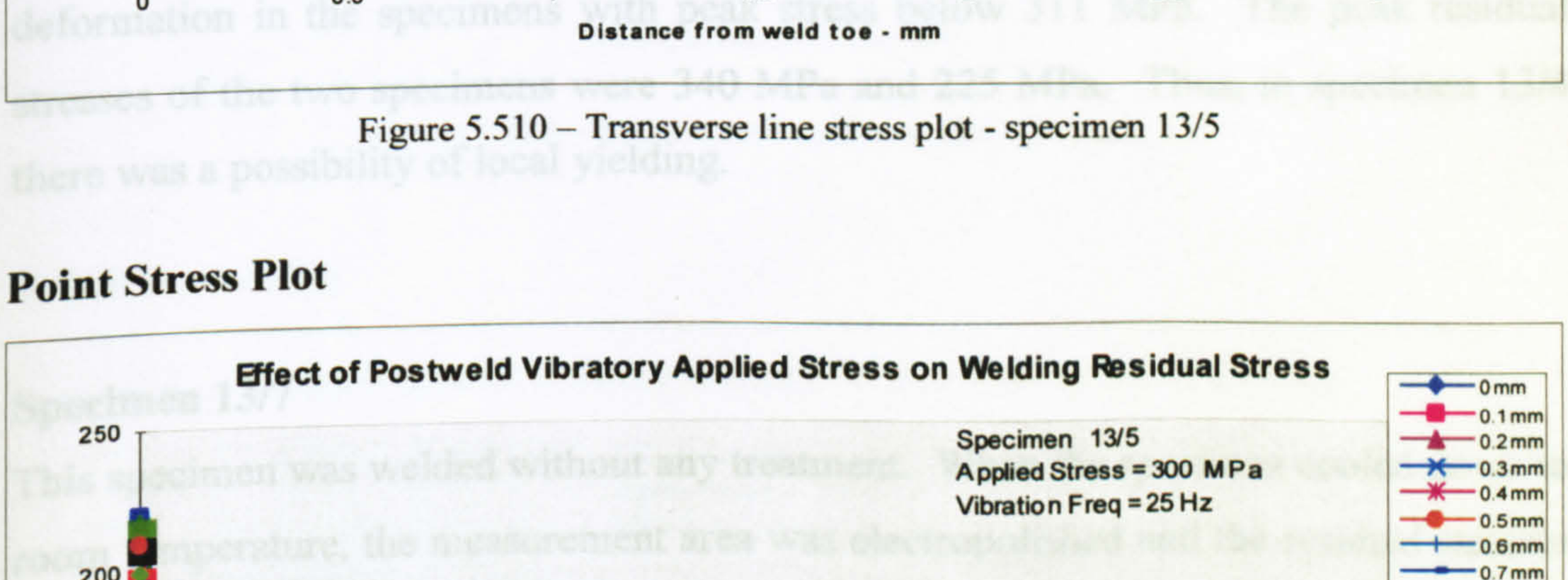

Figure 5.511 – Transverse point stress plot - specimen 13/5

Discussion of Result - Specimens 13/4 and 13/5

In both electropolished specimens substantial reductions in the residual stresses were observed (~100 MPa) along the complete measurement line in the first 5 seconds of treatment. The residual stresses were found to decrease by 45% in the first specimen and 60% in the second specimen. The subsequent vibration intervals showed a relatively small amount of stress reduction.

The reduction in the residual stresses of the electropolished specimens was found to be higher than that of the reductions in the as welded specimens. The reason of that difference was unknown but it was assumed that electropolishing process removed the distorted crystals then the regular crystals were on the measurement surface that showed the actual reduction in the residual stresses.

The applied stress of this batch was ±300 MPa, thus there was not any plastic deformation in the specimens with peak stress below 311 MPa. The peak residual stresses of the two specimens were 340 MPa and 225 MPa. Thus, in specimen 13/4 there was a possibility of local yielding.

Specimen 13/7

This specimen was welded without any treatment. When the specimen cooled down to room temperature, the measurement area was electropolished and the residual stresses were measured on the selected line (Figure 5.13). The electropolishing conditions were similar to the electropolishing conditions of the previous two specimens (specimen 13/4 and 13/5). The specimen was vibrated - applying various levels of dynamic stresses. In every level of applied stress, the time of vibration was stepped to investigate the time effect or stress stabilisation. The applied dynamic stress levels were ±118 MPa, ±175 MPa, ±230 MPa, ±285 MPa, ±333 MPa, and ±366 MPa. The results of the different stress steps were plotted separately as line and point stresses. At the end, the summary plot is included where the residual stresses after the last time interval of each stress step was included.

Residual Stress Plots of Specimen 13/7 Stress Level ±118 MPa

Line Stress Plot

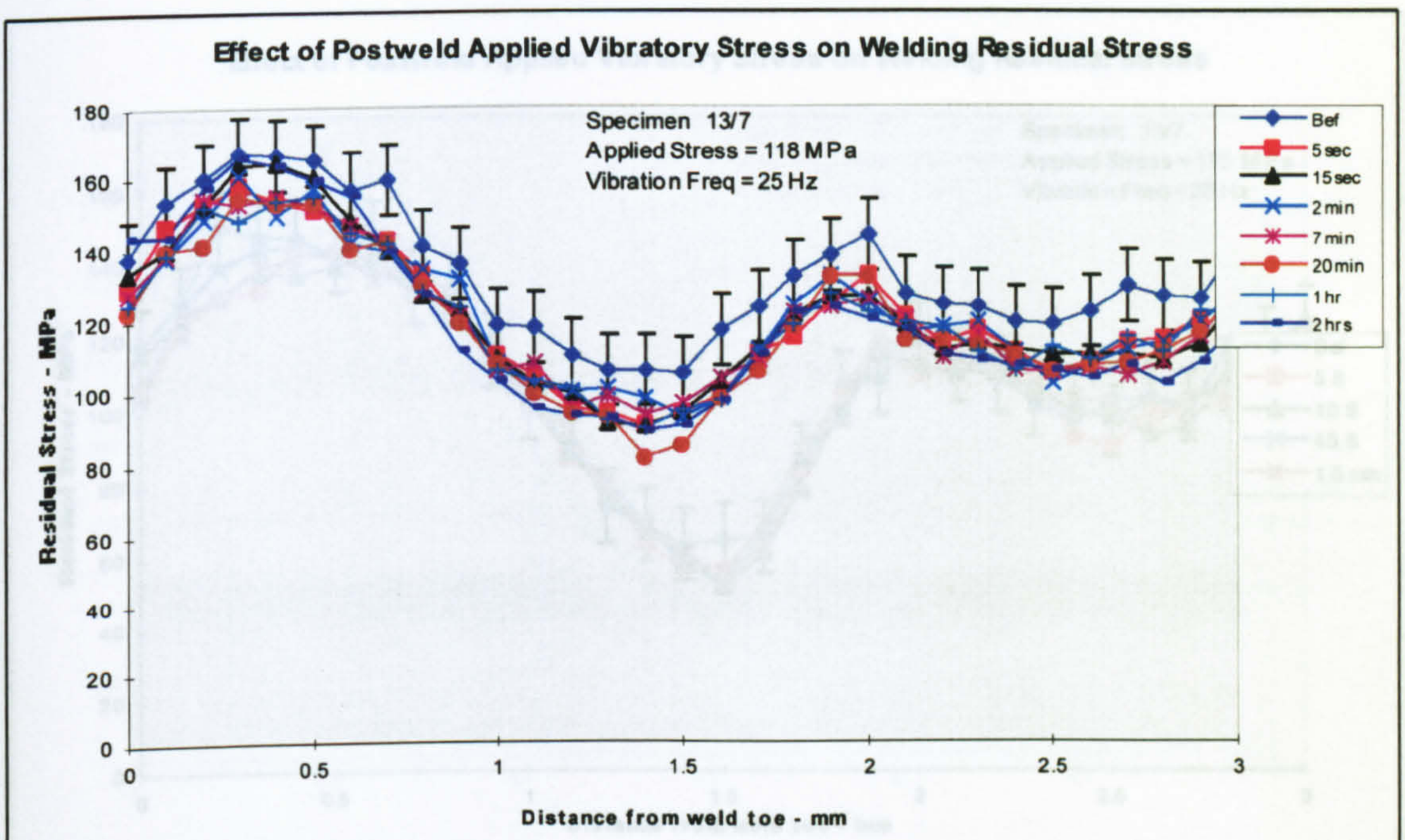

Figure 5.512 – Transverse line stress plot - specimen 13/7

Point Stress Plot

Figure 5.513 – Transverse point stress plot - specimen 13/7

Residual Stress Plots of Specimen 13/7 Stress Level ±175 MPa

Line Stress Plot

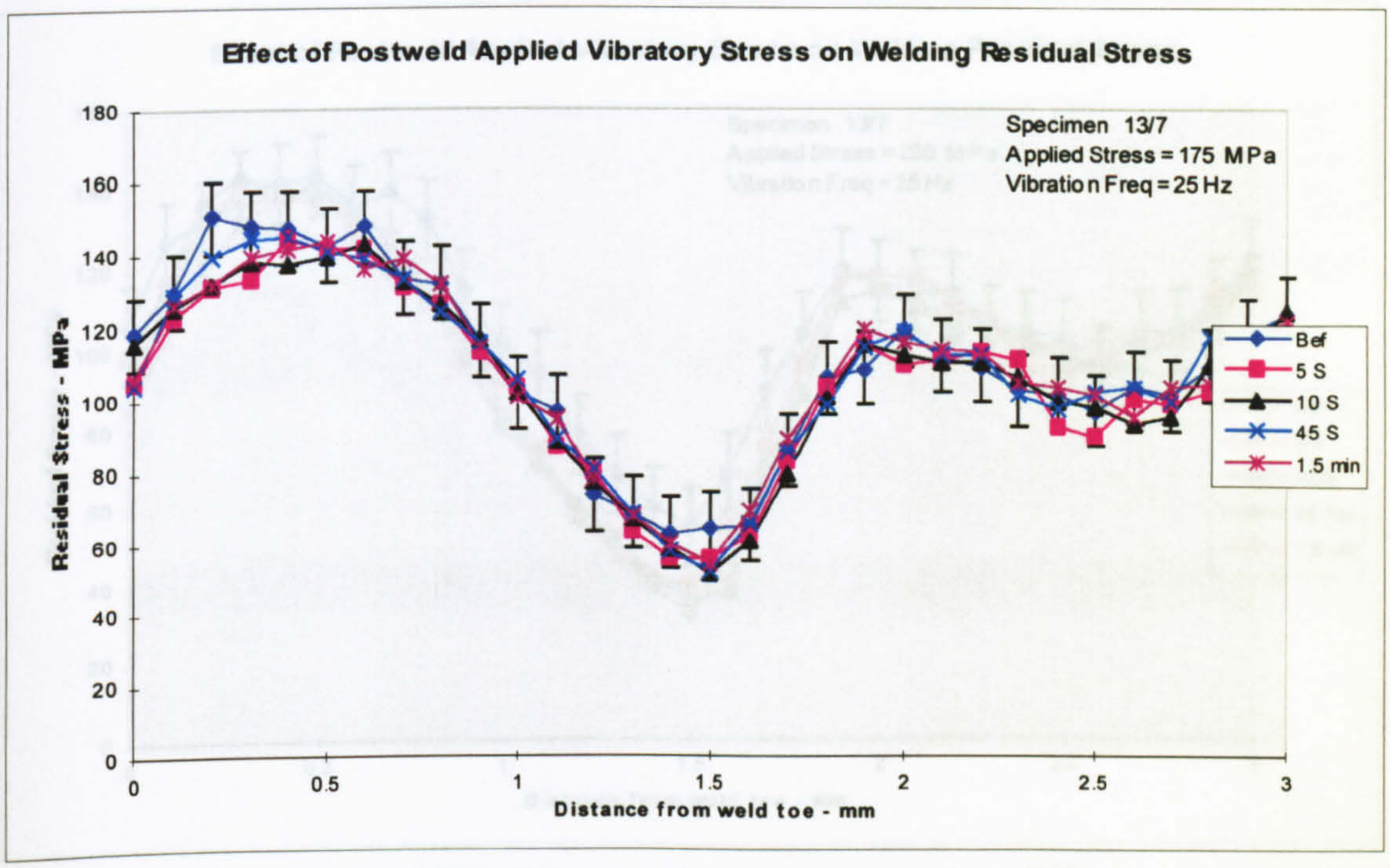

Figure 5.514 – Transverse line stress plot - specimen 13/7

Point Stress Plot

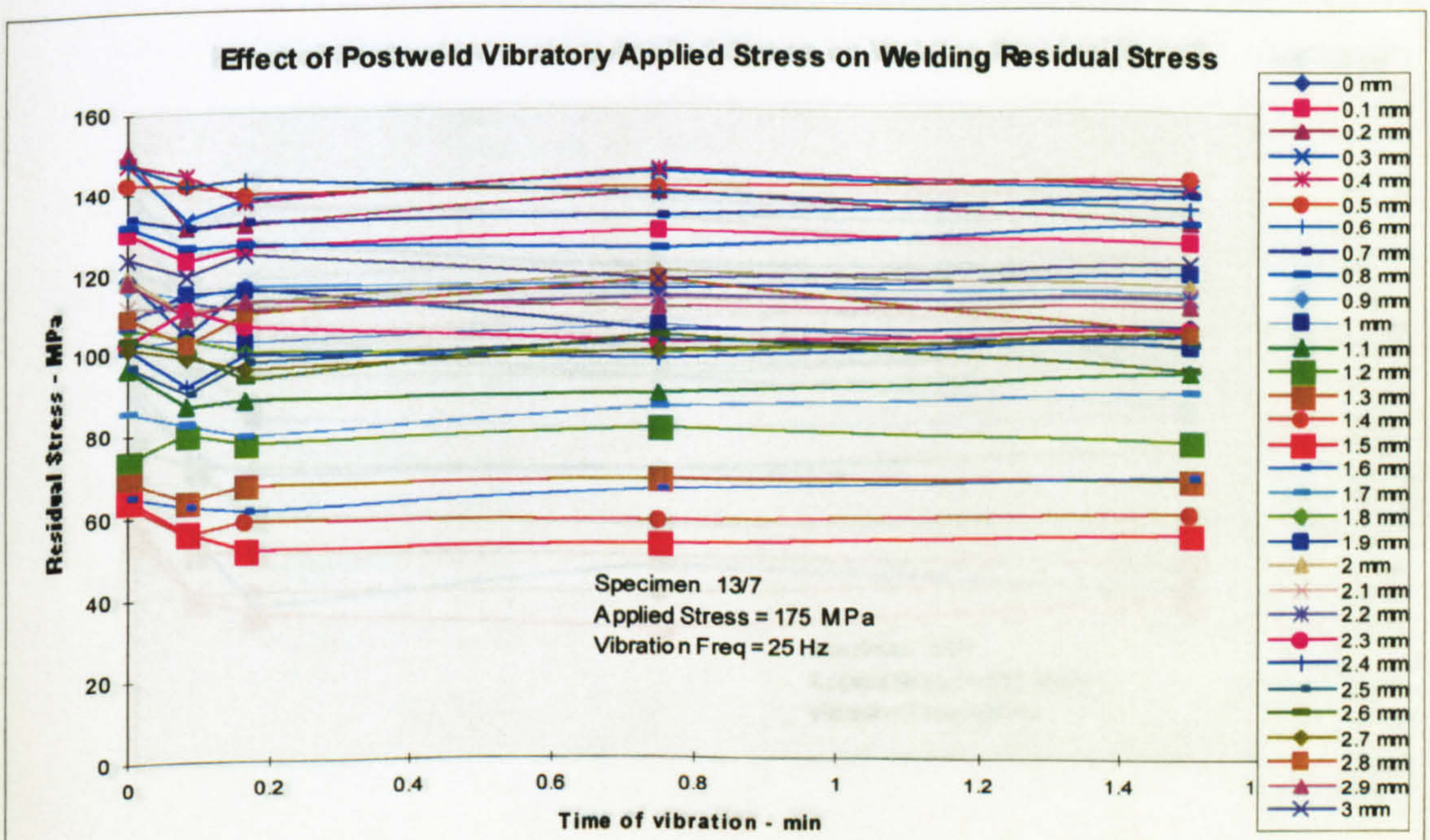

Figure 5.515 – Transverse point stress plot - specimen 13/7

Residual Stress Plots of Specimen 13/7 Stress Level ±230 MPa

Line Stress Plot

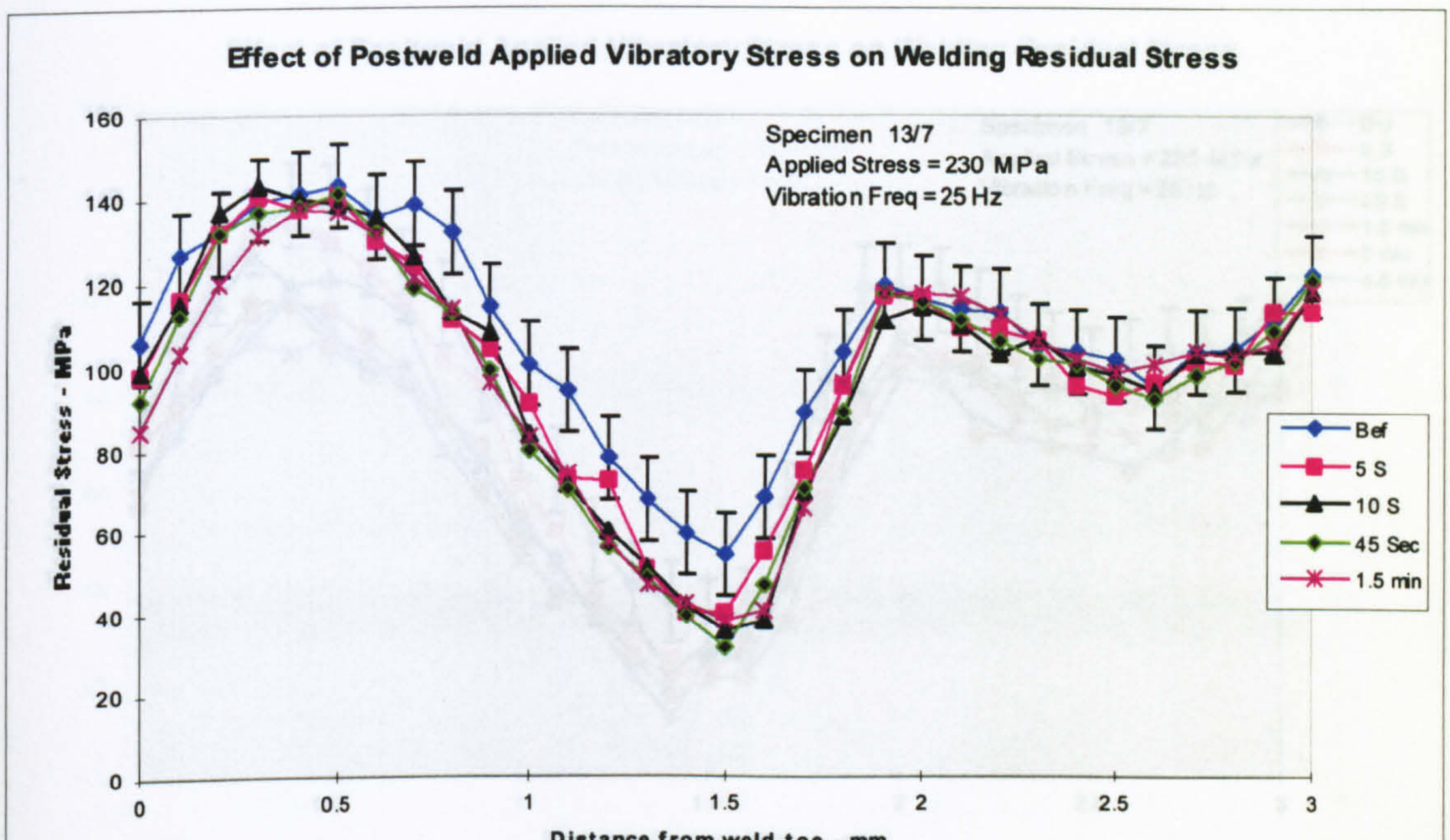

Figure 5.516 – Transverse line stress plot - specimen 13/7

Point Stress Plot

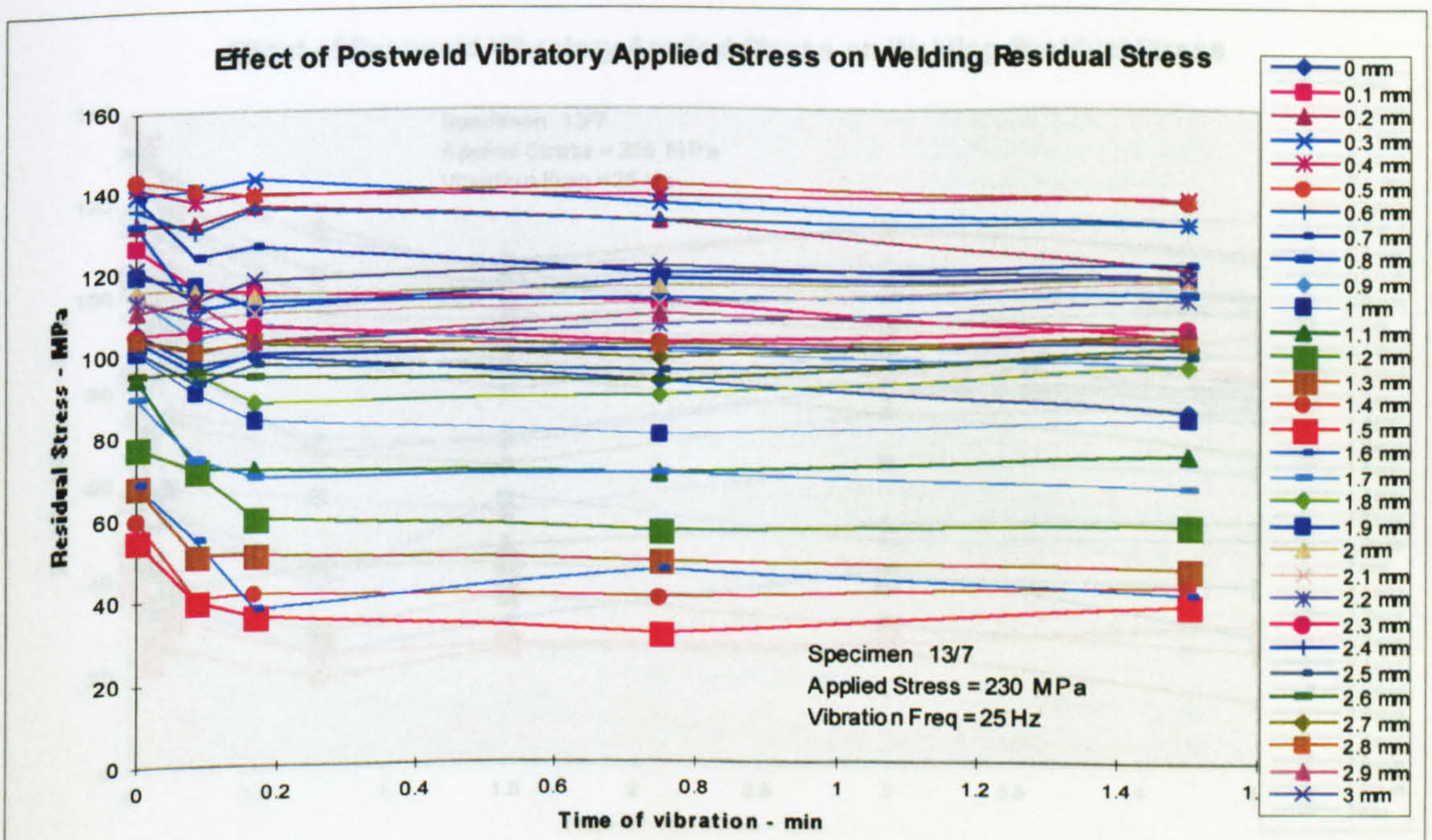

Figure 5.517 – Transverse point stress plot - specimen 13/7

Residual Stress Plots of Specimen 13/7 Stress Level ±285 MPa

Line Stress Plot

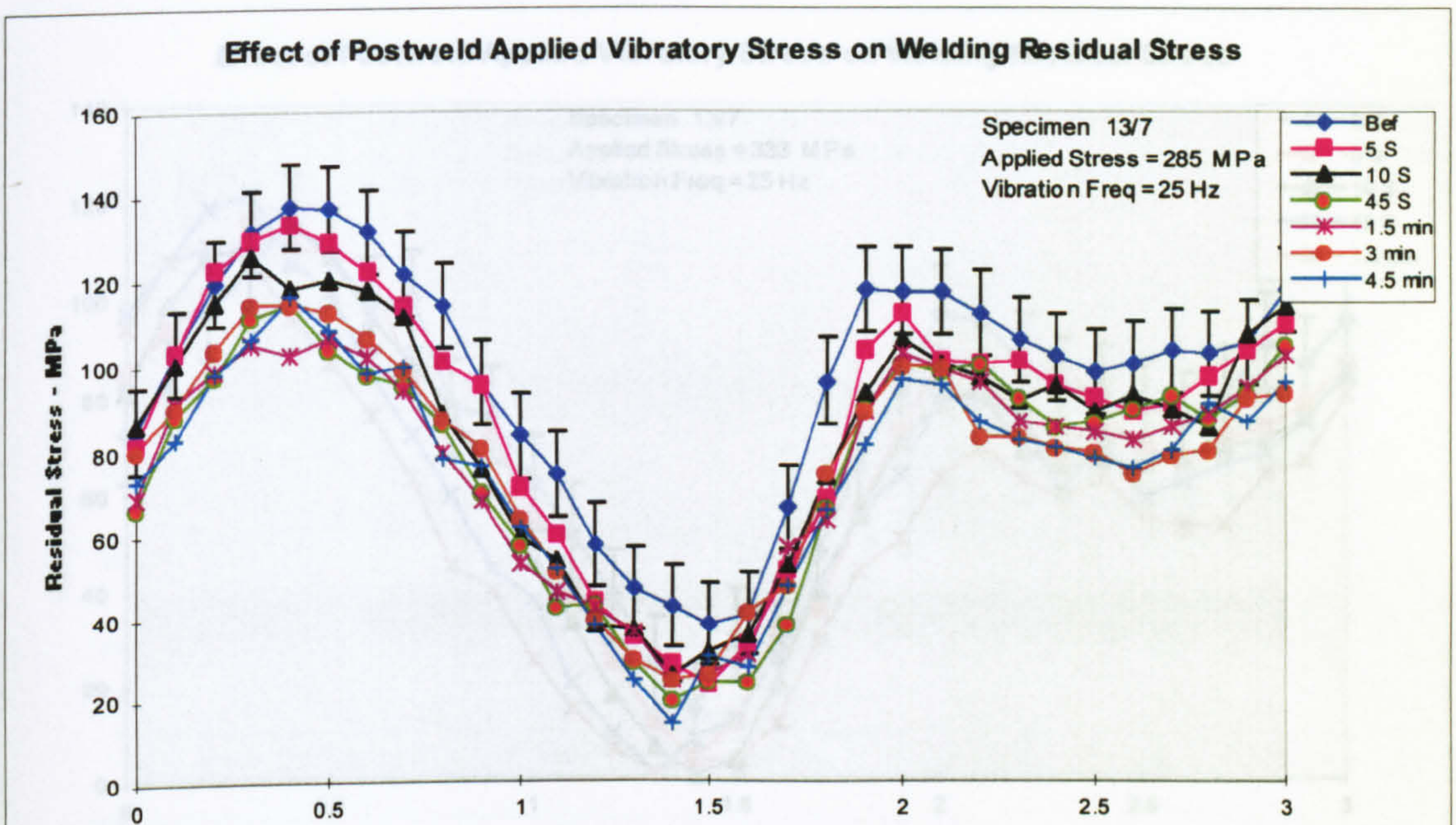

Figure 5.518 – Transverse line stress plot - specimen 13/7

Point Stress Plot

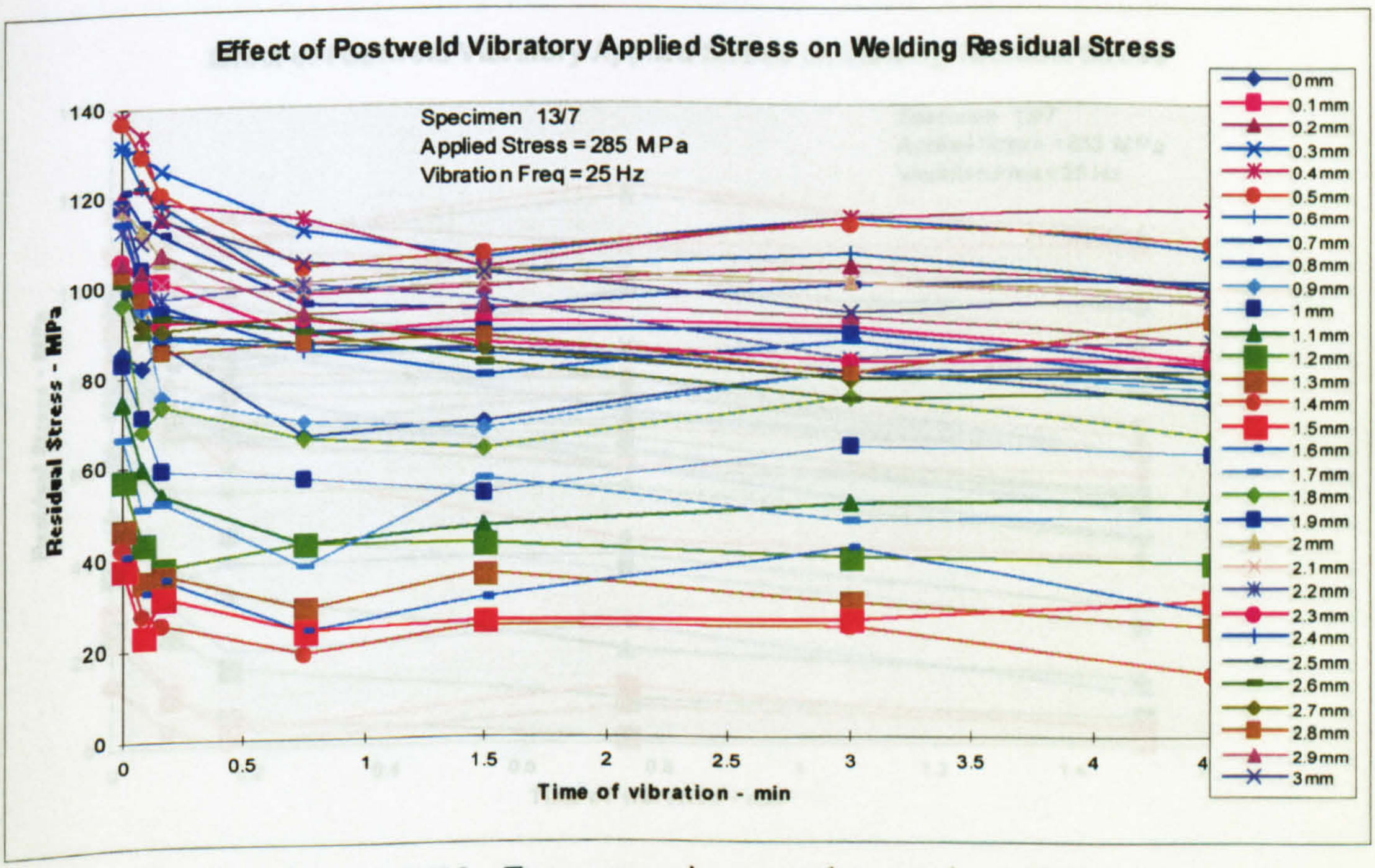

Figure 5.519 – Transverse point stress plot - specimen 13/7

Residual Stress Plots of Specimen 13/7 Stress Level ±333 MPa

Line Stress Plot

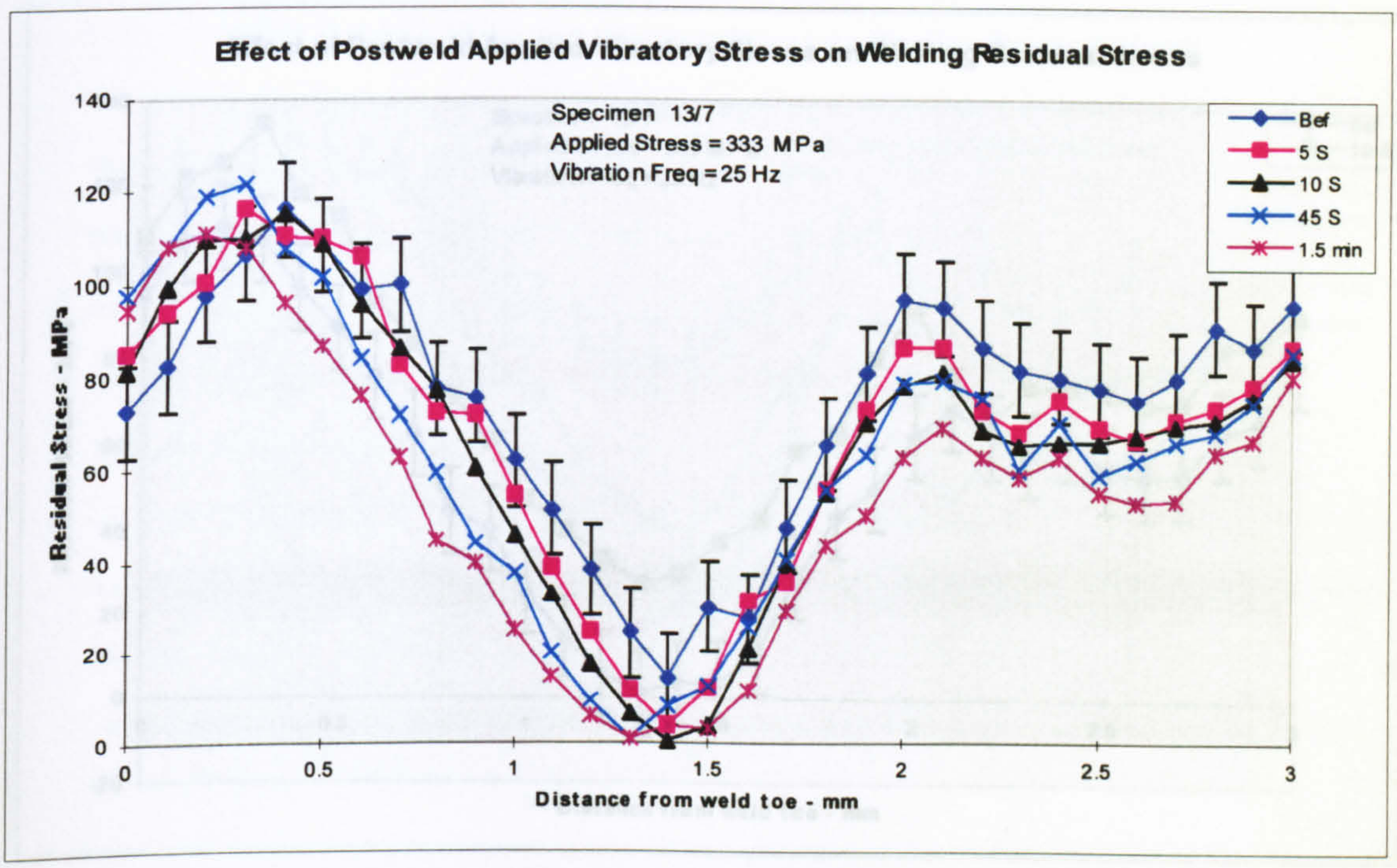

Figure 5.520 – Transverse line stress plot - specimen 13/7

Point Stress Plot

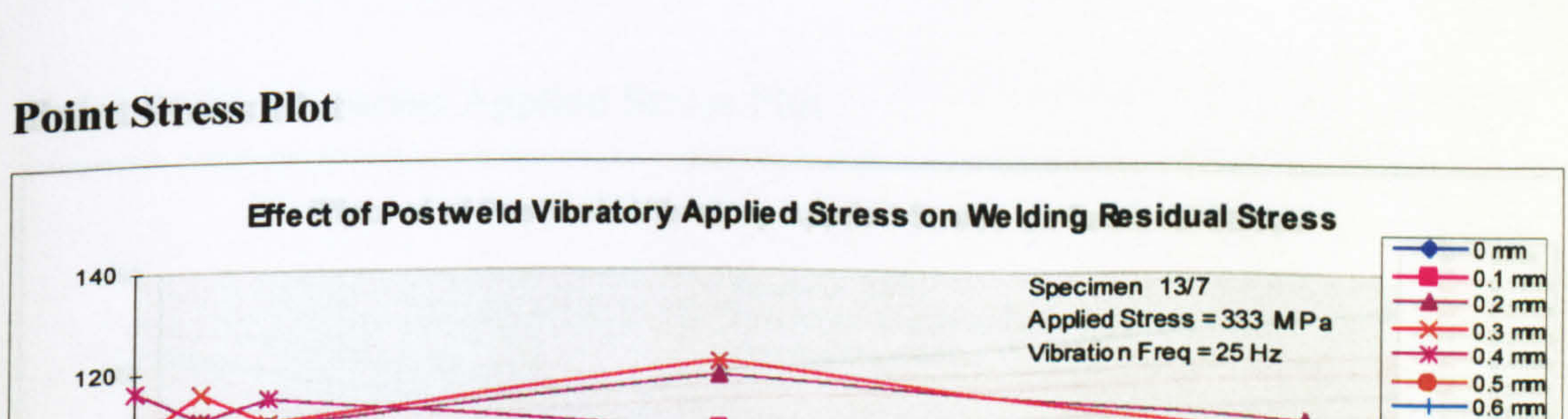

Figure 5.521 – Transverse point stress plot - specimen 13/7

Residual Stress Plots of Specimen 13/7 Stress Level ±366 MPa

Line Stress Plot

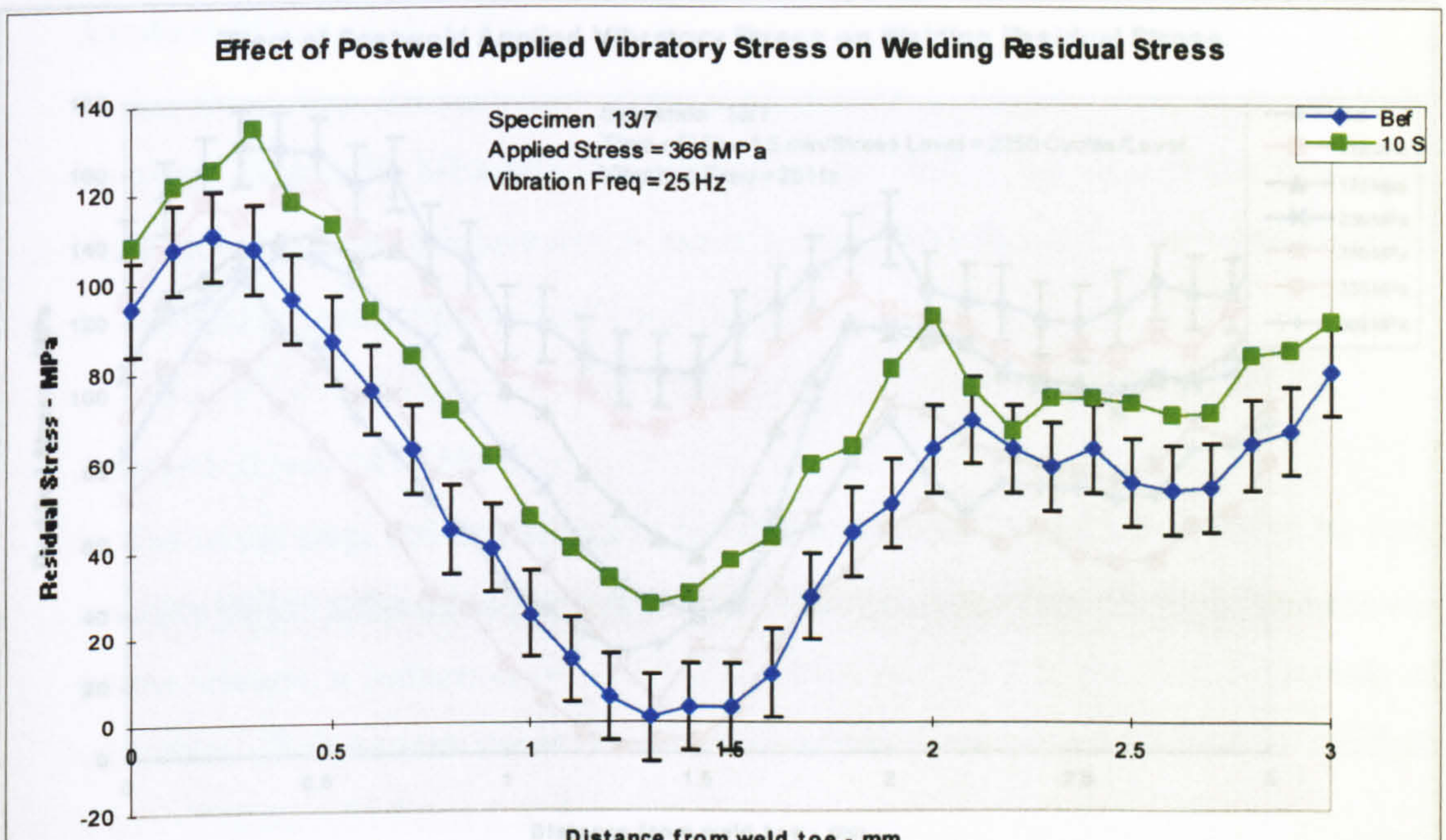

Figure 5.522 – Transverse line stress plot - specimen 13/7

Point Stress Plot

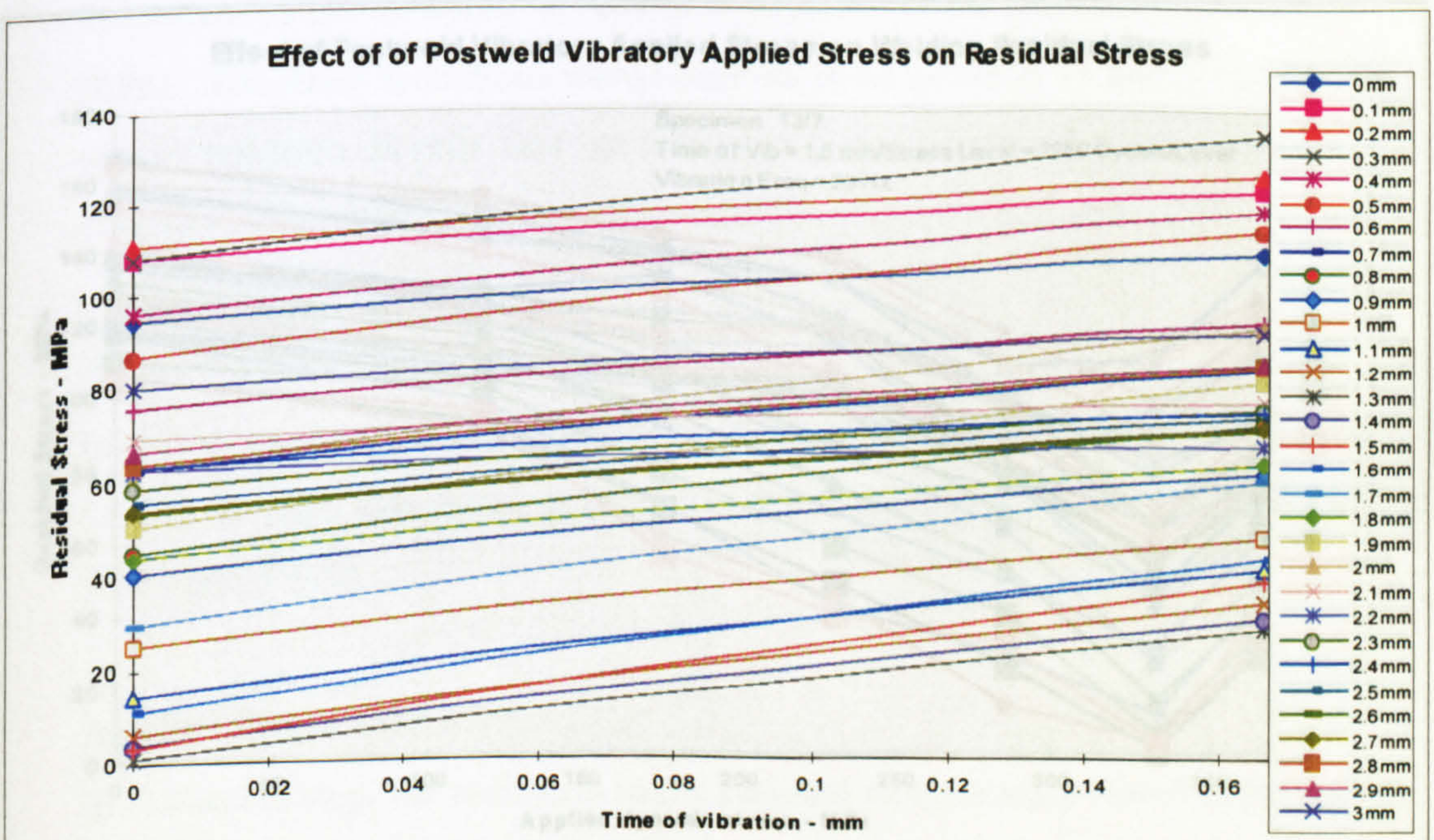

Figure 5.523 – Transverse point stress plot - specimen 13/7

Residual Stress Plots of Specimen 13/7 – Summary plot

Line Stress Plot

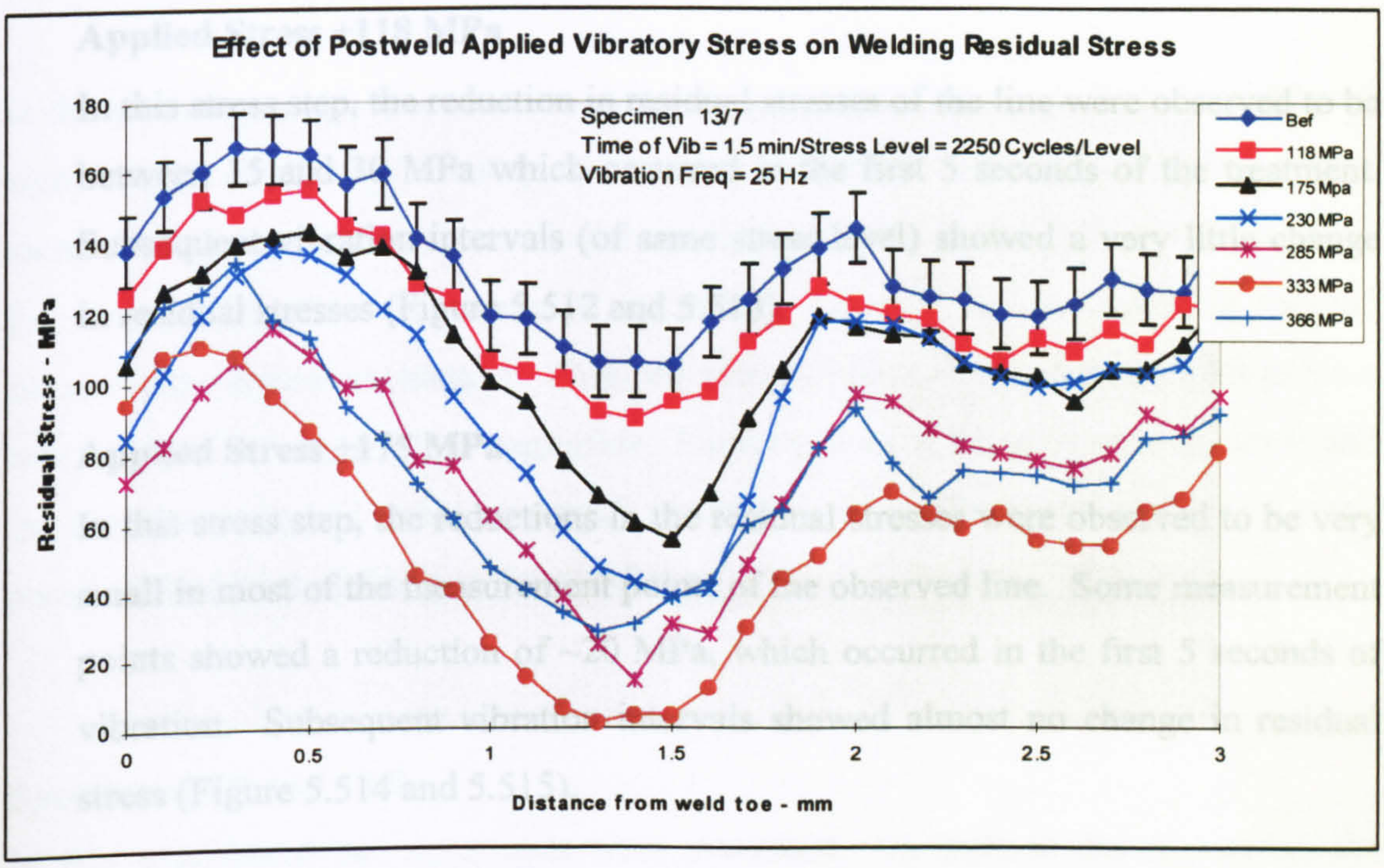

Figure 5.524 – Transverse line stress plot - specimen 13/7

Residual Stress versus Applied Stress Plot

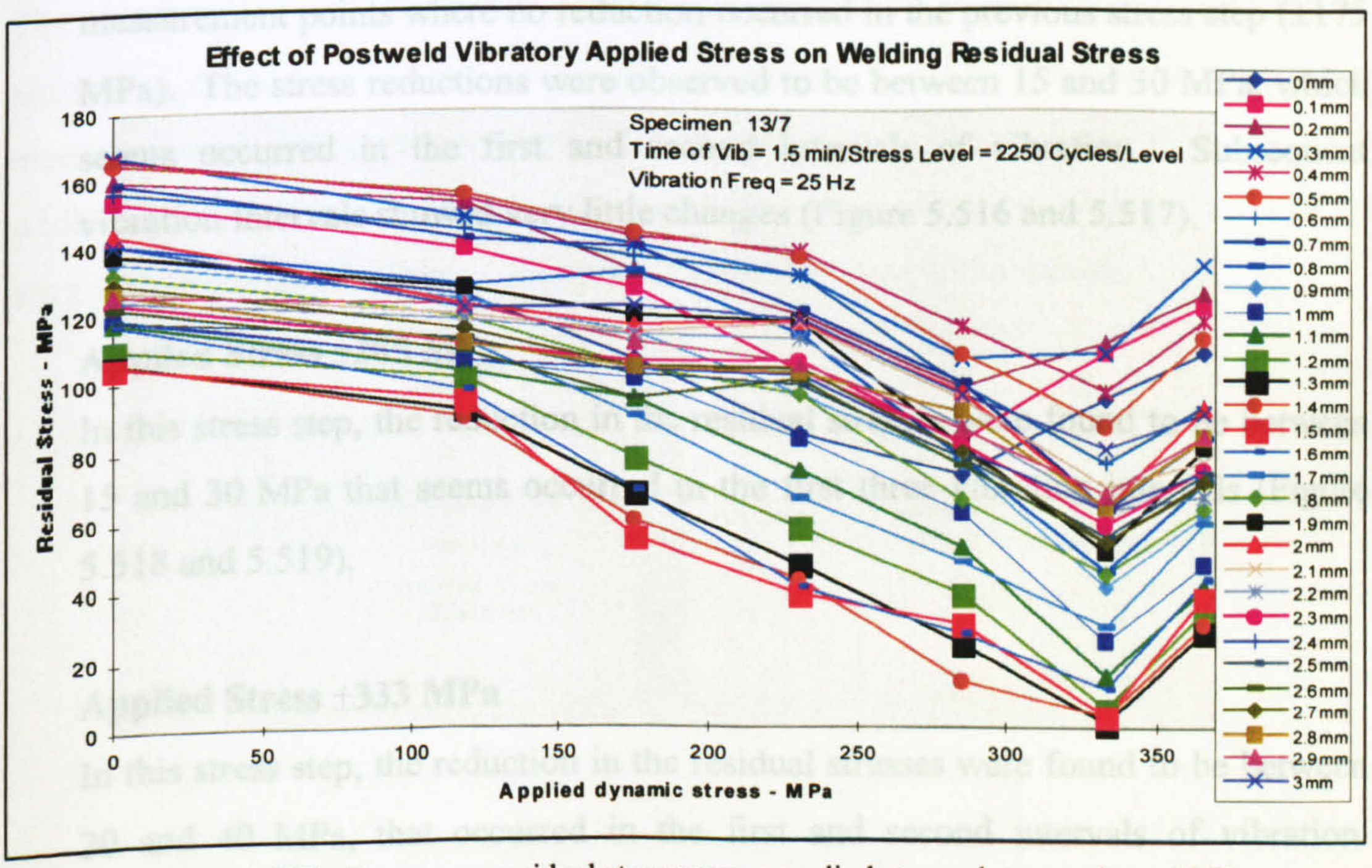

Figure 5.525 - Transverse residual stress versus applied stress plot - specimen 13/7

Discussion of Result - Specimen 13/7

The observed results of this specimen are

Applied Stress ±118 MPa

In this stress step, the reduction in residual stresses of the line were observed to be between 15 and 30 MPa which occurred in the first 5 seconds of the treatment. Subsequent vibration intervals (of same stress level) showed a very little change in residual stresses (Figure 5.512 and 5.513).

Applied Stress ±175 MPa

In this stress step, the reductions in the residual stresses were observed to be very small in most of the measurement points of the observed line. Some measurement points showed a reduction of ~20 MPa, which occurred in the first 5 seconds of vibration. Subsequent vibration intervals showed almost no change in residual stress (Figure 5.514 and 5.515).

Applied Stress ±230 MPa

In this stress step, small reductions in the residual stresses were observed on those measurement points where no reduction occurred in the previous stress step (±175 MPa). The stress reductions were observed to be between 15 and 30 MPa, which seems occurred in the first and second intervals of vibration. Subsequent vibration intervals showed very little changes (Figure 5.516 and 5.517).

Applied Stress ±285 MPa

In this stress step, the reduction in the residual stresses were found to be between 15 and 30 MPa that seems occurred in the first three vibration intervals (Figure 5.518 and 5.519).

Applied Stress ±333 MPa

In this stress step, the reduction in the residual stresses were found to be between 20 and 40 MPa, that occurred in the first and second intervals of vibration. Subsequent intervals showed almost no change (Figure 5.520 and 5.521).

Applied Stress ±366 MPa

In this stress step, the residual stress was increased between 20~40 MPa in all of the measurement points of the line (Figure 5.522 and 5.523).

In the summary plot it was clear that in every stress step, the residual stresses reduced significantly and at the last step the stresses increased. This indicates that due to increase in the applied stress residual stresses decreased. In the different stress steps, the time of vibration was increased by several intervals and the resulting residual stresses were almost unchanged. Thus, the effect of time of vibration on VSR process was found to be very small or negligible. Since the sum of the peak residual stress and the maximum applied stress was much lower than 611 MPa, there was a very small possibility of local yielding in this specimen.

Specimen 13/8 and 13/9

In this experiment two specimens were processed. In both of the specimens, the applied stresses were varied from a lower stress level of ±33 MPa to a maximum of ±366.2 MPa in several steps. The stress steps are shown in the residual stress plots. The specimens were vibrated for 1 minute at each induced stress level. The residual stresses were measured after every step of treatment. The residual stresses were measured on a line shown in Figure 5.526, which was 28 mm away from the mid-width line. The transverse residual stresses of the selected line were plotted as residual stresses against applied stress. Figures 5.527 to 5.530 show the results.

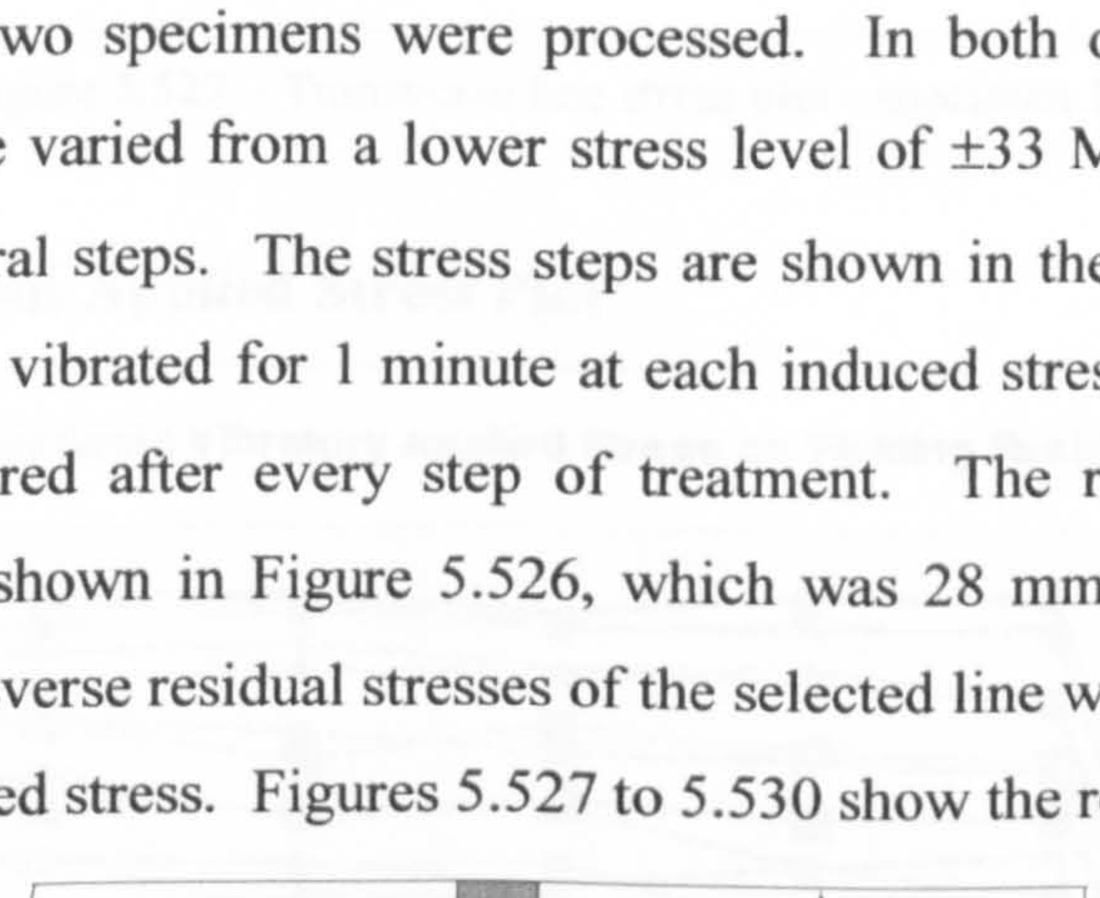

Figure 5.526 – Position of the measurement line for specimens 13/8 and 13/9

Residual Stress Plots of Specimen 13/8

Line Stress Plot

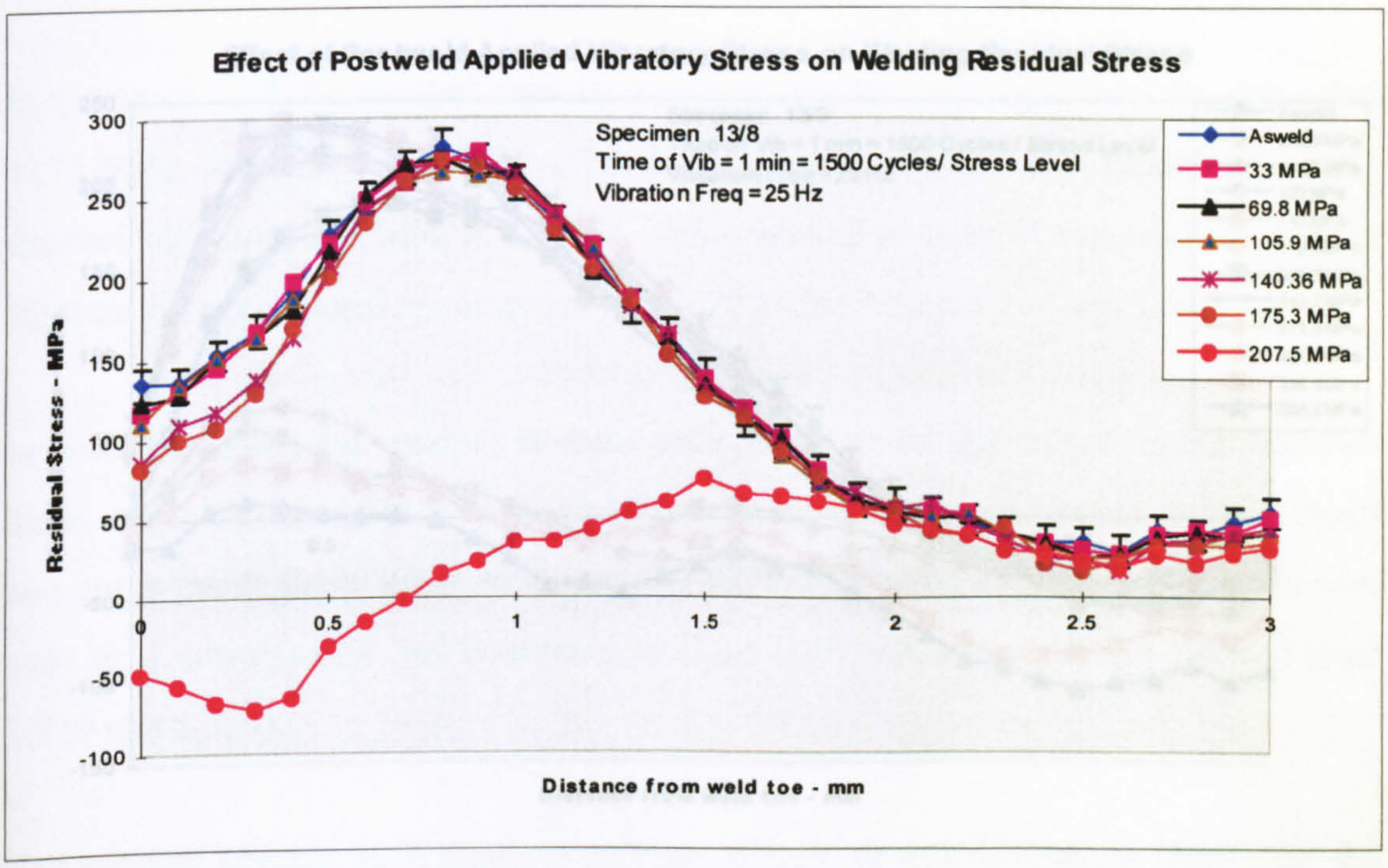

Figure 5.527 – Transverse line stress plot - specimen 13/8

Residual Stress versus Applied Stress Plot

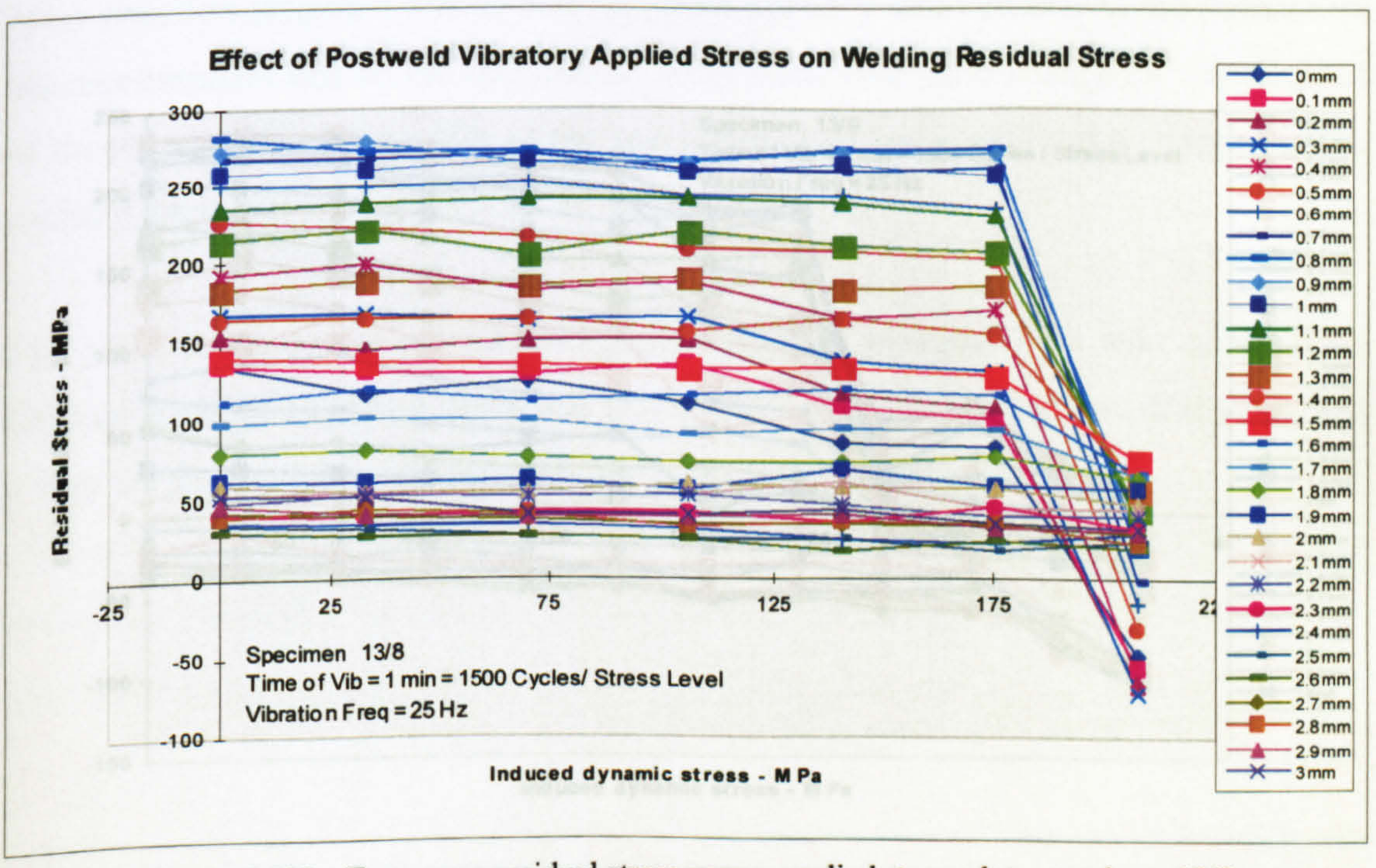

Figure 5.528 – Transverse residual stress versus applied stress plot - specimen 13/8

Residual Stress Plots of Specimen 13/9

Line Stress Plot

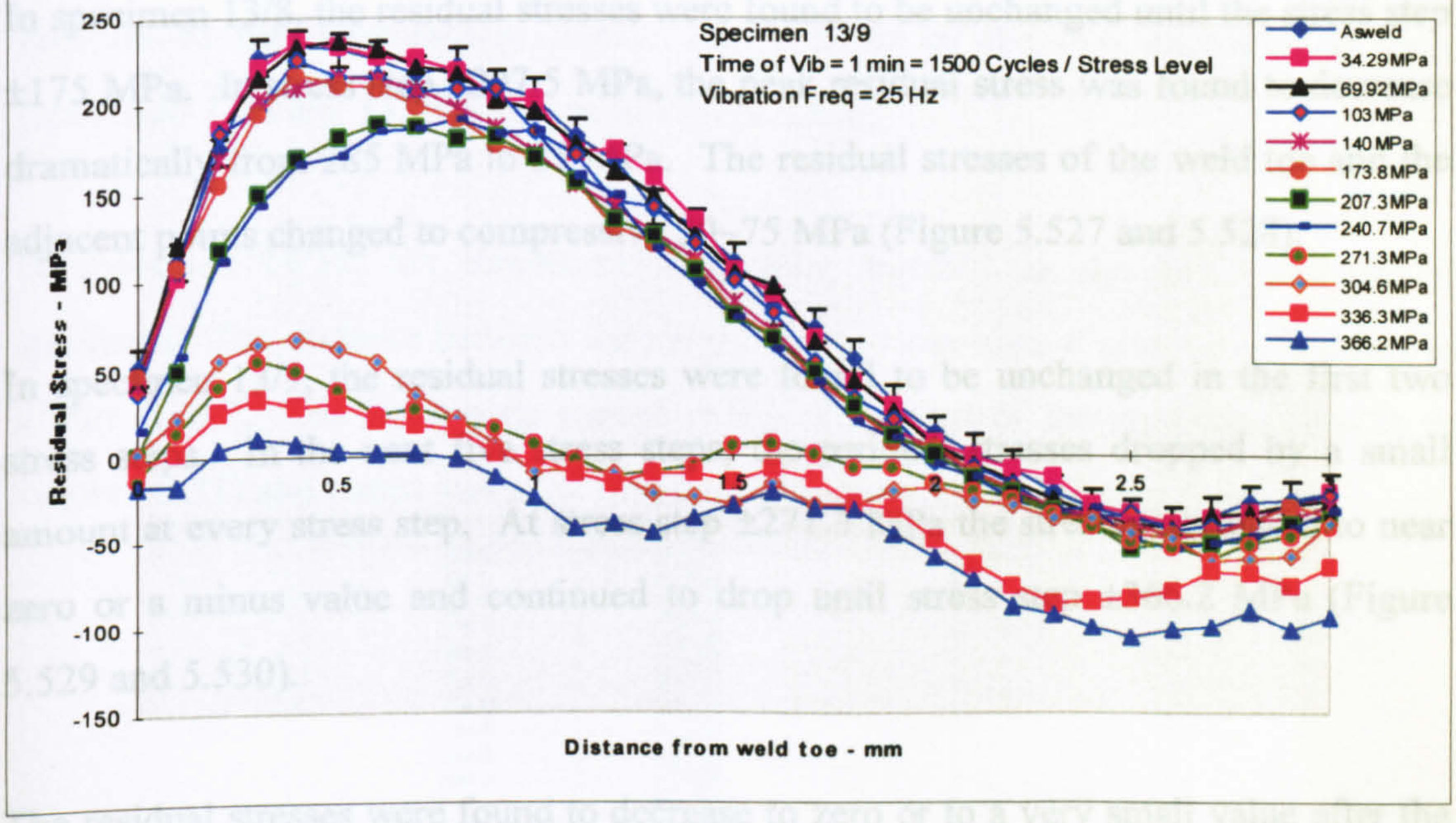

Figure 5.529 – Transverse line stress plot - specimen 13/9

Residual Stress versus Applied Stress Plot

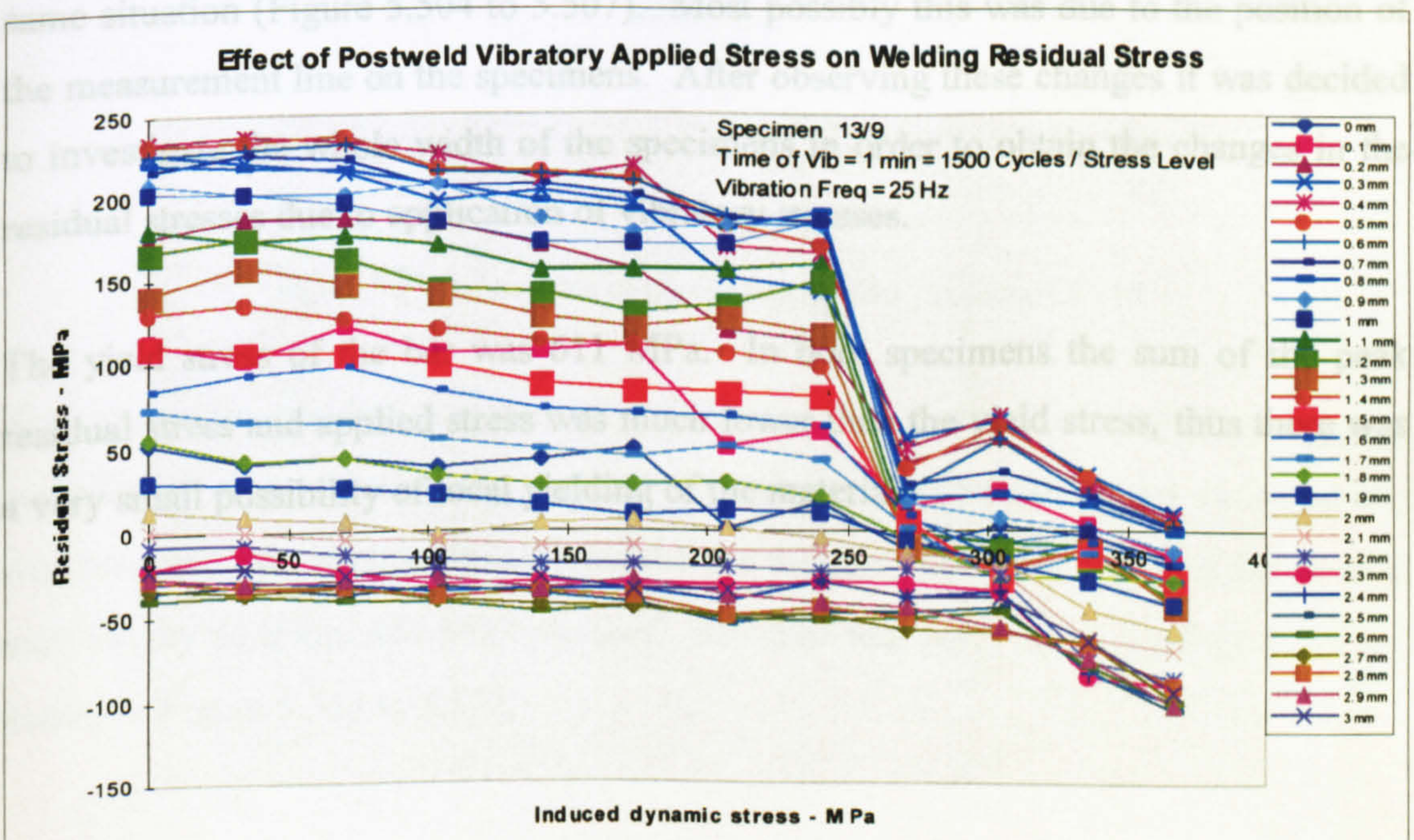

Figure 5.530 - Transverse residual stress versus applied stress plot - specimen 13/9

Discussion of Result - Specimen 13/8 and 13/9

Specimens 13/8 and 13/9 were processed varying applied stress. The time of vibration was 1 minute in every stress step.

In specimen 13/8, the residual stresses were found to be unchanged until the stress step ±175 MPa. In stress step ±207.5 MPa, the peak residual stress was found to decrease dramatically from 285 MPa to 25 MPa. The residual stresses of the weld toe and the adjacent points changed to compressive 50~75 MPa (Figure 5.527 and 5.528).

In specimen 13/9, the residual stresses were found to be unchanged in the first two stress steps. In the next five stress steps, the residual stresses dropped by a small amount at every stress step. At stress step ±271.3 MPa the stresses decreased to near zero or a minus value and continued to drop until stress step ±366.2 MPa (Figure 5.529 and 5.530).

The residual stresses were found to decrease to zero or to a very small value after the application of relatively small applied dynamic stresses. These results were significantly different to the results relating to the other specimens processed in the same situation (Figure 5.504 to 5.507). Most possibly this was due to the position of the measurement line on the specimens. After observing these changes it was decided to investigate the whole width of the specimens in order to obtain the changes in the residual stresses due to application of vibratory stresses.

The yield stress of the bar was 611 MPa. In both specimens the sum of the peak residual stress and applied stress was much lower than the yield stress, thus there was a very small possibility of local yielding of the material.

Specimen 14/10

Specimen 14/10 was processed in order to investigate the phenomenon observed in the previous two specimens (specimen 13/8 and 13/9). In those specimens, the processing conditions were similar to the specimens 13/1 and 13/2 - the only difference being the position of the measurement lines. The position of the two measurement lines (specimen 13/8 and 13/9) is shown in Figure 5.526.

In specimen 14/10, ten transverse lines were selected on the half-width of the specimen. The distance between the neighbouring lines were 4 mm, i.e. x = 4 mm in Figure 5.531. The lines were started at the mid-width of the specimen (line A in Figure 5.531) and ended leaving 2 mm near the edge (line J in Figure 5.531).

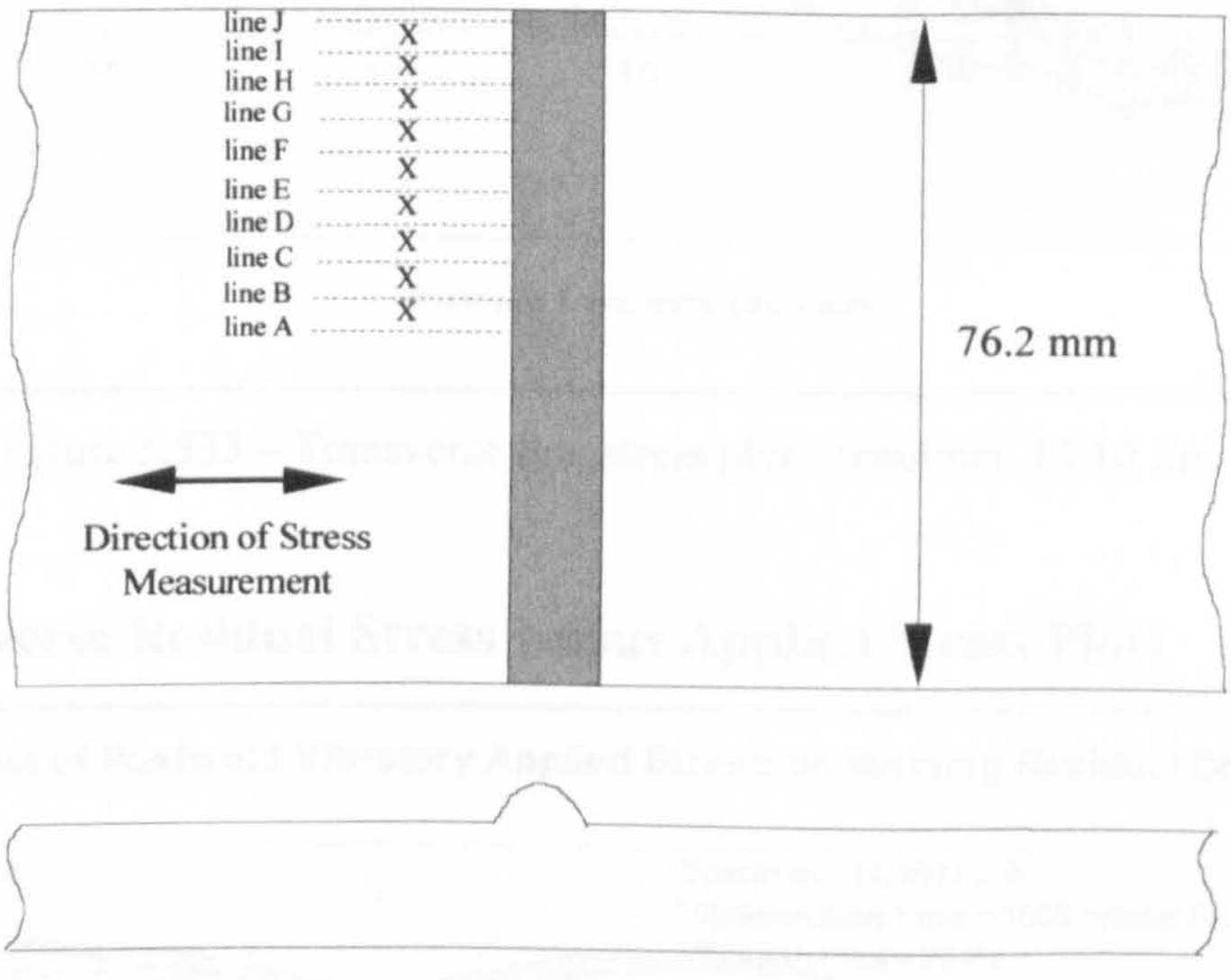

Figure 5.531 - Positions of measurement lines - specimen 14/10

The transverse residual stresses of the lines were measured using the mapping procedure – thus reducing the measurement time considerably. After finishing the area map, the data relating the individual lines was extracted from the map and plotted individually as a line and point stresses. The line and point stresses of the lines are shown in Figure 5.533 to 5.552.

Specimen 14/10 (D = X × 0 mm)

Line A (Line Stresses)

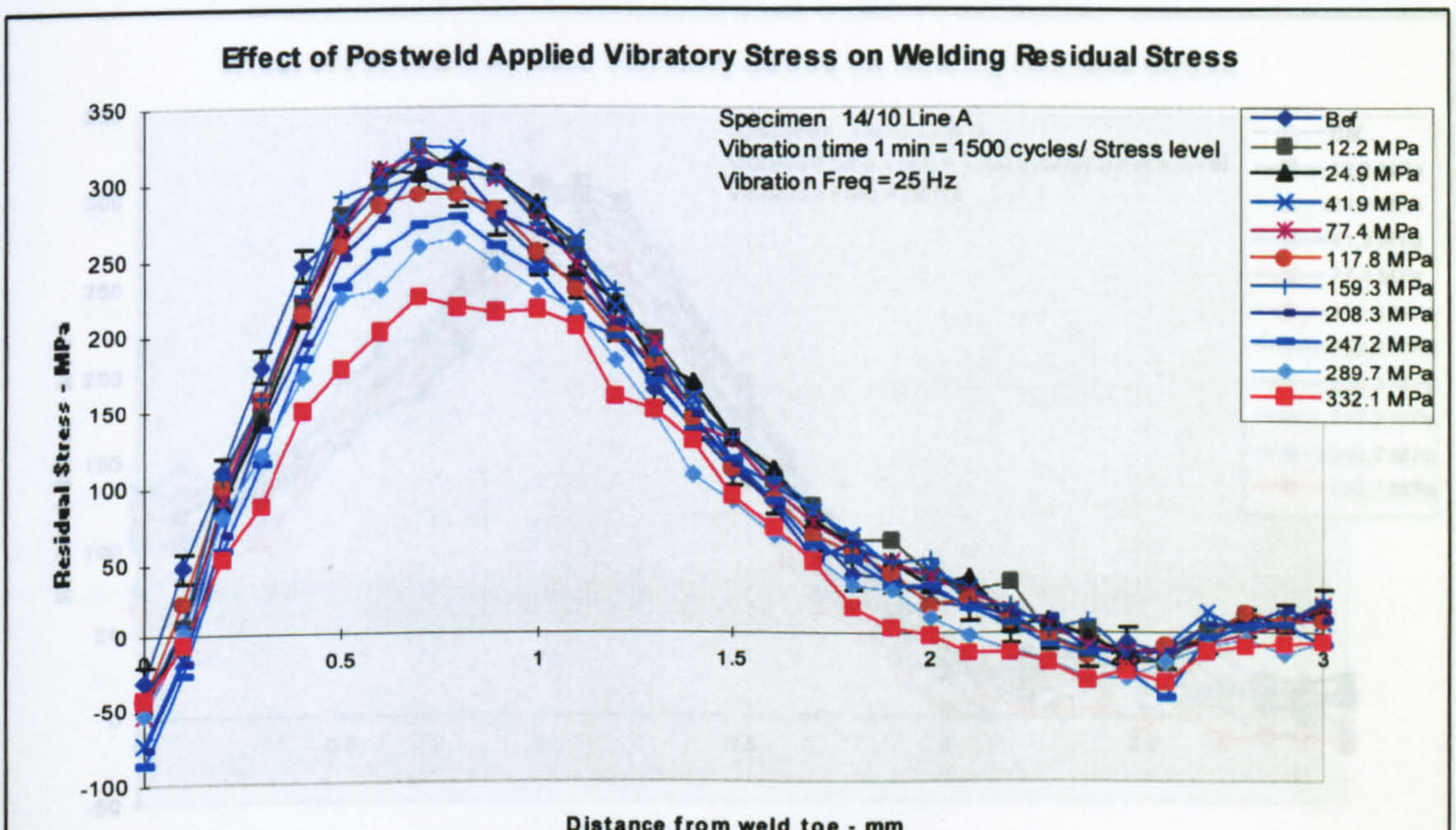

Figure 5.533 – Transverse line stress plot - specimen 14/10 line A

Line A (Transverse Residual Stress versus Applied Stress Plot)

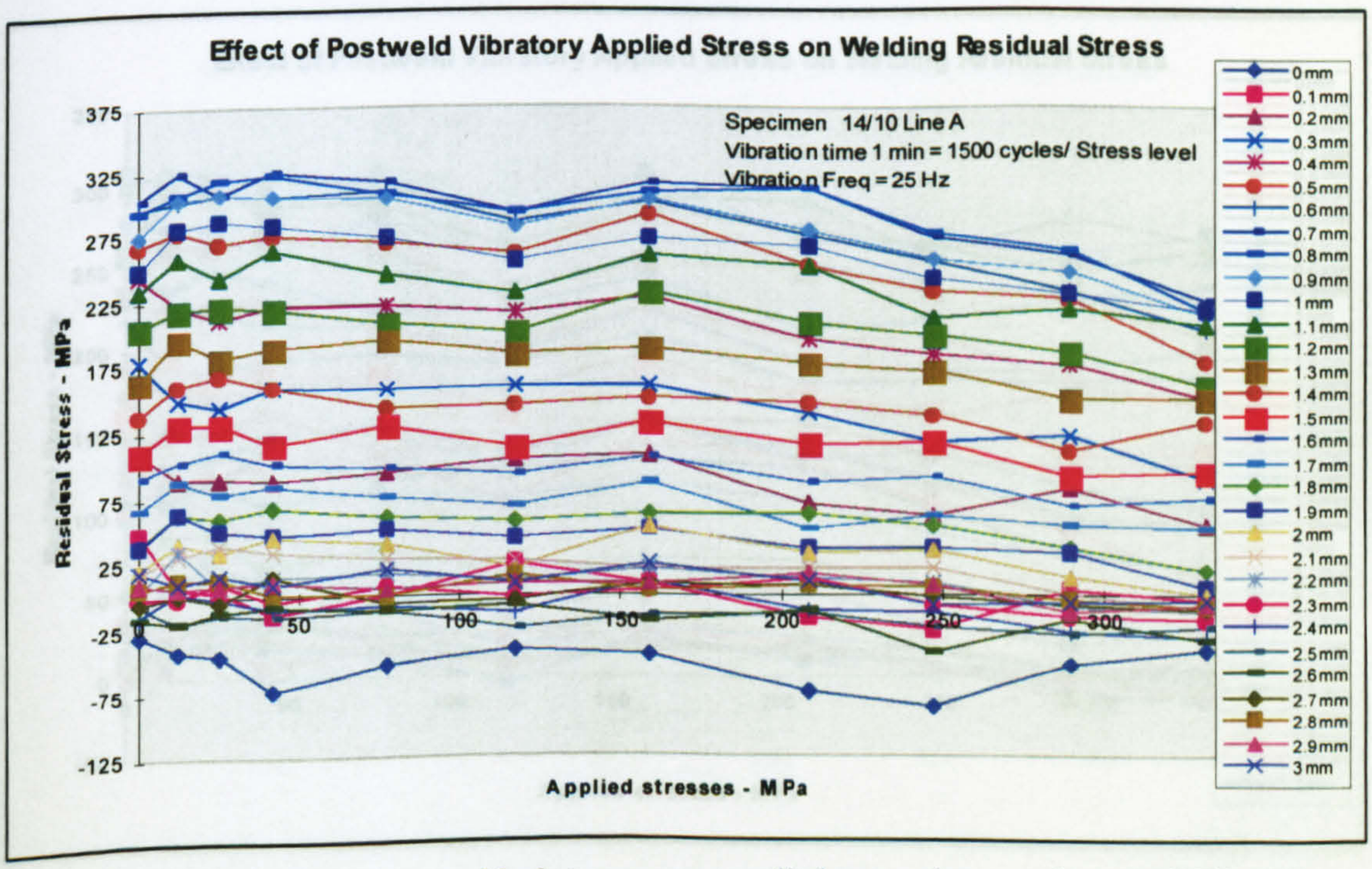

Figure 5.534 – Transverse residual stress versus applied stress plot - specimen 14/10 line A

Specimen 14/10 (D = X × 1 mm)

Line B (Line Stresses)

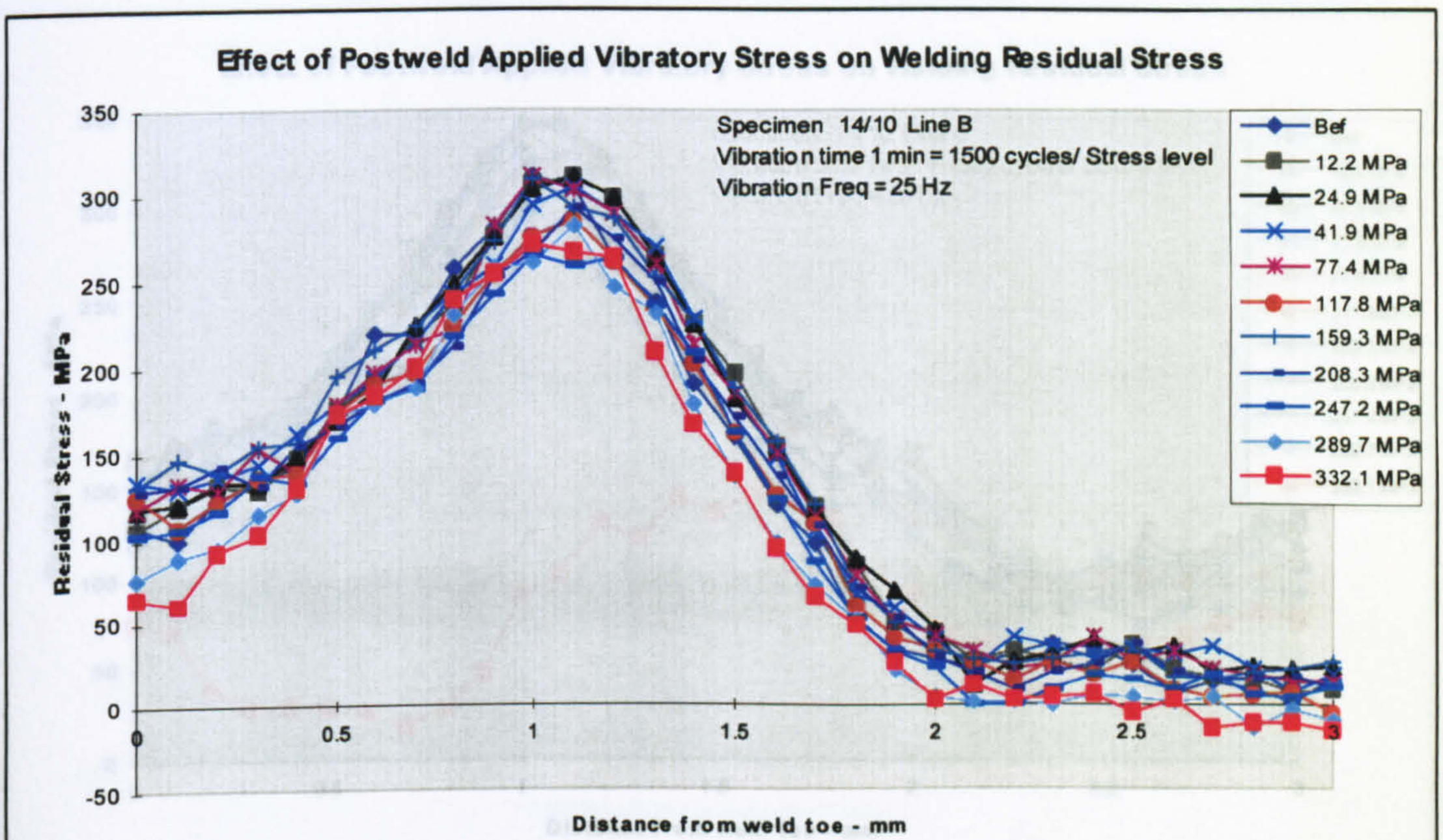

Figure 5.535 – Transverse line stress plot - specimen 14/10 line B

Line B (Transverse Residual Stress versus Applied Stress Plot)

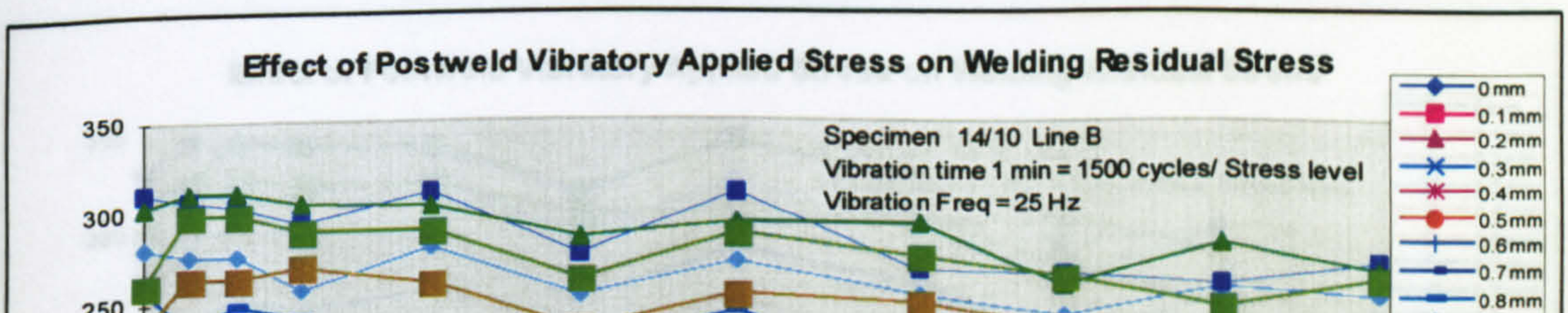

Figure 5.536 – Transverse residual stress versus applied stress plot - specimen 14/10 line B

Specimen 14/10 (D = X × 2 mm)

Line C (Line Stresses)

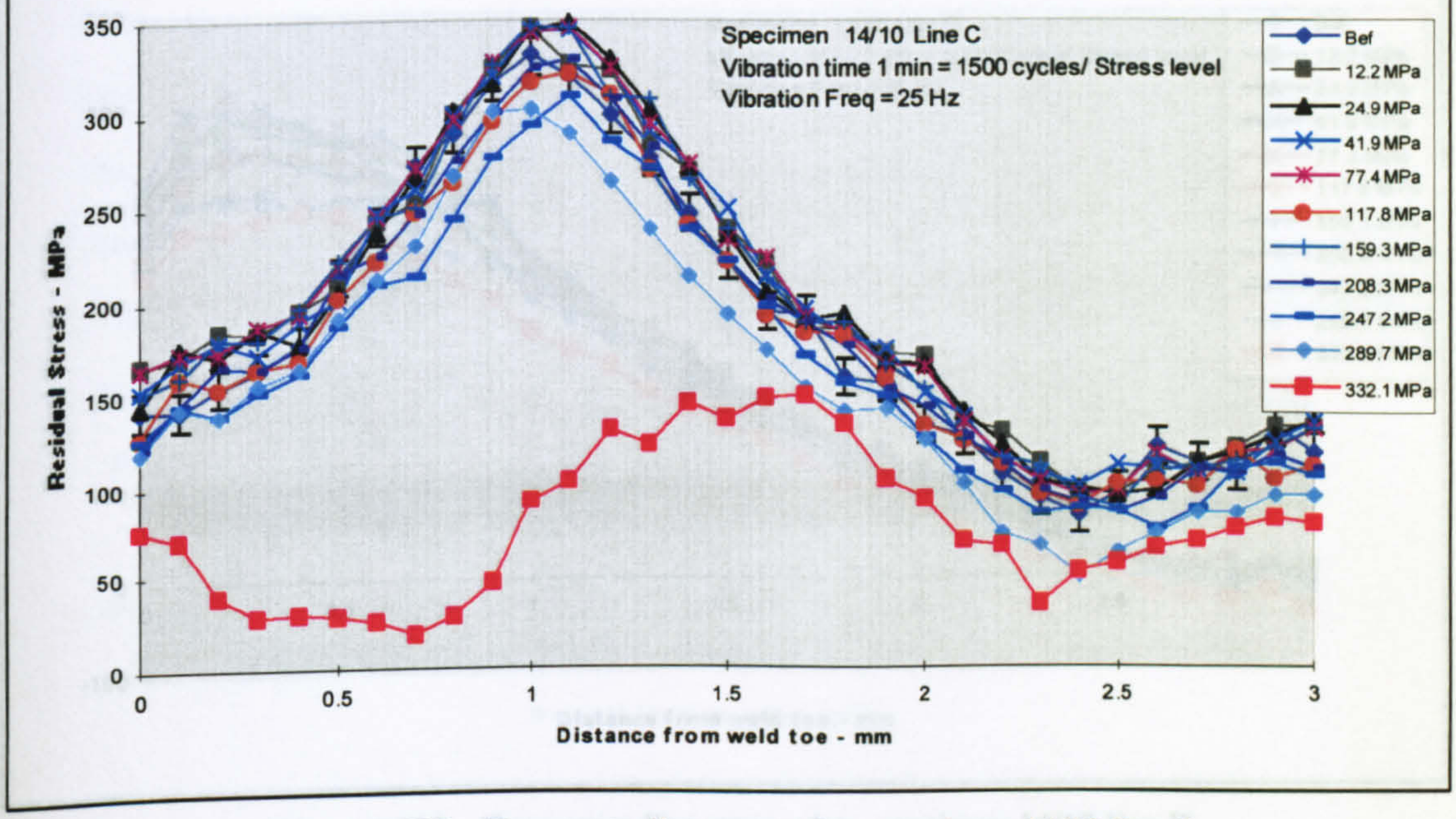

Figure 5.537 – Transverse line stress plot - specimen 14/10 line C

Line C (Transverse Residual Stress versus Applied Stress Plot)

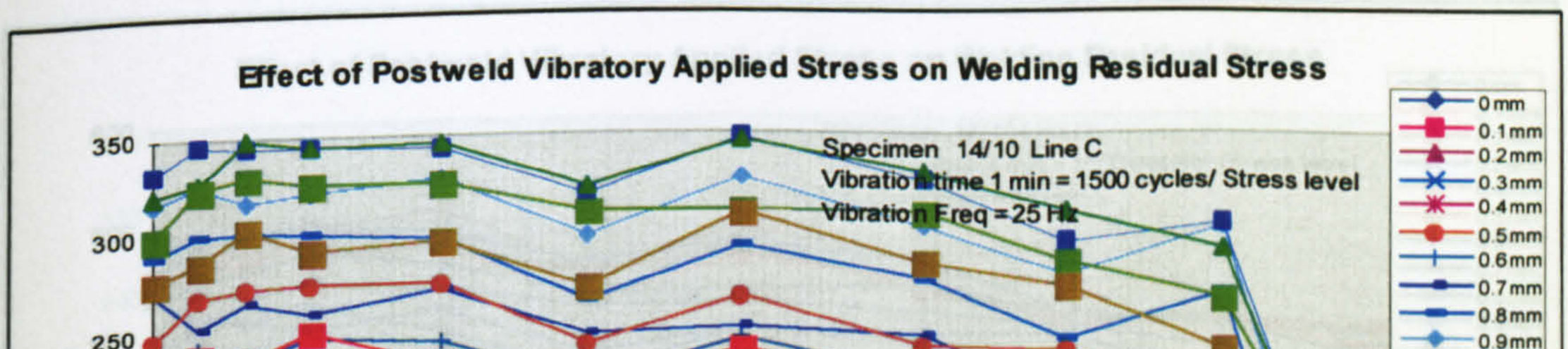

Figure 5.538 – Transverse residual stress versus applied stress plot - specimen 14/10 line C

Specimen 14/10 (D = X × 3 mm)

Line D (Line Stresses)

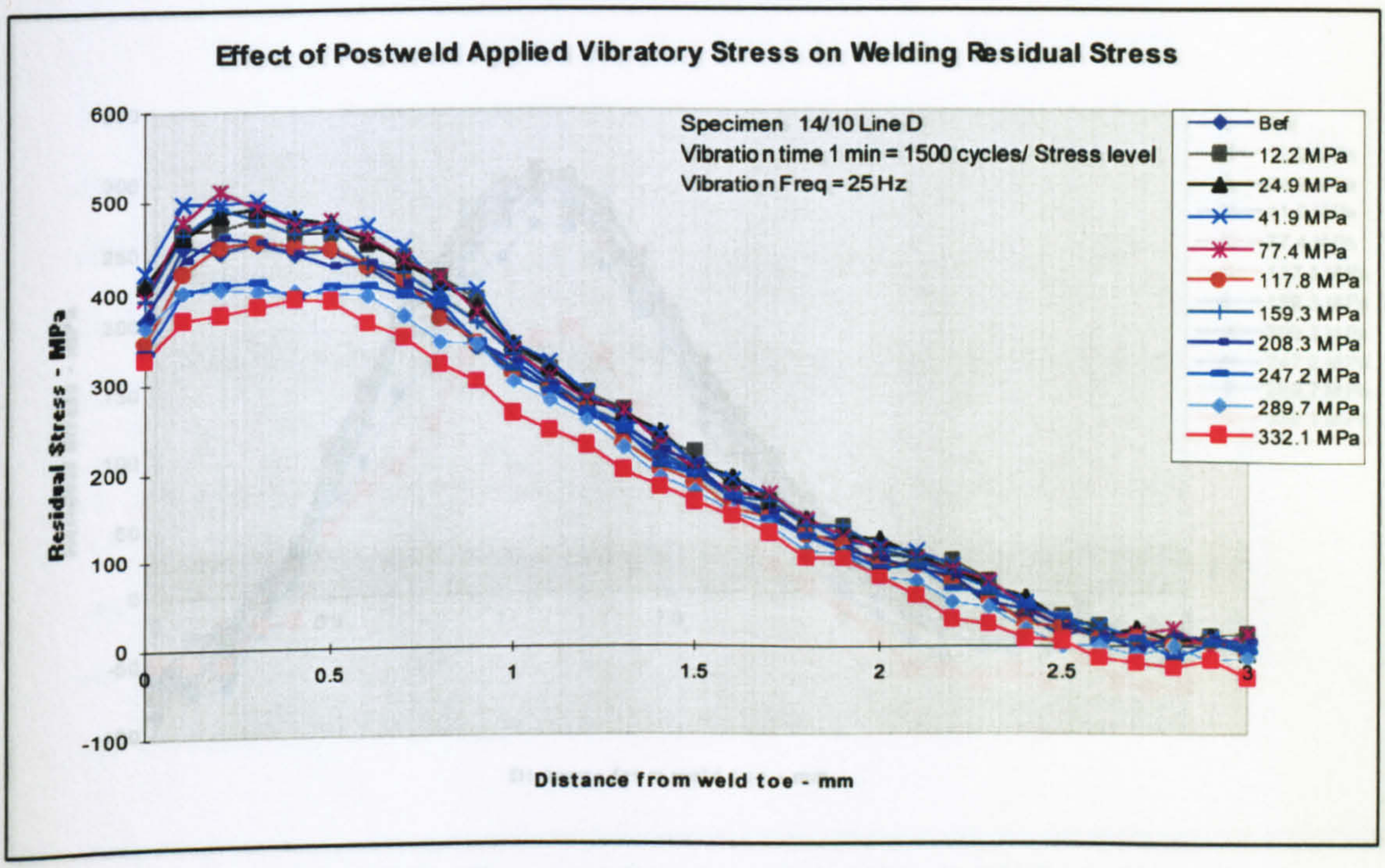

Figure 5.539 – Transverse line stress plot - specimen 14/10 line D

Line D (Transverse Residual Stress versus Applied Stress Plot)

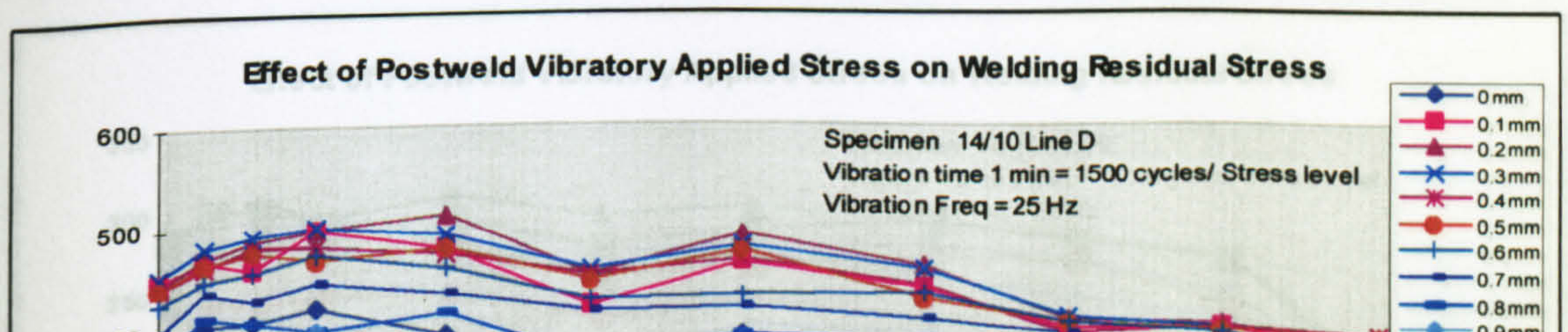

Figure 5.540 - Transverse residual stress versus applied stress plot - specimen 14/10 line D

Specimen 14/10 (D = X × 4 mm)

Line E (Line Stresses)

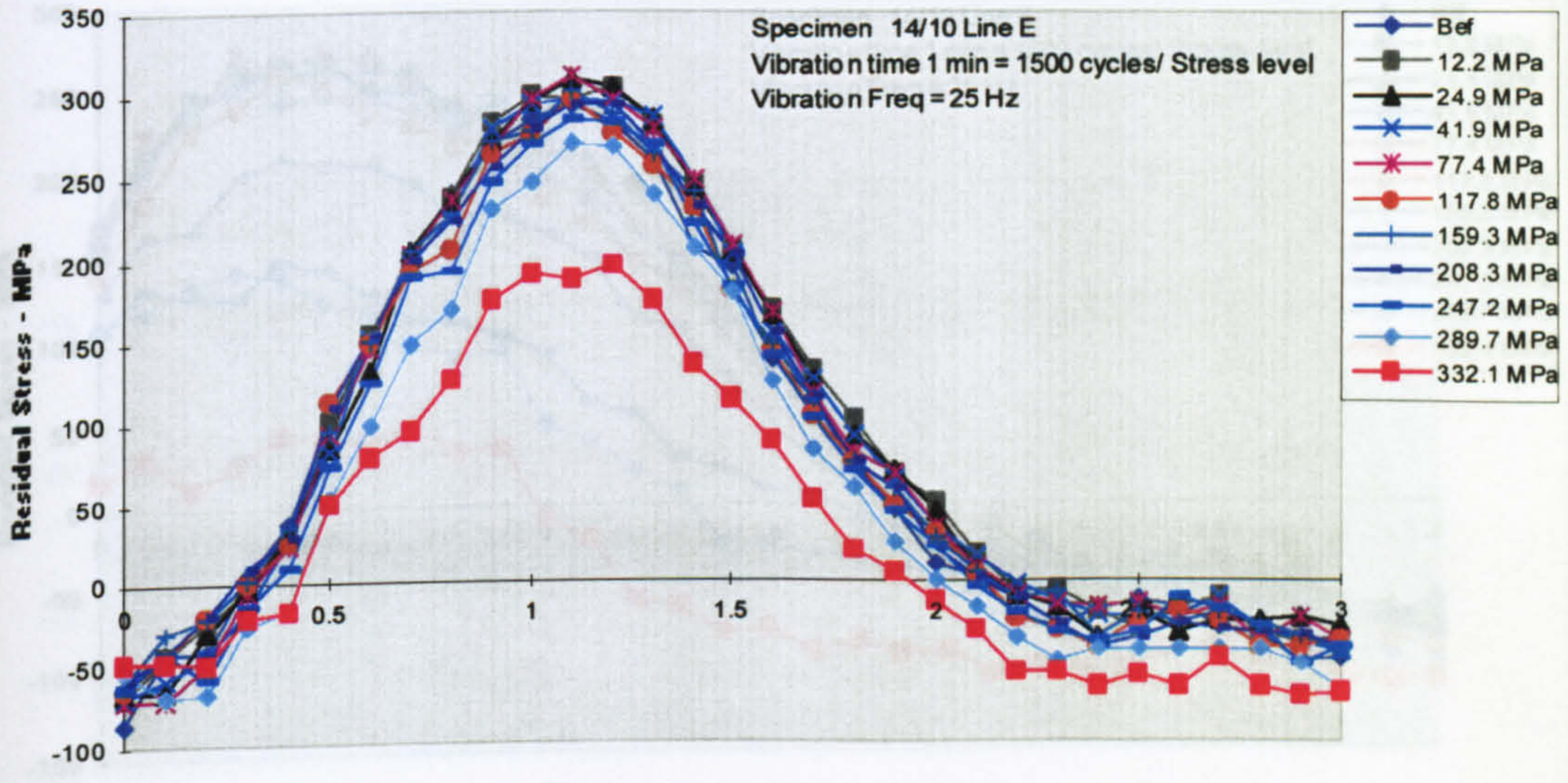

Figure 5.541 – Transverse line stress plot - specimen 14/10 line E

Line E (Transverse Residual Stress versus Applied Stress Plot)

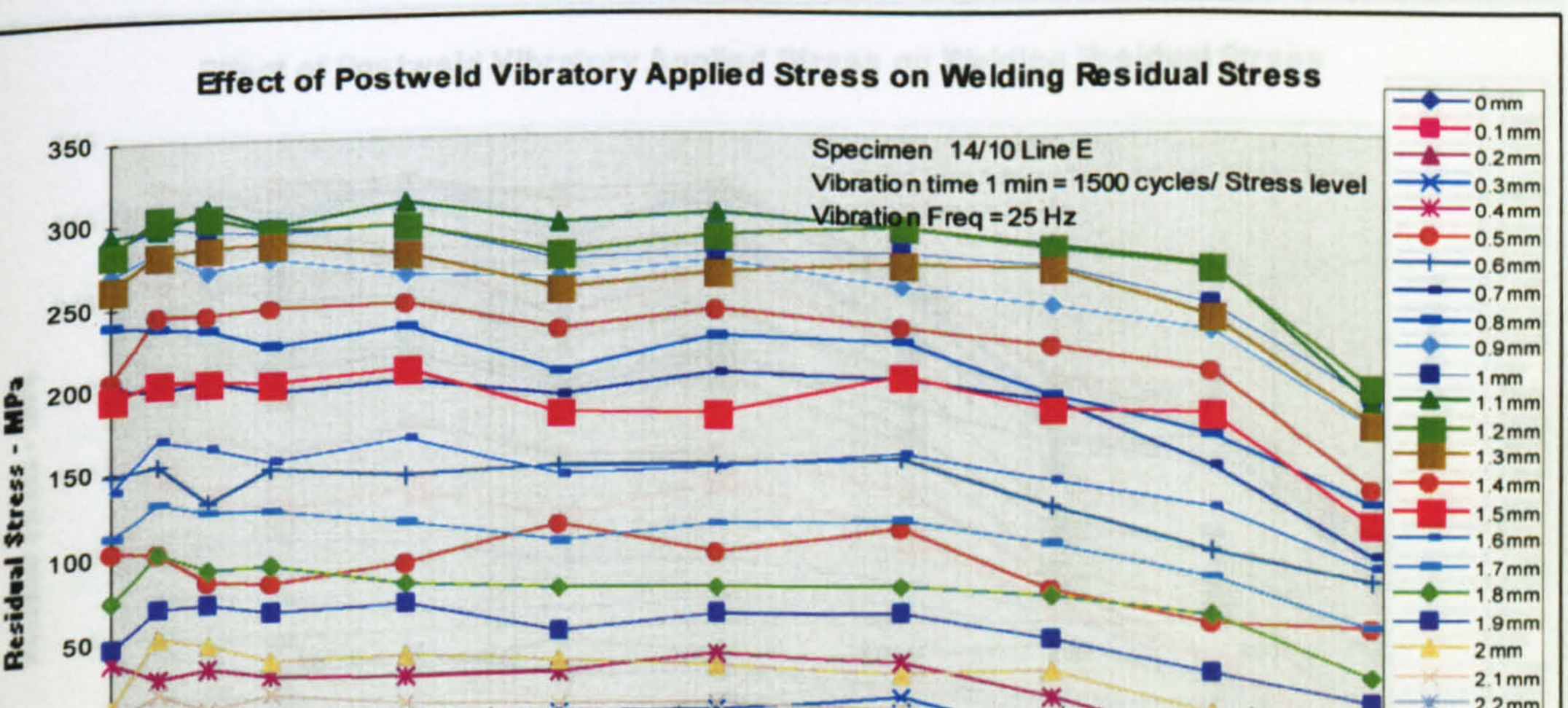

Figure 5.542 – Transverse residual stress versus applied stress plot - specimen 14/10 line E

Specimen 14/10 (D = X × 5 mm)

Line F (Line Stresses)

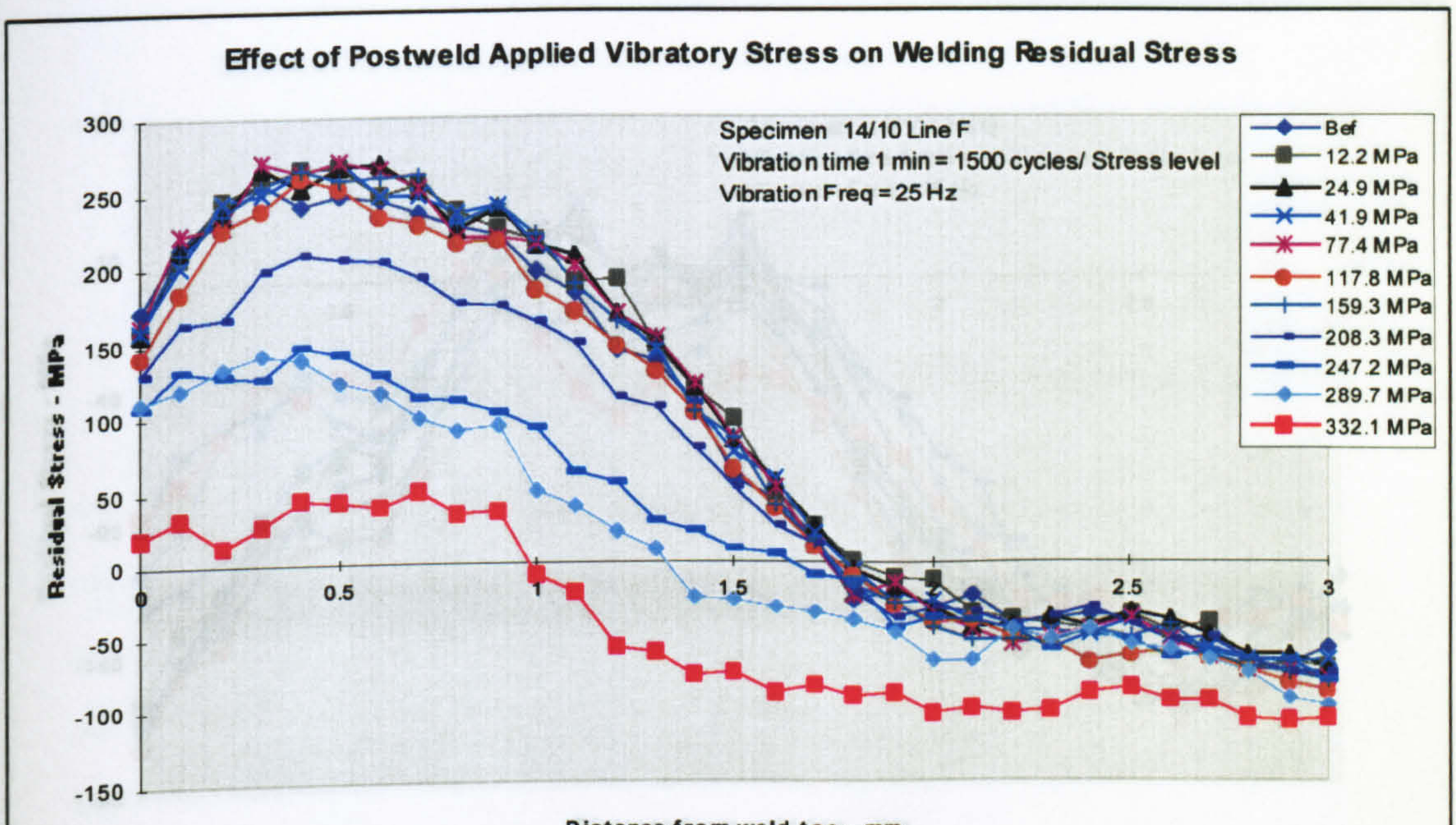

Figure 5.543 – Transverse line stress plot - specimen 14/10 line F

Line F (Transverse Residual Stress versus Applied Stress Plot)

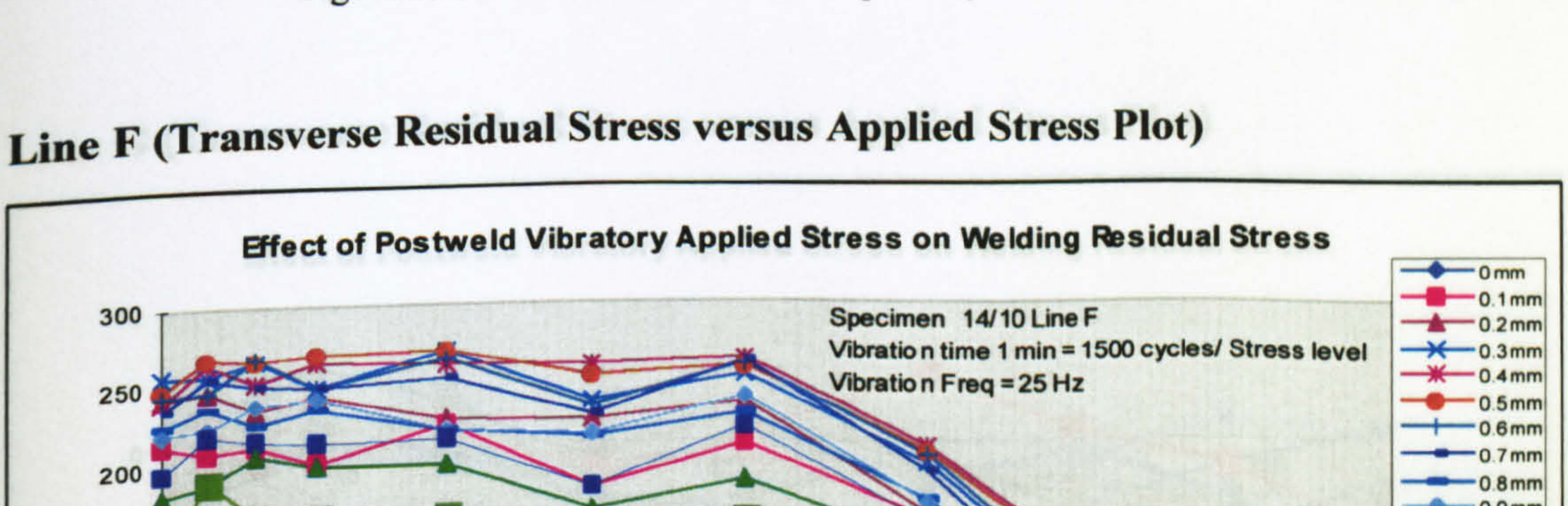

Figure 5.544 - Transverse residual stress versus applied stress plot - specimen 14/10 line F

Specimen 14/10 (D = X × 6 mm)

Line G (Line Stresses)

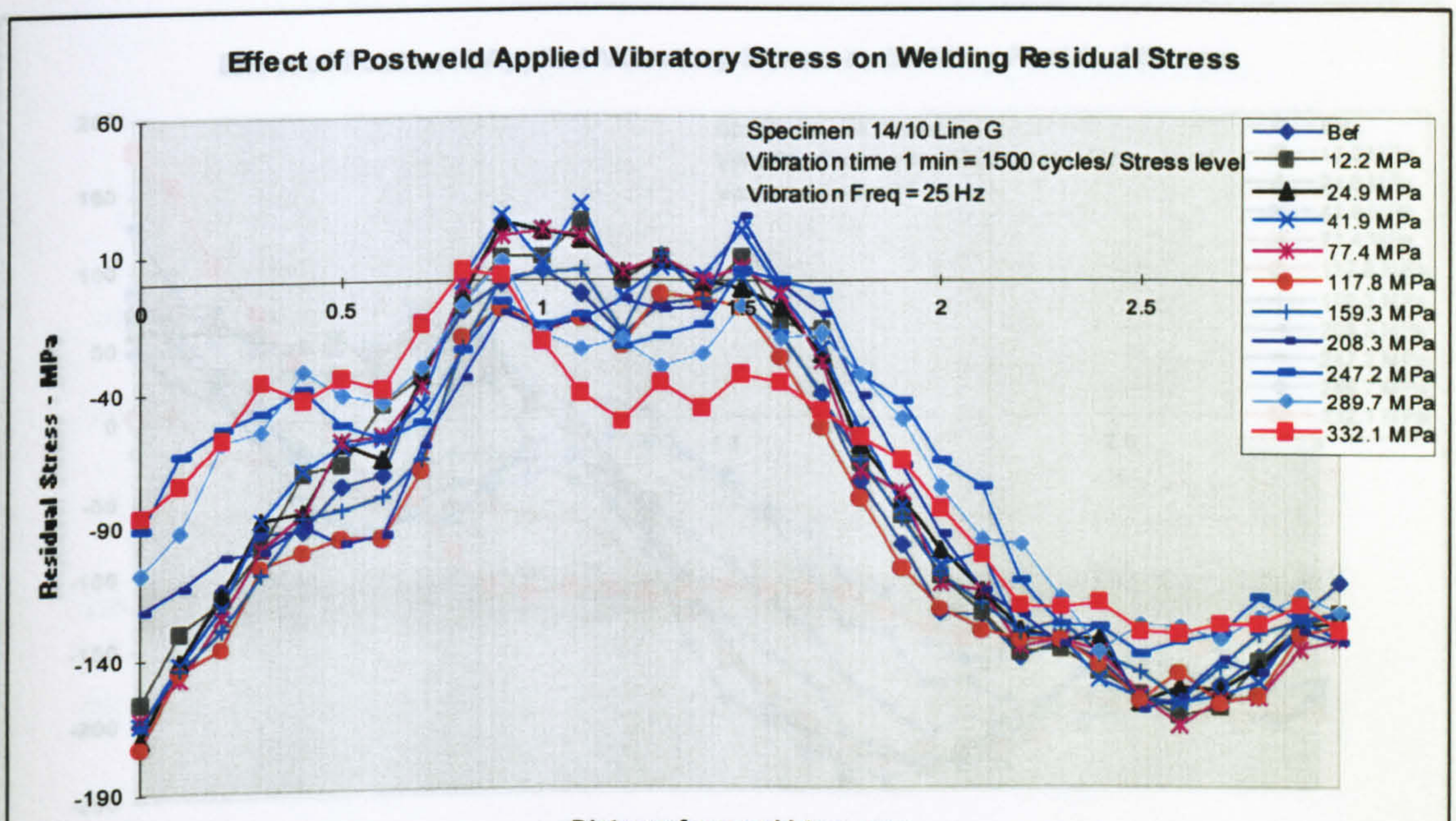

Figure 5.545 – Transverse line stress plot - specimen 14/10 line G

Line G (Transverse Residual Stress versus Applied Stress Plot)

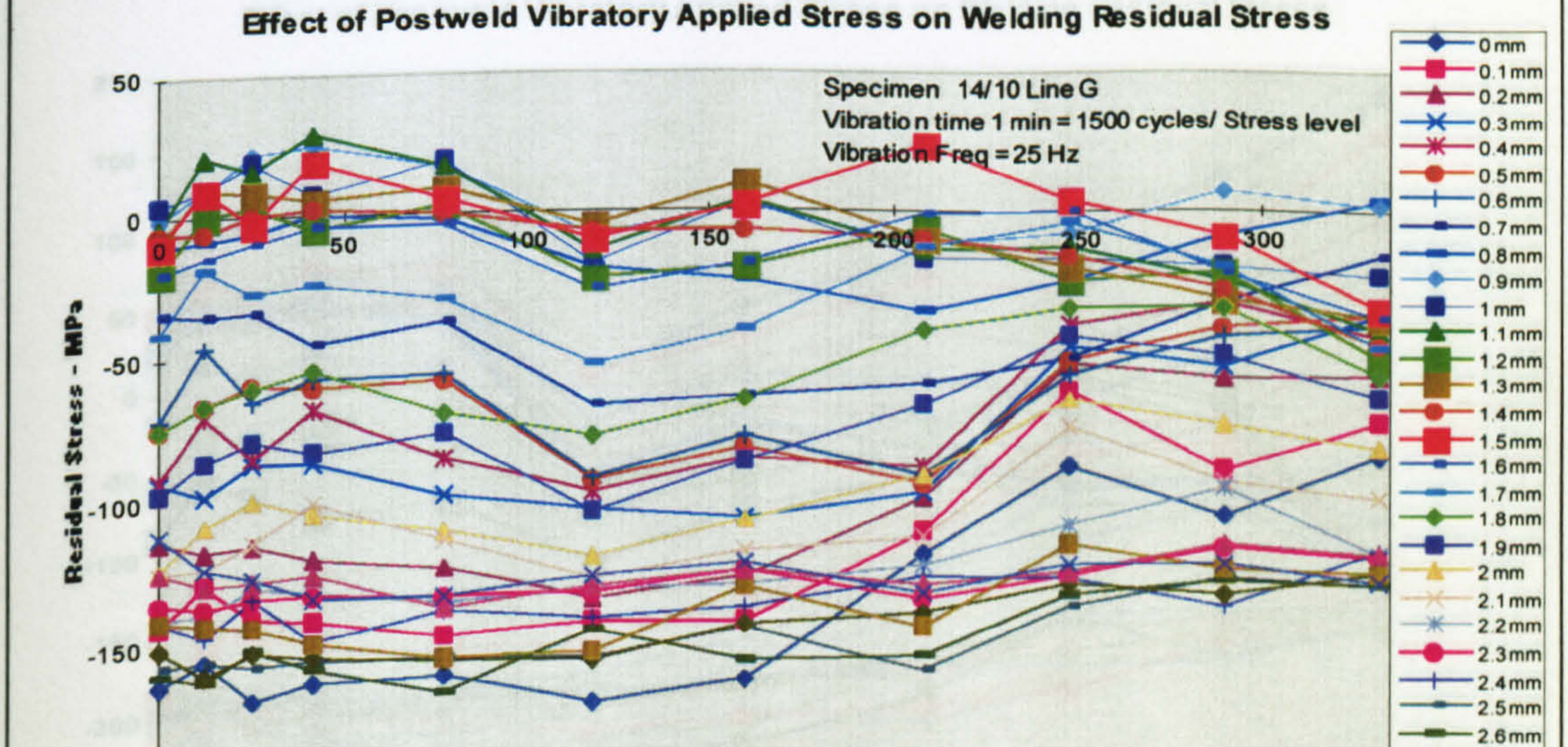

Figure 5.546 - Transverse residual stress versus applied stress plot - specimen 14/10 line G

Specimen 14/10 (D = X × 7 mm)

Line H (Line Stresses)

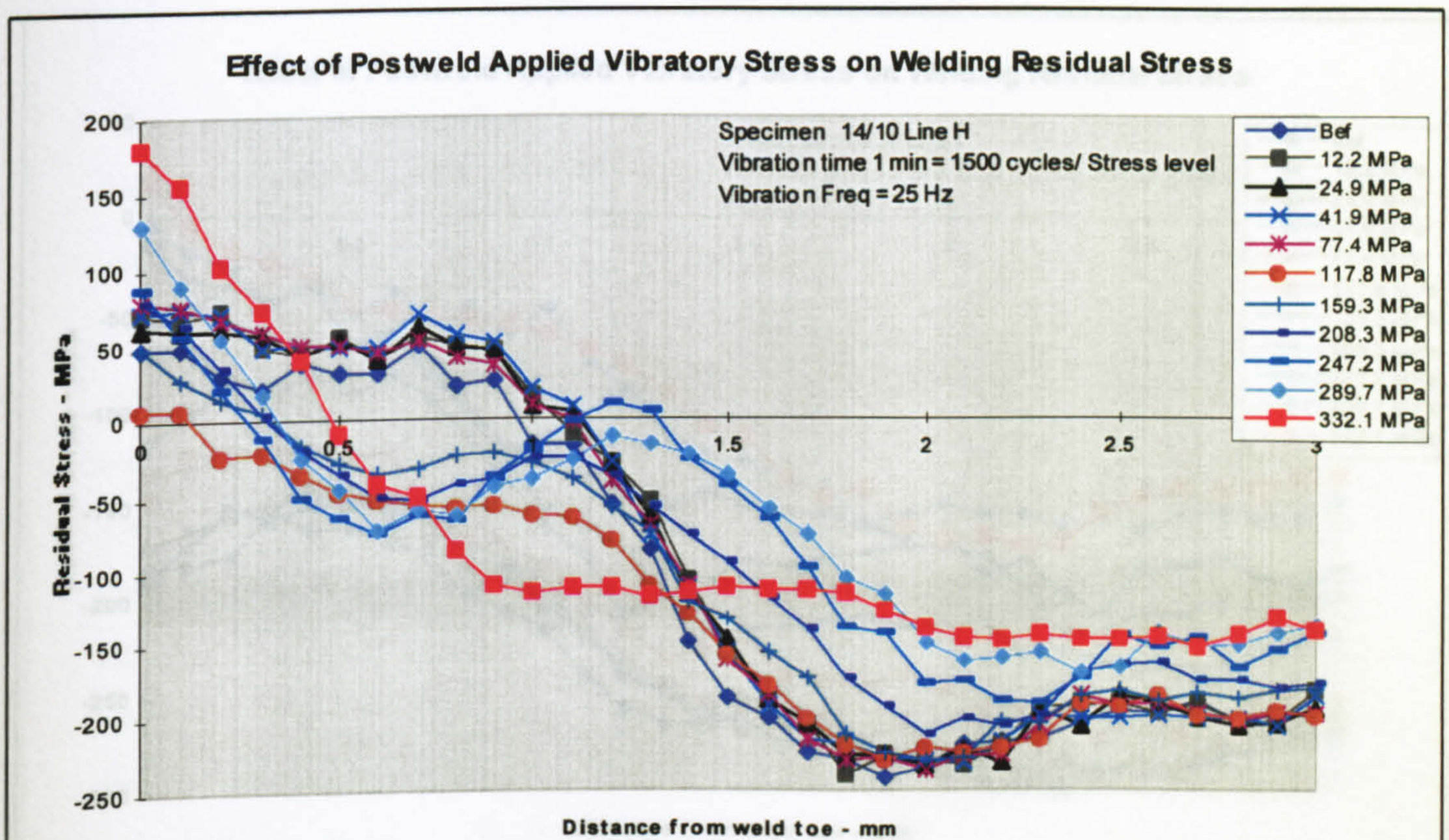

Figure 5.547 – Transverse line stress plot - specimen 14/10 line H

Line H (Transverse Residual Stress versus Applied Stress Plot)

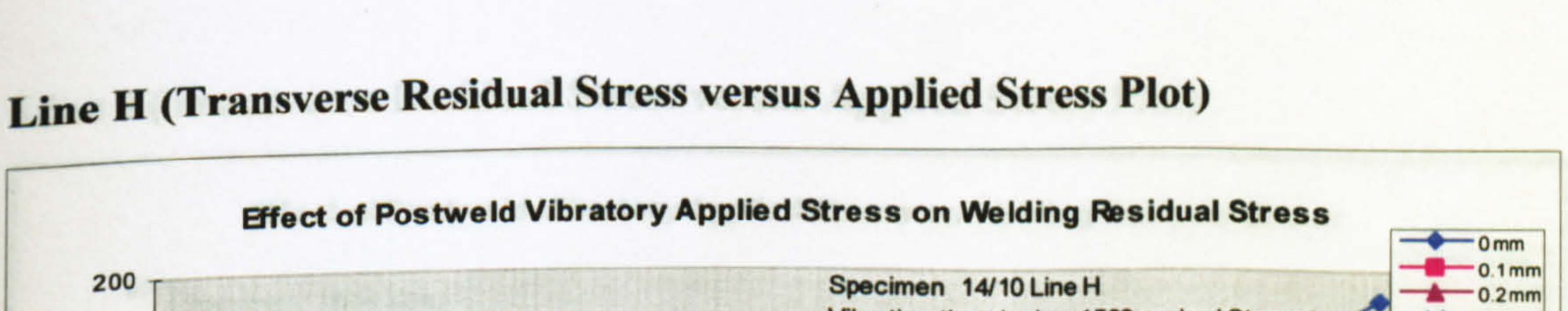

Figure 5.548 - Transverse residual stress versus applied stress plot - specimen 14/10 line H

Specimen 14/10 (D = X × 8 mm)

Line I (Line Stresses)

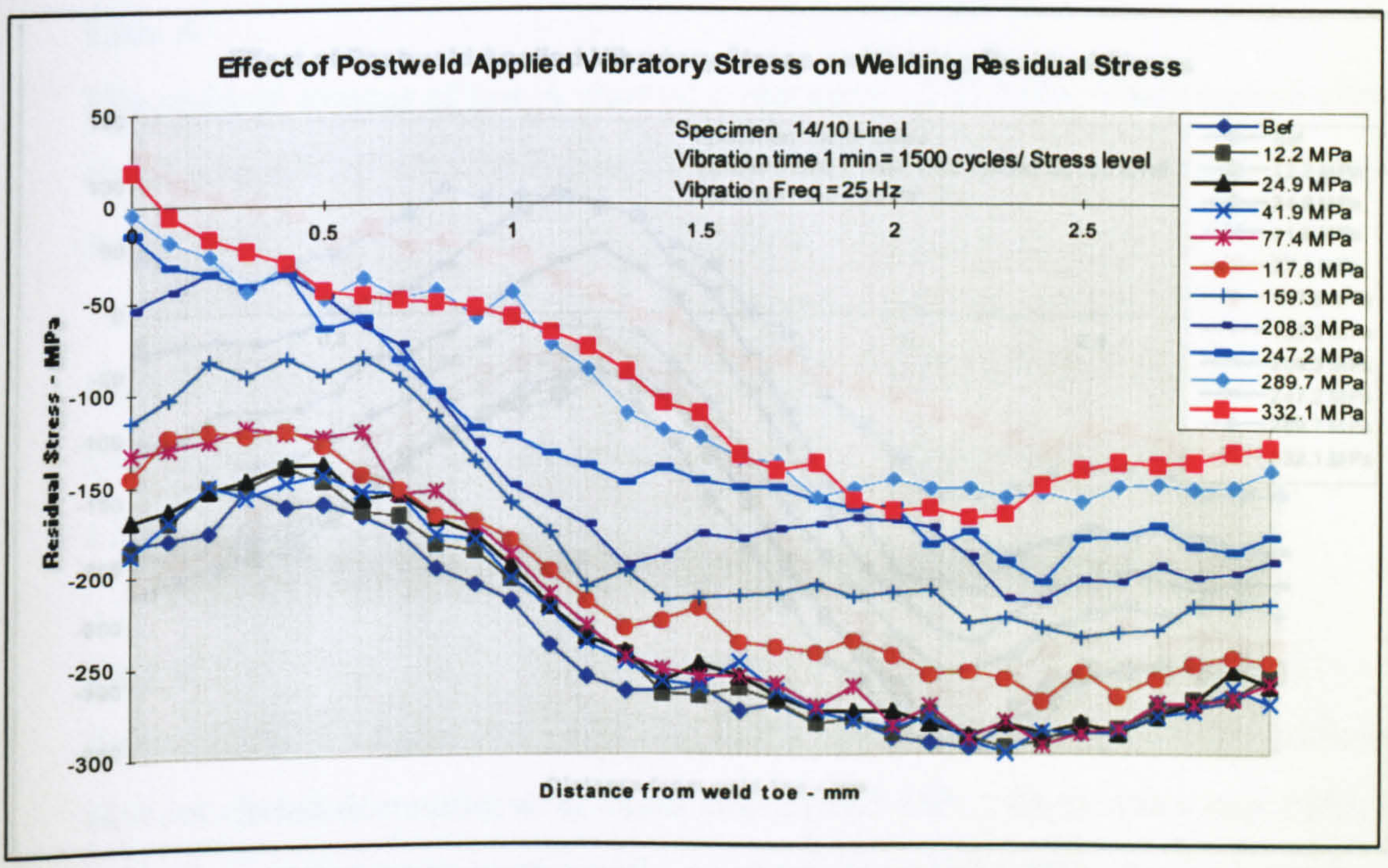

Figure 5.549 – Transverse line stress plot - specimen 14/10 line I

Line I (Transverse Residual Stress versus Applied Stress Plot)

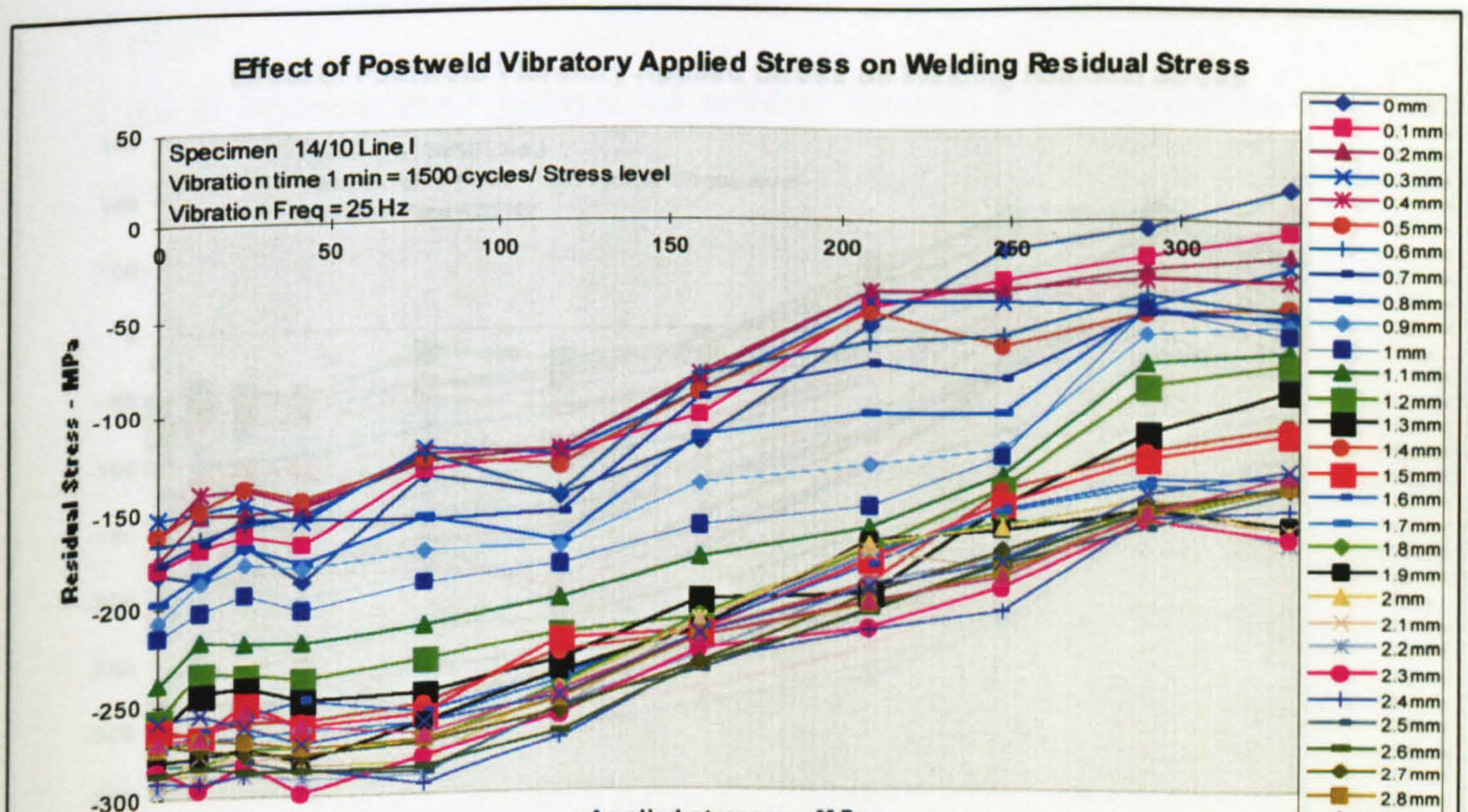

Figure 5.550 - Transverse residual stress versus applied stress plot - specimen 14/10 line I

Specimen 14/10 (D = X × 9 mm)

Line J (Line Stresses)

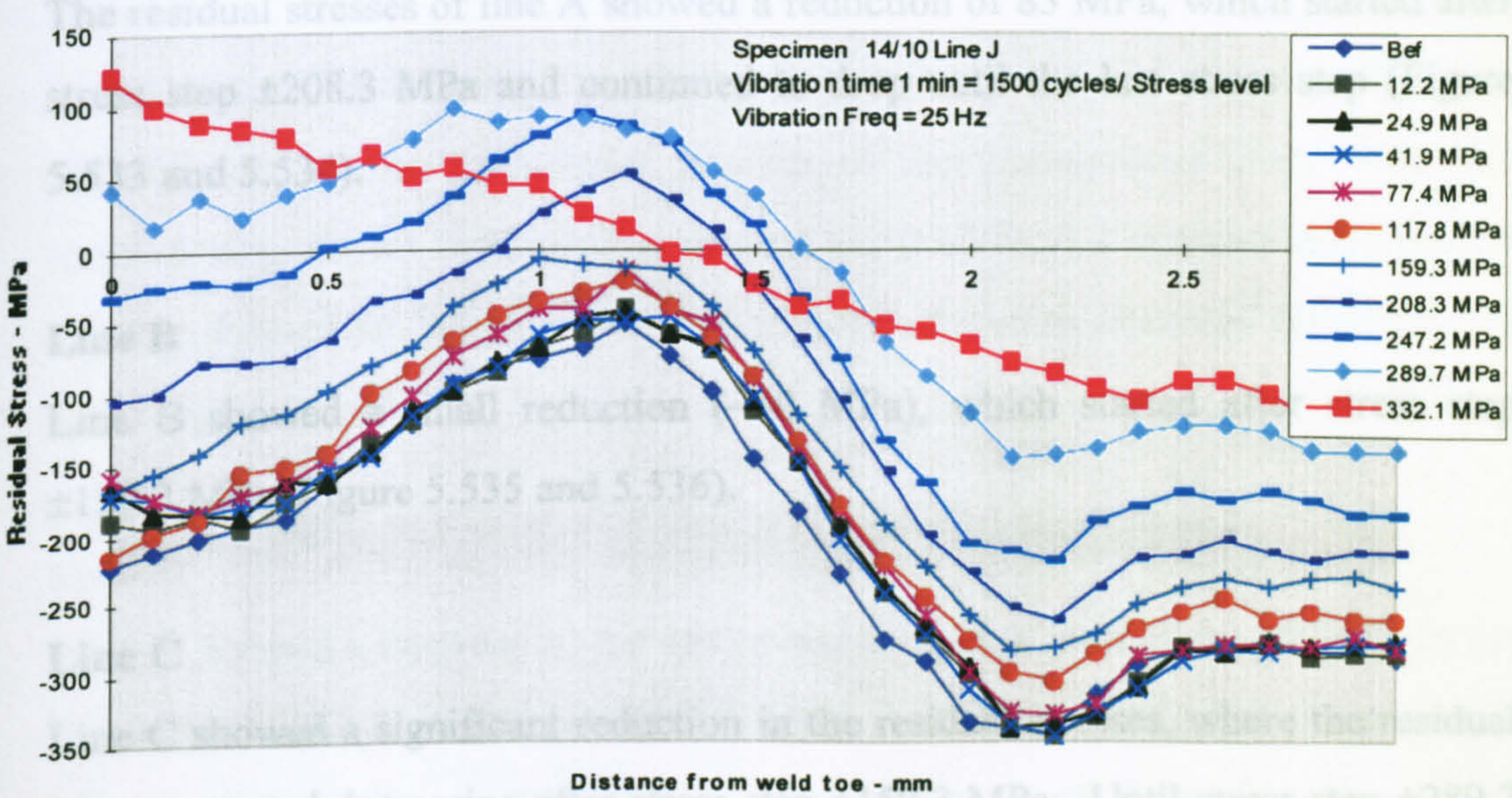

Figure 5.551 - Line stress plot of specimen 14/10 line J

Line J (Transverse Residual Stress versus Applied Stress Plot)

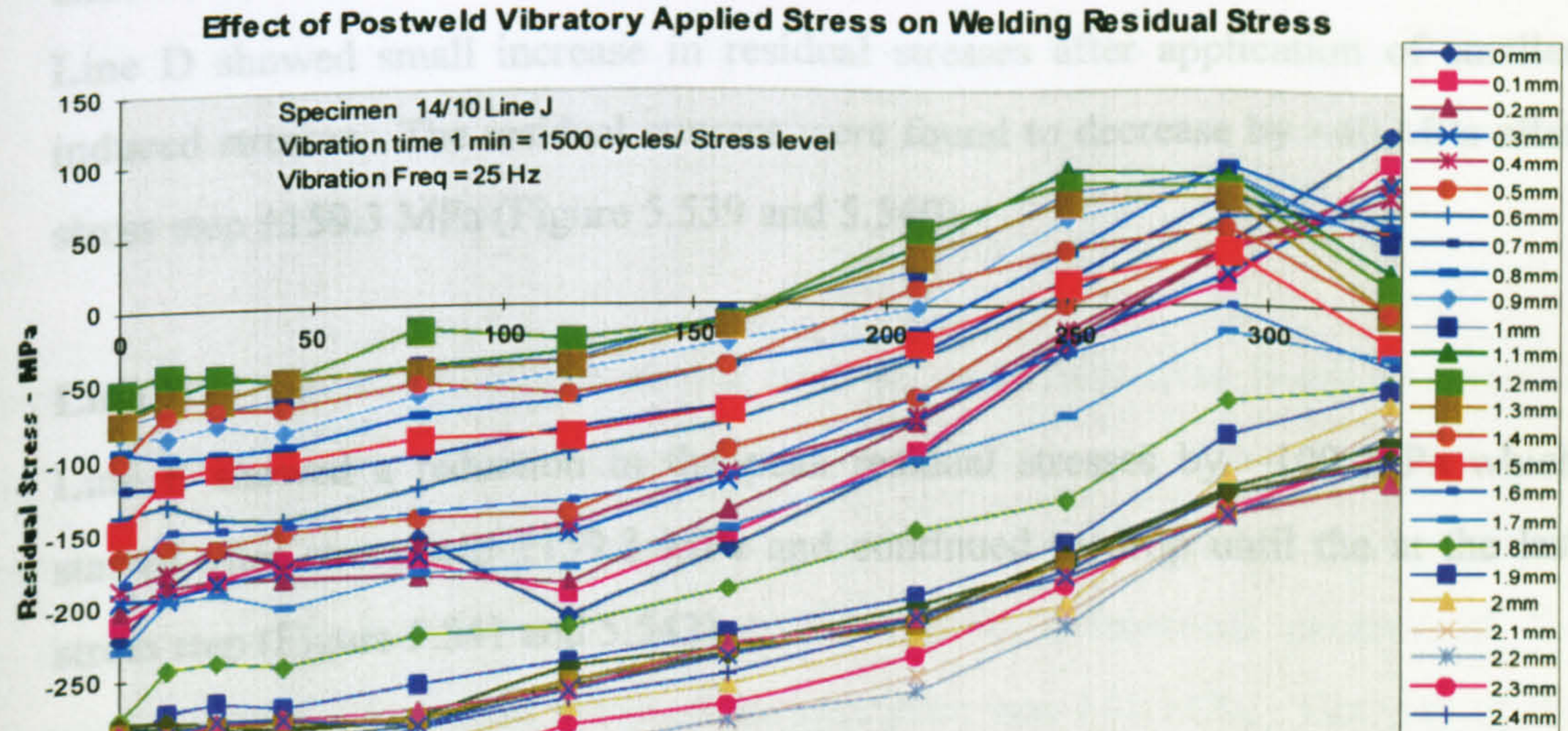

Figure 5.552 - Transverse residual stress versus applied stress plot - specimen 14/10 line J

Discussion of Results - specimen 14/10

The observations on the lines from the result plots are

Line A

The residual stresses of line A showed a reduction of 85 MPa, which started after stress step ±208.3 MPa and continued to drop until the last stress step (Figure 5.533 and 5.534).

Line B

Line B showed a small reduction (~40 MPa), which started after stress step ±159.3 MPa (Figure 5.535 and 5.536).

Line C

Line C showed a significant reduction in the residual stresses, where the residual stresses started decreasing after stress step ±159.3 MPa. Until stress step ±289.7 MPa, the stress reduction was small. At stress step ±332.1 MPa, the peak residual stress reduced from 330 MPa to 115 MPa (Figure 5.537 and 5.538).

Line D

Line D showed small increase in residual stresses after application of smaller induced stresses. The residual stresses were found to decrease by ~40 MPa after stress step ±159.3 MPa (Figure 5.539 and 5.540).

Line E

Line E showed a reduction in the peak residual stresses by ~100 MPa which started after stress step ±159.3 MPa and continued to drop until the at the last stress step (Figure 5.541 and 5.542).

Line F

Line F showed a large reduction, where on and near the weld toe a reduction of 220 MPa was observed (from 270 MPa to 50 MPa). The reduction started after

stress step ±159.3 MPa and continued to drop until stress step ±332.1 MPa. The residual stresses of this line were decreased to compressive or to a near zero values (Figure 5.543 and 5.544).

Line G

Line G showed a different type of distribution in the residual stresses. This was probably due to the geometrical position of the measurement line. This line showed virtually no reduction, in some areas it showed a decrease and in other areas it showed an increase, i.e. only redistribution was observed (Figure 5.545 and 5.546).

Line H

Line H showed a decrease in the compressive residual stresses by 40 MPa in the first stress step. At stress step ±117.8 MPa, a substantial reduction occurred (70 MPa) in the tensile residual stresses. Subsequent stress steps showed a mixed result – the residual stresses in most of the measurement points increased and in some measurement points decreased (Figure 5.547 and 5.548).

Line I & J

Line I and J initially were in high compressive stress, due to the vibratory treatment the residual stress decreased to lower compressive or tensile stresses (Figure 5.549 to 5.552).

Thus, the tensile residual stresses on and near the mid-width were found to decrease and near the edges the compressive residual stresses also decreased, i.e. mathematically increased. In some measurement lines the residual stresses were found to decrease more then others, this may be due to geometrical position of the measurement line. The yield stress of the specimen was 611 MPa. The sum of the peak residual stress and the maximum applied stress was higher than the yield stress, hence there was a possibility of plastic deformation in the specimens.

Specimen 14/11

This specimen was also processed in order to further investigate the findings of specimens 13/8 and 13/9 - the details of which are given in the description of specimen 14/10. In this specimen, four longitudinal lines were selected along the whole width of the specimens - leaving 2 mm from the both edges of the specimen. In the 3 mm distance from the weld toe, four lines were selected for investigation. The first line was on the weld toe. The distances of the second, third and fourth lines from the weld were 1 mm, 2 mm and 3 mm respectively (Figure 5.553). The transverse residual stresses on the lines were measured using the single exposure technique (SET).

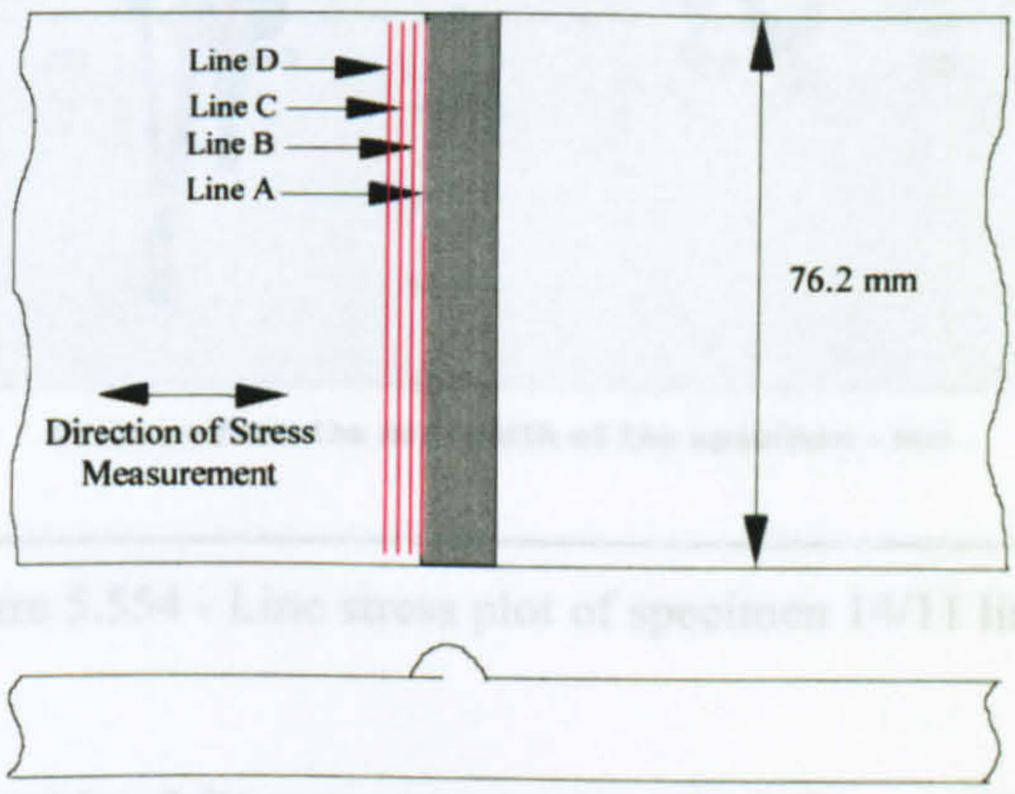

Figure 5.553 - Position of measurement lines - specimen 14/11

The frequency of vibration was 25 Hz and the specimens were vibrated for 1 minute at every stress step. Keeping the frequency and time of vibration constant, the applied stresses were increased from ±55 MPa to ±332.1 MPa in seven steps. Instead of measuring the residual stresses on the separate lines they were measured using the mapping procedure - thus saved measurement time considerably. In the area map of the four lines, the resolution of the measurement points was 1 mm, i.e. 73 points were measured in every line. The data relating to the individual lines were extracted from the area map and plotted as line and point stresses for easy analysis. The line and point stresses of the lines are shown in Figure 5.554 to 5.5561.

Sp-14/11 Line A (on the Weld Toe)

Line Stresses

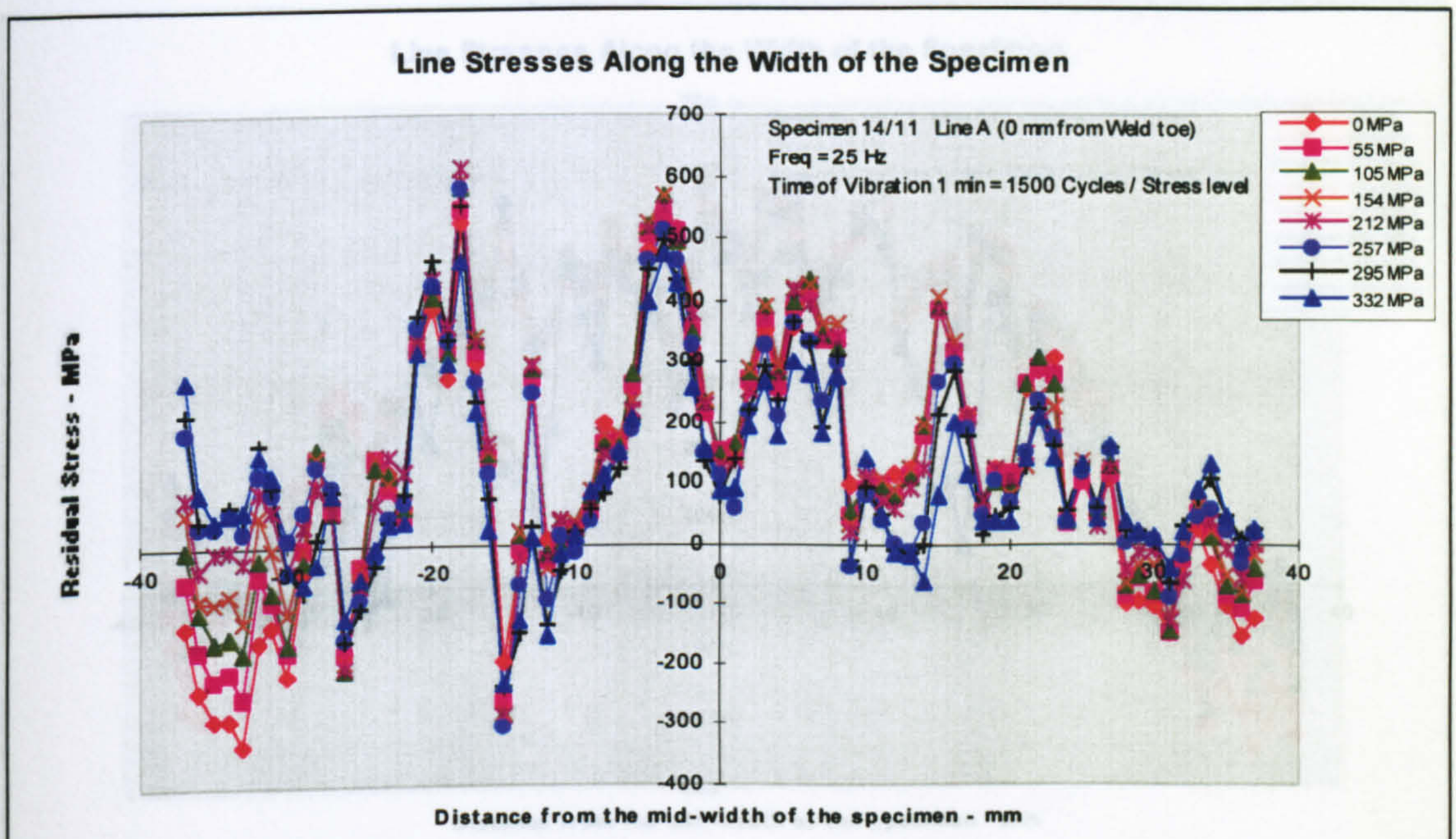

Figure 5.554 - Line stress plot of specimen 14/11 line A

Line A (Transverse Residual Stress versus Applied Stress Plot)

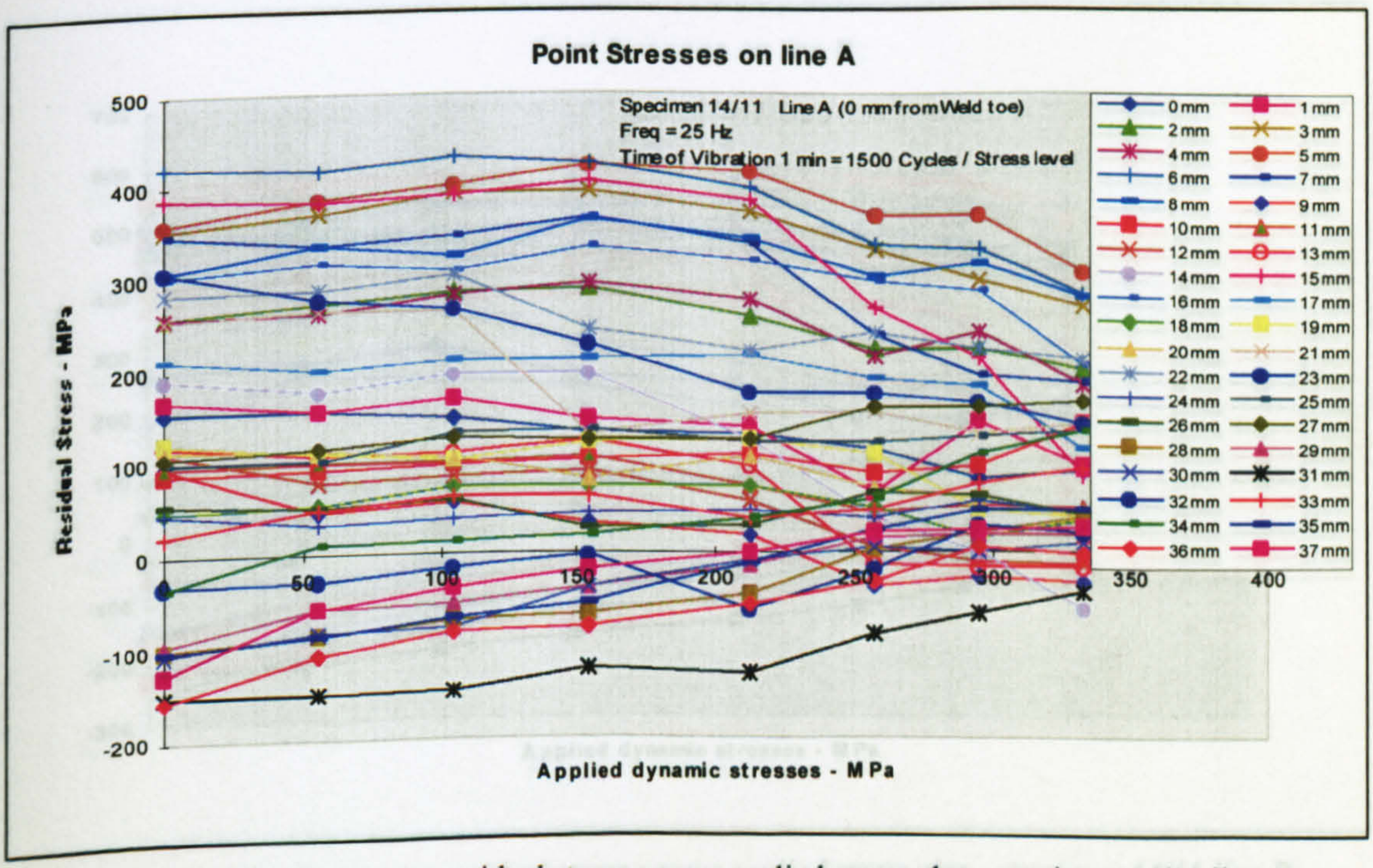

Figure 5.555 - Transverse residual stress versus applied stress plot - specimen 14/11 line A

Sp-14/11 Line B (1 mm from the Weld Toe)

Line Stresses

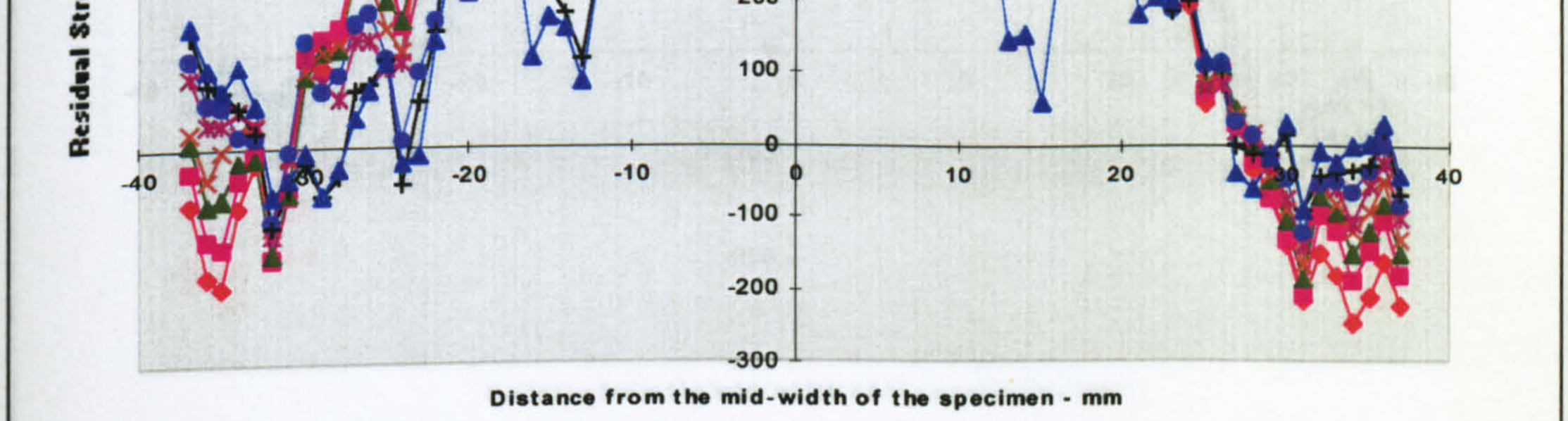

Figure 5.556 - Line stress plot of specimen 14/11 line B

Line B (Transverse Residual Stress versus Applied Stress Plot)

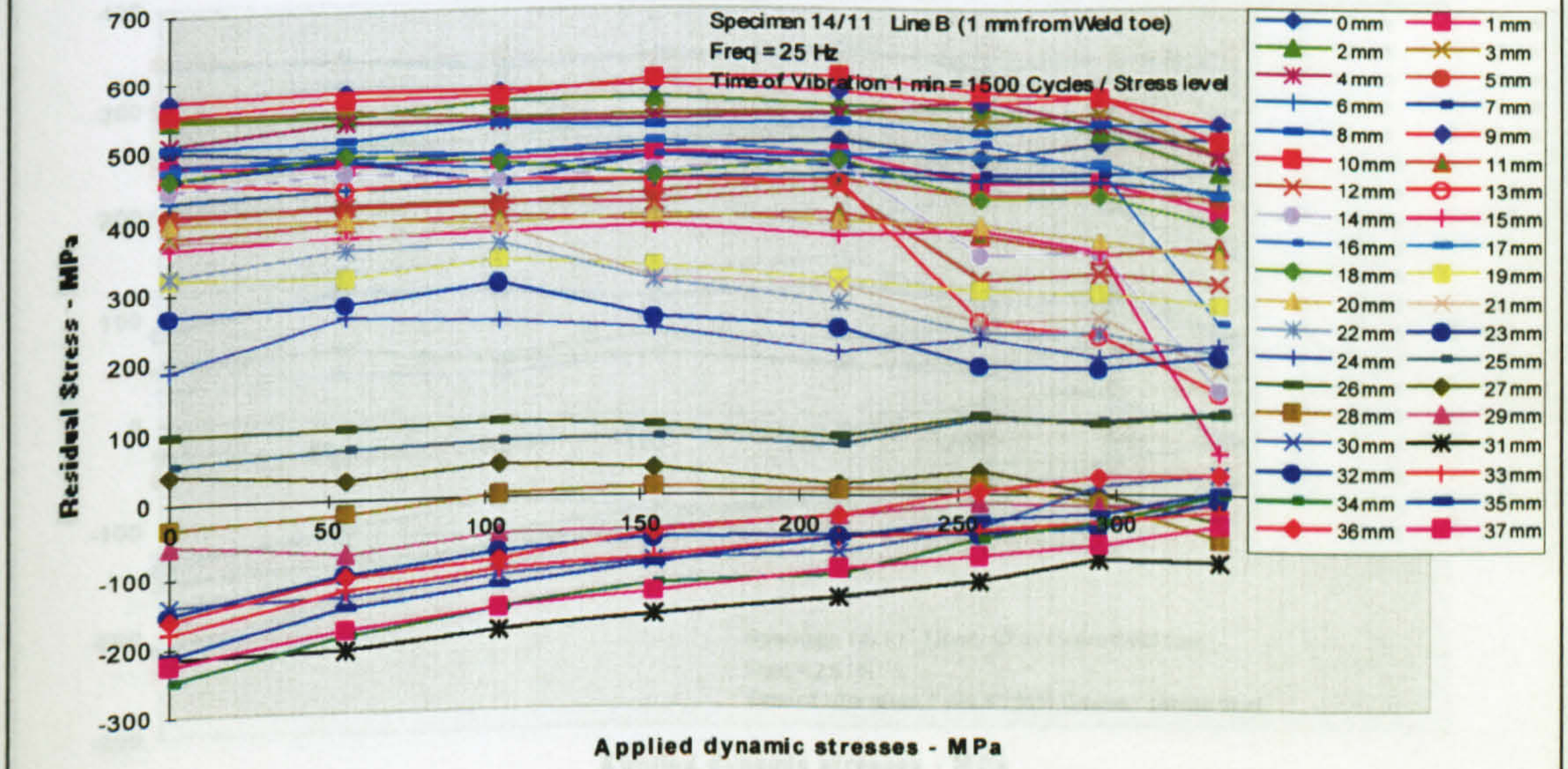

Figure 5.557 - Transverse residual stress versus applied stress plot - specimen 14/11 line B

Sp-14/11 Line C (2 mm from the Weld Toe)

Line Stresses

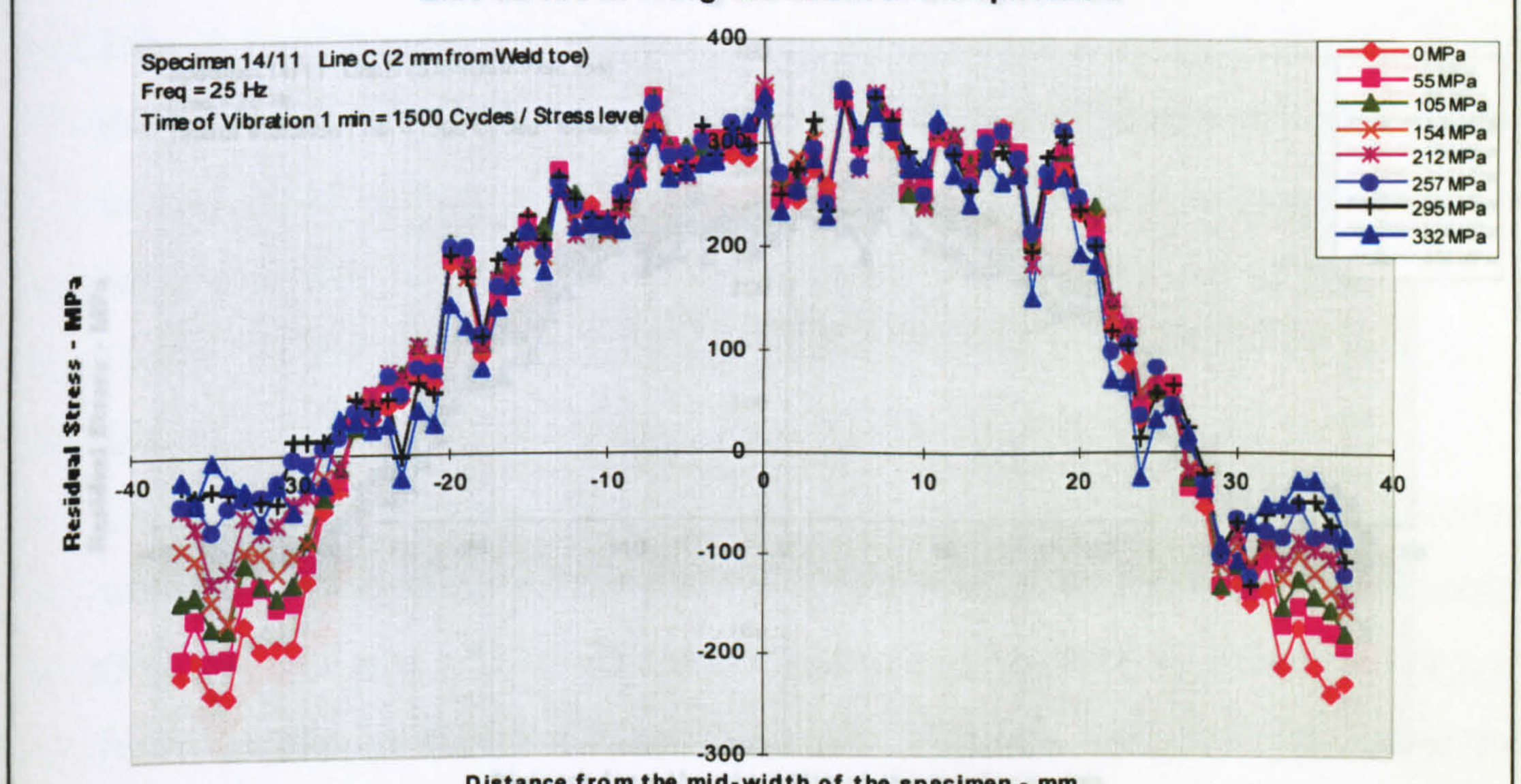

Figure 5.558 - Line stress plot of specimen 14/11 line C

Line C (Transverse Residual Stress versus Applied Stress Plot)

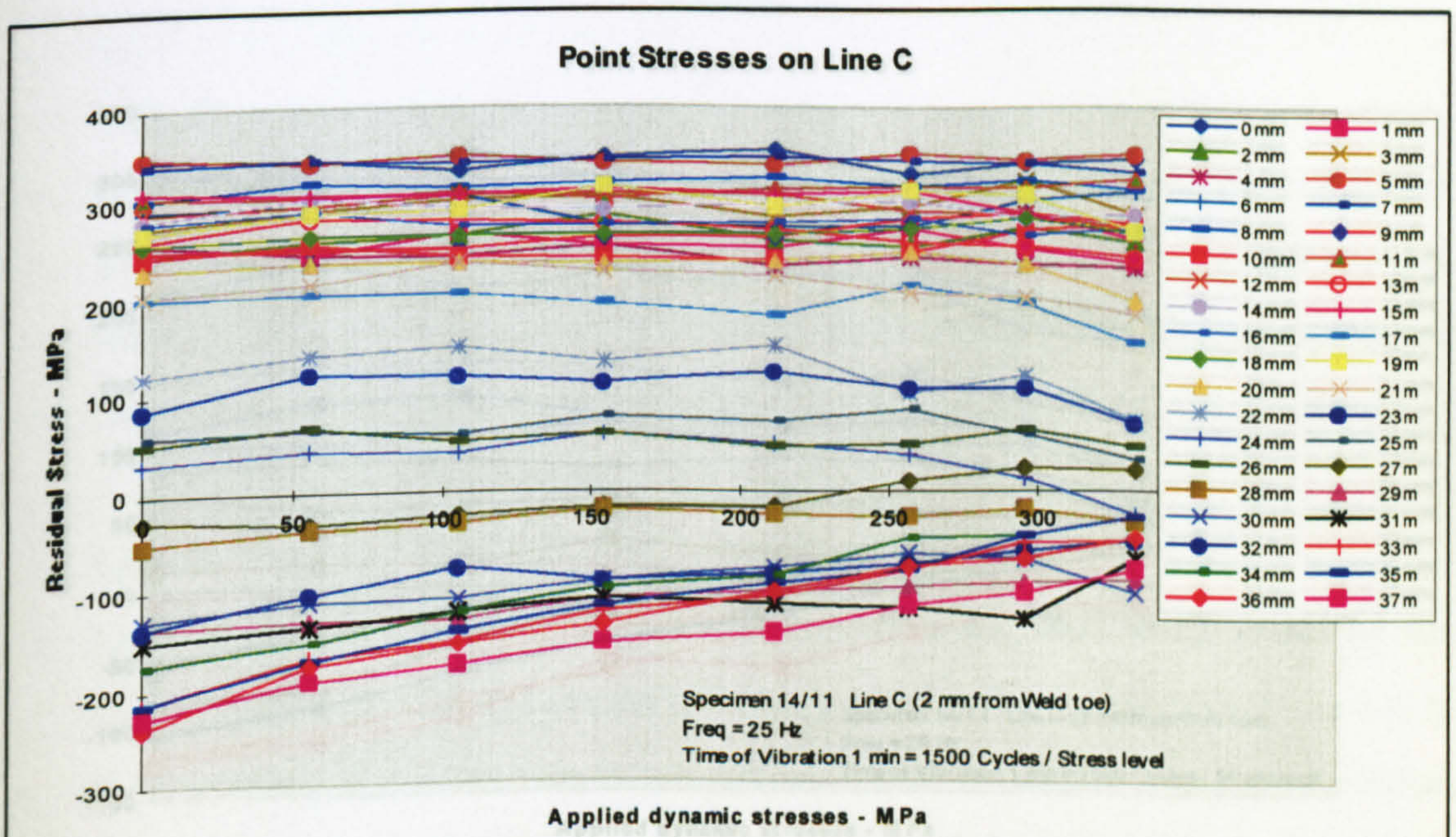

Figure 5.559 - Transverse residual stress versus applied stress plot - specimen 14/11 line C

Sp-14/11 Line D (3 mm from the Weld Toe)

Line Stresses

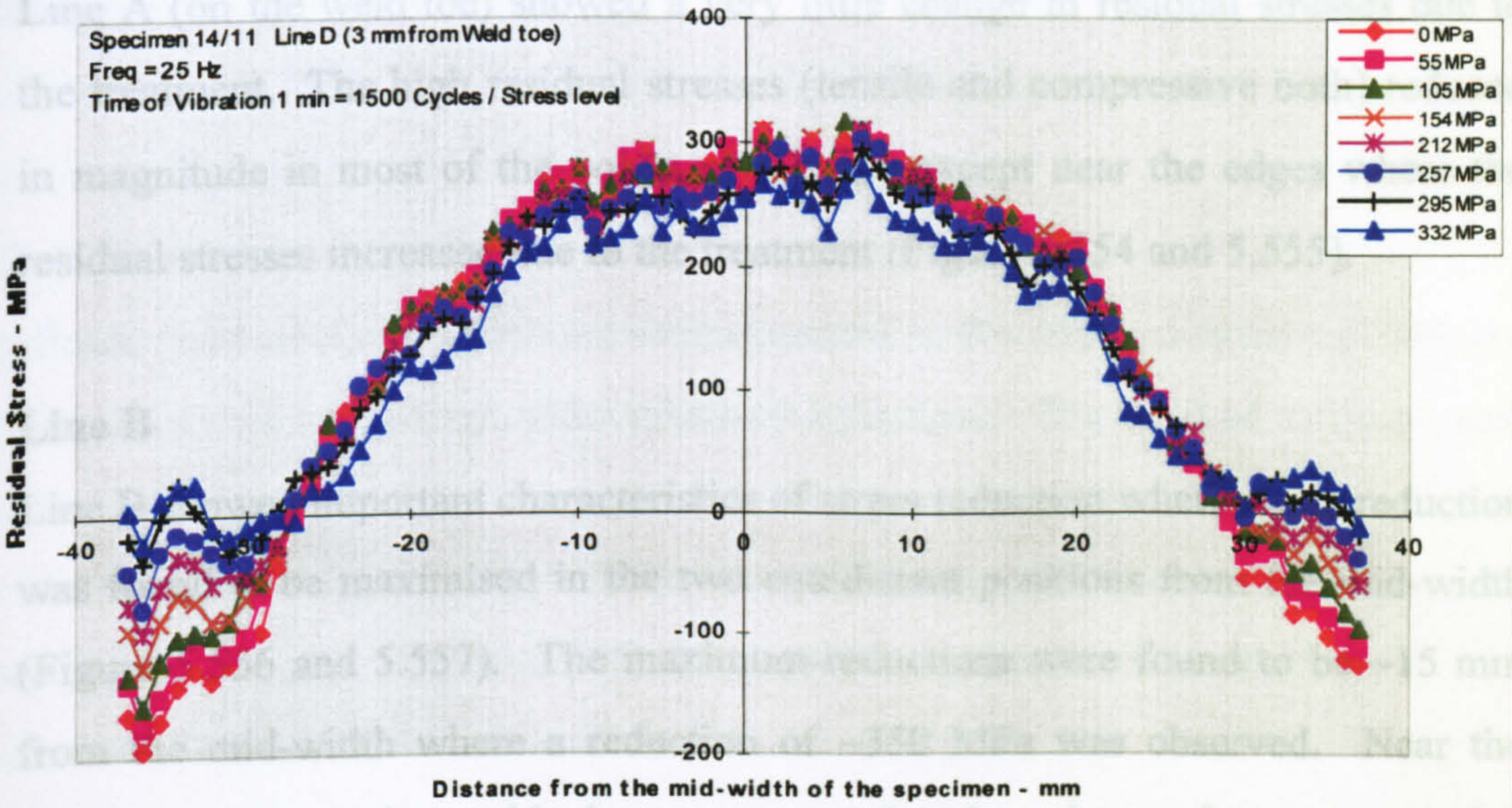

Figure 5.560 - Line stress plot - specimen 14/11 line D

Line D (Transverse Residual Stress versus Applied Stress Plot)

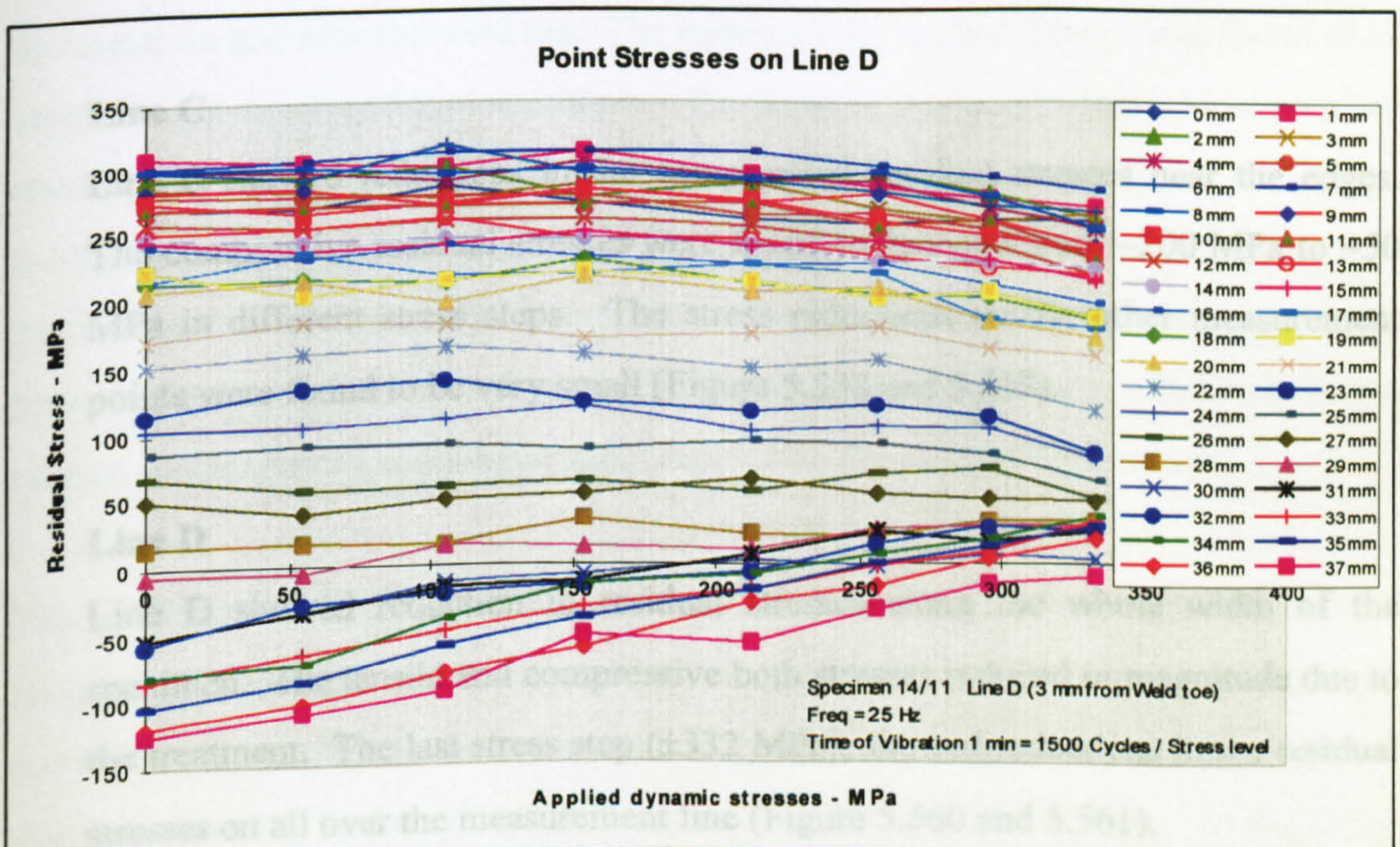

Figure 5.561 - Transverse residual stress versus applied stress plot - specimen 14/11 line D

Discussion of Results - Specimen 14/11

The results of the four different lines of the specimens are

Line A

Line A (on the weld toe) showed a very little change in residual stresses due to the treatment. The high residual stresses (tensile and compressive both) reduced in magnitude in most of the points of the line except near the edges where the residual stresses increased due to the treatment (Figure 5.554 and 5.555).

Line B

Line B showed important characteristics of stress reduction where stress reduction was found to be maximised in the two equidistant positions from the mid-width (Figure 5.556 and 5.557). The maximum reductions were found to be ~15 mm from the mid-width where a reduction of ~350 MPa was observed. Near the edges the compressive residual stresses were found to change from compressive stresses to zero stress or to positive stresses. A detailed discussion of the characteristics of stress reduction from this line is presented in the *summary of result* (Section 5.4.2.4)

Line C

Line C showed reductions in the compressive residual stresses near the edges. The compressive residual stresses were found to decrease from ~200 MPa to ~50 MPa in different stress steps. The stress reductions on the other measurement points were found to be very small (Figure 5.558 and 5.559).

Line D

Line D showed reduction in residual stresses along the whole width of the specimen. The tensile and compressive both stresses reduced in magnitude due to the treatment. The last stress step (±332 MPa), showed reductions in the residual stresses on all over the measurement line (Figure 5.560 and 5.561).

From the results of the four lines it was clear that stress reduction in the heat affected zone (HAZ) was maximum, and, away from the HAZ, stress reduction was not so significant. The peak residual stress in the specimen was ~600 MPa. The applied stress to the specimen was 332 MPa. This suggests that there was a possibility of local yielding due to the applied stresses.

5.4.2.4 Summary of the Results

Significant residual stress reductions were observed in this experiment in the different specimens - subjected to post weld vibratory treatment. The residual stresses were found to change up and down due to the first few short intervals of vibration. It seems that the residual stresses were a little unstable after short intervals of vibration. According to the plot (Figure 5.505) the residual stresses became stable after 1~2 minutes of vibration.

The residual stresses were found to be lesser in the electropolished specimens (specimens 13/4, 13/5, and 13/7), where the residual stress peaks were missing or shifted away from the weld toe. This happened due to the removal of stressed layer of the metal on and near the weld toe. The reduction in residual stresses was found to be higher in the electropolished specimens - the cause of this is unknown. Most possibly electropolishing removed a layer of metal (approximately 50 microns ~ 1.5 grains) from the surface which was severely distorted due to cold rolling processes. Removing the distorted crystal layers from the measurement surface, relatively regular crystals were on the surface where the VSR treatment worked more effectively or the change in the residual stress were read properly by the X-ray diffractometer.

The reduction in the residual stresses were found to be a function of the applied stresses. In specimen 13/7 the residual stresses were found to decrease in every increase in the applied dynamic stresses. Increase in the time of vibration in any stress step was found to be less effective in reduction of the residual stresses. In the lower applied stresses the residual stresses were found to be unchanged due to increase in the

time of vibration. In the higher applied stresses the residual stresses of all over the measurement line was found to increase. The reason of this increase was unknown, most possibly it happened due to strain hardening of the material. Thus, the effect of over treatment was found to be less effect in lower applied stresses but the higher applied stresses works very much against the reduction process of the VSR treatment. This phenomenon is observed in Figures 5.505, 5.507, 5.522 and 5.523, which will be further investigated in experiment IX.

The largest residual stress drops were found to be away from the mid-width of the specimen (specimen 13/8 to 14/11). It was observed that the reduction in the residual stresses of some area started earlier and continued dropping till the last step of treatment. The stress reduction at the mid-width was small. Near the edges, the compressive residual stresses decreased (mathematically increased). The Figure 5.562 shows the stress reduction characteristics along the width of the specimens.

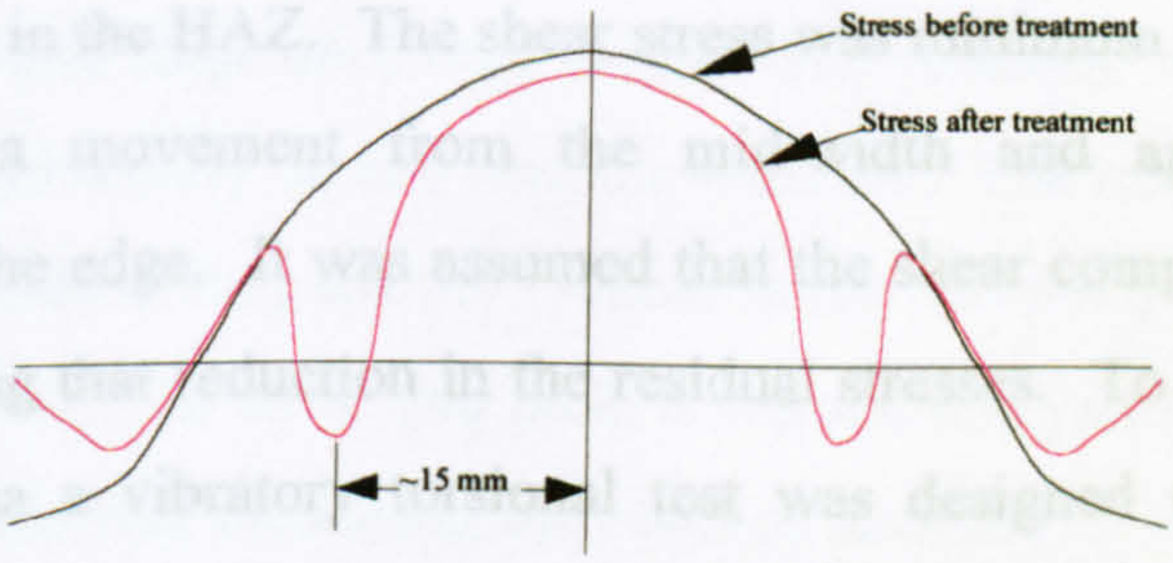

Figure 5.562 - Distribution of residual transverse stress on line B before and after treatment.

Two possible explanations can be given for the characteristics of the residual stress distribution observed in this experiment.

1. It happened due to the equilibrating characteristic of the residual stresses of the specimens. Since the tensile residual stresses of the specimen at the mid-width and adjacent areas are partially relieved and in same time the compressive residual stresses from the edge also reduced or changed to the tensile stresses. To equilibrate the change in the residual stresses in one area, some other area would

show different residual stresses from their own. In those areas, the distributed residual stresses from other areas would superimpose on the residual stresses of their own. In similar way, the residual stresses of the two equidistant area might show lower stresses from the actual stresses of them.

2. It is established from most of the researchers work that the applied stress reduces residual stress, but which component of the applied stress contribute most in relieving in the residual stresses still needs to be established. In this experiment the flat bar (3 inch × 1/4 inch) was vibrated applying dynamic stresses. The applied stresses in the flat bar took a complex shape (shown in FE analysis in Chapter 4) due to some factors - the boundary condition, weld, and width to thickness ratio of the plate etc. It might be possible that one component of the applied stress worked very effectively to relieve the residual stresses that is why some areas showed a large reduction in comparison to other areas. In the FE analysis it was seen that due to the vibratory applied stress a high level of shear stress was found in the HAZ. The shear stress was minimum at the mid-width and increases with a movement from the mid-width and again decreases with approaching to the edge. It was assumed that the shear component of the applied stress was causing that reduction in the residual stresses. To investigate the shear stress phenomena a vibratory torsional test was designed which are shown in Experiment X.

The reduction in the residual stress was found to be maximum in the heat affected zone, this observation brought a strong point in favour of VSR process over thermal and/or other processes. The other treatment processes work on the whole specimen and change the necessary mechanical and chemical properties. Contrary to that the VSR process works in a very localised area and does not change the essential properties of the structure.

5.4.3 Experiment IX:

Investigation of Residual Stress Characteristics During Fatigue Failure.

Abstract

In this experiment four specimens were vibrated to investigate the characteristics of the residual stress just before fatigue failure. In all four specimens high levels of dynamic stress were applied. It was found that the residual stresses were redistributed before failure. Thus, the assumption that the residual stress increased before breaking from Experiment VIII was not confirmed.

5.4.3.1 Introduction

This experiment was designed following the tests on specimens 13/1 and 13/2 (Experiment VIII) where it was observed that the stresses on the weld toe and adjacent area of the specimen were increased significantly before fatigue failure. In those specimens applied dynamic stress was kept constant to ±300 MPa and the specimens were vibrated in several steps until they failed. The resulting residual stresses were found to increase significantly on and near the weld toe. The residual stresses of both of the specimens increased very sharply (visible in the two point stress plots shown in Figure 5.505 and 5.507). In those two plots it seemed that just before fatigue failure every single load cycle was increasing the residual stresses. If these increases in the residual stresses were the characteristic of the material then it would be very dangerous for the structures loaded with high dynamic stresses. According to those two plots it would create a vicious circle of increase in the residual stresses and would accelerate the fatigue failure. To investigate that phenomenon, this experiment was carried out.

5.4.3.2 Experimental Procedure

In this experiment four cold rolled specimens were processed. Two of them were processed as welded and the other two were annealed after welding to relieve the residual stresses then they were processed for this test. Longitudinal and transverse residual stresses were measured for observation. To observe the longitudinal residual

stresses one as-welded and one annealed specimen were used. The other two specimens (one annealed and other as welded) were left for the observation of transverse stresses.

The experimental set-up and calibration constant of this experiment was similar to the set-up and calibration constant of Experiment III. The same welding instruments were used to weld the specimens. The same welding speed controller controlled the welding speed. The annealing conditions are provided in the description of the respective specimens. The residual stresses were measured with the X-ray diffractometer using the mapping procedure. In the area mapping the single exposure technique (SET) was used. In the as-welded specimens the X-ray measurement conditions were similar to the measurement conditions described in Table 5.10. In the annealed specimens the measurement conditions were changed because of distortion of the measurement profiles due to large grain size of the metal. An oscillation of the X-ray head was added to the measurement process which reduced the distortion of the profiles significantly. The number of exposures was increased from 2 to 4 to increase the diffracted X-ray input to the detectors, which decreased the possibility of error. Details of the X-ray parameters for the annealed specimens are shown in the Table 5.52 below.

Table 5.52 – X-ray measurement conditions – annealed specimens

X-ray type	Cr K-Alpha
Bragg Angle	156.1 degree
Measurement angle, β	30 degree
Oscillation of β angle	5 degree
Peak fit	Gaussian
Number of exposure	4

In this experiment the specimens were vibrated applying higher dynamic stresses. The dynamic stress was kept constant and the vibration time was increased in several steps until the specimens broke. The details of the vibratory conditions are shown in the residual stress plots.

5.4.3.3 Experimental Results

Specimen 24/14

This specimen was welded without any treatment. The residual stresses on the selected line (Figure 5.563) were measured and then it was vibrated applying a dynamic stress of ±373 MPa. The specimen was vibrated until it broke, the time intervals of vibration are shown in the plots. On the half width of the specimen 18 lines were selected, leaving 4 mm near the edge. The longitudinal residual stresses of the lines were measured using the mapping procedure, then the data of the individual line were extracted from the map and plotted separately as line and point stress plots. The stress plots of all of the lines showed the same message, instead of the results of all 18 lines the results of selected 3 lines (line A, F, and M) are shown here to save some space.

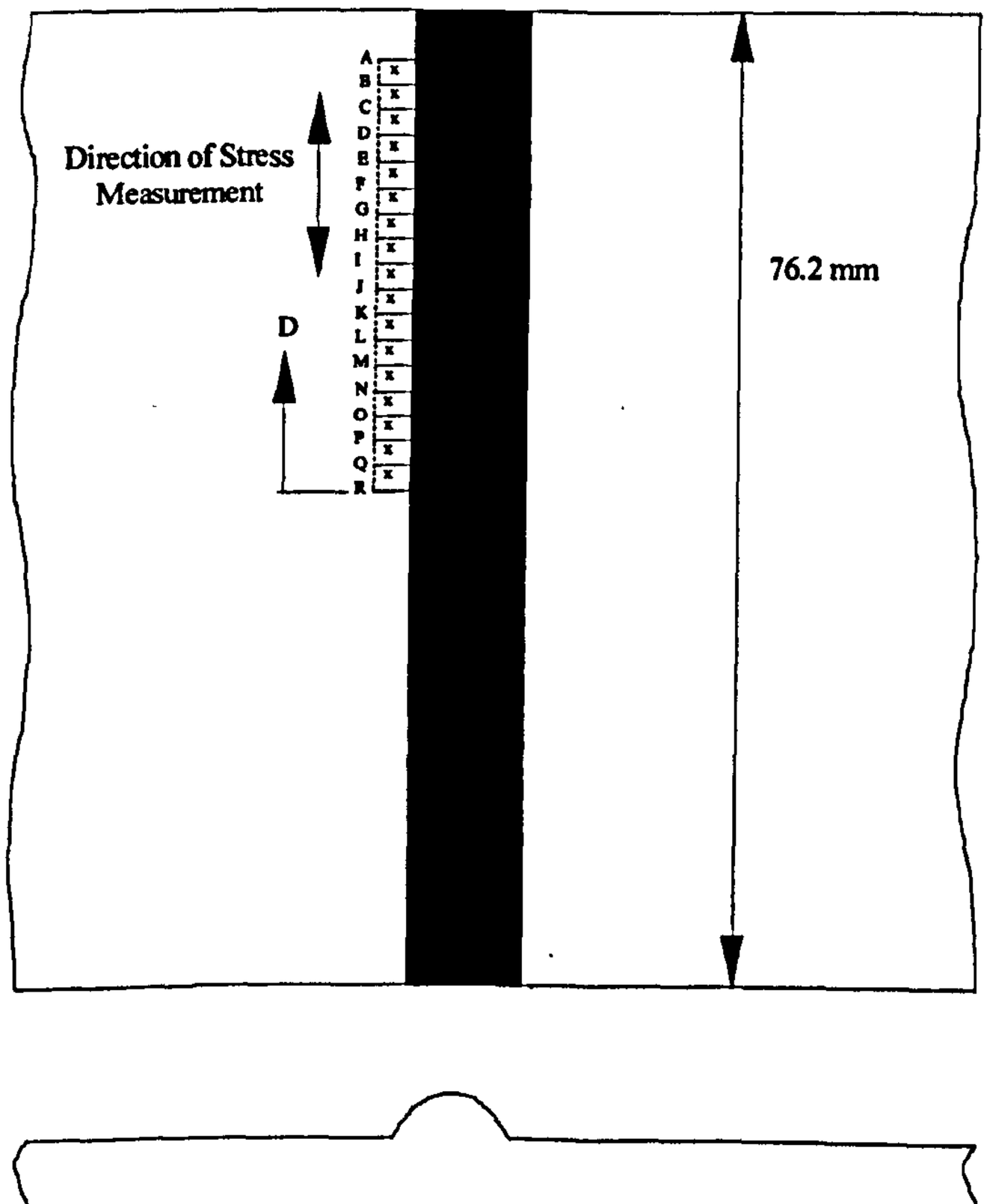

Figure 5.563 - Position of measurement lines - specimen 24/14

Specimen 24/14 (D = 17 × X mm)

Line A (Line Stresses)

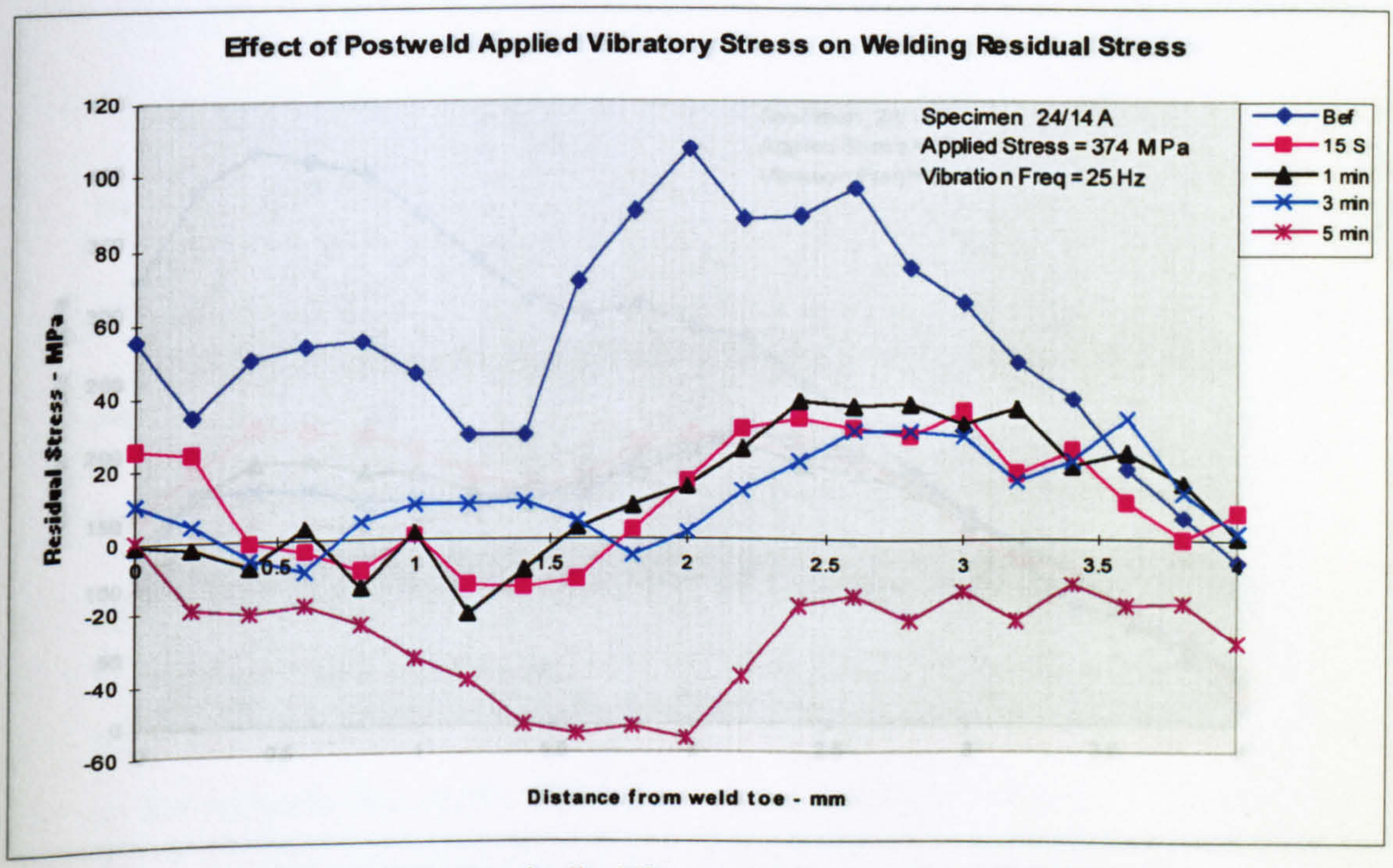

Figure 5.564 – Longitudinal line stress plot - specimen 24/14 line A

Line A (Point Stresses)

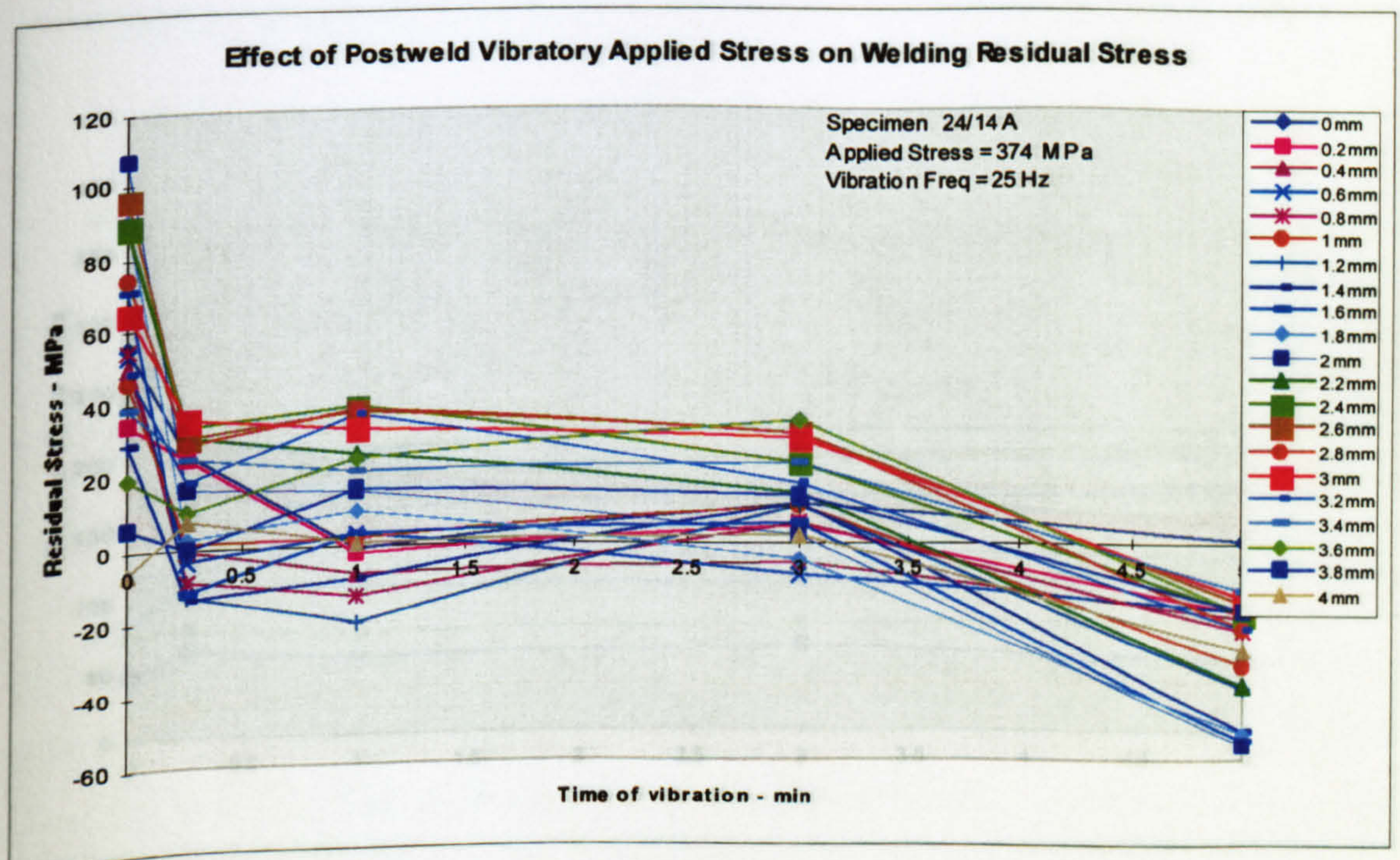

Figure 5.565 – Longitudinal point stress plot - specimen 24/14 line A

Specimen 24/14 (D = 12 × X mm)

Line F (Line Stresses)

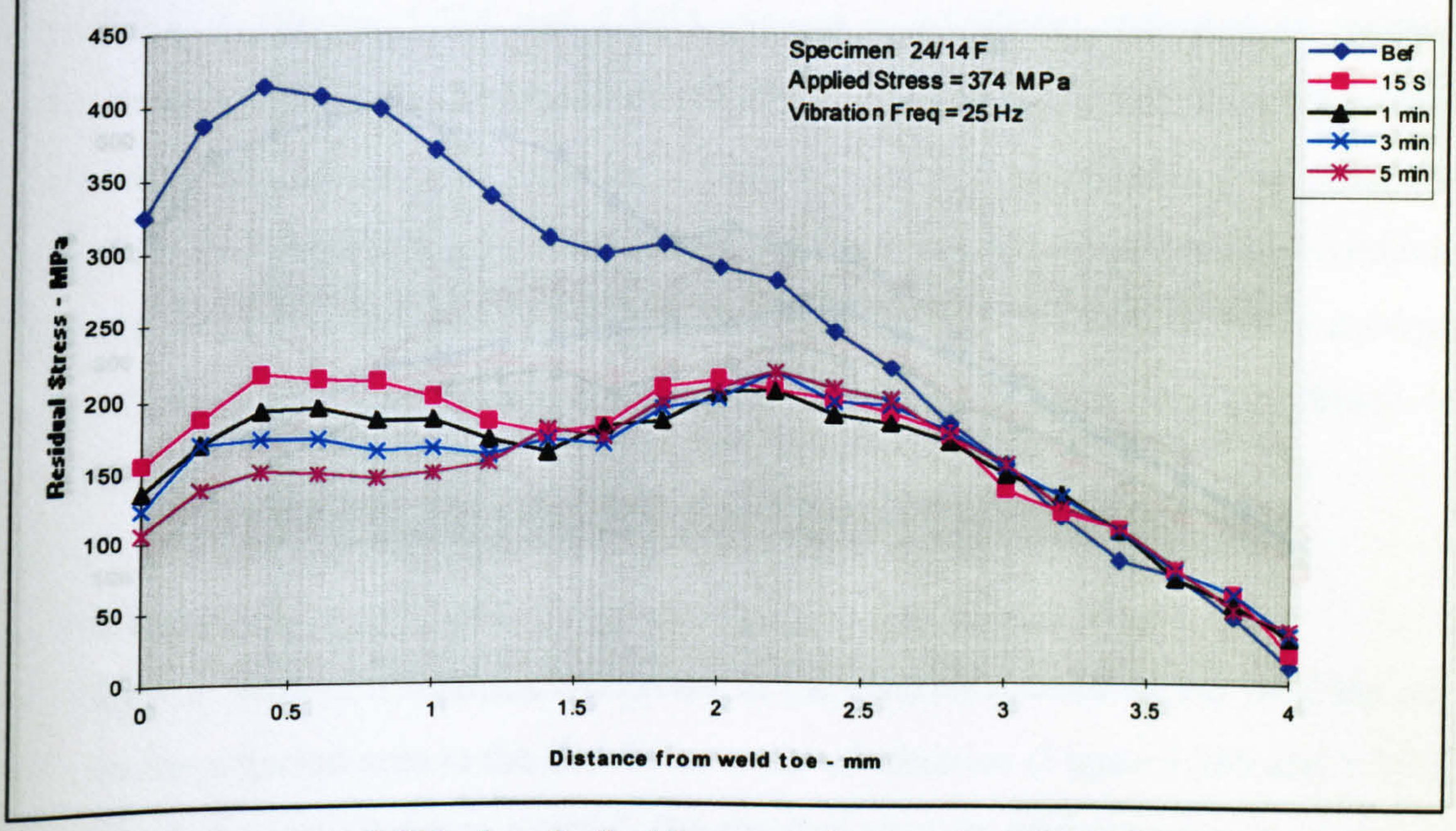

Figure 5.566 – Longitudinal line stress plot - specimen 24/14 line F

Line F (Point Stresses)

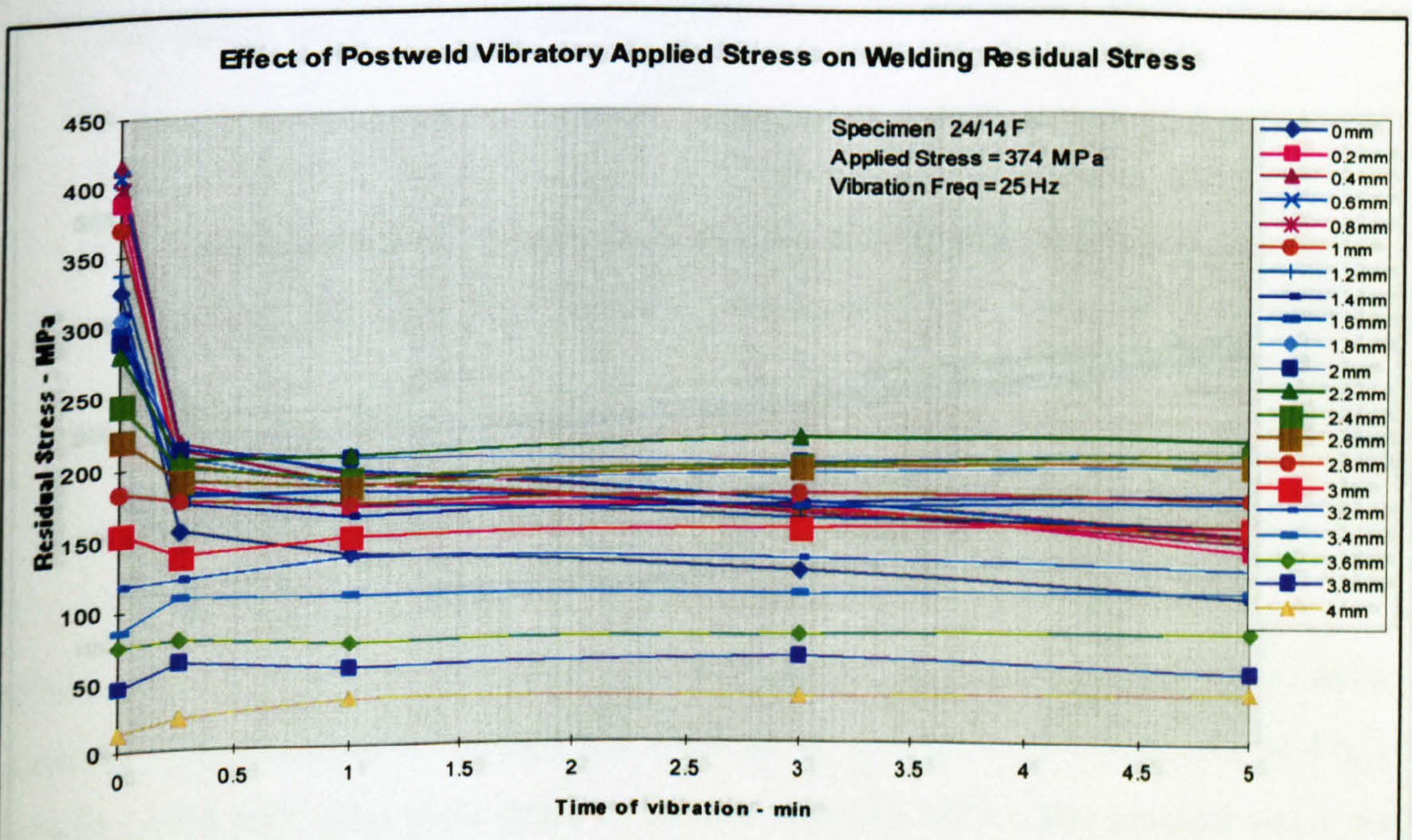

Figure 5.567 – Longitudinal point stress plot - specimen 24/14 line F

Specimen 24/14 (D = 5 × X mm)

Line M (Line Stresses)

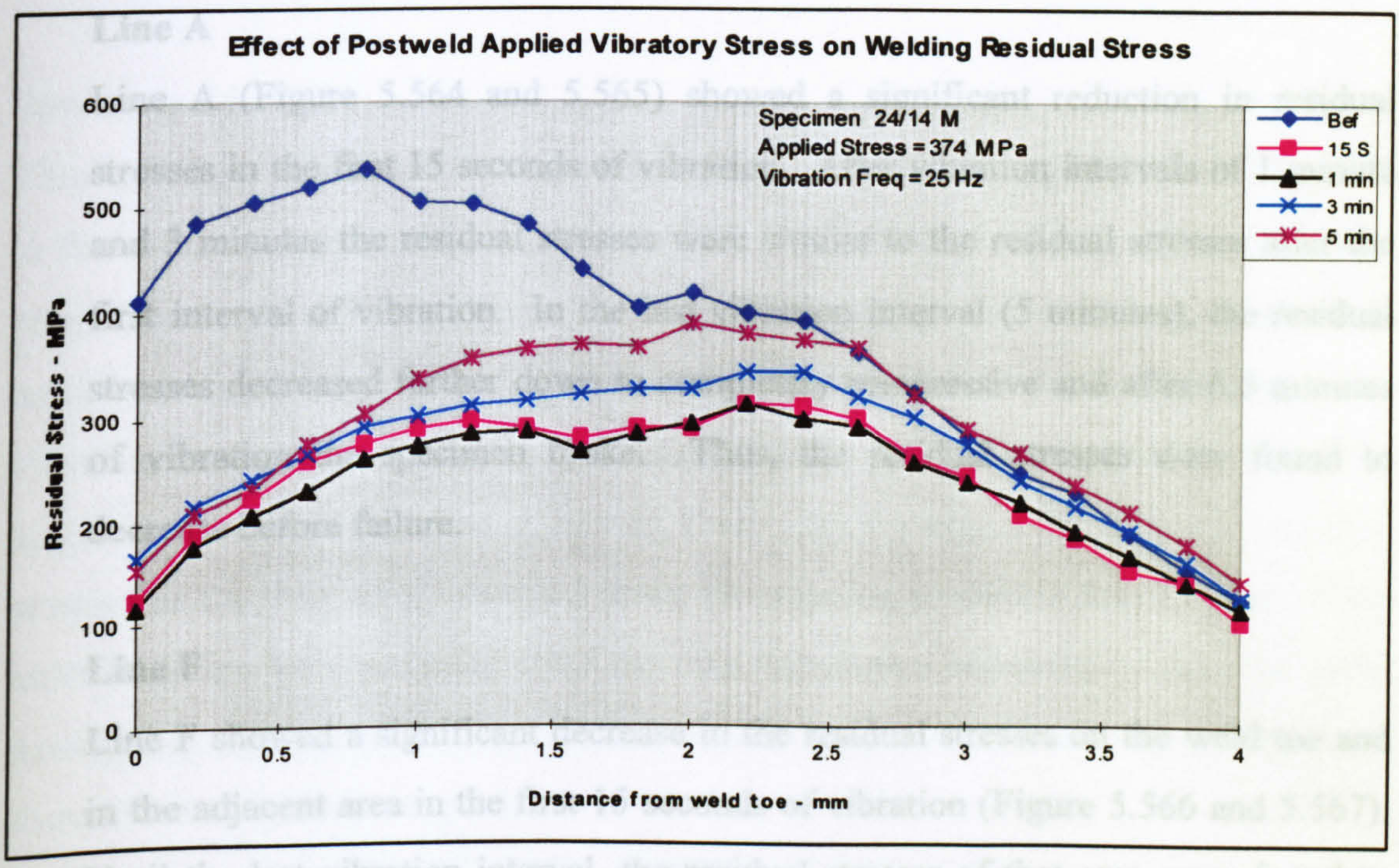

Figure 5.568 – Longitudinal line stress plot - specimen 24/14 line M

Line M (Point Stresses)

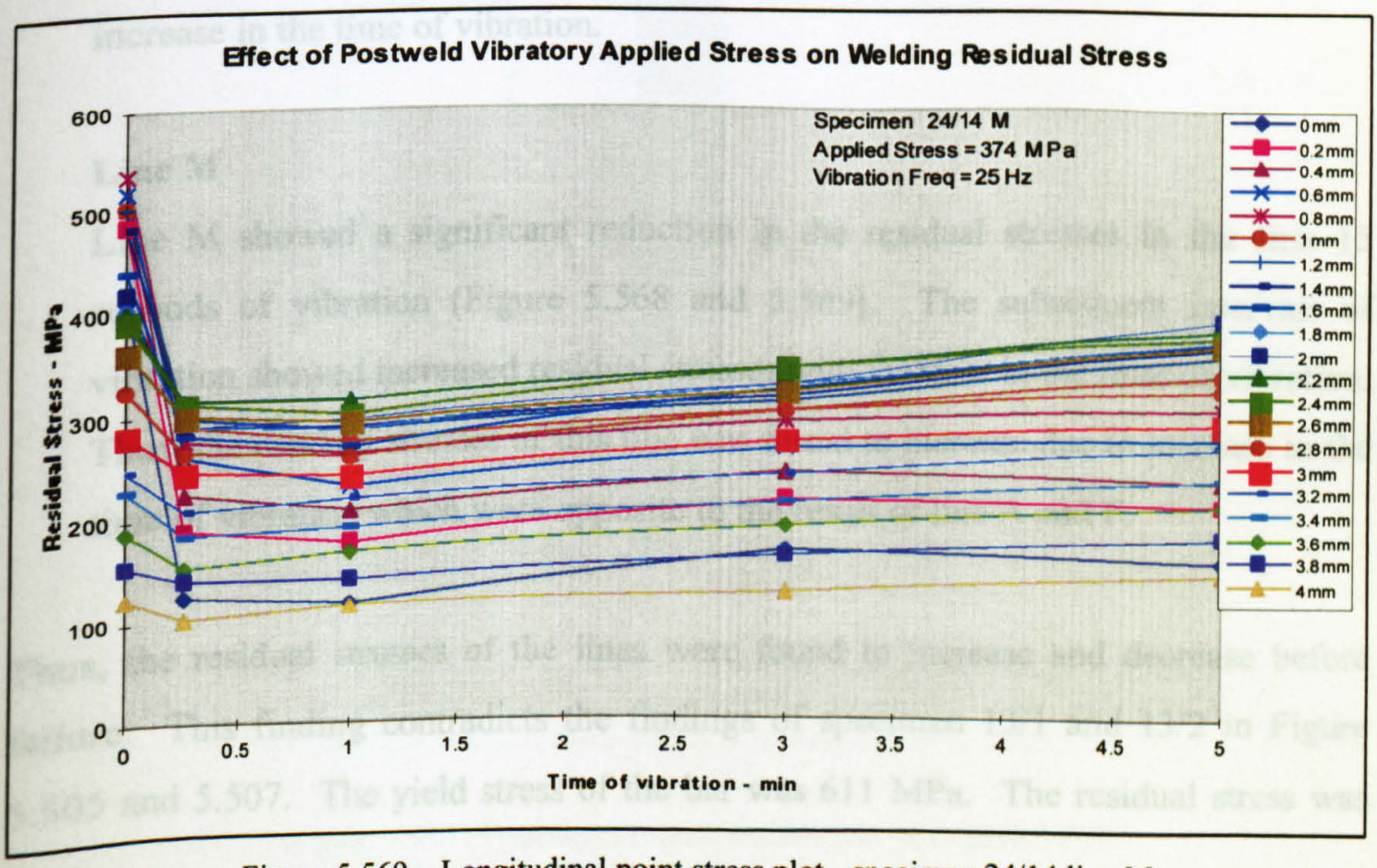

Figure 5.569 – Longitudinal point stress plot - specimen 24/14 line M

Discussion of Result - Specimen 24/14

The results of the selected lines are

Line A

Line A (Figure 5.564 and 5.565) showed a significant reduction in residual stresses in the first 15 seconds of vibration. After vibration intervals of 1 minute and 3 minutes the residual stresses were similar to the residual stresses after the first interval of vibration. In the last vibration interval (5 minutes), the residual stresses decreased further down to completely compressive and after 6.5 minutes of vibration the specimen broke. Thus, the residual stresses were found to decrease before failure.

Line F

Line F showed a significant decrease in the residual stresses on the weld toe and in the adjacent area in the first 15 seconds of vibration (Figure 5.566 and 5.567). Until the last vibration interval, the residual stresses of that area were found to decrease but away from the weld toe (distance range 2.7-4 mm) the residual stresses were unchanged. Thus, in this line the residual stresses decreased with increase in the time of vibration.

Line M

Line M showed a significant reduction in the residual stresses in the first 15 seconds of vibration (Figure 5.568 and 5.569). The subsequent intervals of vibration showed increased residual stresses with increase in the time of vibration. Thus, the residual stresses of this line was found to increase due to increase in the time of vibration which were opposite to the result of line A and F.

Thus, the residual stresses of the lines were found to increase and decrease before failure. This finding contradicts the findings of specimen 13/1 and 13/2 in Figure 5.505 and 5.507. The yield stress of the bar was 611 MPa. The residual stress was

above 500 MPa and the applied stress was ±374 MPa, thus there was a large possibility of local yielding in the treatment process.

Specimen 24/17

This specimen was welded without any treatment. When the specimen cooled down to the room temperature the residual stresses was measured. The measurement lines of specimens are shown in Figure 5.570. The specimen was vibrated in some intervals until it broke where a constant dynamic stress of ±373 MPa was applied. The vibration intervals are shown in the residual stress plots. On the half width of the specimen 19 lines were selected, leaving 2 mm near the edge. The transverse residual stresses of the lines were measured using the mapping procedure then the data of the individual line were extracted from the map and plotted separately as line and point stress plots. Instead of the results of all 19 lines the results of some selected lines are shown here to save some space.

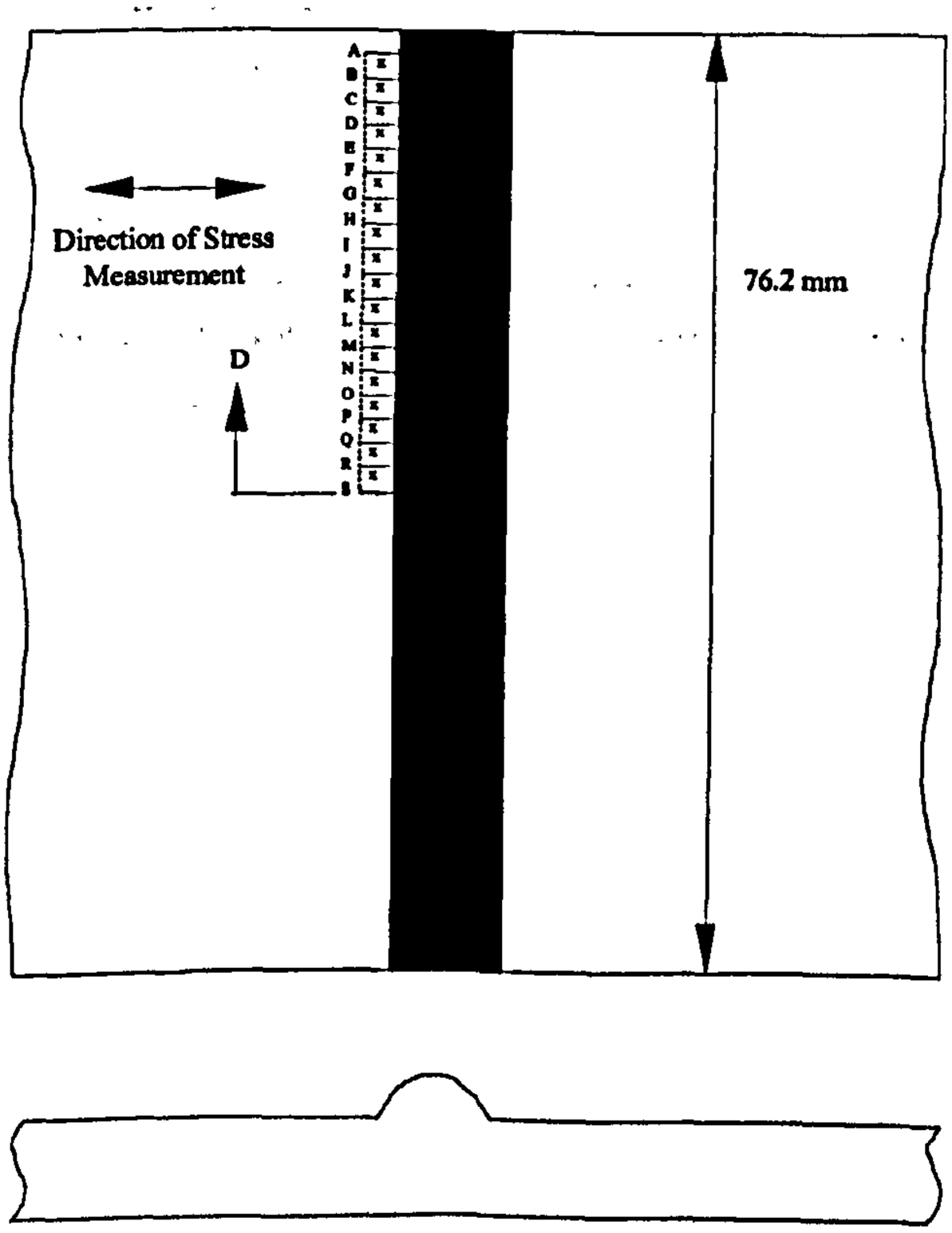

Figure 5.570 - Position of measurement lines - specimen 24/17

Specimen 24/17 (D = 18 × X mm)

Line A (Line Stresses)

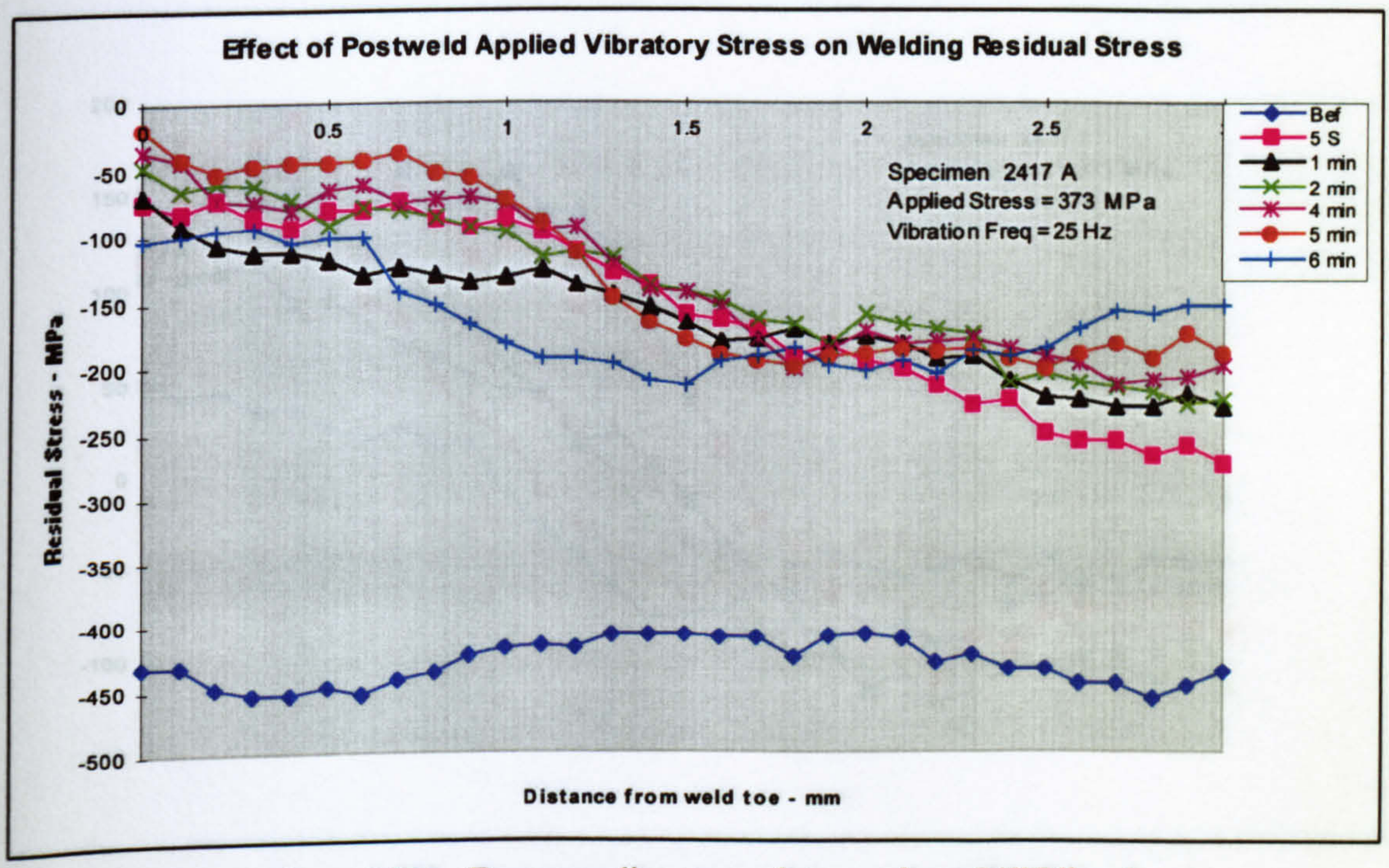

Figure 5.571 – Transverse line stress plot - specimen 24/17 line A

Line A (Point Stresses)

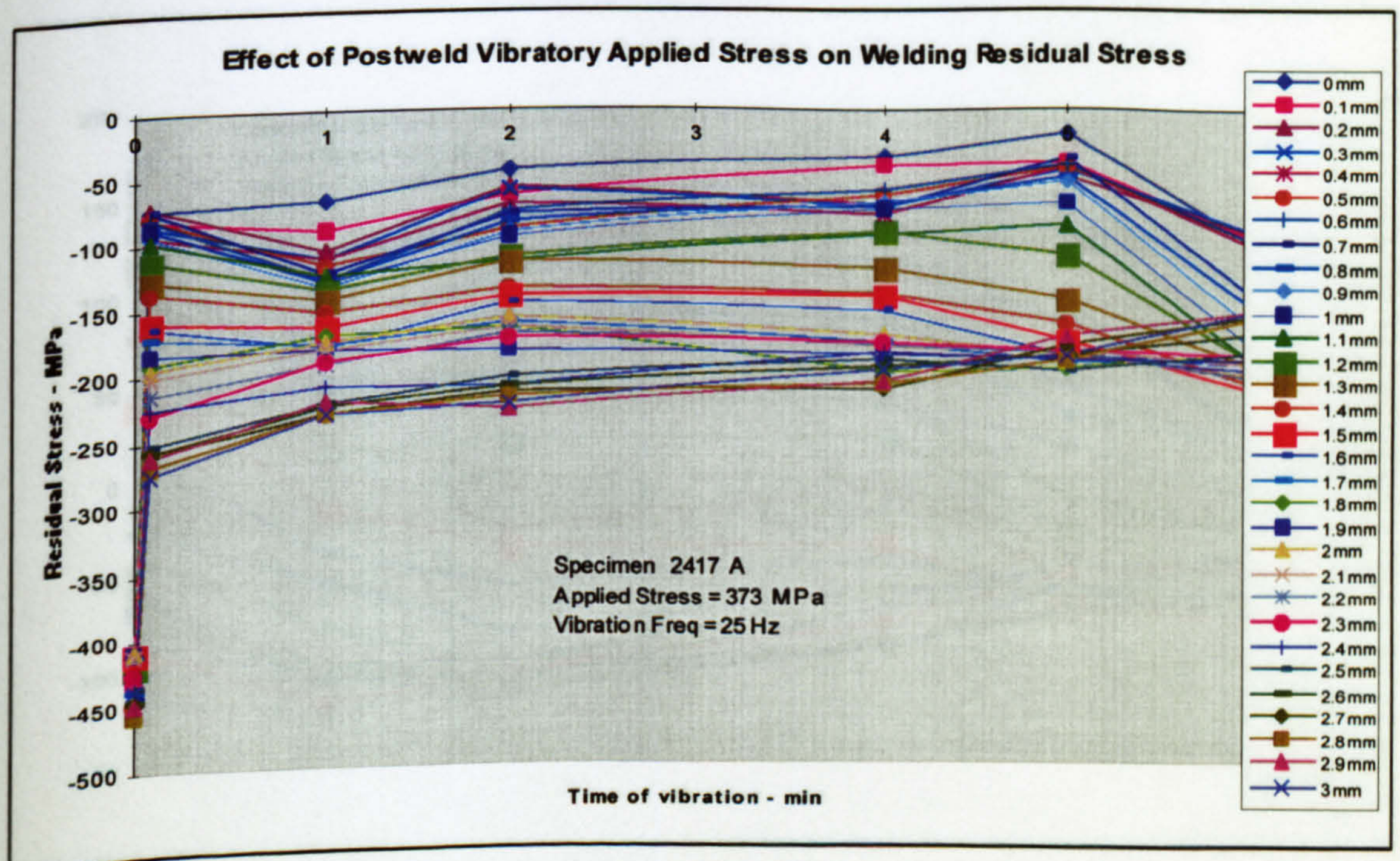

Figure 5.572 – Transverse point stress plot - specimen 24/17 line A

Specimen 24/17 (D = 10 × X mm)

Line I (Line Stresses)

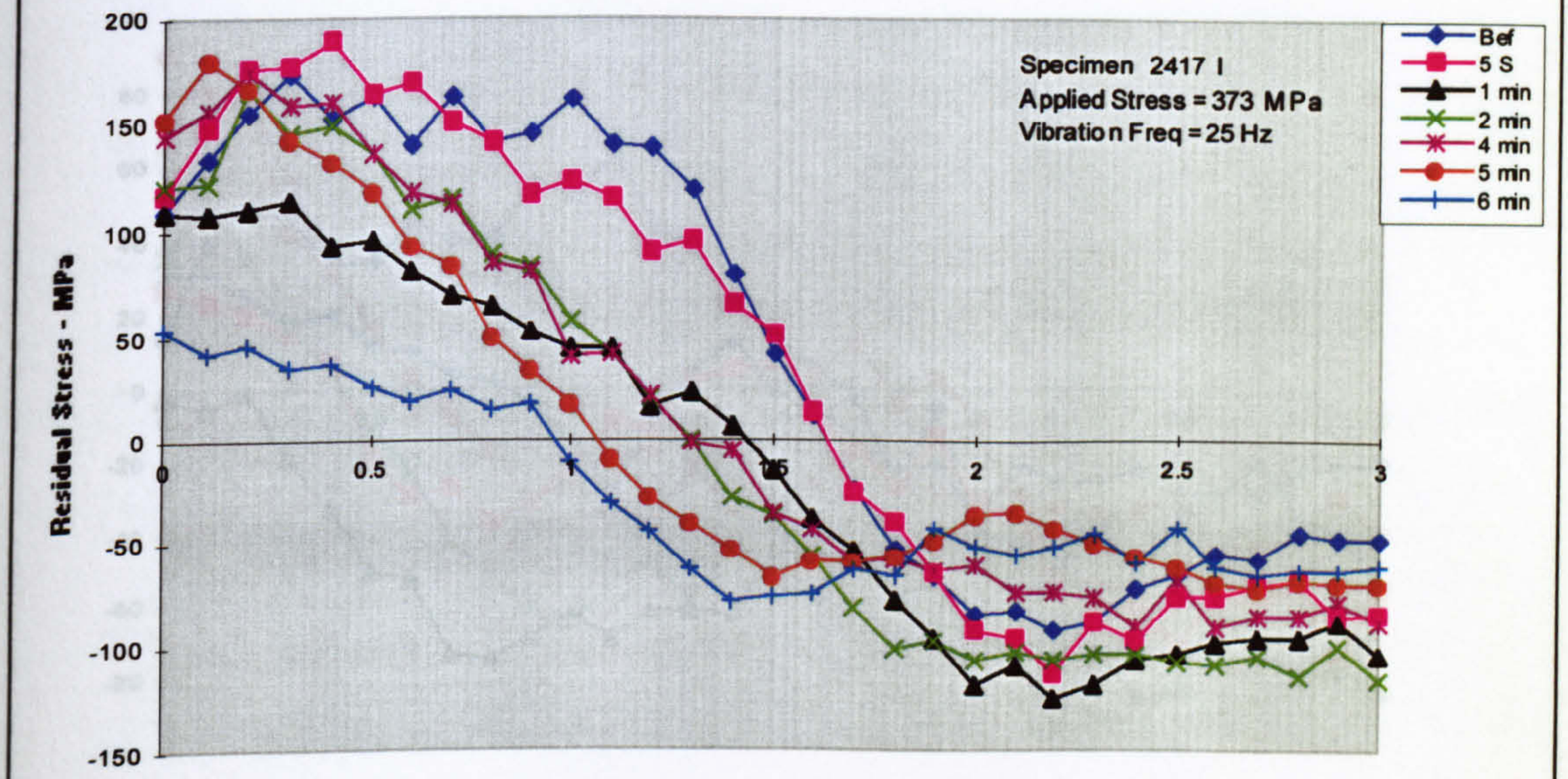

Figure 5.573 – Transverse line stress plot - specimen 24/17 line I

Line I (Point Stresses)

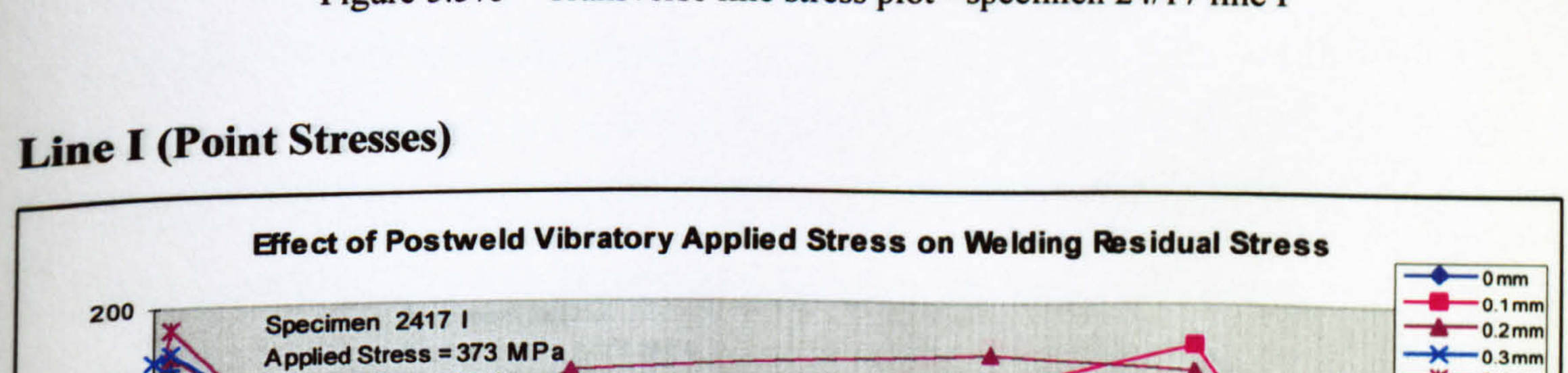

Figure 5.574 – Transverse point stress plot - specimen 24/17 line I

Specimen 24/17 (D = 9 × X mm)

Line J (Line Stresses)

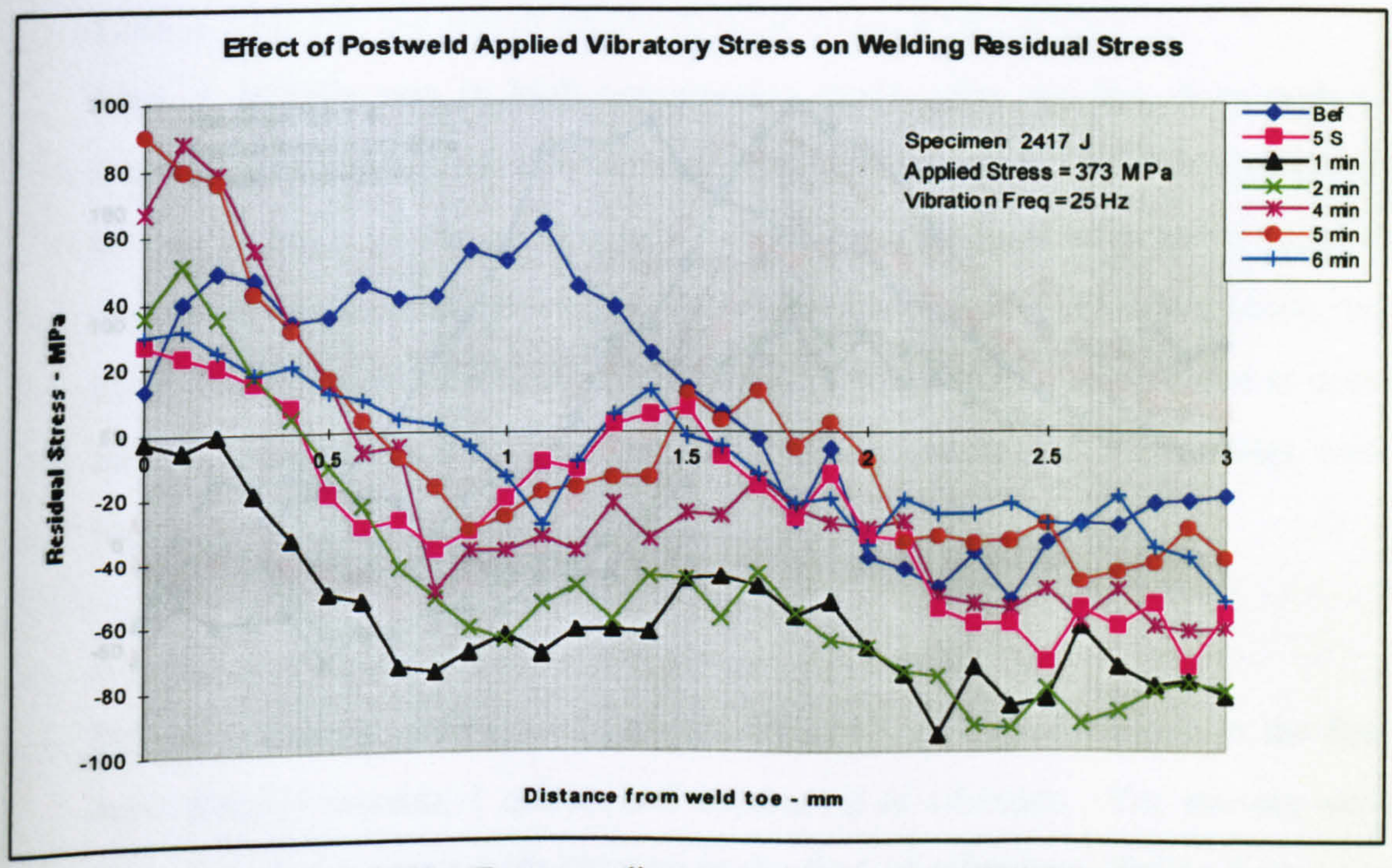

Figure 5.575 – Transverse line stress plot - specimen 24/17 line J

Line J (Point Stresses)

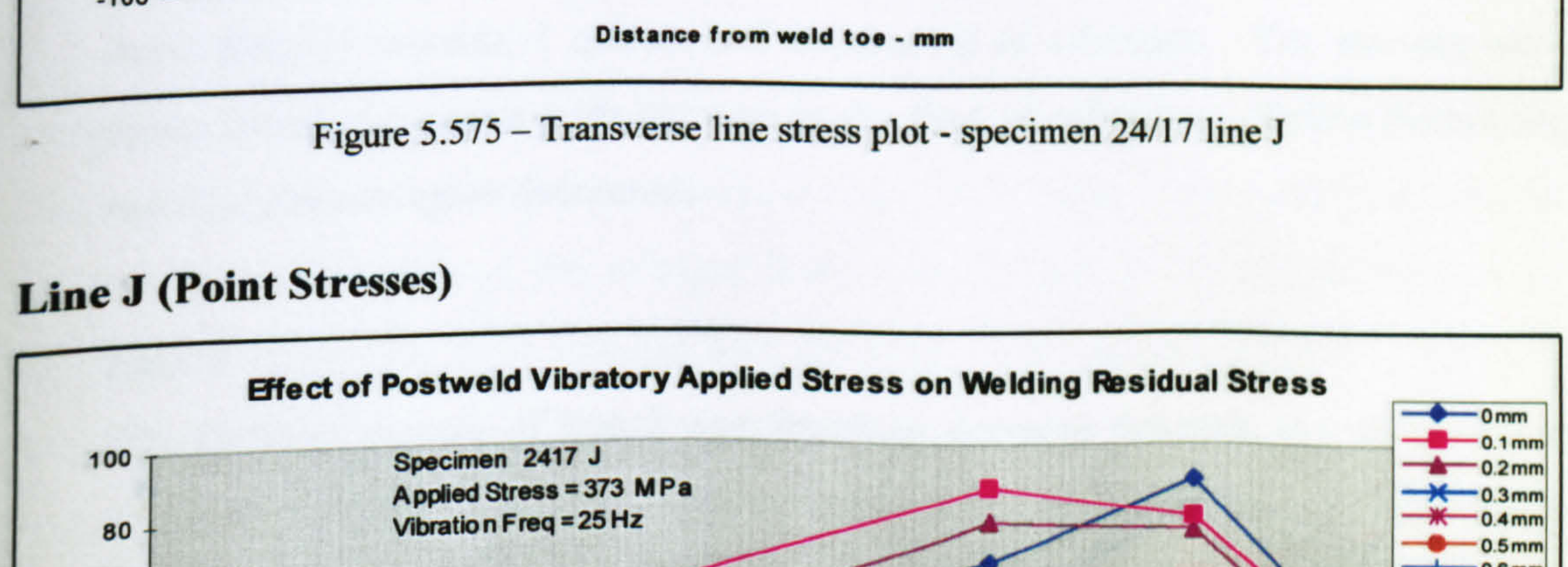

Figure 5.576 – Transverse point stress plot - specimen 24/17 line J

Specimen 24/17 (D = 0 × X mm)

Line S (Line Stresses)

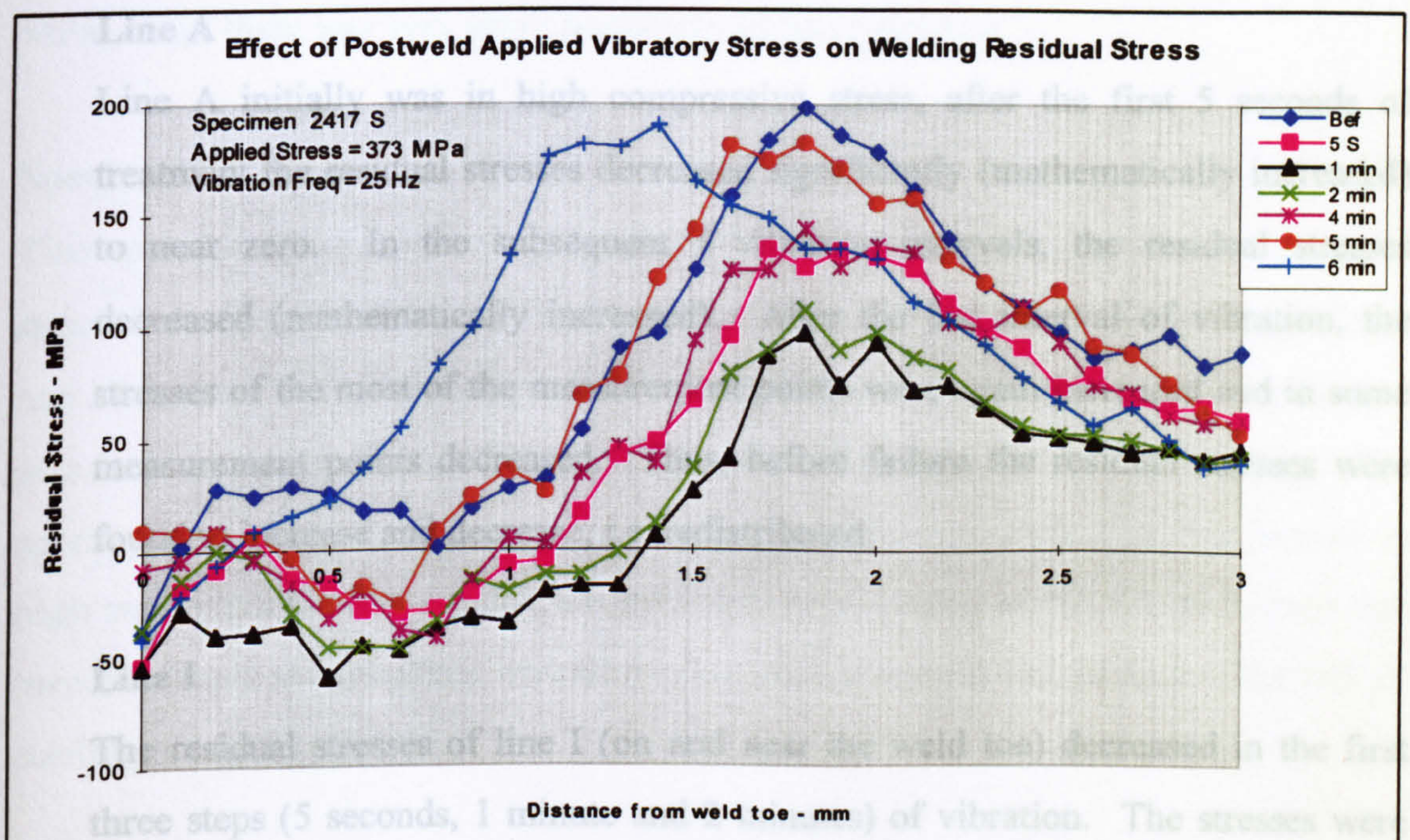

Figure 5.577 – Transverse line stress plot - specimen 24/17 line S

Line S (Point Stresses)

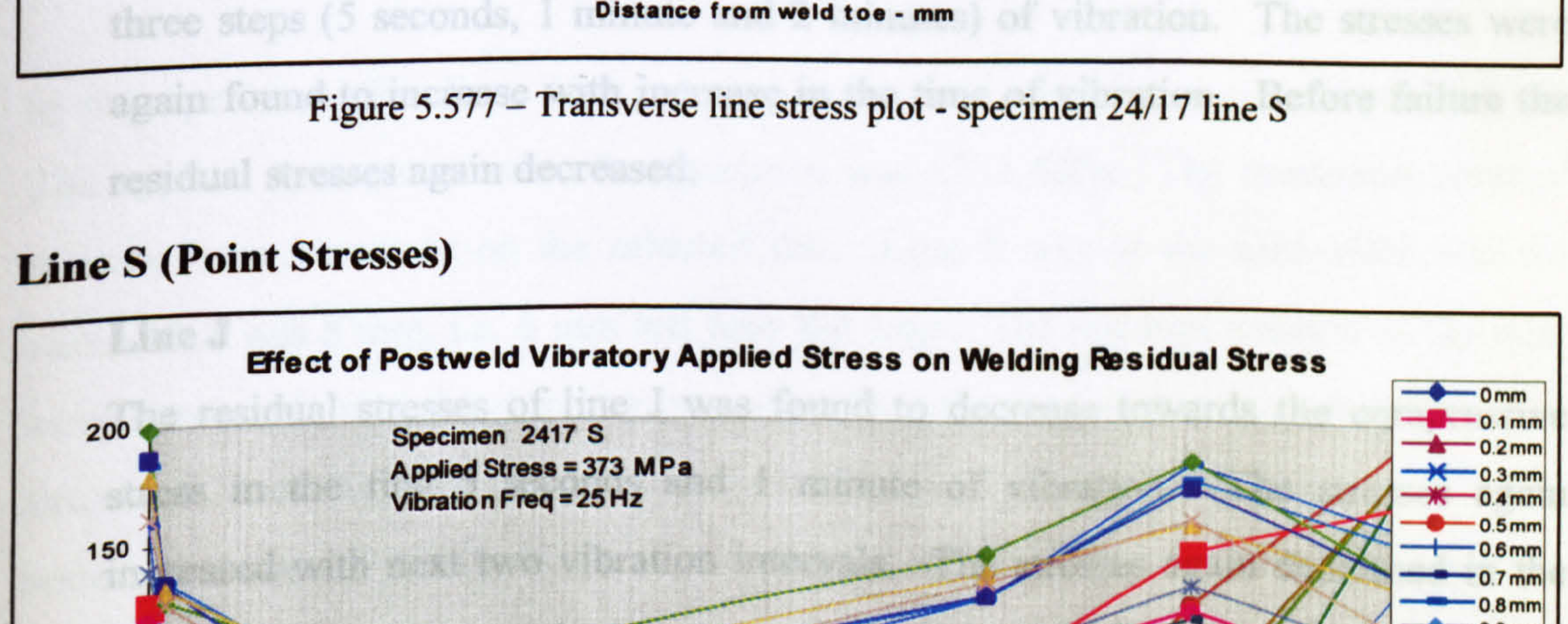

Figure 5.578 – Transverse point stress plot - specimen 24/17 line S

Discussion of Results - Specimen 24/17

The results of the selected lines are

Line A

Line A initially was in high compressive stress, after the first 5 seconds of treatment the residual stresses decreased significantly (mathematically increased) to near zero. In the subsequent 5 vibration intervals, the residual stresses decreased (mathematically increased). After the last interval of vibration, the stresses of the most of the measurement points were again increased and in some measurement points decreased. Thus, before failure the residual stresses were found to increase and decrease, i.e. redistributed.

Line I

The residual stresses of line I (on and near the weld toe) decreased in the first three steps (5 seconds, 1 minute and 2 minutes) of vibration. The stresses were again found to increase with increase in the time of vibration. Before failure the residual stresses again decreased.

Line J

The residual stresses of line J was found to decrease towards the compressive stress in the first 5 seconds and 1 minute of vibration. The stresses again increased with next two vibration intervals. The stresses again decreased in the last two vibration intervals. Some measurement points showed an increase in the residual stresses until the last interval of vibration. Thus, before failure the specimen only redistribution was observed.

Line S

Line S showed a significant reduction in residual stresses in the first 5 seconds and next 1 minute of vibration. The stresses again increased until the fifth vibration interval (5 minutes of vibration). In the last vibration interval, the residual stresses were found to be only redistributed.

Thus the residual stresses of this specimen showed no particular trend just before failure. Only redistribution in the residual stresses was observed. The sum of the applied and residual stress in this specimen was much lower than the yield stress (611 MPa), thus, there was very small possibility of local yielding.

Specimen 24/2

This specimens was made of cold rolled mild steel bar identical to the previous two specimens. Similar to the previous two specimens this specimen was welded without any treatment. Before carrying out the vibration treatment this specimen was annealed in a heat treatment furnace to relieve the residual stresses formed by welding. The specimen was coated with anti-oxidant coating to prevent rusting in the furnace at high temperatures. In annealing the specimens were heated to 913 ^{0}C the furnace was turned off and the specimen was allowed to cool slowly in the furnace. The rate of cooling was not measured.

In this specimen, five lines were selected in the half width (shown in Figure 5.579). The applied dynamic stress to the specimen was ±332 MPa. The transverse residual stresses were measured on the selected line. Line E was at the mid-width and the value of X was 8 mm, i.e. 6 mm left near the edge. The residual stresses of the lines were measured using the mapping procedure then the data of the individual line were extracted from the map and plotted separately as line and point stress plots. The residual stresses of all five lines were measured and plotted. Instead of the results of all five lines, the results of three lines are shown here to save some space.

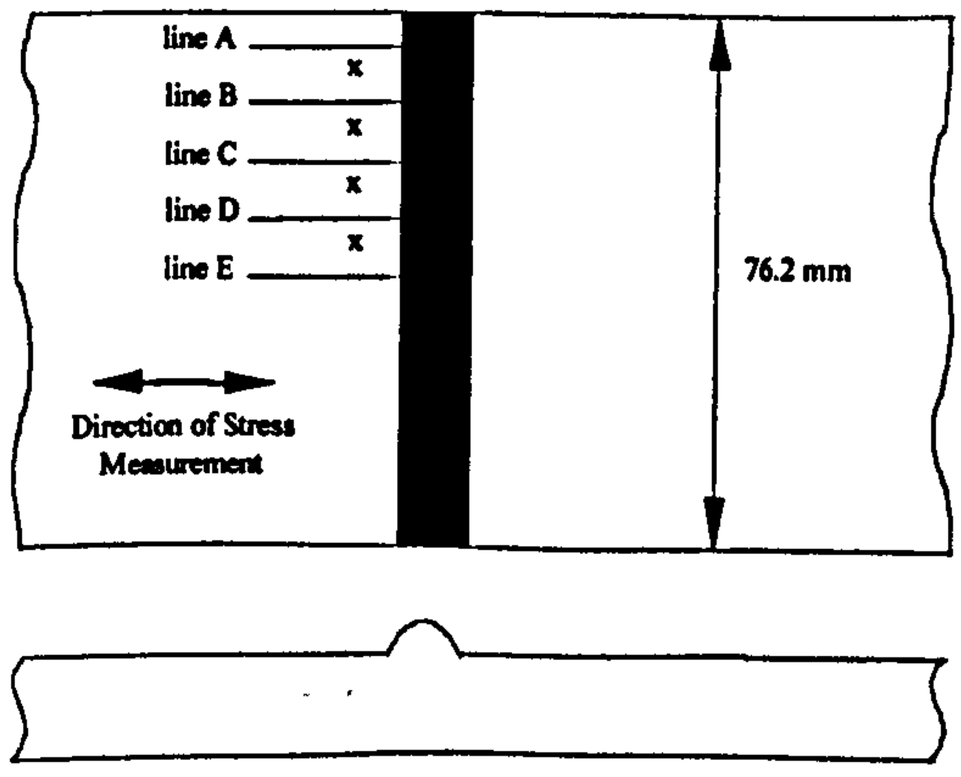

Figure 5.579 - Position of measurement lines - specimen 24/2

Specimen 24/2 (D = X × 4 mm)

Line A (Line Stresses)

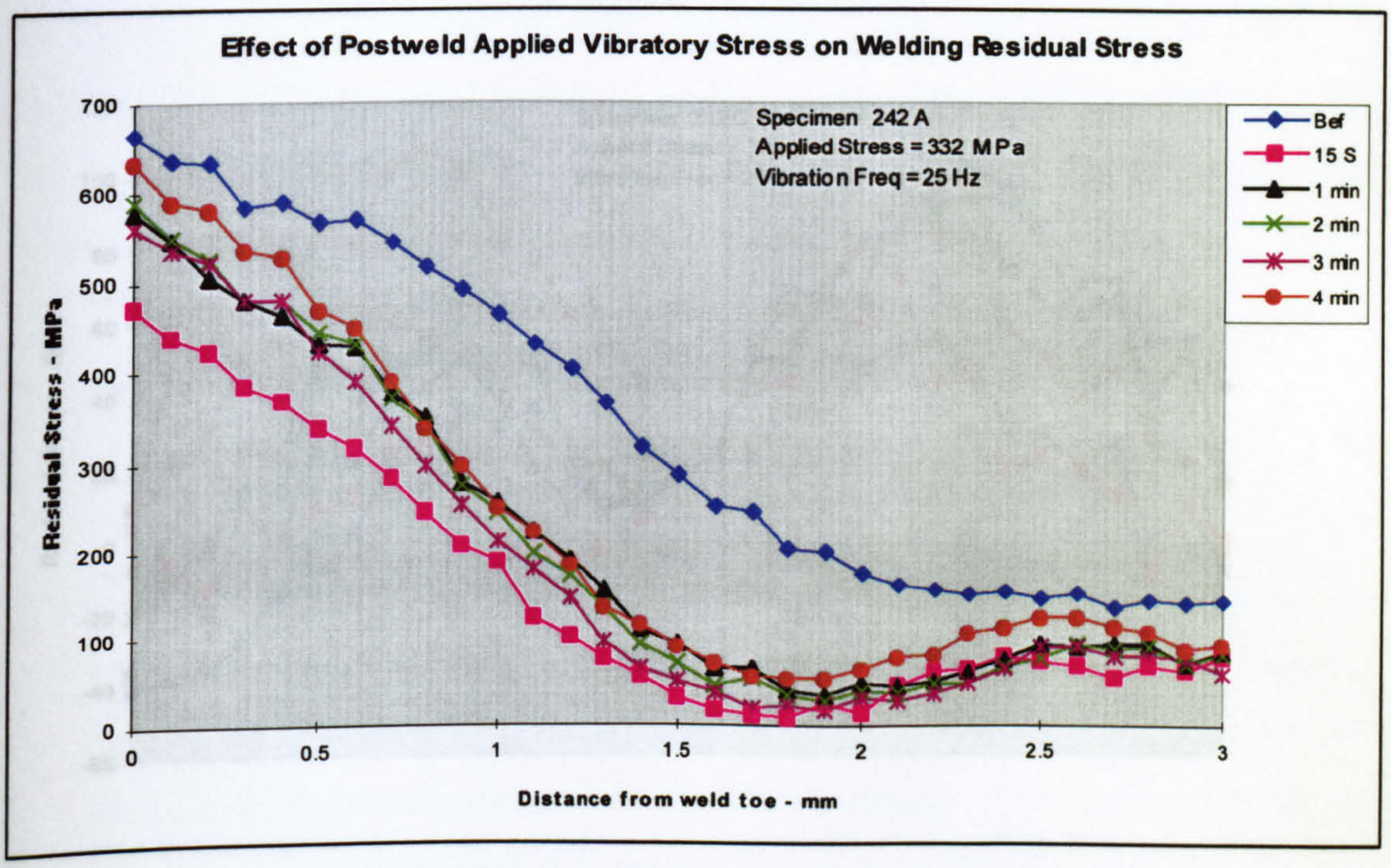

Figure 5.580 – Transverse line stress plot - specimen 24/2 line A

Line A (Point Stresses)

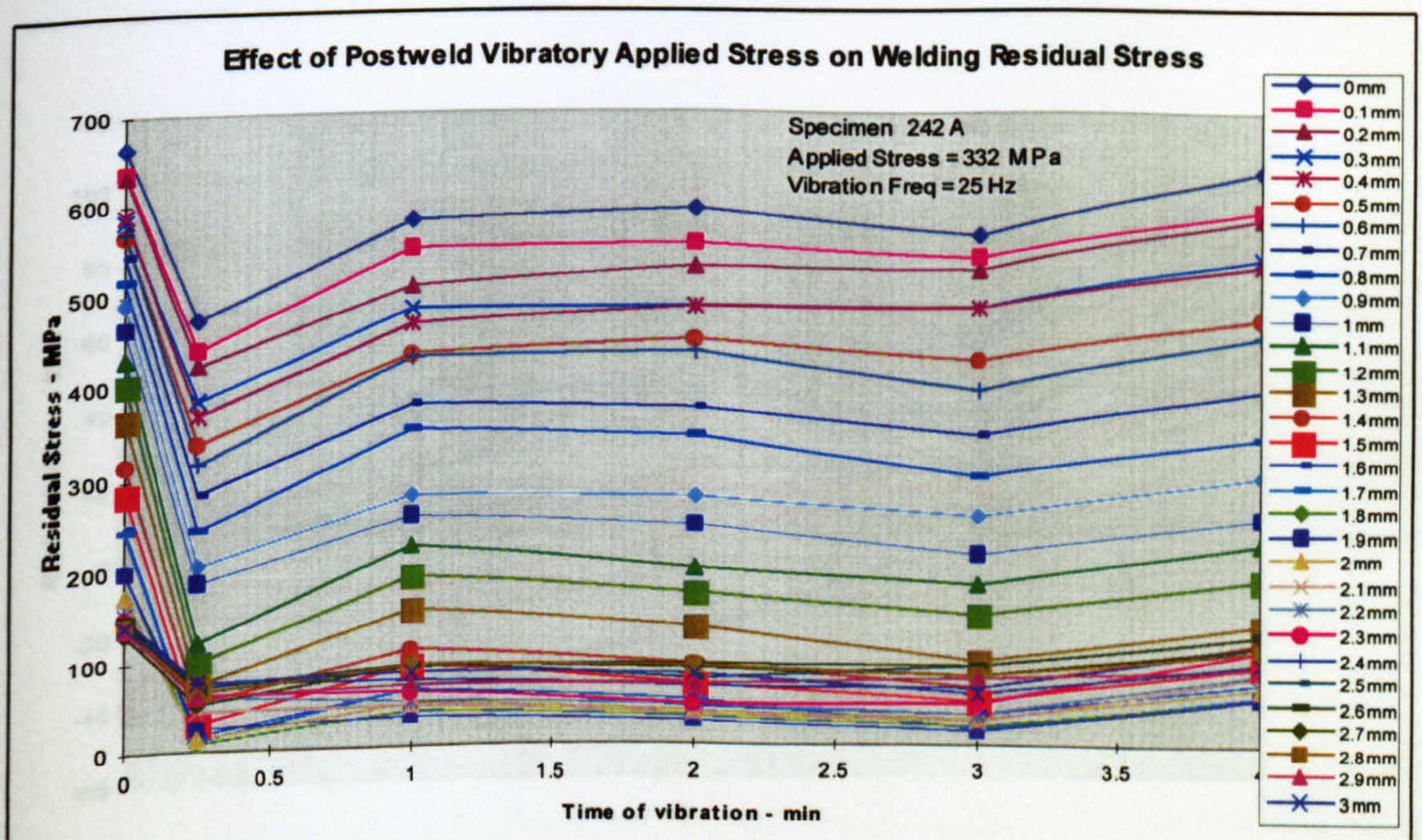

Figure 5.581 – Transverse point stress plot - specimen 24/2 line A

Specimen 24/2 (D = X × 2 mm)

Line C (Line Stresses)

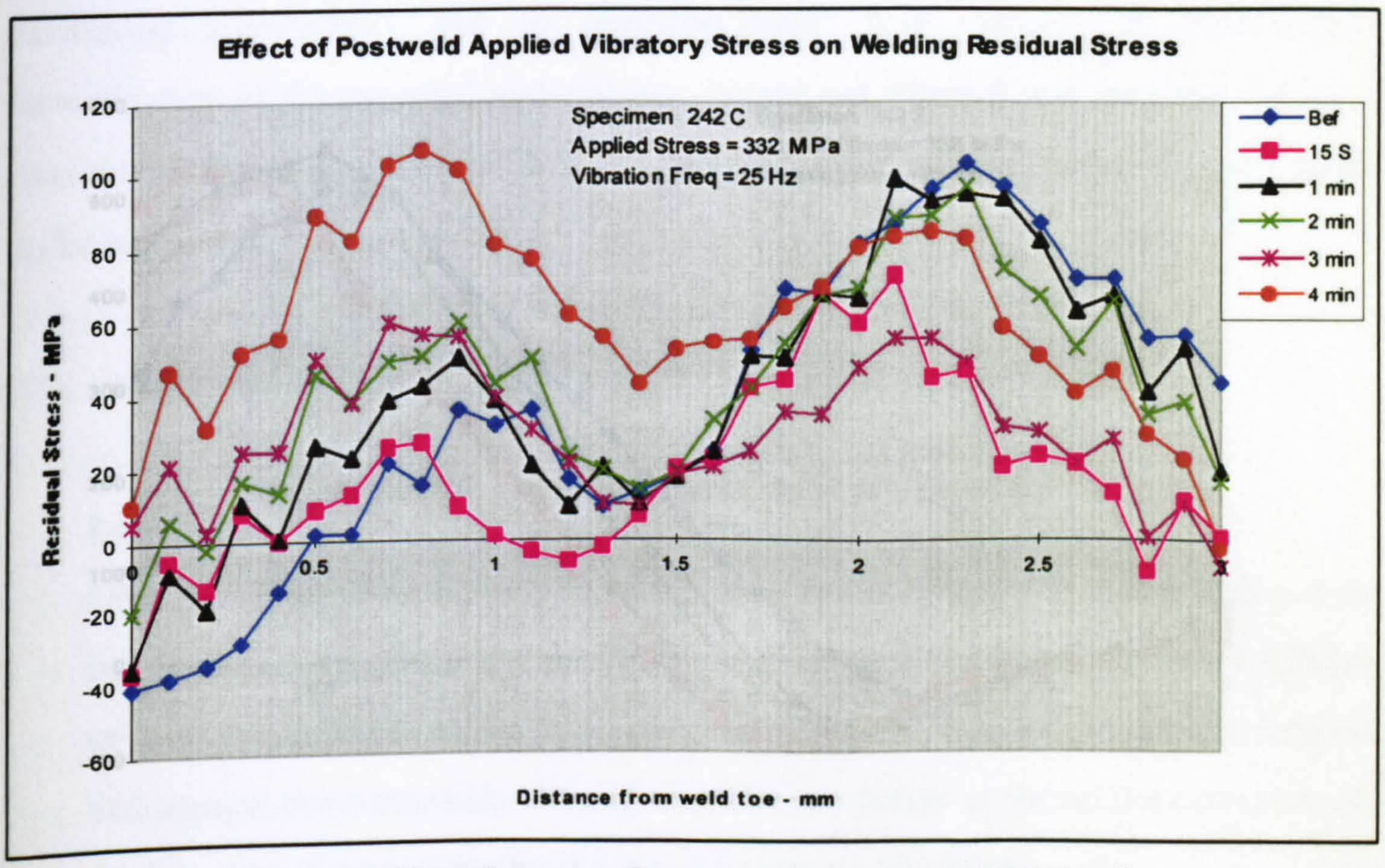

Figure 5.582 – Transverse line stress plot - specimen 24/2 line C

Line C (Point Stresses)

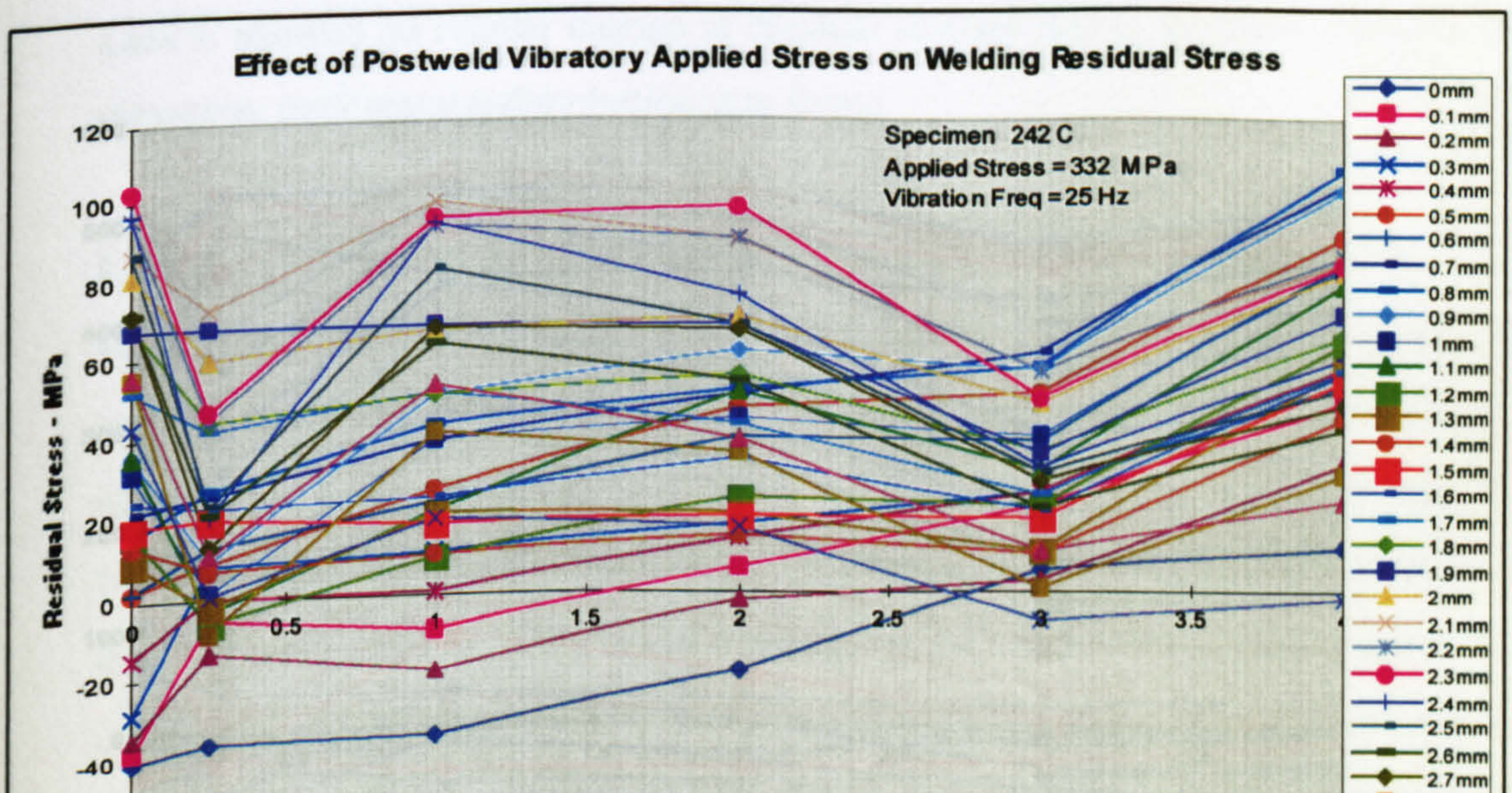

Figure 5.583 – Transverse point stress plot - specimen 24/2 line C

Specimen 24/2 (D = X × 0 mm)

Line E (Line Stresses)

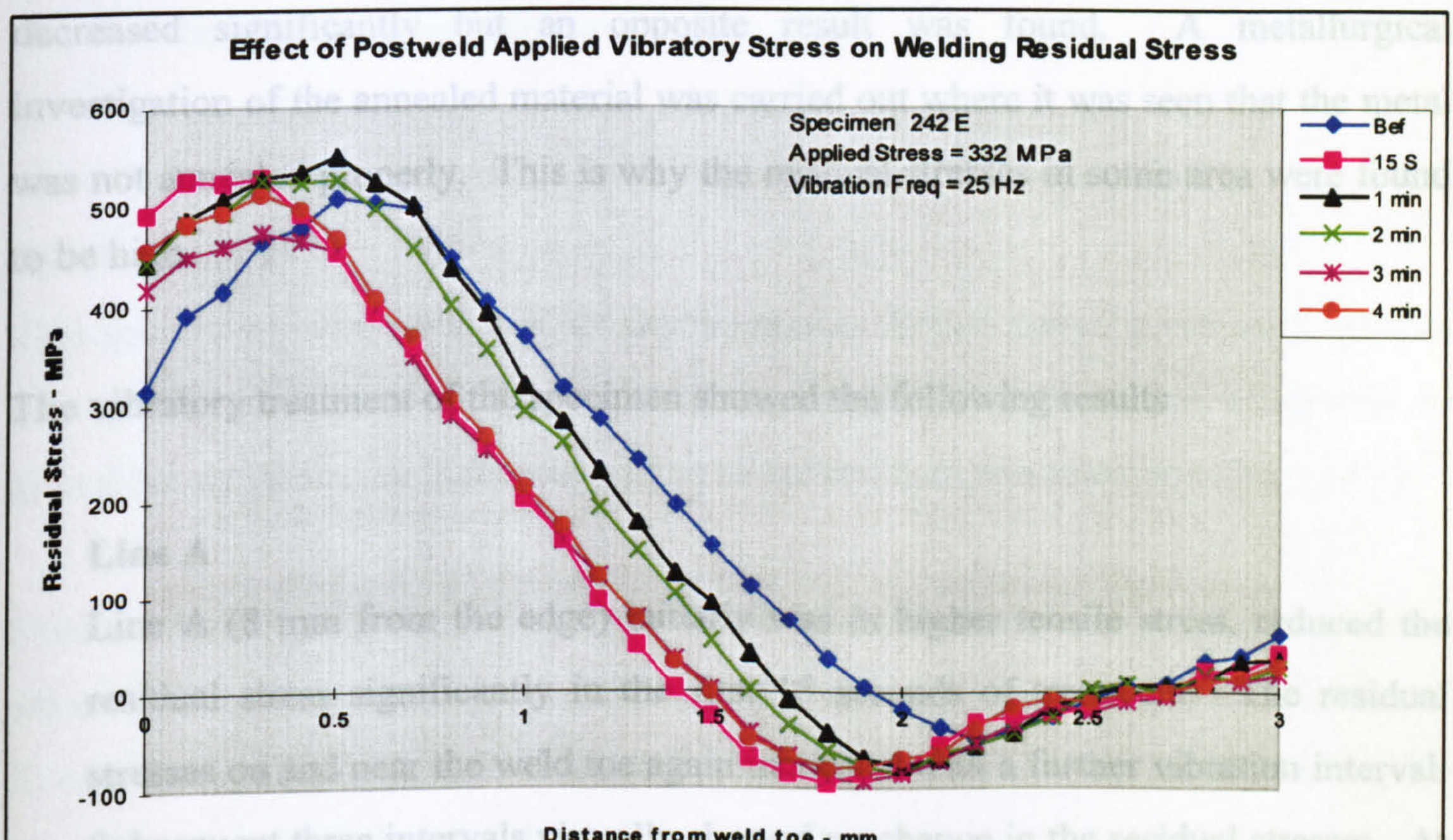

Figure 5.584 – Transverse line stress plot - specimen 24/2 line E

Line E (Point Stresses)

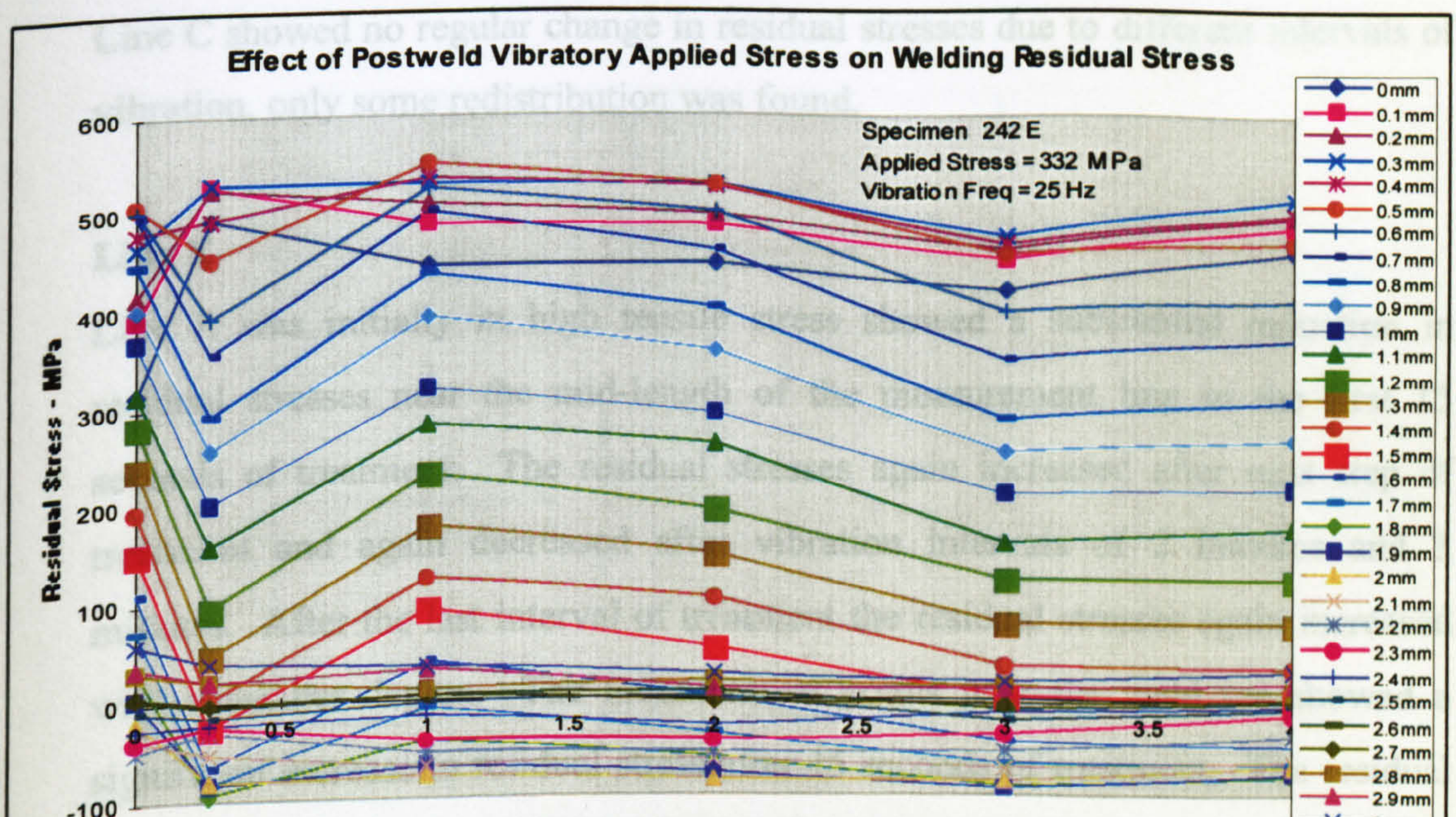

Figure 5.585 – Transverse point stress plot - specimen 24/2 line E

Results of Specimen 24/2

Although the specimen was annealed but surprisingly the residual stresses of two lines (line A and line E) were very high. It was expected that the residual stresses would be decreased significantly but an opposite result was found. A metallurgical investigation of the annealed material was carried out where it was seen that the metal was not annealed properly. This is why the residual stresses in some area were found to be high.

The vibratory treatment of the specimen showed the following results

Line A

Line A (8 mm from the edge) initially was in higher tensile stress, reduced the residual stress significantly in the first 15 seconds of treatment. The residual stresses on and near the weld toe again increased with a further vibration interval. Subsequent three intervals virtually showed no change in the residual stresses. At the last step of treatment, the stress seems increased a little.

Line C

Line C showed no regular change in residual stresses due to different intervals of vibration, only some redistribution was found.

Line E

Line E was initially in high tensile stress showed a substantial reduction in residual stresses near the mid-length of the measurement line in the first 15 seconds of treatment. The residual stresses again increased after next step of treatment and again decreased after vibration intervals of 2 minutes and 3 minutes. After the last interval of treatment the residual stresses again increased with a smaller degree. The measurement points near the weld toe showed a significant increase in residual stress after 15 seconds of treatment. The residual stress peak was found to be shifted towards the weld toe. This result was similar to the result of the specimens 13/1 and 13/2.

Thus, the residual stresses were found to increase and decrease in different measurement points before failure the specimen. No particular trend of change in the residual stresses was observed during the fatigue failure of the specimen. The yield stress of the annealed specimen was not determined.

Specimen 24/13

This specimen also welded without any treatment. Before carrying out any treatment the specimen was annealed to relieve the residual stresses. The conditions of annealing are described in the description of the previous specimen (specimen 24/2).

This specimen was processed applying dynamic stress of ±373 MPa. Ten lines were selected to measure the residual stresses, line J was at the mid-width and the value of X was 4 mm. The longitudinal residual stresses of the lines were measured using the mapping procedure, then the data of the individual line were extracted from the map and plotted separately as line and point stress plots. The results of all ten lines were showing the same message. Instead of the plots of the ten lines, two selected lines are shown here to save some space.

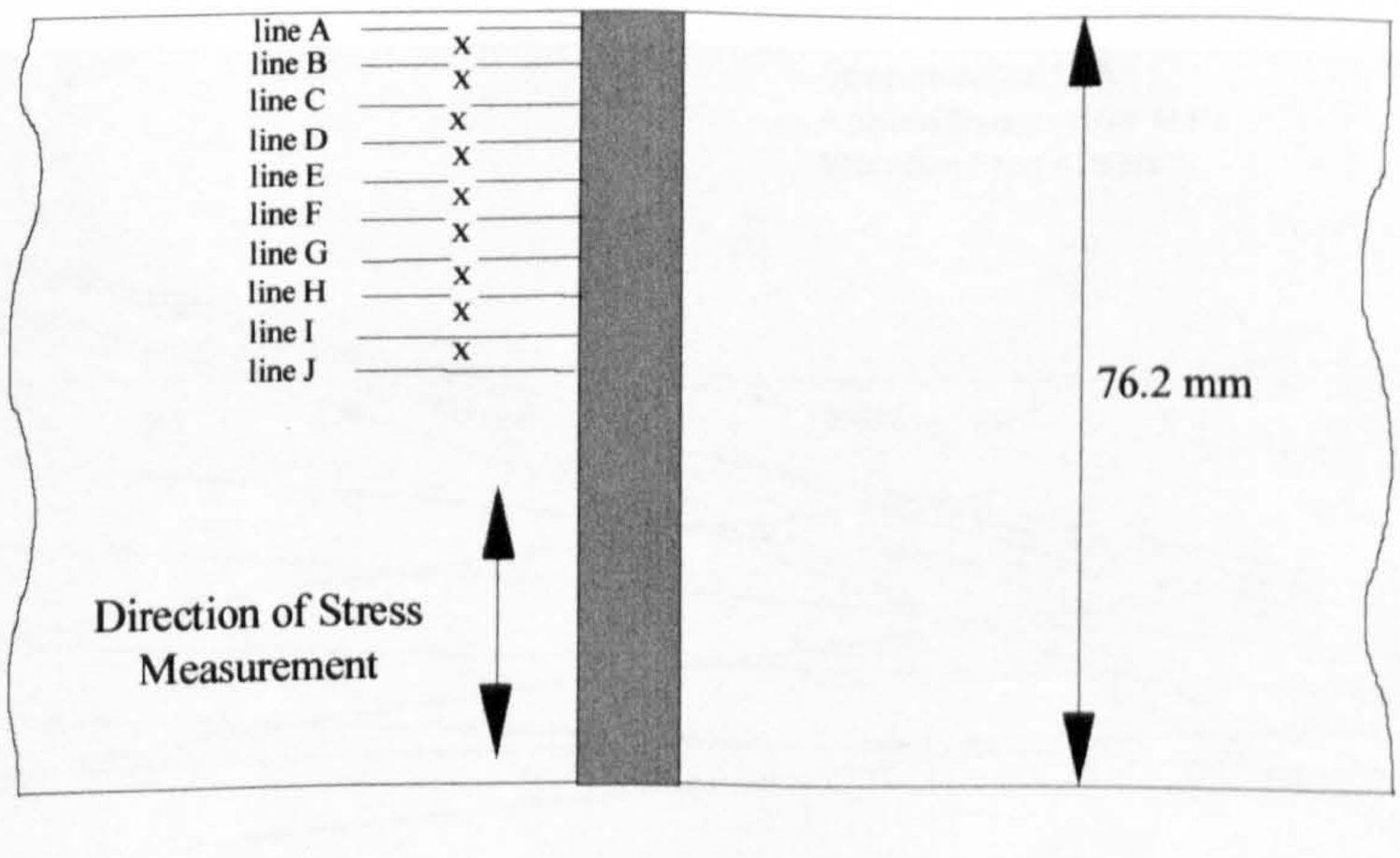

Figure 5.586 - Position of measurement lines - specimen 24/13

Specimen 24/13 (D = 9 × X mm)

Line A (Line Stresses)

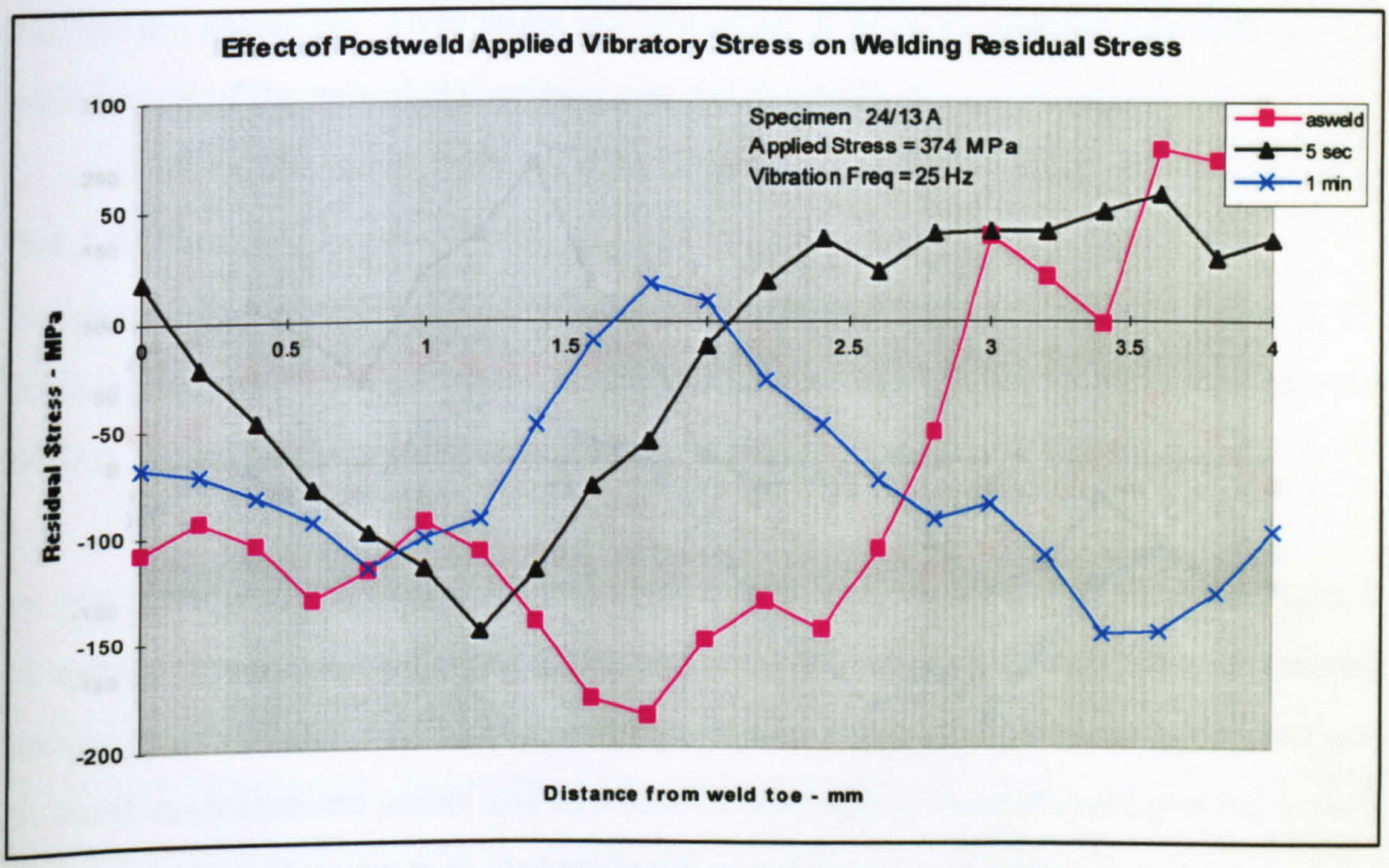

Figure 5.587 – Longitudinal line stress plot - specimen 24/13 line A

Line A (Point Stresses)

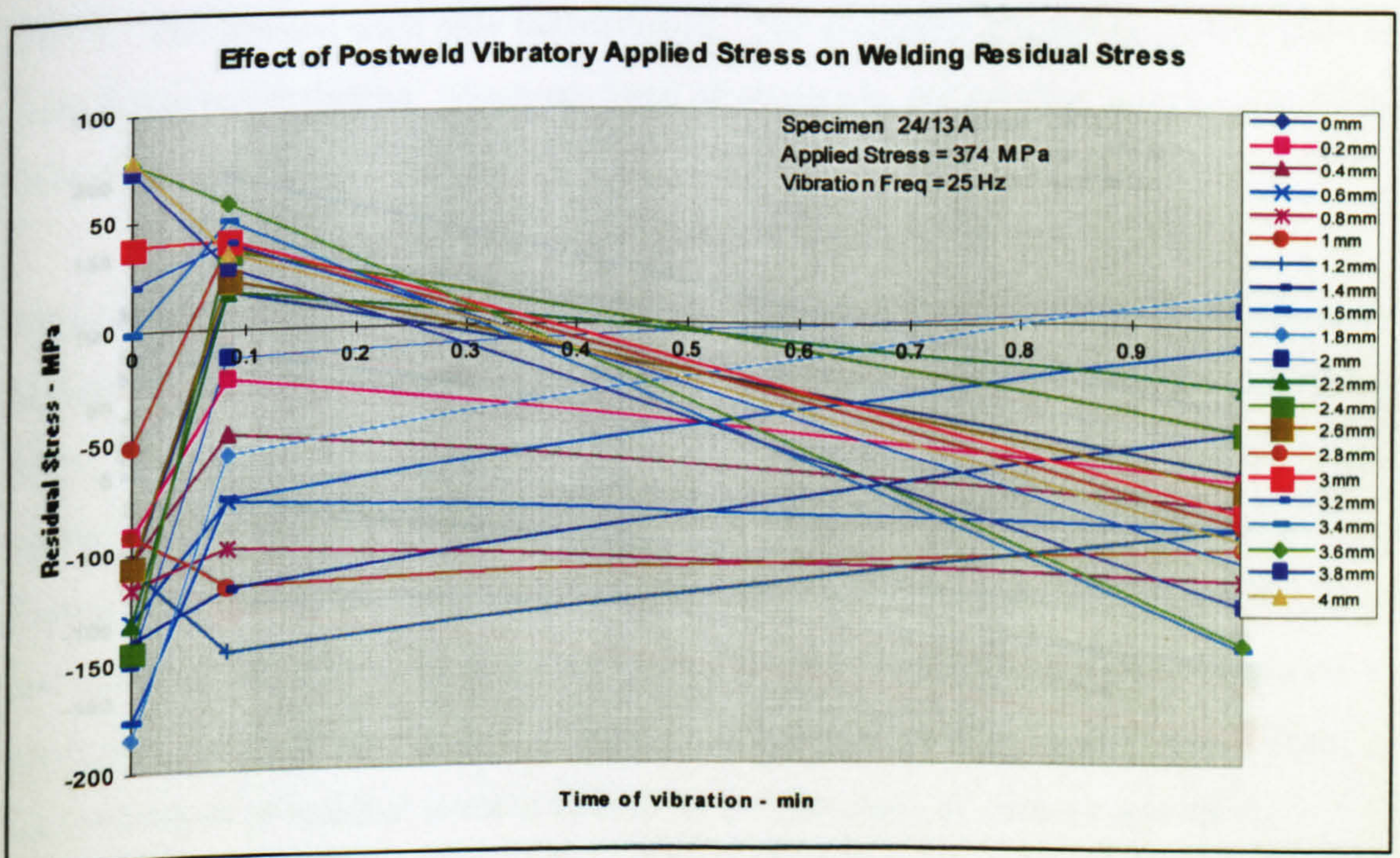

Figure 5.588 – Longitudinal point stress plot - specimen 24/13 line A

Specimen 24/13 (D = 0 × X mm)

Line J (Line Stresses)

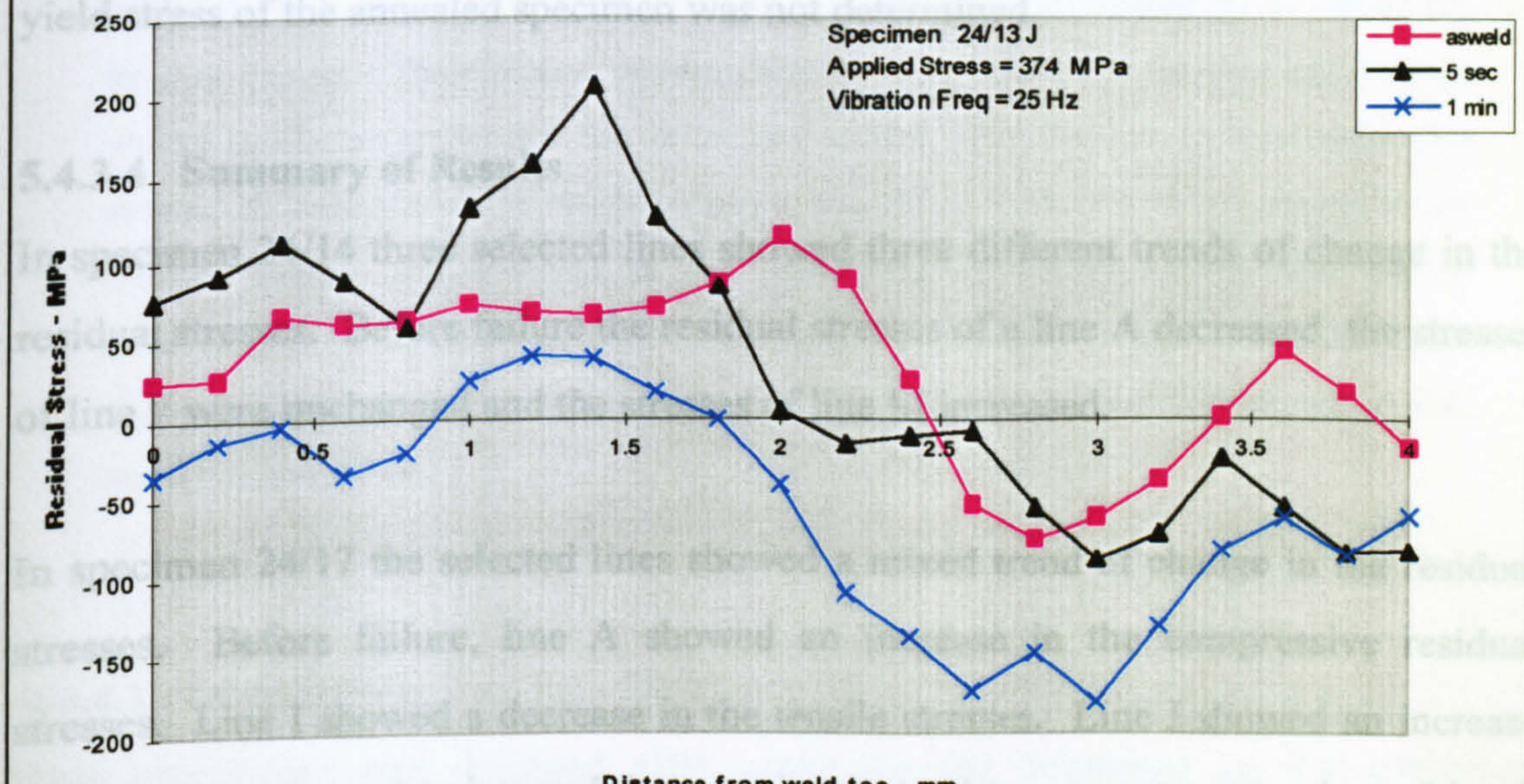

Figure 5.589 – Longitudinal line stress plot - specimen 24/13 line J

Line J (Point Stresses)

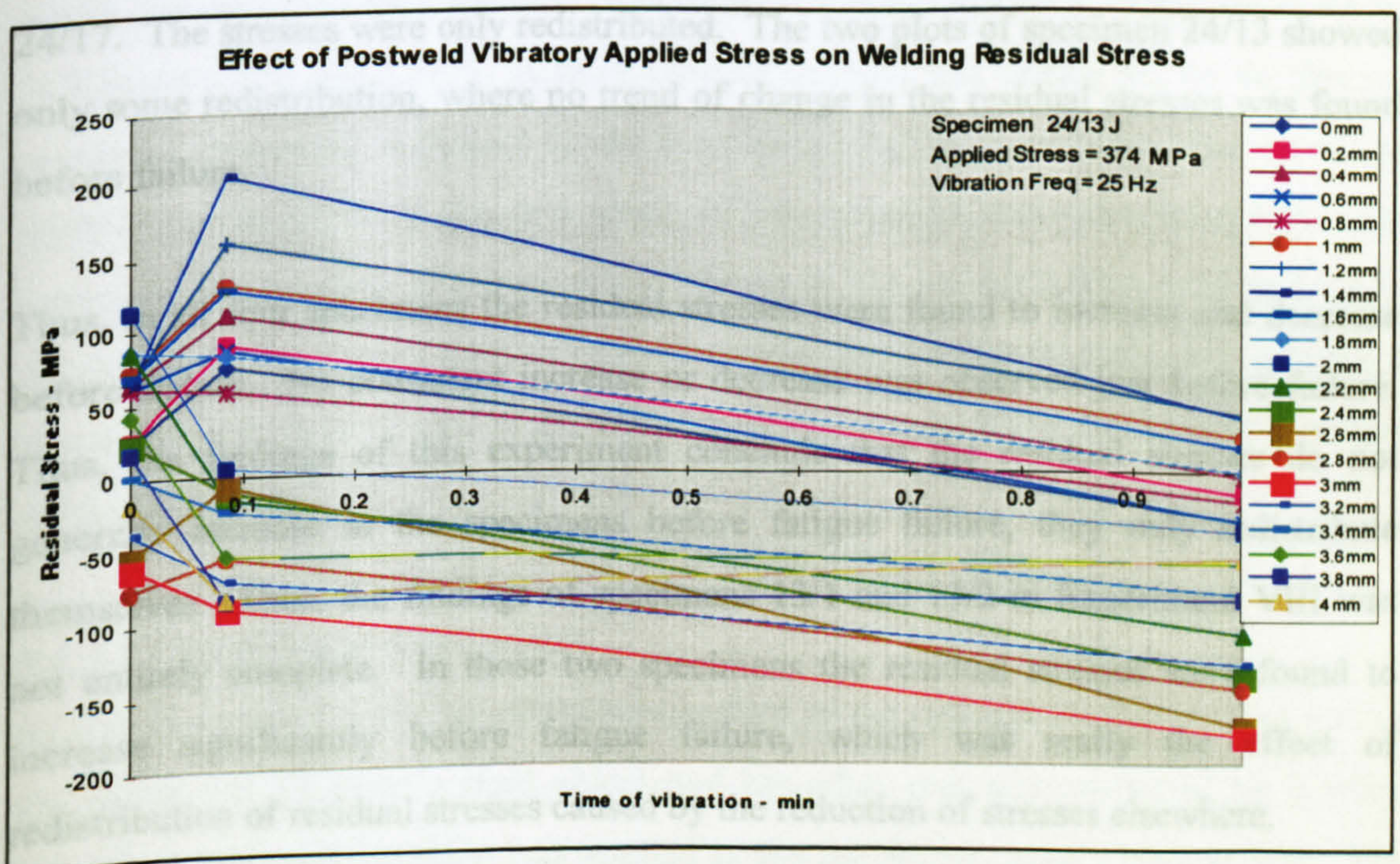

Figure 5.590 – Longitudinal point stress plot - specimen 24/13 line J

Discussion of Results - Specimen 24/13

Out of ten measured lines two lines are included here. In both lines (shown in Figures 5.587 to 5.590) no clear trend of change in the residual stresses were observed before failure the specimen. Only some redistribution of residual stresses was found. The yield stress of the annealed specimen was not determined.

5.4.3.4 Summary of Results

In specimen 24/14 three selected lines showed three different trends of change in the residual stresses. Before failure the residual stresses of a line A decreased, the stresses of line F were unchanged and the stresses of line M increased.

In specimen 24/17 the selected lines showed a mixed trend of change in the residual stresses. Before failure, line A showed an increase in the compressive residual stresses. Line I showed a decrease in the tensile stresses. Line J showed an increase in some measurement points and decrease in some other measurement points. Line S showed mainly increase in the tensile residual stresses.

In all three plots of specimen 24/2 showed a similar results as specimens 24/14 and 24/17. The stresses were only redistributed. The two plots of specimen 24/13 showed only some redistribution, where no trend of change in the residual stresses was found before failure.

Thus, in all four specimens the residual stresses were found to increase and decrease before failure. No consistent increase or decrease was observed just before failure. Thus, the findings of this experiment conclude that the residual stresses do not generally increase in the specimens before fatigue failure, they only redistribute themselves. Thus, the findings of specimens 13/1 and 13/2 in Experiment VIII was not entirely complete. In those two specimens the residual stresses were found to increase significantly before fatigue failure, which was really the effect of redistribution of residual stresses caused by the reduction of stresses elsewhere.

5.4.4 Experiment X:

Investigation of Torsional Stress Effect on Residual Stress and VSR.

Abstract

In this experiment torsional vibratory stress was applied to the specimens to relieve the residual stresses. Three batches of specimens were processed, viz: (a) homogeneous, (b) welded on the circumferential line & (c) spot welded. The first two types of specimens showed no reduction in the residual stresses due to the treatment. Some change in the residual stresses was observed in the higher applied stresses, which was due to redistribution in the residual stresses. The spot welded shafts showed a very important characteristic where the residual stresses were found to decrease significantly with a very small induced stress.

5.4.4.1 Introduction

This experiment was designed after observing the behaviour of the specimens processed in Experiment VIII. In that experiment, flat bar specimens were processed which showed that reduction in residual stress was higher away from the mid-width longitudinal axis. The drop was very high in two equidistant positions from the mid-width and near the edges, the high compressive stresses reduced to nearly zero (shown in Figures 5.556 and 5.562). A finite element analysis was carried out on the flat bar specimen (presented in chapter 4) which indicated that the shear stress was increasing with a movement from the mid-width of the specimen and was decreasing upon approaching the edges of the specimen (shown in Figures 4.12, 4.14, 4.16 and 4.18). At the outset this further analysis of these results showed that the reduction in residual stress was somehow related to the shear stress pattern generated by flexural vibration of the specimen.

5.4.4.2 Experimental Procedure

In this experiment, torsional stress was applied to the cylindrical shafts. One end of the shafts was fixed to a rigid object and the other end was supported by a roller bearing. Torsional vibration was applied to the specimens using a torsion arm. The

experimental set-up for the torsion test is shown in Figure 5.591. The effective induced residual stress was measured by attaching an accelerometer to the torsion arm and suitably conditioning the signals so as to achieve a vibratory amplitude reading at the free end of the shaft. The specimens were subjected to different vibration parameters, which are provided with the description of the specimens.

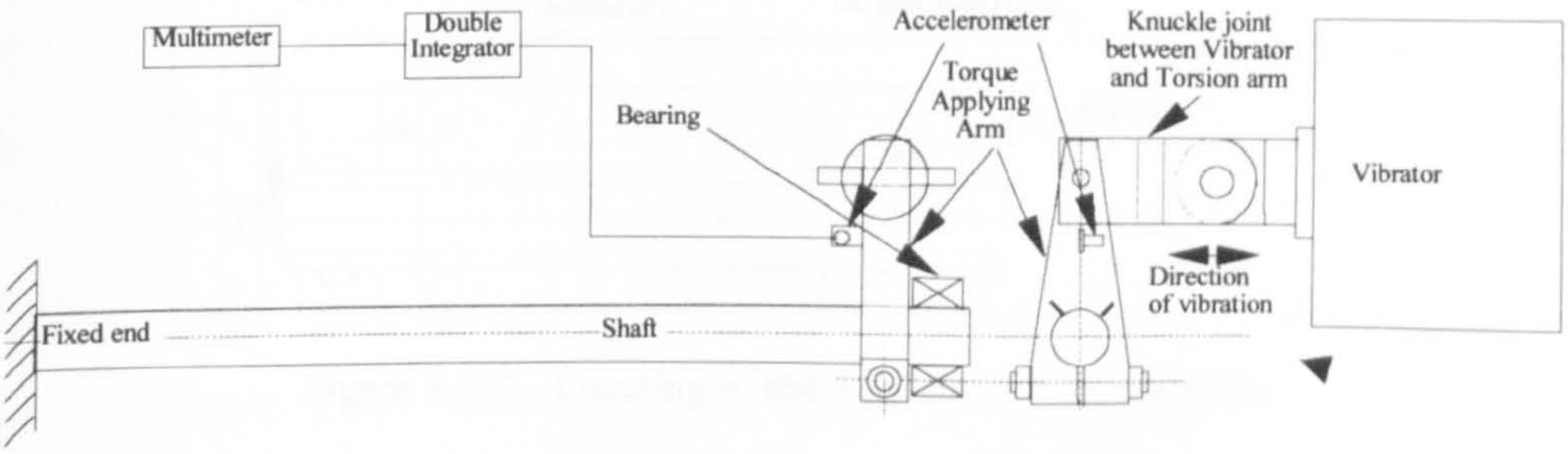

Figure 5.591 – Experimental set-up – torsional test

In this experiment, three batches of shafts were investigated. In batch 1, three hollow shafts (dimensions are presented in Section 5.2.3) were vibrated applying different levels of stresses. Of the three shafts, two were welded to induce some residual stresses then vibratory treatment was carried out as post weld treatment. The third shaft was treated without any welding, i.e. treated as a homogeneous shaft. In batch 2 (different dimensions – presented in Section in 5.2.3), four hollow shafts were investigated, two of them were welded for inducing residual stresses and the other two were treated as homogeneous shafts. In batch 3, six solid shafts (dimensions are presented in Section 5.2.3) were processed. All six shafts were welded to induce some residual stress then subjected to vibration. In all three batches, the set-ups were suitably modified to suit the dimensions of the shafts and applied stress requirements. The applied stress of all three set-ups was calibrated separately.

Residual stress was measured on a longitudinal line on the surface of the shafts. The position of the measurement line is provided with the description of the shaft in Section 5.4.4.4. The residual stresses were measured using the mapping technique. In the measurement single exposure technique (SET) was used. The X-ray measurement conditions were similar to as described in the Table 5.10.

In order to measure the same points of the measurement line, a special jig was prepared to locate the specimens on the goniometer table shown in Figure 5.592.

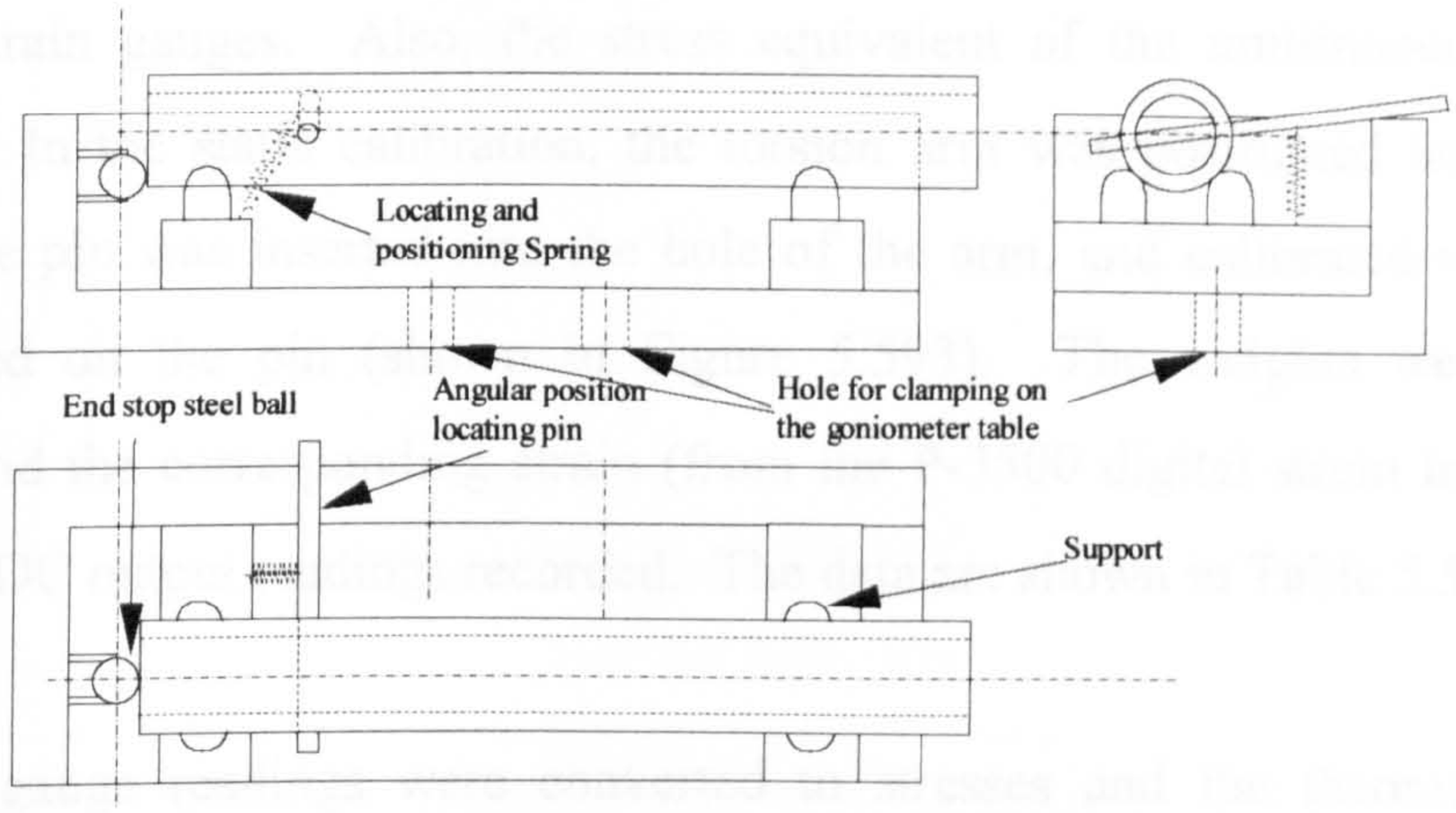

Figure 5.592 - Locating of shaft on the goniometer table.

Four spherical end supports were needed to support the shaft. The axial movement of the shaft was prevented by a steel ball support at one end. The rotational movement was prevented by drilling a small hole in the shaft and inserting a precise slide fit rod in it. The rod was loaded by a tension spring to keep it in the same position every time when a specimen is positioned for measurement. The jig ensured repeatability of the X-ray measured results.

5.4.4.3 Calibration of Applied Stresses

The calibration of the applied stress to the shafts was carried out in two steps. The first being static and the second being the dynamic calibration. The applied strain and hence stress was measured using two strain gauges positioned 45° to the shaft axis and perpendicular to each other. A half bridge configurations was used to obtain the full shear strain value.

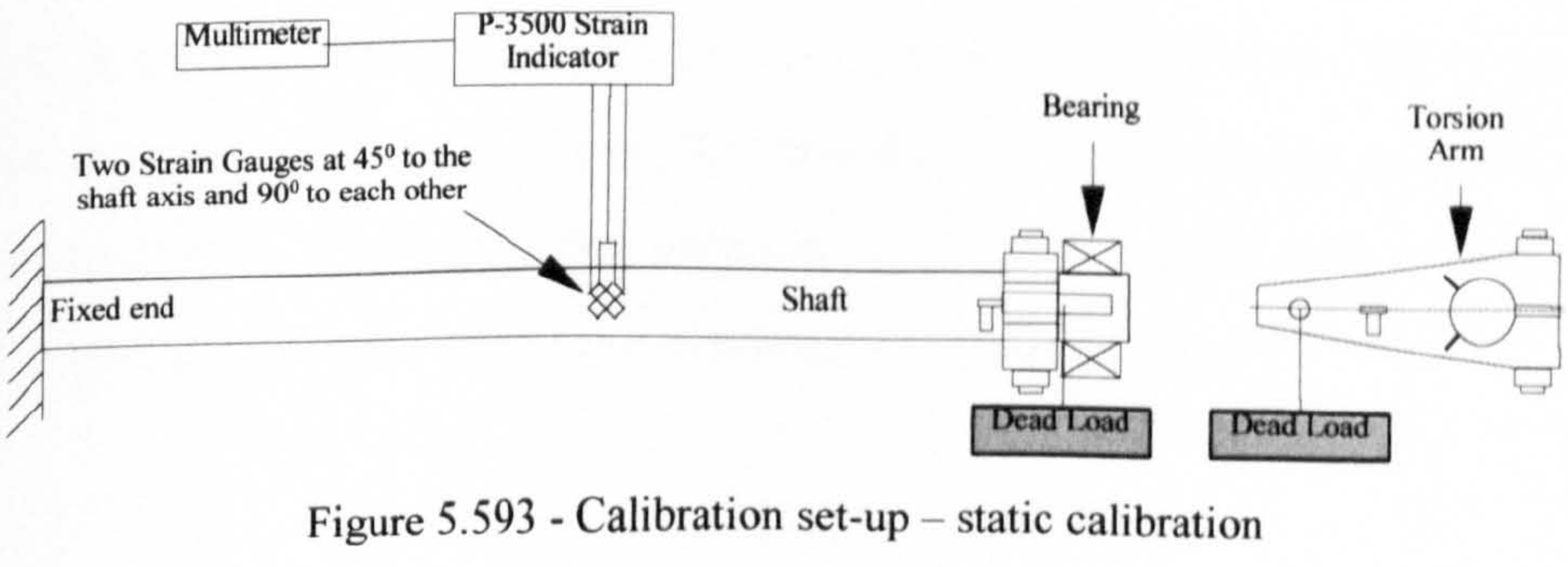

Figure 5.593 - Calibration set-up – static calibration

In the first step the static calibration was carried out, in which the theoretical applied stresses (calculated from torsion formula) were verified with the measured stresses from the strain gauges. Also, the stress equivalent of the multimeter output was calculated. In the static calibration, the torsion arm was positioned horizontally, a precise slide pin was inserted into the hole of the arm, and calibrated weights/loads were hanged on the pin (shown in Figure 5.593). The weights were increased gradually and the corresponding strain (from the P-3500 digital strain indicator) and multimeter DC output readings recorded. The data are shown in Table 5.53 below.

The strain gauge readings were converted to stresses and the theoretical applied stresses were calculated from the applied torque to the shaft. The measured stresses were plotted against the theoretical stresses which are shown below. In the calculation of the stresses the shear modulus was taken as 83×10^9 N/m^2, (from a Materials Handbook). The measured stresses were again plotted against the DC output of the multimeter to obtain an unit mV (multimeter output) equivalent of the measured stresses (shown in Figure 5.595).

Table 5.53 - Calibration of static torsional shear stress.

Load No.	load	Calibrated Load	Total load	Arm length	torque	stress	mic strain	multimeter	stress
	kg	kg	kg	m	Nm	MPa		mV	MPa
0	0	0	0	0.11	0	0	0	-2.7	0
1	0.51	0.505	0.505	0.11	0.547175	0.69655	-8.5	-6.75	-0.7055
2	0.51	0.518	1.023	0.11	1.108435	1.41104	-17.5	-10.8	-1.4525
3	0.51	0.503	1.526	0.11	1.653443	2.10484	-25.5	-14.8	-2.1165
4	0.51	0.509	2.035	0.11	2.204952	2.80691	-34	-18.8	-2.822
5	0.51	0.515	2.55	0.11	2.762962	3.51725	-42.5	-22.95	-3.5275
6	0.51	0.507	3.057	0.11	3.312304	4.21657	-50.5	-27.05	-4.1915
7	0.51	0.506	3.563	0.11	3.860562	4.9145	-59.5	-31.15	-4.9385
8	0.51	0.517	4.08	0.11	4.420739	5.62761	-67.5	-35.25	-5.6025
9	1.02	1.02	5.1	0.11	5.525924	7.03451	-85.5	-43.65	-7.0965

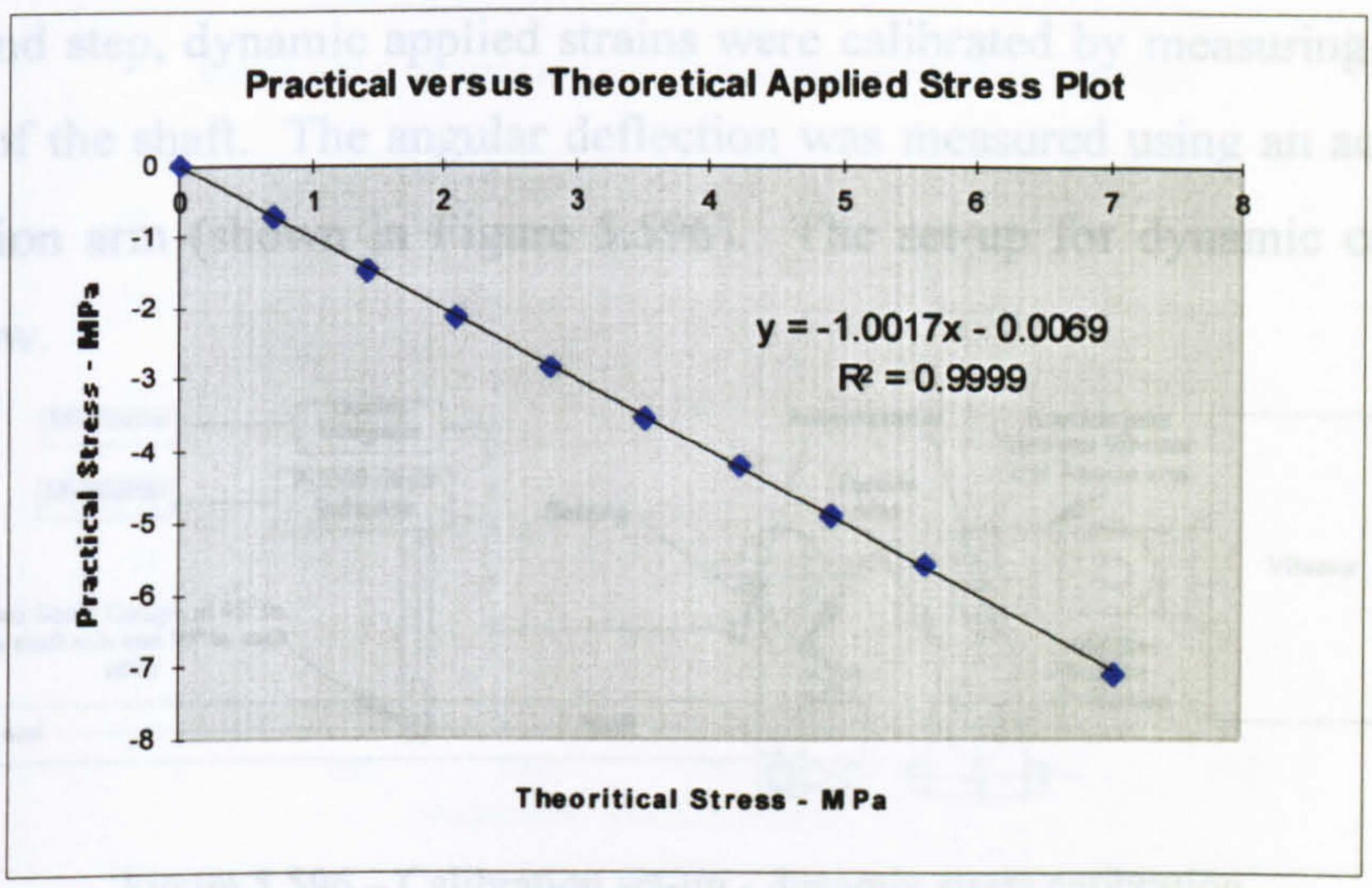

Figure 5.594 – Measured stress versus theoretical stress plot.

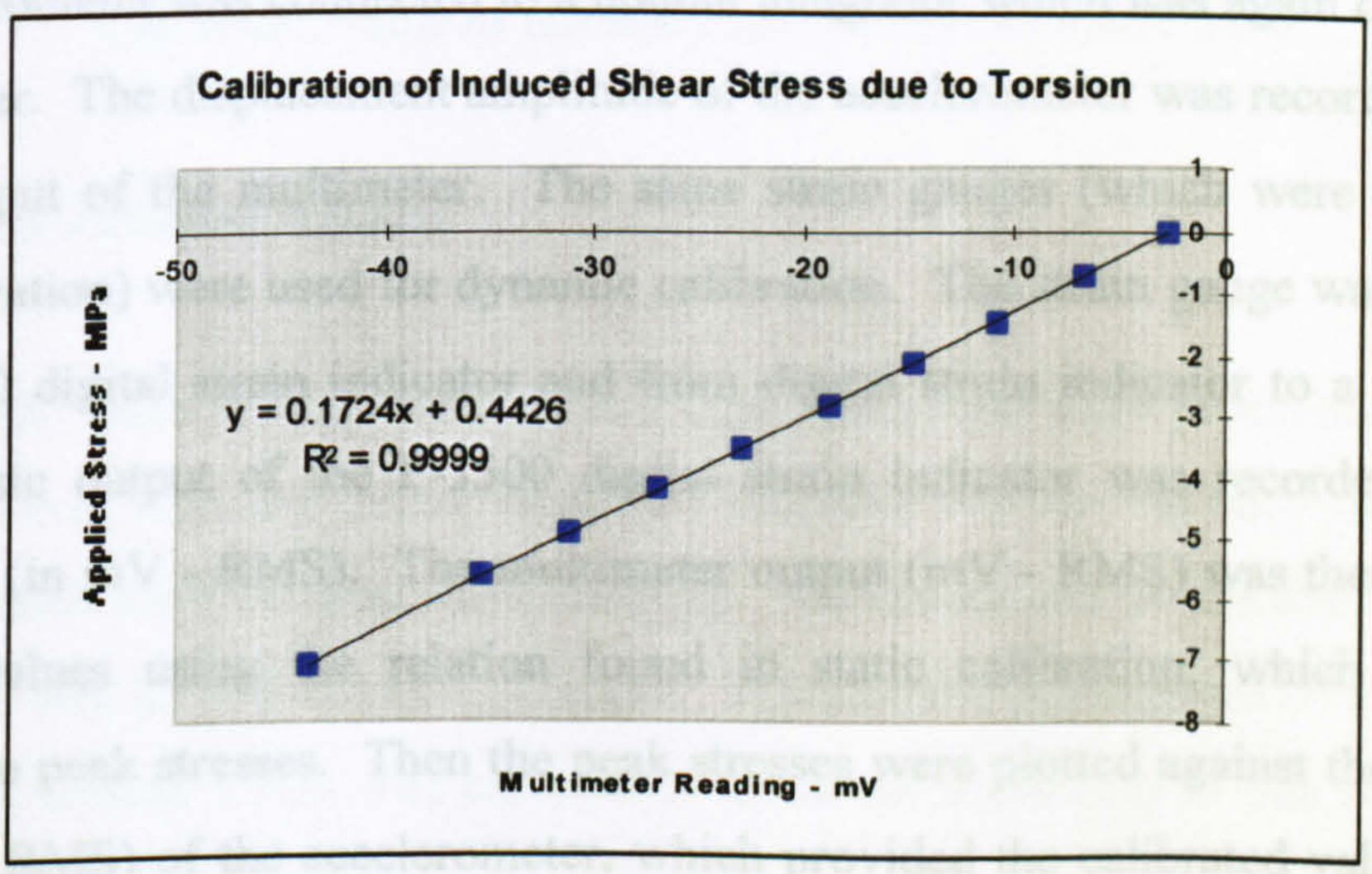

Figure 5.595 – Applied stress verses multimeter output plot.

In the first plot (Figure 5.594), the theoretical applied stresses (from torsion formula) were verified with the stresses calculated from the strain gauges readings. The difference between the two stresses was as low as 0.17 %, which provided confidence in the calibration process. In the second plot (Figure 5.595), the measured stresses (from the strain gauge outputs) were plotted against the multimeter DC output where also good linearity was found. This plot provided the stress equivalent in mV (output of the multimeter). The calibrated value of multimeter output was 1 mV = 0.1724 MPa. This relation was to use in the dynamic stress calculation.

In the second step, dynamic applied strains were calibrated by measuring the angular deflection of the shaft. The angular deflection was measured using an accelerometer on the torsion arm (shown in Figure 5.596). The set-up for dynamic calibration is shown below.

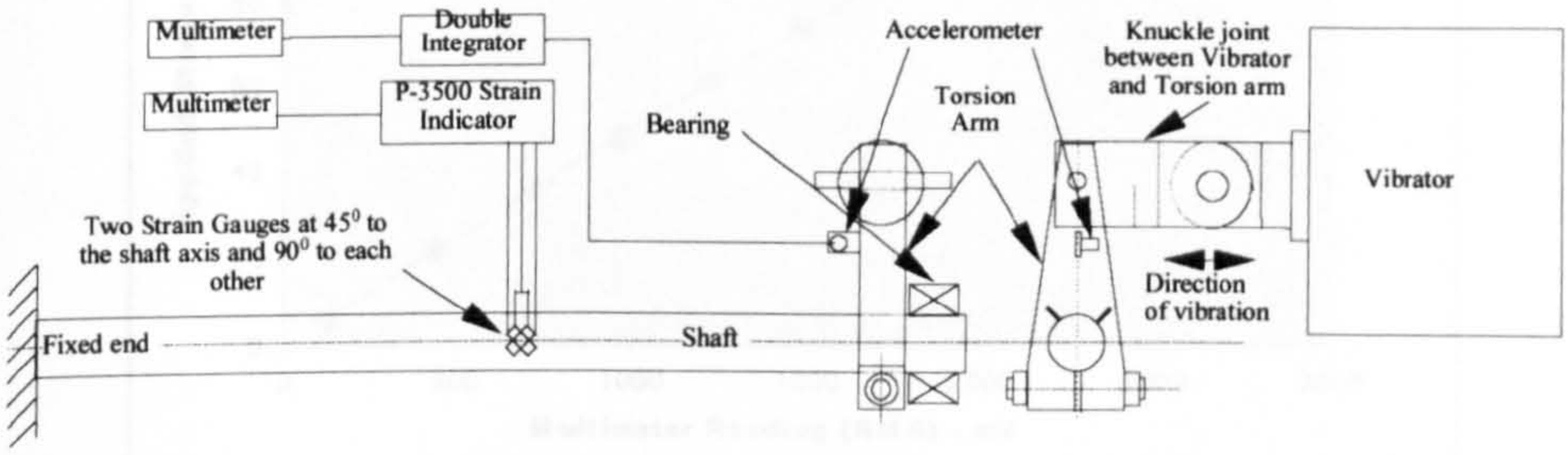

Figure 5.596 – Calibration set-up - dynamic stress calibration.

The accelerometer was connected to a double integrator which was again connected to a multimeter. The displacement amplitude of the accelerometer was recorded in terms of mV output of the multimeter. The same strain gauges (which were used in the static calibration) were used for dynamic calibration. The strain gauge was connected to a P-3500 digital strain indicator and from digital strain indicator to a multimeter. The dynamic output of the P-3500 digital strain indicator was recorded from the multimeter (in mV - RMS). The multimeter output (mV - RMS) was then converted to strain values using the relation found in static calibration, which was again converted to peak stresses. Then the peak stresses were plotted against the deflection outputs (in RMS) of the accelerometer, which provided the calibrated value of stress in terms of deflection output of the accelerometer. Table 5.54 and Figure 5.597 below shows the calibration data and plot.

Table 5.54 - Calibration of Dynamic torsional shear stress.

Disp (rms)	Disp (pk)	Strs (rms)	Strs (pk)	Strs (pk)
	mV	mV	mV	MPa
132	186.704	26.5	37.48232	6.4657
435	615.276	89	125.884	21.715
724	1024.05	147.5	208.628	35.988
978	1383.31	197	278.6421	48.066
1226	1734.09	249	352.1924	60.753
1493.5	2112.45	304	429.9859	74.173
1749.5	2474.54	355	502.1216	86.616
2125.5	3006.36	430	608.2037	104.92
2398	3391.8	484	684.5827	118.09
2686	3799.15	542	766.6195	132.24

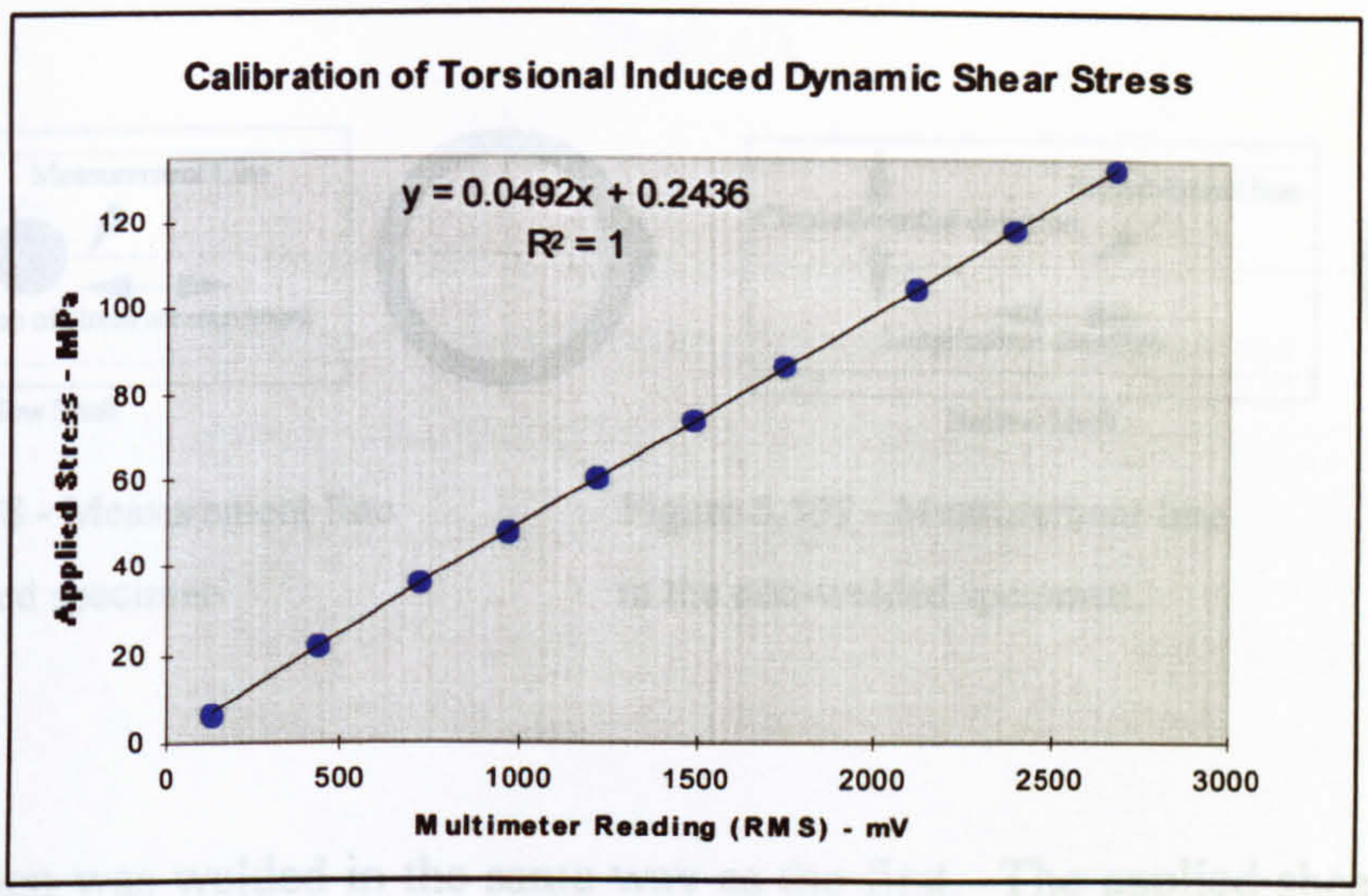

Figure 5.597 - Calibration plot - applied dynamic stress

Calibrated value of out put 1 mV (RMS) = 0.0492 MPa

5.4.4.4 Experimental Results

Batch 1

In this batch, three hollow solid drawn shaft specimens were processed, two were welded and then vibratory treated (shaft 1/1 and shaft 1/2) and the other one treated as a homogeneous shaft (without any welding). The dimensions of the shafts were 25.4 mm OD, 22 mm ID and 430 mm in length. The material descriptions of the shafts are presented in section 5.2.3. The calibration factor for measuring in this set-up was: 1 mV equals 0.0373 MPa.

Shaft 1/1

On this shaft a spot was welded to induce some residual stresses as shown in Figure 5.598. The specimen was allowed to cool down to room temperature and the residual stresses were measured. The specimens were then vibrated as post weld treatment. A longitudinal line near the weld was selected for investigation (Figure 5.598). The longitudinal residual stress of the line was measured. The applied torsional stress to the specimen was varied from 0 to 39.4 MPa in some steps. The details of the applied stresses are shown in the plots. The time of vibration in every stress step was two minutes. The residual stress plots are shown in Figure 5.600 and 5.601.

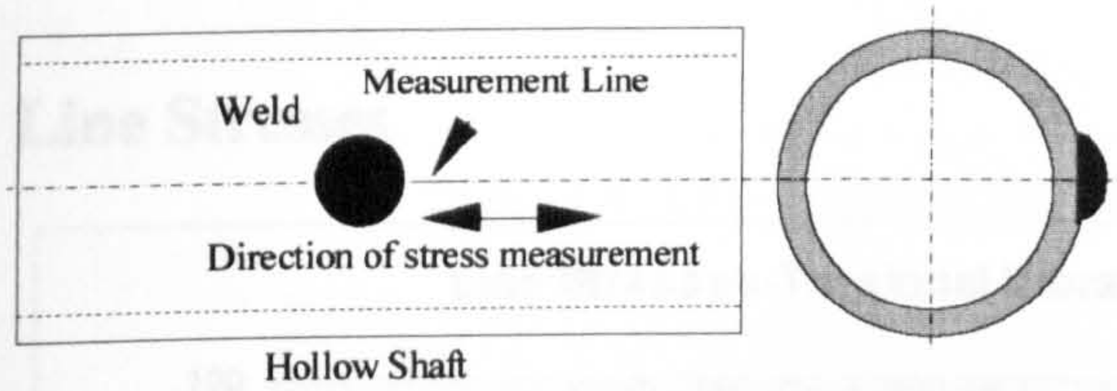

Figure 5.598 - Measurement line in the welded specimen

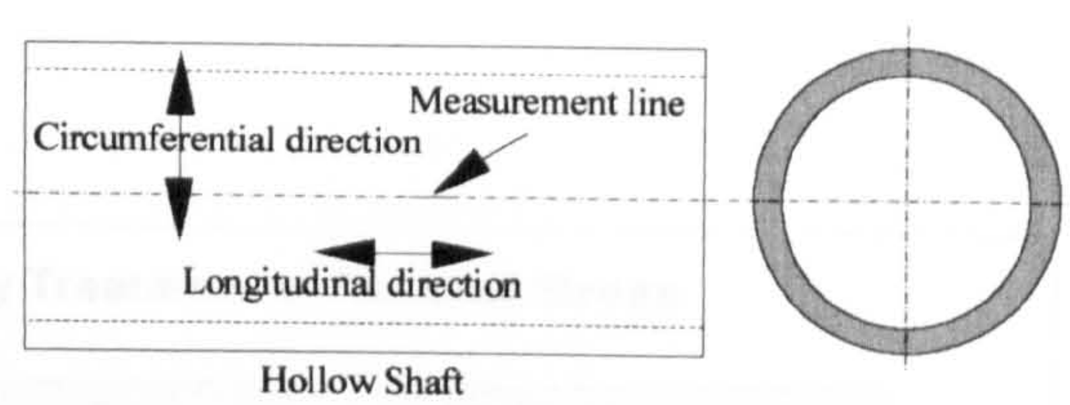

Figure 5.599 - Measurement line in the non-welded specimen.

Shaft 1/2

This specimen was welded in the same way as the first. The applied shear stress was varied from 0 to 65.4 MPa in several steps (shown in the plot). The time of vibration in every stress step was 1 minute. longitudinal residual stress on a 5 mm line (Figure 5.598) was measured. The measurement was started at the weld toe. The line and point stresses are shown in Figure 5.602 and 5.603.

Shaft 1/3

This specimen was processed as a homogeneous shaft. The applied shear stress was varied from 0 to 50 MPa in several steps (details are shown in the plots). In every step the specimen was vibrated for 1 minute (1500 cycles). The longitudinal residual stress was measured along the selected line (Figure 5.599). The line and the point stresses are shown in Figure 5.604 and 5.605.

Shaft 1/1

Line Stresses

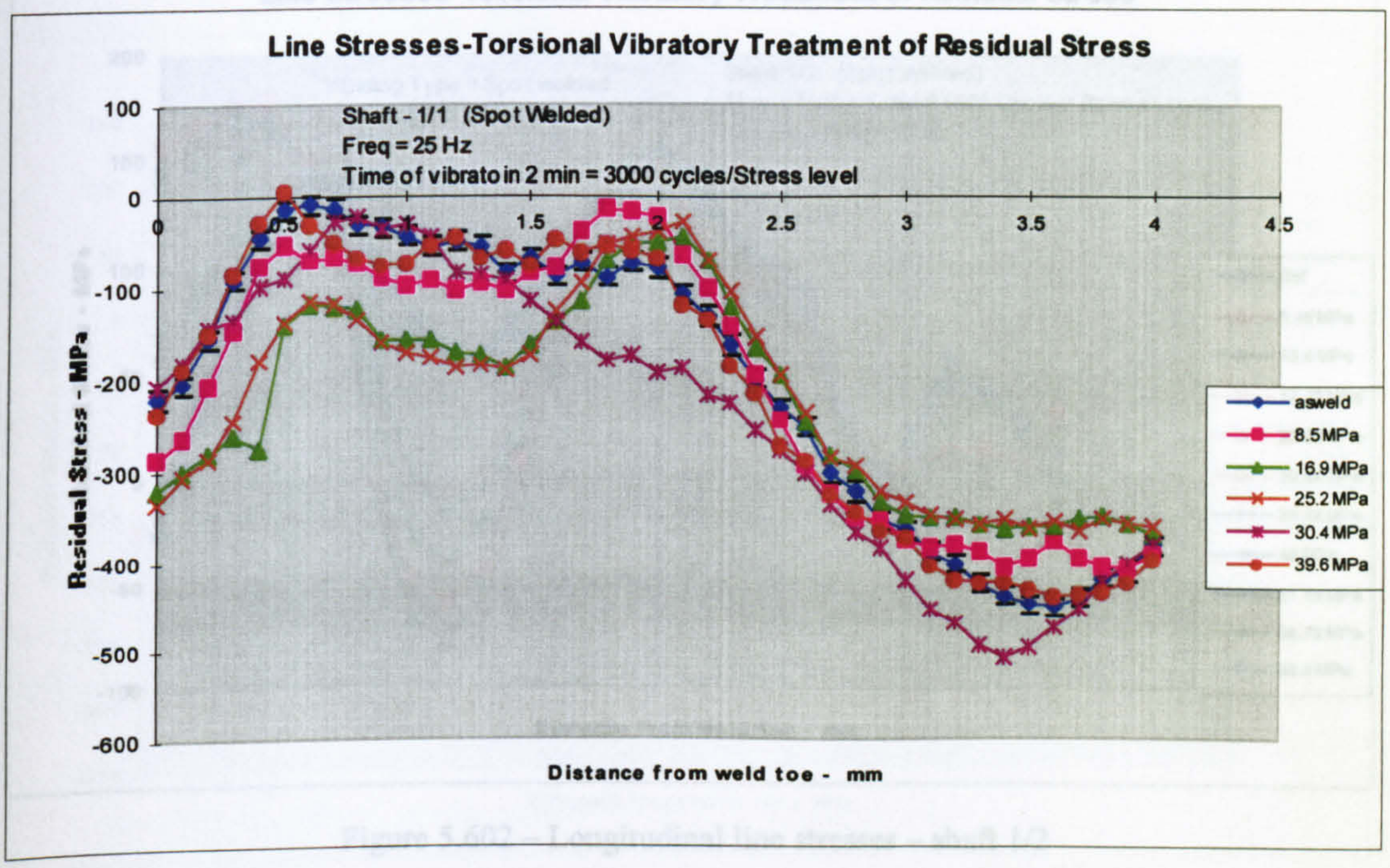

Figure 5.600 – Longitudinal line stresses - shaft 1/1

Point Stresses

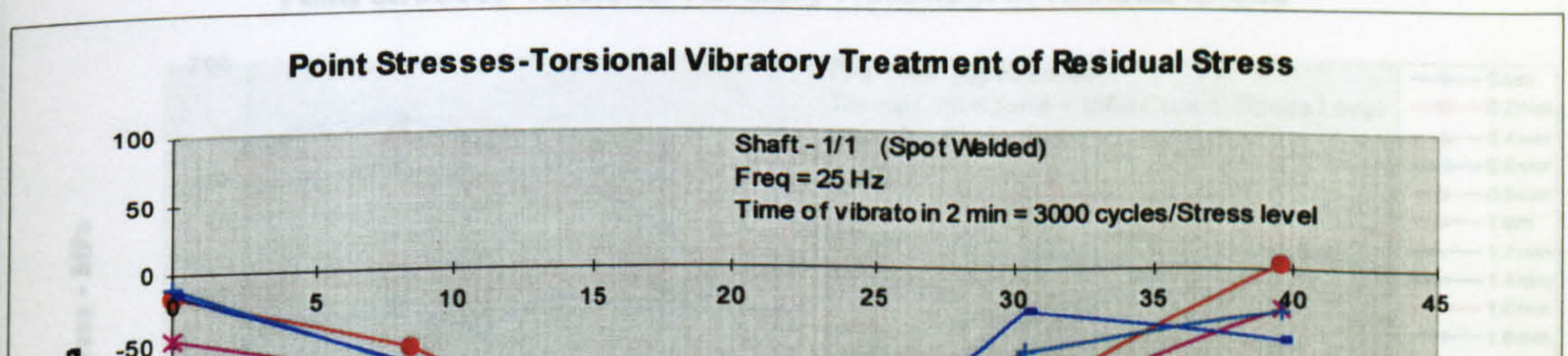

Figure 5.601 – Longitudinal point stresses - shaft 1/1

Shaft 1/2

Line Stresses

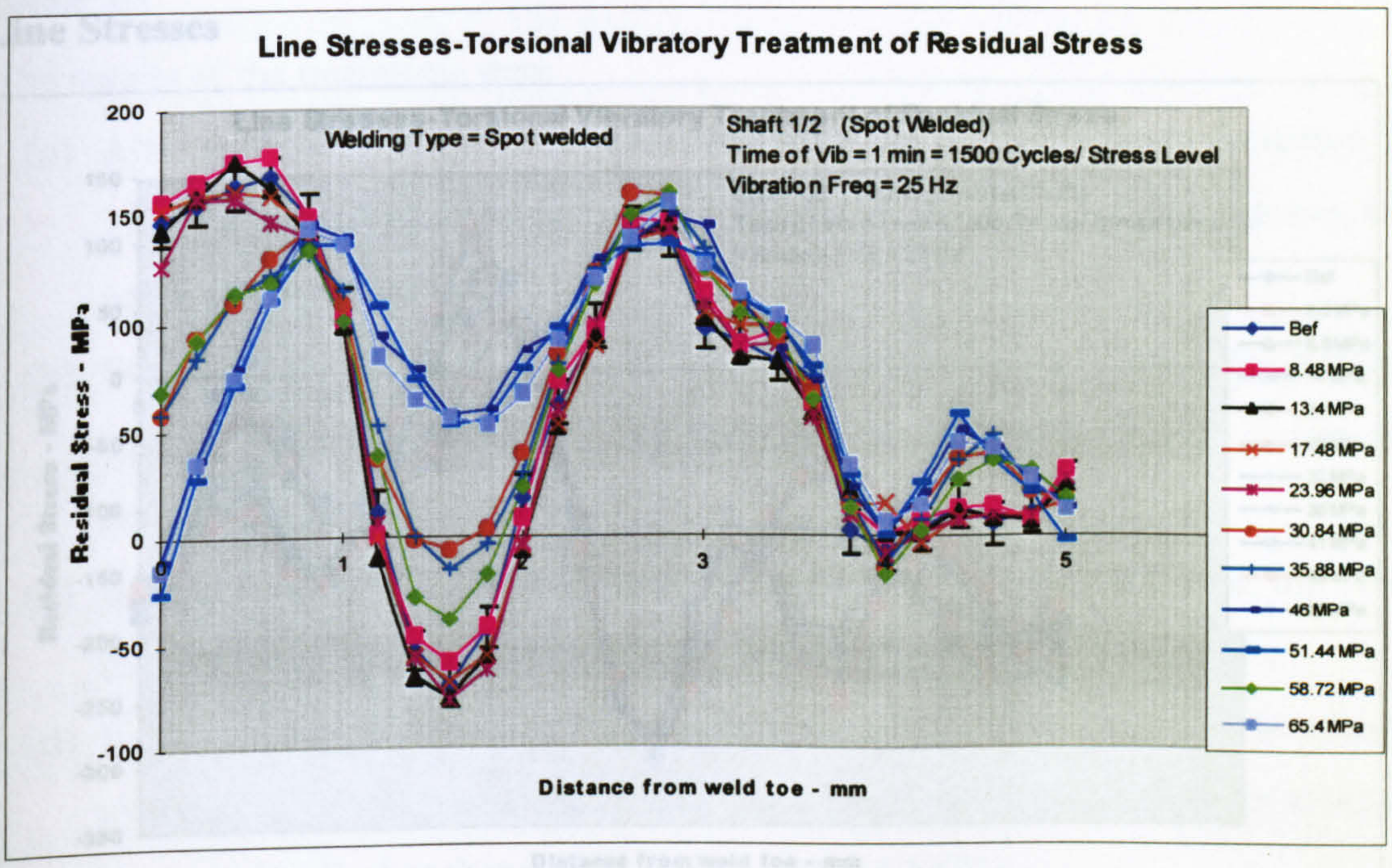

Figure 5.602 – Longitudinal line stresses – shaft 1/2

Point Stresses

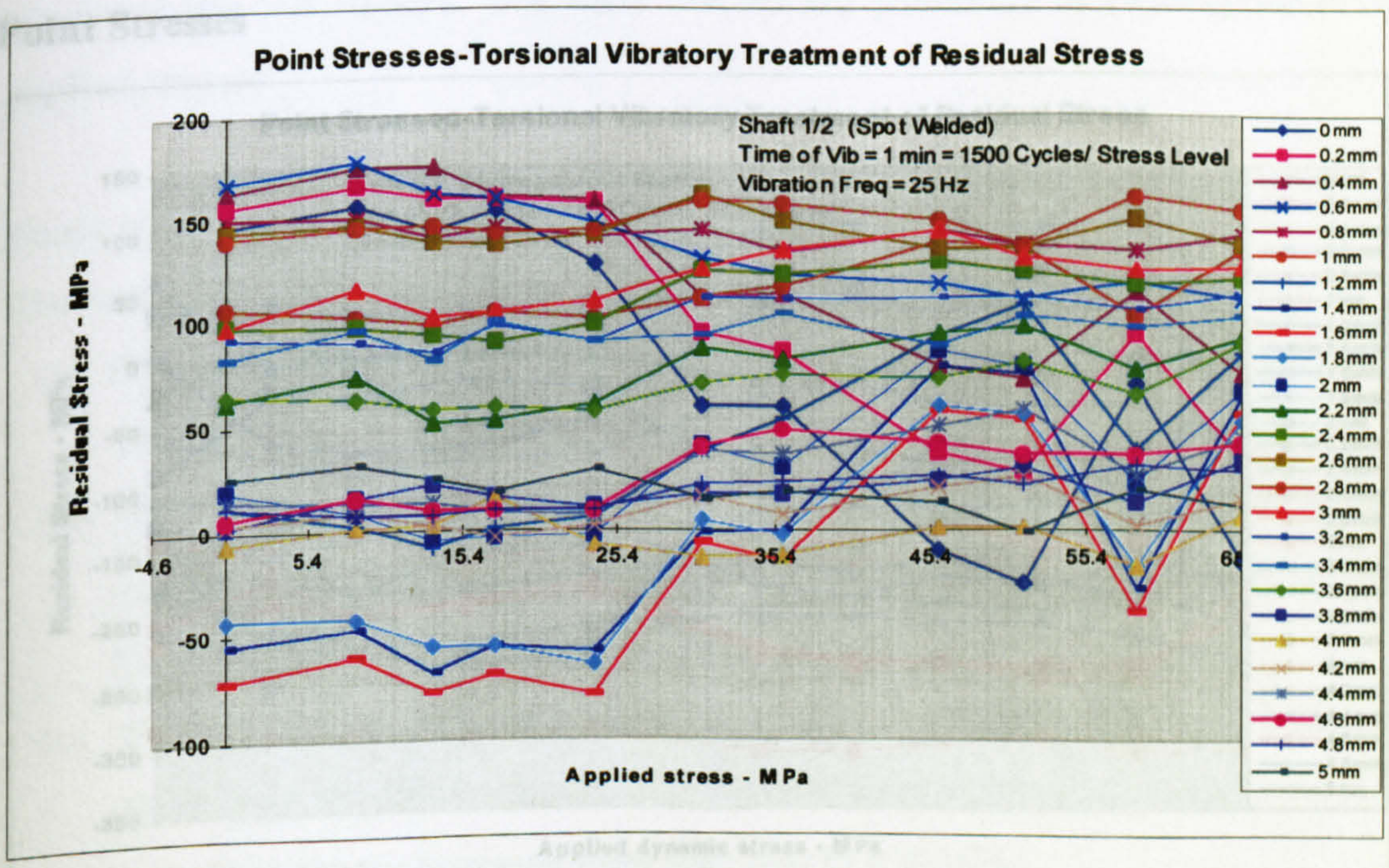

Figure 5.603 – Longitudinal point stresses - shaft 1/2

Shaft 1/3

Line Stresses

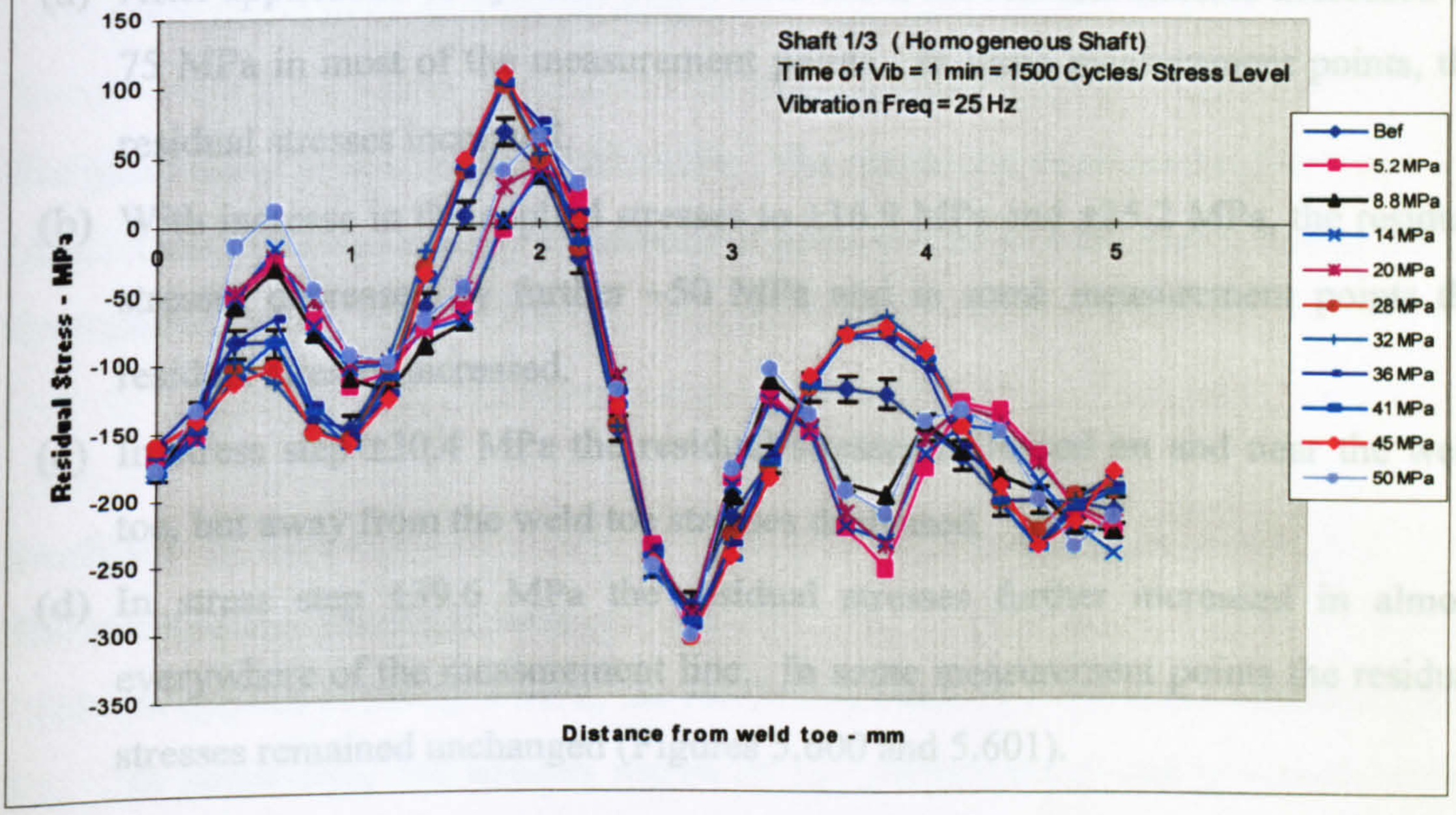

Figure 5.604 – Longitudinal line stress plot - shaft 1/3

Point Stresses

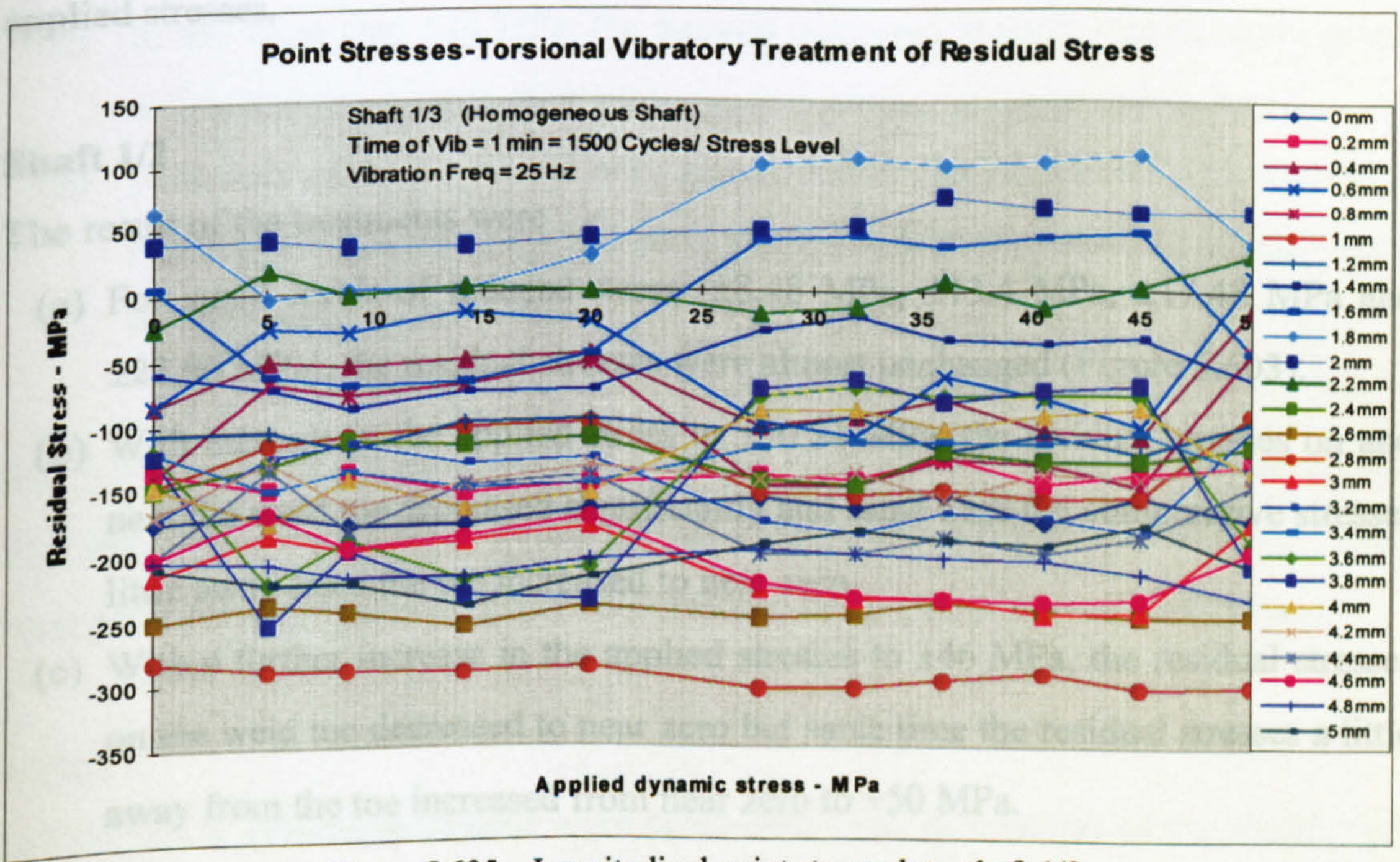

Figure 5.605 – Longitudinal point stress plot - shaft 1/3

Discussion of Result - Batch 1

Shaft 1/1

The results of the treatments were

(a) After application of dynamic stress ±8.5 MPa, the residual stresses decreased by 75 MPa in most of the measurement points. In some measurement points, the residual stresses increased.

(b) With increase in the applied stresses to ±16.9 MPa and ±25.2 MPa, the residual stresses decreased by further ~50 MPa and in some measurement points the residual stresses increased.

(c) In stress step ±30.4 MPa the residual stresses increased on and near the weld toe, but away from the weld toe stresses decreased.

(d) In stress step ±39.6 MPa the residual stresses further increased in almost everywhere of the measurement line. In some measurement points the residual stresses remained unchanged (Figures 5.600 and 5.601).

In this shaft the yield stress of the material was 277 MPa. The maximum stress in the measured line was ~0 MPa, thus, there was not any possibility of yielding due to the applied stresses.

Shaft 1/2

The result of the treatments were

(a) For small levels of induced stress (±8.48 MPa, ±13.4 MPa, ±17.48 MPa and ±23.96 MPa), the residual stresses were almost unchanged (Figure 5.603).

(b) With increase in the applied stress to ±30.84 MPa, the residual stresses on and near the weld toe decreased significantly and same time the compressive stresses little away from the toe increased to near zero.

(c) With a further increase in the applied stresses to ±46 MPa, the residual stresses on the weld toe decreased to near zero but same time the residual stresses a little away from the toe increased from near zero to +50 MPa.

(d) In applied stress step ±51.4 MPa, the residual stresses were similar to the residual stresses of stress step ±46 MPa.

(e) With further increase in the applied stresses to ±58.7 MPa and ±65.4 MPa, the residual stresses were changed but there were not any clear trend i.e. stresses were found to be only redistributed.

The yield stress of this shaft was 277 MPa. The maximum stress on the line was ~170 MPa. Thus there was not any possibility of gross yielding of the shaft material during the treatments.

Shaft 1/3

The result of the treatments were

(a) In applied stress ±5.2 MPa, the residual stresses of some areas decreased, also in some area, the stresses increased i.e. redistribution was observed in this stress step.

(b) In the next three stress steps (±8.8 MPa, ±14 MPa and ±20 MPa), the residual stresses were almost unchanged.

(c) In the stress step ±28 MPa, the stresses increased in some measurement points and decreased in some other measurement points, i.e. again redistributed.

(d) Next four stress steps (±32 MPa to ±45 MPa) showed virtually no change in residual stresses but at the last stress step (±50 MPa) the residual stresses again redistributed.

The yield stress of the shaft material was 277 MPa, the maximum applied stress was ±50 MPa and the maximum residual stress of the measured line was 60 MPa. Thus, most possibly there was no local yielding of the metal due to the induced stresses.

Batch 2

In this batch, several specimens were processed. The dimensions of the shafts were 21.3 mm OD, 13.9 mm ID and 430 mm in length. The test set-ups were modified and

the applied stress was calibrated (as shown in section 5.4.4.3). The calibration constant was 1 mV equals 0.0414 MPa.

Shaft 1/4

This shaft was treated without any weld, i.e. as a homogeneous shaft. The measurement surface was prepared by electro-polishing. The used voltage and current in the electropolishing were 30 V and 3.3 A. The depth of the removed layer was approximately 50 microns. The residual stress of the line was measured then the vibratory treatment was carried out. Circumferential residual stress on a 12 mm line (shown in Figure 5.599) was measured after every step of the treatment. The applied stress was varied from 0 to 118 MPa in 11 steps. The time of vibration was also stepped in treating the shaft in each stress step. The residual stresses after each stress step was plotted. No significant effect of vibratory treatment was observed. Instead of all stress step plots the summary plot is shown here to save some space. In the summery plot, the initial residual stress and the residual stresses after the final interval of treatment of every applied stress step is shown.

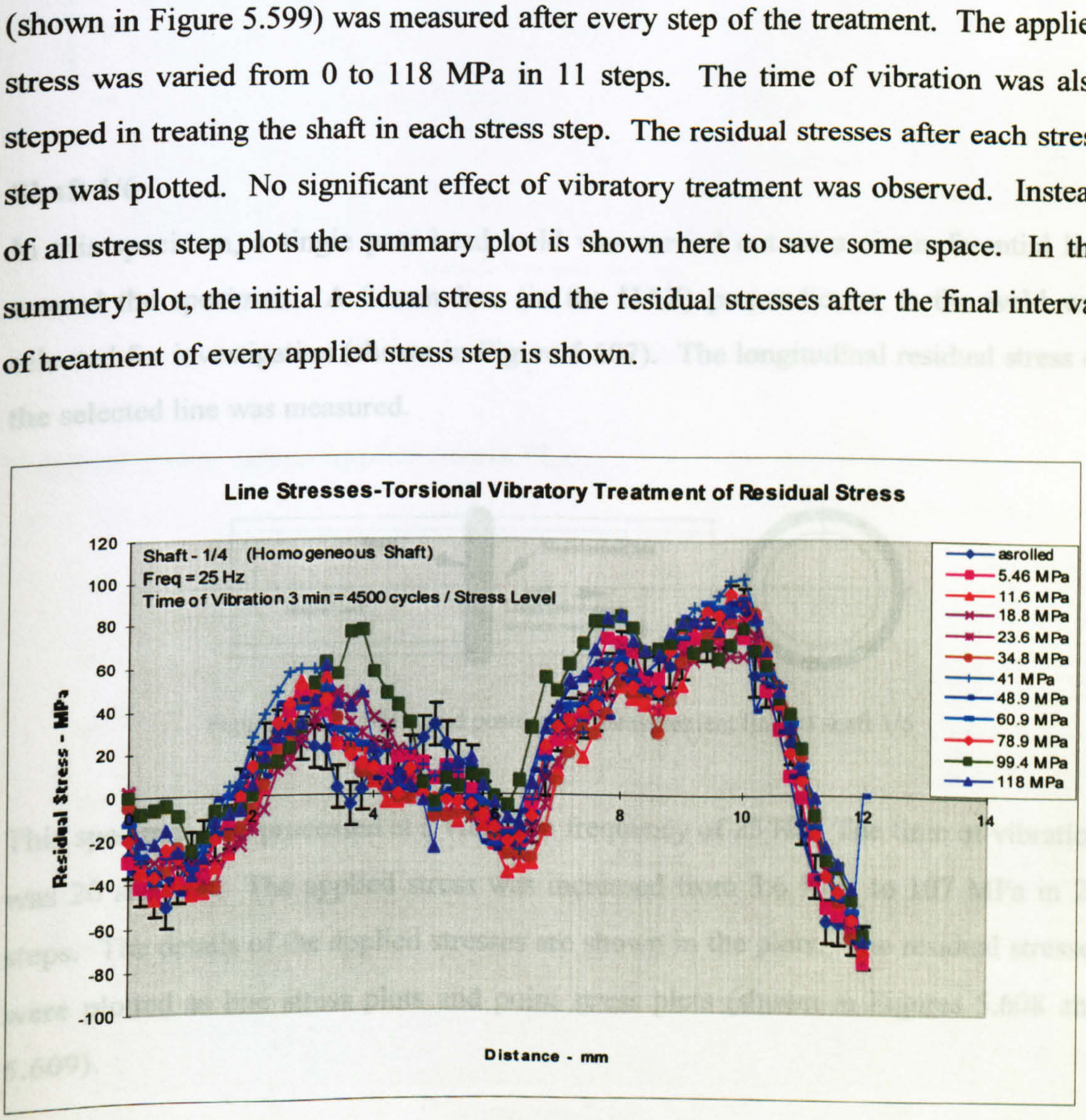

Figure 5.606 – Circumferential line residual stresses - shaft ¼

Discussion of Result – Shaft 1/4

In this shaft, no observable reduction in the residual stresses was observed. The small change in the residual stresses that was observed here was due to different levels of applied stresses was very small.

The yield stress of this shaft material was 350 MPa. The residual stresses of the shaft was small (~75 MPa) and the applied stresses of the treatments were maximum 118 MPa. Thus, the possibility of plastic deformation due to the applied stress was very small.

Shaft 1/6

In this specimen, a single pass bead weld was carried out on a circumferential line around the specimen. A 3 mm line (in the HAZ) perpendicular to the weld was selected for investigation (shown in Figure 5.607). The longitudinal residual stress of the selected line was measured.

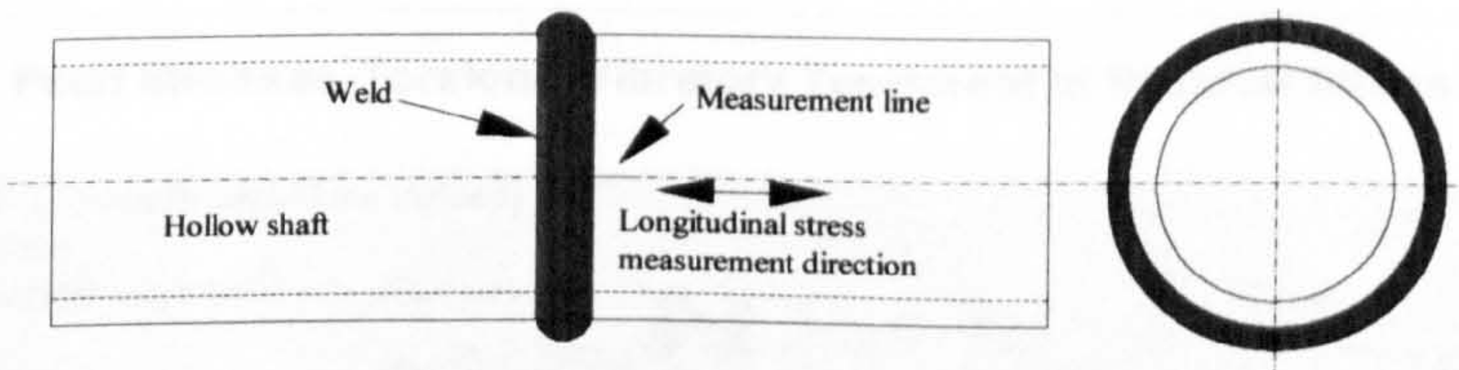

Figure 5.607 - Weld and position of measurement line on shaft 1/6

This specimen was processed at a vibration frequency of 25 Hz. The time of vibration was 20 seconds. The applied stress was increased from 3.6 MPa to 107 MPa in 22 steps. The details of the applied stresses are shown in the plots. The residual stresses were plotted as line stress plots and point stress plots (shown in Figures 5.608 and 5.609).

Shaft 1/6

Line Stresses

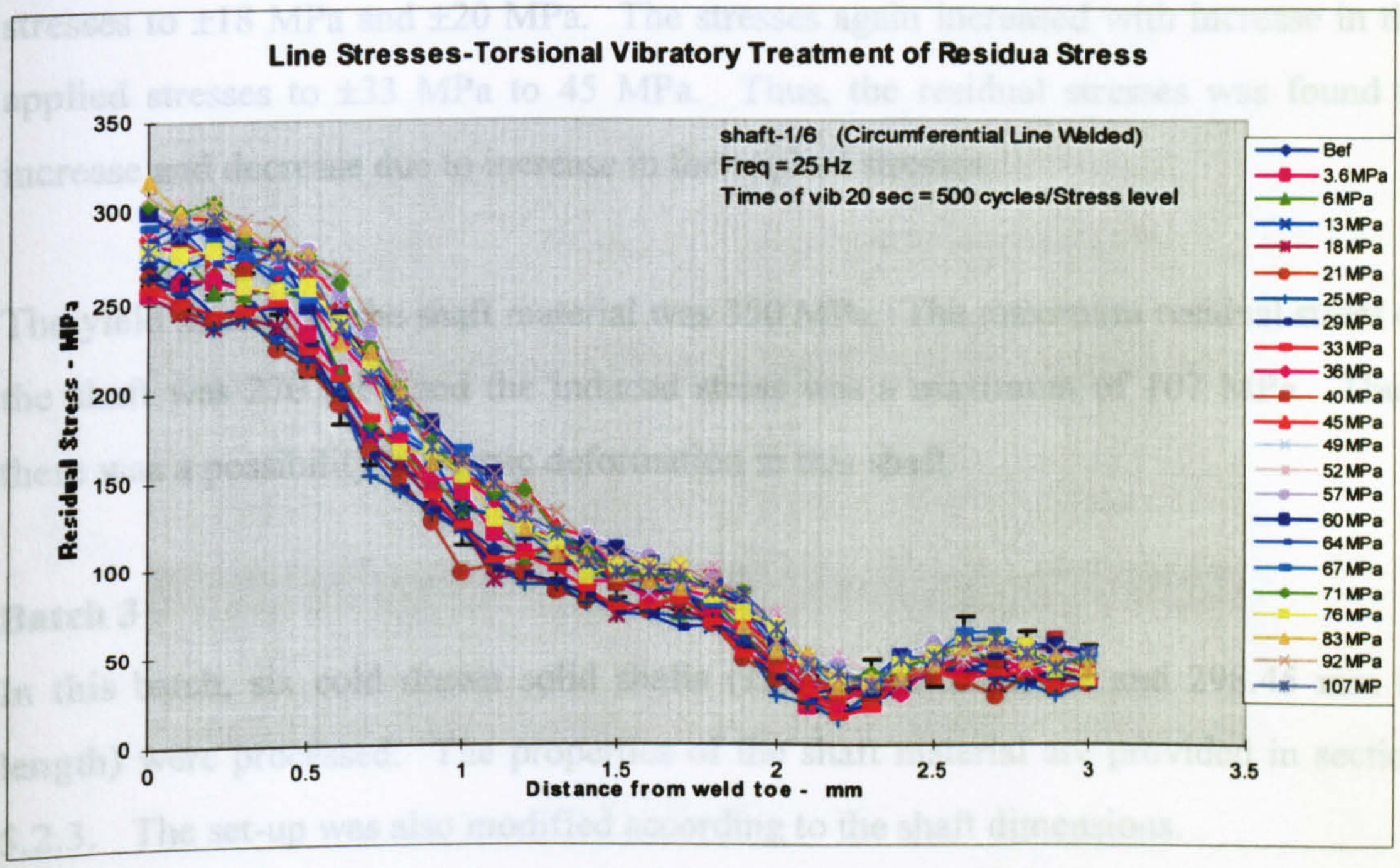

Figure 5.608 – Longitudinal line stress plot - specimen 1/6

Residual Stress versus Applied Stress Plot

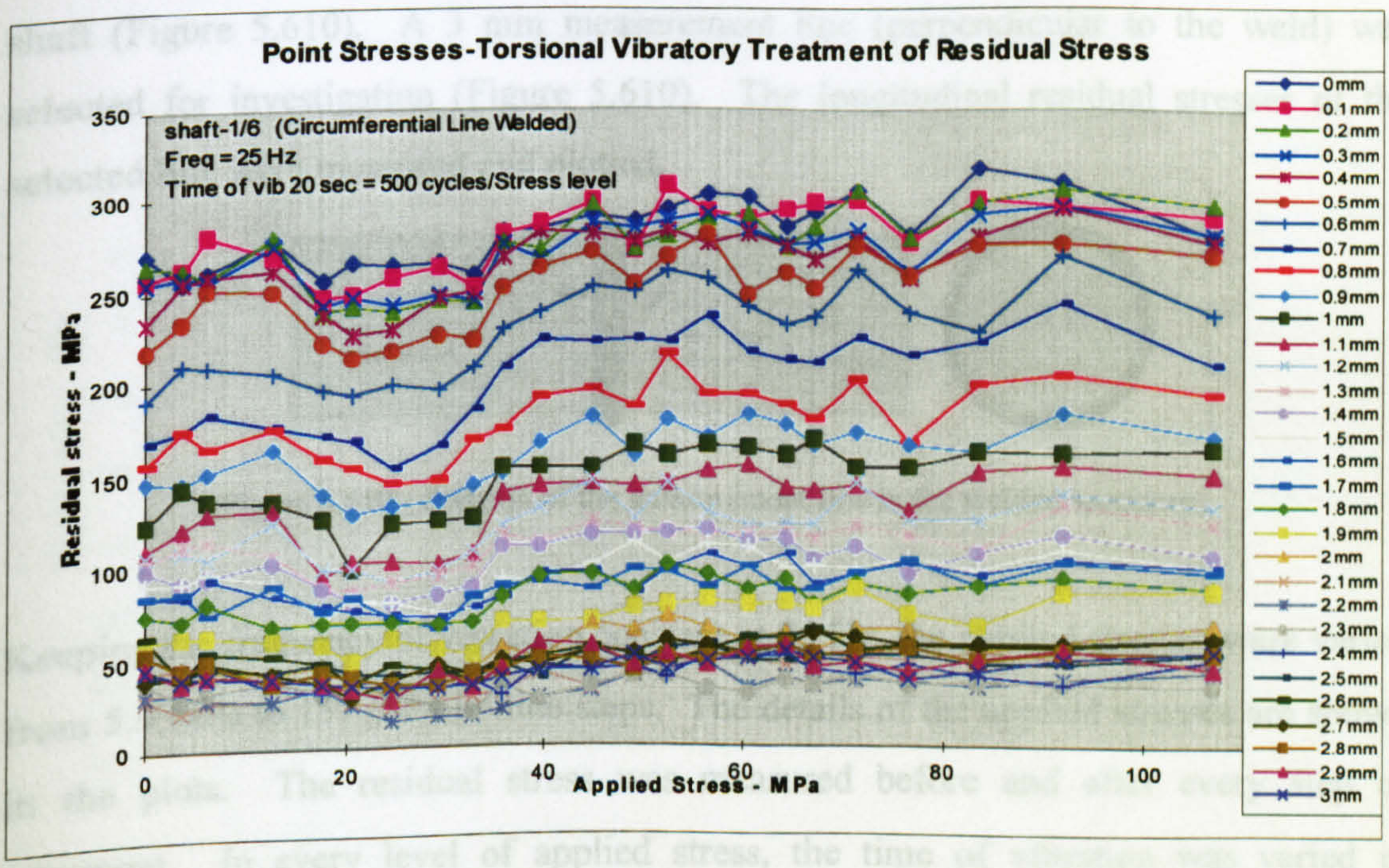

Figure 5.609 – Longitudinal residual stress versus applied stress plot - shaft 1/6

Discussion of Result - Shaft 1/6

In this shaft the residual stresses increased with application of small dynamic stresses (±3.6 MPa and ±6 MPa) but the stresses again decreased with increase in the applied stresses to ±18 MPa and ±20 MPa. The stresses again increased with increase in the applied stresses to ±33 MPa to 45 MPa. Thus, the residual stresses was found to increase and decrease due to increase in the applied stresses.

The yield stresses of the shaft material was 350 MPa. The maximum residual stress of the shaft was 270 MPa and the induced stress was a maximum of 107 MPa. Thus, there was a possibility of plastic deformation in this shaft.

Batch 3

In this batch, six cold drawn solid shafts (15.875 mm diameter and 298.45 mm in length) were processed. The properties of the shaft material are provided in section 5.2.3. The set-up was also modified according to the shaft dimensions.

Shaft 2/1

In this shaft a single pass bead weld was carried out on a circumferential line around shaft (Figure 5.610). A 3 mm measurement line (perpendicular to the weld) was selected for investigation (Figure 5.610). The longitudinal residual stresses of the selected line were measured and plotted.

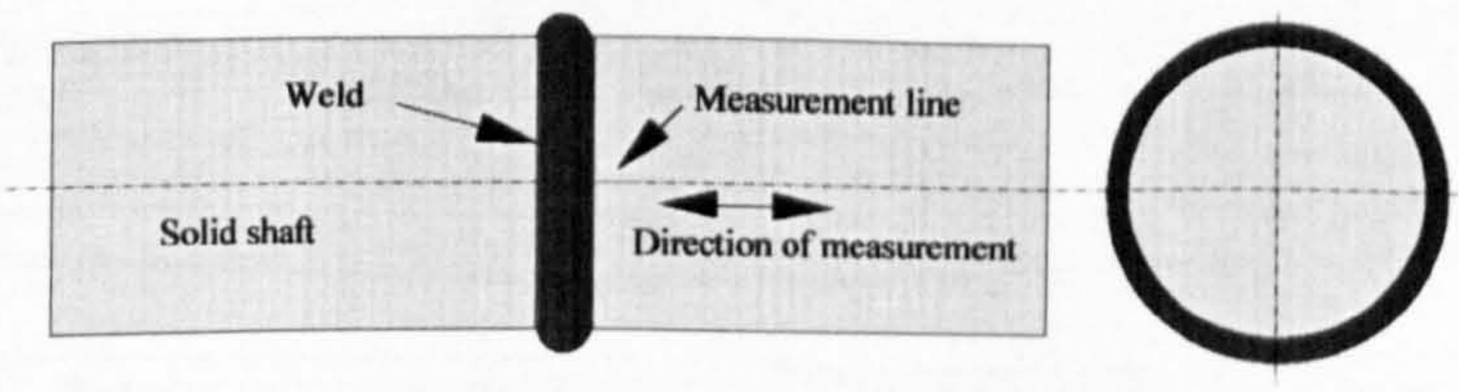

Figure 5.610 - Position of the measurement line in the welded specimen.

Keeping the frequency of vibration constant at 25 Hz, the applied stresses were varied from 5.9 MPa to 157 MPa in nine steps. The details of the applied stresses are shown in the plots. The residual stress was measured before and after every step of treatment. In every level of applied stress, the time of vibration was varied in different steps, which are shown in the relevant stress plots.

Shaft 2/1 – Applied Stress 5.9 MPa

Line Stresses

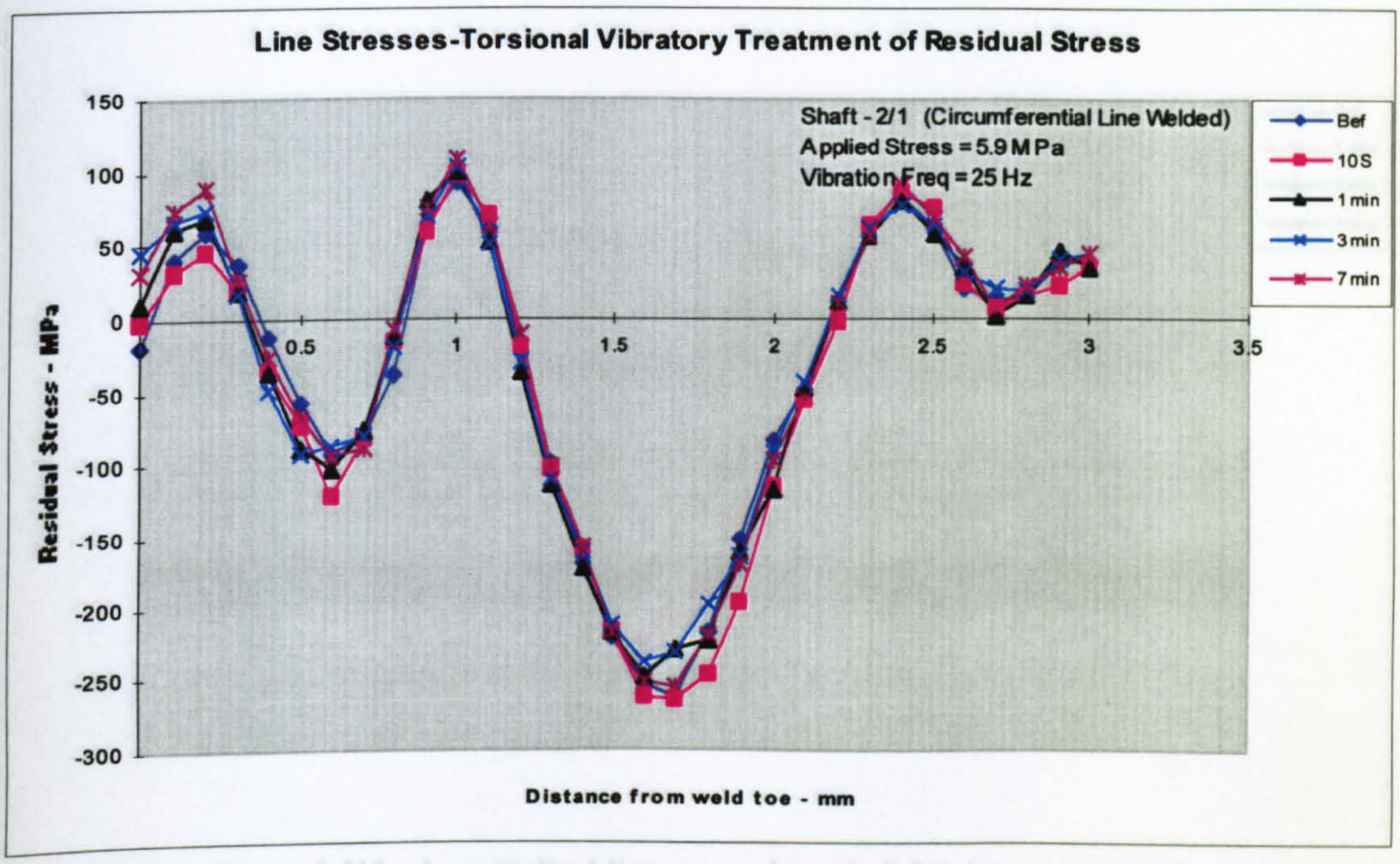

Figure 5.611 – Longitudinal line stress plot - shaft 2/1 (stress step one)

Point Stresses

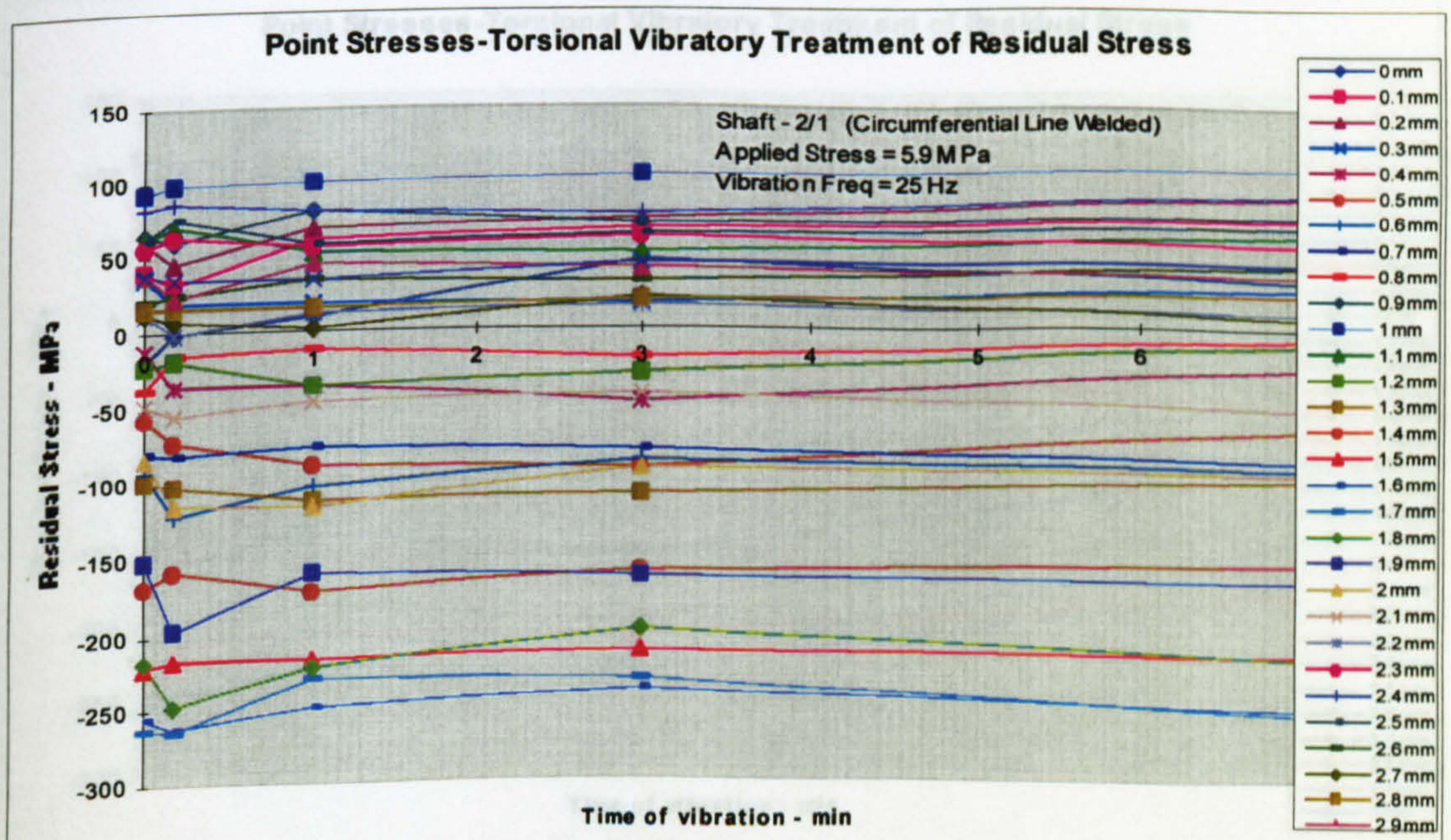

Figure 5.612 – Longitudinal point stress plot - shaft 2/1 (stress step one)

Shaft 2/1 – Applied Stress 15.15 MPa

Line Stresses

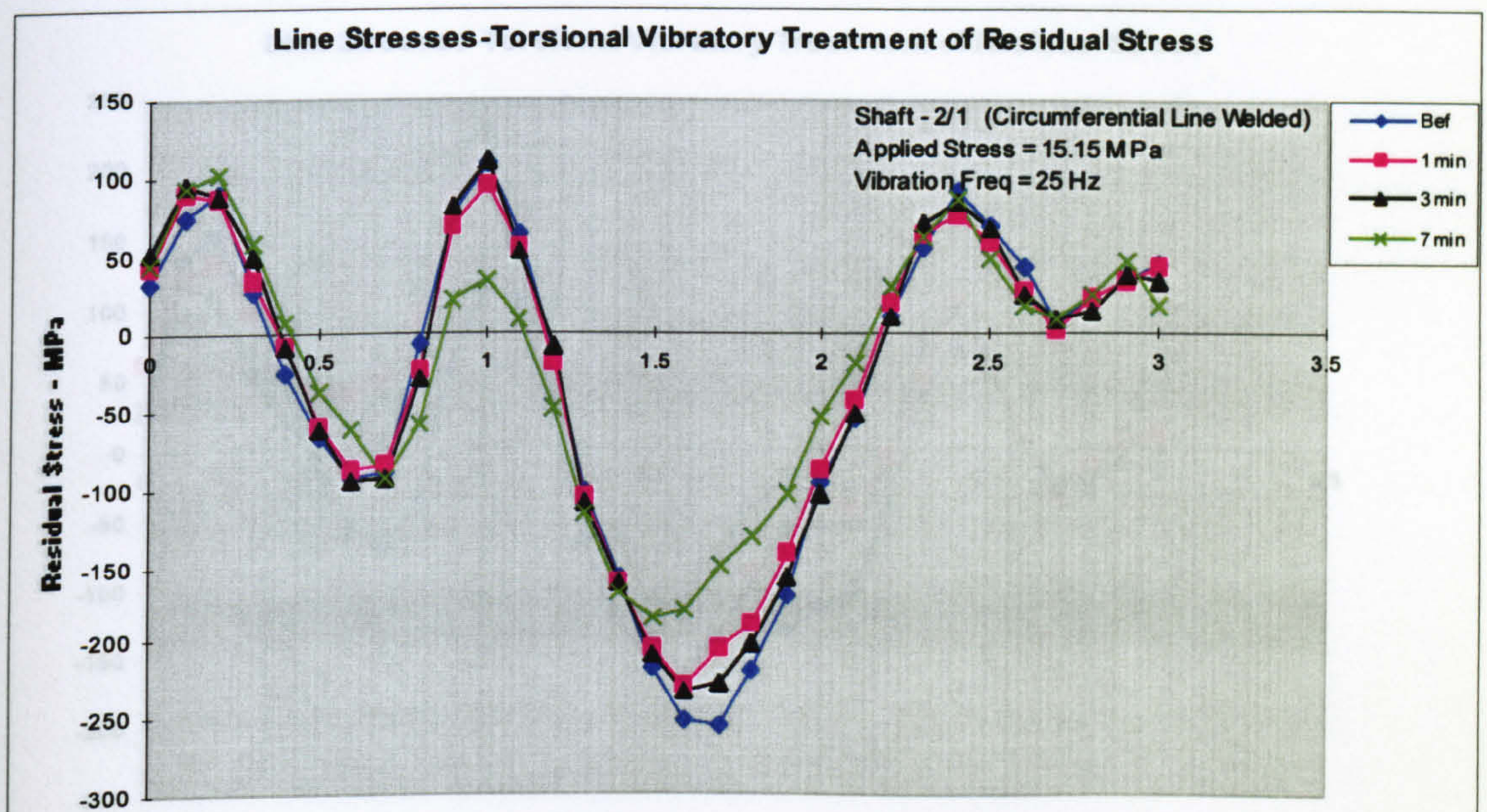

Figure 5.613 – Longitudinal line stress plot - shaft 2/1 (stress step two)

Point Stresses

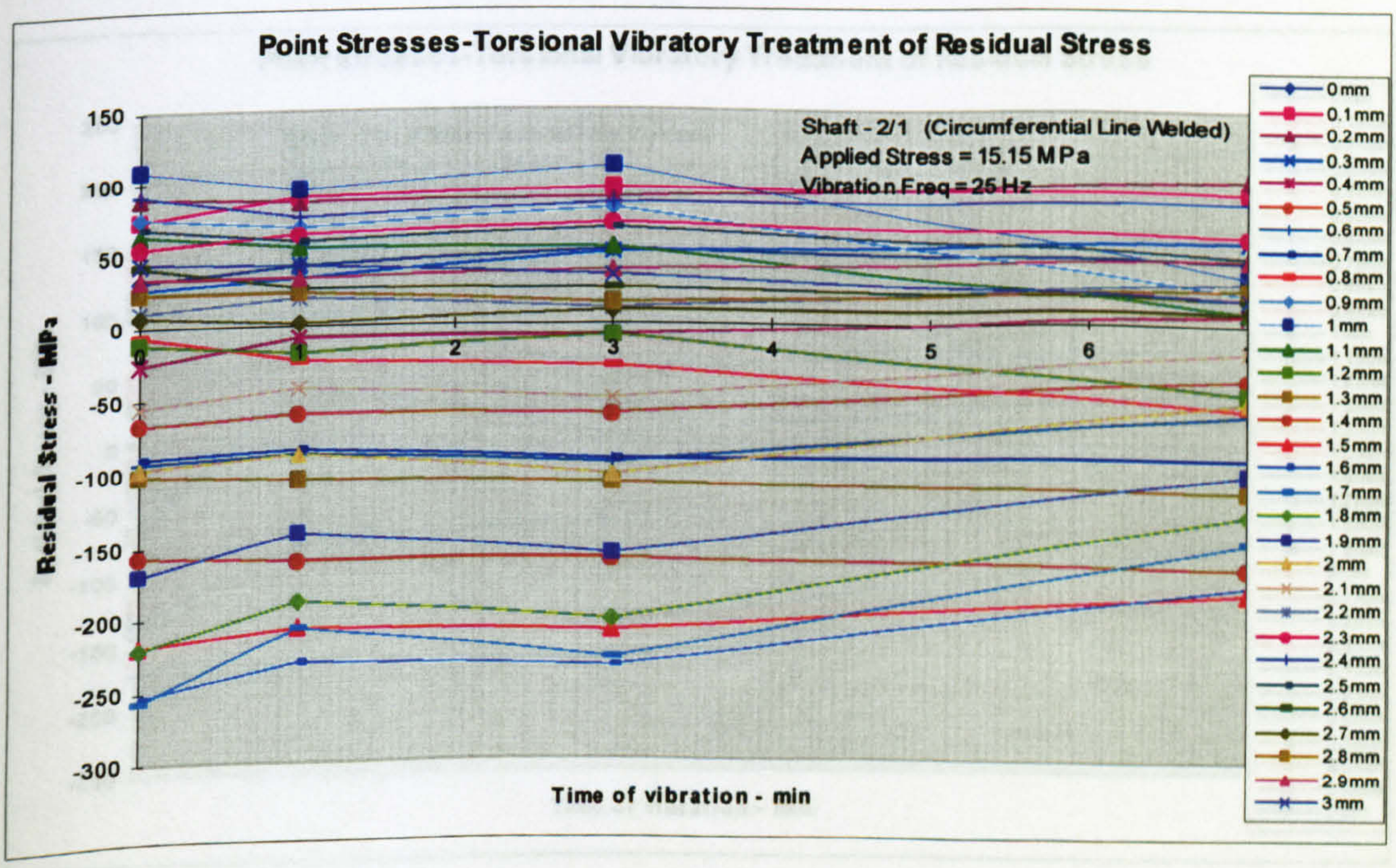

Figure 5.614 – Longitudinal point stress plot - shaft 2/1 (stress step two)

Shaft 2/1 – Applied Stress 123.24 MPa

Line Stresses

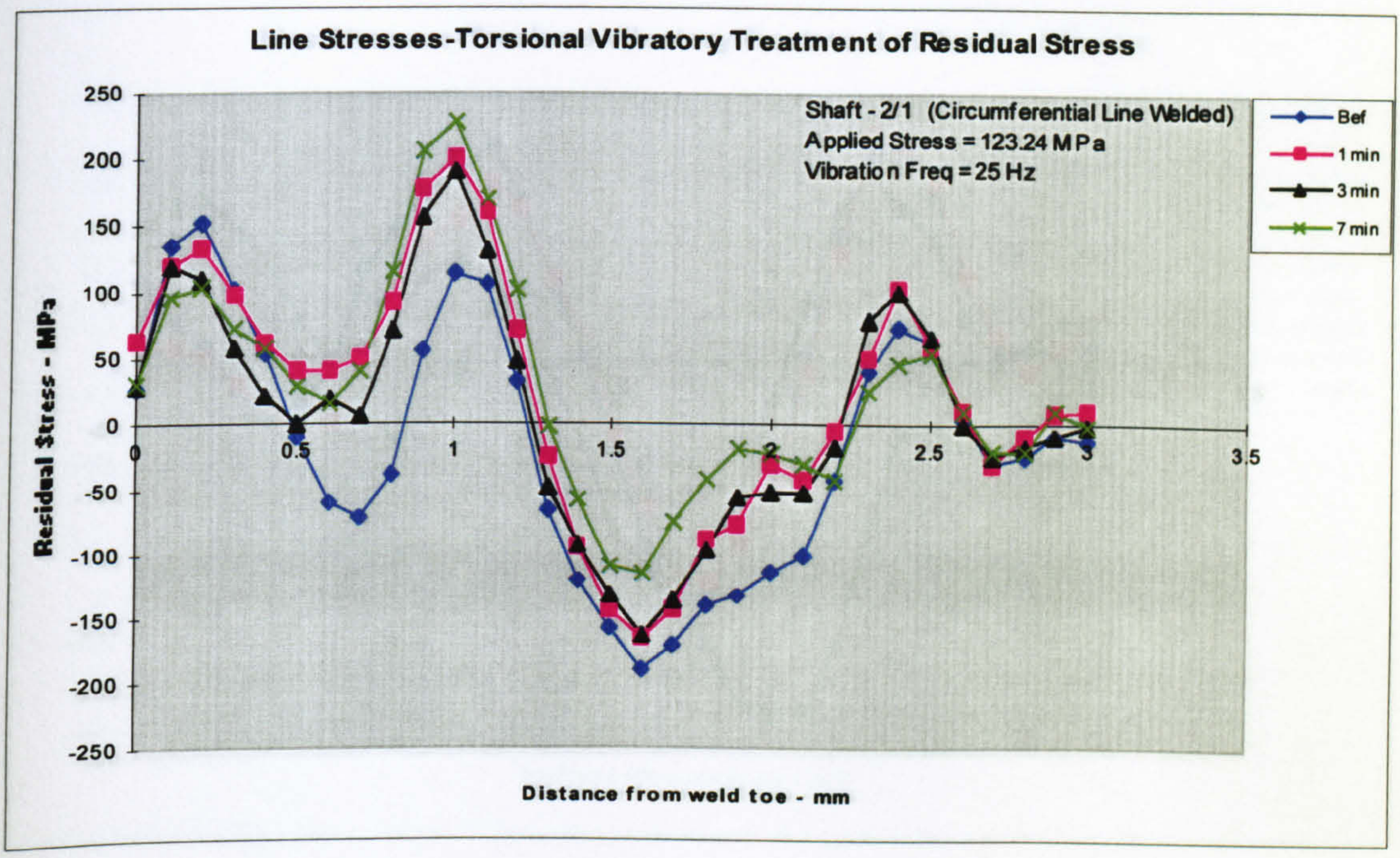

Figure 5.615 – Longitudinal line stress plot - shaft 2/1 (stress step seven)

Point Stresses

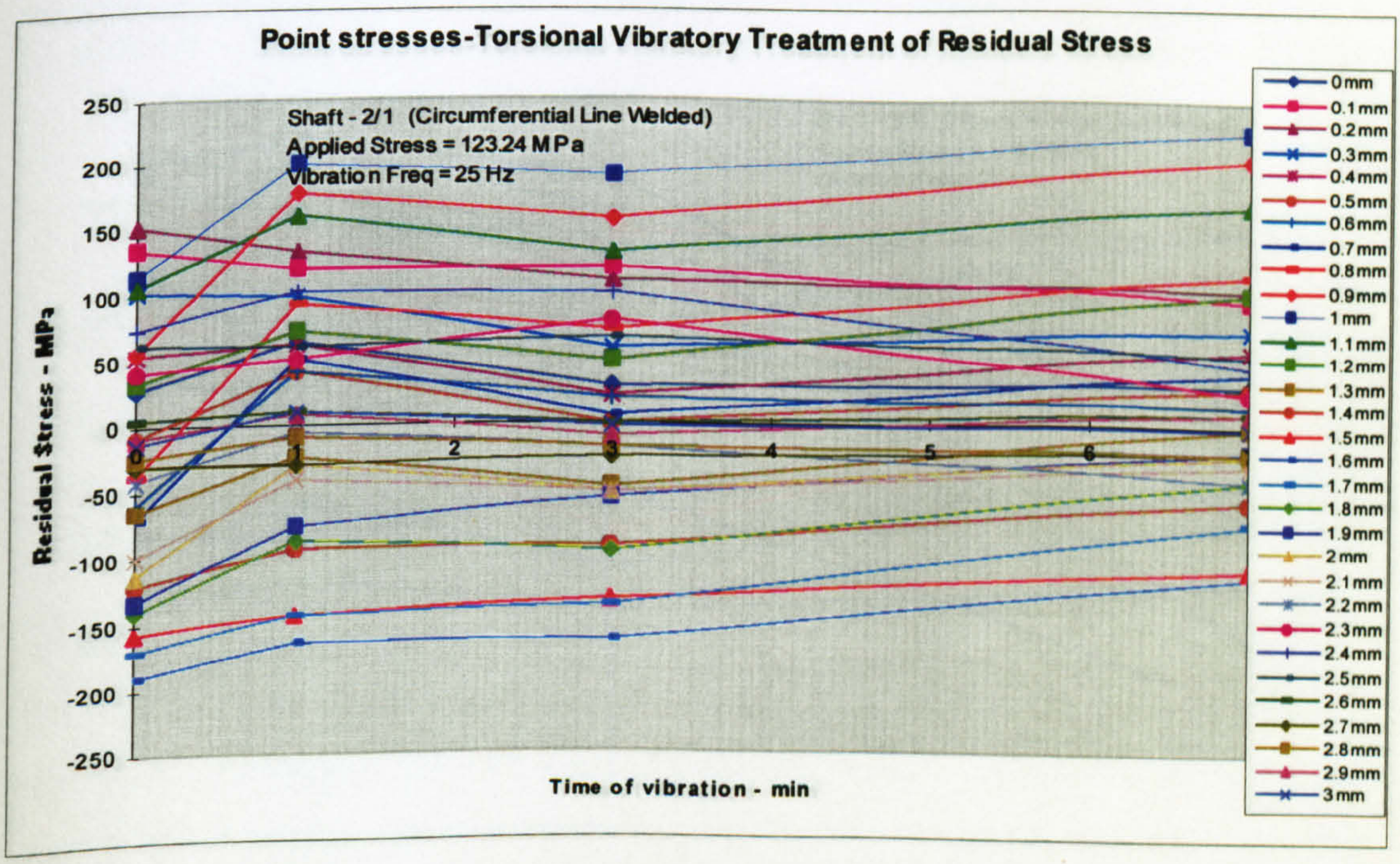

Figure 5.616 – Longitudinal point stress plot - shaft 2/1 (stress step seven)

Shaft 2/1 – Applied Stress 156.7 MPa

Line Stresses

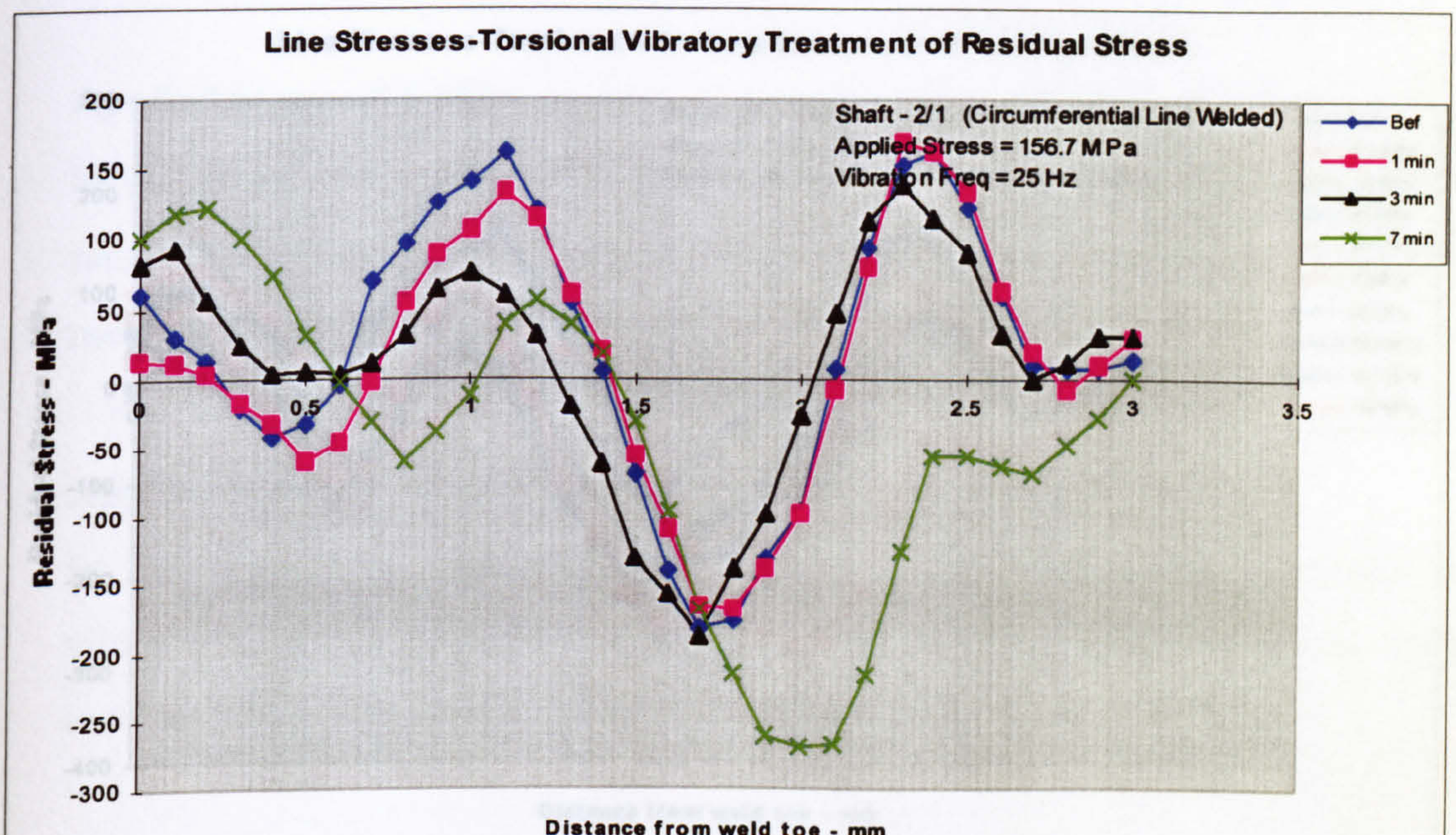

Figure 5.617 – Longitudinal line stress plot - shaft 2/1 (stress step nine)

Point Stresses

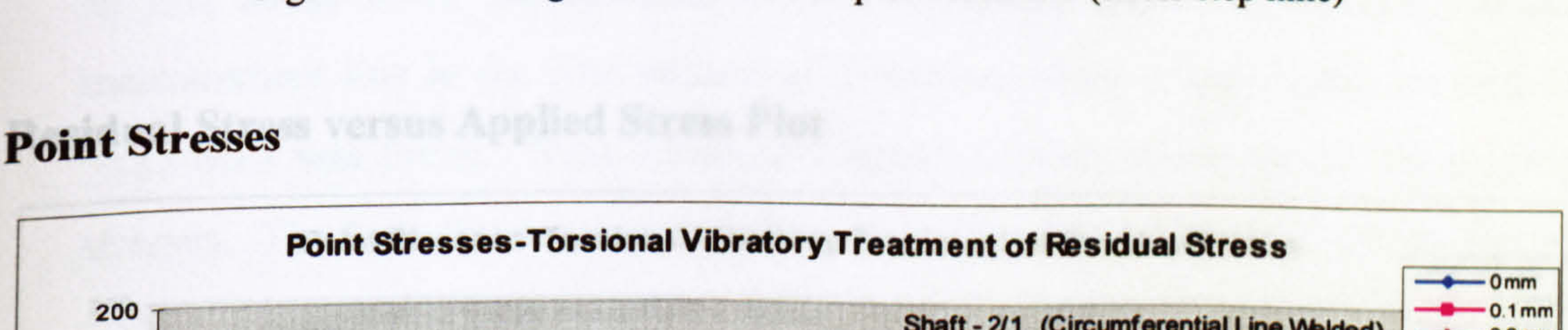

Figure 5.618 – Longitudinal point stress plot - shaft 2/1 (stress step nine)

Shaft 2/1 – Summary plot

Line Stresses

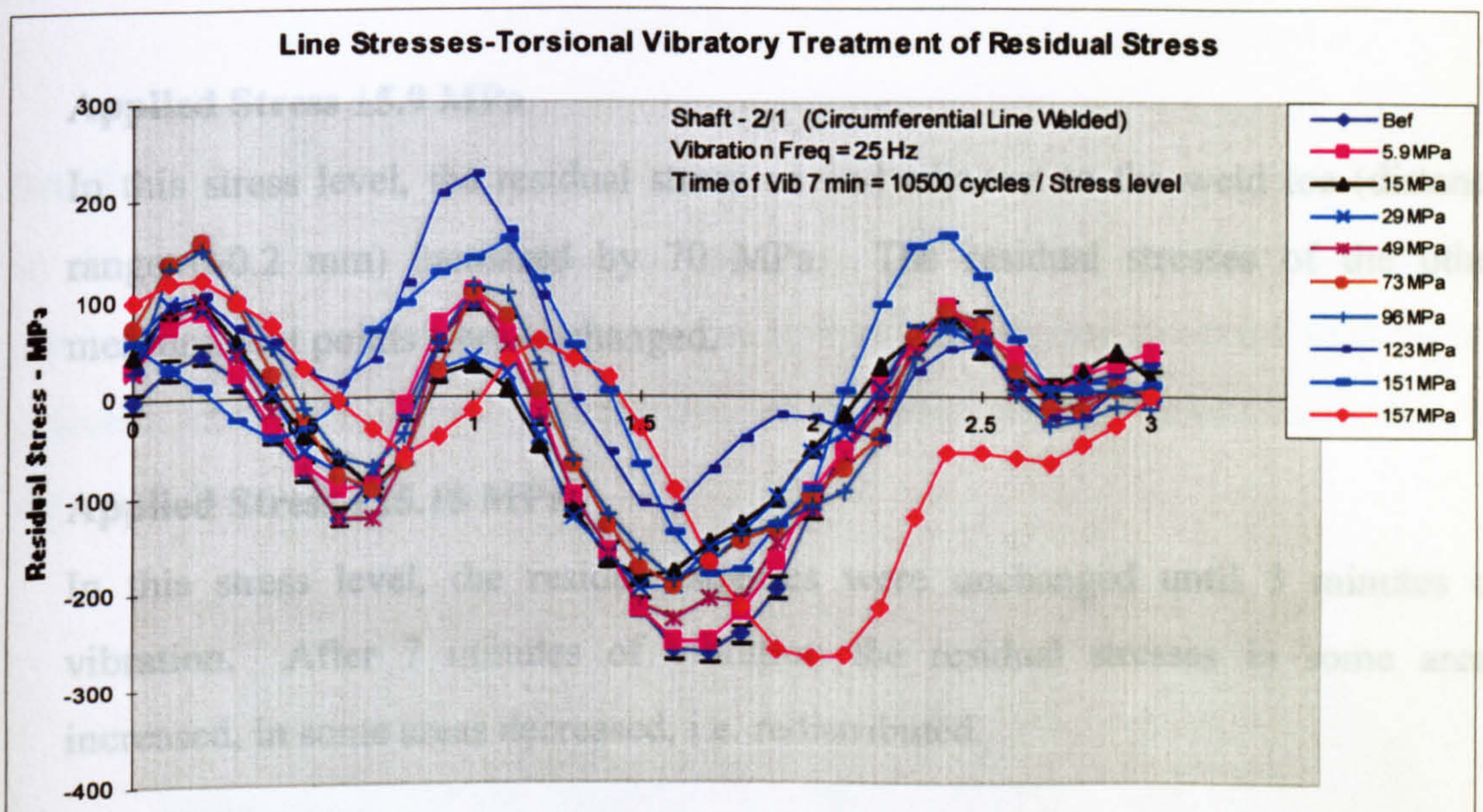

Figure 5.619 – Longitudinal line stress plot - shaft 2/1 (summary plot)

Residual Stress versus Applied Stress Plot

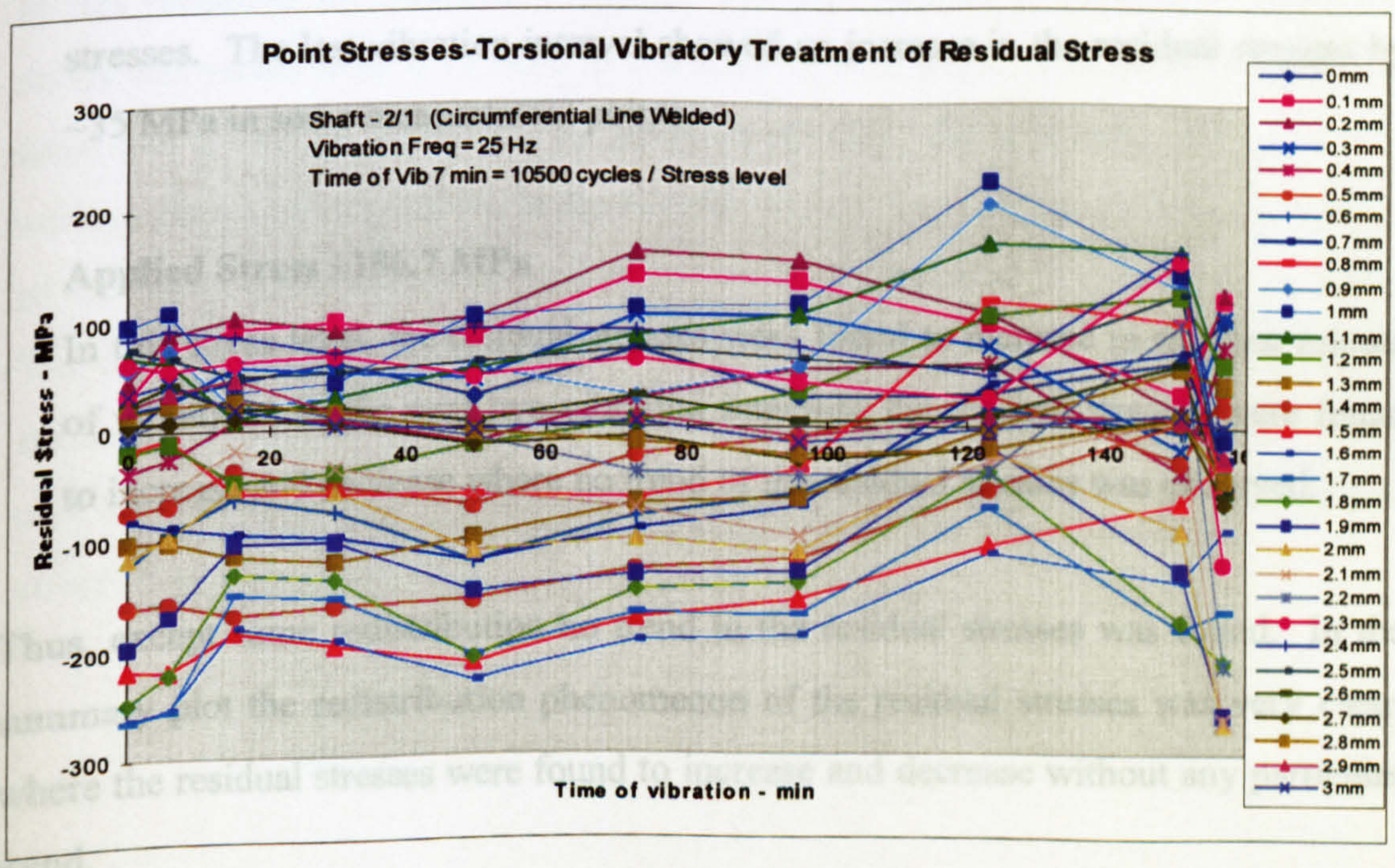

Figure 5.620 – Residual stress versus applied stress plot - shaft 2/1 (summary plot)

Discussion of Results - Shaft 2/1

Although this specimen was vibrated at nine different applied stress levels, only some selected stress levels are shown here to save some space. The results of the steps are

Applied Stress ±5.9 MPa

In this stress level, the residual stress on and adjacent to the weld toe (distance range 0-0.2 mm) increased by 70 MPa. The residual stresses of the other measurement points were unchanged.

Applied Stress ±15.15 MPa

In this stress level, the residual stresses were unchanged until 3 minutes of vibration. After 7 minutes of vibration the residual stresses in some areas increased, in some areas decreased, i.e. redistributed.

Applied Stress ±123.4 MPa

In this stress level, the residual stresses increased almost everywhere of the measurement line in the first minute of vibration, where a maximum increase of ~125 MPa was found. Next vibration interval showed no change in the residual stresses. The last vibration interval showed an increase in the residual stresses by ~35 MPa in some measurement points.

Applied Stress ±156.7 MPa

In this stress level, the residual stresses were found to increase in the first minute of vibration. In the next two vibration intervals, the residual stresses were found to increase and decrease where no trend of the residual stresses was observed.

Thus, except some redistribution no trend in the residual stresses was found. In the summary plot the redistribution phenomenon of the residual stresses was very clear, where the residual stresses were found to increase and decrease without any particular trend.

The yield stress of the shaft was 400 MPa. The maximum applied stress was 156 MPa and the maximum residual stress of the measured line was 100 MPa. Thus, there was not any possibility of local yielding during the treatment.

Shaft 2/2

In this shaft, a spot was welded at the mid-length between the fixed end and the torsion arm (Figure 5.621). A 3 mm line in the HAZ starting from the weld toe was selected for investigation. The position of the weld and the measurement line are shown in Figure 5.621 below.

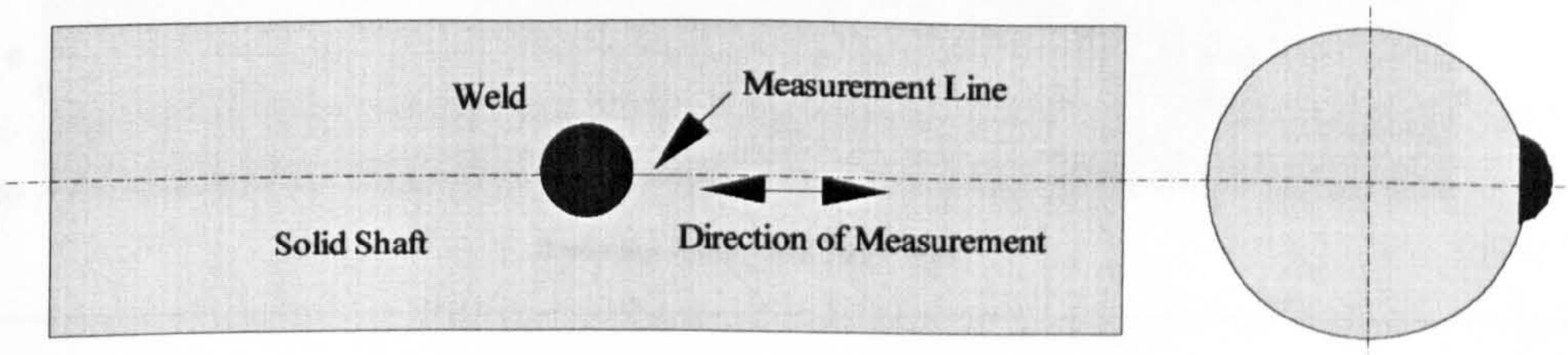

Figure 5.621 - Position of weld and measurement line

In this specimen, the vibration frequency was kept constant at 25 Hz and the applied stress was varied from 6.15 MPa to 156 MPa in nine steps. The details of the stress steps are shown in the plots. At every stress step, the specimen was vibrated at various time intervals (shown in the relevant plots). The longitudinal residual stresses of the selected line were measured before treatment and after every step of treatment. The residual stresses of all applied stress levels were plotted. Residual stress plot of some selected stress levels and the summary plot are included here. In the summary plot the residual stress before vibration and after the last interval of vibration in each stress level is included.

Shaft 2/2 – Induced Stress 6.15 MPa

Line Stresses

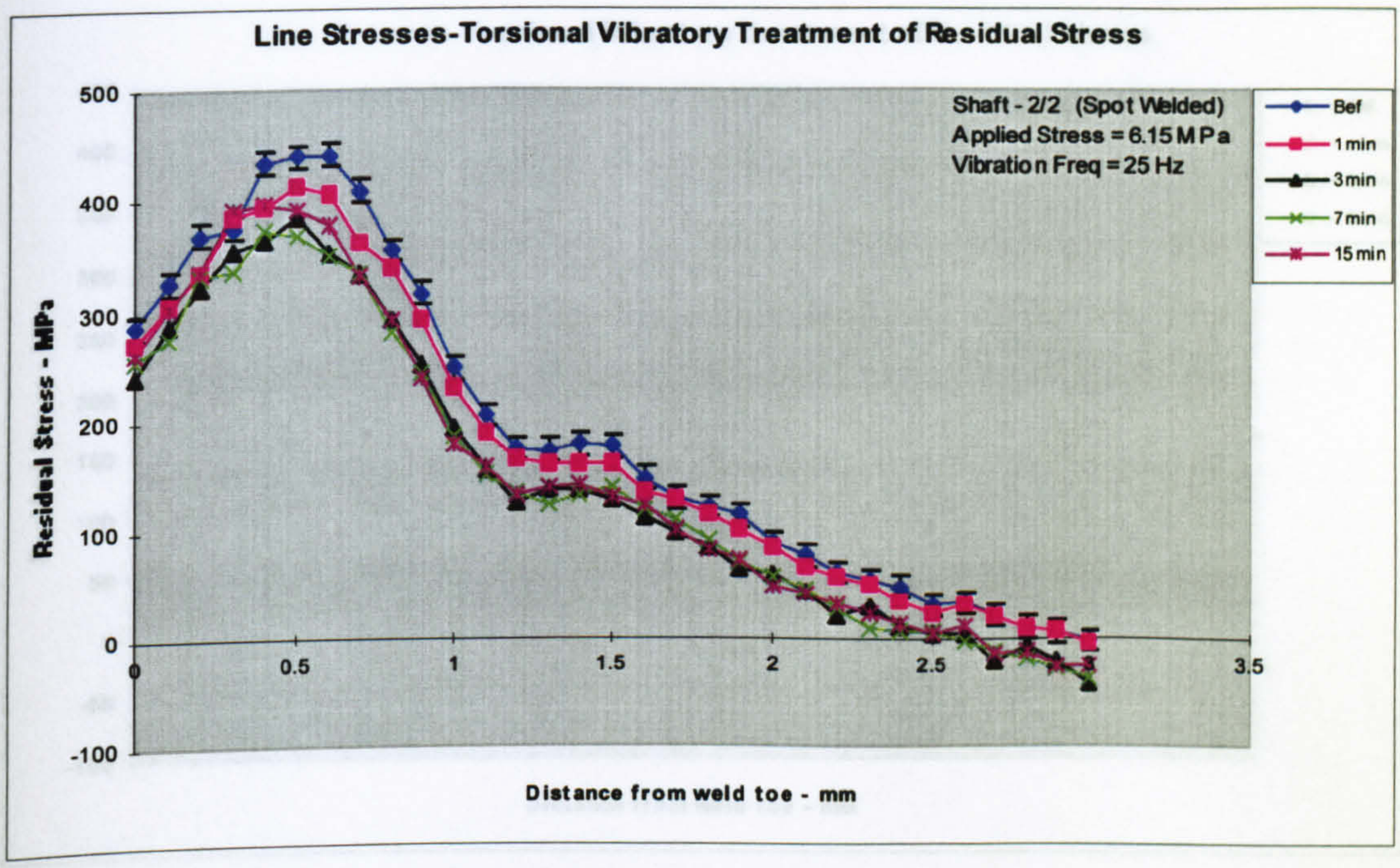

Figure 5.622 – Longitudinal line stresses plot - shaft 2/2 (stress step 1)

Point Stresses

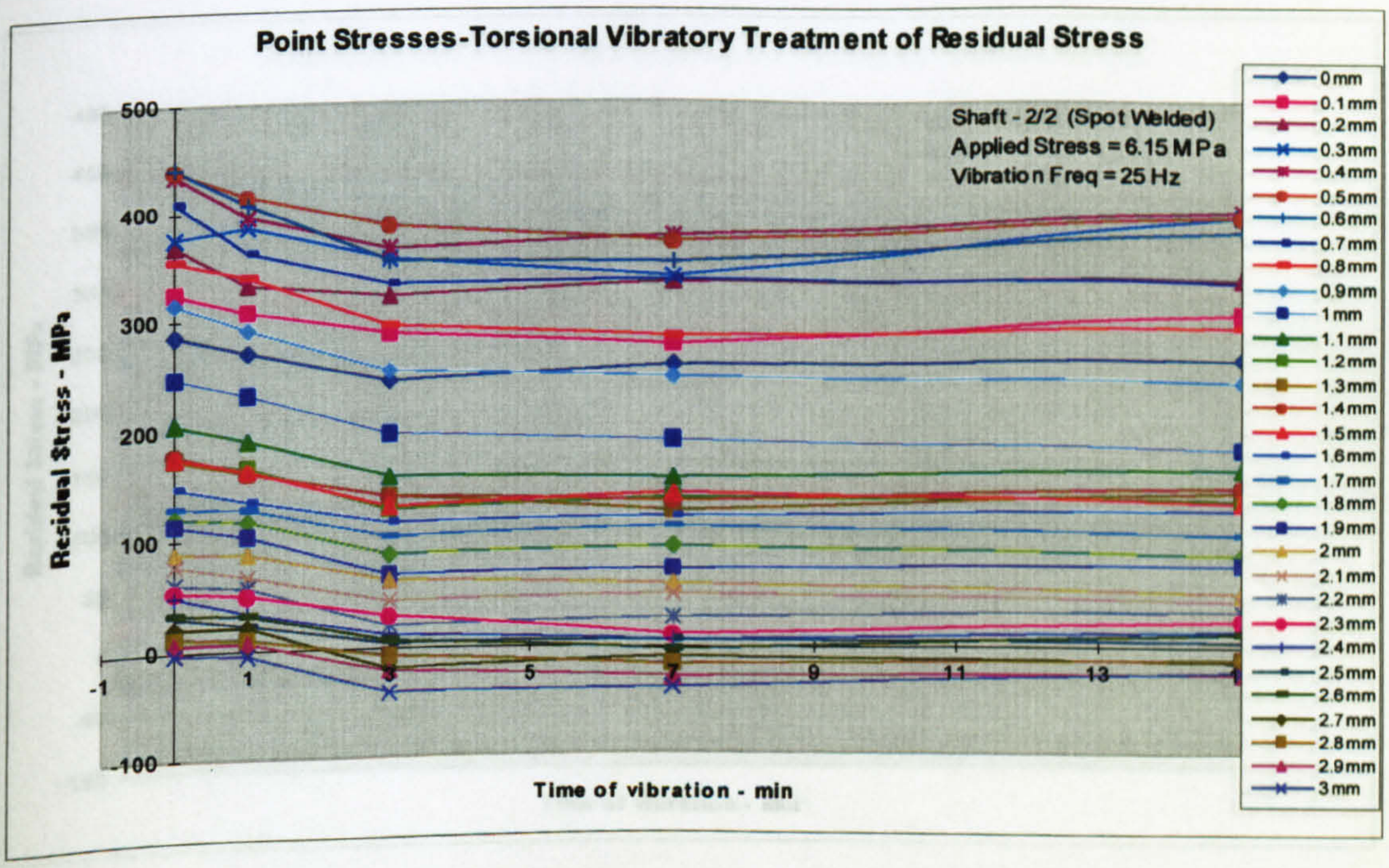

Figure 5.623 – Longitudinal point stresses plot - shaft 2/2 (stress step 1)

Shaft 2/2 – Applied Stress 15.15 MPa

Line Stresses

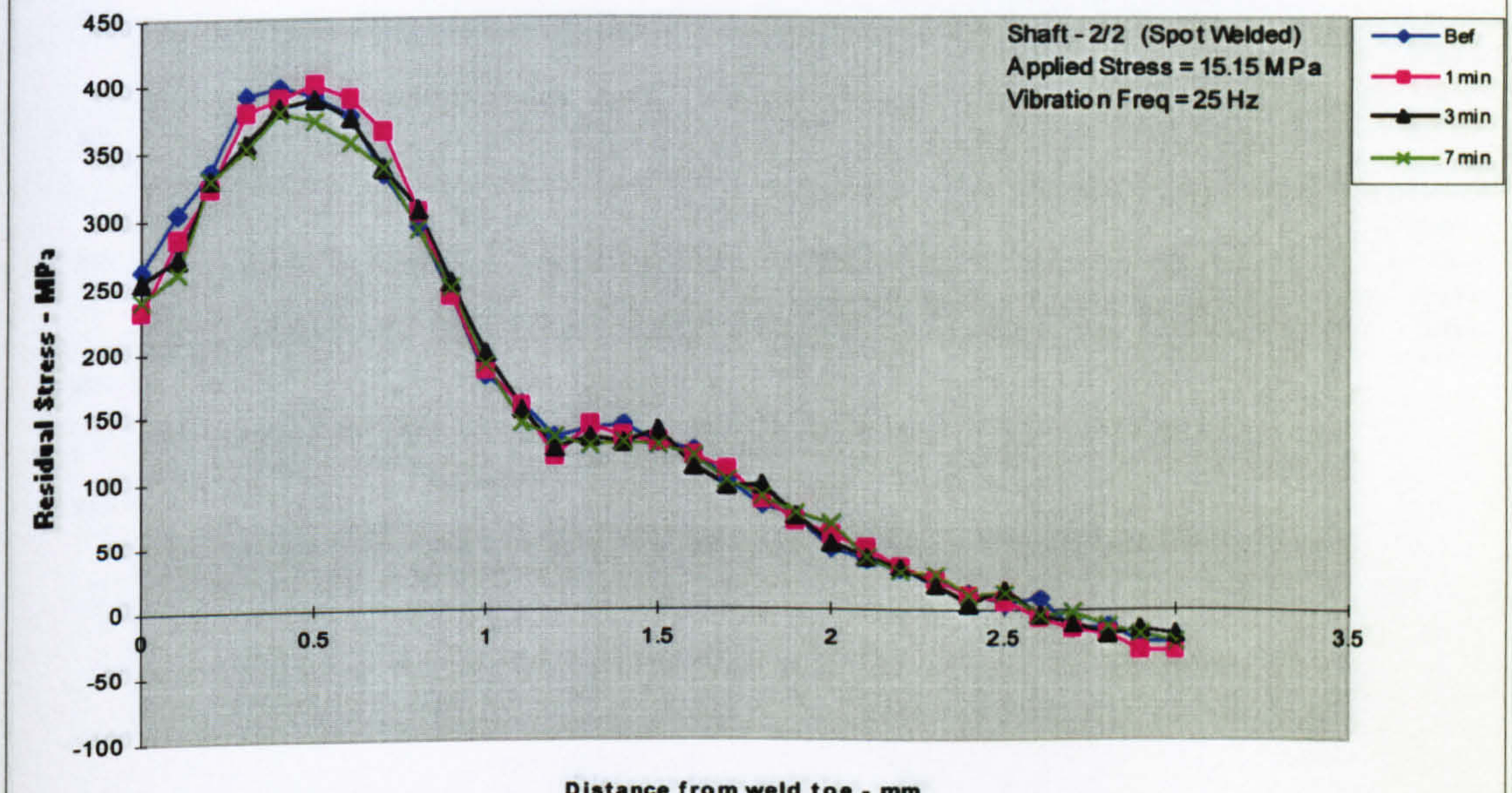

Figure 5.624 – Longitudinal line stresses plot - shaft 2/2 (stress step 2)

Point Stresses

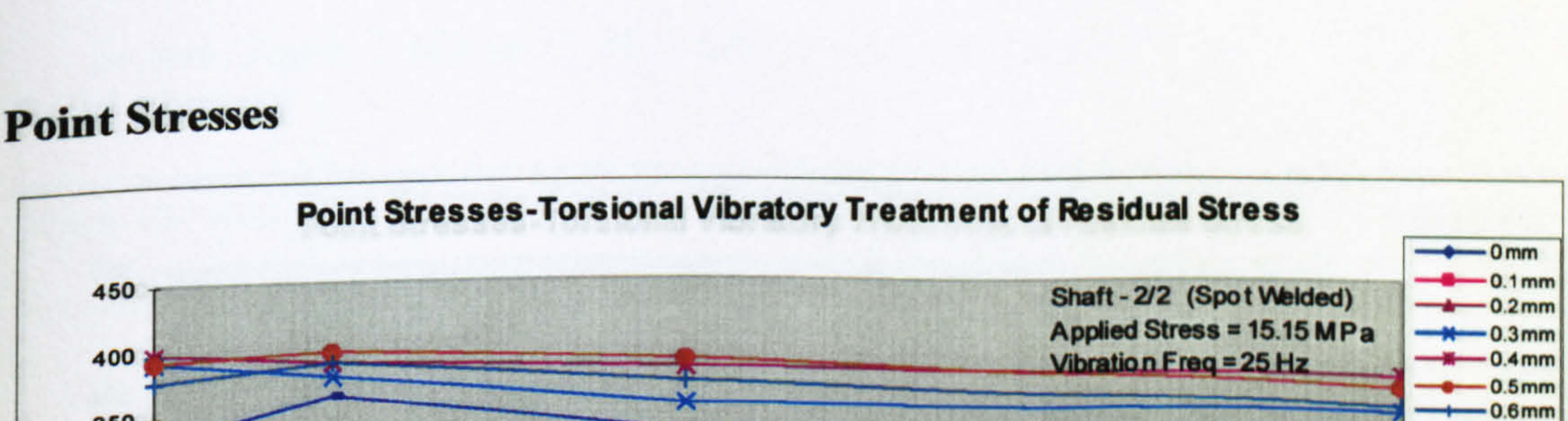

Figure 5.625 – Longitudinal point stresses plot - shaft 2/2 (stress step 2)

Shaft 2/2 – Induced Stress 114 MPa

Line Stresses

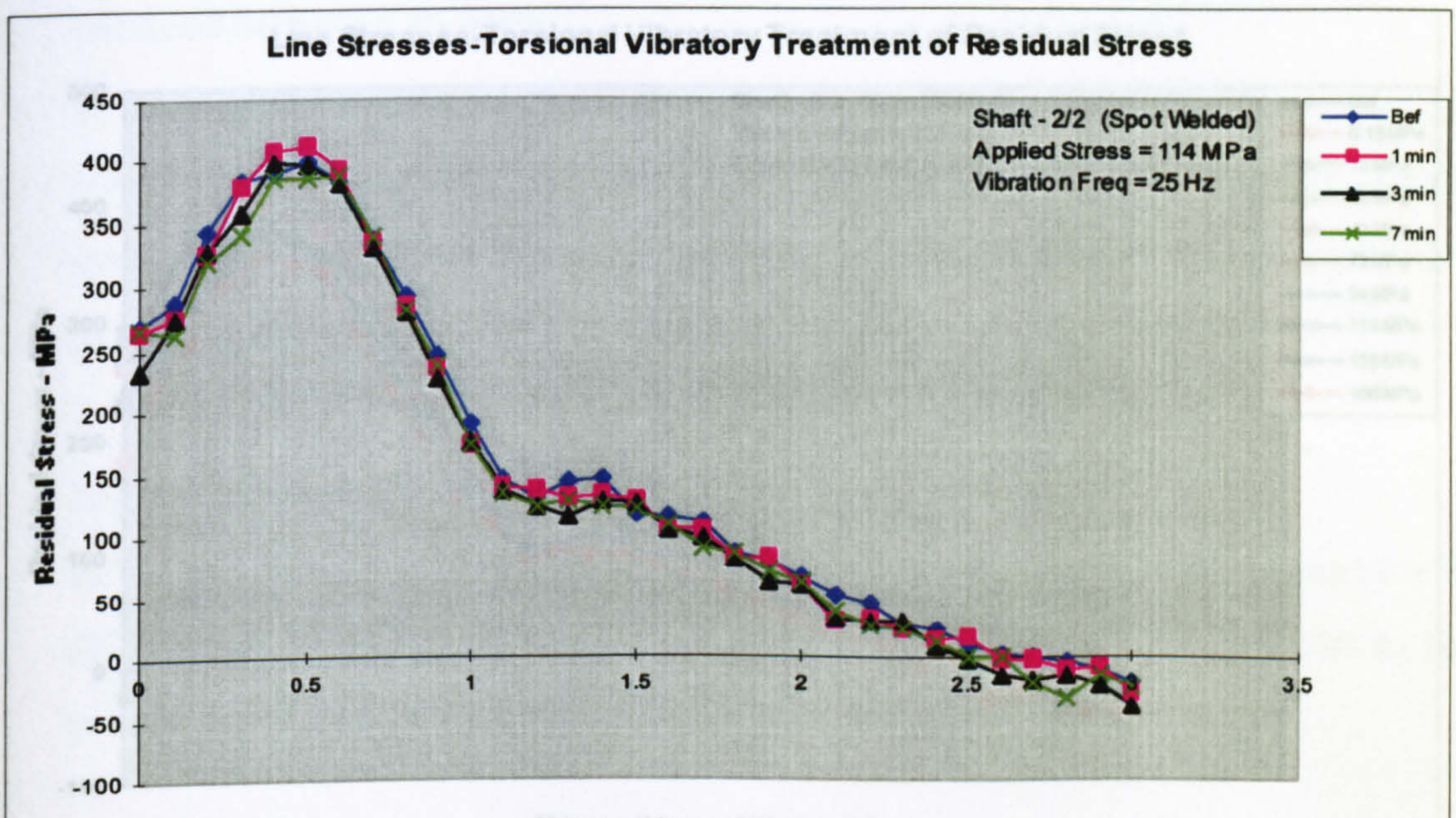

Figure 5.626 – Longitudinal line stresses plot - shaft 2/2 (stress step 7)

Point Stresses

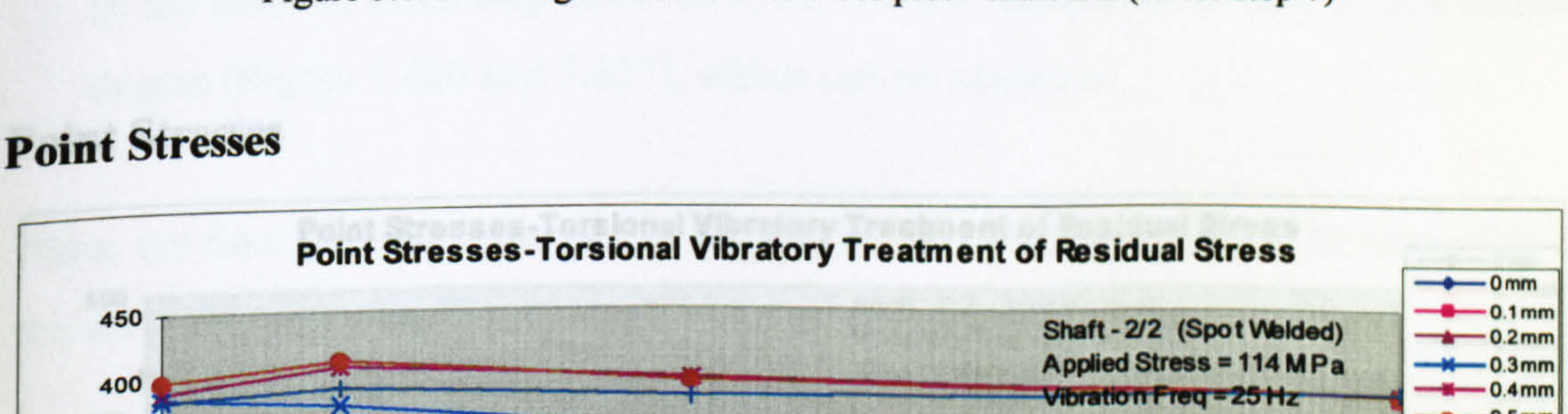

Figure 5.627 – Longitudinal point stresses plot - shaft 2/2 (stress step 7)

Shaft 2/2 - Summary Plot

Line Stresses

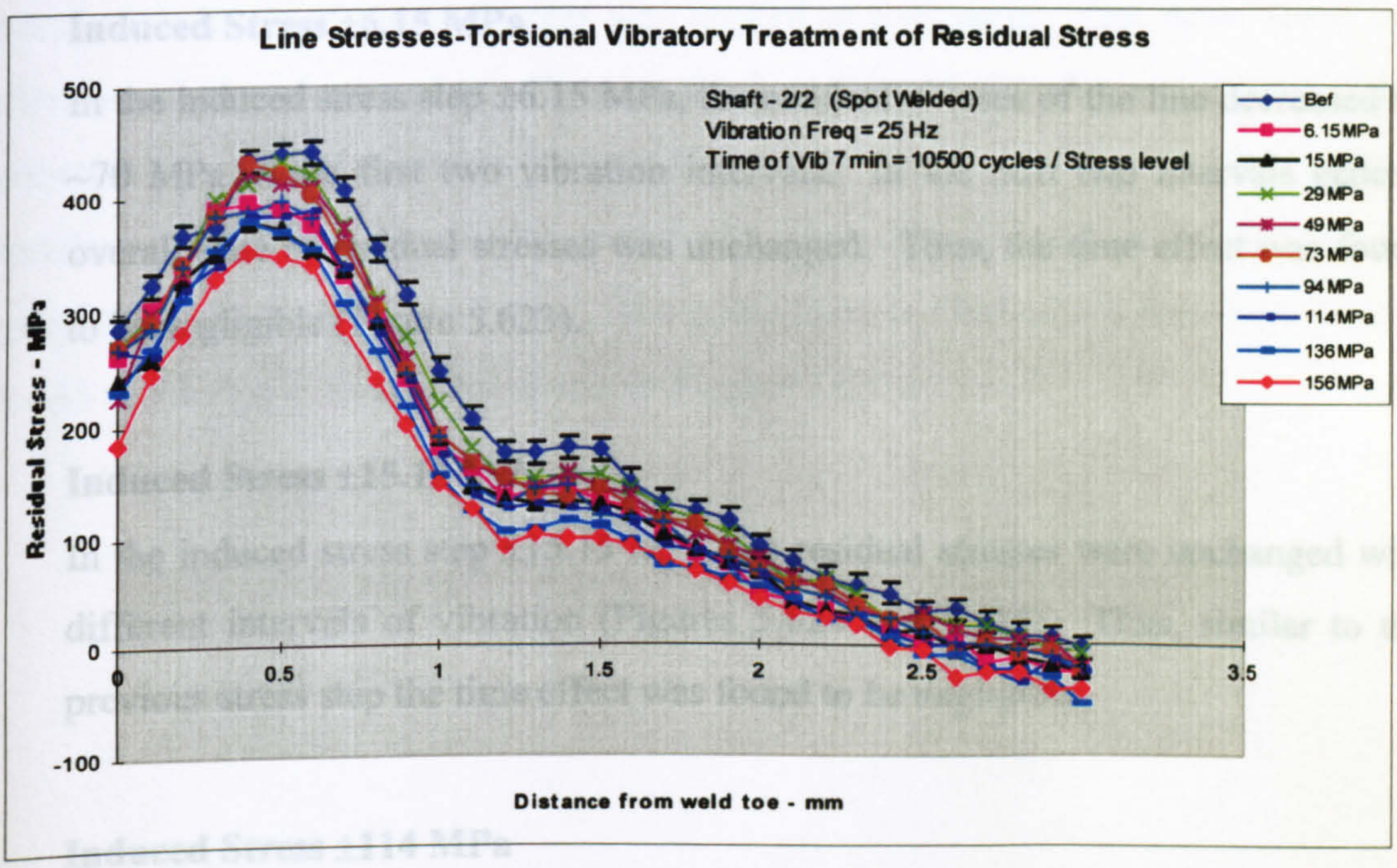

Figure 5.628 – Longitudinal line stresses plot - shaft 2/2 (summary plot)

Point Stresses

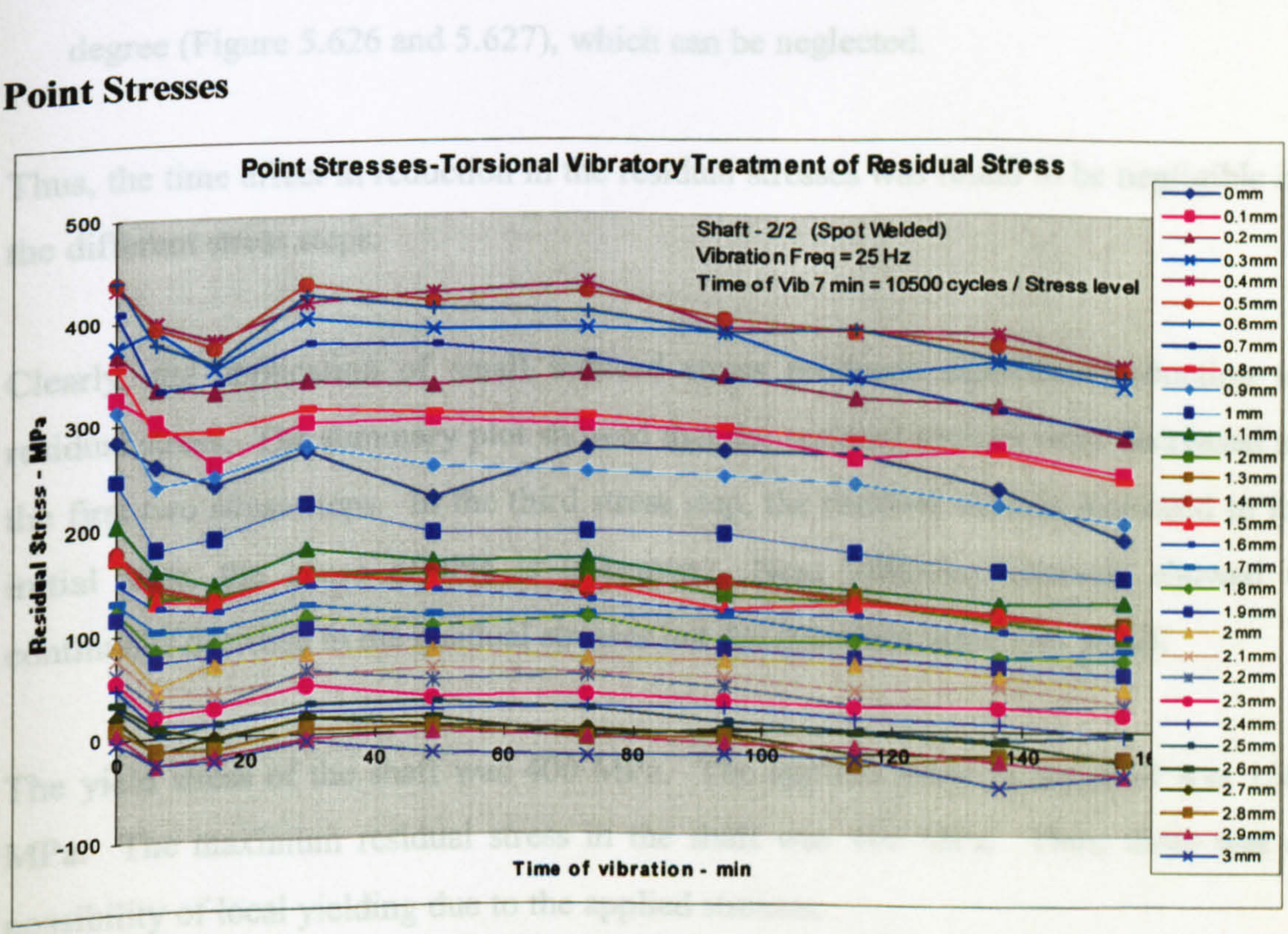

Figure 5.629 – Longitudinal point stresses plot - shaft 2/2 (summary plot)

Discussion of Result - Shaft 2/2

The result of the treatments were

Induced Stress ±6.15 MPa

In the induced stress step ±6.15 MPa, the residual stresses of the line decreased by ~70 MPa in the first two vibration intervals. In the next two intervals general overall state of residual stresses was unchanged. Thus, the time effect was found to be negligible (Figure 5.623).

Induced Stress ±15.15 MPa

In the induced stress step ±15.15 MPa, the residual stresses were unchanged with different intervals of vibration (Figures 5.624 and 5.625). Thus, similar to the previous stress step the time effect was found to be negligible.

Induced Stress ±114 MPa

In the induced stress step ±114 MPa, the residual stresses decreased with a smaller degree (Figure 5.626 and 5.627), which can be neglected.

Thus, the time effect in reduction in the residual stresses was found to be negligible in the different stress steps.

Clearly, the application of small induced stress produces significant reduction in residual stress. The summary plot showed that the residual stresses were decreased in the first two stress steps. In the third stress step, the residual stresses increased to its initial state, the cause of this is unknown. Next vibration intervals showed a continuous decrease in the residual stresses but the decreases were very small.

The yield stress of the shaft was 400 MPa. The applied stress to the shaft was 156 MPa. The maximum residual stress in the shaft was 400 MPa. Thus, there was a possibility of local yielding due to the applied stresses.

Shaft 2/3 and Shaft 2/4

These two shafts were spot-welded as shaft 2/2. The measurement line and the direction of measurement was similar to shaft 2/2 (Figure 5.621). In both shafts, two very small levels of induced stress was applied in two steps. The stress levels are shown with the relevant plots. Keeping the frequency of vibration and applied stress constant the time of vibration was varied as shown in the plots. The longitudinal residual stress was measured before and after every step of treatment. The line and point stress plots are shown below. The stress plots of Shaft 2/3 is shown in Figures 5.630 to 5.633 and shaft 2/4 is shown in Figures 5.634 to 5.637.

Shaft 2/3 – Induced Stress 3.64 MPa

Line Stresses

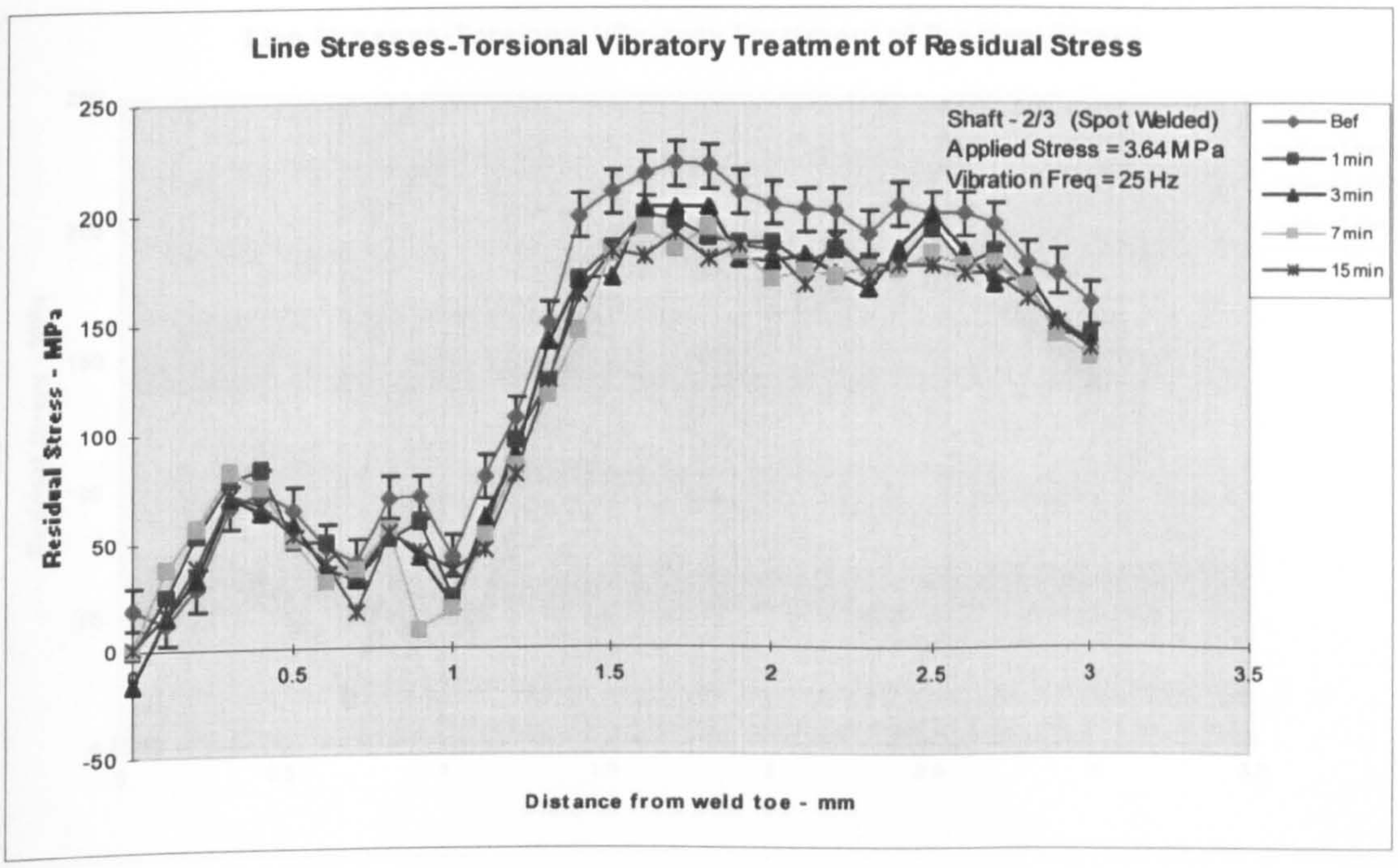

Figure 5.630 – Longitudinal line stresses plot - shaft 2/3 (stress step 1)

Point Stresses

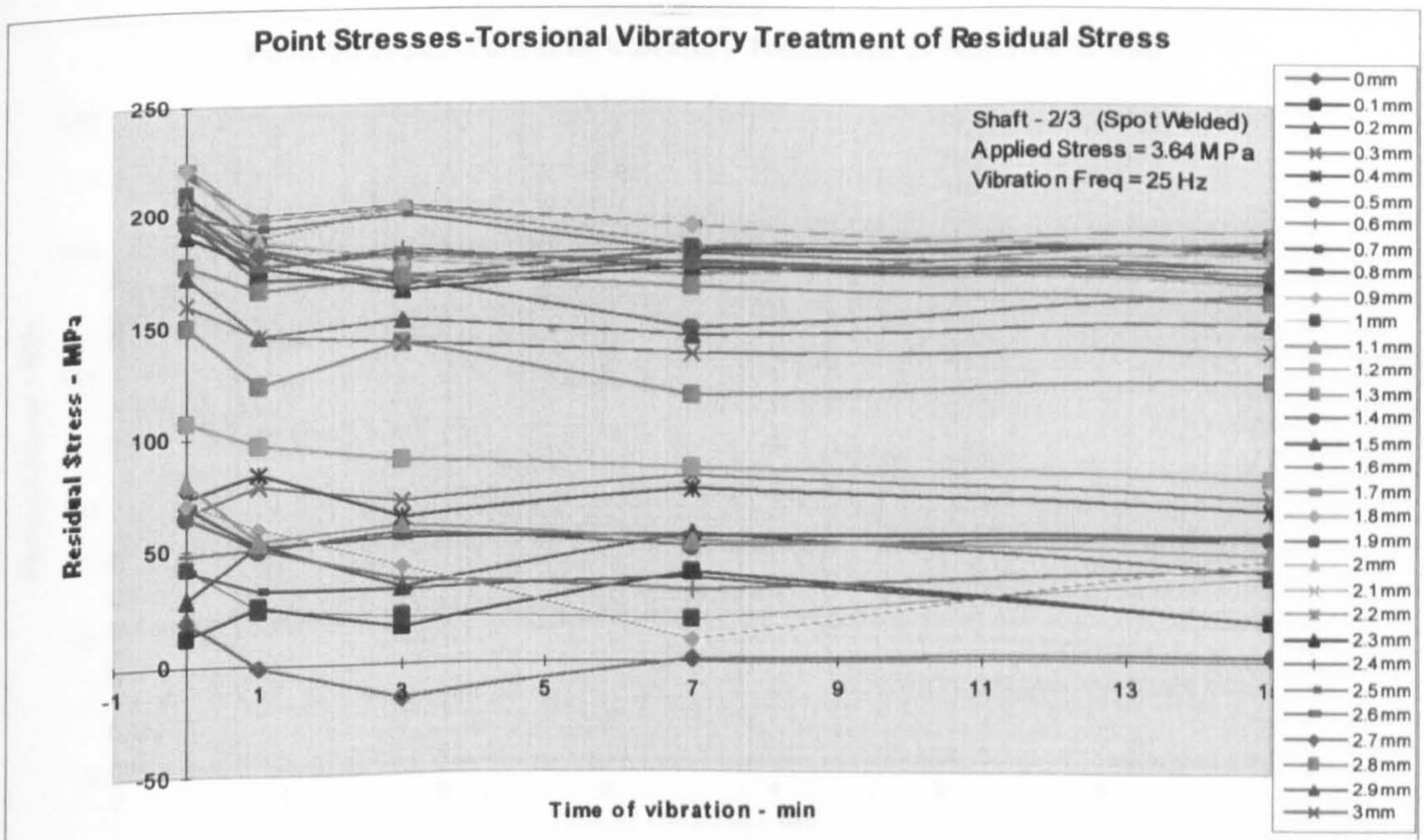

Figure 5.631 – Longitudinal point stresses plot - shaft 2/3 (stress step 1)

Shaft 2/3 - Stress Step 5.75 MPa

Line Stresses

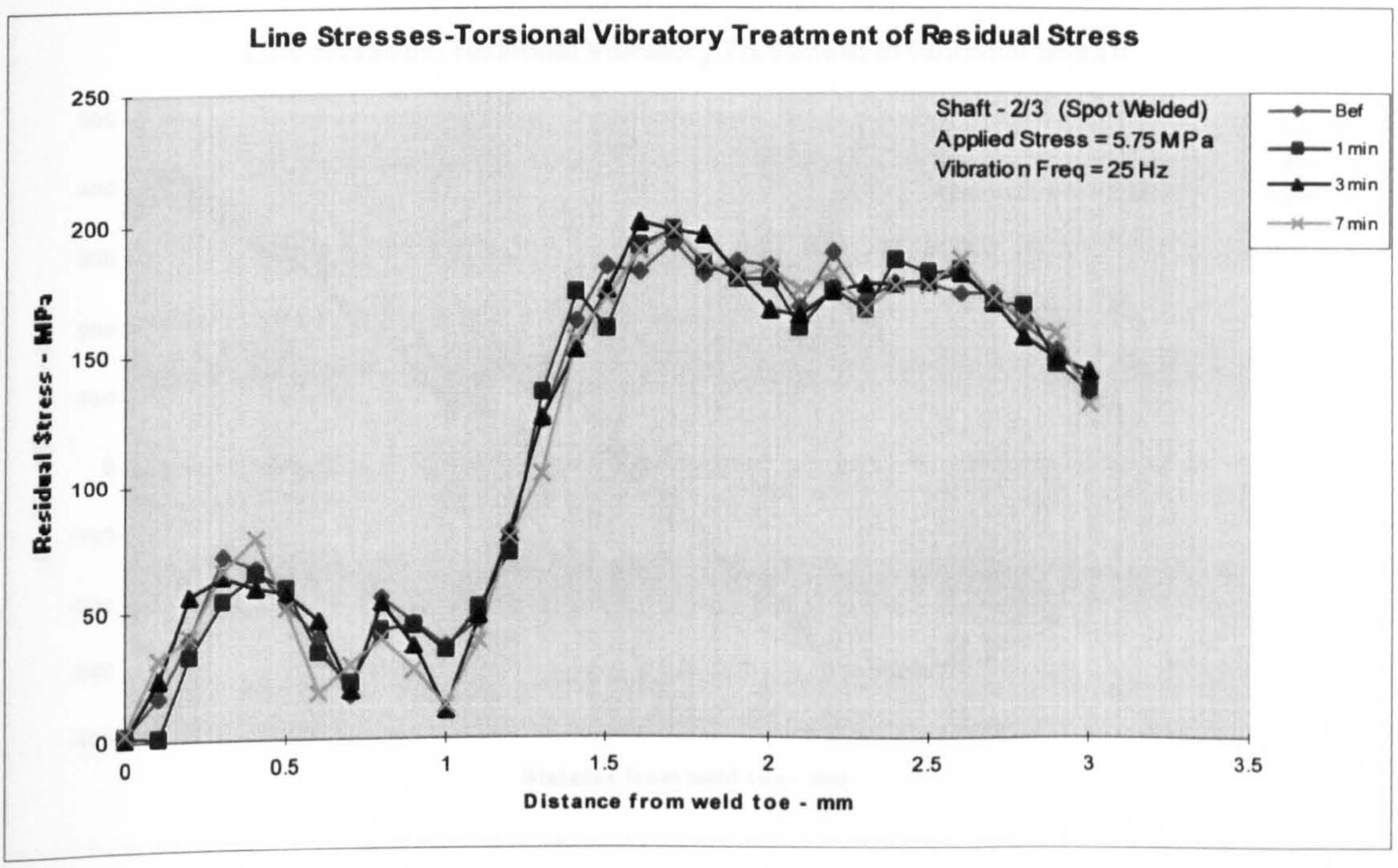

Figure 5.632 – Longitudinal line stresses plot - shaft 2/3 (stress step 2)

Point Stresses

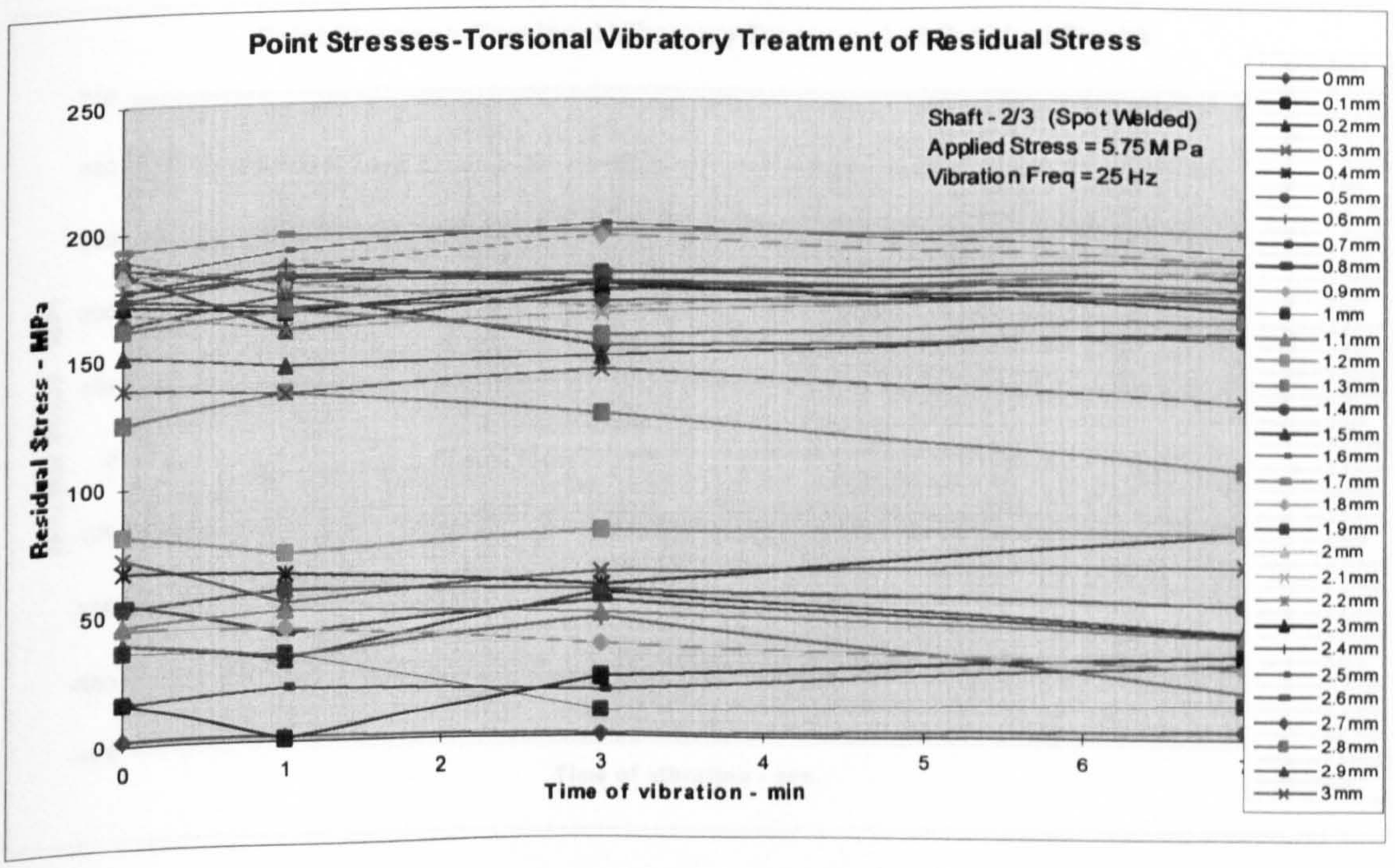

Figure 5.633 – Longitudinal point stresses plot - shaft 2/3 (stress step 2)

Shaft 2/4 - Stress Step 2.95 MPa

Line Stresses

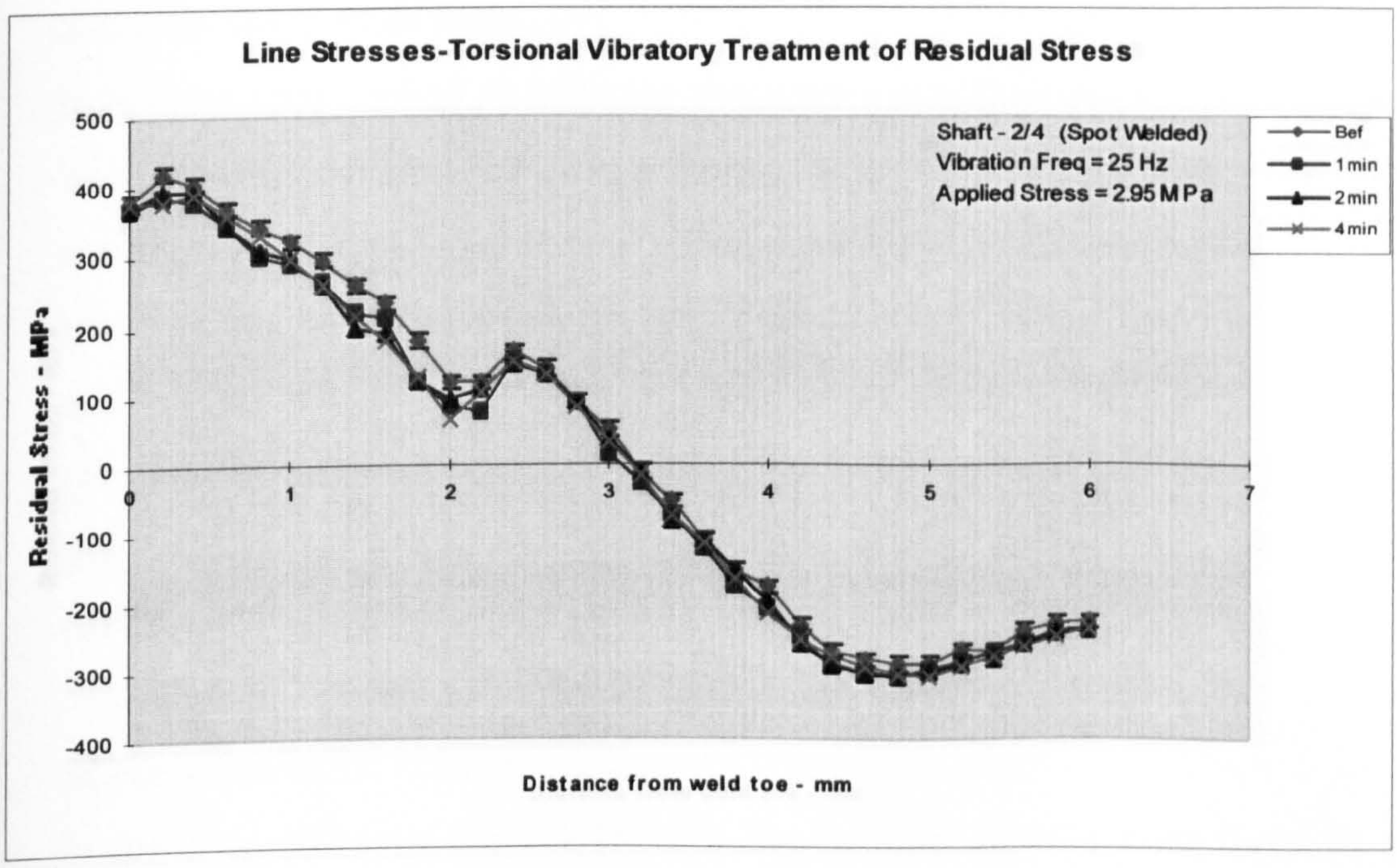

Figure 5.634 – Transverse line stresses plot - shaft 2/4 (stress step 1)

Point Stresses

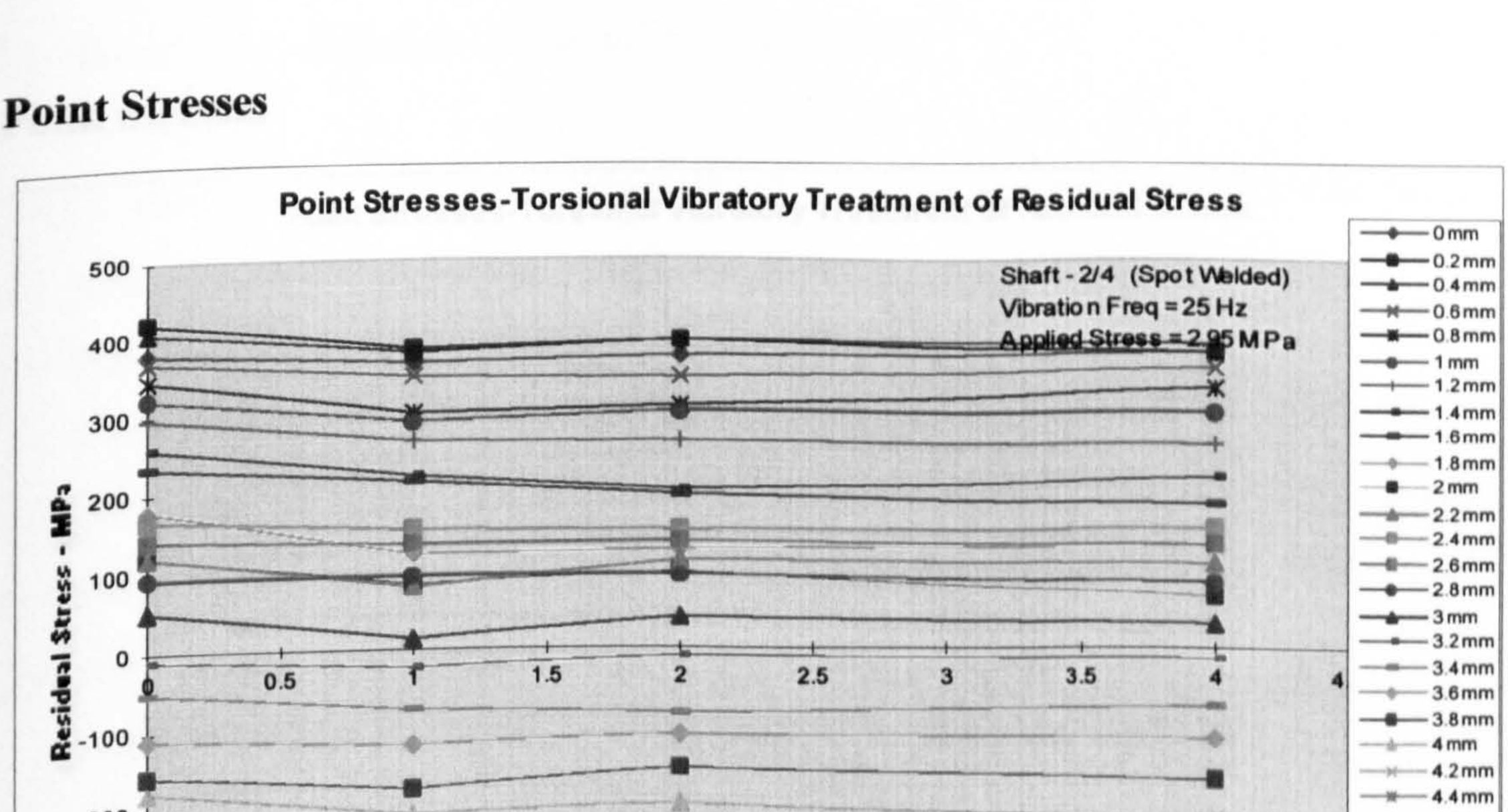

Figure 5.635 – Transverse point stresses plot - shaft 2/4 (stress step 1)

Shaft 2/4 - Stress Step 6.19 MPa

Line Stresses

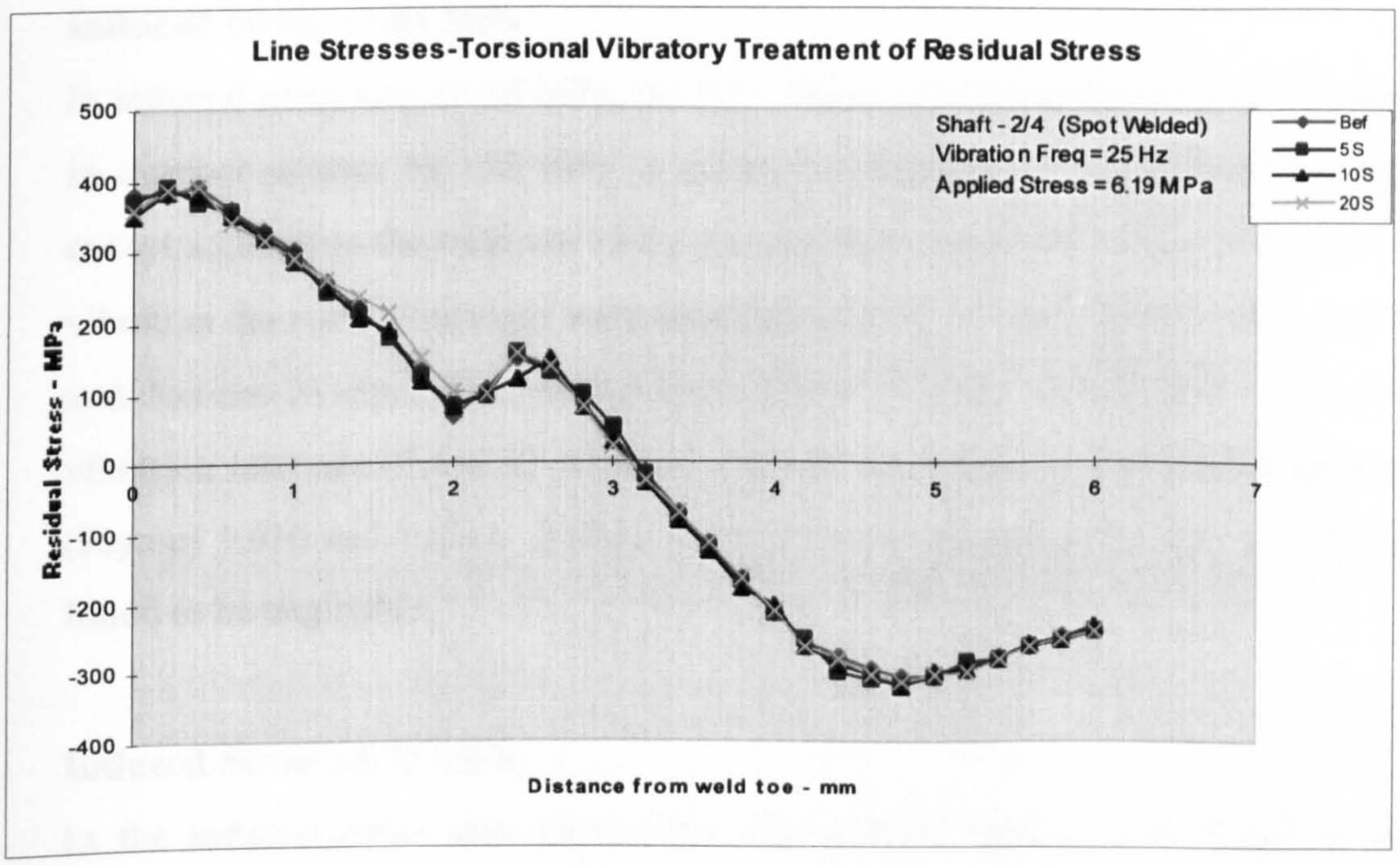

Figure 5.636 – Transverse line stresses plot - shaft 2/4 (stress step 2)

Point Stresses

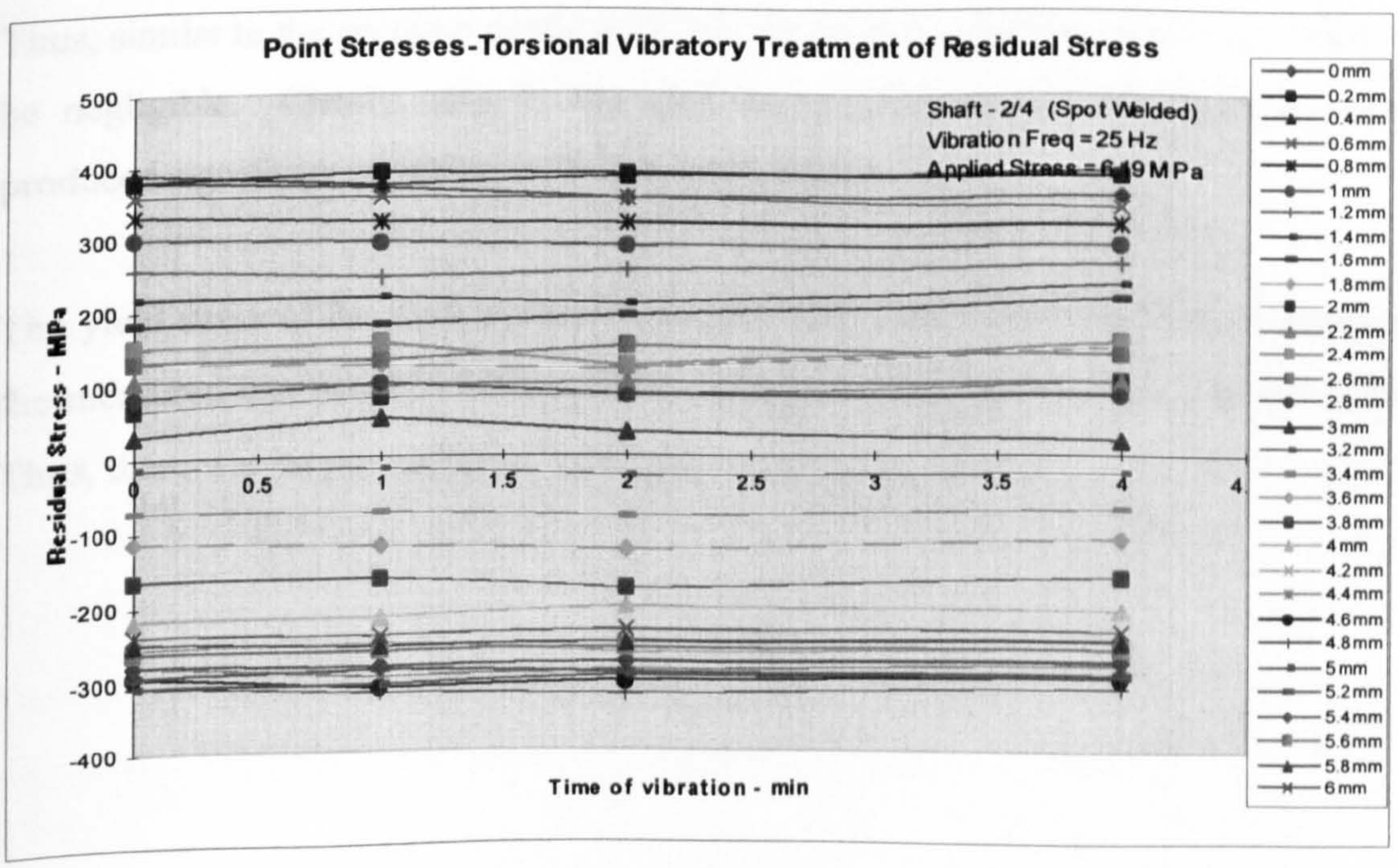

Figure 5.637 – Transverse point stresses plot - shaft 2/4 (stress step 2)

Discussion Result - Shaft 2/3

The results of the treatments of this shaft were

Induced Stress ±3.64 MPa

In induced stress step ±3.64 MPa, the first minute of vibration showed a reduction in residual stresses by ~25 MPa in most of the measurement points of the line except adjacent to the weld toe where no reduction was found. After 3 minutes of vibration the residual stresses were found to increase in some measurement points and decrease in some other measurement points, i.e. only redistributed. Next two vibration intervals (7 and 15 minutes) showed no change in the residual stresses (Figures 5.630 and 5.631). Similar to the previous specimen the time effect was found to be negligible.

Induced Stress ±5.75 MPa

In the induced stress step ±5.75 MPa, the residual stresses were found to be unchanged with different time intervals of vibration. Thus, the time effect was found to be negligible (Figures 5.632 and 5.633).

Thus, similar to the previous shaft (shaft 2/2) the time of vibration effect was found to be negligible. Clearly, also in this shaft the application of small induced stress produced significant reduction in the residual stresses.

The yield stress of the shaft material was 400 MPa. The maximum residual stress of the measured line was 225 MPa and the applied stress to the specimen was 5.6 MPa. Thus, there was no possibility of local yielding the shaft material.

Result of Shaft 2/4

The results of the treatments of this shaft were

Induced Stress ±2.95 MPa

In this stress step, the residual stresses decreased by ~50 MPa on all over the measurement line in the first minute of vibration. In the next vibration intervals, the residual stresses were found to be unchanged (Figures 5.634 and 5.635).

Induced Stress ±6.19 MPa

In this stress step the residual stresses were found to be unchanged with different intervals of treatment (Figures 5.636 and 6.637).

Thus, in the both stress steps, the time effect in reducing the residual stresses were found to be negligible. Similar to shafts 2/2 and 2/3, a significant reduction in the residual stresses were observed due to application of a very small induced stresses.

The yield stress of the shaft material was 400 MPa. The maximum residual stress of the measured line was 420 MPa and the maximum applied stress to the specimen was ±6.19 MPa. Thus, there was a possibility of local yielding of the shaft material.

Shaft 2/5

In this shaft, a spot was welded similar to the previous three shafts. A line was selected in the HAZ for investigation. The stress measurement line was similar to shaft 2/2 (Figure 5.621). The frequency of vibration was 25 Hz. The time of vibration in each in stress step was kept constant to 1 minute. The applied stress was increased from 4.3 MPa to 155.2 MPa in 20 steps and these are shown in the plots. Before and after every step of treatment the longitudinal residual stresses were measured. The plots shown in Figures 5.638 to 5.639.

Shaft 2/5

Line Stresses

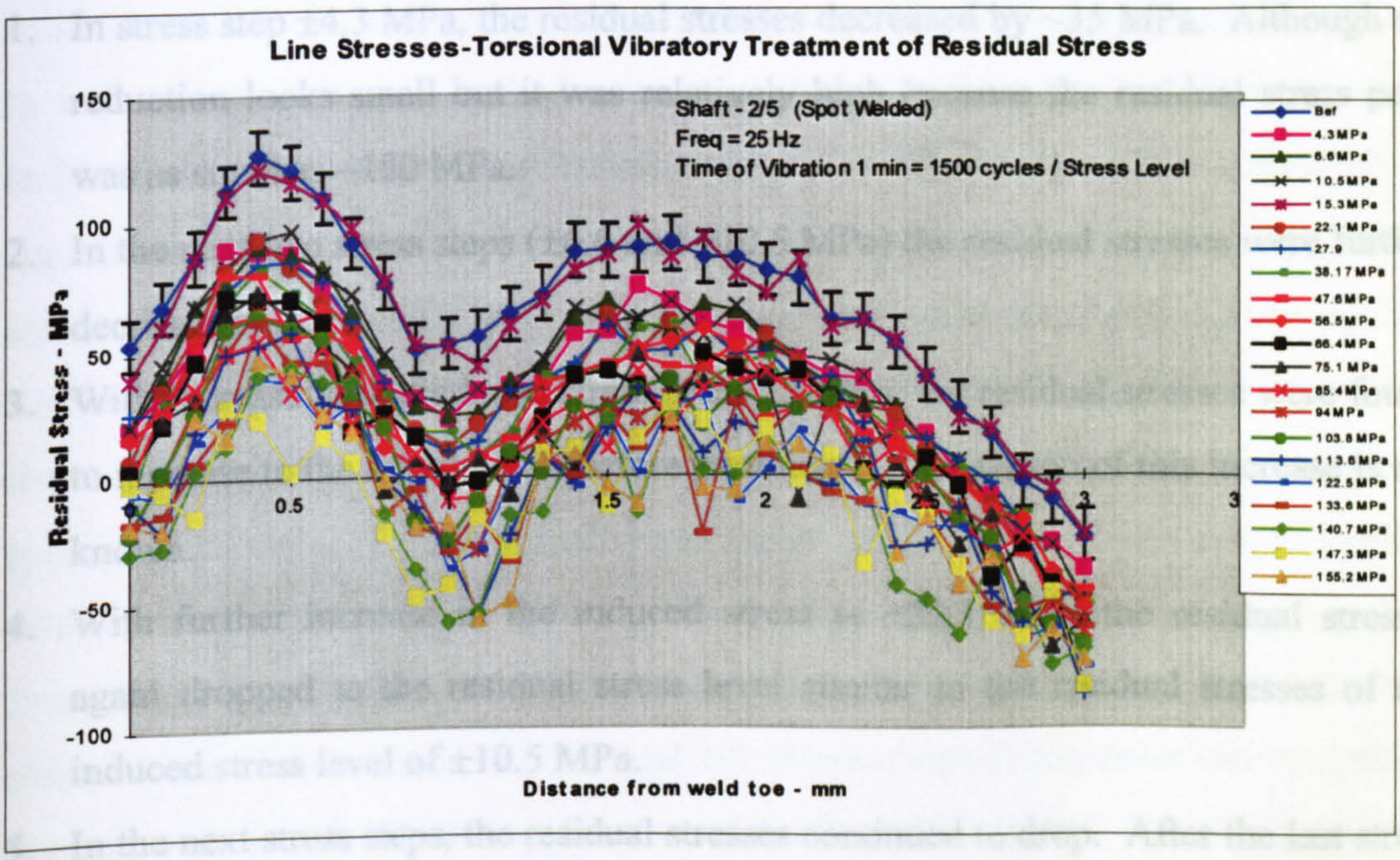

igure 5.638 – Longitudinal line stresses plot - shaft 2/5

Residual Stress versus Applied Stress Plot

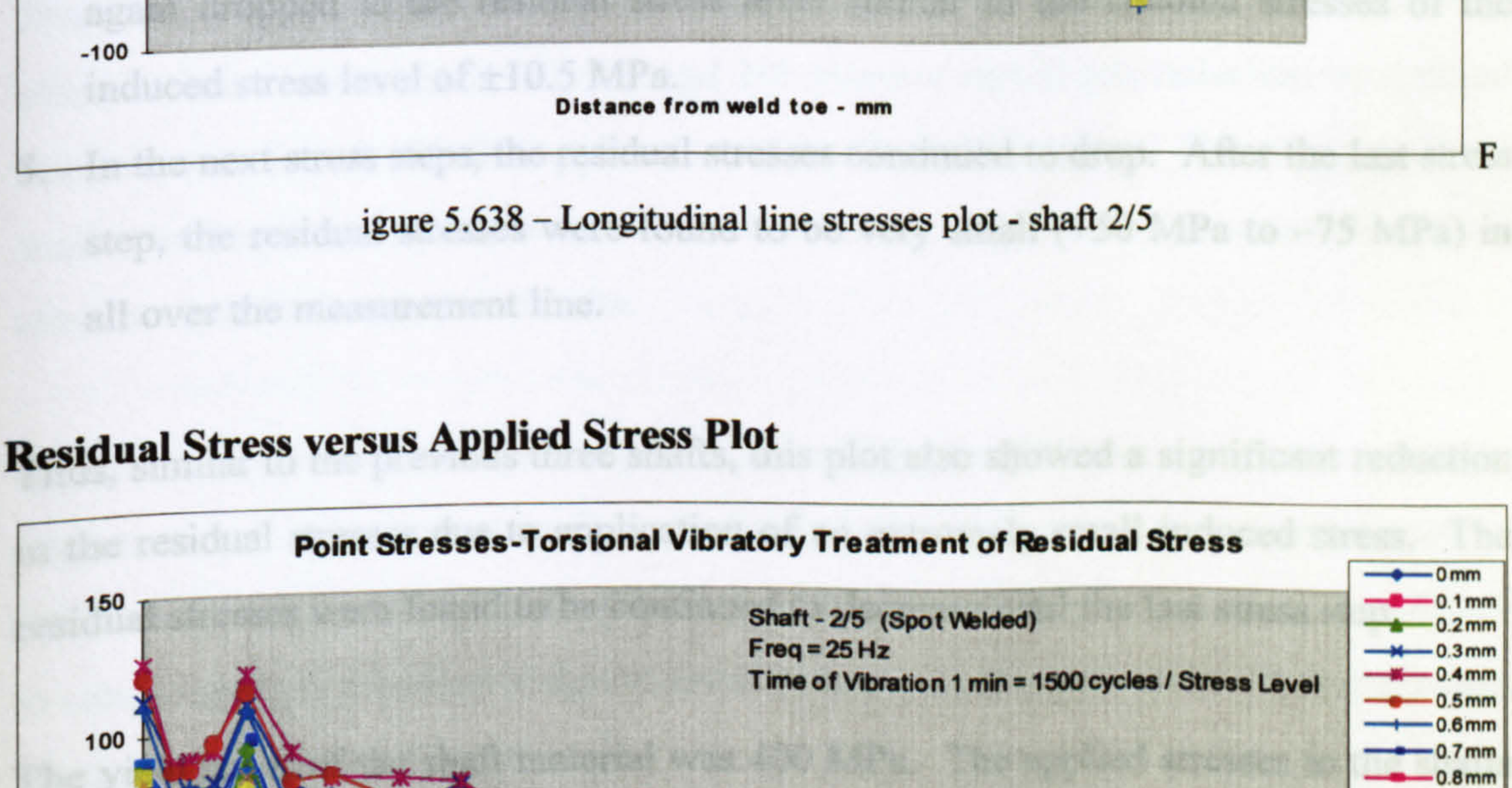

Figure 5.639 – Longitudinal residual stress versus applied stress plot - shaft 2/5

Result of Shaft 2/5

The results of the treatments were:

1. In stress step ±4.3 MPa, the residual stresses decreased by ~35 MPa. Although the reduction looks small but it was relatively high because the residual stress peak was as small as ~150 MPa.
2. In the next two stress steps (±6.6 and ±10.5 MPa) the residual stresses were further decreased.
3. With increase in the induced stress to ±15.3 MPa, the residual stresses were found to increase to the initial level (before treatment). The reason of this increase is not known.
4. With further increase in the induced stress to ±22.1 MPa, the residual stresses again dropped to the residual stress level similar to the residual stresses of the induced stress level of ±10.5 MPa.
5. In the next stress steps, the residual stresses continued to drop. After the last stress step, the residual stresses were found to be very small (+50 MPa to –75 MPa) in all over the measurement line.

Thus, similar to the previous three shafts, this plot also showed a significant reduction in the residual stresses due to application of an extremely small induced stress. The residual stresses were found to be continued to decrease until the last stress step.

The yield stress of the shaft material was 400 MPa. The applied stresses to the shafts were maximum ±155.2 MPa. The maximum residual stress of the measured line was 128 MPa. Thus, there was not any possibility of local yielding of the shaft material.

5.4.4.5 Summary of Results

This experiment was designed to investigate the effect of inducing pure shear stress in the various shaft specimens. Shaft 1/1, and 1/2 showed a significant reduction in residual stress in the weld toe and the adjacent area. The residual stresses were found to redistribute in higher applied stresses. Shaft 1/3 showed some change in the residual stresses but they were relatively small. Shaft 1/4, and 1/6, showed no significant change in the residual stress due to torsional treatment instead they showed some redistribution. Shaft 2/1 did not show any reduction, with higher applied stresses the residual stresses were found to redistribute. Shafts 2/2, 2/3, and 2/4 showed a very important phenomenon, where it was found that a small amount of applied stress reduced the residual stress significantly. Further increases in applied stresses were ineffective in reducing the residual stresses and very large applied stresses led to redistribution of the stresses. Shaft 2/5 showed similar stress reduction characteristics to the shafts 2/2, 2/3 and 2/4 where a significant reduction in residual stresses were found with the application of small applied stress. The stresses of this shaft continued to decrease until the last stress step, this was a contradictory characteristic to the previous shafts.

In some shafts there were some possibility of plastic deformation where relatively large torsional stresses were applied. In those shafts where small stresses were applied which caused a significant reduction in the residual stresses, they were not sufficient to cause any local yielding of the material. It is concluded that some effect other than local yielding caused this reduction.

It was found from these experiments that the reduction in residual stresses was observed on specimens where a spot was welded to induce residual stresses. Homogeneous material shafts and shafts welded around the circumferential line did not show any significant reduction in residual stresses - instead they showed only redistribution at higher applied stresses. The causes of not relieving the residual stresses of the two kinds of shafts are unknown. Both kinds of shafts showed a small level of residual stresses which might be the main cause of this characteristic. For

spot welded shafts, the welding was carried out in fractions of a second and the weld was surrounded by cold parent metal so the weld had to solidify and cool down to room temperature in a very short period. Due to very short cooling time, two things might had happened:

1. Some retained austenite was present in the HAZ and in the weld, which caused some residual stress.
2. The parent metal (HAZ) and the weld transformed into martensite and other phases. Due to very short time of cooling and transformation, the carbon atoms remained interstitially in the BCT or BCC crystal lattice which caused some residual stress.

For the first case, when the shafts were subjected to torsional vibration the retained austenite transformed to martensite and possibly to other phases by a short range diffusion and shear mechanism initiated by the mechanical driving force and the residual stresses was found to decrease. For the second case, due to the applied energy, the carbon atom moved to a suitable place (possibly to the grain boundaries) and formed carbide or remained as free carbon and freed the BCT or BCC thus residual stress was relieved.

Thus, from this experiment, it is found that the residual stresses were not decreased in the same fashion of the other post weld experiments (Experiments VII, and VIII). Only a partial decrease was observed in the shafts where a spot was welded. One would conclude that most probably, shear stress does not work efficiently to relieve all kinds of residual stresses. It works to relieve the residual stresses where the stresses were caused by any unstable/metastable phases of the material. The shear stresses helps to transform the unstable/metastable phase (i.e. retained austenite) into the preceding phases thus the residual stresses are relieved. It is suggested that the other stresses such as thermal stresses cannot be relieved by torsional applied stress.

5.5 Experiment XI:

Cryogenic Treatment Test

Abstract

In this experiment the specimens were submerged into the liquid nitrogen to reduce the residual stresses. Four specimens were submerged into the liquid nitrogen but in all four specimens no reduction in the residual stresses were found. One of the four cryogenic treated specimens were picked up for VSR treatment where a maximum 36% reduction in the residual stresses were found. Thus, the cryogenic method was found to be ineffective in treating mild steel specimens to relieve the residual stresses.

5.5.1 Introduction

A cryogenic treatment was carried out to relieve the residual stresses of the welded hot/cold rolled mild steel bars. This experiment was designed to investigate the retained austenite phenomenon in the mild steel. Frey [52] claimed that cryogenic treatment of Drills and powder metal parts improved fatigue life to 1.5 to 2 times. Bhadeshia [12 to 18] and some other researchers have stated that the presence of retained austenite induces substantial amount of residual stresses. From the metallurgical characteristics of the experimenting steel (0.18 wt % C), the possibility of retained austenite was very low (Figure 1.25). This experiment was carried out to investigate the effect of the cryogenic treatment on the residual stresses caused by different phases present in the structure.

5.5.2 Experimental Procedure

In this experiment four specimens were processed. Of the four specimens two of them (one hot rolled and one cold rolled) were bead welded as previous specimens (Figure 5.10). Other two were left to treat as homogeneous materials. The specimens were sliced to fit in the small opening of the liquid nitrogen container using a band saw where a low feed was used to reduce possibility of any heat affected transformation.

The specimens were sliced from both sides of them to remove the non-uniformity of the weld due to starting and ending of the weld (Figure 5.640).

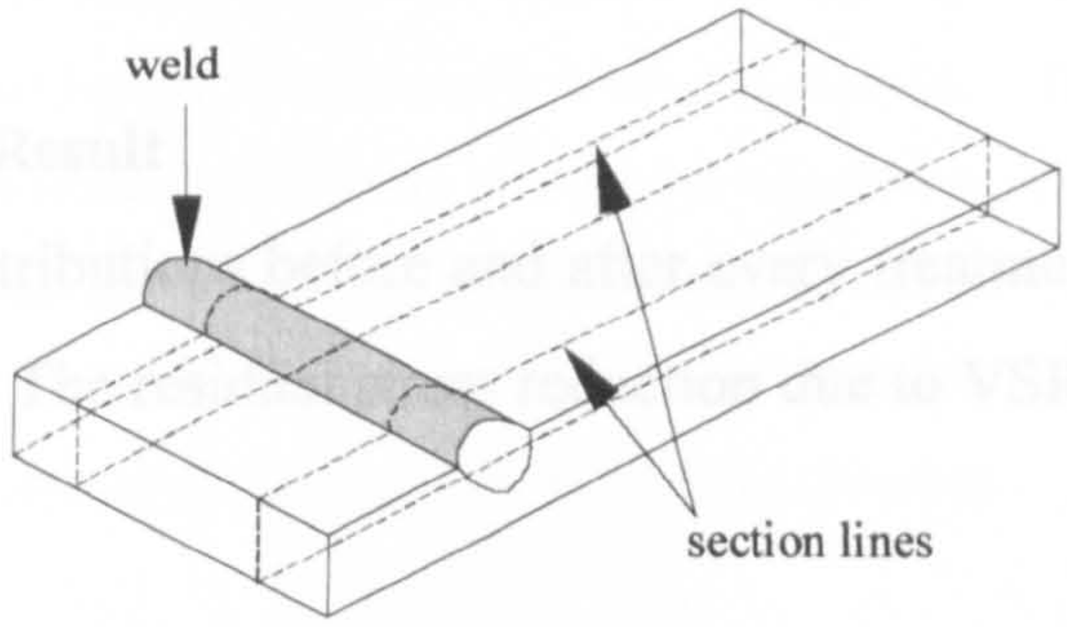

Figure 5.640 - Specimens for cryogenic treatment

In all of these specimens the residual stresses were measured using the X-ray diffractometer before submerging into liquid nitrogen. The specimens were kept in the liquid nitrogen for half an hour then the specimens were removed and kept in the atmosphere to bring them to the normal temperature. The residual stresses of the specimens were then re-measured. The X-ray stress measurement conditions were similar to as described in Table 5.10. The stresses were measured using the mapping technique, where single exposure technique (SET) was used.

The measurement of the residual stresses was carried out using the same X-ray measurement jig as used in Experiment I (shown in Appendix II). The jig was modified a little to locate the specimens in same positions in every step of treatment.

After finishing this part of investigation the hot rolled welded specimen was picked up for vibratory treatment. A dynamic applied stress of ±250 MPa was applied to the specimen. The specimen was vibrated in that stress level for different time intervals which are shown in the result plot.

The experimental set-up for vibratory treatment was similar to the set-up of experiment III. The same calibration constant (as in Experiment III) of applied stresses was used. The length of the specimens and the position of the weld were

similar to the specimens in Experiment III. Crystallographic investigation of the cryogenic treated specimens was not carried out.

5.5.3 Experimental Result

The residual stress distributions before and after every treatment is shown in the plot below (Figure 5.641). The residual stress reduction due to VSR treatment is visible in the plot.

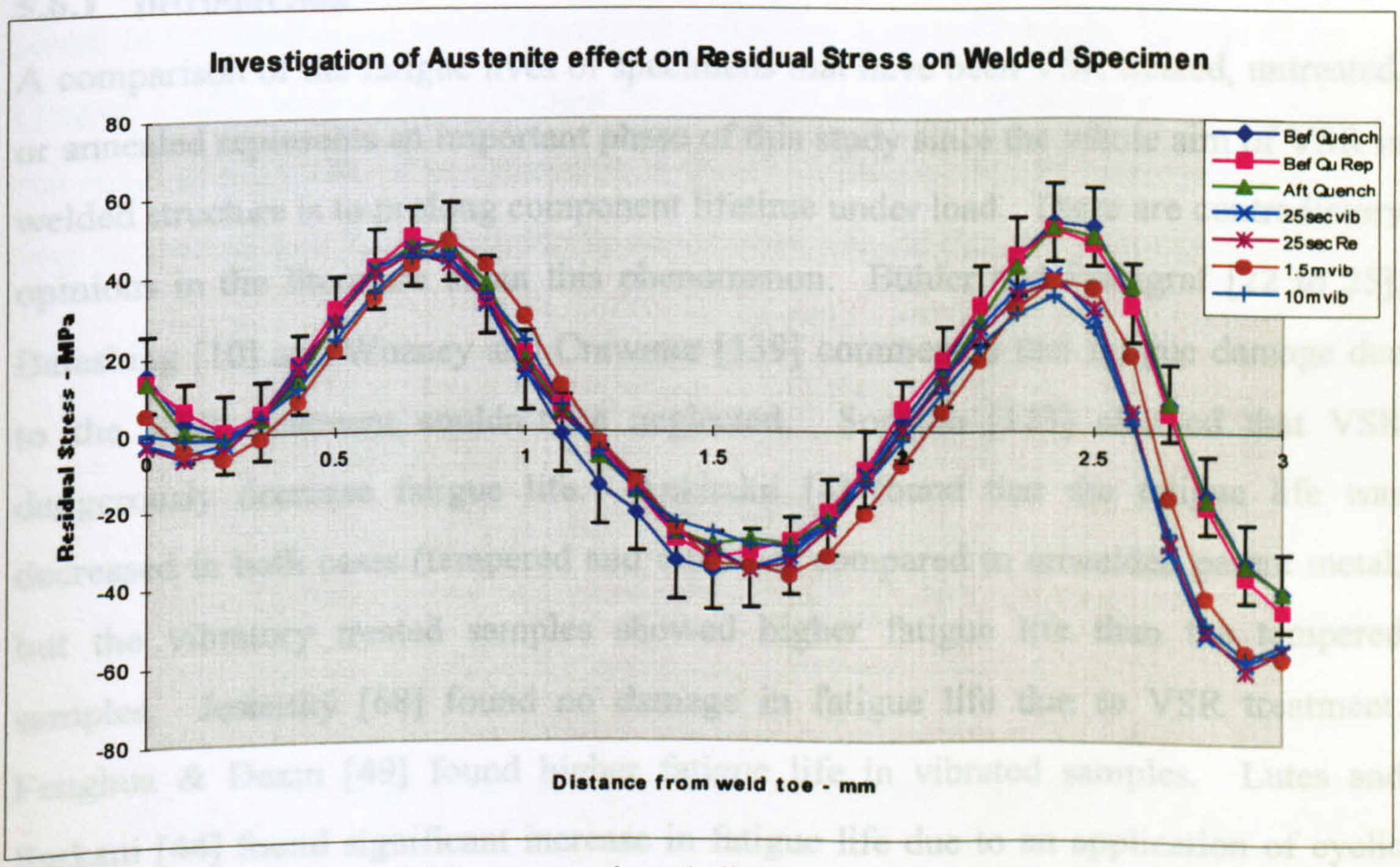

Figure 5.641 - Cryogenic and vibratory treatment result plot

5.5.4 Summary of Results

In all four specimens (homogeneous, welded, hot rolled and cold rolled steels), no reduction in residual stresses was observed due to submerging into liquid nitrogen. On the contrary, VSR treatment showed a reduction of the residual stress from 55 MPa to 35 MPa (Figure 5.641), a reduction of more than 36% in some areas.

5.6 Experiment XII: Fatigue Test

Abstract

In this experiment the fatigue life of the specimens were tested to make a comparison between vibrated, unvibrated and thermally treated specimens. The fatigue life of the thermally treated specimens were found to decrease significantly, on the other hand the VSR treated specimens showed an increase between 16.8 to 30.4 %. To determine the relationship between the residual stress and the fatigue life two batches specimens were processed, where no relationship between those two was observed.

5.6.1 Introduction

A comparison of the fatigue lives of specimens that have been VSR treated, untreated, or annealed represents an important phase of this study since the whole aim of VSR in welded structure is to prolong component lifetime under load. There are contradictory opinions in the literature about this phenomenon. Bühler and Pfalzgraf [22 to 25], Balashing [10] and Wozney and Crawmer [139] commented that fatigue damage due to the VSR treatment couldn't be neglected. Sonsino [123] claimed that VSR dangerously decrease fatigue life. Ankirskii [4] found that the fatigue life was decreased in both cases (tempered and vibrated) compared to unwelded parent metal, but the vibratory treated samples showed higher fatigue life than the tempered samples. Jesenský [68] found no damage in fatigue life due to VSR treatment. Fenghua & Dexin [49] found higher fatigue life in vibrated samples. Lutes and Sarkani [44] found significant increase in fatigue life due to an application of cyclic higher stresses. In this experiment some vibrated, unvibrated and thermally treated specimens were fatigued to make a comparison between their fatigue lives. Some specimens were also processed to find out a relationship between residual stresses and fatigue lives. It was believed that higher residual stress would decrease the fatigue life and lower residual stress would do the opposite.

5.6.2 Experimental Procedure

This experiment was carried out in three batches of specimens where annealed, vibratory treated and untreated specimens were fatigued to compare the fatigue life. The specimens were vibrated applying a constant dynamic stress until they broke. The

residual stresses were measured before carrying out fatigue test the result of which is shown with the relevant batches. The residual stresses were measured using the X-ray diffractometer. The conditions of measurements were similar to the conditions described in Table 5.10. The residual stresses were measured using the mapping technique where the selected lines were measured as a stress map. Single Exposure Technique (SET) was used in the measurement.

To make the specimen free of any applied stress in the static condition, i.e. DC shift of the dynamic stress, care was taken to mount the specimen on the vibrator. The applied stress to the specimens were determined using the accelerometer on the top of the jig (Figure 5.642) which was calibrated by attaching an strain gauge at the mid-width in the HAZ of the weld. The calibration is shown in Section 5.3.3.3. The accelerometer was connected to a signal conditioner and then to a calibrated chart recorder.

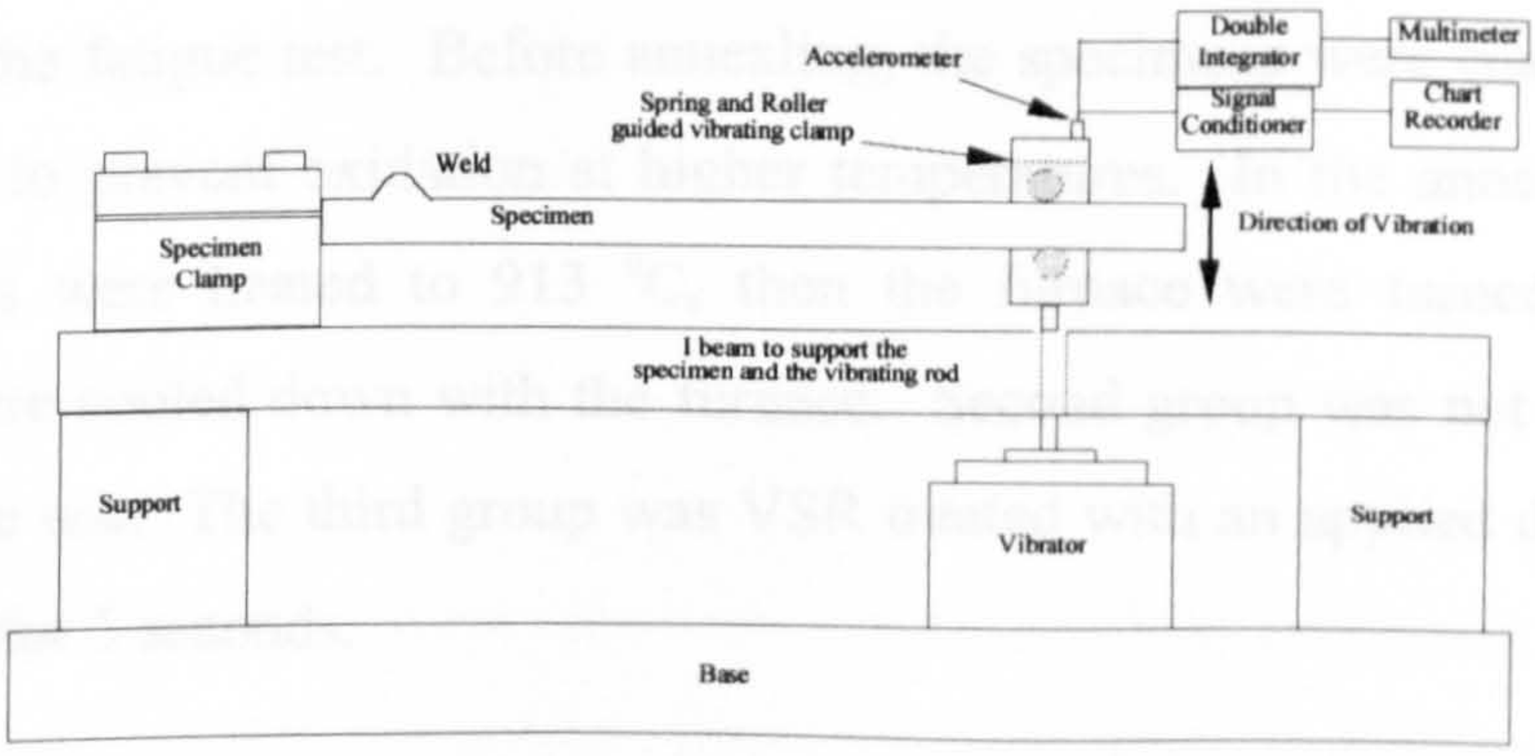

Figure 5.642 - Set-up for VSR treatment and fatigue test

The chart was used to record the fatigue life of the specimens. Prior to use of the chart to the experiments the chart speed was calibrated. The fatigue lives of the specimens were determined by measuring the length of the chart. The chart length was converted to the time of vibration then to number of cycles. In this context the chart recorder was found to be very useful, because it showed the transition period (Shown in Figure 5.643) very clearly. Before breaking the specimens the signals on the chart recorder were very smooth again after breaking it become very smooth, but in the time of breaking the signals were not smooth instead it was very inconsistent.

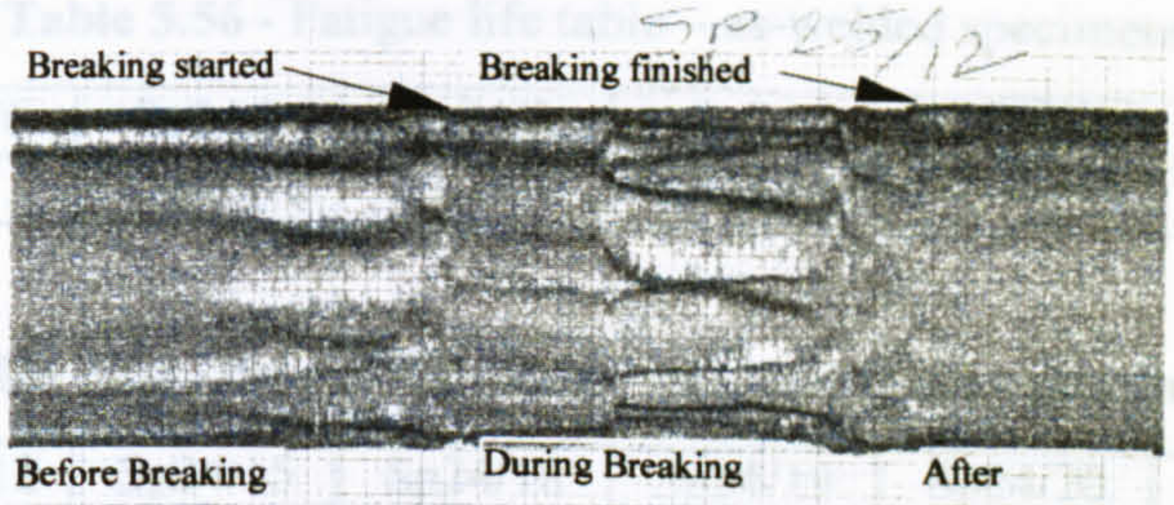

Figure 5.643 - Chart recorded signals before, during, and after breaking

5.6.3 Experimental Results

Batch 1

In batch 1, the test was carried out on three groups of specimens (six in a group). In all three groups, cold rolled flat bar specimens were bead welded. The condition of welding and removing from the welding rig was controlled carefully to keep the specimens in same condition. The first group of specimen was annealed before carrying out the fatigue test. Before annealing, the specimens were coated with anti-oxidant paint to prevent oxidation at higher temperatures. In the annealing process, the specimens were heated to 913 ^{0}C, then the furnace were turned off and the specimens were cooled down with the furnace. Second group was not treated at all, left for fatigue test. The third group was VSR treated with an applied dynamic stress of ±365 MPa for 5 seconds.

The fatigue test was carried out at a vibration frequency of 25 Hz applying a dynamic stress of ±205 MPa. The specimens were vibrated until they broke. While breaking, it was observed that the crack initiated at the mid-width of the specimen (at the weld toe) and propagated towards the edges. This observation complied with the dynamic stress distribution in Finite Element analysis (Chapter 4), where it was found that the direct stress was maximum at the mid-width and minimum near the edges. The fatigue lives of the first batches were.

Table 5.55 - Fatigue life table - annealed specimens

Specimen	Sp-24/1	Sp-24/3	Sp-24/4	Sp-24/5	Average
No. of Cycles	85169.96	136727.7	212555.5	154294.8	147187

Table 5.56 - Fatigue life table – as-welded specimens

Specimen	Sp-24/6	Sp24/7	Sp24/8	Sp24/9	Sp24/10	Sp24/11	Average
No. of Cycles	271617.7	240302.8	233000	278982.9	273157.2	267795.3	260809.3

Table 5.56 - Fatigue life table - vibratory treated specimens

Specimen	Sp-24/12	Sp24/15	Sp24/18	Sp24/19	Sp24/20	Sp24/21	Average
No of Cycles	319865	347825.6	272415.8	412920	236115	238531	304612.1

Discussion of Result - Batch 1

In all three specimens groups same applied stresses were used (±205 MPa). The average fatigue life of the annealed specimens was 147187 cycles. The as welded specimens showed an average life of 260809 cycles and the vibratory treated specimens showed an average life of 304612 cycles.

Thus, the VSR treated specimens showed the maximum fatigue life where the fatigue life was increased by 16.8% in comparison to the as-welded specimens. The annealed specimens showed the least fatigue life, where a reduction in the fatigue life was 43.5%.

Batch 2

In this batch, two groups of specimens were processed. First group was fatigue tested as-welded and the second group was vibratory treated prior to the fatigue test. The specimens were VSR treated at a frequency of 25 Hz using an applied stress of ±370 MPa for 5 seconds. Before carrying out the fatigue test the residual stress of the specimens were measured on all nine lines in Figure 5.644 below. The fatigue test was carried out using applied stress ±205 MPa.

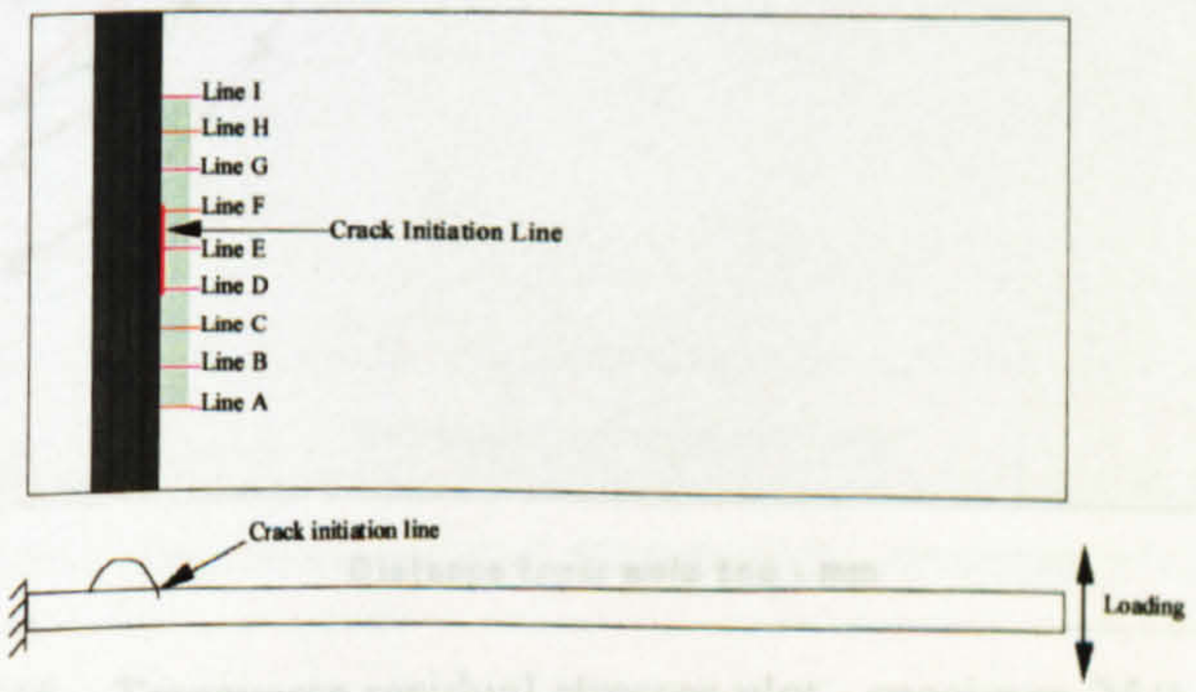

Figure 5.644 - Stress measured lines and lines of crack initiation

The residual stress plots of VSR treated and untreated specimens are shown in the following pages.

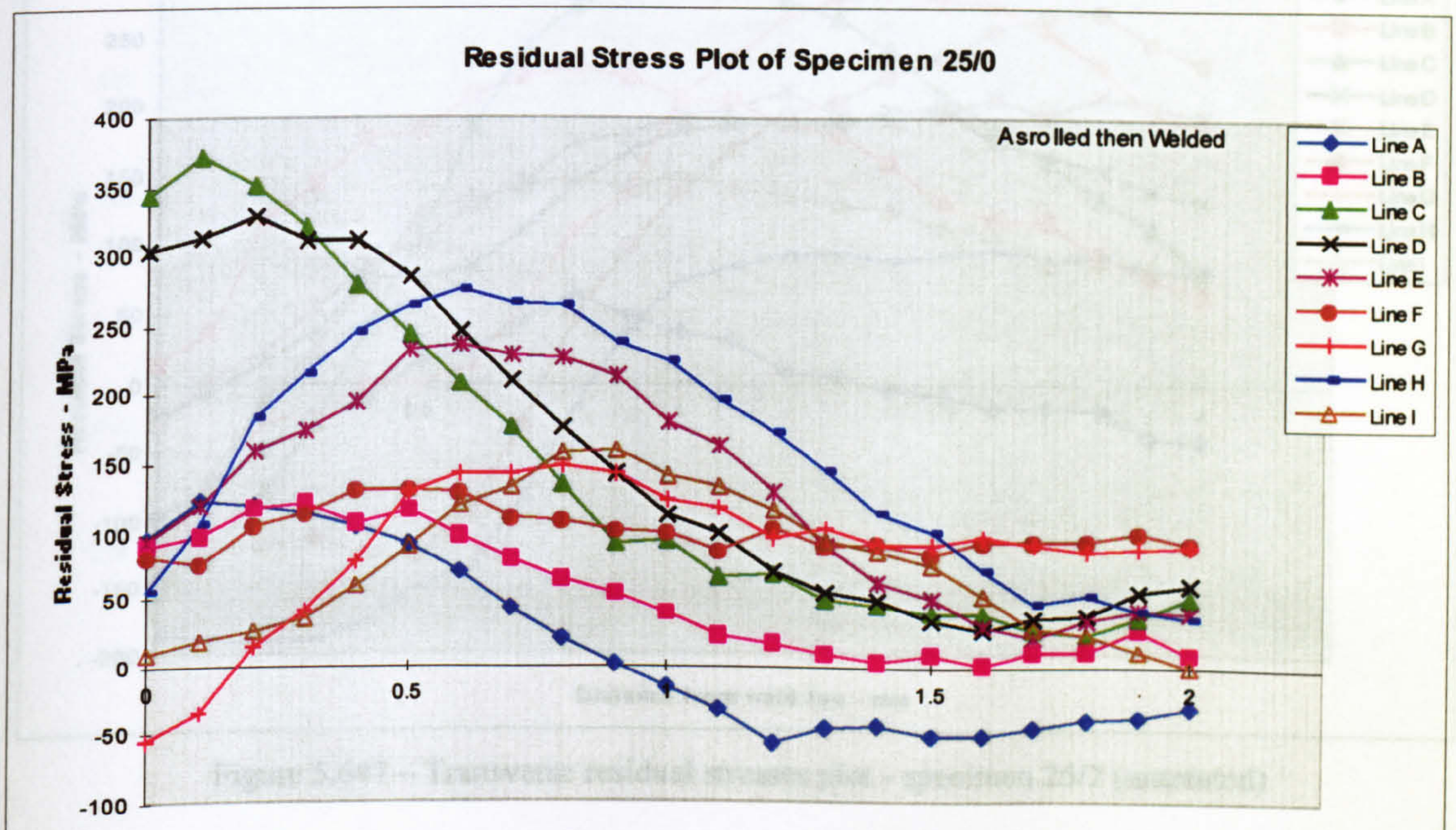

Figure 5.645 – Transverse residual stresses plot - specimen 25/0 (untreated)

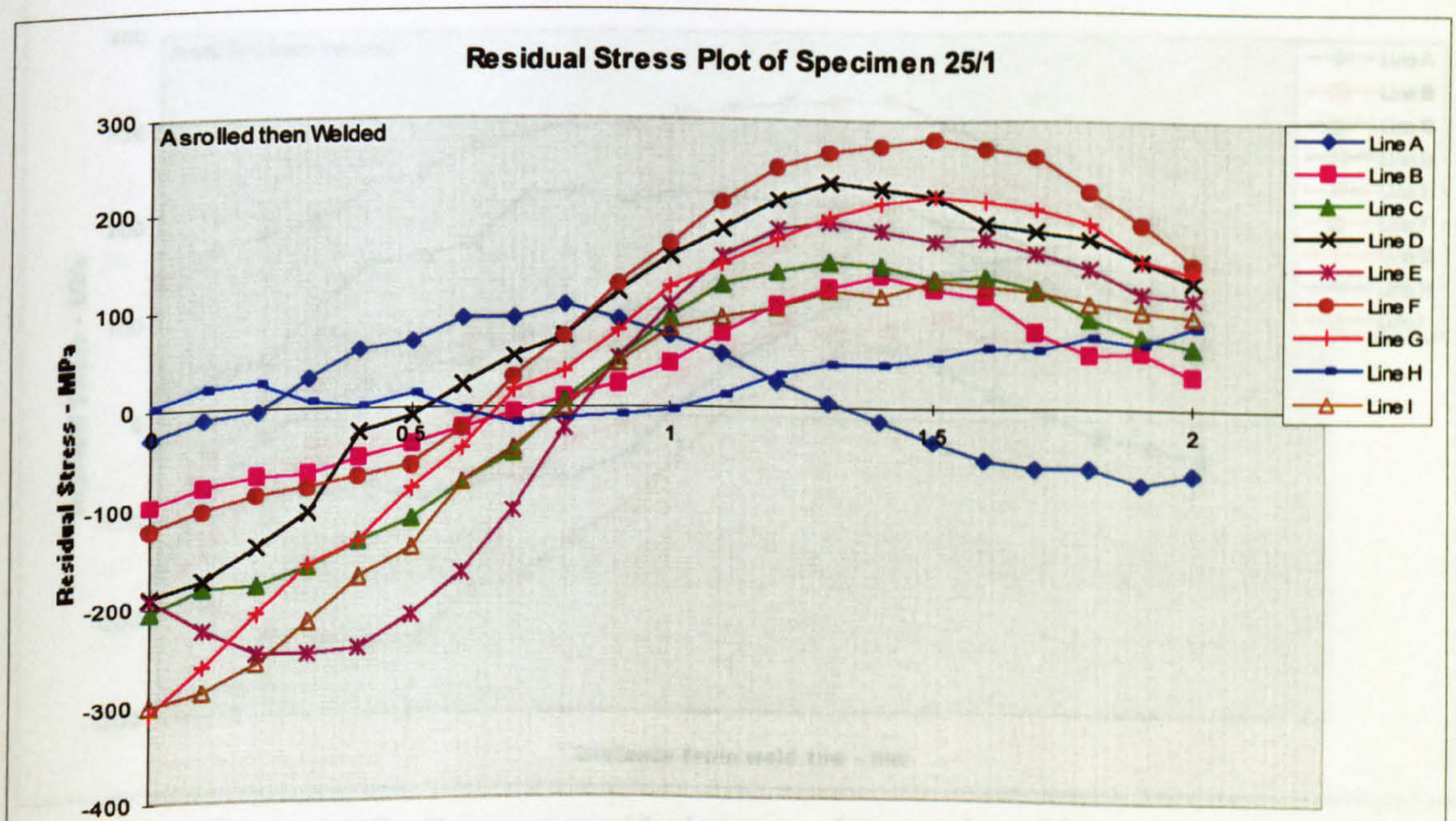

Figure 5.646 – Transverse residual stresses plot - specimen 25/1 (untreated)

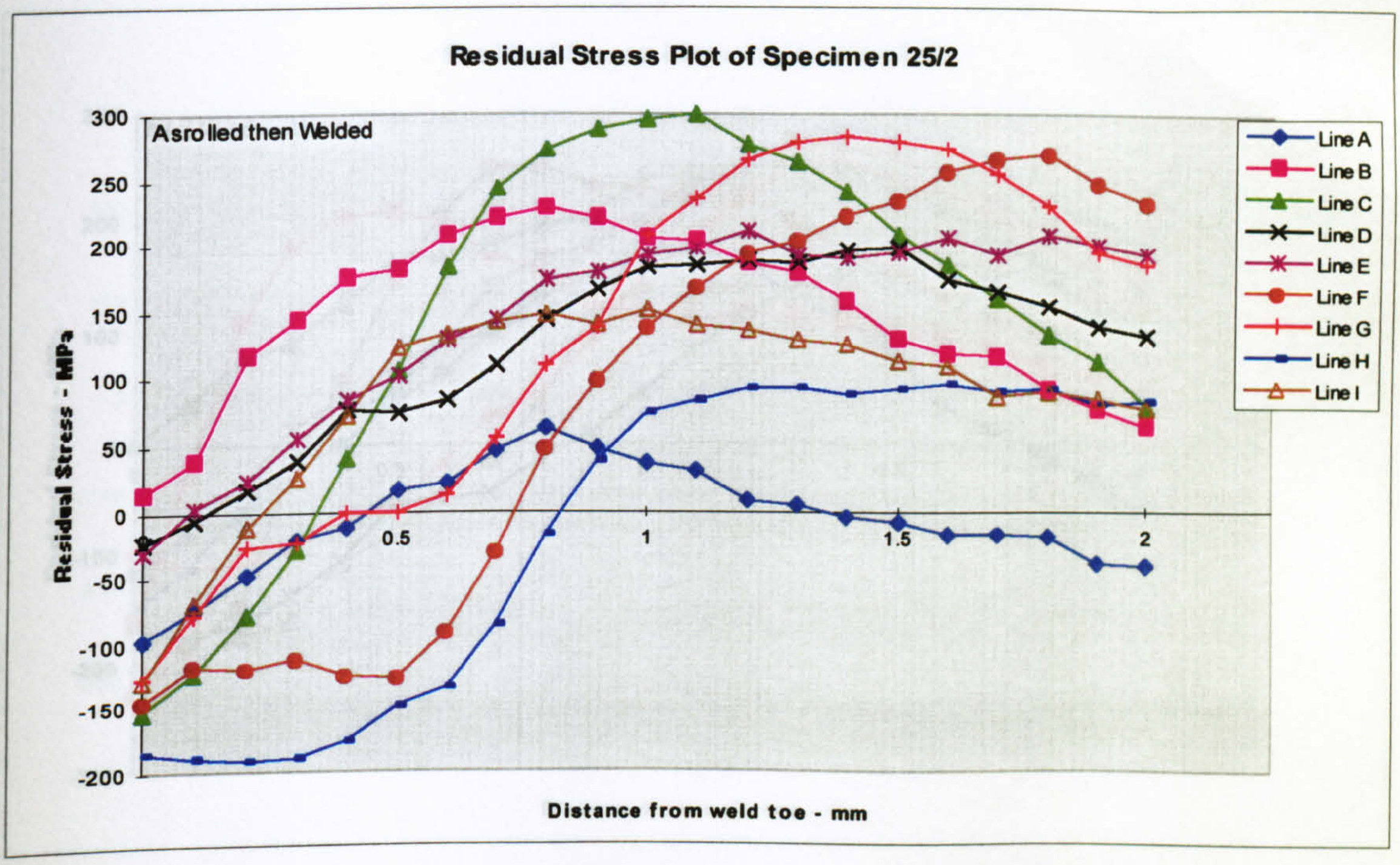

Figure 5.647 – Transverse residual stresses plot - specimen 25/2 (untreated)

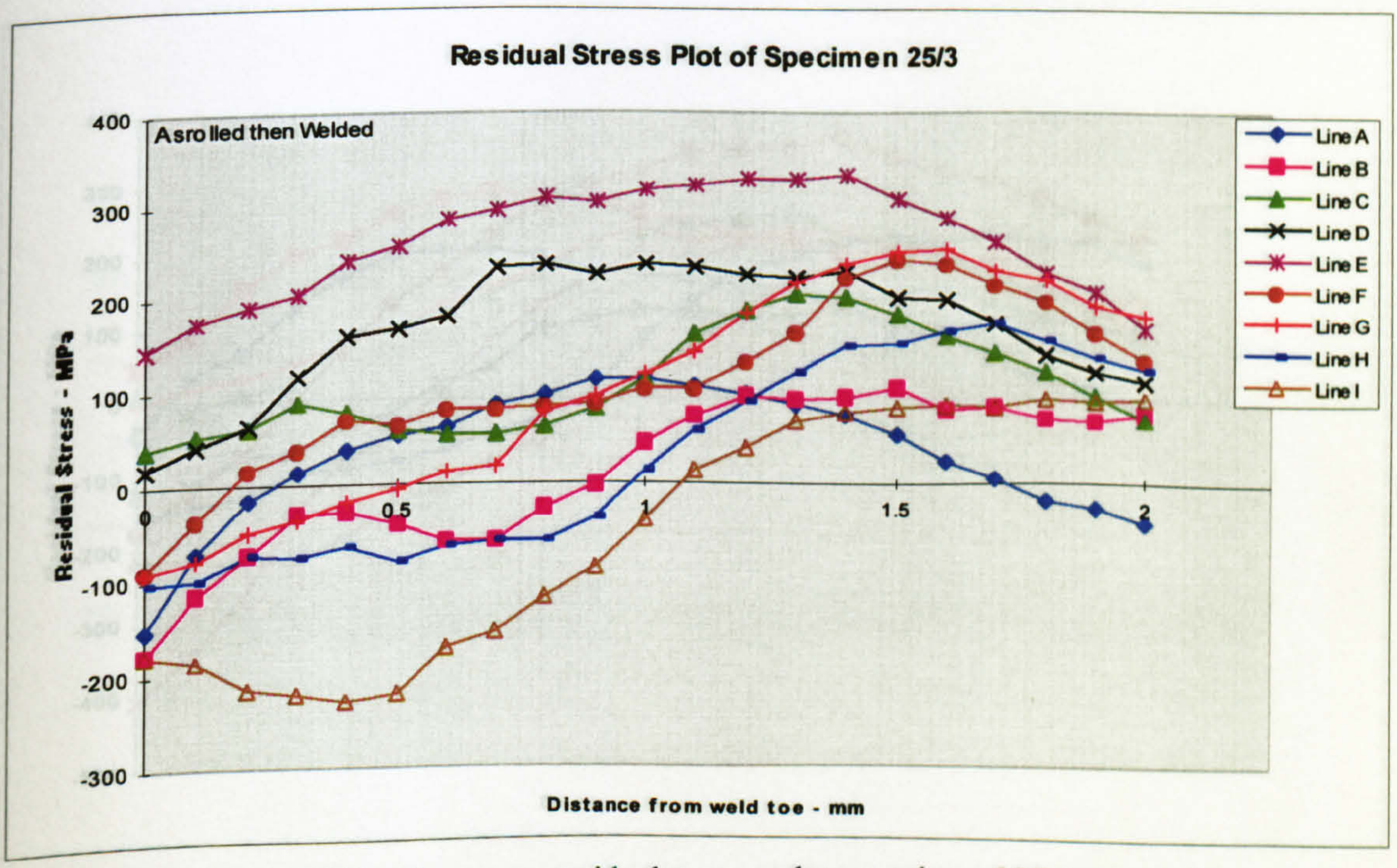

Figure 5.648 – Transverse residual stresses plot - specimen 25/3 (untreated)

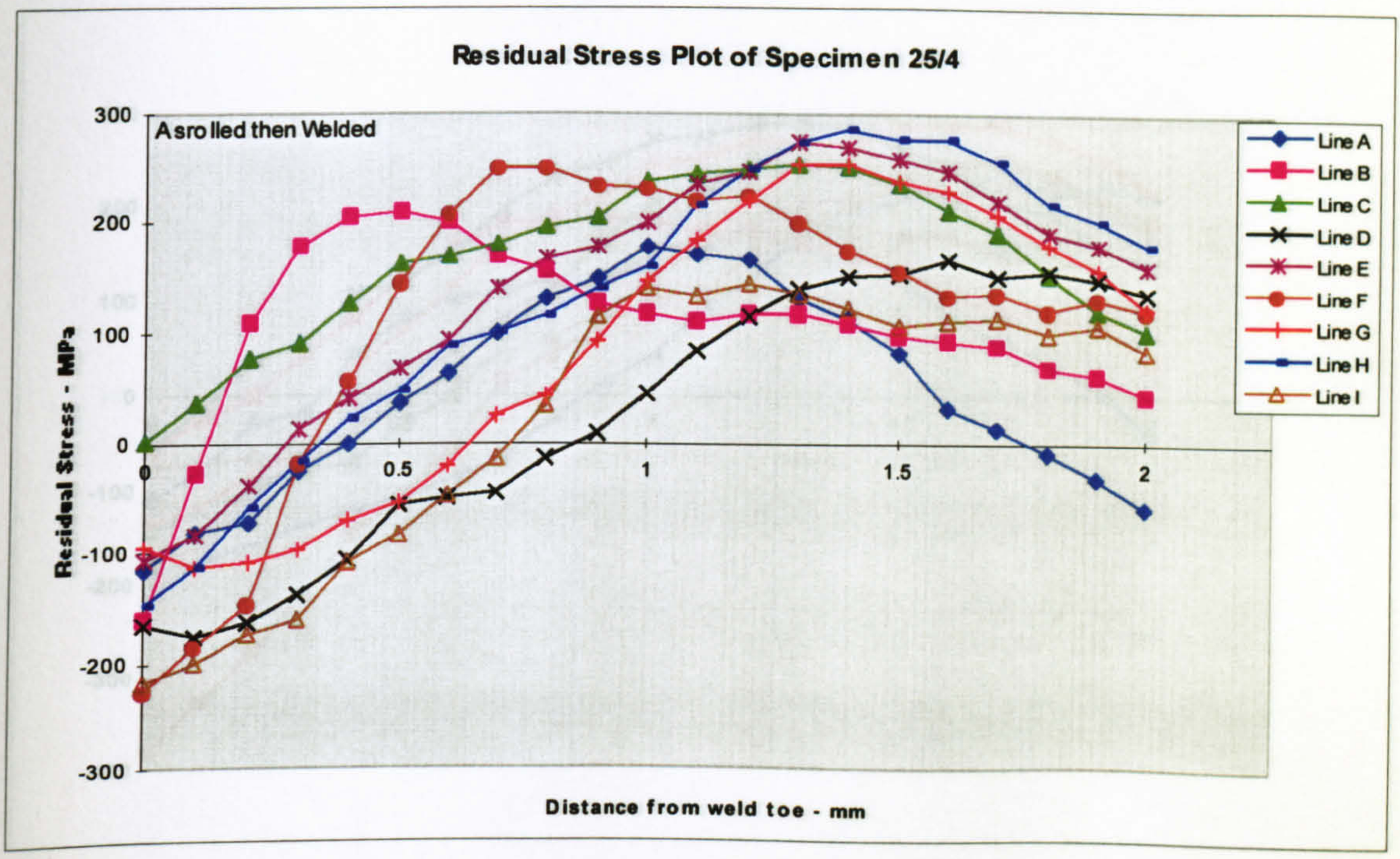

Figure 5.649 – Transverse residual stresses plot - specimen 25/4 (untreated)

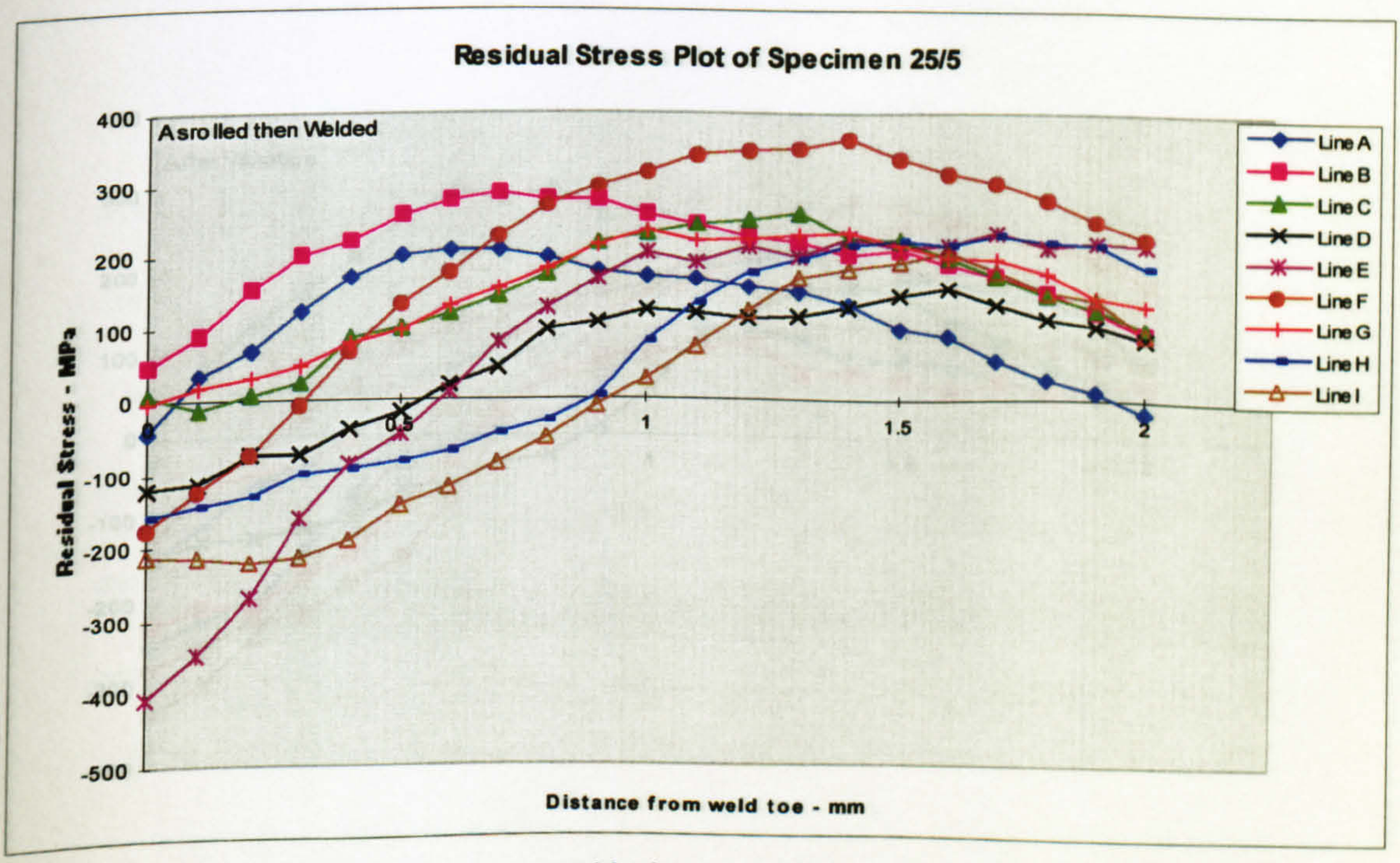

Figure 5.650 – Transverse residual stresses plot - specimen 25/5 (untreated)

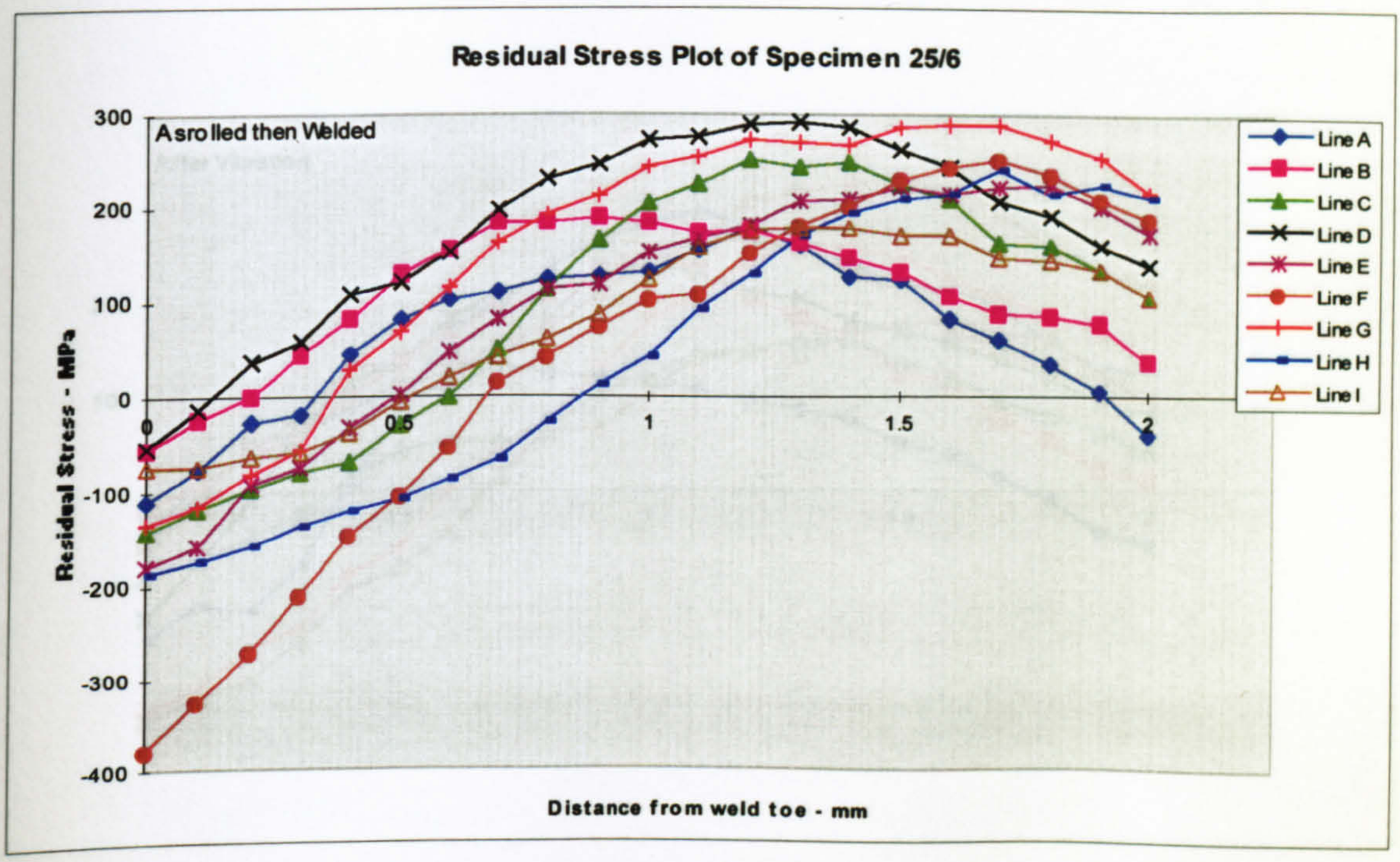

Figure 5.651 – Transverse residual stresses plot - specimen 25/6 (untreated)

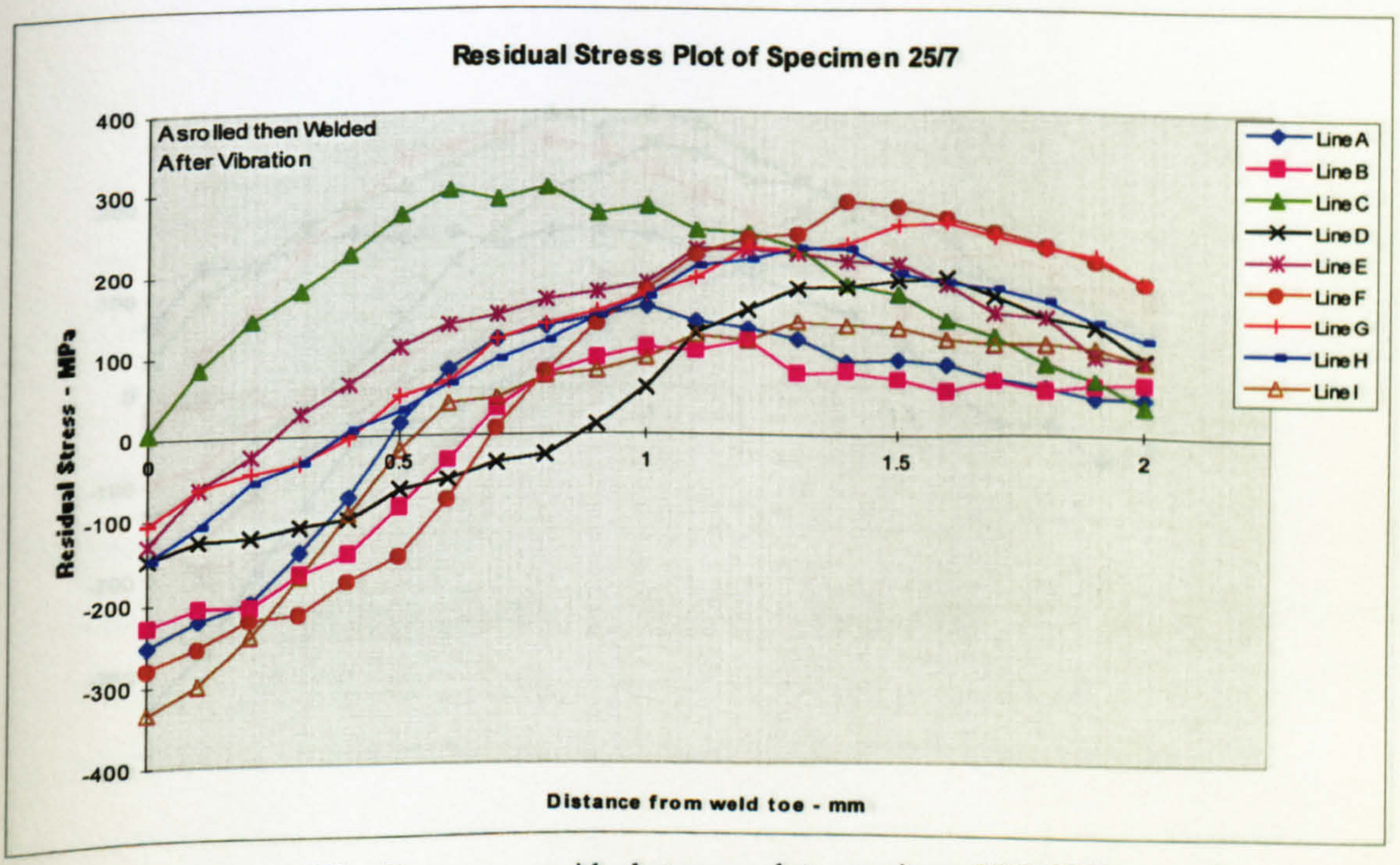

Figure 5.652 – Transverse residual stresses plot - specimen 25/7 (VSR treated)

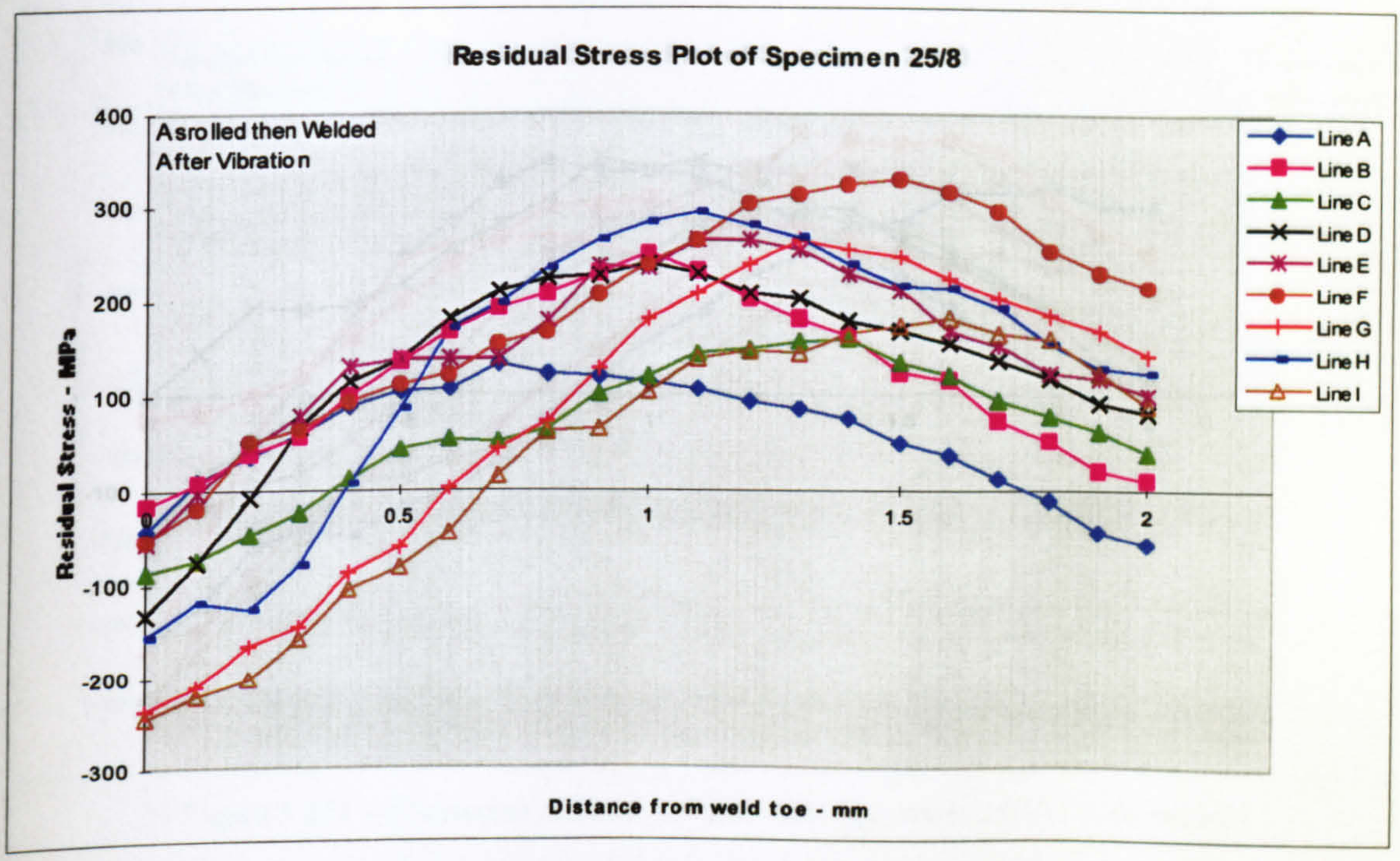

Figure 5.653 – Transverse residual stresses plot - specimen 25/8 (VSR treated)

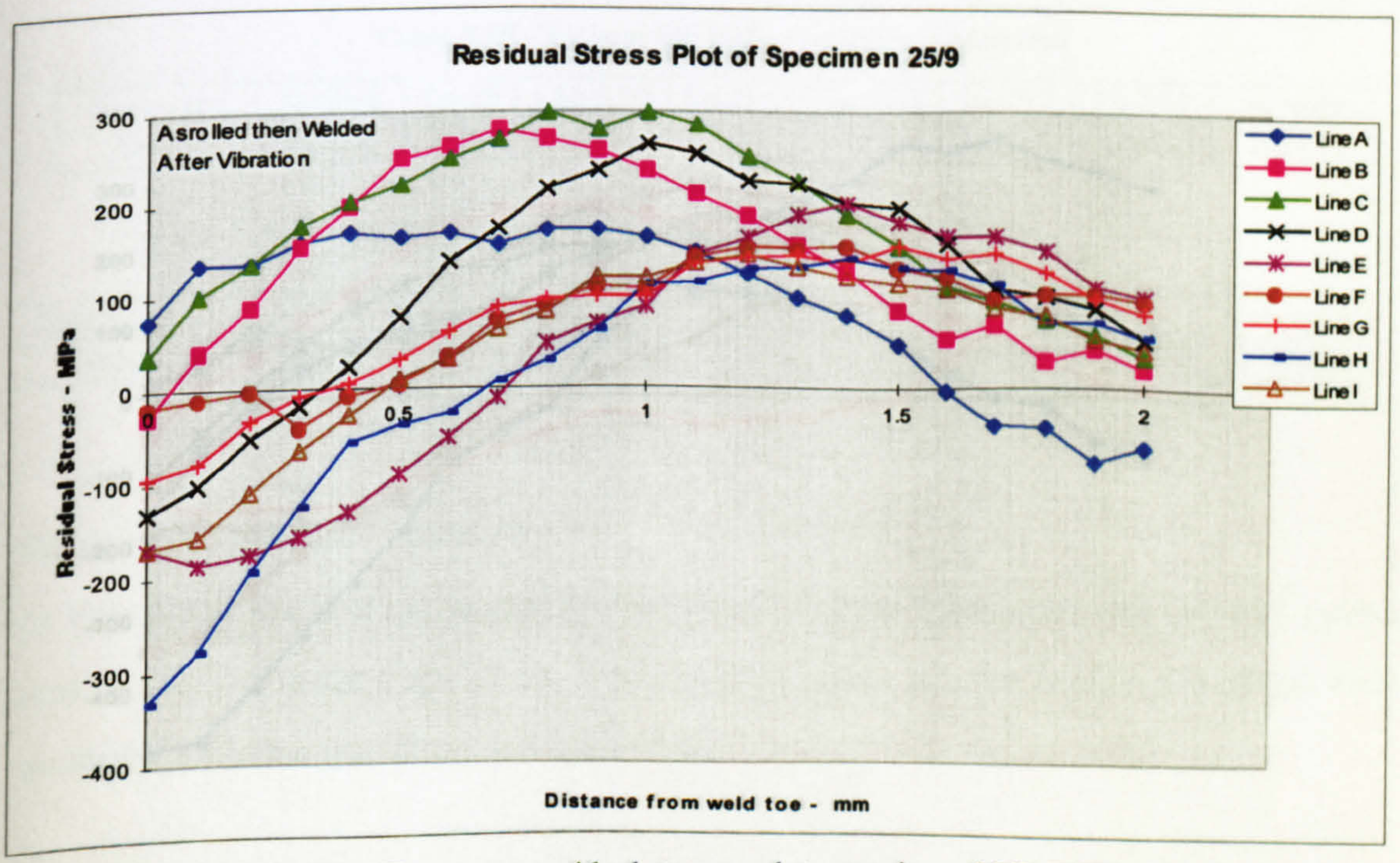

Figure 5.654 – Transverse residual stresses plot - specimen 25/9 (VSR treated)

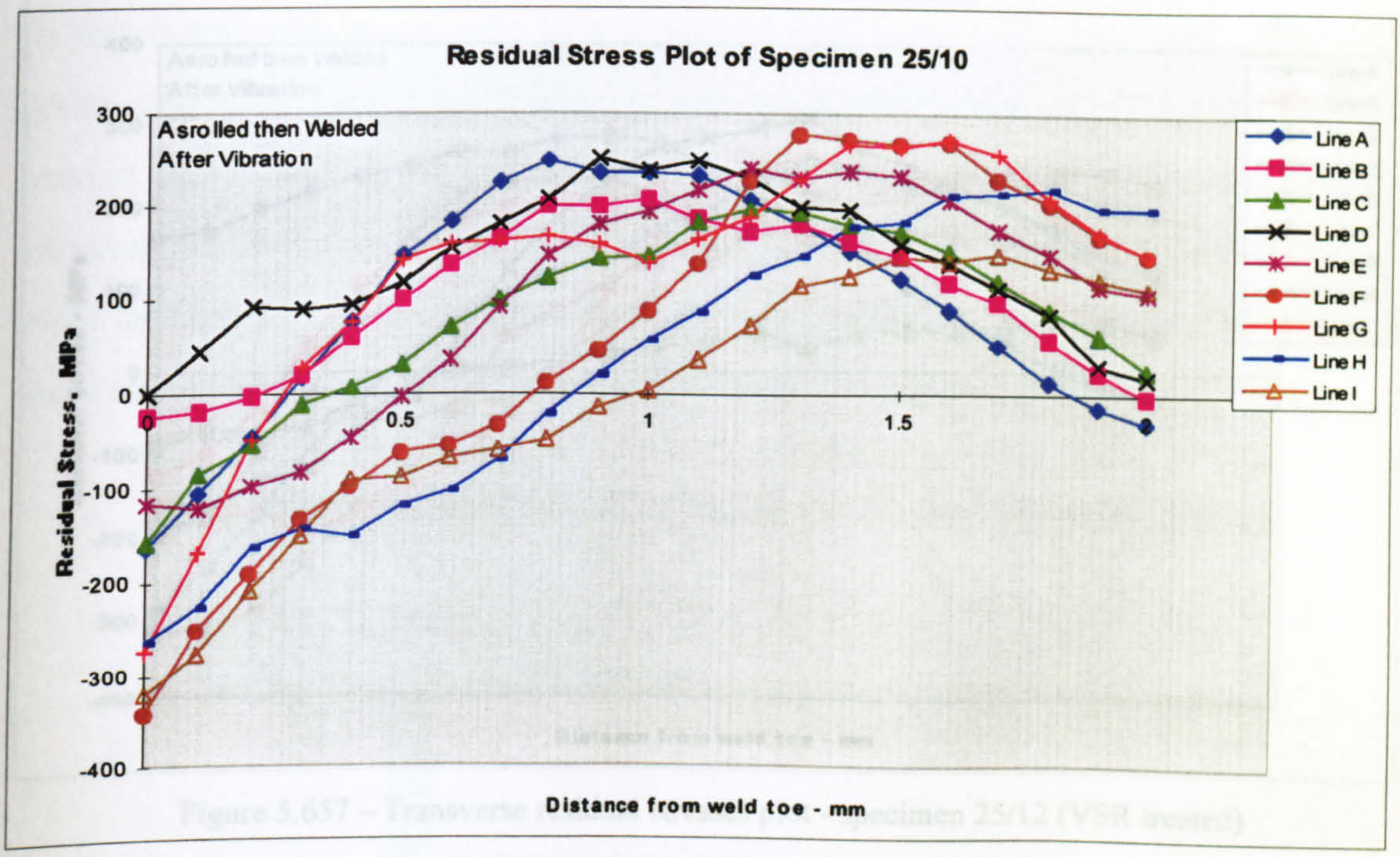

Figure 5.655 – Transverse residual stresses plot - specimen 25/10 (VSR treated)

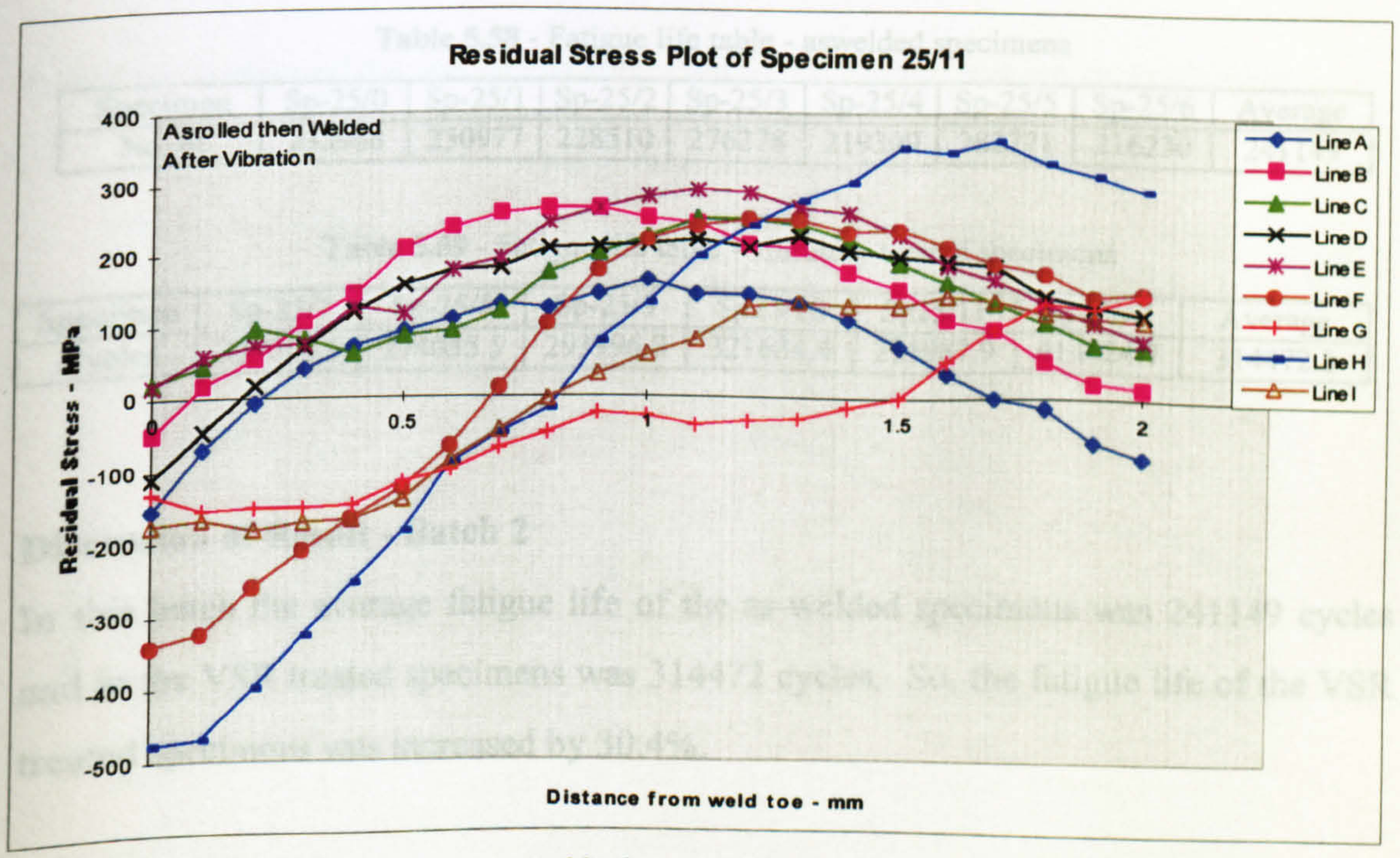

Figure 5.656 – Transverse residual stresses plot - specimen 25/11 (VSR treated)

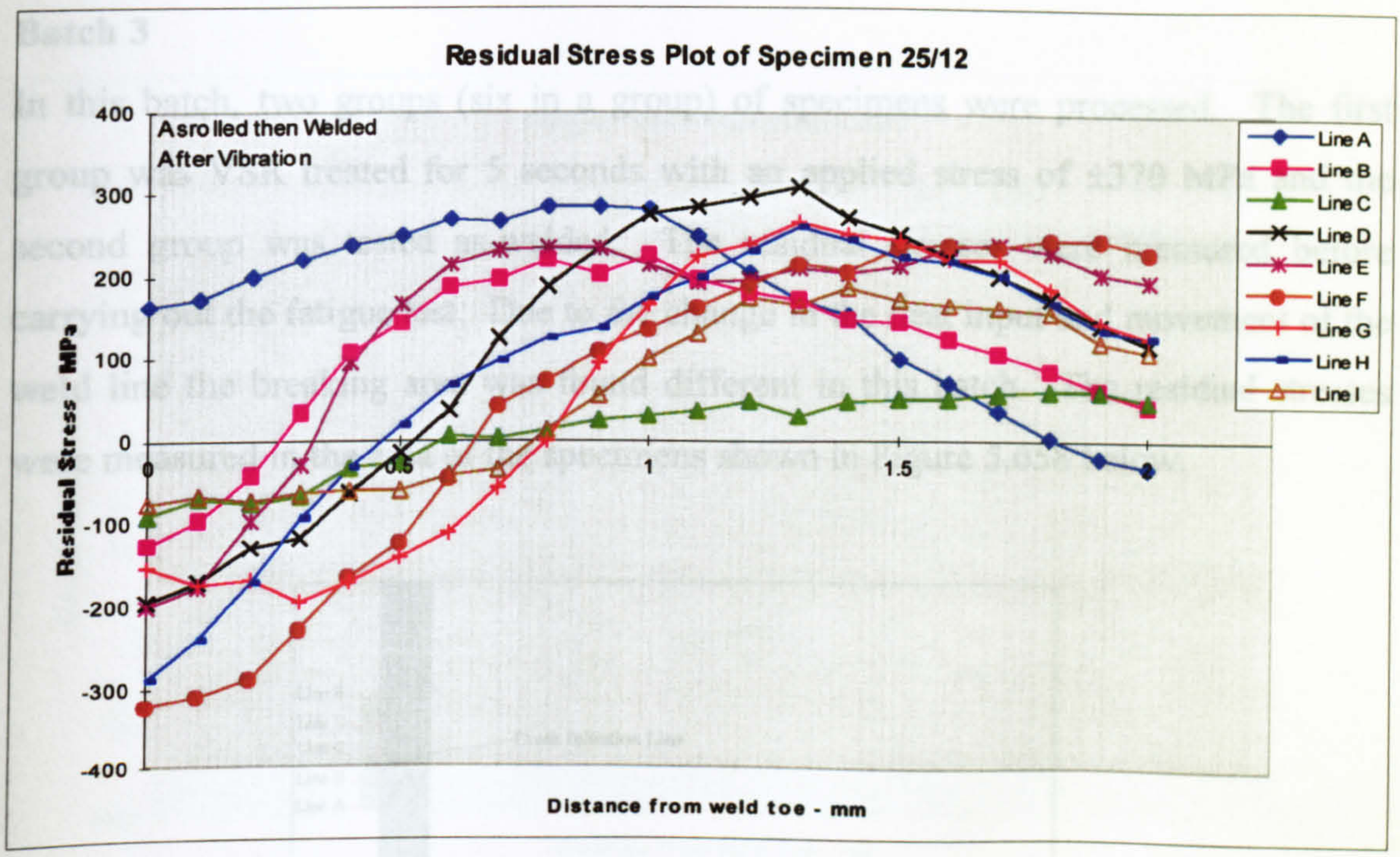

Figure 5.657 – Transverse residual stresses plot - specimen 25/12 (VSR treated)

The fatigue life of the VSR treated and untreated specimens of this group are shown in the tables below (Table 5.58 and 5.59).

Table 5.58 - Fatigue life table - aswelded specimens

Specimen	Sp-25/0	Sp-25/1	Sp-25/2	Sp-25/3	Sp-25/4	Sp-25/5	Sp-25/6	Average
No. of	233968	230977	228510	276278	219309	282771	216230	241149

Table 5.59 - Fatigue life table - vibratory treated specimens

Specimen	Sp-25/7	Sp-25/8	Sp-25/9	Sp25/10	Sp25/11	Sp25/12	Average
Cycles	327084.5	274055.5	293996.8	321684.4	255987.9	414024.7	314472.3

Discussion of Result - Batch 2

In this batch the average fatigue life of the as-welded specimens was 241149 cycles and in the VSR treated specimens was 314472 cycles. So, the fatigue life of the VSR treated specimens was increased by 30.4%.

The residual stresses and the fatigue lives was found not to be linked to each other, i.e. no relationships were observed between the residual stresses and the fatigue lives of the specimens.

Batch 3

In this batch, two groups (six in a group) of specimens were processed. The first group was VSR treated for 5 seconds with an applied stress of ±370 MPa and the second group was tested as-welded. The residual stresses were measured before carrying out the fatigue test. Due to the change in the heat input and movement of the weld line the breaking area was found different in this batch. The residual stresses were measured in the area of the specimens shown in Figure 5.658 below.

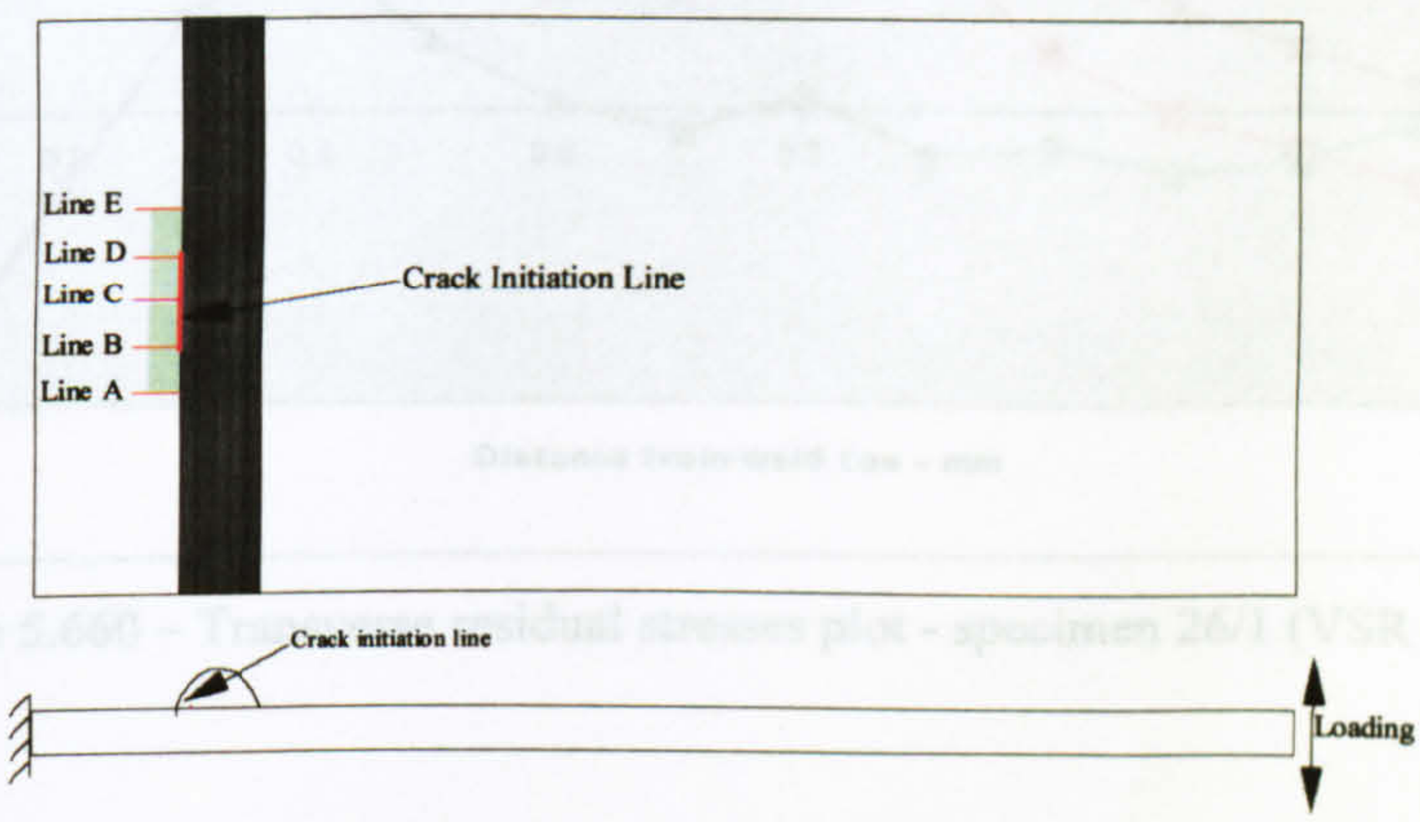

Figure 5.658 - Location of measurement lines

Residual stresses of the specimens subjected to the fatigue test are shown below

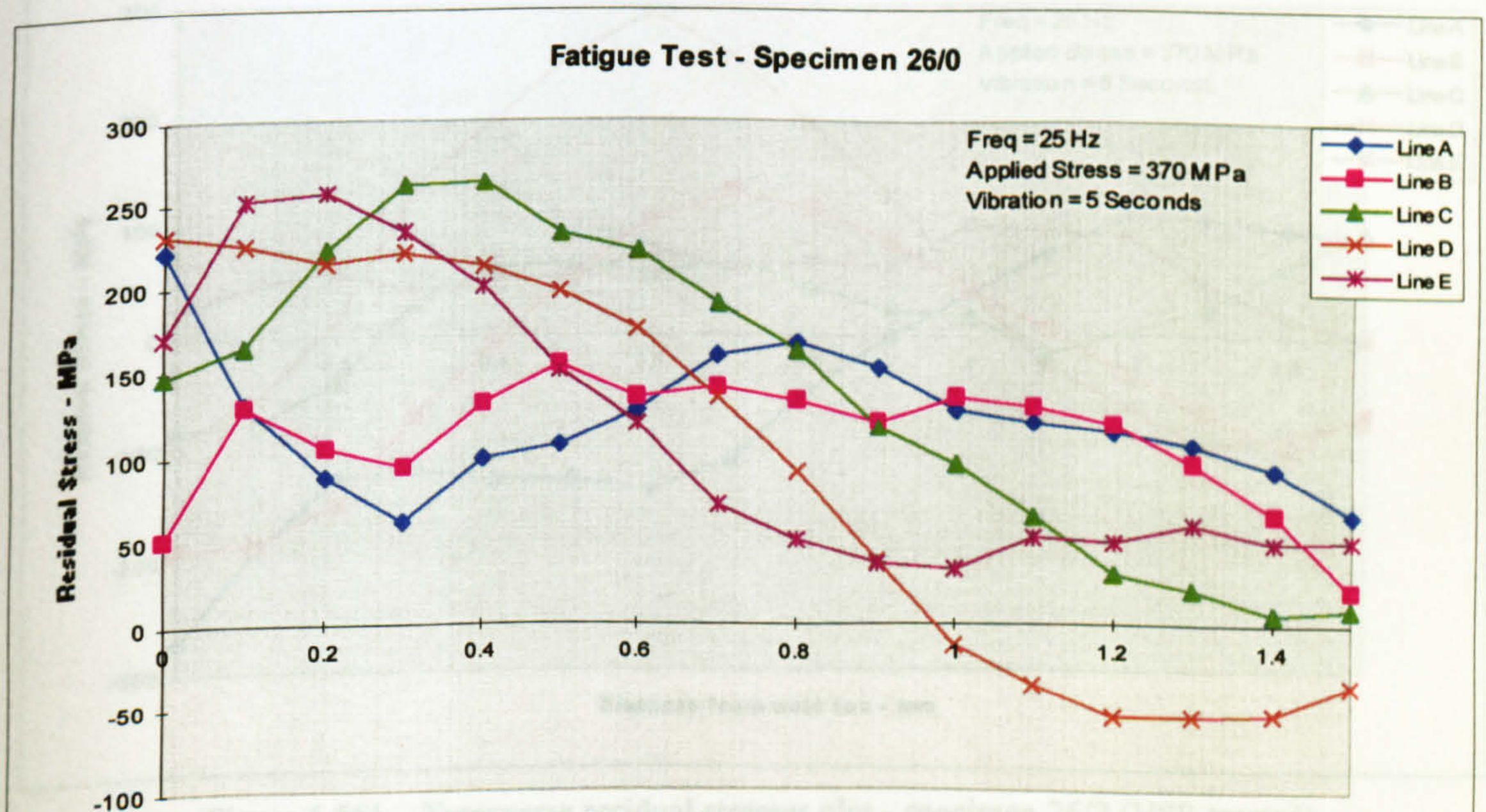

Figure 5.659 – Transverse residual stresses plot - specimen 26/0 (VSR treated)

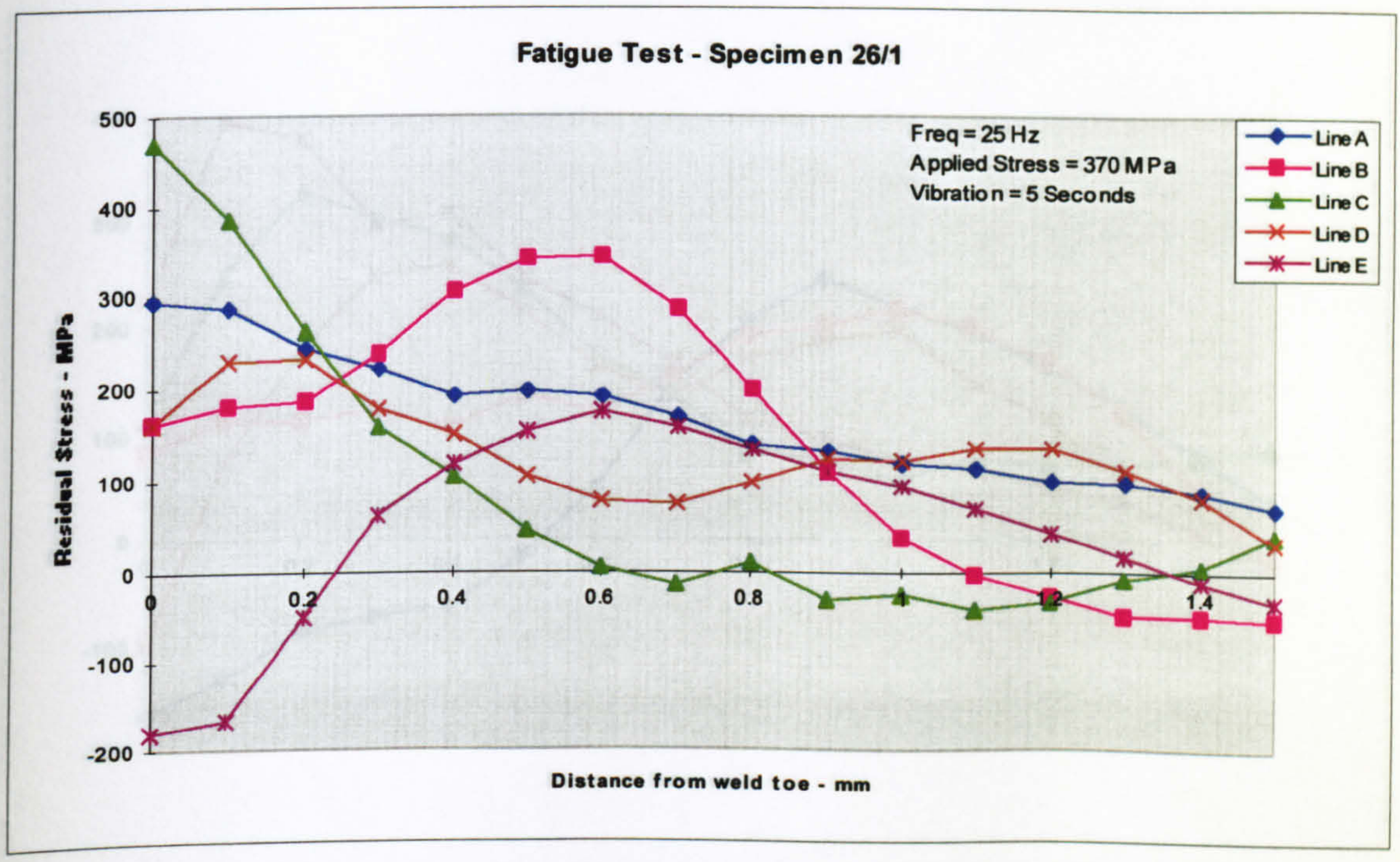

Figure 5.660 – Transverse residual stresses plot - specimen 26/1 (VSR treated)

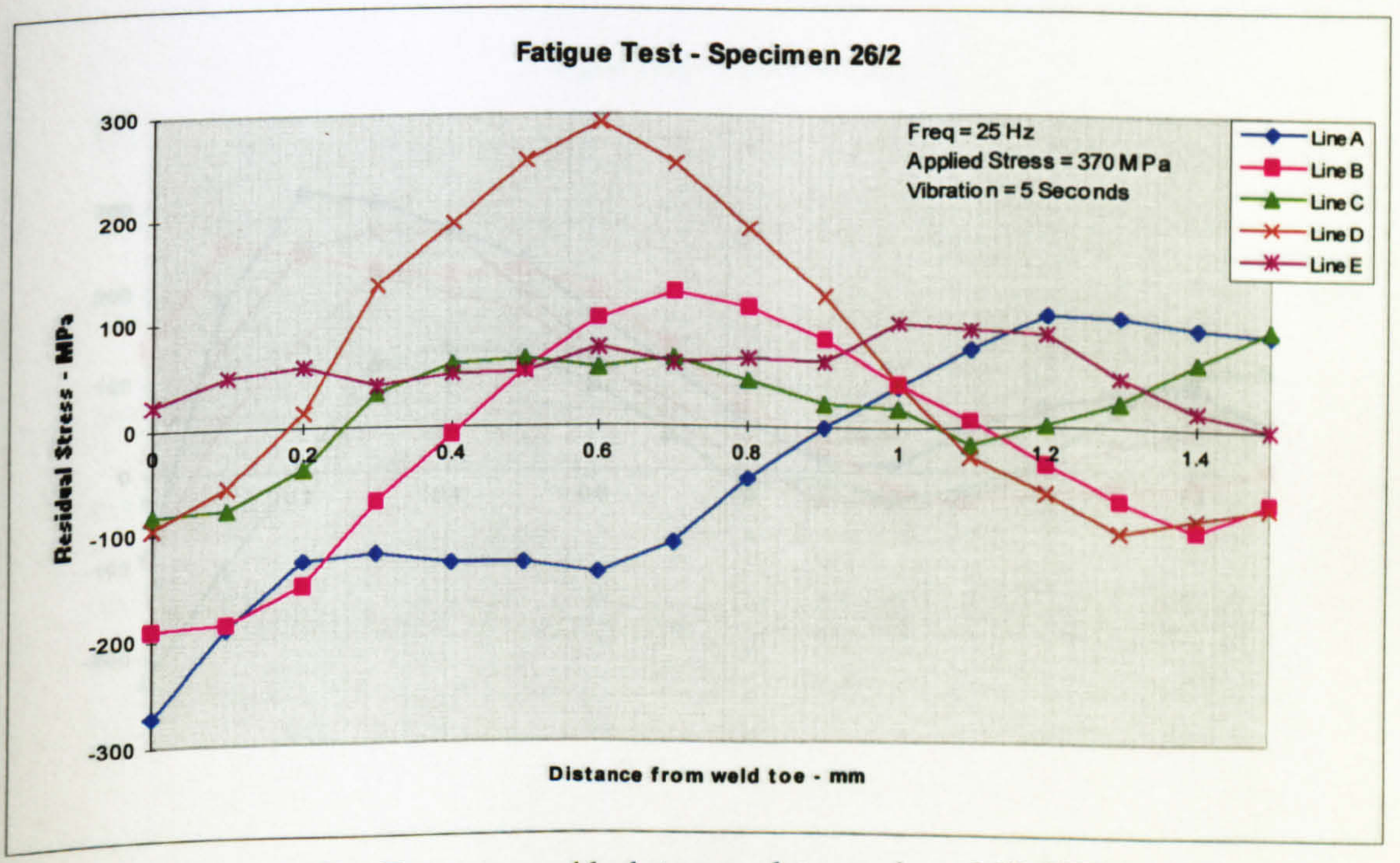

Figure 5.661 – Transverse residual stresses plot - specimen 26/2 (VSR treated)

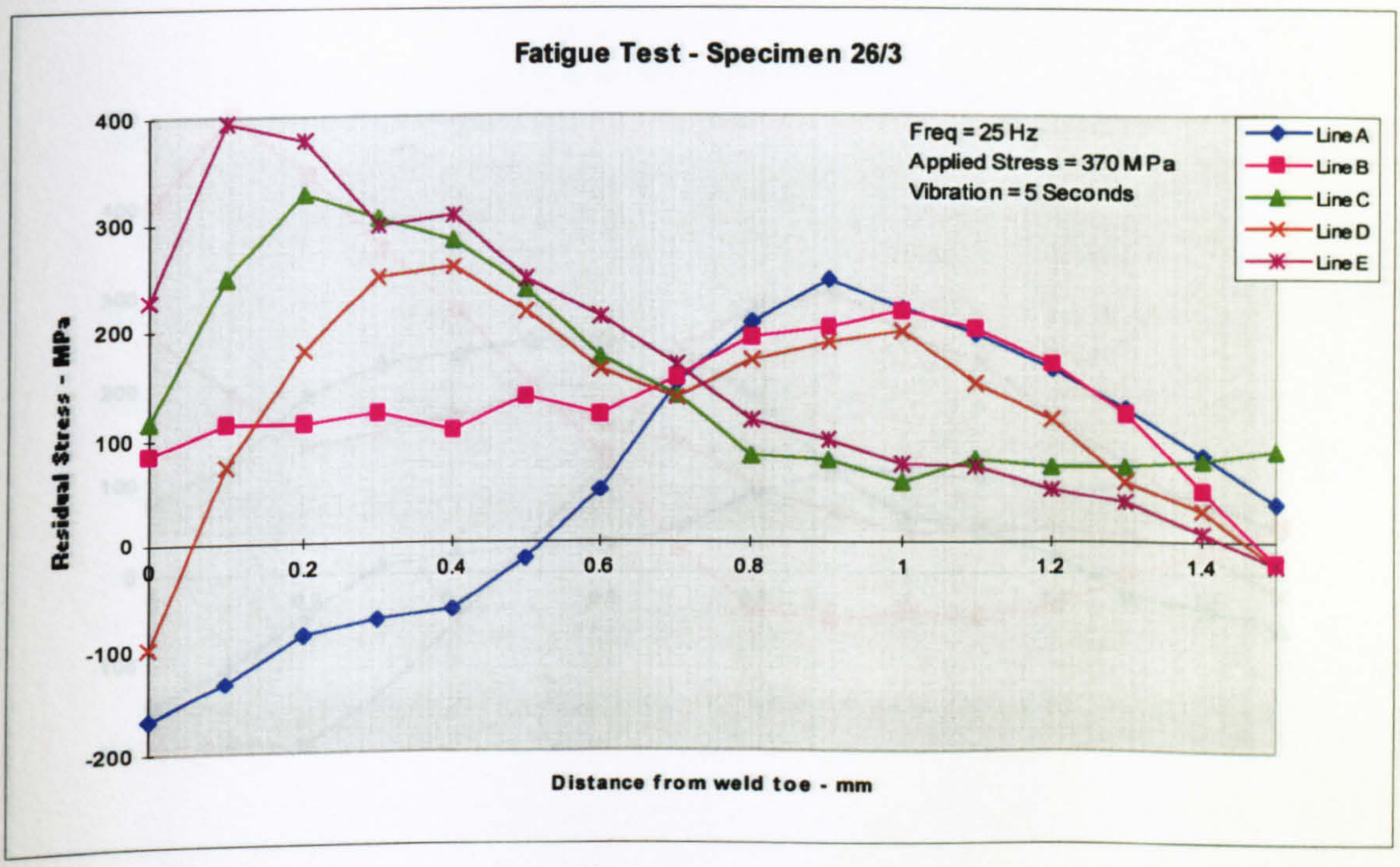

Figure 5.662 – Transverse residual stresses plot - specimen 26/3 (VSR treated)

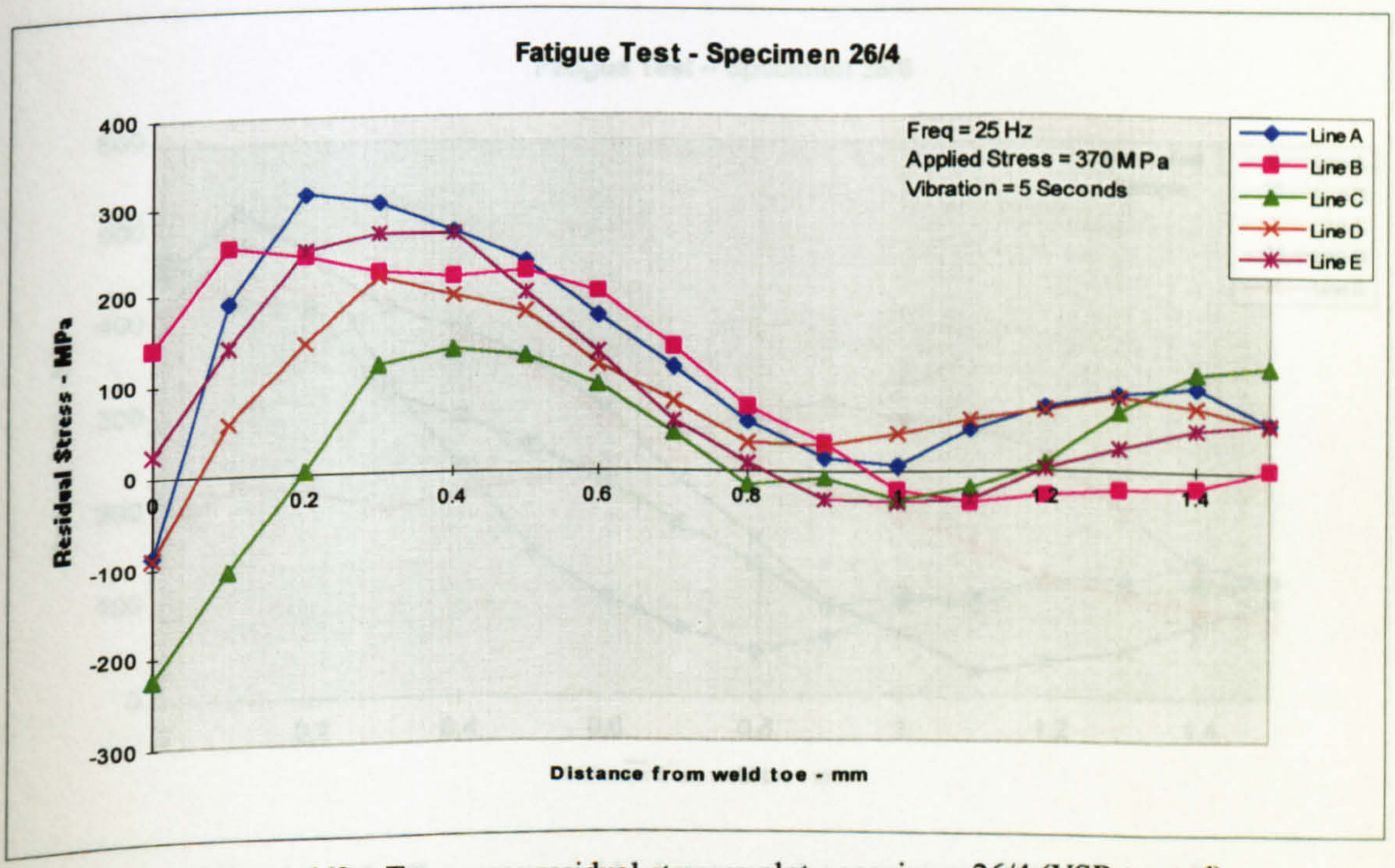

Figure 5.663 – Transverse residual stresses plot - specimen 26/4 (VSR treated)

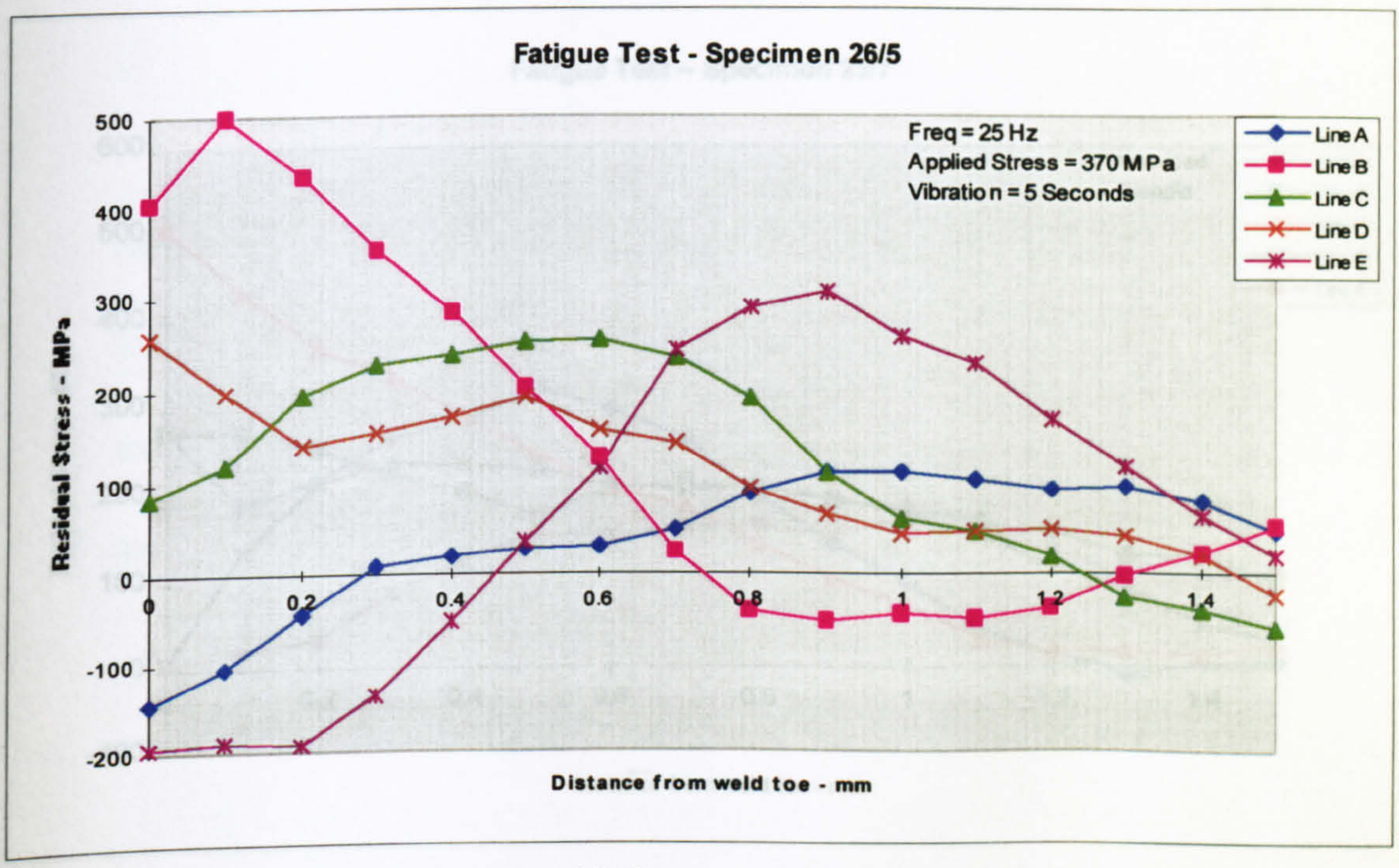

Figure 5.664 – Transverse residual stresses plot - specimen 26/5 (VSR treated)

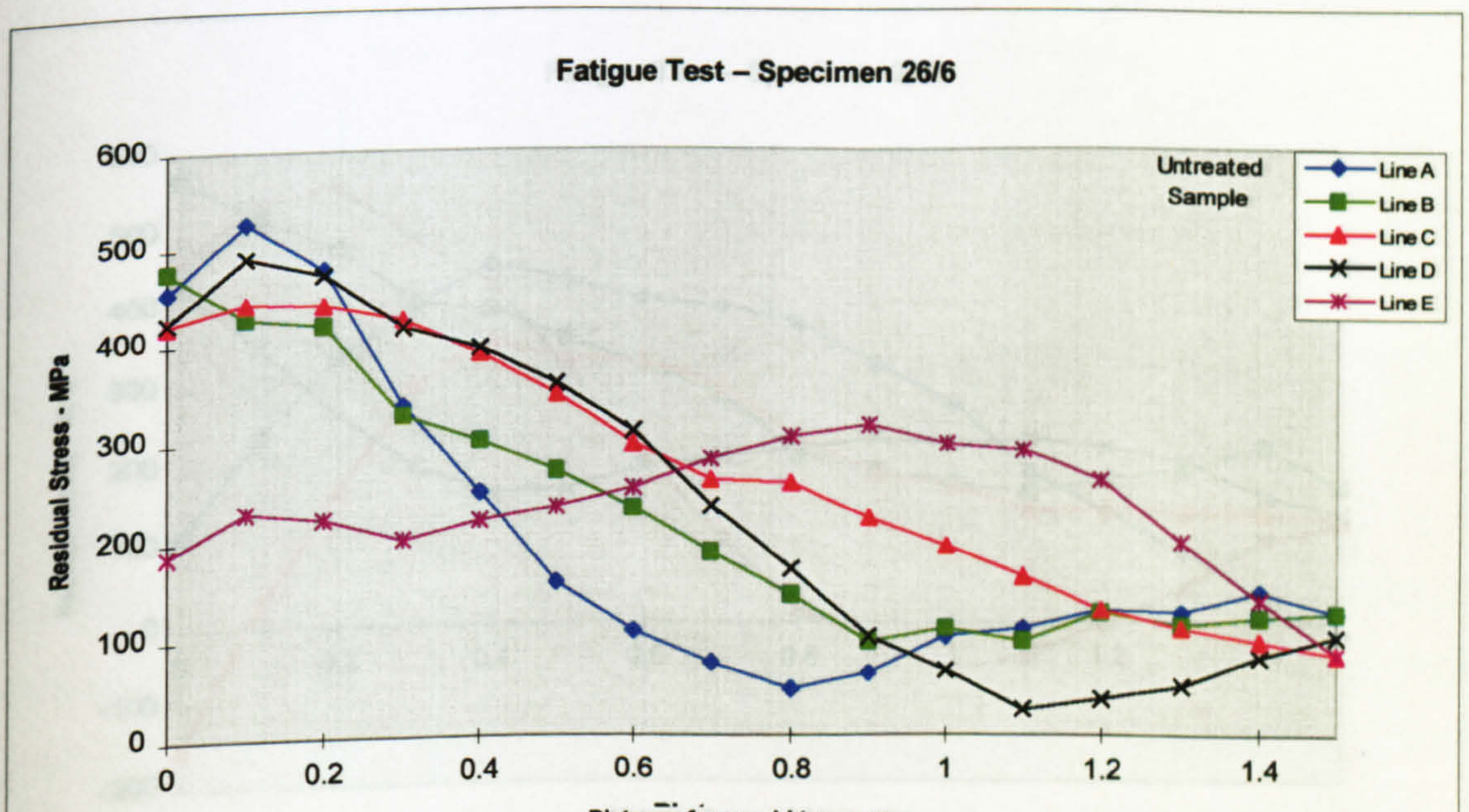

Figure 5.665 – Transverse residual stresses plot - specimen 26/6 (untreated)

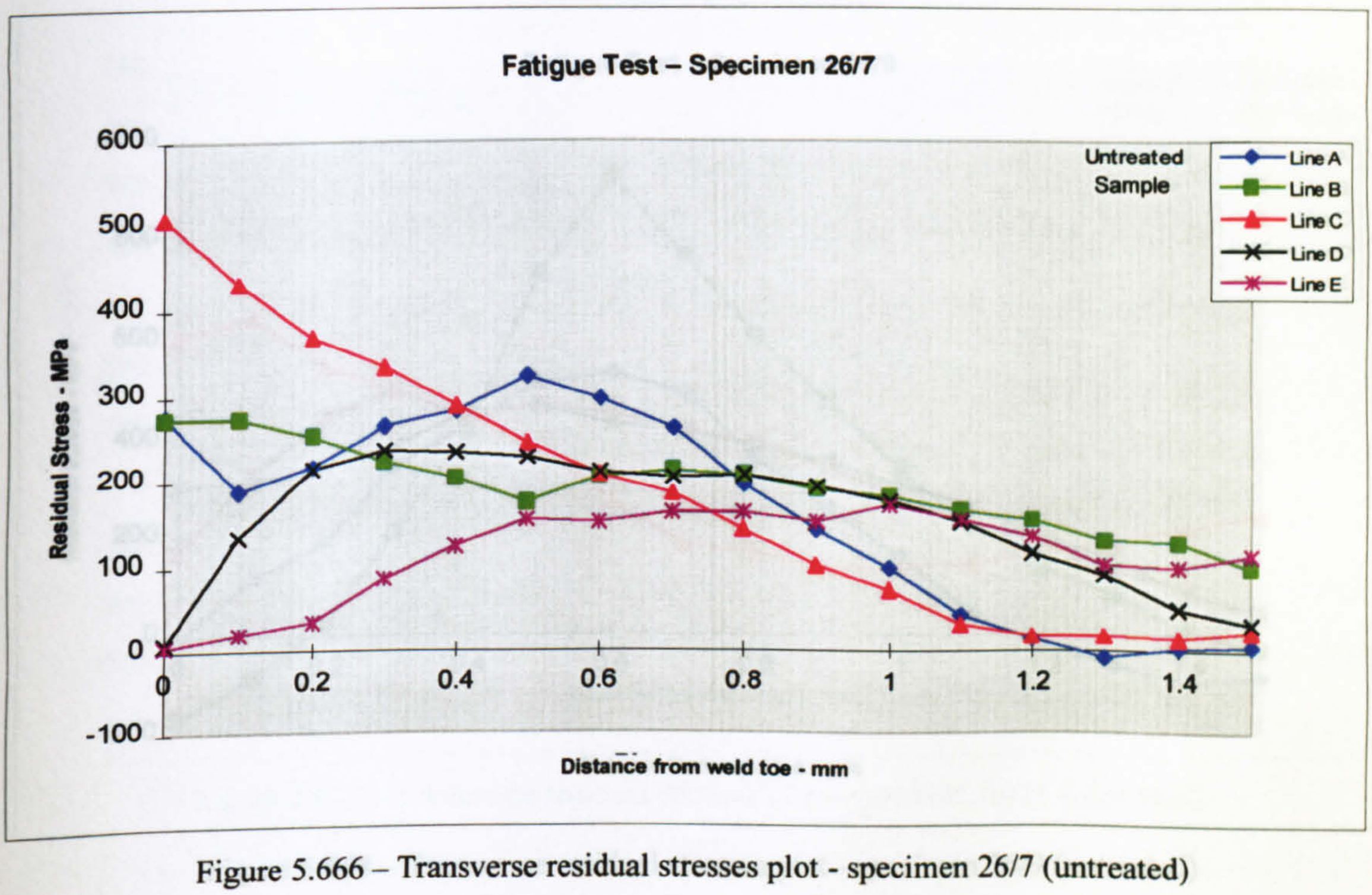

Figure 5.666 – Transverse residual stresses plot - specimen 26/7 (untreated)

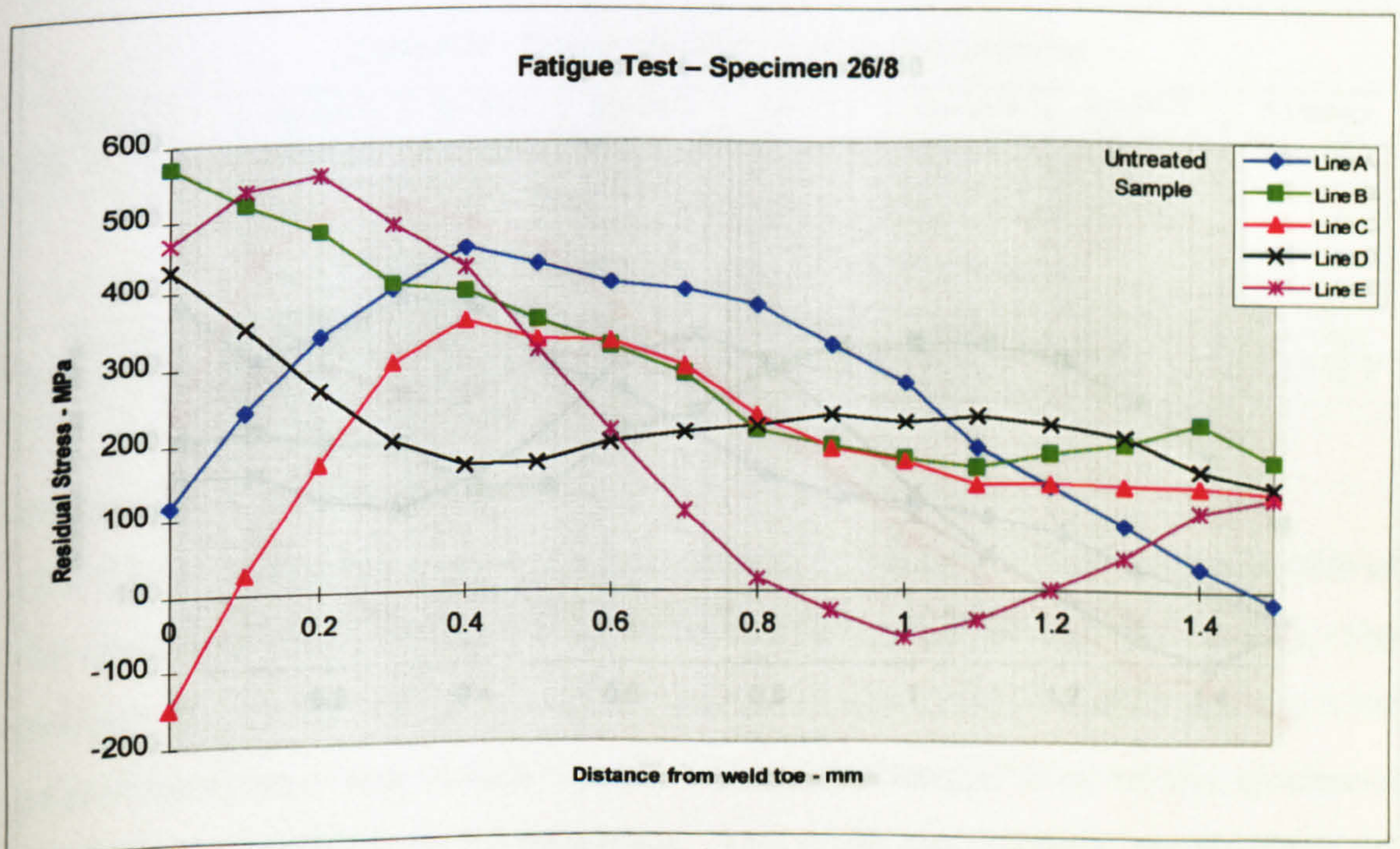

Figure 5.667 – Transverse residual stresses plot - specimen 26/8 (untreated)

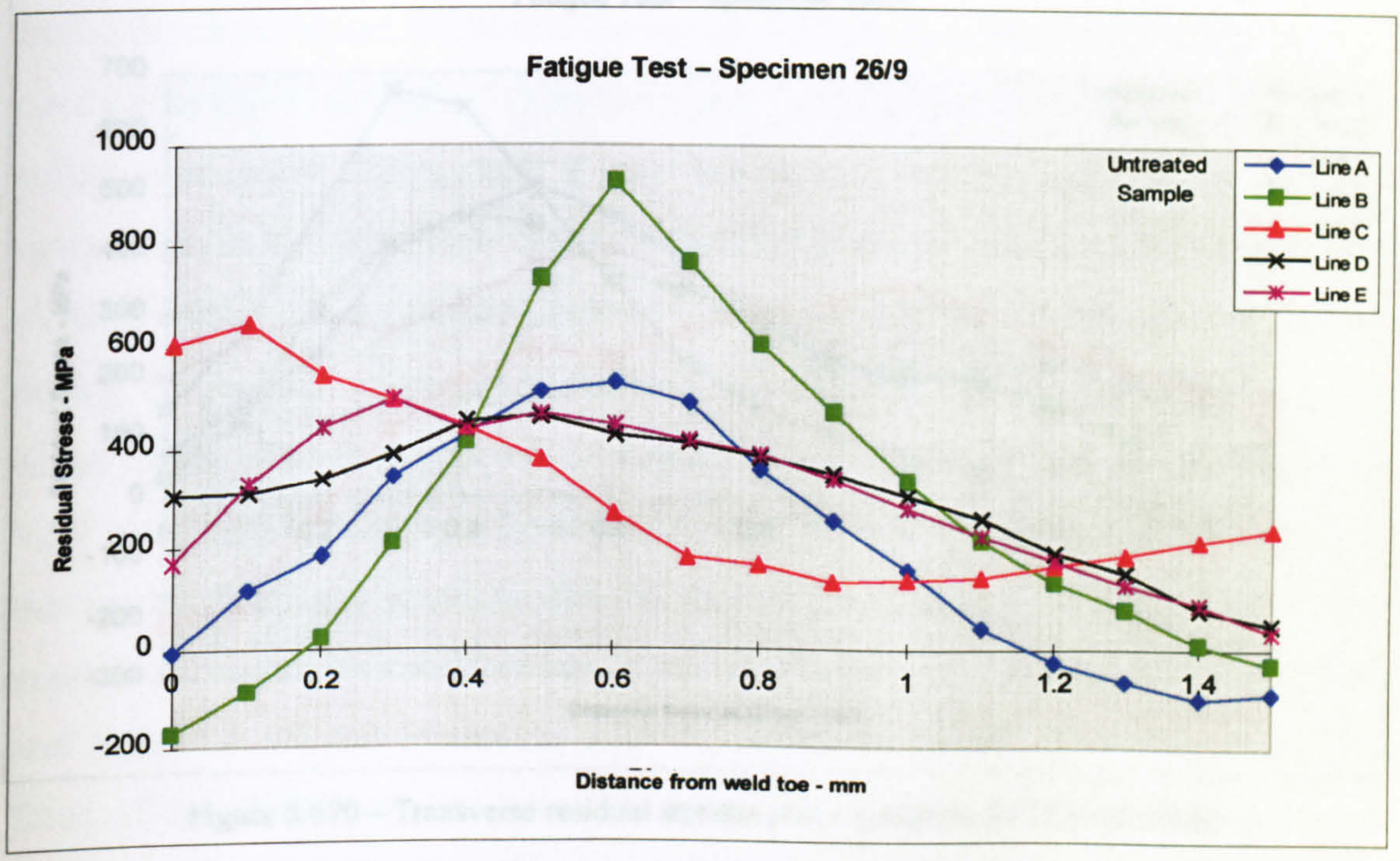

Figure 5.668 – Transverse residual stresses plot - specimen 26/9 (untreated)

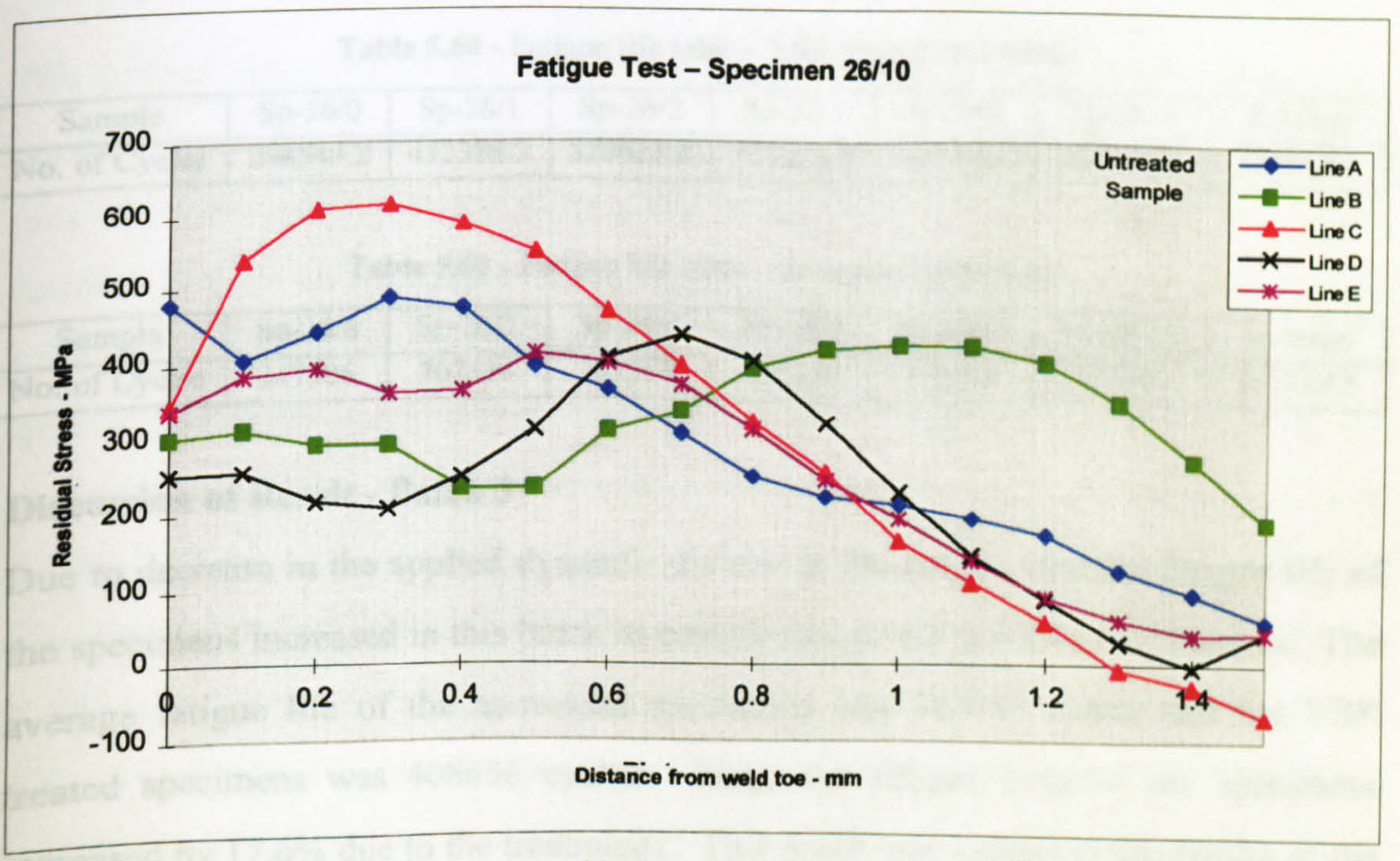

Figure 5.669 – Transverse residual stresses plot - specimen 26/10 (untreated)

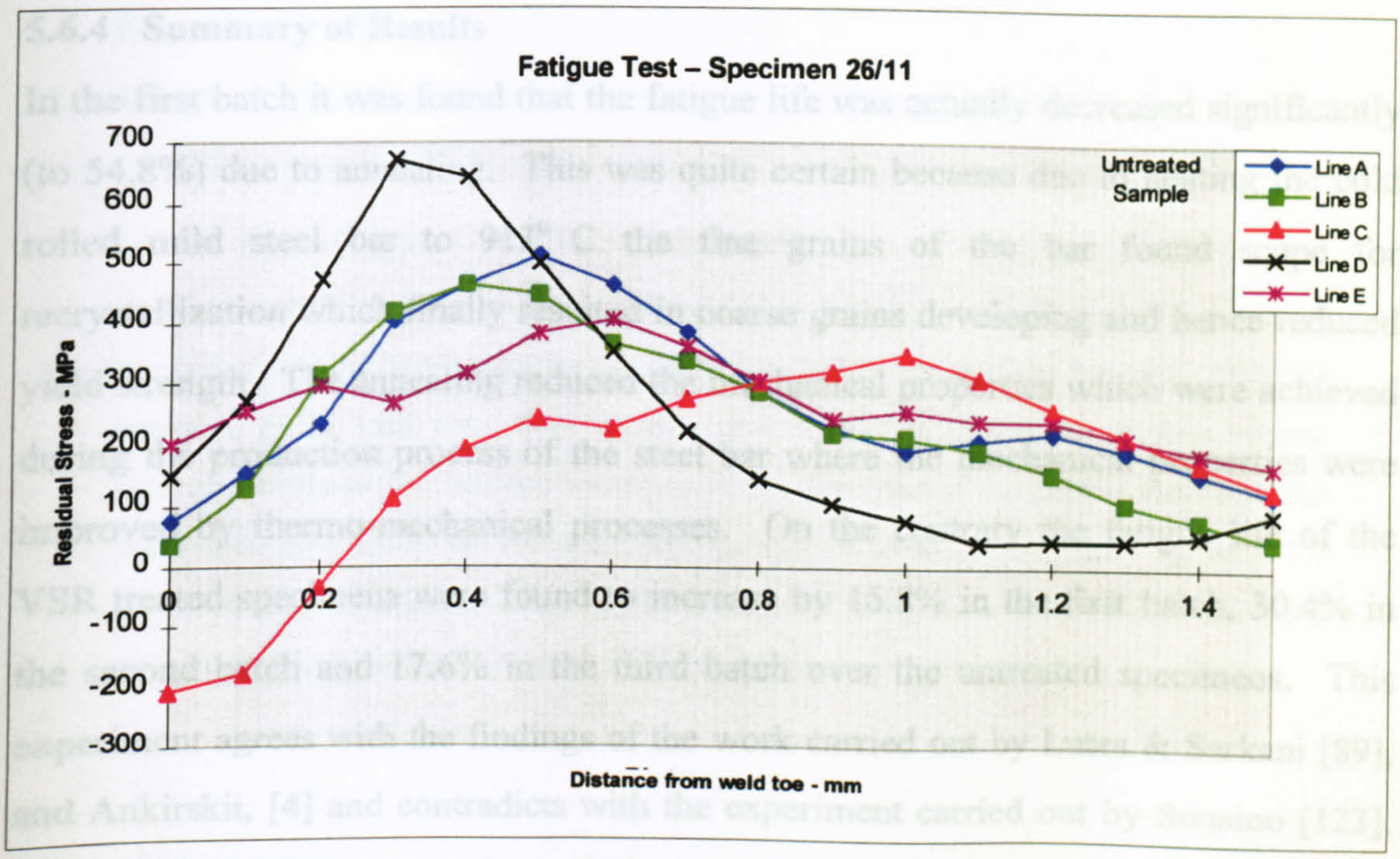

Figure 5.670 – Transverse residual stresses plot - specimen 26/11 (untreated)

Fatigue lives of all twelve samples were tested using applied stress ±164.4 MPa. The life of the specimens were found as

Table 5.60 - Fatigue life table - VSR treated specimens

Sample	Sp-26/0	Sp-26/1	Sp-26/2	Sp-26/3	Sp-26/4	Sp-26/5	Average
No. of Cycles	298544.2	452388.3	320622.8	500926.9	426706.8	449147.8	408056.1

Table 5.61 - Fatigue life table – as-welded specimens

Sample	Sp-26/6	Sp-26/7	Sp-26/8	Sp-26/9	Sp-26/10	Sp-26/11	Average
No. of Cycles	347306	307514	391276	339359	314015	381086	346759.3

Discussion of Result - Batch 3

Due to decrease in the applied dynamic stresses in the fatigue test, the fatigue life of the specimens increased in this batch in comparison to the previous two batches. The average fatigue life of the as-welded specimens was 346759 cycles and the VSR treated specimens was 408056 cycles. Thus, the fatigue lives of the specimens increased by 17.6% due to the treatments. This result was similar to the results of the previous two batches. Similar to the previous batch (batch 2) no relationship was observed between the residual stresses and the fatigue lives.

5.6.4 Summary of Results

In the first batch it was found that the fatigue life was actually decreased significantly (to 54.8%) due to annealing. This was quite certain because due to heating the cold rolled mild steel bar to 913^0 C the fine grains of the bar found scope for recrystallization which finally resulted in coarse grains developing and hence reduced yield strength. The annealing reduced the mechanical properties which were achieved during the production process of the steel bar where the mechanical properties were improved by thermo-mechanical processes. On the contrary the fatigue life of the VSR treated specimens were found to increase by 16.8% in the first batch, 30.4% in the second batch and 17.6% in the third batch over the untreated specimens. This experiment agrees with the findings of the work carried out by Lutes & Sarkani [89], and Ankirskii, [4] and contradicts with the experiment carried out by Sonsino [123]. Thus, if the VSR treatment is carried out with application of a high dynamic stress ($\pm\sigma_Y$) with a small number of cycles, it does not decrease its fatigue life instead it increase. Because of the small number of specimens processed and since only two levels of stresses were applied in the fatigue test the σ-N curve was not drawn.

The second objective of this experiment was to obtain a relationship between the residual stresses in the specimens and the fatigue life. The residual stress on the weld toes were compared with the fatigue life values, where it was assumed that higher residual stresses would show a lower fatigue life and the lower residual stress would show the opposite. In the second batch, the residual stresses on the weld toe were small (most of the specimens were in compressive residual stresses) which were not predicting the fatigue life of the specimens (Figures 5.645 to 5.657 and table 5.58 & 5.59). In the third batch, the heat input was changed to obtain the residual stress peak near the toe, but still it was not predicting of the fatigue life of the specimens (Figures 5.659 to 5.670 and table 5.60 & 5.61). In both batches, the stresses and fatigue life did not correlate. It might be due to the ductile property of the mild steel as Pattinson and Dugdale [105] stated.

5.7 Experiment XIII:

Metallurgical Investigation of Vibratory Treated Specimens

Abstract

In this experiment vibratory stress was applied to the specimens while they were being welded to observe its effect on the microstructure and hardness of the material. Different positions of the weld plate were observed and it was found that the crystals became columnar in shape and oriented according to the directions of the applied stresses. The orientation direction of the columnar crystals appears to be approximately Millar [111] direction with the direction of the applied stresses. The hardness of the metal was found to increase by 25% with application of vibratory stresses.

5.7.1 Introduction

This experiment was designed to investigate the effect of vibration on the transformation products of the weld. When vibration is applied to the structures during welding and cooling, the weld and the surrounding area experience dynamic stresses during solidification and transformation, which triggers the transformation of austenite to its succeeding phases. Bhadeshia [15] showed that due to the presence of uniaxial stress transformation products of the weld (martensite, acicular ferrite etc.) become anisotropic. Ernst [47] noticed grain refinement of a welded structure because of the application of vibration during welding/solidification. Campbell [28] noticed that grain refinement occurred in castings due to the application of vibration during casting.

It is established from different researchers that during-welding or post-weld vibration treatment reduces the residual stresses and vibration refines the crystal structure of the metal. This infers that there might be some kind of relationship between the crystal structures of the weld and the residual stresses. This experiment was carried out to investigate the effect of vibration/applied stress on the crystal structure and the hardness of the material.

5.7.2 Experimental Procedure

To carry out this investigation a 76.2 mm × 6.35 mm cross section bright mild steel plate was bead welded. Some specimens were welded without any treatment and some were vibrated, applying different amplitudes while they were being welded. The set-up for this experiment was the same as that shown in Figure 5.100. The applied stress calibration process was similar to that described in section 5.3.3.3. Two batches of welding-vibrated specimens were investigated. The specimens were cut, polished, etched then an optical microscope was used for observation and taking photographs. The specimens were cut using a Struers Discottom-2 cutting machine. In the etching process 2% nital (2 parts nitric acid and 98 parts methanol) was used as the etching agent. The welding of the specimens was carried out using the experimental set-up as in Experiment III. A constant speed of the welding was maintained using the stepper motor driven welding torch carrier (Figure 5.15A). Two different welding conditions were used for two different groups of specimens. For the first group, a relatively low heat input (25 V 195 A) was used and the weld speed was 252 mm/min. For the second group, the heat input was increased to a higher value (25.5 V 204 A) and weld speed was reduced to 212 mm/min to increase the width of the heat affected zone (HAZ) to carry out a detailed investigation in the HAZ1 (Figure 1.6). Investigation was carried out in the welds and in the HAZ (weld toe, and the side opposite the weld). The microstructure of the parent metal is shown in Figure 5.671.

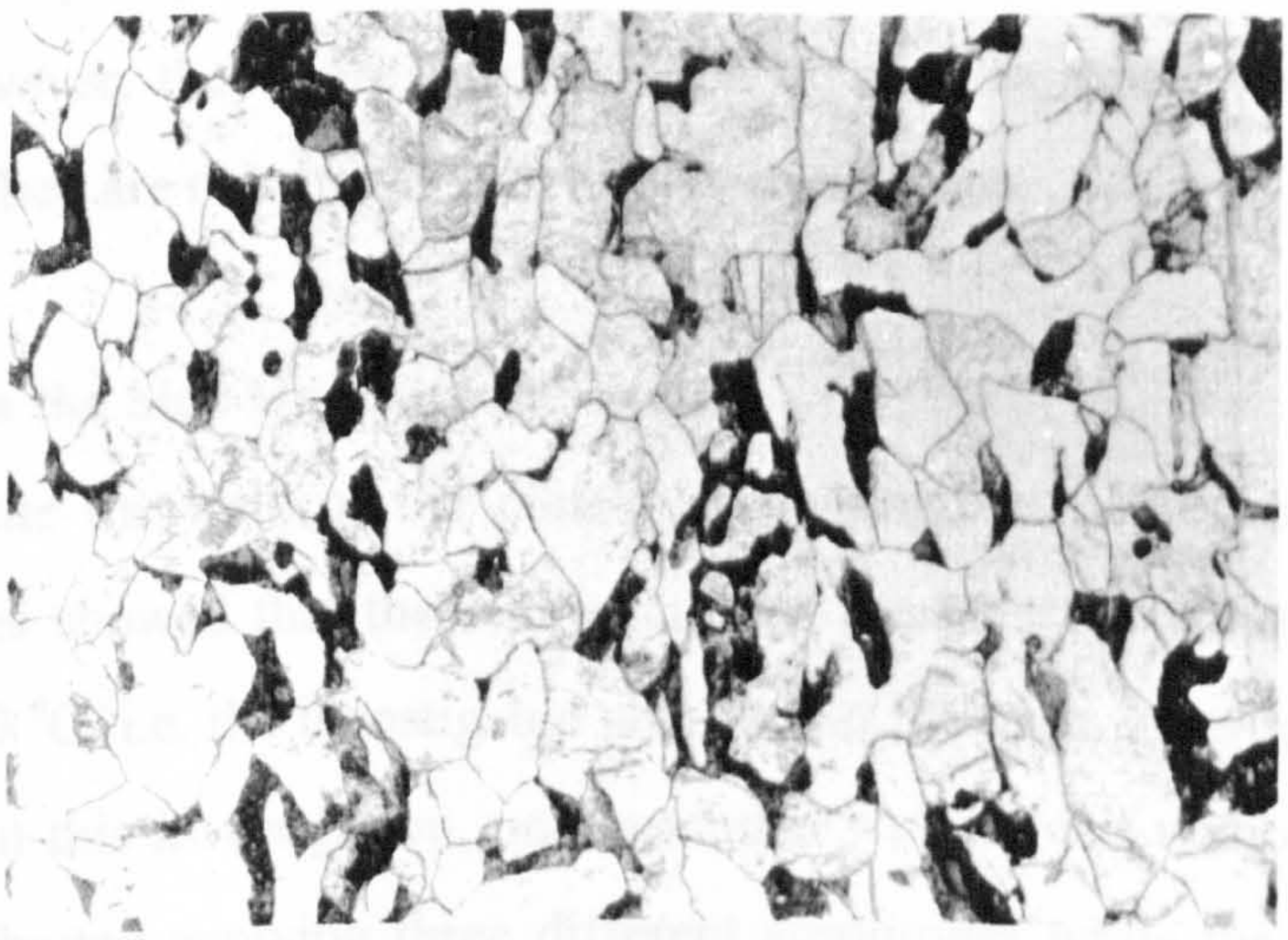

Figure 5.671- Microstructure of the parent metal (× 400)

5.7.3 Experimental Results

Investigation of Weld and Weld toe

Investigation was carried out in the weld and adjacent HAZ. The weld was ground to the parent metal level then the weld and weld toe was polished and etched as shown in Figure 5.672 below.

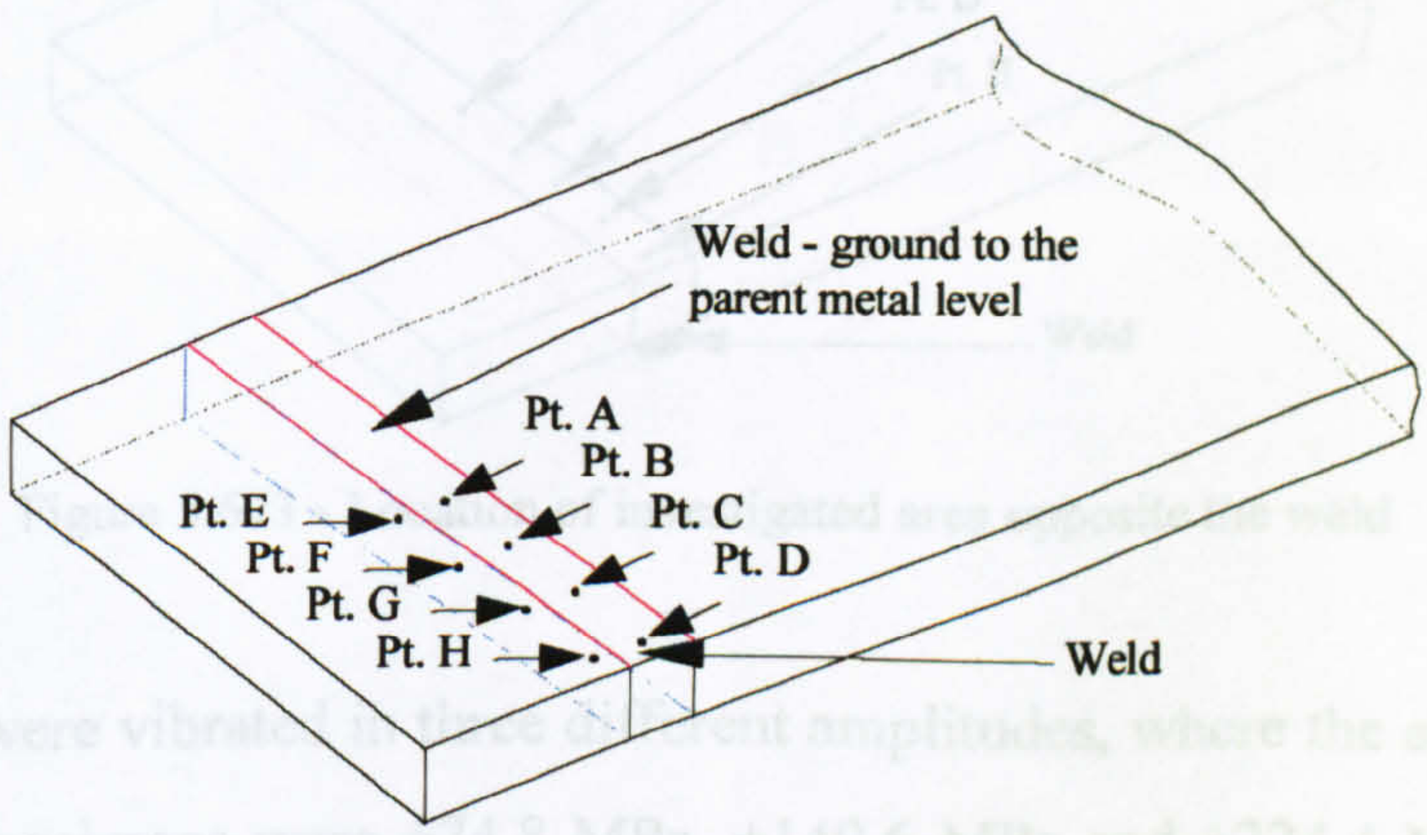

Figure 5.672 - Position of the investigated area on the weld

In the low heat input welds, the HAZ was very small. This made it difficult to observe the characteristics of the microstructure in detail. However, no significant difference of the microstructures between vibrated and unvibrated/control specimens were found.

In the high heat input specimens some differences of microstructures in the HAZ were observed. However, they were not clear due to the very small width of the grain growth zone. They are not shown here to save some space.

Investigation in the Side Opposite the Weld

The side opposite the weld of the plate was investigated. The observation in the crystal structures showed that the temperature of the investigated area was between 1150 ^{0}C to 1300 ^{0}C, i.e. the investigated area was in the grain growth zone (shown in Figure 1.19). In this investigation, one specimen was welded without any vibration and six were vibrated applying three different amplitudes while the specimens were

being welded. For the unvibrated/control specimens five points in the half-width of the weld centre line were investigated and these points are shown in Figure 5.673.

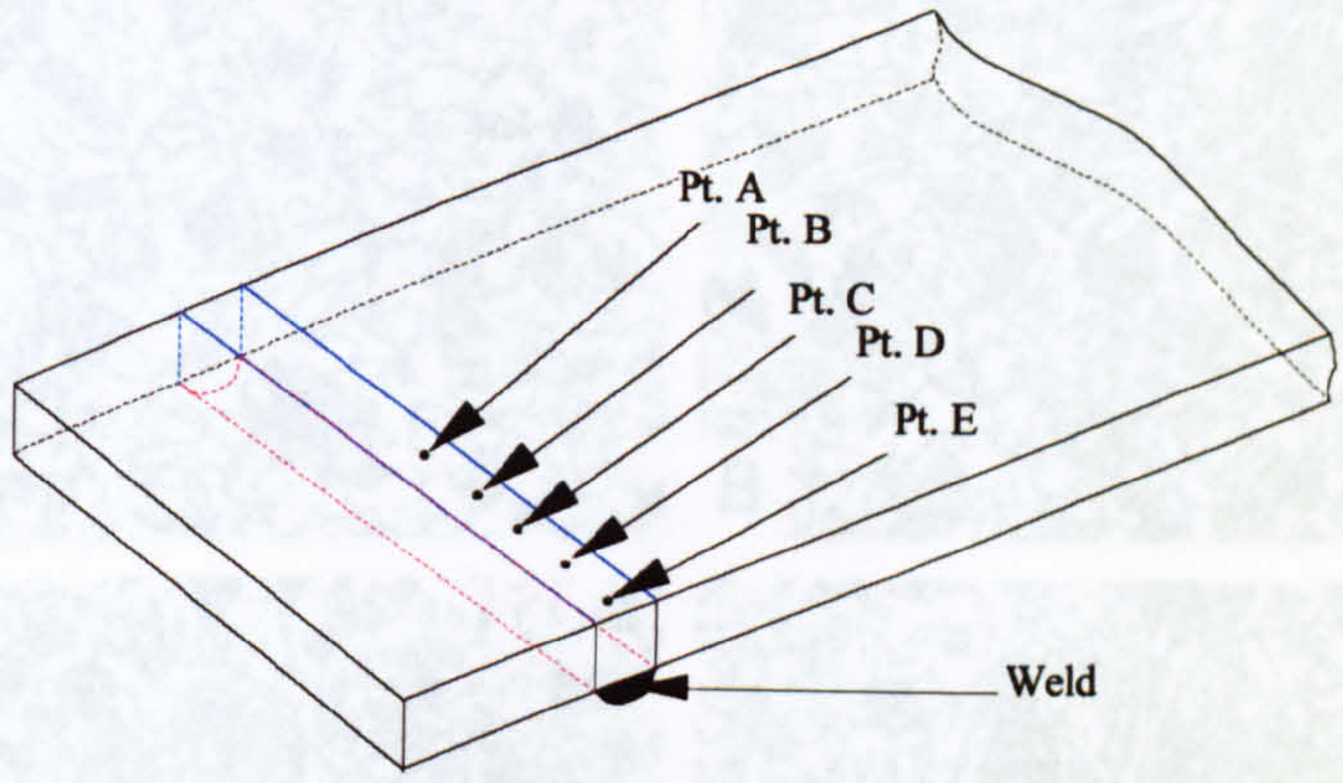

Figure 5.673 - Location of investigated area opposite the weld

The specimens were vibrated in three different amplitudes, where the applied dynamic stresses to the specimens were ±74.8 MPa, ±149.6 MPa and ±224.4 MPa. Vibration of the specimens started with the start of welding and continued for 2 minutes. The welding time was 21.5 seconds. In applied stress amplitude ±74.8 MPa, no differences in the microstructures were observed, at stress amplitude ±149.6 MPa, some differences were observed. However, they were not so clear. At stress amplitude ±224.4 MPa, the differences were very significant. The microstructures of one of the two specimens processed with induced stress ±224.4 MPa is shown here. In this specimen, seven points in the half width in the side opposite the weld line were observed (Figure 5.674).

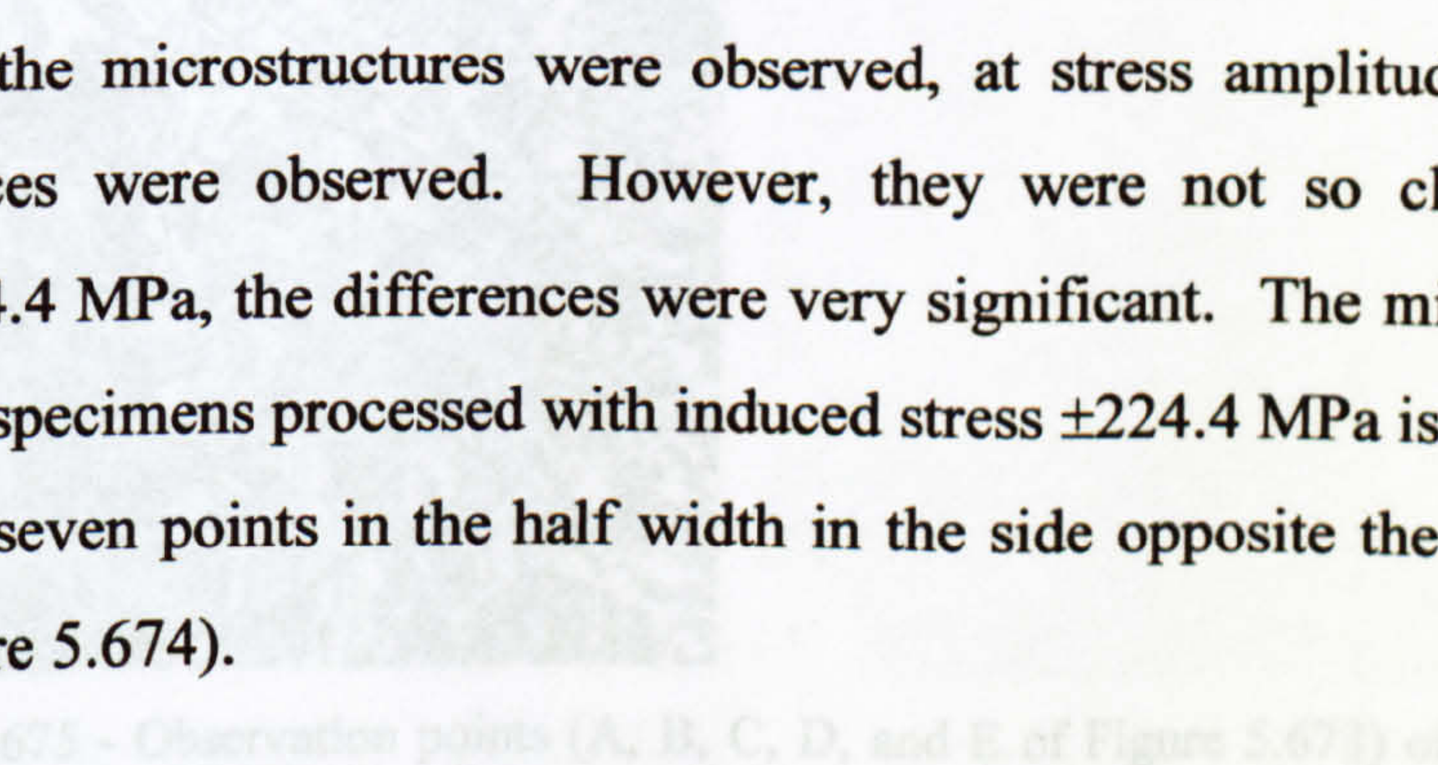

Figure 5.674 - Observation points of the vibrated specimens

Microstructures of the Control Specimens

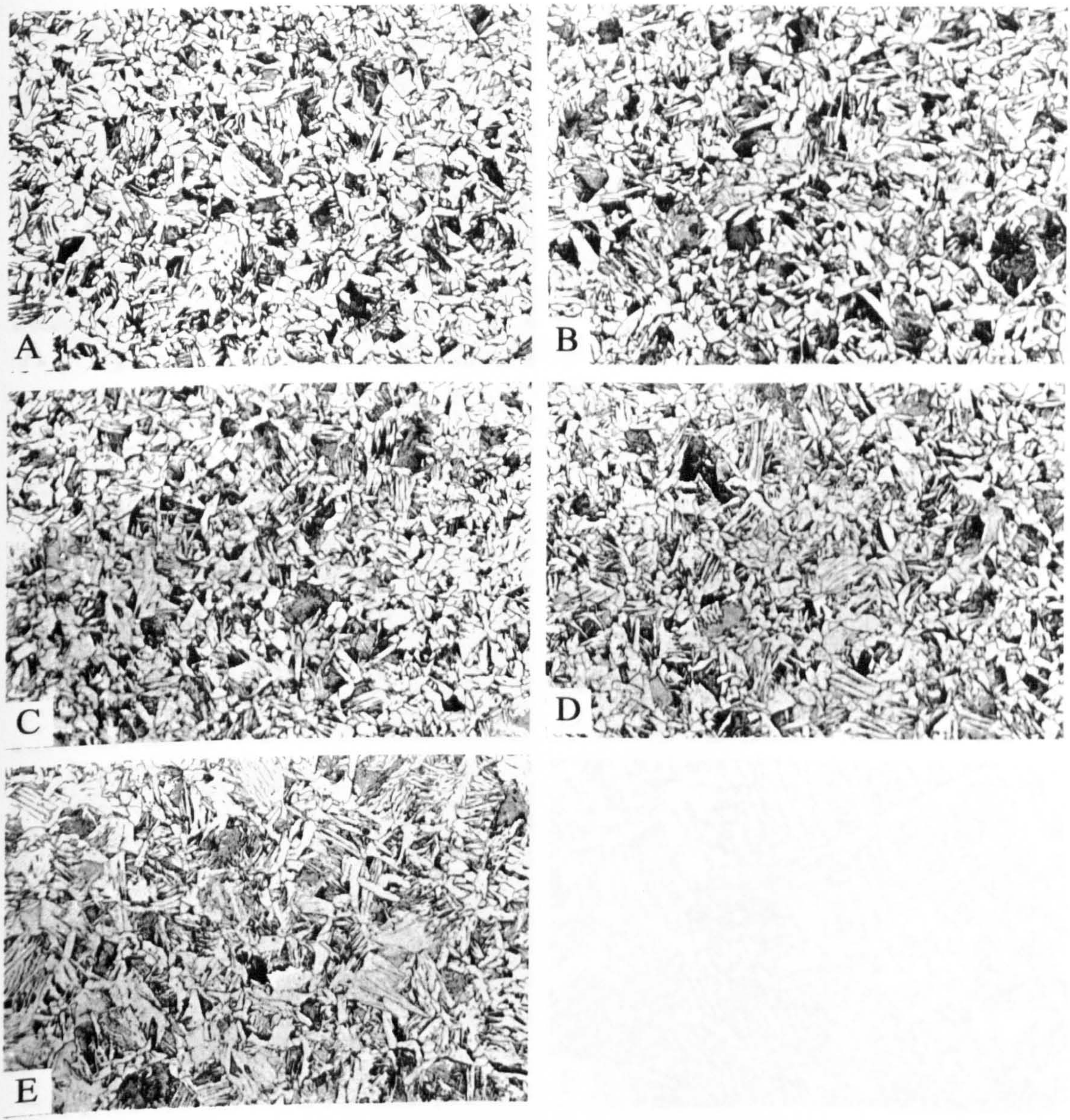

Figure 5.675 - Observation points (A, B, C, D, and E of Figure 5.673) of the control specimen (× 200)

Microstructures of Specimen 1 (Induced Stress ±224.4 MPa)

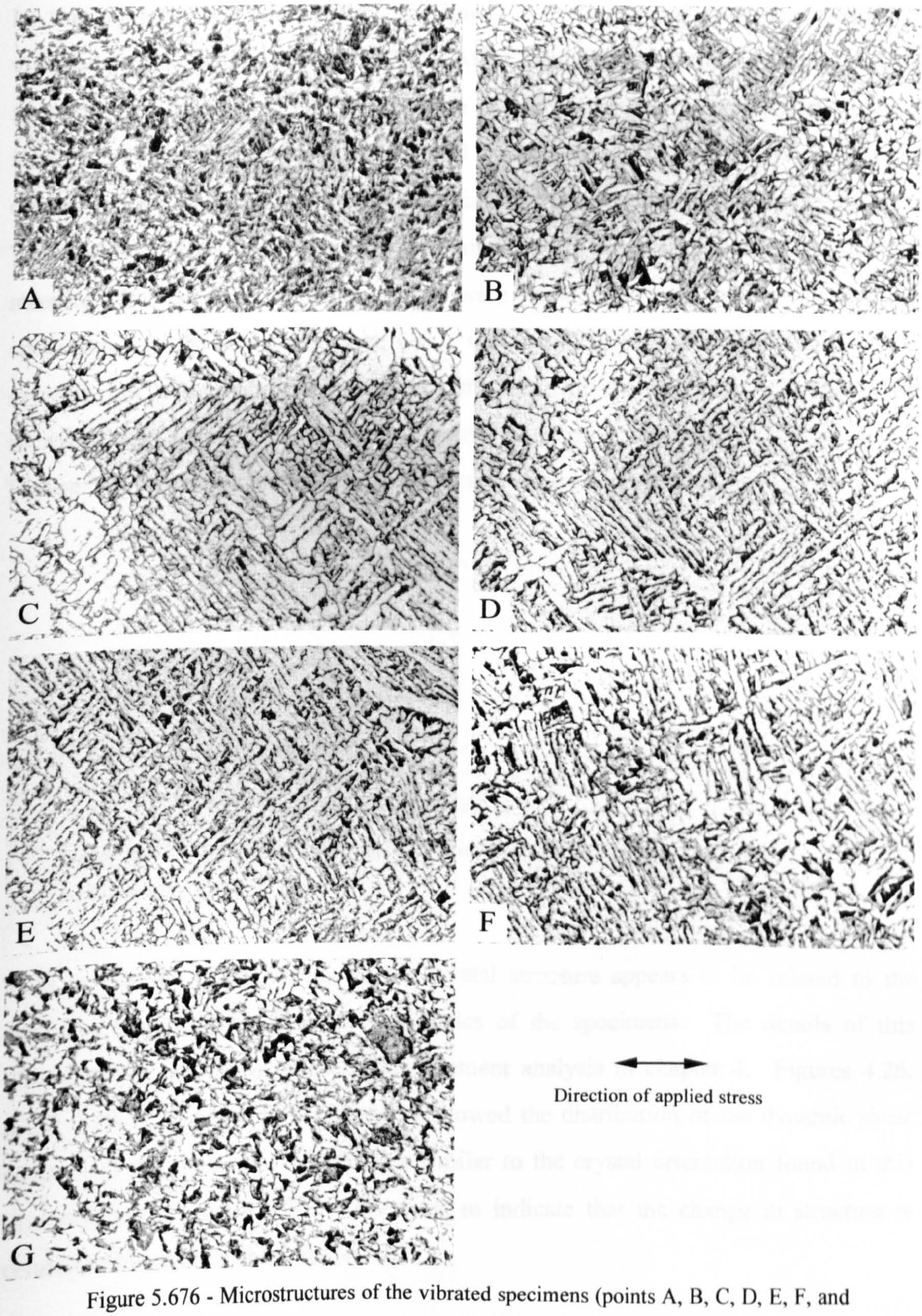

Figure 5.676 - Microstructures of the vibrated specimens (points A, B, C, D, E, F, and G of Figure 5.674) (× 200)

Discussion of the Result – the Side Opposite the Weld

In this investigation, the control specimens were compared with the specimens vibrated with an applied stress of ±224.4 MPa. The microstructure of the unvibrated specimens was found to be chaotic, with no particular arrangement of the crystal structure. The vibrated specimens showed a completely different picture, in that the crystals were found to be arranged according to the direction of the applied stresses. The ferrite crystals were found to form at *ca.* $\pm 45^0$ to the direction of the applied stresses. The orientations of the crystals were found to be position dependent in the specimen. At the mid-width there was a very small or negligible orientation of the crystals but with a movement towards the edge of the specimen the orientation increased and again very near to the edge the orientation was found to be very small. Figure 5.677 explains the trend of the crystal structure arrangements.

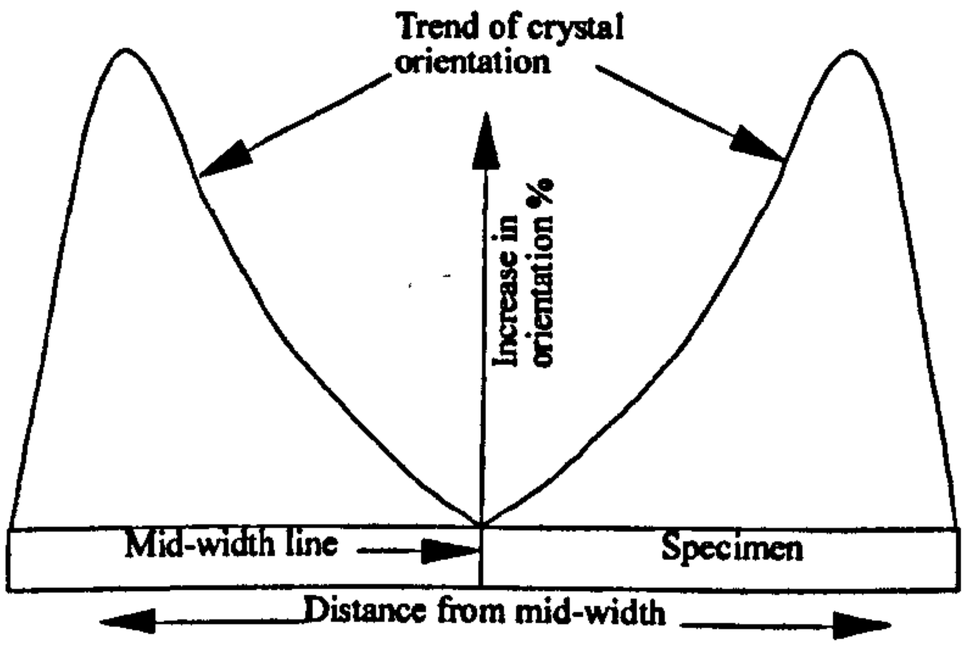

Figure 5.677 – Trend of crystal orientation with a movement from the mid-width (schematic).

This orientation of the change in the crystal structure appears to be related to the dynamic applied shear stress characteristics of the specimens. The details of this characteristic are shown in the Finite Element analysis in chapter 4. Figures 4.26, 4.28, 4.30, 4.32 and 4.34 in Chapter 4 showed the distribution of the dynamic shear stresses in the specimens which were similar to the crystal orientation found in this investigation (Figure 5.677). This tends to indicate that the change in structure is related to the applied shear stress.

Investigation on the Weld

This investigation was carried out to observe the vibration effect on the weld metal. The weld top surface was suitably polished and etched. The control specimen was compared with specimens subjected to an applied stress of ±224.4 MPa. The points of observation are shown in the Figure 5.678. The microstructures of the unvibrated specimen and the specimens vibrated applying ±224.4 MPa are shown in Figures 5.679 and 5.680.

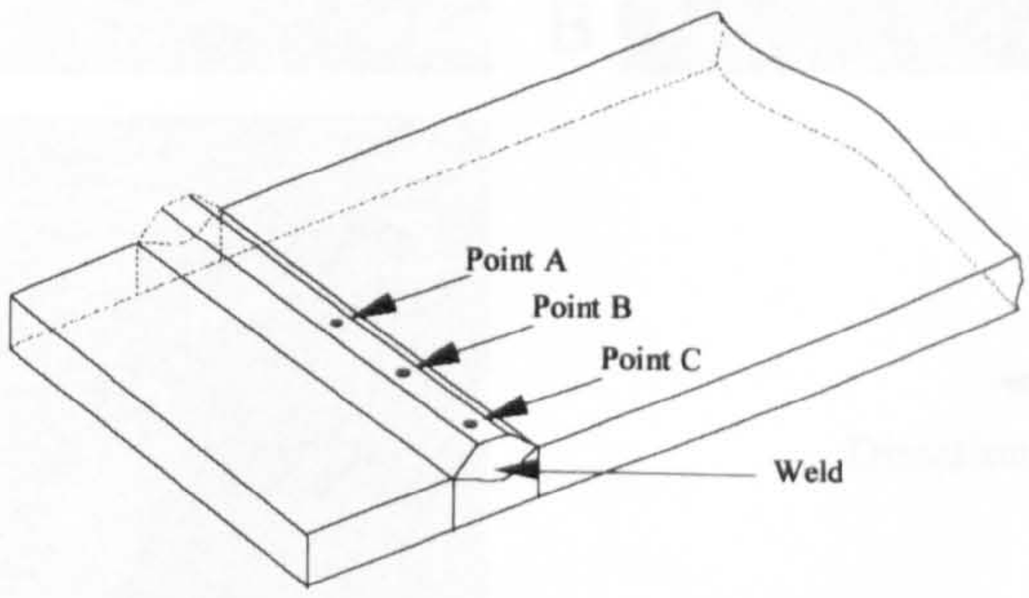

Figure 5.678 - Position of three investigated points on the weld

Microstructures of Control Specimens

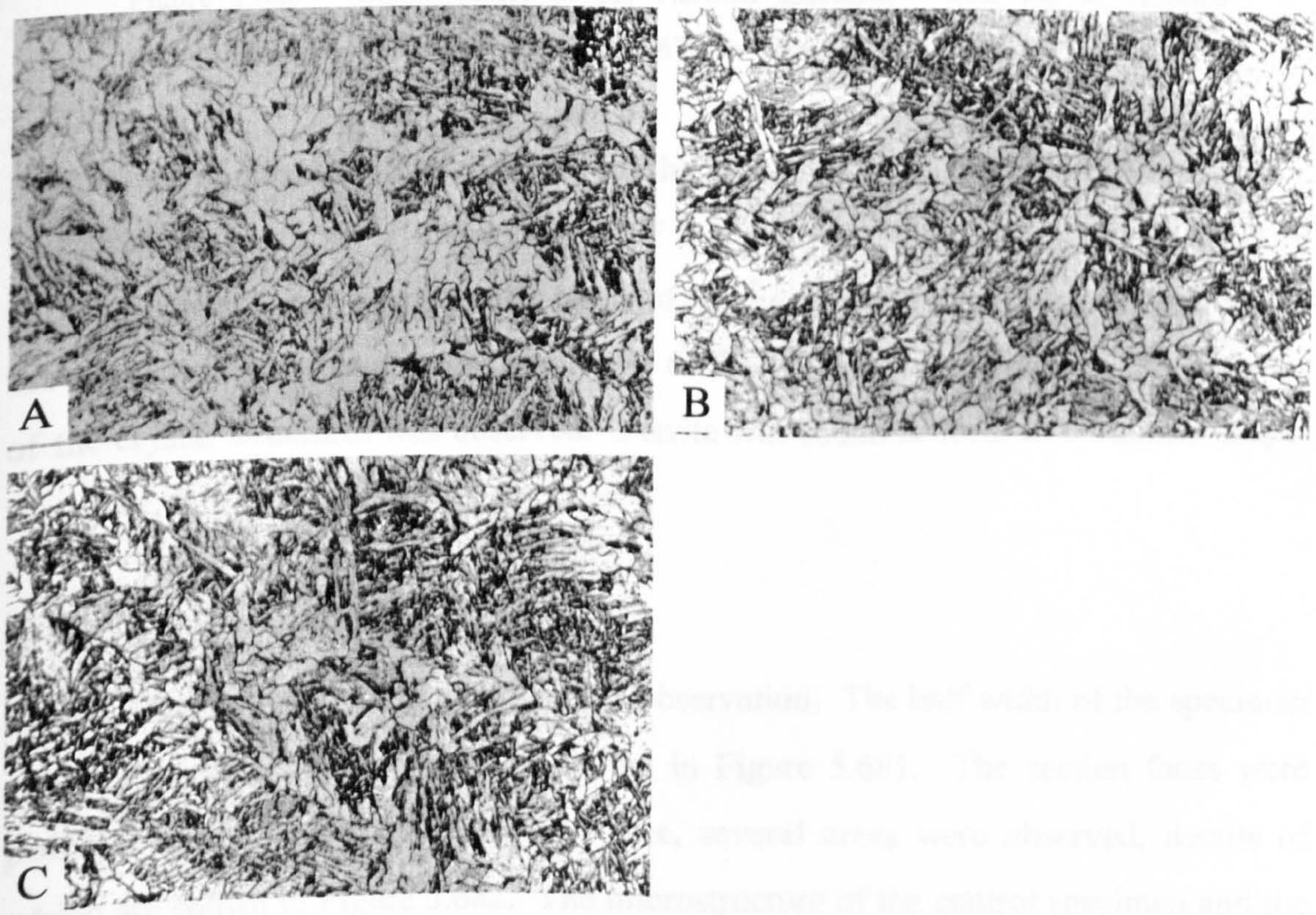

Figure 5.679 - Microstructure of the control specimens - weld top (points A, B and C of Figure 5.678) (× 200)

Microstructures of Specimens with applied Stress ±224.4 MPa

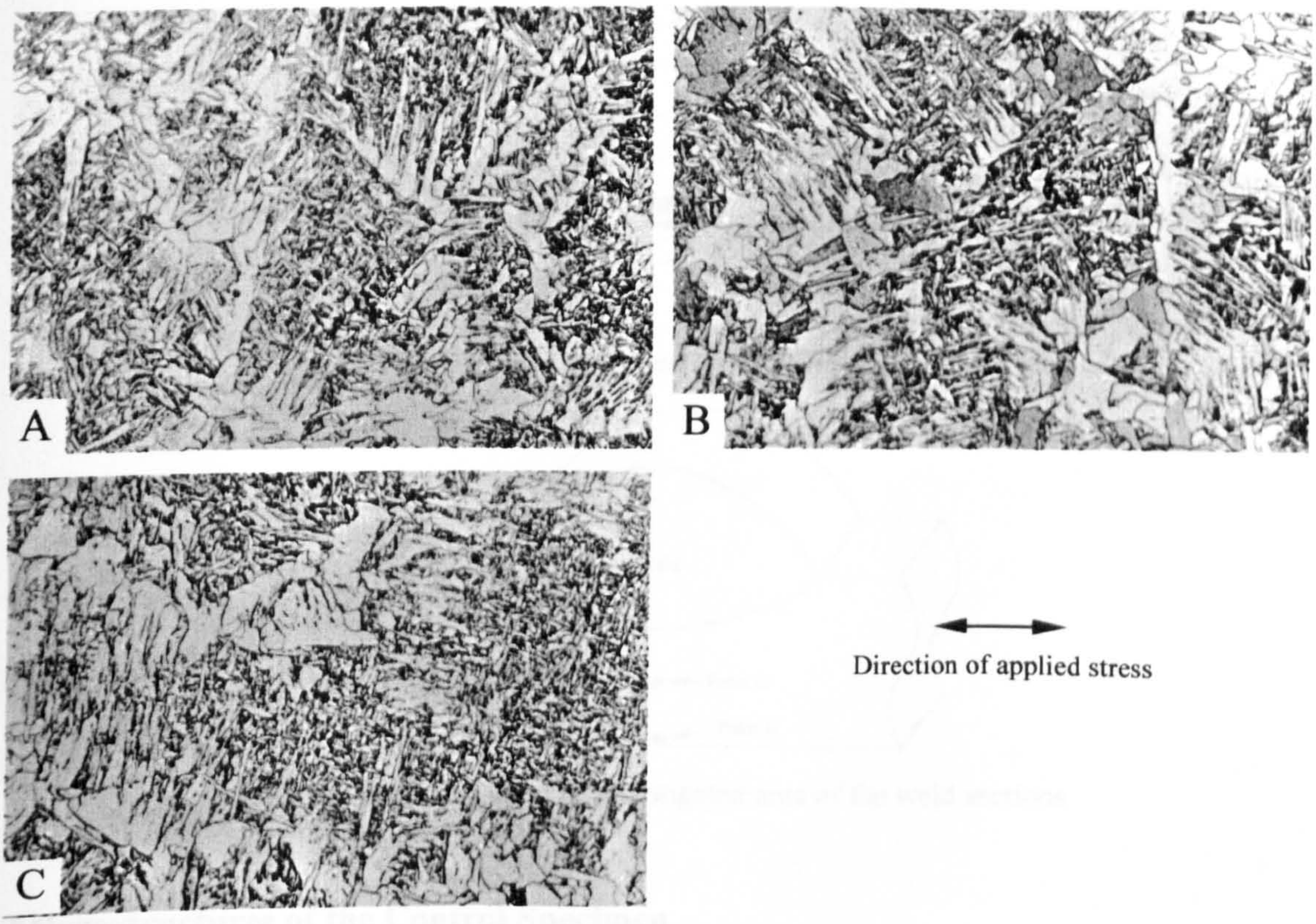

Figure 5.680 - Microstructure of the vibrated specimen - weld top of vibrated specimen (points A, B, and C of Figure 5.678) (× 200)

Discussion of Results - Investigation on the Weld

The crystal structures of the weld top of the control specimens showed a random pattern structure with no particular trend of arrangement of the crystal structures. In the specimens vibrated at stress amplitude of ±224.4 MPa, some pattern arrangement of the crystal structures was observed. Ferrite was found to form in columnar shape. However, this pattern was not very clear.

Investigation in the Sectioned Weld

In this step, the welds were sectioned for observation. The half width of the specimen was sectioned into three pieces as shown in Figure 5.681. The section faces were polished and etched. On the section face, several areas were observed, details of which are shown in Figure 5.682. The microstructure of the control specimen and the three sections vibrated applying ±224.4 MPa are shown in Figure 5.683 and 5.684.

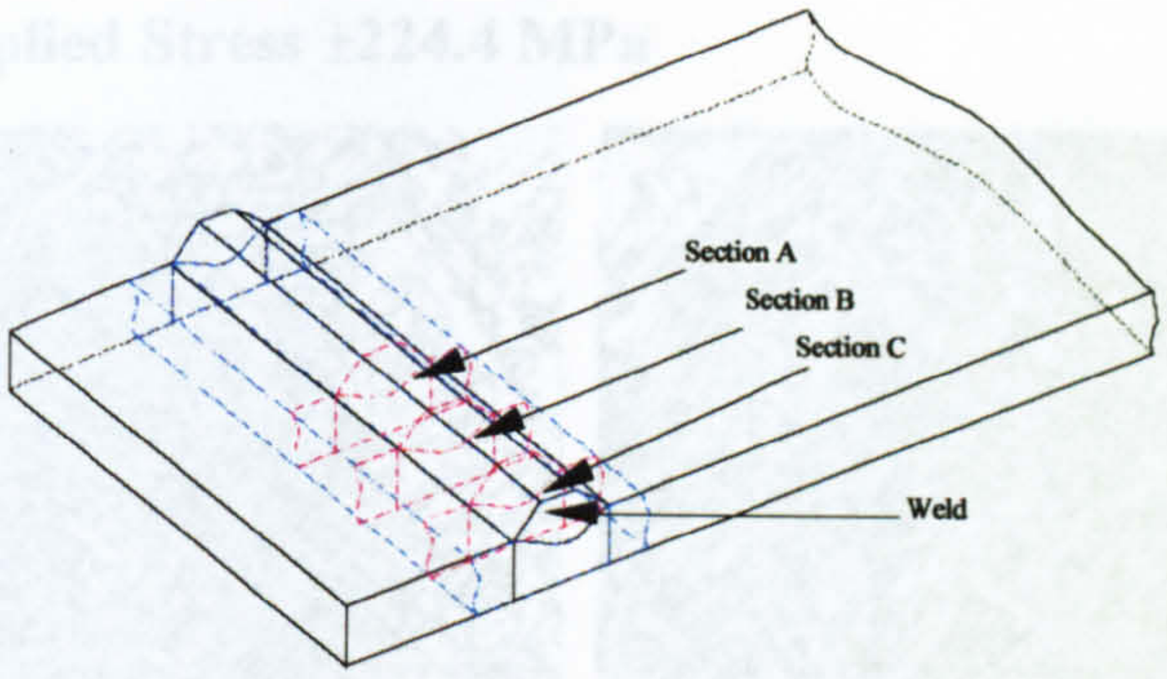

Figure 5.681 - Position of the sectioned area under investigation

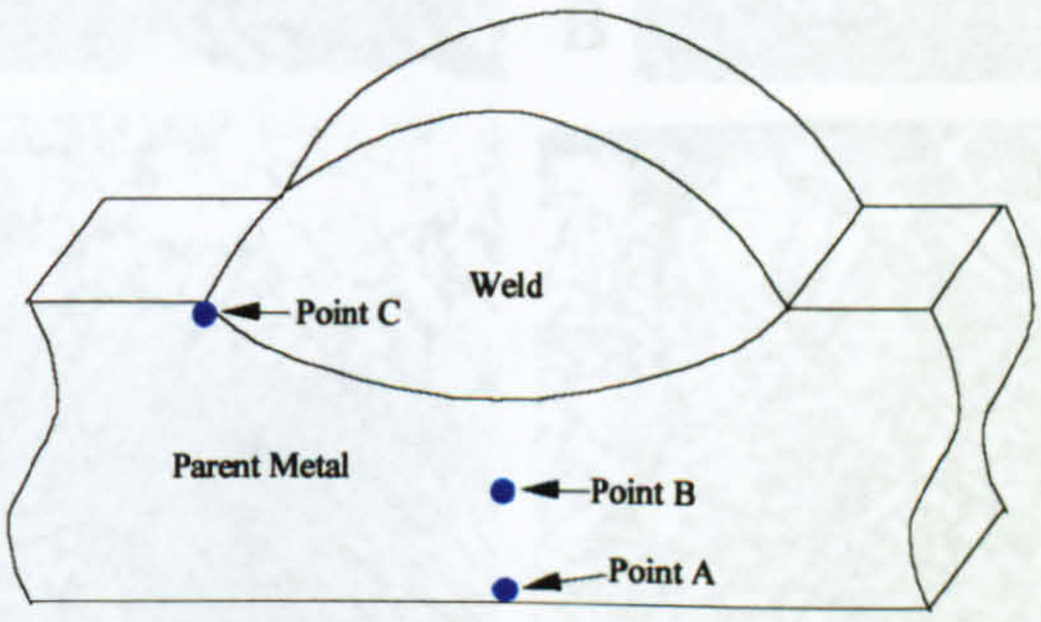

Figure 5.682 - Position of investigated area of the weld sections

Microstructures of the Control Specimen

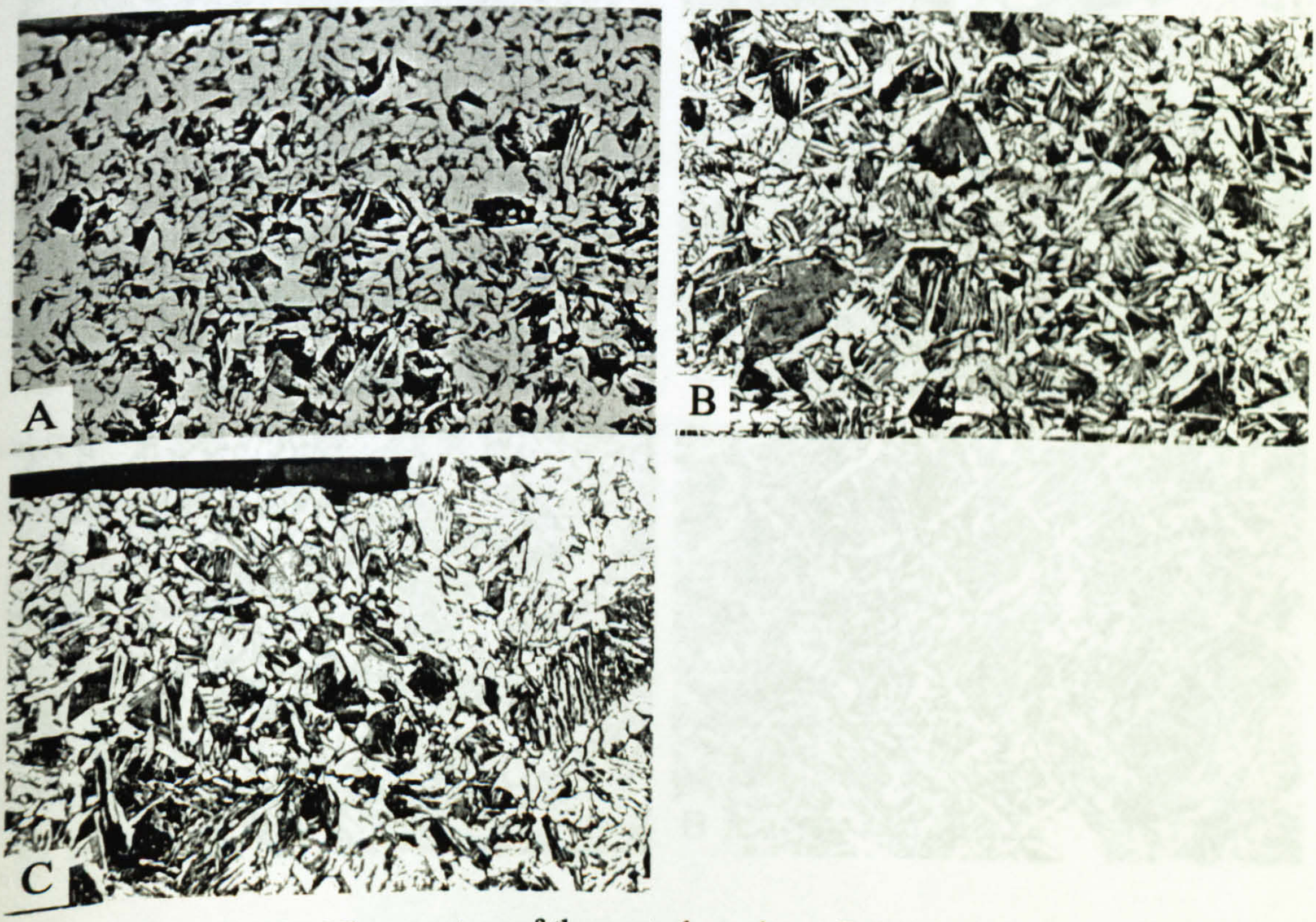

Figure 5.683 - Microstructure of the control specimen (Points A, B and C of Figure 5.682) (× 200).

Specimens with Applied Stress ±224.4 MPa

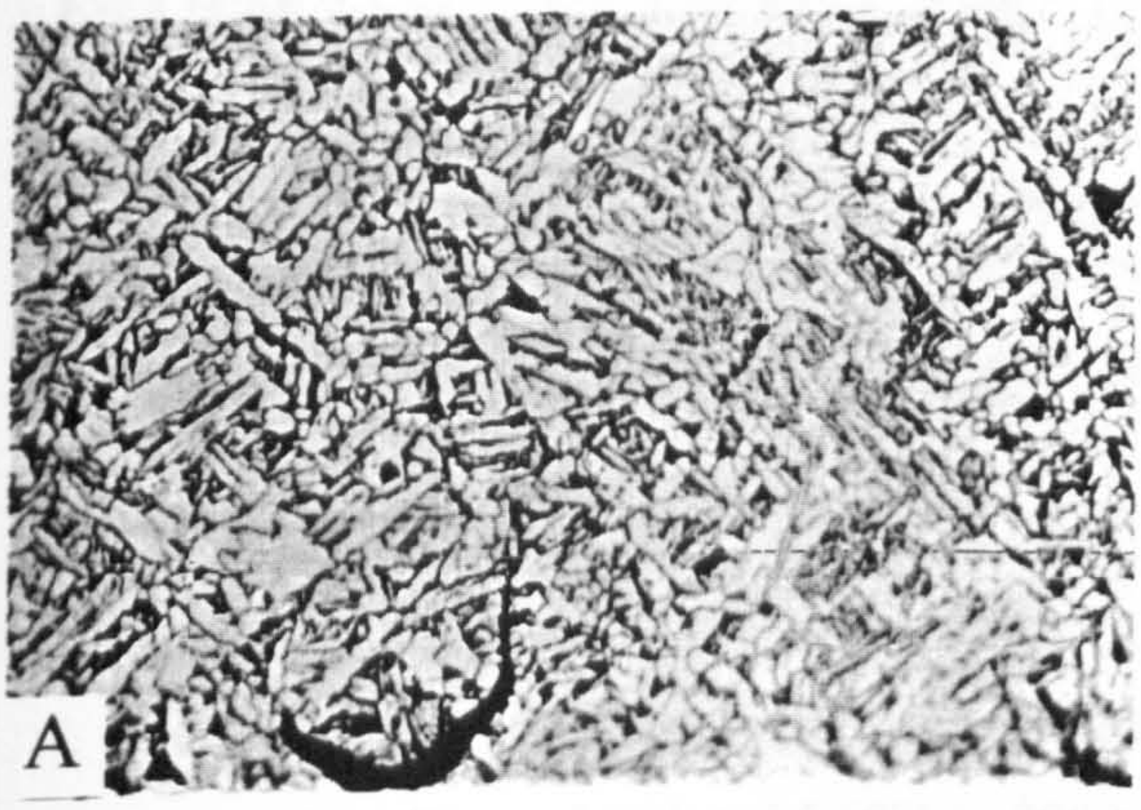

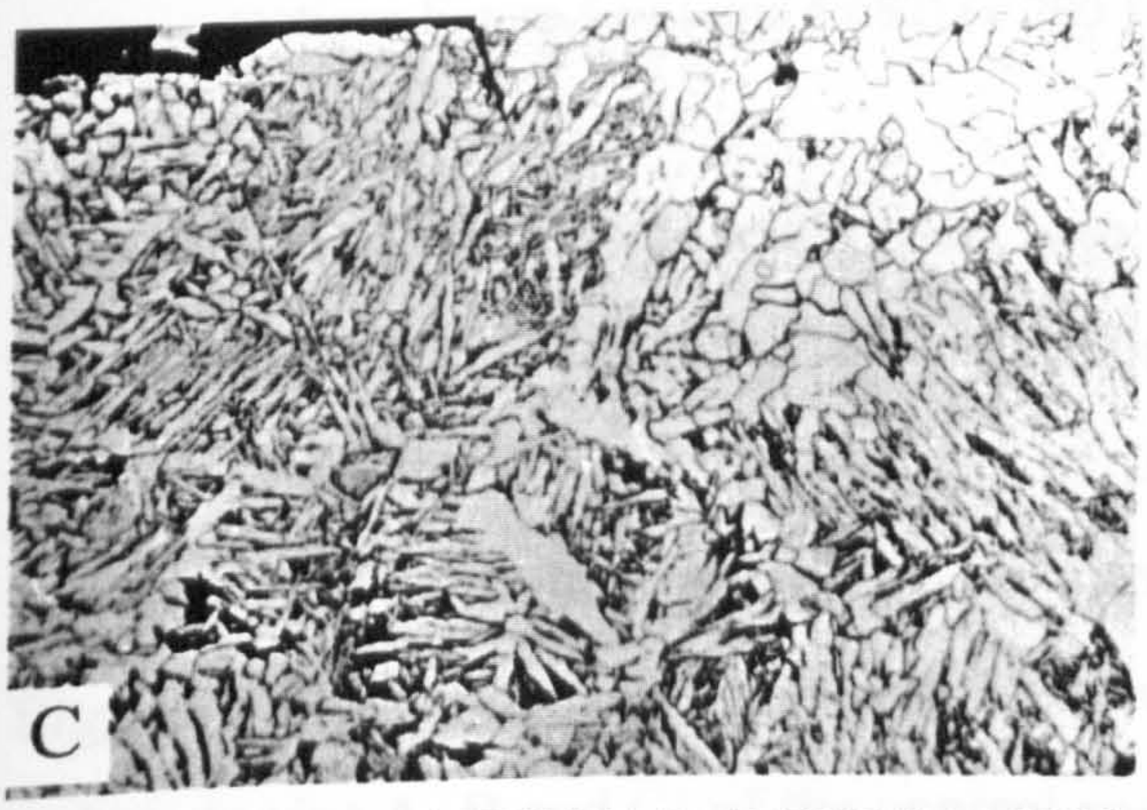

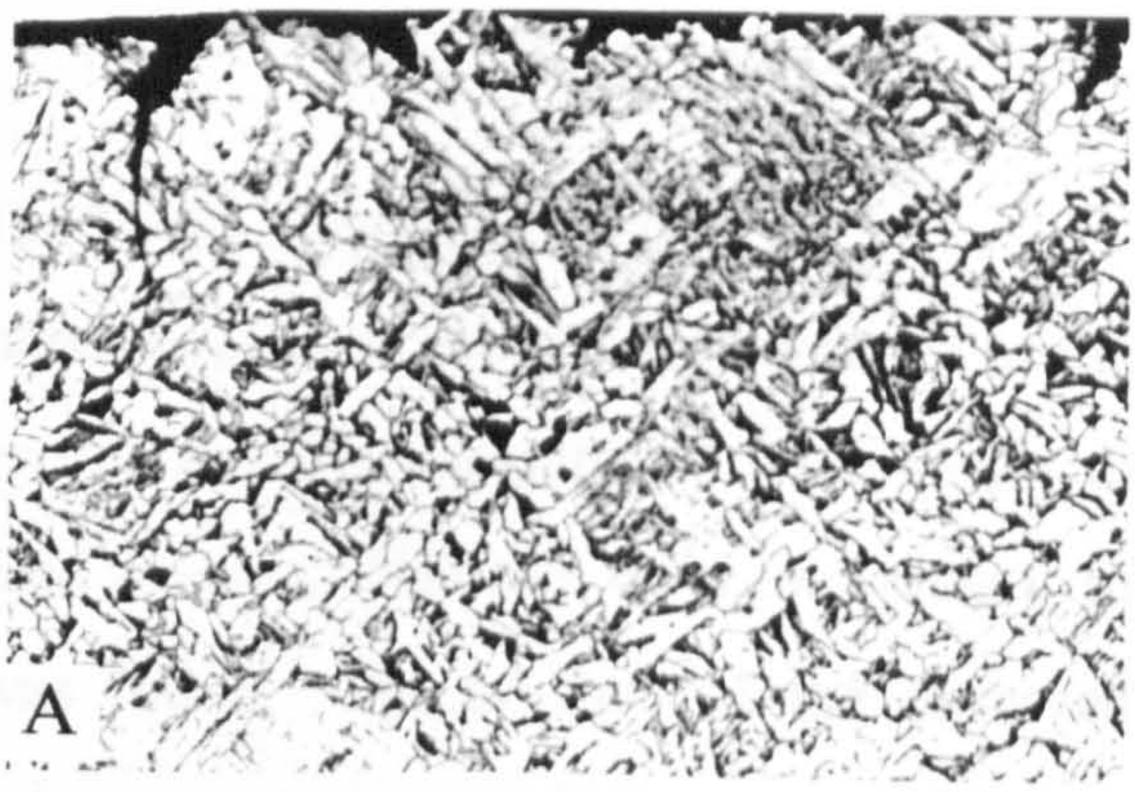

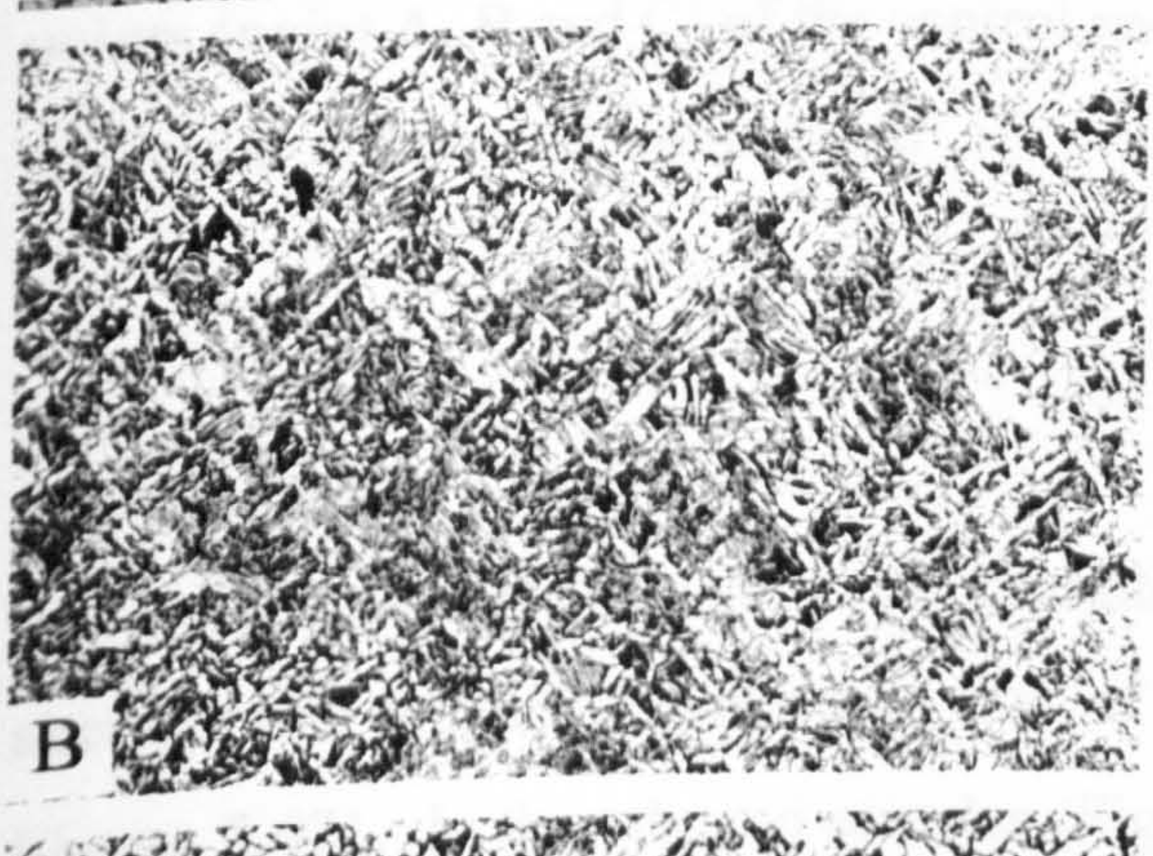

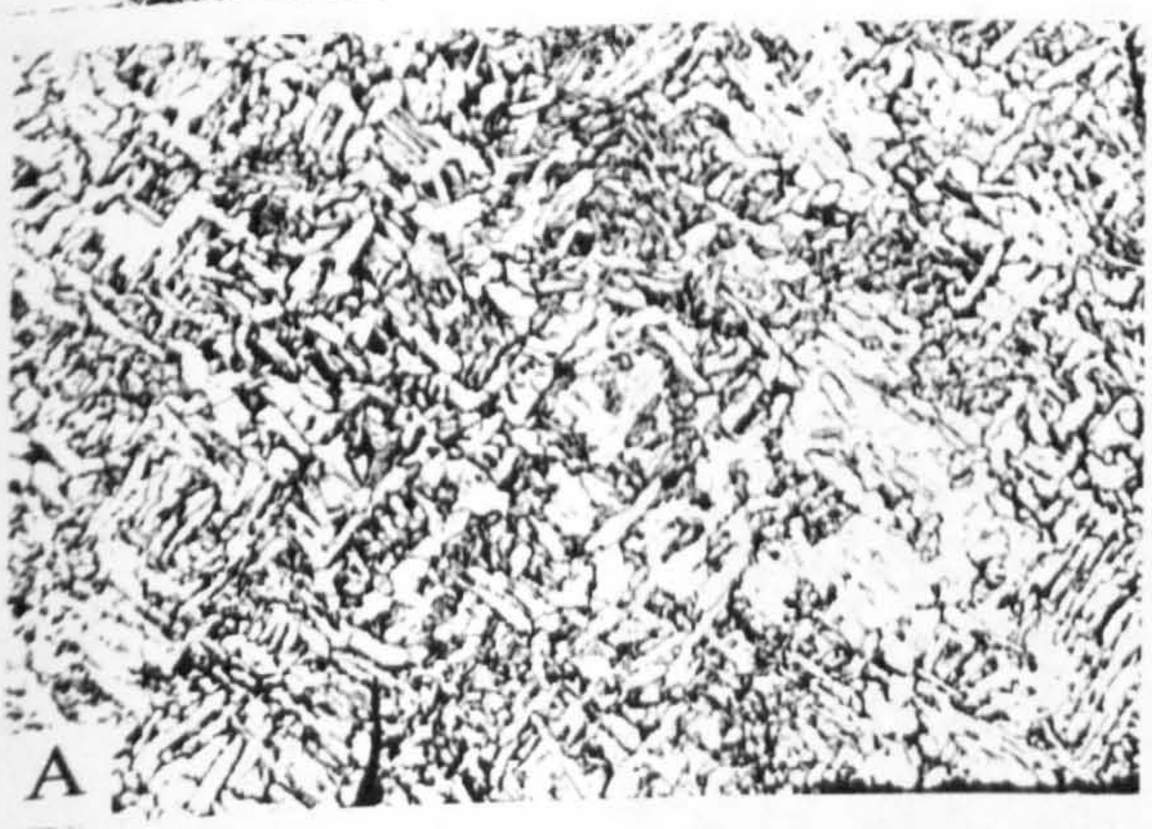

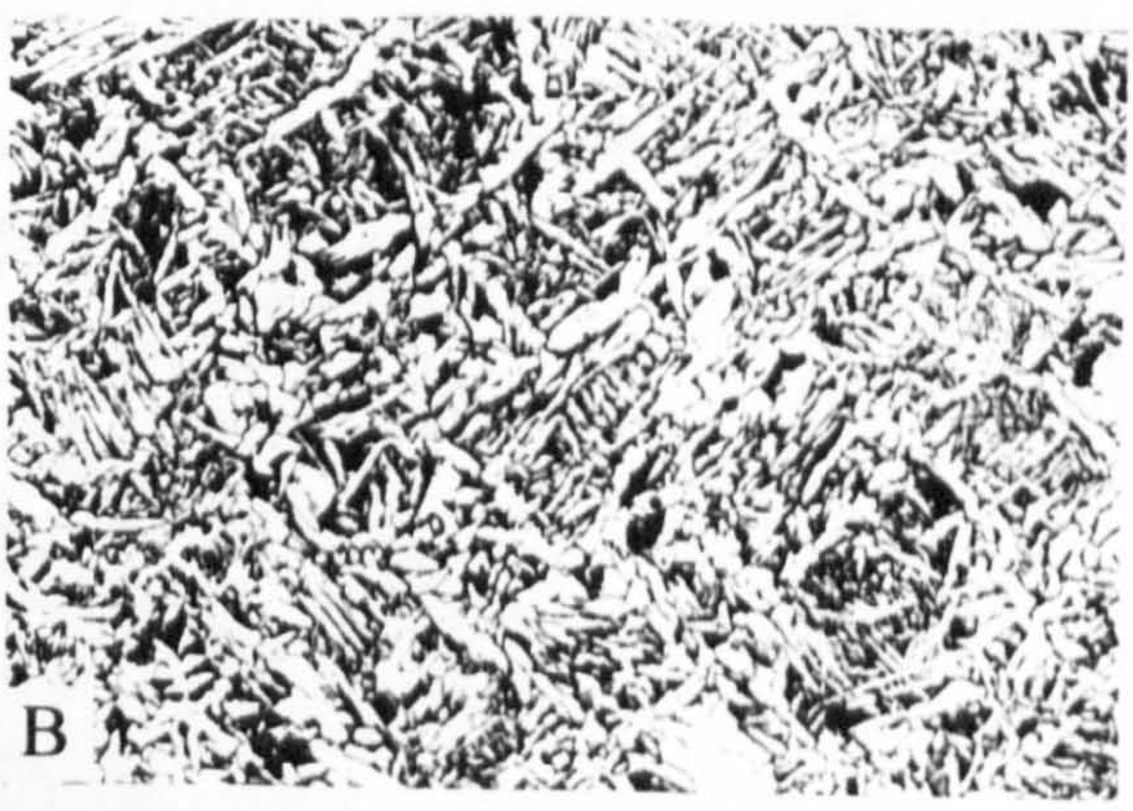

Direction of applied stress

Figure 5.684 - Microstructure of vibrated specimens (points A, B, and C of the three sections Figure 5.681 and 5.682) (× 200)

Discussion of Result - Investigation into the Weld Section

On point A and B of Figure 5.682, the vibrated specimens showed cross pattern of the crystal structures (Figure 5.684). The ferrite crystal cross patterns were found to form *ca.* $\pm 45^0$ with the direction of the applied stresses. Near the weld toe (plots C in Figure 5.682), no particular orientation was found. The crystals of the observed points (point A, B and C) of the control specimens were in a random pattern, where no particular orientation was present.

Comparison of Crystal Size

For comparison of the size of the crystals, point A (of Figure 5.682) of a vibrated section was magnified similar to that of the magnification of the parent metal of Figure 5.671. In the vibrated samples (Figure 5.685) the grain sizes were found to be refined and changed into columnar shape due to the vibratory stresses.

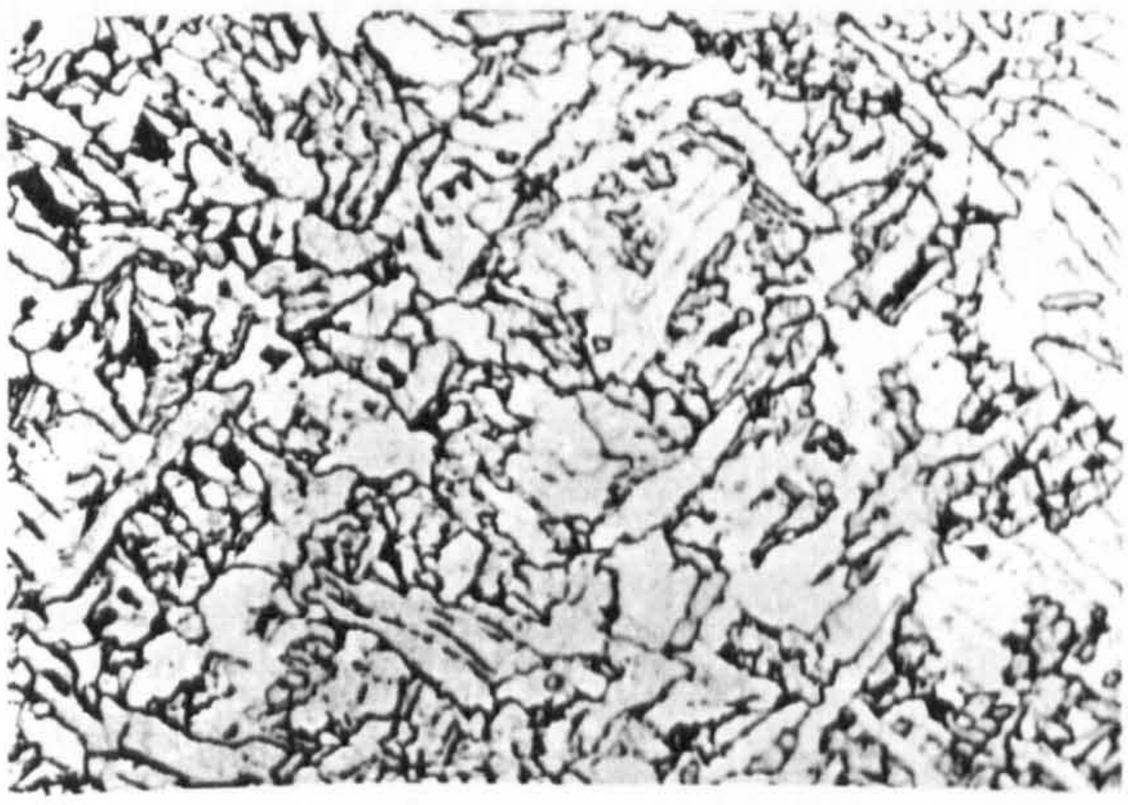

Figure 5.685 - Microstructure of point A of Figure 5.681 (× 400).

Observation of Crack Tip

Due to the high amplitude of vibration during solidification of the weld metal, cracks were formed in the weld. The crystal orientation in the surrounding of the crack was investigated. The Figure 5.686 below shows the crack tip and surrounding area where the effect of the stress is visible around the crack.

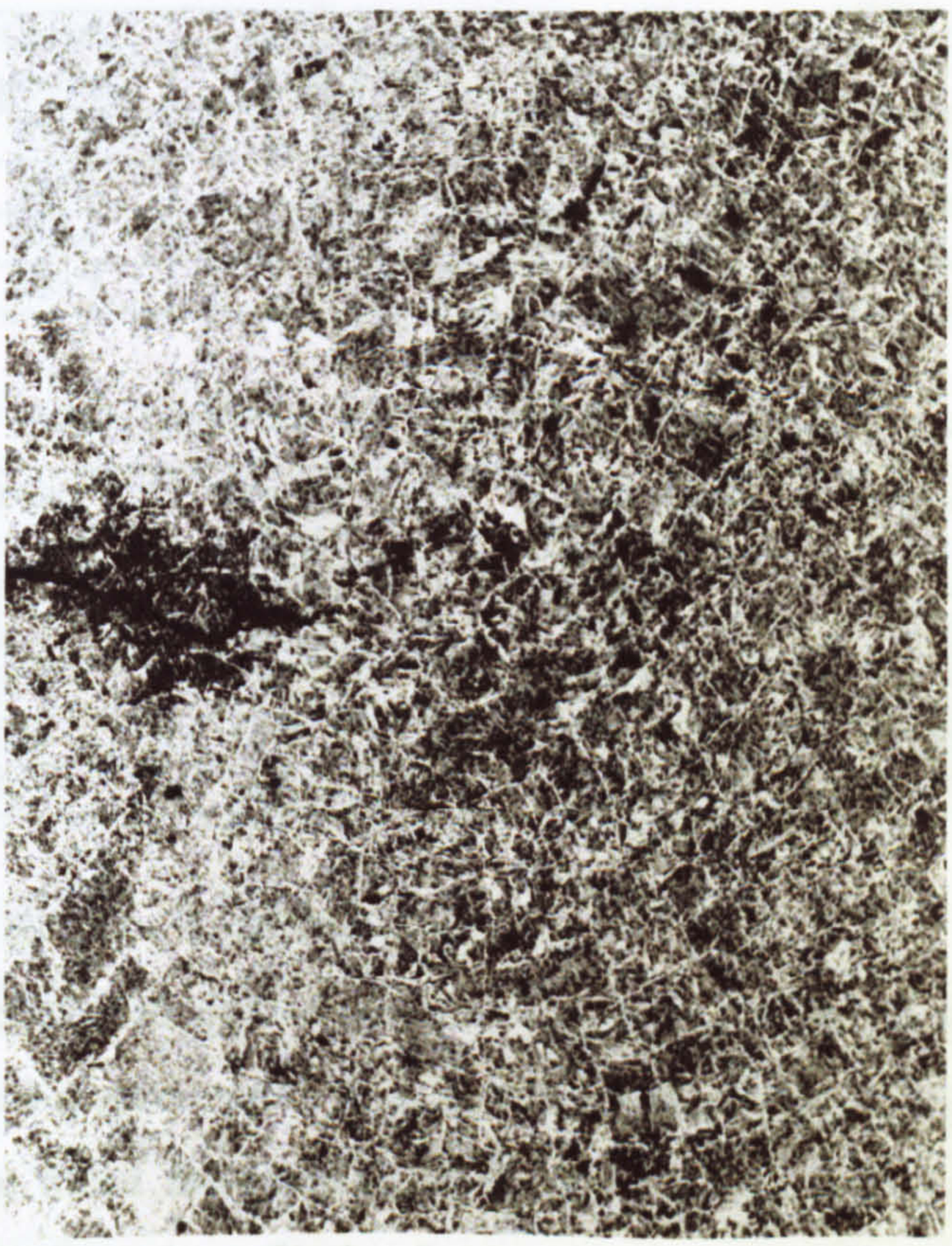

Figure 5.686 - Microstructure of crack tip and surrounding area (× 100)

The above photograph shows that the ferrite was formed as a line. The ferrite line started from the crack tip and continued to a significant distance. This characteristic clearly indicates that the crystals formed in the cyclic stressed situation become highly oriented.

Investigation of Hardness of the Specimens

The hardness of the control specimens and specimens subjected to vibration were measured. A Vickers Hardness Testing machine was used to measure the hardness of

the polished specimens. A 30-Kg load was used in the testing. Two groups of specimens were tested. In the first group, a total four points were measured (point A, B, C, and D of Figure 5.673). In the second group, all five points (A, B, C, D and E) of Figure 5.673 were measured. The hardness of the two groups are shown in the two tables (Tables 5.62 and 5.63) below.

Table 5.62 - Vickers hardness of vibrated and control specimens (group 1)

Measurement point	Control specimen	Applied stress ±149.6 MPa	Applied stress ±224.4 MPa	Maximum increase in hardness
Point A	177.4	158.7	180.6	1.8 %
Point B	161.5	162.6	188.7	16.8 %
Point C	165.4	159.3	190.8	15.3 %
Point D	158.7	159.8	189.4	19.3 %

Table 5.63 - Vickers hardness of the vibrated and control specimens (group 2)

Measurement point	Control specimen	Applied stress ±224.4 MPa	Maximum increase in hardness
Point A	159.8	185.9	16.33 %
Point B	160.4	188	17.2 %
Point C	158.7	193.6	21.99 %
Point D	161.5	194.4	20.3 %
Point E	165.9	208.1	25.4 %

Discussion of the Result - Hardness Test

The specimens subjected to applied stress ±149.6 MPa showed similar hardness to the hardness of the control specimens. With increase in the induced stress to ±224.4 MPa, the hardness of the metal increased up to 19.3%. In the second group the induced stress was ±224.4 MPa, where the hardness were found to increase up to 25.4% in comparison to the control specimens.

Thus, in both groups the hardness of the specimens increased significantly due to application of high amplitude vibration. This result complies with the findings of Campbell [28].

5.7.4 Summary of Results

The result of these tests showed that the crystal structure of the vibrated specimen was regularly arranged due to application of vibration. In the control specimens no regular orientation of the crystals (Figure 5.675, 5.679, and 5.683) was found.

On the weld (Figure 5.678), no significant difference between vibrated and unvibrated specimens could be observed. It happened due to the geometry of the weld. The applied stress on the investigated points was very low which was not sufficient to cause any change in the crystal structure of the metal.

At the weld toe, no significant difference between the crystals of vibrated and control specimens was observed. The length of the HAZ on the weld toe was small. Due to the small width of the section, the change in the crystal structures was not clear.

On the side opposite the weld line, the crystals were found to be highly oriented in the specimens subjected to higher applied stresses. The orientations of the crystals were found to be sensitive to the position on the welded bar. The trend of the formation of oriented crystals appears to be related to the applied dynamic shear stresses in the specimens and is explained earlier in section 5.7.3.

The orientation of the crystals of the specimens were observed from two perpendicular planes of the weld (Figure 5.686A). If the direction in the specimen are represents by a "Millar Index" type specimen axes, the ferrite crystals pattern when viewed parallel to the Y and Z axis appears at *ca.* $\pm 45^0$ (Figure 5.676 and 5.684) corresponding to a [011] and [110] type.

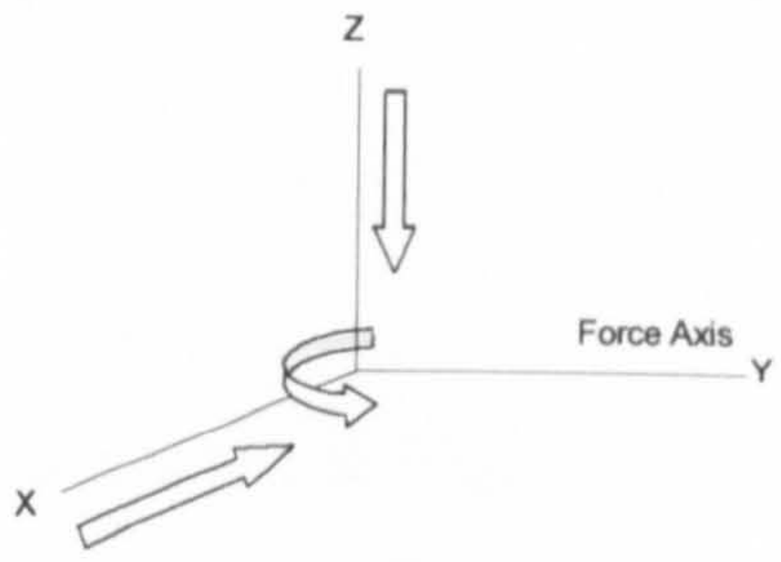

Figure 5.686A – Viewing direction of the crystal orientations

This implies that the orientation was not 45^0 to either of the two tested planes instead the orientation was close to [111] direction with the applied stress, if the direction of the applied stress is parallel to the X axis.

Grain refinement was observed in the vibrated specimens. The grain size of the parent metal and vibrated metal are shown in Figure 5.671 and 5.685. From the figures it is clear that the grains were refined and became columnar shape due to application of vibration.

In the hardness test the hardness of the vibrated specimens were found to increase significantly. The specimens subjected to applied stress of ±149.6 MPa showed no increase in the hardness in comparison to the control specimens. The specimens subjected to applied stress ±224.4 MPa showed a large increase, where a maximum of 25.4 % increase was observed.

In the investigation of crack tip, it was observed that the ferrite crystals were formed in a very regular shape. The ferrite crystals were formed as a line starting from the crack tip and continued to a significant distance. The ferrite formation appears to be following the stress distribution around the crack tip.

5.8 Experiment XIV: Modal Analysis

Abstract

In this investigation the Modal Analysis of the '8' frame was carried out to determine the dynamic properties of the structure. This study found that the position of the bungee supports becomes insignificant if the proper bungee are chosen. These provide very clear FRF curves and hence clear mode shapes. The size and position of the accelerometer used in the Modal Analysis was found to be very important, where the modal properties were found to change due to the size and position of the accelerometer. In the FE analysis, the natural frequencies of the out of plane modes of the structure provided by the shell model agreed with the practical ICATS result. For the in-plane modes, the natural frequencies of the beam model were more in agreement with the practical ICATS result.

5.8.1 Introduction

Modal Analysis of the experimental structure is a necessary preliminary before carrying out VSR treatment. This analysis provides the necessary dynamic properties of the structure. The Modal Analysis data can be used for VSR treatment of the structure. A brief theoretical Modal Analysis was presented in Section 3.1. In this study, several types of specimens were processed, which are described in Section 5.2. In all those specimens, the '8' frame was the most complex structure, where a detailed Modal Analysis was needed to determine the dynamic properties. The other specimens used in this investigation were simple beam (cantilever or four point supported) and shaft. Instead of practical modal analysis of those structures, the FE modal and harmonic analysis of the structures were carried out and are presented in Chapter 4. The necessary set-up for the modal analysis was prepared. It was decided to repeat some experiments, which were reported in the open literature. Also some new features were investigated. They are presented in Section 5.8.3.

5.8.2 Experimental Procedure

The modal analysis test set-up is shown in Figure 5.687 below. The software package used for Modal Analysis is ICATS 4.1C (designed by Imperial College London), for acquisition the software package used the BERAN 402 Frequency Response Analyser,

which acquires the data and generates the sine-wave input for the control of the Vibrator (LDS PA 500)(LDS-Ling Dynamic Systems). The control of the vibrator uses the power supply (LDS FPS 1) which also supplies the vibrator (LDS V530). For the data acquisition there are three PCB (series 353) accelerometers and a PCB force transducer, whose signals, after being amplified in the signal conditioner (PCB 4 Channel) gives the data back to the BERAN, which in turn sends the response back to the ICATS Modal testing package.

Test Set-up Modal Analysis

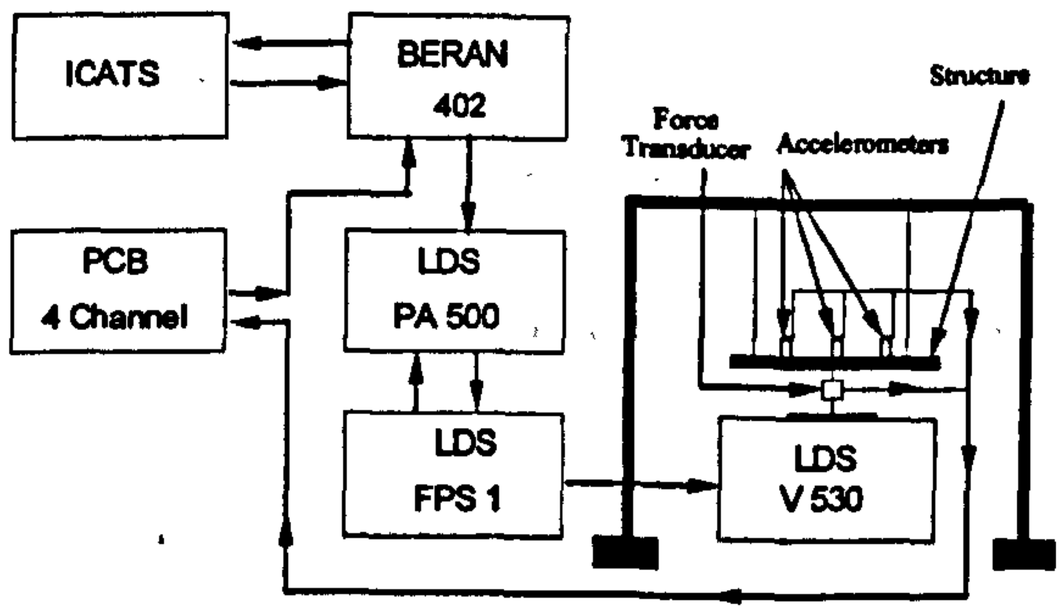

Figure 5.687 - Test set-up of Modal Analysis.

5.8.3 Experimental Results

Several features of the structure were studied, the detailed description of which are presented below.

5.8.3.1 Studies of Bungee Position Effect on Natural Frequency

For a free/free vibration the influence of bungees support should be negligible for a proper condition. It was observed by Moersheim [95a] that in higher modes, the bungees influence the resonance frequency. For mode 5 he showed how this altered the natural frequency, from 7 to 8 Hz. In this experiment the influence of bungee support was again investigated and a different result was found. This study shows that the influence of bungee support becomes insignificant if proper elastic supports are used. In this experiment five tests were carried out by supporting the structure in different arrangements of the elastic band supports, and all other things remained constant.

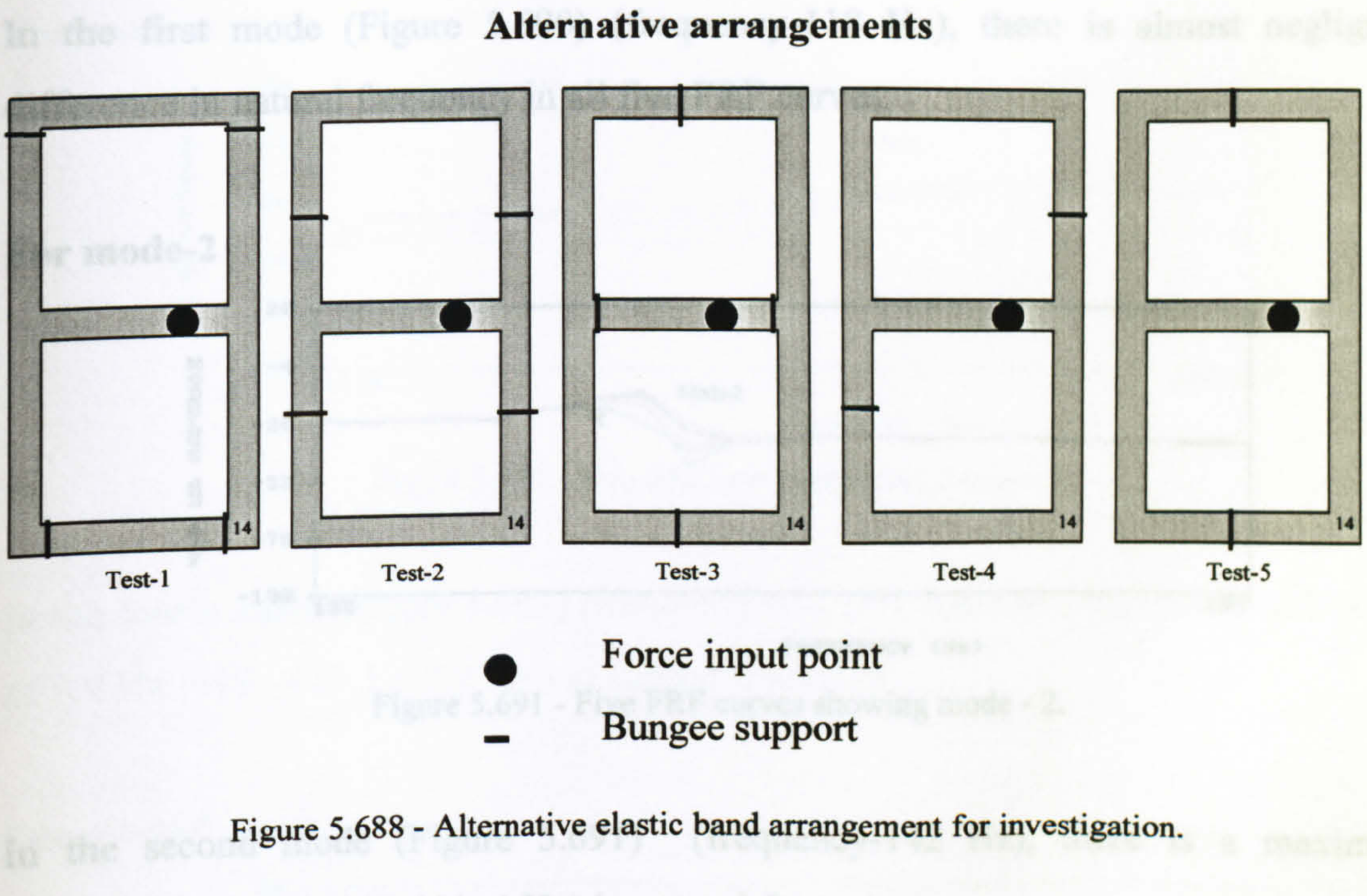

Figure 5.688 - Alternative elastic band arrangement for investigation.

The FRF curves plotted below contains five sets of curves of the same measurement point (point-14). They were taken from five tests as shown in Figure 5.688. The detailed analysis and comparisons of five individual curves are shown below.

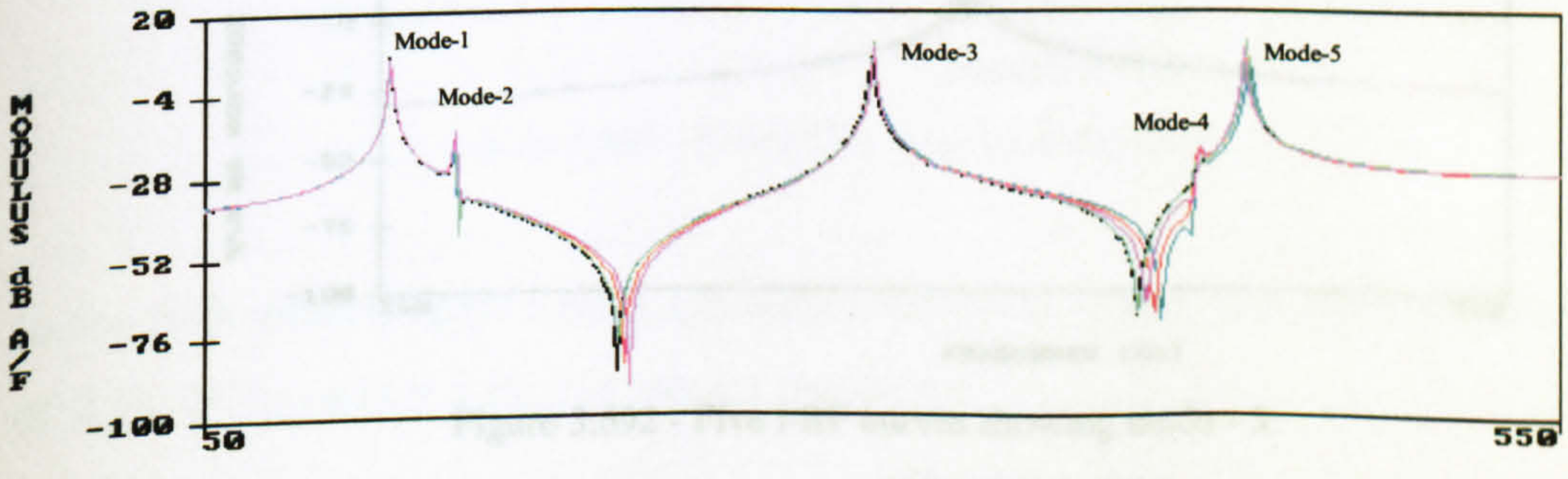

Figure 5.689 - FRF curve for five plots for five arrangement.

For mode-1

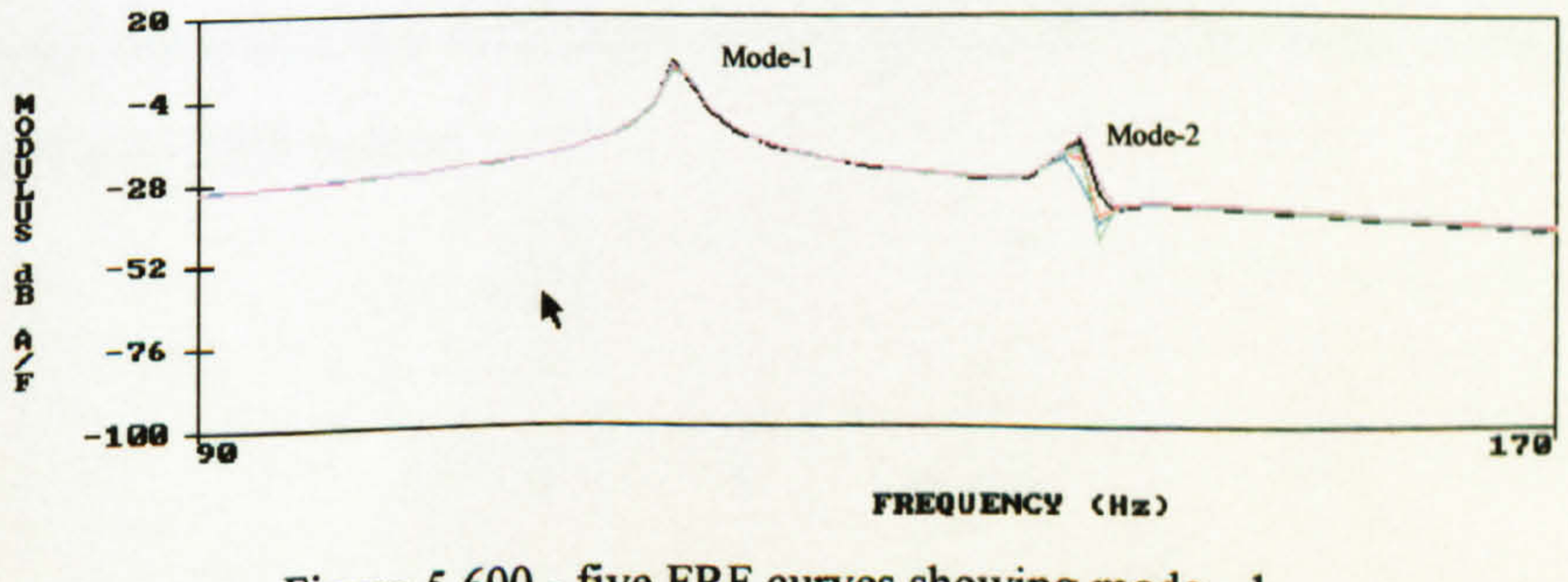

Figure 5.690 - five FRF curves showing mode - 1.

In the first mode (Figure 5.690) (frequency-118 Hz), there is almost negligible difference in natural frequency in all five FRF curves.

For mode-2

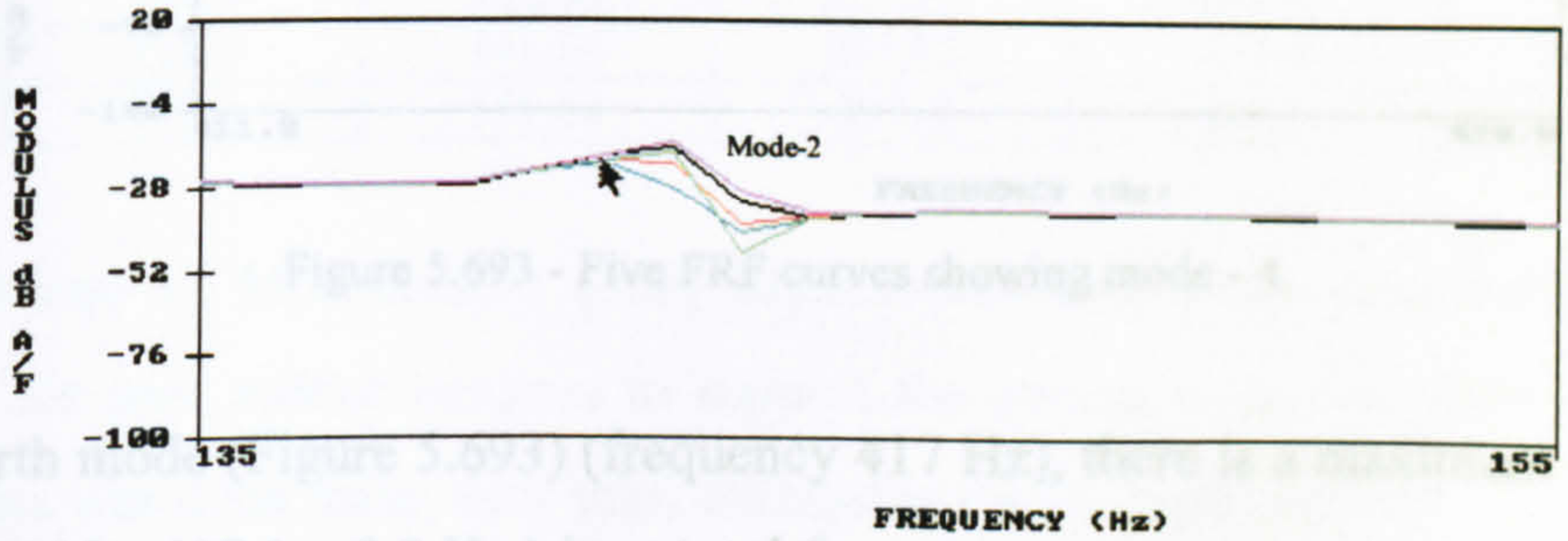

Figure 5.691 - Five FRF curves showing mode - 2.

In the second mode (Figure 5.691) (frequency-142 Hz), there is a maximum difference of 1 Hz (142-141=1 Hz) in natural frequency.

For mode-3

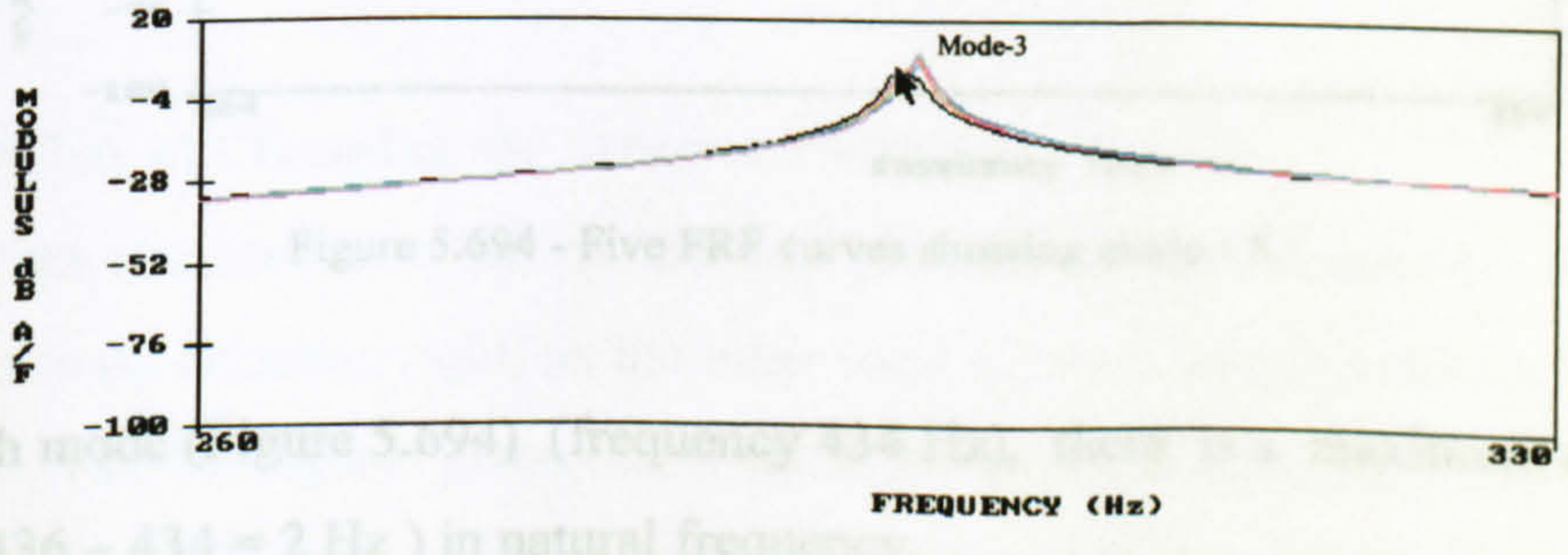

Figure 5.692 - Five FRF curves showing mode - 3.

In the third mode (Figure 5.692) (frequency 296 Hz), there is a maximum difference of 1.1 Hz (297.1 - 296 = 1.1 Hz) in natural frequency.

For mode-4

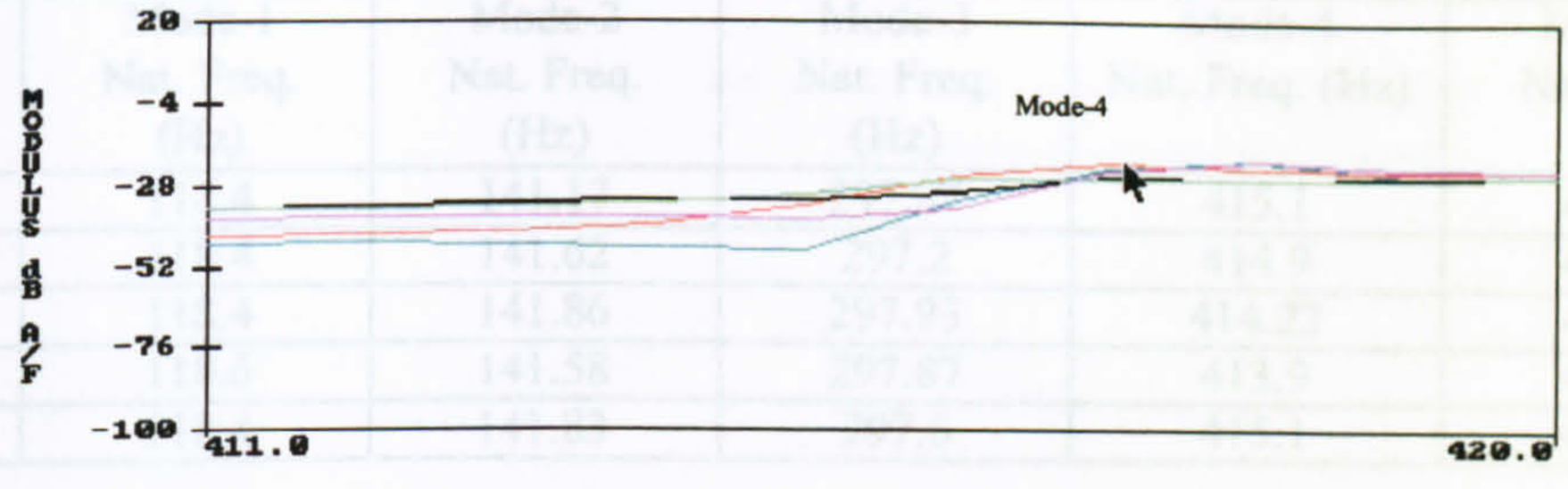

Figure 5.693 - Five FRF curves showing mode - 4.

In the fourth mode (Figure 5.693) (frequency 417 Hz), there is a maximum difference of 0.9 Hz (418 - 417.1 = 0.9 Hz) in natural frequency.

For mode-5

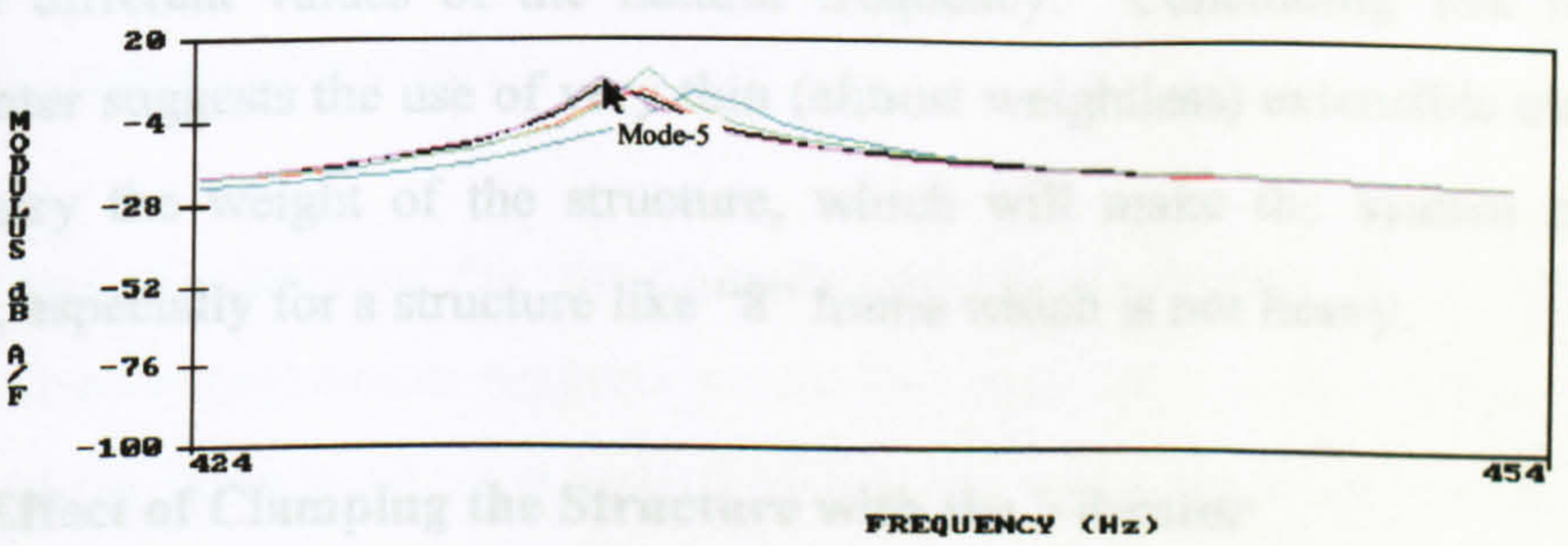

Figure 5.694 - Five FRF curves showing mode - 5.

In the fifth mode (Figure 5.694) (frequency 434 Hz), there is a maximum difference of 2 Hz (436 – 434 = 2 Hz) in natural frequency.

After analysing the FRF curves of all node points, the overall natural frequency was determined, and found very close value of natural frequency for each test. For the first mode there was almost negligible difference in natural frequency and in the higher modes there found a difference of less than 2 Hz. The result of these five tests is given in Table 5.64 below.

Table 5.64 - Comparison of analysis result for five arrangements

	Mode-1 Nat. Freq. (Hz)	Mode-2 Nat. Freq. (Hz)	Mode-3 Nat. Freq. (Hz)	Mode-4 Nat. Freq. (Hz)	Mode-5 Nat. Freq. (Hz)
Test-1	118.4	141.17	297.87	415.1	436.4
Test-2	118.4	141.62	297.2	414.9	434.8
Test-3	118.4	141.86	297.93	414.22	434.6
Test-4	118.6	141.58	297.87	413.9	435.0
Test-5	118.4	141.83	297.6	415.1	434.8

The difference of Moersheim's [95a] experiments and these experiments are the bungees. He used rubber bungees to support the structure, on the other hand these experiments was done using very thin, extensible elastic band supports. Moersheim's bungees were too stiff in relation to the structure weight, so, the bungees damped the vibration of the structure. The different value of damping on different points generated different values of the natural frequency. Concluding this result, this experimenter suggests the use of very thin (almost weightless) extensible elastic cord, just to carry the weight of the structure, which will make the system a free-free condition, especially for a structure like "8" frame which is not heavy.

5.8.3.2 Effect of Clamping the Structure with the Vibrator

Clamping the structure with the vibrator is a problem in modal analysis. Too tight a clamp makes the structure rigid, on the other hand a loose clamping affects the natural frequency. The two figures given below show the effect of loose clamping on natural frequency, where the peak of FRF curves for an accelerometer positioned on the force input point is lower than the other measurement points of the structure.

1 Using Large Accelerometer

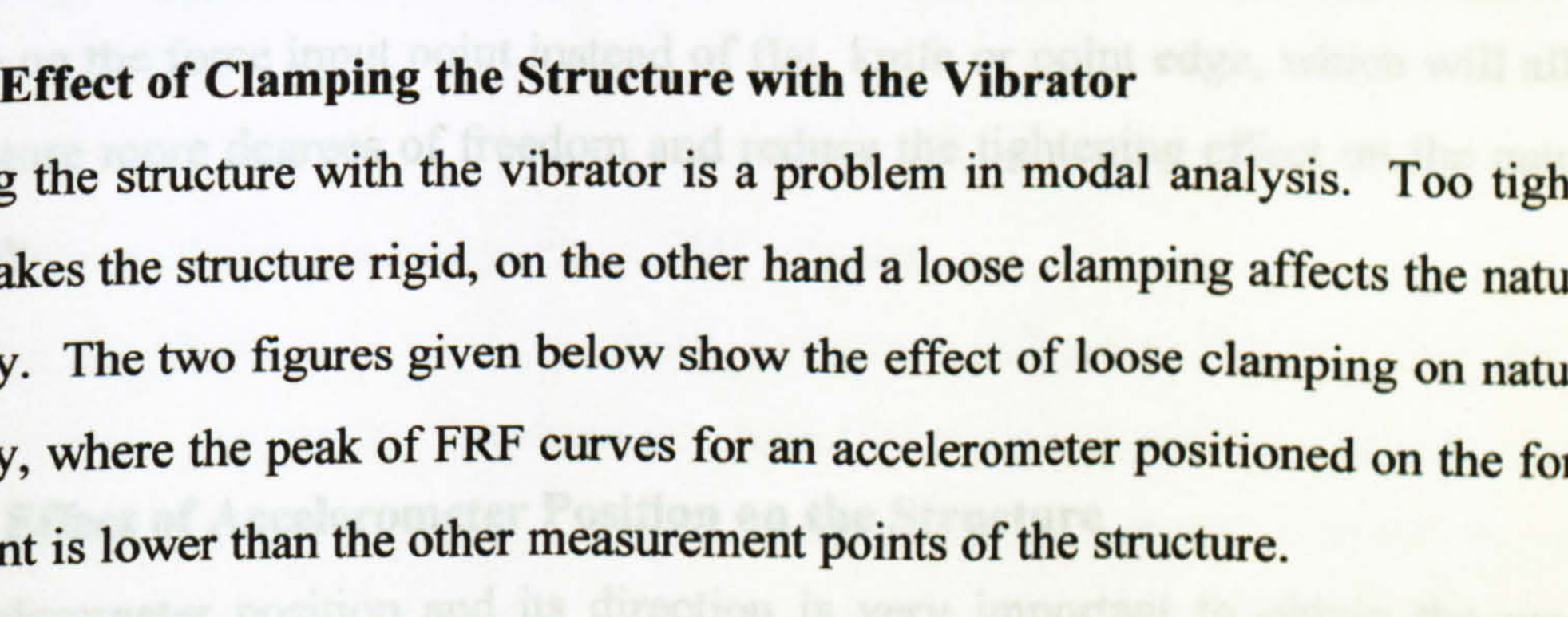

Figure 5.695 - Comparison of FRF curve for large accelerometer.

2. Using Small Accelerometer

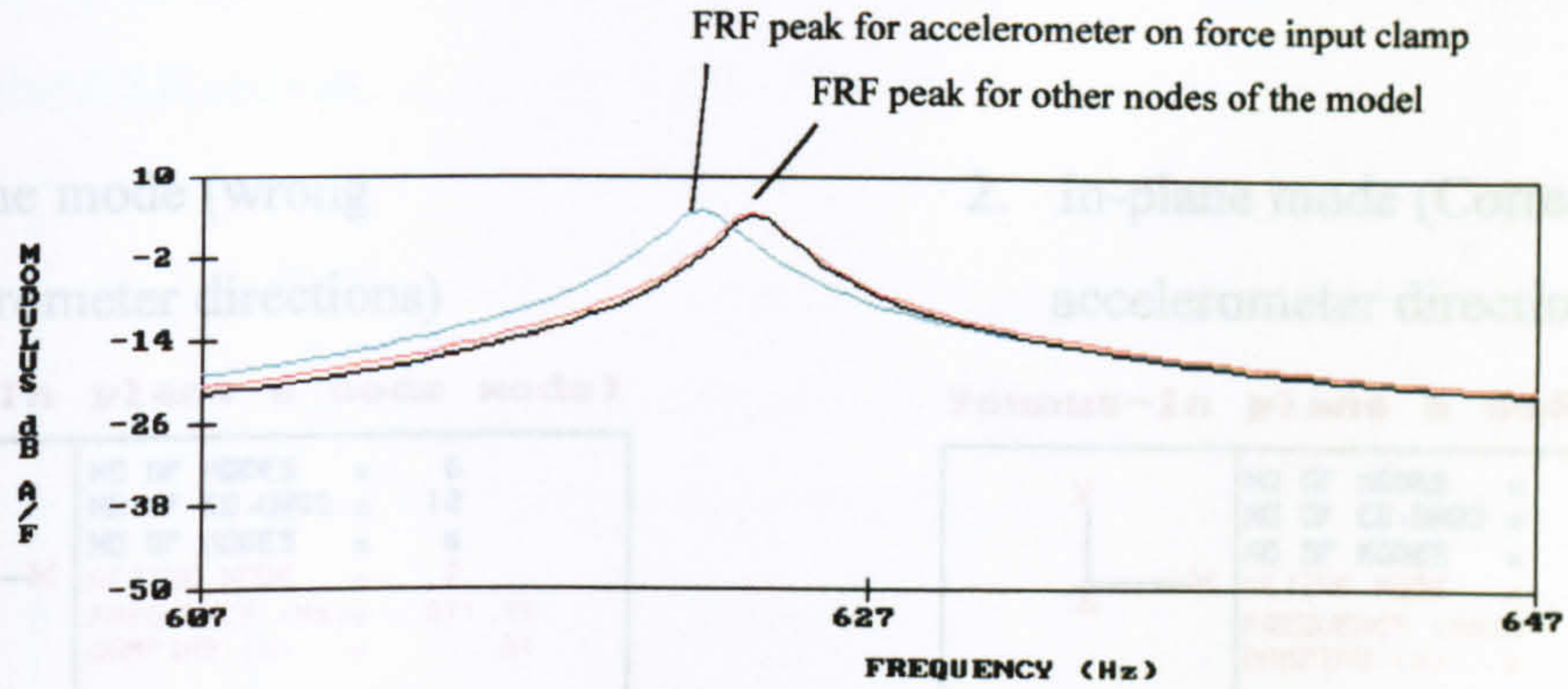

Figure 5.696 - Comparison of FRF curve for small accelerometer.

Observation on the two plots above show that large accelerometers increase the mass more than the smaller accelerometer, so the peak of FRF curves go more down in the case of the large accelerometer.

The problem of clamping the structure should be eliminated using some special measure. This experimenter suggests to use two steel balls in the clamp to hold the structure on the force input point instead of flat, knife or point edge, which will allow the structure more degrees of freedom and reduce the tightening effect on the natural frequency.

5.8.3.3 Effect of Accelerometer Position on the Structure

The accelerometer position and its direction is very important to obtain the modal properties of the structure. The accelerometers should always be positioned on the same specific point of the structure for repeatability of the result. The direction of the accelerometers on the structure plays a key role in finding the modal properties. The accelerometer position on the structure always should be in either the positive or in negative direction. The effect of positive and negative mixed positioned accelerometers is shown below. The mode shapes in the first case (wrongly positioned accelerometers) is not similar to that in the FE model, and in the second

case (accelerometers positioned in right way) the mode shape is very similar to the FE model.

1. **In plane mode (wrong accelerometer directions)**

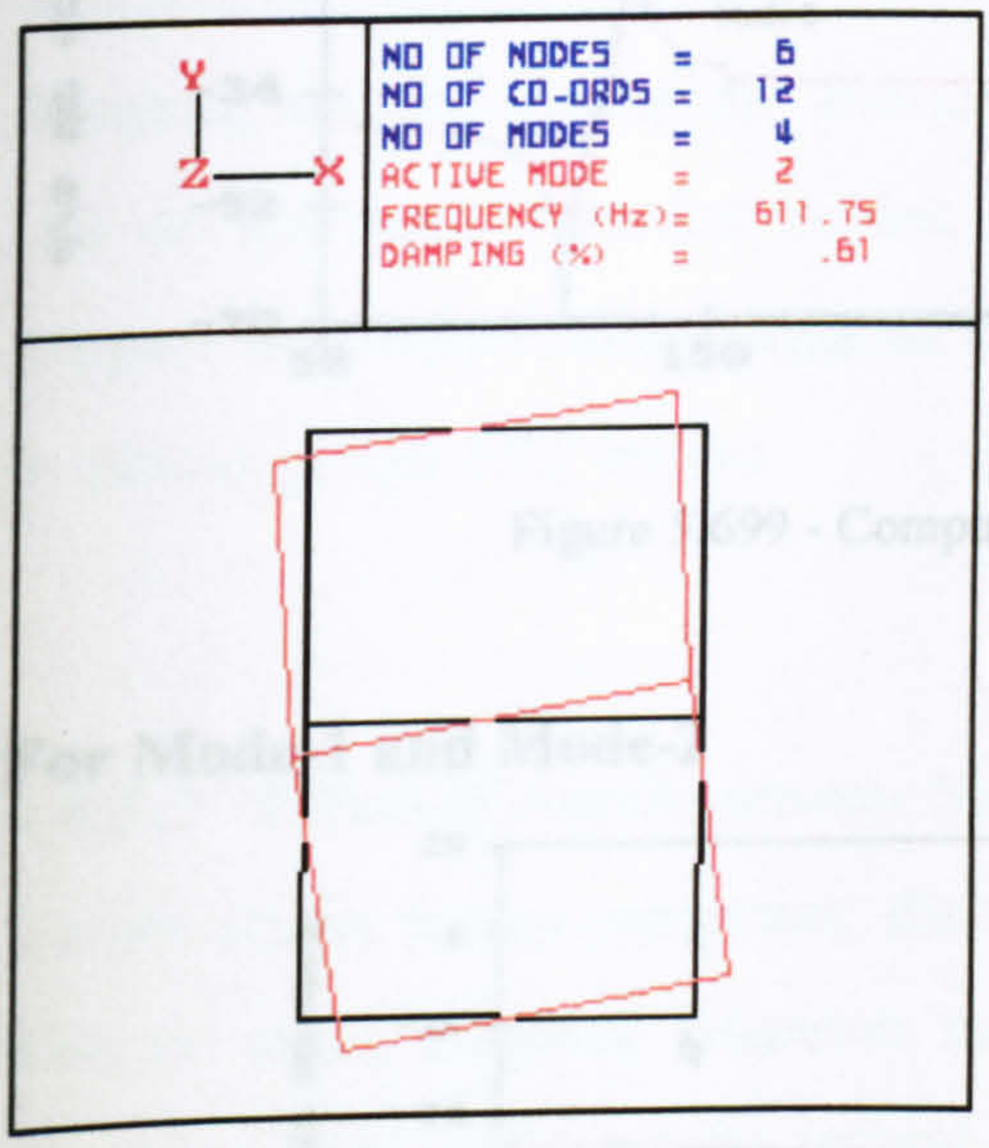

Figure 5.697 - In plane mode (Incorrect).

2. **In-plane mode (Correct accelerometer direction**

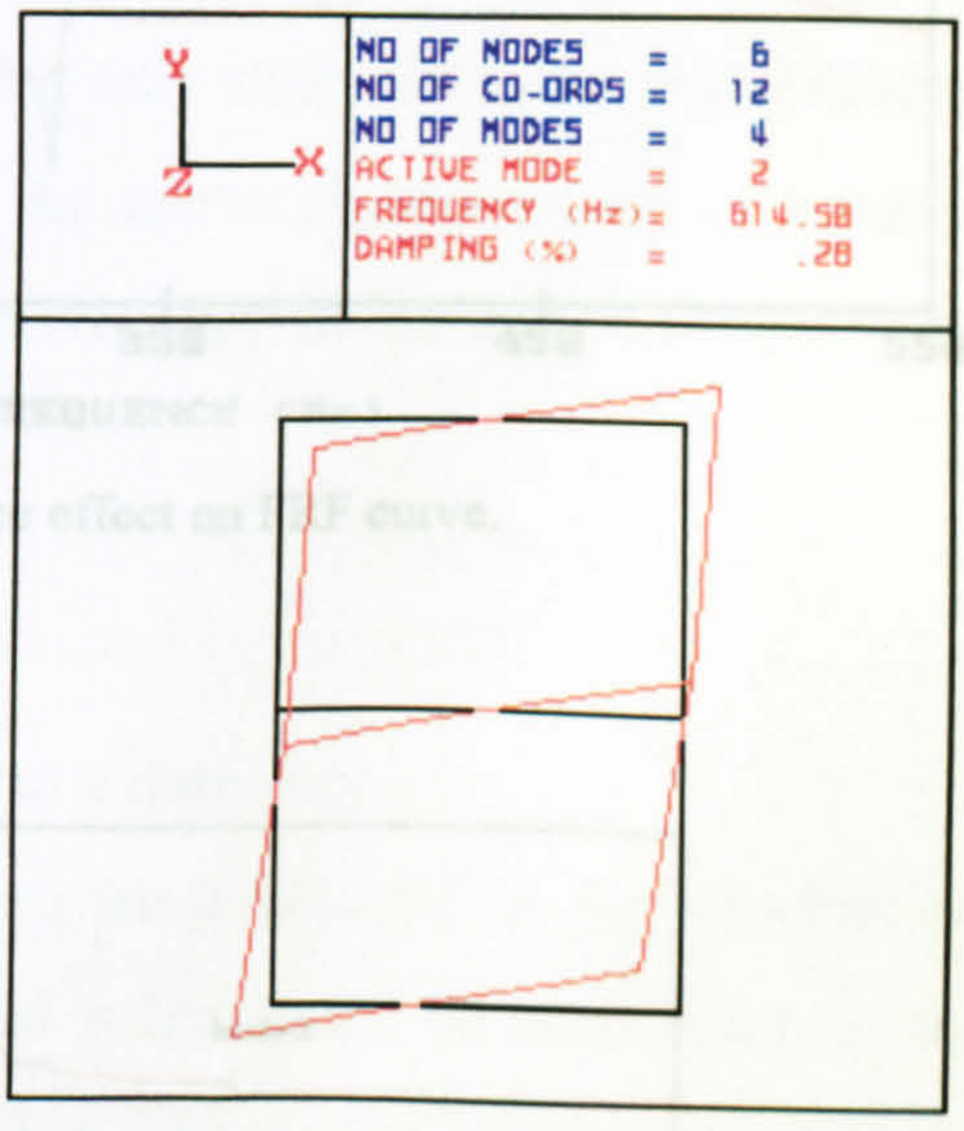

Figure 5.698 - In-plane mode (correct).

5.8.3.4 Effect of Bungee Support on FRF Curves

Supporting the structure is most important, because it influences the modal properties of the structure. Supporting the structure should be with low stiffness springs, which should be very small in weight in relation to the structure, otherwise it will increase the mass of the structure, & hence affect the natural frequency. Using springs and other auxiliary arrangements sometimes becomes very difficult. Rubber ropes can be an alternative to the spring supports, because these are elastic, easily extensible and flexible. The choice of rubber rope is very important, because they need to be elastic, very thin, almost weightless, yet strong enough to carry the weight of the structure. In a previous study a relatively thick bungee was used and resulted in FRF curves which showed non-linearities. In this experiment the effect of bungees (bungee weight, flexibility and extensibility) is investigated. The red FRF curve is from a relatively thick bungee support and the blue one is from thin elastic bands.

The figure below, shows five modes, mode-1, mode-2, mode-3, mode-4, and mode-5. Here mode-1, mode-2 and mode-3 is discussed below to compare the bungee support effect on the FRF curves.

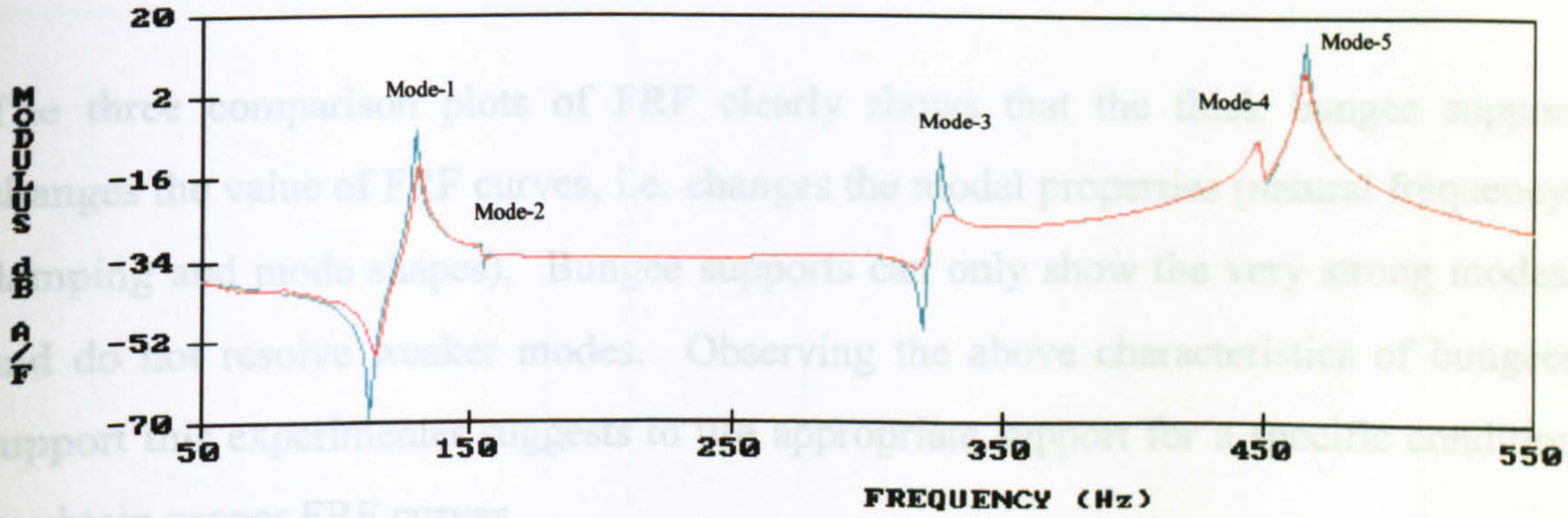

Figure 5.699 - Comparison of bungee effect on FRF curve.

For Mode-1 and Mode-2

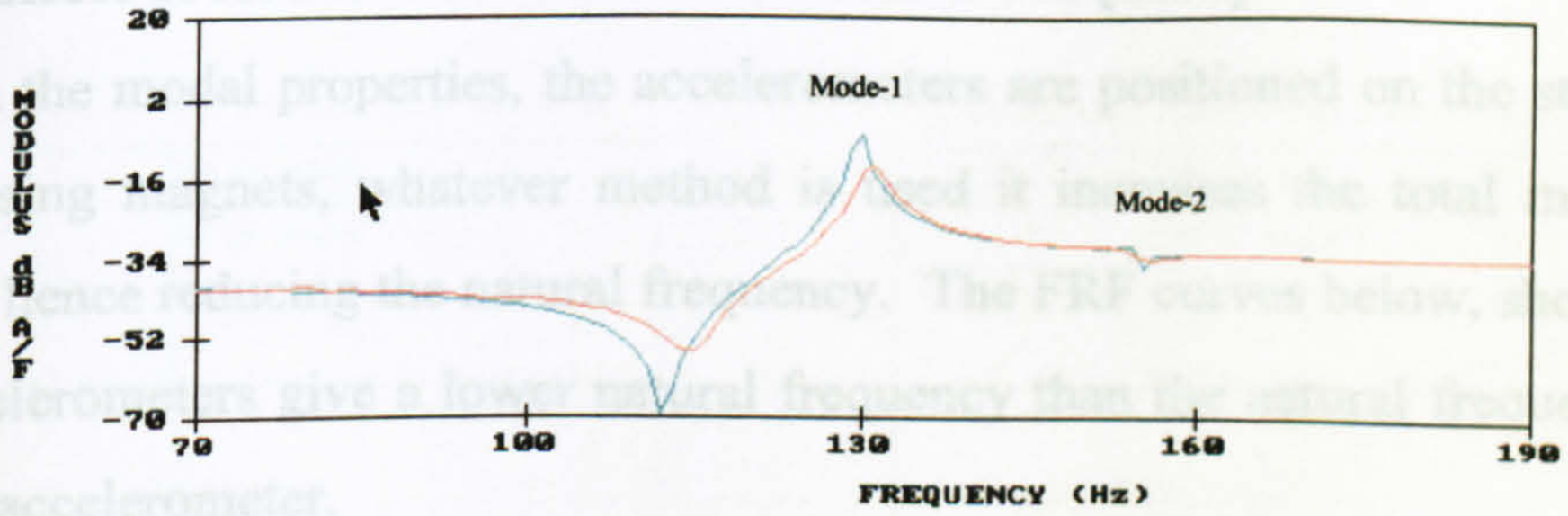

Figure 5.700 - Comparison of FRF curve for mode - 1 and - 2.

In the first mode the peak frequency of the thick bungee is 130.7 Hz and for the thin elastic band is 129.6 Hz. For the second mode from the thick bungee support does not look like a mode, but the FRF curve of the elastic band clearly shows that it is a mode.

For Mode-3

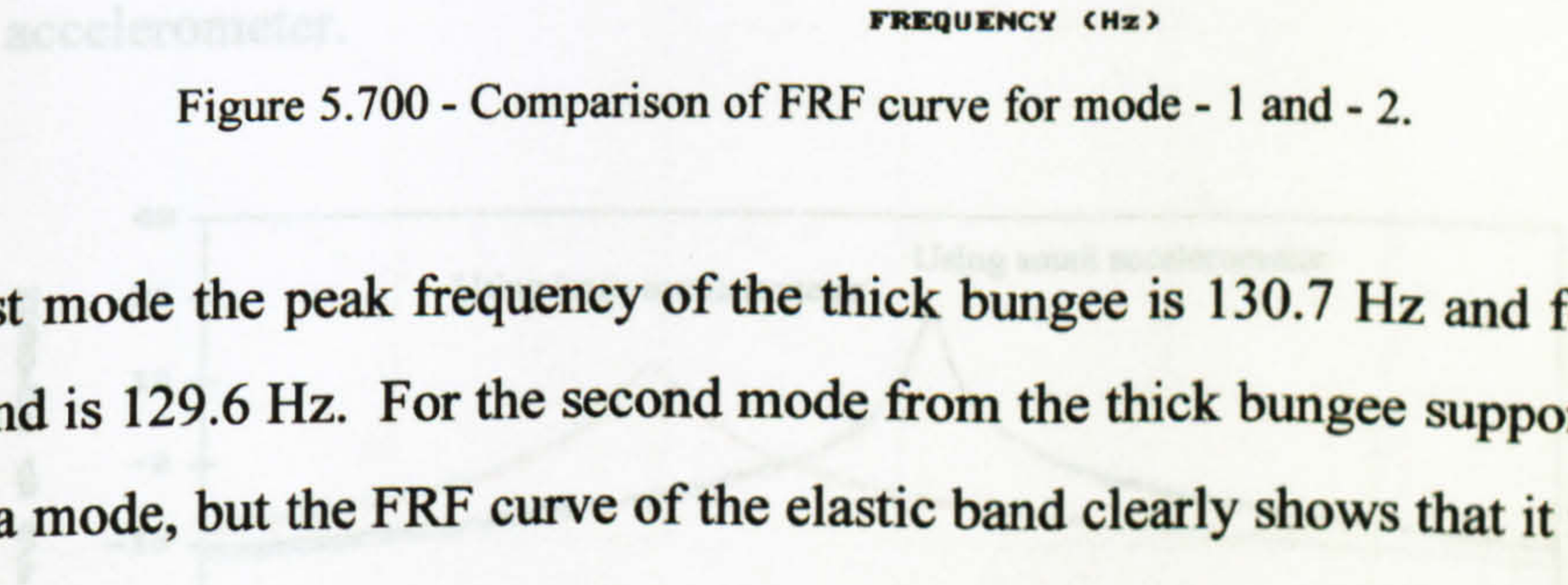

Figure 5.701 - Comparison of FRF curve for mode - 3.

For the third mode (frequency 326.5 Hz), the thick bungee FRF curve does not show any mode (is not resolved sufficiently for identification or analysis), but the FRF curve from thin elastic band clearly shows the mode.

The three comparison plots of FRF clearly shows that the thick bungee support changes the value of FRF curves, i.e. changes the modal properties (natural frequency, damping and mode shapes). Bungee supports can only show the very strong modes, and do not resolve weaker modes. Observing the above characteristics of bungees support this experimenter suggests to use appropriate support for a specific condition to obtain proper FRF curves.

5.8.3.5 Effect of Accelerometer Size on Natural Frequency

To obtain the modal properties, the accelerometers are positioned on the structure by wax or using magnets, whatever method is used it increases the total mass of the structure, hence reducing the natural frequency. The FRF curves below, show that the large accelerometers give a lower natural frequency than the natural frequency using the small accelerometer.

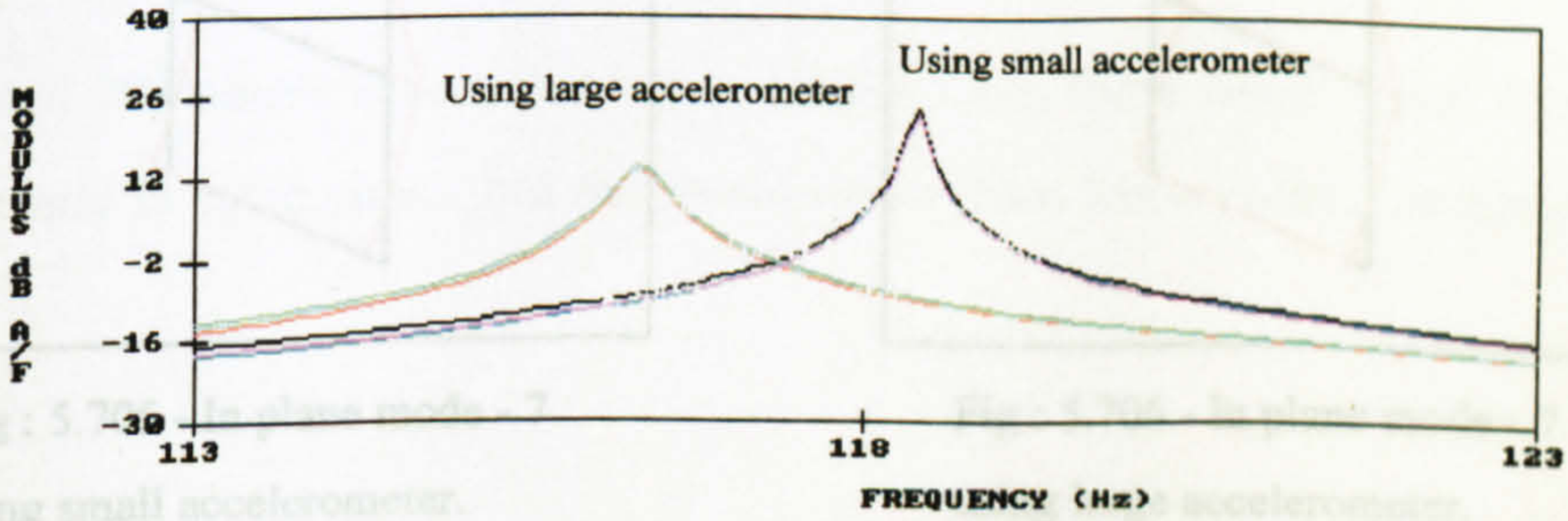

Figure 5.702 - Effect of accelerometer size on FRF curve.

The two in-plane modes shown below were measured using small and large accelerometers, and in both cases, the natural frequency found was less using the large accelerometer than the natural frequency using the small accelerometer

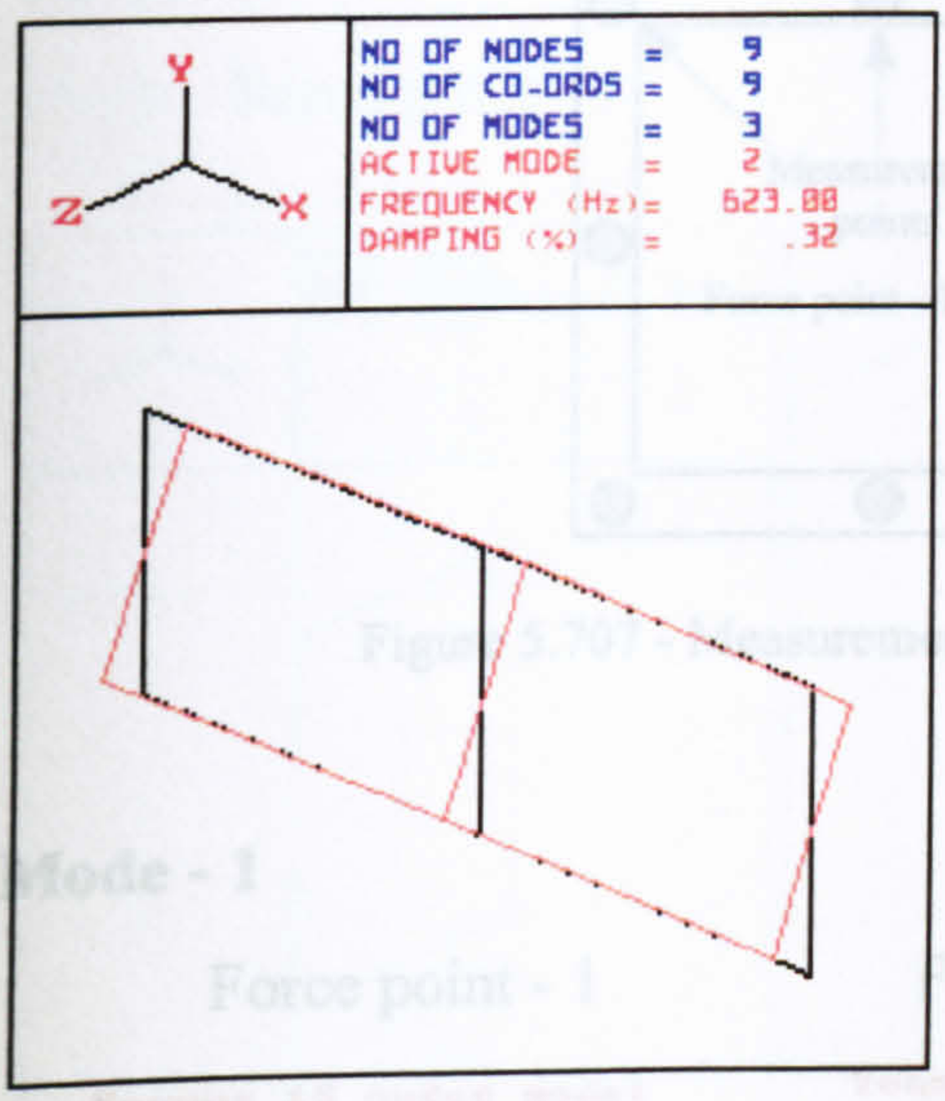

Figure 5.703 - In plane mode - 6 using small accelerometer.

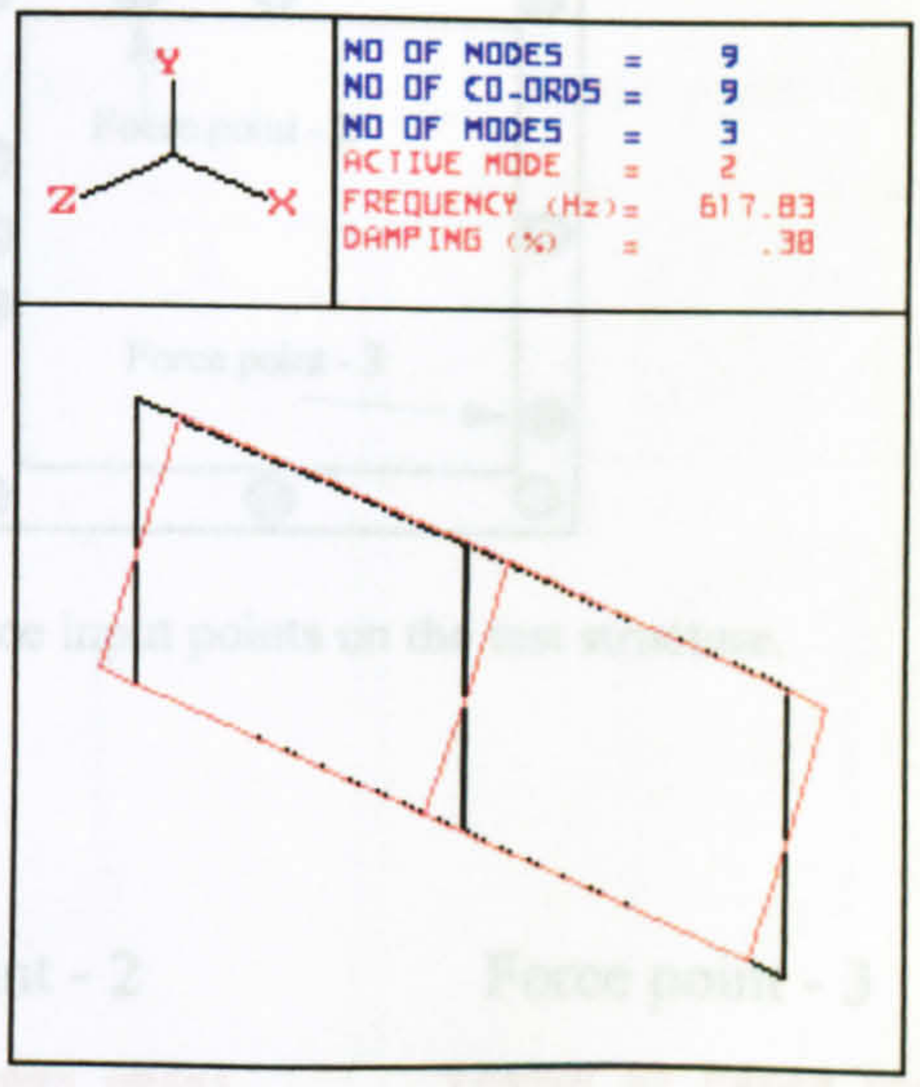

Figure 5.704 - In plane mode - 6 using large accelerometer.

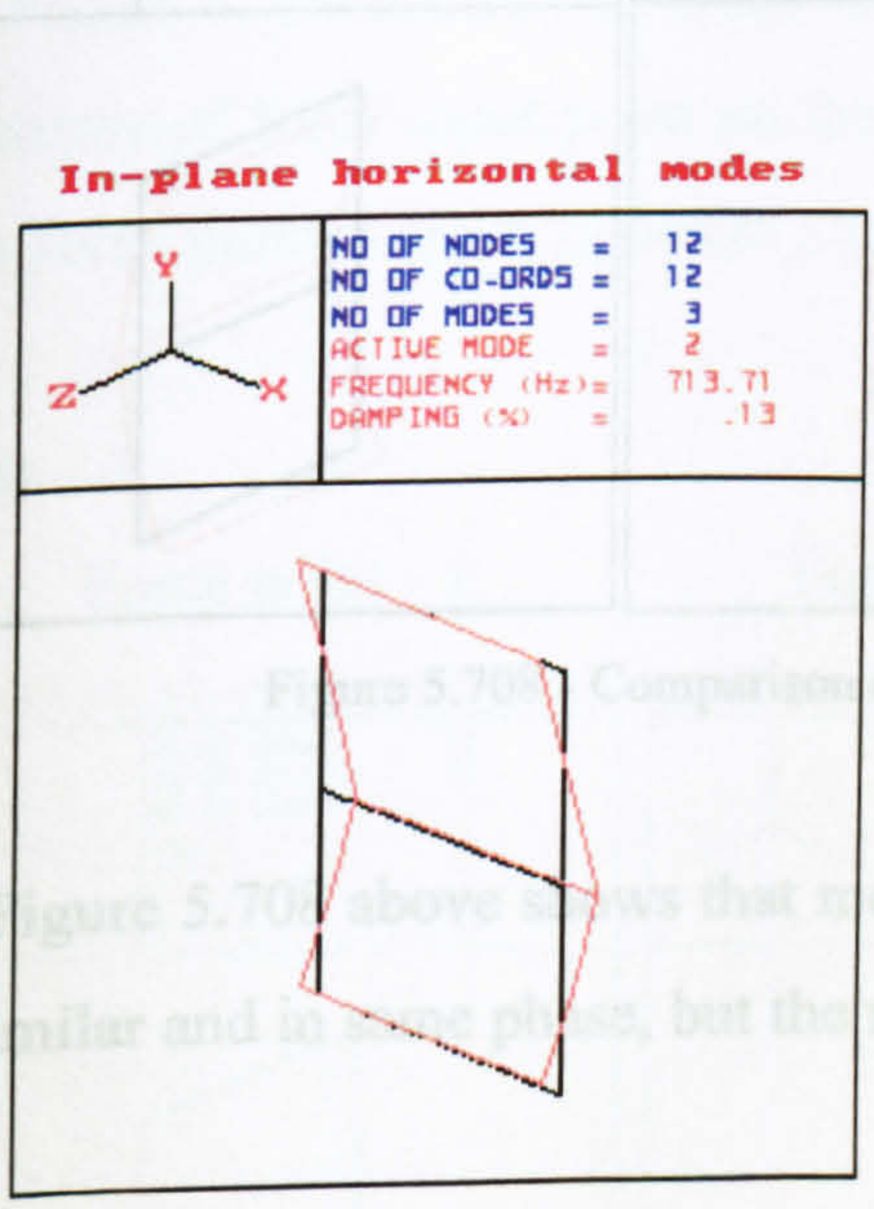

Fig : 5.705 - In plane mode - 7 using small accelerometer.

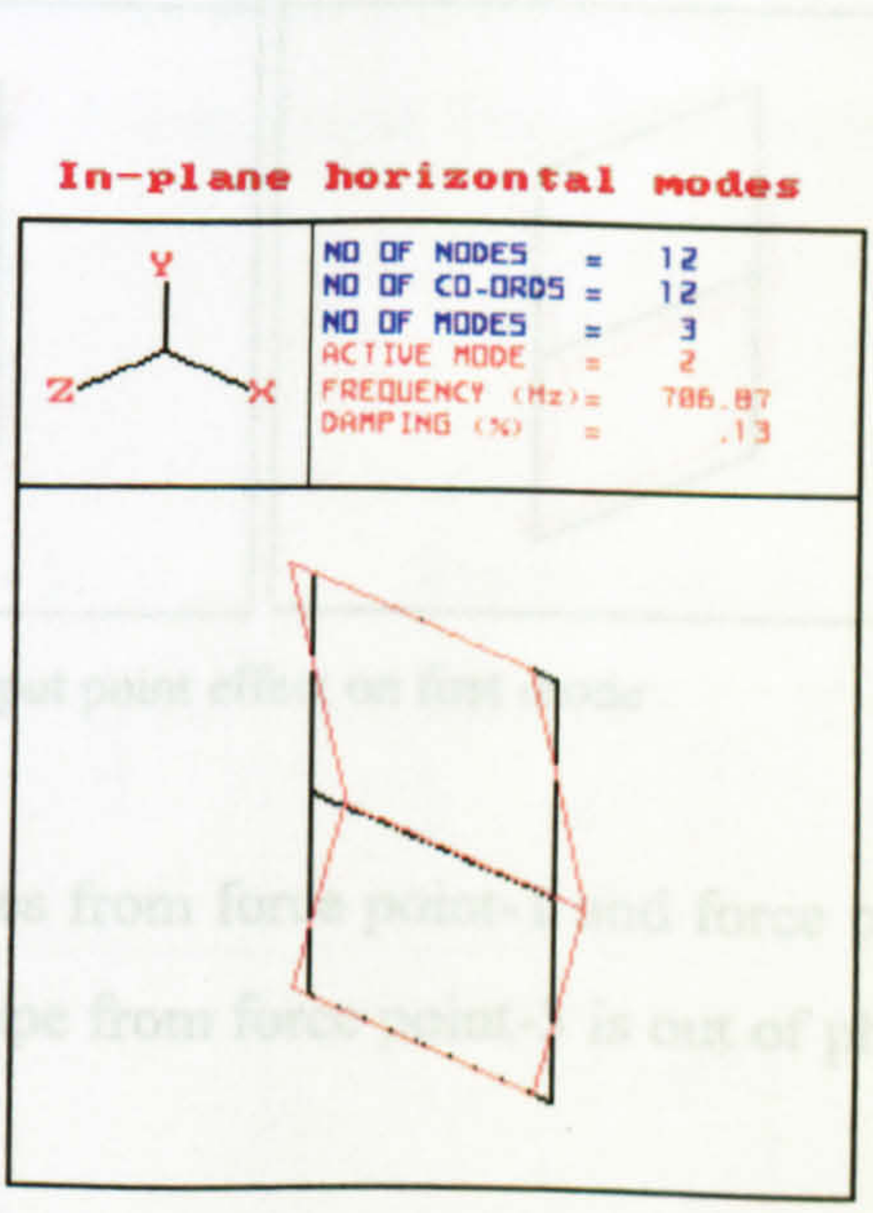

Fig : 5.706 - In plane mode - 7 using large accelerometer.

5.8.3.6 Influence of Force Input Point on Natural Frequency and Mode Shape

The force input point has a major influence on natural frequency. In this experiment three force input points (shown in figure below) are used to check the influence of force input point on the natural frequency and to obtain the correct mode shapes. Here the experimenter used a specimen 6.35 mm thick, all other dimensions were the same.

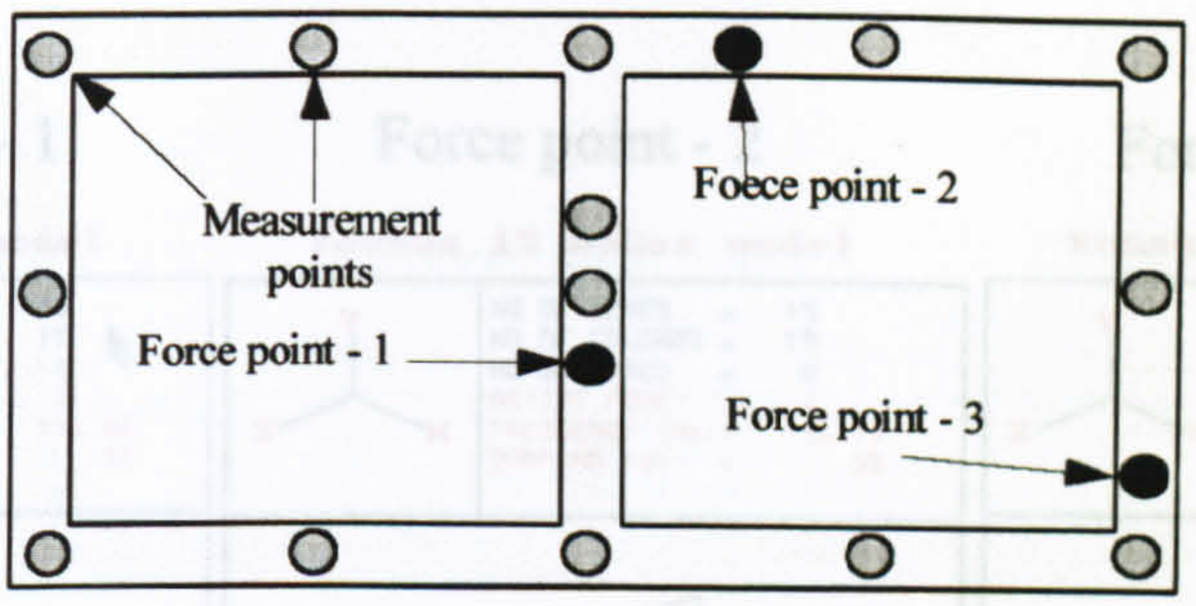

Figure 5.707 - Measurement and force input points on the test structure.

Mode - 1

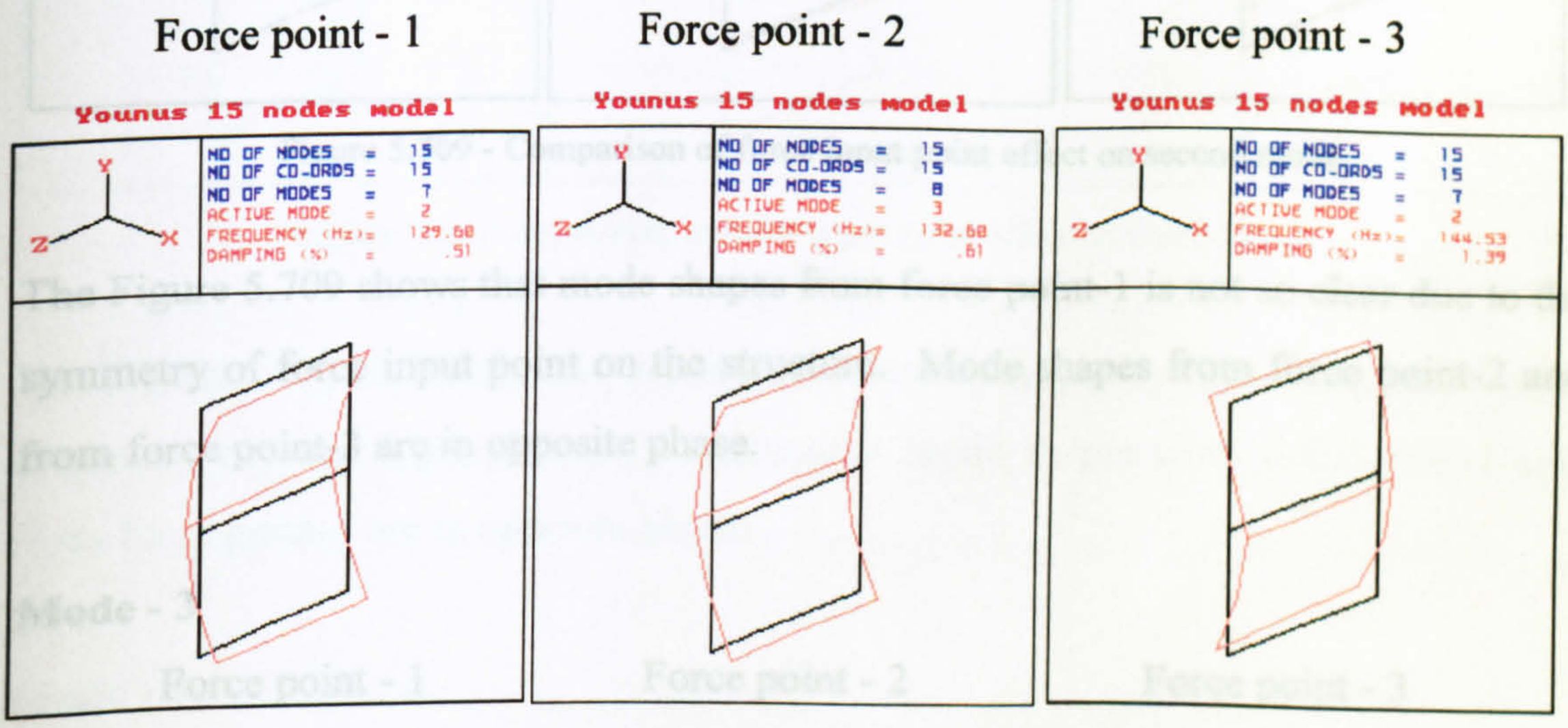

Figure 5.708 - Comparison of force input point effect on first mode

The Figure 5.708 above shows that mode shapes from force point-1 and force point-2 are similar and in same phase, but the mode shape from force point-3 is out of phase.

Mode - 2

Force point - 1 | Force point - 2 | Force point - 3

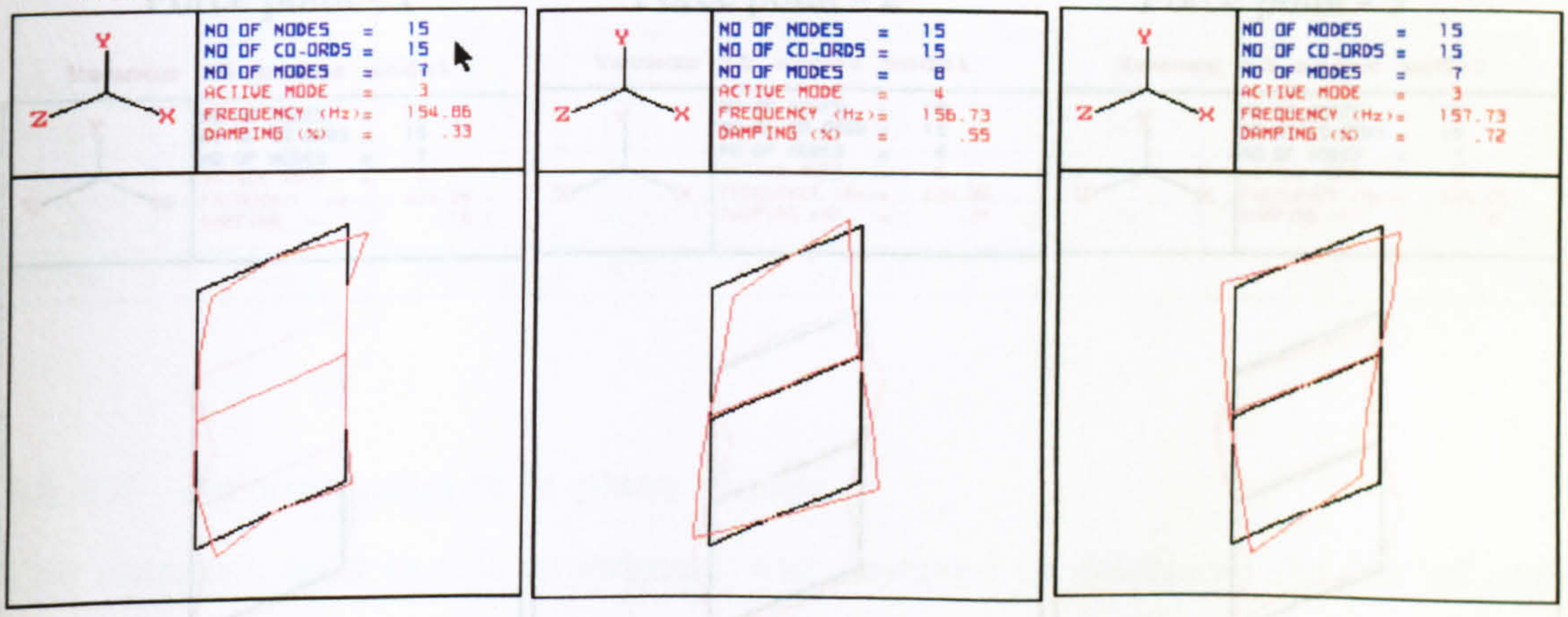

Figure 5.709 - Comparison of force input point effect on second mode

The Figure 5.709 shows that mode shapes from force point-1 is not so clear due to the symmetry of force input point on the structure. Mode shapes from force point-2 and from force point-3 are in opposite phase.

Mode - 3

Force point - 1 | Force point - 2 | Force point - 3

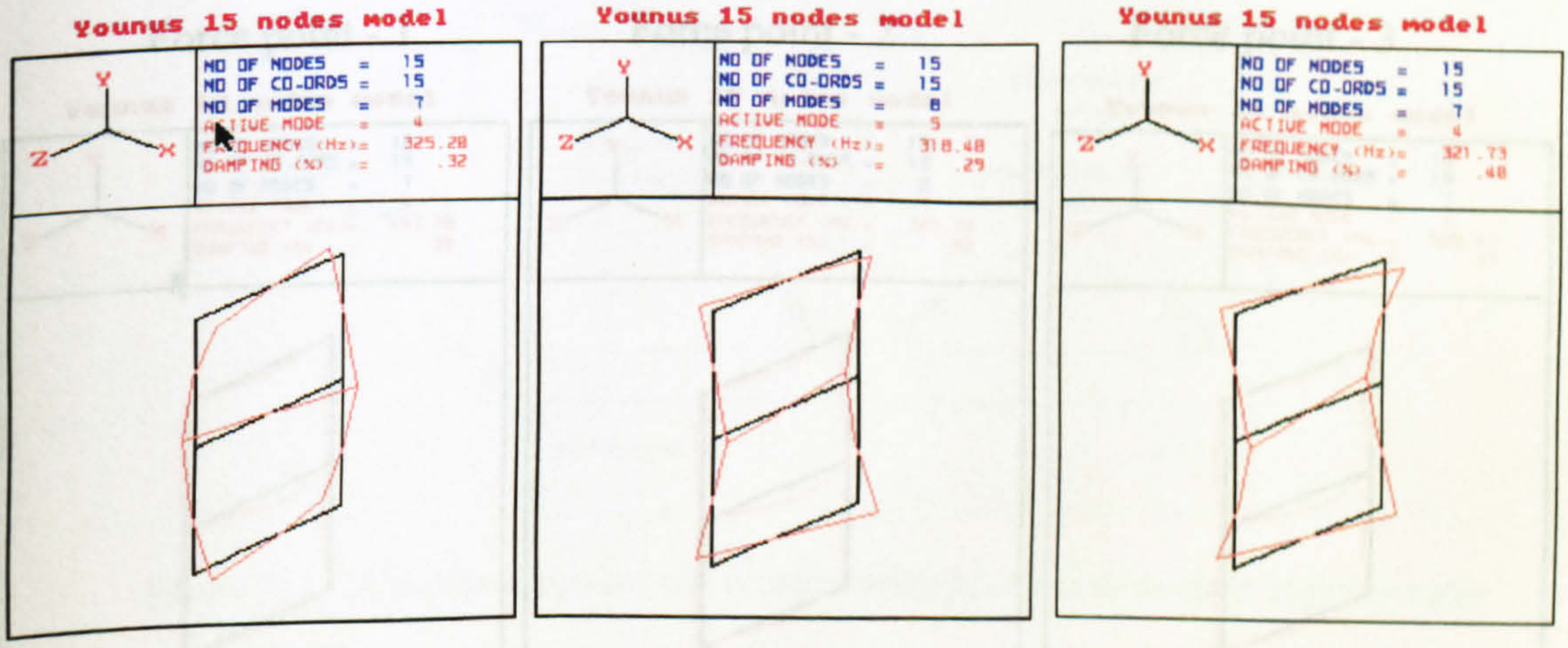

Figure 5.710 - Comparison of force input point effect on third mode

Mode shapes from force point-2 and from force point-3 are in same phase, but mode shape from force point-1 is in opposite phase.

Mode - 4

Force point - 1 | Force point - 2 | Force point - 3

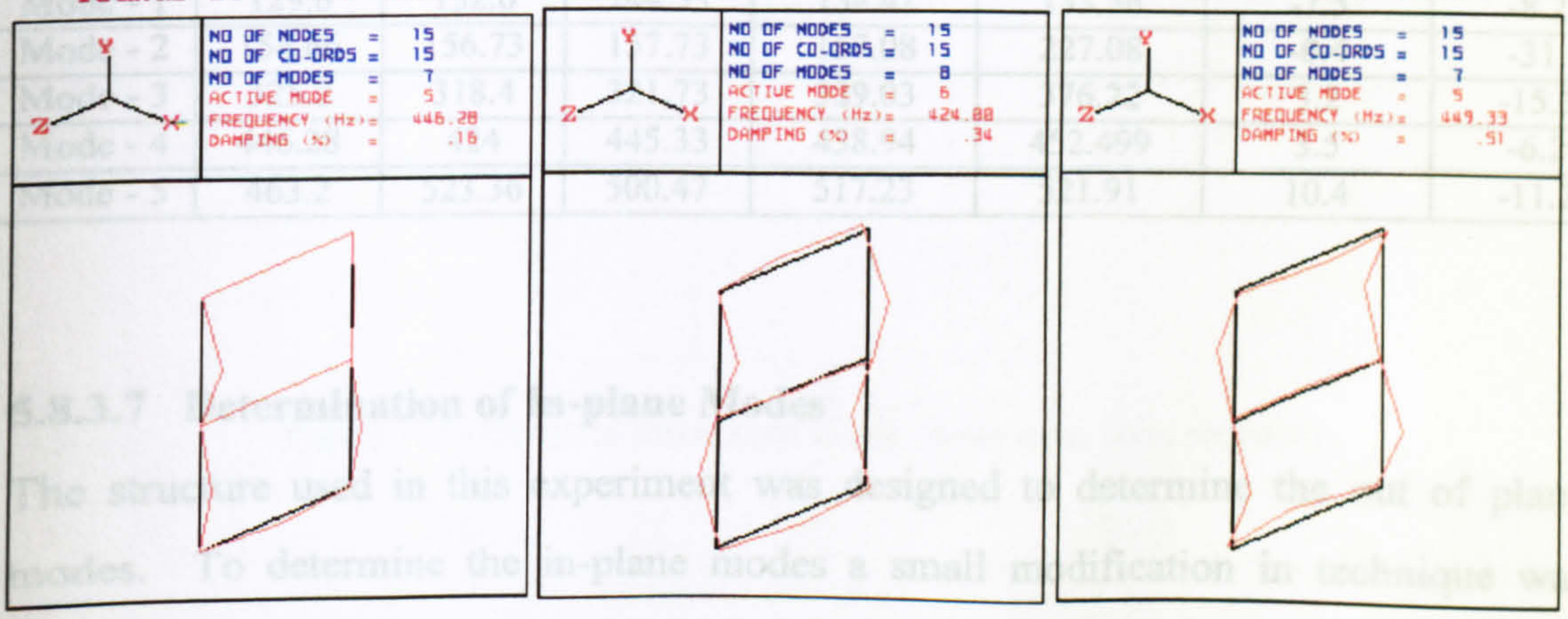

Figure 711 - Comparison of force input point effect on fourth mode

The Figure 5.711 shows that the mode shape from force point-1 is not so clear due to symmetry of force input point of the structure. Mode shapes from force point-2 and from force point-3 are in opposite phase.

Mode - 5

Force point - 1 | Force point - 2 | Force point - 3

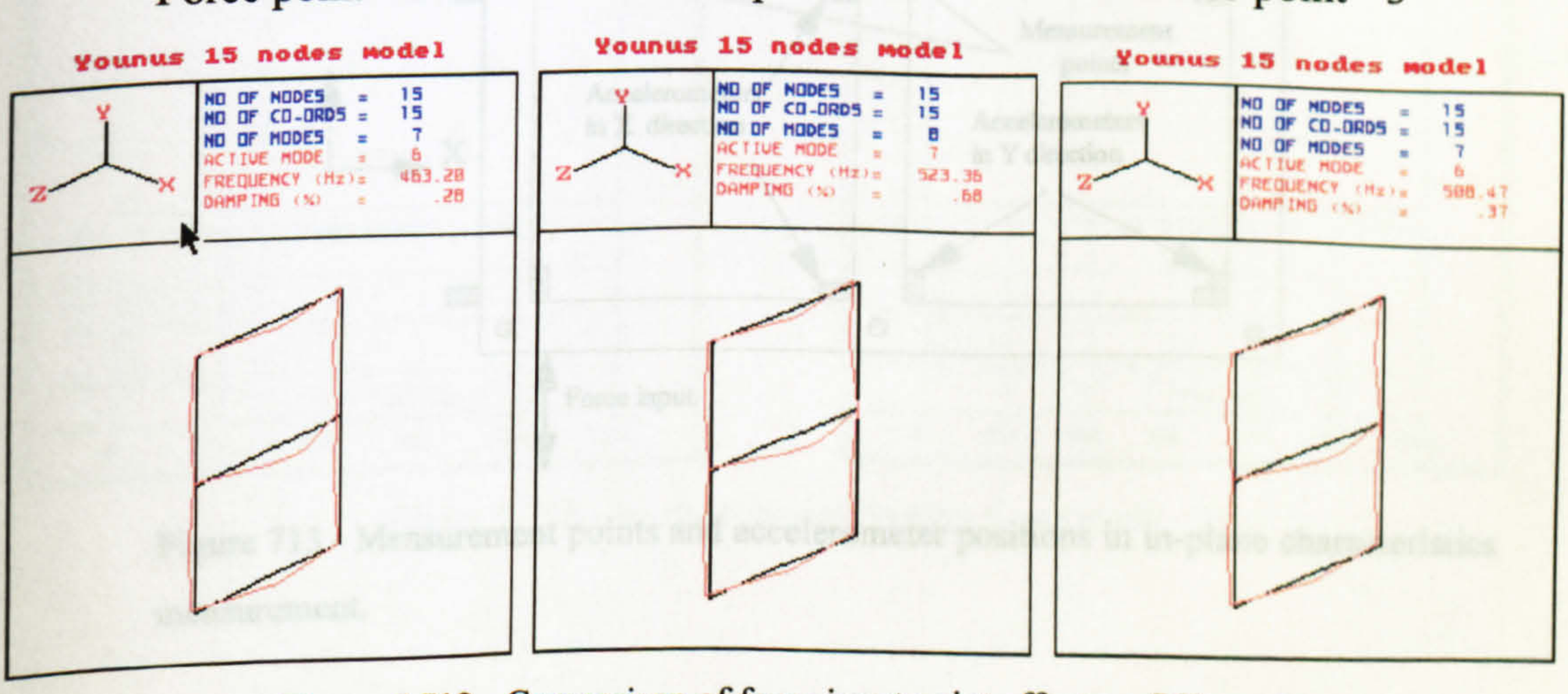

Figure 5.712 - Comparison of force input point effect on fifth mode

The Figure 5.712 above shows that mode shapes from force point-1, force point-2 and from force point-3 are in same phase and similar.

Table 5.65 - Comparison of ICATS model with ANSYS model – out of plane modes

	Force point-1	Force point-2	Force point-3	ANSYS shell model	ANSYS beam model	Max. Diff. shell model	Max. Diff. beam model
Mode - 1	129.6	132.6	144.53	134.42	133.56	-7.5	-8.21
Mode - 2	154.66	156.73	157.73	157.08	227.08	-0.4	-31.9
Mode - 3	325.2	318.4	321.73	329.03	376.22	3.2	-15.36
Mode - 4	446.28	424	445.33	438.94	452.499	3.5	-6.29
Mode - 5	463.2	523.36	500.47	517.23	521.91	10.4	-11.24

5.8.3.7 Determination of In-plane Modes

The structure used in this experiment was designed to determine the out of plane modes. To determine the in-plane modes a small modification in technique was applied. A six measurement point model was created in ICATS, and the accelerometers were positioned on the specimen as near as possible to the measurement points. In this case, only six measurement points were possible to position the accelerometers in both in X and Y directions. In this experiment a 6 mm thick structure was used. The node points and position of accelerometers are shown in figure below.

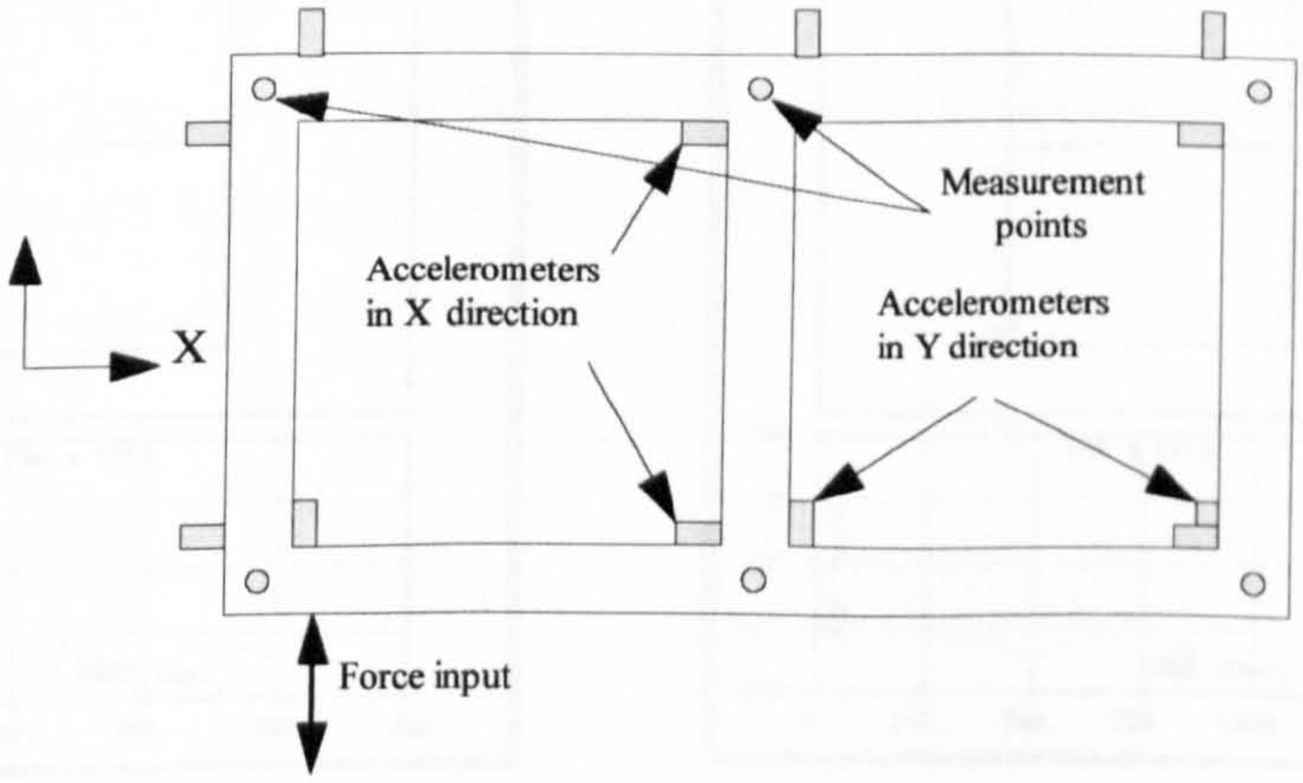

Figure 713 - Measurement points and accelerometer positions in in-plane characteristics measurement.

A force input clamp was designed to allow maximum degrees of freedom and to avoid rigidity. The force input points was made like a roller to do so (figure given below).

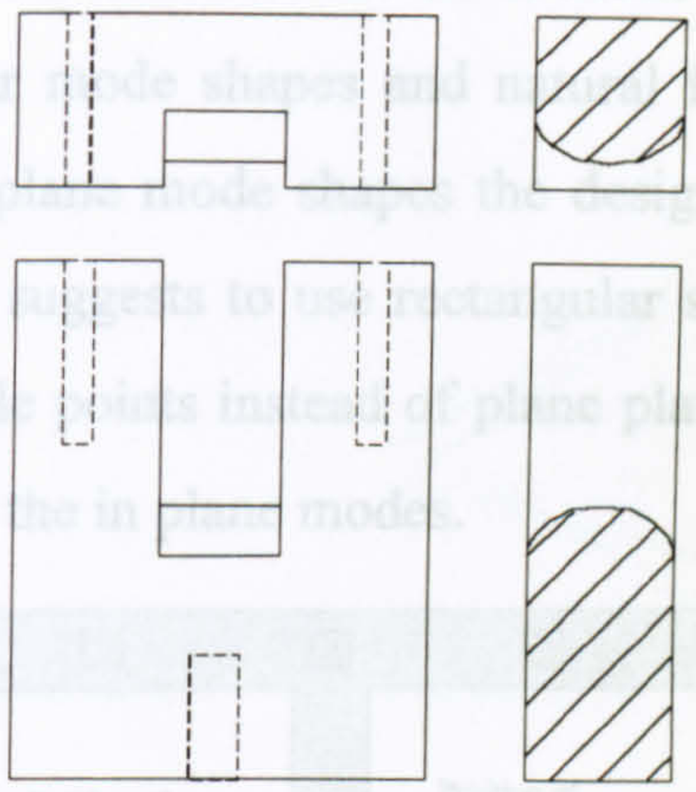

Figure 714 - Designed force input clamp (force input point rounded).

In this experiment two in plane modes (mode-6 and mode-7) were determined,

1. Mode - 6

2. Mode - 7

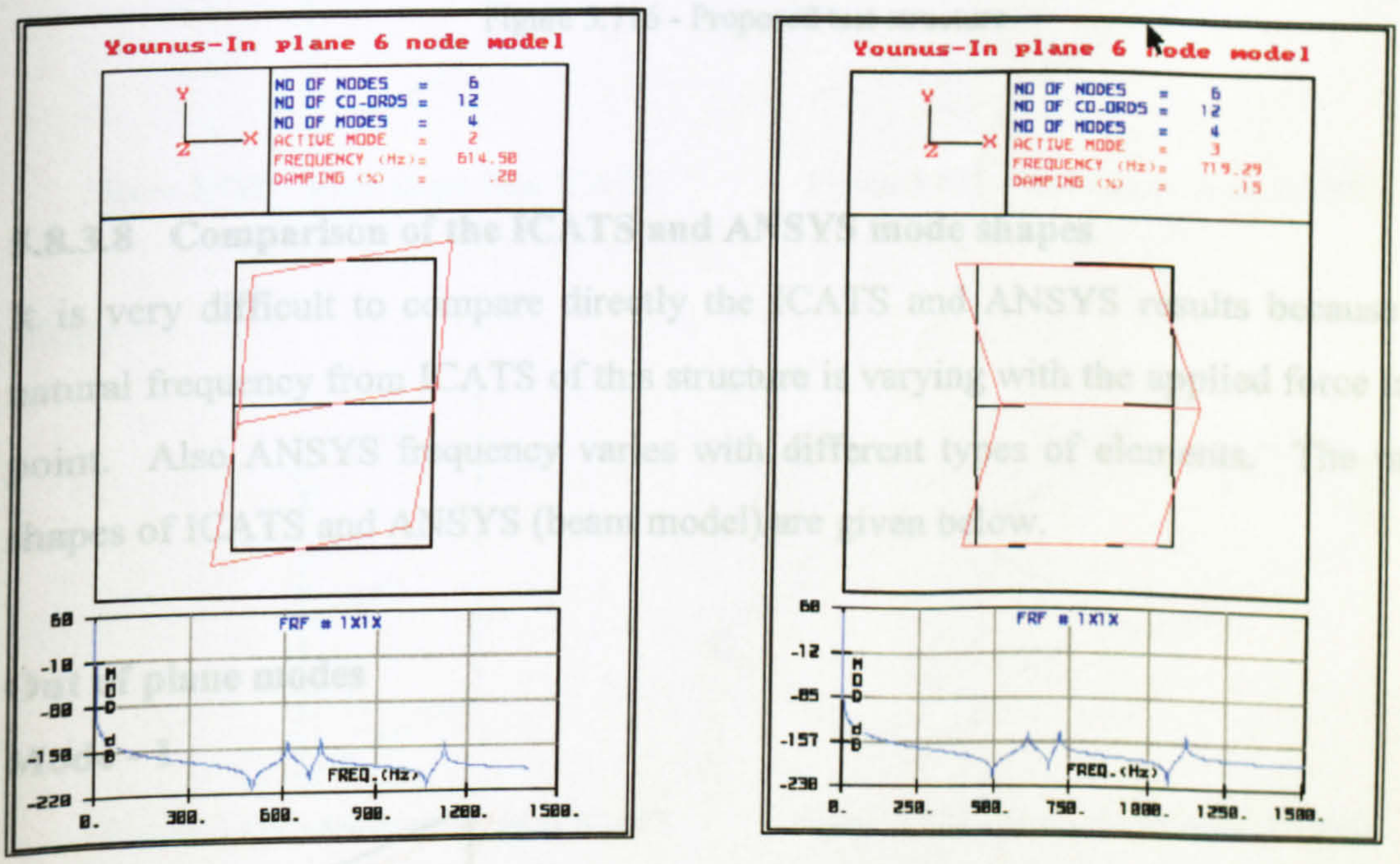

Figure 5.715 - In-plane modes (mode - 6 and mode - 7)

Table - 5.66 - Comparison of ICATS model with ANSYS model – in-plane modes

	ICATS	ANSYS shell element model	ANSYS beam element model	Differencc with shell model %	Difference with beam model %
Mode - 6	614.5	654.69	619.728	6.5	-0.84
Mode - 7	719.29	745.77	712.426	3.6	0.96

This accelerometer position did not show the exact mode shape and natural frequency but it showed a very similar mode shapes and natural frequency as in the ANSYS model. To obtain exact in-plane mode shapes the design of the structure should be changed. This experimenter suggests to use rectangular solid knobs (positioned in X and Y directions) on the node points instead of plane plate. The figure of the model given below is suggested for the in plane modes.

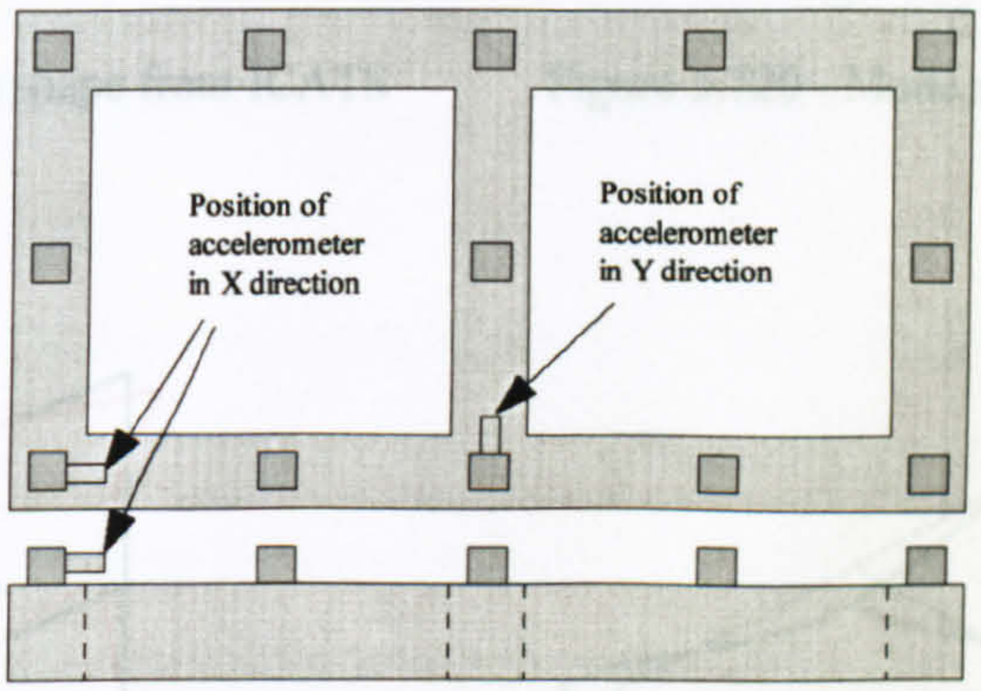

Figure 5.716 - Proposed test structure

5.8.3.8 Comparison of the ICATS and ANSYS mode shapes

It is very difficult to compare directly the ICATS and ANSYS results because the natural frequency from ICATS of this structure is varying with the applied force input point. Also ANSYS frequency varies with different types of elements. The mode shapes of ICATS and ANSYS (beam model) are given below.

Out of plane modes

Mode - 1

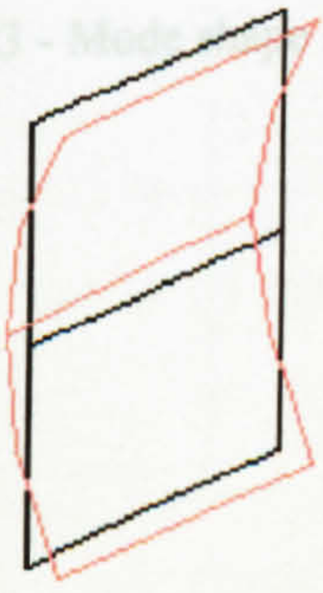

Figure 5.717 - Mode shape from ICATS

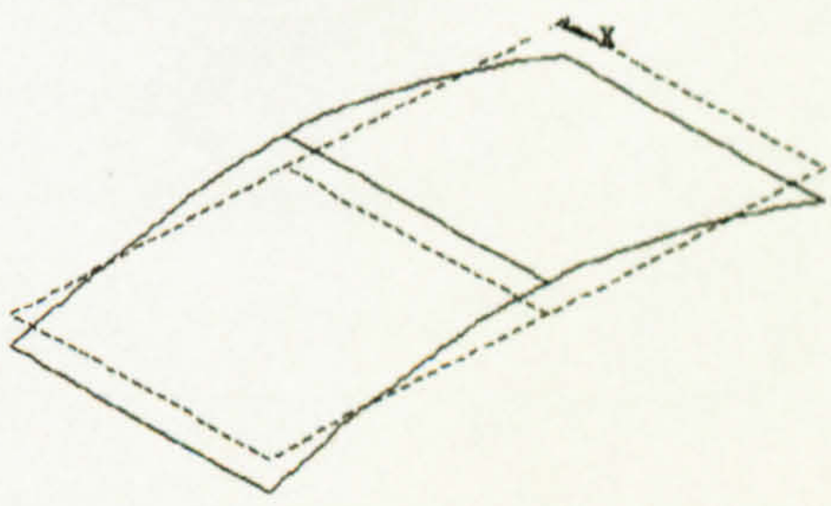

Figure 5.718 - Mode shape from ANSYS

Mode - 2:

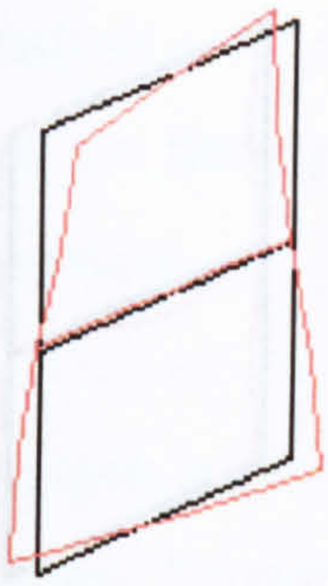

Figure 5.719 - Mode shape from ICATS

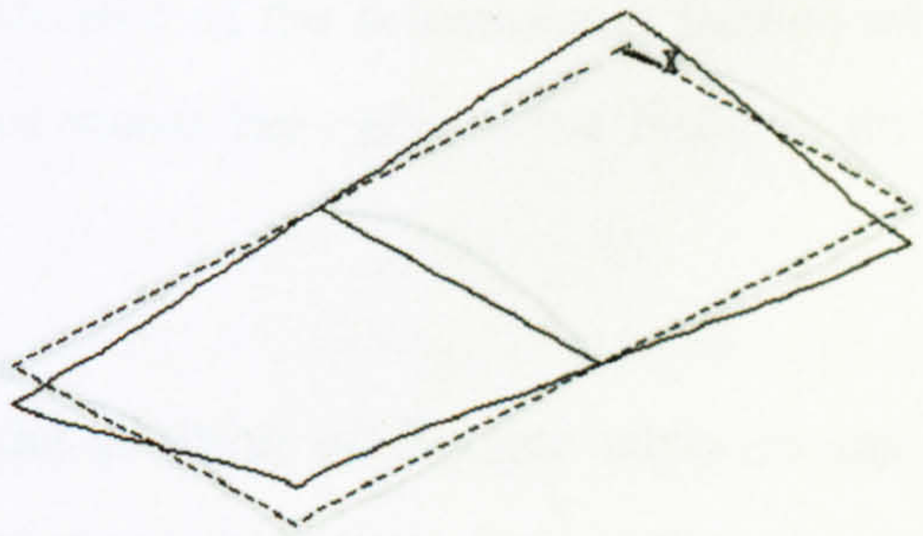

Figure 5.720 - Mode shape from ANSYS

Mode - 3

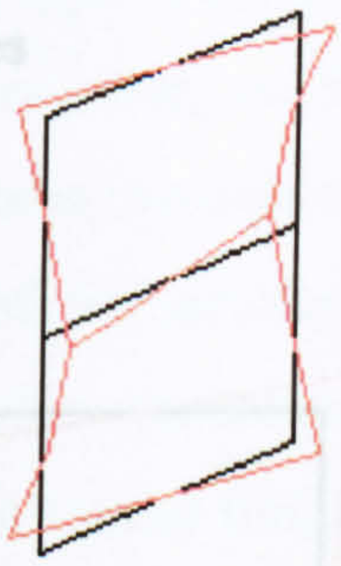

Figure 5.721 - Mode shape from ICATS

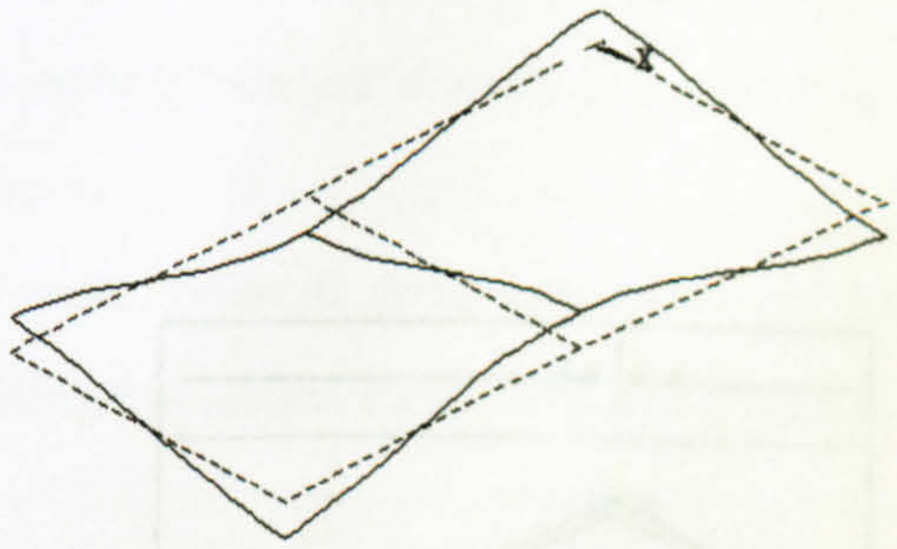

Figure 5.722 - Mode shape from ANSYS

Mode - 4

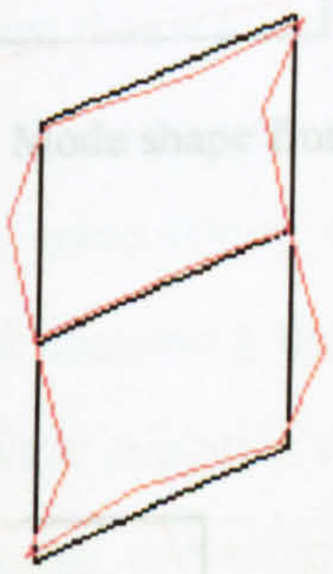

Figure 5.723 - Mode shape from ICATS

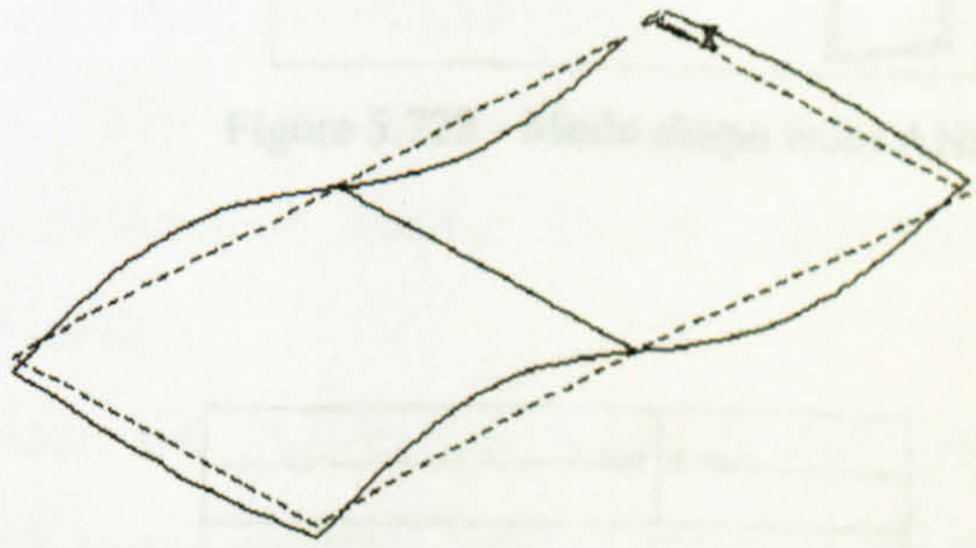

Figure 5.724 - Mode shape from ANSYS

Mode - 5

Figure 5.725 - Mode shape from ICATS

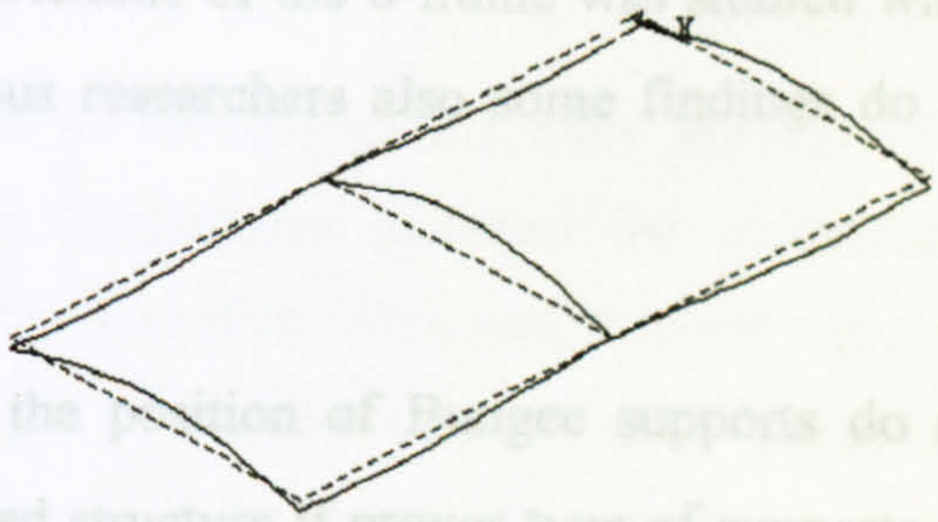

Figure 5.726 - Mode shape from ANSYS

In-plane modes

Mode - 6

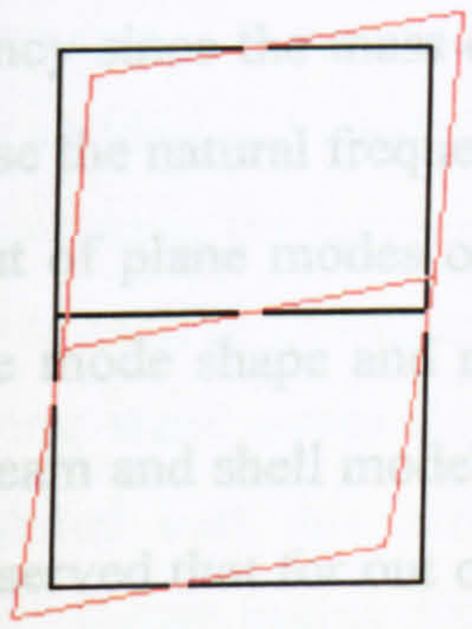

Figure 5.727 - Mode shape from ICATS

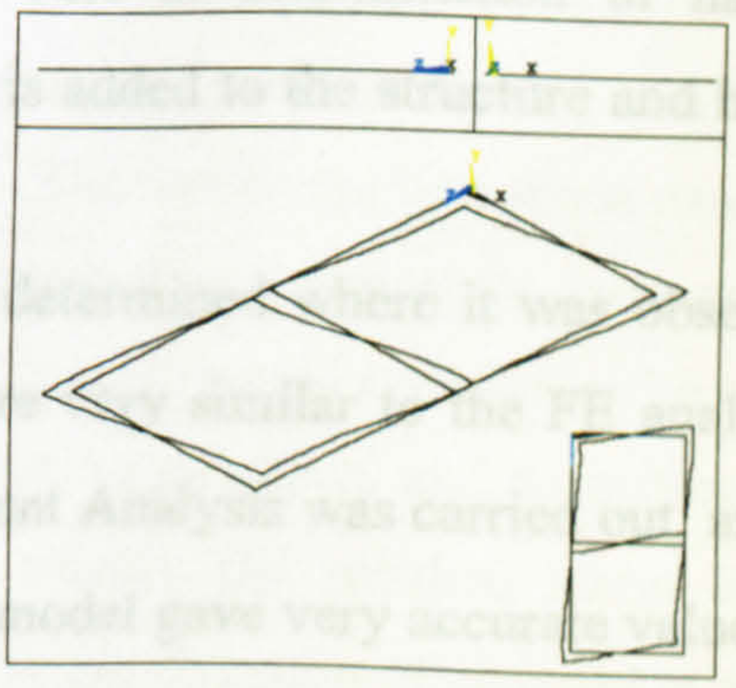

Figure 5.728 - Mode shape from ANSYS

Mode - 7

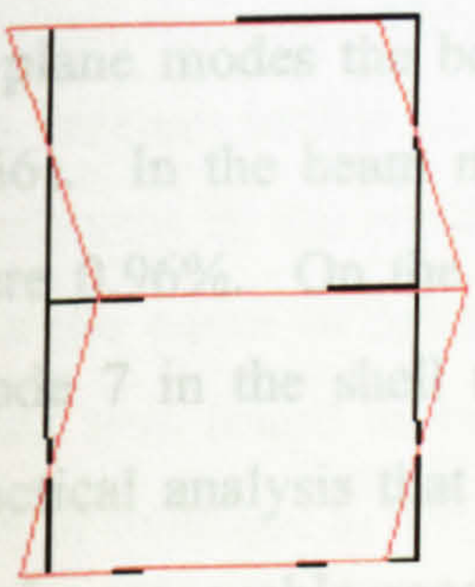

Figure 5.729 - Mode shape from ICATS

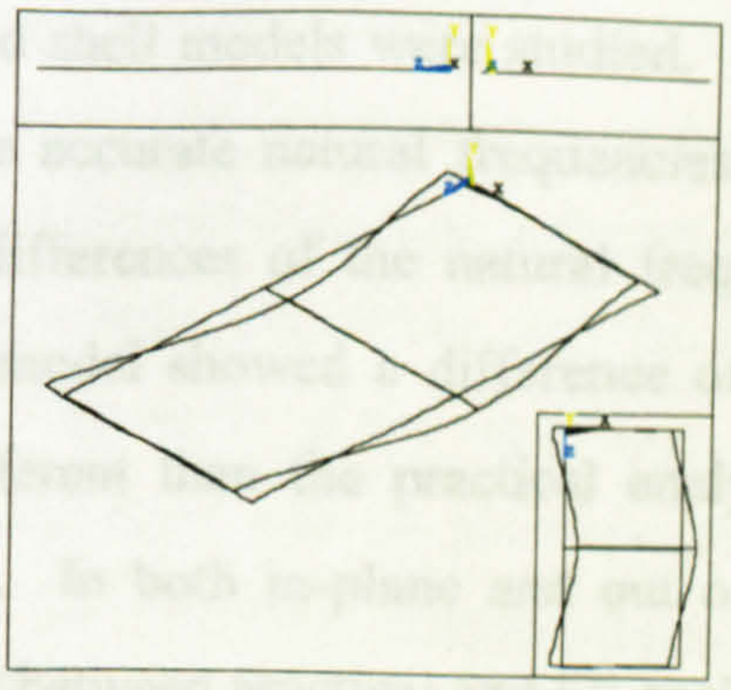

Figure 5.730 - Mode shape from ANSYS

5.8.4 Summary of Results

In the modal analysis some important characteristic of the 8-frame was studied which verified some of the findings of the previous researchers also some findings do not confirm certain results.

1. Study of Bungee support showed that the position of Bungee supports do not change in natural frequency of the studied structure if proper type of supports are used. It is a contradictory finding of Moersheim [95a] where a difference of 7 to 8 Hz was shown for bungee position.
2. The proper type of bungee shows a sharp FRF curve where the natural frequencies become very clear; on the other hand a strong bungee damps the structure and modes become invisible or obscure.
3. The size of the accelerometer plays a vital role in determination of natural frequency since the mass of the accelerometer is added to the structure and hence decrease the natural frequency.
4. The out of plane modes of the structure were determined where it was observed that the mode shape and natural frequencies are very similar to the FE analysis. Both beam and shell models of the Finite Element Analysis was carried out, and it was observed that for out of plane modes shell model gave very accurate values of the natural frequencies (Table 5.65). The maximum difference of the natural frequencies were found to be 10.4% in the shell model. On the other hand the beam model showed a difference of 31.9%.
5. In the in-plane analysis again both beam and shell models were studied. For the in-plane modes the beam model gave more accurate natural frequencies (Table 5.66). In the beam model the maximum differences of the natural frequencies were 0.96%. On the other hand the shell model showed a difference of 6.5%. Mode 7 in the shell model was found different than the practical analysis, in practical analysis that mode was not found. In both in-plane and out of plane modes reasonable good agreement was found between practical and FE analysis.
6. Accelerometer positioning was found to be very important in the determination of the natural frequency and the mode shapes.

Discussion of the Main Points Arising from the Experimental Programme

This investigation was arranged in stages to investigate different aspects of the vibratory treatment process. Initially the programme included the treatment of specimens with applied static stress, rigid body motion vibration, flexural vibration, and post-weld treatment. In the various stages of the investigation, other phenomena appeared which were felt to be essential parts of the whole programme and were investigated further as will be discussed in the following paragraphs. The residual stresses were calibrated to make sure that the measured values were exact. After calibration of the diffractometer and the X-ray elastic constant the instrument error band was reduced to ±10 MPa.

Reviewing the research described in this thesis, it is apparent that the treatments "during-welding" were not as successful as expected at the outset, as the overall effect was not decisive. A static stress was applied to the specimens while the specimens were being welded and cooled to observe its effect. The tensile applied stress caused a general decrease in the residual stress all over the measurement line while compressive applied stress caused an increase. Bhadeshia [15] found oriented crystals in the metal after applying static stress above the martensite start temperature, and accordingly it was anticipated that this effect would radically modify the residual stress level. Although the ferrite grains did show an alignment in the direction of maximum shear stress, there was not an associated change in the nature of the residual stress distribution.

Rigid body motion vibration was applied to the specimens to determine the effect on the residual stresses. Although some researchers have claimed success in reducing the residual stresses in this way there was some doubt because there is no induced stress in the specimens in the rigid body motion and it is a basic hypothesis that the induced stress is the cause of relief of residual stresses. The result of the rigid body motion treatment was found to be as it was expected, and there was no particular trend of increase or decrease in the residual stresses due to the rigid body motion vibration.

Flexural vibration experiments were carried out where dynamic stresses were applied to the specimens while the specimens were being welded and cooled. Two types of

specimens were processed applying flexural vibration, these being cantilever beam and four roller supported beam. The result of the treatments of the cantilever beam was found to be mixed; longitudinal residual stresses were found to decrease with application of small stresses but increase in the time and amplitude of vibration did not decrease the residual stress any further. The transverse residual stresses were found to increase with application of smaller applied stresses and after a certain level of applied stress the residual stress decreased.

In the next experiment of the flexural vibration four-roller-supported beams were processed. Two pieces of metals were joined together to make a similar situation to that of real welds. Similar to the cantilever beam specimens vibration was applied to the specimens while they were being welded and cooled. The result of the treatment was found to be scattered, and no conclusions could be made from the result.

To treat the specimens selecting a range of yield stress (during cooling), the four-roller-supported beams were used. The yield stress is much lower in the heat affected zone of the weld while it is being cooled and it should be easy to deform plastically by applying low amplitude vibration whereas a high applied stress is required at the room temperature. It was expected that this experiment would bring positive results, but again a very high scatter of stress distributions were found where there were no particular trends. There may be several reasons for this scatter; for example specimen geometry, material properties, movement of the weld line etc. However, the result is inconclusive. It may be suggested however that a detailed research programme could be devised where a computer program would follow the temperature variation of the specimen and apply different amplitudes of vibration according to the temperature.

After the negative results of the above two experiments, the work of Aoki and Nishimura [7] was simulated, with the specimens modified to suit to the dimensions of the existing X-ray cabinet. In a fashion similar to the previous two experiments, a very high scatter in the residual stresses was found and no particular trend in the residual stresses was observed due to the vibratory treatments. These results confirmed doubts about the general application of the experiments carried out by Aoki and Nishimura.

In the "during-welding" treatments discussed above, the static applied stress and

flexural vibration (where a bead was welded) showed trends of change in residual stresses. In all of the other experiments a lack of a trend in the data precluded any clear interpretation. This may be due to the variable material properties of the experimental structures, or may be inherent in the process.

After the mixed results of the "during-welding" treatments, welded specimens were vibrated at room temperature as "post-weld" treatment. In the "post-weld" treatment the residual stresses of the same specimen was measured before and after vibration and there were therefore no effects of material property differences. Thus any increase or decrease in the residual stresses were very clear. The "post-weld" treated specimens showed significant reduction in the residual stresses. Some important phenomena were observed in this investigation. The residual stresses were found to decrease to a higher degree in electropolished specimens. The reason of this was unknown, but it is assumed that electropolishing process removed the surface layer whose properties would be different from the bulk of the specimen.

The residual stresses were found to decrease most in two positions equidistant from the mid-width of the specimens. After a finite element analysis of the dynamic stress distribution in the specimen, it was assumed that either induced shear stress or the equilibrium characteristics of residual stresses caused this. To investigate these assumptions a torsional treatment experiment was carried out. In the torsional test the residual stresses were found to decrease significantly with the application of very small stresses. Further increase in induced torsional stress did not cause any more reduction, instead it caused only redistribution in the residual stresses. This finding was similar to the findings of Bouhelier [20], where he vibratory treated a welded gear box and found a significant reduction in the residual stress with application of a small alternating stress. One may conclude that this reduction in residual stress in this case may not be the effect of plastic deformation, but may have been due to the presence of retained austenite in the weld and in the heat affected zone.

In the "post-weld" treatment another characteristic was observed. In two specimens it was observed that residual stress increases significantly just before fatigue failure. To investigate this further, specimens were vibrated applying a high dynamic stress in steps until they broke. In every step the residual stresses were measured. It was found that the residual stress was only redistributed before fatigue failure. Thus the

assumption of increase in residual stress before fatigue failure was not confirmed.

Cryogenic treatment of welded specimens was carried out. The aim of this investigation was to find out if there were any stresses caused by the austenite phase present in the standard welded specimens. No reduction in residual stress was found due to the treatment. One would conclude that there was no retained austenite in the experimental structures, or not enough to affect the residual stress.

The aim of this research was to relieve residual stress and improve mechanical properties, i.e. increase fatigue life. To investigate the vibration effect on the residual stresses and fatigue life, a fatigue test was carried out. In this investigation the specimens were divided into three groups where each group was pre-treated. The first group was annealed, the second group was vibratory treated and the third group was left untreated. The result of the fatigue tests showed that annealing reduced and VSR treatment increased fatigue life. The reason for this result is quite clear, annealing reduced residual stress at the cost of the mechanical properties which were achieved during the thermomechanical treatment of the rolling process. On the other hand VSR treatment did not damage any mechanical property, instead it relieved the residual stresses or work hardening occurred in the heat affected zone which increased the mechanical properties. In this investigation an attempt was made to relate the fatigue life and residual stresses, but a high scatter was found and no definite conclusion was possible. Pattinson and Dugdale [105] stated that in low carbon steels the residual stresses diminished in the initial few load cycles thus the remaining load cycles do not have an effect on fatigue life.

A metallographic investigation of "during-welding" vibrated specimens were carried out, where the crystal orientation and the hardness of the specimens were checked. At low applied stresses no significant difference between vibrated and unvibrated specimens were observed. In the high amplitude vibration the crystals were found to be oriented in the [111] direction with the applied stresses and the hardness was found to increase significantly. A finite element analysis showed that the orientation of the crystals was directly related to the shear stress induced in the specimens. This finding is similar to the findings of Campbell [28]. Who applied vibration to solidifying cast iron and found a significant increase in mechanical properties.

General Conclusions

Before making a general conclusion of this work, it should be remembered that the conclusions are strictly applicable to the Mild Steel specimens used. This research was directed into several areas. Each will be evaluated separately.

X-ray Measurement

The calibration of the X-ray measurement showed that the error in the residual stress measurement could, with care, be reduced to less than ±10 MPa, which increased confidence in the residual stress measurements. The jigs used in the residual stress measurement provided good repeatability and increased the confidence further.

VSR Treatment

Looking back at the progress of the research described in this thesis, it is apparent that VSR treatment process followed two main directions: namely "during welding" and "post weld" treatments. In "**during welding**" treatments, several methods were applied to reduce the residual stresses, but no overwhelming success was achieved. The conclusions of the "during welding" treatments are

1. The effect of static tensile stress applied to the specimens (during welding) was found to decrease the residual stresses. On the other hand compressive applied stresses did the opposite, where the residual stresses were found to increase with application of the static stresses.

2. Rigid body motion vibration treatment was also found to be ineffective in reduction of residual stress, where the residual stresses were found to increase or decrease marginally without any particular trend.

3. Reduction in residual stress was observed in the flexural vibration mode. The longitudinal residual stresses were found to decrease with application of small levels of induced stresses (±48 MPa). With further increase in the applied stresses or the time of vibration no additional effect was found. The transverse

residual stresses showed a different characteristic, where the residual stresses were found to increase with application of small induced stresses. At higher levels of induced stress the residual stresses decreased. Increase in the time of vibration showed increased residual stresses.

4. High frequency vibration was also found to be ineffective in reducing the residual stresses. High frequency vibration showed no reduction in the longitudinal stresses but showed an increase in the transverse residual stresses. The cause of this increase was unknown, the most possible explanation would be the dislocation density was increased due to the high frequency vibration which showed increased residual stresses. One would conclude that VSR is not a function of the applied energy, since if so, then the high frequency vibration would show the maximum reduction, where the maximum power of the vibrator was used. Instead it showed the opposite result.

5. A limited amount of research was carried out selecting the yield stress range of the Mild Steel, but the residual stresses were found to increase and decrease without any particular trend. Further investigation is necessary.

6. The work carried out by Aoki and Nishimura (7) was repeated in this investigation, where no clear trend in the residual stresses were found. This implies that their findings were related to the specimen material used.

In the "post weld" treatment, the main findings may be summarised as follows.

1. The residual stresses were found to decrease with an increase in the applied stresses. The effect of an increase in the time of vibration was found to be negligible for lower applied stresses. In the higher applied stresses (> 200 MPa), increase in the time of vibration was found to be damaging to the structure. In the post-weld treatments the reduction in residual stress were found to be significant in all the samples. It was observed that the time of vibration had either a very small or no effect if the applied stress is small, but for large applied

stresses the residual stresses were found to be only redistributing until the onset of fatigue failure. The amplitude of vibration was found to play a large role in reducing residual stress but no straight forward relation between applied stress and reduction of residual stress was observed. Some researchers modelled the VSR as

$$\sigma_{orig} + \sigma_{app} - \sigma_Y = \sigma_f$$

Or

$$\sigma_f = \frac{\sigma_{orig} + \sigma_Y}{2} - \sigma_{app}$$

Where σ_f = Final level of residual stress

σ_{orig} = Original residual stress

σ_Y = Yield stress

σ_{app} = Applied stress

In this study, a general relation similar to the above two was not observed; this may be due to a complex redistribution in the residual stress. The residual stress reduction in the post-weld treatment was found to decrease in a particular fashion (Figure 5.562), where the above type of relation could not be modelled. The reduction in residual stresses was found to be maximised in two positions equidistant from the mid-width. It was thought initially that the induced shear stress in the plate caused that reduction since the shear stress peaked at these locations, but further work found that the shear stress on its own was not the cause.

2. Electropolished specimens showed a larger reduction in residual stresses in comparison to the as-rolled specimens. The reason for this larger reduction was unknown. It may be hypothesised that the electropolishing has removed the surface layer of highly deformed material that is present due to the friction and redundant shear consequent on the cold rolling process and it became easier for VSR treatment to reduce residual stress from the less deformed surfaces.

3. The residual stresses of the specimens were found to redistribute before fracture. The hypothesis that the residual stresses increase before failure was found to be void.

4. In the torsional test the residual stresses were found to redistribute only in the homogenous and peripheral-line welded shafts. In the spot-welded shafts, where a very short time was taken to cool down, a very important characteristic was found. The residual stresses were found to decrease significantly with application of very small stresses (less than ±3 MPa). This implies that the stress reduction in this case certainly was not due to any plastic deformation. There are maybe two possible explanation of that stress reduction

   (a) Possibly this reduction happened due to the movement of carbon atoms from the BCT or BCC where the carbon atom was stuck due to the very short cooling time.

   (b) Some austenite was retained in the weld or in the HAZ, which caused the residual stresses, and the shear stress helped transformation of the austenite to its succeeding phases and hence the residual stresses were relieved.

Cryogenic Treatment

Cryogenic treatment of the mild steel showed no effect on residual stresses, contrarily the VSR treatment of the same specimen showed a reduction of 36%. The possible explanation of this phenomenon may be that the cryogenic treatment did not work because the residual stress was not due to microstructural phases, (i.e. due to presence of retained austenite) instead it was due to thermal expansion and contraction (explained in Figure 1.2 and 1.3). The VSR treatment caused some local plastic deformation hence the residual stresses were reduced.

Fatigue Test

The fatigue life of the specimens subjected to VSR treatment increased by up to 30% and the thermally treated specimens showed a decrease of fatigue life by 33%. The fatigue life of the annealed specimens was reduced because the annealing process

damaged some important mechanical properties, which was achieved by the thermo-mechanical treatment during the rolling process.

Metallurgical Investigation

The results of the metallurgical investigation may be summarised as follows

1. The microstructural investigation of the post-weld vibrated and unvibrated specimens showed no difference between them although a significant reduction in residual stresses was found in the vibrated specimens. This might be due to the use of the optical microscopy, where the magnification was not enough to see the changes at the microstructural level due to the VSR treatment.
2. The specimens welded in the presence of high vibration amplitude showed grain refinement of the crystals and a special arrangement of the ferrite crystals. The ferrite crystals were found to form in a cross pattern where the direction of ferrite crystal orientation was close to the [111] direction with the applied stress axis.
3. The hardness of the vibrated specimens was found to increase by a maximum of 25%.

Modal Analysis

In the Modal Analysis several important characteristics of the structure was found as follows.

1. The bungee support position becomes insignificant if the proper type of bungee are used, which also makes the mode shapes more clear.
2. The size and position of the accelerometer shows some changes in the modal properties, and so those should be chosen carefully.
3. The natural frequency of the out of plane modes of the '8' frame was very similar to the natural frequencies of the shell model of the FE analysis; on the other hand the beam model showed the natural frequencies similar to the in-plane modes.

Recommendation for Further Work

With the development of modern stress scanning technology this work has got a scope for a true exploration. The "during welding" treatment method is the most important side of investigation, which is a key area in engineering production. In this study, investigations were initiated applying varying yield stresses of the cooling material. Due to the time limitation of this experimenter only a brief study was carried out. A detailed review of this would prove interesting.

The study of VSR should include further microstructural investigation. Electron microscopy may be used because conventional optical microscopy did not show any structural difference between the post-weld vibrated and unvibrated specimens.

In the "post-weld" treatment electropolished samples showed higher stress reduction, and further investigation is necessary. In the torsional stress effect investigation, a minute induced stress caused a significant reduction in the residual stresses and further investigation is necessary. This researcher mainly worked on cold rolled mild steel bar, the work could usefully be extended to other kind of steels non-ferrous metals etc.

References

1. "Standard Test Method for Determining the Effective Elastic Parameter for X-Ray Diffraction Measurements of Residual Stress," *Annual Book of ASTM Standards*, Vol. 03.01. February 1992
2. "Tool life Grows in Magnetic fields." *Machinery and Production Engineering*, 2 June 1989
3. Ananthagopal, K. P; Narayana, G. S; Prasannakumar, S. "Effect of Vibratory Stress Relieving on Dimensional Stability of Fabricated Structures." *Proceedings of the National Welding Seminar*, October, 1986, pp. 1-13
4. Ankirskii, B. M. "Effect of Vibration and Heat Treatment on the Mechanical Properties of the Metal and Welded Joints in 20K Steel." *Welding Production*. March 1995. Svar. Proiz., 1985, No. 3, pp. 19-21
5. Anon. "Relieving Stresses Without Heat. *Tooling and Production*." 1978, Vol. 44, pt. 9, pp. 62-64
6. Anuta, A. E. "The Modal Equations and Equal Frequencies in Definite Systems." *Computers and Structures*. Vol. 60, No. 3. pp. 357-367, 1996
7. Aoki, S; Nishimura, T. "Analytical Model Improvement of Residual Stress of Welding Joint using Vibration." *Current Topic in Computational Mechanics*, PVP-Vol. 305, Presented at The 1995 Joint ASME/JSME Pressure Vessels and Piping Conference, Honolulu, Hawaii, July 23-27, 1995, pp. 75-79.
8. Aoki, S; Nisimura, T; Hiroi, T; Amano, Y. "Reduction of Residual Stress of Welded joint Using Vibration." *Nippon Kikai Gakkai Ronbunshu, C Hen/ Transactions of the Japan Society of Mechanical engineers, Part C*. Vol. 61, No. 592, 1995, pp. 4800-4804
9. Bae, K. Y; Na, S. J; Park, D. H. "A study of Mechanical Stress Relief (MSR) Treatment of Residual Stresses for one-pas Submerged Arc Welding of V-grooved Mild Steel Plate." *Proceedings of the Institute of Mechanical Engineers Part B. Journal of Engineering Manufacture*. 1994, Vol. 208, No. B3, pp. 217-227
10. Balasingh, C; Seshadri, M. R; Srinivasan, M. N; Ramaseshan, S. "Vibrational Stress-Relief of Cast Iron Castings." *Indian Foundry Journal*, 1983, pp. 129-136
11. Belassel, M; Lebrun, J. L; Bettembourg, J. P. "Effect of Low Cycle Fatigue on Residual Stresses Evolution in an Eutectoid Steel; Study of the Bauschinger Effect by X Ray Diffraction." *Proceedings of the Fourth International Conference on Residual Stresses*. June 8-9, 1994. Baltimore, Maryland, USA, pp. 844-853
12. Bhadeshia, H. K. D. H. "A Short Communication: Carbon Content of Retained Austenite in Quenched Steels." *Metal Science*. Vol. 17, March 1983, pp. 151-152
13. Bhadeshia, H. K. D. H. "An Aspect of the Nucleation of Burst Martensite." *Journal of Materials Science* **17** (1982) 383-386
14. Bhadeshia, H. K. D. H. "Modelling of steel welds." *Materials Science and Technology*, February 1992 vol. 8, pp. 123-133
15. Bhadeshia, H. K. D. H. "Possible effects of Stress on Steel Weld Microstructure." *Mathmatical Modelling of Weld Phenomena-2*. ISBN 0-901716-63-4, 1995, pp. 71-118
16. Bhadeshia, H. K. D. H; David, S. A; Vitek, J. M; Reed, R. W. "Stress Induced transformation to Bainite in Fe-Cr-Mo-C Pressure Vessel Steel". *Materials Science and Technology*, August 1991, Vol. 7, pp. 686-698
17. Bhadeshia, H. K. D. H; Edmonds, D. V. "Bainite in Silicon Steels: New Composition-Property Approach Part 1." *Metal Science*. Vol. 17, Sept' 1983, pp. 411-425
18. Bhadeshia, H. K. D. H; Waugh, A. R. "Bainite: An atom-probe study of the incomplete reaction phenomenon." *Acta metallurgica*. Vol. 30, pp. 775-784, 1982

19. Botros, B. M. "Residual Stresses in Welded Steel Structure-II." *SME Technical Paper (Series)* , MF80-305, 1980

20. Bouhelier, C; Barbarin, P; Deville, J. P; Miege, B. "Vibratory Stress Relief of Welded Parts." *Mechanical Relaxation of Residual Stresses, ASTM STP 993*, L. Mordfin, Ed., American Society for Testing and Materials, Philadelphia, 1988, 58-71

21. Brauss, M. E; Pineault, J. A."Residual Strain Measurements of Steel Structures." NDE-Vol. 13, *NDE for the Energy Industry, ASME* 1995

22. Bühler, H; Pfalzgraf, H. G. "Discussion on the Reduction of Residual Stresses in work pieces made of Cast Iron." *Werkstatt und Betreib.* **171** (2) (1964), pp. 36-43

23. Bühler, H; Pfalzgraf, H. G. "Investigation into the Reduction of Residual Welding Stresses by Alternating Stress Tests or Mechanical Vibration." *Schweisse und Schreiden*, **16** (5) (1964), pp. 178-184.

24. Bühler, H; Pfalzgraf, H. G. "Investigation into the Removal of Internal Stresses in Cast Iron and Steel by Mechanical Vibration and Continued holding in the atmosphere." *V. D. I. Verlog*, **56** (1962)

25. Bühler, H; Pfalzgraf, H. G. "Mechanical Relief of Residual Stress in Castings (Relief of Casting Stresses by Jolting)." *Foundry Trade Journal*, May 13, 1965, pp. 567-569

26. Burton, B. "Theoretical analysis of annealing behaviour of mixed distribution of dislocation loops, voids, and gas bubbles: comparison with annealing behaviour of irridiated reactor component." *Materials science and technology*, July 1992 Vol. 8, pp. 602-610

27. Callister, W. D., Jr. "Materials Science and Engineering: An Introduction." Third Edition ISBN 0-471-30568-5

28. Campbell, J. "Effect of Vibration During Solidification." *International Metals Reviews*, No. 2, 1981, pp. 71-108

29. Carfagno, M. G; Noorai, F. S; Brauss, M. E; Pineault, J. A. "X-Ray Diffraction Measurement of Stresses in Post-Tensioning Tendons." *IABSE Symposium San Francisco*, 1995, Vol. 73/1

30. Cheever, D. L; Rowlands, E. W. "Vibrational Stress Relief: The Answer to the Dimensional Control ?" *Welding Design and Fabrication*, 1977, Vol. 50, Pt. 10, pp. 90-92

31. Clapp, P. C; Zhao, Y; Rifkin, J. A. "Transformation Toughening Simulate at Different Length Scales." *Materials Research Society Symposium Proceedings*. Vol-350, pp. 299-311, 1994

32. Claxton, R. A. "Vibratory Stress Relieving – Practice & Theory." Methods and Media. *The Institute of Metallurgical Technician, 1979.* ISBN/ISSN: 0901462071, pp. 34-45

33. Claxton, R. A. "Vibratory Stress Relieving- Part I : Theory." *Verifact.* Vol. 10, No. 1, February 1983, pp. 16-20

34. Claxton, R. A. "Vibratory Stress Relieving- Part II : Practice." *Verifact.* Vol. 10, No. 2, June 1983, pp. 11-16.

35. Claxton, R. A. "VSR Offers Cost Savings to Fabrication." *Welding Review*, August, 1983, pp. 148-152.

36. Claxton, R. A: Claxton, J. "Vibratory Stress Relieving – Its advantages and Limitions as an Alternative to Thermal Treatments." *Heat Treatment of Metals*. 1974, Vol. 1 pp. 131-137

37. Claxton, R. A; Lupton, A. "Vibratory Stress Relieving of Welded Fabrications." *Welding and Metal Fabrication.* December 1991, pp. 541-544.

38. Danko, J. C. "Effect of residual stress on the Stress-Corrosion Cracking of Austenitic Stainless Steel Pipe Weldments. Practical Application of Residual Stress Technology." *Conference Proceedings, Indianapolis, Indiana, USA*, 15-17 May 1991.

39. Dawson, R. "Residual Stress Relief by Vibration." *PhD Thesis*. The University of Liverpool. 1975

40. Dawson, R; Moffat, D. G. "A Study of the Effectiveness of Vibratory Stress Relief." *Proceedings of the Fourth Canadian Conference of Applied Mechanics, Montreal*, 1973, pp. 391-392

41. Dawson, R; Moffat, D. G. "Vibratory Stress Relief: A Fundamental Study of its Effectiveness." *Journal of Engineering Materials and Technology*, Vol. 102, No. 2, pp. 169-176, 1980

41a. Design Manual on the European recommendations for the fire safety of steel structures. European Convention for Constructional Steelwork. Technical Note No. 35, Brussels, 1985.

42. Dexter, R. J; Kaufmann, E, J; Fisher, J. W; Stout, R. D. "Comparison of Fatigue Resistance of various Longitudinal Weld Joints." *Offshore Technology Conference*. 1993

42a Dobson, B. J; "A Straight Line Technique for Extracting Modal Properties from Frequency Response Data." *Mechanical Systems and Signal Processing* (1987) 1(1), 29-40

43. Easterling, K. "Introduction to the Physical Metallurgy of Welding." Butterworth-Heinemann Ltd. ISBN 0 7506 0394 1

44. Eigenmann, B; Schulze, V; Vöhringer, O. "Surface Residual Stress Relaxation in Steels by Thermal or Mechanical Treatment." *Proceedings of the Fourth International Conference on Residual Stresses*, June 8-10, 1994, Baltimore, Maryland, USA, pp. 598-607

45. Enke, F. "Artificial Ageing of Casting with Enke Vibrators." *Machinery*. Vol. 94, April 8, 1959, pp. 794-795.

46. Entrekin, C. H. Jr. "Effect of Stress Relief on Microalloyed Weld Metal Impact Properties." *Suppliment to the Welding Journal*, August, 1983. Paper presented at the 64th AWS Annual Convention held in Philadelphia, Pennsylvania, during April 24-29, 1993

47. Ernst, S. "Effect of Mechanical Vibration on Weld Solidification Structure." *WE*. 714. Spring 1986, pp.1-13

48. Ewins, D. J. "Modal Testing: Theory and Practice." Reprint, June 1986

48a Ewins, D. J; Gleeson, P. T, "A Method for Modal Identification of Lightly Damped Structures." *Journal of Sound and Vibration* (1982) 84(1), 57-79

49. Fenghua, S; Dexin; F. "Tests of Residual Stress on Welded Structure under Vibratory Stress Relief." *Journal of Dalian University of Technology*. Vol. 34, No. 4, August 1994, pp. 390-393

50. Finch, D. M; Burdekin, F. M. "Effects of Welding Residual Stresses on Significance of Defects in Various Types of Welded Joints." *Engineering Fracture Mechanics*, Vol. 41, No. 5, pp. 721-735

51. Free, J. A; Goff, R. F. D. P. "Predicting Residual stresses in Multi-pass Weldments with the Finite Element Method." *Computers and Structures*. Vol. 32, No. 2, pp. 365-378, 1989

52. Frey, R. "Cryogenic Treatment Improves Properties of Drills and P/M Parts." *Industrial Heating*, September 1983, 21-23

53. Fuchs, H. O; Mattson, R. L "Measurement of Residual Stress in Torsion Bar Springs." *Proceedings of the Society for Experimental Stress Analysis*. Vol. 4, No. 1, 1946, pp. 64-73

54. George, T; Parker, E. R; Ritche, R. O. "Susceptibility to Hydrogen Attack of a thick-section 3Cr-1Mo-1Ni Pressure-Vessel Steel-Role of Cooling rate." *Materials Science and Technology*. March 1985 Vol. 1, pp. 198-208.

55. Gifford, D. J. "Vibratory Stress Relief." *Metals Australasia*, 1984, pp. 10-11

56. Gnirss, G. "Vibration and Vibratory Stress Relief. Historical Development, Theory and Practical Application." *Welding in the World*. Vol. 26, No. 11/12, pp. 284-291, 1988

57. Gozman, Y. B. "Controlled Vibratory Stress Relief for Stabilizing Dimension of Parts." *Soviet Engineering Research*. Vol. 10, No. 4, pp. 116-121, 1990

58. Granato, A; Lücke, K. "Application of Dislocation Theory to Internal Friction Phenomena at High Frequencies." *Journal of Applied Physics*. Vol. 27, No. 7, 1956

59. Granato, A; Lücke, K. "Theory of Mechanical Damping Due to Dislocation." *Journal of Applied Physics*. Vol. 27, No. 6, 1956

60. Gray, T. G. F; Spence, J; North, T. H. *Rational Welding Design*. Newnes Butterworths, 1975

61. Guan, Q; Guo, D. L; Li, C. Q; Leggatt, R. H. "Low Stress Non-Distortion (LSND) Welding-A New Technique for Thin Materials." *Welding International*, Vol. 8, No. 7, 1994. Welding Research Abroad. Nov' 1995, Vol. 41, No. 11, pp. 41-48

62. Hebel, G. Jr. "Subresonant Vibrations Relieve Residual Stress." *Metal Progress*, November 1985, pp. 51-55.

63. Hebel, T. A Better Way to Relieve Stress, *American Machinist and Automated Manufacturing*, December 1986, pp. 70-72.

64. Holden, T. M; Root, J. H; Fox, J; Porter, j; Pineault, J. A; Brauss, M. E. "Diffrection Measurements of Linewidth in Plasticity Deformed and Fatigued HY-80 Materials." *NDE-Vol. 13, NDE for the Energy Industry*, ASME 1995

65. Honeycombe, R. W. K; Bhadeshia, H. K. D. H. "Steels: Microstructure and Properties" 1995, ISBN 0 340 58946 9

66. Horger, O. J; Neifert, H. R; "Improving Fatigue Resistance by Shot-Peening." *Proceedings of the Society for Experimental Stress Analysis*, Vol. 2, 1944

67. Houck, F. "Putting Vibration to Work." *Mechanical Engineering*. Vol. 88, No. 9, 1966, pp. 48-50.

68. Jesensky, M. "Vibratory Lowering of Residual Stresses in Weldments." *Proceedings of IIW Conference 1987 on Stress Relieving Heat Treatment of Welded Construction*, pp. 153-160.

69. Ji, V; Lebrun, J. L; Dias, A. M; Batista, A. C. "Study of monotonic and cyclic deformation of 5083 Aluminum allow by X Ray diffraction profile analysis and transmission electron microscopy observation." *Proceedings of the Fourth International Conference on Residual Stresses*. June 8-9, 1994. Baltimore, Maryland, USA, pp. 1230-1237

70. Jo, J; Kleinosky, M. J; Swanson, R. E; Kozaczek, K. J; Ruud, C. O. "Determination of Surface and Depth Profiles of Residual Stresses in HY-100 Weldment." *3rd International SAMPE Metals Conference*, October 20-22, 1992

71. Jo, J; Wang, X. L; Kleinosky, M. J; Green, R. S; Hubbard, C. R; Spooner, S. "Evaluation of Stress Relief Treatments Using Diffraction." *Proceedings of the Fourth International Conference on Residual Stresses*. June 8-9, 1994. Baltimore, Maryland, USA.

72. Josefson, B. L; Karlsson, C. T. "Transformation Plasticity Effect on Residual Stresses in a Butt-Welled Pipe." *Transactions of the ASME*, Vol. 114, No. 3, 1992, pp. 376-378.

73. Josefson, L; Andersson, M. "Welding Stress Redistribution in a Butt Welded Pipe during Later Mechanical and Thermal Loading." *Journal of Pressure Vessel Technology, Transactions of the ASME*, November 1988, Vol. 110, No. 4, pp. 402-404

74. Jye-Long, L; Bhadeshia, H. K. D. H." A methodology for the prediction of time-temperature-transformation diagram." *Materials Science Engineering*, A171 (1993) 223-230

75. Kaldas, M. M; Dickinson, S. M. "The Flexural Vibration of Welded Rectangular Plates." *Journal of Sound and Vibration*, Vol. 75, No. 2, 1981, pp. 163-178

75a Kennedy, C. C; Pancu, C. D. P. "Use of Vectors in Vibration Measurement and Analysis." *Journal of Aeronautical Sciences*. Volume 14, Number 11, 1947, pp. 603-625.

76. Klauba, B. B. "Precise Control of Vibratory Stress Relief." *Tooling and Production*, November 1983, pp. 64-67.

77. Klauba, B. B; Adams, C. M. "A Progress Report on the use and understanding of Vibratory Stress Relief." *AMD (Symposia Series) (American Society of Mechanical Engineers, Applied Mechanics Division)*. Vol. 52, November 1982, pp. 47-58.

78. Klotzbücher, E; Kraft, H. "Vibratory Stress Relieving-An Alternative to Thermal Stress Relieving?" *Residual Stresses in Science and Technology*. (1987) pp. 959-966

79. Kuo, H. K; Cohen, J. B. "Changes in Residual Stress, Domain Size and Microstrain During the Fatigue of AISI 1008 Steel." *Materials Science and Engineering*, **61** (1983) 127-136

80. Landolt, D. "Fundamental Aspects of Electropolishing." *Electrochemica Acta*. Vol. 32 No. 1, pp. 1-11, 1987

81. Larsson, L. E; Spiegelberg, P. "The Gradual Change of Residual Stresses during Bending Fatigue of Induction-Hardened steel." *Scandinavian Journal of Metallurgy* **2** (1973) 19-23

82. Larsson, T. B; Tronskar, J. P. "Influence of Vibrational stress relief on Welding Stresses and Cracking Susceptibility." *VERITEC Marine Technology Consultant. VERITEC Report.*No. 84-3158, March 1984.

83. Lin, Y. C; Chou, C. P. "A New Technique for Reducing the Residual Stress Induced by Welding in type 304 stainless steel." *Journal of Materials Processing Technology*. **48** (1995) 693-698

84. Lindgren, Lars-Erik. "Temperature Fields in Simulation of Butt- Welding of Large Plates." *Communications in Applied Numerical Methods*. Vol. 2, pp. 155-164, 1986

85. Lu, J. "Handbook of Measurement of Residual Stresses." *Society for Experimental Mechanics, Inc. (SEM)*. ISBN 0-88173-229-X FP

86. Lu, J: Flavenot. J. F. "Residiul Stress Relaxation during Cyclic Loading. Influence of Mechanical Properties and Prediction by the Calculation." *Memoires et Etudes Scientifiques Revue de Metallurgie*, Nov 1988, Vol. 85, No. 11, pp. 615-626

87. Lu, J; Bouhelier, C; Lieurade, H. P; Baralle, D; Miege, B; Flavenot, J. F. "Study of Residual Welding Stress using the Step-by-Step Hole Drilling and X-Ray Diffraction Method." *Welding of the World/Le Soudage dans le Monde*. Vol. 33, No. 2, pp. 118-128, 1994

88. Lu, Y. M; Ju, F. D. "Structural Damage Configurations Subject to Modal Oscillations." *American Society of Mechanical Engineers Design Engineering Division (Public), DE, ASME*, New York, NY, USA, 1991, Vol. 38, pp. 1-7

89. Lutes, L. D; Sarkani, S. "Decay of Residual Stress in Stochastic fatigue." *Journal of Structural Engineering*, January 1996, pp. 92-98

90. Maekawa, Y; Nakagiri, A; Maeda, H. "The Behaviour of Surface Residual Stress Relief and Lattice Defect Density with Mechanical Vibration in FC 25 Cast Iron." *Nippon Kikai Gakkai Ronbunshu, A Hen*. Vol. 52, Part 477 pp. 1295-1299, 1986

91. Manceau, J. F; Robert, L; Bastein, F. O; Oytana, C; Biwersi, S. "Measurement of Residual Stresses in a Plate Using a Vibrational Technique- Application to Electrolytic Nickle Coatings." *Journal of Microelectromechanical Systems*, Vol. 5, No. 4, December 1996, pp. 243-249.

92. Masubuchi, K. "In-Process control and Reduction of Residual Stresses and Distorsion in Weldments." *Practical Application of Residual Stress Technology, Conference Procedings, Indianapolis, Indiana*, USA, 15-17 May 1991.

93. Matsuzaki, A; Bhadeshia, H. K. D. H; Harada, H. "Stress Affected Bainitic Transformation in a Fe-C-Si-Mn Alloy." *Acta Metallurgica et Materialia*. Vol. 42, No. 4, pp. 1081-1090, 1994

94. McGoldrick, R.T; Saunders, H. E. "Some Experiments in Stress-Relieving Casting and Welded Structures by Vibration." *Journal of the American Society of Naval Engineers*. Vol. 55, No. 4, 1943, pp. 589-609.

95. Miettinen, J. "Calculation of Solidification-Related Thermophysical Properties for Steels." *Metallurgical and Materials Transactions B*. Vol. 28B, April 1997, pp.281-297

95a Moersheim, R. Vibratory Stress Relief, University of Strathclyde, Summer - 1995.

96. Mohanty, O. N. "On the Stabilization of Retained Austenite: Mechanism and Kinetics." *Materials Science and Engineering B32* (1995) 267-278

97. Moore, H. F. "A Study of Residual Stress and Size Effect and a Study of the Effect of Repeated Stress on Residual Stresses due to shot peening of two steels." *Proceedings of the Society for Experiment Stress Analysis*, Vol. 2, 1994, pp. 170-177.

98. Nakagiri, A; Hirai, K; Shinke, N; Yamano, T. "The residual Stress Relief Under Mechanical Vibration and Subsequent Dimensional Change in Copper and Brass." *Proceedings of the Fourth International Conference on Residual Stresses*, June 8-10, 1994, Baltimore, Maryland, USA, pp. 1300-1305

99. Nakagiri, A; Maeda, H; et. al. "The Behaviour of Vibrational Surface Residual Stress Relief in FC 25 Cast Iron." *Nippon Kikai Gakkai Ronbunshu, A Hen.* Vol. 50, Part 452 pp. 751-757, 1984

100. Nayama, M; Akitmo, N. "Development of Stress Relief method for Weld Joint of Pipe using Ice Plug." *Yosetsu Gakki Ronbunshu*, Feb-1994, Vol-12, Part-1, pp.132-136.

101. Nguyen, T. N; Wahab, M. A. "The Effect of Residual Stresses on Fatigue of Butt Joints." *Welding Journal*, February 1996, Vol. 75, No. 2

102. Ohol, R. D; Nagendra Kumar, B. V; Noras, R. A. "Measurement of Vibration-Induced Stress Relief in Heavy Fabrication Industry." *Mechanical Relaxation of Residual Stress, ASTM STP 993*, L. Morfin, Ed., American Society for Testing and Materials, Philadelphia, 1988, pp. 45-57

103. Ohtake, Y. "Identification Method for Estimating Residual Stress Distribution due to Butt-Welds of Thin Plates by Boundary Element Method." *Nippon Kikai Gakkai Ronbunshu, A Hen/ Transactions of the Japan Society of Mechanical engineers*, Part A. Vol. 61, No. 589, pp. 2068-2072, 1995

104. Parlane, A. J. A. "Vibrational Stress Relief." *The Welding Institute Research Bulletin*, 1977, pp. 339-341

105. Pattinson, E. J; Dugdale, D. S. "Fading of Residual Stresses due to Repeated Loading." *Metallurgia.* 1962, pp. 228-230

106. Petershagen, H. F; Hoffmeister, H. "Fatigue Properties of Hyperbaric Dry Repair Welds." *Offshore Technology Conference*, 1993

107. Pineault, A. J; Brauss, M. E; Vinarcik, M. J. "Characterizing Residual Stresses Induced by Rolling in Crankshaft fillets using X-Ray Diffraction." *Proceedings of the 1995 SEM Spring Conference and Exhibit*, June 12-14, 1995, Grand Rapids, Michigan, USA, pp. 521-524.

108. Polnov,V. P; Mogilner, M. N; Gudonis, I. B; Shukyalis, A. V. "Vibration Working of Formed and Welded Fittings Parts." *Chemical and Petroleum Engineering (English translation of Khimicheskoe I Neftyanoe Mashinostroeni).* Vol. 18, No. 5-6, pp. 248-250, 1992

109. Porter, D. A; Easterling, K. E. "Phase Transformation in Metals and Alloys." Second Edition 1992, ISBN 0 421 45030 5

110. Povolo, F; Tinivella, R. J; Botteri, G. B. "Some considerations about stress-relaxation in bending when an internal stress is present." *Journal of Materials science*, 27 (1992) 6590-6596

111. Povolo, F; Tinivella, R. J; Reggiardo, J. F; Botteri, G. B. "Stress relaxation in bending of type AISI 304 stainless steel at 773 and 823 K." *Journal of materials Science*, 27 (1992) 1505-1513

112.Ragozin, Y. I; Polianin, I. V. "A New Express-Method of Residual Stresses Relief in Metals and Ceramics." *Proceedings of the Fourth International Conference on Residual Stresses*. June 8-9, 1994. Baltimore, Maryland, USA, pp. 926-931

113.Reed, R. C; Bhadeshia, H. K. D. H. "A Simple Model for Multipus Steel Welds." *Acta Metallurgica et Materialia*. Vol. 42, No. 11, pp. 3663-3678, 1994

114.Rich, S. R. "Quantitative Measurement of Vibratory Stress Relief." *Welding Engineer*, 1969, pp. 44-45

115.Rogers, D. H. "An Extension of a Theory of Mechanical Damping Due to Dislocations." *Journal of Applied Physics*. Vol. 33, No. 3, 1962

116.Rosenthal, D. "The Theory of Moving Heat Source of Heat and its Application to Metal Treatments." *Transactions of the ASME*, November, 1946, pp. 849-866

117.Sedek, P. "Vibratory Stabilization of Welded Constructions – Experiments and Conclusions." *Proceedings of IIW- Conference 1987 on Stress Relieving Heat Treatment of Welded Construction*, pp. 145-151.

118.Shanker, S; Wood, W. E; Khan, K. H. "Effect of Vibratory Stress Relief treatments on Residual Stress in Mild Steel Butt Welds." *12th National SAMPE Technical Conference*, October 7-9, 1980, pp. 776-786

119.Shen, W; Chen, W; Chen, S; Zhio, S. "Explosive Relieving of Residual Welding Stresses." *Proceedings of the Fourth International Conference on Residual Stresses*. June 8-9, 1994. Baltimore, Maryland, USA, pp. 1220-1225

120.Shipway, P. H; Bhadeshia, H. K. D. H. "The Effect of Small Stresses on the Kinetics of the bainite transformation." *Materials Science Engineering*, A201 (1995) 143-149

121.Smith, J. J; Farrar, R. A. "Influence of Microstructure and Composition on Mechanical Properties of some AISI 300 series Weld Metals." *International Materials Review*. Vol. 38, No. 1, 1993, pp. 25-51.

122.Solov'eva, E. A; Petrov, A. F; Chikalidi, O. G; Kim-Khenkina, A. M. "Vibration Treatment of Metal Parts." *Chemical and Petroleum Engineering (English translation of Khimicheskoe I Neftyanoe Mashinostroeni)*. Vol. 27, No. 1-2, pp. 48-49, 1991

123.Sonsino, S. M; Müller, F; deBack, J; Gresnigt, A. M. "Influence of Stress Relieving by Vibration on the Fatigue Behaviour of Welded Joints in Comparison to Post-weld Heat Treatment." *Fatigue and Fracture of Engineering Materials and Structures*. Vol. 19, No. 6, pp. 703-708, 1996

124.Taggart, R; Merchant, H. C; Bodre, R. A. "Vibration Stress Relief in Single Crystals." *AMD (Symposia Series) (American Society of Mechanical Engineers, Applied Mechanics Division)*. Vol. 52, 1982, pp. 59-73

125.Tech Briefs: "On-site Stress Relief combats Weld Cracking." *Tooling and Production*, April, 1986, page-114.

126.Tewari, S. P; Shanker, A. "Effect of Longitudinal Vibration on the Mechanical Properties of Mild Steel Weldments." *Proceedings of the Institute of Mechanical Engineers*, Vol. 207, pp. 173-177.

127.Tryfyakov, V. I; Mikheev, P. P; Kudryavtsev, Y. F. "Ultrasonic Impect Peening Treatment of Welds and Its Effect on Fatigue Resistance in Air and Seawater." *Offshore Technology Conference*, 1993, pp.183-193

128.Tsukamota, S; Harada, H; Bhadeshia, H. K. D. H. "Metastable phase solidification in electron beam welding of dissimilar stainless steels." *Materials Science and Engineering*, A178, 1994, 189-194

129. Ueda, Y; Yuan, M. G. "Prediction of Residual Stresses in Butt Welded Plates Using Inherent Strains." *Journal of Engineering Materials and Technology*. October 1993, Vol. 115, pp. 417-423

130. Vlasenko, V. I; Senyukov, V. L. "An Investigation of the Relaxation of Static Stresses in Chromium-Nickel Steel Specimens in Cyclic loading." *Strength of Materials*, 1990, Vol. 22, Pt. 3, pp. 359-363

131. Volkov, V. V; Orzhekauskas, S. I. "Vibratory Stress Relief of Titanium Structures." *Vibration Engineering*, Vol. 2, pp. 59-66, 1988

132. Wahi, K. K; Maxwell, D. E. "An Analysis of the Relaxation of Residual Stresses by using Vibrational Conditioning." *Transactions of the International Conference on Structural Mechanics in Reactor Technology*, 1979, L13/3, pp. 1-8.

133. Walker, C. A.; Waddell, A. J; Johnston, D. J. "Vibratory Stress Relief-an Investigation of the underlying Processes." *Proceedings of Institute of Mechanical Engineers*, Vol. 209, 1995, pp. 51-57.

134. Wang, X; Wang, S; Hua, L. "Transformation Behaviour of Austenite in Steel under Condition of Stress-Strain and Its Application." *Journal of Material Science and Technology*. Vol. 11, 1995, pp. 440-442.

135. Weng, C. C; Chen, J. J. "Study on Residual Stress Relief of Welded Structure Steel Joints." *Journal of Materials in Civil Engineering*, May 1993 Vol. 5 No. 2

136. Weymuller, C. R. "Stress Relieve Early to Avoid Trouble Later." *Welding Design and Fabrication*, 1983 Vol. 56, Pt. 5, pp. 31-36

137. Withers, P. J; Edwards, L. "Strain Scanning: Getting Inside Information." Repriented from *Materials World*, 1996 January Issue, Vol. 4, No. 1, pp. 9-11

138. Wohlfahrt, H. "Residual Stresses as a Consequence of Welding." *Adv in Sur Treat: Technol – Appl – Eff. Vol 4: Residual Stresses*, 1987, pp. 39-58. Pergamon Press, Oxford, England. IS: 0-08-034062-8

139. Wozney, G. P; Crawmer, G.R. "An Investigation of Vibration Stress Relief in Steel." *Welding Research Suppliment*, 1968, Vol. 23, Pt. 9, pp. 411-419

140. Xie, Z. L; Liu, Y; Hänninen, H. "Stabilization of Retained Austenite due to Partial Martensitic Transformations." *Acta Metallurgica et Materialia*. Vol. 42, No. 12, pp. 4117-4133, 1994

141. Yasheng, W; Lanlin, H. "A New Method of Calibrating Strain Release Coefficients in Measuring Welding Stresses." *Strain*. February 1994

142. Ye, X. Y; Zhou, Z. Y; Yang, Y; Zhang, J. H; Yao, J. "Determination of the Mechanical Properties of Microstructures." *International Conference on Solid-State Sensors and Actuators, and Eurosensors and Proceedings*. 1995, Vol. 2, pp. 100-103

143. Zacharia, T; Vitek, J. M; Goldak, J. A; Debroy, T. A; Rappaz, M; Bhadeshia, H. K. D. H. "Modeling of Fundamental Phenomena in Welds." *Modelling and Simulation in Material Science and Engineering*. 3 (1995) 265-288

144. Zaveri, K. "Modal Analysis of Large Structures – Multiple Exciter Systems" ISBN 87 87355 03 5

145. Zhang, G; Shi, Y; et. al. "Study and Application of Vibration Relieve Residual Stress." *Zhuzao/ Foundry*, 1989 Part 1, pp. 19-22

Appendices

Appendix I: Microstructural Phases

The microstructural phases discussed in section 1.3.1 are shown here.

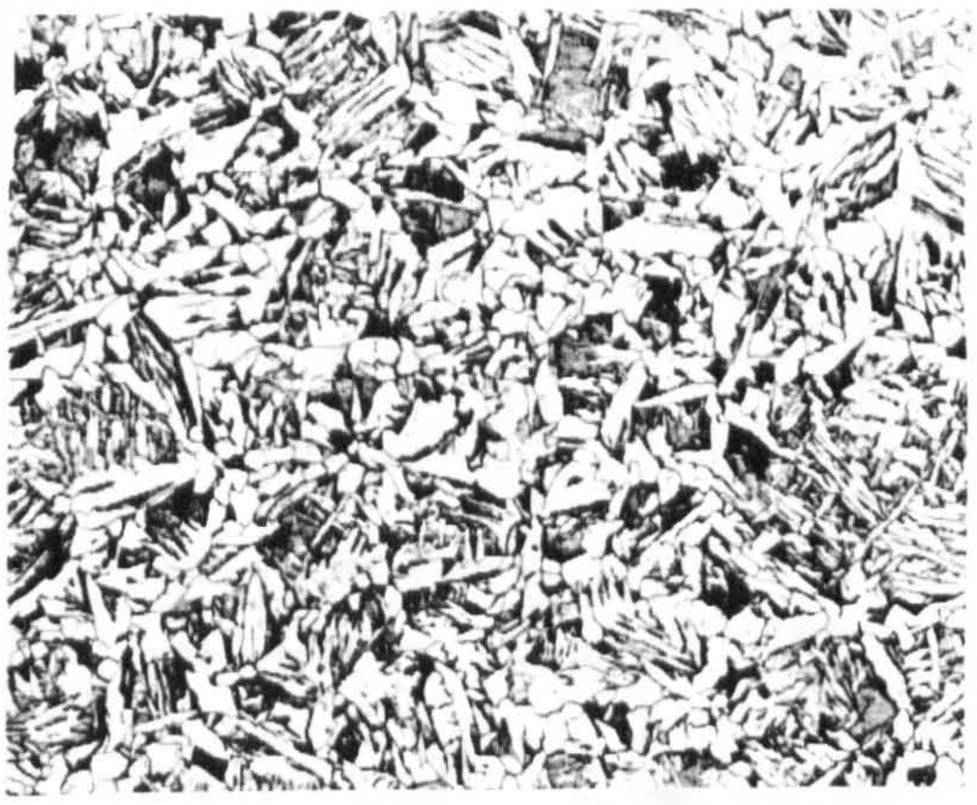

Figure A - Acicular ferrite

Figure B - Allotriomorphic ferrite

Figure A shows a mixture of acicular ferrite and bainite. Acicular ferrite is white a bit columnar, but the boundaries is not rounded, instead it is zigzag. In Figure B the allotriomorphic ferrite is presented. The allotriomorphic ferrite is formed in the grain boundaries (white band).

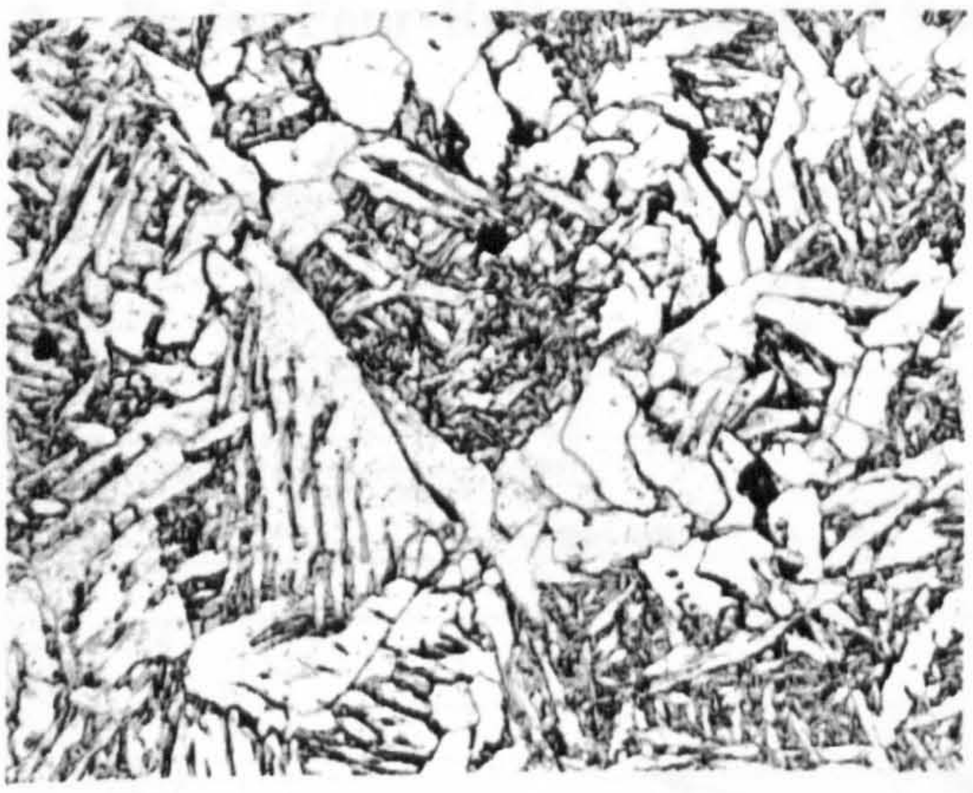

Figure C - Bainite

Figure D - Widmanstätten ferrite

The bainite structure is shown in Figure C above. The bainite formation started from the grain boundaries and formed like fingers. The needle like pattern of the Widmanstätten ferrite is shown in Figure D.

Appendix II: X-ray Measurement Jigs

1. Jig for Cantilever Beam Specimens

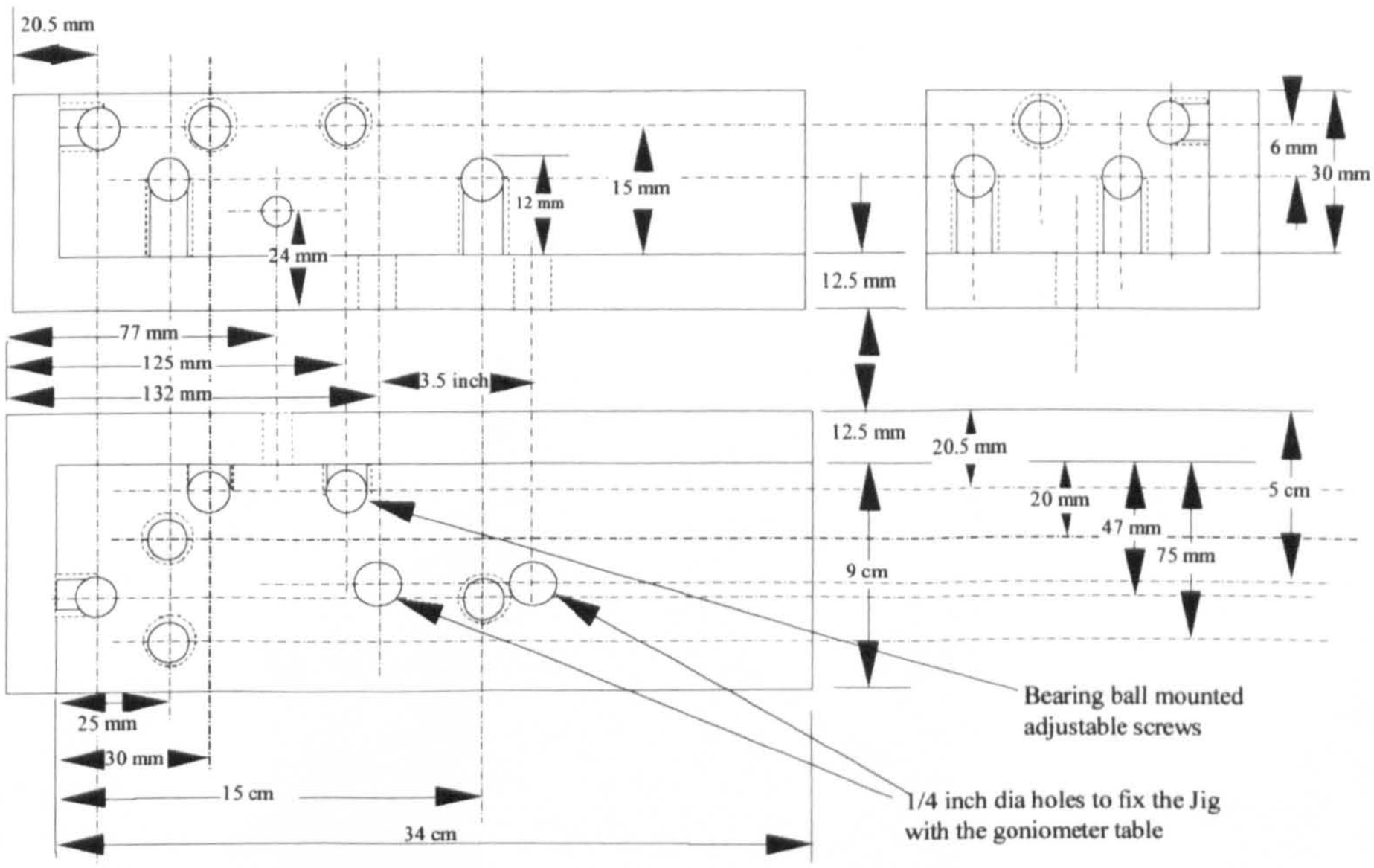

2. Jig for Four-Roller-Supported Beam Specimens